

A J O M C

Asian Journal of Organic & Medicinal Chemistry

Volume 6, Number 4

October - December, 2021

ISSN: 2456-8937



<http://ajomc.asianpubs.org>



Asian Publication Corporation
Sahibabad (India)
<http://asianpubs.org>

Editor-in-Chief

Dr. Bimal K. Bainik

Vice President of Research & Education Development
Community Health Systems of South Texas
Edinburg, USA

Asian Journal of Organic & Medicinal Chemistry

Editor-in-Chief

Bimal Krishna Banik

Professor and Senior Researcher
Department of Mathematics and Natural Sciences
College of Sciences and Human Studies
Deanship of Research Development
Prince Mohammad Bin Fahd University, Kingdom of Saudi Arabia

Editorial Advisory Board

Prof. (Dr.) Doralyn S. Dalisay

Head, Department of Pharmacy

College of Pharmacy and Medical Technology University of San Agustin Iloilo City, Philippines

Prof. (Dr.) Hongchao Zheng

Center for Integrative Chemical Biology and Drug Discovery,

UNC-Chapel Hill, Chapel Hill, NC 27599

Prof. (Dr.) Marek Cyprian Chmielewski

Institute of Organic Chemistry

PASKasprzaka 44/5201 - 224 Warsaw 42,

P.O. Box 58 Poland

Prof. (Dr.) Joaquín Tamariz

Department of Organic Chemistry, National School of Biological Sciences,

National Polytechnic Institute. Prol. Carpio and Plan de Ayala, 11340 Mexico City, DF, Mexico

Dr. Biswa Mohan Sahoo

Department of Pharmaceutical Chemistry

Vikas College of Pharmacy, Vissannapeta, Krishna Dist.

Andhra Pradesh, India

Dr. Pranjal Baruah

Department of Applied Science

Gauhati University, Guwahati, India

Dr. Jhuma Ganguly

Department of Chemistry

Indian Institute of Engineering Science and Technology

Shibpur, India

Dr. Chittaranjan Sinha

Department of Chemistry

Jadavpur University, Kolkata, India

Dr. Aman Bhalla

Assistant Professor

Department of Chemistry & Center of Advanced Studies in Chemistry

Panjab University, Chandigarh

Dr. Hemant Vilas Chavan

Department of Chemistry

A.S.P. College, Devrukh, Ratnagiri, India

Dr. Seema P Mengshetti

Emory University, E469

Laboratory of Biochemical Pharmacology

Health Sciences Research Building

1760 Haygood Drive, Atlanta GA 30322

Dr. Shovan Mondal

Department of Chemistry

Syamsundar College, Shyamsundar, Purba Bardhaman, India

Asian Journal of Organic & Medicinal Chemistry

Special Issue

On

**Current Trend on Research in Applied Science, Management and
Technology**

CONTENTS

Research Papers

Design and Analysis of Flow Patterns and Thermal Behaviour in a Refrigeration Truck using CFD 712 – 722

Archana J, Punitharani K and Jayachitra R

Optimization of Inventory Management in Manufacturing Firms 723 – 737

B. Vaishnavi and R. Ilakkiya

Application of Visual Intelligence for Detection of Physical Damages in Objects 738 – 742

A. Chitra and Gowtham Balaji B

Solving Lorenz System of Equation by Laplace Homotopy Analysis Method 743 – 750

G. Sai Sundara Krishnan, R. Malathy and S. R. Saratha

Mahalanobis-Taguchi System for Simultaneous Feature Extraction and Prediction for Cancer Diagnosis 751 – 757

Aneetha A. Sand Priya R

Automated Detection of the Severity of Diabetic Retinopathy Using Pre-Trained Cnn 758 – 762

R. Vidhyapriya and N. Ravitharajalakshmi

Covid Detection from Chest X-Ray Using Cnn 763 – 768

Ajith Sam Raj S, Hari Ram R and Dr. B. Kalpana

Cancer Treatment Planning Using Computed Tomographic Images 769 – 777

Padmapriya B

A Non-Invasive Early Diagnosis of Osteoarthritis Using Random Forest and Ann 778 – 784

Anisha C.D and Arulanand N

Breast Cancer Prediction Using Machine Learning Algorithms 785 – 795

Kavitha Chinniyan and Roobini Subramani

A Review on Gait Analysis and Supporting Systems to Sense and Prevent Elderly Fall 796 – 804

R. Ramachandran and P. Kanakaraj

Ergonomic Design and Fabrication of Trolleys Used in Hospitals 805 – 817

R. Jayachitra, P. Nidharsan, S. J. Jason Samraj and M. Ranjith Kumar

Chest Radiographic Images Enhancement and Segmentation for Feature Analysis and Lung Nodule Detection	818 – 825
<i>Gopalakrishnan S</i>	
Predicting Parkinson's disease Based on Gait Pattern using Machine Learning Techniques	826 – 834
<i>Sridevi U. K, Hashini S, Janani K and Varsha P. S</i>	
An Evaluation on Theories and Models in Eye Anatomy Interconnected Side Effects and Pro-Longed Diseases	835 – 842
<i>Sowmiya M, Banu Rekha B and Malar E</i>	
A Review on Urinary Sediment Particles and Related Kidney Diseases	843 – 848
<i>Suhail K and Brindha D</i>	
Latent TB Infection (LTBI) Identification through Microscopic Images	849 – 855
<i>Brindha D</i>	
Bladder Prolapse Images Using Preset Sedimentary Particle Recognition	856 - 863
<i>Kathy Jessica P and Brindha D</i>	
Detection and Mitigation of Mitm Attack in Software Defined Networks	864 – 870
<i>Saritakumar N, Anusuya K V and Balasaraswathi B</i>	
A Low-Phase Noise PII for 5G Application	871 – 875
<i>Radha Krishnan K R, Subha Rani S and Shivasubramaniyarajan V M</i>	
A Study on Job Stress among Women Bank Employees with Special Reference to Malabar Region of Kerala	876 – 881
<i>Amrutha S. and V. Santhi</i>	
Enhancement of Overall Equipment Effectiveness in Automotive Parts Manufacturing Industry	882 – 889
<i>S. Adithya and T. Anantharaj</i>	
Quantifying the Effectiveness of Digital Content Marketing	890 – 894
<i>Aarthi Mai A S and Monisha C</i>	
Ergonomic Assessment of Muscular Fatigue Associated with Overhead Tasks in Pump Assembly Using Surface Electromyography (SEMG)	895 – 902
<i>Ashok P, Madhan Mohan G and Nevhetha N</i>	
Step Ahead to Computer Vision - Leveraging Facial Expression Recognition Using GPU-Enabled Resnet-50 and Squeezenet CNN Architectures	903 – 911
<i>Karpagam G R, Akash V S, Sanjaya Prabbakar M S, Jaya Vignesh R, Naveen V and Hari Prasath R</i>	

Design and Development of Medicated Sanitary Napkins with Selected Medicinal Herbs	912 – 927
<i>Subathra. B</i>	
Model Based Calibration for Off-Road Vehicles	928 – 933
<i>Benjamin Shiloh Davidson, Neelakrishnan S and Abhirama Sastry D.V.V.S.S.S</i>	
Shear Capacity of Reinforced Concrete Beam with Vertical Stirrups	934 – 937
<i>Ramesh Babu G and Sivakumar C G</i>	
Planning of Bus Rapid Transit System for Coimbatore City Using GIS	938 – 944
<i>Mohammed Insaf Z, Sivakumar C G and Elangovan K</i>	
Analytical Study on the Optimum Damper Placement on the Seismic Response of RC Framed Structures	945 – 951
<i>Gaanavaruni Rodriguez L F and Sivakumar C G</i>	
Hidden Community Detection in Social Networks using Path Matrix	952 – 961
<i>Sundar C, N Ilayaraja and Ranjani R</i>	
Development of Combination Herbal Microencapsulated Healthcare Apparel for Skin Discolouration	962 – 969
<i>K. Chandrasekaran</i>	
IOT Based Secured Patient Healthcare System	970 – 976
<i>B. Nivedetha</i>	
Covid-19 Severity Detection	977 – 983
<i>M. Prethi and Ila. Vennila</i>	
An Intelligent System Using Deep Learning Techniques to Prevent Human-Animal Conflicts in Agricultural Lands	984 – 995
<i>M. Kathiresh, P. Sweetey Jose, R. Neelaveni and C.T. Sangavi Chellam</i>	
Advances in Sentiment Analysis of Twitter Data	996 - 1005
<i>T. Raveena, P. Saranya, Marx Rajangam and Engels Rajangam</i>	
Design and Hardware Implementation of Three-Phase Multi-Level Active Front End PWM Rectifier	1006 – 1014
<i>R. Srinivashkannan, M. Sundaram, B. Vinod, J.Chelladurai and M. Anand</i>	
Estimation of Remaining Useful Life (RUL) for Turbofan Engines Using Automl: A Self Service Analytics Approach	1015 – 1023
<i>Banu Rekha B, Somasundaram B, Manoj J and Ramesh S</i>	
Improving Sewing Line Performance and Rejection Analysis in a Garment Industry	1024 – 1031
<i>Mathivanank, Jayachitra R, Punitharani K and Prabhakarank</i>	

Design of a Smart Waste Segregation System	1032 – 1046
<i>R. Jayachitra, Udit Sanyal, Ayush Singh and Thangaraju Naveen</i>	
Fabrication of Rice Husk Gasifier Stove by Improving Efficiency	1047 – 1052
<i>Kannan K, Babu S and Dhiraviyapandiyam P</i>	
Study of Heat Transfer Characteristics during Phase Change in a Latent Heat TES System	1053 – 1061
<i>Muthamilselvan N and Kannan K</i>	
Productivity Improvement in Robot Welding through Experimentation by Varying Process Parameters	1062 – 1069
<i>Jayachitra R and Viswanathan P</i>	
Design and Analysis of Flow Patterns and Thermal Behaviour in a Refrigeration Truck Using CFD	1070 – 1080
<i>Archana J, Punitharani K and Jayachitra R</i>	
A Phoneme-Based Method to Recognise Visual Speech Using Deep Learning Model	1081 – 1088
<i>Bineeshia J, Vinoth Kumar B, Monirhithikka S. P and Sarayumiththira V. C</i>	
An Extensive Survey on Memetic Differential Evolution	1089 – 1100
<i>Prakash J and Vinoth Kumar B</i>	
Design and Fabrication of Control Circuit for Boost Converter of Solar Panel in Wind-Solar Hybrid System	1101 – 1107
<i>P. Sweetie Jose, P. Subha Hency Jose and Amirtha R. S</i>	
Ensemble Based Approach for Early Prediction of Alzheimer’s Disease	1108 – 1117
<i>Kavitha C, Narmatha R, Aishvarya G, Sharadha K, Tamil Vani S and Lavanya G</i>	
Deep Learning Based Sign Language Interpreter	1118 – 1129
<i>Kavitha C, Roshini M, Akshaya M, Selvapriya K, Poornimasri P and Vikasinit</i>	
Soukya - Virtual Rehabilitation and Monitoring	1130 – 1137
<i>K. Sathiyapriya, Navenkumar D, Priyadarsan M, Mokshith M and Preetham B</i>	
Detection of Sensitive Data Exposure in Images	1138 – 1146
<i>Amir Faizal, Dhilip Sanjay S, Naveen P, Vishnu Vardhan, Mouleeswaran S and L. S. Jayashree</i>	
Precision Agriculture – Coimbatore Based Crop Suggestion System Using MI and IOT	1147 – 1158
<i>N Gopika Rani, Sneha Sridharan, Gayathri B, Poovizhi Mangai K, Praja S. S and Shivathmica C</i>	
Effective Industrial Workstation Design Using Ergonomic Analysis for Employees in a Pump Manufacturing Industry	1159 – 1170
<i>Jayachitra R and Arunprabhu R</i>	

Box-Behnken Analysis on Crystallinity of Microwave Air Plasma Treated Micro Crystalline Cellulose (MCC) Powder	1171 – 1182
<i>K. Vaideki, M. Surendhar and C. Veeramani</i>	
Analysis on OAT Systems for RFID Devices	1183 – 1189
<i>Senthil Prabha R, Sangeetha B, Ravitharajalakshmi N and Keerthi P</i>	
Optimized Semantic Mapping of XML Elements	1190 – 1194
<i>Sangeetha B, Senthil Prabha R, Ravitha Rajalakshmi N and Srilam K</i>	
Hybrid Feature Selection Using Multiple Feature Ranking and Clustering Techniques	1195 – 1200
<i>Vandna V, Renukadevi T N, Indhumadhi M, Janani R, Iswaryaa G P and Ramesh A. C</i>	
RAGE - A Versatile Drug Target for Alzheimer's disease	1201 – 1214
<i>Palaniswamy Rani*, Balasubramanian Ayshwariya and Saravana Kumar Vinodh</i>	
Recurrent Neural Network Based Predictive Virtual Machine Migration in Hybrid Cloud	1215 – 1219
<i>E.G. Radhika, S. P. Rajamohana and K. Khavya</i>	
Leadership and Employees' Attrition in Manufacturing Companies	1220 – 1224
<i>Shankar R</i>	
Static Analysis of Vulnerabilities Using LUA	1225 – 1231
<i>R Senthilprabha, Ravitha Rajalakshmi N, B Sangeetha and Kaaviya S</i>	
Ameliorated End-To-End Deep Learning System for Self Learning Cars	1232 – 1240
<i>R. Thirumahal and Balajimuthazhagan T</i>	
Predicting Autism Spectrum Disorder Using Stacking Based Ensemble Model	1241 – 1248
<i>K. Anitha Kumari, V. Nivethidha, D. Apoorva, T. Subitsha and S. Muhil Varsini</i>	
Color Correction Using Color Checkers	1249 – 1254
<i>Senthil Kumaran V and Hashini S. S</i>	
Efficiency Improvement in an Assembly Line by Using Line Balancing Method and Valve Stream Mapping	1255 – 1265
<i>R. Jayachitra and K. S Gowtham Kumar</i>	
Numerical Investigation of Coated AISI 4140 Steel by Nitrided Substance	1266 – 1271
<i>Babu S, Raja V, Dinesh Kumar R, Madhan Muthu Ganesh K and Mohamed Anwaru</i>	
Process Improvement Transformation in Petroleum Using Neural Network Approach	1272 – 1277
<i>R. Ramprakash and V. Jaiganesh</i>	

The Impact of Inventory Management Practice on Firm's Competitiveness and Organizational Performance 1278 – 1291

B. Vaishnavi and R. Ilakkiya

Thermal Performance Analysis of the Sustainable Solar Air-Conditioner System by Solar Cooling Tube 1292 - 1296

Babu S, Hariprakasham K, Premkumar T, Subaasini M G and Mathanbabum

Design and Analysis of Flow Patterns and Thermal Behaviour in a Refrigeration Truck using CFD

Archana J, Punitharani K and Jayachitra R

Department of Mechanical Engineering, PSG College of Technology, Coimbatore

ABSTRACT

The demand and scope of the refrigerated transport system, plays a crucial role in cold supply chain. Refrigerated trucks are designed to maintain a low temperature inside the cabin in order to transport food product without any spoilage. The airflow patterns and thermal behavior are the two major factors influencing the storage quality of the food products. The contemporary work is focused towards the design and analysis of flow pattern and thermal behavior inside the truck cab in for transportation of chick in live condition. It is observed that, poorer air velocity and better product temperature at their end of the truck cabin. So, the number of plenum hole and positions are changed to obtain a rapid and uniformity in cooling of product. A Computational Fluid Dynamics (CFD) modeling is agreed out for examination and comparison of the temperature, velocity and pressure circulation in the actual refrigerated truck and the modified truck design.

Keywords: Refrigerated truck, thermalbehaviour, airvelocity, pressure, plenum holes and Computational fluid dynamics.

I. INTRODUCTION

In India road transport is a main mode of transport for goods and chattels over large distances. The atmospheric temperature in few parts of India touches 45°C. In such condition reports shows that the temperature inside the cabin of a transport truck even exceeds 55°C. Especially for chick transportation, refrigeration trucks are used widely by the poultry industries. The ambient air in the truck is maintained at 15°C to 21°C. Upholding of even temperature throughout the cabin is essential in order to preserve the quality, safety and shelf life of product within the refrigerated enclosure, the temperature level and its similarity are directly governed by airflow pattern. The design of the air-distribution system should permit This air flow to compensate heat fluxes exchanged over the insulated walls or generated by the products. This process is vital in order to decrease temperature difference throughout the refrigerated truck. The VCRS (Vapour compression refrigeration system) is used in the truck, the input power to initiative the compressor of the refrigeration system is haggard from the power of the engine shaft. Refrigerant R134a is commercially used in domestic refrigerator all over the world. R134a has poor ozone depletion potential and has excessive global warming potential with a value of 1430. This research is commenced to high point the airflow characteristics, temperature and heat transfer related problematic issues of the refrigerated truck. Thus, by changing the number of plenum holes and its position to obtain a uniform cooling effect inside the cabin. A Computational Fluid Dynamics (CFD) modelling is agreed out for examination and comparison of the temperature, velocity and pressure circulation in the actual refrigerated truck and the modified truck design.

OBJECTIVES:

- To design the refrigeration truck cabin for storage of food products using software Solidworks-2019
- Then analyse the flow pattern and thermal behavior inside the truck by means of CFD (Computationalfluidynamics)software.
- To obtain the uniform flow distribution in the truck cabin by varying the air velocity and plenum size.

II. HEAT LOAD CALCULATION

Heat load factors naturally studied in a cold storage design

$$Q_{total} = Q_{product} + Q_{air} + Q_{infiltratedair} + Q_{walls} + Q_{equipment} + Q_{person}$$

Given conditions: Capacity – 576 kg

Initial temperature – 42 °C

Storage temperature – 18 °C

Specific heat – 4.65 kJ/kg-k

Transporting time – 10 hours

i. Product load: $Q = m \times CP \times (T_0 - T_1)$

$$Q = 576 \times 4.65 \times (42 - 18)$$

$$Q = 64281.6 \text{ kJ}$$

$$= \frac{64281.610}{3600 \times 60} = 1.79 \text{ kW}$$

Respiration load:

$$Q = 576 \times 11.72$$

$$= 6.751 \text{ kW}$$

$$\text{Total product load} = 1.79 + 6.751$$

$$= 8.54 \text{ kW}$$

$$\text{Ton of refrigeration} = \frac{8.54}{3.52} = 2.43 \text{ TR}$$

ii. Airload:

Volume of air = Total truck volume – Total volume of product

$$= 16.96 - 7.88 = m^3$$

$$\text{Density of air} = \rho = 1.117 \text{ kg/m}^3$$

RT

$$\text{Mass of air} = 1.117 \times 8.92$$

$$= 10 \text{ kg of air}$$

$$Q_{\text{air}} = mCP(\Delta T)$$

$$= 10 \times 1.005 \times (40 - 18)$$

$$= 221.1 \text{ kJ}$$

Given conditions: Capacity – 576 kg

ii. Transmission load:

- PPGI thickness (T_1) – 0.5 mm
- Thermal conductivity (k_1) – 0.0299 W/m.K
- PUF thickness (T_2) – 79 mm
- Thermal conductivity (k_2) – 0.028 W/m.K
- Stainless steel (T_3) – 0.5 mm
- Thermal conductivity (k_3) – 14.2 W/m.K
- Opposite two walls will have similar area, thus
- wall₁: 9.513 m²
- wall₂: 20 m²

wall ₁	73.74 kJ
wall ₂	155.03 kJ
Total	228.77 kJ

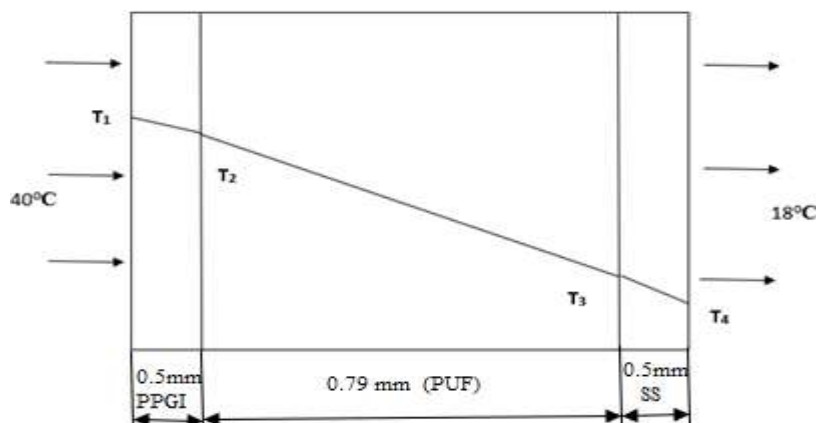


Fig.1 Heat transfer through insulation wall

$$k_1 = 0.02998 \text{ W/m.K}$$

$$k_2 = 0.028 \text{ W/m.K}$$

$$k_3 = 14.2 \text{ W/m.K}$$

$$O = \frac{\Delta T}{(\frac{\Delta X}{KA})}$$

$$R_1 = \frac{0.01667}{A}; R_2 = \frac{2.821}{A}; R_3 = \frac{3.086 \times 10^{-5}}{A}$$

$$R_{NET} = \frac{2.837}{A} \text{ K/W}$$

From above calculation,

$$Q = 6.3 \text{ W/m}^2$$

$$T_2 = 39.89^\circ\text{C}; T_3 = 22.12^\circ\text{C}$$

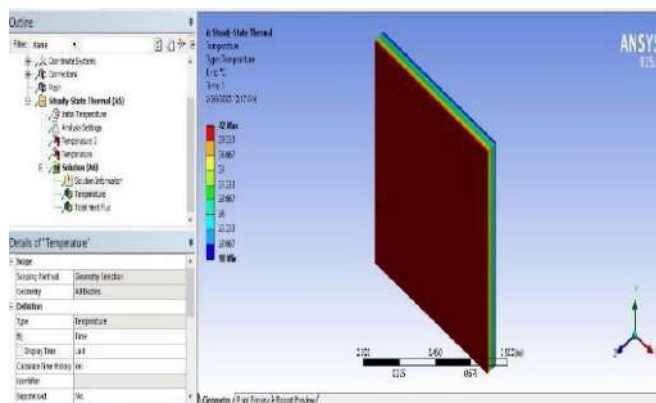


Fig.2 Steady-state thermal analysis of insulation material

The thermal analysis of insulation material at steady-state condition is shown in the figure 2. The PUF (Polyurethane foam) reduces the heat transfer rate, when compared to other insulation materials.

$$\text{Airload} + \text{transmission load} = 221.1 + 228.77$$

$$= 449.87 \text{ kJ} = 0.0124 \text{ kW}$$

$$\text{Total load} = 8.54 + 0.0131 = 8.55 \text{ kW} = 2.43 \text{ TR}$$

Safety factor	0.3
Ton of Refrigeration	3 TR

III. SELECTION OF REFRIGERANT AND REFRIGERATION SYSTEM COMPONENTS

A. Selection of Refrigerant

The selection of a refrigerant plays a major role in refrigeration system for various applications. It should be selected based on its physical, chemical and thermodynamic properties. Refrigerant R134 a is a hydro fluoro carbon (HFC) that has zero potential to root the depletion of the ozone layer and few green house effect. R134 a is the non-flammable and non-explosive, has toxicity within limits and decent chemical stability. Coming from the HFC(hydrofluorocarbons) family of refrigerants, R134a is also known as tetrafluoroethane(CH₂FCF₃).

No	Properties	R-134a
1	Boiling Point	-14.9° For -26.1°C
2	Auto-Ignition Temperature	1418° For 770°C
3	Ozone Depletion Level	0
4	Solubility in Water	0.11% by weight at 77°F Or 25°C
5	Critical Temperature	252° For 122°C
6	Cylinder Colour Code	Light Blue
7	Global Warming Potential (GWP)	1430

Table1. Properties of R134a refrigerant

B. Refrigeration Cycle

Before a detailed examination of truck cabin for the operating conditions, it is compulsory to understand how the air conditioning system works.

Mechanical refrigeration is talented by endlessly circulating, evaporating, and condensing a fixed supply of refrigerant in a closed system. Low pressure and low temperature super heated refrigerant vapor from the evaporator enter the compressor (State 1) and departs as high pressure and temperature superheated vapor (State 2).

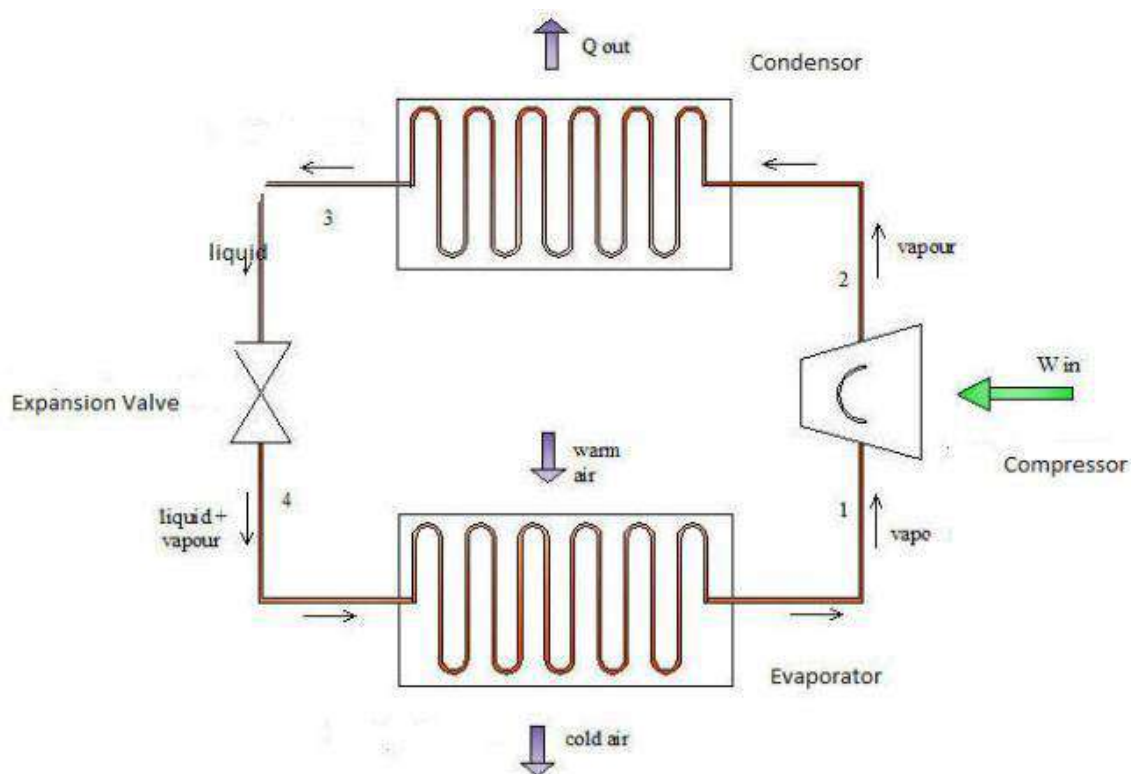


Fig.3 Refrigeration Cycle Equipment

This vapor arrives the condenser where heat is disallowed to out door air that is required over the condenser coils. The refrigerant vapor is cooled to the saturation temperature (State 2s), condensed to a liquid (State

3s), and cooled below the saturation point (State3a). The high-pressure liquid is required through an expansion valve into the evaporator (State4). The pressure in the evaporator is much lower than the pressure in the condenser, so the refrigerant arrives the evaporator as a liquid-vapormix at low temperature and pressure. The refrigerant soaks up the heat from warm indoor air that is blown over the evaporator coils. The refrigerant is totally evaporated (State1s) and heated above the saturation temperature before entering the compressor. The indoor air is cooled and dehumidified as it streams over the evaporator and repaid to the living space. The refrigeration cycle is shown in Figure4.

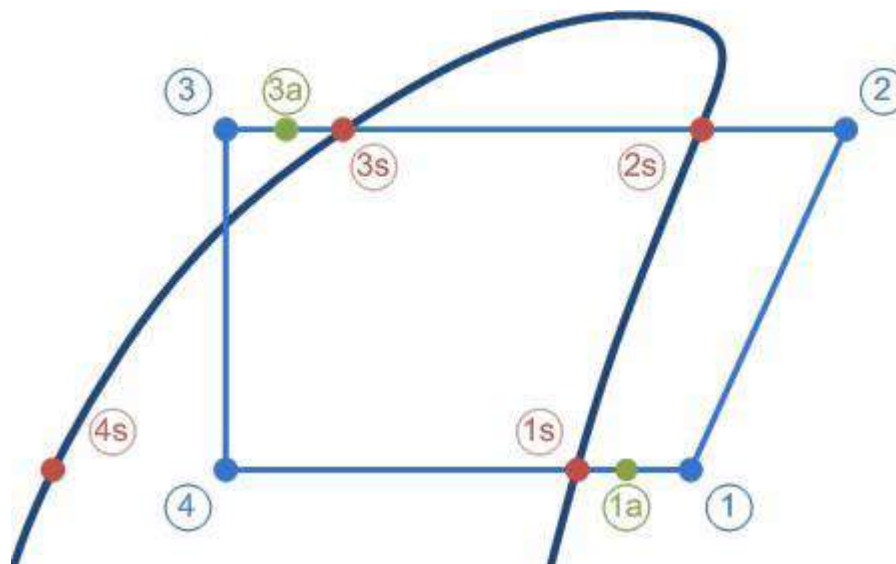


Fig.4 Pressure– Enthalpydiagram

	T	P	h	s
Description	[°C]	[bar]	[kJ/kg]	[kJ/kg.K]
1. Compressor suction	18.0	4.147	412	1.749
2. Compressor discharge	82.6	14.55	460/1	1.809
2s. Condensation dewpoint	54.0	14.55	425.8	1.709
3s. Condensation bubble point	54.0	14.55	278.8	1.259
3a. Condenser out	52.0	14.55	275.6	1.25
3. Including Additional sub cooling	52.0	14.55	275.6	1.25
4. After expansion valve	10.0	4.147	275.6	1.268
4s. Evaporation Bubble point	10.0	4.147	213.8	1.049
1s. Evaporation dew point	10.0	4.147	404.5	1.723
1a. evaporator	18.0	4.147	412	1.749

Table2. Performance details of refrigerant at various stages

With the above collected data, the mass flow rate, compressor work, condenser work and coefficient of performance are calculated by using the below formulas is as follows,

• **Work done by evaporator**

$$Q_L = m(h_1 - h_4)$$

$$10.55 = m(412 - 275.6)$$

$$m = 0.077 \text{ kg/s}$$

• **Work done by Compressor**

$$W_{in} = m(h_2 - h_1)$$

$$= 0.11(460.1 - 412)$$

$$W_{in} = 3.7 \text{ kW}$$

• **Work done by Condenser**

$$Q_H = m(h_2 - h_3)$$

$$= 0.077(460.1 - 275.6)$$

$$Q_H = 14.21 \text{ kW}$$

• **Work done by Compressor**

$$\text{COP} = 2.25$$

C. Selection of refrigerant components

There are four basic components of refrigeration system viz. compressor, condenser, expansion valve and evaporator. The compressor is considered the heart of the refrigeration system.

In our project, the selection of compressor is based on the Danfoss Cool-selector software and on market survey which suits to work well with R134 a refrigerant. The compressor selected is reciprocating compressor with 0.077 kg/s mass flow rate. The purpose of the evaporator is by using the liquid refrigerant to remove unwanted heat from the product. The liquid refrigerant limited within the evaporator is boiling at low pressure. The evaporator coils are created of copper and provided with aluminum fins.

It causes more uniform distribution of cooling effect inside the truck cabin. The expansion valve is situated at the finale of the liquid line, before the evaporator. The valve then reduces the pressure of the refrigerant as it passes over and done with the orif ice, which is located inside the valve. The expansion valve selected is TE5-55 thermostatic expansion valve. The commitment of the condenser is to extract heat from the refrigerant to the outside air. A natural air-cooled condenser is selected as the condenser type, with coil surface area is 12.47 m² and coil fin spacing 8 mm. The details of the selected refrigeration components are given in the table 3.

SI. No	Component	Description
1	Discharge Pressure Gauge(Pd)	14.55 bar
2	Suction Pressure Gauge(Ps)	4.147 bar
3	Compressor type	Reciprocating compressor
4	Mass flow rate in evaporator	0.077 kg/s
5	Compressor power supply [V/Ph/Hz]	220-240/3/50-60
6	Coil surface area	12.47 m ²
7	Coil fin spacing	8 mm
8	Fan quantity & size	2 nos. & 600 mm
9	Air volume	3500

Table 3. Refrigeration system components

IV. DESIGN OF TRUCK CABIN

In this project work, small-scale refrigerated trucks of 3 – ton capacity were considered. These types of trucks are the most common vehicle used in the food cold-chain.

The refrigerated truck had length, width and height of 4232 mm, 1852 mm and height 2164 mm, respectively.

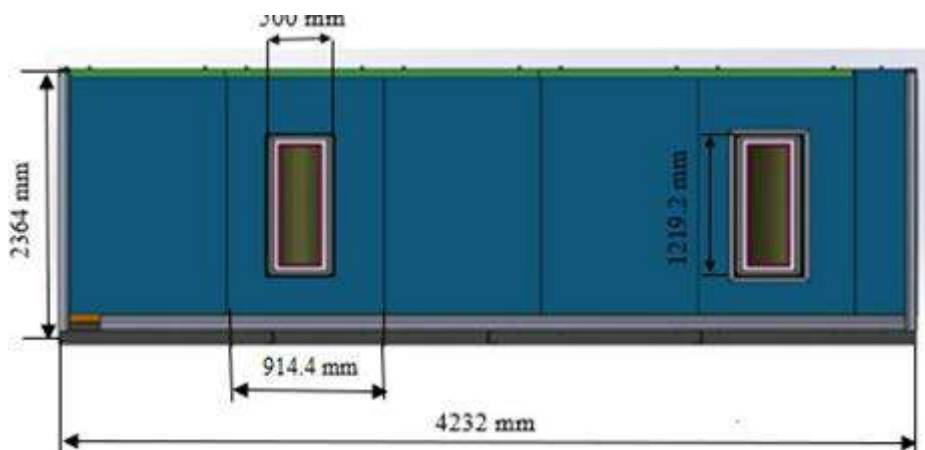


Fig.5 Truck cabin design

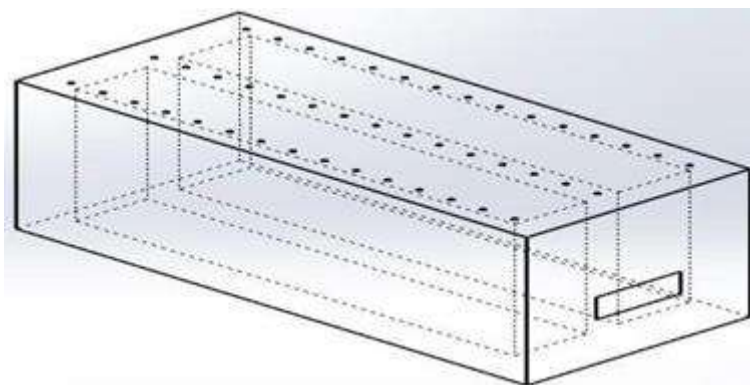


Fig.6 Truck cabin geometry

The geometry of the truck cabin consists of trolleys which are placed inside the boxes. There are 72 trolleys are placed in each trolley box. Totally 8 trolleys are arranged inside the truck cabin. In the truck, plenum plate is placed on the upper side of the cabin. The plenum plate consists of 46 holes, where the cold air blows over the product.

The above truck cabin geometry is used to perform simulation of air flow and heat dissipation using computational fluid dynamics (CFD). In the actual system contain of two plenum plate are shown in the figure 6. The dimension of two plenum plates is not same. One plenum plate consists of uniform holes on both sides, but in another plate only one side holes are placed. Hence, the trolley on one side gets uniform cooling of product than the other.

Modified truck cabin design:

The simulation results, lead to some modification in the actual system design. This will increase the flow rate of air and remove the product heat more effectively compared to the actual system.

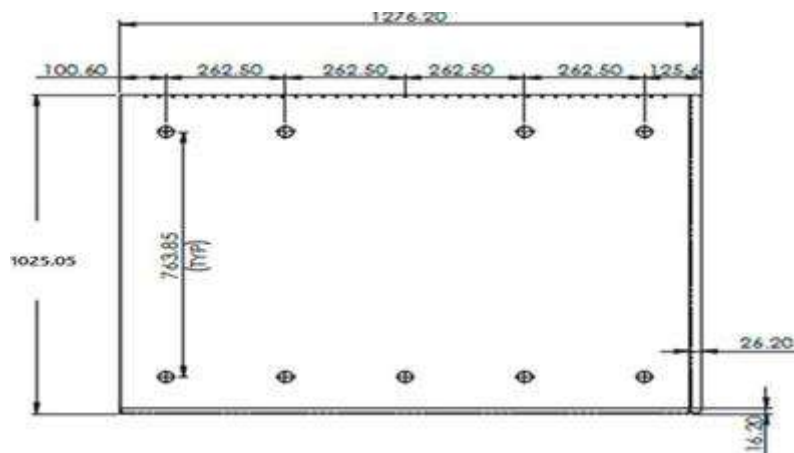


Fig.7 Modified plenum design (All dimensions are in mm)

For obtaining uniform cooling effect inside the cabin, the plenum plate design is modified is shown in figure 7. So, the two plenum plates are designed with same dimension, which leads to get uniform air distribution on both side of the trolley. The air filter area is also increased with length and width of 700 mm and 600 mm. Its helps to circulate more air inside the cabin.

V. COMPUTATIONAL MODELLING AND MESHING

Initially import the geometry file from Solid works to Ansys software. Then create a named section and name the plenum holes as inlet and air filter area on the side of the cabin as outlet.

A. Meshing & Boundary conditions

The commercial software package ANSYS Fluent was new for the generation of the model. The cooling performance of a loaded cold truck in cooling process using transient three-dimensional computational fluid dynamics model. The model accounted for turbulence by worth of the standard k- Epsilon 00model with standard wall profiles. The air inside the refrigerated chamber is assumed to be in compressible fluid. The cut-cell cartesian methodology is used, where the mesh fits perfectly with the geometry, falling the number of inaccuracies that propagate through the rest of the domain.

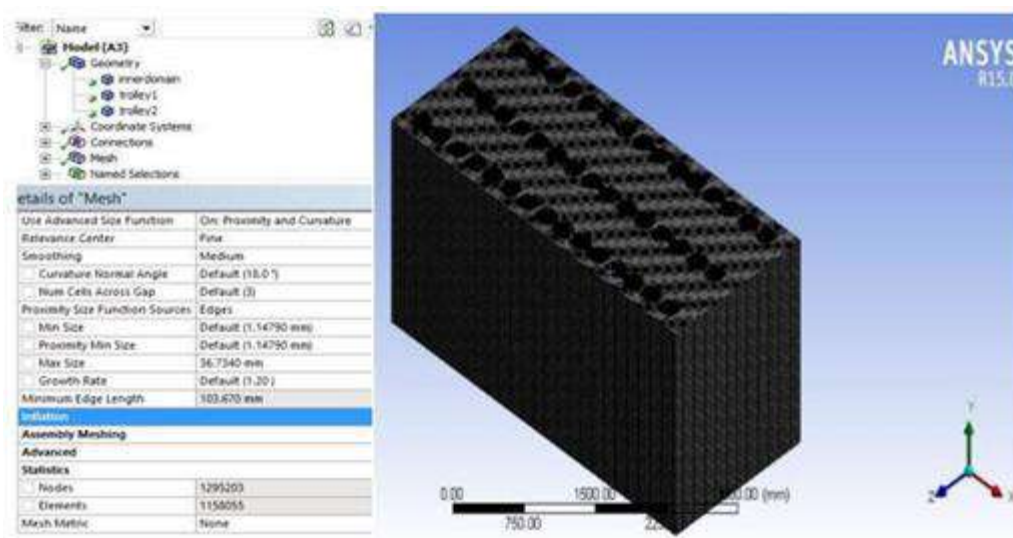


Fig.8 Meshed Model

To account for the effects of turbulence, the SST k-Epsilon model was employed. The transient state condition is used to run the simulation, because the temperature of the product is changed according to the time. The applied boundary conditions for the analysis is shown in the tables below

S.No	BoundaryZones	BoundaryConditions
1	Inlet	Velocity inlet
2	Outlet	Pressure Outlet

Table 4. Boundary Conditions

S.No	Solver	Options
1	Type	Energyon
2	Time	Transient
3	Viscous	K-Epsilon
4	Material	Chick
5	velocity	5m/s&6m/s

Table 5. Model setup

Thus, the SST k-Epsilon turbulent model is used, which reasons for transport of turbulent shear stress and gives highly accurate predictions. It solves for two variables: k – the turbulence kineticenergy and ϵ – the rate of dissipation. It is well – suited for high Reynolds number.

VI. RESULT AND DISCUSSION

A. Velocity – Contour of Actual Truck

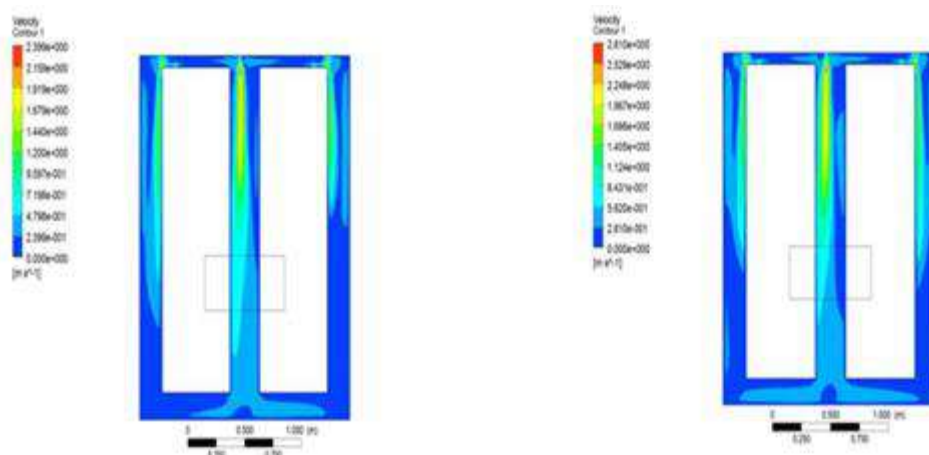


Fig.9 Front view and of truck cabin – velocity contour at 5 &6 m/s

This above result shows, that the average velocity of air inside the cabin for 5 and 6 m/s inlet condition is 2 m/s and 2.5 m/s. Therefore, average velocity inside the cabin is more in second inlet condition.

B. Temperature – Contour of Actual Truck

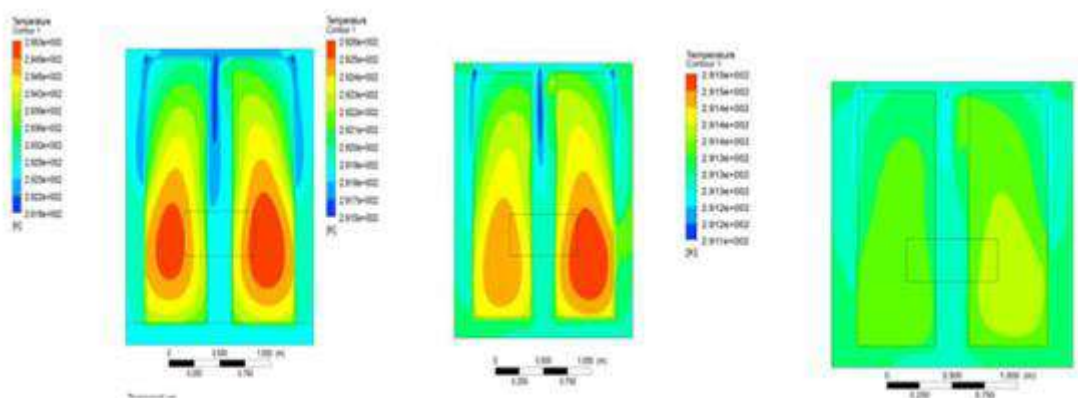


Fig.10 Front view of truck cabin–Temperature contour at 5m/s at (1hr,2hr &3hr)

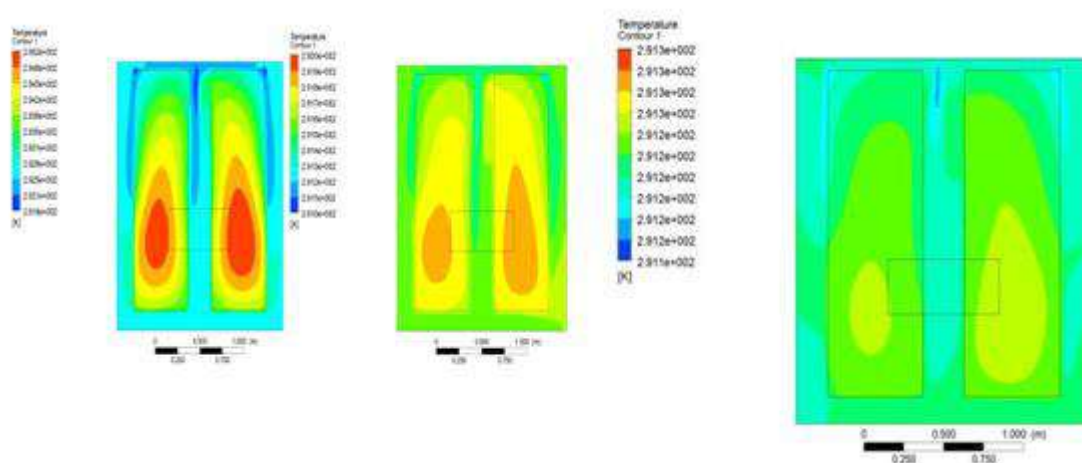


Fig.11 Front view of truck cabin–Temperature contour at 6m/sat (1hr,2hr &3hr)

For both 5 m/s and 6 m/s inlet condition, the temperature contour for different time period is shown in the fig 10 & 11. The time taken to attain 18°C is almost 3 hours in both the inlet condition. It is clearly understood, that the temperature of one trolley is reduced quickly compared to others.

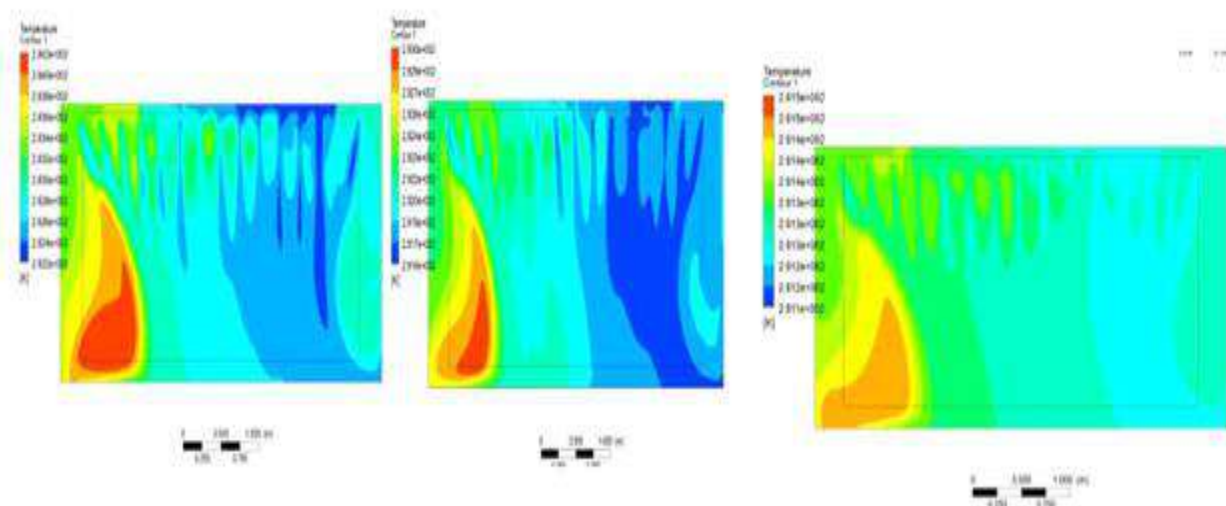


Fig.12 Side view of truck cabin–Temperature contour at 5m/s at (1hr,2hr &3hr)

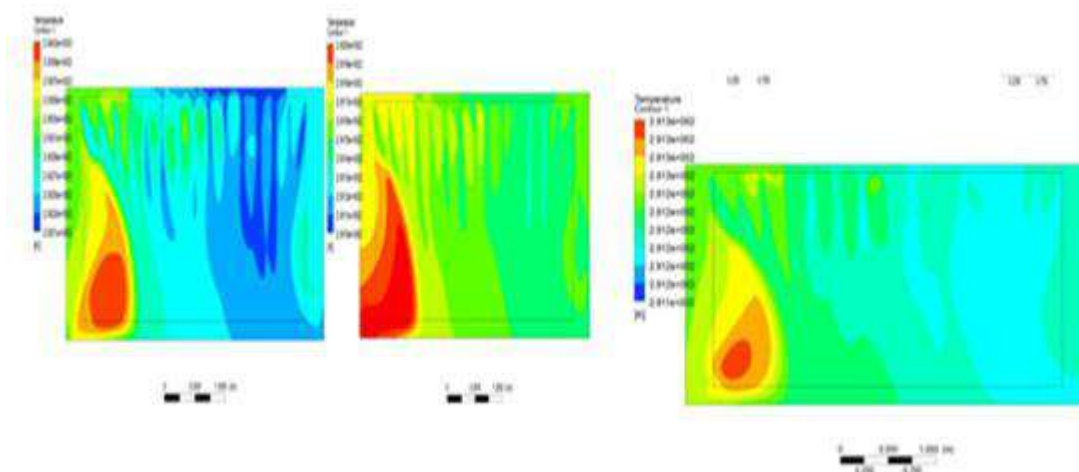


Fig.13 Side view of truck cabin–Temperature contour at 6 m/s(1hr,2hr&3hr)

Some amount of heat is still presented on the back side of the truck is shown in the fig 12 & 13. So non-uniform cooling of product is experiencing inside the truck cabin for both the inlet condition.

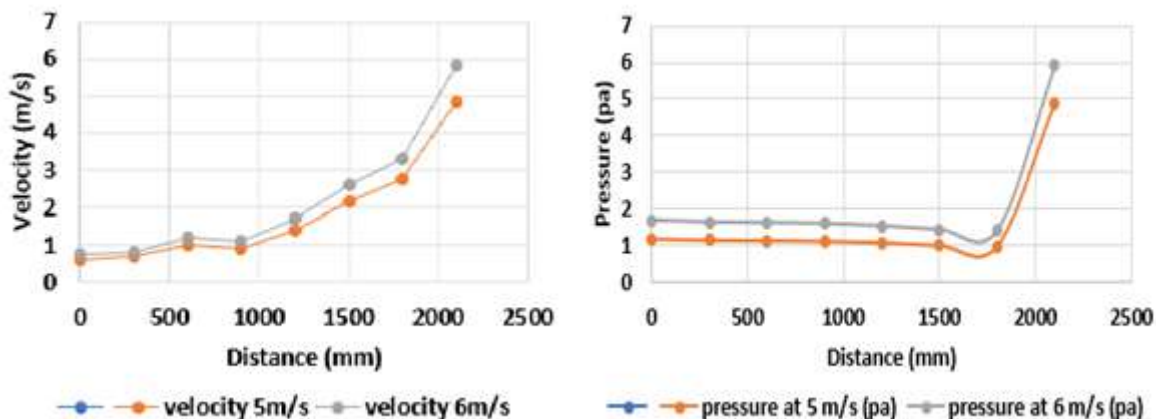


Fig14.Velocity and pressure distribution graph at 5m/s & 6m/s

For both the inlet condition 5 m/s and 6 m/s, the velocity and pressure distribution over the various plane are given in the graph 14.

C. Temperature–Contour of Modified Truck

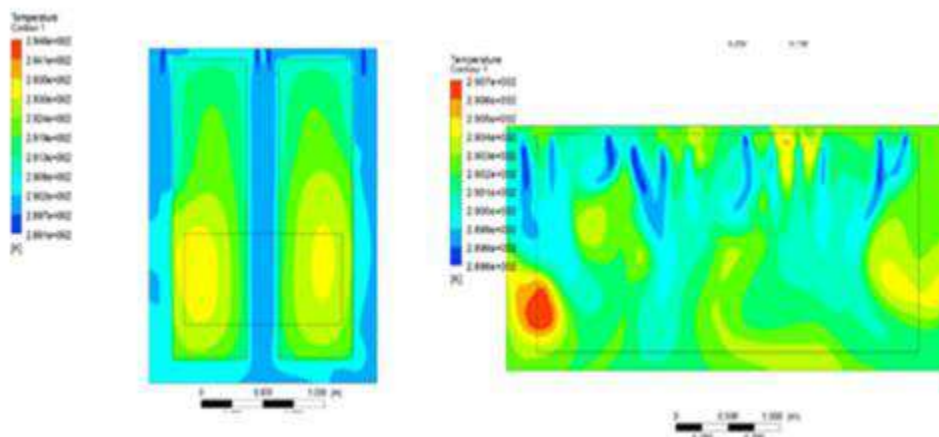


Fig.15 Front & Side view of truck cabin–Temperature contour at 5m/s at (1hr)

From the above figure, it is clearly understanding, that both the trolley attains uniform cooling and temperature on the back-side of the truck cabin is also removed.

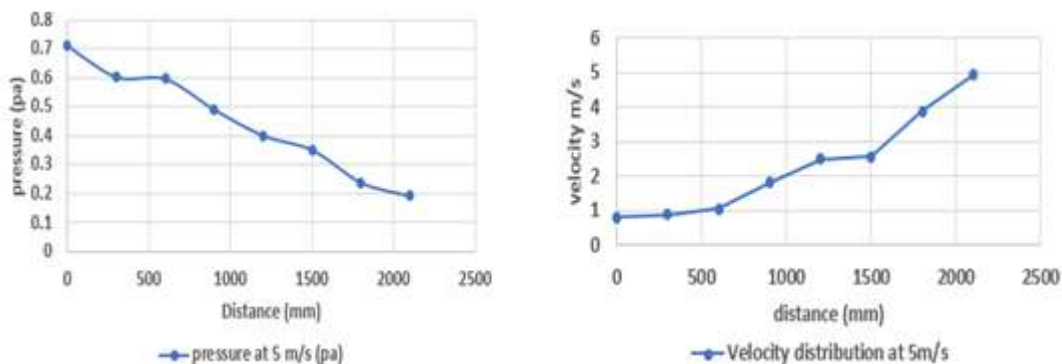


Fig16. Pressure and velocity distribution graph

From these results, it is evident that, the modified truck design is more efficient than the Actual truck design. The average velocity inside the truck cabin is 2.5 m/s. Hence the time taken to obtain a required cooling effect is reduced from 3 hours to 1 hour.

VII. CONCLUSION

The Actual truck cabin is designed by using Solid works – 2019. Then the Computational Fluid Dynamics (CFD) modelling and comparison of the temperature, velocity and pressure distribution inside the truck cabin is carried out. Thus, the result shows non – uniform air flow pattern and cooling effect of the product. So, the truck design is changed by increasing the number of plenum holes and positions are changed to obtain a rapid and uniformity in cooling of product. Hence the time taken to obtain a required cooling effect is reduced from 3 hours to 1 hour. From the analysis, it is evident that the modified truck design is more efficient than the Actual truck design.

REFERENCES

1. Amr Kaood, Essam E. Khalil and Gamal M. El-Hariry, “Flow Patterns and Thermal Behaviour in a Large Refrigerated Store, Faculty of Engineering” Cairo University, Egypt, Volume 13, Issue 2 Ver.III, PP81 - 92, 2016.
2. Turkey Yildiz, “CFD Characteristics of Refrigerated Trailers and Improvement of Air flow for Preserving Perishable Foods Department of Information Technology (B.I.D.B.), Izmir Institute of Technology, 35430 Izmir, Turkey, 2019.
3. [3] Moureh, J., Menia, N., & Flick, D. Numerical and experimental study of air flow in a typical refrigerated truck configuration loaded with pallets. *Computers and Electronics in Agriculture*, 34 (1-3), 25–42, 2002.
4. Mehran Islam, Asif Kabir, Arnab Mustafi Arka, and Md. Ashiqur Rahman. “Assessment of the Transport Refrigeration System in Bangladesh and Numerical Simulation of the Refrigeration Performance” *AIP Conference Proceedings* 2121, 030013, 2019.
5. Tanaka, F., & Konishi. The use of CFD to improve the performance of a partially loaded cold store. *Journal of Food storage and transportation*, 35 (6), 874–880, 2012.
6. Yi, T., Jing, X.I.E., Jin-feng, W., Chen, M., & Yi, Z. Computational Fluid Dynamics Simulation about Comparison of Different Forms of Return Air in a Small Cold Store, 517, 1133–1138, 2012.
7. Getahun, S. Ambaw A. Delele M. Meyer C.J. Opara, U.L. “Analysis of air flow and heat transfer inside fruit packed refrigerated shipping container: Part I—Model development and validation” *J. Food Eng.*, 203, 58–68, 2017.
8. Han J.W, Zhao C.J, Yang X.T, Qian J.P, Xing B, “Computational fluid dynamic simulation to determine combined mode to conserve energy in refrigerated vehicles” *J. Food Process. Eng.* 39, 186–195, 2016.
9. Alam S, “A Proposed model for Utilizing Exhaust Heat to run Automobile Air-conditioner”, The 2nd Joint International Conference on Sustainable Energy and Environment 21-23 November 2006, Bangkok, Thailand, 2006.
10. Amit M. Patel and Prof. R. I. Patel, “Optimization of different Parameters of cold storage for energy conservation”, *International Journal of Modern Engineering Research*. Vol.2, Issue3, 2012

Optimization of Inventory Management in Manufacturing Firms

B. Vaishnavi and R. Ilakkiya

Department of Mechanical Engineering, PSG College of Technology, Coimbatore, India

ABSTRACT

Inventory management system is generally considered to satisfy the needs of the customer. Hence appropriate use of inventory is essential. To further investigate the process, this study aims to use the multi bin system instead of forward cover system. As part of Just in Time Lean manufacturing, the Multi bin system is an indication, flag, or signal within the manufacturing production process that triggers product creation and supply. The length of inventory management system maintenance is also investigated in order to determine the lowest cost incurred or the longest period that can still be tolerated for tracking inventory management system. The findings show that the formula under investigation is appropriate for a multi-bin system, and that periodic review policy should be used to compute inventory management system

Keywords — Inventory management, ABC analysis, Multi bin system, Periodic review policies, Continuous review policies

1. INTRODUCTION

Inventory management, which is a part of the internal company's function, is one of the areas of supply chain management. If the firm can properly and efficiently manage its inventory system, it may be able to save money on operational costs. Good stock management will maximise corporate benefits, whereas vice versa lead to lack of stock control and will result in a loss of company benefit [1]. The continuous review policy and the periodic review policy are two replenishment policies that are frequently utilised in practise. According to the continuous review policy, the inventory status is continually maintained, and ordering according to lot size (Q) was done when the level reached the designated inventory reorder threshold. The periodic review policy indicates that the inventory status was tracked at regular periodic intervals and reorders were made to raise the inventory level to the predefined point. These inventory system policies aren't exhaustive, but they're good enough to address issues with the inventory management system's security. The effectiveness and efficiency of an inventory management system may have a major impact on supply chain management, improving cycle service levels and lowering costs [2]. The benefit of a continuous review strategy is that it may solve situations where demand is strong, but the drawback is that order quantities are changeable. The supplier is more likely to make mistakes, thus clients who bought the fixed order quantity are preferred. With the periodic review policy, the situation is the inverse [3]. Kanban is a Lean manufacturing subsystem that was designed to monitor inventory levels, component production, and supply [4]. The supplier can classify and analyse Kanban variants using his or her knowledge of the construction and accumulation of Kanban systems. The Kanban system is classified as a dual card Kanban system for signalling production and a transportation Kanban system for signalling transportation. During periods of high demand uncertainty, buffer maintenance is required to calm production flow and reconfigures the Kanban System to reduce inventory. As a consequence, Kanban systems enable mixed model production as well as appropriate inventory levels, resulting in shorter product delivery times and more efficient use of resources such as manpower and machinery [5]. Without excellent inventory management, the firm will never accomplish a low-cost plan. The inventory divided into four categories such as Raw material inventory, work-in-progress inventory, finished goods inventory, and maintenance, repair and operational inventory [6]. Because stocks are critical to an organization's success, managing them may be difficult due to storage and holding expenses, as well as limited space in a manufacturing plant. Due to the variety of real-life scenarios, inventory management is a difficult problem to solve [7]. To ensure a successful supply of raw materials, the Kanban method necessitates supplier commitment to offering quick services. Essentially, the Kanban method simply necessitates a minimal number of stocks in the production line, with inventories equal to output numbers. As a result, supplier commitment is critical in ensuring that manufacturing lines run smoothly and effectively. Quality, desire to collaborate, technical expertise, geography, and pricing are five essential characteristics to consider while selecting suppliers. Just in time aims to remove stocks rather than transfer them to a different point in the supply chain. And, cooperation is the key to achieving this. The Japanese Kanban manufacturing method is frequently misunderstood as a basic just-in-time management strategy, a notion that aims to keep inventories to a minimum. The Japanese Kanban method entails more than fine-tuning production and supplier scheduling systems, in which stocks are kept to a minimum by only ordering what is needed in production and work in progress is continuously monitored [8].

II. METHODOLOGY

The process for developing a Kanban system as well as procurement policies are provided as follows that includes gathering essential parameters is the first step in developing a Kanban system and calculating Kanban quantity. Finally establishing a pull mechanism and rule. Whereas the procedure for developing procurement policy includes collecting relevant data, Safety stock, reorder point, economic order quantity calculations and average inventory level calculations. Contrasting the policies of continuous and periodic evaluation.

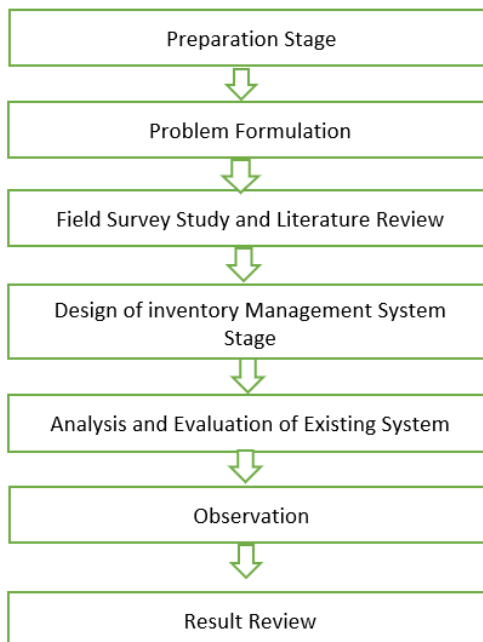


Figure 1: Methodology of the Process

III. CASE STUDY

The research methodology is directly translated to the case study. The procedures involved in the methodology are explained as below

1. Forward cover system

The 'Push system,' which sought to retain a big inventory of product according to consumer projection, is at the heart of traditional production strategy. However, this has been a significant problem for individuals, since raw material stockpiles have increased, production processes have become disjointed, and unnecessary stock has been produced. The problems with the front cover system are that the requirements which are not met must be identified, this need must be placed in the context of procurement, there must be a high degree of leadership and staff commitment, and the capacity to make a strong enough forward commitment to produce the needed market pull. Forward contracts include counterparty credit risk because no money is exchanged at the outset. Because one can rely on the counterparty to deliver the asset, which might end up to lose money if the counterparty defaults between the initial agreement date and the delivery date.

1.1 Procurement policy

- Capital investment in inventories is high
- Raw material inventory is high as compare to usage.
- Safety stock amount for each product is high as compared to usage

2. ABC analysis

ABC analysis is a method of inventory classification that divides into three categories: A, B, and C. The most valuable goods are A, while the least valuable items are C. The ABC analysis in Ats-Elgi limited is listed in table 1 and 2

A Category – 5% to 10% of the items represent 70% to 75% of the money value.

B Category – 15% to 20% of the items represent 15% to 20% of the money.

C Category – The remaining number of the items represent 5% to 10% of the money value.

TYPE OF ITEM	NUMBER OF ITEM	INVENTORY VALUE
A-ITEM	291	30999531.82
B-ITEM	469	5831012.144
C-ITEM	1951	1918426.878

Table 1: Type of item and Inventory value

TYPE OF ITEM	% OF USAGE	% OF INVENTORY VALUE
ITEM A	11%	80%
ITEM B	17%	15%
ITEM C	72%	5%

Table 2: Percentage of Usage and Percentage of Inventory value

3. Multi bin Kanban system

The supplier tops up the bins at regular intervals in a multi-bin Kanban system. They frequently have numerous locations inside the plant, and the operators will simply take full bins and return empty bins for restocking. The following is how the Multi-bin system works. Items are organised into many containers. The first bin is placed on top of the second bin, or in front of it. On the bottom of each bin is a reorder card. The first bin is the only one from which material is taken. When the first bin is full, it is swapped out for the second. The reorder card is used to replenish the first bin's contents. While waiting for the material on order to arrive, material is pulled from the second bin. When the new material arrives, it is placed in the empty bin, and the reorder card is placed back in its original location in the bin. The practise is repeated until all of the material in one bin has been used up. The reordering card is then used to refill the material.

Description	Replenishment lead time(days)	Batch size	Number of cards
Wheel aligner kit dya 1000w	90	4	6
Kit wh f7d	90	11	6
Power pack with motor assy-f	90	6	6
Blower fan model ta/r 18-18	90	12	3
Vacuum pump	90	32	3
Wrench impact 1/2" sp1140ex	90	8	7
Wrench ratchet 1/2" sp1133sx	90	8	7
Power pack	90	4	3
Burner bentona - b30a/as47cpu	60	12	3
Electric 3hp ind motor	60	47	4
3hp electric motor b3 b14	60	19	7

Table 3: Proposed batch size and number of cards for Multi bin system

IV. BASIC SIMULATION USING C PROGRAM

1. Flow chart using c program

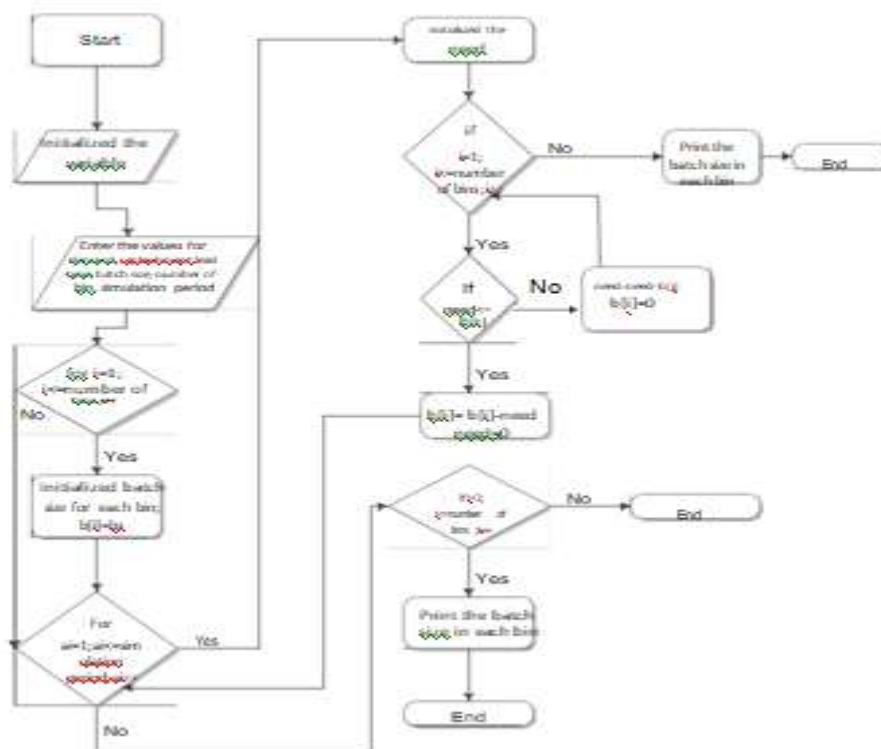


Fig 2: Flow chart using c program

2. C Program code

```
#include<stdio.h>
#include<conio.h>
void main()
{
int ai,i,d,bs,nb,nee,m,lt,tmp=0,opt,b[100]; clrscr();
printf("\n Enter demand value = ");
scanf("%d",&d);
printf("\n Enter number of bins = "); scanf("%d",&nb);
printf("\n Enter batch size = " );
printf("\n Enter manufacturing lead time in months = " ); scanf("%d",&lt);
printf("\n The Monthly demand is = %d\n Number of bins
= %d\n Batch size = %d\n Manufacturing lead time =%d months \n ",d,nb,bs,lt);
printf("\n Enter the simulation period in months ="); scanf("%d",&m);
for(i=1;i<=nb;i++)
{
b[i]=bs;
printf("\n Bin %d = %d",i,b[i]);
}
for(ai=1;ai<=m;ai++)
```

```

{
nee=d;
for(i=1;i<=nb;i++)
{
if(nee<=b[i])
b[i]=b[i]-nee;
nee=0;
}
else
{
nee=nee-b[i];
tmp=tmp+b[i];
b[i]=0;
}
}
for(i=1;i<=nb;i++)
{
printf("\n\n Bin %d = %d",i,b[i]);
}
getch();
}
    
```

V.SIMULATION USING ARENA

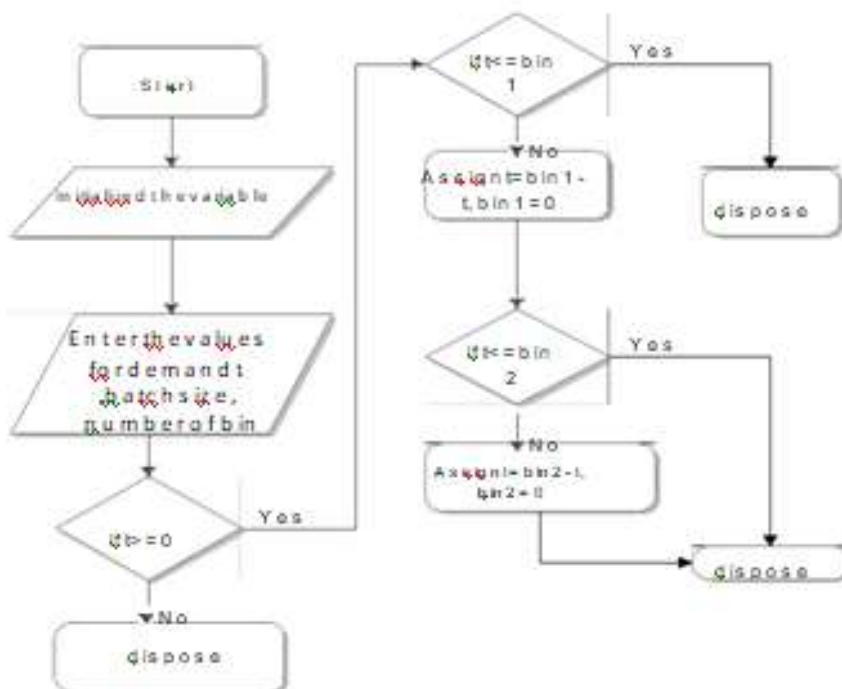


Fig 3: Flow chart-2 bin system

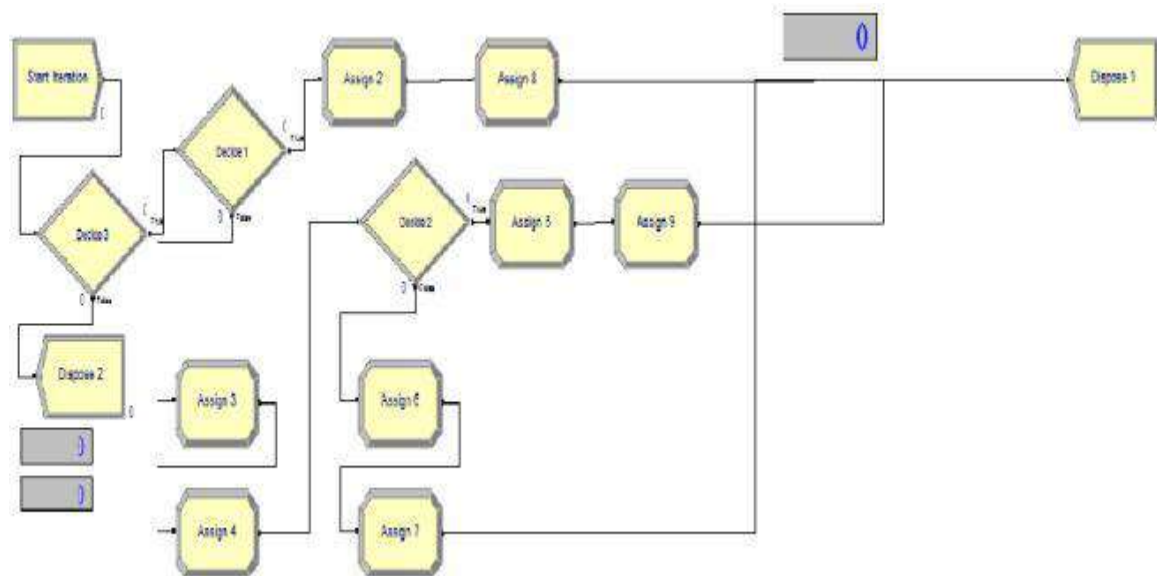


Fig 4: Simulation model-2 bin system

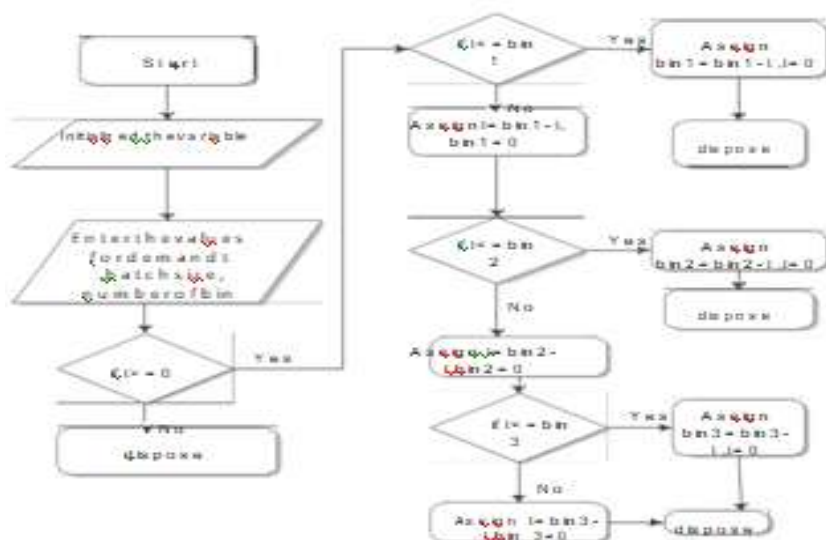


Fig 5: Flow chart-3 bin system

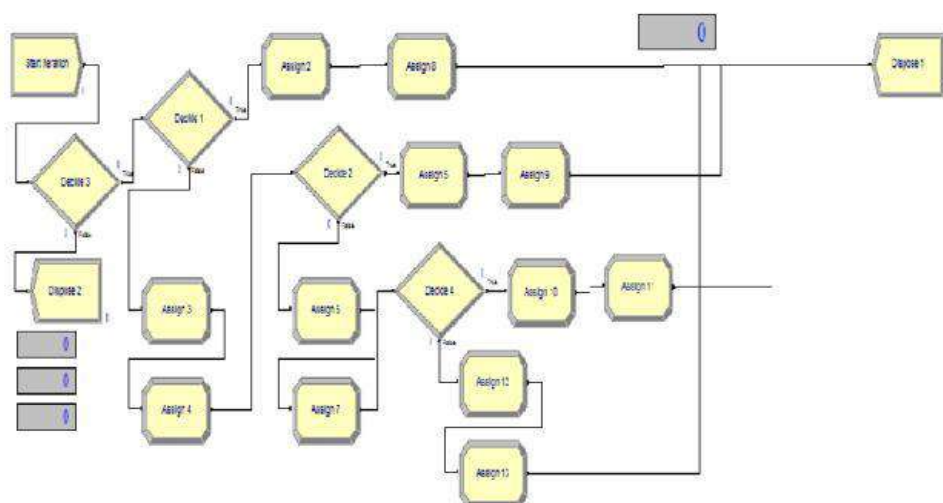


Fig 6: Simulation model-3 bin system

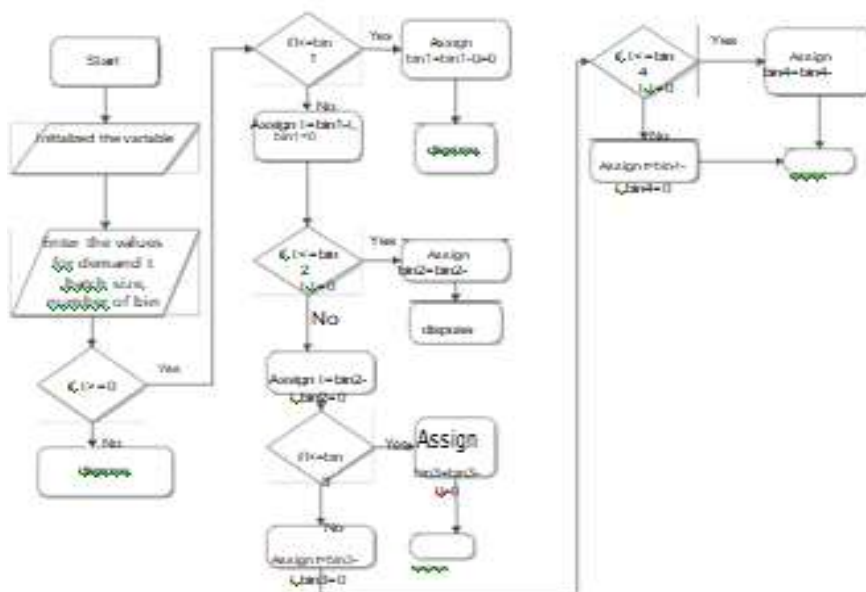


Fig 7: Flow chart-4 bin system

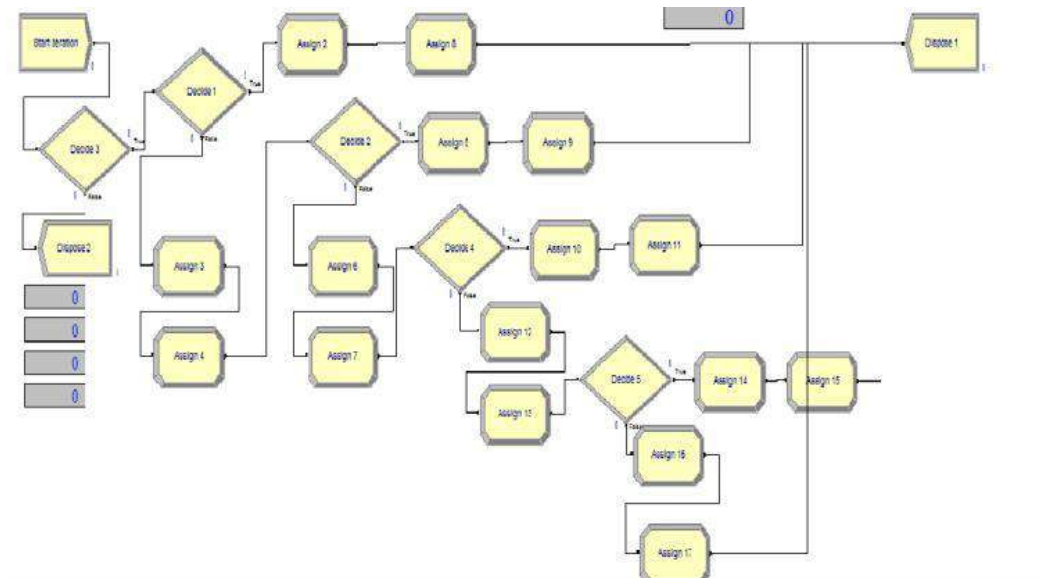


Fig 8: Simulation model-4 bin system

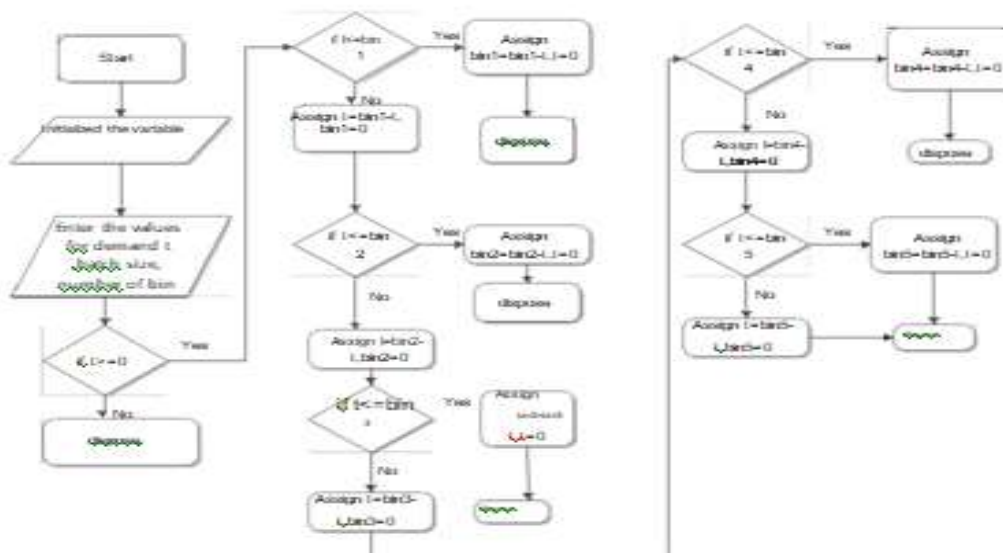


Fig 9: Flow chart-5 bin system

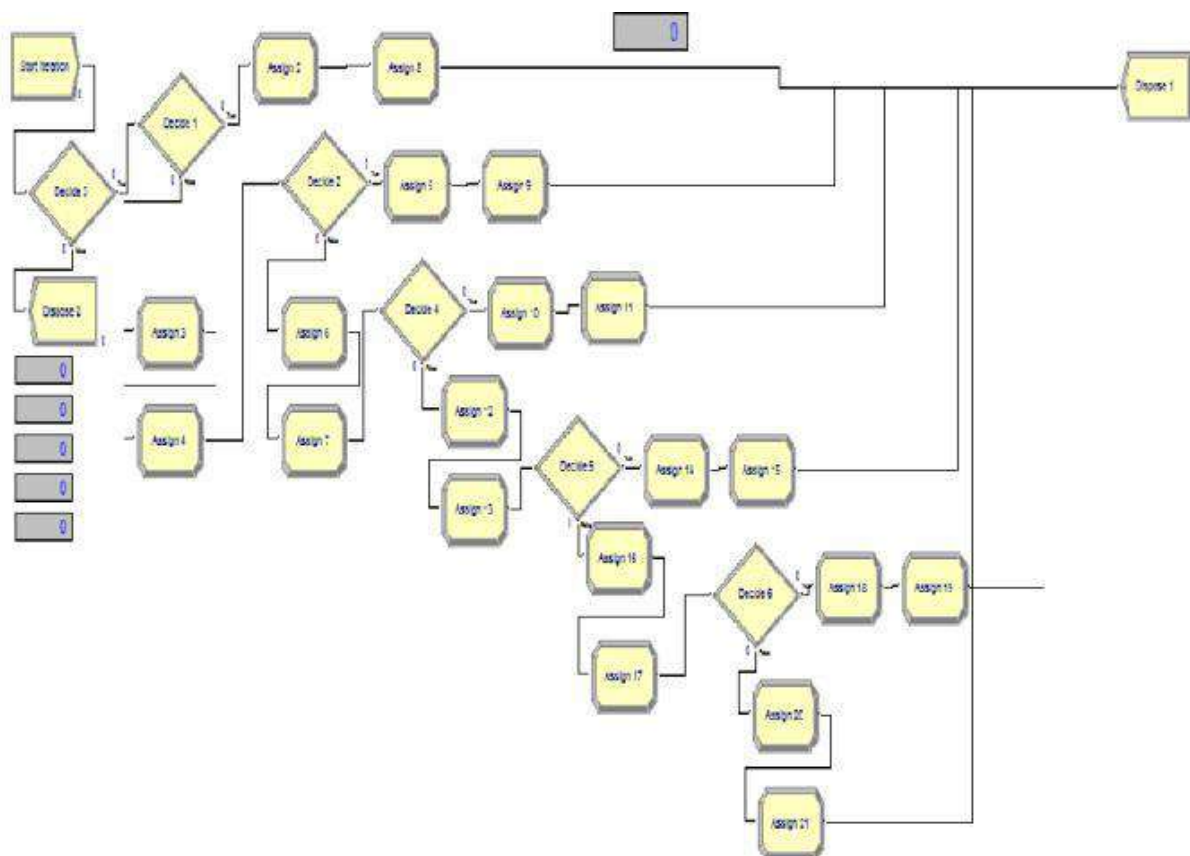


Fig 10: Simulation model-5 bin system

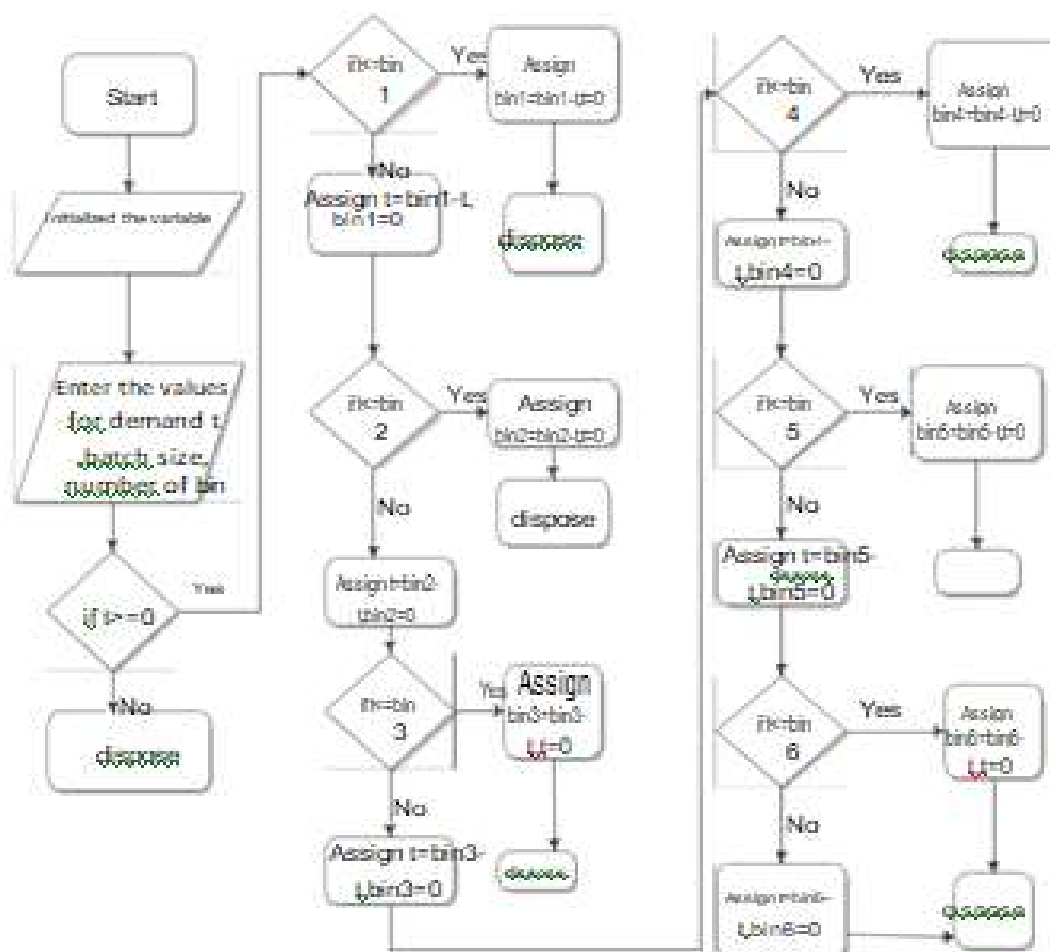


Fig 11: Flow chart-6 bin system

$Fs-1 = \text{normsinv}$

$\sigma_{T+L} = \text{standard deviation of demand during } T+L$

$T = \text{review interval}$

$L = \text{average lead time for replenishment}$

$D = \text{average demand per period}$

$\sigma_D = \text{standard deviation of demand per period}$

$\sigma_L = \text{standard deviation of demand during lead time } DT+L = \text{mean demand during } T+L$

$OUL = \text{order up to level}$

$AIL = \text{average inventory level}$

$Q = \text{lot size}$

$D_e = \text{annual demand}$

$S = \text{order cost per lot}$

$h = \text{holding cost}$

$c = \text{unit cost}$

1. Comparison of continuous review policy and periodic review policy

Description	Cycle inventory	Average inventory level	Average inventory value(rupees)
Power pack with motor assy-f	17	26	374887
Sensor head kit truck align	1	1	240278
Blower fan model ta/r 18-18	17	55	682351
Ramp assembly	5	8	110270
Vacuum pump	48	118	414696
Wrench impact 1/2" sp1140ex	24	41	217398
Wrench ratchet 1/2" sp1133sx	24	44	123035
Blower 8000 cmh italy.ta-s15	1	3	28489
Electric 3hp induction motor	93	137	732998
Oxygen sensor	46	78	207501

Table 4: Proposed continuous review policy inventory system

Description	Order up to level	Average inventory level	Average inventory value(rupees)
Power pack with motor assy-f	38	14	212450
Sensor head kit truck align	2	2	400464
Blower fan model ta/r 18-18	73	48	599265
Ramp assembly	16	25	335875
Vacuum pump	161	95	332052
Wrench impact 1/2" sp1140ex	60	27	139376
Wrench ratchet 1/2" sp1133sx	63	30	82697
Blower 8000 cmh italy.ta-s15	4	2	24378
Electric 3hp induction motor	208	92	494674
Oxygen sensor	116	57	151304

Table 5: Proposed periodic review policy inventory system

VII.RESULTS AND DISCUSSION

1. Analysis of Procurement policy

Safety stock, Reorder level, Average inventory level, Average inventory value and savings in inventory cost were analysed. Based on the results of the inventory policy of each item, it is evident that the Periodic review policy is having less inventory value as compare to continuous review policy

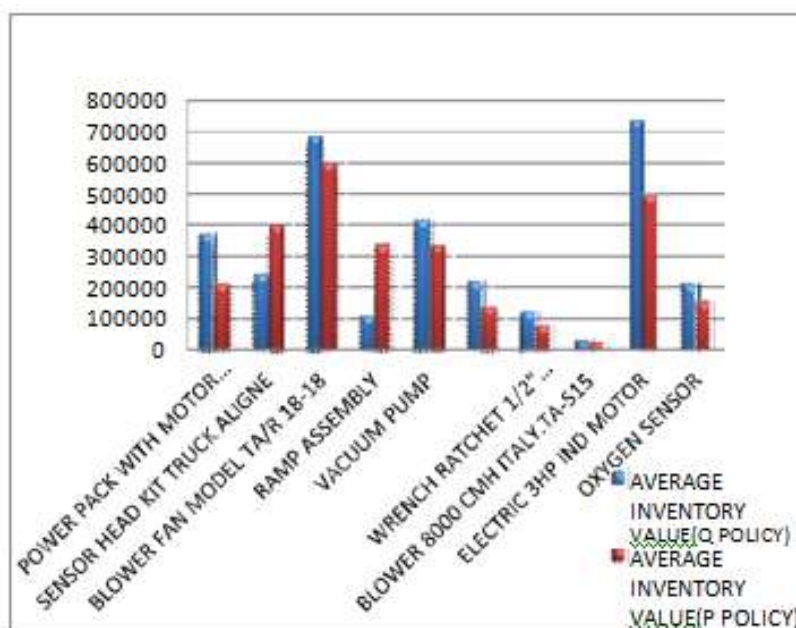


Fig 13: Comparison of average of inventory value

Description	Average inventory value (q-policy)	Average inventory value (p-policy)	Average Inventory Cost value (old)	Q-policy savings (%)	P-policy savings (%)
Power pack with motor	374887	212450	1316531	72	83
Sensor head kit truck align	240278	400464	2838854	92	91
Blower fan model ta/r 18-18	682351	599265	2314605	71	74
Ramp assembly	110270	335875	1980629	94	83
Vacuum pump	414696	332052	1648759	75	80
Wrench impact 1/2" sp1140ex	217398	139376	438373	50	68
Wrench ratchet 1/2" sp1133sx	123035	82697	247959	50	67
Blower 8000 cmh	28489	24378	851863	97	97
Electric 3hp induction motor	732998	494674	5149854	86	90
Oxygen sensor	207501	151304	1395075	85	89

Table 6: Comparison of p-policy savings (%) and q-policy savings(%)

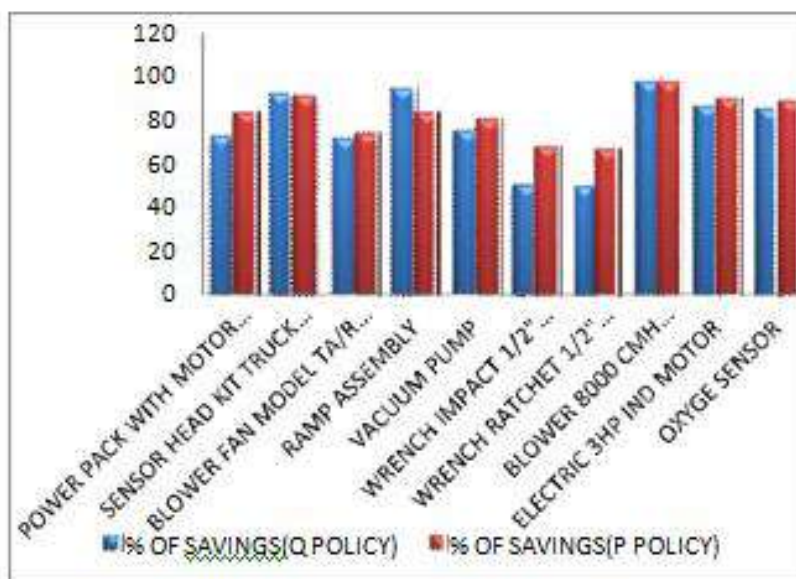


Fig 14: Comparison of p-policy savings (%) and q-policy savings (%)

2. Analysis of multi bin Kanban system

Based on simulation result, multi bin system keeps down the inventory cost as compared to forward cover system.

Description	Apr'15 - qty	May'15 - qty	June'15 - qty	July'15 - qty
Wheel aligner kit dwa 1000w	2	3	2	2
kit wb f7d	2	12	7	3
Power pack with motor assy-f	3	2	6	6
Sensor head kit truck align	0	0	0	0
Blower fan model ta/r 18-18	26	51	17	41
Vacuum pump	13	13	10	9
Wrench ratchet 1/2" sp1133sx	5	4	4	4
Power pack	39	36	18	34
Blower 8000 cmh italy.ta-s15	5	4	4	4
Power pack	39	36	18	34
Bumer bentone - b30a/as47cpu	17	20	9	14
Electric 3hp ind motor	62	83	40	35
3hp electric motor b3 b14	39	49	97	82

Table 7: Forward cover system-inventory in terms of quantity

Description	Apr'15 - value	May'15 - value	June'15 - value	July'15 - value
Wheel aligner kit dwa 1000w	372505.1	542765.3	384651.2	393834.5
Kit wb f7d	110825.5	681200.9	397367.2	166226
Power pack with motor assy-f	50550	29400	88200	88200
Sensor head kit truck align	0	0	0	0
Blower fan model ta/r 18-18	81897.66	160645.4	53548.47	141260.6
Vacuum pump	36220.73	36220.73	27862.1	25075.89
Wrench ratchet 1/2" sp1133sx	53967.75	43174.2	43174.2	43174.2
Power pack	334501.8	309722.4	158168.5	299795.7
Blower 8000 cmh italy.ta-s15	53967.75	43174.2	43174.2	43174.2
Power pack	334501.8	309722.4	158168.5	299795.7
Burner bentone - b30a/as47cpu	407839.2	490315	217252.5	344241.2
Electric 3hp induction motor	351557.4	470633.2	209792.8	184292.5
3hp electric motor b3 b14	222337.1	279346.6	534211	453382.1

Table 8: Forward cover system-inventory value in terms of rupees

Description	April 15- qty	May15- qty	June15 qty	July15 qty
Wheel aligner kit dwa 1000w	2	3	1	2
Kit wb f7d	2	4	8	1
Power pack with motor assy-f	1	2	4	5
Sensor head kit truck align	0	0	0	0
Blower fan model ta/r 18-18	6	6	6	6
Vacuum pump	20	25	30	35
Wrench ratchet 1/2" sp1133sx	6	8	10	4
Power pack	3	4	4	4
Blower 8000 cmh italy.ta-s15	0	0	0	0
Power pack	24	48	1	24
Burner bentone - b30a/as47cpu	16	8	8	12
Electric 3hp induction motor	16	32	1	16
3hp electric motor b3 b14	24	30	36	23

Table 9 : Multi bin system-inventory in terms of quantity

Description	April 15- value	May 15- value	June15 value	July15 value
Wheel aligner kit dwa 1000w	415147	622720	103787	415147
Kit wb f7d	119931	239863	479725	29983
Power pack with motor assy-f	7350	29400	51450	73500
Sensor head kit truck align	0	0	0	0
Blower fan model ta/r 18-18	74180	74180	74180	74180
Vacuum pump	70189	87737	105284	122831
Wrench ratchet 1/2" sp1133sx	16717	22290	27862	11145
Power pack	25761	34348	34348	34348
Blower 8000 cmh italy.ta-s15	0	0	0	0
Power pack	206073	412146	8586	206073
Burner bentone - b30a/as47cpu	392266	196133	196133	294199
Electric 3hp induction motor	85813	171627	5363	85813
3hp electric motor b3 b14	135162	168953	202744	129531

Table 10: Multi bin system-inventory value in terms of rupees

VIII.CONCLUSION

The organizations should use the inventory keeping approach that best suits their operation to meet the aforementioned goals. The just-in-time strategy, which has been shown to be beneficial in keeping the proper quantity of inventory and preventing stock-outs, should be explored as an alternative here. Hence the Effective inventory control management is acknowledged as one of the areas in which any organization's management should develop expertise.

REFERENCES

1. S. Chopra and P. Meindl, *Supply Chain Management Strategy, Planning and Operation*, 4th Ed, Pearson, 2010.
2. F. D. Hedrick et al, "Inventory Management. Purchasing for Owners of Small Plants," *Buying for Retail Stores and Inventory Management*, 2012.
3. C. Laeiddee, "Improvement of Re-Order Point for Drug Inventory Management at Ramathibodi Hospital," Master Thesis, Mahidol University, 2010.
4. Muris LageJunior, MoacirGodinhoFilho, Variations of the kanban system: Literature review and classification, *Int. J. Production Economics* 125 (2010) 13–21
5. Sipper, D, Bulfin Jr, R.L. *Production: Planning, Control, and Integration*, Mcgraw-Hill, New York, 1997.
6. Performance, *Academy of Management Journal*. Vol.38, No.5, p. 1325-1360. Heizer, J. and Render, B. 2005. *Flexible Version: Operation Management*, 7th edition, New Jersey: Prentice Hall.
7. Kobbacy K., Liang Y. 1999. Towards the development of an intelligent inventory management system, *Integrated Manufacturing Systems*. p. 354-366.
8. Donald W., 2003. *Inventory Control and Management*, 2nd Edition, John Wiley & Sons Ltd.

Application of Visual Intelligence for Detection of Physical Damages in Objects

A. Chitra and Gowtham Balaji B

Department of Computer Applications PSG College of Technology, India

ABSTRACT

The main aim of the project is to find the physical damages of the object through images by comparing with the original image of the object at the time of sales or delivery. In this project, the images taken at the time of inspection are compared to the original images (those taken at the time of delivery / sales), and the damaged portions are highlighted and recorded for future reference. This comparison process involves analyzing the objects in images and modelling in 3D viewpoint, so that the comparison can be more accurate and robust even in case of any distortion, noise and change in illumination. As the comparison involves homographic object modelling, the target identification will be more accurate even in the case of change in orientation, lighting and external noise on the target object.

1. INTRODUCTION

Many tools are available for Image Comparison in various platforms; in addition to that many service vendors provide API support for image comparison that are platform independent. Such tools can be used for detection of physical damages of the objects but those tools break down the actual image into many small images and further into a two-dimensional array of pixel, where each pixel has its own color properties. By comparing images in this manner, the tools highlight the dissimilarities / differences. These tools require the image of original object (without damages) in similar orientation, lighting, angle, position, etc..

For example, let us consider a scenario, where a car is damaged at a rural location, in such case the car should not be moved until the damage is inspected. Getting the picture of original object in the similar scene is impossible. In such scenarios, the above discussed comparison methodology will not be accurate. Hence, an application is required, that is robust and should overcome this scenario and identify the damages irrespective of orientation, illumination and environmental lighting noises.

1.1 FEATURE EXTRACTION

Data captured in real world applications are high dimensional and use of such data in algorithms like computer vision, object identification, objects classification etc.. yield low accuracy and overfitting of data [1], [2], [5], [7] and [9]. This issue is solved using features extracted from the images. The use of features aid in transformation invariant object detection and identification. Features are also invariant to illumination and 3D camera viewpoint in most of the cases. The complexity of feature extraction can be reduced by application of techniques like cascade filtering [1], [6], [4] and [8].

1.2 SCALE INVARIANT FEATURE TRANSFORM (SIFT)

SIFT is a method to identify salient feature points in an image. In addition to the feature points, features describing a small region around the point can also be obtained. The features thus obtained are invariant to scaling and rotation. The features thus obtained are invariant to scaling and rotation, colour of the pixel and minor image artifacts. First the key points are identified by looking for the intensity changes. Difference of Gaussians is used. As the key points are either maxima or minima in the images segments used, both location and scale of the key points can be determined. It is better to avoid the points on edges as key points. Then based on the dominant orientations of the points in a small window around the key point, its orientation are fixed. For each of the key points descriptors are determined.

HOMOGRAPHY

Homography is used to get warped versions of the original image. This is useful in applications like image rectification, image registration etc. Two images are related to homography if both are taken from same camera but from different angle or both images are viewing the same place from a difference angle. Homography is applicable only when there is no translation.

2 SYSTEM ANALYSES

This phase of the document contains the details of the existing systems, their drawbacks and the proposed system details that are to be developed.

2.1 EXISTING SYSTEM

There are existing off-the-shelf open source software's available for image comparison, that performs comparison with pixels of the two images under process. Some of the examples are ImageMagick,

PerceptualDiff, Resemble.js, etc.,. The above mentioned software's compare the image pixels and highlight the differences. The main challenge in this type of image comparison software's is that the images under comparison should be taken under similar orientation, lighting, angle and illumination [3], [7], and [9].

2.2 PROPOSED SYSTEM

Proposed system is built to compare the images by modelling the objects in the images in 3D viewpoint and compare the corresponding objects in the other image and determine the similarities and differences irrespective of orientation, illumination, and angle of the images. The objects after comparison will be highlighted, in this case, the damages are the objects and the same will be highlighted in the image under comparison.

In addition to the damage detection, this application allows damaged image contribution feature for interested users to upload the images of damaged objects for fine tuning the dataset and increase accuracy on further usage. Each contribution will be verified manually and added to the dataset by the administrator.

2.3 REQUIREMENTS SPECIFICATION

This phase of the document contains the requirements specified for the application development and execution, both in technical and non-technical aspects.

2.3 FUNCTIONAL REQUIREMENTS

Functional requirements are product features or functions that developers must implement to enable users to accomplish their tasks. Below mentioned requirements are fundamental for application developed. Physical damages of the object are to be detected by comparing the image of damaged object with the dataset and highlight the damaged parts.

2.4 NON-FUNCTIONAL REQUIREMENTS

Following are the non-functional requirements considered:

Reliability:

Reliability also known as the accuracy of the results in predicting the required user attributes.

Data Integrity:

Data Integrity is the assurance of the accuracy and consistency of data over the entire life-cycle of the application execution.

Performance:

Performance is the way of functioning of the application and the extent to which the application is responsive to the app to the end-user while detecting the physical damages.

Scalability:

Scalability of the application is the potential of an application to grow in time, being able to efficiently handle more and more requests per minute.

3. SYSTEM DESIGN

This section of the document contains the UML diagram(s) created during the design phase of the application development.

3.1 USE CASE DIAGRAM

There are two types of users with different roles and access levels. First is the generic user, the application can be used to identify damages and highlight the same of the car by uploading the image, the output (damage highlighted) image can be downloaded for further usage. In addition to the damage detection, the generic user can contribute to dataset by uploading damaged object images in order to update the dataset for more accurate results. Second role is the admin, that will be manually validating the contributions and approve the images that are to be integrated with the dataset in order to restrict in-appropriate contributions.

Figure 1 shows the use case diagram of the application to detect physical damages of the object under comparison.

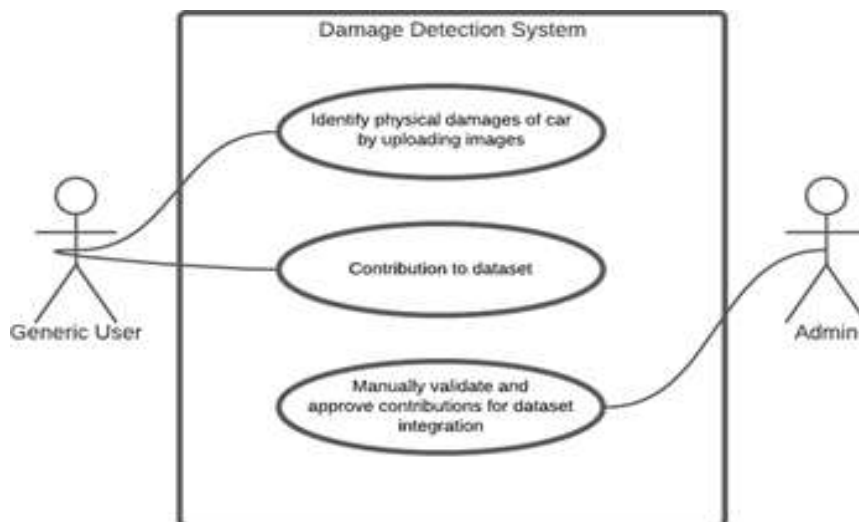


Fig 1 Use Case Diagram of the application.

3.2 FLOWCHART

Figure 2 depicts the steps involved in identifying the physical damages of the objects from uploading the image to server until the detection.

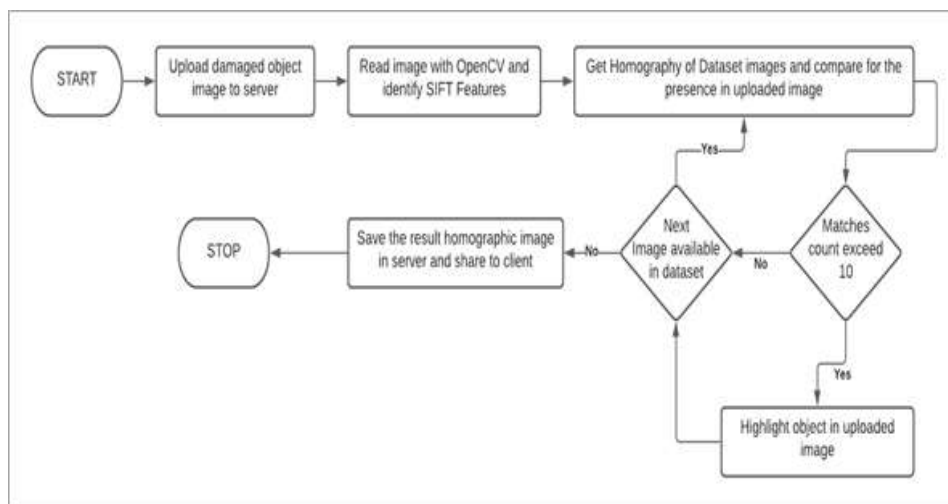


Fig 2 Flow chart of the application.

As the first step, the generic user will be uploading the image of the damaged object to the server, a copy of uploaded image will be saved in the server, later the same image will be read with OpenCV library and the SIFT features (briefly explained section 4 of the document) of the uploaded images are extracted. As next step, each image of the dataset will be iterated, homography of the objects are found and compared for the presence in the uploaded image. If the count of the matches exceeds 10, the corresponding object is highlighted and next image of the dataset is iterated. Once all the images in dataset are iterated, the result image is saved to the outputs directory of the server and link is shared to the client, from where the user can download the highlighted image for further usage.

3.3 MODULES OF THE APPLICATION

The application consists of two modules mainly, one of them is to identify the physical damages and highlight the same, and the other module is to contribute damage object images in order to increase dataset prediction accuracy for future usage. Once the user contribution is done, the same is validated manually by the user and approved for dataset integration.

4. EXPERIMENTAL STUDY AND DATA SET

Experiments were conducted to test and validate algorithms proposed.

CAR DAMAGE DETECTION

Experiments were conducted to test and validate our proposed algorithm to show significant changes in finding the damaged parts in images while comparing with the original car image is shown in figure 4.



Figure 3 Single Car Damage Detection

CAR DAMAGE DATASET

KSGGLR Car Damage Dataset consists of images of the damaged cars. A portion of the collection is shown in Figure 4. From the image of a damaged car, the damaged portions are split and used as objects in homographic comparison.

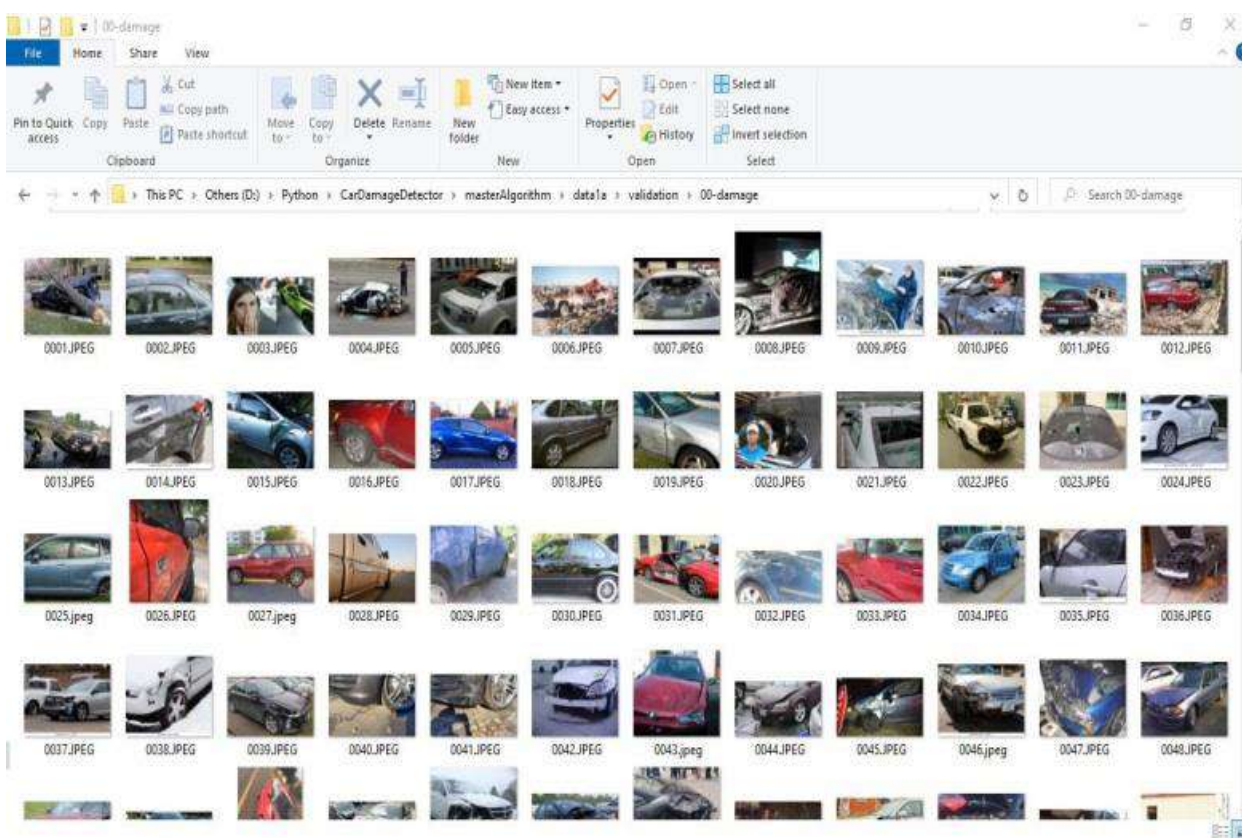


Fig 4 KSGGLR Car Damage Dataset

5 CONCLUSION

The physical damages of the objects are detected using visual intelligence and the damaged parts will be highlighted in the output image so the user would be able to analyze it efficiently for further usage. As this detection involves homographic comparison, the objects under comparison need not to be in similar angle or posture so as to identify the damage. As an additional feature, the users can contribute damaged object images for enriching the dataset and improve the accuracy of the results on further predictions. Those contributions will be validated manually and added to the dataset only after the approval of the system admin in order to eliminate in appropriate contributions by anonymous users.

REFERENCES

1. Lowe, D. G. (2004). Distinctive image features from scale-invariant key points. *International journal of computer vision*, 60(2), 91-110.
2. Karami, E., Prasad, S., & Shehata, M. (2017). Image matching using SIFT, SURF, BRIEF and ORB: performance comparison for distorted images. *arXiv preprint arXiv:1710.02726*.
3. Jayawardena, Srimal. (2013). Image Based Automatic Vehicle Damage Detection. Doctoral Thesis , The Australian University
4. Patil, K., Kulkarni, M., Sriraman, A., & Karande, S. (2017, December). Deep learning based car damage classification. In *2017 16th IEEE international conference on machine learning and applications (ICMLA)* (pp. 50-54). IEEE.
5. Dong, W. S., Gao, P., Li, C. S., Luo, W. H., Yao, R. J., Yuan, T., & Zhu, J. (2020). U.S. Patent No. 10,628,890. Washington, DC: U.S. Patent and Trademark Office.
6. Singh, R., Ayyar, M. P., Pavan, T. V. S., Gosain, S., & Shah, R. R. (2019, September). Automating car insurance claims using deep learning techniques. In *2019 IEEE Fifth International Conference on Multimedia Big Data (BigMM)* (pp. 199-207). IEEE.
7. Balci, B., Artan, Y., Alkan, B., & Elihos, A. (2019). Front-View Vehicle Damage Detection using Roadway Surveillance Camera Images. In *VEHITS* (pp. 193-198).
8. Waqas, U., Akram, N., Kim, S., Lee, D., & Jeon, J. (2020). Vehicle Damage Classification and Fraudulent Image Detection Including Moiré Effect Using Deep Learning. In *2020 IEEE Canadian Conference on Electrical and Computer Engineering (CCECE)* (pp. 1-5). IEEE.
9. Kumar, S. S., & Devaki, K. (2020). Assessing Car Damage using Mask R-CNN. *arXiv preprint arXiv:2004.14173*.

Solving Lorenz System of Equation by Laplace Homotopy Analysis Method

G. Sai Sundara Krishnan¹, R. Malathy² and S. R. Saratha³

¹Applied Mathematics and Computational Sciences PSG College of Technology Coimbatore, India

²Department of Mathematics SNS College of Engineering Coimbatore, India

³Department of Mathematics Kumaraguru College of Technology Coimbatore, India

ABSTRACT

The Laplace Homotopy Analysis Method via Modified Riemann-Liouville Integral has been explored from a new perspective. The important items are assimilated, and the result is proven using well-defined evidence. A combination of the homotopy analysis approach and the suggested integral transform is used to find fractional differential equations.

Index terms—Homotopy, Homotopy Analysis Method, Laplace Transform, Fractional Differential Equations

I. INTRODUCTION

Many researchers have recently become interested in the theoretical studies of various integral transforms as a methodical mathematical strategy for converting fractional differential equations into simple algebraic formulas. Chowdhury et al (2007) introduced MHPM to handle the Lorenz system in the literature. The DTM was used by Mossa et al (2008) to solve a non-linear differential equation.

Jumarie (2009) presented a fractional-order Laplace's transform definition for functions that are fractionally differentiable but not differentiable. Alomari et al (2011) modified the DTM to achieve continuous and analytic solutions for each interval when solving non-linear fractional differential equations. The Laplace transform was first introduced to the field by Liang et al (2015). Medina et al (2017) investigated the effect of the fractional Laplace Transform incorporated in the Riemann-Liouville Fractional Derivative. For various fractional linear differential equations with constant coefficients, Silva et al (2018) studied the pleasant fractional derivative. The integral transform is used in conjunction with the Homotopy Analysis Method to solve nonlinear differential equations (HAM). Hariharan (2017) proposed the homotopy analysis technique (HAM) for solving a few partial differential equations in the literature. Mohammed et al (2017) used modified Laplace Homotopy Analysis to solve a nonlinear system of fractional partial differential equations. The Fractional Laplace Transform through Modified Riemann-Liouville derivative [Jumarie (2009)] is the subject of this work. It is coupled with HAM, which was proposed by Liao (1992), to create a novel hybrid approach called Laplace Homotopy Analysis through Modified Riemann-Liouville Integral. Nonlinear fractional differential equations can be solved using this hybrid approach. Edward Lorenz was the first to study the Lorenz system, which is a set of ordinary differential equations. For specific parameter values and starting circumstances, it is renowned for having chaotic solutions. The Lorenz attractor, in particular, is a collection of chaotic Lorenz system solutions.

This research motivates to study the Fractional Laplace transform via Modified Riemann-Liouville [Jumarie (2009)] and it is combined with HAM introduced by Liao (1992), which provides the new hybrid technique Laplace Homotopy Analysis method via Modified Riemann-Liouville Integral. Non-chaotic behaviour is obtained in this work by employing modal series solutions with Rayleigh number R parameter values below the critical value. Throughout this study, we assume $\sigma = 10$, $b = -8/3$, and change the Rayleigh number R to get different dynamical behaviours and assess the recommended approach. Pandemonium is well known to occur around the critical parameter value $R = 24.74$. [10]

II. PRELIMINARIES

This part contains the essential definitions for the study, as well as other fundamental results that can be found in Jumarie (2009).

Definition 2.1: The Mittag-Leffler function which is a generalization of exponential function is defined as

$$E_{\zeta}(z) = \sum_{n=0}^{\infty} \frac{z^n}{\Gamma(\zeta n + 1)} \quad (1)$$

where $\zeta \in \mathbb{C}$, $R(\zeta) > 0$.

Definition 2.2: The continuous function $g : \mathbb{R} \rightarrow \mathbb{R}$, $t \rightarrow g(t)$ has a fractional derivative of order $k\zeta$. For any positive integer k and for any ζ , $0 < \zeta \leq 1$, the Taylor's series of fractional order can be expressed as

$$g(t+h) = \sum_{k=0}^{\infty} \frac{h^{\zeta k}}{(\zeta k)!} g^{(\zeta k)}(t), \quad 0 < \zeta \leq 1$$

Definition 2.3: (Modified Riemann Liouville derivative) Let $q : \mathbb{R} \rightarrow \mathbb{R}$, denote a continuous (but not necessarily differentiable) function. i. Assume that $q(y)$ is a constant K . Then its fractional derivative of order ζ is

$$D_y^\zeta = K\Gamma^{-1}(1 - \zeta)y^{-\zeta}, \zeta \leq 0, \quad (2)$$

$$= 0, \zeta > 0$$

ii. When $q(y)$ is not a constant, then we will set

$$q(y) = q(0) + (q(y) - q(0)), \quad (3)$$

in which, for negative ζ , one has

$$D_y^\zeta(q(y) - q(0)) = D_y^\zeta q(y) = D_y(q^{(\zeta-1)}(y)). \quad (4)$$

When $n \leq \zeta < n + 1$, we will set

$$q^{(\zeta)}(y) = (q^{(\zeta-n)}(y))^{(n)}, n \geq 1. \quad (5)$$

In order to find the fractional derivative of compound functions, equation (6) is used.

$$d^\zeta q \cong \Gamma(1 + \zeta) dq, 0 < \zeta < 1. \quad (6)$$

Definition 2.4: If $0 < \zeta < 1$, then

$$D_y^\zeta y^\eta = \Gamma(\eta + 1)\Gamma^{-1}(\eta + 1 - \zeta)y^{\eta-\zeta}, \eta > 0, \quad (7)$$

or, if $\zeta = n + \theta$, $n \in \mathbb{N}$, then

$$D_y^{n+\theta} y^\eta = \Gamma(\eta+1)\Gamma^{-1}(\eta+1-n-\theta)y^{\eta-n-\theta}, 0 < \theta < 1, \quad (8)$$

II. FRACTIONAL LAPLACE TRANSFORM VIA MODIFIED RIEMANN-LIOUVILLE INTEGRAL

Definition 3.1: Let $k(y)$ denotes a function that vanishes for the negative value of y . Its Laplace's transformation $L_k(y)$ of order defined by the following expression, where it is finite:

$$L_\epsilon[k(y)] = K_\epsilon(s) = \int_0^\infty E_\epsilon[-s^\epsilon y^\epsilon]k(y)(dy)^\epsilon, \quad (9)$$

$$= \lim_{M \rightarrow \infty} \int_0^M E_\epsilon[-s^\epsilon y^\epsilon]k(y)(dy)^\epsilon, \quad (10)$$

where $s \in \mathbb{C}$, and $E_\epsilon(u)$ is the Mittag-Leffler function $\sum u^k / (k\epsilon)!$.

Theorem 3.1: if $L_\epsilon[k(y)] = K_\epsilon(s)$ then

Scaling property

$$(i) L_\epsilon[k(ay)]_s = \frac{1}{a} L_\epsilon[k(y)]_{\frac{s}{a}}, \quad (11)$$

shifting Property

$$(ii) L_\epsilon[k(y - b)] = E_\epsilon(-s^\epsilon b^\epsilon)L_\epsilon[k(y)], \quad (12)$$

frequency Shifting Property

$$(iii) L_\epsilon[E_\epsilon(-c^\epsilon y^\epsilon)k(y)]_s = L_\epsilon[k(y)]_{s+c}, \quad (13)$$

derivative Property

$$(iv) L_\epsilon[-y^\epsilon k(y)]_s = D_s^\epsilon L_\epsilon[k(y)], \quad (14)$$

laplace transform of fractional derivative

$$(v) L_\epsilon[k^\epsilon(y)] = s_\epsilon L_\epsilon[k(y)] - \Gamma(1 + \epsilon)g(0). \quad (15)$$

Theorem 3.2: Let the convolution of the two functions $k(y)$ and $l(y)$ of order ϵ is given by

$$(k(y) * l(y))_\epsilon = \int_0^y k(y-u)l(y)(du)^\epsilon, \quad (16)$$

then one has the equality

$$L_\epsilon[(k(y) * l(y))_\epsilon] = L_\epsilon[k(y)]L_\epsilon[l(y)]. \quad (17)$$

Coming up next are the main ends for the Laplace fractional change of standard functions, as displayed in Table 1:

Laplace Fractional transform of standard functions		
S.N	$g(y)$	$L_c[g(y)] = G_c(s)$
1	1	$\frac{1}{s^\epsilon} \Gamma(\epsilon + 1)$
2	t^ϵ	$\frac{1}{s^{\epsilon+1}} \Gamma^2(\epsilon + 1)$
3	$t^{2\epsilon}$	$\frac{1}{s^{2\epsilon+1}} \Gamma^3(\epsilon + 1) \Gamma(3)$
4	$t^{n\epsilon}$	$\frac{1}{s^{(n+1)\epsilon}} \Gamma^{n+1}(\epsilon + 1) \Gamma(n + 1)$
5	$E_c[a^\epsilon y^\epsilon]$	$\frac{1}{(s-a)^\epsilon} \Gamma(\epsilon + 1)$
6	$E_c[-a^\epsilon y^\epsilon]$	$\frac{1}{(s+a)^\epsilon} \Gamma(\epsilon + 1)$
7	$E_c[i^\epsilon a^\epsilon y^\epsilon]$	$\frac{1}{(s-ia)^\epsilon} \Gamma(\epsilon + 1)$
8	$E_c[-i^\epsilon a^\epsilon y^\epsilon]$	$\frac{1}{(s+ia)^\epsilon} \Gamma(\epsilon + 1)$
9	$\sin(a^\epsilon y^\epsilon)$	$\frac{a^\epsilon}{(s^2+a^2)^\epsilon} \Gamma(\epsilon + 1)$
10	$\cos(a^\epsilon y^\epsilon)$	$\frac{s^\epsilon}{(s^2+a^2)^\epsilon} \Gamma(\epsilon + 1)$
11	$\sinh(a^\epsilon y^\epsilon)$	$\frac{a^\epsilon}{(s^2-a^2)^\epsilon} \Gamma(\epsilon + 1)$
12	$\cosh(a^\epsilon y^\epsilon)$	$\frac{s^\epsilon}{(s^2-a^2)^\epsilon} \Gamma(\epsilon + 1)$
13	$E_c[a^\epsilon y^\epsilon] \sin[b^\epsilon y^\epsilon]$	$\frac{b^\epsilon}{(s^2-a^2)^\epsilon + b^{2\epsilon}} \Gamma(\epsilon + 1)$
14	$E_c[a^\epsilon y^\epsilon] \cos[b^\epsilon y^\epsilon]$	$\frac{(s-a)^\epsilon}{(s^2-a^2)^\epsilon + b^{2\epsilon}} \Gamma(\epsilon + 1)$
15	$E_c[a^\epsilon y^\epsilon] \sinh[b^\epsilon y^\epsilon]$	$\frac{b^\epsilon}{(s^2-a^2)^\epsilon - b^{2\epsilon}} \Gamma(\epsilon + 1)$
16	$E_c[a^\epsilon y^\epsilon] \cos[b^\epsilon y^\epsilon]$	$\frac{(s-a)^\epsilon}{(s^2-a^2)^\epsilon - b^{2\epsilon}} \Gamma(\epsilon + 1)$

The Laplace transform will be utilized related to the fractional homotopy analysis way to deal with tackle both linear and nonlinear differential conditions (Fractional Homotopy Analysis method).

IV. FRACTIONAL LAPLACE HOMOTOPY ANALYSIS METHOD (FLHAM)

Consider the fractional time nonlinear differential condition with the accompanying beginning condition:

$$D^\epsilon v(y, t) + R(y, t) + Nv(y, t) = q(y, t), \quad v(y, 0) = k(y), \tag{18}$$

where D^ϵ is the fractional differential operator $D^\epsilon = \frac{\partial^\epsilon}{\partial t^\epsilon}$, R is the differential linear operator, N is the differential non linear operator and $q(y, t)$ is source term.

To solve the non-linear partial differential condition, embrace the accompanying organized method:

Step 1: Apply fractional laplace transform, the equation (18),

$$L_c[D^\epsilon v(y, t)] + L_c[Rv(y, t)] + L_c[Nv(y, t)] = L_c[q(y, t)]. \tag{19}$$

Step 2: Applying the derivative of fractional Laplace transform, The condition (19), can communicate as

$$L_c[v(y, t)] - \frac{1}{s^\epsilon} \Gamma(\epsilon + 1)v(y, 0) + \frac{1}{s^\epsilon} L_c[Rv(y, t)] + \frac{1}{s^\epsilon} L_c[Nv(y, t)] - \frac{1}{s^\epsilon} L_c[q(y, t)] = 0. \tag{20}$$

Step 3: The nth order deformation equation

$$v_n(y, t) = \chi_n v_{n-1}(y, t) + hL^{-1}[R_n(v_{n-1}(y, t))], \tag{21}$$

where,

$$R_{n-1}[v_{n-1}(y, t)] = [L_c[v_{n-1}(y, t)] - \frac{1}{s^\epsilon} \Gamma(\epsilon + 1)v(y, 0) + \frac{1}{s^\epsilon} L_c[Rv_{n-1}(y, t)] + \frac{1}{s^\epsilon} L_c[Nv_{n-1}(y, t)] - \frac{1}{s^\epsilon} L_c[q(y, t)],$$

where,

$$\chi_n = \begin{cases} 0 & n \leq 1 \\ 1 & n > 1. \end{cases}$$

V. APPLICATION

Consider the well-known Lorenz system in this study.

$$D^\zeta x = \sigma(y(t) - x(t)) \tag{22}$$

$$D^\zeta y = Rx(t) - y(t) - x(t)z(t) \tag{23}$$

$$D^\zeta z = x(t)y(t) + bz(t) \tag{24}$$

where convective velocity, temperature differential between descending and ascending flows, and mean convective heat flow are proportional to x , y , and z , and σ , b , and the so-called bifurcation parameter R are real constants. with the initial condition $x(0) = c_1$, $y(0) = c_2$, $z(0) = c_3$.

$$\frac{d^\zeta x}{dt^\zeta} = \sigma(y(t) - x(t)) \quad (25)$$

$$\frac{d^\zeta y}{dt^\zeta} = Rx(t) - y(t) - x(t)z(t) \quad (26)$$

$$\frac{d^\zeta z}{dt^\zeta} = x(t)y(t) + bz(t) \quad (27)$$

with the initial condition $x(0) = c_1, y(0) = c_2, z(0) = c_3$.
 Apply L_ζ on both sides of the equation (25)

$$L_\zeta\left[\frac{d^\zeta x}{dt^\zeta}\right] = L_\zeta[\sigma(y(t) - x(t))] \quad (28)$$

$$s^\zeta L_\zeta[x(t)] - \Gamma(\zeta + 1)x(0) = \sigma[L_\zeta(y(t) - x(t))] \quad (29)$$

$$s^\zeta L_\zeta[x(t)] - \Gamma(\zeta + 1)x(0) = \sigma[L_\zeta(y_{m-1}(t)) - L_\zeta(x_{m-1}(t))] \quad (30)$$

The n th order deformation equation for $x(t)$ is defined as

$$R_n[x_{n-1}(t)] = [L_\zeta[x_{n-1}(t)] - \frac{1}{s^\zeta}\Gamma(\zeta + 1)x(0)(1 - \chi_n) - \frac{1}{s^\zeta}\sigma L_\zeta[y_{n-1}(t)] + \frac{1}{s^\zeta}\sigma L_\zeta[x_{n-1}(t)]] \quad (31)$$

$$R_n[y_{n-1}(t)] = [L_\zeta[y_{n-1}(t)] - \frac{1}{s^\zeta}\Gamma(\zeta + 1)y(0)(1 - \chi_n) - \frac{1}{s^\zeta}RL_\zeta[(x_{n-1}(t)) + \frac{1}{s^\zeta}L_\zeta[y_{n-1}(t)] + \frac{1}{s^\zeta}L_\zeta[\sum_{i=0}^{m-1} x_i(t)z_{m-1-i}(t)]]] \quad (32)$$

$$R_n[z_{n-1}(t)] = [L_\zeta[z_{n-1}(t)] - \frac{1}{s^\zeta}\Gamma(\zeta + 1)z(0)(1 - \chi_n) - \frac{1}{s^\zeta}L_\zeta[\sum_{i=0}^{m-1} x_i(t)y_{m-1-i}(t)] - \frac{1}{s^\zeta}bL_\zeta[z_{n-1}(t)]] \quad (33)$$

On both sides of the equation (31),(32), and (33), use the inverse fractional Laplace transform

$$x_n(t) = \chi_n x_{n-1}(t) + hL^{-1}[R_n(x_{n-1}(t))] \quad (34)$$

$$y_n(t) = \chi_n y_{n-1}(t) + hL^{-1}[R_n(y_{n-1}(t))] \quad (35)$$

$$z_n(t) = \chi_n z_{n-1}(t) + hL^{-1}[R_n(z_{n-1}(t))] \quad (36)$$

On solving the (34) (35) (36) equations for $n=1,2,3,4,\dots$

$$x_1(t) = h\sigma(-c_2 + c_1) \frac{t^\zeta}{\Gamma(\zeta + 1)}$$

$$y_1(t) = -h(Rc_1 - c_2 - c_1c_3) \frac{t^\zeta}{\Gamma(\zeta + 1)}$$

$$z_1(t) = -h(c_1c_2 + bc_3) \frac{t^\zeta}{\Gamma(\zeta + 1)}$$

$$x_2(t) = [h\sigma(-c_2 + c_1) \frac{t^\zeta}{\Gamma(\zeta + 1)} + h^2\sigma(Rc_1 - c_2 - c_1c_3) \frac{t^{2\zeta}}{2\Gamma^2(\zeta + 1)} + h^2\sigma^2(-c_2 + c_1) \frac{t^{2\zeta}}{2\Gamma^2(\zeta + 1)}]$$

$$y_2(t) = [h(Rc_1 - c_2 - c_1c_3) \frac{t^\zeta}{\Gamma(\zeta + 1)} + h^2(Rc_1 - c_2 - c_1c_3) \frac{t^\zeta}{\Gamma(\zeta + 1)} - Rh^2\sigma(-c_2 + c_1) \frac{t^{2\zeta}}{2\Gamma^2(\zeta + 1)} - h^2(Rc_1 - c_2 - c_1c_3) \frac{t^{2\zeta}}{2\Gamma^2(\zeta + 1)} - h^2c_1(c_1c_2 + bc_3) \frac{t^{2\zeta}}{2\Gamma^2(\zeta + 1)} + h^2\sigma(-c_2 + c_1)c_3 \frac{t^{2\zeta}}{2\Gamma^2(\zeta + 1)}]$$

$$z_2(t) = [h(c_1c_2 + bc_3) \frac{t^\zeta}{\Gamma(\zeta + 1)} + h^2(c_1c_2 + bc_3) \frac{t^\zeta}{\Gamma(\zeta + 1)} + c_1h^2(Rc_1 - c_2 - c_1c_3) \frac{t^{2\zeta}}{2\Gamma^2(\zeta + 1)} - h^2\sigma(-c_2 + c_1)c_2 \frac{t^{2\zeta}}{2\Gamma^2(\zeta + 1)} + bh^2(c_1c_2 + bc_3) \frac{t^{2\zeta}}{2\Gamma^2(\zeta + 1)}]$$

Similarly $x_3, x_4, \dots, y_3, y_4, \dots$ and z_3, z_4, \dots can be assessed, and a sequence of solutions can be found as follows:

$$x(t) = \sum_{n=0}^N x_n(t) \quad (37)$$

$$y(t) = \sum_{n=0}^N y_n(t) \quad (38)$$

$$z(t) = \sum_{n=0}^N z_n(t) \quad (39)$$

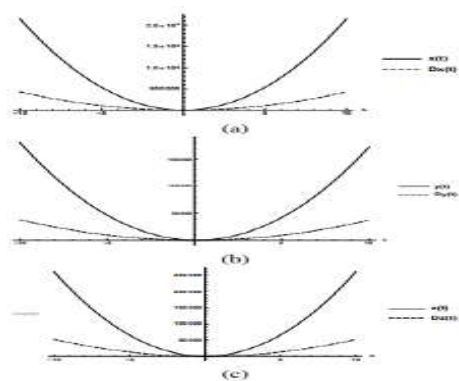


Fig. 1: The h-curve for the Lorenz system of equation $x(t)$ (1a), $y(t)$ (1b) and $z(t)$ (1c) with the convergence region for the auxiliary parameter ($h \in [-1, 0]$).

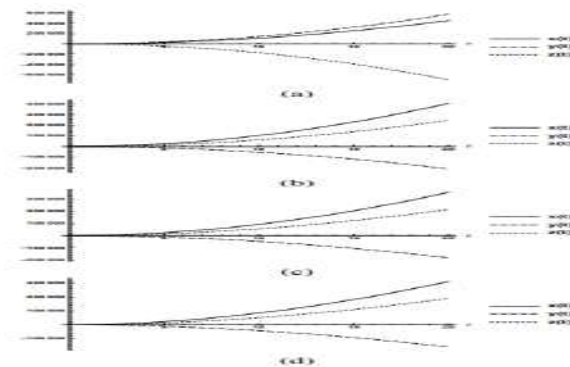


Fig. 2: The Non chaotic Solution curves for Lorenz system of equation when $\zeta=1, 0.98, 0.96, 0.94$ respectively (2a), (2b), (2c), (2d)

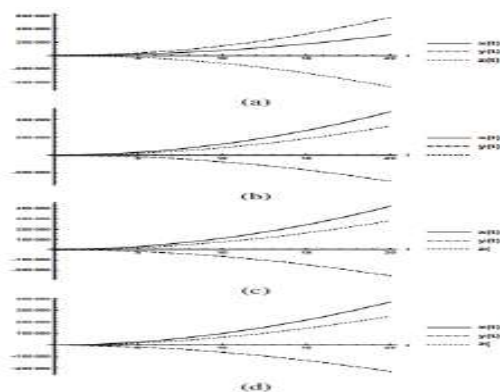


Fig. 3: The Chaotic Solution curves for Lorenz system of equation when $\zeta=1, 0.98, 0.96, 0.94$ respectively (3a), (3b), (3c), (3d) To decide the values of h we plot the h-curve for the equation (37), (38) and (39) in various figures from 11 – 13.

From these figures ,it is noted that the convergence region of h lies between the range $h \in [-1, 1]$. The solution curve of the Lorenz system are displayed in figure 7 – 8 for the different values of ζ . (i.e, $\zeta = 0.94, 0.96, 0.98, 1$) and for a comparison with A.K.Alomari et al [1].we set $\sigma = 10, b = -8/3$ we take initial conditions $x(0) = -15.8, y(0) = -17.48, z(0) = 35.64$ as in [1]. which demonstrates the excellence of the proposed Lorenz system.

TABLE I: Numerical results of Non Chaotic Solution for Lorenz system of equation when $x(t),y(t),z(t)$ for the fractional parameter $\zeta = 1$ that are compared among the two methods LHAM, HAM.

t	x(t)		y(t)		z(t)	
	LHAM	HAM	LHAM	HAM	LHAM	HAM
0	-15.8	-15.8	-17.48	-17.48	35.64	35.64
0.1	-6.1754	-6.1754	17.7329	17.7329	36.2734	36.2734
0.2	26.0584	26.0584	81.5131	81.5131	1.94479	1.94479
0.3	80.9014	80.9014	173.861	173.861	-67.3458	-67.3458
0.4	158.354	158.354	294.776	294.776	-171.598	-171.598
0.5	258.415	258.415	444.258	444.258	-310.813	-310.813
0.6	381.086	381.086	622.308	622.308	-484.99	-484.99
0.7	526.365	526.365	828.925	828.925	-694.128	-694.128
0.8	694.254	694.254	1064.11	1064.11	-938.229	-938.229
0.9	884.753	884.753	1327.86	1327.86	-1217.29	-1217.29
1	1097.86	1097.86	1620.18	1620.18	-1531.32	-1531.32

TABLE II: Numerical results of Non Chaotic Solution for Lorenz system of equation when $x(t),y(t),z(t)$ for the fractional parameter $\zeta = 0.98$ that are compared among the two methods LHAM, HAM.

t	x(t)		y(t)		z(t)	
	LHAM	HAM	LHAM	HAM	LHAM	HAM
0	10	10	0	0	10	10
0.1	12.112	12.805	7.67927	7.3261	14.8467	15.2658
0.2	38.4705	41.1666	2.53492	1.16086	34.2577	35.8881
0.3	88.1468	94.1153	-14.7983	-17.8402	67.7334	71.3427
0.4	160.717	171.207	-44.0691	-49.415	115.031	121.374
0.5	255.899	272.143	-85.1156	-93.3944	175.984	185.808
0.6	373.479	396.7	-137.819	-149.653	250.469	264.512
0.7	513.288	544.7	-202.084	-218.094	338.385	357.381
0.8	675.182	715.992	-277.834	-298.633	439.647	464.326
0.9	859.042	910.449	-365.003	-391.203	554.184	585.271
1	1064.76	1127.96	-463.533	-495.743	681.932	-1531.32

TABLE III: Numerical results of Non Chaotic Solution for Lorenz system of equation when $x(t),y(t),z(t)$ for the fractional parameter $\zeta = 0.96$ that are compared among the two methods LHAM, HAM.

t	x(t)		y(t)		z(t)	
	LHAM	HAM	LHAM	HAM	LHAM	HAM
0	10	10	0	0	10	10
0.1	15.295	14.0435	7.94651	7.17223	15.295	16.2133
0.2	35.5032	45.7982	2.40102	-0.529008	35.5032	38.9782
0.3	69.6115	103.203	-15.3279	-21.71	69.6115	77.1807
0.4	117.143	185.341	-44.7415	-55.8294	117.143	130.293
0.5	177.777	291.606	-85.5242	-102.543	177.777	197.961
0.6	251.276	421.549	-137.446	-161.598	251.276	279.92
0.7	337.448	574.81	-200.329	-232.799	337.448	375.958
0.8	436.136	751.095	-274.023	-315.982	436.136	485.899
0.9	547.203	950.15	-358.406	-411.012	547.203	609.594
1	670.532	1171.76	-453.369	-517.77	670.532	-1531.32

TABLE IV: Numerical results of Non Chaotic Solution for Lorenz system of equation when $x(t),y(t),z(t)$ for the fractional parameter $\zeta = 0.94$ that are compared among the two methods LHAM, HAM

t	x(t)		y(t)		z(t)	
	LHAM	HAM	LHAM	HAM	LHAM	HAM
0	10	10	0	0	10	10
0.1	12.9953	15.4907	8.20776	6.93477	15.7878	17.2969
0.2	41.7532	50.9384	2.22729	-2.45825	36.8311	42.3856
0.3	93.3793	113.064	-15.9186	-25.9604	71.5903	83.4944
0.4	166.644	200.452	-45.4889	-62.7352	119.363	139.808
0.5	260.751	312.181	-86.0223	-112.258	179.689	210.79
0.6	375.117	447.573	-137.188	-174.149	252.223	296.04
0.7	509.28	606.093	-198.727	-248.114	336.697	395.242
0.8	662.863	787.303	-270.433	-333.912	432.885	508.138
0.9	835.547	990.831	-352.129	-431.342	540.6	634.504
1	1027.06	1216.35	-443.664	-540.23	659.676	774.151

TABLE V: Numerical results of Chaotic Solution for Lorenz system of equation when $x(t),y(t),z(t)$ for the fractional parameter $\zeta = 1$ that are compared among the two methods LHAM, HAM.

t	x(t)		y(t)		z(t)	
	LHAM	HAM	LHAM	HAM	LHAM	HAM
0	-15.8	-15.8	-17.48	-17.48	35.64	35.64
0.1	-9.7304	-9.7304	10.6004	10.6004	41.8903	41.8903
0.2	11.8384	11.8384	67.2031	67.2031	24.4124	24.4124
0.3	48.9064	48.9064	152.328	152.328	-16.7937	-16.7937
0.4	101.474	101.474	265.976	265.976	-81.728	-81.728
0.5	169.54	169.54	408.145	408.145	-170.391	-170.391
0.6	253.106	253.106	578.838	578.838	-282.781	-282.781
0.7	352.17	352.17	778.052	778.052	-418.9	-418.9
0.8	466.734	466.734	1005.79	1005.79	-578.747	-578.747
0.9	596.798	596.798	1262.05	1262.05	-762.323	-762.323
1	742.36	742.36	1546.83	1546.83	-969.626	774.151

TABLE VI: Numerical results of Chaotic Solution for Lorenz system of equation when $x(t), y(t), z(t)$ for the fractional parameter $\zeta = 0.98$ that are compared among the two methods LHAM, HAM.

t	x(t)		y(t)		z(t)	
	LHAM	HAM	LHAM	HAM	LHAM	HAM
0	10	10	0	0	10	10
0.1	14.5384	15.364	9.75975	9.26264	17.2731	17.8248
0.2	47.9105	51.1228	1.51521	-0.418838	43.6977	45.8443
0.3	109.045	116.156	-23.8592	-28.1408	88.6316	93.3838
0.4	197.445	209.942	-66.0136	-73.5382	151.758	160.11
0.5	312.775	332.13	-124.722	-136.375	232.861	245.794
0.6	454.786	482.454	-199.819	-216.477	331.776	350.265
0.7	623.275	660.702	-291.171	-313.706	448.373	473.384
0.8	818.074	866.698	-398.671	-427.947	582.539	615.033
0.9	1039.04	1100.29	-522.226	-559.103	734.181	775.112
1	1286.04	1361.34	-661.754	-707.091	903.216	615.033

TABLE VII: Numerical results of Chaotic Solution for Lorenz system of equation when $x(t), y(t), z(t)$ for the fractional parameter $\zeta = 0.96$ that are compared among the two methods LHAM, HAM.

t	x(t)		y(t)		z(t)	
	LHAM	HAM	LHAM	HAM	LHAM	HAM
0	10	10	0	0	10	10
0.1	15.1429	16.9522	10.0782	8.98843	17.9128	19.1219
0.2	49.9584	56.8052	1.24451	-2.87955	45.4098	49.9851
0.3	112.265	127.178	-24.6996	-33.6825	91.1899	101.156
0.4	201.084	226.994	-67.0605	-82.6669	154.631	171.946
0.5	315.77	355.537	-125.398	-149.352	235.317	261.892
0.6	455.84	512.276	-199.392	-233.386	332.934	370.647
0.7	620.913	696.787	-288.79	-334.492	447.231	497.934
0.8	810.67	908.718	-393.387	-452.445	578.002	643.523
0.9	1024.84	1147.77	-513.008	-587.053	725.068	807.216
1	1263.2	1413.69	-647.503	-738.149	888.276	615.033

TABLE VIII: Numerical results of Chaotic Solution for Lorenz system of equation when $x(t), y(t), z(t)$ for the fractional parameter $\zeta = 0.94$ that are compared among the two methods LHAM, HAM.

t	x(t)		y(t)		z(t)	
	LHAM	HAM	LHAM	HAM	LHAM	HAM
0	10	10	0	0	10	10
0.1	15.8212	18.7946	10.3855	8.59375	18.6138	20.6007
0.2	52.155	63.099	0.915056	-5.67976	47.2329	54.5463
0.3	115.672	139.126	-25.6283	-39.762	93.8828	109.556
0.4	204.93	245.212	-68.2145	-92.4884	157.65	184.568
0.5	318.993	380.271	-126.201	-163.127	237.93	278.88
0.6	457.17	543.5	-199.125	-251.147	334.276	391.967
0.7	618.916	952.054	-286.626	-356.137	446.333	523.417
0.8	803.786	908.718	-388.414	-477.76	573.808	672.889
0.9	1011.4	1196.42	-504.241	-615.733	716.451	840.091
1	1241.43	1466.98	-633.898	-769.812	874.049	672.889

The observation from Tables I,II,III,IV,V,VI,VII,VIII show that the suggested approach has a high level of agreement with HAM This study shows that LHAM is a good mathematical tool for tackling fractional Laplace Homotopy Analysis Method problems. The above tables clearly shows the changes in the Non Chaotic and chaotic situations in Lorenz system of equation with the fractional parameter $\zeta = 1, 0.94, 0.96, 0.98$.

VI. CONCLUSION

In this present work continuous solution for fractional Lorenz system of equation is obtained by Fractional Laplace Homotopy Analysis Method Via Modified Riemann-Liouville Integral. This solutions are exactly coincide with the solution of A.K.Alomari et al [1].

REFERENCES

1. A.K. Alomari A new analytic solution for fractional chaotic dynamical systems using the differential transform method (2011).
2. Alomari, M.S.M., Noorani, R., Nazar, C.P., Li, C.P., Homotopy analysis method for solving fractional Lorenz system, *Commun Nonlinear Sci Numer Simulat* (2009).
3. Bagyalakshmi, M., Sai Sundara Krishnan, G., Tarig Projected Differential Transform Method to solve Fractional Non linear Partial Differential Equations, *Boletim da Sociedade Paranaense de Mathematica*, (2018).
4. B.K. Dutta and L.K. Arora, Fractional Elzki's Transform, PhD thesis, North Regional Institute of Science and Technology, Nirijuli-791109, Arunachal Pradesh, (2014).
5. Fernando S. Silva, Davidson M. Moreira and Marcclo A. Moret, Conformable Laplace Transform of Fractional Differential Equation, (2018).
6. Guy Jumarie Laplace's transform of fractional order via the Mittag Leffler function and modified RiemannLiouville derivative, *Applied Mathematics Letters* (2009).
7. Guy Jumarie, Table of some basic fractional calculus formulae derived from a modified Riemann-Liouville derivative for non-differentiable functions, *Applied Mathematics Letters*, (2008).
8. G. Hariharan, A. Homotopy analysis method for the nonlinear partial differential equation arising in engineering, *International journal for Computational Methods in Engineering Science and mechanics*, (2017).
9. Gustavo D. Medina, Nelson R. Ojeda, Jose H. Pereira and Lui G. Romero, Fractional Laplace Transform and Fractional Calculus, *International Mathematical Forum*, (2008).
10. Lorenz, E.: Deterministic nonperiodic flow. *J. Atmosph. Sci.* 20, 130 (1963)
11. M. Mossa Al-sawlha, M.S.M. Noorani On Solving the Lorenz System by Differential Transformation Method, (2008).
12. M.S.H. Chowdhury, I. Hahim, S. Momani The multistage homotopy-perturbation method- A powerful scheme for handling the Lorenz system, (2007).
13. Song Liang, Ranchao Wu, Liping Chen, Laplace Transform of Fractional Order Differential Equation, *Electronic Of Differential Equation*, (2015).
14. Zaid M. Odibat, Cyrille Bertelle, M.A. Aziz-Alaoui, Gerard H.E. Duchamp A multi-step differential transform method and application to non-chaotic or chaotic systems (2009).

Mahalanobis-Taguchi System for Simultaneous Feature Extraction and Prediction for Cancer Diagnosis

Aneetha A. S and Priya R

Department of Applied Mathematics & Computational Sciences, PSG College of Technology, Coimbatore, India

ABSTRACT

The Mahalanobis Taguchi system is a diagnosis and forecasting technique for analyzing multivariate data by combining Mahalanobis distance and Taguchi's robust engineering. The Mahalanobis distance is a statistical method for determining the similarities between normal and abnormal observations. Taguchi's orthogonal array and signal to noise ratio is powerful in selecting significant features from the dataset. In this paper, Mahalanobis Taguchi system is adopted to analyze the reoccurrence of breast cancer after treatment. A dataset from the UCI machine learning repository is utilized for this purpose. This is accomplished through the use of a dataset from the UCI machine learning repository. The suggested system comprises of a preprocessing phase to translate categorical features into numeric values, followed by the construction and validation of the Mahalanobis space using Mahalanobis distance, and finally the Taguchi method to find the relevant features. The diagnosis and forecasting model are built using the above-mentioned features. The performance of the system is validated using k-fold technique, and prediction is made using central limit theorem.

Keywords: Mahalanobis Distance, Orthogonal Array, Signal – to – Noise ratio, Breast Cancer, Prediction, Forecasting, Central limit theorem

1. INTRODUCTION

Medical diagnostics categorization can successfully aid physicians in disease diagnosis and forecast treatment outcomes in the realm of health care (Zhu et al., 2018). In medical diagnostics, efforts have been undertaken to enhance the efficacy of early detection and predicting. According to global statistics, breast cancer is one of the most prevalent diseases among women globally, accounting for the majority of new cancer cases and cancer-related deaths, making it a serious public health concern in today's society. Breast cancer accounts for around 12% among all newly diagnosed cancers in women and 25% over all cancers. (Hiba Asri et al. / Procedia Computer Science 83 (2016) 1064 – 1069)

Since the past decade, many researches analyze and forecast the diseases that contribute to the society, especially on women health. For the early detection of breast cancer, various data mining approaches and machine learning models have been used. Simple data mining techniques like decision trees, K-Nearest Neighbor, and Bayesian networks focus on the model's features. However, the relation that exists between such features is not given importance. A few have combined the data mining techniques with feature selection algorithms or optimization techniques to perform feature selection for enhanced predictive accuracy. Both relevant feature selection and prediction are performed via the Mahalanobis-Taguchi System (MTS).

The MTS is a diagnostic and prediction technology that was developed for analysing and detecting efficient features in multivariate data without making any statistical distribution assumptions. Genich Taguchi developed it by combining Mahalanobis Distance (MD) with Taguchi's robust engineering. MD is used to build a multidimensional measure scale and define the Mahalanobis space (MS) using the normal profile, which serves as the scale's reference point. MD is calculated for the abnormal profiles based on the reference point, which validates the MS. Taguchi's robust engineering technique selects the features that significantly contribute to the analysis and prediction. To identify the essential qualities, Taguchi's approach employs Orthogonal Arrays (OAs) and Signal-to-Noise Ratios (SNR). The prediction model is developed with the features selected using MD values and central limit theorem is utilized for threshold calculation. MTS is used for predicting the possibility of reoccurrence of breast cancer after the treatment of the disease.

The second section of the paper gives a few broad ideas on the literatures related to analysing breast cancer dataset and the applications of MTS in forecasting and prediction. The third section gives the detailed description of the method and the dataset description while the fourth section gives the experimental results and its analysis. The last section concludes the results obtained and its future scope.

2. RELATED LITERATURES

This section briefly explains literatures pertaining to the prediction and forecasting approaches for breast cancer diagnosis, and Mahalanobis – Taguchi System. Hans-Olov Adami et. al (1985) started their analysis on the

relation between age and relative survival of women with breast cancer in Sweden. Rinal Doshi et al. (2014) predicted reoccurrence of breast cancer using four different clustering algorithms. Two out of these, namely k-means and farthest first algorithms were found to be efficient for this prediction. They also found that hierarchical cluster method gives a high error rate. Hiba Asri et al. (2016) used machine learning techniques to create four distinct models based on the Wisconsin Breast Cancer (original) datasets: C4.5, NB, SVM and KNN. They examined the performance of the aforementioned four models based on accuracy, precision, sensitivity, and specificity, and reported that SVM is effective in predicting and diagnosing breast cancer.

In a research on the MTS, Chao-Ton Su (2017) found that the development of an MTS model is unaffected by data distribution, which aids in the resolution of class imbalance difficulties such as having limited medical diagnosis data for chronic diseases. Mahmoud EI- Banna(2017) proposed modified Mahalanobis Taguchi system for binary classification approach using nonlinear optimization model. Its objective was to minimize the Euclidean distance between MTS classifier ROC curve and the theoretical optimal point. Based on the above literatures, an attempt is made in this research work to forecast and predict the reoccurrence of breast cancer.

3. PROPOSED SYSTEM

3.1 Mahalanobis-Taguchi System (MTS)

MTS is a popular data classification approach that uses pattern recognition. It is a hybrid of MD and Taguchi techniques. MD is a generalised distance that is being used to determine the resemblances among unknown and known sample datasets by determining the distance in multidimensional spaces and accounting for any features or variables that may exist. Furthermore, the Taguchi technique is used to enhance the system and examine the contribution of each feature, lowering dimensionality by removing features that do not bring value to the study and making it more resilient. The general architecture of MTS begins with the construction of Mahalanobis Space (MS) using normal records, followed by the validation of MS using abnormal records, the discovery of parameters using orthogonal arrays and signal to noise ratio, and finally the identification and decision-making phase.

A. Construction of Mahalanobis space:

Consider a dataset having an 'n' normal samples and 'm' abnormal samples with 'k' features. MS is constructed by standardizing the normal samples of the dataset, and then calculating the MD values. The data mean (x_i) and standard deviation (S_i) for each feature (i) is calculated using the formula given below.

$$x_i = \frac{\sum_{j=1}^n x_{ij}}{n} \quad \text{and} \quad S_i = \frac{\sqrt{\sum_{j=1}^n (x_{ij} - x_i)^2}}{n-1}$$

Standardization of normal samples Z_{ij} is calculated using

$$Z_{ij} = \frac{(X_{ij} - x_i)}{S_i}$$

where, x_i represents the mean of the i^{th} feature, S_i represents the standard deviation of i^{th} feature, X_{ij} represents the values in the i^{th} record and j^{th} features. After normalizing, the MD value is calculated for all the normal samples using equation

$$MD_j = \frac{1}{k} ([Z_1, Z_2, Z_k] [C^{-1}] [Z_1, Z_2, \dots, Z_k]^T)$$

where, k represents the number of features, C^{-1} represents the inverse of covariance matrix, $Z_j = (Z_{1j}, Z_{2j}, \dots, Z_{kj})$, j ranges from 1 to n . To calculate MD, we need to find inverse of Covariance i^{th} matrix, C

$$C = [c_{ij}]$$
$$c_{ij} = \frac{\sum_{l=1}^n Z_{il} \cdot Z_{jl}}{n}$$

B. Validation of Mahalanobis space:

For validating the MS, records outside the normal MS, abnormal records, are considered to assess if the identified feature set are appropriate for model construction. Consider a set of 'm' abnormal samples with 'k' features. MD_j is computed after each abnormal sample is normalised using the mean and standard deviation of normal samples. The mean of MD_j of both normal and abnormal samples is compared. The average of MD_j of

abnormal samples is greater than MD_j of normal samples, then the measurement scale is identified to be “good”, otherwise repeat the above process with a new set of normal samples.

C. Identification of useful features

On successfully obtaining a “good” measurement scale, Taguchi design is employed to identify features relevant for model development. Orthogonal Array (OA) and Signal-to-Noise (S/N) ratio tools are used for this purpose. An OA is a 2D array in which the columns represent features and the rows reflect the combination of those characteristics (runs). The main objective of OA is to check whether the columns are independent of one another. The existence of corresponding features is represented by Level 1 in the OA, whereas the absence of corresponding features is represented by Level 2. The number of characteristics and levels that OA can accept, determines its size. The general representation of the OA is L_n(2ⁿ⁻¹), here n represents no. of runs (rows) where n values should be in multiples of 4, and n-1 represents no. of columns. For instance, if k contains 13 features, value of n is set as 16 runs (rows), since no. of columns are greater than feature set, it is eliminated. The SN ratio is a metric for measuring the precision of a measurement scale. The higher the S/N ratio, the better, as per MTS.

In OA, for first run, consider the features with value as 1 in first row and calculate the MD for the abnormal records. For second run, calculate the MD value by considering the features with value as 1 in second rows. Similarly, for nth run, calculate the MD value for the abnormal records by considering the features with value as 1 in nth row. The resultant for the OA will be an n*k matrix with n representing total no. of runs and k representing total no. of abnormal records. Calculate S/N ratio for each run using

$$S/N = -10 * \log \left(\frac{1}{t} \left(\sum_{i=1}^t \frac{1}{MD_i} \right) \right)$$

where t is the number of abnormal samples. Calculating the gain with S/N ratios identifies the essential features. Each feature's gain is calculated using the following formula:

$$\text{gain} = S/N^{\text{level1}} - S/N^{\text{level2}}$$

where S/N^{level1} is the average of S/N ratio having value as 1 in corresponding column indicating that the feature is included and S/N^{level2} is the average of S/N ratio having value as 2 in corresponding column indicating that the feature is excluded. If a feature's gain value is positive, it is deemed appropriate in medical diagnosis; otherwise, it is removed during model construction.

3.2 Diagnosis Model Construction

After identifying the relevant feature based on gain value, the diagnosis and forecasting model is developed based on those selected features of both normal and abnormal samples. The model is developed using MD values of normal samples with the selected feature. The records in 'n' normal samples and 'm' abnormal samples after removing unnecessary features are considered.

Using 'n' normal samples, calculate new MD values for normal and abnormal samples based on new mean, standard deviation, and covariance matrix. Since, the model has been constructed by k-Fold Cross-Validation technique in order to eliminate the disparity among records. The dataset is divided into training data to develop the model and test data to evaluate the model. In k-fold methods, for training data, collect the (k-1)/kth of normal samples from original dataset and calculate mean, standard deviation and covariance matrix for those normal samples. Calculate the MD value for each observation. The model developed with (k-1)/kth training samples is evaluated using 1/kth test sample. The process is repeated for k times and average is taken as overall system performs. The new reduced measurement scale is established using the identified relevant features.

3.3 THRESHOLD

The Threshold is calculated using the method of central tendency, using the formula $\mu \pm \sigma * \alpha$, where μ is the mean and σ is the standard deviation of the MD values of normal samples, α is considered as level of significance which ranges from -3 to +3. MD values are generated for any unknown samples using the mean, standard deviation, and covariance matrix of normal known samples. The new MD value of the unknown sample is in the threshold range then the decision is made that unknown sample is normal otherwise it is considered as abnormal.

4. EXPERIMENT ANALYSIS AND DISCUSSIONS

This section includes the features of the breast cancer dataset are described first, followed by a discussion of the MTS results.

4.1 Data Source:

The Breast Cancer dataset was taken from UCI machine learning repository, consists of 9 features and 286 samples with a class label. In 286 samples, 201 normal samples, records corresponding to non-reoccurrence of breast cancer after treatment, and 85 abnormal samples, records corresponding to reoccurrence of breast cancer after treatment. The features age, tumor size, Inv-nodes contain numeric values and remaining six features have categorical values and a binary class, whether there is possibility of reoccurrence or non - reoccurrence. The nine features are explained in detail and their possible values are also given in table below. The preprocessing is carried out by assigning numerical equivalence for the categorical values for developing the MTS model for diagnosis and forecasting.

Table: 1 Dataset Description

Features	Feature Description
Age	The patient's age at the time of diagnosis. (a numerical value)
Menopause	Whether the patient is in the pre-menopausal or post-menopausal stage at the time of diagnosis (categorical value)
Tumor size	The tumor's largest diameter after it has been removed (numeric value)
Inv-nodes	The number of auxiliary lymph nodes found to have metastatic breast cancer on histological evaluation (numeric value)
Node-caps	The tumour may replace the lymph node before penetrating the capsule and invading the surrounding tissues. (Yes/No)
Degree of malignancy	The tumor's histological grade (range 1-3). (1,2,3)
Breast	Breast cancer can arise in either breast. (Left and right)
Breast quadrant	The breast can be divided into four quadrants. (left upper, left lower, right upper, right lower, center)
Irradiation	Radiation therapy is a cancer treatment that uses high-energy rays to kill cancer cells (yes, no)
Class	Reoccurrence (abnormal) and non-reoccurrence (normal) of condition after treatment.

4.2 RESULTS AND DISCUSSIONS:

The construction of MS is constructed based on the history of medical test report after performing preprocessing. Initially, the mean and standard deviation of the 201 normal samples is calculated. The calculated mean and standard deviation for each feature is given in Table

Table: 2 Mean and SD for Normal Samples

Features	1	2	3	4	5	6	7	8	9
Mean	4.711	1.483	5.637	0.319	0.128	1.905	0.512	1.179	0.1841
SD	0.998	0.549	2.210	0.876	0.334	0.697	0.501	1.244	0.3885

After standardization, verify the samples to have their mean and standard deviation is 0 and 1 respectively. If the samples are standardized then they are used to calculate covariance matrix and then MD values. The MD values of the normal samples are presented in Table along with average of MD value

Table: 3 MDs for Normal Samples

Features	1	2	3	4	200	201	Average
MD	1.0609	1.8519	1.0397	0.7914	0.559	0.893	1.000

The 85 abnormal samples used in MS validation will be standardized using the mean and standard deviation of the normal samples, and MD values will be generated using the normal samples' covariance matrix. The MD values of the abnormal samples are given in Table below along with its average MD value

Table: 4 MDs for Abnormal Samples

Features	1	2	3	85	Average
MD	2.9906	0.8121	2.5836	2.6301	2.8358

The average MD value for abnormal samples is 2.8358. Since the MDs of abnormal have higher distances than the normal which is 1.000. The constructed measurement scale is considered as a “good” scale, means efficient records are selected in this validation step.

Identification of relevant Features is carried in order to identify useful set of features using OA's and SN ratios. Since there are 9 features, we required a two-level OA, L₁₂(2¹¹) array is selected. L₁₂(2¹¹) means two-level array with 12 combinations (runs) and 11 columns. The 9 features are allocated to first 9 columns in this array others are eliminated. The MD will be computed for all the 12 runs. For all 12 runs, larger-the-better SN ratios are computed. For abnormal MDs, the SN ratio will be determined. The Level 1 and Level 2 values for each feature should be determined using the calculated SN ratio. For Column 1, Level 1 will be calculated by adding all the SN ratio values whose features are included and Level 2 will be calculated by adding all the SN ratio values whose features are excluded. The sample OA table and gain for the features are given below

Table: 5 Orthogonal Array with SN ratio and gain

	F1	F2	F3	F4	F5	F6	F7	F8	F9
SN+	-0.801	2.142	-0.276	0.134	-0.668	-0.222	0.571	-0.722	-0.089
SN-	-0.228	-2.164	-0.759	-1.095	-0.376	-0.806	-1.398	-0.014	-0.920
Gain	-0.573	4.305	0.483	1.229	-0.292	0.584	1.970	-0.708	0.831

The gain value for the features “Age, Node-caps and Breast quad” has negative values. So, we can eliminate those features from the original dataset and the efficient features are considered for model development.

The Diagnosis model is constructed using K-fold cross-validation technique with relevant 6 features. The original sample is randomly partitioned into k equal size subsamples, in this work, k is kept as 5 and in each of the 5 folds 4/5th samples were used for training data and 1/5th samples were used for test data. Calculate the covariance matrix to calculate the MD values for normal samples and abnormal samples by taking inverse of covariance matrix of normal samples. The threshold range is calculated using the central limit theorem which utilizes the mean and standard deviations of the MD values of normal samples. Calculate the MD values for test data which contains 1/5th of normal samples and 1/5th of abnormal samples. MD values of the test data are compared with the threshold range, if MD value lies in the range then they are correctly classified as normal (non- recurrence) otherwise consider as misclassified. Based on the test data the system performance is evaluated using accuracy, specificity and sensitivity. The results obtained in each fold for all the metrics are given the figure 1.

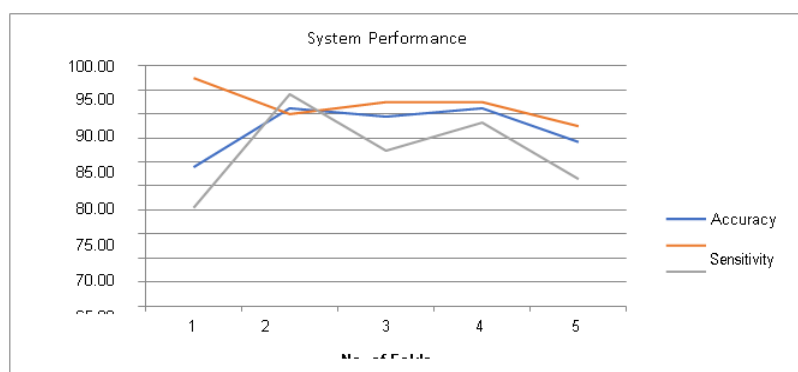


Figure 1: Performance Metrics for Breast Cancer Dataset

From the figure 1 it is shown that the second fold is able to produced better results when compared of other four sets. The comparison is based on three performance indicators: accuracy, specificity, and sensitivity. The proposed technique's accuracy is 91.23 %, its sensitivity is %, and its specificity performance is 94.12 %, which is higher than existing techniques

5. CONCLUSION

In this paper, the proposed Mahalanobis - Taguchi system for simultaneous feature extraction and prediction has been developed for combining both selecting relevant features and also the predicting the normal and abnormalities. The MTS model was tested using a benchmark breast cancer dataset to predict breast cancer recurrence after treatment. The proposed model is able to perform better with the results obtained on the evaluation metrics are accuracy is 91.23%, sensitivity is 90% and specificity is 94.12% respectively. In future work, we aim at employing this proposed model for predicting all types of medical diagnosis, which has binary classification.

REFERENCES

1. Adami, H. O., Malker, B., Holmberg, L., Persson, I., & Stone, B. (1986). The relation between survival and age at diagnosis in breast cancer. *New England Journal of Medicine*, 315(9), 559-563.
2. Aljawad, D. A., Alqahtani, E., Ghaidaa, A. K., Qamhan, N., Alghamdi, N., Alrashed, S., ... & Olatunji, S. O. (2017, February). Breast cancer surgery survivability prediction using bayesian network and support vector machines. In 2017 International Conference on Informatics, Health & Technology (ICIHT) (pp. 1-6). IEEE.
3. Avalappampatty Sivasamy, A., & Sundan, B. (2015). A dynamic intrusion detection system based on multivariate Hotelling's T2 statistics approach for network environments. *The Scientific World Journal*, 2015.
4. Buenviaje, B., Bischoff, J. E., Roncace, R. A., & Willy, C. J. (2015). Mahalanobis– Taguchi system to identify preindicators of delirium in the ICU. *IEEE journal of biomedical and health informatics*, 20(4), 1205-1212.
5. Chang, Z. P., Li, Y. W., & Fatima, N. (2019). A theoretical survey on Mahalanobis- Taguchi system. *Measurement*, 136, 501-510.
6. Daniels, B., Corns, S. M., & Cudney, E. A. (2012, May). Introduction of R-LCS and comparative analysis with FSC and mahalanobis-taguchi method for breast cancer classification. In 2012 IEEE Symposium on Computational Intelligence in Bioinformatics and Computational Biology (CIBCB) (pp. 283-289). IEEE.
7. El-Banna, M. (2017). Modified Mahalanobis Taguchi system for imbalance data classification. *Computational intelligence and neuroscience*, 2017.
8. Gan, D., Shen, J., An, B., Xu, M., & Liu, N. (2020). Integrating TANBN with cost sensitive classification algorithm for imbalanced data in medical diagnosis. *Computers & Industrial Engineering*, 140, 106266.
9. Haldar, N. A. H., Khan, F. A., Ali, A., & Abbas, H. (2017). Arrhythmia classification using Mahalanobis distance based improved Fuzzy C-Means clustering for mobile health monitoring systems. *Neurocomputing*, 220, 221-235.
10. Joshi, J., Doshi, R., & Patel, J. (2014). Diagnosis of breast cancer using clustering data mining approach. *International Journal of Computer Applications*, 101(10), 13-17.
11. Kharya, S. (2012). Using data mining techniques for diagnosis and prognosis of cancer disease. arXiv preprint arXiv:1205.1923.
12. Muhamad, W. Z. A. W., Jamaludin, K. R., Saad, S. A., Yahya, Z. R., & Zakaria, S. A. (2018, June). Random binary search algorithm based feature selection in mahalanobis taguchi system for breast cancer diagnosis. In AIP Conference Proceedings (Vol. 1974, No. 1, p. 020027). AIP Publishing LLC.
13. Padmapriya, B., & Velmurugan, T. (2014, December). A survey on breast cancer analysis using data mining techniques. In 2014 IEEE International Conference on Computational Intelligence and Computing Research (pp. 1-4). IEEE.
14. Pal, A., & Maiti, J. (2010). Development of a hybrid methodology for dimensionality reduction in Mahalanobis–Taguchi system using Mahalanobis distance and binary particle swarm optimization. *Expert Systems with Applications*, 37(2), 1286-1293.
15. Sarvestani, A. S., Safavi, A. A., Parandeh, N. M., & Salehi, M. (2010, October). Predicting breast cancer survivability using data mining techniques. In 2010 2nd International Conference on Software Technology and Engineering (Vol. 2, pp. V2- 227). IEEE.
16. Su, C. T. (2017). Mahalanobis-Taguchi system and its medical applications. *Neuropsychiatry*, 7(4), 316-320.
17. Su, C. T., & Hsiao, Y. H. (2008). Multiclass MTS for simultaneous feature selection and classification. *IEEE Transactions on Knowledge and Data Engineering*, 21(2), 192- 205.
18. Su, C. T., & Hsiao, Y. H. (2008). Multiclass MTS for simultaneous feature selection and classification. *IEEE Transactions on Knowledge and Data Engineering*, 21(2), 192- 205.
19. Taguchi, G., & Jugulum, R. (2002). *The Mahalanobis-Taguchi strategy: A pattern technology system*. John Wiley & Sons.

20. Wang, N., Zhang, Z., Zhao, J., & Hu, D. (2019). Recognition method of equipment state with the FLDA based Mahalanobis–Taguchi system. *Annals of Operations Research*, 1-19.
21. Xiao, X., Fu, D., Shi, Y., & Wen, J. (2020). Optimized Mahalanobis–Taguchi System for High-Dimensional Small Sample Data Classification. *Computational Intelligence and Neuroscience*, 2020.
22. Yue, W., Wang, Z., Chen, H., Payne, A., & Liu, X. (2018). Machine learning with applications in breast cancer diagnosis and prognosis. *Designs*, 2(2), 13.

Automated Detection of the Severity of Diabetic Retinopathy Using Pre-Trained Cnnnts

R. Vidhyapriya and N. Ravitharajalakshmi

Department of Biomedical Engineering, PSG College of Technology, Coimbatore, India

ABSTRACT

Recently Deep Learning framework has been employed in various fields to aid in the development of automated systems. Medical field require the help of machine intelligence for diagnosis of various diseases and drug discovery. An eye condition caused by long-term diabetes is diabetic retinopathy. Diabetes destroys the small blood vessels inside the retina, the light-sensitive tissue at the back of the eye, causing it to bleed. This study focuses on extracting features from DR pictures and using them to train Multi-class SVM for classification using famous CNN models dubbed Alex-Net that were successful in the IMAGENET competition (ILSVRC). The model is evaluated using a Kaggle dataset with a large heterogeneous DR Dataset.

Keywords - Alex-net; Convolutional Neural Network (CNN); Diabetic Retinopathy.

1 INTRODUCTION

Diabetes is a disease that occurs due to the inadequate secretion of insulin; which is essential in balancing the blood sugar level. Diabetes may damage the entire circulatory system, including the retinal portion of the eye, resulting in Diabetic Retinopathy if it is not treated early (DR). The blood vessels in the retina are permanently damaged by DR. According to the fact sheet published by World Health Organization (WHO), about 15% of the population are affected by DR. Earlier clinical diagnosis method include screening of retinal images acquired through fundus camera by ophthalmologist. Due to the increasing prevalence of the disease, there is a growing need for scientific tool to assist in the diagnosis of DR at an earlier stage and also to assess the severity of the disease in progressive stages.

The automated diagnosis was traditionally modeled as a classification problem (i.e.) categorizing the images based on the features that could better characterize the classes to which an image belongs to. Previous techniques retrieve hand crafted features for representing an image which requires domain knowledge. The process of feature extraction is found to be time -consuming in the entire classification pipeline. Recently, Convolutional Neural Network (CNN) is being heavily used in the field of image processing to classify images. CNN is different from the fully connected neural networks like Multilayer perceptron by sharing the weights between the neurons to exploit the local connectivity of a pixel. But, training a CNN is a CPU intensive process as it requires a large number of convolution operations to be carried out between the filters and images. Hence, the work used weights of pre-trained CNN to learn the abstract features of the DR image and SVM for classification. The AlexNet CNN model is utilized in this study. In the model of AlexNet, the number of layers that are connected fully is three and the pooling layers are available and additionally it has a Softmax layer. As features, the output of the last completely linked layer is utilized. Section II provides a broad survey of the previous works in the field of automated diagnosis. Section III presents an overview of the Image dataset used for the work and also outlines the preprocessing steps employed to glean the images. Section IV provides a brief description on the Alex-Net architecture, its layers and connectivity. Section V outlines the working of Multi-class SVM and evaluation metrics for assessing the performance of the technique. Section VI presents the conclusion and future work

2 LITERATURE SURVEY

This section lists few works in the domain of medical image analysis which has used CNN for feature extraction, image classification and segmentation. CNN, when used for classification predicts the class label for entire image. For segmentation, it predicts a value for each pixel; based on whether it corresponds to the region of interest. Alban et al [1] used a convolutional neural network to develop a supervised technique for blood vessel segmentation in diabetic retinopathy pictures. The Random Forest classifier is then used to determine the severity of the DR illness using the segmented blood vessels. Extensive testing is done on the DRIVE and STARE public retinal imaging databases. Though blood vessels represent severity, there are additional abstract characteristics such as lesions and blood clots that might help in correct picture categorization.

Hu et al. [4] suggested using deep convolutional neural networks to directly categorize hyper-spectral pictures in the spectral domain. Hyper-spectral pictures are created by taking several photos of an item at various frequencies. So that the objects complete characteristic may be retrieved. This method is very popular in the

remote sensing application as certain features of interest could be visible or highly available only under specific frequency. Convolution, pooling, fully linked, and output layers make up the suggested architecture. Cao et al. [3] offered a domain-specific introduction to diabetic retinopathy pictures and disease phases. They devised an algorithm for exudate extraction since the presence of exudates is a key indicator of diabetic macular edema. The programme was evaluated on a small picture library and compared to a human grader's performance. The identification of exudates and their usage in categorization resulted in a 92.8 percent mean sensitivity and a 92.4 percent mean predictive value

The National Eye Institute has outlined a standardized description for each of the severity class in the DR image. There are four severity scales, the first three scribes

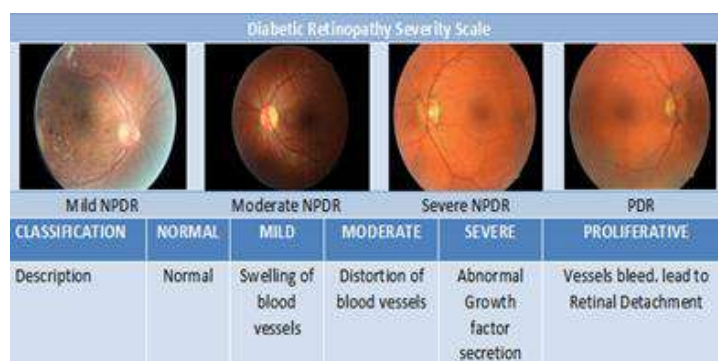


Figure1:Severity of Diabetic Retinopathy Images

Describes non-proliferative DR (NPDR) and the last one describes proliferative DR (PDR). The severity scales are then characterized through a progression of four stages as illustrated in Figure 1.

3 DATASET

3.1 Overview

This research makes use of a dataset kept by EyePacs and made available through Kaggle[8] under an open license. It consists of high-resolution retina pictures collected under various imaging settings (i.e., the images are of varying resolution and captured with various cameras, affecting the image's visual appearance). [6]

<Subjectid left/right> is the label for the pictures. A physician labels the entire dataset with a value between 0 and 4 based on the severity of the image according to the following scale.

0 -indicates that there is no DR.

2 -Indicates that it is Reasonable

3 -Identifies as critical

4 - Proliferative DR

3.2 PREPROCESSING

The images are downsized to 256 * 256 in order to input the image to the network. As the images are heterogeneous in nature, background elimination and contrast adjustment are done. The edges are detected using sobel operators. It identifies the edges based on the derivative of the pixel with respective to the neighboring pixels. The output of the preprocessing module is shown below.

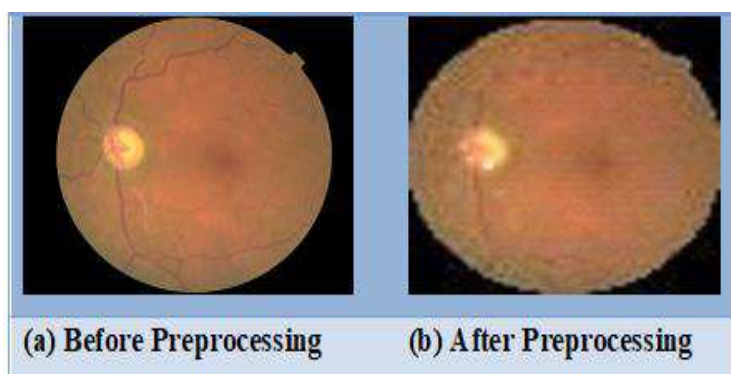


Figure 2: Preprocessed Images

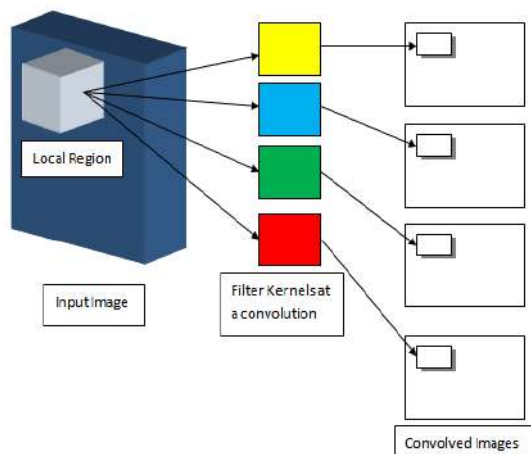


Figure 3: Convolutional Neural network Architecture

4. CONVOLUTIONAL NEURAL NETWORK

In the field of image processing, convolution is a crucial procedure. To detect edges and contours in a given picture, filter kernels are convolved with the input image. The model predicts the weights associated with the filter kernels in a convolutional neural network to extract the best representative features in the pictures. [7]

4.1 ALEXNET

In this work, the CNN model used for feature extraction is AlexNet[5]. The Network architecture was successful in one of the world's difficult image recognition challenge. This model convolves the image through series of filters and is down sampled through pooling layers. There are many such layers of convolution as the input passes through. Convolution layer learns series of kernels to extract abstract features in it. The various layers of AlexNet are shown in the Figure 4. The advantage of the convolution layer includes weight sharing between the neurons and its capability to preserve the local connectivity of the pixels.

The input was convolved through all of the convolution and fully connected layers of the network using the pre-trained weights of AlexNet shared through caffe models. The input image is represented by the output of the final fully linked layer, which has 4096 neurons. The Obtained input vectors are then subjected to multi-class SVM for the task of classification.

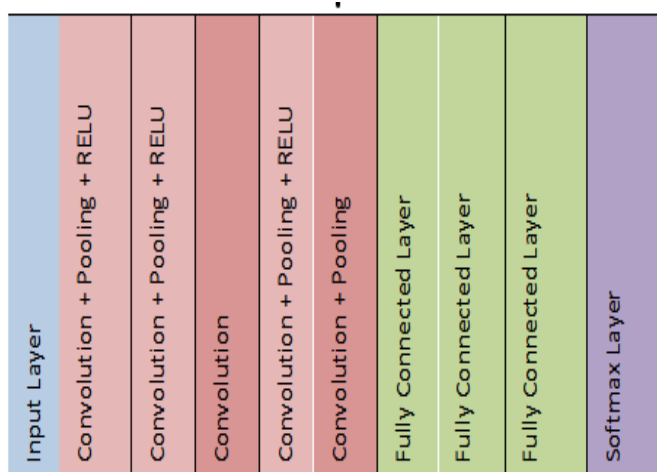


Figure 4 Layers in Alex Net Architecture

5. MULTI-CLASS SVM

A supervised learning approach that is normally used to classify and predict data is the support vector machine. It's a two-class classifier that creates an n-dimensional hyper-plane to distinguish two classes' patterns. The created hyper-plane is used as a template for classifying new patterns. The SVM can be extended to work with multiple classes using two approaches: One Vs One and One Vs Rest. In this work, one vs. rest approach is used. It models the m-class problem as m-binary problems where each classifier constructs a hyper-plane to separate patterns of one class against the others [2]. In the decision phase, a pattern is associated with the class depending on the classifier which provides a positive score.

5.1. EVALUATION METRICS

Table 1: Sample Distribution in Each Class

Classes	Number of Samples (In %)
0	30
1	20
2	10
3	20
4	20

The model is assessed using the Hold-out technique, which uses two-thirds of the dataset for training and one-third for validation. The accuracy metric is used for evaluation. The following equations are used to determine the model's accuracy:

$$\text{Accuracy} = \frac{\text{Number of correctly classified patterns}}{\text{Total Number of patterns}}$$

The model under consideration has an accuracy of 80%. The model cannot be fine-tuned further since the dataset contains sparse vectors. As a result, Principal Component Analysis is employed to minimize the dimensionality of feature vectors, and the best linear combination of features is selected to describe the patterns. The grid search method is used to identify the number of primary components that might be utilized to better describe the feature vector. Figure 6 depicts the accuracy attained for various numbers of main components. When more than 40 components are examined, the model works effectively. Hence PCA derived vectors containing 40 features are utilized for classification.

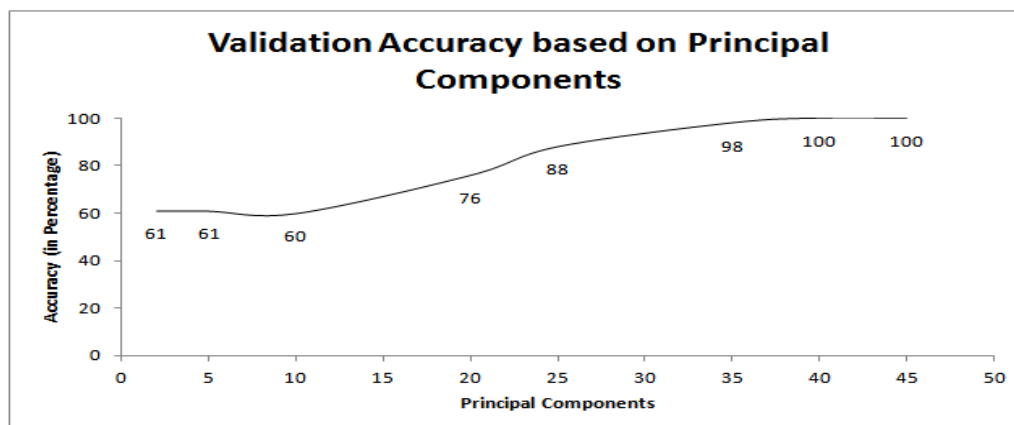


Figure 6: Validation accuracy based on principal component analysis.

6 CONCLUSION

In this work, the cross-domain pre-trained Convolution Neural Network (CNN) model called Alex-net is used as feature extractor for representing the medical diabetic retinopathy images. The extracted features are then used for assessing the severity of the disease using Multi-class SVM. The performance of the classifier is about 92%. The features are extracted from fully connected layer of Alex Net model. The work can be extended by considering the extraction of features from different convolution layers and find its effectiveness in representing the images.

REFERENCES

1. Marco Alban, Tanner Gilligan "Automated Detection of Diabetic Retinopathy using Fluorescein Angiography Photographs" Stanford University, 2016.
2. Wei Hu, Yangyu Huang, Li Wei, Fan Zhang, and Hengchao Li "Deep Convolutional Neural Networks for Hyperspectral Image Classification" Journal of Sensors, Article ID 258619, 12 pages, 2015.
3. G. Cao B. Wei Y. Zheng G. Yang S. Yang, Y. Yin. "Hierarchical retinal blood vessel segmentation based on feature and ensemble learning". Journal on Neurocomputing Volume 149 Pages 708-717, 2015
4. Bhat P. S. Acharya U. R. Lim C. M. Nayak, J. and M Kagathi. "Automated identification of different stages of diabetic retinopathy using digital fundus images" Journal of Medical Systems, Volume 32, Issue 2, pages 107-15. 2008

5. Alex Krizhevsky, Geoffery E Hinton, "ImageNet classification with deep convolutional neural networks", Proceedings of the 25th International Conference on Neural Information Processing Systems, Pages 1097-1105, 2015
6. K. Ng J. Suri O. Faust, R. Acharya. "Algorithms for the automated detection of diabetic retinopathy using digital fundus images": Springer Science, Journal of Medical Systems, Volume 36 pp 145-157, 2012
7. P. Massin A. Erginay T. Walter, J. Klein. "A contribution of image processing to the diagnosis of diabetic retinopathy detection of exudates in color fundus images of the human retina" IEEE transactions on Medical Imaging Volume 21, Issue 10, 2002.
8. <https://www.kaggle.com/c/diabetic-retinopathy-detection>.

Covid Detection from Chest X-Ray Using Cnn

Ajith Sam Raj S, Hari Ram R and Dr. B. Kalpana

Department of Computer Applications PSG College of Technology, India

ABSTRACT

With the breakout of COVID-19, the entire world has been stunned. COVID can be detected by RT-PCR tests, antigen tests, and other methods. However, only medical imaging, such as a chest X-ray or computerized tomography, can determine the extent of infection (CT-Scan). Deep learning approaches for analyzing and understanding medical imaging will aid in the detection of COVID on time. However, most extant studies suffer some obstacles, including a small dataset, insufficient generalizability, and other restrictions. To address these issues, A CNN-based Chest X-Ray image categorization technique is proposed in this research. The proposed model aids in the detection of COVID, Pneumonia, and a healthy individual. On the training data set, the model was 96 percent accurate, and on the validation data set, it was 93 percent accurate. The results reveal that the suggested model outperforms comparative models in terms of prediction, accuracy, and sensitivity, demonstrating its utility in computer-assisted diagnosis.

Keywords: Deep Learning, CNN, COVID, Chest X-Ray.

INTRODUCTION

The Novel CoronaVirus (COVID-19) was first discovered in December 2019 in Wuhan, China, and has now spread to nearly 213 nations, infecting millions of people. COVID-19 was declared a pandemic by the World Health Organization in March 2020. According to WHO data, more than 219 million individuals have been infected with the disease, with 4.5 million deaths reported as of October 1, 2021.[1]

Early detection of COVID-19 is critical not only for patient care but also for public health since it allows patients to be isolated and the pandemic to be controlled. Because of the disease's novelty, strategies to combat it were unknown in the beginning, but researchers saw a screening and prompt diagnosis of infected patients, as well as their separation from the general population, as critical measures. Rapid detection of infected patients and monitoring of positive cases is the first and most crucial step in controlling this pandemic. Many researchers and the WHO have proposed various diagnostic procedures for the quick identification of COVID-19, with the reverse transcription-polymerase chain reaction (RT-PCR) test being the most notable.[2]

X-radiation, often known as X-ray, is a type of electromagnetic penetrating radiation. These rays penetrate through the required human body parts, creating photographs of the body part's inside features. The X-ray image is a black-and-white portrayal of the inside body parts. One of the oldest and most widely used medical diagnostic tests is the X-ray. The image of the thoracic cavity, which includes the chest and spine bones as well as the soft organs such as the lungs, blood vessels, and airways, is used to identify chest-related disorders such as pneumonia and other lung ailments[6]. Computed tomography (CT) is a more sensitive and specific detection tool for COVID-19 than chest X-ray imaging, and lung involvement and ground-glass opacities (GGO) can sometimes be seen on CT even before the beginning of clinical symptoms and before a positive RT-PCR test. This means that COVID-19 problems can often be recognized in the lungs before the onset of the first clinical signs and a positive RT-PCR result.[3]

CT scans are expensive and damaging to one's health because they use a lot of radiation. The use of a chest X-ray is another effective method of detecting COVID-19 infection. In comparison to CT scans, chest X-rays are less expensive and safer. Pneumonia can also be detected with chest X-rays. Deep Learning (DL) methods have demonstrated exceptional accuracy in the accurate interpretation of medical images. Deep learning-based solutions are attractive since they are scalable, automated, and straightforward to implement in clinical settings.[4]

Image detection using Convolutional Neural Network

Convolutional neural networks (ConvNets or CNNs) are one of the most common types of neural networks used to recognize and classify images. CNN's are commonly used in domains such as object detection, face recognition, and so on. CNN image classifications take an input image, processes it, and categorizes it into several groups (Eg., Dog, Cat, Tiger, Lion). An input image is seen by computers as an array of pixels, with the number of pixels varying depending on the image resolution. It will see $h \times w \times d$ (h = Height, w = Width, d = Dimension) based on the image resolution.[8]

To train and evaluate deep learning CNN models, each input image will be passed through a sequence of convolution layers using filters (Kernels), Pooling, fully connected layers (FC) as shown in Fig 1, and the Softmax function to classify an object with probabilistic values ranging from 0 to 1.

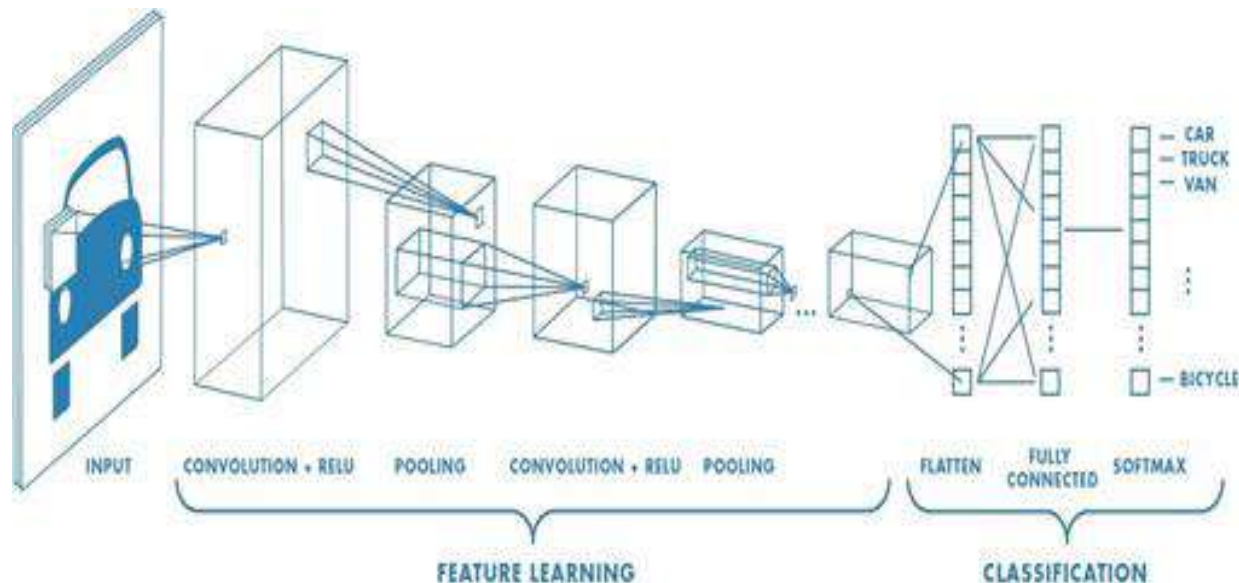


Fig 1 CNN Architecture.

The first layer to extract features from an input image is convolution. By learning visual attributes with small squares of input data, convolution preserves the link between pixels. It's a mathematical process with two inputs: an image matrix and a filter or kernel. Convolution of an image with various filters can be used to accomplish tasks such as edge detection, blurring, and sharpening. Stride is a component of convolutional neural networks, which are neural networks that are optimized for image and video compression. Stride is a filter parameter in a neural network that controls the amount of movement across an image or video. If the stride of a neural network is set to 1, for example, the filter will move one pixel (or unit) at a time. Because the size of the filter has an impact on the encoded output volume, the stride is frequently set to a whole number rather than a fraction or decimal.[9]

Filters do not always precisely fit the supplied image. There are two possibilities: To accommodate the picture, padding it with zeros (zero-padding) is necessary. Remove the portion of the image where the filter didn't work. This is known as valid padding, and it maintains only the image's legitimate parts. Non-linearity is a term used to describe a phenomenon (ReLU). For a non-linear operation, ReLU stands for Rectified Linear Unit. $f(x) = \max(0, x)$. Why is ReLU important? The goal of ReLU is to add non-linearity to our ConvNet. Because the data we want our ConvNet to learn in the real world is non-negative linear numbers. In addition to ReLU, other nonlinear functions such as Tanh and sigmoid can be employed. The majority of data scientists choose ReLU since it outperforms the other two in terms of performance.[10]

When the photos are too huge, the pooling layers portion would lower the number of parameters. Spatial pooling, also known as subsampling or downsampling, decreases the dimensionality of each map while preserving crucial data. There are several types of spatial pooling such as Pooling to the maximum, Pooling on the Average, Pooling of sums, The largest element from the corrected feature map is used in max pooling[11]. The average pooling could be calculated by taking the largest element. Sum pooling refers to the sum of all elements in a feature map. We flattened our matrix into a vector and fed it into a fully connected layer, similar to a neural network, in the FC layer. The feature map matrix will be transformed to a vector (x1, x2, x3,...) in this step. We put these attributes together to make a model using the fully linked layers. Finally, we use a softmax or sigmoid activation function to identify the outputs as COVID-19, Pneumonia, or Normal individual.[12]

IMPLEMENTATION

The data set was obtained via Kaggle. This data set is made up of a variety of publicly available datasets. The data set is divided into two folders (train and test), each with three subfolders (COVID19, PNEUMONIA, NORMAL). The dataset contains 6432 x-ray pictures, with test data accounting for 1288 images. This data set is a collection of various publicly available data.[7]. A sample of the data set has been shown in Fig 2.

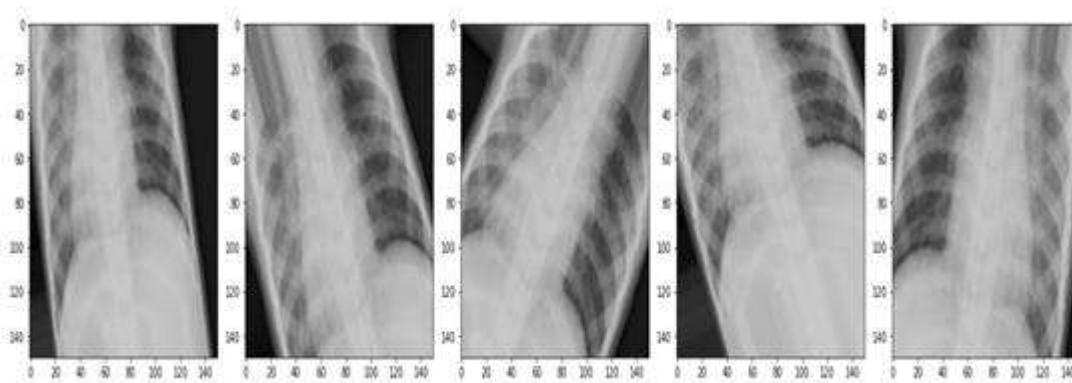


Fig 2 Sample data.

The model has been built using the CNN with Relu as an activation function in the input layer and the softmax layer as an activation function in the output layer. The optimizer employed here is Adam, and the loss function is sparse categorical cross-entropy. We used three convolution layers, three max pooling layers, and three drop out layers in this experiment. There are 2,028,228 parameters in all as shown in Fig 3.

```
Model: "sequential"
-----
Layer (type)                Output Shape              Param #
-----
conv2d (Conv2D)              (None, 148, 148, 32)     896
max_pooling2d (MaxPooling2D) (None, 74, 74, 32)       0
conv2d_1 (Conv2D)            (None, 72, 72, 64)       18496
max_pooling2d_1 (MaxPooling2 (None, 36, 36, 64)       0
conv2d_2 (Conv2D)            (None, 34, 34, 128)      73856
max_pooling2d_2 (MaxPooling2 (None, 17, 17, 128)     0
conv2d_3 (Conv2D)            (None, 15, 15, 256)      295168
max_pooling2d_3 (MaxPooling2 (None, 7, 7, 256)       0
dropout (Dropout)            (None, 7, 7, 256)        0
Flatten (Flatten)            (None, 12544)            0
dense (Dense)                 (None, 128)              1605760
dropout_1 (Dropout)           (None, 128)              0
dense_1 (Dense)               (None, 256)              33024
dropout_2 (Dropout)           (None, 256)              0
dense_2 (Dense)               (None, 4)                1028
-----
Total params: 2,028,228
Trainable params: 2,028,228
Non-trainable params: 0
```

Fig 3 Model Summary

The number of epochs is 300. It took around 8 hours to train the model. After that, the model file was downloaded and made available as an API. It's more like a SaaS. To host the model as an API the following steps are followed.

This detector has been deployed in Heroku because it is free and simple to set up. The source code along with the model was then published to GitHub. A requirement text file has been created that contains all of the imported libraries that the project requires to execute. After that, a runtime file is needed to tell Heroku which type of Python function is required. Then it needs a profile with a statement that tells the website how to launch the project.

For this project the chosen website is Heroku as it's free and easy to deploy. The completed source and executable files are into GitHub. The requirement file which will have all the imported libraries, a profile that has a statement that will tell how to run the project on the website are also uploaded to GitHub. We will also need to have a runtime file that will tell Heroku which type of python function is required. Once GitHub code is linked to Heroku, it will take care of the rest. Following that, the website will be launched.

The user can upload the Chest X-ray to be examined, as shown in Figure 4. The model will forecast the output once the image has been successfully uploaded. If the uploaded Chest X-ray image is contaminated with COVID-19, the result will be as shown in Figure 5. The outcome will look like Fig 6 if the supplied Chest X-ray image is clear of COVID-19 and Pneumonia. If the uploaded Chest X-ray image is infected with pneumonia, the result will be as shown in Figure 7.



Fig 4 : Upload the Chest X-ray image



Fig 5: COVID19 predicted Chest X-ray.



Fig 6 : A healthy Chest X-ray



Fig 7: Predicts pneumonia infected Chest X-ray.

On the basis of chest X-ray pictures, we have presented an automated intelligent approach for differentiating COVID-19 patients from non-patients. Our method analyses the structure of a chest X-ray image in real-time identifies COVID-19 patients using hidden patterns and eliminates the requirement for manual pre-processing.

Our suggested approach can detect COVID-19 patients with an accuracy of 93–99 percent, according to empirical findings acquired from 6432 chest X-ray pictures of patients.

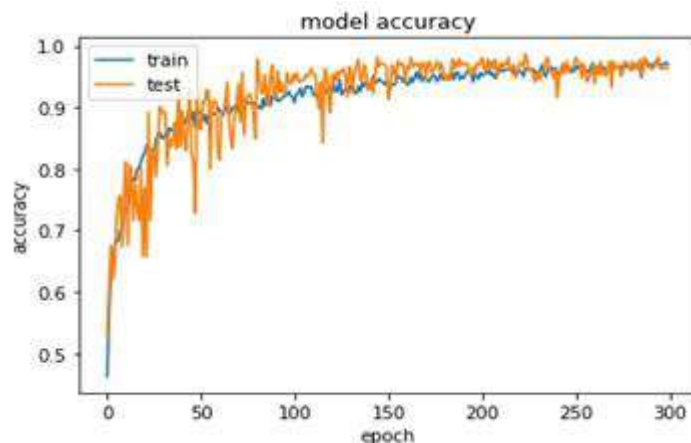


Fig 8 Model Accuracy graph.

A model accuracy graph or a learning curve shows how the model is performing on the train and test data. Overfitting is a term used to describe a model that performs poorly on testing data but performs well on training data. Underfitting is defined as a model that cannot both model and generalise to new data. We may deduce that our model is a good fit from Fig 8 because it performs well on both train and test data.

CONCLUSION

Since Chest X-rays are widely available from nearby clinics or hospitals at a reasonable cost, they can be utilized to detect COVID-19 infections. Our COVID-19 detector, which is based on CNN, outperformed the competition in terms of precision, accuracy and loss. It is suggested that Deep Learning approaches be used for COVID-19 diagnosis using our CNN-based COVID-19 detector.

An end-to-end fully automated CNN model for COVID-19 identification from chest X-ray pictures was provided in this paper. The proposed CNN model had a 96% accuracy rate. The imaging test can help to detect COVID-19 quickly and, as a result, help to control the disease's spread. The imaging techniques of Chest radiography and CT are helpful in the diagnosis of COVID-19 disease.

There are some drawbacks to the proposed system. To begin with, the sample size is comparatively small and needs to be raised in order to assess the generalizability of the constructed system. If more data is discovered in the next few days, this will be overcome. Second, it only looks at the posterior-anterior (PA) perspective of X-rays, thus it can't tell the difference between other X-ray views like anterior-posterior (AP), lateral, and so on. Finally, COVID-19 photos with various illness symptoms are difficult to classify. Finally, comparison of the performance of the suggested system to that of radiologists is yet to be done. As a result, a future study will include a comparison of the suggested method with radiologist findings.

REFERENCES

1. WHO Coronavirus (COVID-19) Dashboard and Vaccination data.
2. Yicheng Fang, Huangqi Zhang, Jicheng Xie, Minjie Lin, Lingjun Ying, Peipei Pang, et al., "Sensitivity of chest CT for COVID-19: Comparison to RT-PCR", *Radiology*, pp. 200432, 2020.
3. Shan F, Gao Y, Wang J, Shi W, Shi N, Han M, Xue Z, Shi Y " Lung infection quantification of COVID-19 in CT images with deep learning". arXiv preprint arXiv:2003.04655, 1–19.
4. Covid-19 Sample Collection Management System - Indian Council of Medical Research.
5. Ritu Gill, Archana Rohilla., "Lung disease detection using X Rays in COVID-19 victims - Journal of Emerging Technologies and Innovative Research"
6. Convolutional Neural Network - Tensorflow documentation.
7. <https://www.kaggle.com/prashant268/chest-xray-covid19-pneumonia>
8. Ritu Gill, Archana Rohilla, Yash Dhankhar., "Deep Convolutional Neural Network–Based Computer-Aided Detection System for COVID-19 Using Multiple Lung Scans: Design and Implementation Study" - Journal of Medical Internet Research., September 2021, Volume 8, Issue 9

9. Areej A. Wahab, Ashraf Yunis. "COVID-19 Detection in X-ray Images using CNN Algorithm" - IEEE Conference Publication.
10. Aijaz Ahmad Rashi, Furqan Rustam., "An Efficient CNN Model for COVID-19 Disease Detection Based on X-Ray Image Classification".
11. Mustafa Ghaderzadeh, Farkhondeh Asadi., "Deep Learning in the Detection and Diagnosis of COVID-19 Using Radiology Modalities: A Systematic Review".
12. Moutaz Alazab, Albara Awajan, Abdelwadood Mesleh, Ajith Abraham, Vansh Jatana, Salah Alhyari., "COVID-19 Prediction and Detection using Deep Learning" - International Journal of Computer Information Systems and Industrial Management Applications ISSN 2150-7988 Volume 12 (2020) pp. 168-181
13. Rikiya Yamashita, Mizuho Nishio., "Convolutional neural networks: an overview and application in radiology" Springer open.
14. M Polsinelli, L Cinque, G Placidi., "A light CNN for detecting COVID-19 from CT scans of the chest" - Pattern recognition letters, 2020 - Elsevier

Cancer Treatment Planning Using Computed Tomographic Images

Padmapriya B

Department of Biomedical Engineering, PSG College of Technology, Coimbatore Tamil Nadu, India

ABSTRACT

The Planning systems used for cancer treatment uses Computed Tomography images for locating the diseased region and these images should be free of noises and extra information. The raw images will have couch, which is an additional data and hence it should be removed. The first part of the paper is the development of an algorithm for removal of couch, so that their intervention can be avoided. This paper also deals with the development of a methodology for detection of skin and skin marker. Skin detection is one of the significant roles in planning system as it is the outer boundary of the image. Further skin detection helps in treatment planning where skin markers and reference point are used. The references are placed on skin, hence detection of skin is a mandatory task for such devices. Marker detection supports the placement of needles planned for the cancer treatment.

Keywords—Computed Tomography, Couch, Skin marker, Marker detection, Cancer treatment

INTRODUCTION

Over the world one of the leading causes for death is happened due to cancer. The modern imaging technology helps to treat the cancer effectively such as early detection of tumour, efficient diagnosis, planning of better treatment and early stages detection and monitoring. Variety of medical imaging techniques, such as PET, SPECT, MRI and CT were developed for improving the non-invasive treatment and played central role in clinical oncology. In order to achieve large intersubjective variability and available huge important parameters in molecular images, mostly it is challenging to adapt the same methodical model to define the target in the acquired medical images. Hence, getting of better molecular imaging for medical studies, techniques that fall under image processing were widely used to achieve a better treatment.

OBJECTIVE

The objective of the paper is to implement image processing techniques to perform removal of couch, detection of skin and skin marker in the CT images used in planning the treatment of cancer patients. These preliminary steps will describe the objective of the paper.

Purpose of Couch Removal

The couch removal in CT images is mandatory since couch information can affect the patient's data. In 3D visualization such as digitally reconstructed radiographs or maximum intensity registration or CT fused with another dataset such as PET (Positron Emission Tomography). In CT /PET systems [1], in PET reconstruction attenuation and scatter correction in CT is used. Patient specific and patient boundary has to be estimated accurately by using of scatter correction, patient table removal is used to evaluate the accurate estimation of boundary. In the process of image registration the two images with same image information is consider for registration. The presence of couch in CT image can poorly impact its registration with other modalities [2]. CT image before and after couch removal is shown in Fig. 1.

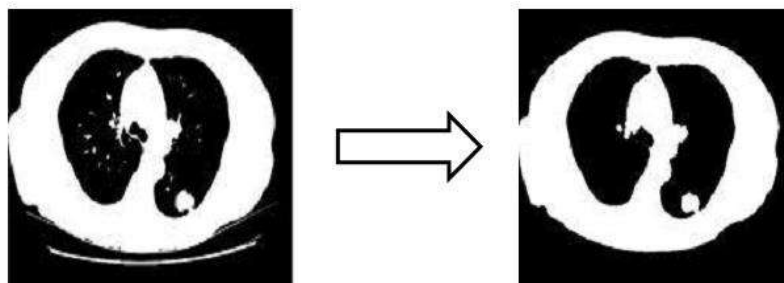


Fig. 1. CT image before and after couch removal.

Purpose of Detection of Skin

In the human body skin is the largest organ with a total area of approximately 20 square feet. Needle insertion during interventional therapies requires the detection of skin for identifying the entry point into the body [3], since skin is the outermost layer. The detection of skin is also important in planning systems where skin markers are used. The placement of skin marker requires the detection of skin in the images which is shown in Fig. 2.

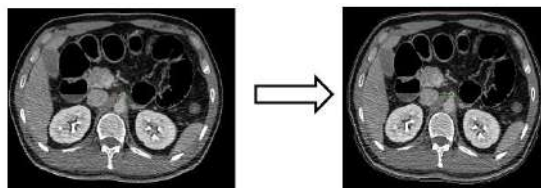


Fig. 2. Detection of skin in CT image.

Purpose of Detection of Skin marker

Multimodal imaging such as CT and MRI visible skin markers are used [4], and image registration or stereotactic indexing also performed by using of one or both imaging types. Index or concave central portion is always available in the marker; digitized pointer is enabled by the above process and to be placed stably within indentation during calibration or marker identification in a surgical context. The other, frame less stereo taxonomy method where a digitized pointer can be used to pick off the position of markers in physical space so as to relate the physical space to two dimensional or three dimensional image data taken from CT or MRI scanning [5]. These applications of skin markers make their identification significant in scanning systems. Skin marker detection is depicted in the Fig. 3.

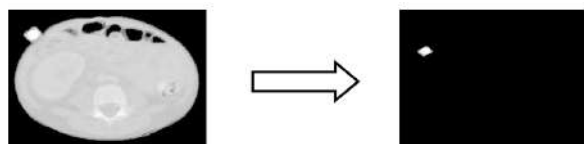


Fig. 3. Detection of skin marker in CT image.

Eclipse C/C++ IDE

Eclipse was started as IBM product. It is open source platforms that facilitates and encourages the development of third party plug-ins. It is the best known integrated development environment. It was originally designed for JAVA but provides good support for C and C++. The benefits of using Eclipse IDE are fast code compiling, open source and extensive. Eclipse is a JAVA based application and hence it requires JAVA runtime environment (JRE) [6-7].

OpenCV Library

OpenCV is a library of programming functions containing all the standard algorithms for computer vision. Functions are implemented in C/C++, Python and Java. OpenCV libraries can run on Windows, Linux, Android and Mac systems. The latest version is 2.4.4. It was developed by Willow Garage. The basic functionalities and data structures are imgproc, highgui, calib3d, core, features 2d and objdetect. Imgproc deals with image processing functions such as blurring, histograms, registration, tracking and detection. Core relates the basic functionalities and data structures. Highgui correlates high-level graphical user interfaces. Features2d interfaces feature detection and description algorithms. Data structures and functions belong to the namespace CV. Therefore to access the functionality “using namespace CV” directive has to be used. OpenCV allows one to efficiently encode the algorithm for computer vision [8-9]. It runs much faster than MATLAB. It allows incorporating external libraries therefore solutions to serious problem can be found easily.

DATASET COLLECTION

Couch Removal

The datasets for couch removal was selected with an idea to check the accuracy of algorithm in all the possible cases such as the image with a single couch line, image with two couch lines and absence of couch [10]. The algorithm was designed in such a way that it displays the information in console window if no couch is present in the input image taken. The proposed methodology works well with all images. Some of the sample images are shown in Fig. 4 (a) & (b).

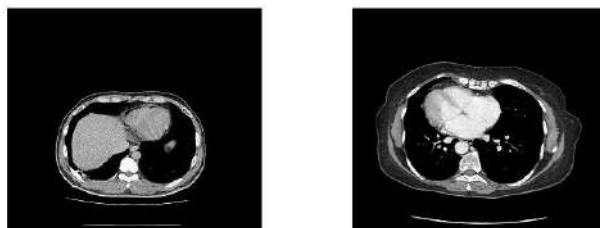


Fig. 4. (a) CT image with two couch lines (b) CT image with single couch line

SKIN DETECTION

The idea behind skin detection in CT images is to enhance or represent skin, the outer boundary of image by different colour. Skin is represented by two distinct layers. Since two layers were detected, the accuracy of algorithm was tested by choosing datasets in which detected layers were connected with areas present inside the boundary. Fig. 5(a) and (b) were the sample images used for testing the accuracy of skin detection algorithm.

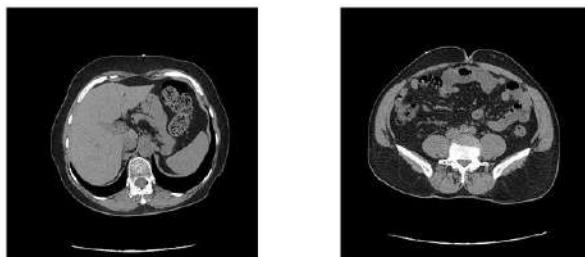


Fig. 5. (a) Skin Detection Image1 (b) Skin Detection Image2

Skin Marker Detection

The datasets selected for skin marker detection includes images with no skin marker, images with single skin marker and images that contain multiple skin markers. Examples of input images are depicted in Fig. 6 (a) & (b).

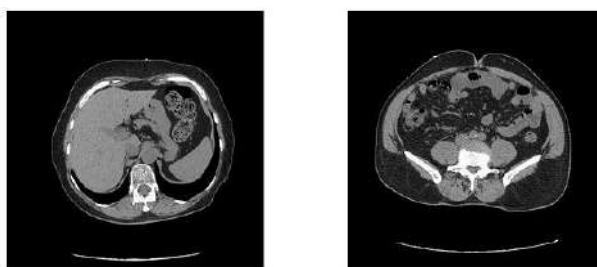


Fig. 6. (a) Skin MArker Image1 (b) Skin Marker Image2

PROPOSED METHODOLOGY

Removal of Couch

The first step is to detect the couch present in image. The search for couch was made from bottom of the image. Threshold was used to find the first high intensity pixel; this is taken as seed point. To confirm that the detected seed point is a couch pixel the neighbouring pixel's intensities were compared with zero. If the condition fails the information was displayed in the console window. If all the intensities were zero the detected point was taken as couch point. Flood fill algorithm was applied to fill the couch line with intensity equal to black. Thus the first couch line was removed. After applying flood fill, the next seed point was identified. After detection of second seed point, the same checking condition and process used for the first couch line was applied. Applying the process twice helps in removal of multiple couches present in image. The work flow of couch removal is shown in Fig. 7.

ALGORITHM:

- Step 1: Read input image
- Step 2: Detect first seed point
- Step 3: Check whether seed point is present in couch
- Step 4: If seed point is not in couch, show the information
- Step 5: If seed point is there, apply flood fill operation
- Step 6: On removal of first couch line, find next seed point
- Step 7: Check presence of second seed point
- Step 8: If not, consider removal of couch 1 as final
- Step 9: If there, apply flood fill operation
- Step 10: Display the image after performing the operation

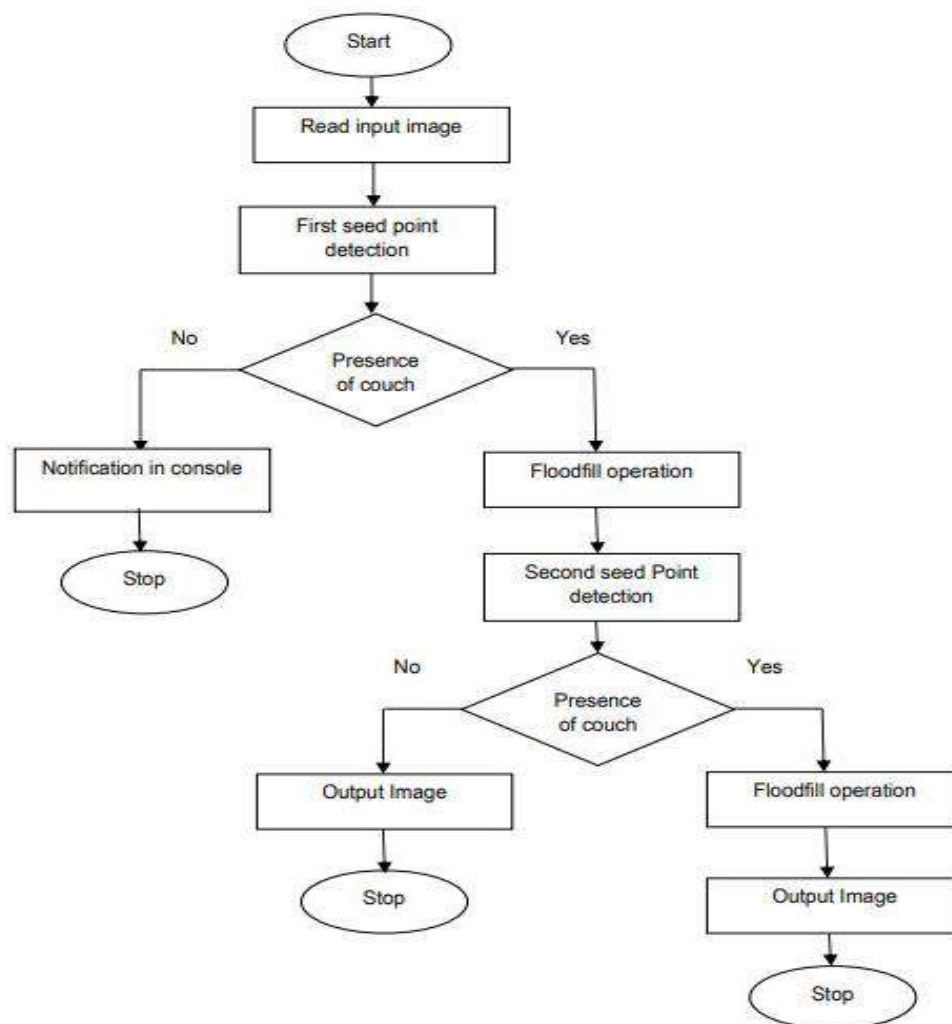


Fig. 7. Work flow of Couch Removal

SKIN DETECTION

The Detection of skin starts with the pre-processing steps such as dilation, this step enhances the skin layer. Identification of seed point was the next step; the search was made from top of the image. Canny edge detection was applied after detection of seed point. By using flood fill operation colour was assigned to the outermost edges. The coloured edges were extracted separately. The difficulty in skin detection was displaying the second layer without branches. For this process, the layers were first separated from each other. The extracted first layer was named as Mask1. After applying morphological operations, second layer was extracted without branches and that was named as mask2. Mask 1 and Mask 2 was combined using bitwise or operation and this was used as the final output mask. This mask was merged on the input image. In the resultant image the edges were shown in different colour. Thus the objective of skin detection was attained. Below mentioned skin detection algorithm flow chart is depicted in Fig. 8.

ALGORITHM:

- Step 1: Read input image
- Step 2: Apply dilation to image for outer boundary
- Step 3: Detect seed point & used its intensity value
- Step 4: Apply canny edge detection
- Step 5: Apply colour to outer layer use of food fill
- Step 6: Extract only outer colour edges
- Step 7: Use of canny and food fill, obtain first layer of skin
- Step 8: Taken this outer first layer of skin as mask 1.

- Step 9: Bit wise operation on mask 1 for enhancement.
Step10: Take first layer intensity as threshold value.
Step11: remove noise using food fill and threshold tech.
Step10: Take first layer intensity as threshold value.
Step12: To attain branches free second layer (mask 2).
Step13: Use Gaussian blur, food fill.
Step14: use bit wise operation on mask1 and 2.
Step15: Merge outer most layer for final result.

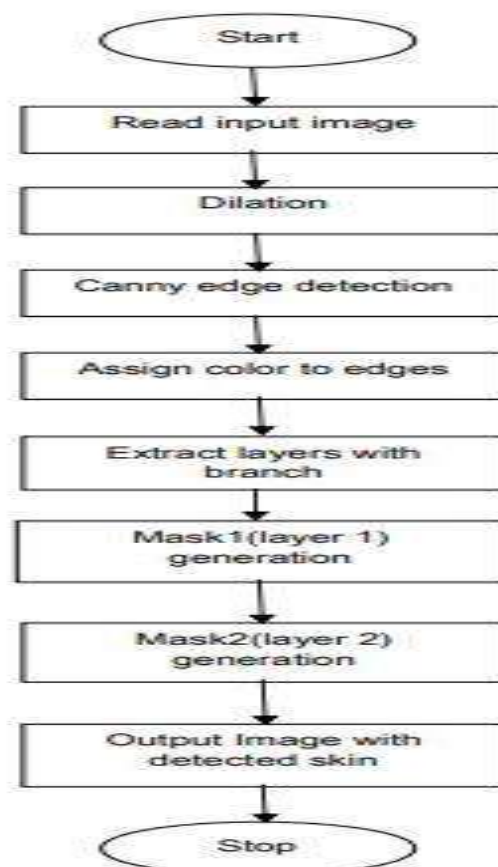


Fig. 8. Work flow of Skin Detection

SKIN MARKER DETECTION

The objective is to represent the skin marker present in input image with a different colour so that its presence is enhanced. The preliminary requirement for skin marker enhancement is the detection of outermost layer which is skin. Hence skin detection algorithm was used before proceeding with marker identification. The Mask obtained as the result of algorithm was used for further operations. Marker's intensity will be greater than skin intensity. Hence threshold method was used for its identification. On absence of skin marker the information was displayed in console window. If marker was present a different colour was applied to it. Thus the final image will have enhanced marker. Skin detection algorithm flow chart is clearly depicted in Fig. 9.

ALGORITHM:

- Step 1: Read input image
Step 2: Apply dilation to image
Step 3: Use Contours operation for get external layer
Step 4: Apply smoothening to get outer boundary
Step 5: use food full, bitwise, threshold to get mask

Step 6: This mask contains outer layer & skin marker

Step 7: Apply threshold to obtain mask

Step 8: check skin marker presence & obtain a result.

Step 9: If not, show the information.

Step10: If skin marker is present apply colour.

Step11: Combine the coloured skin marker with input.

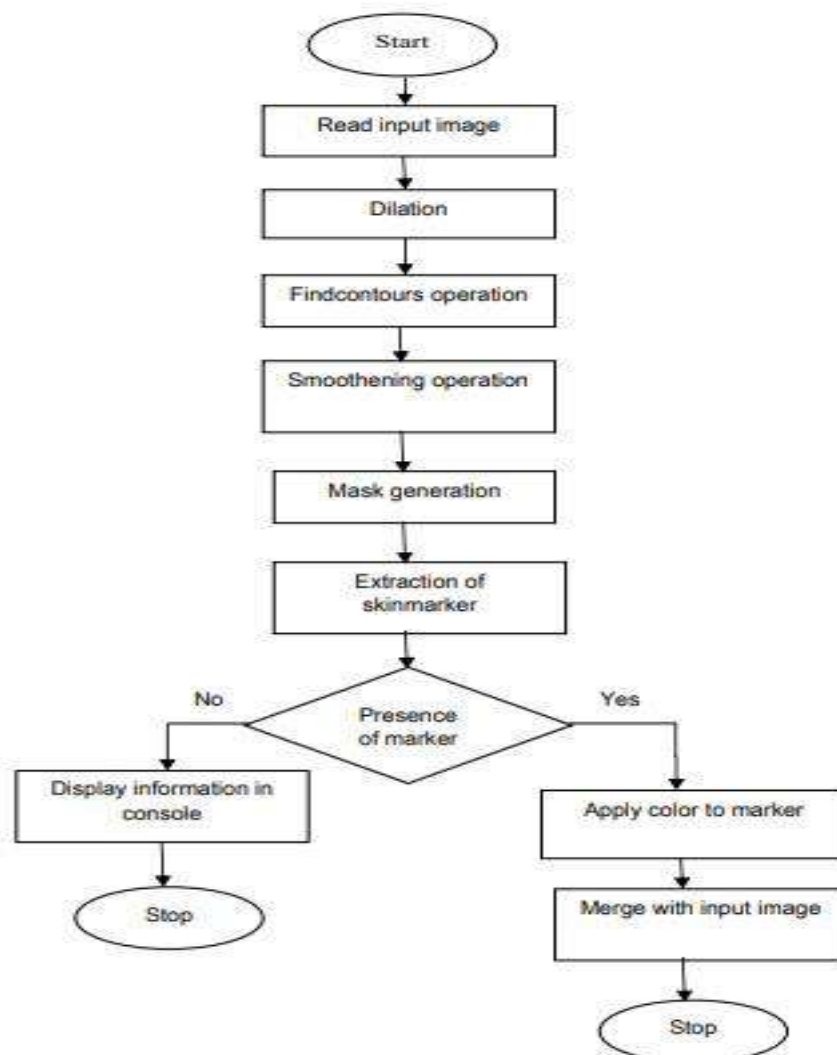


Fig. 9. Work flow of Detetction of Skin Marker

CHALLENGES FACED

The challenge in couch removal was detecting the presence of multiple couch lines and removal of couch when it occurs closer to the image. Seed point detection helps to overcome these challenges.

In skin detection difficulties faced was detecting the second layer without branches. Using morphological operation and thresholding second layer can be obtained properly.

RESULTS AND DISCUSSION

The outputs obtained for the proposed algorithm is given below.

REMOVAL OF COUCH

The output of images containing one couch line and two couch lines are shown in Fig. 10 and Fig. 12 respectively. On removing couch in input image, the interference of its intensities when processing volume of interest was eliminated. When no couch was present, the information was displayed in console. The output image for such case was shown in Fig. 11 and Fig. 13 respectively.

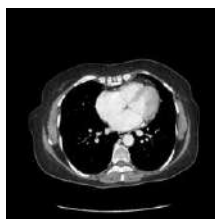


Fig. 10. Input image with single couch line

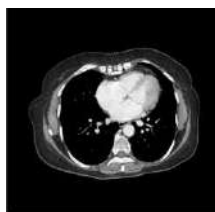


Fig. 11. Couch removed output image

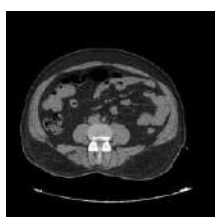


Fig. 12. Input image with two couch line



Fig. 13. Couch removed image



Fig. 14. Input image without couch

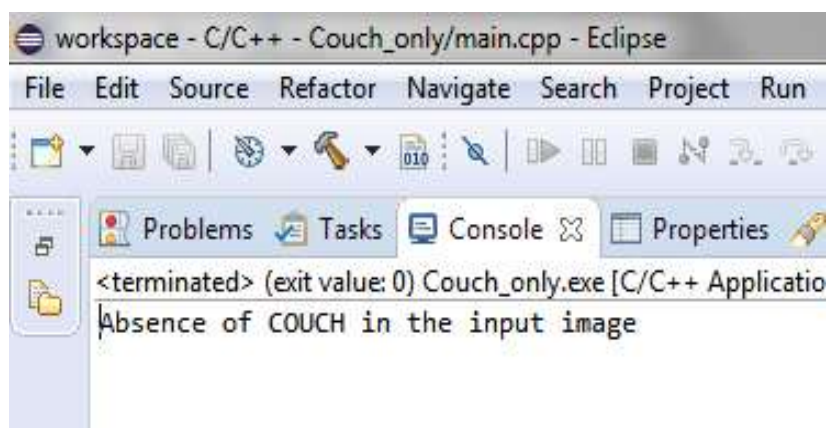


Fig. 15. Information in console

The input image without couch is shown in Fig. 14 & information in console is shown in Fig. 15.

DETECTION OF SKIN

The input image for skin detection is shown in Fig. 16 and skin enhanced output image is shown in Fig. 17. Applying colour to the skin makes its identification much simpler for the user.

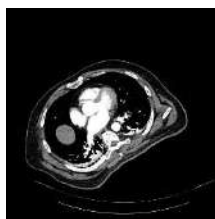


Fig. 16. Input image for skin detection

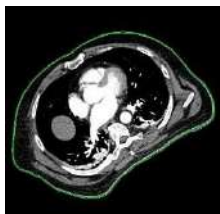


Fig. 17. Skin enhanced image

Detection of Skin Marker

The input image with skin marker and without skin marker is shown in Fig. 18 and Fig. 20. Fig. 19 is the processed image in which skin marker is shown in a different colour. When skin marker was not present in input image, the notification of its absence was given in console window. This output was shown in Fig. 21.



Fig. 18. Input image with skin marker

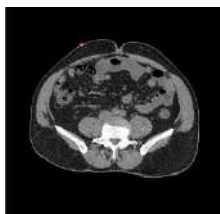


Fig. 19. Skin marker enhanced image

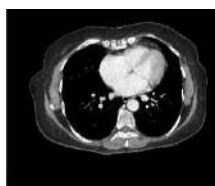


Fig. 20. Input image without skin marker

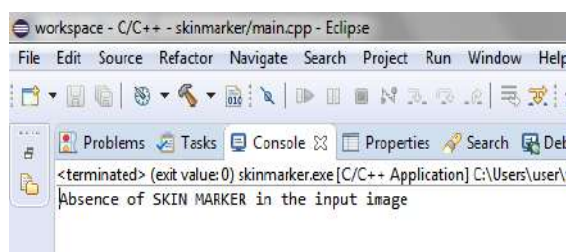


Fig. 21. Notification in console

CONCLUSION AND FUTURE WORK

The proposed steps are to ensure an efficient utility of CT images without the interference of artifacts in treatment planning system. Our future work will be to improve the detection of skin in the images when an external object touches skin in input images. When machine part touches the outermost layer the connectivity check algorithm was disturbed by external object intensity. Hence an effective way of implementing skin

detection during the occurrence of machine parts has to be implemented. Further, when the entire three algorithms were executed in a single paper, skin was displayed in only layer. Our further improvement will be, to find a method that displays skin as two layers when the algorithm was executed in a single paper.

REFERENCES

1. Kim, Jinman, Youmo Hu, Stefan Eberl, David Feng, and Michael Fulham. "A fully automatic bed/linen segmentation for fused PET/CT MIP rendering." (2008): 387P-387P.
2. Florian Weiler, Christoph Brachmann, Nadine Traulsen, Rinoud Nijhuis, "Fast automated non-linear contour propagation for adaptive head neck therapy", 2012.
3. Moussallem M, Valette PJ, Traverse-Glehen A, Houzard C, Jegou C, Giammarile F. New strategy for automatic tumor segmentation by adaptive thresholding on PET/CT images. *J Appl Clin Med Phys*. 2012 Sep 6;13(5):3875. doi: 10.1120/jacmp.v13i5.3875. PMID: 22955656; PMCID: PMC5718227.
4. K.K. Anilkumar, V.J. Manoj, T.M. Sagi, A survey on image segmentation of blood and bone marrow smear images with emphasis to automated detection of Leukemia, *Biocybernetics and Biomedical Engineering*, 10.1016/j.bbe.2020.08.010, (2020).
5. Harada-Shoji, Narumi, Takayuki Yamada, Takanori Ishida, Masakazu Amari, Akihiko Suzuki, Takuya Moriya, and Noriaki Ohuchi. "Usefulness of lesion image mapping with multidetector-row helical computed tomography using a dedicated skin marker in breast-conserving surgery." *European radiology* 19, no. 4 (2009): 868-874.
6. "Introduction to Eclipse IDE", Available on: <https://www.seas.upenn.edu/~cis1xx/resources/eclipse.html>.
7. "How to install Eclipse Neon", Available on: https://www3.ntu.edu.sg/home/ehchua/programming/howto/EclipseCpp_HowTo.html
8. "Introduction to Opencv", Available on: https://www.cse.unr.edu/~bebis/CS485/Lectures/Intro_OpenCV
9. "How to install opencv on windows with minGW", Available on: <http://kevinhughes.ca/tutorials/opencv-install-on-windows-with-codeblocks-and-mingw>
10. Tokuda, J., Song, S. E., Tuncali, K., Tempany, C., & Hata, N. (2013, September). Configurable automatic detection and registration of fiducial frames for device-to-image registration in MRI-guided prostate interventions. In *International Conference on Medical Image Computing and Computer-Assisted Intervention* (pp. 355-362). Springer, Berlin, Heidelberg.

A Non-Invasive Early Diagnosis of Osteoarthritis Using Random Forest and Ann

Anisha C.D and Arulanand N

Department of CSE PSG College of Technology Coimbatore, India

ABSTRACT

Osteoarthritis or degenerative arthritis is one of the joint disorders which affects the cartilage. This type of joint damage, if left untreated in the early stage will lead to degeneration of joints. There is a need for a non-invasive early diagnosis of osteoarthritis which is made possible through the usage of Machine Learning Techniques. Surface Electromyography signal (sEMG) is a non-invasive manner of collecting muscle data from the surface of the skin, which is cheaper and easier to capture from the individuals. The proposed framework uses the dataset retrieved from the UCI repository. It consists of sEMG data of three movements namely Gait, Flexion and Extension procured from the lower limb of the normal and abnormal subjects. The time series data can't give meaningful information for classification, so the data is sampled and the sampled sEMG signal data is pre-processed using Butterworth Band Pass Filter which is then fed to feature extraction stage wherein Time Domain (TD) features are procured. The extracted features are fed to the Random Forest classifier and Artificial Neural Network (ANN) classifier. The evaluation metrics used to analyse the prediction of the classifier are Confusion Matrix, Accuracy, Precision, Recall and F1 Score.

Keywords— Osteoarthritis, Butterworth band pass, Time Domain, Random Forest, ANN

I INTRODUCTION

Osteoarthritis or degenerative arthritis is a progressive disorder wherein it affects the cartilage of the joints. [1][3] This disorder affects the lower limb functionality.[5]. The prevailing Osteoarthritis diagnosis system is invasive and costly. Therefore, it is necessary to use surface Electromyography Signals (sEMG) which is a non-invasive method for collecting data from individuals. sEMG represents the electrical potentials recorded from the individual while performing movements.[15]. The movements considered includes Gait which refers to walking, extension of the leg from the sitting position and flexion of leg up from the standing position.

Signal Processing is the vital step in sEMG data classification. The filtering of signals removes the noise in the sEMG signal Machine Learning Algorithms are used for Classification in more efficient manner.

The organization of the paper is as follows: Section II presents the related works which provides the techniques used in the paper, Section III presents the methodologies used in the proposed system and Section IV provides the results analysis and Section V presents the Conclusion and the future work.

II RELATED WORKS

In [1] Jean de Dieu Uwisengeyimana proposes a Knee pathology diagnosis using Support Vector Machine (SVM) and deep learning Neural Network and the sEMG is processed using Overlapped windowing technique. Least-Squares Kernel, Linear Discriminant Analysis (LDA) are used for classification in [2] for the data which involves control subjects and Rheumatoid arthritis and hip osteoarthritis. Different Machine Learning and Deep learning algorithms were compared to classify the osteoarthritis individual data from healthy subject data in [3] and a discussion on quantum perspective is also provided. Xin chen et al in [5] presents Entropy based Measures are used to distinguish Knee Osteoarthritis (KOA) individuals from control subject. The three types of Entropy measures considered are Approximate entropy, Sample Entropy and Fuzzy Entropy.

Jihye Lim et al, in [16] has presented the deep learning method to predict the occurrence of the Osteoarthritis using the statistical information of the patients. Principal Component Analysis (PCA) is used for generation of features.

Multi-Layer Perceptron, a type of Artificial Neural Network (ANN) has been used for the assessment of the Knee Injuries from the surface Electromyography signals and goniometric signals wherein these signals sent to the processing stage of time-frequency space obtained from the spectrogram and wavelet transform.[17].

Nima Befrui et al in [18] has presented a Vibro-arthrography based diagnosis for Knee Osteoarthritis. The normalized features are extracted from vibratory signals which is processed using segmentation stage, normalizing stage using Hann Window. The Linear Support Vector Machine (SVM) has been used for classification with input as normalized feature vectors obtained from the raw vibratory signals.

A Multi Model based Knee Osteoarthritis has been presented in [19], The X ray images has been processed using Convolutional Neural Network (CNN), clinical information and the baseline characteristics are fused using Gradient Boosting Machine (GBM).

From the related works, it is evident that the osteoarthritis prediction was mainly performed using the sEMG time series data and X ray Images data. The prominent classifiers used were Artificial Neural Network (ANN), Support Vector Machine (SVM), Linear Discriminant Analysis (LDA) for sEMG data and Convolutional Neural Network (CNN) for X-ray Images.

III. METHODOLOGIES

Figure 1 depicts the proposed framework with the flow of the process. The proposed system uses Butterworth Bandpass filter to the input signal wherein it provides an averaged smooth signal and performs better than the filters used in the existing system [1]. Another improvisation incorporated to the existing system is the construction of the hyperparameter space for the Random Forest Classifier, identifying and implementing the exact preprocessing technique essential for each classifier in the analysis which impact in the accurate prediction.

A. Dataset Description

The sEMG dataset is retrieved from the publicly available UCI repository. The dataset consists of sEMG recordings of 11 Healthy subjects and 11 Abnormal subjects who exhibit osteoarthritis. The five muscle positions considered for the collection are Recto Femoral, Biceps Femoral, Vasto Medial, EMG Semitendinoso, Flexo-Extension of the lower limb. The movements performed by the subjects are gait which refers to the walking movement, leg extension from a sitting position, and flexion of the leg up from the standing position. Figure 2,3,4 represents the above specified movements. The sources of the figures are specified in [21][22][23].

B. Data Processing- Splitting of Data

Each sEMG data of an individual is unique. The dataset considered for the process involves one Normal subject sEMG data and one Abnormal subject sEMG data. Table 1 represents the input given to this splitting process and the output obtained from this process. The data is split into 100 samples for the range of instances from 5000 and 200 samples for the range greater than 10000 instances.

C. Signal Processing – Filtering and Feature Extraction

The sEMG data obtained from splitting process is filtered using Butterworth band pass filter as Butterworth provides a thin frequency signal and band pass filter provides the average of low pass and high pass filter.[13] The filtered signal is then sent to the feature Extraction stage wherein 17 Time Domain Features are extracted.[11][12]

D. SPLITTING OF TRAIN AND TEST SET

The extracted features are split into 80% training set and 20% testing set. Table 2 represents the Training and Testing set split.

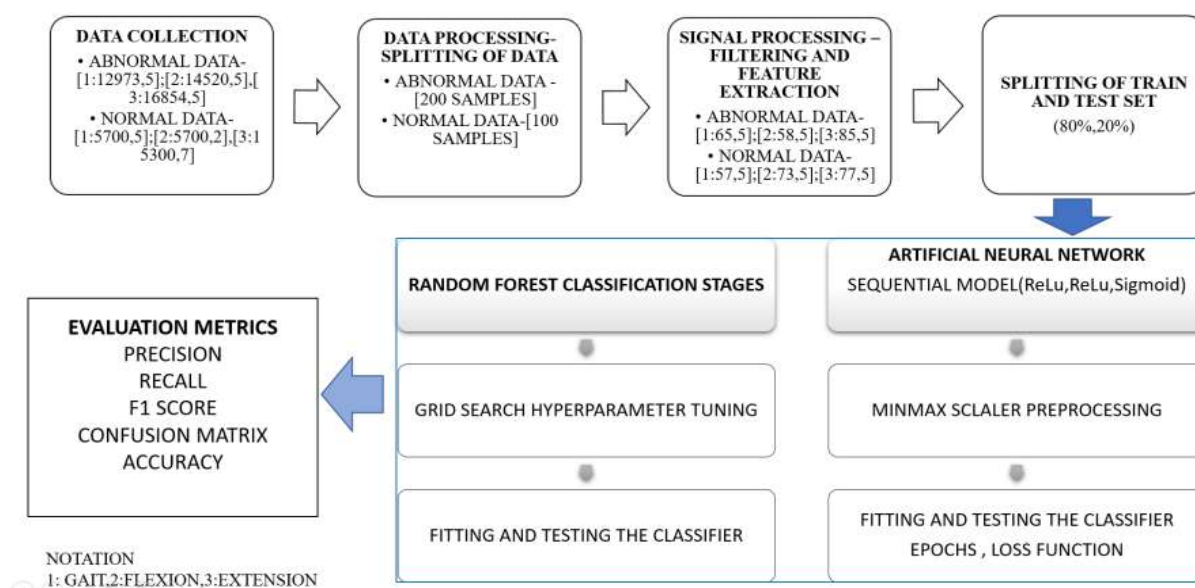


Figure 1 – Proposed Framework

Table 1 - INPUT TO SPLITTING STAGE

MOVEMENT	ACTUAL INSTANCES IN DATASET	SAMPLES SPLIT	AFTER SPLIT OUTPUT INSTANCES
GAIT	{Normal :(5700,5); Abnormal:(12973,5)}	{Normal: 100 Abnormal :200}	Normal:57 Abnormal:65 {122,5}
FLEXION OF LEG UP	{Normal :(14520,5); Abnormal:(12973,5)}	{Normal: 200 Abnormal :200}	Normal:73 Abnormal:58 {131,5}
SITTING-EXTENSION	{Normal :(11403,5); Abnormal:(16854,5)}	{Normal: 200 Abnormal :200}	Normal:77 Abnormal:85 {162,5}

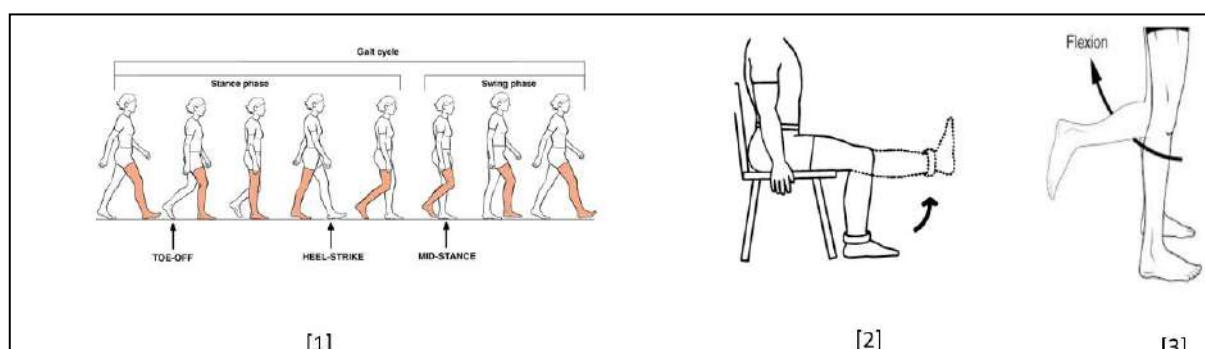


Figure 2 – Movements in the dataset [1] Gait (walking) [2] Extension from sitting position [3] Flexion of leg up from standing position.

Table 2- Training and Testing Set Split

MOVEMENT	TRAINING SET INSTANCES	TESTING SET INSTANCES
GAIT	97	25
FLEXION OF LEG UP	104	27
SITTING-EXTENSION	129	33

E. CLASSIFICATION

The classification algorithm considered are Random Forest and Artificial Neural Network (ANN).

1. Random Forest Classifier

i. Working Principle of Random Forest Classifier

Random Forest is an ensemble algorithm wherein it uses majority voting technique. [8]. The parameter bootstrap in the Random Forest Classifier specifies the sampling of data, if the bootstrap is set to True then the dataset is split into samples and send to each decision tree, if it set to false then the whole dataset is sent to each decision tree. The number of decision tree is specified using number of estimators. Each decision tree in the forest is trained using bootstrap approach and Each decision tree provides prediction which is then combined using majority voting approach.

ii. Hyperparameter Tuning – Grid Search Method

The hyperparameters are the prominent parameters for the classifier which directly influences the performance. They are tuned using Grid Search Method to increase its performance. It forms all possible combinations from the hyperparameter space and finds the best combination.[6][7].

The hyperparameters of the Random Forest are n_estimators and Bootstrap.

- n_estimators: corresponds to the number of decision tree in the forest, the value for n_estimators is provided based on the number of features in the dataset.
- Bootstrap: It is Boolean value, True indicates that the dataset sample is split and send to each decision tree otherwise the whole dataset is sent to each decision tree.

The hyperparameters Space of the Random Forest is presented in the table.

Table 3 – Hyperparameter Space – For All Three Movement Classes

MOVEMENT	HYPERPARAMETER INPUT SPACE	HYPERPARAMETERS OUTPUT
GAIT	n-estimators= {1,33}, Bootstrap= {True, False}	n_estimators=31, Bootstrap=True
FLEXION OF LEG UP	n-estimators= {1,33}, Bootstrap= {True, False}	n_estimators=1, Bootstrap=True
SITTING-EXTENSION	n-estimators= {1,33}, Bootstrap= {True, False}	n_estimators=3, Bootstrap=True

iii. Fitting and Testing the Classifier.

The classifier is fitted to the training set and the trained classifier is tested using the testing set.

2. Artificial Neural Network (ANN)

i. Working Principle of ANN

Artificial Neural Network consists of an input layer, the hidden layers and the output layer. The activation function used for the hidden layers are ReLu, for two layers and Sigmoid for one layer.[9] The number of epochs parameter specifies the number of iterations required to train the classifier. The number of epochs is set to 2000 by trial and error method.

ii. Min Max Scaler Preprocessing

The dataset is preprocessed using min max scaler for providing better results from ANN. The dataset is preprocessed by standardizing the values in the dataset to the range of [0,1]. [10]

iii. Fitting and Testing the Classifier

The classifier is fitted to the training set by execution of the specified number of epochs and tested using the testing set wherein the prediction is done for the unknown data.

F. Evaluation Metrics

1. Confusion Matrix

The confusion matrix is 2 X 2 Matrix as it is a binary classification. The 0 indicates the presence of Osteoarthritis and 1 indicates the healthy status. The confusion Matrix is constructed based on True Positive (TN), True Negative (TN), False Positive (FP) and False Negative (FN).[14]

2. Accuracy:

Accuracy is computed using the formula:

Accuracy = Total number of correctly classified instances / Total number of instances.

3. Precision:

It is the number of positive instances correctly classified divided by the total number of positive instances in the test set [20].

4. Recall:

It is the number of positive instances correctly classified divided by the total number of predicted instances (True Positive + False Negative)

5. F1 Score:

It is weighted average of Precision and Recall.

IV RESULT ANALYSIS

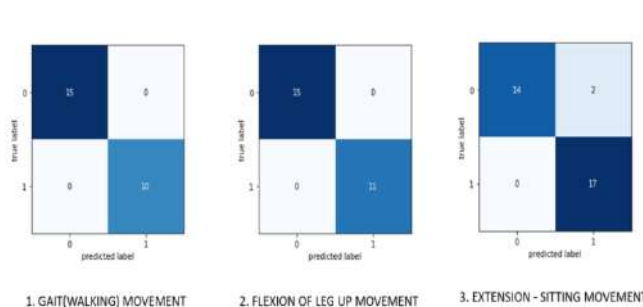


Figure 3 – Confusion Matrix of Random Forest Classifier

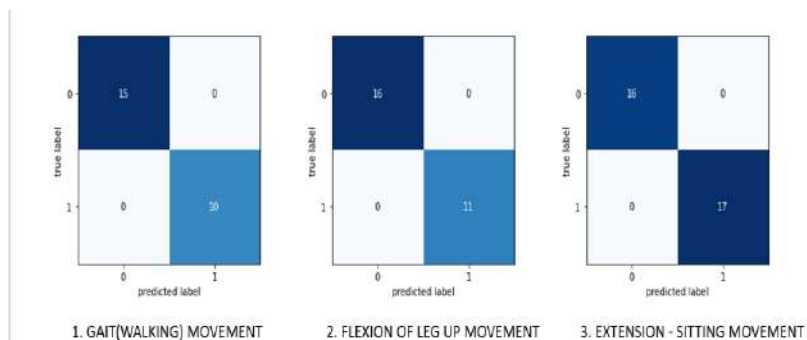


Figure 4 – Confusion Matrix of Artificial Neural Network (ANN)

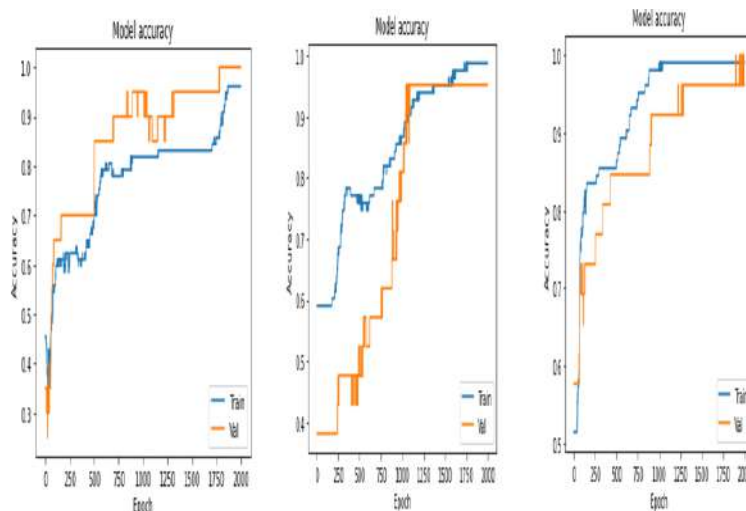


Figure 5 – Accuracy Graph of Epochs in ANN for three movements

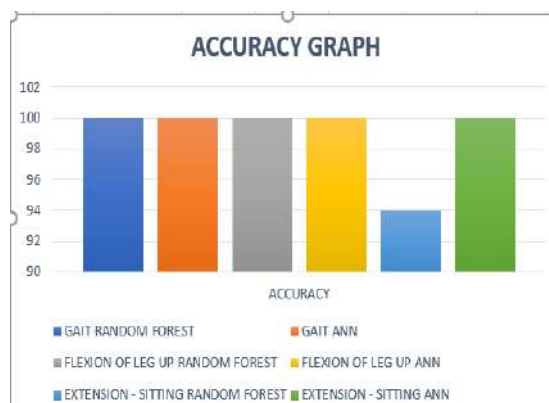


Figure 6- Accuracy Graph of Random Forest and ANN for all movements.

Table 5 – Accuracy, Precision, Recall and F1 Score

Movement	Classifier	Accuracy	Precision	Recall	F1 Score
Gait	Random Forest	1.00	1.00	1.00	1.00
	ANN	1.00	1.00	1.00	1.00
FLEXION OF LEG UP	Random Forest	1.00	1.00	1.00	1.00
	ANN	1.00	1.00	1.00	1.00
SITTING-EXTENSION	Random Forest	0.94	0.95	0.94	0.94
	ANN	1.00	1.00	1.00	1.00

INFERENCES FROM THE RESULTS

Figure 3,4 represents the Confusion Matrix of Random Forest and ANN. Figure 5 presents the accuracy obtained in each epoch for ANN. Figure 6 presents the accuracy obtained by Random Forest and ANN for all three movements. Table 5 presents the Evaluation results specified using Accuracy, Precision, Recall and F1 Score.

1. The Random Forest classifier correctly distinguishes Abnormal subjects from healthy subjects for the movement Gait and Flexion. It produces **100%** accuracy for Gait and Flexion movement and **94%** accuracy.
2. The ANN classifier correctly distinguishes Abnormal subjects from healthy subjects for all the three movements. It produces **100%** accuracy for three movements.
3. The Epochs is set to 2000 which is set by trial and error method.
 - i. Initially when Epochs was kept at 1000 the accuracy obtained was 87.5% but when Epochs increased to 2000 the accuracy obtained was 100%.
 - ii. Epochs which corresponds to the number of iterations plays a vital role in improving accuracy.

V. CONCLUSION

The proposed Framework provided movement-based analysis for the discrimination of osteoarthritis patients from healthy subjects. The movement considered for the classification of Osteoarthritis are Gait, Flexion and Extension. The Random Forest and ANN both provided 100 % accuracy for the movement Gait and Flexion. ANN provided a higher accuracy of 100 % than the Random Forest for the movement Extension. The appropriate pre-processing stage are Hyperparameters Tuning of Random Forest and Min Max Scaling of Random Forest which are based on the nature of the classifier is one of the reasons for yielding good accurate results. The proposed Framework performs better than the existing system [1]. The results obtained prove that the classifiers are efficient in early diagnosis of the osteoarthritis. The future work is to test the algorithms on the real time data which is to be collected from the lower limb and to automate the complete process.

REFERENCES

1. Jean de Dieu Uwiseneyimana et al, "Diagnosing Knee Arthritis Using Artificial Neural Network and Deep Learning", Biomedical Statistics and Informatics, 29 March 2017.
2. Sumitra S Nair et al, The Application of Machine Learning Algorithms to the Analysis of Electromyographic Patterns of Arthritis Patients, IEEE Transaction on Neural Systems and Rehabilitation Engineering, Vol 18, No2, April 2010.
3. Serafeim Moustakidis et al, "Application of Machine Intelligence for Osteoarthritis classification: A Classical Implementation and Quantum Perspective, Quantum Machine Intelligence, 29 September 2019.
4. Kokkotis et al, "Machine Learning in Knee Osteoarthritis: A review", Osteoarthritis and Cartilage Open, 17 April 2020.
5. Xin Chen et al, "Entropy Based Surface Electromyogram Feature Extraction for Knee Osteoarthritis Classification, IEEE Transactions and Journal, 2016.
6. Pedregosa et al., "Scikit-learn: Machine Learning in Python", JMLR 12, pp. 2825-2830, 2011.
7. Buitinck et al., "API design for machine learning software: experiences from the scikit-learn project", 2013.
8. Gerard Biau et al, "Analysis of a Random Forests Model", Journal of Machine Learning Research 13 (2012).
9. Vidushi Sharma et al, "A Comprehensive Study of Artificial Neural Networks", International Journal of Advanced Research in Computer Science and Software Engineering, Volume 2, Issue 10, October 2012
10. Saranya et al, "A Study on Normalization Techniques for Privacy Preserving Data Mining.", International Journal of Engineering and Technology (IJET), 2013
11. J. Too, A. R. Abdullah, N. Mohd Saad, and W. Tee, "EMG Feature Selection and Classification Using a Pbest-Guide Binary Particle Swarm Optimization," Computation, vol. 7, no. 1, 2019.
12. J. Too, A. R. Abdullah, and N. Mohd Saad, "Classification of Hand Movements based on Discrete Wavelet Transform and Enhanced Feature Extraction," Int. J. Adv. Comput. Sci. Appl., vol. 10, no. 6, 2019.
13. Dipak C. Vaghela et al, "Design, Simulation and Development of Bandpass Filter", International Journal of Engineering Development and Research, Volume 3, Issue 2 1015
14. Hossin, Mohammad & M.N, Sulaiman., "A Review on Evaluation Metrics for Data Classification Evaluations.", International Journal of Data Mining & Knowledge Management Process, 2015.

15. Jiajia Wu, “sEMG Signal Processing Methods: A Review”, IOP Conf. Series: Journal of Physics: Conf. Series 1237 (2019)
16. Jihye Lim et al, “A Deep Neural Network-Based Method for Early Detection of Osteoarthritis Using Statistical Data”, International Journal of Environmental Research and Public Health — Open Access Journal, 2019
17. M. Herrera-González, G. Martínez-Hernández, J. Rodríguez-Sotelo and O. Avilés-Sánchez, “Knee functional state classification using surface electromyographic and goniometric signals by means artificial neural networks”, Ing. Univ., vol. 19, no. 1, pp. 51-66, Ene., Jun., 2015.
18. Nima Befrui et al, “Vibroarthrography for Early Detection of Knee Osteoarthritis Using Normalized Frequency Features”, Medical & Biological Engineering & Computing, February 2018.
19. Tiulpin, A., et al, “Multimodal Machine Learning-based Knee Osteoarthritis Progression Prediction from Plain Radiographs and Clinical Data.”, Sci Rep 9, 20038 (2019). <https://doi.org/10.1038/s41598-019-56527-3>.
20. Goutte C. et al, “A Probabilistic Interpretation of Precision, Recall and F-Score, with Implication for Evaluation.” In: Losada D.E., Fernández-Luna J.M. (eds) Advances in Information Retrieval. ECIR 2005. Lecture Notes in Computer Science, vol 3408. Springer, Berlin, Heidelberg. 2005.
21. Nazia Gillani, “Human Gait Phase Detection using Convolution Neural Network-Based Prediction Engine”, innovate FPGA.
22. “DVT: Guidelines for Activity and Exercise”, North American Thrombosis Forum.
23. Tonye Ogele CNX, “Anatomy and Physiology”, OpenStax.

Breast Cancer Prediction Using Machine Learning Algorithms

Kavitha Chinniyar and Roobini Subramani

Department of Computer Science and Engineering, PSG College of Technology Coimbatore, India

ABSTRACT

Breast Cancer is one of the major causes of death in women. Treatment against malicious cancer in tissue has led to numerous visual examinations for Breast cancer. In cancer research, classification of tissue samples is necessary for cancer diagnosis. This can be done with the help of quantitative inference and extraction models to prevent tissue from further growth. The classification of tissues surrounding the malicious cancer cells into benign and malignant categories is extremely challenging task to predict using data mining algorithms. In this paper, a novel quantitative inference of breast cancer tissues is examined using semi-supervised mechanism. In semi-supervised approach, the records in dataset are clustered using farthest first clustering. The clustered records are classified using Artificial Neural Network and Naive Bayesian classifiers. The proposed method is evaluated using k-fold cross validation. The Wisconsin Original breast cancer dataset from UCI Repository is used to test the efficiency of the proposed model. The experimental results demonstrate that, the proposed technique produces the best accuracy of 98.0% for Artificial Neural Network and 95.2% for Naive Bayesian Classifier. Among them, Artificial Neural Networks has proved to be one of the best classifier with 2.8% of improved accuracy.

Keywords— Artificial Neural Network, Prediction, Accuracy, Decision Tree, Simulated Annealing

I. INTRODUCTION

Machine learning methods are extensively used in medical application which includes identification and classification of tumours. Machine learning is improving in diagnostics, to predict outcomes, and begins to scratch the surface of personalized care. It is mainly used as an aid for cancer diagnosis and prediction. Researchers have recently involved in pertaining the machine learning techniques towards cancer prediction and prognosis. Machine learning is a more powerful arena because it allows decisions to be made which could not be possibly made using conventional methodologies [15]. Predictive analytics is one of the areas in data mining which deals with extracting information from data and used to predict the trends and behaviour patterns. Predictive analytics is a high level statistical method which has an ability to build predictive models [16]. Breast cancer is an important research topic in medical science. Breast cancer is the most common invasive cancer among women, with more than one million cases and deaths occurring worldwide annually. The most effective way to reduce breast cancer death is to detect at an earlier stage [28]. The main objective is to predict the breast cancer in advance that ensures a long survival of patients. A complicated test for the main diagnosis of breast cancer makes it difficult to obtain the results as cancer or non-cancer [18]. In predictive analytics, predicting the outcome of a disease is one of the most fascinating and challenging tasks. The machine learning algorithms could be used directly to find the final result as cancer or non-cancer by exploiting various data mining techniques. There are several possible solutions for early diagnosis with accurate prediction of breast cancer such as supervised and unsupervised learning [23]. Supervised Learning includes Decision tree, a popular classification approaches in knowledge discovery and data mining, which classifies the labeled trained data into a tree or rules [21], Artificial Neural Network (ANN) is a mathematical model or computational model based on biological neural networks, K- nearest neighbor (Knn) is used to classify the building model [26], SVM built optimal separating boundary between datasets to solve optimization problem and the association rule discovery techniques to construct classification systems [22]. Unsupervised learning includes clustering which discovers useful patterns within the data. Semi -Supervised learning is also called as inductive learning which is used to infer the correct label for unlabeled dataset [17].

II. RELATED WORK

MeghaRathi and VikasPareek [4] suggest a framework which has Data Pre-processing, Feature selection, Feature Subset and different classifiers for making prediction. The data pre-processing is used to remove data-inconsistency and irrelevant data. The feature selection is used to extract subset of features using MRMR (Maximum Relevance and Minimum Redundancy) algorithm. It is used for selection of features and to improve the accuracy of classifiers by selecting subset of features. Four classifiers such as End Meta, Naive Bayes, SVM (Support Vector Machine), and FT (Function Tree) is used. After extracting the relevant features from the data set, classifier is applied to check the performance in terms of accuracy. The classifiers are trained using training set, and then classification algorithm is applied one by one and SVM with MRMR produces better results. The

disadvantage is selected features are correlated strongly and it is mutually far away from each other due to which it has high correlation and redundant features.

Hamid Mohamadi, JafarHabibi, Mohammad SanieeAbadehand HamidSaadi [7] proposes a simulated annealing based Fuzzy Classification System (SAFCS). SAFCS generates a fuzzy if-then rules and temperature initialization. The procedure is repeated k times. Then temperature is decremented using cooling parameter and iterates until the stopping criterion is reached. SAFCS is compared with C4.5 which is based on entropy criteria and pruning techniques, in order to discard the parts of a tree. These classification methods are applied to different datasets, among them SAFCS achieves better results in terms of accuracy for both training set and testing set. The disadvantage of SAFCS is difficult to fix the cooling parameter and time consuming.

Animesh Hazra, Subrata Kumar Mandal, Amit Gupta [8] the main objective is to find the smallest subset of features that can ensure a best accurate classification of breast cancer. It compares three classifiers Naïve bayes, SVM and ensemble classifier. After pre-processing, the comparison is carried out in three ways such as Feature selection using Pearson correlation coefficient, Pearson correlation with binning and principal component analysis. The Pearson correlation is used to reveal about how much the class attributes and attributes of data set are related based on which the features are ranked. In second methodology after data cleaning and Pearson correlation coefficient, discretization of binning technique was applied. In the next method, feature extraction was performed with principal component analysis (PCA) after pre-processing. Then classification technique was applied, among all classifiers naïve bayes provides better accuracy percentage and time complexity. The disadvantage is execution time for prediction model and PCA maps the data into lower dimensional space due to which performance of classifier is degraded.

Mohamed Junaid.K.A, [10] discusses about two layer neural network back propagation algorithm. During learning phase, the network learns by adjusting the weights and takes longer learning time. As a result, parallelization techniques are used to speed up the computation process and outperforms in terms of accuracy. As a result of two layer neural networks, parallelization techniques are used to speed up the computation process and outperforms in terms of accuracy. The disadvantage of this approach is too many hidden neurons and difficult to train the network.

Deepshree A.Vadeyar, Yogish H.K [11] focuses on farthest first clustering for reorganization of website structure to improve user navigation. The websites are considered as a graph, each node as a web page, redirecting URL between pages as edges and links are represented as 1/0. The clusters are formed in which URL acts as objects for cluster and a threshold criterion is set for clusters [5]. The website structure depends on the threshold criterion of the clustering. It is difficult to assign the threshold criterion is the disadvantage.

SunitaSoni, O.P.Vyas [12] discusses about association rule mining, associative classifiers and advanced classifier rule mining. Classification using association rule mining is a predictive analytics technique which discovers a subset of rules to predict an accurate classifier called Classifier Association Rule (CAR). The advanced CAR provides better accuracy which depends on set of rules before applying classifiers. The associative classifiers using Fuzzy association rule, deals with sharp boundary problems. The fuzzy and weighted associative classifier provides a greater accuracy when compared to other associative classifiers. The disadvantage is difficulty in handling temporal data which is being dynamic. The rules predicted are not static and it has additionally related attributes.

Ibrahim M. El-Hasnony, Hazem M. El-Bakry, Ahmed A. Saleh [13] discusses a hybrid methodology of K-means, Feature reduction with feature selection (FRFS) and discernibility K-nearest neighbor (D-Knn) classifier. The hybrid feature selection and data reduction method is used for combining the rough set features and calculating the attribute dependencies. The classifier makes decisions at each point and classifies the data by contrasting test set is called Instance based learning (IBL). Knn assumes that class label for each record is same for nearest neighbor which is simple that helps to enhance its predictive accuracy. The disadvantage is to determine value of parameter computation cost is quite high.

III. METHODOLOGIES

The following are the research methods employed in this paper.

A. Data collection and Pre- Processing

The dataset is collected from UCI Machine learning data repository of Wisconsin (Original) Breast cancer dataset (WBC). WBC has 699 instances, 2 class labels (2 for Benign/4 for Malignant) and 11 attributes. The attributes are integer valued. The WBC dataset is provided in Table I.

Table I. Dataset Description

S.NO	ATTRIBUTE	DOMAIN
1.	Sample Code Number	Id number
2.	Clump Thickness	1-10
3.	Uniformity of Cell Size	1-10
4.	Uniformity of Cell Shape	1-10
5.	Marginal Adhesion	1-10
6.	Single Epithelial Cell Size	1-10
7.	Bare Nuclei	1-10
8.	Bland Chromatin	1-10
9.	Normal Nucleoli	1-10
10.	Mitoses	1-10
11.	Class	2-benign, 4-malignant

The dataset contains missing values ‘?’ is pre-processed by single imputation method, i.e., the mean value of a variable. The advantage is sample mean remains unchanged [25].

B. Fuzzy C-Means Clustering

The clustering has been classified as soft clustering and hard Clustering. In hard clustering, the data point belongs to exactly one cluster. In Soft Clustering, the data point can belong to more than one cluster [14]. The Fuzzy C-Means Clustering (FCM) algorithm is an unsupervised and soft clustering algorithm, which introduces the fuzziness for an object. The main limitations are sensitive to noises, minimizes an objective function and difficult to select appropriate parameters. The algorithm is provided in Table II.

In algorithm, where

K= Number of Iterations

V_j = j^{th} cluster center

m= Fuzziness Index [1,∞]

C= Number of Cluster Center

μ_{ij} = membership of i^{th} data to j^{th} cluster center

d_{ij} = Euclidian distance between i^{th} data and j^{th} cluster center

x_i = Original data point

n = Number of Data Points

Table II.Fuzzy C-Means Clustering Algorithm

<p>Algorithm: Fuzzy C-means Clustering Algorithm</p> <p>Input : Pre-processed dataset</p> <p>Output : Clustered cancer dataset</p> <ol style="list-style-type: none"> 1. Randomly ‘C’ Cluster centres are selected. 2. Calculate fuzzy membership matrix. $\mu_{ij} = 1 / \sum_{k=1}^c (d_{ij} / d_{ik})^{(2/m-1)}$ <ol style="list-style-type: none"> 3. Compute Fuzzy centers ‘V_j’ using $V_j = \left(\sum_{i=1}^n ((\mu_{ij})^m x_i) / \sum_{i=1}^n ((\mu_{ij})^m) \right), \forall j = 1, 2..c$ <ol style="list-style-type: none"> 4. Repeat 2 & 3 until minimum J value is achieved $J(u, v) = \sum_{i=1}^n \sum_{j=1}^c ((\mu_{ij})^m) (\ x_i - v_j\ ^2)$

C. Simulated Annealing

Simulated Annealing is an iterative method which is mainly used as an optimization search paradigm to escape from local minima and to achieve global optima. This optimization can be done by accepting moves which degrades the probability on a parameter called temperature. The temperature is gradually decreased by using cooling schedule [1]. The algorithm behavior ends when the temperature reaches to zero. The parameter required for simulated annealing are starting temperature, final temperature and temperature decrement. The final cluster structure depends on how the cooling is performed [9]. The ideal cooling rate is difficult to compute. The temperature decrement is given by,

$$f(t) = t \alpha \quad (1)$$

Where,

t = time in minutes, which lies between [1, ∞]

α = Cooling rate which lies between 0.5 - 0.99

D. Decision Tree [C4.5]

Decision Tree is a supervised algorithm which can be used for classification problems. C4.5 is also a type of decision tree which is improved from ID3 algorithm by dealing with both continuous and discrete attributes, missing values and pruning trees [2]. C4.5 builds decision trees from a set of training data by calculating the information gain for each attribute. The complexity of a decision tree is, the tree becomes unstable even when there is a small change in entropy value [21]. It will result in a generation of different tree. The sub trees replicated several times.

$$\text{Entropy}(S) = -\frac{p}{p+n} \log_2 \left(\frac{p}{p+n} \right) - \frac{n}{p+n} \log_2 \left(\frac{n}{p+n} \right) \quad (2)$$

The attribute with highest information gain is taken as a root for decision tree [27]. In the equation 2, where

p = Number of positive classes

n = Number of negative classes.

The algorithm steps are provided in Table III.

Table III. Decision Tree [C4.5] Algorithm

```
Algorithm: Decision Tree (C4.5)  
Input : Training dataset (D)  
Output : Decision Tree (T)  
Tree{  
if D is "pure" OR other stopping criteria met then  
    terminate  
end if  
for all attribute a ∈ D do  
    Compute information gain to split on 'a'  
end for  
abest = Best attribute according to gain calculated  
Tree = Create a decision node that tests abest in the  
    root  
Dv = Induced sub – datasets from D based on abest  
for all Dv do  
    Treev = C4.5(Dv)  
    Attach Treev to the corresponding branch of tree  
end for  
return Tree
```

E. Farthest First Clustering algorithm

Farthest First clustering is a type of Hard Clustering algorithm in which one data point can belong to only one cluster [20]. It is similar to K-Means clustering algorithm it chooses centroids and assigns objects in cluster with max distance. Farthest first clustering solves k-center problem and it is very efficient for large set of data. In farthest first algorithm, the mean for calculating centroid is not required which takes centroid arbitrary and distance of one centroid from other is maximum [24]. After calculating centroid, the points with minimum

distance are assigned to clusters. The algorithm is provided in Table IV.

Table IV. Farthest First Clustering Algorithm

<p>Algorithm: Farthest First Clustering</p> <p>Input : Pre-processed dataset</p> <p>Output : Clustered cancer dataset</p> <p>Steps :</p> <ol style="list-style-type: none"> 1. Pick any data point and label it as point 1 2. For $i=2,3,\dots,n$ 3. Find the unlabelled point furthest from $\{1,2,\dots,i-1\}$ and label it as i. //Use $d(x,S) = \min_{y \in S} d(x,y)$ to identify the distance of a point from a set 4. $\pi(i) = \operatorname{argmin}_{j < i} d(i,j)$ 5. $R_i = d(i, \pi(i))$
--

F. Naïve Bayesian

In machine learning, naïve bayes algorithm is a simple probabilistic classifiers based on Bayes theorem with strong independence assumptions between the features [6]. Naive Bayes classifiers are highly scalable which requires a number of parameters to be linear and the number of variables (features/predictors) for training the model. Naive Bayesian classifier is based on Bayes' theorem and the theorem of total probability. The Advantages of Naïve Bayesian Model are:

- It is a simple classifier because it has an underlying probabilistic model.
- Requires only small amount of data to train the model.
- If the independence assumption holds well, NB Classifier performs well and provides better results.

The probability with vector $x = \langle x_1 \dots x_n \rangle$ belongs to hypothesis h is,

$$P(Y | X_1, \dots, X_n) = P(X_1, \dots, X_n | Y) / P(X_1, X_2, \dots, X_n) \quad (3)$$

Where, X = Number of predictors.

Y = Class of probability.

Table V. Back Propagation Algorithm

<p>Algorithm: Back propagation algorithm</p> <p>Input : Training dataset</p> <p>Output : Network model</p> <p>Steps :</p> <ol style="list-style-type: none"> 1. Initialize the weights and biases 2. The weights in the network are initialized to random numbers from the interval $[-1, 1]$. 3. Feed the training Sample 4. Propagate the input forward and we compute the net input and output of each unit in hidden and output layer. 5. Back propagate the error. Error is computed using $Err_k = O_k(1 - O_k)(T_k - O_k)$ 6. Weight function is $\Delta w_{ij} = (l) Err_j O_i$ 7. Biases is given by $\Delta \theta_j = (l) Err_j$

G. Artificial Neural Network

The artificial neural network (ANN) was implemented using back propagation architecture. Each of the layers has certain elements called as neurons, which has input layer, hidden layer and output layer. The input layer is selected based on the features and output layer has two neurons either as benign or malignant [15]. The transfer

function is computed as a weighted sum of input signals. The learning capability of an artificial neuron is achieved by adjusting the weights of neurons. Initially, the process is carried out as forward pass, then back propagation is applied to achieve target node. Back Propagation learns by iteratively processing a set of clustered samples. For each sample, weights are modified to minimize the error between network's classification and actual classification Process [29]. The algorithm of ANN is provided in Table V. The advantages of ANN are [30]:

- ANN is used to solve complex problems.
- Less effort is required to train the network model.
- Implicitly detects Complex non – linear relationship between dependent and independent variables.
- Ability to detect all possible interactions between predictor (attributes) variables.

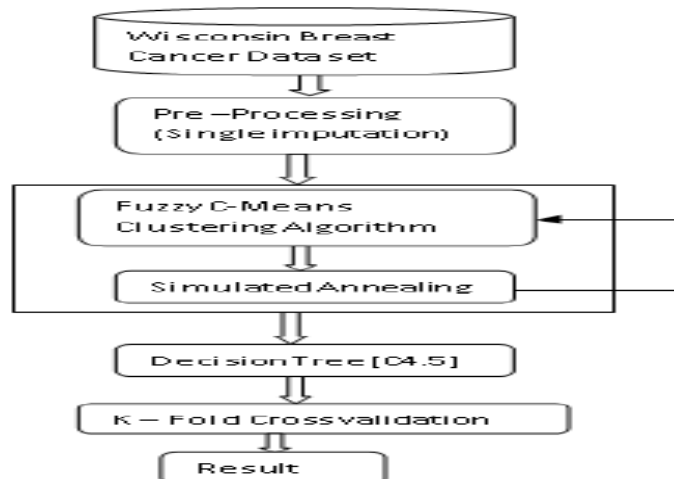


Figure. 1. Existing System Flow Chart

IV. SYSTEM DESIGN

In existing method, the combined approach such as Fuzzy C-means clustering with Simulated annealing and Decision tree (C4.5) classifier is used for diagnosis of breast cancer. The detailed working of the existing module is described as follows:

A. EXISTING SYSTEM

The dataset from UCI repository is used for prediction, in which single imputation pre-processing technique was used. Then in order to predict labels, FCM clustering is processed [1] on dataset which is then optimized using Simulated Annealing. In FCM, 'm' is a fuzziness index which measures the tolerance for clustering and its value lies between [1, ∞]. If the value of 'm' is larger, it has larger overlapping between clusters. m=1 for crisp and 2 for fuzzy clustering. In this research [19], m=1.4 is chosen as fuzzy index. Then, the clustered data is annealed for which the cooling schedule is chosen as $f(t)=4$. The starting and final temperature is chosen as minimum and maximum of a feature in a random manner. After clustering with annealing, C4.5 classifiers are used to classify the clustered dataset and labels are predicted either as Benign or Malignant. The model is then cross validated using K-fold cross validation, here K=10. The existing system flows as it is being provided in figure 1.

B. Disadvantages of existing model

The drawbacks of existing model are:

- FCM clustering takes $O(ndc^2i)$ as a computation time to cluster the dataset and optimized by simulated annealing

Where,

n = Number of Data Points.

d = Number of dimensions.

c = Number of Clusters.

i = Number of Iterations.

- FCM provides K-center problem ie. Distances between cluster centers should satisfy the theory, triangle of inequality.
- Computationally expensive, difficult to fix thresholds and cooling rate.
- In decision tree, normally over fitting occurs, then pruning is required due to which accuracy gets decreased.

C. PROPOSED SYSTEM

In proposed model, farthest first clustering and Naïve Bayesian model is used for diagnosis of breast cancer. Farthest first clustering is used to cluster the pre-processed dataset as given in table 3. In existing work, simulated annealing was used to optimize the clusters. The farthest first clustering does not provide local optimum even in worst case so it does not require optimization. Farthest first clustering always provides global optimum so, it guarantees to provide optimal solution. In our proposed model, two clusters are considered because it has only two labels such as benign and malignant. After clustering, Naïve Bayesian model and Artificial Neural Network is used to classify the clustered data and labels are predicted either as Benign or Malignant. Then, it is cross validated using K-fold cross validation. In this $k=10$, the dataset is divided into 10 equal subsets. Each subset acts as testing set, whereas the rest of the partition acts as training set. This procedure is repeated ten times so that each partition is used to test only once. The proposed system flows as it is being provided in figure 2.

D. Advantages of Proposed model

The advantages of proposed model are:

- FFC Clustering computation time is $O(nk)$

Where, n = Number of data points.

k = number of clusters.

- FFC achieves global optimum because it does not require iteration cluster formation takes place in a single pass.
- Farthest first solves K-center problem ie.,it achieves triangle of inequality property.
- Artificial Neural Network (ANN) and Naive Bayesian provide optimal solution because it performs well does not over fit.
- It is a simple classifier with high accuracy.

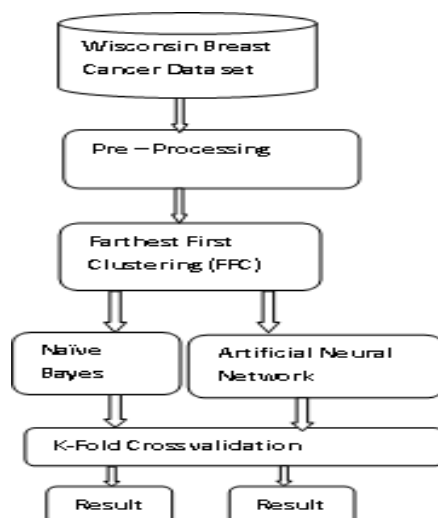


Figure 2. Proposed System Flow Chart

V. EXPERTIMENTS AND RESULTS

E. PERFORMANCE METRICS

In this experiment, the medical data related to breast cancer classification is initiated with the preprocessing using mean imputation which is followed by the farthest fast clustering. The clustered data is classified using artificial neural network and naive Bayes, to predict the tumors. The performance of classifier is validated based on error rate and mean accuracy. The performance metrics are precision, recall, F-Measure, error rate and accuracy [20].

F. PRECISION

Precision is a ratio of true positive tuple and all positive tuple in a dataset. It is used to measure the exactness or quality. Precision is given by,

$$\text{Precision} = \frac{TP}{TP + FP} \quad (4)$$

G. RECALL

Recall is a ratio of true positive tuple against positive and negative tuple. Recall is the measure of completeness or quality. It is also called as sensitivity. Recall is given by,

$$\text{Recall} = \frac{TP}{TP + FN} \quad (5)$$

H. F-MEASURE

F – Measure is also called as F – Score. F –Measure is a mean of precision and recall. F- Measure value varies from 0 to 1. If the value of F-Measure is higher, then it is said to be a better classifier. It is given by,

$$\text{F-Measure} = 2 * \frac{\text{Precision} * \text{Recall}}{\text{Precision} + \text{Recall}} \quad (6)$$

I. ACCURACY

The classifiers accuracy is an important metric for evaluation. It is a ratio of positive tuples and negative tuples against all the tuple. It is given by,

$$\text{Accuracy} = \frac{TP + TN}{TP + TN + FP + FN} \quad (7)$$

J. ERROR RATE

The error rate is an essential measure for evaluation. Lower error rate is said to be a better classifier. Error rate determines the error between the prediction and actual. It is given by,

$$\text{Error Rate} = \frac{FP + FN}{TP + TN + FP + FN} \quad (8)$$

Table VI: Confusion Matrix For Decision Tree [C4.5]

Testing & Training (%)	True positive (TP)	True Negative (TN)	False positive (FP)	False Negative (FN)
50 -50 %	219	0	130	0
60 – 40 %	172	0	108	0
75 - 25 %	110	0	65	0
80 – 20%	118	0	22	0
90 – 10 %	43	0	27	0

Table VII: Confusion Matrix For Naïve Bayes Model

Testing & Training (%)	True positive (TP)	True Negative (TN)	False positive (FP)	False Negative (FN)
50 -50 %	282	50	0	17
60 – 40 %	212	56	1	11
75 - 25 %	143	24	0	8
80 – 20%	110	22	0	8
90 – 10 %	57	10	0	3

K. CONFUSION MATRIX

The confusion matrix is used to describe the performance of a classifier. True positive (TP) refers to positive tuple and True Negative (TN) refers to negative tuple classified by the basic classifiers. False Positive (FP) refers to positive tuple but predicted as negative and False Negative (FN) refers to negative tuple but predicted as positive which is incorrectly classified by the classifiers. The training dataset is used to train the classifiers. The correctly classified instances and incorrectly classified instances for existing model ie., Decision Tree

[C4.5] is provided in the table VI. The Proposed model ie., Naïve Bayes model in table VII and Artificial Neural Network is provided in table VIII.

Table VIII: Confusion Matrix For Artificial Neural Network [Ann]

Testing & Training (%)	True positive (TP)	True Negative (TN)	False positive (FP)	False Negative (FN)
50 -50 %	291	49	1	8
60 – 40 %	218	56	1	5
75 - 25 %	145	24	0	6
80 – 20%	114	22	0	4
90 – 10 %	58	10	0	2

Table IX: Performance Metrics Evaluated For Fuzzy C-Means Clustering (Fcm) With Simulated Annealing (Sa) And Decision Tree C4.5

Testing & Training (%)	Precision	Recall	F-measure	Accuracy (%)	Error-rate
50 -50 %	0.6275	1.000	0.771	62.7%	0.3725
60-40%	0.614	1.000	0.760	61.4%	0.386
75-25%	0.6285	1.000	0.771	62.8%	0.3715
80-20%	0.84	1.000	0.91	84%	0.16
90-10%	0.614	1.000	0.760	61.4%	0.386
Balanced Average	0.6648	1.000	0.7944	66.4%	0.3352

Table X.: Evaluation Metrics Obtained For Farthest First Clustering And Naïve Bayesian Model

Testing & Training (%)	Precision	Recall	F-measure	Accuracy (%)	Error-rate
50 -50 %	1.000	0.943	0.970	95.1%	0.049
60-40%	0.9953	0.9506	0.9723	95.7%	0.043
75-25%	1.000	0.947	0.972	95.4%	0.046
80-20%	1.000	0.9322	0.964	94.2%	0.06
90-10%	1.000	0.95	0.974	95.7%	0.043
Balanced Average	0.9990	0.9445	0.9704	95.2%	0.048

L. RESULTS

The experiments have been done on R-studio of version 3.0.3. The results for existing and proposed model are shown in Table IX, X and X1. The table describes the performance of the model in terms of accuracy, precision, recall, f-measure and error rate. The result shows that the classifier with Farthest First Clustering (FFC) provides better accuracy with lower error rate. The Farthest First Clustering clusters the data with maximum distance. The quality of clusters depends on distance between the cluster centers should be farther and the cluster is said to be well formed. Farthest first clustering satisfies the criteria when compared to Fuzzy C-Means Clustering. The Farthest First Clustering with Artificial Neural Network provides a better balanced accuracy of 98.0%, lower error rate of 2% with all testing and training phases because ANN has a capability to solve a complex and mimic problem. Due to that, ANN can be used for many real world applications which give better results.

VI. CONCLUSION

In this paper, the prediction model for breast cancer is constructed by using classifiers with clustering. The performance of a model is analyzed by comparing the different classifiers with clustering. The Farthest First Clustering provides a better prediction compared to fuzzy clusters. The farthest first clustering with Naïve Bayes and Artificial Neural Network classifier provides balanced accuracy of 95.2% and 98.0%. Therefore, Farthest First Clustering [FFC] with Artificial Neural Network achieves an improved accuracy of 2.8% because ANN is a powerful machine learning algorithm. ANN is suggested as a better prediction model for diagnosis of breast cancer to ensure the long survival of patients. In future, ANN with genetic algorithm can be made as a hybrid model to predict the disease which evolves a huge remark in medical science [31].

REFERENCES

1. Sudipta Acharya, Sriparna Saha and Yamini Thadisina, "Multiojective Simulated Annealing-Based Clustering of Tissue Samples for Cancer Diagnosis", IEEE Journal of Biomedical and Health Informatics, vol 20, no.2, March 2016.

2. Sonia Singh and Priyanka Gupta, "Comparative Study Id3, Cart and C4.5 Decision Tree Algorithm: A Survey", International Journal of Advanced Information Science and Technology (IJAIST), vol.27, no.27, July 2014.
3. K.Vembandasamy, T.Karthikeyan, "Novel outlier detection in diabetics Classification Using Data Mining techniques", International Journal of Applied Engineering Research, ISSN 0973 – 4562, Vol 11, 2016.
4. MeghaRathi, VikasPareek, "Hybrid Approach to predict Breast Cancer using Machine Learning Techniques", International Journal of Computer Science and engineering, May 2016.
5. Digambar A Kulkarni, Vijaylaxmi K Kochari, "Detection of Breast Cancer Using K Means Algorithm" in International Journal of Emerging Technology and Advanced Engineering Volume 6, Issue 4, April 2016.
6. Murat Karabatak, "A new classifier for breast cancer detection based on Naïve Bayesian in Measurement", Elsevier Science Direct, 2015.
7. Hamid Mohamadi, JafarHabibi, Mohammad SanieeAbadehand HamidSaadi," Data Mining with a simulated annealing based fuzzy classification system", Elsevier Science Direct, pp.1824 – 1833, Nov 2013.
8. AnimeshHazra, Subrata Kumar Mandal, Amit Gupta, "Study and Analysis of Breast Cancer Cell Detection using Naïve Bayes, SVM and Ensemble Algorithms", International Journal of Computer Applications (0975 – 8887) Volume 145 – No.2, July 2016.
9. Wei Yang, Luis Rueda, AliouneNgom, "A Simulated Annealing Approach to Find the Optimal Parameters for Fuzzy Clustering Microarray Data", Elsevier Science Direct, December 2014.
10. Mohamed Junaid.K.A, "Classification Using Two Layer Neural Network Back Propagation Algorithm", Scientific research publishing, June 2016.
11. Deepshree A.Vadeyar, Yogish H.K, "Farthest First Clustering in Links Reorganization", International Journal of Web & Semantic Technology (IJWesT) Vol.5, No.3, July 2014.
12. SunitaSoni, O.P.Vyas,"Using Associative Classifiers for Predictive Analysis in Health Care Data Mining", International Journal of Computer Applications (0975 – 8887) Volume 4 – No.5, July 2010.
13. Ibrahim M. El-Hasnony, Hazem M. El-Bakry, Ahmed A. Saleh, "Classification of Breast Cancer Using Softcomputing Techniques", International Journal of Electronics and Information Engineering, Vol.4, No.1, PP.45-54, Mar. 2016.
14. Tejwant Singh and Mr. Manish Mahajan, "Performance Comparison of Fuzzy C Means with Respect to Other Clustering Algorithm", International Journal of Advanced Research in Computer Science and Software Engineering (IJARCSSE), vol 4, Issue 5, pp.89-93, May 2015.
15. M.Sheha, M.S. Mabrouk, and A. Sharawy, "Automatic detection of melanoma skin cancer using texture analysis," Int. J. Comput. Appl., vol. 42, no. 20, pp. 22–26, Mar. 2012.
16. Knox H.Todd, "Cancer facts and figures 2012," American Cancer Society, Atlanta, GA, USA, 2012.
17. U. Maulik, A. Mukhopadhyay, and D. Chakraborty, "Gene-expression based cancer subtypes prediction through feature selection and transductive SVM," IEEE Trans. Biomed. Eng., vol. 60, no. 4, pp. 1111–1117, 2013.
18. S.C. Dinger, M. A. Van Wyk, S. Carmona, and D. M. Rubin, "Clustering gene expression data using a diffraction inspired framework", Biomed. Eng. Online, vol. 11, no. 1, p. 85, 2012.
19. S. Saha, A. Ekbal, K. Gupta, and S. Bandyopadhyay, "Gene expression data clustering using a multiobjective symmetry based clustering technique," Comput. Biol. Med. vol. 43.11, pp. 1965–1977, 2013.
20. DelshiHowsalya Devi R and Dr. M Indra Devi, "Outlier Detection Algorithm Combined With Decision Tree Classifier for Early Diagnosis of Breast Cancer", International Journal of advanced engineering and technology(IJAE), vol. VII, Issue II, pp.93-98, April-June 2016.
21. K.Sivakami, "Mining Big Data: Breast Cancer Prediction using DT - SVM Hybrid Model", International Journal of Scientific Engineering and Applied Science (IJSEAS), vol.1, Issue5, pp.418-429, August 2015.

22. SmrutiRekha Das, Pradeepta Kumar Panigrahi, Kaberi DaS and Debahuti Mishra, "Improving RBF Kernel Function of Support Vector Machine using Particle Swarm Optimization", International Journal of Advanced Computer Research, vol-2, no-4, Issue-7, ISSN : 2249-7277 December 2012.
23. Cuong Nguyen, Yong Wang and Ha Nam Nguyen, "Random forest classifier combined with feature selection for breast cancer diagnosis and prognostic", J. Biomedical Science and Engineering, pp.552-560, May 2013.
24. S.Kharya, D.Dubey, and S.Soni, "Predictive Machine Learning Techniques for Breast Cancer Detection" International Journal Computer Science and Information Technologies, Vol. 4, Issue 6, pp.1023-1028, Nov – Dec 2013.
25. K.Arutchelvan and Dr.R.Periyasamy, "Cancer Prediction System Using Data mining Techniques", International Research Journal of Engineering and Technology (IRJET), ISSN: 2395-0056, Vol.02, Issue 08, Nov a2015.
26. J.S.Raikwal and KanakSaxena, "Performance Evaluation of SVM and K-Nearest Neighbour Algorithm Over Medical Data Set" , International Journal of Computer Applications, vol.50, no.14, pp.35-39, July 2012.
27. Jahanavi Joshi, RinalDoshi, "Diagnosis and prognosis of Breast Cancer using Classification rules", International Journal of Engineering research and General Science, Vol 2, Issue 6, October – November, 2014.
28. Souad Demigha, "Data Mining for Breast Cancer Screening", IEEE Spectrum, Sep 2015.
29. R. R. Janghel, Anupam Shukla, Ritu Tiwari "Breast Cancer Diagnosis using Artificial Neural Network Models ", IEEE Spectrum, Aug 2010.
30. Mihir Borkar, Prof. Khushali Deulkar, Abhinav Garg, "Prediction of Breast Cancer Using Artificial Neural Networks", International Journal of Engineering Research & Technology (IJERT), ISSN: 2278-0181, Vol. 4 Issue 09, Sep 2015.
31. M.Deepika*, L.Mary Gladence, R.Madhu Keerthana, "A review on prediction of Breast Cancer using various Datamining Techniques", Research Journal Of Pharmaceutical, Biological and Clinical Sciences (RJPBCS), ISSN : 0975-8585, Jan- Feb 2016.

A Review on Gait Analysis and Supporting Systems to Sense and Prevent Elderly Fall

R. Ramachandran and P. Kanakaraj

Department of Fashion Technology, PSG College of Technology, Coimbatore-641004, India

ABSTRACT

The elderly people are facing more physical and psychological problems. It has been estimated that major number of elderly people are injured due to recurrent falls which may also lead to death at certain cases. The elderly people have low bone density which makes fractures and cracks in the bone more severe leading to surgery for recovery. But the doctors will not suggest surgery on elderly people as it takes longer recovery period compared to younger people. The money spent on fractures and surgeries on elderly people is usually high. The elderly people will require a caretaker beside them the whole day which makes the elderly people dependent.

From the statistic data of regional review on —Falls in elder people, it has found that the elderly people end up falling majorly in sitting. In the perspective of preventing elderly from injury due to major fall, lot of preventive systems to sense and detect fall have been designed. The available safety wears protect the elderly only when they end up falling in x or y directions. But it is important to protect elderly people when they fall in sitting position. In this connection a detailed study on falling motions of the elderly people has been done and recorded in terms of angular velocity and angular acceleration and presented here.

Keywords: elderly fall, fall preventers, gait analysis, gait parameters, support systems, wearable air bag

I. INTRODUCTION

India is the second packed country having 7.7% of people maturing more than 60 years. Old fall is one of the main problem looked by everyone and is considered as "Geriatric Monsters". The repeated fall causes mortality and indisposition among the more seasoned people and realizing poor cerebral and physical condition. Strong inadequacy, in taking even more extreme pharmaceuticals, assistive device usage, step shortcomings are a part of the risk segments of fall. In an examination, surveying prosperity conditions in old people, it had been found that the recurrence of tumble to be 14%. Repetitive falls happens as a result of where it tallies causes require evaluation of focal remedial conditions which require progressively preventive measures.

With the true objective to improve old therapeutic issues progressively preventive advances ought to be taken. The one area where we can help older with getting away from torment is that the injuries happen due to fall. There are various prosperity organizations are being driven by administrative and non-authoritative relationship concerning the expectation of older fall wounds and its preventive measures. Physical injuries in view of fall will diminish the noticeable quality of life and limits their execution of ADL's (Activity of Daily Living). Head wounds and breaks are most noteworthy issues due to older fall. In like manner the older people need to stay in mending community for longer period as their recovery from bone split will take longer time than progressively young people. A portion of the time the patients need to encounter therapeutic systems like plating on account of anomalous condition of break which will before long on the grounds that greater torment to persevering. Consequently a couple of tests are being done on stroll of the older people step by step works out, to assess the chances of fall due their poor walk system.

Lot of supportive systems has been developed to detect and prevent the fall of elderly people. The system that senses the angle of fall and send communication to medical assistance so that immediate attention can be given those who are residing without any assistance. Few systems apart from sensing, prevents the heavy damage to the bones especially hip fractures, with the help of textile materials. This paper reviews the factors influencing the fall of elderly people with gait analysis and the different methods used for sensing and preventing the fall of elderly.

II. CAUSES OF FALLS IN THE ELDERLY

Falls are the main cause for injury-related visits to hospitals and the prime cause for accidental deaths of senior citizen around the age 65 and above. The death rate resulting from fall increase every year with 70% in elderly people above the age 75. A survey says that 90% of these fall result in hip fractures in persons over 70 years of age.

Risk factors for falls

The more established age individuals at 75 years old or more and the general population who are living alone in homes and so on are more prone to fall. The persons with changes in nervous system, science of the body developments (i.e., impeded response time; postural precariousness are having a higher risk of fall [1].

Common causes of falls

Falls because of parity issue, step unsettling influence and visual issue are the fundamental physical shortfalls bringing about falls. Different causes incorporate liquor utilization, Central Nervous System (CNS) issue and unending conditions like Neuromuscular issue, recently cleaned floors or wet floors, for example, in restroom, dim light, rugs or mats that are not appropriately anchored, reaching for capacity regions, for example, cabinets, stairs [2].

Intrinsic Factors

Because of physical and mental changes identified with maturing, the vast majority of the elderly individuals turn out to be more helpless to falls when they confront any test. Patients with inborn conditions, for example, vertigo, tumor and lower leg shortcoming are at higher dangers of falling which results in wounds. Adjustment in psychological, musculoskeletal, visual and vestibular capacities, constant maladies and various solutions add to falls.

The medications associated with higher risks of falls include tricyclic antidepressants and heterocyclic antidepressants. Particular Serotonin Reuptake Inhibitor (SSRI) antidepressants are free of reactions of tricyclic antidepressants. So SSRI antidepressants are more secure to utilize [1].

Extrinsic factors

Extrinsic factors incorporate poor lighting, perilous staircase and sporadic floor surfaces. Amid routine exercises, slight elderly individuals fall and harm themselves in home. Energetic more established individuals partake in powerful exercises and experience the ill effects of unintentional falls, for example, in stairs or new territories path from home [1].

III DISORDER THAT CAUSE FALLS IN THE ELDERLY

Visual impairment

Vision is one of the important factor in stabilizing the balance by means of supporting the nervous system with regular and continuous update of information for positioning and moving the body parts in relation to the environment. Impaired vision can have antagonistic impact on the capacity to embrace the everyday exercises.

Poor vision lessens the postural security of the elderly individuals. Visual misfortune is correctable in more seasoned individuals by normal eye examinations, utilization of right endorsed glasses, cataract medical procedure [3].

MOBILITY

Loss of mobility is found as social, mental, and physical results. Loss of mobility is because of more established age, low physical action, corpulence, debilitated quality and balance, and ceaseless illnesses, for example, diabetes. Mobility depends intensely upon equalization. Standard exercise can enable the body to manufacture quality and stay flexible. As you age, energy levels can decrease; this can be reduced by eating a healthy diet.

DEPRESSION

Depression among the older people is a serious problem. Elderly populations are at high risk of depression which may cause fall among them. Incapacity, Poor Social Support and health are some of the factors which causes serious depression on the older people.

It is clear that depression as an illness is a common factor among the older people. This can be avoided by not letting the elder people to live alone [4].

FUNCTIONAL DISABILITY

Incapacity in the elderly can be gathered into two different ways. One is who can deal with their day by day exercises with the assistance of mechanical gadgets and the other one is who have various medical issues and extreme restrictions in mental and physical working that require exceptionally escalated levels of consideration.

The elderly populace is at more serious danger of being less sound than the non-elderly populace. The disability was relatively less among men than among women [3].

Systolic blood pressure

Increased blood pressure is the major risk factor for cardiovascular diseases, which also leads to falls in the elderly people. Blood pressure ought to be begun gradually in more seasoned individuals and expanded progressively. This evades a sudden drop in blood pressure levels. There are numerous ways of life changes that we can make to bring down the danger of hypertension and to maintain a strategic distance from fall wounds. They are, cut down on salt, drink less liquor, do not smoke and oversee pressure [2].

IV GAIT ANALYSIS

METHODS OF ANALYSIS

Alvaro Muro-de-la-Herran [27] introduced a review of the techniques utilized in analysis and recognition of the human step from three unique methodologies: picture preparing, floor sensors and sensors set on the body. Advancement in new innovations has driven the improvement of a progression of gadgets and systems which take into account target assessment, making measurements more proficient and effective and providing researchers with reliable data.

Human gait can be classified into two methodologies and they dependent on

- i. NWS - non-wearable sensors
- ii. WS - wearable sensors

NWS setup is where the sensors are found and get information on the step when the elders fall on a specified walkway.

Whereas, WS setup makes it conceivable to examine information outside the research center and get data of human gait during the individual's regular exercises. There is likewise a third classification of hybrid setup that utilizes both of the two techniques.

NWS setup shall be grouped into two sub categories:

Those dependent on image processing (IP); and Those dependent on floor sensors (FS).

IP structures collect information about human gait with at least one optical sensor and take objective measurements of unique parameters through advanced image manipulation. Simple or computerized cameras are the for the most part generally utilized devices. Different kinds of optic sensors are used. The FS frameworks depend on sensors situated along the floor on the alleged force platform where the gait data is estimated through pressure sensors and ground reaction force sensors (GRF) which estimates the force applied by the subject's feet on the surface when subject falls.

Gait Parameters

From the clinical perspective, the significance of human gait investigation be positioned in the circumstance that gait issue influence a high level of the total populace. The principal symptoms of some neurological illnesses are improper balance, an fundamentally slower pace, with a phase showing sustain on the both the feet.

A fundamental ailment described by lower bone mass and weakened bone micro architecture, which implies more delicate bones and more serious danger of breaks. In the elderly, physical exercise majorly affects osteoporosis since it altogether anticipates falls, which are the greatest hazard factor for this age aggregate. In this way, assessment of gait quality might be profitable for early diagnosis.

Gait speed is a simple test that can distinguish subgroups of elderly patients who run a higher danger of death and serious grimness following heart medical procedure. Researchers evaluate patients' health by utilizing different techniques that measure the parameters which represent to the human gait such as velocity, step or walk length, width of the step, distance covered etc.

Recent research in gait analysis, contrasting the advantages and disadvantages of unique techniques, does not include the need to extend the WS framework's estimated threshold, although the objective evaluation of a variety of parameters is the ultimate goal of providing clients with day-to-day exercise during long-term panic periods [27].

Changing gait speed changed the age coefficient size from 62 to 86% for temporal variability measures, 25% for phase length fluctuations, and 5 to 12% for phase width anomaly [28].

Elderly fall hazard evaluation and forecast dependent on gait analysis

To build up a basic fall forecast framework, a three dimensional accelerometer and a mobile phone are used. Accelerometer provides a cost efficient method to monitor a human walking. In the gait assessment stability and symmetry of the step are checked and ascertained and henceforth the person's walk can be assessed. This gait assessment model is used to predict the fall risks of walking subjects. This gait assessment has given better investigation results, for example, better execution of forecast and effectiveness [5].

Normal gait analysis

Automatic adjustment can be done by human body to achieve balance and stability. Normal walking legs with exchanging arms normally swing development, and the development bearing of one arm is distinctive with the bilateral leg, yet predictable with the opposite side of the leg. The situation of lower leg and knee, hip edge changes amid movement for coordination. The walking speed diminishes with ageing [5].

V FALL PREVENTION METHOD

Fall preventers

The fall preventers decrease the need for emergency treatment but not so successful. The hip protector pads shown in the fig.1 are placed into the garments in the right position in the place of hip area. It is not successful because the pocket containing the pad can move from the hip area during falls and it restricts the daily activities so it is refused to be used by the seniors [6]. The air bag coat has an accelerometer that recognizes falls and triggers the road impact [7].



Figure 1. Hip protectors

FALL DETECTORS

The fall detector comprises of wristband composed of triboelectric generator and a lithium battery associated with coordinated sensors, controllers and remote units. The stretchable conductive nylon covered with Ethoxylated Polyethylenimine is utilized as terminals, interconnections amplify the work execution of triboelectric generator. The electrical vitality created in generator however body developments energize the battery. The 3-pivot accelerometer and the hardware record human body movements and sends data. This sends the message to versatile phone [8].

VI WEARABLE AIRBAG SYSTEM

The requirements of wearable airbag are listed as follows:

- It must have the capacity to distinguish the fall and ensure the wearer during standing or strolling.
- It should be compact and less in weight.
- It must be able to distinguish daily activities and falls, inflate only during the fall occurrence [20].
- It must be less expensive [21].

Reliability of the Airbag System

- The sensor and the system should not bring damage to the subject at any situation.
- The airbag must be loaded up with adequate measure of gas before the subject falls on the ground [21].

Motion Tracking Sensors

3-axis accelerometer

The 3-axis accelerometer estimates increasing speed in x, y and z-axes which in different terms it quantifies angular acceleration [9].

Gyroscope

The angular velocity in x, y and z-directions is measured using Gyroscope and is used along with 3-axis accelerometer for motion tracking [10].

Proximity sensor

A proximity sensor sends an electromagnetic field or electromagnetic radiation and searches for return signal. The question identified by the sensor is known as proximity target. It detects the adjacent nearness of close-by question with no physical contact [11].

Geomagnetic sensor

Geomagnetic sensors are utilized to give and set reference as for gravity by estimation of Earth's attractive field. But difficulty is change in magnetic fields during movements [12].

Barometer sensor

Barometer is utilized to quantify the environmental weight. The air pressure changes with change in separation and stature regarding the ocean level [14]. The barometer is likewise used to quantify the height [17].

Inertial sensor

Inertial sensors are based on inertia. It is generally accessible as Inertial estimation Unit (IMU) which made out of accelerometer, gyroscope and furthermore magnetometer some of the time [15].

Thus the IMU unit is utilized to distinguish the increasing speed and rakish speed of the human body. The 6-hub inertial sensor estimates the 3-axis acceleration and 3-axis angular velocity [16].

MEMS sensor

A micro electromechanical framework is a little machine that has both mechanical and electric parts. The span of MEMS can go from millimeters to micrometers. MEMS are the micro machines. Many Applications were available.

Example: Tiny gyroscope, barometers, accelerometers, microphones to support mobile apps [13].

Electronic Setup in Fall Prevention System

Setup 1

Accelerometer, gyroscope, magnetometer, and altimeter. The above set up gives better execution. The barometer in the system is used for the measurement of altitude variations during the fall is necessary to prevent the backward falls but it creates noise making it unsuitable during use. To achieve accurate altitude estimation standard data has been fixed and programmed in altimeter.

Lithium battery which had been inbuilt protection from high voltage, high current and less voltage. MCU went with micro SD is utilized to store information from the sensors [17].

Set up 2

MEMS Sensor containing tri-axial accelerometers, gyroscope for reducing space and power consumption, magnetometers and proximity sensors.

MCU is a battery. Micro controller is used to analyses and processes the data [18].

Setup 3

Accelerometer, gyro sensor, geomagnetic sensor [19].

Setup 4

6-Axis inertial module (3-axis accelerometer+3-axis gyroscope), Inclination sensor, micro controller.

Setup 5

MEMS sensor, micro controller, servo BMS-380MAX, bluetooth module. The total size of the system is 5.6cm*2.3cm*1.5cm.

Design of Wearable Airbag System

Airbag framework has coat securing head, neck, hip and thighs. Two airbags are utilized in the framework one air sack is put at the back ensuring the head and the neck with 470*330mm and has a volume of 10L and the other airbag is placed at waist region folded inside the pouch protecting the hip and thigh region with 250*450mm and has a volume of 10L. The two air bag weighs 1.1 kg and it is worn as jacket. Alkaline battery is used here. The gas cartridge weighs about 160g and the gunpowder used is 100mg. The system is reusable [20].

The airbag system in the form of belt has been developed weighing 253.5g, including compressed CO₂ cylinder of 42.5g. Receiving the signal from the electronic set up the response time of the inflator is 0.133 seconds. The total time taken for the inflation of airbag is 0.6 seconds[22].The weight of CO₂ cartridge is 12g(with 8mm in diameter and length 85 mm).The volume of the air bag is $1.88 \times 10^{-3} \text{ m}^3$ [23].

The airbag developed in the form of hip belt which is reusable with a built in LED battery lasting up to seven days and the battery can be charged again with the help of USB cable [24].It prevents hip fracture and give protection to the thigh region. The gas cartridge is the main part to be supplanted in the plan [24]. It shields all the hip territory from the highest point of your hips to the center of your thighs.

Waist mounted device to determine the fall in people. Android application in smart phones sending fall alarms from the subject to the related person of the subject [17].Full bodysuit with numerous sensors to secure hip and abdomen bone fracture. WIFI module is utilized in giving alert services [18]. Pelvic ergonomic wearable airbag system is invented in the form of belt, the sensors and the airbag is kept inside the belt. If the fall occurs the airbag made of polyurethane is deployed preventing the wearer [19].

Working Mechanism of Wearable Airbag System

The gyroscope and accelerometer is utilized to measure the current position of the human body. The deliberate information is exchanged to the CPU consistently. In the event that the CPU decides the fall event the signal is sent to the driving area. The airbag is sent by the initiation of inflator and shields the wearer from damage [19]. The gas is filled inside the cartridge. The trigger signal sent by the sensor is utilized to discharge the gas from the cartridge and swell the airbag [20]. After the sending of the airbag vent gaps noticeable all around packs discharges the air inside the airbag keeping the wearer from crash [19].

The mechanism which is shown in the fig.2 is relatively same as notice in the past strategy as opposed to utilizing whirligig and accelerometer independently 6-axis inertial module is utilized to measure the current position of the subject and microcontroller is used to send information instead of CPU[21].

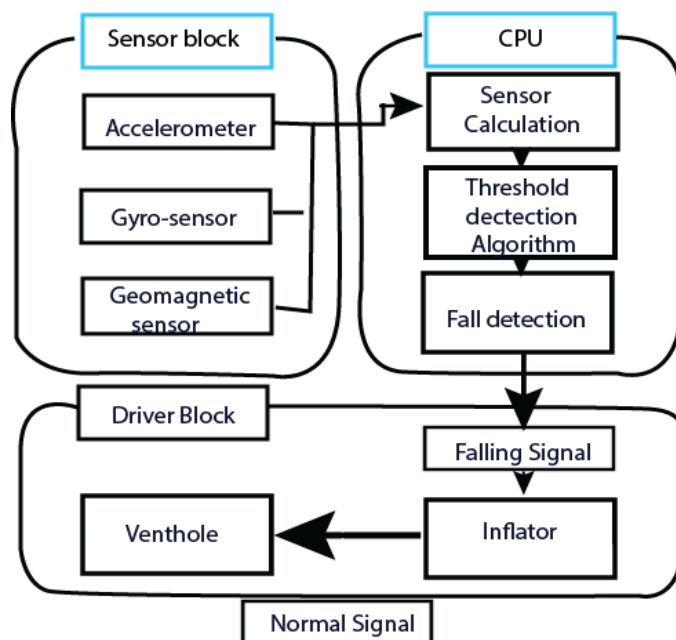


Figure 2. Block diagram of mechanism

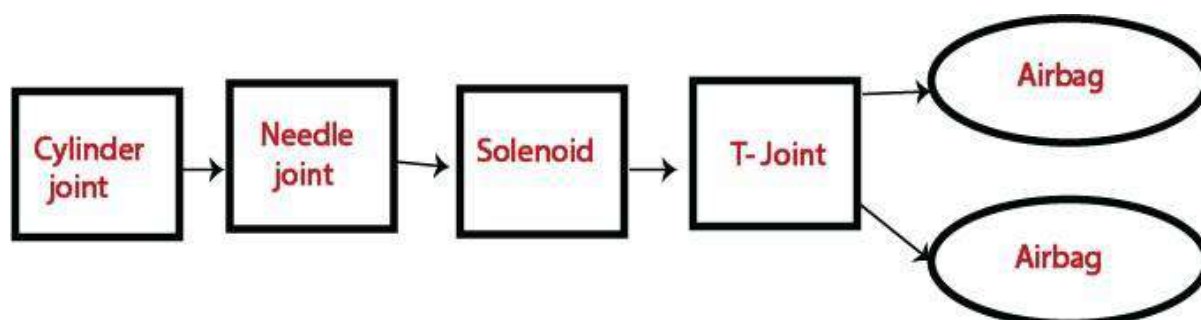


Figure 3. Block diagram of gas circuit mechanism

AS CIRCUIT SYSTEM

The fig. 3 shows the gas circuit system which consists of air source, air pipe, valve and airbags. The parts of the gas circuit system are shown in the figure. The compressed carbon dioxide is the gas used. This gas is colorless, tasteless, non-toxic, not combustion-supporting and nonflammable. This gas is effectively accessible in the market and more affordable. The solenoid valve of 2 mm breadth and administrator weight scope of 0-7.2MPa is utilized. The airbag is built utilizing nylon fabric [21].

It has punch kept on launcher that contains spring and a locking switch. The spring is kept at the compressed position. At the point when Actuator presses the locking switch, the spring kept in packed position is expanded and the punch quickens towards the pressurized chamber. The CO₂ gas is discharged from the hole among punch and the barrel. The discharged gas is transmitted through 16 cm long pipe to discharge the airbag [22, 25].

The speeding up flag among the fall is like one that happens during free fall. The situation of the sensor, furthermore, the Signal to Noise Ratio (SNR) of a low speeding up esteem that accepted that a counteractive action quickening worth would be underneath $\pm 3 \text{ m/s}^2$. A fall happened when the speeding up was under $\pm 3 \text{ m/s}^2$ and the precise speed surpassed 0.52 rad/s . The result revealed that a fall happened when the triaxial speeding up was below $\pm 3 \text{ m/s}^2$ and the precise speed exceeded 0.52 rad/s . The key issues in fall damage anticipation are the time it takes for the airbag to blow up and wrong swelling caused by the calculation.

Any fall-location framework must be exceptionally dependable. Their proposed calculation had an exactness of 93%. Mistakes happened when the free-fall condition showed up before the precise speed surpassed 0.52 rad/s . This came about because of an inconsistency in the location times for speeding up and precise speed. The subject reacted to the fall by twisting the knee and falling on the knee. So, the body turned less, and the precise speed was lower. In the case that the subject did not expect a protective posture, the angular speed would have been sufficiently huge to distinguish [26].

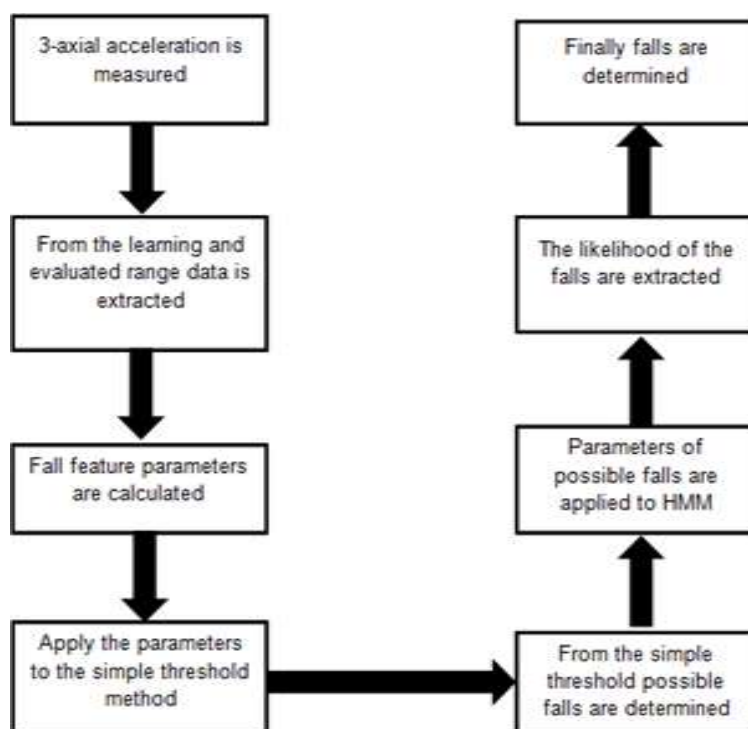


Figure 4. Flow diagram of fall detection system

VII CONCLUSIONS

The dissemination of fall history among the subjects over 60 years demonstrates that, 51.5% had fallen. Out of which 21.3% revealed breaks and 79.6% had different wounds. Among which 26.4% were females and 16% were guys.

Inability and mental misery were related with fall history and recurrence of fall. Higher incapacity and resultant expanding trouble was noticeable among those with an earlier fall history following 60 years. There is an endless loop where, because of poor saw well-being and dismalness there is expanded propensity to fall which itself prompts expanding incapacity and misery. It had been discovered that over 90% of hip cracks occur

because of fall of individual over 70 years. In the situations where BMI (Body Mass Index) is lower than 19.02 does not had breaks. Additionally elderly individuals who are practicing frequently, 60% did not have hip breaks when they fall. This is a result of general exercise kept them from fall wounds by better neuromuscular control

Various fall detective and preventive systems developed using 3 axis gyroscope sensors. These systems are highly effective in preventing the injury especially in the hip region of the elderly people. Various sensors and electronic and IT developments aid towards making the fall preventive system more effective and efficient. Usage of textile materials in air bags is highly prominent and further developments in synthetic fibre technology will help to design and develop hip janitorial belts with lesser cost and easily wearable.

REFERENCES

1. George F. Fuller Falls in the Elderly, April, 2000.
2. Goodarz Danaei MD et al. The Lancet, Vol.377, 9 pages, P. 568-577, February 2011.
3. S K West, B Munoz, et al. , Function and visual impairment in a population-based study of older adults, Vol.38, P.72-82, Jan, 1997.
4. John RM Copeland, Aartjan TF Beekman, et al. Depression among older people in Europe , February 2004.
5. T. Hsiao-Weckler, Biomechanical and age-related differences in balance recovery using the tether-release method, Issue: 18(2):179-87.
6. GongbingShan, XiangZhang, Mingliang Meng, Brandie Wilde, A Biomechanical Study for Developing Wearable Sensor System to Prevent Hip Fractures among Seniors, July 2017.
7. Carlos Gonçalves, Alexandre Ferreira da Silva, et al., Wearable E-Textile Technologies A Review on Sensors, Actuators and Control Elements, March 2018.
8. Sungmook Jung, Seungki Hong, et al., Wearable Fall Detector using Integrated Sensors and Energy Devices, Nov 2015.
9. <https://learn.sparkfun.com/tutorials/accelerometer-basics/all>, Citation on October 2018.
10. <http://sensorwiki.org/doku.php/sensors/gyroscope>, Citation on October 2018.
11. https://en.wikipedia.org/wiki/Proximity_sensor, Citation on October 2018.
12. <https://www.pnicorp.com/rm3100/> Citation on October 2018.
13. <https://internetofthingsagenda.techtarget.com/definition/micro-electromechanical-systems-MEMS> Citation on October 2018.
14. <https://www.britannica.com/technology/barometer> Citation on October 2018.
15. <http://www.kostasalexis.com/inertial-sensors.html/> Citation on October 2018.
16. <https://www.tu.com/index.php?route=tublog/blog&id=56> Citation on October 2018.
17. Dr.M.Meenakumari et al, Advances in Natural and Applied Sciences, P 94-100. May 1 2017.
18. Beomgeun Jo, Youngho Lee, et al. Design of Wearable Airbag with Injury Reducing System.
19. ToshiyobTramura, Senior Member, Takumi Yoshimura, Masaki Sekine, A Wearable Airbag to prevent Fall Injuries, November 2009.
20. Qi Zhang, Huiqi Li, et al., Design and Relialization of a wearable hip-Airbag system for Fall Protection, November 2013.
21. Guangyi Shi, Cheung Shing Chan, et al., Towards a Mobile Airbag System Using MEMS Sensors and Embedded Intelligencel.
22. GuangyiShi, Cheung, Mobile Human Airbag System for Fall Protection Using MEMS Sensors and Embedded SVM Classifier, March 2009.
23. www.techguide.com.au/news, May 22, 2018.
24. BeogeunJo, Young Lee, Jaemin Kim, Design of wearable Airbag with Ijury Reducing System.

25. Dongha Lim, Chulho Park, Fall-Detection Algorithm Using 3-Axis Acceleration:Combination with Simple Threshold and Hidden Markov Model, Journal of Applied Mathematics, September 2014.
26. IEEE transactions on information technology in biomedicine, toshiyotamura, senior member, A wearable airbag to prevent fall injuries, Nov 2009.
27. Alvaro Muro-de-la-Herran, BegoñaGarcía-Zapirain and Amaia Méndez-Zorrilla, Review on Gait Analysis Methods: An Overview of Wearable and Non-Wearable Systems, Highlighting Clinical Applications, Feb 2014.
28. Michele L. Callisaya, Leigh Blizzard1 etal., Ageing and gait variability , a population-based study of older people, Age and Ageing 2010; 39: 191–197, January 2010.

Ergonomic Design and Fabrication of Trolleys Used in Hospitals

R. Jayachitra, P. Nidharsan, S. J. Jason Samraj and M. Ranjith Kumar

Department of Mechanical Engineering, PSG College of Technology, Coimbatore, India

ABSTRACT

Trolleys are used to transport material from one location to another by human effort. In PSG Hospitals the trolleys are employed for laundry and food transport applications. When the trolley is fully loaded, the person who is pushing or pulling the trolley in slopes experiences a great difficulty and if he/she continues to perform such tasks regularly he/she may experience a work related musculoskeletal disorder. Musculoskeletal disorder causes pain in joints, muscles and ligaments. This may lead to several factors such as absenteeism of the worker, reduce the efficiency of worker, decrease productivity, etc. The project involves the ergonomic analysis of the existing trolley using force sensing electronic equipment and ergonomic analysis software to visualize stress caused to the workers. The project aims to design a new trolley with a lesser weight by making appropriate changes in the trolley design to reduce the stress caused to the workers with the aid of structural and ergonomic analysis. Further the project aims to develop a battery powered electrical driving system to incorporate with the existing heavy trolleys to assist the worker in slopes.

Keywords: Trolleys, Hospitals, transport material, Load

II. INTRODUCTION

Ergonomics is the activity of designing or arranging products and systems in workplaces, so that they are comfortable and fit the people who use them. Ergonomics applies to the design of anything that involves people – workspaces, health and safety, sports and leisure. The aim of Ergonomics or ‘human factors’ is to learn about human abilities and limitations, and then apply this learning to better people’s interaction with their specific environments.

The trolley is an equipment to transport material from one location to another by human effort. The sole purpose of trolley is to reduce human effort and increase the load carrying capacity of human by the usage of mechanical linkages, mechanism and the principles of mechanical advantages.

The repetitive and strenuous work during physical labour or any other type of work causes a broad range of health problems associated with work-related musculoskeletal disorders (MSDs). These health problems range from minor aches and pains, discomfort, to more serious medical conditions which can lead to more severe and permanent disabilities. Low back pain and work-related upper limb disorders are the most well-known MSDs. The first is mainly related with manual handling while the latter are associated with task repetition and awkward or difficult work postures. Lower limb work-related MSDs have been acknowledged as severe disorders which is related to occupational activity.

III. LITERATUREREVIEW

During the past decade or so, lot of work has been done by the researchers around the globe to determine the force evaluation to push / pull the trolley, ergonomic analysis and the work related musculoskeletal disorders. Few significant works which are used for our analysis is presented below.

A. Design of food trolley for hospitals

Anuraj et al., (2013) noticed a specific problem in hospital food service system. The basic need was identified for a better food trolley, which could reduce maintenance and simplify the hospital food service. The final design satisfied major user needs such as handles for usability, ergonomics and modular design shelves.

B. Force evaluation on trolley

Chan yew tow et al. (2015) conducted a force evaluation test on a supply trolley which weight around 280 kg using a mechanical gauge to find the pull and push forces on the trolley. A test to find the static and dynamic friction co-efficient of the wheel of trolley was also conducted. The values where estimated 30 kg for static force and 9 kg for dynamic force.

Matthaisjager et al. (2007) performed study on load lumbar spine in flight attendant during pulling and pushing of trolley in aircrafts and studied the various compression load on the disk of the spine. The force was also evaluated for inclined surface and a 14% increase in force was found on the spine.

C. Factors causing MuskuloSkeletal disorder

Andreas Argubi-Wollesen et al. (2016) studied the important factors that causes musculoskeletal strains by pushing or pulling the carts. The study investigated on different factors that causes musculoskeletal strain. The factors include (1) forces acting externally (2) handling task (pull and push) (3) cart load / weight (4) design and handle position (5) experience of a task. The study was done and the most influential factor of strain was proved to be external load on cart weight .

D. Automatic trolley using sensors

Deepali Pandita et al. (2017) studied the difficulty in moving the shopping trolley because of heavy weight of stuff. So to overcome this problem, automatic moving shopping trolley using sensors were designed. This consists of IR sensors, DC motors that helps the customers to push or pull the trolley with ease.

IV. OBJECTIVES AND METHODOLOGY

In Hospitals, Industries and many other work places, the workers are used in transferring food materials and other necessary items from one place to other using trolley. The problem here is the trolley design is not good enough to carry heavy loads in slopes as it may injure the person if anything goes wrong or the person is weak to pull or push such loads. Also some delicate and expensive items are carried using trolley and if the person who uses trolley loses control, the items may be affected.

The person who pushes or pulls the trolley may also be affected by work related musculoskeletal disorders which may cause serious problems to the person. This may be loss to the hospital as well as the person who does the job.

A. OBJECTIVES

The main objectives of this project are,

- To conduct an ergonomic study of the trolleys using force sensing electrical unit and 3DSSPP software.
- To design and fabricate new trolley considering ergonomic factors to avoid the un-usability of the trolley due to overweight and also to reduce the cost of the trolley.
- To design an electrical system to drive the existing heavy weight trolleys and the cost estimation to be calculated.

B. METHODOLOGY

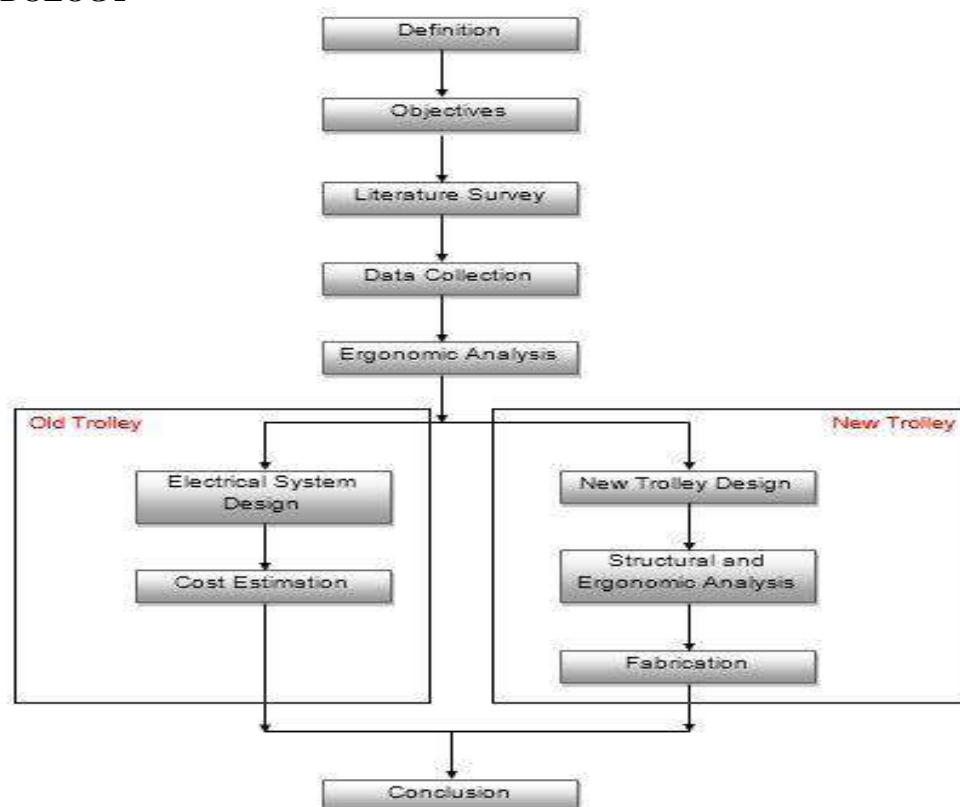


Fig. 1. Methodology of the project

The figure 1 shows the methodology of the project. The project started with the problem definition with the help of worker interaction and data collection. Further literature review is done using the relevant journals and articles for the solution possibilities. After literature review the required data are collected. The data collected include the trolley dimension, Working condition and anthropometric data of the trolley operators. And with the data collected ergonomic analysis is carried out to test the usability of the existing trolley.

After ergonomic analysis, the existing trolley is found to be unsafe and two solutions were derived. One is to design and fabricate a new trolley with reduced weight to reduce the stress caused to the trolley operators and another solution is to incorporate an electrical driving system to assist the worker in operating the existing heavy trolley in difficult working conditions.

V. DATA COLLECTION

A. Construction of the trolley



Fig. 2. Closed trolleys used to serve general wards in PSG hospitals

DETAILS

- Dimension - 96×63×90 cm
- Handle distance from trolley – 12 cm (45°)
- Handle height from ground – 118 cm
- Handle diameter – 3.34 cm
- Trolley wheel diameter – 15 cm
- Door Dimension – 40×90×2 cm
- Number of plates (capacity) – 45 to 50 plates.

Plate (special ward)

- Plate weight – 2.5 kg
- Plate Material – Stainless steel
- Plate Dimension - 39×28×5 cm

Plate (general ward)

- Plate weight – 2.35 kg
- Plate Material – Stainless steel
- Plate Dimension – 33.5×28×6 cm

Hot box with rice

- Dimension - 17×10 cm
- Handle – 2 cm (4 ends)

B. Food distribution cycle

The food is supplied to the patients in hospitals three times per day and so the operators have to use the trolley for three cycles. The weight of the food that is carried for one cycle per patient and the time of delivery is given below.

- Morning (7 AM), Weight of food = 1.7 to 1.85 kg per plate

- Afternoon (12 PM) Weight of food = 2.25 to 2.35 kg per plate
 - Night (7.30 PM) Weight of food = 1.8 to 2 kg per plate
1. Total distance travelled by the trolley in a cycle = $167+167 = 334$ m
 2. The total time taken for one cycle = 35-45 minutes

The time taken by one cycle depends on

- Number of patients
- Each ward accommodates 8 patients
- To serve a single ward with 8 patients it takes 3 minutes.

Total Trolley Running time = 16-18 minutes

C. ANTHROPOMETRIC DETAILS

S.NO	HEIGHT(cm)	WEIGHT(kg)
1	165	52
2	160	58
3	164	59
4	158	75
5	175	58
6	177	58
7	180	69
8	185	68
9	165	54
10	160	55

Table. 1. Anthropometric Details

The anthropometric details of 10 operators who are using in the trolley in general ward is noted.

The anthropometric data of the trolley operators are listed in the Table 4.1 and the data is used in the ergonomic analysis to evaluate the stress involved with individual workers.

VI. STRUCTURAL ANALYSIS

The modelling of the trolley was generated using catia V5 software which uses constructive solid geometry techniques to develop models. Three models of the trolley were developed for to estimate the weight of the trolley, conduct structural analysis on the trolley and incorporation of an electrical system into the trolley. The three trolleys are

1. Existing closed type trolley
2. New closed type trolley

A. Weight Analysis

The model in the Figure 3 was developed by initially constructing separate part and then assembling them with proper surface constrains between each part.

Constrains were given as weldment to stimulate the effects of weld in the analysis. The density data of the stainless steel was inserted into the model to extract the weight of the old trolley.

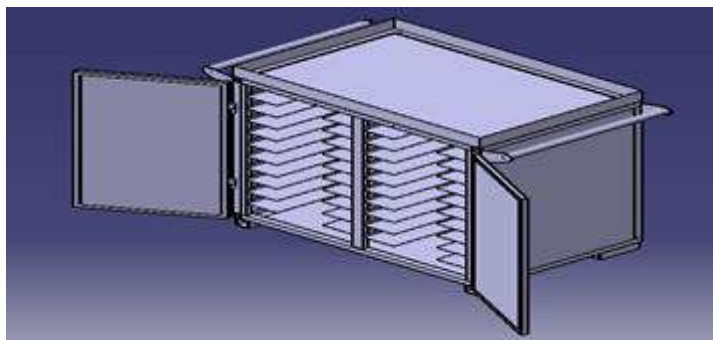


Fig. 3. Existing trolley

The empty weight of the trolley was estimated to be 135 kg as shown in the Figure 4.

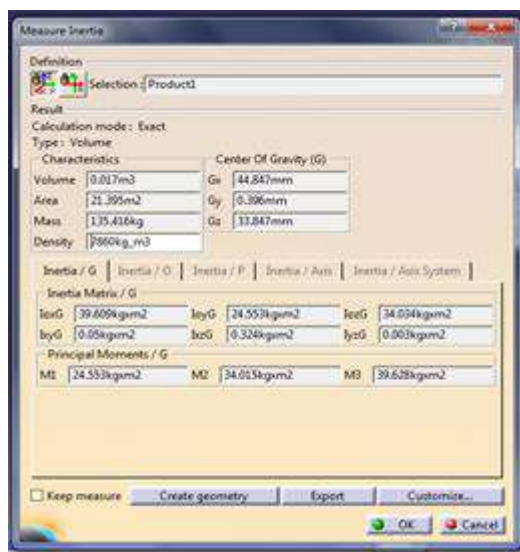


Fig. 4. Weight of the existing trolley

The new trolley was designed according to the plate dimension to increase the compactness of the design and reduce the weight without compromise in centre of gravity of the trolley. The steel section where chosen after consultation with a manufacturers of kitchen wear expert and the narrow down the section with greatest strength to weight ratio.

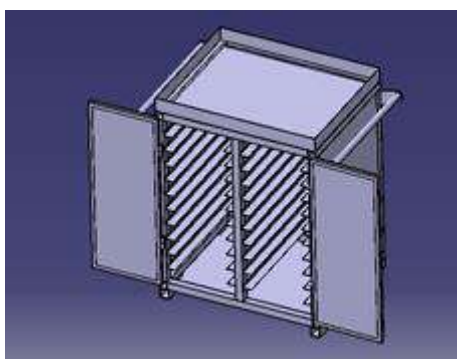


Fig. 5. New trolley

The trolley was designed based on these sections as individual part and assembled with as a single assembly with proper surface constrain to get accurate stimulation. the density data where inserted and the weight of the trolley was found to be 77 kg which is 45% reduction in the weight compare to pervious trolley

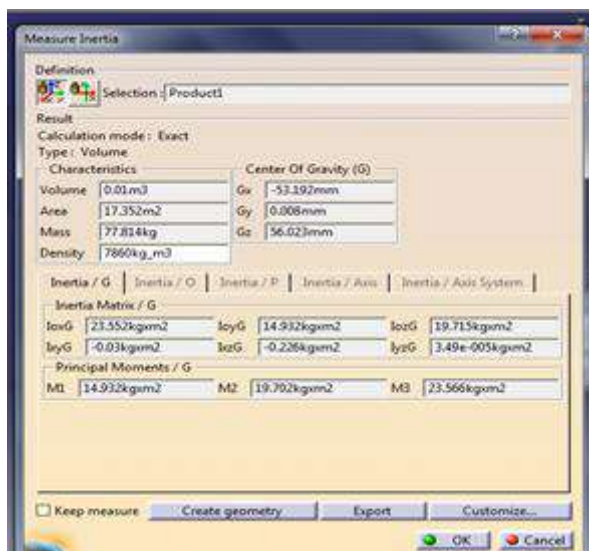


Fig. 6. Weight of new trolley

B. STRUCTURAL ANALYSIS

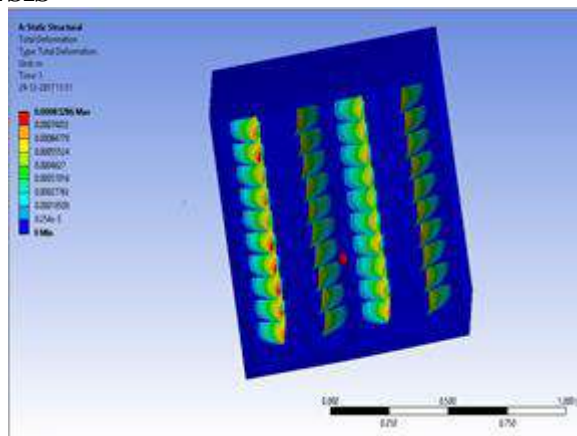


Fig. 7. Structural analysis of existing trolley

The existing trolley is modelled and analysed in ANSYS with the load data from the data collection section as shown in the Figure 7 and the following inferences were made.

- The trolley was over design for the application and further reduction in the weight of the trolley is possible which will enhance in improving the ergonomics of the trolley
- Excess vacant space in between was present in the trolley, which can be reduced according to the plate dimensions, which will reduce the material required to construct the frame and overall cost
- The stress is found to be uniform across the trolley and within the stress limit
- The displacement of the tray is 8mm which also within the fatigue limit of the trolley

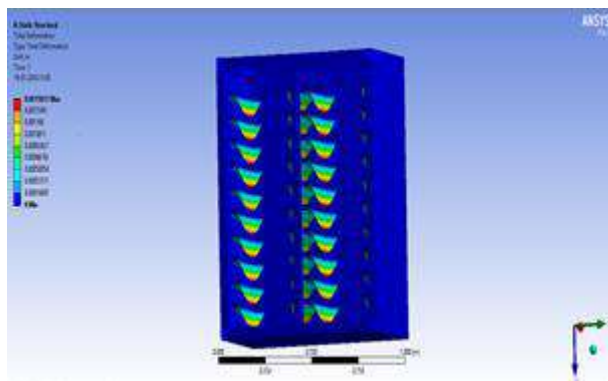


Fig. 8. Structural analysis of new trolley

The new trolley is analysed in the ANSYS as shown in the Figure 7 and the weight is evaluated as shown in the Figure 8 and the following inferences are made.

- The weight of the trolley has reduced by 45% when compare to old trolley to 77 kg with the centre of gravity increased by 5 mm , which don't effect the performance of the trolley
- The stress analysis on the trolley proved the trolley is within the stress limit of the material
- The displacement of the 1.5 mm is observed in the tray and a fatigue failure analysis of the tray is done to estimate the possible failure of the tray

VII. ERGONOMIC ANALYSIS

The ergonomic analysis is the major concern for our project. It gives the major data regarding the fatigue at different part of our body. Also the balance while performing a task is analysed. The ergonomic analysis is done using 3DSSPP software.

The ergonomic study involves the trolley handle pushing and pulling force evaluation using force sensing unit, trolley handle height measurement and operator posture measurement using Goniometer and ergonomic evaluation of the measured load under operating postures using 3DSSPP software.

The ergonomic analysis includes the contribution two units namely

- Force sensing unit
- 3DSSPP software

A. Force sensing unit

The force sensing unit is to evaluate the force applied to the trolley handle, which is an important factor in the ergonomic analysis. The force data from the sensing unit is given as input to the ergonomic software. The force sensing unit contains

- CZL 601 40 kg load cell to measure the force applied.
- HX711 Load cell amplifier to convert analog to discrete signals.
- Arduino uno, 32-bit Micro-processor to interpret the data to computer.
- Arduino uno Serial monitor to display the data on computer

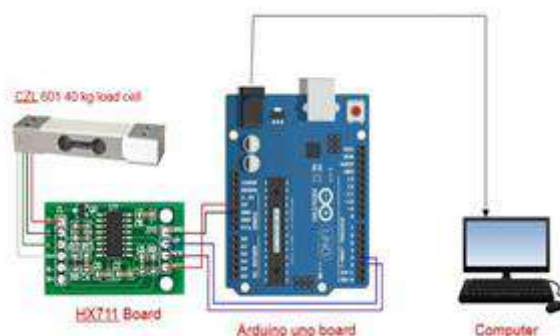


Fig. 9. Force sensing unit.

B. Load cell results for different working conditions

S.NO	CONDXION	RUBBER WHEEL (In kg)		POLYURETHANE (In kg)	
		INITIAL	ROLLING	INITIAL	ROLLING
1	CONCRETE - PUSH	26.37	12.75	10.25	6.25
2	CONCRETE - PULL	20.375	10.2	8	3.75
3	MARBLE - PUSH	16.625	7.65	3.75	2.5
4	MARBLE - PULL	11.4	5.525	2.75	1.5
5	SUDDEN OBSTACLE	12.92	-	12.75	6.5
6	RAMP PUSH	35	21.75	20.25	8.75
7	RAMP PULL	33.125	20	15.5	7.5

Fig. 10. Load cell results

The trolley is operated under different conditions which are involved in the day-to-day trolley operation with the load cell attached to the handle. The load cell provides the force given by the hand on the trolley and thus the force acting on the hand in all the working conditions is evaluated and displayed in the computer with the help of force sensing unit and tabulated in the figure 10.

C. Introduction to 3DSSPP

3D Static Strength Prediction Program predicts the static strength requirements for different tasks namely pushes and pulls lifts, presses. An approximate job simulation comprising of posture data, male/ female anthropometry, force parameters is provided by the program.

Output includes the percentage of men and women who have the strength to perform the described job, spinal compression forces and data comparison according to NIOSH guidelines.

3DSSPP can be used as an aid in the physical demands evaluation of a prescribed job.

The 3DSSPP analysis is performed for three different anthropometric data. The analysis is done by keeping the height of the person as 160 cm, 165 cm and 175 cm. The analysis is done under different floor conditions as mentioned below

- Concrete
- Marble
- Ramp



Fig. 11. Operator posture

The Task Input Summary shown in the Figure 12 displays a summary of the data entered under the Task-Input Menu items including the:

- Hand locations,
- Joint angles,
- Additional joint forces,
- Hand force magnitude and direction, and
- Anthropometric data.

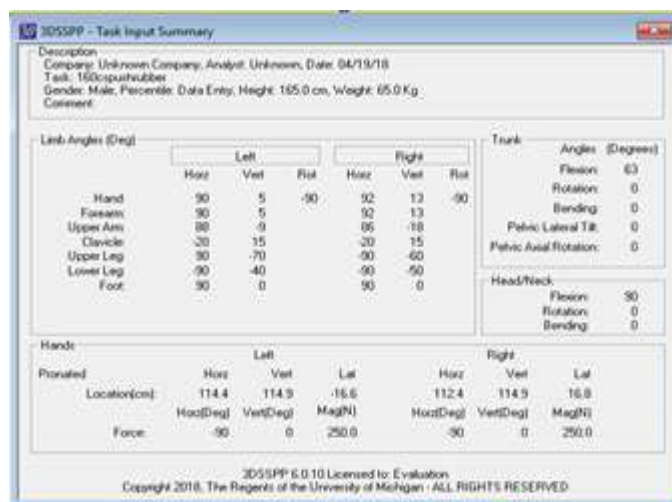


Fig. 12. Posture input data

The strength capability of the selected gender and anthropometry at the major joints are displayed. The lowest value for each joint obtained from the strength capabilities calculated for the joint actions on the left and right side of the body is displayed. The smallest of axial rotation strength, lateral bending strength and flexion/extension strength is the torso value. The SDL (Strength Design Limit) designation is defined by the green to yellow transition in the bar graphs and is set at 75% for women or 99% for men. The SUL (Strength Upper Limit) designation, on the other hand, is defined by the yellow to red transition and is set at 1% for women or 25% for men.

The 3D low back compression force at L4/L5 above the percent capable values is displayed in both a numeric value and a bar graph. The disc compression force predictions are compared with the Back Compression Design Limit (BCDL = 770 pounds or 3400 newtons) and the Back Compression Upper Limit (BCUL= 1430 pounds or 6400 newtons) as specified by NIOSH. In the bar graph the Back Compression Design Limit (BCDL) is delimited by the green to yellow transition and the Back Compression Upper Limit (BCUL) is delimited by the yellow to red transition.

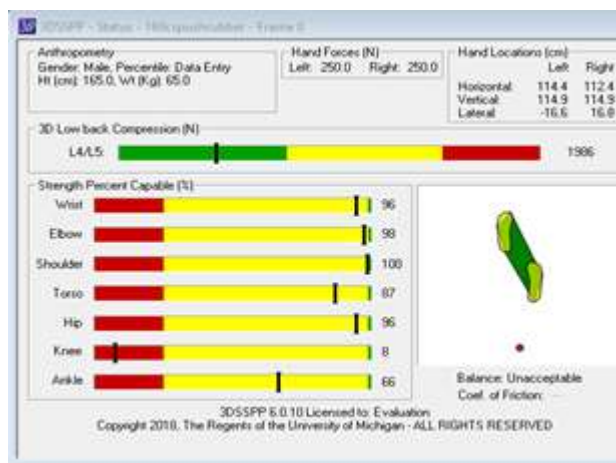


Fig. 13. 3DSSPP Results

D. INFERENCE

The L4/L5 3D Low back compression value is taken into account and a bar graph is drawn for the following operations for three different human heights as shown in the Figure 14

- Concrete pull
- Concrete push
- Tiles pull
- Tiles push
- Ramp pull
- Ramp push

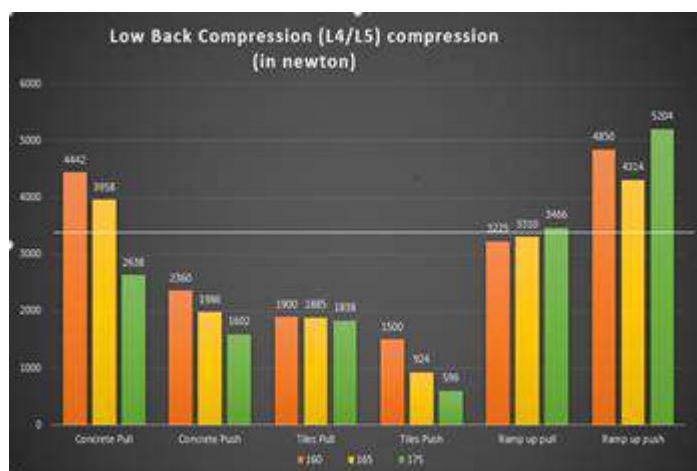


Fig. 14. L4/L5 Low back compression comparison

The concrete, Ramp push and pull operation produces undesirable lower back compression which is above the Back Compression Design Limit of 3400 newtons thereby ensuring the process to be unsafe. The ergonomic study is conducted on the existing trolleys using force sensing electrical unit and 3DSSPP software, and the result showcases that the existing trolleys causes discomfort to the operator as the lower back compression limit is higher under certain conditions.

Then the ergonomic analysis is done for the new trolley with the following assumptions

- Mass of the new trolley – 77.8 kg
- Friction co-efficient of the wheels is found from the previous trails of existing trolley and since the same wheels are used for the new trolley, the same co-efficient of friction is used.
- With the load data and the co-efficient of friction the hand force is calculated for all the working conditions for new trolley

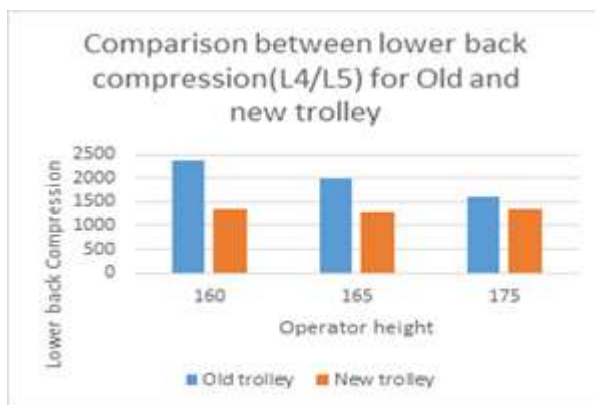


Fig. 15. Lower back compression comparison for new trolley and existing trolley

The Figure 15 clearly shows that the lower back compression in the existing trolley exceeds safe limit whereas the lower back compression in the new trolley does not exceed the safe limit thereby making the new trolley to be safe to operate under all working conditions.

VIII. ELECTRICAL DRIVING SYSTEM

The Electrical driving system consists of a battery powered motor to drive the wheels of the existing trolley. The Electrical driving system reduces the stress caused to the operator by assisting him in handling the trolley during difficult work conditions. The Electrical system consists of the following units namely,

- The Permanent Magnet DC motor
- The Battery
- The Speed reduction gearbox
- The Wheel assembly

The Electrical driving system involves the following activities in the selection of the components

- Torque requirement of the trolley is to be calculated.
- Battery power requirement of the motor to be calculated.
- The wheel has to be selected.

The Figure 16 shows the arrangement of the above mentioned components in the trolley. And the torque required to pull trolley is calculated.

- Total weight of trolley (excluding food) = 161.047 kg
- Total weight of vessels = 50 vessels \times 2.35 kg = 117.5kg
- Other vessels = 20 kg
- Total weight = 298.54kg ~ 300kg.
- Considering the electrical assembly to be 20 kg
- Gross Vehicle Weight = 320 kg
- Radius of Wheel tire = 0.127 m (10inch wheel assumed)
- Weight on each wheel = 80 kg
- Top speed (V_{max}) = 1.5 m/s (average human walking speed)
- Inclination angle = 4°
- Time to attain top speed = 10 seconds

Total tractive effort = Rolling Resistance + Grade Resistance + Acceleration Force

Rolling Resistance = $320 \times 0.0125 = 4$ kg (0.0125 is the Surface Friction for Concrete)

Grade Resistance = $320 \times \sin 4^\circ = 20.09$ kg (4° is the inclination angle)

Acceleration force = $(320 \times 1.5) / (9.81 \times 10) = 4.88 \text{ kg}$

Total Tractive Effort = 28.97 kg

Drive wheel torque = $28.97 \times 0.127 \times 1.15 = 4.231 \text{ kg.m} = \mathbf{41.5 \text{ Nm}}$

(0.127 is the wheel diameter, 1.15 is the resistance factor)

The required torque of the trolley is found to be **41.5 Nm**

- Total distance travelled by the trolley in a

Cycle = $167 + 167 = 334 \text{ m}$

- The total time taken by a cycle = 35-45 minutes
- The time taken by one cycle depends on
- Number of patients
- Each ward accommodates 8 patients
- To serve a single ward with 8 patients it takes 3 minutes.
- Total Trolley Running time = 16-18 minutes
- Motor Power = 372.85 Watts
- Voltage = 24 V
- Ampere = 15 A

The Battery required is found to be 24V 15Ahr DC battery.

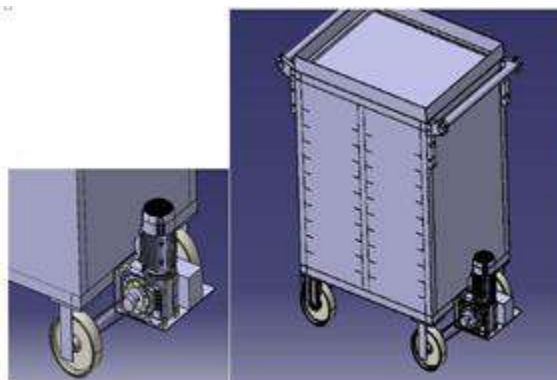


Fig. 16. Electrical driving system

S.NO	REQUIREMENT FOR THE SYSTEM	SELECTED COMPONENT	COST (Rs)
1	TORQUE = 41.5 Nm	24V 0.5HP 1500RPM PMDC MOTOR WITH 20:1 WORM GEARBOX	10500/-
2	24V 15Ahr DC BATTERY	12V 16Ahr MOTOR (2nos)	4200/-

Fig. 17. Cost estimation

The torque requirement of the trolley is 41.5 Nm, so a motor which has the capability provide that torque should be selected. With the help of WEN technology, the torque is calculated from the power and speed of the motor, with that technology the 24V 0.5HP 1500 rpm PMDC motor gives the torque of 47.5Nm

The battery power requirement is 24V 15Ahr DC battery, the commercially available battery is 12V 16Ahr, so two battery are purchased and connected in series thereby the required output 24V 16Ahr is achieved.

The figure 17 shows the selected components with the cost per unit.

IX. CONCLUSION

The ergonomic study is conducted on the existing trolleys using force sensing electrical unit and 3DSSPP software under different working conditions, and the result showcases that the existing trolleys causes discomfort to the server as the lower back compression limit is higher under certain conditions.

Thus the result showcases that the existing trolleys are unfit to be operated by the operator as it causes the L4/L5 to compress more than the safe limit as shown in the Figure 14. And there is a need to replace the trolley with a light new trolley or with an assisting electrical driving system.

Thus the Figure 15 shows that the lower back compression has fallen in the new trolley due to weight reduction and the compression value of the new trolley lies below the safe value which shows that the new trolley safe for the user to operate at all working conditions.

The Figure 18 compares cost of both existing trolley and the new trolley and it is observed that the cost of new trolley lesser than that of the existing trolley since the material procurement is lesser due to dimensional modifications and since the fabrication is done in the PSG hospitals maintenance department, the fabrication cost is not included.

COST OF THE TROLLEY (Rs)	
EXISTING	NEW
54500/-	24750+/-

Fig. 17. Comparison of cost of existing and new trolley

The Electrical driving system is designed to drive the existing trolley in all working conditions and the cost estimation for the fabrication of the electrical driving system is quoted. With the Electrical driving system the trolley operation becomes safe and simple as the entire power is given by the motor itself.

In future hand trolleys can be powered with high power electrical driving system which carries a series of trolley with the operator on board, which empowers a single operator to handle two or more trolleys. The system resembles the way in which the trolleys are coupled in series in airports. The Stainless steel can be replaced with a lighter food grade material to reduce the weight of the trolley. An intelligent electronics unit can be developed which indicates the plate of the particular patient in a common ward which reduces the serving time.

ACKNOWLEDGMENT

At this pleasing moment of having successfully completed my project, we wish to convey our sincere thanks and gratitude to our college PSG College of technology for providing all possible facilities. We would like to express our sincere thanks to Dr.R.Rudramoorthy, Principal, PSG College of Technology for his kind patronage. We wish to convey our heartfelt thanks to Dr.P.R.Thyla, Professor and Head, Department of Mechanical Engineering, who has greatly helped in the success of the project by giving valuable suggestions and providing us with the necessary permission for usage of equipment and facilities required. We wish to express our heartfelt gratitude to our tutor Mr.V.Vijayakumar, Assistant Professor, Department of Mechanical Engineering for his useful suggestions throughout the project work. We adequately pronounce our sincere gratitude and indebt thanks to our project guide Dr.R.Jayachitra, Assistant Professor, Department of Mechanical Engineering for her inspiration, valuable guidance throughout the venture of this project. With great pleasure and deep gratitude, we express our sincere thanks to all the staff members of Mechanical Engineering Department whose assistance played a big role in this project and have been of immeasurable value. We take great pleasure in thanking our family and friends for their continuous support and encouragement whenever we needed them the most. Without the fruitful grace of Almighty nothing would have been possible and place our thanks for Him.

REFERENCES

1. Andreas Argubi – Wollesen, Bettina Wollesen, Martin Leitner and Klaus Mattus (2016) "Human body mechanics of pushing and pulling: Analyzing the factors of task- related strain on the musculoskeletal system", Safety and Health at work, Volume 4, Issue 8, pp. 11-18.

2. Anuraj, N.P., Srinivasa and Vignesh Ravichandran, (2013) "Design of a food trolley for hospitals in India", *sasTech journal*, Volume 12, Issue 2, pp. 90-98.
3. Chan Yew Tow and KamWaiKuen (2015), "Force evaluation and comparison for supply trolley in hospitals", *Procedia manufacturing*, Volume 3, Issue 1, pp. 1861-1864.
4. Deepali Pandita, Ashwini Chauthe and Nikhil Jadhav, (2017) "Automatic Shopping Trolley using sensors", *International Research Journal of Engineering and Technology (IRJET)*, Volume: 4, Issue 4, pp. 2670-2673.
5. Haslama, R.A., Boocock, M., Lemon, P. and Thorpe, S, (2012) "Maximum acceptable loads for pushing and pulling on floor surfaces with good and reduced resistance to slipping", *Safety Science*, Volume 40, Issue 1, pp. 625-637.
6. Jesper Sandfeld, Christian Rosgaard, Bente Rona Jensen, (2014) "L4-L5 compression and anterior/posterior joint shear forces in cabin attendants during the initial push/pull actions of airplane meal carts", *Applied Ergonomics*, Volume 45, Issue 1, pp. 1067-1075.
7. Jon Boyer, Jia-hua Lin, Chien-chi Chang, (2013) "Description and analysis of hand forces in medicine cart pushing task", *Applied Ergonomics*, Volume 44, Issue 1, pp. 48-70.
8. Macro J.M. Hoozemans, Allard J. Van Der Beek, Monique H.W. Frings-Dresen, Frank J.H. Van Dijk and Luc H.V. Van Der Woude, (1998) "Pushing and Pulling in relation to musculoskeletal disorders : a review of risk factors", *Ergonomics*, Volume 41, Issue 6, pp. 757-781.
9. Matthais Jaeger, Kirsten Sawatzki, Ulrich Glitsch and Alwin Luttmann, (2007) "Load on the lumbar spine of flight attendants during pushing and pulling trolleys aboard aircraft", *International Journal of Industrial Ergonomics*, Volume 37, Issue 11-12, pp. 863-876.
10. Na JinSeo, Thomas J. Armstrong and Justin G. Young, (2010) "Effects of handle orientations, gloves, handle friction and elbow posture on maximum horizontal pull and push forces", *Ergonomics*, Volume 53, Issue 1, pp. 92-101.
11. Nimbarte, Ashish D., Moore, Christopher and Sun, Yun, (2013) "Kinematics of cart pushing and pulling under different loads and surface gradient conditions", *Occupational Ergonomics*, Volume 11, Issue 2-3, pp. 75-84.
12. Resnick, Marc L., and Chaffin, Don B, (1995) "An ergonomic evaluation of handle height and load in maximal and submaximal cart pushing", *Applied Ergonomics*, Volume 26, Issue 3, pp. 173-178.

Chest Radiographic Images Enhancement and Segmentation for Feature Analysis and Lung Nodule Detection

Gopalakrishnan S

Department of Biomedical Engineering PSG College of Technology Peelamedu, Coimbatore

ABSTRACT

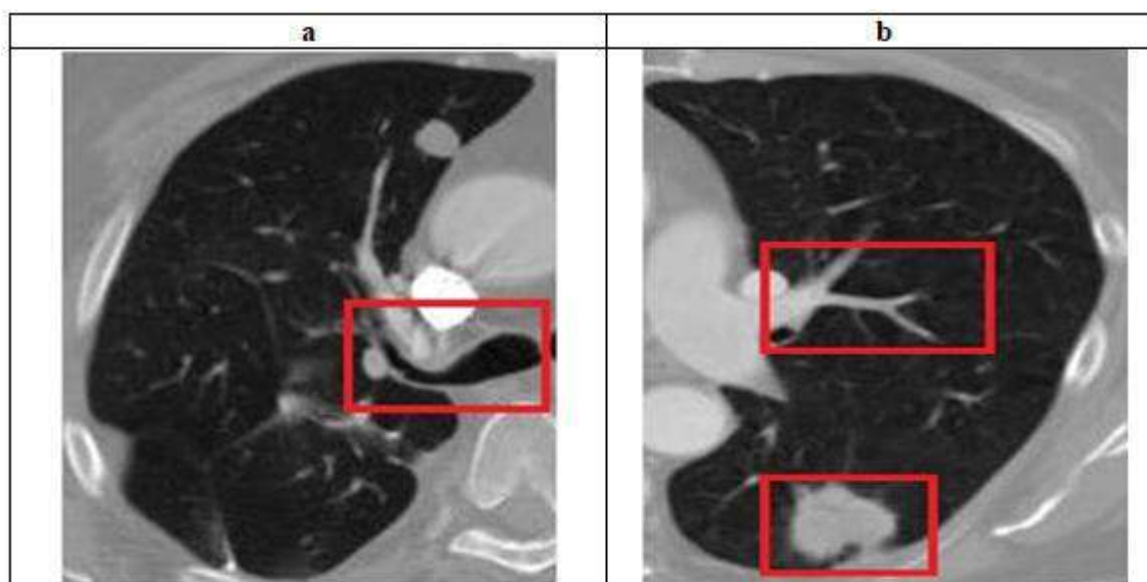
Lung cancer is becoming a serious disease in the world causing a huge number of deaths. Since, lung cancer detection is very challenging in its early stage. Computed Tomography (CT) is proven an efficient, non-invasive screening method for lung cancer. The dense anatomical structures around the lung Nodules in the CT image increases the complexity of the Nodule detection process. In this work, we propose a computer aided detection (CAD) system for lung nodule. The proposed method is based on enhancement, segmentation and feature analysis. The experimental results shows that there is a potential for employing the system for computer-aided detection of lung Nodule.

Keywords: Lung Nodule, Computer Aided Detection, Segmentation, Feature Analysis, image enhancement

1. INTRODUCTION

Lung cancer, the major cause of cancer deaths, among other cancers worldwide. The mortality rate of lung cancer is almost equal to that of colon, breast, prostate and pancreatic cancer put together[1]. WHO South-East Asia Region reports 162003 lung cancer incidence and mortality of 146216 cases in the region in the year 2012 [2]. The highest mortality rate is due to the difficulty of detecting it in an earlier stage. Therefore, the nodules must be detected before it turns to a malignant stage. The Low Dose Computed Tomography (LDCT) can detect malignant lung nodules at an early stage. The chance of surviving the inception of lung cancer depends largely on how early they are diagnosed and how well they are treated. Most of the victims were diagnosed with the final stage of lung cancer, resulting in a very low five-year survival of about 16% [3]. Periodical screening can help us in diagnosing a lung cancer at an initial stage and increases the survival rate. Screening is looking for early sign of lung cancer before a person has any symptoms.

The National Lung Screening Trial (NLST), a large, high quality randomized, controlled study validated that the LDCT scan reduce the risk by 20% than the conventional chest X-ray screening [4]. With the advancement in Computed Tomography (CT) imaging technology in the past decade, the quantity of data is increases continuously. Currently, an average of 350 image slices per examination can be acquired. This additional data improves the accuracy of disease diagnosis; however, it increases the complexity of examination procedure. Nodule detection in CT image is extremely difficult because of smaller in size, reduced contrast and its location within an area of complicated lung anatomy. Computerized nodule detection schemes have been shown to substantially increase diagnostic accuracy in radiological imaging. The importance of lung CT images and its complicated anatomical structure motivates the research community to develop a computer-aided algorithm to assist radiologist in reading chest radiographic images.



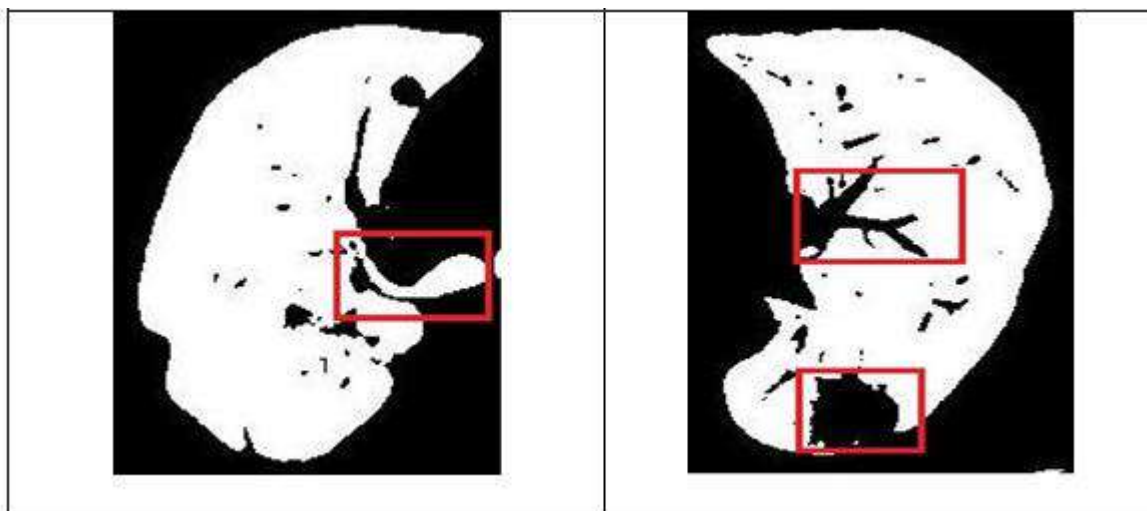


Fig. 1. The limitations of intensity thresholding segmentation techniques:

(a) airways included; (b) pleural nodules and pulmonary vessels were excluded.

The development of Computer Aided Analysis (CAA) begins in the 1960s and research papers describing techniques for computer aided detection of abnormalities in chest radiographs began to appear in the 1970s. A first attempt at fully automatic Computer Aided Diagnosis or Detection (CAD) system was proposed in 1987 and was based on work developed earlier in this decade [5]. A typical CAD system consists of preprocessing, enhancement, segmentation, candidate extraction, feature extraction and classification. The first five steps deals image processing and the final classification is considered a pattern recognition problem. Though a number of methods have been proposed in the literature to improve each of the steps but the problem is wide open and yet to be improved. The rest of the paper is organized as follows: Section 2 describes image data and proposed methodology for detecting lung nodules. Section 3 presents the results obtained in our work and discusses its significance.

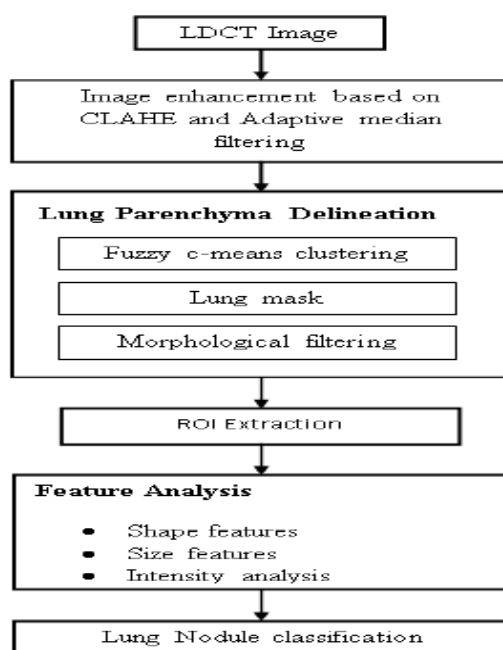


Fig. 2. Proposed lung parenchyma segmentation algorithm

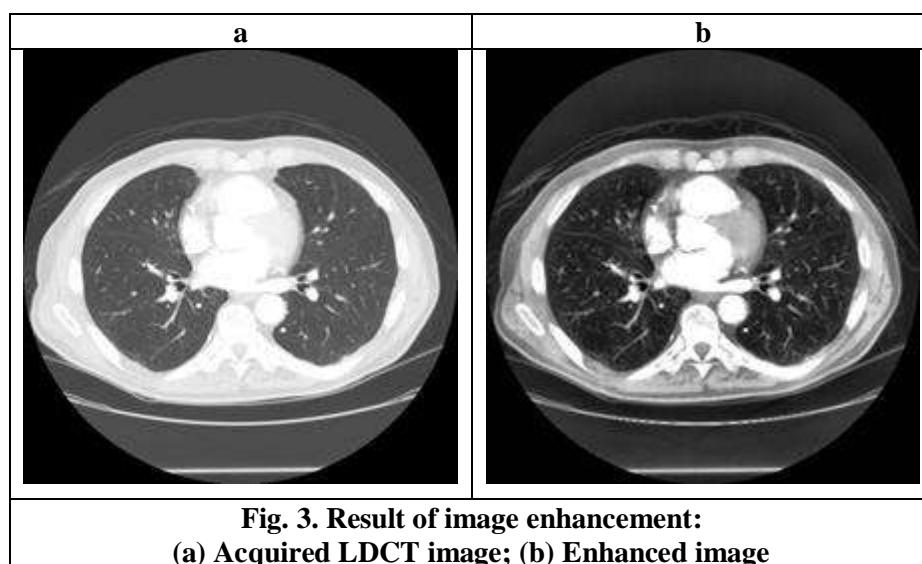
2. MATERIALS AND METHODS

Lung Image Database Consortium (LIDC) is a publically available reference database for lung Nodules. We have randomly chosen 126 cases from LIDC database for evaluating the performance of the proposed methodology [6]. One of the simplest image segmentation employed in many of the previous work is intensity thresholding [7, 8] but, the problem associated with thresholding techniques is it produces poor segmentation result at region like lung parenchyma is depicted in Fig.1. Thresholding is combined with region filling and

deformable model was proposed to improve the segmentation accuracy [9]. The block diagram of the proposed methodology is shown in Fig.2. It consists of the following stages: image enhancement, segmentation ROI detection, feature analysis and classification.

2.1 Lung Parenchyma Enhancement

Enhancement of lung parenchyma in the low dose computed tomography is an essential pre-processing step to improve the visibility of the lung nodule among other anatomical structures. The recommended enhancement technique is based on the combination of two techniques: Contrast Limited Adaptive Histogram Equalization (CLAHE) and Adaptive Median Filtering (AMF). The conventional histogram equalization procedure improves the contrast of the image but, it has a tendency to amplify the noise. CLAHE enhance the local contrast of the image and it operates on a small image region. The level of contrast introduced is depends on the property of the region and it is controlled by controlling the slope of the Cumulative Distribution Function(CDF) of the transformation function. In our work, we use exponential target distribution and the slope of the distribution is 1.5. The contrast-enhanced image is further processed to reduce the noise; an adaptive median filtering is preferred since it performs well at higher noise level. Unlike median filtering, it changes its size of the median region based on the noise distribution [10]. The result of the acquired and enhanced CT image is given in Figure 3.



2.2 Delineation of Lung Parenchyma

Segmentation of lung parenchyma from other part of chest CT image will concise the searching area of CAD system and reduces its complexity. The important requirement of the lung segmentation algorithm is, it should exclude trachea and preserve juxtapleural nodule. Keeping this in mind, we propose an unsupervised technique based on fuzzy c-means clustering followed by lung border refinement and mask processing for accurate delineation of lung parenchyma. Conventional clustering algorithm assign each data point to only one cluster. In contrast, Fuzzy clustering allows data points to belong to more than one cluster based on the degree of the membership function associated with each cluster [11]. Here, the membership function and the cluster center is randomly initialized and iteratively updated as long as the objective error function is minimized. The performance of Fuzzy c-Means Clustering (FCMC) in the case overlapping data is better as compared with k-means algorithm.

In order to take care of the juxtapleural Nodule and trachea, the segmented lung field undergoes morphological filtering process. Erosion and dilation are the two fundamental morphological operations from which can define following operations: closing and opening. Closing operation is achieved by dilation is followed by erosion.

$$I \cdot S = (I \oplus S) \ominus S \quad (1)$$

Opening operation is achieved by erosion is followed by dilation.

$$I \circ S = (I \ominus S) \oplus S \quad (2)$$

Where S, is the structuring element.

The set operation for erosion is given by

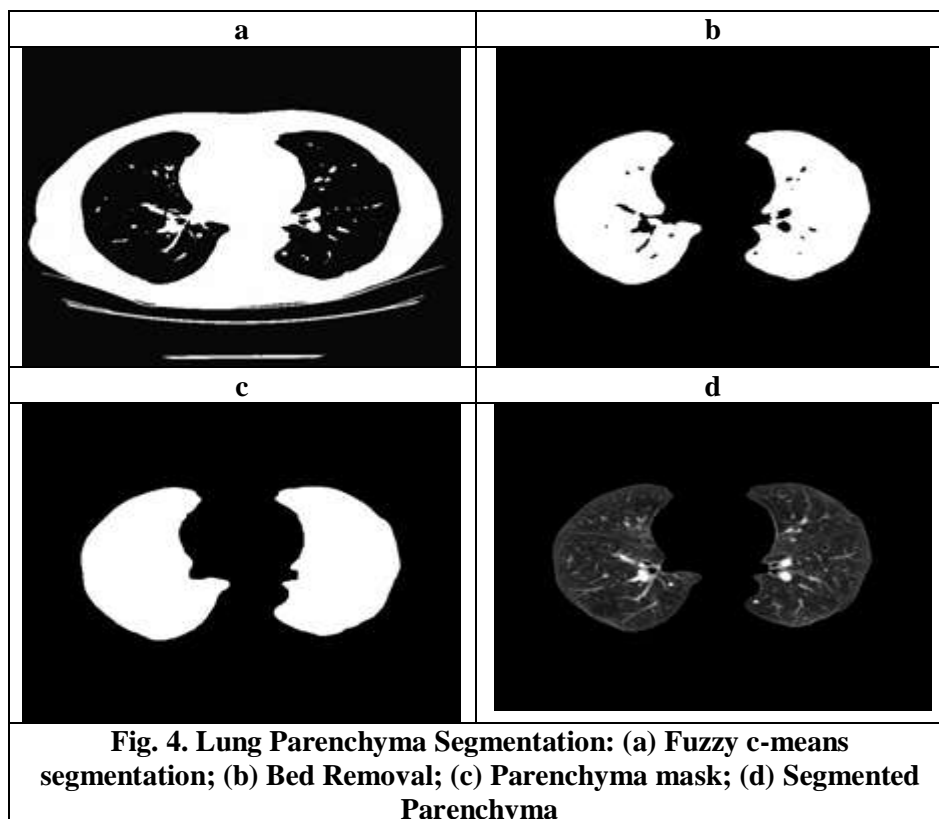
$$I \ominus S = \{P \in Z^2 \mid (P + Q) \in I, Q \in S\} \quad (3)$$

Where, \ominus is an erosion operator.

The set operation for dilation is given by

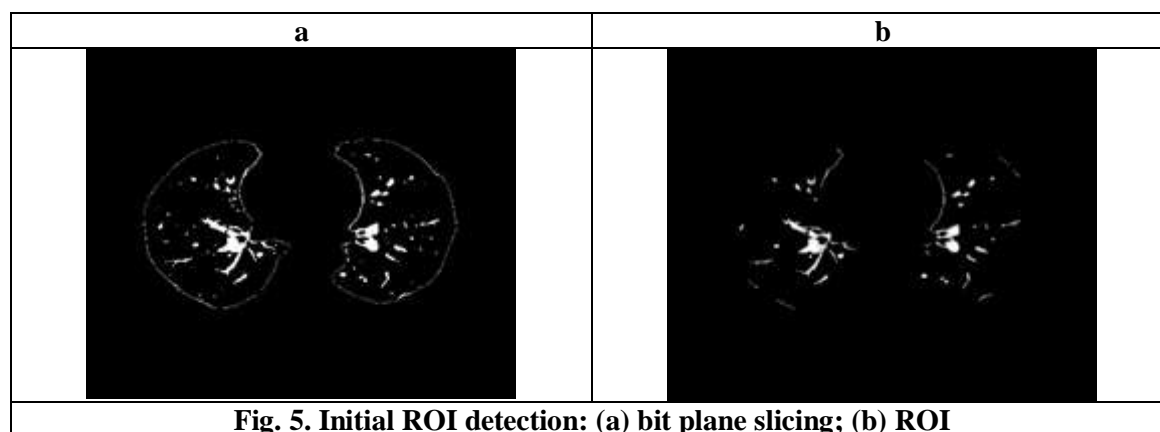
$$I \oplus S = \{(P + Q) \mid P \in I, Q \in S\} \quad (4)$$

It helps to fill holes in the foreground that are smaller than the structuring element (S). Filling of the holes inside the lung parenchyma is carried out using the closing function where the holes of particular size can be closed. The rolling ball algorithm that uses ball shaped structure elements is applied on the boundary to retain the pleural nodules. The lung parenchyma can be extracted by multiplying the mask with the original image. The results of the lung delineation is given in Fig.4.



2.3 Region of Interest

In order to facilitate the analysis of lung Nodule, the objects like lung Nodule are detected from the segmented lung parenchyma. The lung Nodules are usually has higher intensity therefore; the initial ROI detection is based on either intensity thresholding or bit-plane slicing. The problem associated with the above mentioned method is it will not detect Nodules with lower intensity level [12, 13]. In this work, we employ a multi-level thresholding for ROI detection. The ROI detection result is given in Fig.5. This method will not exclude any Nodule results very less False Negatives (FN).



2.4 Feature Extraction

The extracted ROIs can be distinguished as either Lung Nodule or other anatomical structure (vessels) by analyzing their size, shape and intensity features [14]. We consider the following features for the analysis ROI:

2.4.1 Area

Area of the segmented object is calculated by counting the number of pixels in the object region and it is multiplied by the spatial resolution of the pixel.

$$A = N * R \quad (5)$$

2.4.2 Circularity

Circularity is otherwise called Irregularity index which specifies the roundness of an object. The irregularities in the tumor are computed by the following formula

$$C = \frac{4\pi A}{p^2} \quad (6)$$

The value of circularity index ranges from 0 to 1. For perfect circles, its value is 1 and its value decreases as their irregularities increases.

2.4.3 Convex Hull

The convex hull of a set of points S in the plane is the enclosing convex polygon with the smallest area and perimeter of that region. A polygon is said to be convex only if the segment connecting any two points lie entirely within the polygon. The advantage of convex hull, it helps to detect spherical structures.

2.4.4 Convex Area

It gives the number of pixels in the convex image. Convex image is the representation of convex hull in the form of binary image.

2.4.5 Solidity

Solidity provides the proportion of the pixels in the convex hull that are also in the required region. Solidity is measured by the following formula:

$$S = \frac{\text{Area}}{\text{Convex Area}} \quad (7)$$

2.4.6 Major Axis Length

Major axis is the longest diameter of an ellipse and it passes through the foci, center, and vertices of an ellipse. The length of major axis (in pixels) is given by the formula:

$$\text{Major Axis Length} = f_1 + f_2 \quad (8)$$

Where, f_1 and f_2 are the distance from each focus to any point in an ellipse.

2.4.7 Minor Axis Length

Minor axis is the shortest diameter of an ellipse and it passes through the center of ellipse which is perpendicular to the major axis. The length of minor axis (in pixels) is given by the formula:

$$\text{Minor Axis Length} = \sqrt{(f_1 + f_2) - f^2} \quad (9)$$

Where, f is the distance between foci.

2.4.8 Eccentricity

It is the ratio of the distance between the foci of the ellipse over the major axis length. The value of eccentricity ranges from 0 to 1. Eccentricity is calculated by the formula:

$$E = \frac{c}{a} \quad (10)$$

Where, c is the distance between center and focus and a is the distance between foci and vertex. If the value equals 1 it forms an absolute circle. If its 0 it forms a line.

2.4.9 Maximum Intensity

The clinical importance of maximum intensity is to improve the detection of pulmonary nodules from blood vessels. It specifies the highest intensity range in the region.

2.4.10 Minimum Intensity

It specifies the low intensity range in the region. Since our ROI is not very low in intensity, this feature helps to eliminate the false positive.

2.4.11 Mean Intensity

It identifies the average of all intensities in the region. Some of our ROIs satisfy this intensity feature.

2.4.12 Equivalent Diameter

The value which indicates the diameter of a circle with the matching area as the region. The equivalent diameter is computed by the formula.

$$E_{dia} = \sqrt{\frac{4A}{\pi}} \quad (11)$$

2.4.13 Perimeter

It is determined across the border of the region by calculating the distance between each adjoining pair of pixels. In simple terms it is counting of pixels along the border. If the border has some disjoints then the results are unpredicted.

2.4.2 Background Intensity

The pixels around the nodule shows some significance change in intensities. The background pixels around the objects of interest is segmented as shown in Fig.6. The following intensity features were calculated:

- Background Maximum Intensity
- Background Minimum Intensity
- Background Mean Intensity

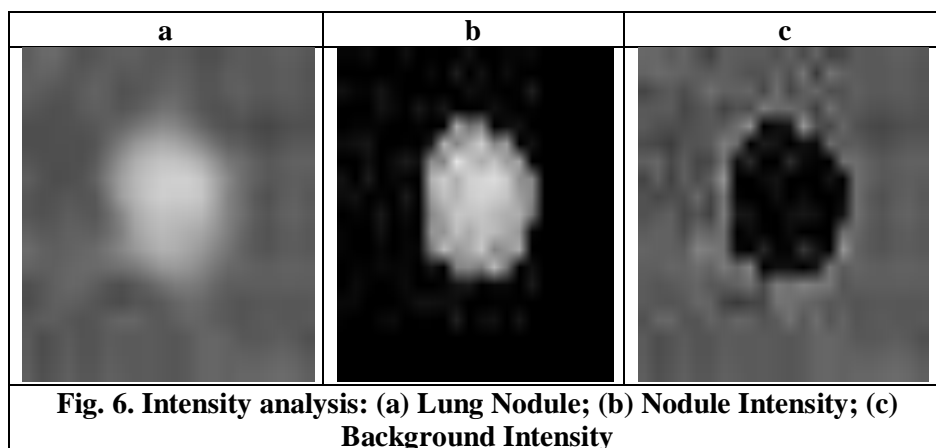


Fig. 6. Intensity analysis: (a) Lung Nodule; (b) Nodule Intensity; (c) Background Intensity

3. RESULTS AND DISCUSSION

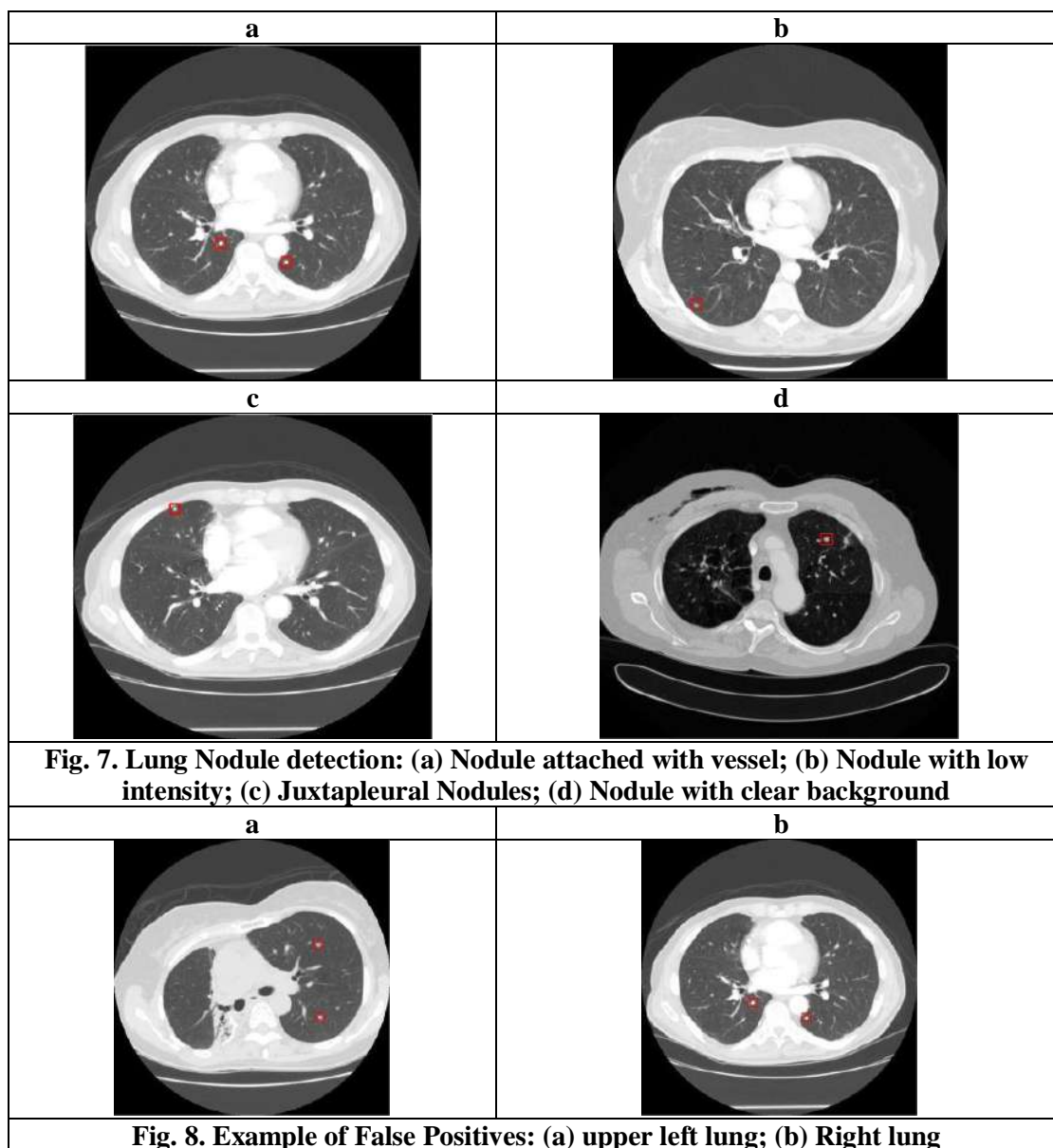
The results of feature extraction for different objects present in the lung region is given in Table 1. The results shows that the extracted features has potential for discriminating Nodule and other objects.

Table 1. Various feature values of different objects in the lung parenchyma

Features	Non-nodule	Nodule
Area	47.0±11.83	60±8.19
Perimeter	38.1±14.51	27.56±3.22
Eccentricity	0.9±0.04	0.50±0.17
Circularity	0.6±0.15	0.99±0.16
Convex hull	22.8±4.03	31±2.76
Convex area	86.8±15.51	63±4.11
Solidity	0.8±0.12	0.95±0.09
Equivalent diameter	9.3±2.78	8.74±1.78
Major axis length	15.8±4.48	9.51±3.48
Minor axis length	6.4±1.83	8.23±1.68
Max. Intensity	235.3±14.20	255±7.32
Min. Intensity	129.5±2.38	142±45.8

Mean Intensity	171.3±6.17	187.28±11.23
Background Max. Intensity	75.0±7.83	87±9.47
Background Min. Intensity	13.8±6.70	12±5.68
Background Mean Intensity	33.4±8.30	47.87±8.19

We have chosen 126 images from the LIDC database which produces 4032 objects, the above mentioned features were calculated for these objects. We employed random forest classifier [15], with 10 fold validation which gives the following classification results: specificity (87.3%), sensitivity (86.3%) and accuracy (86.8%). The final lung Nodule segmentation in the original image is given in the Fig.7. Since we have considered only a low level features the classifier produces some false negatives. An example of Nodule detection with false positives is given in Fig.8.



4. CONCLUSION

We have presented an unsupervised methodology for enhancement and delineation of lung parenchyma. The results show that accurate segmentation and contrast enhancement improve the accuracy of the final Nodule classifier. We have considered 16 features to classify nodules from non-nodules. In future, the false positives can be reduced further by considering high-level features and eliminating the false negatives in order to gain maximum efficiency for our CAD system.

REFERENCES

1. Siegel, Rebecca, et al. "The impact of eliminating socioeconomic and racial disparities on premature cancer deaths." *Ca-a Cancer Journal for Clinicians* 61.4 (2011): 212-236.

2. Lung Cancer Incidence and Mortality South-East Asia Region in 2012 Available at <http://www.globocan.iarc.fr/factsheets/cancers/lung.asp>. Accessed may 10, 2016
3. Midthun, David E. "Screening for lung cancer." *Clinics in chest medicine* 32.4 (2011): 659-668.
4. National Cancer Institute -National Lung Screening Trial. Available at <http://www.cancer.gov/types/lung/research/nlst>. Accessed may 10, 2016
5. Van Ginneken, Bram, Bart M. terHaarRomeny, and Max A. Viergever. "Computer-aided diagnosis in chest radiography: a survey." *Medical Imaging, IEEE Transactions on* 20.12 (2001): 1228-1241.
6. Armato III, Samuel G., et al. "The lung image database consortium (LIDC) and image database resource initiative (IDRI): a completed reference database of lung nodules on CT scans." *Medical physics* 38.2 (2011): 915-931.
7. Tong, Jia, Wei Ying, and Wu Cheng Dong. "A lung cancer lesions detection scheme based on CT image." *Signal Processing Systems (ICSPS), 2010 2nd International Conference on*. Vol. 1. IEEE, 2010.
8. Yao, Jianhua, John Bliton, and Ronald M. Summers. "Automatic segmentation and measurement of pleural effusions on CT." *Biomedical Engineering, IEEE Transactions on* 60.7 (2013): 1834-1840.
9. Kim, D-Y., et al. "Pulmonary nodule detection using chest CT images." *ActaRadiologica* 44.3 (2003): 252-257.
10. Lei, Peng. "Adaptive median filtering." *Seminar Report, Machine Vision*. Vol. 140. 2004.
11. Chuang, Keh-Shih, et al. "Fuzzy c-means clustering with spatial information for image segmentation." *computerized medical imaging and graphics* 30.1 (2006): 9-15.
12. Lin, Daw-Tung, Chung-Ren Yan, and Wen-Tai Chen. "Autonomous detection of pulmonary nodules on CT images with a neural network-based fuzzy system." *Computerized Medical Imaging and Graphics* 29.6 (2005): 447-458.
13. Kiran, Thapaliya, and Goo-Rak Kwon. "An advanced segmentation using bit-plane slicing technique in extraction of lungs region." *Internet (AH-ICI), 2011 Second Asian Himalayas International Conference on*. IEEE, 2011.
14. Böröczky, Lilla, Luyin Zhao, and Kwok Pun Lee. "Feature subset selection for improving the performance of false positive reduction in lung nodule CAD." *Information Technology in Biomedicine, IEEE Transactions on* 10.3 (2006): 504-511.
15. Breiman, Leo. "Random forests." *Machine learning* 45.1 (2001): 5-32.

Predicting Parkinson's disease Based on Gait Pattern using Machine Learning Techniques

Sridevi U. K, Hashini S, Janani K and Varsha P. S

Department of Applied Mathematics and Computational Sciences, PSG College of Technology, India

ABSTRACT

Parkinson's disease (PD) is a nervous system cognitive decline condition which mostly affects the motor function. The first indications show a common balance loss and instable body movements. Existing method to assessing and measuring gait abnormalities in PD have proven complex, difficult and inadequate in detecting abnormal movement behaviours. The data available from Physionet Gait database, a predictive analytical model is developed to identify abnormal movement behaviours in the gait patterns of seniors. Machine learning algorithms were implemented to the Parkinson disease collection, and analysis was conducted using Logistic Regression, Decision Trees, KNN and Random Forest. The findings show a learning performance and a prediction accuracy of 85% was obtained. Machine learning methods supply a powerful method for analysis, diagnosis and treatment of human gait.

Keywords— Gait Pattern, Machine Learning, Logistic regression, Random forest, K-NN

I. INTRODUCTION

Walking is something the average citizen is likely not giving much attention to. Walking has been our most common mode of travel, but an unwillingness to move or be active will transform a life of a person significantly. This can impair our freedom, and can also cause major short- and long-term health issues. Many people are walking about for years with little or no difficulty, not in regular pattern or asymmetric gait trends. Due to accidents the natural walking pattern may change and will lead to irregular gait patterns and needs medical treatments. This research analysis on walking patterns runs and can recognize the regular trends of gait that may be an indication to Parkinson's disease. The level identification helps to identify pain-causing problems as well as introduce and assess therapies to resolve anomalies.

Parkinson's disease is a chronic neural disorders condition causing indications of both the movement and non-motor. The most severe disorder of Parkinson's is severe neurological disorders mobility condition. PD requires a different of engine and non-motor features that description which varies somewhat among patients. Parkinson's is an evolutionary disease in neurology that induces motor and non-motor symptoms. Treatment offers pain relief but no existing therapy was shown to delay disease illness.

PD clinical studies include a method of assessing disorder seriousness by evaluating motor symptoms, assessing the ability to complete everyday cognitive tasks, and treatable medicine reaction. The Parkinson's disease phase and seriousness is an important consideration when making successful treatment choices. While the disease rating scale of the Parkinson offers an important framework for assessing the most significant characteristics of PD, it does not provide for PD classification. The scales used in the study of activities of daily life are the Unified Parkinson Disease Rating Scale (UPDRS) and Hoehn and Yahr (HY). PD study studies include a means of evaluating disease intensity by analyzing movement symptoms, assessing the capacity to perform everyday operational tasks, and indicative treatment responsiveness. Perlmutter etal (2009) provided useful guidelines about these assessments using ranking scales. While these are the most commonly used PD assessment scales, these scales still have significant disadvantages to be addressed when using them for scientific purposes.

Aich et al (2019) has discussed that the study on Parkinson's disease (PD) contribution to the cognitive disorder category which obviously impacts the neurons and shows the effect in terms of movement, speech and other brain disorders. Researchers are focusing towards the diagnosis and control of Parkinson's disease for the past few years, using both the speech analysis and the evidence from the gait study. Parkinson's disease (PD) is a neural disorder condition and mainly identified by symptoms of the motor and non-motor. PD prediction is carried out in the work of Anisha and Arulanand (2020) using classification accuracy since the outcomes of predictions are improved by integrating the same or related models. Parkinson's disease prognosis and development is a crucial concern for physicians as there is a variety in criteria taken into medical considerations making the diagnosis process more complex. Different datasets were systematically examined and extended to analyses the risk of disease and its development through machine learning.

Most of the famous works referred to the successful application of artificial intelligence methodology to test the disorder at various stages by walking patterns as well as person talks in associated information. Thus, in this

paper an attempt was made to differentiate PD group from safe comparison group based on voice recordings with feature selection and various classification method. Mandal et al (2017) created a prediction accuracy model to diagnose the PD patients. The accuracy, sensitivity, specificity is obtained using the logistic regression and machine learning algorithms.

II. LITERATURE STUDY

Parkinson's disease is a general neurology issue which influences the living conditions of individuals, contributing in particular to locomotive defects like postural dysfunction and posture abnormalities. Gait signal is among the essential indications of PD patients to recognize neurological dysfunction due to a failure in part of the brain functionality. In order to classify the Parkinson's gait, different classification methods using neurophysiological gait factors were discovered earlier. Zeng et al (2019) suggested a method for the analysis of walking style between PD patients and control subjects depending on neural learning algorithm

The interdependent complexity of the signs and persistence of Parkinson's in its initiation simplifies clinical diagnosis and clinical study understanding. Therefore, the research of methods that can forecast PD development is of great importance. In Ahmadi Rastegar's study (2019), samples from a medically described data were used in combination with machine learning algorithms to forecast survival rate. Using the standardized error analysis as an output metric, the statistical measures were for the intensity rates of movement symptoms.

Tsiouris et al (2017) research was suggested on a decision-making system to turn the motor indications of the UPDRS representation. The method estimates the Hoehn & Yahr rating scale of a Parkinson's person was importance because this specific measure is adequate to reflect diagnosis, extent of symptoms and development of the phase and disorder. Data mining algorithms are being used for the first time to improve the efficiency of Hoehn & Yahr stage prediction within a DSS. A category algorithm is learned in its central utilizing UPDRS information from the motor assessment, and subsequent cases can be further continuously categorized to give advice and enhance the final choice of the doctor. Using collected UPDRS data from PD patients' various methods of assessment and feature recognition approaches were assessed.

Prashanth et al (2018) suggested a conceptual and enhanced PD staging scale, and the creation of statistical models to determine the level and intensity of disease using machine learning techniques. Besides this, the value of aspects in PD is also measured using Random Forests. The results shows that SVM's statistical models, random forests classifier and probabilistic conceptual framework scored well It is suggested that associated with algorithms, UPDRS can formulate useful applications for forecasting PD stages that can support physicians in the treatment process.

Zhao et al (2010) studied the effects to determine advancement in neurological disease by evaluating the time required to migrate from one H&Y process towards the next phase and by analyzing measures correlated with H&Y crossfades use a massive PD database forward-looking data obtained. Information was collected from the National Institute of Neuroscience in Singapore movement disorder database. Survival research was introduced to analyze the time required to advance across different phases of H&Y. Cox regression modeling has been used to analyze the relationship at the gateway for each H&Y period between base measures and the development to another phase. Analysis of Cox regression showed that diagnosis, longer period of PD and greater increase movement ratings of UPDRS were correlated with a considerably faster development across different H&Y stages.

Gender and nationality have never been connected with cognitive decline. In summary, H&Y progression duration is a beneficial measurement of progression of the disease in PD and can be used to assess clinical strategies and diagnostic aspects in PD in clinical trials. Deep brain stimulation (DBS) is the preferred clinical method for Parkinson's disease of mild to severity. Moreover, limited research evaluated its effectiveness in extreme PD as established by the updated H&Y level. Research by Kahn et al (2019) assesses the continuing and treatment effects of DBS in acute PD. From 2008 to 2014, report obtained retrospectively data on 15 patients diagnosed with DBS with serious PD. The comparative evaluation of the updated rating scale and the movement section of the UPDRS III were used for quantitative evaluation of extent and progress of motor function, collectively. Regular doses of daily doses of anti parkinson's medications have been used to assess drug burden improvements. Evidence were analyzed using univariate analyzes and conducted the statistical test. The rating scales analysis the problems associated with Parkinson's diseases sensitivity and risk.

Dávid et al (2019) examined the association between adjustments in the movement test portion of the Movement Disorder Society-sponsored Unified Parkinson's Disease Rating Scale (MDS-UPDRS). The ratings

during most of the acute levodopa test and calculated a threshold level on both the Parkinson's disease composite scale (PDCS) suggesting statistically significant improvements. MDS-UPDRS helps to identify the patients with the Parkinson disease. The correlation is high between MDS-UPDRS and PDCS motor scores and the clinical relevant responses shows the reliability of the test.

Balestrino et al (2019) research was conducted to evaluate the existence of Parkinson's disease symptoms, their occurrence by movement subtype, and wellbeing -related better-quality relationships using the currently tested Parkinson's Composite Disease Scale. Association. Symptom occurrence was measured by item rating. MDS-UPDRS types were transformed onto the PDCS using ROC analysis and Youden approach to obtain a similar grouping dependent on the PDCS results. In the research the same approach has been used to predict rates of occurrence from many other tests. The correlation and multiple linear regressions analyzed the relationship between PDCS and quality of life The comparative PDCS-based formula given these cut-off values with this grouping as measure.

Açııcı et al (2017) proposed a specific development of wearable sensor data mining to assess gait level of the patients with Parkinson's disease. The learning implements a supervised Random Forest-based algorithm that analyses the collected from sensors to determine the movement of patients with these detectors. The attempt to derive from their gait patterns which would be accurate in identifying healthy and ill person. The research outcomes on a comparison framework showed that the suggested approach could strongly exceed established literature-reported methods.

III. METHODOLOGY

Parkinson's disease is a developmental cognitive difficulties that induces motor functions and non-motor symptoms. Medication offers pain relief but no existing medication was shown to delay neurological decline. PD study experiments use a process of scoring disorder seriousness by analyzing motor signs, examining the ability to accomplish everyday cognitive functions, and diagnosable treatment responsiveness. The Parkinson scale which are consider are Hoehn Yahr Scale, UPDRS Scale and UPDRSM Scale. Figure 1 shows the Parkinson's disease rating method of classification.

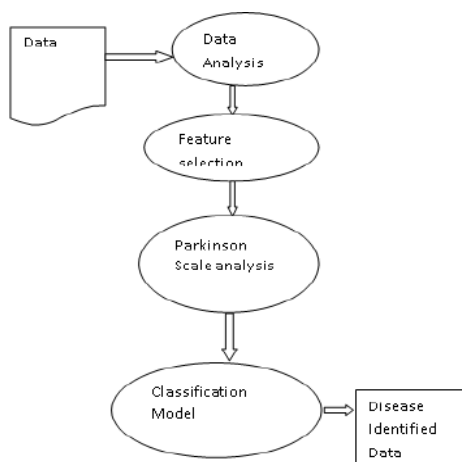


Figure.1 Gait pattern classification using Parkinson scale analysis

The two most widely used assessment method of the Hoehn and Yahr scale, and the Disorder Score Scale of the Unified Parkinson. Every one of these ranking levels, providing specific guidance about how to conduct such scores, is outlined. Whereas these are the most commonly established PD score measures, such measurements still have major drawbacks to be recognized when used them for medical purposes. There are many different value levels that can be used to classify an individual or group level of Parkinson's disease To distinguish individuals into either safe or parkinsonian groups using different methods of identification such as K nearest neighbors (K-NN), the multinomial Logistic regression, random forest and decision tree algorithms. Extraction of the attribute is acquired from human activity, and it is also effective of grouping people with or without disease. Evaluation of the gait trends among disease symptoms and control subjects. The Gait attributes are as follows:

1. Target : whether the person has PD or not
2. Subject number
3. Gender

4. Age
5. Height in meters
6. Weight in kilograms
7. Hoehn-Yahr scale : Symptoms for disease progress
8. UPDRS : Unified Parkinson's Disease Rating Scale
9. TUAG : Time up and go is a simple measure of mobility
- 10.Speed_01 (m/sec) : speed maintained to walk 1 meter
- 11.Speed_10 (m/sec) : speed maintained to walk 10 meter

The supervised learning using machine learning methods used to generate a model that would generalize to disease classification. The classification system has four components:

1. A feature representation of the input. For each input observation $x(i)$, this will be a vector of features $[x_1, x_2, \dots, x_n]$.
2. A classification function that computes y , the estimated class, via $p(y|x)$. The function $f(c,x)$ represent the classification of x to the class c .
3. An objective function for learning, usually involving minimizing error on training examples.
4. An algorithm for optimizing the objective function uses the stochastic gradient descent algorithm.

The logistic regression uses maximum likelihood estimation. The estimated parameters values are adjusted iteratively until the maximum likelihood value for the estimated parameters is obtained. The disease severity in each patient was examined using the Hoehn and Yahr Scale and the unified Parkinson's disease Rating Scale (UPDRS) parts Multinomial logistic regression is employed to assess the disease to the patient. Multinomial aim is to create a framework that will link predictors to the probability of dropping at particular target levels. Let $P_j, j=1,2,\dots,J$ be the probability of mapping in the j^{th} level of a target variables Y . The primary objective was to build a model for P_j that takes the predictor values x , where $\sum_i p_j = 1$. The method identifies the best the category for best classification. The response is to create all logits equal to one of the rates, which is called the tier of the threshold. When it is possible to interpret one of the goal criteria as unique from each other, it is normal to use it as the guideline. The logistic regression model was then

$$\log\left(\frac{P_j}{P_j}\right) = \beta_{0j} + \beta_{1j}x_1 + \dots + \beta_{kj}x_k, \quad j = 1,2, \dots, J - 1$$

Where β_{0j} is the intercept parameter and $\beta_{0j}, \dots, \beta_{kj}$ is the vector of j dimensional slope parameters. The model incorporates equations, each of which is based on a distinct set of parameters β . The weights is the learning rate. The initial weights are assigned and the new weights learning is done using the formal:

new_weight = existing_weight - learning_weight * gradient

$y = 0.20960829 * \text{gender} + 0.24066011 * \text{age} - 0.0160451 * \text{height} - 0.05383171 * \text{weight} + 1.13601452 * \text{HoehnYahr} + 0.46693391 * \text{'UPDRS'} + 0.26705249 * \text{'UPDRSM'} + 0.22108785 * \text{'TUAG'} + 0.01986023 * \text{'speed_01'} + 0.02669533 * \text{'speed_10'} + 11.45224632$

Hoehn and Yahr score can be used in the classification of disease stages. The Unified Parkinson Disease Rating Scale (UPDRS) identifies the decline in motor unction and difficulties in activities of daily living. The performance of the model during testing is quantified by the scoring value and for every person the Parkinson disease was predicted with the probability value obtained. The Parkinson's disease classification cut-off value was kept as 0.5 and the patient's data were classified into PD patients or non-PD patients by the logistic regression model. The model is compared with random forest and KNN algorithm. Random forest algorithm takes the randomly generated training sets and corresponding the decision trees are generated and the selected

attributes ‘m’ are done by optimal splitting of the node. Each tree is allowed to grow integrally, without being pruned. By considering the decision tree the test data are classified and the output categories are determined.

IV. EXPERIMENTAL RESULTS

The patient’s data are collected from the reference given in Goldberg et al (2003) and it is available in Physionet (<https://physionet.org/content/gaitpdb/1.0.0/>) based on the Gait pattern. This collection includes gait measurements from 93 patients and the average age considered is 66.3years. In specific PD cases there are significant variations between changes in conditions and the results of various treatments. Additionally, with a significant number of interventions and clinical studies, few definitive data on significant treatment relation to functional improvements in PD signs have been obtained. There are various reasons for these failures: first, the shortcomings in effect verification and analysis of existing disorder features; second, challenges in deciding treatment parameters; third, issues in identifying responsive disease development biomarkers. The big downside is that disorder occurs well before the first troubling motor signs are noticed by an actual patient. The gender based group on attribute score HoehnYahr and Tuag for the dataset was given in the Table 1 and Table 2

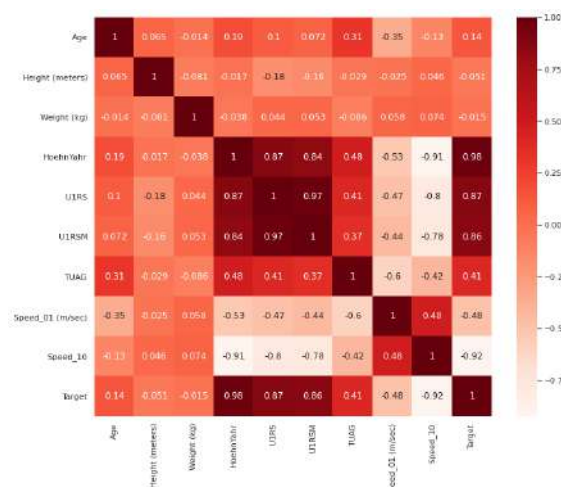


Figure 2 Correlation matrix of gait features

Table.1 Gender based Data Analysis based on Hoehn Yahr

Gender	Age	Height	Weight	HoehnYahr
Female	64.4705	65.460	62.397	1.1764
Male	65.602	50.439	77.387	1.326

Table.2 Gender based Data Analysis based on UPDRS AND TUAG

Gender	UPDRS	UPDRSM	TUAG	Speed_01	Speed_10
Female	14.235	8.676	10.145	1.1045	0.134
Male	19.693	12.132	10.006	1.1285	0.103

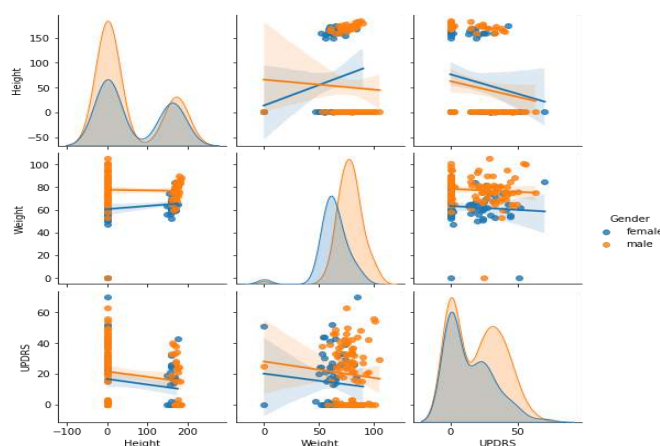


Figure 3 Gender based variable interactions

The gender based variable interaction attributes are shown using the figure 3. The correlation matrix of the gait features was analysed and was given in Figure 2. The high correlation indicates the gait characteristics and optimal features for classification of PD needs to be determined. The features extracted mainly univariate selection using chi-square and feature importance is obtained based on the correlation and tree based classifier. The correlation value above 0.5 was taken as relevant feature and given in the table 3 and Figure 4.

Table. 3 Features selected

Feature	Value
HoehnYahr	0.975055
U1RS	0.871941
U1RSM	0.857827
Speed_10	0.923113
Target	1.000000

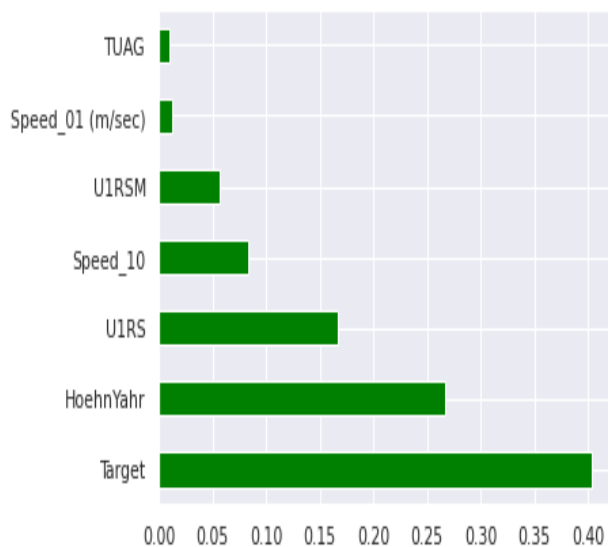


Figure.4 Feature extracted for Gait analysis

A regression capturing the relation between one variable and another, eg Age and TAUG Score plot is given in the figure 5.

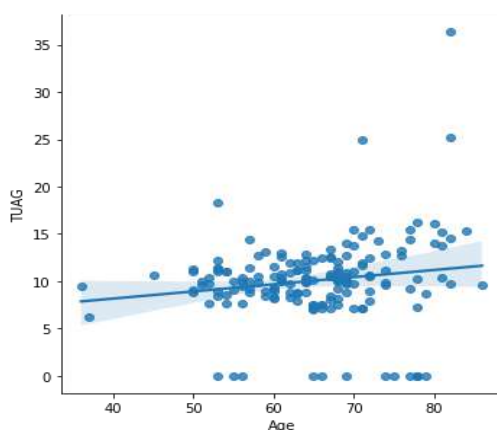


Figure 5 Regression analysis on Age and TAUG

The method used are Logistic regression, k-nearest neighbour grouping, decision tree, random forests to model predictions. Figure 4 shows the features extracted for gait analysis. The non-parametric model KNN is inefficient in identifying the data nodes with neighbours. The parametric model LR can quickly derive information from the adjusted coefficient. The output of the LR is analysed by rating the training model and measuring the forecasted PD likelihood for each person. The method calculate the number of cases in the testing dataset correctly identified as PD patients or properly categorized as non-PD patients. The cut off value of 0.5 for the expected likelihood of Parkinson's disease was kept for logistic regression model. The best coefficient will results in the algorithm estimating the outcome for the class that is very near to 1 but for the other class, the

result quite close to 0. The rationale for maximum likelihood of logistic regression is that an experiment in order finds quality for the parameters, which minimizes the likelihood error expected by the algorithm to others in the dataset. The features associated for the development of Hoehn-Yahr and UPDRS classification done on the different analysis including the patient's age and suffering from disease. Collinearity is treated better by decision tree than LR.

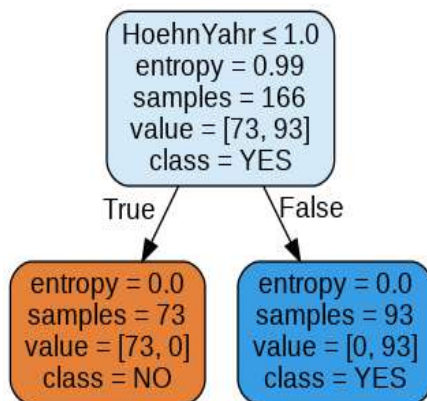


Figure. 6 Decision tree classifier for Hoehn Yahr scale

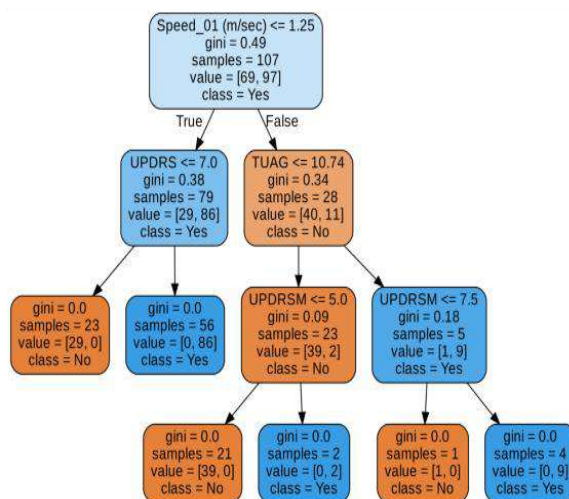


Figure.7 Random forest classifier for gait analysis

In Random Forest average was chosen as the performance expected. The Random Forest model would be less likely to over fit than the Decision tree, which will have a more specific approach. Random Forest is better and much more reliable than the decision trees. Unless the rating of the Hoehn Yahr scale is less than or equal to 1 then Parkinson's disease could be the subject. Figure 6 shows the decision tree based on the Hoehn Yahr scale. The Random Forest (RF) is a "ensemble learning" strategy that consists of the collection of a significant number of decision trees, consisting in a reduction of difference relative to the single decision trees. Using information gain feature selection and Sequential Forward Selection the features from all features that was identified as the most important. All features are evaluated according to the attributes of their information gain. Figure 7 shows the random forest classifier tree for gait analysis.

Table. 4 Classification Report for K-NN model

	Precision	Recall	F1-score	Support
dual-task walking	1.00	0.29	0.44	7
Rhythmic Auditory Stimulation	1.00	1.00	1.00	15
Treadmill walking	0.69	1.00	0.81	11
Accuracy			0.85	33
Macr avg	0.9	0.76	0.75	33
Weighted avg.	0.90	0.85	0.82	33

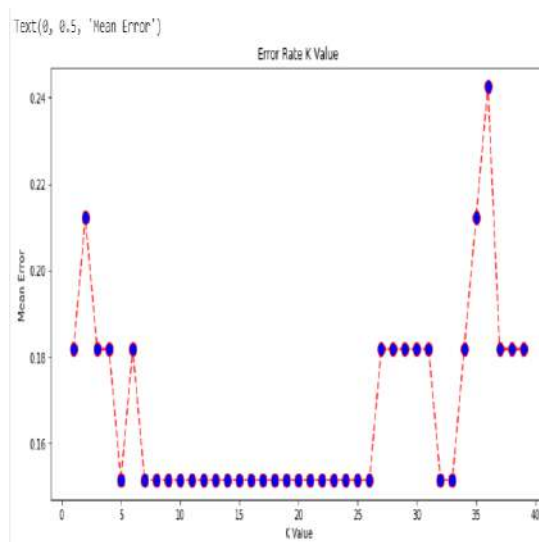


Figure.8. K-NN model Error rate for k value between 1 and 40

All gait characteristics were included in the model and the machine learning model can be adopted in feature learning and classification.

Table. 5 Accuracy of Models

Model	Accuracy
Logistic regression	0.8324
Decision Tree	0.8598
KNN	0.86021
Random Forest	0.86026

Different split ratios for training and testing (70/30%, 80/20%, and 90/10%) were used, due to similar results and to have more data for training, 90% data for training and 10% for independent testing were used in final analysis. KNN Model predicts class based on the distance metrics and gets the most frequent class. The predicted class is based on the sorted order based on a distance values. The study data is collected from 3 different gait characteristics taken from Physionet dataset are dual task walking, Rhythmic auditory stimulation and Treadmill walking and the classification report is given in the table 4 and error for different k values are given in the figure 8. Table 5 shows the result of 10-fold cross validation on the datasets. The accuracy for the logistic regression was 83.24% and the variance is 0.17%. Random forest, KNN model has given the accuracy of 86%. Machine learning model on gait pattern analysis helps in identification of Parkinson diseases at earlier stage may help to give better treatment. Further model learning was done by hyper-parameter tuning and feature reduction methods that may increase test classification results.

V. CONCLUSION

The research combines the traditional statistical averaging methods and diagnosis of PD with different machine learning approaches. Accurate identification of human gait patterns includes the collection and standardization of gait patterns, choice of specific gait attributes and analysis of gait abnormalities. The results are highly patient-dependent and couldn't provide accurate information to forecast the actions of new patients. The prediction based methods to machine learning offer basic rules for forecasting patient's assessment based on the Parkinson's disease classification scales. Comparative analysis of learning algorithm results found that for new cases, random forests exhibited greater precision and proper generalization. The approach of machine learning can give a simple tool to investigate the patterns of gait and identify disorders.

REFERENCES

- Açııcı K., Erdaş Ç.B., Aşuroğlu T., Toprak M.K., Erdem H., Oğul H. (2017) A Random Forest Method to Detect Parkinson's Disease via Gait Analysis. In: Boracchi G., Iliadis L., Jayne C., Likas A. (eds) Engineering Applications of Neural Networks. EANN 2017. Communications in Computer and Information Science, vol 744. Springer, Cham. https://doi.org/10.1007/978-3-319-65172-9_51
- Ahmadi Rastegar, D., Ho, N., Halliday, G.M. *et al.* (2019). Parkinson's progression prediction using machine learning and serum cytokines. *npj Parkinsons Dis.* 5, 14

3. Aich, Satyabrata & Kim, Hee-Cheol & younga, Kim & Hui, Kueh & Absi, Ahmed & Sain, Mangal. (2019). A Supervised Machine Learning Approach using Different Feature Selection Techniques on Voice Datasets for Prediction of Parkinson's Disease. 1116-1121. 10.23919/ICACT.2019.8701961.
4. Aich, Satyabrata & Sain, Mangal & Park, Jinse & Choi, Ki-Won & Kim, Hee-Cheol. (2017). A mixed classification approach for the prediction of Parkinson's disease using nonlinear feature selection technique based on the voice recording. 959-962. 10.1109/ICICI.2017.8365279.
5. C. D. Anisha and N. Arulanand, "Early Prediction of Parkinson's Disease (PD) Using Ensemble Classifiers," 2020 International Conference on Innovative Trends in Information Technology (ICITIIT), Kottayam, India, 2020, pp. 1-6, doi: 10.1109/ICITIIT49094.2020.9071562.
6. Balestrino, R., Hurtado-Gonzalez, C.A., Stocchi, F. *et al.* (2019). Applications of the European Parkinson's Disease Association sponsored Parkinson's Disease Composite Scale (PDCS). *npj Parkinsons Dis.* 5, 26
7. Pintér, Dávid & Martinez-Martin, Pablo & Janszky, József & Kovács, Norbert. (2019). The Parkinson's Disease Composite Scale Is Adequately Responsive to Acute Levodopa Challenge. *Parkinson's Disease.* 2019. 1-8. 10.1155/2019/1412984.
8. Goldberger AL, Amaral LAN, Glass L, Hausdorff JM, Ivanov PCh, Mark RG, Mietus JE, Moody GB, Peng C-K, Stanley HE. *PhysioBank, PhysioToolkit, and PhysioNet: Components of a New Research Resource for Complex Physiologic Signals* (2003). *Circulation.* 101(23)
9. Kahn L, Mathkour M, Lee SX, Gouveia EE, Hanna JA, Garces J, Scullen T, McCormack E, Riffle J, Glynn R, Houghton D, Lea G, Biro EE, Bui C, Sulaiman OA, Smith RD, (2019),
Long-term outcomes of deep brain stimulation in severe Parkinson's disease utilizing UPDRS III and modified Hoehn and Yahr as a severity scale, *Clin Neurol Neurosurg.* 179:67-73.
10. Mandal, Dr. Indrajit & N.Sairam,. (2012). New machine-learning algorithms for prediction of Parkinson's disease. *International Journal of Systems Science.* 45. 10.1080/00207721.2012.724114.
11. R Prashanth, S. Dutta Roy, (2018), "Novel and improved stage estimation in Parkinson's disease using clinical scales and machine learning", *Neurocomputing*, 305, pp. 78-103.
12. Perlmutter JS. Assessment of Parkinson disease manifestations. *Curr Protoc Neurosci.* 2009 Oct;Chapter 10:Unit10.1. doi: 10.1002/0471142301.ns1001s49. PMID: 19802812; PMCID: PMC2897716
13. Saxena, Merry & Ahuja, Sachin. (2020). Comparative Survey of Machine Learning Techniques for Prediction of Parkinson's Disease. 248-253. 10.1109/Indo-TaiwanICAN48429.2020.9181368.
14. K. M. Tsiouris et al., "Mining motor symptoms UPDRS data of Parkinson's disease patients for the development of Hoehn and Yahr estimation decision support system," 2017 IEEE EMBS International Conference on Biomedical & Health Informatics (BHI), Orlando, FL, 2017, pp. 445-448, doi: 10.1109/BHI.2017.7897301.
15. Zhao YJ, Wee HL, Chan YH, Seah SH, Au WL, Lau PN, Pica EC, Li SC, Luo N, Tan LC. (2010), Progression of Parkinson's disease as evaluated by Hoehn and Yahr stage transition times, *Mov Disord.* ,25(6):710-6. doi: 10.1002/mds.22875.
16. Zeng, Wei & Yuan, Chengzhi & Wang, Qinghui & Liu, Fenglin & Wang, Ying. (2019). Classification of gait patterns between patients with Parkinson's disease and healthy controls using phase space reconstruction (PSR), empirical mode decomposition (EMD) and neural networks. *Neural Networks.* 111. 10.1016/j.neunet.2018.12.012.

An Evaluation on Theories and Models in Eye Anatomy Interconnected Side Effects and Pro-Longed Diseases

Sowmiya M¹, Banu Rekha B^{2*} and Malar E³

^{1,3}PSG Institute of Technology and Applied Research, Coimbatore, India

^{2*}Department of Biomedical Engineering, PSG College of Technology, Coimbatore, India

ABSTRACT

Concentrates on connected with eye vasculature are acquiring consideration as of late because of the harmless nature and the information encased in vascular primary imaging helps in the finding of different fundamental sicknesses like cardiovascular illnesses, Diabetic Retinopathy (DR), hypertension and stroke. The construction of veins in the retina gives adequate degree to concentrate on the underlying and practical qualities of the circulatory framework. This paper gives an organized audit on the hypothesis and model of the eye, foundational infections and retinal imaging strategies, with an emphasis on foreseeing Cardiovascular Disease (CVD) risk factors from retinal pictures and the meaning of Artificial Intelligence methods in anticipating illnesses.

Keywords— Digital image processing, Eye anatomy, Cardiovascular disease, Retina.

INTRODUCTION

Eye endows with the vision of sight to observe the world around us. The main significant parts of the eye are cornea, pupil, iris, cornea, retina, choroid and sclera. Retinal layers convert the light into neural signals which is processed in the visual cortex of the brain. Vascular changes in veins, arteries and capillaries within the eyes affect the circulatory system includes. Since retina allows direct non-invasive examination of the circulation, which will be useful in diagnosing both eye and systemic diseases. Ocular diseases like age related macular degeneration, glaucoma and systemic diseases include diabetic retinopathy, hypertension, and cardiovascular diseases can be predicted by examining the anatomical structures of retinal images [1].

Advancement in imaging techniques developed several medical imaging devices to capture the different parts of the eye and observe the pathological signs. Fundus photography and Optical coherence Tomography are widely used techniques to capture the retinal images [1]. Growth in Computer-Aided Diagnosis (CAD) has anticipated giving the ophthalmologists suggestions for diagnosing and treating the diseases. It not only guides the clinicians with objective opinion, but also suggests the progression of diseases for routine screening and early detection. With the development of Artificial Intelligence (AI) techniques, analyzing and examining the medical images provides higher accuracy of prediction of diseases. This paper reviews the research on retinal imaging techniques, the most prevalent diseases discover from retinal images, and the role of AI in diagnosing ocular diseases.

CLINICAL BACKGROUND

Anatomy of the eye

Figure 1 represents the structure of the eye. Eye structure consists of various anterior and posterior chambers. The outer layer contains transparent cornea, and the sclera. The cornea consists of tissues that help to focus the light. The eye color is determined by the iris that is also involved in controlling the pupil through its set of muscles. Pupil is termed as the opening in the middle of the iris part. The amount of light entering into the eye is manipulated through this opening. Retina is situated in the inner eye that consists of light sensitive cells. The lights that are reflected from an object fall on retina and are converted into electrical signals. These signals are sent to the brain for processing through the optic nerve. The optic nerve is a thick bundle of nerve fibers attached to the back of the eye[2]. It transmits visual information from the retina to the brain.

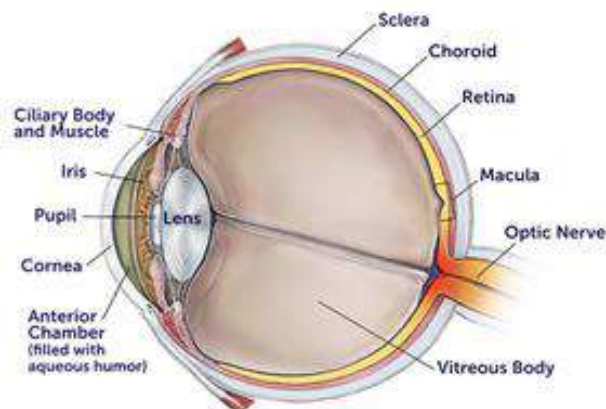


Fig 1. Cross sectional view of the Human Eye [1]

OPTIC DISK

The area where the optic nerve connects the brain to the retina and the size is about very few mm in diameter. This area is called the optic disc. It is the point through which major blood vessels enter the retina. The central point of the optical disc is called the optic cup. Severity of glaucoma can be assessed through the variation in this cup to disc ratio. However, the ratio and inclination of main vessels vary in eyes [2].

MACULA

The macula is the middle of the retina, which is responsible for sharp and fine vision. The macular area looks darker and has a diameter of approximately 5 mm. The center of the macula contains fovea which produces visual acuity with the help of cone cells. Age related macular degeneration severely impair the central vision which is diagnosed by fluoresce in angiography and optical coherence tomography [2]. Exudates in the macular region may be originated in diabetic retinopathy, and age-related macular degeneration

RETINA

The retina has layer of sensitive tissue, located near the optic nerve head. Photoreceptors associated process the incoming light and send the signals on to the brain. Retinal blood vessels include arteries, veins and its branches. The vessel carries oxygen and nutrients are called as arteries, where veins supply low oxygen blood to the heart. Color and caliber will distinguish the arteries and veins. The arteries appear in bright red color with narrow width. Veins have wider width, and dark red color. The ratio of the width of an artery to a vein is 2:3 for normal subject.

Retinal Imaging Modalities

Retinal imaging techniques have been developed rapidly to diagnose the retinal and systemic diseases. It acquires a detailed picture of the interior eye which shows the retina, blood vessels, and optic disk. Imaging techniques enable non-invasive evaluation of vascular structures. This helps the ophthalmologist to discover vision loss, distinct diseases and check the health of eyes. The review presents the widely used fundus imaging modality with a clinical application. Figure 2 shows the fundus photography.

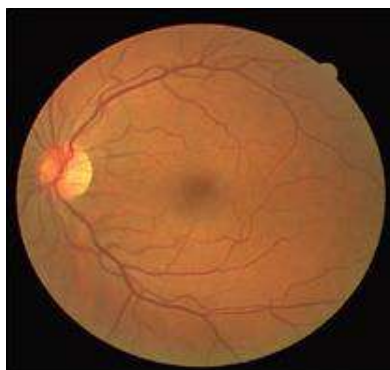


Fig 2. Fundus image [3]

Fundus photography is widely utilized in clinics for to monitor the severity of systemic diseases especially diabetic retinopathy, cardiovascular disease. Optical coherence tomography (OCT) is preferred for examining the choroidal vascular structure and macular edema. Fluorescence in angiography is used to monitor the patient's condition on a routine basis.

Fundus camera captures the structure of retina, blood vessels and optic disk in two-dimensional (2D) view. Field of view gives the angle range of the image for magnification. Traditionally used fundus cameras provide 30° to 45° field of view [1]. Imaging beyond 50° is called wide-field photography and it can be increased with the help of montage patterns. Figure 3 shows the montage image. German ophthalmologist in 1891 obtained the first photographic images of the retina, which shows the blood vessels [1]. Gullstrand developed the fundus camera, which is widely used to image the retina. The modality would be chosen based on its safety and cost, since fundus imaging had persisted as the primary method of retinal imaging.

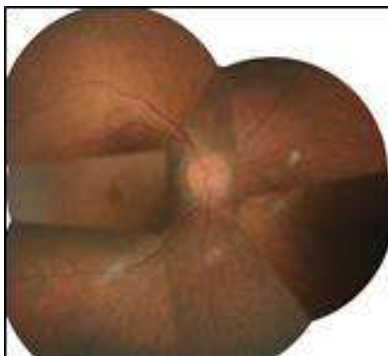


Fig 3. Montage fundus image of the right eye of a patient [4]

The next modality is fluorescent angiography technique, where a fluorescent dye is injected into the blood stream. As dye passes through the blood vessels, photographs reveal the abnormality or pathological signs in the retina. OCT that stands for Optical Coherence Tomography generates 3D cross-sectional images of the retina. Since this is a non-invasive technique, it has found wide popularity. Using OCT, the retinal layers could be differentiated to examine the retinal diseases.

Fundus photography is used for mass screening and detection of various ocular and systemic conditions.

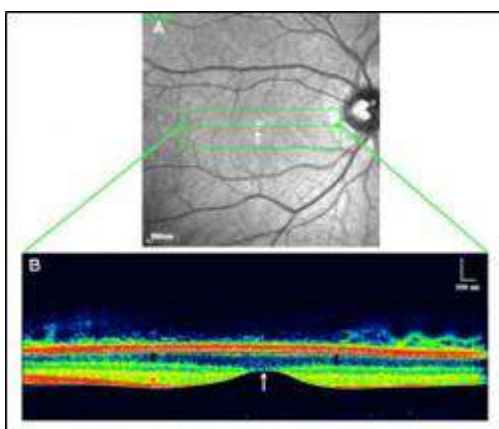


Fig 4. Fundus photo and Optical coherence tomography images [5]

Retinal and Systemic Diseases

Retinal vasculature shares the microcirculation with heart and brain; various diseases show their progression in the retina. This section gives an overview of the most dominant diseases that can be examined via retinal images. The diseases include age-related macular degeneration (AMD), glaucoma, diabetic retinopathy which are the common cause of blindness. Therefore, understanding their implications and severity stage provides earlier detection and treatment in clinical fields.

A. DIABETIC RETINOPATHY

Diabetic retinopathy (DR) is a complication of diabetics which damages the retinal blood vessels. It occurs due to high blood sugar levels in subjects [5]. In early stages, vessel swelling, bleeding and bulging of capillaries occur in the retina which is categorized as non-proliferative diabetic retinopathy. It develops the abnormal lesions like Microaneurysms (MAs), hemorrhages, exudates and cotton wool spots [6]. MAs occur due to bulging of retinal capillaries and it appears as small, round dots in fundus images. The count of MAs has a relationship to examine the severity of DR. The diameter of MAs ranges from 10 μm to 100 μm . Exudates are yellowish white fatty lipids with irregular shape and size. Hemorrhages are larger than MAs which appear in dot and flame shape [6]. Figure 5 illustrates the retina with lesions. In advanced stage, abnormal blood vessels will

grow on the retinal surface called as proliferative diabetic retinopathy. It leads to complication of vitreous hemorrhage, retinal detachment, blindness. Figure 5 shows the retina with abnormal lesions.

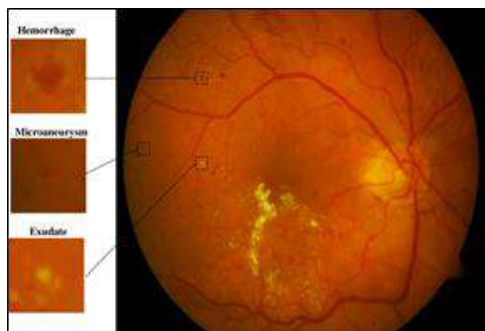


Fig 5. Retinal Fundus Image with abnormal lesions for DR [6]

B. Age-related macular degeneration (AMD)

Age-related macular degeneration (AMD) leads to gradual damage to the macula, which is responsible for central vision. It occurs for people over the age of 60 years. Aging and family history are the significant risk factors for AMD. There will be no early-stage symptoms for AMD. The two types are dry AMD and wet AMD. In dry AMD, yellowish deposits accumulated in the macula. In Wet AMD, there will be growth of new blood vessel into the macula which leaks fluid into the retina. Figure 6 shows the effect of AMD.

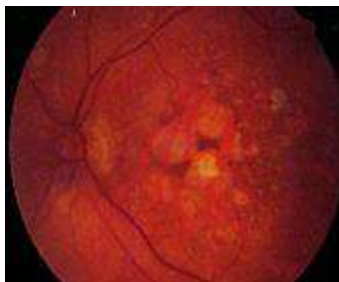


Fig 6. Age-related macular degeneration [7]

C. GLAUCOMA

Glaucoma is the cause of blindness, which damages the optic nerve and produces the loss in visual field [3]. Main risk factor of glaucoma is elevated intra ocular pressure (IOP) that damages the blood vessels and optic nerves as shown in Figure 7. Also optic disk is damaged which is replicated in varying optic disk cup ratio. Glaucoma is called as 'sneak thief of sight' because it damages the nerves without any early symptoms. Early detection and treatment will diminish the visual loss due to glaucoma.

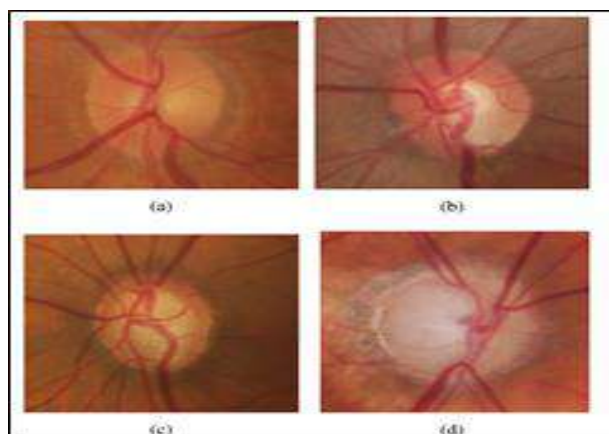


Fig 7. Retinal Fundus Images

(a) No Glaucoma (b) Early Glaucoma (c) Moderate Glaucoma and (d) Severe Glaucoma [3]

D. CATARACT

Protein in the eye prevents the lens to send clear images to the retina which forms a cloudy area in the lens. Cataract causes blurry vision, double vision, fading of colors. The cataracts develop slowly and become severe for adults resulting in visual disorders. The symptoms include diabetes, smoking, obesity, eye injury. Cataracts can be cured by surgery where artificial lens replace the damaged lens [8].

CARDIOVASCULAR DISEASE

Cardiovascular diseases remain the leading cause of mortality even though advances in prevention and diagnosis therapy available. It places a substantial burden on the economies of low- and middle-income countries. Many people are diagnosed late in the progression of disease and may die in younger age. The risk factors include high blood pressure, cholesterol, smoking, alcohol consumption, obesity which are modifiable and other case includes age, gender, and genetic history. Though many studies are available to predict CVD risk from risk factors, still there remains a need for early-stage prognosis and risk stratification.

The clinical test includes Coronary Computed Tomography, ECG to diagnose CVD, research studies show the interest in non-invasive mode of identifying the risk of CVD. The retina offers an opening to study in vivo the structure and pathology of the human circulation. Retinal vasculature can be observed non-invasively which provide the pathway to examine heart diseases, hypertension, stroke, diabetics. Microvascular alterations provide significant information to examine the systemic diseases. Cardiovascular diseases are characterized by changes in the vascular structure of retina. There have been numerous researches showing the relationship between vessel calibre changes and its development to heart diseases. Medical image analysis is stepping to transition into AI-powered medical professions. DL has been used to detect diabetic retinopathy, glaucoma, macular edema and age-related macular degeneration from retinal images. Also, DL is used for screening and monitoring major eye diseases for patients in primary care settings. DL in fundus imaging may be considered as a screening tool to identify early risk factors of CVD. This paper outlines the initiative of predicting cardiovascular risk factors from retinal images.

The retinal circulation shares various features with the heart and cerebral microcirculation. As the eye's vasculature structure is easily examined from retinal images, which may indeed be a window to the heart. Changes in the microvasculature structure can be used for the diagnosis of cardiovascular diseases. Cardiovascular diseases include hypertension, coronary heart disease, diabetes, and obesity. Systemic conditions have association with vascular changes in the retina.

Small changes in the blood vessels within the eyes affect the vascular, circulatory and cerebral system. Vessel caliber and vascular morphology are the significant biomarkers derived from fundus photography.

Reduction in the width of the retinal arterioles to venules (AVR) is a predictor of diseases like hypertensive retinopathy, stroke and CVD occurrence. Specifically, in women narrower retinal arterioles and wider venules was associated with the extent of CAD. AVR is calculated as ratio of Central Retinal Artery Equivalent (CRAE) and Central Retinal Vein Equivalent (CRVE). From the vessel segmentation graph, ROI is fixed around OD. Six arterioles and venules having width greater than 30 μm are considered inside ROI. The CRAE and CRVE are determined by using the modified Knudston formula.

Widened venules have more effect in cardiovascular diagnosis. Arteriovenous nicking and occlusions are observed due to vascular damage [1]. Figure 8 shows the signs of CVD in retinal images. Diabetic retinopathy is caused by the damage to the retinal blood vessels. The major cause of this damage is uncontrolled rise of blood sugar levels. Among adult diabetic patients, heart disease and stroke are estimated to the leading cause of death [9].

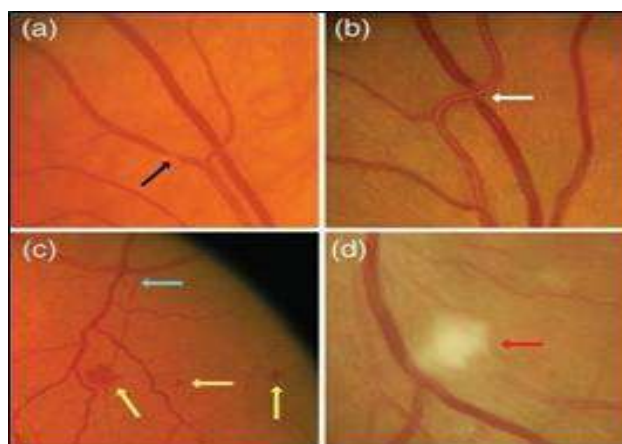


Fig 8. Vascular abnormalities

a) Black arrow: arteriolar narrowing, b) White arrow: arterio-venous nicking, c) Yellow arrow: hemorrhage, Blue arrow: microaneurysm, d) Red arrow: cotton wool spot [9]

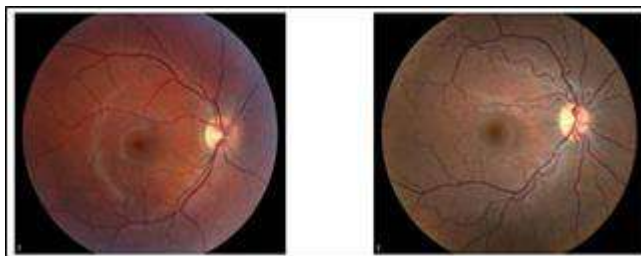


Fig.9. a) Normal image b) Image with tortuous blood vessels

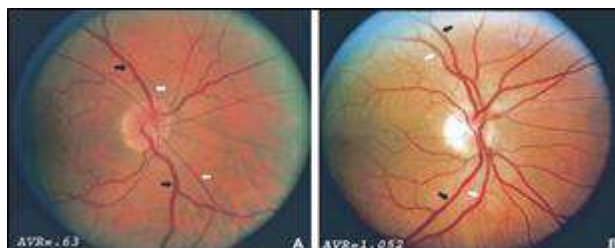


Fig 10. White arrow: arteriolar diameter; black arrow - venular diameter [10-11]

Retinal vascular morphological parameters such as branching angle, fractal dimension and vessel tortuosity are also used to measure the risk of CVD [12]. The typical vascular structure of retina is shown in Figure 11. Retinal vascular attributes are extracted from segmented retinal images. Branching patterns of the blood vessels vary from simple to complex. Fractal dimension of the images are proportional to the complexity of the branching patterns. The tortuosity of the blood vessel curvature is a function of the curvature along the path of the vessel, and the total length of the path of blood vessel. A smaller tortuosity value indicates the straightening of the vessel. From the branching pattern, daughter vessels are identified at each bifurcation of the vessel and the subsequent vessels. The first angle subtended at the division is termed as the branching angle. The average branching angle of the blood vessels including arterioles and venules are found through the arteriolar branching angle and venular branching angle.

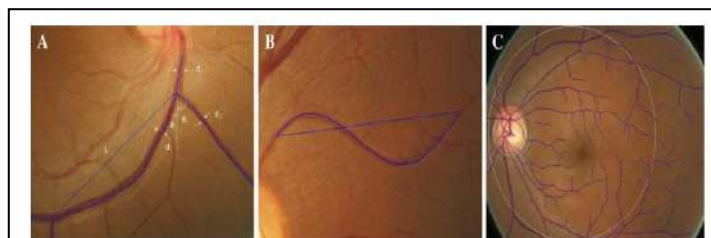


Fig. 11. a) Branching angle, b) Tortuosity c) Branching pattern [12]

VII. Clinical Applications of AI in Ophthalmology

Medical images contain millions of datasets that can be examined and identify the pattern using artificial Intelligence (AI). The aim of machine learning and deep learning techniques are to detect and quantify the pathological features in retinal disease. AI algorithms have provided accurate performance in the detection of diabetic retinopathy and age-related macular degeneration [13]. This section discusses the summary of the AI methods for ophthalmic applications, limitations in clinical deployment and future research.

The machine learning algorithms are classified into supervised learning and unsupervised learning. In the researches that employed the machine learning algorithm, the steps involved the development stage, such as pre-processing, feature extraction, dimensionality reduction and classification/segmentation.

Pre-processing is performed in different approaches, image quality improvement, noise removal, contrast enhancement, illumination adjustment. It leads to improve the vessel region for further analysis. Some of the pre-processing method identified from the survey, channel extraction, channel conversion, histogram equalization, gamma correction, filtering.

Supervised learning can be used for the following scenarios,

- Classification: To categorize the image based on disease type or stage.
- Segmentation: To extract the regions of interest based on anatomy or the lesions occurring in an image.
- Prediction: To predict the future outcomes or occurrence of disease.

AI based medical device is developed in April 2018 by the US to detect the severity of DR. The device is named as iDx-DR, where the image is automatically categorized into mild DR) or not. They tested the device with 900 diabetic patients and achieved an accuracy of 87.4% for positive result. This automated system provides the support for ophthalmologists and diagnose the severity of diseases.

AI techniques are developed for the diagnosis of AMD. Deep learning algorithms are used to detect AMD with a sensitivity of 93% and specificity of 89% for the dataset of 72,610 fundus images [14]. OCT has the potential to examine signs of AMD that are not observable on fundus image. OCT based AI system was modeled using 3265 images and validated in 367 individuals with sensitivity and specificity of 93% [15]. In clinical settings, fundus photographs have been shown to be useful in diagnosing AMD at earlier stages. Integrated models are also developed to combine the OCT images and visual field data [16]. It provides an accuracy of 82% (only OCT), 84% (only visual field) and 87% (both).

Many systemic diseases like hypertension, atherosclerosis and obesity are diagnosed from retinal images using Artificial Intelligence (AI) techniques. Poplin et al. established a model with dataset having fundus images of 2, 84,335 for predicting cardiovascular risk factors. Features like age, sex, smoking habit, blood pressure were identified with high accuracy [17]. There are some studies which demonstrate the effect of systemic diseases on age and sex. ResNet 152 architecture is developed and trained for age and sex prediction without any pathological diseases. The trained model was tested in four datasets which contains images from normal, hypertension, diabetes, and smoking participants. From the study, we identified that vascular conditions and ageing process have different effects in retinal image. CNN architecture is trained with retinal database obtained from Diabetic Retinopathy screening programme. It consists of 5 convolutional and 3 fully connected layers. The objective of the model is to predict the smoking status. The images were contrast enhanced or skeletonized. The contrast enhanced model outperforms skeletonized with an accuracy of 88.8%. Also, research suggests the alterations in the architecture of the vasculature alone are not adequately predictive markers for the accurate detection of the smoking status of a cohort with diabetes. Automated algorithms will provide the support to diagnose the diseases from retinal images.

VII. CONCLUSION

Assessment of the retinal vasculature has been recognized as a painless and financially savvy method for distinguishing eye and foundational infections like diabetic retinopathy, hypertension, glaucoma, macular degeneration, cardiovascular dangers. Anomalies in retinal conduits and veins, arrangement of sores are the huge biomarkers for the location of sicknesses. Fundus photography and optical soundness tomography are the generally involved imaging procedures to catch the picture of eye for the finding of above infections. Studies have underscored the significance of Artificial Intelligence methods in diagnosing the infections, which gives proactive clinical consideration to patients and lessens the manual work of clinicians. The examination work can be stretched out to utilize Artificial Intelligence procedures to foresee the gamble of CVD in light of elements extricated through picture handling methods from fundus camera pictures. Despite the fact that contemporary investigates guarantee to have anticipated CVD risk, they are significantly founded on pictures procured from information bases as well as information gathered in created nations and have their own impediments. Thus, there is a need to make a powerful philosophy inside Indian setting for forecast of CVD risk utilizing retinal pictures. Improved profound learning calculations can likewise be used to inspect the retinal vasculature and recognizing CVD risk.

VIII. REFERENCES

1. Michael D. Abramoff, Mona K. Garvin, Milan Sonka, "Retinal Imaging and Image Analysis", IEEE reviews in Biomedical Engineering, 2010, vol. 3, pp.169-208.
2. Nema H. V, Nitin Nema, "Textbook of Ophthalmology, Jaypee Brothers Medical Publishers (P) Ltd, 5th Edition, 2008.
3. Caroline Viola Stella Mary M., Elijah Blessing Raj Singh, Ganesh R. Naik, "Retinal Fundus Image Analysis for Diagnosis of Glaucoma: A Comprehensive Survey", IEEE Access, 2016, Vol. 4, pp.4327-4354.
4. Amit B. Jain, Vadivelu Jaya Prakash and MunaBhende, "Techniques of Fundus Imaging", 2015, Vol. XXXIII, pp. 100-107.
5. Kolb H, "Simple Anatomy of the Retina", In: Kolb H, Fernandez E, Nelson R, editors. Webvision: The Organization of the Retina and Visual System [Internet]. Salt Lake City (UT): University of Utah Health Sciences Center; 1995-. PMID: 21413391, 2005.

6. Valverde C, Garcia M, Hornero R, Lopez-Galvez MI, “Automated detection of diabetic retinopathy in retinal images”, *Indian Journal of Ophthalmology*, 2016, vol.64, pp.26-32.
7. Gehrs KM, Anderson DH, Johnson LV, Hageman GS, “Age-related macular degeneration--emerging pathogenetic and therapeutic concepts”, 2006, *Journal Annals of Medicine*, Vol. 38, Issue No.7.
8. Chi-Ting Horng, Han-Ying Sun, Hsiang-Jui Liu, Jiann-Hwa Lue, Shang-Min Yeh, “Predicting the Incidence of Human Cataract through Retinal Imaging Technology”, *International Journal of Environmental Research Public Health*, 2015, Vol.12,pp.14800–14810.
9. Josef Flammer, Katarzyna Konieczk a, Rosa M. Bruno, Agostino Viridis, Andreas J. Flammer, Stefano Taddei, “The eye and the heart”, *European Heart Journal*, 2013, vol. 34, pp.1270–1278.
10. Vinayak S. Joshi, Joseph M Reinhardt, Michael Abramoff, “Automated measurement of retinal blood vessel tortuosity”, *SPIE Proceedings and conference*, 2010.
11. Gerald Liew ,JieJin Wang, *Retinal Vascular Signs: A Window to the Heart*, *CARDIOLOGIA*,2011.
12. Wang SB, Mitchell P, Liew G, Wong TY, Phan K, Thiagalingam A, Joachim N, Burlutsky G, Gopinath B “A spectrum of retinal vasculature measures and coronary artery disease”, *Atherosclerosis*, 2018, 268, pp. 215-224.
13. Daniel Shu Wei Ting, Louis R Pasquale, Lily Peng, John Peter Campbell, Aaron Y Lee, Rajiv Raman, Gavin Siew Wei Tan, Leopold Schmetterer, Pearse A Keane, Tien Yin Wong, “Artificial intelligence and deep learning in ophthalmology”, *British Journal of Ophthalmology*, 2018, Vol. 103, Issue No.2.
14. SajibSaha, Marco Nassisi, Mo Wang, Sophiana Lindenberg, Yogi Kanagasingam, Srinivas Sadda, Zhihong Jewel Hu, “Automated detection and classification of early AMD biomarkers using deep learning”, *Scientific reports*, 2019.
15. Venhuizen FG, van Ginneken B, Liefers B, et al., “Deep learning approach for the detection and quantification of intraretinal cystoid fluid in multivendor optical coherence tomography”, *Biomedical Optics Express*. 2018; 9: 1545–1569.
16. Vizzeri G, Balasubramanian M, Bowd C, et al. Spectral domain-optical coherence tomography to detect localized retinal nerve fiber layer defects in glaucomatous eyes. *Opt Express*. 2009;17(5):4004–4018.
17. Poplin, R., Varadarajan, A., Blumer, K., Liu, Y., McConnell, M., Corrado, G., Peng, L. and Webster, D., “Prediction of cardiovascular risk factors from retinal fundus photographs via deep learning”, *Nature Biomedical Engineering*,2018, 2(3), pp.158-164.

A Review on Urinary Sediment Particles and Related Kidney Diseases

Suhail K and Brindha D

Department of Biomedical Engineering PSG College of Technology, Coimbatore, Tamil Nadu, India

ABSTRACT

Kidney and urinary tract diseases are identified by detecting various particles present in the urine sediment. The different urine sediment particles are Red Blood Cells, White Blood Cells, Epithelial Cells, Crystals, fungi, and Casts. Microscopic examination of urine sediments reveals the presence of these particles. Traditionally urine sediment examination is performed by using centrifuge urine samples. Machine learning and deep learning methods utilize images of urine sediments to perform automated urine sediment microscopy. The results from this analysis determine various types of urine particles present in the sample. Thus it aids in the diagnosis of different kidney and urinary tract diseases such as haematuria, kidney stones, and urinary tract infections.

Keywords: RBC, WBC, Epithelial cells, UTI, Haematuria

1. INTRODUCTION

Nowadays kidney diseases are common and are affected by millions of people worldwide. Kidney and urinary tract related problems causes' death of 830000 people every year. 18467000 people having disability-adjusted life due to renal diseases [1]. Kidney stones are commonly found to be in industrial countries which affect 1 in every 1000 people annually [2].

Kidney diseases can be diagnosed by the examination of urine sediment particles by identifying the presence of various particles in the urine sediment images namely, RBC, WBC, crystals, casts, fungi, epithelial cells, etc. Urine sediments can be analysed by two types of examinations namely, physical method and chemical method. Microscopic analysis of urine sediments are carried out when these two methods detects any unusual result. The microscopic method for urinalysis based on urine sediment images detects the presence of different types of particles present in the corresponding urine sample. The presence of such particles indicates various kidney-related diseases. This paper describes the particles found in urine sediments and diseases caused by the presence of various urine particles.

2. Urine Sediment Particles

Urine sediments usually consists of various particles such as erythrocytes (RBC), leukocytes (WBC), Mycetes, Crystals, Casts, Fungi, bacteria and epithelial cells. Urinalysis examines the presence of urinary particles for diagnosing various kidney diseases.

2.1 RBC

A Red Blood Cells (RBC) also called Erythrocytes commonly found in blood cells. Erythrocytes are usually biconcave disc-shaped cells and their major product is hemoglobin. RBCs are the carriers of oxygen and carbon dioxide in the human body [3]. An Erythrocyte has an average diameter of 8 micrometers. Oxygen movement from pulmonary capillaries to tissue capillaries to exchange carbon dioxide is carried out by erythrocytes.

There are mainly two types of RBC found in urine sediments. An RBC having a smooth surface with a round or biconcave-shaped structure is called isomorphic RBC and an RBC having a contour with irregularity in their structure are called dysmorphic RBC [4]. The two types of RBCs are shown in Figure 1. Dysmorphic cells having a wide morphological spectrum includes acanthocytes [5]. Distortion in the cytoskeleton of RBC is the main reason for the dimorphism in RBCs. The distortion is caused due to the passage of red cells through the renal tubules and through the glomerular membrane gaps.

Other than these two types of RBCs, various types of RBCs that are present in the urine of haematuria patients are sickle cells, anisocytes, and poikilocytes and their presence in the urine is very rare. Sickle cells were observed in patients having sickle cell disease or sickle cell traits. There is a mild chance for occurrence of Haematuria in the urine of the patients with sickle cell trait and is 3-4% [3]. An RBC with varied cell size is called anisocytes and an RBC with varied cell shape is called poikilocytes.

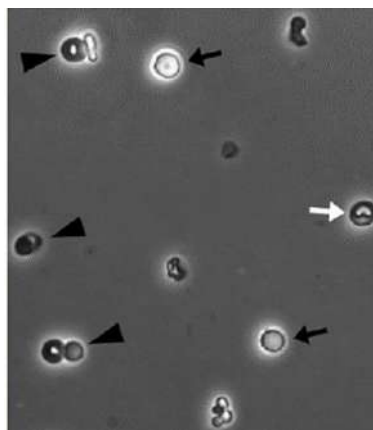


Fig 1 Black arrows represents Isomorphic cells, white arrows represents dysmorphic cells, and arrow heads represents acanthocyte [2]

2.2 WBC

White Blood Cells (WBC) also called leukocytes are a type of blood cell in the human body usually found in blood and lymph. Structure WBC is shown in figure 2. WBCs are part of the immune system in the body [6]. There are mainly five types of leukocytes namely neutrophils, eosinophils, basophils, lymphocytes, and monocytes [7].



Fig 2: White blood cells.

Half of the WBC population is occupied by neutrophils. Neutrophils are the primary cells for the immune system that respond to a bacteria or virus entered into the body. Once released from bone marrow neutrophils die after 8 hours. But 100 billion neutrophils are produced every day [8]. Basophils occupy only 1% of the total WBC concentration. They mount a nonspecific immune response to pathogens. Basophils release histamine and some other chemicals by stimulation [9]. Lymphocytes are mainly two types and they are B cells and T cells. T cells directly kill foreign particles in the body and B cells are responsible for humoral immunity. B cells produce antibodies that remember an infection when the body is affected by that particular infection a second time [10]. Monocytes occur around 5% to 12% of WBC and their function is to clean up the dead cells by migrating into tissues [11]. Eosinophils cover 5% of the white WBC in the bloodstream and are present in high concentration in the digestive tract [12].

Leukocytes travel through different organs of the body to monitor problematic germs or infections in the various organs of the body. Normally a few levels of leukocytes are found in urine. The presence of a high concentration of leukocytes in the urine may indicate various infections in the kidney or urinary tract. Diseases identified by the presence of a high number of WBC in urine are bladder infections, kidney stones, kidney infections, urinary system blockage, and holding in urine. Presence of leukocytes in urine cause different symptoms that include shivering and fever, lower back and side pain, acute pelvic pain, nausea or vomiting and long term pelvic pain [13].

2.3 CRYSTALS

Urine may contain many chemical particles. Sometimes these chemical particles form a solid salt-like structure called crystals. Normally crystals can be present in the urine sediment of healthy persons caused by the slight excess of protein or vitamin C. Many of the urine crystals are not harmful. However, urine crystals are the indicators of various kidney diseases. The presence of crystals in the urine may cause fever, presence of blood cells in urine and it may lead to jaundice and fatigue. The different categories of crystals commonly found in

urine are calcium carbonate crystal (figure3), uric acid and hippuric acid, cysteine (figure 4), calcium oxalate crystal etc. [14].

Uric acid crystals may be barrel, plate-like, or diamond-shaped structures and are orange-brown or yellow in color. The uric acid deposition in the urine may due to the Protein-rich diet or it may be the result of chemotherapy or kidney stones. Taking enough amount of water and keeps hydrated is the best way to treat the crystals. Calcium oxalate crystals are colorless and having dumbbell or envelope-shaped it is heavily associated with kidney stones. Kidney stones can be formed by the presence of a high number of oxalate. Hippuric acid may rarely see in urine. It may be yellow-brown or clear and have needle-like prisms or plate-like shapes. It also appears in the urine of healthy individuals. Calcium carbonate crystals resemble round discs with smooth surfaces and appear in the urine as a light brown color. Cysteine causes crystal formation and kidney stones. Kidney stones produced by cysteine are larger than the kidney stones produced by the other types of crystals. Cysteine crystal formation is a very rare condition and it may be due to genetic problems [15].

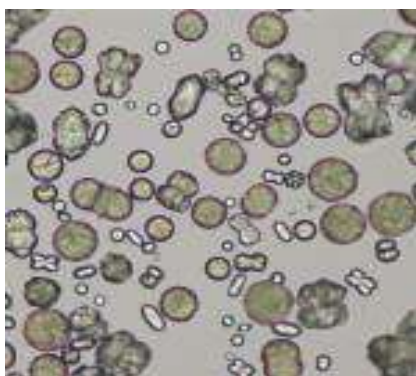


Figure 3: Calcium carbonate crystals

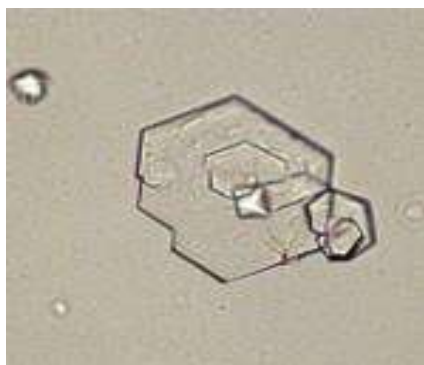


Figure 4: Cysteine

2.4 CASTS

Casts are tiny tube-shaped particles in urine sediment which is formed by the crystallisation of protein in the kidney nephrons [16]. Casts represent the biopsy of the kidney. The presence of casts in the urine indicates the existence of kidney diseases. Based on the morphological features casts are classified as Hyaline casts, RBC casts, WBC casts, Bacterial casts, epithelial casts, granular casts, waxy casts, fatty casts, etc. [16]. The hyaline cast is secreted by renal tubular cells which are produced by the solidification of Tamm-Horsfall micro-protein. Hyaline casts are found in normal individuals and are considered to be non-specific. The presence of hyaline cast causes decreased urine flow due to exercise, vomiting, or fever. However, the high amount of hyaline casts may indicate damage to the kidney due to the reduction of blood flow to the kidneys [17]. In healthy individuals, a small amount of hyaline cast is found between 0 -2 casts per low power field. Hyaline casts cause increased acidity in urine and highly concentrated urine. The cellular cast is composed of either RBC, WBC, or epithelial cells. It may be difficult to identify the type of cell which produces cellular cast. The presence of RBC in the cast may be due to the leakage of RBCs through the glomerular membrane. WBC casts are composed of neutrophils in WBC and it may indicate the infection to the kidney cells. The presence of WBC casts or RBC-WBC mixed casts causes acute glomerulonephritis.

Epithelial casts are formed by the renal epithelial cells and it is a serious condition that causes viral disease and exposure to toxic substances such as mercury, various drugs, etc. Epithelial cast as shown in figure 5.



Figure 5: Epithelial casts

2.5 Epithelial Cells

Epithelial cells are normally found at the surface of the body such as skin, blood vessels, urinary tract, etc. presence of a large number of epithelial cells indicates the infection to the kidneys or kidney diseases. Based on the shape and size epithelial cells are categorized as renal tubular epithelial cells, squamous epithelial cells, and transitional epithelial cells as shown in Figure 6, Figure 7, and Figure 8 respectively [18]. Renal tubular epithelial cells also called renal cells which are the common epithelial cells found in the urine of most healthy individuals. An increased number of renal epithelial cells might be due to kidney disorders. Squamous epithelial cells are the biggest cells commonly found in female urine and it has come from the vagina and urethra. Transitional epithelial cells are common in older adults and found in the male urethra and renal pelvis.

The normal count of urine epithelial cells in humans are 1-5 cells per high power field. The moderate number above the normal count indicates yeast, urinary tract infection (UTI), and kidney or liver diseases. The presence of more than 15 renal cells indicates the improper functioning of the kidney. The occurrence of squamous epithelial cells in the urine sample causes the contamination of the urine.

The occurrence of large number of epithelial cells in the urine indicates that the patient is at higher risk condition. The higher count of epithelial cells might be due to kidney stones, diabetes, family history of chronic kidney disease (CKD), or enlarged prostate.

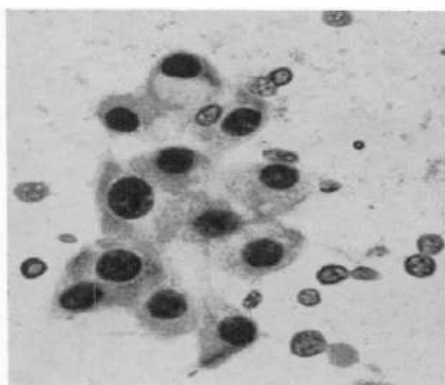


Figure 6: renal epithelial cells in urine sample

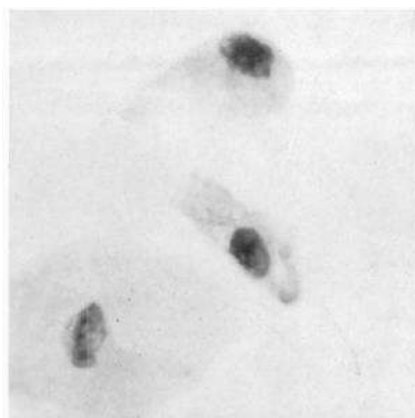


Figure 7: Squamous epithelial cell

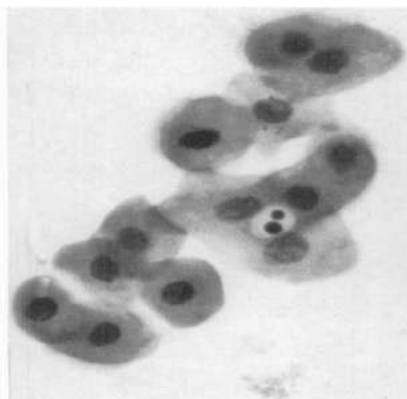


Figure 8: Transitional epithelial cell

2.6 FUNGI

Urinary tract infection due to fungi is caused by the candida species called candiduria. Candida fungi are the most common pathogenic fungi in the urinary tract of both males and females. Fungal infections in the urine primarily affect the bladder and kidneys. High-risk patients with candiduria may lead to cystitis by the presence of bladder inflammation.

3. CONCLUSION

This literature described various types of particles present in urine sediment samples and various types of diseases diagnosed by the presence of these particles. The urinary particles described in this paper are erythrocytes, leukocytes, Epithelial Cells, Crystals, fungi, and Casts. The presence of urinary particles in the urine sample may indicate the various types of kidney diseases such as urinary tract infections, Haematuria, kidney stones, bladder cancer, and chronic kidney diseases. Urine sediment particles can be detected by using manual microscopic examination and by automated examination by using machine learning and deep learning framework. Manual microscopic examination is a time-consuming and labour-intensive process. Automated urine sediment microscopy can be performed by using urine microscopic images.

REFERENCES

1. Dirks, John, Giuseppe Remuzzi, Susan Horton, Arrigo Schieppati, and S. Adibul Hasan Rizvi. "Diseases of the kidney and the urinary system." *Disease control priorities in developing countries* 2 (2006): 695-706.
2. Morton, A. Ross, Eduard A. Iliescu, and James WL Wilson. "Nephrology: 1. Investigation and treatment of recurrent kidney stones." *Cmaj* 166, no. 2 (2002): 213-218.
3. Klinken, S.P., 2002. Red blood cells. *The international journal of biochemistry & cell biology*, 34(12), pp.1513-1518.
4. Poloni, J.A.T., Bosan, I.B., Garigali, G. and Fogazzi, G.B., 2012. Urinary red blood cells: not only glomerular or nonglomerular. *Nephron Clinical Practice*, 120(1), pp.c36-c41.
5. Köhler, H., Wandel, E. and Brunck, B., 1991. Acanthocyturia—a characteristic marker for glomerular bleeding. *Kidney international*, 40(1), pp.115-120.
6. ("Definition of white blood cell - NCI Dictionary of Cancer Terms - National Cancer Institute," n.d.)<https://www.cancer.gov/publications/dictionaries/cancer-terms/def/white-blood-cell>
7. ("Types and Function of White Blood Cells (WBCs)," n.d.)<https://www.verywellhealth.com/understanding-white-blood-cells-and-counts-2249217>
8. Mayadas, T.N., Cullere, X. and Lowell, C.A., 2014. The multifaceted functions of neutrophils. *Annual Review of Pathology: Mechanisms of Disease*, 9, pp.181-218.
9. Cromheecke, J.L., Nguyen, K.T. and Huston, D.P., 2014. Emerging role of human basophil biology in health and disease. *Current allergy and asthma reports*, 14(1), p.408.
10. Hoffman, W., Lakkis, F.G. and Chalasani, G., 2016. B cells, antibodies, and more. *Clinical Journal of the American Society of Nephrology*, 11(1), pp.137-154.
11. Karlmark, K., Tacke, F. and Dunay, I., 2012. Monocytes in health and disease—Minireview. *European Journal of Microbiology and Immunology*, 2(2), pp.97-102.

12. McBrien, C.N. and Menzies-Gow, A., 2017. The biology of eosinophils and their role in asthma. *Frontiers in medicine*, 4, p.93.
13. ("Leukocytes in the urine: Causes, symptoms, and diagnosis.,"n.d.)<https://www.medicalnewstoday.com/articles/314165>
14. Bradley, M., 1982. Urine Crystals—Identification and Significance. *Laboratory Medicine*, 13(6), pp.348-353.
15. Khan, S.R., Glenton, P.A., Backov, R. and Talham, D.R., 2002. Presence of lipids in urine, crystals and stones: implications for the formation of kidney stones. *Kidney International*, 62(6), pp.2062-2072.
16. Ringsrud, K.M., 2001. Casts in the urine sediment. *Laboratory medicine*, 32(4), pp.191-193.
17. Hiremath, S. and Lerma, E.V., 2018. HISTORY AND PHYSICAL DIAGNOSIS. *Nephrology Secrets: First South Asia Edition-E-Book*, p.3.
18. Kern, W.H., 1971. Epithelial cells in urine sediments. *American journal of clinical pathology*, 56(1), pp.67-72.

Latent TB Infection (LTBI) Identification through Microscopic Images

Brindha D

Department of Biomedical Engineering, PSG College of Technology, Coimbatore, India

ABSTRACT

Latent Tuberculosis (TB) infection is an inescapable, irresistible, lethal sickness in emerging nations. Mycobacterium tuberculosis, the causative microorganism, is imparted by means of contaminated sputum. Early finding and treatment becomes crucial to forgo deadly results. Customarily, determination of tuberculosis is finished by the manual minute assessment of sputum spreads utilizing Ziehl-Neelsen stain (ZN stain) strategy which requires human skill and time and accordingly becoming drawn-out. These constraints brief the requirement for robotization of assessment and discovery of TB microorganisms. In this work, a PC supported framework for TB analysis in view of division through shading deconvolution is created for ID of the bacilli in infinitesimal sputum smear pictures. The Mycobacterium are segregated utilizing angle proportion. This computerized strategy intends to reduce down the assessment expenses, handling time and human mistake accordingly working on by and large productivity.

Keywords: Latent TB infection, Microscopic sputum phantasmagorias, Computerized verdict

1. INTRODUCTION

Tuberculosis (TB) is a potentially harmful disease caused by Mycobacterium tuberculosis. The disease may be classified as pulmonary TB or extra pulmonary TB depending on whether it affects the lungs or other parts of the body like liver, kidneys, bone, brain or central nervous system. According to WHO report, a massive 9.4 billion new cases are identified and 1.68 million deaths are reported worldwide annually [1,2]. Prevention relies on screening programs and vaccination with Bacillus Calmette Guerin vaccine.

1.1 Characteristics:

Tuberculosis is a widespread disease caused by different types of Mycobacterium, usually Mycobacterium tuberculosis. It typically targets the pulmonary system may also create problems to other organs. The disease is transmitted mainly through air through via cough, sneeze or sputum of an affected individual. Mycobacterium tuberculosis is a small, aerobic, non-motile bacillus. The distinctive clinical character of the species is the high lipid conten. It is a slow rated bacteria which divides every 16 to 20 hours [3]. The bacterium is surrounded by a lipid bilayer membrane. Naturally, the bacteria can grow mostly inside the human body but it is possible to develop in the laboratory using invitro culture method also. Mycobacterium tuberculosis (MTB) can be identified from microscopic examination of histological stains or sputum samples. Even after cleansing with acid, MTB has an amount of stain in it, so it is called as acid-fast bacillus (AFB). The commonly used AFB staining technique is Ziehl Neelsen (ZN) stain, which stains the pathogen pink in contrast with blue background (Figure 1.1.1). Auramine- rhodamine stain can also be used followed by fluorescence microscopy. Four other TB-causing mycobacterium are inclusive in the M.Tuberculosis complex: M.bovis, M.africanum, M.canetti and M.microti. The former species has ceased to be a major causative agent after the advent of pasteurized milk in developed countries. M.africanum and M.canetti have grounds confined predominantly to African races. M.microti is rare and encountered in immune deficient people. M. leprae, M.avium and M. kanasii are other significant pathogenic Mycobacterium. The latter two are called Non-Tuberculosis Mycobacterium (NTM) as they cause neither leprosy nor TB but a pulmonary disease akin to TB.



Figure 1.1.1 Mycobacterium Tuberculosis

1.2 Signs and symptoms:

Tuberculosis infection is not always contagious as our immune system can safeguard us initially revealing no noticeable symptoms. This TB category, referred to as latent TB, causes infection but the pathogen remain in

the body in dormant state. It can be contagious and communicable if timely treatment is not administered. An estimated 2 billion people are reported to have latent TB. On the other hand, the contagious version, or the active TB causes illness and variety of symptoms which may manifest within few weeks of infection or some years. Common symptoms of active TB are Persistent cough lasting beyond 2 weeks, Chest pain, Loss of weight, Loss of appetite, Fever and chills, Fatigue, Night sweats. Symptoms may vary in Extra pulmonary TB. For instance, back pain is observed in spinal infection whereas infection in kidneys may cause loss of blood through urine.

1.3 Transmission:

As said earlier, transmission of TB is through infected droplets released by patients while talking, coughing or sneezing. Mostly people get infected due to prolonged or frequent contact with infected individuals. The disease is communicated only when it dwells in an active form, otherwise latent TB is not infectious. Transmission can be controlled by administration of drugs to people with active infections. A person with an incidence of TB takes minimum 3 to 4 weeks before being capable of spreading the infection.

1.4 Microscopy staining techniques:

Direct microscopy is useful in identification of pathogen after staining the sputum sample. The three common staining procedures are:

1.4.1.1 Ziehl-Neelsen Method:

This classical Acid-fast staining technique can stain the bacterium bright red by the retention of carbol-fuchsin dye against blue background developed by methylene blue counter stain, which are otherwise resistant to Gram stain due to high lipid content in cell wall in the form of mycolic acids (Figure(1.4.1.1)). The species are heat fixed on the slide and viewed on microscope under oil immersion. AFB cultures accompany AFB stain for improved predictive value negative.

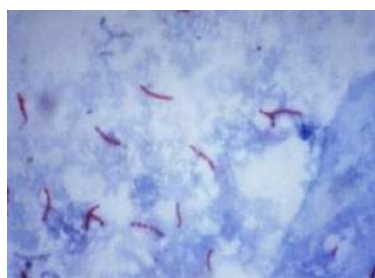


Figure 1.4.1.1 Ziehl Neelsen stain

1.4.1.2 KINYOUN METHOD:

This is a cold staining technique unlike the Ziehl-Neelsen technique. It uses more concentrated carbol-fuchsin dye to stain the bacteria bright red on the slide. After decolorizing other species with acid alcohol, the slide is flooded with methylene blue to counter stain and dried (Figure (1.4.1.2)). The slides can be examined under high magnification (400x) or oil immersion for stronger evidence.

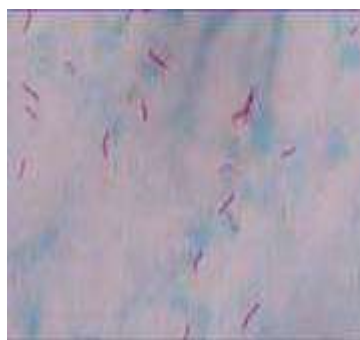


Figure 1.4.1.2 Kinyoun stain

1.4.1.3 Auramine-Rhodamine Method:

This histological technique uses a mixture of Auramine O and Rhodamine B dyes, Auramine binds to mycolic acid in cell wall. Permanganate is used as counter stain post decolorizing. The detection requires a fluorescence microscope equipped with BG-12 exciter filter and an OG1- barrier filter. Acid-fast bacteria appear as brightly fluorescent against dark field (Figure(1.4.1.3)). It is more quick, affordable and more sensitive, therefore it is often used screening tool.

Manual examinations of microscopic sputum smear images consume time and are prone to error. Thus, automation of examination is proposed in this work by computer aided diagnosis system using image processing technique aiming to minimize the effort, time and cost thereby enhancing early diagnosis.



Figure1.4.1.3 Auramine Rhodamine stain

2. LITERATURE REVIEW

Forero and Cristóbal, 2003; Forero et al, 2004; Forero et al, 2006, proposed segmentation of microscopic sputum smear images by Adaptive thresholding and K-means clustering in their but the results were not absolutely accurate. Sadaphal et al, (2008) proposed tuberculosis identification by multi stage colour based Bayesian segmentation followed by artifact removal by shape comparison. Superimposed AFB clusters, extreme stain variation and low depth of the field were the challenges. The results of research by Ibnu et al, (2010) published in "Development of Algorithm for Tuberculosis Bacteria Identification Using Colour Segmentation and Neural Networks" are based on Neural Networks. The testing result by using 15 hidden layers showed an accuracy of about 88% [8]. Castaneda et al, (2010) in their work, "Automated Tuberculosis screening using image processing tools" employed edge detection and mathematical morphology to extract the bacilli. This method showed specificity over 90% but it is applicable only on samples stained with Auramine and not ZN stain images. Khutlang et al, (2010) in their work "Classification of Mycobacterium tuberculosis in Images of ZN-Stained Sputum Smears" proposed segmentation using a combination of two-class pixel classifiers. This method could not be implemented for automatic segmentation. In this work, computerized automation of TB diagnosis is realized by identification of Mycobacterium from microscopic sputum smear images using segmentation techniques [10].

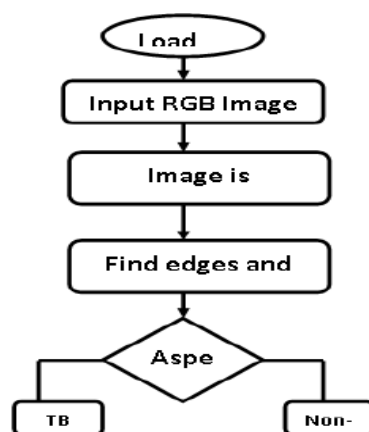


Fig. 2. Flow chart for the proposed system

3. METHODOLOGY

In this work, an algorithm based on segmentation which is a common method in image processing is developed for identification of mycobacterium tuberculosis bacilli in microscopic sputum smear images. Segmentation is used to extract region of interest. Feature extraction also helps us to identify the exact object in image.

3.1 Colour Segmentation Based On K-Means Clustering

Our objective is to distribute the pixels in the original image into groups based on coherence in properties like colour and texture and extract information from the image. K-means clustering is an unsupervised clustering algorithm that intends to distribute n observations into k clusters in which each observation belongs to the cluster with the nearest mean. This method produces exactly k different clusters of greatest possible distinction. Given a set of features (x_1, x_2, \dots, x_n) , where each feature is a d -dimensional real vector, k -means clustering algorithm tries to partition the n features into k ($k \leq n$) sets $S = \{S_1, S_2, \dots, S_k\}$, in order to reduce the total intra-cluster variance,

$$V = \sum_{i=1}^k \sum_{x \in S_i} (x - \mu_i)^2 \quad (3.1)$$

The algorithm here is supplied with a two dimensional image as an input and then the algorithm is applied in the following sequence:

- The initial assignment of points to clusters can be done randomly.
- The mean of each group is calculated.
- The distance of every point from each group is estimated by its distance from the corresponding group mean. Each point is assigned to the cluster it is nearest to.
- The above two steps are repeated till the sum of squares within group errors cannot be lowered any more.

In k-means clustering, the actual requirement is only one cluster to be segmented. But the acquired output has two clusters that are overlapping (Figure 3.1.1). Since the output is not accurate other methods are tried.

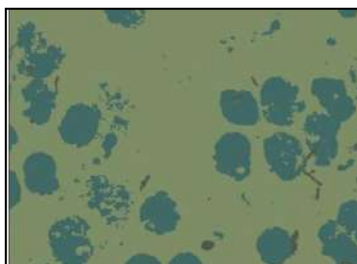


Figure 3.1.1 Image segmented using k means clustering

3.2 Colour Segmentation Based On Siox

SIOX stands for Simple Interactive Object Extraction and is a solution for extracting foreground from still images with very little user interaction. It has hands free selection tool that is used to specify the region of interest which contains foreground objects to be extracted. The algorithm initially creates colour signatures i.e. set of representative colours for background and foreground. Next, all image points are assigned to nearest neighbour in the colour signature and the output mask is generated. The output can be refined by morphological operations like erode, dilate, and blur which helps to remove the unwanted details present in the image. As with any segmentation algorithm, this algorithm doesn't guaranty exact segmentation. The disadvantage of SIOX is that it dependence on the colour characteristics. Though colour characteristics is considered to be one of well distinguished feature with respect to images, the method fails to handle the camouflage. If there is common shades shared with both the the foreground and background f similar colours, the method might produce an outputt with parts missing or incorrectly classified as foreground (Figure 3.2.1).



Figure 3.2.1 Image segmented using SIOX

3.3 Colour Thresholding

Thresholding is a simple segmentation technique which simply converts a gray scale image into a bi-level image. In 8 bit gray scale images and colour images there are 256 intensity graduations which can be assigned to a pixel. Thresholding works by separating the pixels which fall in a desired range of intensity values from those that do not. Thresholding is an effective method for extracting distinct features in an image. An effective thresholding algorithm preserves logical and semantic content. The two types of thresholding are:

- A. Global thresholding algorithm: Global thresholding can be applied when all the pixels of background and foreground are fairly consistent by using a single threshold for all image pixels.
- B. Local or adaptive thresholding: As the name implies, this technique uses different threshold values for different local areas in an image.

The output acquired by thresholding is quite accurate but the drawback of this technique is that the threshold range varies for each of the images and thus is dependent on manual adjustment of threshold values for different images (Figure 3.3.1). Not fulfilling the cited aim of automation of TB detection, next approach was made by colour deconvolution.

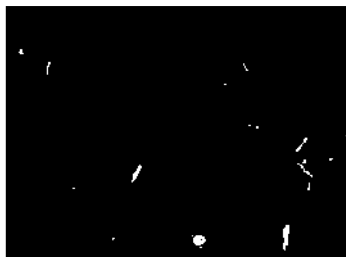


Figure 3.3.1 Threshold image

3.4 COLOUR DECONVOLUTION

Colour deconvolution is a sophisticated algorithm for image segmentation [11]. In this technique, the original RGB image is transformed depending on information from the user about the three colours into images representing the stain densities. The diagnostic information provided by the contrast of individual stains in mixtures of multiple stains with different spectral absorption characteristics is restored.

The intensity of transmitted light from the specimen with stain concentration is described by Bouguer-Lambert-Beer law as,

$$I(\lambda) = I_0(\lambda) \cdot e^{-\delta(\lambda) \cdot c} \quad (3.4.1)$$

where $I_0(\lambda)$ is the incident intensity, $\delta(\lambda)$ is the optical density for a unified layer of thickness; c is the concentration of the stain.

For a mixture of absorbing stains, spectral absorbance $A(\lambda)$ can be expressed as $A(\lambda) = -\ln\left(\frac{I(\lambda)}{I_0(\lambda)}\right) = \sum_i(\delta_i(\lambda) \cdot c_i)$ (3.4.2)

Each pure stain has three characteristic absorbance for each of the three RGB channels and hence three characteristic optical densities. $\vec{d}_i = \begin{bmatrix} d_{red,i} \\ d_{green,i} \\ d_{blue,i} \end{bmatrix}$ (3.4.3)

Assume there are three stains in the sample, each contributes linearly to light absorption. Then for given sample with three stains, the resultant optical density,

$$\vec{d} = \begin{bmatrix} d_{red} \\ d_{green} \\ d_{blue} \end{bmatrix} = \begin{bmatrix} a_{r1x} & a_{r2x} & a_{r3x} \\ a_{g1x} & a_{g2x} & a_{g3x} \\ a_{b1x} & a_{b2x} & a_{b3x} \end{bmatrix} \begin{bmatrix} c_1 \\ c_2 \\ c_3 \end{bmatrix} = M\vec{c} \quad (3.4.4)$$

where M is the convolution matrix, and \vec{c} is the concentration of the three stains.

To ease calculation, optical density vector \vec{d} and concentration vector \vec{c} are normalized by dividing respective unit vectors

$$\hat{D} = \hat{M}\hat{C} \quad (3.4.5)$$

Stain concentration thus can be found as

$$c = M^{-1}D \quad (3.4.6)$$

The matrix M^{-1} is the deconvolution matrix which can be found if the optical densities of each individual stain is known and hence find the individual concentration of the stains. This method was superior in ZN stained image segmentation over other methods. This method has best accuracy since it is based on stain used to colour the slides (Figure 3.4.1). However, it also segments other small particles besides TB bacteria. This calls for further clarification to exactly extract the rod shaped TB bacilli only.

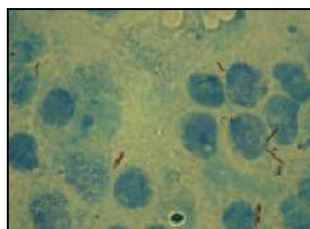


Figure 3.4.1Original Image

The microscopic images are given as input for colour deconvolution process . In ZN stained sputum images the background is stained blue colour in contrast to red stained AFB Mycobacterium Tuberculosis. From the built in vectors, Brilliant blue vector is selected as it is best related to the concept. The image is split by deconvolution into three channels one of which consists of only red coloured TB cells(Figure 3.4.2). But slide staining is a manual procedure and hence shades of stain colour may vary in different slides giving rise to possibility of detection of other cells or particles in pink regions. So the shape describing property is used to discriminate TB from Non TB cells.After deconvolution, the image is converted into binary image to find the edges(Figure 3.4.3 &3.4.4). The edges are then detected for cells and particles in the binary image.



Figure3.4.2 Deconvolved Image



Figure3.4.3 Binary Image

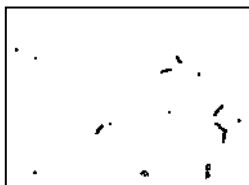


Figure 3.4.4 Image after edge detection

The particles present in the image are analyzed using the option analyze particles where the circumference is set in order to extract only the rod shaped bacteria(Figure 3.4.5). Still other particles may not be removed.Next, region of interest from the image is selected and the properties are studied. From the featured properties, the aspect ratio seems to be varied for TB and Non TB cells. Aspect ratio is the ratio of major axis to minor axis. If the aspect ratio is greater than 3.5 the cell is distinguished as TB cell otherwise it is a Non TB cell.



Figure3.4.5 Image after particle analysis is done

4 RESULTS AND DISCUSSION

This work highlights the various segmentation methods for image processing for the automation of TB detection from microscopic sputum smear images. The images are initially captured from a camera attached to microscope magnifying the ZN stained sputum slides. A set of 50 images each were captured from both TB positive and TB negative slides and subjected to segmentation. Colour deconvolution has proved to be the most efficient technique when compared to other segmentation methods. One of the three resulting images from colour deconvolution contain the segmented bacilli. As this method relies on colour for segmentation, various

undesirable particles maybe included in the segmented images. Further distinction of TB bacteria from Non TB cells is done by one of the shape describing factors namely aspect ratio which varies for TB and other cells.

5 CONCLUSION

Hence a PC supported framework for identification of TB microorganisms from minuscule sputum smear pictures is examined. Shading deconvolution and component extraction help to segregate the TB microbes from the slides. This procedure is basic, modest and wide coming to in arising economies. This method can be additionally stretched out for comparative discovery and finding in different illnesses. This procedure diminishes exhaustion via robotization and end of visual investigation of pictures. This PC supported framework has a serious level of exactness, explicitness and quicker discovery ability. Hence this computerized identification limits time, cost, human mistake and disposed of the requirement for talented expert.

REFERENCES

1. Castañeda B, Aguilar NG, Ticona J, Kanashiro D, Lavarello R, Huaroto L , “Automated Tuberculosis Screening Using Image Processing Tools.” Pan American Health Care Exchanges, March, 2010.
2. Chadha V, K . Epidemiology of Pulmonary Tuberculosis. In. Jindal K (Eds), Textbook of pulmonary and critical care medicine, New Delhi, Jaypee Brothers Medical Publishers, 2011.
3. Forero M and Cristóbal G, Automatic identification techniques of tuberculosis bacteria., Proceedings of the SPIE 5203, Applications of Digital Image Processing XXVI, 71,2003.
4. Forero MG, Sroubek F, Cristóbal G , Identification of tuberculosis bacteria based on geometric and color. Real Time Imaging, Vol.10 No.4,2004, pp.251-262.
5. Forero M, Cristobal G, Desco M . Automatic identification of Mycobacterium tuberculosis by Gaussian mixture models. Journal of Microscopy, 223,2001,pp.120–132.
6. Ibnu Siena , Kusworo Adi, Rahmat Gernowo & Nelly Mirnasari , Development of Algorithm Tuberculosis Bacteria Identification Using Color Segmentation and Neural Networks, International Journal of Video & Image Processing and Network Security, Vol.12, No.4, 2010, pp.9-13.
7. Kashyap S and Malay Sarkar, Pulmonary Tuberculosis: Clinical Features and Diagnosis In. Jindal K (Eds) Textbook of pulmonary and critical care medicine, New Delhi, Jaypee Brothers Medical Publishers, 2011.
8. Khutlang et al, Classification of Mycobacterium tuberculosis in images of ZN-stained sputum smears, IEEE Transactions On Information Technology In Biomedicine, Vol.14, No.4, 2010, pp.:949-57.
9. Ruifork A.C. and Johnston D.A .Quantification of histochemical staining by color deconvolution". Analytical and Quantitative Cytology and Histology, The International Academy of Cytology and American Society of Cytology, Vol.23 No.4, 2001, pp. 291-9.
10. Southwick F, Pulmonary Infections. In. Southwick F(Eds). Infectious Diseases: A Clinical Short Course, 2nd ed. McGraw-Hill Medical Publishing Division, 2007.
11. Sadaphal P, Rao J, Comstock GW, Beg MF . Image processing techniques for identifying Mycobacterium tuberculosis in Ziehl-Neelsen stains, The International Journal of Tuberculosis and Lung Disease , Vol.12 No.5, 2008, pp.579-582.

Bladder Prolapse Images Using Preset Sedimentary Particle Recognition

Kathy Jessica P and Brindha D*

Department of Biomedical Engineering, PSG College of Technology, India

ABSTRACT

For diagnosing kidney and urinary parcel issues, urinalysis is the trial of pee to recognize and inspect silt. The consequences of pee dregs examination might be utilized to help with conclusion and treatment. Manual pee silt assessment is emotional and work escalated. It involves a standard volume of pee as well as a few chambers to count the urinary components. It is pivotal to group and right away distinguish the different sorts of sedimentary particles, including erythrocytes, leukocytes, epithelial cells, precious stones, mycete and epithelial hubs. The proposed procedure utilize Detectron2's Faster R-CNN execution utilizing one of their base models or designs to robotize the acknowledgment and characterization of pee sedimentary particles. The system proposed think about pee molecule identification as article discovery, and use cutting edge CNN-based object location methods. This outcomes in F1 scores for each class of silt and mAP values. The work additionally analyzed the time intricacy of various models used to recognize Urine sedimentary particles with Detectron2. PC vision errands are a subset in Artificial insight and can be utilized to investigate a picture utilizing profound learning.

Keywords— Preset Sedimentary Particle Detection, Bladder prolapse, Detectron2, Faster R-CNN.

I. INTRODUCTION

Healthy individuals should have clear, sterile urine. Some sedimentary particles found in urine samples can indicate the presence of corresponding diseases. Microscopic urinalysis can detect particles in urine that may help to diagnose dysfunction, infection, inflammation, or other diseases of the urinary tract. It is possible to determine if the patient has urinary tract inflammation by looking at the number of leukocytes present in their urine. If the patient also has Erythrocytes, it could be that they have urinary tract calculi.

The Manual microscopic analysis using the human eye is one of the most important parts of the test. It is time-consuming, labor-intensive and intuitive. This requires the use of Artificial Intelligence and computer vision to analyze the results. Automatic detection and classification of urine particles is achieved by identifying the regions that contain target objects, and then extracting them. Deep learning is also gaining popularity due to its recent advances and state-of-the-art results in various tasks related to computer vision [1]. Diverse research has used deep learning to classify and detect different types of Urinary sedimentary particle.

Deep learning projects for Urinary Sedimentary particles detection and classification involve tasks such as collecting images, creating labels and then building deep learning models using the data. To provide labels and bounding boxes for different types of sedimentary particles, the labeling process takes time and requires a lot of human labor. This work describes state-of-the-art object detection techniques to identify sedimentary particles.

The proposed methodology involves the labeled data currently available and suggests a strategy for generating more labeled information. Our contributions include:

- The current state-of-the-art object detection techniques and their application to Urinary Sedimentary particle classification and detection tasks are explored.
- Experimenting with the dataset [2] to create a single model using Detectron2
- Visualizing and qualitatively evaluating predictions made.

II. RELATED WORK

A. Object detection using Deep Learning

Deep learning is an advanced method for object detection. There are numerous works in the literature on this topic. Region-Based Convolutional Neuro Networks (Rot-Based CNNs) are the most widely used technique. There are also various versions of You Only Have One (YOLO) which are popular.

R-CNNs take a lot of time to train, as there are many stages involved in the training process. The predicting stage can also take a while. In terms of training and prediction rate, the standard R-CNN is slow. To solve these issues, Girshick suggests Fast R-CNN [3]. R CNN is not the same as fast R-CNN. Instead, it is taught as a single model. Fast R-CNN's architecture examines images and provides candidate locations. To extract the features from the candidates, the images are then put through a pre-trained image classification model (e.g. ResNet [4] VGG-16[5]). After the features have been extracted, a pooling layer is applied. The final step is to

create two fully connected layers. For label classification and bounding box regression, two more completely linked heads are added.

Although Fast R-CNN reduces prediction and training time frames, it still necessitates the creation of region suggestions for each image using any image processing technique. To solve this difficulty, Ren et al. [6] offer a quicker model as Faster R-CNN. It has the main advantage of incorporating region proposals into the final model by using Region Proposal Networks (RPN). This is possible through the use of two smaller networks. Region Proposal Network (RPN) and Fast R-CNN are the two sub-networks in concern. Region proposals, bounding box classification, and regression can all be used to train these two sub-networks at the same time. These strategies increase object detection speed and accuracy, while reducing training time.

YOLOv2 [7], YOLOv3[8], YOLOv4[9] - are some of the most popular object detection algorithms. There are many YOLO versions. Each version has a different architecture and uses different techniques. All YOLO variants use the same core strategy: a single neural network. Images, ground-truth boxes/segments, and labels are used as inputs. The bounding box labels and the matching labels for the objects discovered on the image are the outputs. The image is divided into grids of cells. Bounding boxes are used to anticipate objects using the features from each cell. This technique has the benefit of being easier to train and predict, but it does have several drawbacks.

To summarise, YOLO has many advantages in terms of fastness, and a faster R-CNN is more accurate in terms of accuracy. Single Shot Detection [10] on the other hand, provides a better blend of speed and precision. SSD computes a feature map from input images and uses anchor boxes of different sizes and aspects. It is similar to Faster R-CNN. Because the inputs have different receptive fields, SSD predicts the bounding boxes sizes. It is possible to observe that larger bounding boxes are predicted more easily if the features of the convolutional layers are deeper than vice versa.

B. Deep learning-based urine sedimentary particle detection

David M. Roxel[11] proposed manual microscopic inspection of urine. This involves centrifugation followed by high-power (x100) and low-power(x400) observation. The results identify refractile fats bodies and crystals. False negative results were obtained, which is why it is expected that the number of cases will vary between 3 and 37%. Corey Cavanaugh[12] and Mark A. Perazella[10] also conducted a comparison of manual and automated urinalysis. He compared and analyzed different automated urine analyzers such as Cobas-6500 (IQ-200), Cobas u 601, etc. He highlighted the benefits of automated urine analysers over manual methods, such as lower labor costs, better correlation results, higher specificity, and greater sensitivity. Rui Kang, et.al.[2] used CNN to eliminate the manual examination of microscopic urine images. They found that they had a lower labor cost, good correlation results, and a higher specificity and sensitivity.

Abdul Aziz[13] and colleagues[7] proposed an unsupervised method of extracting objects from urine images using U-net. For the extraction of objects methods such as Otsu's, Niblack's, and Sauvola are used. U-net can be trained to extract these objects. The proposed method yielded an artifact-to-object ratio of 0.71. This is lower than the average.

Xiaohong Zhang et.al.[14] also proposed a multi-view urine-cell recognition method based upon multi-view deep residual learning. This was to overcome multi-view grey change in cells and information loss in natural states. There are nearly 17 convolutional layers. Squeeze-and-Excitation block is introduced to screen useful features to improve the sensitivity of the network to information features, thereby effectively extracting deep features in the urine images. The proposed method has state-of-the-art classification accuracy and reduces network computing time. It is concluded from the works that the recognition accuracy of the deep learning algorithms is larger than traditional artificial feature extraction methods.

The automated urine analysis is more accurate than manual methods and gives you precise results. Manual methods are subjected to errors, labour-intensive. Automated urinalysis is cost-effective and also with reduced time of evaluation. One stage automated urinalysis models are slower than Two-stage approaches due to the external region proposal network. Modern models can produce accurate results, and they can also recognize confusing categories of urine sediments.

III.METHODOLOGY

The methodology involves exploring the dataset to understand the data and then proceed by splitting the overall dataset further into the training, testing, and evaluation sets. The training data is split randomly while making sure to capture all the classes that have to be recognized. The validation set enables us to evaluate the hyper-parameters for our architectures quantitatively and finally. The proposed methodology use the test set to

determine the accuracy and other parameters. Regarding deep learning model architectures, the process start with the commonly used model architectures for Urinary sedimentary particle detection and classification tasks. The proposed methodology then proceed with techniques to improve the base model by changing hyper-parameters. In order to obtain higher accuracy, the proposed methodology perform data augmentations to increase our dataset. A brief idea about the various steps involved are depicted in Figure 1. For this challenge, the evaluation criteria is based on the F1 score defined to balance the precision and recall. Also mAP values and test time per image of all models are compared with our proposed model, namely Detectron2

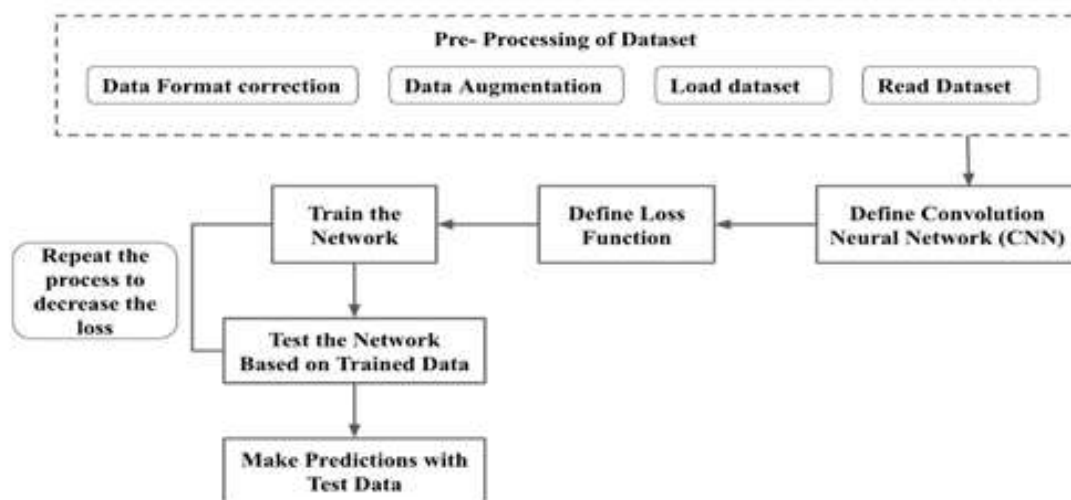


Fig. 1. Work Flow Block Diagram

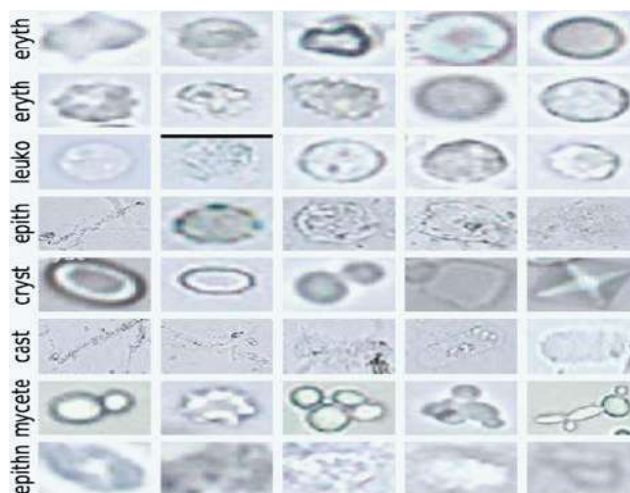


Fig.2. Samples of Urinary Sedimentary particles.

A. Dataset Preparation

The proposed methodology involves microscopic urine image database, which is annotated with ground truth boxes by medical professionals, to conduct this research. There are 5,376 annotated photos in our database. Each image's annotations are stored in.xml files. All of the images are coloured and 800×600 pixels in size, which are multiples of 32, obviating the necessity for zero padding prior to CNN training.

Erythrocyte (eryth), Crystal (cryst), cast, leukocyte (leuko), epithelial cell (epith), mycete, and epithelial nuclei are among the seven types of urine sediment particles included in the image dataset (epithn). Eryth, leuko, crystal, mycete, and epithn are only annotated in high-power fields, while epith and cast are only annotated in low-power fields. Figure 2 shows the seven types of urinary sedimentary particles found in the database, as well as their subdivisions in varied shapes.

The complete dataset is divided into three sets: Training, Validation, and Testing. The proposed methodology use 70 percent of data for training, 20 percent for validation, and the remaining 10% for testing from each of the seven classes. Table 1 shows the total number of images with annotations utilised across the entire dataset.

Table I No Of Annotations In Images Used For Training, Validation And Testing From Each Class

Classification Type	# Training	# Validation	#Testing
Eryth	15,270	4,363	2,182
leuko	4,318	1,233	618
Epith	4,322	1,235	618
Cryst	1,150	328	166
Cast	2,564	732	367
Mycete	1,458	416	209
Epithn	480	137	70

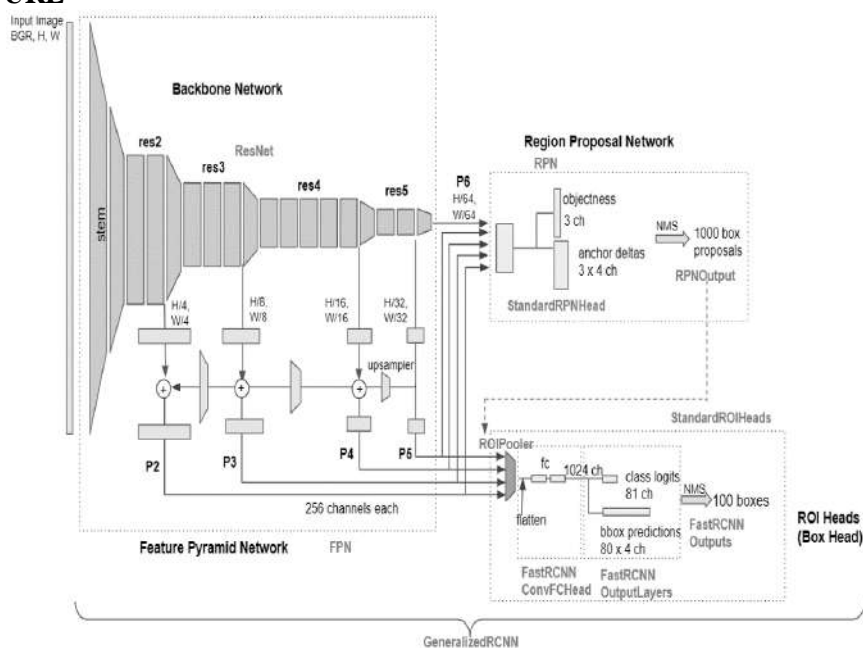
B. Data Augmentation

Data augmentation is a term used in artificial intelligence to describe techniques that add slightly modified copies of current data or newly created synthetic data from existing data to increase the quantity of data accessible. It acts as a regularizer and helps avoid overfitting when training a machine learning model. Artificial intelligence's oversampling is intimately linked to it.

In our project, the proposed method have performed 7 rotations for each image, and each rotation is incremented by 45°. The rotation angles are 45°, 90°, 135°, 180°, 225°, 270°, 315°. The reason for performing rotations as our augmentation technique is because the orientation of the particles can be at any angle.

CLoDSA, an open-source package, was used to implement the rotation approach (that stands for Classification, Localization, Detection, Segmentation Augmentor). CLoDSA is written in Python and uses OpenCV and SciPy as libraries. CLoDSA allows us to conduct various augmentation techniques such as flipping, scaling, adding noise, and so on. The CLoDSA library works on any operating system and is not dependent on any specific machine learning framework.

C. ARCHITECTURE



Point Rend works on detectron2 and Mask RCNN as base components. The network utilizes the feature pyramid network concept as backbone. The FPN network helps in detecting small or large objects with high accuracy

Backbone Network:

This network is in charge of obtaining feature maps from the images in the training dataset. The base network generates images of various scales. P2 (1/4 scale), P3 (1/8 scale), and P4 (1/16 scale) are the output features. Convolutional neural networks were used to process photos P5 (1/32 scale) and P6 (1/64 scale). As inputs, the FPN network uses batch size, image height, and width. As output parameters, channel size and stride are employed. Different scales will be applied to a single image that is processed into the input sensor (4,8,16,32,64 for p2,p3,p4,p5,p6..Outputs)

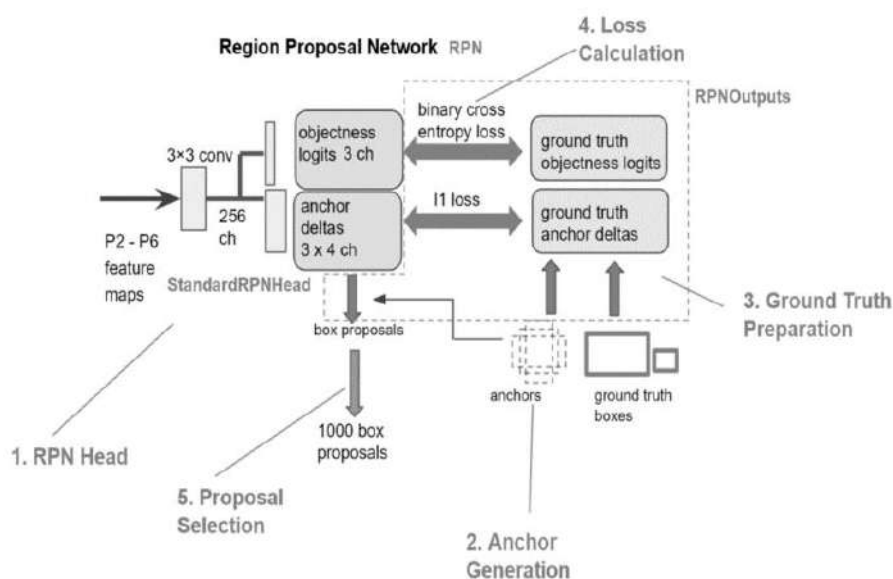
Read image function to load and transform images. An image named 'filename' is loaded. The loaded image is transformed using predefined transformers (such left-right flip), and then the image tensor, whose shape is (channel height, width, width, etc.) is registered.

Transform annotations: If the image is flipped or rotated, the box coordinates will be changed to the new location. The 'annotations' of the dataset are transformed by the transformations performed on the images.

Convert annotations into instances: This function is used to convert annotations into instances. Annotations labelled 'bbox' are registered to the Boxes object that can store a list bounding boxes. Annotations containing 'category_id' are converted to torch tensors.

The Region Proposal network: Detects object regions using multi-scale features. 1000 box proposals are generated by default, with confidence scores.

Help in detection region of interest from multi scale feature maps and creates 1000 box regions with confidence scores. The Regions with high confidence scores will be considered for further processing



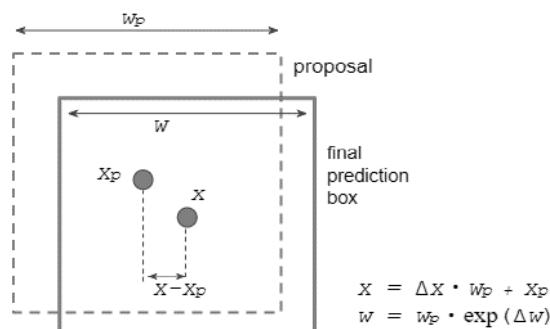
RPN is a cascade convolutional neural network. It has 3 convolutional neural networks and five levels of filters. These feature maps generated from filters are fed into convolutional neural network one by one. Anchor generation helps in connecting between Objectness map and ground truth boxes. Different anchor sizes are used to identify the optimal region of interest on the image. The anchors are placed on the grid cells that are having equitant size to the feature maps.

The proposed method calculates Intersection of Union between the predicted bounding box locations and ground truth labelled data. IOU thresholds Box head: IOU thresholds Box Head. A non-maximum suppression is applied to feature sets created using RPN network. This allows for fine-tuned box locations that allow classification of objects. The Box Head will use the proposed boxes to extract ROIs from feature maps. To speed up the training process, ground-truth boxes can be added to the expected propositions. After ROI Pooling, the feature maps are cropped to create rectangle regions. These are used to identify the proposal boxes. The features that have been cut are then given to the head networks. Mask R-CNN4 has two types of heads: mask heads and box heads. The Fast RCNN Convolutional FCHead Box Head in Base R-CNN NFP is the only one that can classify the item within the ROI. It also fine-tunes both the shape and position of the box.

Two loss functions, localization loss and classification loss applied to fine tune the model based on the validation datasets

Localization Loss: Predictions from foreground are picked and compared with ground truth targets. The tensor values used are relative sizes of the ground truth boxes compared to the proposal boxes

Classification Loss: As the proposed method deals with multiple classes, soft max is the ideal choice of the neural network. Foreground, background and prediction scores are calculated by comparing against the ground truth label dataset.



IV. RESULTS AND EVALUATION

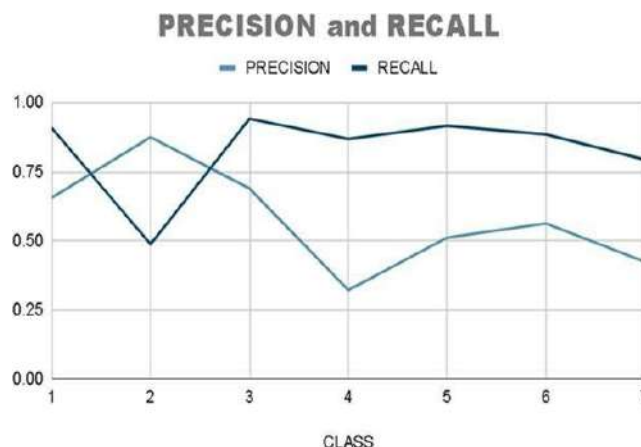
Proposed convolutional neural network models are validated based on 3 parameters:

Time Complexity: A convolution is the sum of the row-wise dot products of a filter $W \in \mathbb{R}^{k \times d}$ with a region matrix $A \in \mathbb{R}^{k \times d}$, where k is the length of the filter and d is the depth dimension (e.g. dimensionality of word embedding space).

- $O(d)$ for one dot product (d multiplications + $d-1$ additions)
- The method perform in total k dot products (there are k rows in W and A), which amounts to $O(k \cdot d)$
- And finally, at the layer level, the proposed methodology apply the filter over the input $n-k+1$ times (where n is the length of the input), let' say n times since $n \gg k$. This gives us a final complexity of $O(n \cdot k \cdot d)$.

Accuracy: To validate model accuracy, the proposed idea used precision, recall, and f1 score. The proposed model uses better key performance indicators than state-of-the art research models.

classes	cast	Cryst	Epith	epithn	eruyth	leuko	Mycete
Precision	0.656	0.975	0.69	0.322	0,512	0.563	0.424
Recall	0.909	0.488	0.942	0.869	0.916	0.885	0.794
F1 Score	0.762	0.626	0.769	0.469	0.656	0.688	0.552



Mean Average Precision: Computer vision uses mAP as an evaluation metric for object detection. Localization and classification are two different things. Localization is the determination of where an instance is located (e.g. Bounding box coordinates and classification are used to identify what the instance is.

$$MAP = \frac{\sum_{q=1}^Q AveP(q)}{Q}$$

The mean average precision (mAP). where Q is the number of queries in the set and $AveP(q)$ is the average precision (AP) for a given query, q .

To qualitatively evaluate the findings, the methodology involved also depict the predicted bounding boxes with corresponding labels and their scores, as shown in Figure 3. Predictions and ground truth values agree fairly well. The proposed method proved that the result is extremely sat for automatic urine sediment analysis. Also compared and contrasted the most up-to-date historical models in Table 2. Our suggested model, Detectron2, demonstrated to have a higher mAP value in terms of image segmentation of large and medium-sized objects. The main benefits of utilising Detectron2 include obtaining a superior and similar mAP when compared to other models described by Rui Kang [13] with only 4 hours of training time. In under 4 hours, 10,000 iterations on a huge augmented dataset were learned. Thus for 0.5 IOU, It is possible to get mAP values close to 90% with our proposed model.

TABLE II: Comparisons between our detection results and those of other networks

Net	Anchor scales	mAP	Eryth	Leuko	epith	cryst	cast	Mycete	Epithe t	test time (sec/img)
ZF	{1282, 2562, 5122 }	0.723	0.607	0.749	0.845	0.86	0.658	0.781	0.566	0.44
	{642, 1282, 2562, 5122 }	0.796	0.853	0.809	0.855	0.86	0.671	0.861	0.665	0.045
	{322, 642, 1282, 2562, 5122}	0.779	0.859	0.805	0.854	0.85	0.657	0.863	0.57	0.046
	{642, 1282, 2562 }	0.757	0.748	0.823	0.846	0.85	0.642	0.82	0.568	0.044
VGG-16	{1282, 2562, 5122 }	0.757	0.599	0.772	0.874	0.79	0.708	0.874	0.679	0.102
	{642, 1282, 2562, 5122 }	0.802	0.842	0.818	0.868	0.87	0.716	0.877	0.621	0.104
	{322, 642, 1282, 2562, 5122}	0.795	0.854	0.825	0.857	0.85	0.724	0.876	0.576	0.104
	{642, 1282, 2562 }	0.762	0.743	0.822	0.863	0.76	0.712	0.88	0.558	0.104
ResNet-50	{1282, 2562, 5122 }	0.77	0.613	0.831	0.853	0.85	0.757	0.873	0.615	0.219
	{642, 1282, 2562, 5122 }	0.784	0.761	0.824	0.86	0.82	0.768	0.859	0.595	0.219
	{322, 642, 1282, 2562, 5122}	0.804	0.876	0.812	0.86	0.85	0.747	0.874	0.605	0.22
ResNet-101	{1282, 2562, 5122 }	0.761	0.606	0.83	0.864	0.8	0.769	0.875	0.578	0.268
	{642, 1282, 2562, 5122 }	0.773	0.841	0.814	0.848	0.85	0.749	0.863	0.446	0.267
	{322, 642, 1282, 2562, 5122}	0.801	0.872	0.809	0.839	0.85	0.772	0.883	0.581	0.268
PVANet	{482, 962, 1442, 2562, 5122}	0.841	0.884	0.843	0.871	0.88	0.765	0.89	0.76	0.072
Proposed Model : Detectron2	{64,128,1282, 2562, 5122,642, 1282, 2562, }	0.8429	0.886	0.8459	0.878	0.886	0.766	0.8913	0.7625	0.014



Fig.6. Predicted Image outputs

I. CONCLUSION

The philosophy recommends practiced Detectron2 to regard pee molecule acknowledgment as article discovery and utilize the wellknown CNN-based procedure Faster R-CNN as the premise recognition system. They don't need division what's more, can gain task-explicit highlights beginning to end. One of the most major problems in the medical services industry is the discovery of pee particles and hence needs exact, precise and inventive techniques to distinguish them. The philosophy included is a FPN-based convolutional brain network model to perceive unmistakable kinds of pee particles in this distribution. In contrast with existing profound learning brain organizations, the proposed models accomplished better best in class execution. It is feasible to introduce a few sorts of occasion division models in later examinations to research the size of every molecule under pee molecule grouping.

REFERENCES

1. Pham, N. V. Nguyen, and T. Dang, "Scagcnn: Estimating visual characterizations of 2d scatterplots via convolution neural network," in Proceedings of the 11th International Conference on Advances in Information Technology, ser. IAIT2020, July 2020.
2. R. Kang, Y. Liang, C. Lian, and Y. Mao "CNN-Based Automatic Urinary Particles Recognition." ArXiv abs/1803.02699 (2018)
3. R. Girshick, "Fast r-cnn," Proceedings of the IEEE international conference on computer vision, pp. 1440–1448, 2015.
4. K. He, X. Zhang, S. Ren, and J. Sun, "Deep residual learning for image recognition," Proceedings of the IEEE conference on computer vision and pattern recognition, pp. 770–778, 2016.
5. K. Simonyan and A. Zisserman, "Very Deep Convolutional Networks for Large-Scale Image Recognition" "Computer Vision & Pattern Recognition, 2014.
6. S. Ren, K. He, R. Girshick, and J. Sun, "Faster R-CNN: Towards Real-Time Object Detection with Region Proposal Networks," IEEE Transactions on Pattern Analysis and Machine Intelligence, vol. 39, no. 6, pp. 1137–1149, 2017.
7. J. Redmon and A. Farhadi, "Yolo9000: better, faster, stronger," Proceedings of the IEEE conference on computer vision and pattern recognition, pp. 7263–7271, 2017.
8. Joseph Redmon, Ali Farhadi "yolov3: An Incremental Improvement, Computer Vision & Pattern Recognition 2018.
9. Bochkovskiy, C. Y. Wang, and H.-Y. M. Liao, "YOLOv4: Optimal Speed and Accuracy of Object Detection", Computer Vision & Pattern Recognition 2020.
10. W. Liu, D. Anguelov, D. Erhan, C. Szegedy, S. Reed, C. Y. Fu, and A. C. Berg, "SSD: Single Shot MultiBox Detector" 2016.
11. Roxelia D. M. Urinalysis. In: Walker HK, Hall WD, Hurst JW, editors. Clinical Methods: The History, Physical, and Laboratory Examinations. 3rd edition. Boston: Butterworths; 1990. Chapter 191.
12. Cavanaugh C, Perazella MA. Urine Sediment Examination in the Diagnosis and Management of Kidney Disease: Core Curriculum 2019. Am J Kidney Dis. 2019;73(2):258-272. doi:10.1053/j.ajkd.2018.07.012
13. A. Aziz, H. Pande, B. Cheluvareja and T. R. Dastidar, "Improved Extraction of Objects from Urine Microscopy Images with Unsupervised Thresholding and Supervised U-net Techniques," 2018 IEEE/CVF Conference on Computer Vision and Pattern Recognition Workshops (CVPRW), 2018, pp. 2311-23118, doi: 10.1109/CVPRW.2018.00299.
14. Zhang X, Jiang L, Yang D, Yan J, Lu X. Urine Sediment Recognition Method Based on Multi-View Deep Residual Learning in Microscopic Image [published correction appears in J Med Syst. 2020 Mar 12;44(4):84]. J Med Syst. 2019;43(11):325. Published 2019 Oct 23. doi:10.1007/s10916-019-1457-4

Detection and Mitigation of Mitm Attack in Software Defined Networks

Saritakumar N, Anusuya K V and Balasaraswathi B
PSG College of Technology, Coimbatore, India

ABSTRACT

Software Defined Network (SDN) is the networking architecture that segregates the activities of the control plane from the data plane. Man In The Middle (MITM) is a type of digital attack in a network where the attacker utilizes duplicated ARP messages by spoofing the attacker's MAC address with the authorized user's IP address. This paper sorts out the ARP spoofing, which is the suite of MITM attacks using IP-MAC address bindings. SDN is emulated using Mininet and the MITM attack over this network is done using arpspoof, which is the segment of the tool named Dsniff. For the evaluation of the proposed algorithm, various network parameters are compared and analyzed in both RYU and POX controllers. As a result, the proposed algorithm mitigates the MITM attack successfully by dropping the attacked packets.

Keywords: ARP Spoof, Dsniff, Mininet, MITM attack, SDN.

1. INTRODUCTION

In this digital world, wired and wireless technologies play the predominant role as they reduce human efforts. Since the number of users increases due to its flexibility, the network becomes more complex. To deal with such complex networks, SDN is used.

SDN is the networking architecture that decouples the data plane from the control plane and thereby greatly minimizing the network complexity. The control plane is responsible for providing instructions about directing the traffic through the network and forwarding data traffic to the data plane in the path specified by the control plane. The OpenFlow (OF) protocol [2] provides flow tables to direct the network traffic flow.

The infrastructure layer comprises network routers and switches to forward the data traffic. The controllers in the control plane control the network infrastructure by monitoring the topology, statistics, and state, etc. The application layer is developed by users interested in developing the applications by leveraging the network information such as topology, state, and statistics of the network.

The control layer and application layer are communicated through a North bound interface in which the applications notify the network requirements such as data, bandwidth, etc., so that the network can deliver those resources. The bottom layers such as the control layer and infrastructure layers having switches and network nodes are communicated through the Southbound interface used to identify the network and implement the data sent by the northbound interface.

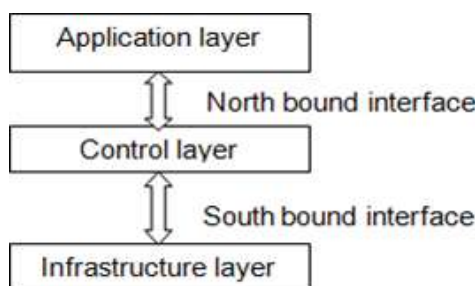


Fig.1. SDN Architecture

Since SDN [4] uses centralized architecture, security is a major concern. If the attacker fakes the controller as legitimate, then there has been the chance of data stolen from the end-user. It is necessary to mitigate those attackers so that users can use the network without any inconvenience.

2. LITERATURE REVIEW

The paper [3] explains different kinds of MITM attacks, such as ARP or TCP based MITM attacks. CMD obtains the forwarding rules of the infrastructure layer from the northbound API of the SDN controller, generates a real-time Global Flow Table, and starts the real time MITM attack detection using generated Global Flow Table. The design of the MITM attack detection algorithm is based on the topology and connection of network flow. The MITM attack detection mentioned in this paper analyzes the contents of network packets, which is simple and efficient.

The paper [8] proposes two scenarios to describe the methodology of MITM attack in different controllers like OpenDayLight (ODL), Open Network Operating System (ONOS) and RYU. The simulation results indicate that the attackers can control the SDN controller easily and the communication between the control layer and infrastructure layer is not secure. This paper recommends the tool named snort which is based on an IPS intrusion prevention system and an ARP spoof pre-processor.

The paper [1] investigates the potential threats of MITM attacks on the OpenFlow control channel and proposes a lightweight countermeasure using Bloom filters. Bloom filter monitor system is implemented in OpenvSwitch and Floodlight controller and the result shows that the method is lightweight and efficient. As the result, the attack detection is achieved within a short time and there are negligible delays in traffic.

The paper [5] eliminates the problem of ARP poisoning attack which is the key factor for many other network attacks such as MITM, DOS and session hijacking. Two scenarios are introduced to resolve the ARP spoofing problem based on whether a network host will be assigned a dynamic or a static IP address such as SDN_DYN and SDN_STA. Since, the controller has recorded the MAC-IP paired map in all attempts, the ARP spoofing attack has failed.

3. PROBLEM STATEMENT

This paper focuses mainly on the Man in the Middle attack considered as one of the security threats in the network. In a MITM attack, the attacker spoofs between the conversation of sender and receiver and eavesdrops on the information sent by those users. By this, an attacker can easily steal the sensitive information of the end-user. This type of attack can be detected by monitoring the incoming packets based on their IP and MAC addresses. Since this attack is detected at an earlier stage, the attacker cannot gain control of stealing the data.

4. SYSTEM DESIGN

The system design comprises SDN network architecture with an SDN controller detached from the data plane. The Open V Switch is used in the infrastructure layer and its operation is based on the instructions provided by the controller in the control layer.

Mininet [7] is the network emulator used to create SDN virtual environment. It utilizes virtual hosts and switches in a single OS kernel. The virtual hosts and switches are used to create network topology. The hosts run on Linux based operating system and the switches support OpenFlow protocol.

The proposed methodology is implemented on both RYU and POX controllers. RYU is the open-source controller that uses OpenFlow or other protocols to provide instructions to the forwarding plane on the handling of traffic flows in the network. POX is the popular controller for developing network applications in SDN using Python programming language for OpenFlow devices.

arp spoof - the poisoning tool, a suite of Dsniff tools written in python with CLI is used to spoof the MAC address of legitimate hosts.

5. IMPLEMENTATION

Whenever the PACKET_IN message arrives at the destination from the sender, initially it passes the switches and is sent to the firewall of the controller, if the details of the destination host are not found on the switch. Thus the proposed algorithm is fused in the firewall of the controller.

5.1 Attack Generation

As a part of the MITM attack, an ARP spoof [9] is generated using the Dsniff tool. By using this tool, an attacker would redirect packets from the target host intended for the client host by sending ARP replies. Thus the attacker sniffs the traffic on a switch.

As a result, the attacker replicates the own MAC address to the target and hence the ARP table [10] gets updated. Subsequently, all the packets from the client receive the attacker and the attacker can redirect the packets or modify the packets or even steal the data easily.

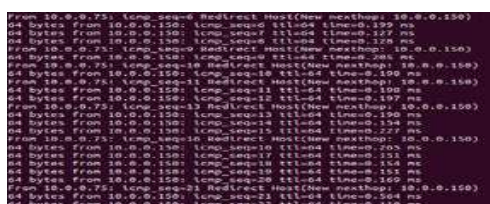


Fig.2. Redirected packets from the target host

5.2 Attack Detection

There are several ways to detect ARP spoofing in SDN such as

- Based on traffic patterns
- Based on IP-MAC address bindings
- Based on flow graphs

Since the attacker places its own MAC address between target and client, the ARP table [6] gets updated with replicated MAC address. Every switch maintains an ARP (Address Resolution Protocol) table that stores the MAC and IP addresses of the network devices and is used to find the corresponding MAC addresses of the hosts. Thus by analyzing packets after ARP spoofing, the MAC address gets replicated between the hosts with the different IP addresses found in the ARP table.

Here, the detection is based on IP-MAC addresses bindings. Once the topology gets initialized, the controller dynamically allocates MAC addresses for every IP address in the network. The controller stores the created MAC address in the mac_to_port table. During the attack, the attacker duplicates its own MAC address and spoofs the arrived packets. But the controller is unaware that whether the arrived packets have legitimate MAC addresses or duplicated MAC addresses.

5.3 Attack Mitigation

As a part of the MITM attack, an ARP spoof is generated using the Dsniff tool. Attacker redirects packets from a target host intended for client host by casting ARP replies. Thus the attacker replicates the attacker’s MAC address to the target so that the ARP table gets updated. Subsequently, all the packets from the client are received by the attacker.

Due to arpspoof, the ARP table gets updated with reproduced MAC address. ARP table is maintained by all switches which are used to store the IP and MAC addresses of the network devices. By this process, the attacker can redirect, modify or steal the data from the client.

The OpenFlow switch maintains the flow table with four entries related to ARP protocol, Ethernet source address, Ethernet destination address, IP source address, an IP destination address. But the controller forwards packets only based on the MAC address.

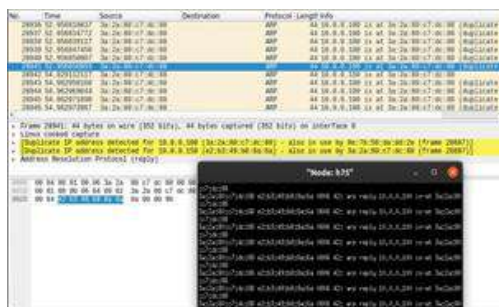


Fig.3. Attack detection

IP addresses of hosts are obtained and configured IP addresses and corresponding MAC addresses are stored in the mac_to_ip table. If the arrived packet is ARP, then the source IP and MAC addresses are obtained. The incoming MAC address is compared with the MAC address that is stored in the table. If the MAC address entry is found in the table, then the corresponding IP address is analyzed. If the corresponding IP address is unmatched with the incoming IP address, then the attack is detected.

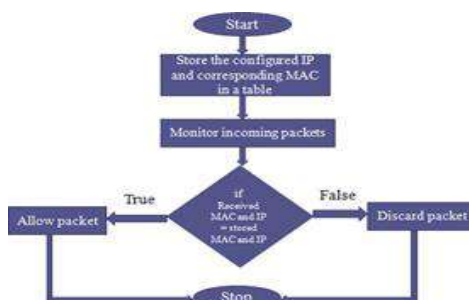


Fig.4. Proposed methodology

6. RESULTS AND DISCUSSIONS

The proposed methodology is carried out on the POX and RYU controllers with a network emulator, Mininet. POX and RYU controllers are based on python programming language and run on OpenFlow protocol version v1.0.

Algorithm 1 MITMmitigation

```

Input: Arrived packets
Output: Dropping attacked packet

1: procedure FUNCTION
2:   Monitor arrived packets
3:   for (packet = 1; packet <= i; packet++) do
4:     Store IP and MAC in mac_to_ip table
5:     if (incoming MAC = stored MAC) then
6:       Allow packet
7:     else:
8:       Packet drop
9:     end if
10:  end for
11: end procedure
    
```

6.1 Network topology

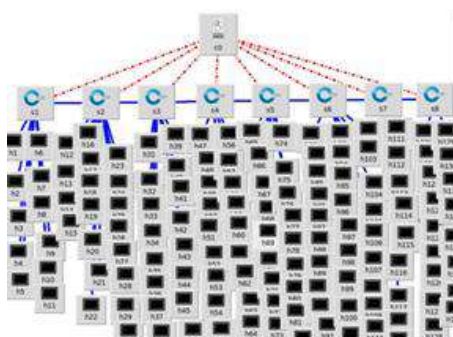


Fig.5. Network topology

Fig.5 shows a tree network topology created using Mininet with 200 hosts, 8 switches, and a remote controller. The remote controller can be either an RYU or POX controller.

6.2 Network Setup

Table 1. System specification

Parameters	Values
Processor	Intel(R) Core(TM) i3 -5005U CPU @2.00GHz
RAM	4 GB
Diskspace	255 GB
Operating System	Windows 10
Application Software	Virtual Box Mininet Version 2.2.1

6.3 Experimental Results

The controller compares the received IP address and MAC address with the configured IP and MAC address.

```

arp(dst_ip='10.0.0.150',dst_mac='ce:95:34:e8:53:4a',hlen=6,hwtype=1,opcode=2,plen=4,
proto=2048,src_ip='10.0.0.100',src_mac='a2:25:1c:3c:be:b0')
{'a2:25:1c:3c:be:b0': '10.0.0.75', '46:3c:cb:4c:83:65': '10.0.0.100', 'ce:95:34:
e8:53:4a': '10.0.0.150'}
10.0.0.75
10.0.0.100
ARP spoof detected
Packet drop
    
```

Fig.6. Dropping the arpspoofed packets

In Fig.6, when compared to the configured and received IP addresses, there is a mismatch in those IP addresses and thus the ARP spoofing gets detected and thus the packet gets dropped.

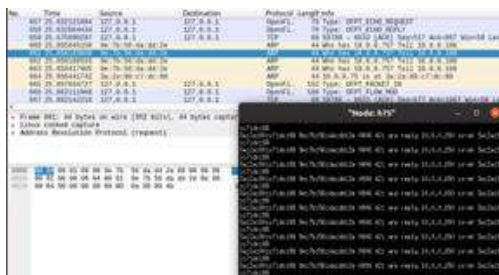


Fig.7. Analysis of dropped packets in Wireshark

Fig.7 shows that the filtered-out attacker’s spoofed the MAC address from the controller and directs only the legitimate MAC and IP addresses.

6.4 CPU Utilization

Performance evaluation is done to ensure the mitigation algorithm under MITM attack under various conditions. The CPU utilization is observed for switches with two controllers named POX and RYU before and after implementing the mitigation algorithm. The CPU utilization metric is based on average CPU usage over a certain period.

Table 2. CPU utilization for POX

Number of hosts	Before mitigation (%)	After mitigation (%)
50	70.8	61.2
100	80.5	76.6
150	87.2	78
200	88.4	82.6

Table 2 infers the CPU utilization for the POX controller before and after attack mitigation. The result analysis shows that CPU utilization has reduced after the prevention mechanism.

Fig 8 represents the graphical CPU Utilization for before and after mitigation of MITM attack. During the attack, as the number of hosts increases the CPU utilization increases. After implementing the mitigation algorithm, CPU utilization gets reduced up to 10% in POX.

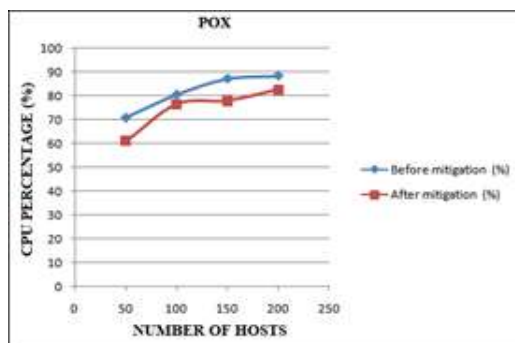


Fig.8. CPU utilization for POX

Table 3 infers that the CPU utilization for the RYU controller before and after attack mitigation. The result analysis shows that CPU utilization has reduced after the prevention mechanism.

Fig 9 represents the graphical CPU utilization before and after mitigation of the MITM attack. The plot represents the number of hosts versus the CPU resource used respectively during the MITM attack. As the number of hosts increases the CPU utilization increases. The CPU utilization gets decreased up to 20% during the mitigation in the RYU controller.

Table 3. CPU utilization for RYU

Number of hosts	Before mitigation (%)	After mitigation (%)
50	71.4	47.4
100	74.1	59.2
150	76.3	64
200	77	70.9

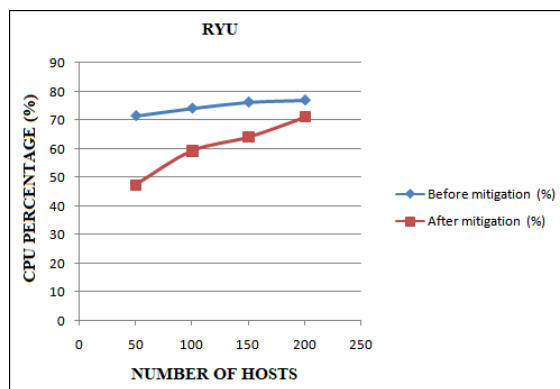


Fig.9. CPU utilization for RYU

6.5 Execution Time

It is necessary to calculate the execution time to evaluate the efficiency of the algorithm. The calculation of execution time is done in both POX and RYU controllers.

Table 4. Execution time for controllers

NUMBER OF HOSTS	POX (us)	RYU (us)
50	1.6	3.6
100	1.8	1.4
150	3	1.6
200	9	3.6

Fig.10 depicts the execution time required for the POX and RYU Controllers. The plot represents the number of hosts versus the time required for the execution of the mitigation algorithm.

As the number of hosts increases, execution time also gets increased. For the implemented algorithm, the execution time utilized by the RYU controller is only 5% of that found using the POX controller.

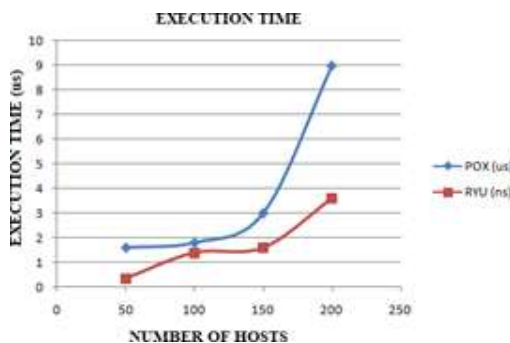


Fig.10. Execution time for POX vs RYU

7. CONCLUSION AND FUTURE WORK

With the detection algorithm implanted into the 2 controllers, two different behaviors are observed. This solution is not only efficient in detection, but it also has minimal code addition to the controller program and does not increase CPU load in either normal or attack conditions. POX controller takes more time to process the packets once an attack occurs but consumes less CPU usage than that of the RYU controller.

The execution time is directly proportional to the number of hosts in the network. The execution time taken in the RYU controller is reduced by 5% when compared with the POX controller. The future scope is to make our mitigation algorithm to detect different kinds of MITM attacks such as SSL hijacking, DNS spoofing, IP spoofing, etc.

REFERENCES

1. Cheng Li, Zhengrui Qin, Ed Novak, Qun Li, Member, IEEE, "Securing SDN Infrastructure of IoT-Fog Networks from MitM Attacks," IEEE Internet of Things Journal, 2017.
2. XIA Jing, CAI Zhiping, HU Gang, and XU Ming, "An Active Defense Solution for ARP Spoofing in OpenFlow Network," Chinese Journal of Electronics, Vol.28, No.1, Jan.2019.
3. Kai Zhang and Xiaofeng Qiu, "CMD: A Convincing Mechanism for MITM Detection in SDN," IEEE International Conference on Consumer Electronics (ICCE), IEEE, 2018.

4. Tri-Hai Nguyen and Myungsik Yoo, "A hybrid prevention method for eavesdropping attack by link spoofing in software-defined Internet of Things controllers", *International Journal of Distributed Sensor Networks*, Vol 13 (II), 2017.
5. Mohammad Z. Masoud, Yousef Jaradat, and Ismael Jannoud, "On Preventing Arp Poisoning Attack Utilizing Software Defined Network (SDN) Paradigm", *IEEE Jordan Conference on Applied Electrical Engineering and Computing Technologies (AEECT)*, 2015.
6. Talal Alharbi, Dario Durando, Farzaneh Pakzad, "Securing ARP in Software Defined Networks", *IEEE 41st Conference on Local Computer Networks*, 2016.
7. Chaitra N. Shivayogimath and N.V. Uma Reddy, "Performance Analysis of a Software Defined Network Using Mininet," *Springer Artificial Intelligence and Evolutionary Computations in Engineering Systems* pp 391-398, Feb. 2016.
8. Anass Sebbar, Mohammed Boulmalf and Mohamed Dafir, "Detection MITM Attack in Multi-SDN Controller", *IEEE*, 2018, pp.583- 587
9. Zeynab Sasan, Majid Salehi, "SDN- based Defending Against ARP Poisoning Attack", *Journal of Advances in Computer Research*, Vol.8, No.2, May 2017.
10. Ahmed M.AbdelSalam, Ashrad B. El-Sisi and Vamshi Reddy.K, "Mitigating ARP Spoofing Attacks in Software-Defined Networks", *ICCTA*, 2015.

A Low-Phase Noise PLL for 5G Application

Radha Krishnan K R, Subha Rani S and Shivasubramaniyarajan V M
Department of ECE, PSG College of Technology, Coimbatore, India

ABSTRACT

In this paper, the performance of PLL with different topologies and technologies are discussed. A PLL can be used as frequency synthesizers in the 5G transceivers; such PLLs require high demand in performance i.e., low phase noise and jitter. There are many design techniques available to achieve good performance. Among the various blocks that constitute a PLL, the most critical one is voltage control oscillator which trades off with performance for area. For upcoming 5G transceivers both area and performance are important. So design techniques which should be able to satisfy the both are needed. The work aims at reducing the phase noise of the PLL less than 100 dBc/Hz at 1MHz.

Keywords—phase lock loop, frequency synthesizers, charge pump, VCO, phase noise, jitter.

I. INTRODUCTION

The mobile bandwidth requirement increases day by day and current 4G bandwidth are not sufficient to the data traffic. As a consequence, higher bandwidth is required which implies higher frequency i.e., in gigahertz and leads to the development of 5G technology. With the advent of 5G, there are so much pressing needs on performance of various building blocks (both analog and digital). Of all of them, frequency synthesizers which produce gigahertz clock should meet stringent requirements- for example jitter of clock should be less than 100fs and phase noise well below the - 100dBc/Hz are required. Below some of the most advanced techniques are discussed.

II. TECHNIQUES

A. SUBSAMPLING

In this sub sampling technique, high frequency VCO signal is sampled by low frequency signal. This technique eliminates the power consumption by frequency divider and noise of the same. So, the power consumption and noise of overall frequency synthesizers improves. The PLL which is used in this technique under-samples the high frequency oscillator output with low frequency clock reference. Moreover, the noise which is N^2 times that of PD/CP is eliminated which itself is an added advantage. Difficulty of integration and limited acquisition range are the drawbacks of this technique. But this has to be overcome because limited acquisition range limits this PLL to be used as high frequency generators in mm-wave. However, the drawbacks can be overcome by pulse width control which operates the subsampling PD/CP.

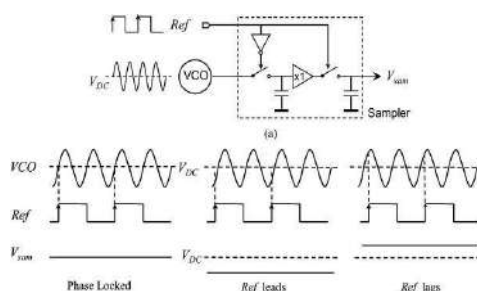


Fig 1. Conceptual and timing diagram of subsampling PLL.

A traditional PFD/CP can also be utilized with a dedicated dead zone which prevents any degradation in jitter performance. So, the integrated jitter and the phase noise of the subsampling PLL is greatly improved which is shown in the table. The conceptual and timing diagram are shown in the Fig. 1.

B. IN PHASE INJECTION BASED QVCO

Many in-phase current injection networks have been introduced for low phase noise and less jitter. But those network uses RC or LC circuits to achieve the purpose. In this [2], the injection technique is based on network which is not dependent on the frequency. There are lots of advantages like oscillation stability, less phase error due to mismatches which arises due to asymmetric layout variations or process variations, and low phase noise [2]. To prevent the usage of the inductor which can cause numerous problems in layout, a special circuit called low power inductor less circuit has been introduced. The charge pumps are prone to more spurs in voltage which can be eliminated by using unity gain amplifier by low pass cascaded by RC circuit. The in-phase coupling is realized in the IPIC quadrature voltage control oscillator which reduces the phase noise and jitter

considerably. It is implemented in standard low power 65nm technology to further improve the FoM (figure of merit) of the PLL. The phase noise is around -90dBc/Hz for 1MHz and reference spur is around -54.45dBc. Thus, this method of designing PLL has great compliance with IEEE std 802.15.3c and also other 60 GHz standards.

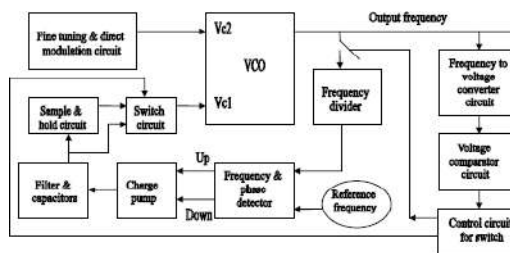


Fig. 2. Architecture for PLL for non-continuous operation of constituent blocks

C. NON-CONTINUOUS OPERATION FOR ULTRA-LOW POWER

A method is proposed in the [3] to bring down power consumption of the PLL to very large extent while still keeping the performance on par. This kind of PLL find application in bio-medical equipment; these do not have the frequency divider in the PLL to be operated continuously [3] because these are placed inside the body where temperature is sufficiently constant; therefore, frequency deviation due to temperature is minimum. A control circuit is designed to switch on and off the frequency divider, charge pump, etc. There are two tuning point associated with this PLL; the first point allows to tune for wide range and other to tune for narrow range [3]. The PLL architecture is shown in the Fig 2. Using this technique, the circuit is able to operate with low power as much as 0.23 mW and with low phase noise of around -100dBc/Hz at 1MHz.

D. HYBRID ARCHITECTURE FOR LOW JITTER

The ring oscillators are good for wide range tunability, while LC oscillator is good for low phase noise. Both wide range tunability and achieving low phase noise are contradicting factor. This architecture combines both the ring-oscillator PLL and LC oscillator PLL for achieving the above stipulated features. This architecture has also come up with 360-degree phase adjustment [4]. In this architecture LC PLL and the ring oscillator PLL are cascaded together to meet the required tunability and phase noise.

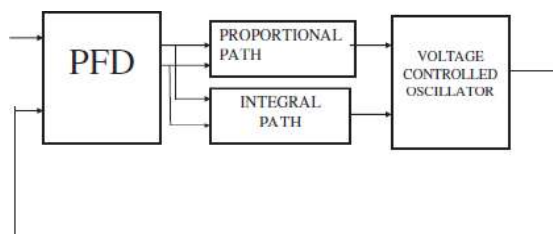


Fig.3. LC PLL

The block diagram for LC PLL is shown in Fig.3. The block diagram for ring oscillator PLL is shown in Fig.4. The major demerit in the architecture is area overhead due to the LC oscillator PLL. However increased bandwidth leads to reduction in the area of loop filter. Due to an extra LC PLL [4], the power consumption is comparatively larger than other PLL structures but this trades off with low jitter and low phase noise. The RMS jitter is around 21 ps and peak to peak jitter is around 19ps with tunable range of 4.5 to 8.25 GHz [4].

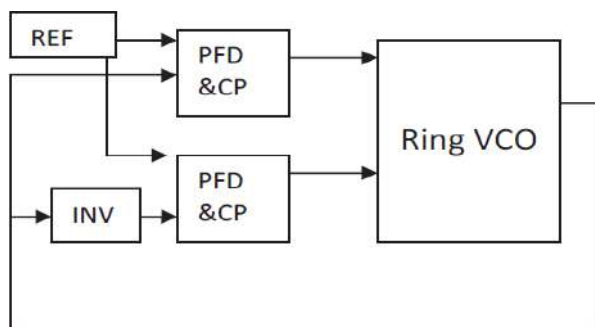


Fig.4. RO PLL

The loop filter resistance is realized with a MOS transistor operated in a linear region i.e., deep triode region so that PVT variation does not affect the loop stability much and robust stability is ensured at high frequency.

E. CASCADED ARCHITECTURE

The design for future 5G transceivers demand the high pressing needs on the performance of clock synthesizers. But as the frequency increases, there is more phase noise and jitter also get worsened. Hence designing such high frequency PLL with the desired performance is highly difficult. Moreover, often the clock synthesizers need to synthesize the frequency which is not integral multiple of reference clock but fraction of it; this makes the condition even worse. Hence in this [5], it is proposed to use cascaded PLLs which are of different type i.e., fractional PLL is cascaded with integral PLL. Moreover, instead of multiplying local oscillator frequency with huge number, say 40 or 50, it is stepped up to some intermediate frequency by one PLL and it is further stepped up to desired frequency level by the other. The architecture is shown in the Fig.5.

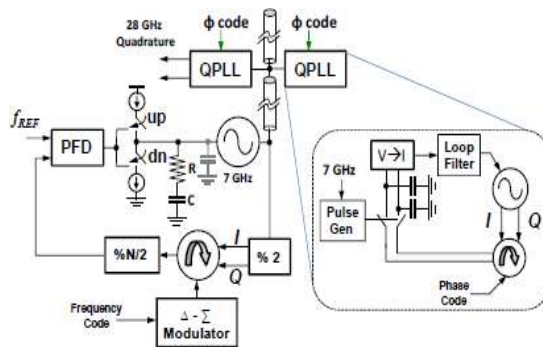


Fig.5. Cascaded PLL architecture.

In the traditional cascade PLL architecture, fraction division is performed outside the PLL. But in this architecture the fractional part is included in the second stage. Moreover, the fractional architecture is of subsampling [1] type which reduces the power consumption which improves the FoM (Figure of Merit) of the PLL. In the first, reference frequency is first stepped up to 7GHz and it is further stepped up to 28 GHz by the fractional PLL. As a result of subsampling technique in the second PLL, the phase noise multiplied by N^2 are eliminated.

The PLL of type II is used as first stage which fractionally converts 230 MHz clock frequency into 7GHz frequency and it implements the phase rotator to achieve fractional division, unlike in traditional PLL which uses the normal divider circuit. Converting 7GHz frequency signal to 28GHz signal is really a difficult task. A conventional PFD which divides such a high frequency is nearly impossible and moreover the area required for the divider which divides a 28GHz signal by 4X times is very large. The above point implies that there should be some modification, which provides good performance to PLL, in the divider and PFD circuits. So, the concept of subsampling i.e. divider-less sampling [1] comes into picture. Hence in the second PLL subsampling concept is used and PFD is modified with sample and hold circuit which is called Sample and Hold Phase Detector (SHPD). The main problem with the SHPD is that it is prone to locking false frequency, which can be eliminated with additional circuitry.

III. PROPOSED WORK

The proposed work targets low phase noise among other architectures discussed here. The phase noise contribution mainly comes from the devices those are being used. The higher length of the devices used, lesser will be the noise in the circuit. But since the device length used is 180nm, the noise is quite considerable. So noise can be controlled by any kind of feedback mechanism, since PLL is based on feedback circuit that would be quite useful for the purpose. Noise of the circuit is reduced when negative feedback mechanism is used-roughly the noise is divided by loop gain of the loop, so by increasing the loop gain, one can control noise, thereby achieving low phase noise. Increasing the operational amplifier output resistance helps to improve the loop gain. From the table I, the results are tabulated, comparing to the other architectures, the low phase noise is achieved by increasing the loop gain. The architecture used for the work is shown fig 6. The architecture is normal only but the way it is implemented is different.

TABLE I PERFORMANCE COMPARISON ACROSS THE ARCHITECTURES

Parameter/ techniques	Sspll [1]	IPIC [2]	Ultra-low power [3]	Hybrid architectue [4]	Cascae architecture [5]	Work proposed
Technology	0.18um	65nm	65nm	250nm	65nm	0.18um

CMOS						
Phase noise	-235dBc/Hz @200kHz	-191dBc/Hz@ 1MHz	106dBc/Hz @ 1MHz	N/A	-114 dBc/Hz@ 1MHz	-99dBc/Hz @1MHz
Power consumption	7.6mW	24mW	0.23mW	22.1mW	26.9mW	N/A
Output Frequency/ tuning range	2.2 GHz	60GHz	405MHz	4.5GHz- 8.25GHz	28GHz	1.5GHz
Jitter	0.15 RMS-ps	N/A	N/A	21 RMS-ps	66.7fs	5ps

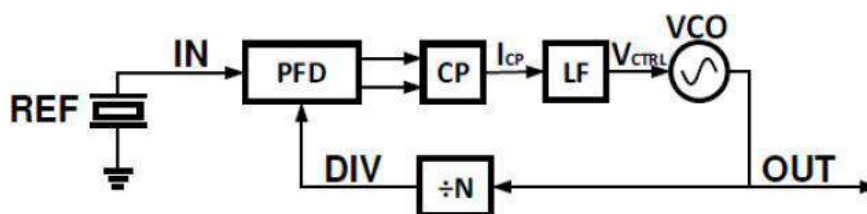


Fig 6 PLL architecture

IV. RESULTS

The circuit is simulated in the cadence spectre simulator for all corners. The one that is tabulated is for the worst cascorner. The KVCO vs frequency is shown in the fig 7.

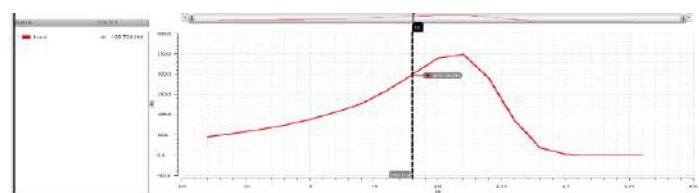


Fig 7. KVCO vs frequency

The phase noise gives the accuracy of the frequency that is produced. The phase noise vs frequency is shown in fig 8. From the figure, it is clear that as relative frequency increases around the central frequency, the phase noise reduces.

Hence as previously stated, the phase noise of the PLL has come down due to the circuit design technique employed.

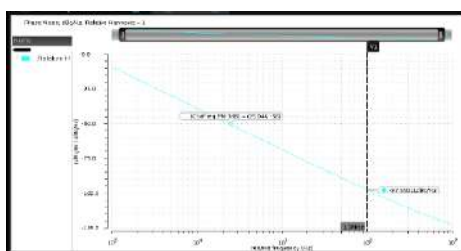


Fig 8. Phase Noise vs relative frequency

V. DISCUSSION

The table I summarizes the performance of PLL across the different architectures. Among them, the lowest possible technology that has been used to implement is 65nm which is quite high for this type of complex circuit. When considering the phase noise, cascade structure performance is good and also its output frequency is also pretty high compared to the most of topologies. When there is a need to design for ultra – low power PLL, one can look into [3] which gives very much reduction in the power but at the cost of relatively low output frequency. For 5G transceivers, which requires high frequency range around some 100 GHz, one can choose the IPIC based architecture which has low phase noise. The clock jitter determines the performance of the circuits which are time-critical and also very important for the circuits working in high frequency. As for clock jitter, the cascaded architecture does better. Moreover, the cascaded architecture incorporates so many optimal techniques to implement the PLL, for example it uses Quadrature PLL which also leads to low noise compared

to the conventional PLL. The most important component in the PLL is VCO which contributes roughly around 40 percent of the total noise in the PLL. So careful designing of the VCO is very important. Further, there are many topologies available for VCO, for example differential VCO comes with area overhead but it provides low noise comparatively among other VCO topologies. As it has been discussed earlier, that LC oscillator provides low phase noise but comes with narrow tunable range which is in contrast to the ring oscillator type. The type of architecture to be chosen is based on the requirement.

VI. CONCLUSION

Thus, several topologies have been discussed and the merits and demerits of them are also discussed. Also choosing particular topology over other also comes with certain trade-offs. From the performance table one can be able to identify topology that suits the requirements. Also for upcoming 5G ICs the above discussed topologies will certainly help. The PLL thus discussed are implemented not below 65nm technology. So there are definitely many challenges in designing PLL well below the 60nm technology as the second order effects are more pronounced. Despite this, noise contribution is very much as the technology shrinks. The work shows that even with 180nm one can achieve less 100 dBc/Hz @1MHz.

REFERENCES

1. X. Gao, E. A. M. Klumperink, M. Bohsali, and B. Nauta, "A low noise sub-sampling PLL in which divider noise is eliminated and PD/CP Noise is not multiplied by N²" in IEEE journal of solid-state circuits, vol. 44, no. 12, December 2009
2. Xiang Yi, Member, IEEE, Chirn Chye Boon, Senior Member, IEEE, Hang Liu, Jia Fu Lin, Student Member, IEEE, and Wei Meng Lim, "A 57.9-to-68.3 GHz 24.6 mW Frequency Synthesizer with In-Phase Injection-Coupled QVCO in 65 nm CMOS Technology" in IEEE journal of solid-state circuits, vol. 49, no. 2, February 2014
3. Bahram Ghafari, Leila Koushaeian, and Farhad Goodarzy Victorian Research Laboratories, National ICT Australia Dept. of Electrical and Electronic Engineering, "New architecture for an ultra low power and low noise PLL for biomedical applications"
4. R.Prithivi Raj, S.Balaji, Dr K.S.Srinivasan, S.Senthilnathan M.E (VLSI Design), Dept. of ECE, Easwari Engineering College, Chennai, India, "Low Jitter Hybrid Phase Locked Loop" in 2012 Third International Conference on Emerging Applications of Information Technology (EAIT)
5. Waleed El-Halwagy, Student Member, IEEE, Amlan Nag, Philip Hisayasu, Member, IEEE, Farshid Aryanfar, Senior Member, IEEE, Pedram Mousavi, Senior Member, IEEE, and Masum Hossain, Member, IEEE, "A 28-GHz Quadrature Fractional-N Frequency Synthesizer for 5G Transceivers With less than 100-fs Jitter based on cascaded PLL architecture" in IEEE transactions on microwave theory and techniques, vol. 65, no. 2, february 2017
6. M.Ferriss, et. al., "A 13.1-to-28GHz fractional-N PLL in 32nm SOI CMOS with a $\Delta\Sigma$ noise-cancellation scheme," IEEE ISSCC2015, pp.1-3, Feb. 2015.
7. V.Szortyka, et. al., "A 42 mW 200 fs-Jitter 60 GHz Sub- Sampling PLL in 40 nm CMOS," IEEE JSSC, Sep. 2015.
8. M. Hekmat, et. al. "A 25 GHz Fast-Lock Digital LC PLL with Multiphase Output Using a Magnetically-Coupled Loop of Oscillators," IEEE JSSC, vol.50, Feb. 2015.
9. V. F. Kroupa, Frequency Synthesis: Theory and Design, London, U.K.: Griffin, 1973.

A Study on Job Stress among Women Bank Employees with Special Reference to Malabar Region of Kerala

Amrutha S. and V. Santhi

Department of Humanities, PSG College of Technology, Coimbatore

ABSTRACT

Human resource is the most valuable resource for an organization. They are responsible and capable of making valuable contributions. Banking is one of the sectors in which the percentage of women employed is higher. The major challenge now they face is job stress. In this study, the fifteen job content variables have been chosen as the stress-causing variables and among them, eight variables were found to be significant. They are workload, technological changes, personal and family issues, marketing stress, career growth, target achievement, job rotation and training opportunities. Among the demographic factors, age, Job designation and native place of the women employees have significant relation with the job stress. These factors contribute about 63% of the total stress caused among women employees in the banking sector at Malabar region of Kerala. The primary data were collected from women employees working from both private as well as public sector bank through a structured, tested questionnaire. These findings could help banks eliminate numerous stress-inducing variables in the workplace.

Keywords: Job Stress, Commercial Banks, Women Bank Employees, Demographic Variables, Job Content Variables, Malabar region of Kerala

INTRODUCTION

In today's world, Stress Management is one of the main areas which require more attention. This is very particular concerning the financial sector. Everyone is exposed to tension and anxiety as they get through their job. The banking industry, which is the country's economic backbone, sits at the top of the list. Job stress is a typical workplace issue that affects all professionals, regardless of the type of their work. It is a major problem causing occupational health problems and a significant cause for economic loss. It can even cause both psychological and physiologic problems. Employees may exhibit numerous stress symptoms as a result of their stress, which can have a negative impact on their job performance. People who are stressed may become jittery, uncooperative, and prone to losing their cool. Employees must conquer this ailment in order to be more productive at work and have a better life.

Indian women are getting themselves out of traditional old ways and have placed themselves in diversified areas. They have shown their presence in all the areas and have showcased their talents, skill sets, knowledge and thereby bringing success in all stages of the job that they have taken up. Job opportunities in the banking sector have created a good opportunity for them to find employment in the sector and many are placed at the topmost positions of many major banks. Work-life and personal life are very much related. The job stress felt by the women is high and at times find it difficult to balance the work and personal life. So there should be some remedies to reduce the stress among them and motivate them to bring about the best in them.

REVIEW OF LITERATURE

Inter role distance, role stagnation, role expansion conflict, role erosion, role overload, role conflict, personal inadequacy; self role distance, role ambiguity, and resource insufficiency are among the 10 types of organisational stressors identified by Patnaik (2014). According to Kahn and Quinn (1970) "stress is the outcome of the fact of the assigned work role that caused harmful effect for the individual. Occupational stress is considered as a harmful factor of the work environment. In a study conducted by Claudia-Neptina Manea et al (2013) proposed that the level of stress, social attitudes in different position of bank employees have significant relationship between them. Murphy (1995) proposed that organisational and individual pressures might be divided into five areas in his work. Organizational factors, job/task characteristics, organisational culture/climate, Interpersonal Relationships, and employee personal attributes are the aspects to consider. According to the study conducted by Harish Shukla and Rachita Garg (2013), like any other business, banking sectors in the Indian economy is deemed to be one of the most competitive, despite several challenges in terms of technological breadth, diversity, and globalisation. It creates a stressful environment to majority of employees when they are unable to cope with frequent work changes.

Cobb (1975) said that the over responsibility imposed on the employees create severe stress among workers. Cooper and Marshall (1976) came to a conclusion about workplace stress. They suggest that different

environmental factors or stressors, such as role ambiguity, task overload, role conflict, and poor working conditions, can create workplace stress. These factors ultimately affect the performance of an employee. Khattak, Jamshed Khan et al. (2011)¹ in his study had identified many factors that significantly causes the stress among employees. In his study he found out that technology is one of the most influencing factors that cause job stress. According to N. V. Ramachandran and Dr. R. Rajendran (2018). Employment instability and insufficient planning, role invasion and fortification, and a lack of position definition, as well as an abundance of work, are all sources of workplace stress among marketing executives. Ashfaq Ahmed et al (2013) proposed that are under a great transaction of stress. In their study, Dr.R.PrakashBabu and K.Vembu (2014) conclude that Women employees are under a lot of stress because of things like position ambiguity, duty overload, a lack of supervisory assistance, and technological developments.

RESEARCH QUESTION

- Do women working in the banking sector find their job stressful?
- What are the factors that contribute to work stress among women bank employees in Malabar region of Kerala?
- Based on demographic parameters, what are the disparities in the amount of stress-causing among women bank employees?
- What is the hierarchy of factors that cause job stress among women employees in the banking sector?

MODEL OF THE STUDY

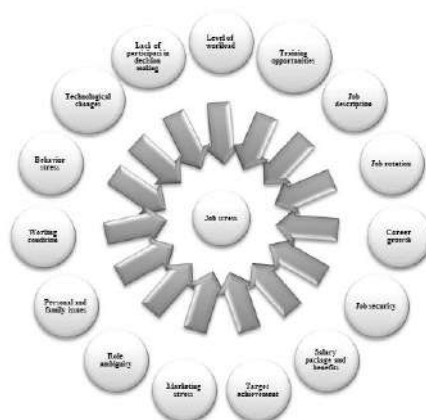


Fig1.Pictorial representation of the model

OBJECTIVE OF THE STUDY

1. To examine the variables that contributes to job stress.
2. To study the differences in the level of stress due to demographic factors.
3. To determine the hierarchy of factors that contributes to job stress.

RESEARCH METHODOLOGY

The study was conducted at Malabar region of Kerala. Primary data have been collected from the women banks who are working across different branches in the Malabar region of Kerala. The final instrument was administered to 105 respondents, across the country, of which 92 data was used for the analysis after editing to accommodate the missing value. Respondents were from all age groups from age 20 to 58. The data was collected in a descriptive method. A pilot study was conducted by collecting data from 15 respondents' in order to check the robustness of the scale. The Cronbach alpha value was 0.73. Secondary data was gathered from a variety of sources, including books and papers published in reputable management journals, as well as websites, corporate records, and annual reports. The Statistical tools used in the study are Percentage Analysis, Weighted average, Correlation, Regression and factor analysis.

Analysis of demographic characteristics and job content variables of respondents:

The demographic Variables reveal some of the results that have been lifted by the respondents are listed as follows

Age of the respondents: Among the 11.43% respondents who belong to the age category of 18-25 years finds their job is highly stressful.62% of the respondents who belong to the age group of 25-35 years feel their job is

stressful, 27.5 % of the respondents feel their job is not stressful and the rest of the respondents have a neutral mentality towards the job stress. Another interesting factor that can be seen from the result that as age increases the level of stress felt by the employees also increases.

Marital status: From the total respondents, about 51.4% of the respondents were married. Among the married respondents 72% of respondents find their job as stressful, 17% of respondents find their job is not stressful and the rest of the respondents have a neutral approach. Among the 45.7% unmarried respondents, 56% feel their job is stressful, 37% feel no stressful and the rest of the respondents have a neutral approach. The widowed respondents find their job as highly stressful.

Educational qualification: From the total respondents, about 37% of the undergraduates' respondents, 71.4% of respondents find their job as stressful, 21.4% respondents find their job is not stressful and the rest of the respondents have a neutral approach. Among the 48.5% postgraduate respondents, 62% feel their job is stressful, 31% feel no stressful and the rest of the respondents have a neutral approach. Among the respondents who have done professional courses, 60% of respondents find their job as highly stressful and the rest 40% have a neutral approach.

Experience of the respondents: Respondents who are having below 2 years of experience belongs to 34% of the total respondents. Among them 60% of the respondents find their job as stressful, 33% of respondents do not find their job as stressful and the rest 7% have a neutral approach. Among the 20% of respondents who are having 6-10 years of experience, 71% of the respondents are very much stressed, 14% of finds the job as not stressful and the rest finds responded as neutral.

Job designation: All the respondents in the middle-level management find their job as stressful. 64% of the respondents from the junior level management find their job as stressful and 60% of respondents from the clerical respondents find the job is stressful. From this, it is evident that the stress level increases as the employees get to higher designations.

Native Place: Among the 23% respondents whose belongs to the rural area, 75% of respondents find their job is highly stressful, 12.5% of the respondents find their job as not stressful and the rest finds it neutral, 60% respondents who belong to semi-urban area, 57% among them feel their job is stressful, 38 % of the respondents feels their job is not stressful and the rest 5% of respondents have a neutral mentality towards the job stress. 83% respondents from the urban area feel their job as stressful and the rest 17% have a neutral mentality towards job stress.

The Job content variables reveal some of the results that have been lifted by the respondents are listed as follows

Table 1. Job content Variable

<i>variables</i>	Mean	Weighted Mean	Rank
Marketing	3.57	3.12	4
Career growth	3.46		5
Technologies	3.23		6
Target	3.97		1
Workload	3.65		2
Family	3.6		3
Job ambiguity	2.8		11
Secured feeling	2.74		12
Working condition	2.69		13
Salary	2.48		14
Moral values	2.4		15
Training	3.2		7
Job rotation	3.14		8
acceptation	3		9
clarity	3		9
Participation in Decision making	2.97		10

According to the above table, the mean value shown, the respondent view about the factors impacting the respondents' perceptions of job stress among women employees in the banking sector is extremely important.

The dimensions of the following variable, Job stress, are given more weight by the respondents. The opinions of the respondents are ranked based on the mean value.

Table 2. Ranking based mean value of the job content variables

Variables	Mean	Rank
target	3.97	1
workload	3.65	2
family	3.6	3
marketing	3.57	4
Career growth	3.46	5
technologies	3.23	6
training	3.2	7
Job rotation	3.14	8

FINDINGS AND DISCUSSION

It can be determined that among the fifteen job content variables chosen for the study which are workload, lack of participation in decision making, Technological changes, Behaviour stress, Working condition, Personal and family issues, Role ambiguity, Marketing stress, Target achievement, Salary package, and benefits, Job security, Career growth, job rotation, work overload, No proper job description, and Training opportunities, eight variables are found to be significant. They are workload, Technological changes, Personal and family issues, Marketing stress, career growth, target achievement, job rotation and training opportunities. These factors contribute about 63% of the total stress cause to women employees. Six demographic variables were chosen for the study which is Age, Native places, Job designation, Work experience, Educational qualification, Family status. Among them Age, Native places and Job designation show significant relation with the job stress among the women bank employees.

Marketing has a positive correlation with job stress. It influences 67% on the stress among the women bankers. Target which has a positive correlation with job stress influences 70% on the stress among the women bankers. Job rotation which is a very common practice in banking contributes almost 29% to the stress among women. Training which improves an employee's overall development shows a significant influence over the stress causing variables. It has an inverse relation with the stress level. the stress level among the women employees can be decreased as the bank provide frequent and affective training to the employees. It could almost decrease about 47% of the stress among the women bankers. The career growth has a positive correlation which influences 54% on the stress among the women bankers. Banking is one of the areas where the updation of technology is happening in a faster way. This creates a stress among the women employees to adapt to the change in the technology. It influences almost 33% on the stress among the women bankers. Workload shows a positive correlation with job stress that influences almost 57% on the stress among women bankers. Another major factor that significantly contribute to the stress level is the Personal and family life. The analysis shows that the stress level contribute a negative correlation with job stress that is if an employee has a supporting and happy personal life she feels less stressful. This variable can affect almost 49% on the stress level among the women bankers.

Demographic variables are most relevant variable when we are more focusing on an individual basis. In this study three demographic variables show significant relation with the stress causing variables. Age is one of the significant variables that can influence the stress of a women bank employee. In the study we can see that the stress level increases with increase in the age of the individual. The next factor that has a significant is Native places. Women employee whose native place is rural area seems to be more stressful compared to women whose native place belongs to urban areas. Designation of the employee is the variable that significantly affects the stress level of the employees. The employee at the higher position feels more stressful compared to the low level employees. The analysis shows that Work experience, Educational qualification and Family status do not have significance over the stress generating variables.

Work-life balance for women employees in the banking industry is the norm. Women, when compared to men, have a harder time reconciling their personal and professional lives. Women's work-life balance is critical to their overall health and productivity, as well as their overall financial prosperity. Unlike the ancient time of women staying at home and doing just the work hold activities, things have changed a lot. Now women are self-dependent and this facilitates Women's empowerment. It has become a significant topic of discussion in today's

scenario. The empowerment of women enhances the quality and the number of human resources available for development. This reduces the problems regarding gender inequality and in the future enhances a life without any gender bias.

SCOPE OF THE STUDY

From the above study, it is evident that nowadays women working in the banking industry face job stress. As we all know the stress always decreases one's efficiency and thus resulting in low output. So by taking into consideration all our stress-causing factors the management can take adequate measures to eradicate such difficulties in the future. In terms of individual perceptiveness, he or she can individually evaluate those factors that cause job stress and take steps to improve their personal as well as professional life. This ultimately helps them to maintain a work life balance.

CONCLUSION

India's banking system is undergoing significant changes. Rather of clinging to their old ways of doing business, they have devised new ways to improve their operations. This has had both beneficial and negative consequences for the company's employees. According to the study, women working in the banking industry are under huge stress. There could be a variety of reasons for this. According to the study, various demographic and latent job content factors have a role in their job stress. Workload, technological changes, personal and family concerns, marketing stress, career growth, target achievement, job rotation, and training opportunities are some of the job content variables. Among the demographic factors, age, Job designation and native place of the women employees contribute to job stress. Each person's level of stress is different. It's high time for management to take actions to alleviate stress on a regular basis.

REFERENCE

1. E. George and Z. K.A., "Job related stress and job satisfaction: A Comparative Study Among Bank Employees," *Journal of Management Development*, vol. 34, no. 3, pp. 316–329, 2015.
2. B. B.ujwala and Dr. Mukesh Kumar V Dr. Mukesh Kumar V, "A study on workplace stress and its impact on job performance among bank employees in Chittoor (DIST)," *International Journal of Scientific Research*, vol. 2, no. 9, pp. 223–225, 2012.
3. D. I. Satpathy, D. B. Patnaik, and B. Mitra, "Review of literature-stress management in IT sector," *Indian Journal of Applied Research*, vol. 4, no. 2, pp. 7–9, 2014.
4. H. Swain and S. Mohapatra, "A Comparative Study of Leadership Factors Affecting Public and Private Sector Banks in India: An Employee Perspective", *Prabandhan: Indian Journal of Management*, vol. 6, no. 9, p. 28, 2013. Available: 10.17010/pijom/2013/v6i9/60028 [Accessed 7 October 2021].
5. "The Influence of Gender on Conflict Management Styles: A Study among Employees of Public Banks in Ethiopia", *International Journal of Science and Research (IJSR)*, vol. 5, no. 3, pp. 577-582, 2016. Available: 10.21275/v5i3.nov161916.
6. H. Kahn and C. Cooper, "A note on the validity of the mental health and coping scales of the occupational stress indicator", *Stress Medicine*, vol. 7, no. 3, pp. 185-187, 1991. Available: 10.1002/smi.2460070310.
7. "Occupational Stress And Job Satisfaction Among Working Women In Banks", *Paradigm*, vol. 16, no. 1, pp. 29-38, 2012. Available: 10.1177/0971890720120105.
8. C. COOPER and J. MARSHALL, "Occupational sources of stress: a review of the literature relating to coronary heart disease and mental ill health", *Journal of Occupational Psychology*, vol. 49, no. 1, pp. 11-28, 1976. Available: 10.1111/j.2044-8325.1976.tb00325.x.
9. P. Murphy, "Corporate ethics statements: Current status and future prospects", *Journal of Business Ethics*, vol. 14, no. 9, pp. 727-740, 1995. Available: 10.1007/bf00872326.
10. C. Manea, C. Salceanu, C. Chiper and I. Chiper, "Occupational Stress and Tolerance of Bank Employees", *Procedia - Social and Behavioral Sciences*, vol. 92, pp. 495-500, 2013. Available: 10.1016/j.sbspro.2013.08.707.
11. M. Alaparathi, "Impact of Financial Innovations on Job Stress among Employees of Select Private and Public Sector Banks, Andhra Pradesh, India", *International Journal of Economics and Management Studies*, vol. 7, no. 7, pp. 96-102, 2020. Available: 10.14445/23939125/ijems-v7i7p112.

12. A.Ahmed, "Effects of Job Stress on Employees Job Performance A Study on Banking Sector of Pakistan", *IOSR Journal of Business and Management*, vol. 11, no. 6, pp. 61-68, 2013. Available: 10.9790/487x-1166168.
13. M. Chakkachampambal, "A Study on Occupational Stress Among Women Employees in Private Banking Sector with Special Reference to Thrissur District", *International Journal of Advanced Research in Science, Communication and Technology*, pp. 204-212, 2021. Available: 10.48175/ijarsct-1935.
14. S. Sharma, P. Basumatary and B. Hazarika, "job stress and its impact on the performance of bank employees: a study on select banks in kamrup metro district", *international journal of management*, vol. 11, no. 12, 2020. Available: 10.34218/ijm.11.12.2020.129.
15. S. Menon, "Job Stress at Workplace and Recession: A Study of Stress in Employees of Selected Banks in Mumbai", *Prabandhan: Indian Journal of Management*, vol. 3, no. 11, p. 26, 2010. Available: 10.17010/pijom/2010/v3i11/61178.
16. Mohsin Zafar, "Impact of online service quality on customer satisfaction in banking sector of Pakistan", *AFRICAN JOURNAL OF BUSINESS MANAGEMENT*, vol. 5, no. 30, 2011. Available: 10.5897/ajbm10.379.
17. D. R. Lavuri, "Job Related Stress on Employees Performance: A Comparative Study of Public Bank and Private Bank," *American Research Journal of Business and Management*, vol. 4, no. 1, 2018.
18. Dr. Karshan B. Chothani, "Job satisfaction and occupational stress among public and Private Bank Employees," *International Journal of Indian Psychology*, vol. 2, no. 2, 2015.
19. D. S. Biswal, "Occupational Stress among Female Bank Employees: Comparative Study of Indian Bank's," *Journal of Advanced Research in Dynamical and Control Systems*, vol. 12, no. SP7, pp. 2450-2456, 2020.
20. C. Rexrode, "The Woman With the Most Stressful Job in Banking," *The Wall Street Journal*, 04-Apr-2016. [Online]. Available: <https://www.wsj.com/articles/the-woman-with-the-most-stressful-job-in-banking-1459798440>. [Accessed: 07-Oct-2021].
21. C. E. O. P. and F. of T. F. B. Jeffrey Pilcher, "Two-Thirds of Bankers Are So Stressed, They May Quit Their Job," *The Financial Brand - Banking Trends, Analysis & Insights*, 23-Oct-2016. [Online]. Available: <https://thefinancialbrand.com/61903/banking-manager-work-stress/>. [Accessed: 07-Oct-2021].
22. S. Purkait., "Impact of Occupational Stress on Quality Work Life among Employees in Banking Sector: A Study in West Bengal Region.", *International Journal of Advanced Research*, vol. 4, no. 7, pp. 1215-1222, 2016. Available: 10.21474/ijar01/1026.
23. D. Jacob, "Occupational Stress And Job Satisfaction Among Working Women In Banks", *Paradigm*, vol. 16, no. 1, pp. 29-38, 2012. Available: 10.1177/0971890720120105 [Accessed 7 October 2021].
24. Prof. (Dr.) Manju Agrawal, Sabrina Shajeen Alam, and Dilruba, "Job satisfaction and job stress among bank employees in Rajshahi City: A field study," *International Journal of Indian Psychology*, vol. 3, no. 2, 2016.

Enhancement of Overall Equipment Effectiveness in Automotive Parts Manufacturing Industry

S. Adithya and T. Anantharaj
PSG College of Technology, Coimbatore, India

ABSTRACT

Injection moulding is one of the most commonly used production processes for the fabrication of automobile component. A significant development actions have taken place in the management of equipment and productive systems to reduce the wastage of energy resources and time. The overall equipment effectiveness (OEE) is a technique to measure the effectiveness of the machines. It helps in systematically analysing the processes and identifying the potential problems affecting the utilization of the machines. Thus a maintenance program should be implemented to increase the productivity and to improve the quality. Total productive maintenance (TPM) is a systematic approach to maintaining and improving the integrity of production and quality through which effectively utilize the machines, equipments, processes and employees rather than new investments. TPM aims at increasing the availability of the existing equipment and improve its performance. In the case study on the OEE of injection moulding process is measured and increased through availability, TPM, better utilization of resources and a maintenance program.

Keywords: Lean Manufacturing (LM), lean tools, Total productive maintenance, kaizen sheet

1. INTRODUCTION

LM is a systematic process that aims at consistent reduction of waste through constant development in pursuit of perfection. Implementation of LM uses less resources as compared with conventional mass production approaches namely, less product development engineering hours and less on site inventory and so forth. LM is a systematic approach to reduce the waste within a manufacturing system without sacrificing productivity. It also takes into account waste created through unevenness in workloads and overburden.

The ultimate aims of LM are

- Improve quality
- Increase productivity
- Eliminate waste
- Reduce cost

There are 7 types of waste to be eliminated

- Inventory
- Transportation
- Motion
- Waiting
- Over production
- Over processing
- Defects

1.1 Overall Equipment Effectiveness (OEE)

OEE measures how effectively a production operation is carried out or an equipment is utilized. Calculating the OEE is a critical element of any serious methods to reduce machines and processes related wastes.

Elements of OEE

1. Availability losses

- Setup
- Breakdown

2. Performance losses

- Minor stoppages
- Speed losses

3. Quality losses

- Start-up losses
- In-process losses

OEE calculates the production time that is actually productive or to simply put it finds the gap between actual and potential performance of a production unit. Finding of OEE and the losses will give insights on how to methodically develop the production processes.

OEE is the product of Availability, Performance and Quality, it takes into account all losses resulting in a measure of actual productive production time.

Availability: The ratio of operating time or run time and planned operating time. Operating time is planned operating time minus down time.

Performance: The account of all that causes the production process to perform at less than maximum possible speed.

Quality: The account of parts that do not meet the requirements including the components that need rework. It is the ratio of accepted components to total components produced.

$$\text{OEE} = \text{Availability} \times \text{Performance} \times \text{Quality}$$

(World class = 85 %)

$$\text{Availability} = \frac{\text{Actual operating time}}{\text{Planned operating time}} \times 100$$

(World class = 90 %)

$$\text{Performance} = \frac{\text{Designed cycle time} \times \text{Output}}{\text{Operating time}} \times 100$$

(World class = 95 %)

$$\text{Quality} = \frac{\text{No. of accepted parts produced}}{\text{No. of total parts produced}} \times 100$$

(World class = 99 %)

1.2 Total Productive Maintenance (TPM)

TPM is an improvement methodology which enable continuous and fast improvement of the production processes through use of employees' involvement, employees' empowerment and closed-loop measurement of results. There are eight pillars of TPM and each pillar has their own task to perform. The eight pillars are

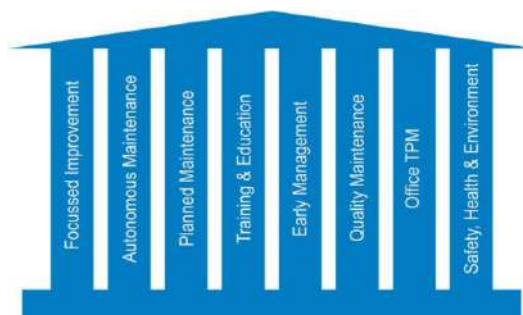


Fig. 1: 8 pillars of TPM 5S Tool

5S is the foundation of TPM. It describes how to organize a workplace for efficiency. 5S as a broader construct as visual control, visual workplace or visual factory.

Seiri (sort): Separate the necessary and unnecessary items from the workplace and discard what is not required.

Seiton (set in order): Arrange the items or tools in order such way that it can be easily selected for use. It reduces waiting and searching time.

Seiso (sweep): Cleaning the workplace systematically and uses cleaning as inspection. It helps the operator become more involved in the work and aware about the condition of the equipment.

Seketsu (standardize): Standardize and schedule the first three 'S' practices. Develop a work structure that supports the new practice.

Shitsuke (sustain): Translates to "do without being told" sustain the practices, conduct regular audits, implement training and self-discipline.

Autonomous maintenance, in this pillar independent maintenance is carried out by the operator. The operators are educated and trained in basic maintenance activities such as cleaning, lubricating, calibration of equipment etc. so that maintenance department can concentrate on more serious problems like break downs. This pillar is a basic preventive maintenance activity to reduce or eliminate break downs and empowers the operator makes him more involved in the work and increases the lifetime of the equipment.

Focused improvement, cross functional teams are formed to solve problems of critical or crucial machines by doing large number of small improvements. Right tools are used to find the root cause of problems and solving the problems. Focussed improvements involves activities that maximize the OEE through elimination of losses.

Planned maintenance, the objective of this pillar is to maintain the equipment at optimal process conditions and improve the service life of the equipment. Planned maintenance is scheduling of maintenance in advance based on the frequency of breakdowns and failures of equipment.

Quality maintenance, the objective of this pillar is to detect, prevent and eliminate errors during production. It focusses on providing right quantity at the right time. Defects lead to reworks, reworks lead to more usage of energy and resources, thus quality maintenance is crucial as it aims at preventing defects.

Early equipment maintenance, it is to ensure that the new machinery is used at its optimal level earlier than usual after the installation through the knowledge gained from the maintenance and management of the previous machines. It uses input from the operator and other individual going to use the equipment before installation for better utilizing the equipment.

Education and training, this pillar bridges the gap that exists when it comes to TPM. Lack of education and training leads to improper application of tools and wrong results. Without proper education and training the roles of the employee and tools can be misunderstood which may lead to more problems than solution.

Healthy safety and environment, this pillar aims at providing a working environment free of harmful elements that is environment which safe and healthy for his wellbeing. All the health and safety risks are to be eliminated.

Office TPM, it concentrates on all area that provides administrative and support functions in the organization. Its work is eliminating losses and waste from these departments. This pillar ensures that all process support the optimisation of manufacturing process.

1.3 Lean tools and techniques

LM tools and techniques used are

- 5S
- TPM
- Kaizen

2. LITERATURE REVIEW

- [1] Vijay lahri et al, (2015) has given a study on implementation of OEE on CNC milling machine and table type boring. The inefficiency losses were classified into three categories for better understanding of the manufacturing process. Through the implementation of OEE the bottleneck and hidden losses were found thus enabling to reduce them and improve the effectiveness of the machines.
- [2] Raghavendrakashyap K. et al, (2014) has done a case study on various defects that occur in an injection moulding process. The author found the effect of machine process parameters on wall thickness variation defects. Through design of experiments the process parameters were optimized and wall thickness variation defects were reduced.

- [3] Ranteshwarsingh et al, (2012) has done a study on automation of OEE calculation through hardware and software development. Based on different machine parameters and flow chart, algorithm and software was developed to automatically measure the OEE. Hardware controller was developed to overcome the problem using stopwatch. OEE calculation was made automatic and the losses can be identified and analysed using the software.
- [4] Vijaykumar S.R. et al, (2014) has given a case study on improving the OEE in injection moulding industry, the paper implies that maintenance management of the productive system is important to reduce wastage of energy and resource. In this work, the OEE of the injection moulding processes was increased from 61 % to 81 % through the better utilization of resources, execution of availability, high quality products and also raised employees' morale and confidence.
- [5] Jitendrakumar (2016) has done a case study on OEE improvement by TPM implementation. In this paper TPM was implemented in a thermal power plant and its effectiveness after the TPM implementation was increased which is measured from the OEE calculation after TPM implementation.
- [6] Khedkar S.B. et al, (2012) has given a work study on execution of 5S in plastic injection moulding industry. The objective of the paper is to improve the utilization of the storage space of raw material and finished goods through 5S implementation. Layout of the plant was studied and 5S was implemented and there were significant improvements to productivity, efficiency and housekeeping.
- [7] Vikashdwivedi et al, (2014) has given a case study on injection moulding process to improve the quality. Six sigma DMAIC methodology and root cause analysis were used to identify the causes for the black speck on the part surface and through TPM implementation improvements were made to reduce the defects.

3. DATA ANALYSIS

Manufacturing data

- Shift time
- Tea breaks time
- Meal breaks time
- Down time
- Idle run rate
- Total quantity produced
- Total quantity rejected

Support variables

$$\text{Down time} = \text{ideal time} + \text{changeover and setup time} + \text{flow or shortage of material time} + \text{breakdown or failure time} + \text{meeting time}$$

4. DETAILED WORK

OEE Calculation for Machine-1 before TPM implementation

Designed cycle time = 45 seconds

Number of shifts per day = 2

Number of days in a month = 26

Total down time = 162 hours

Planned operating time = 572 hours

Actual operating time = Planned operating time –

Total down time

$$\text{Availability} = \frac{\text{Actual operating time}}{\text{Planned operating time}} \times 100$$

Availability = 71.6 %

Total quantity produced = 27546

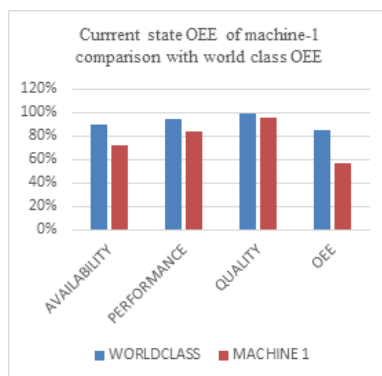


Fig. 2: OEE of Machine-1

Total quantity rejected = 915

$$\text{Performance} = \frac{\text{Designed cycle time} \times \text{Output}}{\text{Operating time}} \times 100$$

Performance = 83.9 %

$$\text{Quality} = \frac{\text{No. of accepted parts produced}}{\text{No. of total parts produced}} \times 100$$

Quality = 96 %

$$\text{OEE} = \text{Availability} \times \text{Performance} \times \text{Quality}$$

OEE = 57 %

OEE calculation for Machine-2 before TPM implementation

Designed cycle time = 40 seconds

Number of shifts per day = 2

Number of days in a month = 26

Total downtime = 177 hours

Total quantity produced = 23055

Total quantity rejected = 340

Planned operating time = 572 hours

Actual operating time = Planned operating time –

Total down time

$$\text{Availability} = \frac{\text{Actual operating time}}{\text{Planned operating time}} \times 100$$

Availability = 69 %

$$\text{Performance} = \frac{\text{Designed cycle time} \times \text{Output}}{\text{Operating time}} \times 100$$

Performance = 64.8 %

$$\text{Quality} = \frac{\text{No. of accepted parts produced}}{\text{No. of total parts produced}} \times 100$$

Quality = 98.5 %

$$\text{OEE} = \text{Availability} \times \text{Performance} \times \text{Quality}$$

OEE = 44.1 %

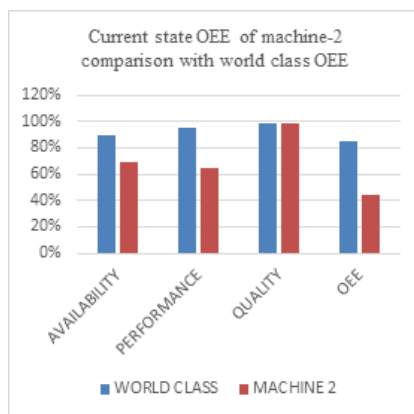


Fig. 3: OEE of Machine-2

OEE calculation of Machine-1 after TPM implementation

Designed cycle time = 45 seconds

Number of shifts per day = 2

Number of days in a month = 26

Total downtime = 121 hours

Total quantity produced = 32049

Total quantity rejected = 676

Planned operating time = 572 hours

Actual operating time = Planned operating time –

Total down time

$$\text{Availability} = \frac{\text{Actual operating Time}}{\text{Planned operating time}} \times 100$$

Availability = 78.6 %

$$\text{Performance} = \frac{\text{Designed cycle time} \times \text{Output}}{\text{Operating time}} \times 100$$

Performance = 88.8 %

$$\text{Quality} = \frac{\text{No. of accepted parts produced}}{\text{No. of total parts produced}} \times 100$$

Quality = 68.43 %

$$\text{OEE} = \text{Availability} \times \text{Performance} \times \text{Quality}$$

OEE = 68.43 %

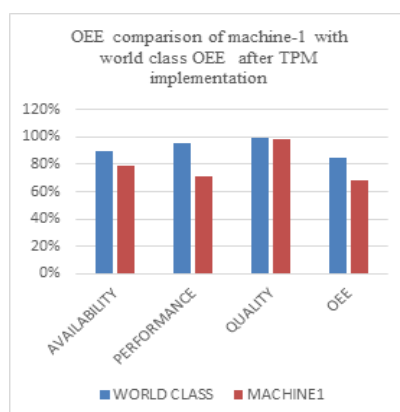


Fig. 4: OEE of Machine-1 after TPM implementation

OEE calculation of Machine-2 after TPM implementation

Designed cycle time = 40 seconds

Number of shifts per day = 2

Number of days in a month = 26

Total down time = 139 hours

Total quantity produced = 27908

Total quantity rejected = 388

Planned operating time = 572 hours

Actual operating time = Planned operating time –

Total down time

$$\text{Availability} = \frac{\text{Actual operating Time}}{\text{Planned operating time}} \times 100$$

Availability = 75.6 %

$$\text{Performance} = \frac{\text{Designed cycle time} \times \text{Output}}{\text{Operating time}} \times 100$$

Performance = 71.6 %

$$\text{Quality} = \frac{\text{No. of accepted parts produced}}{\text{No. of total parts produced}} \times 100$$

Quality = 98.5 %

$$\text{Oee} = \text{Availability} \times \text{Performance} \times \text{Quality}$$

OEE = 53.3 %

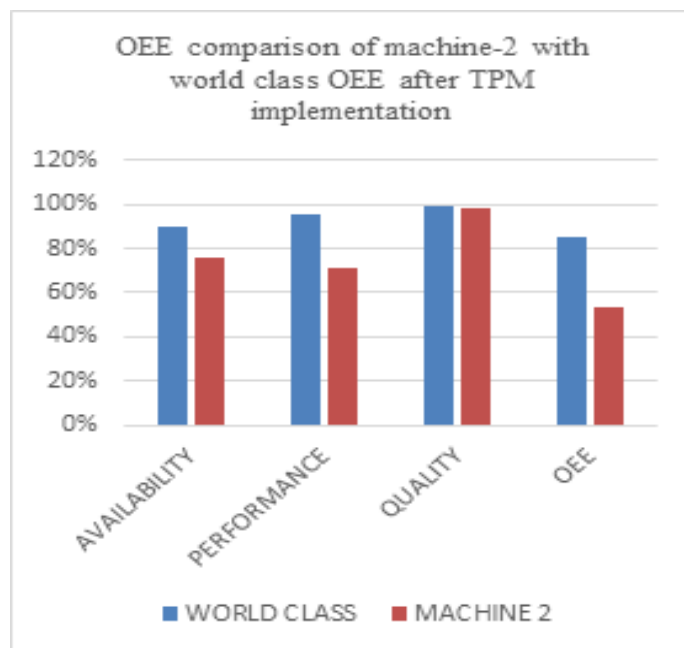


Fig. 5: OEE of Machine-2 after TPM implementation

Table 1: OEE of Machine-1 and Machine-2 after TPM implementation

	Availability	Performance	Quality	OEE
World class	90 %	95%	99 %	85 %
Machine-1	78.6 %	88.8%	97.8 %	68.43 %
Machine-2	75.6 %	71.6 %	98.5 %	53.3 %

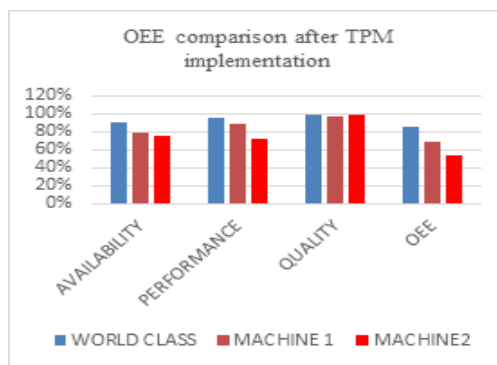


Fig. 6: OEE comparison after TPM implementation

5. RESULT

After the implementation of total productive maintenance (TPM) and 5S techniques the OEE of Machine 1 was increased from 57 % to 68.3 % and OEE of Machine 2 was increased from 44.1 % to 53.3 %.

6. CONCLUSION

Manufacturing process and the resources for producing the plastic parts have been studied and the breakdowns such as mechanical, electrical and other which occur during operation have been analysed. It is evident that TPM increases the service life of the equipment and improve manpower and machine utilization. Therefore, it is very much important to implement TPM so as to increase the availability, performance, quality and effectiveness of the machines.

ACKNOWLEDGEMENT

We are sincerely grateful to the General Manager, Maintenance Head, Facilitator and the operators who helped as to conclude the study.

REFERENCES

1. Vijay lahri, Prhmod Pathak, "A case study of implementation of overall equipment effectiveness on CNC table type boring and milling machine of heavy machinery manufacturing industry" IOSR journal of mechanical and civil engineering (IOSR-JMCE) e-ISSN 2278-1684-, p-ISSN 2320-33vx, vol-12, ISSUE- 5 (SEP-OCT 2015) PP 63-70
2. K Raghvendrakasyap, M Subha Rao, "A case study on injection moulding Windsor 650 machine parameter at wall thickness variation defect" International Journal of Computational Engineering Research ISSN- 2250-3005 VOL-3 ISSUE-8 AUG-2014
3. Ranteshwar Singh, Ashish M Gohil ,Milesh h shah "A case study on overall equipment effectiveness calculation – automation through hardware and software development" Chemical, Civil and Mechanical Engineering Tracks of 3rdNirma University International Conference (NUicone2012)
4. S.R. Vijayakumar, S. Gajendran "Improvement of Overall equipment effectiveness in injection moulding process industry" IOSR Journal of Mechanical and Civil engineering (IOSR-JMCE) E-ISSN 2278-1684 P-ISSN 2320-334X PP 47-60
5. Jitendrakumar, 5th International Conference on Science and Technology Management (ICSTM-16) ISN 978-93-86171-00-9
6. S.B. Khader R.D Thakre .Y.V Mahentra, Ravi gowda "A study of implementation of 5S techniques on plastic moulding" International Journal of Modern Engineering Research (IJMER) ISSN 2249-6645, VOL- 2 ISSUE 5, SEP- OCT 2012, PP 3653-3656
7. Vikashdwivedi, Mohd. Anas and Mohd. Siraj "Six sigma- applied in quality improvements for injection moulding process" International Review of Applied EngineeringResearch ISSN 2248-9967 VOL-4 NO.4 (2014)

Quantifying the Effectiveness of Digital Content Marketing

Aarthi Mai A S and Monisha C

Department of Computer Applications, PSG College of Technology, Coimbatore, India

ABSTRACT

A global technology leader makes significant investment in content marketing with the goal of building brand awareness and driving engagement. The main objective of this web analytics project is to measure the effectiveness of their content marketing activities in order to optimize the content as per industry needs and building credibility. The dashboard is generated with the data captured by the customers of their websites. The data are then cleaned and imported to the power bi[4] to generate an absolute dashboard. Client can visualize real-time data with interactive dashboard. Based upon the observations, the contents of the activities can be modified to improve the performance and outcome.

The digital content effectiveness is proposed to create a dashboard with visuals of data. These visuals explain about the performance of the website assets. Based upon the visuals the client can make decisions on their investment of their documents. The data's received from the Adobe Analytics will be updated at a quarterly basis and then it is updated to the dashboard. Once the data is updated in the dashboard, new visuals will be created with the imputed data to produce the best results.

Keywords - content effectiveness, dashboard.

I. INTRODUCTION

Measuring digital content is as straightforward or as difficult on build it. It isn't capturing the information and views. It's a method of capturing complete website performance by views, visits, hits or clicks, etc., and to present it to the client as per the request. The digital content effectiveness dashboard contains digital visuals which fascinate the audience and this results in increase of the sales pitch and so the possibility of business alliances and associations instantly. Digital dashboard is then presented to the client to make the client aware of the asset performance of the website.

The content measuring sessions from the traffic to the website measures and tracks individual visitor behavior on the site. The challenge with measuring the effectiveness of content is that metrics [3] alone not the content. The buyer's journey starts from B2Bs is complex, It may be from months and also as years. Content measuring focuses on creating and distributing valuable, relevant, and consistent content to attract and retain a clearly defined audience to drive profitable customer action.

The type of content explains most relevant needs, needs which helps to optimize the path users take from consuming content to becoming engaged customers and brand advocates.

II. EXISTING METHODOLOGY

The digital content effectiveness [1] process works on updating methodology. The client updates the data in a Quarterly basis. Each update is imported in to the system to produce the best accurate live results. The existing system only produces the results for the previous quarters. To improve and achieve better results, the updated data needed to be annexed into system.

III. PROPOSED METHODOLOGY

Power BI is a service tool used for business analytics. The main objective of power BI is to supply interactive visualizations and business intelligence capabilities with an interface easy enough for the client or users to create their own reports and dashboards. Power BI provides cloud-based BI (business intelligence) services, referred to as "Power BI Services", alongside a desktop-based interface, known as "Power BI Desktop". It offers information warehouse capabilities together with information, information discovery and interactive dashboards.

It is used to generate visualization like bar graphs and charts with the help of intelligence tool which converts data from multiple data sources to interactive dashboards and business intelligence.

In digital content effectiveness, power BI plays a major role. A dashboard is created with the help of the power BI analytics tool, which outputs the performance of the assets and information regarding it to the client. The data get processed after each update of website information in a quarterly and monthly basis.

The proposed system shown in figure 3.1. It includes creation of dashboard with visuals of data. These visual explains about the performance of the website assets. Based upon the visuals the client can make decisions on their investment of their documents. The data's received from the adobe analytics will be updated at a quarterly basis and then it is updated to the dashboard. Once the data is updated in the dashboard, new visuals will be created with the input data to produces the best results.

The dashboard is created with filters to view the asset performance in efficient manner, which helps to understand the content performance easily. If the client needs to view any particular quarter data asset performance, the quarter slicer will be used. The cards created in this dashboard helps to view the total counts of the assets viewed and not viewed.

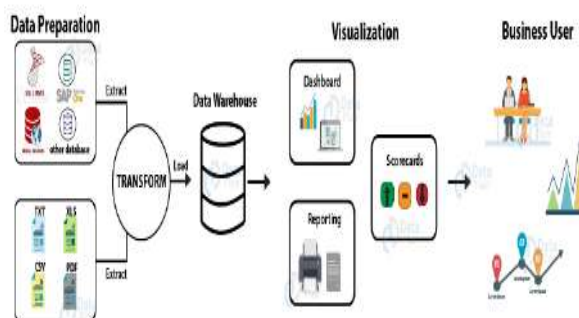


Figure 3.1 Block diagram

Each update is done by updating the data by the existing one. After each update, the data has to be processed by removing duplicated and blanks, removing unwanted data and making relationships to make the dashboard better and achievable. This proposed dashboard helps the client to make changes in their website to improve the performance. Whenever there is a new update it produces clear observation of data. Different type of updated filters are used in each update.

IV. DATA ENGINEERING

Data engineering emphasizes on practical applications of data collection and analysis. This deals with the study of data engineering technique. It converts the raw data into a clean data set.

A. Process in Data Engineering

1. Extracting asset ids from page URL.
2. Splitting evar1 to get country and language.
3. Converting country and language into complete words.
4. Creating column for language extension.
5. Concatenate asset ids and language extension when length of asset id is less than 13.
6. Check for blank columns.
7. Merging cleaned data with metadata based on Asset id.
8. Mapping columns from different datasets using VLOOKUP.
9. Calculating age of asset.
10. Creating platform columns.
11. Updating geographies and countries
12. Video Data Integration
13. Data Validation
14. Merge Video data with Client data

V. SYSTEM FLOW

The figure 5.1 explains about the dashboard flow diagram, which explains about the process of requesting the dashboard from the client end and making the deliverables. This explains from the process of creating the dashboard for delivering it to the client.

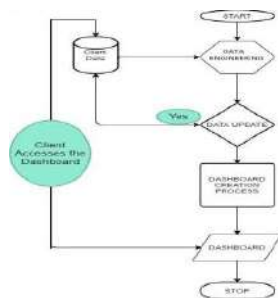


Figure 5.1 Dashboard Flow Diagram

VI. SYSTEM DESIGN

Systems design is the process of defining the architecture, modules, interfaces, and data for a system to satisfy specified requirements. Systems design is an application of systems theory to product development. In figure 6.1 shown detailed description about the modules and system flow of the digital content effectiveness project.

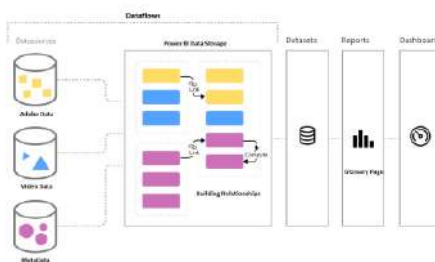


Figure 6.1 System Design

Digital Marketing segments are as follows:

Total assets and viewed assets: Assets are any items on the website that are producing the website traffic and allowing the site to rank in search engines.

Total assets are the overall count of asset in the website and viewed assets are the assets viewed by the visitors of the website.

HVA Views: HVA views are high value action views which seriously affects the organization shown in fig 6.2. Those

information resources, mission/business processes, and critical programs that are of particular interest to potential or actual adversaries. This prediction can be used for long term.

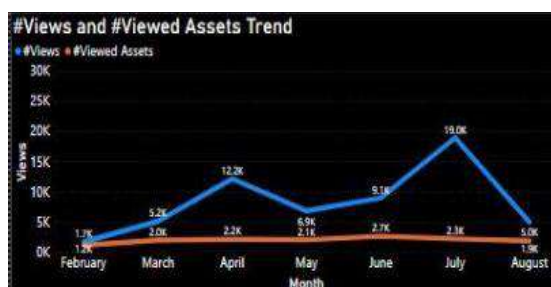


Figure 6.2 High Value Action Views

Page Views: A page view (or page view hit, page tracking hit) is an occurrence of a page being loaded (or reloaded) in a browser. Page views means it is a total number of pages viewed. Page view measurement allows you to measure the number of views you had for a particular page on your website.

Visits: If a user searches a website and at least one page is loaded then it is counted as a visit. Visits indicate a continuous process of using a website. The visit is fundamental for the preparation of most analyses. The visit provides you with information on navigation (initial page, content viewed, exit page) and behavior (duration, loads/page views, bounce rate, etc.). The dashboard design is shown in Fig 6.3.



Figure.6.3 Dashboard design

Traffic Sources: Refers how do visitors find your site

1. **Direct navigation** – It will be through URL, Tracking codes and Bookmarks
2. **Referral traffic** – It is from Web, Social media, Trackable email, Promotion & Branding campaign links
3. **Organic search** – It means queries that sent traffic from major or minor web search engines
4. **Pay Per Click** – It is through sponsored ads and triggered by targeted key phrases

Last Touch Channel: The ‘Last Touch Channel detail’ dimension reports details around the most recent marketing channel a visitor matches with during that visitor’s engagement period (30 days by default). This dimension is valuable in understanding what contributed to the hit matching a marketing channel.

Hero Asset: The Hero asset of sample data is shown in figure 6.4. These assets are larger, higher value assets like E-books or guides. These are the anchors for long-term campaigns with different topic tracks or branches.

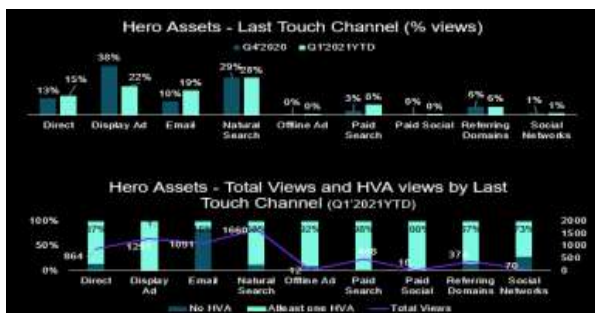


Figure 6.4 Hero Asset

Buyer's Journey: The Buyer’s Journey[2] is the research process a buyer goes through leading up to a purchase. This model helps to understand the sales, buyer’s needs, problems and behavior throughout the buying cycle.

The journey is a three-step process:

1. **Awareness** stage: The buyer realizes the asset and its properties.
2. **Consideration** stage: The buyer considers and researches for the asset in the website.
3. **Decision** stage: The buyer chooses a solution whether to purchase the asset or not.

VI. IMPLEMENTATION

It is developed in power bi using data from adobe analytics. The data will be updated in a quarterly basis and then passed to the dashboard to display the live results, which helps to observe the channel performance, visits, HVA’s and other metrics of the website.

In this methodology, inputs are processed in adobe analytics, which are sent to power bi to create a front-end level dashboard. The data is pushed to the visuals like tables and graphs as per the client request and modulated to generate the dashboard.

VII. CONCLUSION

Digital content effectiveness is developed as a storyboard with different visualization charts and tables to provide ease of use to client to know about the website and asset performance.

REFERENCES

1. Kishan Prajapati, "A Study on Digital Marketing and It's Impacts", Article in Research Gate, Nov 2020.
2. D. Bhagowati and D. M. Dutta, "A study on literature review for identifying the factors impacting digital marketing," *International Journal of Sales & Marketing Management Research and Development*, Aug., vol. 8, no.3, pp. 1-8, 2018.
3. <https://medium.com/strategic-content-marketing/measuring-the-effectiveness-of-digital-content-marketing-insights-from-the-2018-intelligent>
4. David Reske, "Digital Marketing in the Zone - The Ultimate System for Digital Marketing Success", ISBN 978-1-68350-268-5 paperback, Morgan James Publishing, 2017
5. <https://experienceleague.adobe.com/docs/analytics/components/metrics/overview.html>
6. Amrapali Bansal, A. K. Upadhyay, "Microsoft Power BI", *International Journal of Soft Computing and Engineering (IJSCE)*, ISSN: 2231-2307, Volume-7 Issue-3, July 2017

Ergonomic Assessment of Muscular Fatigue Associated with Overhead Tasks in Pump Assembly Using Surface Electromyography (SEMG)

Ashok P, Madhan Mohan G and Nevhetha N

Department of Production Engineering, PSG College of Technology, Coimbatore – 641004, TN, India

ABSTRACT

In small and medium scale industries, manual intervention is inevitable. Lack of automation due to various reasons assemblies carried out manually at workstations. Due to extended standing position during monotonous repetitive tasks such as assembly line tasks may lead to muscle fatigue, then end up in work related musculoskeletal disorders (WMSD). This study is to measure the surface electromyography activity of the muscles for different tasks and report the inferences. In pump assembly the currently used task was normal and over-head. The experiment was simulated in the laboratory environment for the period of five minutes similar to industry conditions. By using rapid upper limb assessment (RULA) the critical muscle is identified for the experiment. Result shows that the slope value of the overhead task is more than the normal condition for the both biceps and upper trapezius muscle indicated as the fatigue. The median frequency decreases as the working time is increased. The muscle fatigue rate is more in the right hand of upper trapezius muscle in overhead tasks. So, the workplace can be redesigned according to anthropometric dimensions.

Keywords: Pump Assembly, Overhead Task, Surface Electromyography, Stages of Pump, Musculoskeletal Disorders.

1 INTRODUCTION

Natural resources include air and water. These are the most important natural resources for the needs of the people to the extent that streams and rivers cannot satisfy it. Submersible pumps are competent, far above in capacity, necessitate very little maintenance and are normally very cost-effective for wells that are more than 90 feet in depth. Submersible pumps are competent, far above in capacity, necessitate very little maintenance and are normally very cost-effective for wells that are more than 50 m in depth. Multi stage submersible pumps are used to draw water from depths more than 50 m. Each stage of these pumps is capable of pumping at least 10 m deep from the ground level [1].

Different categories of processes carried out in manufacturing industries at workstations. These are the integral and essential part of manufacturing industries. Workplaces are a most important part of the manufacturing engineering industry that is desirable to carry out an assortment of categories of jobs. At workplaces, the workers carry out the assigned tasks with high quality proportion to the compatibility and comfort of the workstation. Design of the workstation also plays a vital role in increasing the efficiency of the worker in a safe and comfortable environment; it reduces the effort required by the workers for the tasks to accomplish within allotted time. Improper workstation designs are the main contributor to the development of worker fatigue and then when it proceeds, lead to work related musculoskeletal disorder (WMSD). The efficiency of the worker is reduced thereby the productivity at the manufacturing industries is affected [2]. When the manufacturing industries automated, reduces the amount of manual intervention in manufacturing industries. Automation involves high cost investment at the initial stage of implementation, which might not be affordable by any small and medium scale industries in developing countries like India.

Improperly designed workstations, without any considerations to ergonomic principles force the workers to adopt awkward posture while at work. This leads to pain, then fatigue and finally to permanent disorder. These are permanent injuries to soft tissues and the nervous system. Soft tissues including muscles, tendons, cartilage and ligaments injured while workers are working in not so good postures at work. Soft tissues and the central nervous system affected to deteriorate the motor skills of the workers putting them at high risk. Unsafe work environments contribute high risks.

Manual tasks done using their arms and limbs, when affected; the efficiency of the worker is deteriorated. Cumulative trauma disorder, occupational overexertion syndrome, repetitive stress injuries and soft tissue syndrome are the other names given to work-related musculoskeletal disorders by occupational safety and health professionals certified by national institute of occupational safety and health [3]. Workday should ideally start with no pain at any part of the worker's body. Due to various unfavorable conditions and factors pain, exist for days and weeks even for months, source for permanent disorders to the workers, thereby decreasing the efficiency of the worker.

Workers suffer from exhaustion, weakness, and injury throughout long hours of monotonous repetitive work when appropriate workplace/ working surroundings is not present. This may not directly contribute to reduced productivity and efficiency in an industry. Human factor subjects come about in straightforward systems and purchaser/ consumer products as well. For this reason, the ergonomic principles/ values have been widely used in the design of both consumer and industrially manufactured products. Earlier examples take account of screwdriver handles finished with irregularities to get better finger grip, by ever increasing the friction concerning the skin of the hand and the handle surface.

One of the majority types of job-related injuries are musculoskeletal disorders. Job-related musculoskeletal disorders effect in unrelenting pain, failure of functional ability and work disability, but their initial diagnosis is not easy because they mostly based on grievances of pain and other indications. Hence a appropriate workplace is to be designed to prevail over the beyond issues or to diminish them noticeably. The production of electrical power with pumped brine from well was projected in that report.

The Rapid Upper Limb Assessment (RULA) makes available an investigation of the manikin's upper limbs foundation on variables such as frequency, distance and weight. It is used to analyses numerous components of manikin posture based on a amalgamation of automatically become aware of variables and customer data. It gives the opportunity of adding together tasks specific variables such as whether the manikin is on the outside maintained, if the manikin's arms are functioning crosswise the midline of the body throughout a task, and whether the manikin's feet are evenhanded and in good health condition sustained. These analyses generates a recapitulate report of the task and make available a quantified set of results not anything whether the assignment and positional posture are good enough/ satisfactory or it should be investigated in addition or it should be investigated more but changed soon or should be investigated further but changed straight away. Hence, with the RULA examination can optimize manikin posture in the context of a manual assignment and therefore design improved, and more extensively established, products and workplaces [4].

Myoelectric signals of the muscles are recorded, stored and analyzed using the surface electromyography (SEMG) system that is an experimental technique. Physiological variations of muscle fibers are captured by the myoelectric signal using the surface electromyography system. Myoelectric signals of the muscles are recorded, stored and analyzed using the surface electromyography (SEMG) system, which is an experimental technique.

Physiological variations of muscle fibers are captured by the myoelectric signal using the surface electromyography system. Inferences from the myoelectric signals contribute extensively to the applied ergonomic research. Myoelectric signals in biomechanical studies help in depth understanding of the contributing factor with reference to the tasks carried out by the workers.

Surface electromyography signals are used in applications like physiotherapy, study of sports people, rehabilitation, human machine interaction and also in cognitive ergonomics. Human machine interaction studies product interaction with human body interaction with the industrial products within work conditions. Risks are mitigated by properly designing the workstation.

Applied ergonomic research is used to analyze the risk involved in work, demand created in design and product certification. For the most part in ergonomics, EMG is used for examination of demand, risk avoidance, ergonomics proposals and product documentation [5, 6]. The muscles for the most part affected in the assembly of submersible pumps are biceps brachii and upper trapezius.

2 METHODOLOGY

Ergonomics and Anthropometric considerations are prepared to aid the foundation. In this research, the designing of the place of work for the assemblage of pump is well thought-out [7-10]. The existing workplace considered, difficult/ awkward body postures are recognized and the stress intensity at a variety of parts of the worker's body is calculated.

Initially RULA analysis carried out and it followed by the Surface Electromyography. Based on the consequences of the EMG better improved design of the workplace is recommended. Adopted methodology is illustrated in figure 1.

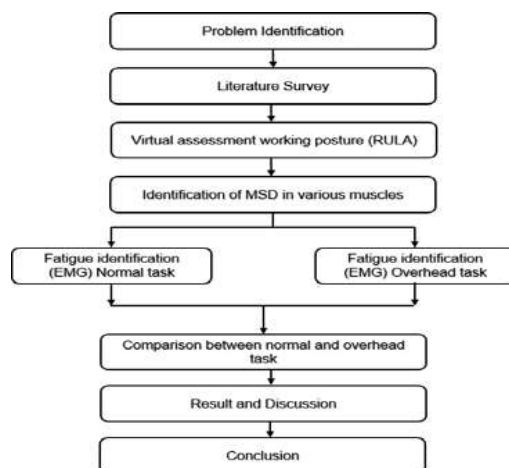
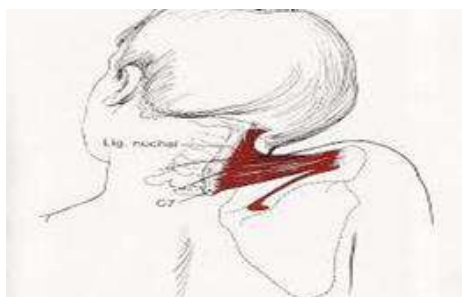


Figure 1. Methodology adopted in this study

3. ANALYSIS PROCEDURE FOR FINDING OUT IMVC (ISOMETRIC MAXIMUM VOLUNTARY CONTRACTION)

Time domain analysis and frequency domain analysis conducted using surface electromyography signals. In time domain analysis, amplitude RMS (root-mean-square) values are normalized to compare data of workers in the common scale, standardization of information. The RMS values in mV converted to data of percentage value against time plotted in x-axis. Percentage values of isometric maximum voluntary contraction are used to compare the data of the participants on a common scale. Different subjects will exert different amounts of output for given input. Output from the subjects depends on many factors, physical and cognitive factors of each of them. Thus the surface electromyography signals obtained from each individual will differ, even though the measurements were taken from the same muscle and same tasks are carried out for fixed time [11]. Normalization and standardization of surface electromyography data will aid to compare and infer from the information obtained without any differences obtained due to the variant occurred by subjects. Differences in values arising between subjects can be eliminated when the data is normalized.



For trapezius descendens (Figure 2), isometric maximum voluntary contraction is carried out following a particular procedure; the person is made to sit erect with hands hanging vertically down. Surface electromyography electrode is placed at 50 % location on the line joining the point on acromion to the vertebra C7 in the spine. The shoulder is twisted around the spine of the vertebrae C7. Clavicle is elevated for the acromial end and pressed to the maximum force to hold for the duration of time with the scapula extended [12]. The head and neck are rotated, pressed against each other to the shoulder elevated with the opposite side direction of the rotated face. In the direction of depression, the shoulder is pressed with applied force of the flexion anterolateral.

Figure 2. Trapezius descendens, isometric maximum voluntary contraction

Isometric maximum voluntary contraction for the biceps brachii (Figure 3) is measured by placing the electrode at the top of the biceps. The subject is made to sit on the chair with the elbow flexed to right angle and force is applied at the top of the wrist, while opposite forces are applied as their resistance. Horizontal posture is maintained for the dorsal side of the forearm downward position [13-15]. The surface electromyography electrodes are placed on the belly of the biceps muscle on the point of the line joining medial acromion and the focca cupit. One third of the distance from the focca cupit is considered to place the sensor. While applying the force one hand can be used on the top of the wrist for the opposition force.



Figure 3. Biceps brachii, isometric maximum voluntary contraction

Worker's productivity shall be increased by incorporating ergonomic principles at work. Worker's efficiency can be increased by fitting man to the specified tasks by designing individual work stations. The study was conducted at an assembly of submersible pump. The aim of the study is to identify the work related musculoskeletal disorders (WMSD) techniques and observation made with respect to the working posture practiced while performing assembly task and design the comfortable working area, which reduces the WMSDs and modify workplace according to the ergonomic principles.

When the depth of the well bore increases, stages in the multistage pump increase. These pumps are assembled for the requirement of the stages. When assembled, it is assembled vertically; cannot be assembled horizontally [16]. Even if the stages are increased, the worker is not given a height platform for inserting the stages. This increases the fatigue load on the worker while inserting each stage to the shaft. Reach height of the shaft differs with the number of stages of the multistage pump. While the worker is assembling multi stages, they are forced to adopt not so good postures that cause pain and fatigue, when prolonged ends up in injuries and disorders. This aggravates tasks that are carried out above the shoulders, overhead tasks. These tasks are to be redesigned properly to increase efficiency and productivity of the workers.

The most important benefit of this virtual evaluation method is that the working posture can exist and be analyzed in a virtual environment with no instantaneous implementations. From above literature it is understood that postural evaluation is carried out for an uncomfortable working posture with manual assembly of submersible pumps in small-scale industrialized industries. Purpose of this study is to reduce WMSD risk in the manual assemblage of submersible pumps. Understanding the risks from the workstations with the help of virtual postural investigations. Recommendations for a newly redesigned workstation shall be integrated and incorporated with ergonomic interferences. To satisfy the purpose, a case study in a small-scale manufacturing industry was carried out.



Figure 4 Assembling in Pump Industry

Workstations are redesigned to require suggestions and recommendations. Dimensions have arrived for Indian anthropometry. Working postures at the manufacturing industries are recorded during performing the task based on questions are photographed and stored for evaluation followed by analysis. The task involves the worker to assemble the stages to the shaft vertically (Figure 4 and Figure 5). As stages increase the shaft is longer and the worker has to lift the block above shoulder level with the load to assemble the multistage pump.



Figure 5. Pump assembly

The jig is presented during assembly of pump helps for correct alignment of multistage pumps and its components during assembling. The workers reaching the top of the shaft to insert a block causes pain at the trapezius muscle. Not so good posture is adopted while doing the task. RULA for the existing workstation is presented in Figure 6.

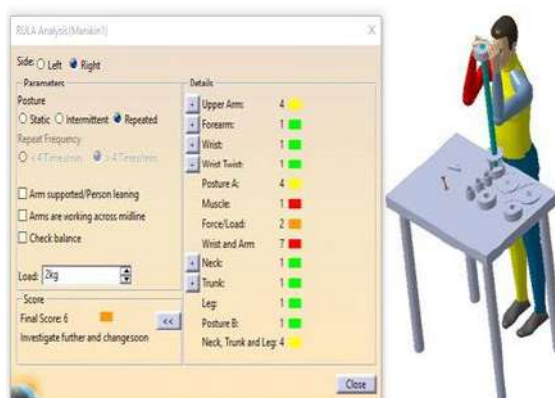


Figure 6 RULA for existing workstation

The experiment was conducted in the laboratory environment for the period five minutes. The muscle selected for the experiment biceps brachii and Trapezius Descendens. Sensor is positioned at a point on the line meeting the medial acromion and the fossa cubit. Biceps brachii muscle on the region of the wrist.

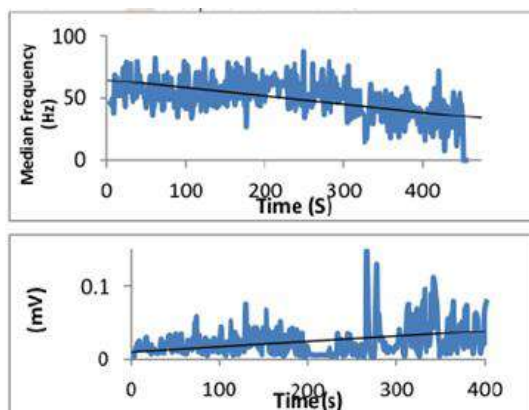


Figure 7 EMG RMS graph of Biceps Brachii Muscle

The graph is plotted between the time and root mean square (RMS) for the biceps muscle in the time domain analysis and 0.14 peak volt produced with respect to the time and the linear increase in the line indicated as fatigue as shown in Figure 7.

The graph is plotted between the time and median frequency for the biceps muscle in the frequency domain analysis and frequency produced with respect to the time and the linear decrease in the line indicated as fatigue as shown in Figure 7.

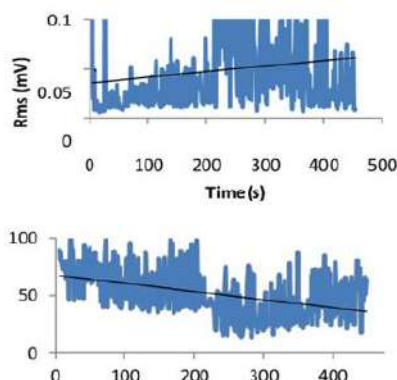


Figure 8. EMG Median Frequency graph of Biceps Brachii

The graph is plotted between the time and root mean square (RMS) in micro volt for the upper Trapezius muscle in the time domain analysis and 0.14 peak volt produced with respect to the time and the linear increase in the line indicated as fatigue as shown in Figure 8.

The graph is plotted between the time and median frequency for the Upper Trapezius muscle in the frequency domain analysis and frequency produced with respect to the time and the linear decrease in the line indicated as fatigue as shown in Figure 8.

Throughout assembly, the employee has to be in motion to the platform to way in the components on or after the provide rack, place in the component from end to end the top end of the shaft and move down to the lesser levels for additional assembling work [17]. This is go behind until a particular number of stages are bring together. After assembling a particular quantity amount of stages, there is no require moving downward to the lower levels and the employee can to perform the task by standing over the platform.

Inside submersible pump assemblage, these postural concerns can happen at what time insertion the components in appropriate position. Multistage pump assemble of the pump, the worker perform the tasks with their arms higher than shoulder level and it is classified as above your headwork (Figure 9).

Above headwork consists of uncomfortable positions, which might produce uneasiness and pain to shoulders and show the way shoulder disorders. When the number of stages increase in multistage pump assembly, the height of the shaft increase [18]. Number of components in the assembly increases. Height of the centre shaft with increase in stages of multistage pump develops into a problem throughout this assembly jobs.



Figure 9. Over head task

3. RESULT AND DISCUSSION

The graph is plotted between the time and root mean square (RMS) for the biceps muscle in the time domain analysis for the overhead task and 0.14 peak volt produced with respect to the time and the linear increase in the line indicated as fatigue as shown in Figure 10.

The graph is plotted between the time and median frequency for the biceps muscle in the frequency domain analysis for the overhead task and frequency produced with respect to the time and the linear decrease in the line indicated as fatigue as shown in Figure 10.

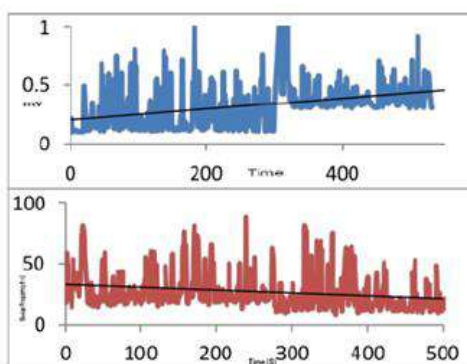


Figure 10. EMG RMS and median frequency graph of Biceps Brachii Muscle

The graph is plotted between the time and root mean square (RMS) micro volt for the upper Trapezius muscle in the time domain analysis for the overhead task and 0.14 peak volt produced with respect to the time and the linear increase in the line indicated as fatigue as shown in Figure 11.

The graph is plotted between the time and median frequency for the Upper Trapezius muscle in the frequency domain analysis for the overhead task and frequency produced with respect to the time and the linear decrease in the line indicated as fatigue.

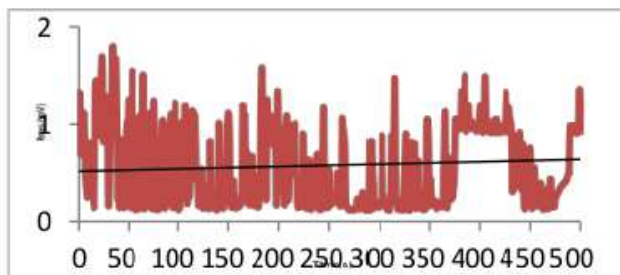


Figure 11. EMG RMS of Trapezius muscle

Table 1 Comparison of Normal and Overhead Work

MUSCLES		NORMAL	OVERHEAD
BICEPS BRACHII	RMS	0.0723	0.325
	MPF	-0.092	-0.0032
UPPER TRAPZEIUS	RMS	0.0112	0.2361
	MPF	-0.632	-0.0052

4. CONCLUSION

The muscle fatigue rate was determined for the biceps and upper trapezius muscle and summarized in the above table. The slope value of the overhead task is more than the normal condition for the both biceps and upper trapezius muscle indicated as the fatigue. The results clearly show that median frequency decreases as the working time increased. The muscle fatigue rate more in the right hand of upper trapezius muscle in overhead task.

REFERENCES

1. V. Balasubramanian, K. Adalarasu, and R. Regulapati, "Comparing dynamic and stationary standing postures in an assembly task," *Int. J. Ind. Ergon.*, vol. 39, no. 5, pp. 649–654, 2009.
2. C. Gavriel, "A comparison of day-long recording stability and muscle force prediction between BSN-based mechanomyography and electromyography," pp. 69–74, 2014.
3. M. M. Liu, W. Herzog, and H. H. C. M. Savelberg, "Dynamic muscle force predictions from EMG : an artificial neural network approach," vol. 9, pp. 391–400, 1999.
4. A. Merlo, D. Farina, and R. Merletti, "Detection From Surface EMG Signals," vol. 50, no. 3, pp. 316–323, 2003.
5. B. Hu, L. Ma, W. Zhang, G. Salvendy, D. Chablat, and F. Bennis, "International Journal of Industrial Ergonomics Predicting real-world ergonomic measurements by simulation in a virtual environment," vol. 41, pp. 64–71, 2011.
6. L. Ma, W. Zhang, D. Chablat, F. Bennis, and F. Guillaume, "Computers & Industrial Engineering Multi-objective optimisation method for posture prediction and analysis with consideration of fatigue effect and its application case," *Comput. Ind. Eng.*, vol. 57, no. 4, pp. 1235–1246, 2009.
7. S. Al-qaisi and F. Aghazadeh, "Electromyography analysis : Comparison of maximum voluntary contraction methods for anterior deltoid and trapezius muscles," *Procedia Manuf.*, vol. 3, no. Ahfe, pp. 4578–4583, 2015.
8. R. M. Enoka and J. Duchateau, "Muscle fatigue : what , why and how it influences muscle function," vol. 1, pp. 11–23, 2008.
9. J. Seghers, A. Jochem, and A. Spaepen, "Posture, muscle activity and muscle fatigue in prolonged VDT work at different screen height settings," *Ergonomics*, vol. 46, no. 7, pp. 714–730, 2003.
10. H. M. Mwawasi, "Feasibility Study of Using a Downhole Pumping System in Menengai Well Mw-17 for Geothermal Utilization," no. 22, 2014.
11. L. Wang and T. S. Buchanan, "Prediction of Joint Moments Using a Neural Network Model of Muscle

- Activations From EMG Signals,” vol. 10, no. 1, pp. 30–37, 2002.
12. D. G. Allen, G. D. Lamb, and H. Westerblad, “Skeletal Muscle Fatigue : Cellular Mechanisms,” pp. 287–332, 2018.
 13. A. Merlo, D. Farina, and R. Merletti, “Detection From Surface EMG Signals,” vol. 50, no. 3, pp. 316–323, 2003.
 14. E. F. Shair, S. A. Ahmad, M. H. Marhaban, S. B. Mohd Tamrin, and A. R. Abdullah, “EMG Processing Based Measures of Fatigue Assessment during Manual Lifting,” *Biomed Res. Int.*, vol. 2017, no. February, p. 3937254, 2017.
 15. N. A. Dimitrova, “Interpretation of EMG integral or RMS and estimates of ‘ neuromuscular efficiency ’ can be misleading in ...,” *J. Electromyogr. Kinesiol.*, vol. 20, no. 2, pp. 223–232, 2009.
 16. R. A. Ekstrom, R. Donatelli, and R. A. Ekstrom, “Surface electromyographic analysis of exercises for the trapezius and serratus anterior muscles Normalization procedures using maximum voluntary isometric contractions for the serratus anterior and trapezius muscles during surface EMG analysis q,” no. May 2003, 2016.
 17. R. Nishanth, “Ergonomic Workplace Evaluation for Assessing Occupational Risks in Multistage Pump Assembly,” *International journal of computer applications*, vol. 113, no. 9, pp. 9–13, 2015.
 18. S. A. Binoosh, G. Madhan Mohan, P. Ashok, and K. Dhana Sekaran, “Virtual postural assessment of an assembly work in a small scale submersible pump manufacturing industry,” *Work*, vol. 58, no. 4, pp. 567–578.

Step Ahead to Computer Vision - Leveraging Facial Expression Recognition Using GPU-Enabled Resnet-50 and Squeezenet CNN Architectures

Karpagam G R, Akash V S, Sanjaya Prabbakar M S, Jaya Vignesh R, Naveen V and Hari Prasath R
Department of Computer Science and Engineering, PSG College of Technology, Coimbatore, Tamil Nadu

ABSTRACT

Facial Expressions convey important cues about person thoughts and shows an individual's intentions within a social-based situation. Emotion detection is considered as a popular topic in the field of computer vision. This paper focuses on extraction of deep features for recognizing the emotions using convolutional neural network from the videos. This system takes the footage of the facial reactions of the person and predict the emotion exhibited by the person every 'n' seconds. Every frame which is extracted from the video is passed through CNN models to predict the emotion exhibited at that particular moment. The methodology of the recognition process used here is ResNet-50 and SqueezeNet. Both these architectures are trained on FER-2013 dataset and tested on video samples to predict the emotions and the point of occurrence. Results obtained from these models are evaluated along with their performance parameters namely confusion matrix, accuracy, precision, recall and f-score.

Keywords— Deep learning, Convolutional Neural Network, Emotion recognition, Facial expression, video emotion analysis, ResNet-50, SqueezeNet, Artificial intelligence, Psychiatric, Neural Networks

1. INTRODUCTION

Video-based Emotion recognition has played a key role in understanding emotions and been used in numerous fields such as medical diagnosis, interactive video games, surveillance and affective computing. Humans express their emotions through facial expressions which is of critical importance in social interactions. The objective of the system is to predict the emotion exhibited by the person in each frame with the timestamp indicating when the frame was extracted from the video. Over the past few years, the design and implementation of emotion recognition systems have become so popular in diagnosing psychiatric patients and improve their emotion states. Psychiatric patients usually seem to be out of touch with the real world. Recognizing the emotions of patients helps the doctors to know the status of the patients and able them to provide a suitable therapy to the patients. Emotion recognition bridges the gap between patient's behavior and the reality that open up a new world of understanding patient's behaviors. In this paper, an approach based on Convolutional Neural Networks (CNN) for facial expression recognition is presented using the GPU feature available in Google colab that helps in speed up the processing and recognizing emotion from videos. Seven universal facial emotions such as angry, disgust, fear, happy, sad, surprise and neutral show distinct signals in face and correspond to key individual emotions of a person.

2. RELATED WORK

Genne et.al., [1] conducted a survey on Facial Expression Recognition using CNN. They extracted the critical features by deep learning methods by updating the weights using back propagation and optimization of errors.

Khanzada et.al., [2] studied about the performance of Deep Learning Algorithms in Emotion Recognition. Vanilla CNN model is with the help of ReLU filters, 3x3x32 same-padding, 2x2 MaxPool layers, a FC layer and a softmax layer.

Gunawan et.al., [3] developed a Video-Based Emotion Recognition Model using Deep Learning. They developed a model which extracts image frames at regular intervals from the video and the images undergoes pre-processing and various CNN architectures are applied for emotion recognition.

Landola et.al., [4] studied about the SqueezeNet model and their advantages over larger model (AlexNet). The three main strategies used when designing the model are: 3X3 filters are used instead of 1X1 filters, reducing input channels of 3X3 filters, to achieve large activation maps, the downsampling is delayed.

Dhankhar et.al., [5] conducted a research on ResNet-50 for Recognizing Facial Emotions. The concept of skip connection was used here. One of the skip connections stacks up the CNN layers together while in the other the original input is added to output of the CNN block.

Millier et.al., [6] conducted a survey on Humanistic Burden in Schizophrenia Patients. This survey studied about the burden of this disease on people all over the world. The search considered several databases, including Embase, Medline, Cochrane Library.

Rassadin et.al.,[7] learned how Compressing Deep Convolution Neural Networks works efficiently in Visual Emotion Recognition. They compressed the deep convolutional neural network using pruning techniques and they followed the ideas of distilling the knowledge, weights hashing, tensor decomposition and binarization.

He et.al., [8] studied about ResNet-50 for Image Recognition. The degradation problem is addressed by introducing a deep residual learning framework.

Based on the literature survey, the following are the lessons learnt

- The preprocessing carried out with image frames associated with the video showed great result and Residual Networks shows better results than many other architectures. [8]
- SqueezeNet which has smaller size and also has less parameters to that of AlexNet but gave similar output accuracy to that of AlexNet. [3]
- ResNet-50 model when coupled with transfer learning produced acceptable results in both Kaggle and KDEF datasets. [4][5]

3. TECHNICAL FRAMEWORK

The following diagram briefly describes the algorithms available to implement the system. This system can be implemented using software or hardware. Since the work involves deep image processing the extract the deep features for predicting the emotion, deep learning technique such as convolutional neural network is chosen. From the CNN architectures, ResNet-50 and SqueezeNet is used. The dataset consists of 3662 training images and 2503 validation images. These images were taken at a 45-degree FOV and are separated into 5 different classes.

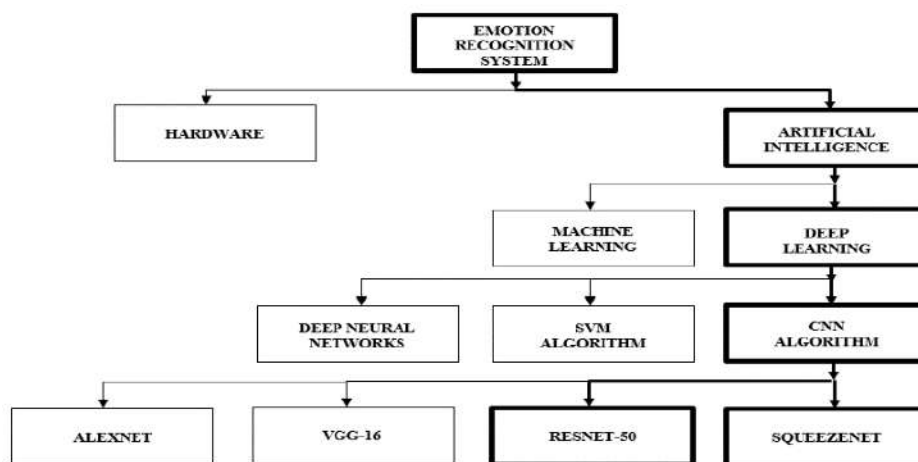


Fig 1 :Technical framework

3.1BACKGROUND

Convolutional Neural Network (CNN/ConvNet) is a powerful deep learning neural network that is most familiar for extracting the important/deep features from the image which is significant for distinguishing one image from the other. ResNet-50 and SqueezeNet are one of the architectures of CNN that is specifically used in image processing.

ResNet-50 also known as Residual Neural network is a type of CNN architecture that utilizes skip connections to overcome the problem of most deep neural networks. Before the introduction of ResNet-50, it was very difficult to construct deep learning models due to vanishing gradients.

This powerful ResNet-50 architecture comprises of five stages where each stage consists of a convolution block and identity block and contains over 23 million parameters. These two blocks consist of three convolutional layers. The shortcut connection skips 3 blocks instead of 2. In ResNet-50 the stacked layers in the residual block will always have 1×1, 3×3, and 1×1 convolution layers. The 1×1 convolution first reduces the dimension and then the features are calculated in bottleneck 3×3 layer and then the dimension is again increased in the next 1×1 layer. In order to reduce and increase the dimension of feature maps before and after the bottleneck layer,

1x1 convolution layer can be used. Since there's no pooling layer within the residual block, the dimension is reduced by 1x1 convolution with strides 2.

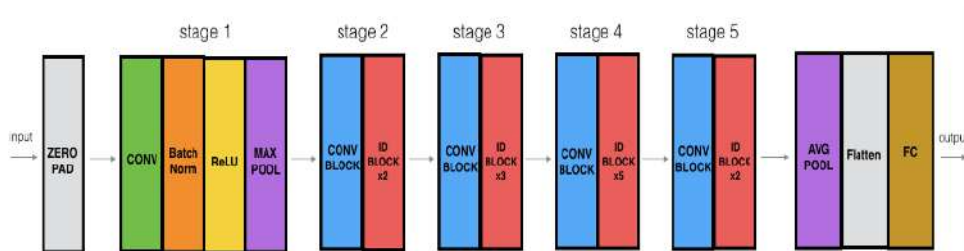


Fig 2: Architecture of ResNet-50

SqueezeNet is the smallest architecture among the CNN architectures that is considered as an alternative for AlexNet. This architecture consists of parameters which are 50x fewer than AlexNet, and gives 3x faster performance. It is comprised of "squeeze" and "expand" layers. Fire Module is used in this architecture which includes a squeeze convolution layer of 1x1 filters, fed to an expand layer that comprises of both 1x1 and 3x3 filters to achieve greater accuracy with small size.[5]

The number of parameters in 1x1 filters are 9x times less than that of 3x3 filters. So, the majority of 3x3 filters can be replaced with 1x1 filters so that the number of parameters is decreased. Create a convolution layer with 3x3 filters. The total number of parameters required for this layer can be computed using the following formula: (total no of input channels) * (no of filters) × (size of the filter). Total no of input channels can be decreased to the size of the filter using squeeze layers. Higher classification accuracy can be achieved with large activation maps which are delayed as a result of down-sampling [5].

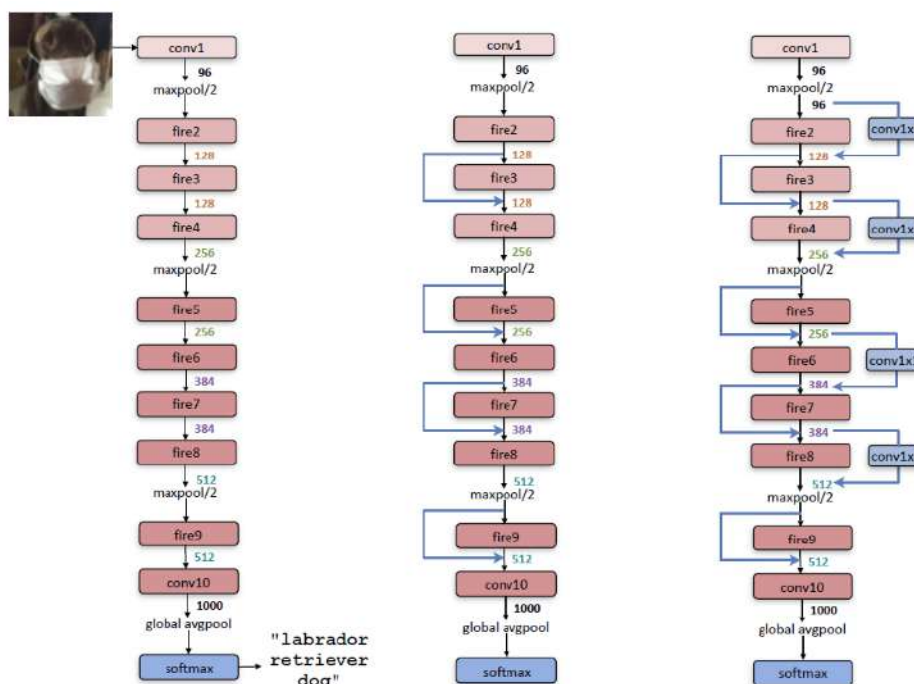


Fig 3 Architecture of SqueezeNet

3.2 DATASET AND FEATURES

Dataset used for the work was FER-2013 dataset. The dataset consists of 48x48 pixel grayscale images of faces. The images in the dataset have been processed in a such way that the face occupies equal amount of space and is centered. FER-2013 consists of seven categories of emotion (0=Angry, 1=Disgust, 2=Fear, 3=Happy, 4=Sad, 5=Surprise, 6=Neutral). FER-2013 dataset consists of nearly 35,000 images. In addition to this, some more images have been added and the total images added to 50,000 images. Dataset were split into two sets: training and testing. Training and testing set contains 40,000 and 10,000 images respectively. The images were stored CSV file with three columns: Label of emotion, image pixels and category (training or testing). After reading each image from the CSV file, we store the pixels of image in separate arrays train_data and test_data and labels in train_label and test_label. Image pixels were normalized and reshaped into 48X48X1 shape for training purpose. In order to acquire much more accuracy and be able to detect the faces in any direction, data

augmentation has been applied by doing some manipulation such as horizontal flip, vertical flip, zoom in and so on.

4. Comparison of CNN Architectures

This table describes the various CNN Architectures alongwith year of release, parameters, depth and remarks.

Architecture Name	Year	Parameters	Depth	Remarks
LeNet	1998	0.060M	5	This standard architecture performs stacking convolution layers with activation function, perform pooling and finally ending the model with fully-connected layers.
AlexNet	2012	60M	8	This architecture introduced Rectified Linear unit (ReLU) as activation function and adding dropout feature.
VGG - 16	2014	138M	19	Homogeneous topology. Use small size kernel
Inception-v1	2015	5M	22	Introduced building the model using modules/blocks rather than stacking convolutional layers.
ResNet-50	2016	23M	50	Popularized the skip connections. Eliminate degradation problem in deeper neural networks. First model to use batch normalization.
SqueezeNet	2016	0.66M	16	Smaller CNN with very fewer number of parameters. It uses fire module to achieve greater accuracy with small size.

Table1: CNN Architectures

5. PROPOSED METHODOLOGY

Conceptual Architecture is the conceptual view(s) of the architecture of a system. The ultimate goal of our work is to evaluate the performance of ResNet-50 and SqueezeNet in predicting the frames extracted from the video file. The following diagram describes the conceptual architecture for our system.

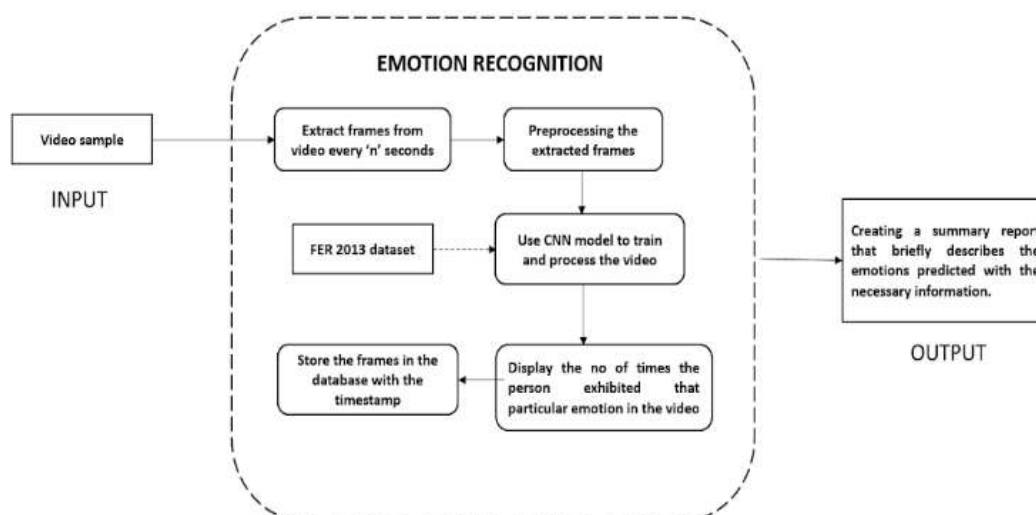


Fig 4: conceptual architecture

PRE-PROCESSING:

This is the first process that is applied to the input video sample. This process includes face detection, gray scale conversion, histogram equalization, image resizing and cropping. Training the CNN Model: With the help of training data, train the model with options such as learning rate, optimizer and loss function. Passing the features from CNN layers: The features which were identified and extracted from the layers are fed to the model for classification of the input. Testing the CNN Model: Use test data for calculating and validating the accuracy of the model.

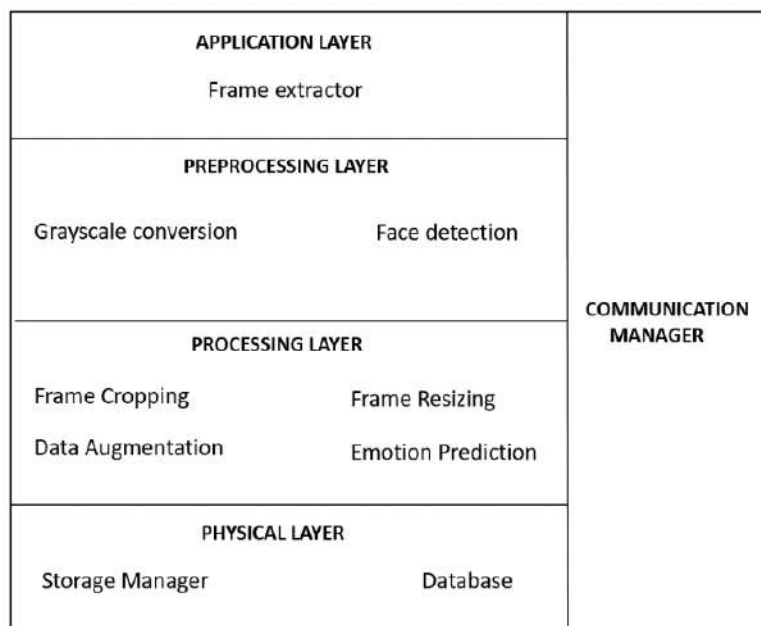


Fig 5: 4-layer architecture

APPLICATION LAYER: This layer takes the video file as an input and extracts image frames from the video for every 'n' second which is given as input to the preprocessing layer.

PREPROCESSING LAYER: This layer preprocesses the frames extracted for predicting the emotion. The image frames extracted from video are given as input to this layer. It applies Grayscale conversion which is converting the frames to grayscale. Once the frames are converted to grayscale face detection process takes place.

PROCESSING LAYER: This layer processes the pre-processed frames for predicting the emotion. Face detected gray-scaled images undergoes processes like Frame Cropping and Frame Resizing. These processes remove undesirable external regions from the image and resizes the image to 48x48 pixels. The CNN models are trained for considerable number of epochs with learning rate, batch size and the emotions are predicted.

PHYSICAL LAYER: This layer helps in storing the images extracted from the video file with the emotion predicted on it.

Communication Manager is common to all the layers that helps layers communication with each other to perform necessary operations.

6. CNN-Enabled Emotion Prediction Algorithm:

6.1 SPLITTING_DATA(DATASET):

1. Read each image from the dataset (CSV file) and store it in an array.

(CSV file consists of three columns "Emotion label", "Pixel of images", "Usage" (Training or Testing)).

2. Create x_train, x_trainlabel, x_test, x_testlabel lists.

3. for each image in array:

If 'Training' in usage:

Append the Pixel to x_train

Append the emotion label to x_trainlabel

If 'Testing' in usage:

Append the Pixel to x_test

Append the emotion label to x_testlabel

4. Perform Normalization on pixels

6.2 MODEL_TRAINING (EPOCHS, BATCH_SIZE, LEARNING_RATE, CALLBACKS):

1. Create a CNN model
2. Perform Data augmentation.
3. Training is carried out until the model achieves a considerable accuracy.
4. Evaluate the model on x_test.

6.3 EMOTION_PREDICTION (INPUT VIDEO):

1. Read the video sample from which you want to predict emotion
2. Create a dictionary with keys as emotion label from 0 to 6 and values as emotion name.
3. sec = 0
4. count = 0

5. frameRate = n // 'n' seconds

6. While there is frame to extract:

Extract the frame

Convert the frame to grayscale

Perform face detection

If face is not detected:

continue with extracting the next frame

else

count = count + 1

Crop the face detected portion of the frame.

Resize the frame size to 28x28 pixels

Use CNN model to predict the emotion

Get the emotion name using dictionary

Save the frame in the database along with the predicted emotion and the timestamp.

7. Display the no of times the patient exhibited that particular emotion in the video by plotting the bar graph.

7. EXPERIMENTAL RESULTS

The experiment was carried out on Google colab platform and FER-2013 was used as a dataset. Colab is a free Jupyter notebook environment that does not require any prior setup and can be run entirely in the cloud. Notebooks can be imported, created and edited by more than one person at the same time. Colab supports popular machine learning libraries such as keras and tensorflow that can be easily loaded in the notebook. Deep learning model usually requires a lot of computational power to run on. Whenever a deep learning model needs to be built, the training phase contains more intensive operations that takes a long time. For this, google colab provides a free GPU which is smaller and has more logical cores than the CPU. GPU allows us to process multiple computations simultaneously for artificial intelligence and deep learning models. Dataset was loaded to google drive in the form of CSV file and get mounted in the colab. Both the models ResNet-50 and SqueezeNet were trained for 3 hours for 160 epochs.

7.1 EVALUATION

Performance metrics like accuracy, f-score, recall and precision were used to evaluate the performance of the two models. These performance metrics show how well the model performs on a test data. Precision tells how 'precise or correctness' the model is by dividing the number of true positives plus the number of false positives where TP = True Positives, FP = False positives, TN = True Negative, FN = False negatives.

Recall is the classification metric that identifies all the relevant instances. It is the model's ability to find all the data points of interest in a dataset.

F1-measure tells that how well the model has performed on the positive class. It is obtained by harmonic mean of recall and precision. It focuses mainly on the positive class.

Accuracy is the widely used performance metric for evaluating the model's performance. It tells the percentage of samples correctly classified by the model.

Performance Parameters	ResNet-50	SqueezeNet
Accuracy	68	64
Precision	72	67
Recall	63	60
F1-Measure	65	61

Table 2: overall performance of ResNet-50 and SqueezeNet:

7.2 RESULTS

The experiment was carried out with two convolutional neural networks ResNet-50 and SqueezeNet with FER-2013 as a dataset with data augmentation applied on the dataset. Both the models were trained for 160 epochs with learning rate 0.001. In order to obtain best classification results, Batch normalization was applied to the dataset. Hyperparameters are tabulated in Table 3. Results are tabulated in Table 4. It shows that both the models achieved the testing accuracy of 70% and 65%. Learning rate is increased as the model reaches closer to the accuracy.

Confusion matrix were computed for both the models that is shown in Figure 6. From the confusion matrix, it can be seen that happy was predicted accurate by both the models when compared to other expressions. The performance metrics such as precision, recall and f1-score were computed for each expression for both the models. Models were tested by giving sample images. ResNet-50 predicted the emotion angry accurately but SqueezeNet shows some spike on disgust and fear. Models were tested on a sample video where the frames were extracted every 2 seconds and the emotion exhibited by the person in each frame was predicted and stored with the timestamp stating when the frame was extracted. Both these models ResNet-50 and SqueezeNet have contrasting features of each other. ResNet-50 is a deep network with 50 layers over 23 million parameters whereas SqueezeNet is a deep network with 5 million parameters and it turns out that ResNet-50 is able to predict more intensive expressions in faces when compared to SqueezeNet.

Hyper-parameters	Value
Optimization algorithm	Adam
Initial learning rate	1.000×10^{-3}
Epochs	160
Batch size	256
Face detection algorithm	Haar-Cascade

Table3: Hyper-parameters used

Models	ResNet-50			SqueezeNet		
	Precision	Recall	F1-measure	Precision	Recall	F1-measure
Angry	0.27	0.80	0.40	0.23	0.70	0.35
Disgust	0.76	0.41	0.53	0.74	0.22	0.34
Fear	0.56	0.35	0.43	0.53	0.20	0.29
Happy	0.92	0.83	0.88	0.86	0.82	0.84
Sad	0.53	0.41	0.46	0.53	0.26	0.35
Surprise	0.77	0.71	0.74	0.80	0.64	0.71
Neutral	0.79	0.52	0.63	0.71	0.64	0.67

Table 4: Confusion Matrix

Performance Parameters	ResNet-50	SqueezeNet
Training Accuracy	75	72
Training loss	0.7669	0.7523
Testing Accuracy	70	65
Testing loss	0.9901	0.9926

Table 5 : performance of ResNet-50 and SqueezeNet in predicting emotions

The prediction of emotions is shown below:

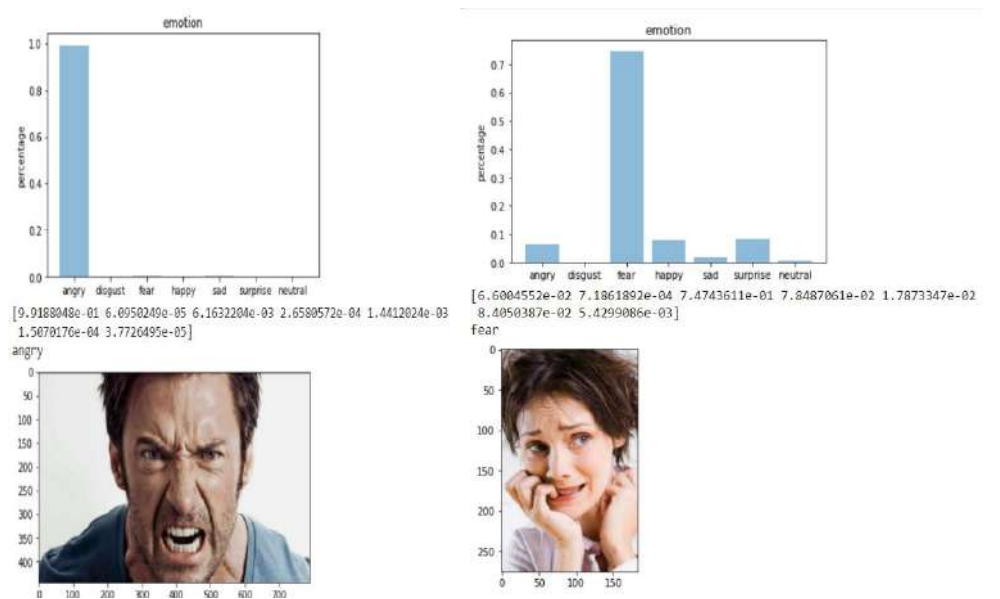


Fig 6 a) ResNet-50

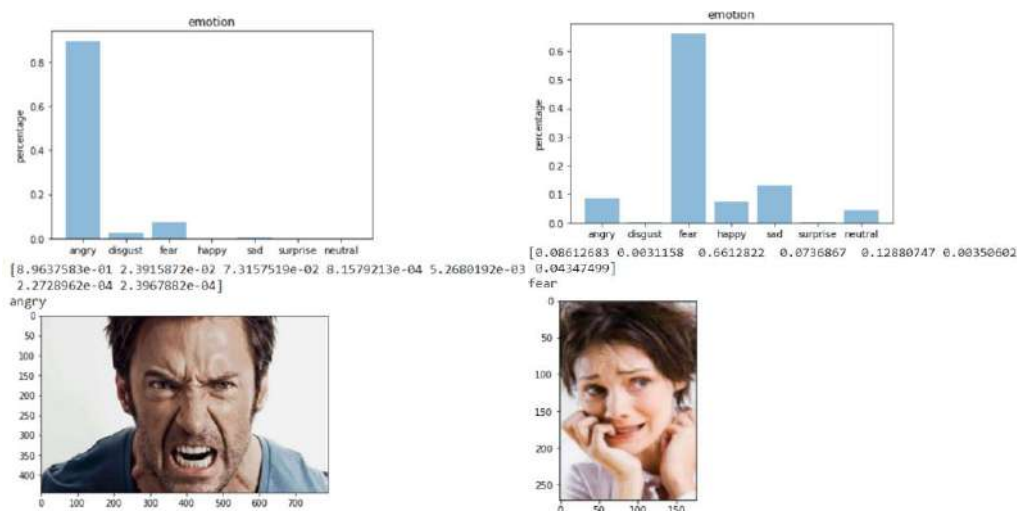


Fig 6 b) SqueezeNet

8.CONCLUSION

In this paper, CNN architectures ResNet-50 and SqueezeNet has been chosen for video-based emotion recognition with google colab. Several CNN models were explored for predicting facial expressions. Both the models have contrasting features with each other and able to recognize expressions of emotion compared to more subtle expressions of the same emotions. Experiment shows the no of times the particular emotion exhibited by the person in the video. This can be useful in providing a treatment to psychiatric patients where the doctor would be able to know how well the patients are improving by analysing the emotions exhibited by them. Different performance parameters were benchmarked on both the models to show the progress and accuracy of the model. In future, work can be further extended by tuning the hyper parameters and developing an ensemble model, including working with other datasets.

REFERENCES

1. Ravichandra Ginne, Krupa Jariwala. (2018). "Facial Expression Recognition Using CNN: A Survey". International Journal of Advances in Electronics and Computer Science, ISSN: 2393-2835, Volume-5, Issue-3, Available at: https://www.ijae.in/journal/journal_file/journal_pdf/12-451-152482308313-16.pdf.
2. Amil Khanzada, Charles Bai, Ferhat Turker Celepcikay. (2020). "Facial Expression Recognition with Deep Learning", Stanford University, Available at: https://cs230.stanford.edu/projects_winter_2020/reports/32610274.pdf.

3. Teddy Surya Gunawan, Arselan Ashraf, Bob Subhan Riza, Edy Victor Haryanto, Rika Rosnelly, Mira Kartiwi, Zuriati Janin. (2020). "Development of Video-Based Emotion Recognition Using Deep Learning". TELKOMNIKA Telecommun Comput El Control, Vol. 18, No. 5, Page No. 2463 – 2471. <https://dx.doi.org/10.12928/TELKOMNIKA.v18i5.16717>.
4. Landola F.N., Han S., Moskewicz M.W., Ashraf K., Dally W.J., Keutzer K. (November 4, 2016). "SqueezeNet: AlexNet-Level Accuracy with 50X Fewer Parameters and <0.5MB Model Size". Under review as a conference paper at ICLR 2017, arXiv:1602.07360v4 [cs.CV].
5. Poonam Dhankhar. (2019). "ResNet-50 and VGG-16 for recognizing Facial Emotions". International Journal of Innovations in Engineering and Technology (IJJET), <http://dx.doi.org/10.21172/ijjet.134.18>.
6. Millier A., Schmidt U., Angermeyer M.C., Chauhan D., Murthy V., Toumi M., Cadi-Soussi N. (2014). "Humanistic burden in schizophrenia: A literature review". Elsevier Ltd, <https://doi.org/10.1016/j.jpsychires.2014.03.021>.
7. Rassadin A.G, Savchenko A.V. (2017). "Compressing Deep Convolutional Neural Networks in Visual Emotion Recognition". 3rd International conference Information Technology and Nanotechnology 2017, Available at:<https://ceur-ws.org/Vol-1901/paper33.pdf>.
8. Kaiming He, Xiangyu Zhang, Shaoqing Ren, Jian Sun. (2015). "Deep Residual Learning for Image Recognition". Microsoft, arXiv:1512.03385v1 [cs.CV].
9. Karpagam G.R., Vinoth Kumar B., Uma Maheswari J., Gao Xiao-zhi. (2020). "Smart Cyber Physical Systems Advances, Challenges and Opportunities". 1st Edition. Boca Raton: Chapman and Hall/CRC. <https://doi.org/10.1201/9780429321955>.
10. Rohit Verma, fer2013, Kaggle, Version1, 2013. Available at: <https://www.kaggle.com/deadskull7/fer2013>
11. Devi I., Karpagam G.R., Vinoth Kumar B. (2018). "A survey of machine learning techniques". International Journal of Computational Systems Engineering, <https://doi.org/10.1504/IJCSYSE.2017.089191>.
12. Yingruo Fan, Victor O.K. Li, Jacqueline C.K. Lam. (2018) "Video-Based Emotion Recognition Using Deeply-Supervised Neural Networks". ACM. <https://dx.doi.org/10.1145/3242969.3264978>.

Design and Development of Medicated Sanitary Napkins with Selected Medicinal Herbs

Subathra. B

Department of Apparel and Fashion Design, PSG College of Technology, Coimbatore, Tamilnadu, India

ABSTRACT

In the modernized world most of the people are very conscious about their health and hygiene. Using of health care products become serious business among the medical professionals and also in the common people. Good health, comfort and social interaction are bound strong by good hygiene. Human life is completely kept safeguarded with the help of textile materials. The clothing provides warmth, comfort and support from infant to elders, ie to the whole life cycle of man-kind. The textile materials are not only providing comfort to the human being, but also to the microbes. Textile and clothing are not only the carriers of micro-organisms such as bacteria and fungi. The inbuilt properties of the textile fibers more suitable for the growth of micro-organisms. So, it develops comfortably. But it cause more derma related issues to the human. Humid and warm environment still stimulate the growth of pathogens growth, which leads to cross infestations and lead to bad odor on the fabric surface. Every women suffer with vaginal yeast infection in their lifetime or series of infection that never treated completely. Nearly 75 percent of all adult women have the bad experience of genital yeast infection atleast once in their lifetime. Itching and perile rash is the symptoms of vaginal yeast infection. Medical treatment may support partially to come out of this problem. But treating these issues with herbal treatment may cure the issue slow and sturdy.

Keywords: Herbs Hygiene, Micro-organism, sanitary napkin.

I. INTRODUCTION

Natural and synthetic fibers are considered as the fundamental of textiles. The fibers are blended together in a different combinations to bring out various textile products. Based on the textile application the combination of fibers are used to achieve specific properties. i.e., these special type of fabrics are upholstery, automobile and industrial products. Cotton has high absorbent property, which made it to use in the fluid absorbent agent in the various fields. In medical field cotton used as absorbent of body fluids such as Urine, blood and other fluids. Polypropylene is a polymer used as an absorbent. it is usually used as an inner layer in diapers and sanitary pads. Among all the natural and synthetic fibers, it is found as thin and lightest. The absorbency properties of cotton and polypropylene gives more comfort to the wearer, but it lead to the easy occupation of microbes on its surface. Humidity and warmth supports the growth of microbes. Microbial infestations possess danger to living and non-living matters. Sometimes obnoxious odor found from the inner wears. The growth of micro-organisms extend as spread of disease, staining and degradation of textile materials etc. Textiles used in healthcare environment have unique microbial problems and their control of a complex task. The micro-organisms of mold, mildew, bacteria, yeast, fungi and virus are the part of our life. The nature of the micro-organisms are cause both good and bad impact among man-kind. In the environment more than thousands species are found. Few micro-organism helps & make our life very easy and healthy, but few are health hazardous. It spoils the performance of textile products and create bad impacts. To enhance the life and performance of textile products antimicrobial finish can be given. In future some kind of finish become standard mandatory finish to maintain quality. Most of the women have experienced badly with vaginal yeast infection during menstruation. Finding the solution for the issue was taken as a challenge.

II. REVIEW OF LITERATURE

Microbial growth, infections and its impacts are found more in the modernized world. The special characteristics of contamination free and infection control are the key parameters of hygienic products. Antimicrobial is the agents' acts against to control, destroy and suppress the growth of microbes and control its stain and odor. These micro-organisms are majorly classified as bacteria and fungi (1)., The bacteria's family has classified as gram positive staphylococcus Aureus and gram negative is E-coli are spore bearing and non-spore bearing types. These are pathogenic and cause cross infections. Complex organism of fungi, mold and mildew has slow growth rate (2). Selecting a suitable materials for the preparation of sanitary napkins and finishing with the quality herbals is place a major role in controlling the microbes.

A. Selection of Fibers

1) Cotton

Fiber is the fundamental raw materials of textile which is more delicate, thin hair like tissue of a plant has small in diameter in relation to length (3). Cotton is a natural fiber that comes from the seedpod of the cotton plant and is used to make many fabric types. It absorbs up to 27 times its own weight in water and has a comfortable soft hand (4).

The main reason for the use of Cotton is, it's good weaving qualities, low cost, high absorption, excellent abrasion & pilling resistance & stability to repeated blending. The Cotton is excellent if preshrunk, and can be safely ironed even at temperature of 425°F. It has excellent to colour fast in wash and wear, wrinkle resistance and is also good if resin treated (5)

2) Polypropylene

Polypropylene is a synthetic material of polymer, which is essentially plastic. As a result its colours won't fade or bleed when washed, because the colors are built into the material (6). Polypropylene is more hydrophobic, meaning that it does not absorb as much water. Since the water cannot be absorbed into the fabric, but it has a tendency to spread evenly throughout the garment which in turn helps the water to evaporate much quicker than a fabric that absorbs and retains the water (7).

B. Selection of Fabric

Fibers are turned as fabric by major three process of weaving, knitting and non-woven. Each fabrication process has its own properties and positives.

1) Woven fabrics

Woven fabrics is constructed by interlacing two sets of yarn that run lengthwise and crosswise, this form the interlacing or weaving. Woven fabrics are classified as to weave or structure according to the manner in which warp and weft cross each other.(8,9) Plain weave is the simplest and most common interlacing method. In this, the warp and weft are of equal tension and spacing and it is equally visible on the surface.

2) Non-woven fabrics

Non-woven fabrics are made by spreading the long fibers along with resin/ solvent and applying more pressure and temperature the fabrics are formed. Fibers are assembled into a uniform web structures in order that a bonding process can be applied to stabilize the tenuous network.(10-15). Non-woven bonded fabrics are made of just like other textiles. The fibers may be very short, only a few millimeters long, but generally they are of similar length to those spun into yarn & may even be so long as to be called 'endless'. Non-woven's are more ecological fabric for certain applications, especially in fields and industries where disposable or single use products are important such as hospitals, schools, nursing homes. It provides specific functions such as absorbency, stretch, softness, bacterial barriers and sterility (16).

C. Importance of Herb

Herbs are the natural plants or parts of natural plants which is grown near to us. Plants are named as herbs due to its unbeatable medicinal values. Ayurveda is the term related to herbal treatment; (17-19) it is an ancient science of India, is accepted system (20).

D. Microbes

The Anti- microbial property of fabric is being considered to be an important and inevitable parameter for garments which are in direct contact with human body. It becomes highly important for all the garments where the chance of Bacteria growth is high and the safety is paramount (21). This includes medical garments, sanitary napkins, socks, underwear, disposable wipes, Carpets. Skin reactions are more common today due to climatic condition and body nature. Allergies are abnormal or hypersensitive responses of immune system to relatively harmless environmental antigens. Sanitary napkin rash usually arises from chemical irritation or due to certain germs present during menstruation (22).

Lot of women worry about the smell of menstrual blood for a number of reasons. Until very recently, it was always taboo to talk about menstruation and so far many people there were only ever negative connotations associated with it. This meant the subject was always kept hidden and women tended to make sure that nobody ever knew that they were having their period (23). Naturally, this led to certain manufacturers jumping onto the brand wagon and producing artificial products that are designed to hide the smell of menstruation, further reinforcing the idea that it is a negative thing (24-26). Vaginal infection is caused due to number of reasons. The principle causes of vaginal infection are bacterial infection, yeast infection and estrogen imbalance (27). To control the activeness of microbes some external steps need to be taken, that must possess the power to control

the development and growth of Micro-Organisms. These processing will collapse the growing environment. These antigens are called as Antimicrobials (28-30).

1) Bacteria

The growth of bacteria spoils the fabric surface and also hazardous to the wearer. Antimicrobial finish on a fabric surface will limit the growth of these organisms. When a product has a negative influence on the vitality of a micro-organism: it is generally termed as anti-microbial; when the bacterium is killed the suffix static is used (32).

2) Fungus

Yeast infections are caused by fungus in vagina, because of the warmth and humid nature of the private part. These vaginal yeast infection caused by the fungus candida albicans. This infection leads to unpleasant symptoms. Anti-fungal agent control the fungus growth, rashes and prevent odor.

E. Anti-Microbial protection

The benefits associated with incorporating antimicrobial agents include the protection of textile and wearer from microbial attack, increasing comfort properties of textiles by the prevention of odor from perspiration, product differentiation and added value (41).

F. Need for Herbal Finish

Commercially more health care products are available, which are made with chemical components Maylead to health and environmental hazards. The natural herbals extracts will control the growth of odor controlling bacteria and cure the issues permanently. Using the herbs to treat the vaginal yeast infection is the best way to get rid of from infection (42). Use of herbs for treating vaginal yeast infection in women is a painless way to get rid of this bacterial disease before it cause further problems. Herbs applied externally ease the inflammation and itching of vaginal infection. Herbs bolster the body's immune response and directly fight the Micro-Organisms that are causing the infection(43).

G Selection of Solvents

Solvent is the media, which is mixed with solute to extract the solution(44-46). Water is a good solvent for the extraction but self-life of the solution is minimum. So, Alcohol or ethanol will acts as a best solvent with good self-life.(47).

H. Selection of Herbal finishing method

Prepared Herbal extraction is applied on fabric surface to improve the quality of fabric and analyze the property of herb. There are more methods followed to do the herbal finish. Exhaust Padding-mangle, dip & dry, direct application, dyeing, micro-encapsulation & cross linking method are the some kind of special finishing methods. Based on the Finishing method the life of finish can be determined (48).

I. Hygienic sanitary pads

In few decades before women usually use cloth to collect their menstrual fluids. Nowadays due to the awareness about the sanitary napkins everyone uses it. (49). Today's pads are also more absorbent, allowing them to be thinner and more effective. Some even have wings wrap around the crotch of underwear, which gives greater protection. Pads can be unscented or deodorant. The deodorant can cause irritation in some women; however, many like the deodorant products, believing it helps to mask odor opines (50).

III. MATERIALS & METHODS

A. Selection of Fabrics

Cotton fibers have one clean advantage over synthetic fibers that is their ability to absorb moisture from the surrounding air as conditions change. This property is often described as breathability, plain weave gauze fabric has more breathability and absorbency. Hence, considering the above factors, the investigator has chosen cotton plain woven fabric for study (51).. A non-woven fabric for the top sheet of an absorbent article has been developed as hygiene product. The liquid permeable top sheet material is said to have improved softness, Liquid inlet and rewet properties. It will find application in sanitary napkins, pant diapers and sanitary pants. Polypropylene non-woven fabric was taken as a layer for napkin (52).

B. Pre-treatment

The preparatory processes to get bleached fabrics from grey fabrics are the heart of the entire process house, which produces dyed, printed & mechanical finished fabrics. In this study to remove sizing materials in woven fabric, the Cotton cloth was soaked in luke warm water for particular time of 30 minutes and dried under sun shade and Non-woven's need not to be pretreated

C. Pilot study

In Pilot Study five natural herbs were taken & tested. The herbs were 1. Curcuma Aromatica 2. Curcuma Zedoaria, 3. Cassia Auriculata 4. Ficus Religiosa 5. **Mimosa pudica**. These herbs were collected & dried under sunshade & Powdered. To extract herbal tincture, three grams of dry powder from each herb (1. Curcuma Aromatica 2. Curcuma Zedoaria, 3. Cassia Auriculata 4. Ficus Religiosa 5. **Mimosa pudica**) were taken and mixed with 50 ml of 80 percentage of Ethanol. The container was closed & kept for overnight. After the overnight incubation the extract was filtered through filter paper & evaporated to concentrate the extract.

Sterile bacteriostasis agar was dispensed in sterile Petri dishes. The herbal extract was tested for its Antibacterial activity by well diffusion method. After solidification of the media, wells of approximately 5 mm were punctured for loading the samples. Broth cultures (24 hours) of the test organisms were used as inoculums. Using sterile cotton swab, the test organisms (*Escherichia coli* & *Candida albicans*) were swabbed over the surface of the agar plate. The samples were loaded on the pre-swabbed agar surface. The plates were incubated at 37°C for 24 hours. After incubation, the plates were examined for the zone of bacterial inhibition around the loaded samples. The size of the clear zone was used to evaluate the inhibitory effect of the solution.

In Ethanol solution Antimicrobial property in herb were not found. So Methanol was tried as solvent to prepare herbal solution. The same procedure was followed again. In this testing found that, Cassia Auriculata and Ficus Religiosa had anti-microbial property. Pilot study results are shown in the table I and Fig.1

TABLE –I Pilot Study Result- Anti Microbial activity of the Extract (Well Diffusion Method)

S. No	Herbal extracts	Antibacterial activity- Zone of inhibition (mm)	
		E. coli	Candida albicans
1.	Curcuma Zedoaria (100 %)	0	0
2.	Curcuma Aromatica (100 %)	8	9
3.	Cassia Auriculata (100 %)	10	14
4.	Ficus Religiosa (100 %)	9	11
5.	Cassia Auriculata (50 %)	0	0
6.	Ficus Religiosa (50 %)	0	0

So, these two herbs were selected for the finishing process. To analyze best antimicrobial property in that herbs, various concentrations of herbs were prepared, the same process was followed. In that testing found that 100 percentage concentration solution gave best result in Antimicrobial property.

D. Selection of herb

Curcuma Aromatica, Curcuma Zedoaria, Cassia Auriculata, Ficus Religiosa, **Mimosa pudica** were selected for pilot study. Because Curcuma Zedoaria herb can be used to remove the dirt from body and it possess the power to cure open wounds. Curcuma Auromatica is commercially well known antimicrobial agent, which is also used to cure skin diseases and prevent infection. Cassia Auriculata used as a bathing powder to control body odor and improve body sheen, it also called as “Herbal Kayakalpa”. **Mimosa pudica** used to cure open wounds along with calcium carbonate. Ficus Religiosa utilized to strengthen the uterus(53).

Among those herbs Ficus Religiosa and Cassia Auriculata were selected for study due to best Antimicrobial property found in the pilot study. Cassia Auriculata is the botanical name for Aavaram poo and it is proven to control and reduce blood sugar levels. Cassia auriculata is an evergreen shrub with bright yellow flowers. It has got many medical properties and it cures many diseases. Figus religiosa is called as Arasa leaf which is heart shaped green leaf has more medicinal value. Herbs selected and treated on fabric is shown in the fig 2.

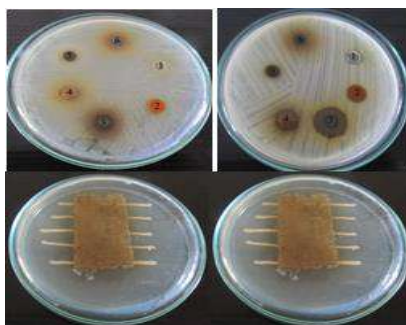


Fig. 1. Pilot study- Anti-microbial test

E. Selection of Finishing Method

There are more methods available in finishing a textile fabric. Dyeing, dip and dry, padding mangle are some of the types. The investigator has selected the dip & dry method to finish the Woven & Non-woven fabric.

Finishing Parameters

Methanol	-	1500ml
Herbal powder	-	100g
Temperature	-	37°C
Time duration	-	24 Hours
Size of fabric - Cotton	-	20"X 40"
Polypropylene	-	10"X 20"

F. Post treatment

Methanol is selected as solvent. The finished fabric kept in hot oven to make it dry completely. In room temperature the finished fabric may have little wetness which may lead the development of microbes in it. So it kept in oven and dried completely.



Fig.2. Herbs & Finished fabrics

G. Preparation of sanitary napkin

Disposable literally means designed for or capable of being thrown away after used or used up. They are bounded by "use and Throw" Concept. Textiles disposables include fiber, yarn, woven, knitted, braided structure and non-woven. Sanitary napkin with the Herbal treated woven & non-woven fabric materials were prepared.

A sanitary napkin basically comprises of three layers; top layer, absorbent layer and barrier sheet. The absorbent layer is the key component of the napkin and the extent to which this layer is able to absorb and retain the fluid determines the efficiency of the napkin. This bulk layer of a napkin is a non-woven web, made of hydrophilic cellulosic staple fibers like wood pulp, cotton linters; viscose. Wings model sanitary napkin was prepared for the study. The herbal finished woven and Non-woven fabric were cut in to 3" X 1" small pieces, and is used to keep inside the sanitary napkin. Below to that piece of fabric, herbal powder of *Vetiveria zizanioides* is kept for fragrance and to control odor. Sanitary napkin making tools and napkins are shown in the fig.3 & 4.

Type 1-First layer is a Polypropylene layer third layer is an absorbent core layer last one Barrier sheet of Polyethylene layer. Between the Polypropylene layer and absorbent core layer an herbal finished fabric is kept. In type 1 napkin *Cassia Auriculata* Herbal finished woven fabric is kept.

Type 2- In type 2 napkin, as second layer *Cassia Auriculata* herbal finished Non-woven fabric is kept.

Type 3- *Ficus Religiosa* herbal finished woven fabric is kept as second layer in the type 3 sanitary napkin.

Type 4- This sanitary napkin is prepared as normal wings style, but *Ficus Religiosa* herbal finished Non-woven fabric is placed inside the type 4 Napkin.



Fig.3.Sanitary napkin makings



Fig.4. herbal sanitary napkins

Table –Ii Nomenclature Of Samples

S.No	Material used	Sample name
1.	Cotton –Woven	CW
2.	Polypropylene - Non- woven	PN
3.	Cotton- Woven - Cassia Auriculata	CWCA
4.	Polypropylene - Non- woven - Cassia Auriculata	PNCA
5.	Cotton – Woven - Ficus Religiosa	CWFR
6.	Polypropylene - Nonwoven - Ficus Religiosa	PNFR

H. Objective Evaluation

1) Anti-bacterial Assessment

The Agar plate method is a qualitative method to determine antibacterial activity of diffusible antimicrobial agents on treated textile materials. Test specimen is cut by hand or with die. The standard samples are circular with diameter of 2.5cm. Prepare the test organisms by taking a cooled flame sterilized inoculation loop and inoculating separate culture tubes of the appropriate broth with the organism to be used, Incubate the cultures at $37\pm 2^{\circ}\text{C}$ for 18- 24 hours. Examine the incubated plates for a growth free zone around the test sample and for cleaning directly beneath the test sample. By the above mentioned AATCC 100 standard method the test samples of Woven and non-woven fabric finished with Cassia Auriculata and Ficus Religiosa, four samples were tested and the zone of incubation were measured. Test results are shown in the table III and Fig.5.

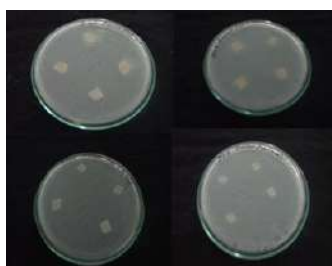


Fig.5.Result of Antibacterial test

Table-Iii Antibacterial Test (Aatcc100)

Samples	Organisms	
	Escherichia coli(mm)	Staphylococcus aureus (mm)

CWCA	11.1±0.1	1.5±0.5
PNCA	No	1.2±0.09
CWFR	12±1.73	1.7±0.41
PNFR	1.03±0.05	No

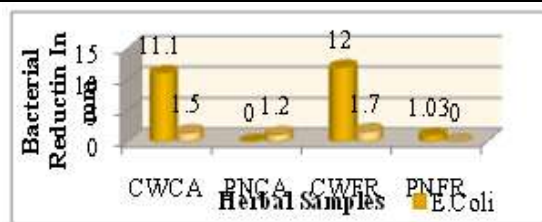


Fig.7. Anti-bacterial Finish

In grading according to the Anti-Bacterial power CWFR graded as very good and CWCA considered as good against Escherichia coli & Staphylococcus aureus. But, Non-woven were not up to the level of woven.

3) Anti- Fungal Assessment

The two purpose of this test method are to determine the susceptibility of textile materials to mildew and rot and to evaluate the efficacy of fungicides on textile materials. In testing minimum of five sample must be prepared and can be visual examined. Cut the samples in 3.8±0.5cm diameter discs from both treated and untreated samples.

Place the Agar solution in container and sterilize in an autoclave at 121°C for 15 min and cool in a position which affords maximum inoculation surface. According to the AATCC 30 standard method the test samples of Woven and non-woven fabric finished with Cassia Auriculata and Ficus Religiosa, four samples were tested and the zone of incubation were measured. Test results are shown in the table III and Fig.6.

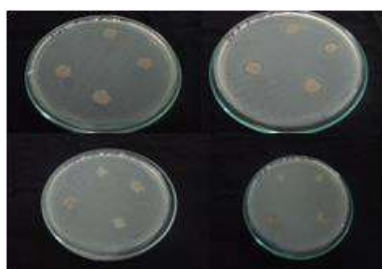


Fig.6.Result of Anti-fungal test

Table –Iv Anti-Fungal Test (Aatcc 30)

Samples	Candida Albicans	
	(mm)	%
CWCA	8±1	72
PNCA	0	0
CWFR	9±1.2	76
PNFR	0	0

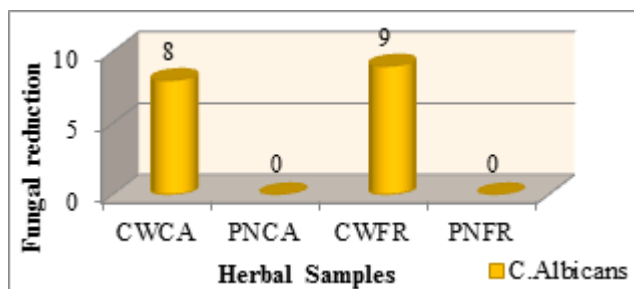


Fig.8. Anti-fungal Finish

It was found that woven finished sample CWCA has 8±1mm (72%) Anti-Fungal reduction, in the sample CWFR had 9±1.2 mm (76%) of fungal reduction against Candida Albicans. Among the Non-woven samples of Cassia Auriculata and Ficus Religiosa had no activity against Candida Albicans. Test results are shown in the table IV and Fig.8.

4) Fabric Weight

The fabric to be weighed is cut using a template size (3.5" X3.5") and weighed using an ohaus Adventure TM weighing balance which is shown in plate (15).This is an electronic balance which gives the direct readings of the samples. Ten reading were taken and average calculated. Test results are shown in the table V and Fig.9.

Table-V Fabric Weight

Sample	Fabric weight (g)		Loss or gain over original		't' value
	Mean	SD	Absolute	%	
CW	39	1.58	-	-	
CWCA	48	1.41	+ 9	+ 23.08	28.46* *
CWFR	47	2.45	+ 8	+ 20.51	4.544* *
PN	25	2.24	-	-	-
PNCA	32	1.58	+ 7	+ 28.00	7.000* *
PNFR	35	1.58	+ 10	+ 40.00	7.906* *

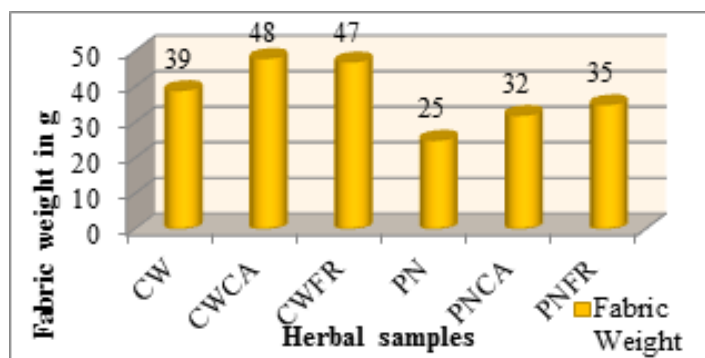


Fig.9.Fabric weight

Sample PNCA, PNFR showed greater increase in fabric thickness when compared with original samples. Non-woven samples thickness was statistically significant.

5) Fabric Thickness

The sample was mounted between the pressure foot and the anvil. The readings were taken at different places ten readings were taken and the mean calculated. This was expressed in milliletre. Care was taken to see the places were away from the selvedge and from wrinkle. Thickness tester is shown in the Plate (16). Test results are shown in the table VI and Fig.10.

Table-Vi Fabric Thickness

Sample	Fabric thickness		Loss or gain over original		't' value
	Mean	SD	Absolute	P5	
CW	0.14	0.02	-	-	-
CWCA	0.19	0.03	0.05	34.72	2.936* *
CWFR	0.19	0.01	0.05	33.61	3.751* *
PN	0.10	0.02	-	-	-
PNCA	0.14	0.01	+0.04	34.71	4.059* *
PNFR	0.15	0.00	+0.05	49.02	4.951* *

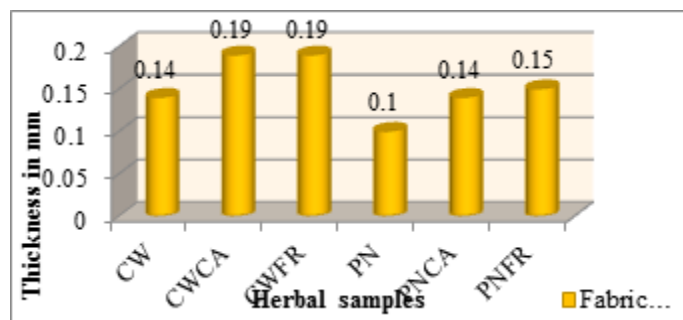


Fig.10 Fabric thickness result

6) Total Weight of Napkin

Sanitary napkin is weighed with the instrument ohaus Adventure TM weighing balance which is shown in plate (15). This is an electronic balance which gives the direct readings of the samples. Ten readings were taken and average calculated. Test results are shown in the table VII and Fig.11.

Table – Vii Total Weight Of Napkin

Sample	Napkin weight(g)		Loss or gain over original		't' value
	Mean	SD	Absolute	%	
Plain	12.55	0.05	-	-	-
CWCA	12.65	0.12	+0.10	0.79	0.294NS
CWFR	12.64	0.11	+0.09	0.71	0.235NS
PNCA	12.60	0.08	0.05	0.39	0.173NS
PNFR	12.62	0.09	0.07	0.55	0.198NS

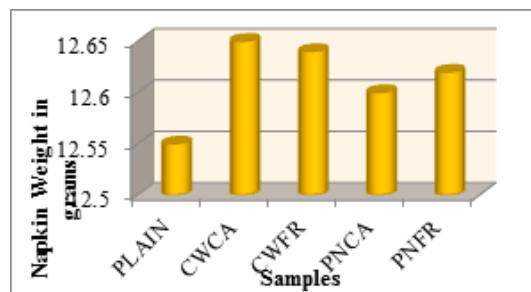


Fig.11. Result of Napkin weight

7) Liquid Strike & Wet Back

Burette, funnel ring stand, electronic conductivity detector and strike through plate were arranged for testing. Ten plies of filter paper above that test specimen kept and dispense with the pipette or burette 5.0 ml of artificial blood solution into the funnel. While keeping the discharge, value of the funnel is closed. Liquid strike and wet off time was taken with stop watch. Lister Tester in plate (17). Results seen in the table VIII & IX, Fig 12 & 13.

Table-Viii Liquid Strike Test

Sample	Liquid strike		Loss or gain over original		't' value
	Mean (s)	SD	Absolute	%	
CW	1.80	0.12	-	-	-
CWCA	1.92	0.03	0.12	6.90	2.150 ^{NS}
CWFR	1.82	0.07	0.02	1.34	0.340 ^{NS}
PN	2.90	0.05	-	-	-
PNCA	3.13	0.08	0.24	8.22	4.350*
PNFR	2.96	0.31	0.06	2.14	0.397 ^{NS}

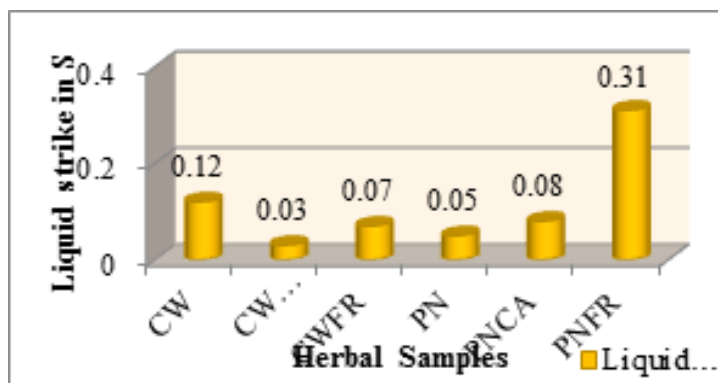


Fig.12. result of Liquid strike test

Table-Ix Wet Back Test

Sample	Wet back (s)		Loss or gain over original		't' value
	Mean	SD	Absolute	%	
CW	0.05	0.03	-	-	-
CWCA	0.05	0.02	0.00	0.00	0.00
CWFR	0.05	0.02	0.00	0.00	0.00
PN	0.06	0.03	-	-	-
PNCA	0.03	0.02	-0.03	-50	0.121 NS
PNFR	0.06	0.02	0.00	-	0.089 NS

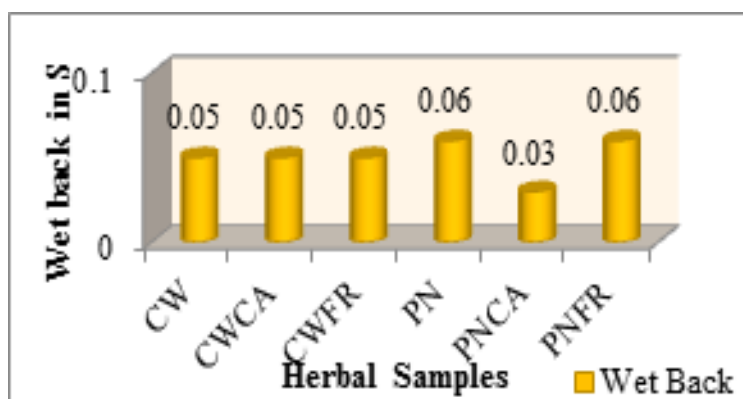


Fig.13. Result of wet back test

Among all those samples, the sample CWCA gets (0.03 s) very less time, the highest seconds shows PNFR (0.31 s). So in this conclude good liquid strike capacity present in the fabric.

8) Absorbency

This test was done to measure the absorbency of sanitary napkin. Napkin was kept on a flat surface plate and 30 ml of prepared colored water was poured on it 15ml per min. The absorption time was noticed with stop clock.

Table-X Absorbency Test

	Absorbency(s)		Loss or gain over original		't' value
	Mean	SD	Absolute	%	
CW	12	1.58	-	-	-
CWCA	13	2.12	1.00	8.33	0.767
CWFR	11	1.73	-1.00	-8.33	0.877
PN	15	1.58	-	-	-
PNCA	15	3.16	0.00	0.00	0.000
PNFR	15	1.58	0.00	0.00	0.000

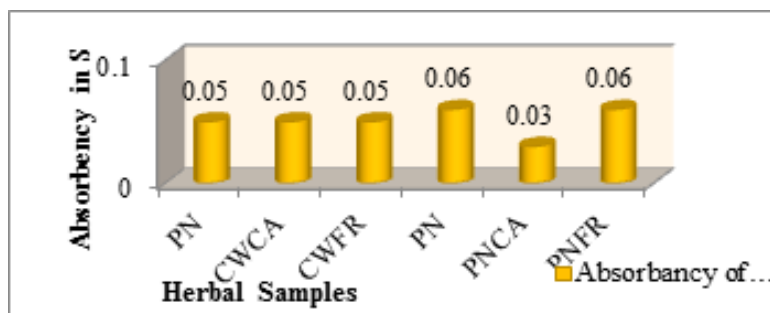


Fig.14. result of Absorbency test

9) pH Value

Test specimen was placed on flat surface and it was wet by pure water. pH paper placed on the wet fabric to analyze the Acid & Alkalinity of test specimen. Colour change in pH paper is noticed and taken as result. pH test results shown in the table XI and Fig.15.

Table-Xi Ph Value Test

Sample	pH value		Loss or gain over original		't' value
	Mean	SD	Absolute	%	
CW	7.2	1.79	-	-	-
CWCA	7.2	1.79	0.00	0.00	0.000
CWFR	7.0	1.58	-0.20	-2.78	0.152
PN	7.0	1.58	-	-	-
PNCA	7.2	0.84	0.20	2.86	0.272
PNFR	7.0	1.00	0.00	0.00	0.000

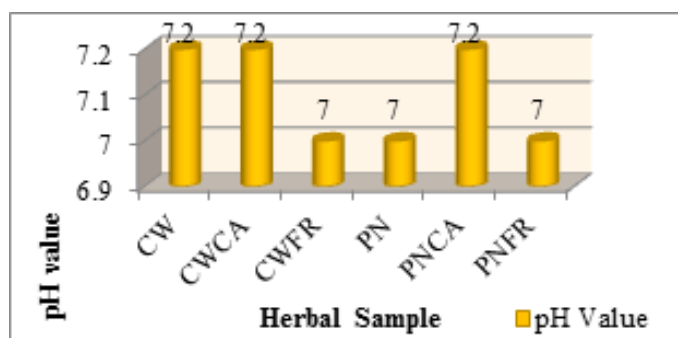


Fig.15. result of pH value

10) Disposability

The disposability test was done to analyze the degradation of material by nature sources. 15 liter of water was taken in a vessel, and in a sanitary napkin the top non-woven layer removed and it soaked in the vessel. A stirrer used continuously to make the napkin to disintegrate. The disintegration is checked and noticed.

11) Field Trial

Field trial is one of the ways to analyze the quality of new product. To conduct the field trial proper sample must be selected under the law of need and the new products have to be given to the sample people to use and can analyze the quality of product by making the sample people to answer the questionnaire.

In this study Cluster sampling Method is adopted. This method involves grouping sample as population and the same characterized cluster is selected for the trail study .This cluster sampling is easier and give good efficiency in the field work.

Field trial was conducted to analyze the quality of sanitary napkins. The Investigator selected 25 working women (middle worker) age between 20-40 years, for the sample study. The Sanitary napkins prepared with herbal treated Woven and Non-woven materials like CWCA, PNCA, CWFR and PNFR were given to the women and instructed to use during their menstruation. The pre-prepared questionnaire were given individually to them and asked to answer it.

Finally the answered questionnaires were collected and analyzed to find the properties of prepared herbal Sanitary napkins. The properties like absorbency, size, comfort, control of irritation, fragrance of Sanitary napkin were analyzed with answered questionnaire. Final products image is shown in the Fig.16.

Table XII ACCEPTANCE LEVEL OF SANITARY NAPKIN

S.No	Napkins	Best Usage of Herbal Treated Sanitary Napkins in Percentage
1	CWCA	80
2	CWFR	95
3	PNCA	25
4	PNFR	20

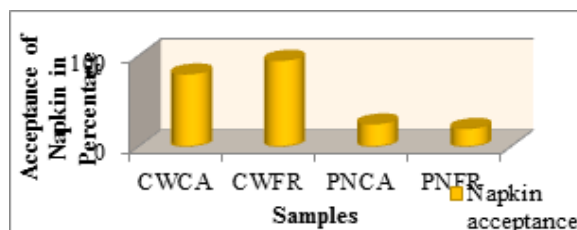


Fig.16. Acceptance of Herbal Napkin



Fig.16. Herbal napkin Femi care product

V.SUMMARY & CONCLUSION

The Prepared Sanitary Napkins were given to selected members of teaching staff and asked them to use during their menstrual period. The properties of Napkins were evaluated with filled questionnaire.

A.Findings of the study

- As for Fabric Weight, the weight gain was observed in woven samples finished with Cassia Auriculata and Ficus Religiosa, when compared to the original. For Non-woven fabric all samples observed weight gain when compared to original samples.
- As for Fabric thickness, all Woven and Non-woven samples, thickness of fabrics were increased when compare with original samples.
- pH value of all Woven and Non-Woven Samples were found as Neutral.
- As for liquid strike test, there was no more difference found in absorption time in finished samples of both Woven and Non-woven. So it concluded that, the herbal finish on fabric not affected the fabrics absorption property.
- As for wet back, in Woven finished samples, there were no differences found in wet off time. But in Non-Woven samples absorption improved.
- The Absorbency of Napkins was found in very good, there was no obstacle seen due to herbal finished fabric in Napkin.
- Total weight of Sanitary Napkins were increased when compared with plain Napkin, but it was not affected the comfort properties of Napkin.
- As for Disposability, the Napkin gets disintegrated in water completely. As for it considering as eco friendly product.

- In Anti-Bacterial results, the Woven fabric finished with *Ficus Religiosa* given very good result comparatively against *E.Coli* and *S. Aureus*. The woven fabric finished with *Cassia Auriculata* graded second as per the Anti-Bacterial result.
- In Anti-Fungal testing, Woven fabrics finished with *Ficus Religiosa*, *Cassia Auriculata* gave nice result against *Candida Albicans*, but Non-Woven fabrics do not have any inhibition against Fungus.
- As for Field trial Flexibility, Absorption, Irritation control, Odor control were found good. CWCA and CWFR Sanitary Napkins were accepted by most of the people (80, 95 % respectively) due to its excellent properties.

VI.CONCLUSION

The Prepared Herbal treated Femicare Sanitary Napkins were evaluated subjectively and objectively. The characteristics of herbal fabric like Liquid strike, wet back, pH value, Absorption of Napkin were found very good (100%). Anti-Bacterial and Anti-Fungal properties were found good (76%) in woven fabric finished with *Ficus Religiosa*, Woven fabric finished with *Cassia Auriculata* graded second (72%) in Anti-microbial property among those fabrics. In field trial, Flexibility, Absorption, Irritation control and odor control resulted 100 percentages. The acceptable level of Femi care Sanitary napkin graded as CWFR (95%), CWCA (80%) PNCA (25%), PNFR (20%) respectively. Overall women satisfactorily gave the statement as Very Good about the Femi care Sanitary Napkin, in all other aspects.

REFERENCE

1. Albrecht's and Lunenschloss.J, "Non-woven bonded fabrics", Halsted press, New York P-44.
2. Anand, Kennedy.J.F, Rajendran.S (2006), "Medical and Health care Technology, Komarapalayam-638 183. Pp-82,84.
3. Anne fritz and Jennifercant (1988), "Consumer textiles", Oxward University press, Wood head publishing series in textiles, Bombay. Pp-202-203.
4. Angappan & Gopalakrishnan (1990), "Textile Testing", SSM Institute of Textile Technology, Komarapalayam-638 183. P- 52.
5. Arindam Basu,(2002) "Textile Testing-Fiber, Yarn & Fabric", SITRA, Cbe-14. P-36.
6. Billie.J.Colloex and Hele.H .Epps, (2000) "Textile Testing and Analysis", Merrill- an imprint of prentice Hall, Upper saddle river, New jersey, Columbus, Ohio.P-8.
7. Bernard. P. Corbman, (2006), "Textiles Fibre and Fabric", Mc-Graw-hill book Publishers, New York, P-68.
8. Dubey.R.C (2008), "The Text book of Bio-Technology", S.Chand company, Ramnager, New Delhi, P-386.
9. Elliot.B.Grover and Hamby.D.S (1999), " Textile Testing and Quality Control" S.Chand company, Ramnager, New Delhi, P-85.
10. Gokarneshen.N (2004), "Fabric structure and Design", New age International Publishers, New Delhi, Pp-1, 16, 28.
11. Horrocks and Anand.S.C (2005), "Hand book of Technical Textiles", Wood head Publishing Ltd, Mumbai.P-162
12. ISO-5725-2 Accuracy (trueness precision) of measurement methods and results- Part- 2. Basic method for the determination of repeatability and reproducibility of a standard measurement method, Pp-1-10.
13. ISO-9073-8, Textiles-Test method for Non-woven's- Part-8,"Determination of Liquid strike through time (Simulated Urine), Pp-1-10.
14. Jacquie Wilson (2001), "Fundamentals of Weaving", Wood head Publishing Ltd. Cambridge, England, Pp-82-89.
15. Kadirvel (2007), "Laboratory Practice in Knitting Technology", Mir. Publisher, Moscow, Pp-203.
16. Kothari.V.K. "Testing and Quality Management", Vol.I, IAFL Publications, New Delhi-110048, Pp-54-62.

17. Manak Bhavan, Bahadur Shah Zefar Marg, (2010), "Hand Book of Textile Testing", Bureau of Indian Standards, Part- II, New Delhi-110002, Pp-4-6.
18. Naik.S.D (1997), "Folk Embroidery and Traditional Handloom Weaving", A.P.H. Publishing Corporation, New Delhi, P-11.
19. Naik.S.D and Wilson.J.A (2006), "Surface Designing of Textile Fabrics", New Age International Publishers, New Delhi, P-5.
20. "Non-woven by BTRA", BTRA Monograph series, The Bombay textile Association, Bombay, Pp-1-4.
21. Prakash (2007), "Central institute for research on Cotton Technology", Adenwala road, Matunga, Mumbai.P-86.
22. Parmer M.S, (2004), "Study on Dimensional properties of Non-woven Fabrics", Man-Made Textile in India, SASMIRA 50th yrs Publication, P- 48.
23. Richard A.Scott, (2005), "Textiles for Protection", Wood head publishing in Textiles, University of Georgia USA
24. Sara.J. Kadolph (2009), "Textiles", Darling Kindersley India Pvt. Ltd, Pp- 215, 221.
25. Sara.J. Kadolph, Anna.L.Langford, Norma hollen, Jane saddler (1993), "Textiles", Mac million Publishing Company, New York, P-184.
26. Singh. V.P (2004), "Introduction to Textiles", Kalyani Publishers, New Delhi, Pp-8,109.
27. Sumant. V.D (1999), "Convection on Natural Dyes", Council of Scientific and Industrial Research, Monaharlal and Co, IIT, Delhi, P-44.
28. Sundar Ram, Krishnaiyer.K.R and Sreenivasan.S (2005), "Hand book of Method of tests for Cotton Fibers, Yarns and Fabrics", Part- II. P-252-256.
29. "Textiles- Test Methods for Non-Woven", ISO 9073-13, First edition, International Standards.Pp-92, 96.
30. Wilson (2001), "Hand Book of Textile Design- Principle of processes and practice", Wood head Publishing Ltd, Cambridge, England, P-82.
31. Wynne.A(1998), "Effects of Organism and Weather" AATCC- Test Methods, Pp-240-245.
32. "Antibacterial Activity Assessment of Textile Materials: Parallel Streak Method", TM-147-2011, AATCC Technical Manual -2012. P-43
33. "Absorbent article for night time use" (2011), Hygiene, April, SITRA, Cbe, P-58.
34. "Antibacterial Activity Assessment of Textile Materials: Agar Plate Method" TM-90-2011, AATCC Technical Manual -2012. Pp-352-355.
35. "Antibacterial Finishes on Textile Materials: Assessment of Antibacterial Activity" (Quantitative Method), TM-100-2004, AATCC Technical Manual -2012.P-356
36. "Antifungal Activity, Assessment on Textile Materials: Mildew and Rot Resistance of Textile Material", TM 30- 2004, AATCC Technical Manual -2012.P-342.
37. Alistair's. Rig and Subbash C.Anand,(2010) Medical Textiles, SITRA, Cbe.P-15
38. Amsamani (2007), " Development of Eco friendly Herbal Antimicrobial Finish on Cotton Fabric using Aloe Barbadosis Mailler" Man- Made Textiles in India, No-4, April -2010, P-146.
39. Anon. (2000). Case Study Project 10. "In: Vetiver Grass: Vetiver and the Environment", Thailand, ORDPB, Bangkok. Pp-78-81.
40. Arunraj, (2011), "Technical Textile and Non-woven Excellence" Issue-2230-8733, Vol.2 No.4, July-September, SITRA, Cbe. P-32.
41. Avinash Mayekar (2009), "Disposable Textiles- Future of India", Non-woven and Technical Textiles, Vol.2, N0.1, January- March (Quarterly), P-9.
42. Chomchalow N. 2001. The Utilization of Vetiver as Medicinal and Aromatic Plants with Special Reference to Thailand. Tech. Bull. No. 2002/1, PRVN / ORDPB, Bangkok, Thailand. Pp-86-88

43. Deepti Gupta (2004), "Mechanism of Dyeing, Synthetic Fibers with Natural Dyes", *Colourage*, No.3, P-23.
44. Deepti Gupta, Sudhir Kumar Khare and Ankur Laha (2004), "Antimicrobial Properties of Natural dyes against Gram- negative bacteria Colouration Technology", *April, Medical Textiles, SITRA, Cbe.* Pp-76-78.
45. [45] Edward Menezes and Mrinal Choudhari (2007), "Special finishes and Effects", *AATCC Review*, &, No.3, March, Pp-43, 44.
46. "Fighting Fungi- A New generation of Antifungal Products" (2012), *AATCC-Review- A journal for "Textile Professionals*, Vol.12, No.3, May- June, P-30.
47. Freddy Gustavo Rewald, "Nonwovens in Automotive Uses", *Nonwovens Industry*, 30, March 2008. P-6.
48. Gauri Goel and Alka Goel (2012), "Outstanding comfort with Polyurethane fibers", *Asian Textile Journal*, Vol.21, January, No.1, Pp-42-45.
49. Geoff fisher (2012), "Hydro entangled Non-woven Fabrics for Absorbent Articles, *Medical Textiles, International News letter Ltd*, March, No.5 P-9.
50. Giustiniani.A, Sharma.N.K (2009), "Design and Structure of composites Non-woven", *Non-woven and Technical Textiles*, Vol.2, N0.3, July- September (Quarterly), P-25-32.
51. Gopal.D (2006), "Anti microbial finishes", *Man-made Textiles in India*, October, Vol.3, No.5, Pp-372-377.
52. Gopalakrishnan.D (2006), "Antimicrobial Finishes", *Man- Made Textiles in India*, Vol.49, No.10, Pp-372-373.
53. Juliard C. (2002). *Vetiver Grass as an Ornamental Decorative Plant*. In: *Vetiver Network Discussion Board*, <dickgrimshaw@vetiver.org>, Feb.2002
54. Chellamani.K.P. et.al. (2012), *Medical Textiles*, *Asian Textile Journal* Vol.21, No.6, April, P-57.
55. Kamat and Sawant, (1998), "Dyeing with cellulosic Fibers using reactive dyeing", *Colourage*, *Colour Publication Pvt.Ltd*, Mumbai, July, Vol.29, No.7, P-61.
56. Keskar.V.H, Jothi Aggarwal, (2005), "Renewable Antimicrobial Finish for nest to skin garments", *Man-made textiles in India*, No.1, P-51.
57. Krishnaveni.V ,Amsaveni.S (2010), " Development of Indian Acalypha herbal antimicrobial finishing of garment for skin diseases", *Non-woven & Technical Textiles*, April –June 2010, Pp-20 -25.
58. Kavery bai. and S Mamatha.G,Hedge (2011), " Antibacterial activity of Garcinia Indica dye", *Journal of the Textile Asociation*, Vol.72, No.4, November –December, P-238.
59. Narayanan.S.S, (2012), "Importance of cotton as a crop and commodity in 21st century", *Asian Textile Journal*, Vol.21, January, No.1, Pp-49-51.
60. Naylor (2001), "The Future of Circular Knitting Productivity", *knitting views*, *Vanker Publications*, New York, March / April, Vol.34, Issue No.4, P-10, P-167.
61. "News points", "BBA Nonwovens", *Nonwovens Industry*, 28 April 1997, P-80.
62. "Non-woven International News", (2012), *Asian Textile Journal*, Vol-21, No.5. May, P-13.
63. Parmer.M.S (2004), "Comparative study on Organic and Conventional cotton", *Asian Textile Journal*, *GPS Kwatra Publications*, Mumbai, June, P- 35.
64. Parthiban, (2012), "European Quality control and Texting Equipments", *Asian Textile Journal*, April, Vol.21, No.4,
65. Pasupathi.R and Kadirval.S (2007), "The Quality of various count Cotton Yarns", *Asian Textile Journal*, *GPS Kwatra Publications*, Mumbai, June, P- 53.
66. Patel (2004), "Inverse relation in fabric", *Indian Journal of Fiber and Textile Research*, *National Institute of Science and Communication and Information resources*, CSIR, New Delhi, March, Vol-28, Pp-50,54.

67. Patel.B.H and Tandel M.G, (2004), "Antimicrobial Finish in Cotton fabric by Natural Extracts", Man-Made Textiles in India, Dec, P-473.
68. Patel.B.H, Patel.K.J, Naik.J.A and Bhavsar.A.M. (2004), "Dyeing and Antimicrobial finishing of Cotton", Man-Made Textiles in India, 47, No.11, Pp-426,427.
69. Philip.A.Smith, (2010), Technical fabric structure", Non-woven Fabrics, P-34.
70. Ragunathan.K (2012), "Absorbent core has concentrically arranged Absorbent Regions", International News letter Ltd, Medical Textiles, January, P-15.
71. Rajkumkar , Ibrahim.M, Khan .A.A (2007), " Antimicrobial Activity of Sapindus Mukorossi and Rheum emodi extracts against H Pylori" World journal of Gastroenterology,12(44), Nov,P-7-13.
72. Ramachandran.T, Rajendrakumar, R.Rajendran (2005), "Antimicrobial Textiles- An Overview", Textile Industry of India, Vol-15, March, P-17.
73. Sakthivel.S, "Technical Textiles and Non-woven- Application of Protective Textiles", The Indian Textile Journal, Vol.122, No.9, June, P-81.
74. Sakthivel.S.et al, (2012) "Development of Non-woven Composites using reclaimed fibers", Asian Textile Journal, Feb, Vol.21, No.2, P-43.
75. Sampath.V.R (2003), "Functional garments", The Indian Textile Journal, Jan, Pp-51, 52.
76. Saravanan.S (2012), "Advanced Textile Composites: Types and Application", Non-woven and Technical Textiles, Vol.4, N0.1, April- June (Quarterly), P-29.
77. Sathyanarayanan.M.P, Bhat N.V, Kokate S.S (2010), "Antimicrobial Finish for Cotton Fabric Herbal Products", Indian Journal of Fibre and Textile Research, Vol-35, No.1, March, P-50.
78. Sekar.N.Dec (2001)," Antibacterial finish on cotton Developments", Colourage, Vol.7, No.48, Pp-37-39.
79. Shakthi sharmila.S (2010) " Eco friendly functional finishes for curative footwear applications", Asian Textile Journals, May, vol-4,No.3, Pp-38-41
80. Shanmugasundram (2007), "Antibacterial finish in Textiles", The Indian Textile Journals, August, P-56.
81. Shefali Massey,(2008)," clothing Hygiene: Its effect on insulation and comfort properties", Man-made textiles in India, May,Vol-2,Pp-172-175.
82. Simon N. 2003. Medicinal vetiver. Proceedings of the Third International Conference on Vetiver and Exhibition, Guangzhou, China.P-65
83. Srikrishnan.M.R.et.al, Textile and Apparel Testing Instruments, Indian Journal of Fiber and Textile Research, National Institute of Science and Communication and Information resources, CSIR, New Delhi, March-2011, Vol-28, Pp-57.
84. "Technical Manual of the AATCC", (2012), Vol.87, AATCC.
85. Oengaew U. Thiramonngkol V, and Teeprasan S,(2003). The vetiver grass ceramic pots. Proceedings of the Third International Conference on Vetiver and Exhibition, Guangzhou, China.
86. Veera Desai Marng (2011), "Medical Non-wovens for Barrier protection" Asian Technical Textiles, Vol.5,No.4, October- December(Quarterly),P-27.
87. Vellingiri.K. Parthiban.M and Viju.S, (2012), "Versatile application of Non-woven - an overview", Asian Textile Journal, January, Vol.21, No.1, P-33.
88. White Curtis (2009), "Medical Textiles", Nonwoven and Technical Textiles, Vol-2, No.2, P: 9-11.

Model Based Calibration for Off-Road Vehicles

Benjamin Shiloh Davidson, Neelakrishnan S and Abhirama Sastry D.V.V.S.S

Department of Automobile Engineering, PSG College of Technology Coimbatore, Tamil Nadu, India

ABSTRACT

The calibration of a new engine is a critical step in its development. This is a costly, time-consuming process that necessitates specialist understanding. This paper explains how to build a combustion model and how to optimise diesel engine parameters in order to produce a model-based calibration. To execute a Design of Experiments using the Taguchi Method, this model employs operating points from the engine speed vs engine torque map as a reference, the paper takes into account five input parameters: boost pressure, fuel pressure, main injection timing, pilot one quantity, and pilot one timing. The work focuses on building a methodology rather than a collection of final models; the key discovery with relation to input data is that some operational points do not allow for any variability, resulting in data that is uninformative for regression algorithms. The model-based calibration using taguchi method is to generate Global and local optimization points. The primary goal of this research is to reduce emissions to meet the standard emission norms and also to reduce the testing time on real engine in order to reduce cost using DoE methods. "calG" is the calibration tool that we have used for the calibration and validated based on the Design of experiment (Taguchi) Method.

Indexterm—engine calibration, taguchi method, design of experiments (DoE) method.

I. INTRODUCTION

Cross-country or off-road vehicles require several characteristics to be ready to run off the beaten path: they must have a coffee ground pressure, they must be compelled to keep their wheels or tracks on the bottom in order to avoid sinking into soft ground, they must have ground clearance in order to avoid becoming stuck with obstructions, and they must be compelled to keep their wheels or tracks on the bottom in order to avoid sinking into soft ground, and they must be compelled to keep their wheels or tracks on the bottom. On wheeled vehicles, this is accomplished by combining a good balance of big or larger tyres with tall and flexible suspension. Wide tracks and flexible suspension on the road wheels let half-track cars achieve this. The decision between wheels and tracks is one of value and quality. The cost of providing and maintaining a half-track drivetrain is higher. Wheeled drivetrains are less expensive and give the fastest speed. The cross-country capabilities of the half-track powertrain is greater.

ORVs have also been blamed for generating a lot of pollution in locations where there isn't usually any. Old-style two-stroke engines, according to the US Forest Service, can cause disability and stress in addition to noise pollution (although certain area units are still in use, they are no longer a part of contemporary cross-country vehicles) "Indirect waste product deposition from two-stroke snowmobile engines will occur in the top layer of snow and afterwards in the related surface and spring water" and "Indirect waste product deposition from two-stroke snowmobile engines will occur in the top layer of snow, followed by surface and spring water. The Environmental Protection Agency of the United States adopted emissions standards for all-terrain vehicles in 2002, which, among other things, "When fully implemented in 2012, are expected to prevent nearly 2 million tonnes of pollution from being released annually, the equivalent of removing pollution from nearly 32 million cars.



Fig.1. Benz off-road truck [11]

These vehicles include any vehicle that can drive on and off a paved or gravel surface. Tractors, cranes, backhoes, and golf carts are examples of off-highway vehicles, which are characterised by their huge tyres with deep, wide treads, adjustable suspension, and perhaps caterpillar tracks.

Off-road vehicles have a large fan base, thanks to their skilfulness. Sport cross-country vehicles are used in a variety of races. The most typical purpose of these vehicles is to look for things that aren't on the ground. Access to rough and low-traction pathways and forest roads is possible with the use of vehicles with greater clearance and better traction.

II. EMISSIONS AND CALIBRATION

A. Emission Standards

- BS II - III On September 21, 2006, outflow guidelines for diesel developing apparatus were adopted.
- The guidelines were divided into two categories.
- BS II— These gauges are based on the EU Stage I standards, but they also include smaller motors that aren't covered by the EU Stage I criteria...
- BS III— These measures are based on the specifications...

The Republic of India (Trem) agricultural tractor standards come into effect in 1999. Starting with the Republic of India (Trem) Stage III A, emission regulations for agricultural tractors were harmonised with those for construction machinery for several engine classes.

On March 5, 2018, the Republic of India enacted Stage (CEV/Trem) IV - V emission standards for diesel non-road engines used in construction and agricultural equipment. The emission requirements for BS (CEV/Trem) IV were matched with EU stage IV standards, whereas the emission requirements for BS (CEV/Trem) V were aligned with EU stage V standards.

Engine performance depends on precise management of an outsized variety of engine management parameters. for instance, today's engine management units (ECUs) modify multiple injections per engine cycle, every with totally different amounts of fuel, adding a lot of parameters to the matter. Engine standardization involves calibration these variables et al. to maximize performance across the operational vary of engine speeds and hundreds.

Table I. Emission Norms For Off-Road Vehicles

EMISSION	CATEGORY	EFFECT	CO	HC	NOx	PM
BS III	37<P<56	01-APR-2010	5.0	4.7 (HC+NOx)		0.025
	56<P<75	01-APR-2011	5.0	0.19	0.4	0.025
	75<P<130	01-APR-2011	5.0	4.0 (HC+NOx)		0.025
	130<P<560	01-APR-2011	5.0	4.0 (HC+NOx)		0.025
BS IV	37<P<56	01-OCT-2020	5.0	4.7 (HC+NOx)		0.025
	56<P<130	01-OCT-2020	5.0	0.19	0.4	0.025
	130<P<560	01-OCT-2020	3.5	0.59 (HC+NOx)		0.025
BS V	37<P<56	01-APR-2024	5.0	4.7 (HC+NOx)		0.015
	56<P<130	01-APR-2024	5.0	0.19	0.4	0.015
	130<P<560	01-APR-2024	3.5	0.19	0.4	0.015

Emission Curve Details for the AL engine:

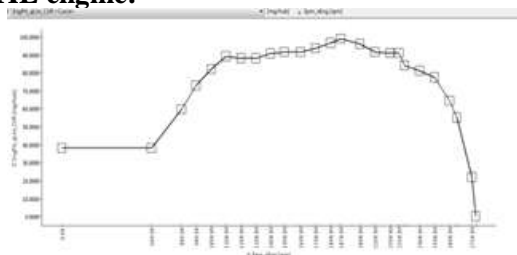


Fig. 2. Ashok Leyland - H series BS III engine

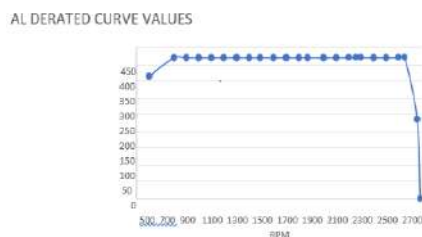


Fig. 3. Ashok Leyland – Derated curve

B. Design of Experiments (Doe)

The Design of Experiments (DoE) methodology addresses this drawback by generating take a look at plans that with efficiency verify the character of the engine responses. we've used Taguchi DoE methodology for generating native points.

Taguchi's methodology

Taguchi strategies are used in the form of mathematical strategies, often known as strong style strategies, created by 'Genichi Taguchi' to improve the quality of factory-made products, and more recently used to engineering, biotechnology, marketing, and advertising. Professional statisticians have praised the aims and improvements brought about by Taguchi methods, particularly Taguchi's invention of styles for detecting variation, but have questioned the incompetence of a number of Taguchi's suggestions.

The procedure is divided into three stages:

- System design
- Parameter (measure) design
- Tolerance design

Five parameters are considered as the emission constrains for the calculation of emission of the engine. The parameters are:

1. Boost pressure
2. Fuel Pressure
3. Pilot 1 timing
3. Main Injection Timing
4. Pilot 1 Quantity

C. Test Data Collection

The test data details are collected from the INCA software available at the lab, the fuel consumption Map is taken, and the parameters are measured.

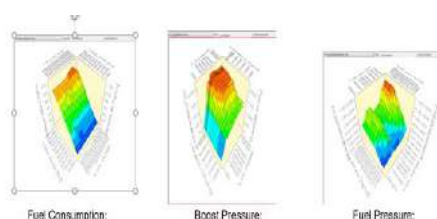


Fig. 4. INCA details

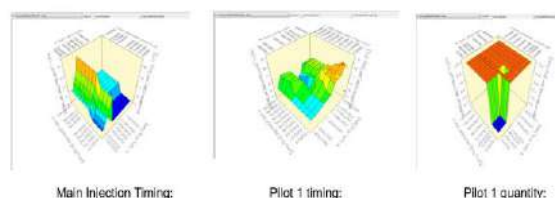


Fig. 5. INCA details

Operating Point

An Operating Points (OP) are points in the operating region that are defined by their engine speed and torque. Because the derated engine speed vs. engine torque map is taken into account. There are a total of 494 operational points, including repeating points where the engine speed and torque values are repeated.

Number of parameters = 5

Number of levels = 5

D. Python Scripting

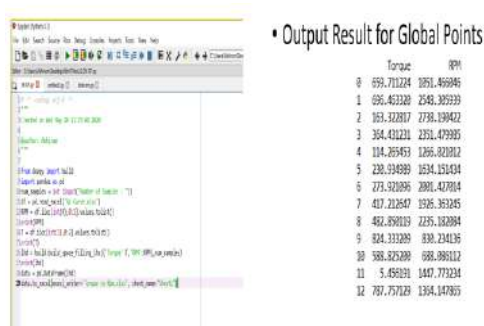


Fig. 6. Python script and result for the global points generation

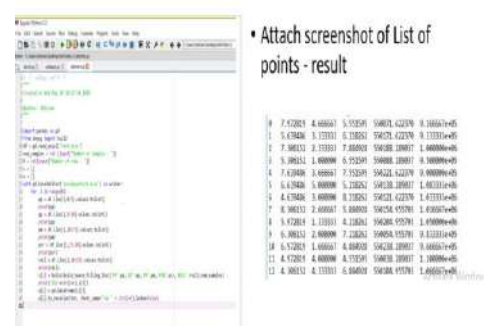


Fig. 7. Python script and result for the local points generation

E. Engine Data Simulation

1) Operating Zone Identification: The operating Zone Identification gives the weightage of the NOx and Soot emissions for which the input data are:

- Steady State Data
- Transient State Data

OUTPUTS:

- Percentage of time this engine contributes throughout steady-state and transient emission cycles
- The engine's contribution to NOx during steady-state and transient emission cycles in percent.
- The engine's contribution to NOx during steady-state and transient emission cycles in percent.
- This engine's contribution to PM during steady-state and transient emission cycles in percent.

2) Optimization of the engine: During emission optimization, NOx and PM trade-off for diesel engines is very critical to achieve the target emissions. CalG uses real world data to make engine simulation model for Raw NOx and Raw PM (Soot) and match with the same real-world data to see the correlation and find the acceptable tuning zone for simulations. With this way, the effect of change in the control variables on raw NOx and raw PM (Soot) can be easily simulated in the acceptable tuning zone

CalG Engine out optimization is based on regression modelling of engine raw NOx and raw soot for engine out emissions. This takes the effect of various parameters which are responsible for engine NOx and soot. We have the option to select the various parameters which will affect the Engine out NOx and soot in CalG user selection window. With this given input, CalG builds engine NOx & soot model and provides data to estimate the coefficients. Now we should perform the regression analysis using statistic tools and upload coefficients to CalG.

INPUTS:

- Engine Part throttle performance data covering the total operating zone and the input parameter variations at each point
- NOx coefficients
- Soot Coefficients

- Emission cycles data.

INPUT PARAMETERS:

- Engine speed
- Torque
- Raw NOx (ppm)
- Raw PM (FSN)
- Input parameters which effect NOx and Soot in the engine
- NOx coefficients
- Soot coefficient

OUTPUT FROM CALG:

- Plot of NOx model validation
- Plots of Soot model validation
- Calibration window to optimize control variables
- Add points of optimization
- Change Control factors
- Observe change in emissions
- We can visually identify the close approximation zone for NOx model and Soot model.
- The zones within $\pm 3\%$ are taken as close approximation zone

Engine Speed	Torque	Fuel pressure	Max injection timing	Intake Manifold pressure	Peak mass air flow	Air/Fuel ratio	Estimated NOx	Estimated Soot
1500	150	1824	15.3	1406	127	18.56	10455	2.3
1500	147.5	1800	15	1370	101	18	12131	2.1
1500	145	1704	15.3	1374	113.75	18.51	12157	2.19
1500	142.5	1624	15.3	1374	113	18	10717	1.76
1500	140	1400	14.7	1415	113	18	14131	1.79
1500	137.5	1318	14.7	1375	114	18	11906	1.81
1500	135	1236	14.7	1376	113	18	9747	1.74
1500	132.5	1154	14.7	1376	114	18	7588	1.67
1500	130	1072	14.7	1376	114	18	5429	1.6

Emission Cycle	Cycle NOx (g/kwhr)		Cycle Soot (g/kwhr)		Options
	Present	Optimized	Present	Optimized	
Steady State	7.288	6.987	0.161	0.1381	Export to excel
Transient State	1.0544	0.8879	0.0465	0.2931	Default optimization

Fig. 9. Engine out optimization – target control variables (For BS II norms)

Engine Speed	Torque	Fuel pressure	Max injection timing	Intake Manifold pressure	Peak mass air flow	Air/Fuel ratio	Estimated NOx	Estimated Soot
1500	150	1824	15.3	1406	127	18	14175	3.3
1500	147.5	1780	15	1370	101	18	11618	2.3
1500	145	1704	15.3	1374	113.75	18	10117	1.61
1500	142.5	1624	15.3	1374	113	18	8617	1.31
1500	140	1400	14.7	1415	113	18	14131	1.79
1500	137.5	1318	14.7	1375	114	18	11906	1.81
1500	135	1236	14.7	1376	113	18	9747	1.74
1500	132.5	1154	14.7	1376	114	18	7588	1.67
1500	130	1072	14.7	1376	114	18	5429	1.6

Emission Cycle	Cycle NOx (g/kwhr)		Cycle Soot (g/kwhr)		Options
	Present	Optimized	Present	Optimized	
Steady State	7.2889	6.815	0.161	0.1346	Export to excel
Transient State	1.0549	0.8717	0.0476	0.2937	Default optimization

Fig. 10. Engine out optimization – target control variables (For BS III norms)

III. RESULT

The real time simulation environment to achieve the target emission factors calG tool was more helpful.

The Global and Local Operating points are reduced using Taguchi Method. Therefore, the total number of operating points have been reduced from 2350 Operating points to 395 operating points by implementation of Taguchi Design for Operating point’s generation.

The target value of NO_x and PM (Soot) are achieved with help of calG tool. To achieve real time simulation environment and to achieve the target emission factors calG tool was more helpful.

IV. CONCLUSION

The Conceptual study of taguchi for engine calibration for reducing time and utilizing the resources (CalG) which is based on the different approaches that helps us in finding the accurate data for the calibration of all the parameters within short time. With the calibration the engine response is optimized by comparing the same with the traditional method and also with the emission constraints. The Design of Experiment (Taguchi method) is used as the offline tool for engine calibration.

REFERENCES

1. Wipke, K.; Cuddy, M.; Burch, S. Advisor 2.1: A user-friendly advanced powertrain simulation using a combined backward/forward approach. *IEEE Trans. Veh. Technol.* 1999, 48, 1751–1761.
2. Guzzella, L.; Sciarretta, A. *Vehicle Propulsion Systems*; Springer Verlag: Berlin, Germany, 2007.
3. Gaevsky, V.; Ivanov, A. *Theory of Ground Vehicles*; MADI: Moscow, Russia, 2007.
4. Kravets, V. *Theory of Vehicles Handbook*; University of Nizhni Novgorod, NNSU: Nizhni Novgorod, Russia, 2007.
5. Bosch, R. *Bosch Gasoline-Engine Management*; Bentley Pub: Cambridge, MA, USA, 2004. 15. Stone, R. *Introduction to Internal Combustion Engines*; Macmillan: Basingstoke, UK, 1985.
6. Jimenez-Palacios, J. *Understanding and Quantifying Motor Vehicle Emissions and vehicle Specific Power and Tildas Remote Sensing*. Ph.D. Thesis, Massachusetts Institute of Technology, Cambridge, MA, USA, February 1999.
7. <https://law.resource.org/pub/in/bis/S13/is.iso.8178.4.2007.pdf>
8. https://en.wikipedia.org/wiki/Off-road_vehicle#Technical
9. <https://dieselnet.com/standards/cycles/nrtc.php>
10. Stein M, "Large sample properties of simulations using Latin hypercube sampling", *Technometrics* 1987;29(2):143–51.
11. https://roadstars.mercedes-benz.com/en_GB/magazine/transport/02-2019/mercedes-benz-offroad-trucks-in-the-desert.html
12. Karsten ROEPKE, "Design of Experiments for Engine Calibration", IAV GmbH, Carnotstrasse 1, Berlin, Germany, 1-2, 2014. https://www.jstage.jst.go.jp/article/sicejl/53/4/53_322/_pdf.
13. Fire Software help, AVL, version 2013.2; DoE and optimization; 2014.
14. Renninger P., Aleksandrov M, "A new method to determine the design space for model based approaches", 2008, DoE in engine development II, Berlin, Germany.
15. Conover, WJ, "On a better method of selecting values of input variables for computer codes", 1975.
16. https://en.wikipedia.org/wiki/Design_of_experiments
17. Manny Uy , Jacqueline K.Telford "Optimization by Design of Experiment Techniques" , 2009.
18. Sall, J., Creighton, L., and Lehman, A., "JMP Start Statistics - the Statistical; Discovery Software, Version 7.0", Third Edition, , SAS Institute, Inc., 2007.
19. Uy, O. M., Hardesty, R. Jr., Fogle, J and Moor, A., "Use of Design of Experiments Techniques to Investigate Resistance Change of Chip Resistors in MESSENGER", SPIE International Conference, San Diego, CA, 21-25 August 2006.

Shear Capacity of Reinforced Concrete Beam with Vertical Stirrups

Ramesh Babu G and Sivakumar C G

Department of Civil Engineering, PSG College of Technology, Coimbatore, India

ABSTRACT

In RC Beams, providing shear reinforcements varies the shear strength of the concrete in more unpredictable manner owing to the complex load transfer mechanism through the beam resulting from the combination of concrete and stirrups. In IS code method, the combined effect in concrete resulting from the use of stirrups and other parameters influencing the shear capacity is not considered. Artificial Neural Network (ANN) will be useful to infer a function from observations and finds application where the hand computations are impractical which involves complexity with large data. ANN model requires a huge set of Shear Strength observation data that is comparable to the data of the beam whose shear strength is to be predicted using ANN. The data required for ANN model training are obtained from previous research publications. The ANN model trained is validated by comparing its Shear Strength with the Shear Strength obtained from Experimental testing. Three beams with different shear span to that of effective depth ratios (a/d ratio) are tested. The results obtained from the experiments are compared with the results obtained from ANN model and IS code method. The IS code method is found to be more conservative while the ANN model gives fairly accurate results. The artificial neural network model for predicting the shear capacity is found effective when compared to the IS code method, which is more conservative. The ANN model is also used to observe the weight of the parameters influencing the shear capacity of reinforced concrete beam which is given in IS code method.

Keywords: Shear Strength, RC beam with Stirrups, Artificial Neural Network, ANN model.

1. INTRODUCTION

The additional shear capacity of reinforced concrete beam with the stirrups is calculated based on the yielding capacity of the stirrups that are perpendicular to the shear crack. But in reality, providing shear reinforcements varies the shear strength of the concrete in more complex way due to the combined effect.

Artificial Neural Network is a computational approach that is self-learning and trained. It finds its application in areas where obtaining the solution becoming difficult when using computer program.

ANN model is created using data from previous research publications. It is then validated with experimental shear capacity results. The experimental investigation includes two-point load test on three beams having different a/d ratio. The shear capacity is also calculated using IS method. The Shear capacity from all the three methods (IS method, ANN model and Experimental test) are compared.

2. ANALYTICAL INVESTIGATION

2.1 INPUT PARAMETERS

Beam width in mm

Effective depth of beam in mm

Ratio of shear span to effective depth

Tension reinforcement percentage

Yield strength of tensile steel in MPa

Concrete compressive strength in MPa

Compression steel area in mm^2

Yield strength of compression steel in MPa

Stirrup area in mm^2

Stirrup spacing in mm

Yield strength of stirrup in MPa

2.2 OUTPUT PARAMETERS

Shear capacity of RC beam in kN

2.3 ACTIVATION FUNCTION

'tansig' function is used as the activation function for the hidden layers

2.4 TRAINING METHOD

The ANN model is trained with Levenberg-Marquardt method (stable and fast). The input parameters and output are tabulated in table 1 and table 2 respectively.

2.5 SIMULATING TRAINED ANN MODEL

Table 1: ANN input parameters

Input Parameter	Beam1	Beam2	Beam3
Width in mm	150	150	150
Depth in mm	156.5	156.5	156.5
a/d ratio	2.87	3.15	4.15
Tensile steel ratio in %	3.27	3.27	3.27
Yield of Tensile Steel in MPa	415	415	415
fck in MPa	32.046	34.444	33.136
Area of compression steel in mm ²	981.25	981.25	981.25
Yield - compression steel in MPa	415	415	415
Area of stirrup in mm ²	28.26	28.26	28.26
c/c spacing of stirrups in mm	115	115	115
Yield of Stirrups in N/mm ²	250	250	250

The output is obtained from trained ANN model for the above input parameters as follows,

Table 2: ANN output

Shear Strength in kN	104.37	97.68	91.28
----------------------	--------	-------	-------

3. EXPERIMENTAL INVESTIGATION

3.1 BEAM DESIGN

The RC beam is designed such a way that the beam always fails by shear when it is subjected to two-point loading. Table 3 gives the beam details. Figure 1 gives the reinforcement details of the beam.

Table 3: Reinforced Concrete beam details

Compression	B (mm)	D (mm)	Reinforcement	Stirrups
2 # 25 mm dia bar	150	200	2 # 25 mm dia bar	2 legged 6 mm dia bar spaced at 115 mm c/c

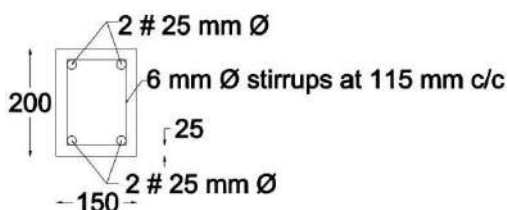


Fig. 1: Reinforcement details of the specimen

3.2 CONCRETE

The mix proportion details for the reinforced concrete beam is shown in table 4.

Table 4: Proportion of mix for M30 grade concrete

Materials	Quantity (kg/m ³)
Cement	394
Fine Aggregate	680.17
Coarse Aggregate (20 mm)	1240.062
Water	210.89

3.3 CASTING ON RC BEAMS

A total of 3 RC beams were used of 1800 mm length. Figure 2 shows the picture of beams casted.



Fig. 2: Casting of Beams

The hardened concrete is then cured for 28 days before testing.

3.4 TEST SETUP

Load test on reinforced concrete beams are conducted under two-point loading. The loads are applied in increment of 2 kN using hydraulic jack until failure of the beam. Deflection is measured at the centre of the span. The experimental setup for beam testing is shown in figure 3.



Fig. 3: Experimental test setup for beam testing

3.5 RESULT

The experimental results are given in table 5.

Table 5: Experimental results

Beam No.	a/d ratio	Ultimate load in kN
1	2.87	202
2	3.51	197
3	4.15	180

4. COMPARISON OF RESULTS

Figure 4 shows the shear strength between IS code method, experimental investigation and ANN model.

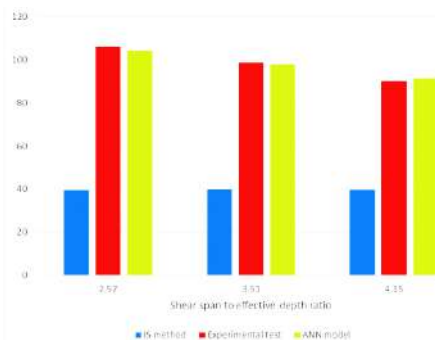


Fig. 4: Shear strength from various methods

5. CONCLUSIONS

- Increase in a/d ratio decreases the Shear capacity of the beam
- The IS code method for calculating Shear capacity is more conservative
- IS code method doesn't take into account some of the Shear capacity influencing parameters
- ANN model provides better prediction for the Shear capacity
- The weights of the input parameters are as follows based on ANN weights,

Input Parameter	Weight factor (max - 10)
Width in mm	1
Depth in mm	5

Shear span to Depth ratio	3
Tensile Reinforcement ratio in %	7
Yield - Tensile Steel in MPa	3
fck - concrete in MPa	6
Compression steel area in mm ²	4
Yield - compression steel in MPa	4
Area of stirrup in mm ²	9
c/c stirrup spacing in mm	10
Yield strength of Stirrups in MPa	6

REFERENCES

1. Abdul Ghaffar, Afzal Javed, Habib ur Rehman, Kafeel Ahmed and M Ilyas, 2010, "Development of Shear Capacity equations for Rectangular Reinforced Concrete Beams" Pak J. Engg& Appl. Sci.-6(2010):1-8
2. Bertha Guijarro-Berdinas, Oscar Fontenla-Romero and Amparo Alonso-Betanzos, 2006, "A very fast learning method for Neural Networks based on Sensitivity Analysis" -Journal of Machine Learning Research 7(2006) 1159-1182
3. Cladera. A, Mari.A.R ,2004, "Shear design procedure for reinforced and high-strength concrete beams using artificial neural networks. art II: beams with stirrups" Engineering Structures-26(2004):927-936
4. Karl-Heinz Reineck, Evan Bentz, BirolFitik, Daniel A. Kuchma, and Oguzhan Bayrak, 2014,"ACI-DAfStb Databases for Shear Tests on Slender Reinforced Concrete Beams with Stirrups"-111(2014), pp1147-1156
5. Mansour.M.Y, Dieleli.M, Lee.J.Y, Zhand.J, 2004,"Predicting the shear strength of reinforced concrete beams using artificial neural networks" Engineering Structures-26, pp781-799
6. Rafiq.M.Y, Bugmann.G, Easterbrook.D.J, 2001, "Neural network design for Engineering applications" Computers and Structures-79(2001):1541-1552
7. Sundaresan. R and Appa Rao. G, 2012, "How uniformly the Indian codes predict the shear strength of concrete beams?" Journal of Structural Engineering-39(2012): 167-177
8. IS 10262:2009," Concrete Mix Proportioning" (First Revision), Bureau of Indian Standards
9. IS 4031: Part – 11 (1988), "Methods of physical tests for hydraulic cement-Determination of Density", Bureau of Indian Standards
10. IS 4031: Part – 5 (1988), "Methods of physical tests for hydraulic cement-Determination of Initial and Final setting times", Bureau of Indian Standards
11. IS 2386: Part – 3 (1963), "Method of test for aggregates for concrete – Specific Gravity, density, voids, absorption and bulking", Bureau of Indian Standards
12. IS 516 (1959), "Method of test for Strength of Concrete", Bureau of Indian Standards
13. IS 456:2000," Plain and Reinforced concrete code of Practice" (Fourth Edition). Bureau of Indian Standards
14. IS 383 (1970), "Specification for Coarse and Fine aggregates from natural sources for concrete", Bureau of Indian Standards

Planning of Bus Rapid Transit System for Coimbatore City Using GIS

Mohammed Insaf Z, Sivakumar C G and Elangovan K

Department of Civil Engineering, PSG College of Technology, Coimbatore- 641004, India

ABSTRACT

To implement BRT system, data regarding vehicle growth, air pollution, car ownership, shares of public transport are collected. Road wise traffic data was collected from TNSTC, Coimbatore City limit fatal data was collected from Commissioner Office, PPD data is collected from various sources. These collected data are overlaid by considering major roads in the city by using Arc View software and the best route is found. By considering present road width of various roads in the city, road elements for BRT system is recommended by the study of other BRT systems in India and as per IRC recommendations.

1. INTRODUCTION

1.1. Introduction to Bus Rapid Transit System

Indian cities are addressing the increase in need for urban mass transit mobility. Roads are designed based on number of users in one hour in a direction. The bus rapid transit system (BRTS) carry 20,000 passengers in one hour in a direction in a single dedicated lane. The project on this system is framed such that no extra cost to commuters is planned while improving service.

One of the major thrusts of the BRTS is to decrease the commuter's dependency on private vehicles and increase the shares of public transport to make urban transportation system environmentally sustainable. Major cities like Delhi, Pune, Ahmedabad, Bhopal, Indore, Rajkot, Jaipur, and Vishakapatnam have implemented BRT system. A BRTS could be developed either by altering the existing infrastructure, vehicles, etc. or by constructing completely dedicated new roads and buses. To meet transit demand, buses or specialized vehicles on roadways or dedicated lanes are used in the system to efficiently transport passengers to their destinations quickly.

Sumalatha and Eshrak[7] focused on a method which selects corridors for introduction of BRTS in Hyderabad. This method deals with the increasing traffic congestion and car ownership, lack of road and transport infrastructure and gradual deterioration of bus transit system. Using data like traffic count, passenger ridership etc., they proposed the BRT system which can be customized easily to fulfill the needs of the community and incorporate low-cost technologies that yields in minimum congestion and more number of passengers.

Vimal Gahlot and B.L. Swami [8] proposed a BRT for the city of Jaipur using GIS. The model objective was to choose the BRT corridor based on spatial distribution of transit trips in the city. To identify the high ridership based BRT corridor, the model uses the demographic, transit trip and land use characteristics of the city. For better understanding, the model provides graphical maps regarding policy making and transit demand pattern using GIS.

1.2. Features of BRT system:

1.2.1. Segregated bus lane:

The most important feature of the system is physically segregated lanes for buses, private motor vehicles and non motorized traffic such as pedestrians and bicyclists.

Segregated lanes help in increasing the average speed of all vehicles and improving the overall traffic flow. The traffic situation can be alleviated by implementing efficiently this system to cause citizens to change their modes of travel from car to bus.

1.2.2. Bus Stations:

The options for bus stations starting from ordinary stops having shelters to complex stations and intermodal terminals containing several amenities, providing platform level boarding and bus information systems (ITS).

1.2.3. Vehicles:

Double doored hybrid A/C buses with flat floor deck were used and options like Automated Vehicle Locator System (AVLS) and GPS devices mounted as primary source of data for tracking purposes[2].

1.2.4. Fare collection:

The option for fare collection ranges from traditional pay-on-board methods to pre-payment method using electronic fare media (e.g., smart cards)

1.2.5. Service and Operational Plan:

A design plan is required to meet the needs of the population and employment centers in the service area and matches the demand for service.

1.2.6. Cost:

The BRT system is quite cost effective since setting it is much more economic as compared to any MRT System, moreover, the maintenance and operational expenses are quite nominal, thus making it a cheap mode of transportation[5].

1.2.7. Other Basic Features:

1. HI-Tech fare verification system, Low-emission vehicle technologies [1].
2. System management through a centralized control center, utilizing ITS applications such as automatic vehicle location.
3. Real-time information displays, clear route maps and signage are visibly placed within stations and vehicles.
4. Low-cost infrastructure elements which increases the speed and reliability of bus service that include bus turnouts, bus boarding points and curb realignments.

2. NEED OF BRTS IN COIMBATORE CITY:

Need of BRTS in Coimbatore city is found by considering the following factors.

2.1. VehicleGrowth:

Total number of vehicle that registered in past three years were collected from Coimbatore RTO and vehicle growth of the city is calculated for the year of 2014 and 2015. (Ref Table 1)

Table 1: Vehicle Growth in Coimbatore City

CATEGORY	2013	2014	2015
Car	15428	16789	18301
Motor Cycle	20123	24432	26621
Scooter	7920	8100	9921
Others	5648	5916	7458
Total	49119	55237	62301

Vehicle Growth in the year 2014 – 12.45

Vehicle Growth in the year 2015 – 12.79

2.2. Air pollution:

The quantum of vehicular pollutants emitted is highest in Chennai. Coimbatore, Salem, Trichy, Madurai and Thirunelveli are the other cities that has significant quantum of vehicular pollutants followed by Chennai, in Tamilnadu. Coimbatore's rapid growth may give impression of the city becoming more polluted by day by day. The city, Comprehensive Environmental Pollution Index, which measures pollution levels, has fallen from 72.38 in 2009 to 53.14 in 2013. Again pollution index has raised to the level of 63.93 in the year 2015. Indeed, in 2009, the Central Pollution Control Board (CPCB) had included Coimbatore among the country's critically polluted cities and banned new industrial units and expansion of existing units. There could hardly be any road user who has not seen government buses emitting excessive smoke. Tamil Nadu State Transport Corporation (TNSTC) officials said that of the nearly 1,180 buses is in TNSTC Coimbatore, around 200 buses faced the problem of emitting excess levels of smoke. More than 30 per cent TNSTC buses are unfit for use as they pollute the environment and cause inconveniences to other road users.

2.2.1. Causes for pollution in city buses:

Mainly poor maintenance of vehicles results in the spewing out of noxious fumes into the atmosphere. There are City Buses that have covered more than seven lakh kilometers are in road for more than six years and also the majority of the buses have crossed seven lakh kilometers in less than five years. There are many buses that have been on the road for 12 to 13 years but have not been taken off the road.

Inadequate funds to replace buses and increasing demand for public transportation are cited as the reasons for old polluting buses continuing to ply on roads.

2.3. Car ownership:

As per the report of MORTH 2012 Coimbatore holds third place when car ownership is calculated per thousand person in city. The density of cars per sq.km has been increasing gradually in Coimbatore city and this has led

to traffic congestion. Especially cars like sedan and hatch backs are replaced by SUVs & XUVs, which occupies lots of space in roads and congest the city roads. (Ref. Table 2)

Table 2: Top Indian Cities with high Car ownership (Per 1000 persons in cities)

City	Cars
Delhi	157
Chennai	127
Coimbatore	125
Bangalore	85
Hyderabad	72
Jaipur	67

Source: MORTH 2012[6]

2.4. Share of public transport:

The share of mode in transport of Coimbatore city reports that people are more dependable to two wheelers and cars than any other mode of transport when comparing major cities in Tamil nadu. Para transit, public transport fleet sizes and estimated ridership are very high in Coimbatore with highest bus boardings of 701456 and highest bus fleet of 655 in Tamilnadu, which ensures the peoples of Coimbatore are more dependable to public transport compare to other major cities. (Ref. Table 3 and Table 4)

Table 3: Share of transport in major Cities of Tamilnadu

City	walk	cycle	bus	Two wheeler & car	Para transit
Coimbatore	28	7	21	35	9
Madurai	28	10	28	18	15
Salem	26	7	20	18	29
Tiruppur	28	10	17	40	5
Trichy	28	10	26	22	14

*mode share in percentage

Source: TNSTC

Table 4: Para transit and public transport fleet sizes and estimated ridership in 2013

CITY	Total Auto fleet	Estimated Auto boarding's	Total TNSTC Fleet	Daily BUS boarding
Madurai	13360	320987	507	636768
Coimbatore	8652	297110	655	701456
Salem	6016	329316	226	229720
Tiruppur	1133	64332	281	198229
Trichy	9843	210837	218	394200

Source: RTO

These are the factors to implement BRTS in Coimbatore City.

3. SELECTION OF ROAD FOR BRTS:

Selection of road is made by considering by following factors:

3.1. Traffic & Passenger Car Units data:

1. In Coimbatore City about 42% of the people depends upon Public transport.
2. Road wise average annual daily traffic in Coimbatore indicate that Avinashi road, Mettupalayam road and Trichy road have highest average peak hour traffic volume of 4530 PCUs.
3. In the city about 10 out of 30 Intersections with peak hour volume of greater than 6000 PCUs.
4. Bus terminal at Gandhipuram and Ukkadam not geared to handle traffic and inter change trips.
5. Truck terminal at Ukkadam and absence of bypass causes 25% of traffic in arterial corridors on account of external - external traffic.
6. Over 20 intersections and mid block locations in the city have high levels of pedestrian-vehicle conflicts.

7. 30% of major arterial road with available road space do not have foot paths.

Table 5 shows the road wise annual average daily traffic.

Table 5. Road wise Annual Average Daily Traffic

Road	AADT PCU
Mettupalayam Road	51422
Sathy Road	40107
Avinashi Road	43390
Pollachi Road	42021
Palakkad Road	26783
Perur Road	26346
Maruthamalai Road	23067
Thadagam Road	18474
Trichy Road	40788

Source: TNSTC

3.2. Fatal data:

Number of fatal and non fatal accidents in city limits increases year by year because of improper road networks, increase in number of vehicles, improper signaling system and lack of facilities for pedestrian crossing. People are dependable for other transit because of inadequate and delaying public transport system. Fatal data are considered in BRT planning in order to identify the black spots and to provide better road network for road users and pedestrians. BRT system can provide fast, comfort, cost effective, & safe urban mobility to the passengers and will reduce the fatal accidents.(Ref. Table 6)

Table 6.Fatal & Non fatal accidents in the 2014

Road	Number of Fatal	Number of non Fatal
Mettupalayam Road	44	301
Sathy Road	48	210
Avinashi Road	51	311
Pollachi Road	21	66
Palakkad Road	26	54
Perur Road	18	53
Maruthamalai Road	11	22
Thadagam Road	31	72
Trichy Road	34	221
Total	284	1310

Source: City Commissioner Office

3.3. PPD data:

Road wise passenger per hour per direction data are collected and converted to passenger per day in order to find the road with high passenger. (Ref. Table 7)

Table 7. Road wise Passenger Per Day data

ROAD	AADT PCU
Mettupalayam Road	119080
Sathy Road	80821
Avinashi Road	131920
Pollachi Road	86732
Palakkad Road	76531
Perur Road	40111
Maruthamalai Road	68521
Thadagam Road	55627
Trichy Road	114430
Total	773773

Source: TNSTC

4. SELECTION OF ROADS BY USING GIS:

1. The road network of Coimbatore city is digitized in Arc View software(Figure 1)
2. Geo-Referencing is made to various locations.
3. Attributes are added to the digitized map(Figure 2)
4. The collected above data are overlaid with respect to the road network which is digitized.
5. Coimbatore city road wise Fatal map (Figure 3), PCU map (Figure 4), PPD map (Figure 5) are generated.



Figure 1: Major roads in Coimbatore city

Shape	ID	name	km	PCU	pop
PointLine	1	shivaj	34	40790	114430
PointLine	2	shivajhi	51	43390	131920
PointLine	3	salwa mangalam	46	40107	80821
PointLine	4	metu polelam	44	51422	113000
PointLine	5	thodasam	31	18474	56227
PointLine	6	mouthanale	11	23967	88321
PointLine	7	peasu	18	26346	40111
PointLine	8	pebbikad	26	26793	79931
PointLine	9	polachi	21	42021	86722

Figure 2: Adding attributes

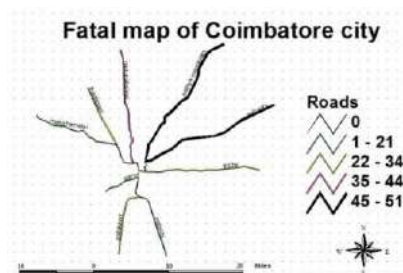


Figure 3: Fatal map of Coimbatore City

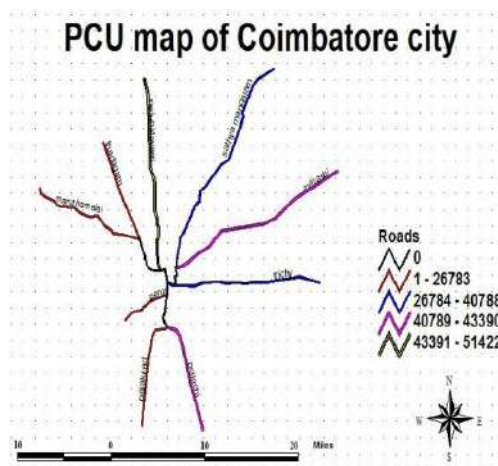


Figure 4: PCU map of Coimbatore City

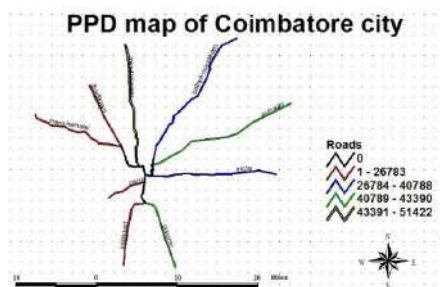


Figure 5: PPD map of Coimbatore City

5. RESULT AND DISCUSSIONS:

It is found that Avinashi road, Mettupalayam road, Sathy road, Trichy road has the major cause to implement BRT system. Phase one in avinashi road 20Km stretch upto Neelambur. In Sathy road 14Km stretch upto Saravanampatty, In Trichy road 15 km stretch upto Ondipudur. In Mettupalayam road 18 km stretch upto Thudiyalur, of total stretch of 67 km can be implemented. These corridors provide essential connectivity and linkages to important towns such as Sular, Neelambur etc.

Phase two can be done by connecting Cowley Brown Road, Nallapalayam Road, and Kamaraj Road, from R.S. Puram to Singanallur, and Palaghat road as shown in Figure 6.



Figure 6: Recommended BRT network

6. BRT ROAD ELEMENTS:

BRT road elements such as BRT lane, Barrier, mixed carriageway, cycle track, parking, foot path are made by considering the available road width in the city by the reference of Ahmadabad BRT system which is a most successful BRT system in India and also by accepting the recommendations of IRC[3][4]. Typical 24M row cross section, 30M row cross section & 36M row cross section are suitable for implementing BRT in Coimbatore city. 24M lane cross section can be implemented in heart of the city with available space, 30M cross section can be implemented in National Highways like Avinashi road Sathy road and Mettupalayam road and 36 m cross section can be implemented in the entrance of Coimbatore city corporation where rural areas connect urban. Details of BRT road elements are also shown in Table 8.

Table 8. BRT Road Elements

24m Row Cross Section	
Foot Path	2350mm
Mixed Carriage way	5500mm
Barrier	500mm
BRT Lane	7300mm
30m Row Cross Section	
Foot Path	2500mm
Parking	2100mm
Mixed Carriage way	6000mm
Barrier	750mm
BRT Lane	7300mm
36m Row Cross Section	
Foot Path	2700mm

Parking	2300mm
Cycle Track	2250mm
Mixed Carriage way	6250mm
Barrier	750mm
BRT Lane	7500mm

7. CONCLUSIONS

The following conclusions are made by this study.

1. BRTS will decrease the traffic congestion in National Highways like Avinashi road, Sathy road & Mettupalayam road, passing the city.
2. Segregated bus lanes makes the buses to increase their speed which can provide fast transportation service in the city.
3. BRTS will also cause citizens to switch travel modes from car to bus which reduce the traffic congestion.
4. Recommended Highway cross sections can be made with very less acquisition in the city.
5. BRTS can serve larger geographical area in the city with frequent operations.
6. BRTS will increase the PPHPD in the city and satisfies the peoples need.
7. This is the best and suitable Mass Rapid Transit system when compare to other transits in Coimbatore city.

REFERENCES

1. "Bus Rapid Transit Planning Guide",2014, Federal ministry for economic corporation and development, Germany (2014), Page no: 175
2. "Bus Rapid Transit Route Planning Project",2010, Western Riverside Council of Governments, California (2010), Page no:18
3. IRC: SP:73-2007, "Manual of standards & specifications - For laning of state Highways".
4. IRC:11-1962, "Recommendation practice for the design and layout of Cycle track"
5. "Pre feasibility study for Bus Rapid Transit system in Hyderabad", 2009, The Institute for Transportation and Development Policy (2009).
6. "Safety in Roads", 2012, Ministry of Road Transport and Highways (2012).
7. Sumalatha, Eshrak, 2015, "Bus Rapid Transit System in Hyderabad, "International Journal of science and Research Technology", volume 4, pp 157-163.
8. Vimal Gahlot, B.L. Swami, 2012, "User oriented planning of bus rapid transit corridor in GIS environment" International Journal of Sustainable Built Environment (2012) 1, pp102–109.

Analytical Study on the Optimum Damper Placement on the Seismic Response of RC Framed Structures

Gaanavaruni Rodriguez L F and Sivakumar C G

Department of Civil Engineering, PSG College of Technology, Coimbatore, India

ABSTRACT

The paper deals with the study of seismic behaviour of RC structures using software. It includes dynamic analysis of structures with the placement of energy dissipating systems and the optimum placement of dampers in the various structures are determined among the various position of dampers. Regular buildings are effective in seismic behaviour due to its property of symmetry. The influence in varying the number and positioning of the dampers in a structure is studied and the most optimum results are suggested, to provide a cost effective arrangement of Pall Friction Dampers which have a cross bracing configuration to provide both the damping effect and bracing behaviour in a structure. In the current scenario, construction industry is demanding taller and lighter structures, which are also more flexible and with low damping value. The study is compared with the structures without dampers, fully dampers placed, diagonally placed, corner placement, middle placement, h/2 from bottom floors placement, alternate placement and diagonal placement in RC multistoreyed buildings with G+5, G+7, G+9, G+11, G+13 and G+15 floors. The paper deals with the effectiveness of a passive dissipative friction damping device in structures to control vibration in structures.

Keywords: Optimum placement, pall friction damper, seismic analysis, SAP2000

1. INTRODUCTION

Earthquake is one of the unpredictable major natural calamities that increases the challenges faced by a structural engineer and threatens the construction industry. Earthquake resistant buildings are gaining importance in the recent times to reduce the damages caused in structures inspite of their highly complicated architectural and structural designs. In order to avoid the collapse of structures during severe earthquakes due to the strong ground shaking, seismic dampers are introduced in buildings. During major earthquakes, the performance of conventional structural systems are highly unlikely to provide required adequacy. Buildings are constructed for moderate seismic loads which only increase cost of the structure by fifteen to twenty five percent of the total construction cost of the building.

Traditional friction dampers can only be designed under a target earthquake of a given intensity. Complied with the current design code, this target earthquake usually has an intensity of the return period of 475 years. Consequently, traditional friction dampers may function well under earthquakes with the intended design level, but may not be functional for earthquakes with lower intensities. Friction dampers absorb vibration energy by friction forces between contacting plates. Normal force required to induce desired slip load is applied through pre-tensioning of the bolts.

From the previous earthquakes the behaviour and the collapse mechanisms of structures were studied and dampers were developed to give an effective measure to reduce the collapse of structures. There are different types of dampers available at present.

Pall friction dampers were made by Pall and Marsh in 1982 which mimics the automobile's brake. The Pall friction damper can be positioned in the intersection of X braces and it includes rigid diagonal bars with friction hinges at their intersection points connected. The first building in which the Pall Friction Dampers was used is in North America (1987). Pall Friction Dampers are used worldwide for development and retrofit in the existing structures. These dampers are utilised for the seismic assurance of in excess of 80 noteworthy structures in India, Unites States and Canada. These are healing centers, media transmission structures, instructive foundations, police base camp, guard establishments, tradition focuses, courthouses, office and private structures.

Caudana Quintanaa H, Petkovskib M, concluded that the main system uses passive control systems. After the control mechanism is introduced, it has no capacity to direct itself under various ground motions. Control systems with frictional components are basic and financially flexible. Be that as it may, the ideal execution of friction based slow control is given by a special arrangement of slip-load limit and position of the dampers noted distinctive execution between Passive friction dampers were utilized as introductory retrofit answer for a low-rise moment resistant steel frame. The ideal placement changed for various number of the dampers and distinctive ground movements.

Fallah, N, Honarparast S proposed that the viability of two types of height-wise distribution of slip load of pall friction dampers in reducing the seismic responses of 2D shear frame. The impacts of two types of distribution decreases of seismic reactions have been investigated. Incorporation of friction dampers in the 10-story frame causes decrease in basic reactions. To counteract the action during earthquakes, these seismic forces generated are dissipated using the introduction of seismic dampers which are energy dissipation devices which resist the structure from damage by means of horizontal and vertical elements.

In this present work, various RC multistoried structures with various stories G+5, G+7, G+9, G+11, G+13 and G+15 are considered for the study. For each chosen building, dampers are placed in various floor levels (Fig.5) and different locations. These were modelled and analysed for gravity loads in STAAD.Pro software and were modelled in SAP2000 software and nonlinear time history analysis was carried out without the dampers and with the varied placement of dampers. Based on the type of structure and characteristics of the dampers, this specific damper for a structure is selected and used to fulfil the requirement.

2. NON LINEAR TIME HISTORY ANALYSIS

The collapse assessment of the modelled structure is done using nonlinear time history analysis. This is a step-by-step analysis carried out to determine the dynamic response of the structure that varies with time for the applied seismic loading of respective earthquake. North ridge ground motion, 1994 is taken from the ATC-63 ground motion criteria.

3. PALL FRICTION DAMPER

A particular type of friction damper is selected (Fig.1,2 and 3) for this study due to its properties, after effects and behaviour under seismic loads. Friction-based structural control is an available strategy for reducing the seismic response of buildings. For economical structural design the Pall Friction Dampers are economically feasible. For new construction and for retrofit of buildings, these dampers are preferred due to their low cost and maintenance free characteristics. Pall and Marsh addressed this problem by connecting the friction dampers by four links at the intersection of frame cross-braces and assuming that the braces could be made to slip both in tension and compression. The resulting device is usually called as Pall frictional damper (PFD) after its inventor.

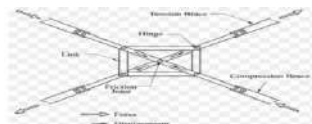


Fig.1. Components of Pall Friction Dampers

3.1 Mechanism of pall friction dampers

The response of the building during vibration can be controlled using friction dampers. These dampers consist of series of treated steel plates to develop reliable friction and are clamped together allowing slippage at predetermined load. The performance of the dampers are reliable, repeatable and have large rectangular hysteresis loops with lesser fade. These are passive energy dissipation devices and, therefore, need no energy source other than seismic forces to operate. The behaviour of these dampers go beyond elastic range. The energy dissipation amount is proportional to the displacement. Hence, the analysis and design should include the use of nonlinear time-history dynamic analysis.

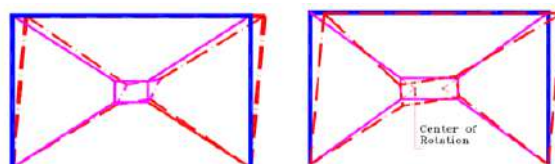


Fig.2. Sliding mechanism of pall friction dampers



Fig.3. Pall Friction Dampers

4. BUILDING DESCRIPTION

The properties chosen for the analysis are as shown below. The modelling of the buildings are as shown in figure 4. Figure 5 shows the placement of dampers in the buildings.

4.1 Properties of the RC Structures

Dimensions of the column: 0.4m x 0.4m

Dimensions of the beam : 0.5m x 0.4m

Height of between the stories : 3m

Length and width of the bays : 6m

Number of bays in both the directions : 4

4.2 Damper properties

Damper type: Plastic (wen)

Section selected for brace: ISLB150 (IS800)

Mass of the brace = 0.05 tonnes

Weight of the brace = 0.534 kN

Area of the brace = 1026 mm²

Length of the brace = 6.71m

Modulus of elasticity = 2×10^5 N/mm²

Stiffness of the brace = $K_e = AE/L = 30640$ N/mm

Yield Stiffness Ratio (post) = 0.0001

Yielding exponent = 10

Yield Strength = Slip load of friction damper = $K_e = 200$

Rotational inertia 1 = 0

Rotational inertia 2 = 0

Rotational inertia 3 = 0

Ce = Effective Damping = 0

4.3 Analysis Results

Tables 1 to 7 give the details of the displacement in various floors for all the buildings for various placements of dampers after analysis.

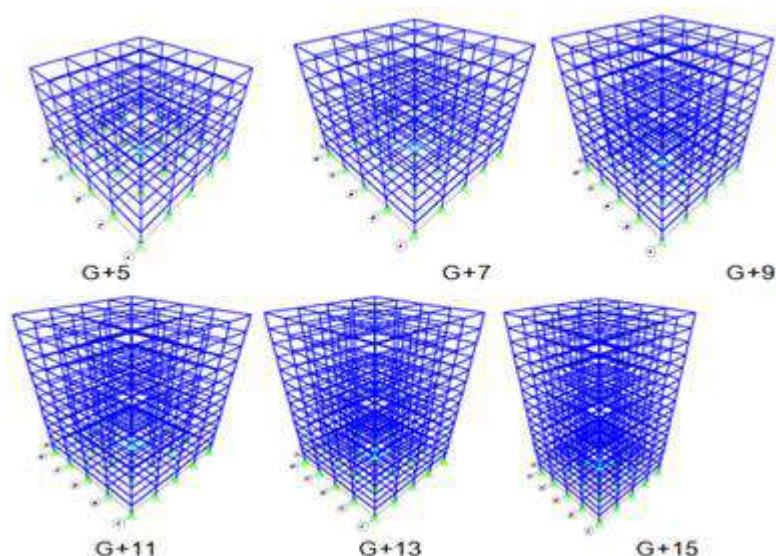


Fig .4.The various RC structures modelled and analysed by time history analysis in SAP2000 software

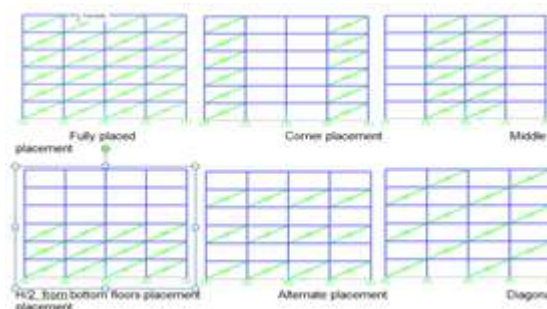


Fig.5. Various damper placements

Table 1 Storey Displacements of G+5 RC structure for the varied damper placement

Floor	Displacements (mm)						
	Without dampers	With dampers	Alternate placement	h/2 floors from bottom	Diagonal placement	Corner placement	Middle placement
G	23.58	13.61	3.27	2.79	11.25	5.17	8.54
I	35.79	25.65	29.75	6.64	22.33	12.27	19.67
II	39.5	36.08	34.47	11.69	36.88	19.43	30.19
III	49.85	44.51	52.88	40.54	45.45	45.99	39.21
IV	56.58	50.04	55.62	50.53	54.36	51.46	46.02
V	60.47	53.61	57.43	56.60	57.99	55.47	59.91

Table 2 Storey Displacements and storey drifts of G+5 RC structure

Floor	Without dampers		Corner placement (optimum placement)		Reduction in storey displacements percentage %	Reduction in storey drift percentage %
	Storey displacements (mm)	storey drift (mm)	Storey displacements (mm)	storey drift (mm)		
G	23.58	23.58	8.52	8.52	63.87	63.87
I	32.45	8.87	15.98	7.46	50.76	15.90
II	40.21	7.76	23.54	7.56	41.46	2.58
III	44.65	4.44	27.77	4.23	37.81	4.73
IV	56.58	11.93	38.98	11.21	31.11	6.04
V	60.47	3.89	42.58	3.6	29.58	7.46
Average					42.43	16.76

Table 3 Storey Displacements and storey drifts of G+7 RC structure

Floor	Without dampers		Corner placement (optimum placement)		Reduction in storey displacements percentage %	Reduction in storey drift percentage %
	Storey displacements (mm)	storey drift (mm)	Storey displacements (mm)	storey drift (mm)		
G	13.68	13.68	11.78	11.78	13.89	13.89
I	28.06	14.38	26.01	14.23	7.31	1.04
II	38.23	10.17	36.1	10.09	5.57	0.79
III	47.69	9.46	45.01	8.91	5.62	5.81
IV	58.37	10.68	51.64	6.63	11.53	37.92
V	64.14	5.77	54.51	2.87	15.01	50.26
VI	65.99	1.85	55.84	1.33	15.38	28.11
VII	71.97	5.98	57.72	1.88	19.80	68.56
Average					11.76	25.80

Table 4 Storey Displacements and storey drifts of G+9 RC structure

Floor	Without dampers		Diagonal placement (optimum placement)		Reduction in storey displacements percentage %	Reduction in storey drift percentage %
	Storey displacements (mm)	storey drift (mm)	Storey displacements (mm)	storey drift (mm)		
G	17.6	17.6	14.92	14.92	15.23	15.23
I	27.45	9.85	23.37	8.45	14.86	14.21
II	32.97	5.52	28.47	5.1	13.65	7.61
III	40.47	7.5	35.63	7.16	11.96	4.53
IV	52.65	12.18	46.52	10.89	11.64	10.59
V	65.33	12.68	57.64	11.12	11.77	12.30
VI	71.92	6.59	62.58	4.94	12.99	25.04
VII	86.01	14.09	74.67	12.09	13.18	14.19
VIII	98.05	12.04	85.15	10.48	13.16	12.96
IX	109.89	11.84	92.64	7.49	15.70	36.74
Average					13.41	15.34

Table 5 Storey Displacements and storey drifts of G+11 RC structure

Floor	Without dampers		h/2 placement (optimum placement)		Reduction in storey displacements percentage%	Reduction in storey drift percentage %
	Storey displacements (mm)	storey drift (mm)	Storey displacements (mm)	storey drift (mm)		
G	17.33	17.33	10.11	10.11	41.66	41.66
I	32.81	15.48	24.7	14.59	24.72	5.75
II	43.39	10.58	33.18	8.48	23.53	19.85
III	54.65	11.26	43.45	10.27	20.49	8.79
IV	61.3	6.65	49.23	5.78	19.69	13.08
V	72.37	11.07	60.05	10.82	17.02	2.26
VI	83.78	11.41	71.09	11.04	15.15	3.24
VII	94.23	10.45	81.35	10.26	13.67	1.82
VIII	101.26	7.03	85.95	4.6	15.12	34.57
IX	112.87	11.61	94.67	8.72	16.12	24.89
X	131.39	18.52	110.78	16.11	15.69	13.01
XI	155.18	23.79	133.62	22.84	13.89	3.99
Average					19.73	14.41

Table 6 Storey Displacements and storey drifts of G+13 RC structure

Floor	Without dampers		h/2 placement (optimum placement)		Reduction in storey displacements percentage%	Reduction in storey drift percentage %
	Storey displacements (mm)	storey drift (mm)	Storey displacements (mm)	storey drift (mm)		
G	21.33	21.33	17.99	17.99	15.66	15.66
I	35.68	14.35	29.31	11.32	17.85	21.11
II	48.96	13.28	41.59	12.28	15.05	7.53
III	61.57	12.61	51.68	10.09	16.06	19.98
IV	75.26	13.69	64.95	13.27	13.70	3.07
V	93.69	18.43	81.96	17.01	12.52	7.70
VI	108.57	14.88	94.32	12.36	13.13	16.94
VII	119.6	11.03	103.75	9.43	13.25	14.51
VIII	132.57	12.97	114.99	11.24	13.26	13.34
IX	147.64	15.07	129.64	14.65	12.19	2.79

X	162.75	15.11	141.67	12.03	12.95	20.38
XI	188.36	25.61	164.23	22.56	12.81	11.91
XII	209.77	21.41	183.33	19.1	12.60	10.79
XIII	227.92	18.15	198.75	15.42	12.80	15.04
Average					13.85	12.91

Table 7 Storey Displacements and storey drifts of G+15 RC structures

Floor	Without dampers		middle placement (optimum placement)		Reduction in storey displacements percentage %	Reduction in storey drift percentage %
	Storey displacements (mm)	storey drift (mm)	Storey displacements (mm)	storey drift (mm)		
G	16.37	16.37	13.6	13.6	16.92	16.92
I	35.19	18.82	27.14	13.54	22.88	28.06
II	51.2	16.01	42.66	15.52	16.68	3.06
III	73.55	22.35	58.78	16.12	20.08	27.87
IV	91.63	18.08	76.64	17.86	16.36	1.22
V	105.69	14.06	87.02	10.38	17.66	26.17
VI	126.32	20.63	103.54	16.52	18.03	19.92
VII	142.71	16.39	119.64	16.1	16.17	1.77
VIII	169.87	27.16	144.78	25.14	14.77	7.44
IX	186.52	16.65	159.67	14.89	14.40	10.57
X	204.64	18.12	175.54	15.87	14.22	12.42
XI	219.12	14.48	187.78	12.24	14.30	15.47
XII	233.77	14.65	201.89	14.11	13.64	3.69
XIII	256.69	22.92	216.67	14.78	15.59	35.51
XIV	287.15	30.46	241	24.33	16.07	20.12
XV	311.53	24.38	254.69	13.69	18.25	43.85
Average					16.63	17.13

5.0 CONCLUSION

The introduction of pall friction dampers in the RC structures shows a considerable change in the displacements and the storey drifts of the structures. The type of optimum placement format of different heights of stories varies with their structural behaviour along with the dampers.

In G+5 and G+7 RC structures, the optimum placement of damper is obtained in the corner placement of dampers with about storey drift reduction of 16.76% and 25.80% respectively. In G+ 9 RC structure, the optimum placement of dampers is obtained in the diagonal placement of dampers with about storey drift reduction of 15.34%. In G+11 and G+13 RC structures, the optimum placement of dampers is obtained in the h/2 from bottom floors placement with about storey drift reduction of 14.41% and 12.91% respectively. In G+ 15 RC structure the optimum placement of dampers is obtained in the middle placement of dampers with about storey drift reduction of 17.31%.

It is concluded from this study that the optimum placement of dampers changes with the height of structure with the behaviour of the structure.

REFERENCES

1. Avtar S. Pall and Cedric Marsh, Members, ASCE, 1982, "On Response Of Friction Damped Braced Frames" published in Journal Of The Structural Division, ASCE 1982; 108(no. St6), pp1313–23.
2. Avtar Pall And R. Tina Pall, 2004, "Performance-based Design Using Pall Friction Dampers- An Economical Design Solution" Proceedings of the 13th World Conference On Earthquake Engineering, Vancouver, B.C., Canada, Paper No. 1955.
3. Babak Esmail Zadeh Hakimi, Alireza Rahnavard, Teymour Honarbakhsh , 2004, "Seismic Design Of Structures Using Friction Damper Bracings" Proceedings of the 13th World Conference On Earthquake Engineering, Vancouver, B.C., Canada, paper No. 3446.

4. Carolina Tovar And Oscar A. López , 2004, “Effect Of The Position And Number Of Dampers On The Seismic Response Of Frame Structures”, Proceedings of the 13th World Conference on Earthquake Engineering Vancouver, B.C., Canada, Paper No. 1044.
5. Caudana Quintanaa H, Petkovskib,M, 2018, “Optimum Performance Of Structural Control With Friction Dampers”, Journal Of Engineering Structures 172, pp 154–162.
6. Fallah.N , S. Honarparast, 2013, “NSGA-II based multi-objective optimization in design of Pall friction dampers”, Journal of Constructional Steel Research, Vol.89, pp 75–85.
7. Pavan Raj. G , Dr. B. Dean Kumar , 2018, “Effect Of The Position And Number Of Friction Dampers On The Seismic Response Of Unsymmetric Building” International Research Journal Of Engineering And Technology (IRJET), Volume: 05 Issue: 05.
8. Shameena Khannavar, M.H.Kolhar and Anjum Algur, 2017, “Seismic Analysis of RC Structures Using Friction Dampers” International Journal for Research in Applied Science & Engineering Technology (IJRASET) ISSN: 2321-9653; IC Value: 45.98; SJ Impact Factor: 6.887, Volume 5 Issue XII.

Hidden Community Detection in Social Networks using Path Matrix

Sundar C, N Ilayaraja and Ranjani R

Computer Applications, PSG College of Technology, Coimbatore, India

ABSTRACT

In social network group of people interact frequently. Detection of such groups is known as Community Detection. Detecting communities is of great importance in sociology, biology and computer science, disciplines where systems are often represented as graphs. A community is defined as a set of nodes that are more densely connected to each other than to the rest of the network nodes. Community detection in social networks helps to find people who are having high connection in social network sites. This paper addresses community detection using path matrix representation of single level. This technique ensures the detection of hidden communities. Hidden Community Detection (HICODE) is helpful to detect the threatened activity patterns in social networks. It can help the investigators to find the persons having connections with the criminals. This work is implemented using NetworkX graph data structure in python which reduces the storage space of social network graphs to detect the communities.

Keywords— social network, community detection, graph, path matrix, NetworkX, python, twitter, HICODE, LCM, Stack, Spyder

INTRODUCTION

A Graph is a non-linear data structure. It consists of a finite set of nodes and a finite set of edges which connects a pair of nodes. The nodes are also called as vertices and the edges are also called as links or arcs that connect any two vertices in the graph. There are various types of graphs depending upon the number of edges and its connectivity. Few important types of graphs which are relevant to community detection is discussed here.

Directed Graph

A directed graph is a set of vertices (nodes) connected by edges, with each edge having a direction associated with it. Edges are usually represented by arrows pointing in the direction the graph can be traversed. In Figure 1 the graph can be traversed from vertex 1 to 2, but not from vertex 2 to 1.

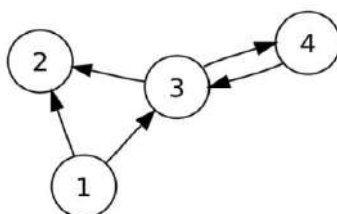


Fig 1 Directed Graph

Undirected Graph

In an undirected graph, the edges are unidirectional, with no direction associated with them. Hence, the graph can be traversed in either direction. The absence of an arrow tells us that the graph is undirected. Figure 2 represents an Undirected Graph without self-loops.

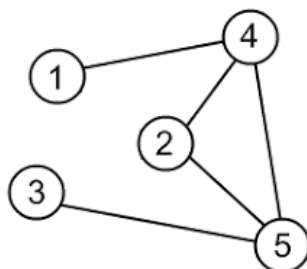


Fig 2 Undirected Graph

Weighted Graph

In a weighted graph, each edge will be associated with a value called weight. This weight represents the importance of an edge. A weighted graph can be either directed or undirected. Figure 3 represents an undirected weighted graph.

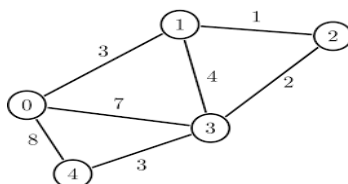


Fig 3 Undirected Weighted Graph

The important application of graph theory is social networks. The application of graph theory in social networks are discussed further

SOCIAL NETWORKS

Graph is the most powerful data structure to represent social network. In a social network graph, the nodes represent persons or individuals who use social networks and the edge represents the interaction between them. In Social network analysis, networks are represented depending upon the interaction and behaviour of nodes. Following are the types of networks used in social networks.

Directed Social Network

It is a type of network with directed edges between the persons. A directed arrow is represented between person P1 and P2 shows that person P1 is connected with person P2 and not vice versa. Twitter is using directed social networks in which the connection is unidirectional. It works based on the following principles.

- 1) People follow you, but you don't follow them back.
- 2) People don't follow you, but you can follow them.

Undirected Social Network

When no direction was assigned to the edge between the persons is known as undirected network. An edge between person P1 and P2 could be considered as P1 and P2 friends. Similarly, P2 and P1 are friends. Facebook follows undirected social network. Generally, all social networks will be represented using undirected graph representation.

Weighted Social Network

In weighted social networks, the edges between persons are characterized by significance described by particular numeric value. These social networks can be either directed or undirected. Telephonic graph follows weighted social network representation where the edges are represented by the number of calls made between two persons or the amount of time two person communicates with each other.

COMMUNITY DETECTION

Community detection is one of the key areas in the social network analysis. Community means a group of persons in social networks. The objective of community detection is to find the clusters in a social network such that persons in the same cluster are highly connected than outside of the cluster. There are three types of communities.

Static Community

The clustering of users in a social network by fixed or unchanged behavior in a social network over a large time span represents the static community structure. The static approach is unable to cover all the necessary characteristics of a network. So, there is a necessity to find a way to capture the dynamism in a network such that interpretable communities could be discovered.

Dynamic Community

Over the period of time interactions between the nodes changes which ultimately reflect change in community structure. With the change in data, the community structure changes. Dynamic communities in a social network deals with interactions change over time. Dynamic network captures the ongoing change of interactions and node positions in the network and updates the communities accordingly.

Overlapping Community

A single person can be occurred in multiple communities. The social networks such as LinkedIn, Twitter, Instagram, and Facebook divide into groups of friends/colleagues/business partners. Naturally, these networks form so many related overlapping communities. In real world, the people characterized by multiple community membership i.e. a student belong to different social groups like family, classmates and friends.

The objective of this paper is to detect static overlapping communities from a large social network graph. The process of detecting communities will be discussed in the upcoming chapters.

LITERATURE REVIEW

Community detection and link prediction is done using adjacency matrix by Sweta Rai [2]. R. Hosseini [1] proposed an improved label propagation algorithm called memory-based label propagation algorithm (MLPA) for finding community structure in social networks. A simple memory element was designed for each node of graph and this element store the most frequent common adoption of labels iteratively.

W. Wang [3] approach was not differentiating the influence ranking but also effectively find communities in both directed and undirected network. These two tasks were incorporating into one integrated framework. It outlines a new perspective on the influence-based connectivity of network graph topology, and define a novel influence centrality and shared-influence-neighbour (SIN) similarity in an integrated framework. The SIN similarity is well-suited as a refined proximity metric for community detection.

N. Barbieri [4] proposed a stochastic framework which assumes that item adoptions are governed by an underlying diffusion process over the unobserved social network, and that such diffusion model is based on community-level influence. It identifies the community membership and the level of influence of each user in each community.

Graphs cannot be stored as such in computer's memory. To represent the graph in computer memory, either adjacency matrix or adjacency list data structure to be used.

Adjacency matrix

Adjacency Matrix is a two-dimensional array of size $V \times V$ where V is the number of vertices in a graph. Let the two-dimensional array be $adj[][]$, a cell $adj[i][j] = 1$ indicates that there is an edge from vertex i to vertex j . Adjacency matrix for undirected graph is always symmetric. Adjacency Matrix is also used to represent weighted graphs where each edge will have a weight associated with it. If $adj[i][j] = w$, then there is an edge from vertex i to vertex j with weight w . Table 1 represents the adjacency matrix representation of the directed graph shown in Figure 4.

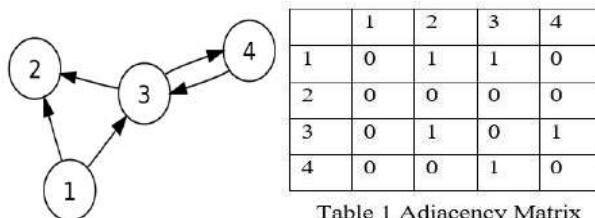


Table 1 Adjacency Matrix

Fig 4 Directed Graph

Adjacency list

An adjacency list is an array of lists. Size of the array is equal to the number of vertices. Let the array be $array[]$. An entry $array[i]$ represents the list of vertices adjacent to the i^{th} vertex. Each entry in the $array[i]$ will have different size depending on the number of adjacent vertices. This representation can also be used to represent a weighted graph. The weights of edges can be represented as lists of pairs. Figure 5 represents the adjacency list representation of a directed graph shown below.

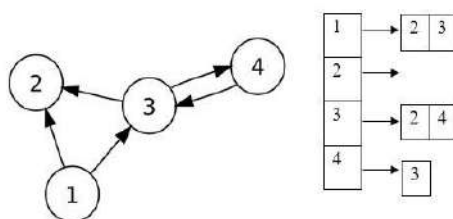


Fig 5 Adjacency list

Limitations of Adjacency Representation

There are some limitations in the adjacency representation of graphs. Adjacency matrix consumes more space that is $O(V^2)$ where V denotes the number of vertices. Even if the graph is sparse (contains a greater number of zeroes), it consumes the same space as $O(V^2)$. Adding a new vertex is also takes $O(V^2)$ time complexity. Since memory for a new row and a new column must be allocated and entries must be filled in the existing adjacency matrix. Adjacency matrix cannot reveal hidden relationships. (i.e.) Communication between two persons always

cannot happen directly. There will be an intermediate person who conveys important and secret information to the other side. But adjacency matrix will not show this hidden relationship.

PATH MATRIX

To overcome the limitation, storage using path matrix of one level is proposed. The path matrix P of a directed graph G having n-vertices is defined as,

$$P_{ij} = \begin{cases} 1 & \text{if there is a path from } V_i \text{ to } V_j \text{ directly or via any node } V_k \\ 0 & \text{otherwise} \end{cases}$$

In path matrix of single level the transitivity property is used. If vertex A is adjacent to vertex B and vertex B is adjacent to vertex C then vertex A is mostly adjacent to vertex C. A new edge from vertex A to vertex C is added in the path matrix. Figure 6 represents a directed graph. Path matrix representation of this graph using transitivity property is as shown in Figure 7.

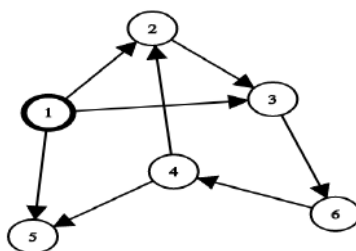


Fig 6 Adjacent Graph

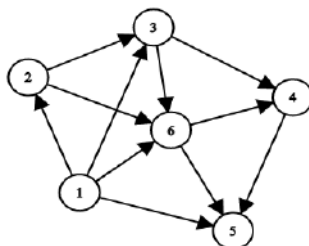


Fig 7 Path Graph

Path matrix also exploits the properties of Adjacency matrix. If $Adj[i,j]=1$ then $P[i,j]=1$. Path matrix is also a $V \times V$ matrix. Path matrix is stored using NetworkX graph data structure in python. It optimizes the storage space. Each edge in the path matrix will be represented as a tuple in Python which is in the form of (i, j) where i is the source vertex and j is the destination vertex. This paper addresses community detection using path matrix representation for both directed and undirected graph.

LCM ALGORITHM

The section illustrates linear time closed item set Miner (LCM) algorithm used in this paper for community detection.

Working Procedure of LCM

Frequent item set mining is one of the fundamental problems in data mining and has many applications such as association rule mining, inductive databases, and query expansion. Using this LCM Algorithm Community detection can be done with the help of path matrix. LCM algorithm works in depth first search manner as shown in Figure 8.

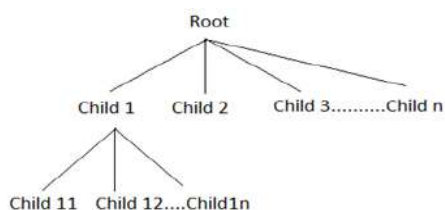


Fig 8 LCM Algorithm Tree

LCM algorithm has three steps. First step is to initialize the root node. Second step is to generate all the first level nodes. Third step is to generate all the remaining level nodes.

Step 1: Root Node Initialization

The root node will be always empty. This algorithm starts with an empty node continuously add vertices one by one and push into stack.

Step 2: First Level Nodes Generation

Expand the root node by creating n children where n is the number of non-isolated vertices in the graph. Each node will point to one vertex of the input graph.

Step 3: Remaining Level Nodes Generation

For each node in the first level expand the children by combining the parent and every adjacent vertex one by one and then push into stack.

For every node find the common vertices and then expand the children by inheriting from parent and then all common vertices one by one.

Working Example

Figure 9 represents the adjacency list of a directed graph. Number of vertices in the graph are six starting from 0 to 5. The LCM algorithm starts with an empty node { }. First level nodes will be expanded starting from 0 to 5 and pushed into stack in reverse order.

0:	1, 2, 3
1:	2, 3
2:	0, 1, 3
3:	0, 1, 2
4:	1, 5
5:	1, 3

Fig 9 Input Data

As LCM algorithm works in depth first manner, the first child is to be considered was node 0. Expand node 0 by inserting all adjacent vertices of 0. Vertex 0 having connection with vertices 1, 2 and 3. So create three children {0, 1}, {0, 2}, {0, 3} and push into the stack in reverse order.

As per the depth first manner, node {0, 1} should be expanded first. Find all the common adjacent vertices of 0 and 1. There are two common vertices {2, 3} between them. Create 2 nodes {0, 1, 2} and {0, 1, 3}. Push these nodes in reverse order into the stack. Similarly expand the children one by one. All the leaf nodes will form communities. Figure 10 represents three level of LCM enumeration tree.

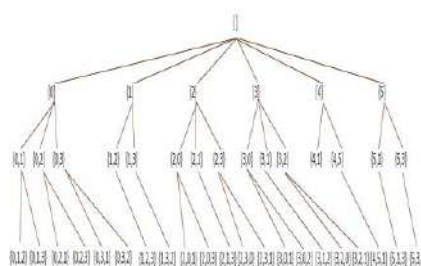


Fig 10 LCM Enumeration Tree Upto Level 3

Pruning Duplicates

It is evident in figure 10 that there are some duplicate nodes generated. Node {0,1,2} is same as node {0,2,1}, {2,0,1}. Because of these duplicate nodes the search space is increased. The efficient LCM algorithm keeps on decreasing the search space because it reduces the number of rows and columns processed each time. LCM algorithm eliminates the previous row and column for next computation of community. Thus, this efficient algorithm takes only half of the running time of LCM algorithm.

0:	1, 2, 3	0:	1, 2, 3
1:	2, 3	1:	2, 3
2:	0, 1, 3	2:	3
3:	0, 1, 2	3:	5
4:	1, 5	4:	
5:	1, 3	5:	

Fig 11 (a) Original Dataset

Fig 11 (b) Modified Dataset

Data set is modified as, first vertex 0 concentrate on all adjacent vertices in the graph. Vertex 1 concentrate only on the adjacent vertices that are greater than 1. Vertex 2 concentrate only on the adjacent vertices greater than 2. For vertex 3, no other adjacent vertices are greater than 3 so it is empty. For vertex 4 only one adjacent vertex 5 which is greater than 4. For vertex 5, no adjacent vertices are greater than 5. So, it is also empty.

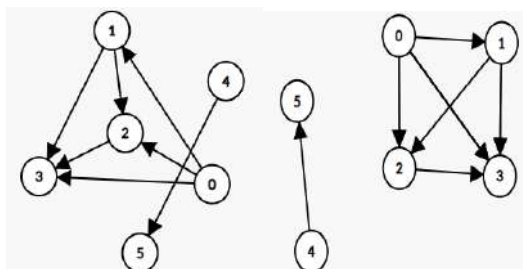


Fig 12 Adjacent Graph Fig 13 Path Graph

Now, the modified dataset shown in Figure 11 (b) will be the input for the LCM algorithm. LCM enumeration tree for the modified graph is shown in Figure 14. From the depth first manner if a node is a subset of previously generated community then prune that branch. So that the search space is reduced

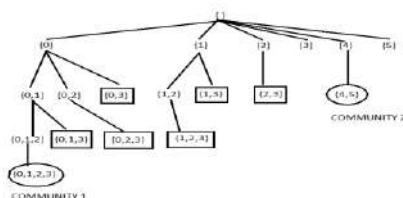


Fig 14 LCM Enumeration Tree

The nodes marked with rectangles are duplicate communities and the encircled nodes are communities.

TOOLS AND TECHNOLOGY

This section describes tools and technologies used in this work to detect communities effectively.

NETWORKX

NetworkX is a “high-productivity software for complex networks analysis” in Python. It consists of various data structures for representing the different types of social networks (directed, undirected, multigraphs). A multigraph will contain multiple edges between two vertices in the graph with different weights.

NetworkX provides extreme flexibility where the vertices can be any hashable object in python and edges can contain arbitrary data. Since NetworkX uses hashing, it is much faster than the other graph-oriented tools. NetworkX also consists of commonly used graph algorithms. NetworkX is a platform independent software package and it is easy-to-use.

NetworkX is not primarily a graph drawing package but it provides basic drawing capabilities by using matplotlib library. For more complex visualization techniques it provides an interface to use the open source GraphViz (graph visualization) software package.

NetworkX’s internal graph data structures are based on an adjacency list representation which is implemented using python dictionary data structure. The graph adjacency structure is implemented as a python dictionary of dictionaries; the outer dictionary is keyed by nodes to values that are themselves dictionaries keyed by neighbouring node to the edge attributes associated with that edge. This structure allows fast addition, deletion, and lookup of nodes and neighbours in large graphs.

SPYDER

Spyder is an open source cross platform integrated development environment (IDE) for scientific programming in the Python language. Spyder integrates with a number of prominent packages in the scientific Python stack, including NumPy, SciPy, Matplotlib, pandas, IPython, SymPy and Cython, as well as other open source software.

FLASK

Flask is a web application framework written in Python. A web application framework represents a collection of libraries and modules that enables a web application developer to write applications without having to bother about low-level details such as protocols, thread management. Flask has many configuration values, with

sensible defaults, and a few conventions when getting started. By convention, templates and static files are stored in sub directories within the application's Python source tree, with the names templates and static respectively.

DATA STRUCTURE AND IMPLEMENTATION

This section focuses on the implementation of LCM algorithm for community detection and the data structures used in this work.

LCM algorithm is implemented using dynamic memory allocation techniques with the help of linked stack data structure to enumerate the communities with zero duplicates. During program execution if any community is found, then new node will be created and added to the linked stack. Size of the linked stack can be changed during run time. Main objective of using dynamic memory allocation is that the program should work for all graphs irrespective of number of nodes in the graph.

DATA STRUCTURE

Stack is a linear data structure in which insertion and deletion of data can take place at only one end called "top". Stack follows Last-In-First-Out (LIFO) principle. Stack has two main operations called push (insert) and pop (delete). Stack implemented using linked list is called as "Linked stack" which is used when the size is initially unknown. LCM algorithm generates the set of all communities. Each community will be considered as a "node" in the linked stack. Each node will have a pointer to the next node. Structure of a node is shown in Figure 15

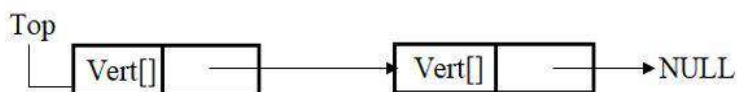


Fig 15. Node representation

A NetworkX graph uses dictionaries to store a graph. Each vertex will act as a key in the dictionary. All adjacent vertices of a particular key will be considered as values. Attributes such as weights, labels, colors, or whatever Python object it can be attached to graphs, nodes, or edges. Each graph, node, and edge can hold key/value attribute pairs in an associated attribute dictionary (the keys must be hashable). Figure 17 represents the NetworkX representation of graph shown in Figure 16.

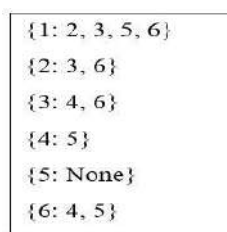
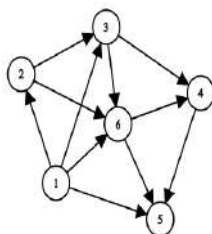


Fig 16. Directed Graph Fig 17. NetworkX

Generate Adjacent Graph

This function will take dataset name and the type of graph as arguments and return the adjacent object of type networkx graph. From the given input dataset, it reads the content add edges into the adjacent object. This function will also plot the adjacent graph and print the details about the adjacent object.

```
def generateAdjacentGraph(datasetname,typeOfGraph):
```

```
import Graph
```

```
fileobj=open(datasetname, "r")
```

```
file_content=fileobj.readlines()
```

```
AdjObject=Graph.MyGraph(typeOfGraph)
```

```
vertex=0
```

```
for line in file_content:
```

```
adjVertices=line.split(' ')
```

```
for adjv in adjVertices:
```

```
AdjObject.addEdge(vertex,adjv)
vertex=vertex+1
AdjObject.plotGraphAdj()
AdjObject.graphStatistics()
return AdjObject
```

Convert to Path Representation

This function will take adjacent object as argument and returns a corresponding path object which uses transitivity property. In path object all edges in the adjacent graph will also present. This function uses stack data structure to achieve transitivity property. After converting into path graph this graph removes self-loops in the graph.

```
def convertAdjToPath(AdjObject):
import Graph
import Stack
PathObject=Graph.MyGraph(AdjObject.gettypeofGraph())
PathObject.addEdges(AdjObject.edges())
for u in AdjObject.vertices():
StObject=Stack.MyStack()
for v in AdjObject.vertices():
if AdjObject.isAdjacent(u,v):
StObject.push(v)
i=StObject.size()
while i>0:
v=StObject.pop()
for w in AdjObject.vertices():
if AdjObject.isAdjacent(v,w):
PathObject.addEdge(u,w)
i=i-1
PathObject=PathObject.removeSelfLoop()
PathObject.graphStatistics()
```

Remove Self Loop

This function will take path graph as an argument and remove the edges connecting to itself.

```
def removeSelfLoop(self):
temp=self.copyGraphObject()
for tuples in self.edges():
if tuples[0]==tuples[1]:
temp.removeEdge(tuples[0],tuples[1])
return temp
```

RESULTS AND OUTCOME

This section discusses the user interface and community detection of Twitter data set used in the work.

User Interface

The user interface consists of a “Choose file” button. If this button is pressed it will be redirected to file explorer window. The user can upload the dataset in text format and can select the type of graph. The input file will be converted into an adjacent object. Then the adjacent object will be converted into a path object using the transitivity property. Then from the path object degree centrality for all vertices will be found. The node with degree centrality zero will be removed. It indicates that a node that doesn't connect with anyone will be removed because it doesn't provide any valid community structure. These nodes are called as isolated vertices. After removing those nodes, the LCM algorithm will detect the communities in the modified path matrix object. Figure 18 shows the user interface design of this work.



Fig 18. User Interface

Community Detection in Twitter

The below figure 19 represents the input dataset of twitter social network of 120 people.



Fig 19. Twitter Data set

Figure 20 represents the generated communities of the data set. The communities are overlapped here. A single node can be present in multiple communities. There are seven valid communities.

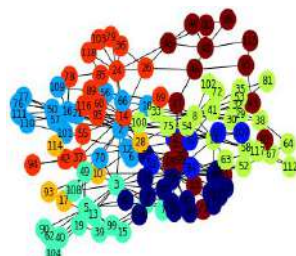


Fig 20. Generated Communities

CONCLUSION

Community are efficiently detected using path matrix representation implemented by LCM algorithm. It reveals the hidden communities in the social network. The dataset can be dynamically extracted from social networks and identifies the HICODE. The future work includes ranking the communities and analysing information about the individual person from their social networking sites like Facebook and Twitter so that it can decide more accurately.

ACKNOWLEDGMENT

We are thankful to Dr. K. Prakasan, Principal In-Charge, PSG College of Technology, Coimbatore for permitting us to take up this work. We extend our earnest gratitude to Dr A. Chitra, Professor and Head, Department of Computer Applications, PSG College of Technology, Coimbatore, for her support, encouragement and above all her ardent motivation.

REFERENCES

1. R. Hosseini and R. Azmi, "Memory-based label propagation algorithm for community detection in social networks," 2015 The International Symposium on Artificial Intelligence and Signal Processing (AISP), 2015, pp. 256-260, doi: 10.1109/AISP.2015.7123488.

2. Rai, Sweta, Shubha Chaturvedi, and Anurag Jain. "Community detection on social media: A review." *International Journal of Scientific Research Engineering Technology* 2.2 (2017).
3. W. Wang and W. N. Street, "A novel algorithm for community detection and influence ranking in social networks," 2014 IEEE/ACM International Conference on Advances in Social Networks Analysis and Mining (ASONAM 2014), 2014, pp. 555-560, doi: 10.1109/ASONAM.2014.6921641.
4. N. Barbieri, F. Bonchi and G. Manco, "Influence-Based Network-Oblivious Community Detection," 2013 IEEE 13th International Conference on Data Mining, 2013, pp. 955-960, doi: 10.1109/ICDM.2013.164.
5. Rao and A. Mitra, "A new approach for detection of common communities in a social network using graph mining techniques," 2014 International Conference on High Performance Computing and Applications (ICHPCA), 2014, pp. 1-6, doi: 10.1109/ICHPCA.2014.7045335.
6. Uno, Takeaki, Tatsuya Asai, Yuzo Uchida, and Hiroki Arimura. "LCM: An Efficient Algorithm for Enumerating Frequent Closed Item Sets." In *Fimi*, vol. 90. 2003.
7. <https://www.python-course.eu/networkx.php>

Development of Combination Herbal Microencapsulated Healthcare Apparel for Skin Discolouration

K. Chandrasekaran

Department of Fashion Technology, PSG College of Technology, Coimbatore-641 004, Tamilnadu, India

ABSTRACT

In this work, 100% bamboo knitted fabric was chosen for the development of healthcare apparel for skin discolouration based on its water absorbency, antimicrobial, thermo regulation and softness characteristics which are very much essential for curing skin related problems. From the study of medicinal herbs, neem, wild turmeric, tulsi and karboga arisi were identified for skin discolouration problem. From the methanol extract of herbal extracts, micro capsules were prepared. The pre-treated bamboo knitted fabric was finished with micro capsules of the combinational medicinal herb extracts (Sample A: Turmeric, Tulsi, Onion powder, & Karbogaarisi Sample B: Turmeric, Neem & Tulsi;) using pad-dry cure method with optimized process parameters. The developed fabric samples were tested for contact allergy test (Patch Test). The comfort properties tests were carried out to test the properties such as air permeability, water vapour permeability, drapeability, thermal conductivity and water absorbency. The t-test results showed that treated samples were significantly better than the pre-treated samples in thermal conductivity, water vapour permeability and air permeability characteristics. In FTIR (Fourier Transform Infrared Spectroscopy) analysis, the presence of active components has been confirmed. The SEM (Scanning Electron Microscopy) analysis also confirmed the presence of microcapsules on the fabric surface. From the test results 100% bamboo knitted fabric treated with the combination herbal extracts of Turmeric, Neem and Tulsi was chosen for developing night wear apparel to care against skin discolouration problem. A wearer trial was conducted who are having the skin discolouration problem and the results show that there is a significant improvement observed in all the cases.

Indexterms— Bamboo fabric, Combination medicinal herb extract, Healthcare apparel, Skin discolouration

I. INTRODUCTION

The World Health Organization emphasizes the use of medicinal plants and their products. India's ancient form of medicine ayurveda had a branch called Ayurveda. "Ayurveda" is based on the Ayurvedic principle that regular contact with a fabric made from the yarns treated with organic herbs and medicinal plant extracts will alleviate metabolic disorders and leads a new line of healthy living. The Ayurveda emphasize the importance of sustaining the planet for upcoming generation. Now-a-days human skin is get in contact with pollution and other toxic substances which leads to skin allergy, skin cancer, skin discoloration etc. Skin discoloration, a change in the color of the skin, is caused due to health problems or side effects of medications. Discoloration is a darkening of the skin in the case of melasma and in the case of another category of skin discoloration i.e. vitiligo, in which a complete loss of pigmentation that results in white skin is noticed. The main aim of the work is to impart medicinal value to 100% bamboo knitted fabric by treating it with microcapsules of organic farm grown medicinal herb extracts to care against the skin discoloration problem by providing it with more comfort to the people who are affected with skin discoloration.

II. RELATED WORKS

The existing scenario of eco-consciousness, consumers expect the production process should be environment-friendly along with the use and durability of the product [1]. In Ayurveda based healthcare textiles, herbal extracts were used for curing various types of diseases by incorporating the herbal substances into the fabric and which in turn enter the body through skin and the healing will take place [2]. Today, the comeback of Ayurvedic polyherbal formulations (use of multiple herbs) have occurred worldwide, most of the times, they got acceptable results and safety, making them one of the highly chosen medicines of selection [3]. The study about herbal synergism highlighted that synergistic actions may be accountable for the medical efficacy of an extensive number of herbal products [4]. *Curcuma aromatic* Salisb. Commonly known as wild turmeric, mentioned as a medication for curing various types of skin diseases. Extensive research works performed in the last few decades establishes the medical potential of wild Turmeric and its extracts [5]. The extracts of the *Ocimum sanctum* Linn. alone and its combination with other medicinal plant extracts were reported with good medicinal efficacy [6].

Neem was used in the treatment for Dermatitis Eczema, Acne, Bacterial, Fungal infections and many skin disorders. It has established its usefulness as a powerful antibiotic. Neem also has revealed its antiviral, anti-fungal and anti-bacterial properties [7]. *Psoralea corylifolia* has been reported to give in noteworthy positive

outcomes in vitiligo (white patches) management [8]. The *invitro* drug release studies using microencapsulated *Terminalia* reported that drug releasing characteristics expected to be a promising area of research in the health care sector [9]. In their research work, Sumithra & Vasugi Raaja used 100% cotton denim fabric and it was given finishing treatment with the combination poly herbal extracts comprising of three herbs in the proportion of 1:3:2 to get antimicrobial activity yielded best results. Micro encapsulation and nano-encapsulation of the herbal extracts were carried out and the study reported that the encapsulated fabric retained good antimicrobial activity even after 30 washes. Chandrasekaran *et al.* (2012) have carried out an inspiring research work to develop polyherbal extracts treated curative garments and highlighted this approach as a supportive curative therapy to cure the specific disease. In this work, it was mentioned that about 16 medicinal herbs used for curing 7 diseases. The study was reported as a substitute method of drug delivery [11]. Wear comfort requirement is essential for bio-functional textiles. To improve the skin sensorial wearing comfort of the bio-functional textiles, hydrophilic treatments with good process parameters along with the use of spun yarns are essential [12]. The moisture management ability of the knitted fabrics can be maximized by the correct selection textile materials. The moisture management in knitted fabrics can be further improved by appropriate finishing treatments. The type of fabric knitted structure reported as more essential for achieving excellent moisture management potential [13]. In line with the findings of several literatures, the present work is aimed on the exploration of the synergistic effect of appropriate combination medicinal herb extracts treatment on the selected textile fabric by adopting the polyherbal concept. The study is aimed to address the problems associated with skin discoloration through healthcare apparel solution.

III. METHODOLOGY

A. Materials

The particulars of the materials such as medicinal herbs, textiles used in the developmental work are given below.

1) TEXTILES

The particulars of 100% Bamboo knitted fabric used for the development of health care apparel are furnished in Table I.

Table I. Knitted fabric particulars

Particulars	100% Bamboo fabric
Fabric structure	Single jersey
Yarn count(Ne)	40s
TPI	21.87
Wales /inch	44.4
Course /inch	33.3
GSM	130
Loop length (mm)	3.2
Tightness factor	13.86

2) Medicinal Herbs

The details of the medicinal herbs utilised for the development of health care apparel are given in Table II.

Table II. Medicinal herbs particulars

Common name for the medicinal herbs used	Botanical name for the medicinal herbs used	Parts used
Neem	Azadirachta indica	Bark
Wild Turmeric	Curcuma aromatica	Rhizome
Holy basil	Ocimum sanctum	Leaves
Karboga arisi	Psoralea corylifolia	Seeds
Onion	Allium cepa	Bulb

B. Methodology

100% bamboo knitted fabric was given the following pre-treatment processes.

1) Scouring

The recipe for the scouring of 100% Bamboo knitted fabric is given in table III.

Table III Recipe for scouring

Sodium hydroxide	10gpl
Sodium carbonate	10gpl
Soap solution	5cc/l
Temperature	90°c
Time	90 minutes
M:L	1:25

2) Bleaching

The recipe for the bleaching of 100% Bamboo knitted fabric is given in table IV

Table IV Recipe for bleaching

Recipe	Half – bleach
Hydrogen peroxide	7 gpl
Sodium silicate	7 gpl
Sodium hydroxide	0.5 g/l
Sodium carbonate	2 g/l
M : L	1:20
Time	60 minutes
Temperature	80 °c
pH	10.5

3) Preparation of herbal extract

The herbs such as wild turmeric, neem, tulsi, and onion and karboga arisi were obtained in the powder form. Microencapsulation was done in two combinations which are named as sample A and sample B. The herbal combination and ratio is given in Table V.

Table V Preparation of herbal extract

Sample Description	Herbal combination	Ratio
Sample A	Wild Turmeric, Tulsi, Onion powder, Karbogaarisi	1:1:1:0.5
Sample B	Wild Turmeric, Neem, Tulsi	1:1:1

In this work, herbal powders were soaked in methanol to extract the active components from the herbs.

4) Microencapsulation process

Microcapsules are formed by using polymer interface method. Microencapsulation was done using the herbal extracts as core material and gum acacia as wall material.

5) Finishing of health care fabrics by Pad-dry-cure method:

The knitted bamboo fabric was first immersed in water and squeezed. After that, fabric was dipped in the microcapsule solution using pneumatic padding mangle; it is squeezed, dried and then cured.

6) Testing of Healthcare Fabrics

To determine the effectiveness of the combination medicinal herb extracts treated 100% bamboo knitted fabric, the following tests have been carried out.

Contact allergy test (patch test)

Fabric surface analysis tests:-

- Fourier Transform Infrared (FTIR) Spectroscopy Analysis
- Scanning Electron Microscope (SEM) Analysis

Comfort property tests

- Air permeability test
- Water absorbency test
- Thermal conductivity test

-Water vapour permeability test

-Drapeability test

6.1 Contact allergy test (patch test)

In patch test, subjects tested were random volunteers representing three male and three females for the present study. In this test, fabrics were patched on the normal skin and monitored for 24 hrs to notice any allergy symptoms which leads to contact dermatitis.

6.2 Fabric surface analysis tests:-

The confirmation of the presence of active components has been done using FTIR (Fourier Transform Infrared Spectroscopy) tester. The confirmation of the presence of microcapsules has been done using SEM (Scanning Electron Microscope) tester.

6.3 Comfort property tests

The air permeability of the fabrics were carried out in KES Air-permeability tester which gives the resistance of the tested fabric to the passage of air using the ASTM D7-96 standard test method for air-permeability of textile fabrics. For water absorbency test, AATCC/ASTM TEST METHOD TS-018 is used. Lee's disc method is used for measuring the thermal conductivity of the fabric. ASTM method E 96-80 test procedure is used for the measurement of water vapour permeability. The drapeability of the developed samples was tested with drape meter by using cusack drape test method.

7) Development of Health Care Apparel for Skin Discoloration

After the testing of developed samples for contact allergy, fabric surface analysis and comfort properties, the sample which excels in both aspects has been selected and night wear apparels were developed.

8) Wearer Trial

The performance of the developed health care apparel was evaluated by conducting a wearer trial for one month duration by giving it to volunteers as given in table VI. The volunteers were given the apparel and instructed to use it especially during the night time and its effects were accessed regularly.

Table VI Wearer trial summary

S.No	Age	Gender	Problem
1	19	Male	Black spots on the skin
2	24	Male	Black spots on the skin

IV.RESULTS AND DISCUSSION

A. Evaluation Of Contact Allergy Test

Patch test was carried out to check the irritation level of the patient. From the test result (Table VII) it is observed that the treated samples showed no irritant reaction on the test subjects except one male in sample A. This clearly confirms that the fabric sample does not cause any irritation to the people who are affected with skin discoloration. This is very important result since the skin discoloration gets worsened due to clothing irritation.

Table VII – Contact Allergy Test Results

Subjects	Sample A	Sample B
Subject 01 (male/21 yr)	-	-
Subject 02 (male/30 yr)	-	-
Subject 03 (male/35 yr)	-	-
Subject 04 (male/22 yr)	-	-
Subject 05 (male/25 yr)	IR	
Subject 06 (male/29 yr)	-	-

B. Analysis of Fabric Surface Characteristics

1. Analysis of FTIR (Fourier Transform Infrared Spectroscopy) test results

The Fourier Transform Infrared Spectroscopy (FTIR) spectrum of pre-treated sample, Sample A & Sample B are given in Figure 1, 2 & 3 respectively.

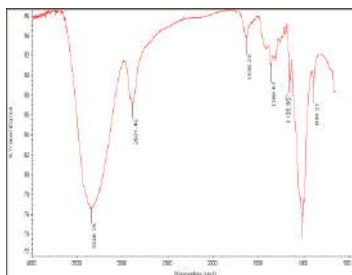


Fig 1 FTIR Spectrum of Pre-Treated Sample

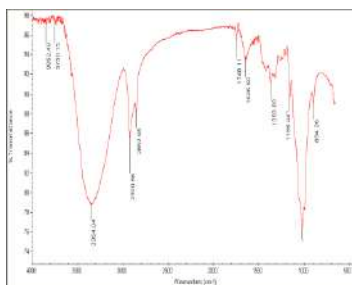


Fig 2 FTIR Spectrum of Sample A

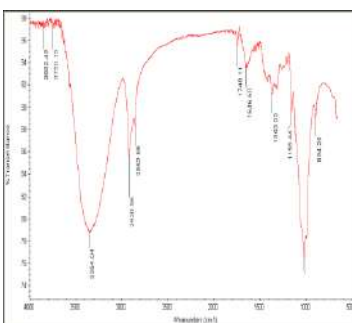


Fig 3 FTIR Spectrum of Sample B

In pretreated sample alkyne C-H group is stretching around 3346.25 cm⁻¹ and C-C group stretching around 1000cm⁻¹.In microencapsulated sample A, in addition to the peak appeared in pretreated sample, C-H alkyne group is stretching more around 3903cm⁻¹ to 3345cm⁻¹ and also a new peak is corresponding to –CH methylene group is stretching around 2920 cm⁻¹ and this is due to the incorporation of active components turmeric, tulsi, onion powder and psoralea corylifolia. In microencapsulated sample B, in addition to the peaks observed in pre-treated, a new peak is observed around 2920 cm⁻¹ where –CH methylene group is stretching which is due to the incorporation of active components wild turmeric ,tulsi and neem.

2. Analysis of SEM (Scanning Electron Microscopy) test results

The scanning electron microscopy (SEM) images of parent pre-treated knitted fabric and treated fabric samples (Sample A & Sample B) are shown in figure 4, 5 & 6 respectively. From the SEM photographs, it is clearly evident that the presence of the applied herbal substances in the form of microcapsules is firmly attached to the fabric seen in Sample A and Sample B.

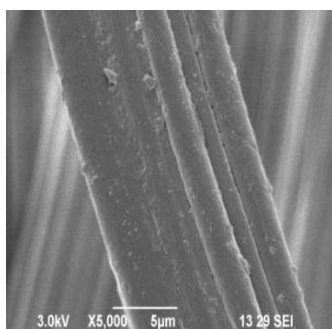


Figure 4 SEM image of pretreated sample

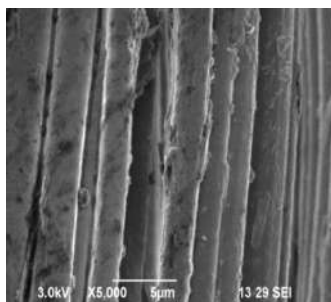


Figure 5 SEM image of Sample A

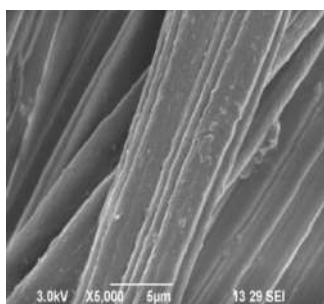


Figure 6 SEM image of Sample B

C. Evaluation of Comfort Property Tests

1. Evaluation of air-permeability characteristics

The air-permeability test results of pre-treated fabric, Sample A and Sample B are given in Table VIII.

Table VIII Air Permeability test results

Air Permeability (Kpa s/m)		
Pretreated	Sample A	Sample B
66.97	78.08	89

From the test results, it is obvious that the knitted fabric samples, which are the single jersey knit structure, offered a higher permeability level than pre-treated fabric. This property can be exploited by developing the apparel with the knitted samples for more complex skin diseases. Since in these diseases, the fabric surface friction with skin may aggravate the diseases. This property also helps to dry out the sweat emitting from the skin easily, which will give wearing comfort to the wearer. The test result reveals that the treated samples (Sample A & B) have more air permeability than pretreated fabric. The t-test result shows that there is a significant difference exists between pretreated sample and treated samples.

2. Evaluation of water absorbency characteristics

The water absorbency test results of pre-treated fabric, Sample A and Sample B are given in Table IX.

Table IX Water absorbency test results

Water absorbency time (seconds)		
Pretreated	Sample A	Sample B
0.24	3.4	1.3

From the results, the time taken for the absorption of water is presented. Greater the time taken, lesser is the water absorbency. In that aspect, water absorbency time increases in the treated sample than the pretreated, this may be due to the addition of microcapsules of herb extracts which might have caused more time to absorb the water and hence the pretreated fabric has greater absorbency than the treated fabric. The t-test result shows that there is a significant difference exists between pretreated sample and treated samples.

3. Evaluation of Drapability Characteristics

The drapability test results of pre-treated fabric, Sample A and Sample B are given in Table X.

Table X Drapability coefficient test results

Drape coefficient			
S.No	Pretreated	Sample A	Sample B
1.	0.4593	0.5380	0.5695

The test results shows that drape ability of treated fabric decreases due to the addition of microcapsules of herb extracts which increases the fabric weight considerably to make it stiffer than the pre-treated fabric. T-test result shows that there is significant difference exist between pretreated and treated samples.

4. Evaluation of water vapour permeability characteristics

The water vapour permeability test results of pre-treated fabric, Sample A and Sample B are given in Table XI.

Table XI Water vapour permeability test results

Water vapour permeability (Grams/sq.metre/day)			
S.No	Pretreated	Sample A	Sample B
1.	528.75	723.5	748.5

The test result shows that the treated samples have more water vapour permeability characteristics than the pre-treated fabric. T-test result shows that there is significant difference exist between pretreated sample and treated samples.

5. Evaluation of thermal conductivity characteristics

The thermal conductivity test results of pre-treated fabric, Sample A and Sample B are given in Table XII.

Table XII Thermal conductivity test results

Thermal conductivity (W/KM)			
S.No	Pretreated	Sample A	Sample B
1.	0.0171	0.0217	0.0208

Thermal conductivity (W/KM)			
S.No	Pretreated	Sample A	Sample B
1.	0.0171	0.0217	0.0208

Thermal conductivity (W/KM)			
S.No	Pretreated	Sample A	Sample B
1.	0.0171	0.0217	0.0208

The study results show that thermal conductivity of the treated fabric samples is better than pre-treated samples. T-test result shows that there is a significant difference exists between pretreated sample and treated samples.

6. Evaluation of Wearer Trial

Based on the contact allergy test, fabric surface characteristics analysis and comfort property test results, the bamboo fabric treated with microcapsules of the combination herbal extract of wild turmeric, neem and tulsi has been chosen for the skin discolouration problem. Using this sample, night wears were constructed and given to two volunteers who are suffering from skin discolouration problem and wearer trial was conducted for a period of one month and the results are as follows.

VOLUNTEER 1:

Gender: Male

Age: 19

Sex: Male

Problem: Black spots on the body

VOLUNTEER 2:

Gender: Male

Age: 24

Sex: Male

Problem: Black spots on the body

The wearer trial results in both the cases show that there is a sign of disappearance of black spots in the affected area. If the apparel is worn for a longer duration the regaining of original skin tone can be effectively seen.

V.CONCLUSIONS

Polyherbal concept is successfully adopted in this research work. 100% Bamboo knitted fabric micro-encapsulated with wild turmeric, neem and tulsi was chosen for caring the skin discolouration problem based on

contact allergy test, fabric surface characteristics analysis and comfort properties test results. The wearer trial was conducted using the night wear apparel developed from the chosen sample. The wearer trial result shows that there is a significant improvement in all the cases. Further if the apparel worn for longer duration still better results may be expected.

ACKNOWLEDGMENT

The author wishes to thank Dr.K.Prakasan, Principal In-charge, PSG College of Technology and Dr.P.Kandhavadi, HOD-Fashion Technology for their help and encouragement in this work. The author wish to thank B.Tech Fashion Technology graduates R.Janani, Nivedhitha Moorthy and P.Sakthivel for their support and contribution in the research work.

REFERENCES

1. G.Thilagavathi and T. Kannaian, "Application of Pricky chaff (*Achyranthes aspera* Linn.) leaves as herbal antimicrobial finish for cotton fabric used in healthcare textiles", *Natural Product Radiance*, vol. 7, no.4, pp 330-334, 2008.
2. Farida, P, Minocheherhomji and Solanki, "Ayurveda: An Innovative Alliance of Ayurveda and Textile: A Review" *Scholars Journal of Applied Medical Sciences*, vol. 3, no. 2F, pp. 925-931, 2015.
3. Parasuraman, S, Thing, GS and Dhanaraj, SA, 'Polyherbal formulation: Concept of Ayurveda', *Pharmacognosy reviews*, vol. 8, no. 16, pp. 73-80, 2014.
4. Ma, XH,Zheng, CJ,Han, LY,Xie, B,Jia, J,Cao, ZW,Li, YX and Chen, YZ, 'Synergistic therapeutic actions of herbal ingredients and their mechanisms from molecular interaction and network perspectives', *Drug delivery today*, vol. 14, no. 11-12, pp. 579-588, 2009.
5. Sikha, A, Harini, A and Hegde Prakash, L, 'Pharmacological activities of wild turmeric (*Curcuma Aromatica Salisb*):a review', *Journal of Pharmacognosy and Phytochemistry*, vol. 3, no. 5, pp. 1-4, 2015.
6. Pingalea, SS, Firke, NP & Markandeya, AG, 'Therapeutic activities of *Ocimum tenuiflorum* accounted in last decade: A review', *Journal of Pharmacy Research*, vol. 5, no. 4, pp. 2215-2220, 2012.
7. Debjit Bhowmik, Chiranjib, Jitender Yadav, K. K. Tripathi and K. P. Sampath Kumar, "Herbal Remedies of *Azadirachta indica* and its Medicinal Application", *Journal of Chemical and Pharmaceutical Research*, 2(1): 62-72, 2010.
8. Hussain, Irshad & Mubarak, Naeem and Abro, Hakim. "Skin Pigmentation Effects of *Psoralea Corylifolia*: A Case Study of Vitiligo" *JIIIMC*, Vol. 14, No.1, 2019.
9. Rathinamoorthy, R and Thilagavathi, G, 'Antimicrobial and In -Vitro Drug Release Studies of Microencapsulated *Terminalia chebula* extract finished Fabric', *International Journal of PharmTech Research*, vol. 5, no. 3, pp. 894-905,2013.
10. Sumithra, M and Vasugi Raaja, 'Micro-encapsulation and nano-encapsulation of denim fabrics with herbal extracts', *Indian Journal of Fibre & Textile Research*, vol. 37, pp. 321-325,2012.
11. Chandrasekaran, K, Ramachandran, T and Vigneswaran, C, 'Effect of medicinal herb extracts treated garments on selected diseases', *Indian Journal of Traditional Knowledge*, vol. 11,no. 3, pp. 493-498,2012.
12. U.C.Hipler and P.C.Elsner, "Current problem in dermatology: bio functional textiles and skin", Switzerland, S.Kargar AG,2006.
13. Hussain, T, Nazir, A and Masood, R, 'Liquid Moisture Management in Knitted Textiles – A Review', *Proceedings of the Third International Conference on Value Addition & Innovation in Textiles (Covitex-2015)*, pp.15-26, 2015.

IOT Based Secured Patient Healthcare System

B. Nivedetha

Department of EEE, PSG College of Technology

1. ABSTRACT

Smart and cost-effective healthcare has been in increasing demand to meet the needs of growing human population and medical expenses. It is very much needed to develop a secured health monitoring system which monitors the heart pulse and oxygen saturation level of a patient to detect abnormalities of health conditions in time and make diagnoses according to the monitored data. The data is sent over internet in order to access it from all over the world, so that the patients can be monitored even from the home. The data sent over internet needs to be encrypted in order to protect it from intruders, and therefore any modifications in the sent data can be avoided. A secured IoT based healthcare system is proposed in this work to monitor the patients continuously and to save their lives. The proposed work allows the organization to store the IoT data on the cloud securely by applying Blowfish encryption and cryptographic concepts.

Keywords: IoT, ECG, Health monitoring, Sensor, Blowfish

2. INTRODUCTION

Internet of Things is the network of physical devices, vehicles, home appliances and other items embedded with electronics, software, sensors, actuators, and connectivity which enable these objects to connect and exchange data. Things are uniquely identified using its embedded computing system and connected with the existing Internet infrastructure. Objects used in IoT can be sensed and controlled remotely across existing network infrastructure. It has direct connection of physical world into computer based systems with improved efficiency, accuracy, low cost and less human intervention. This method helps to improve the lives of patients which includes the elderly, physically, mentally disabled and as well as the chronically ill patients.

3. IoT IN HEALTHCARE

IoT [2] devices are used for remote health monitoring and emergency notification. The health monitoring devices include specialized implants such as pacemakers, wristbands, or hearing aids and sensors for blood pressure, heart rate. Smart beds are implemented in few hospitals to detect the movement of patient in ICU. The patient data are accessible by all the staff and doctors, so a new method is proposed where patient and doctors are able to communicate through mobile application. In hospitals, patients are monitored continuously by measuring their medical parameters continuously. The monitoring has to be continued even when they return to home as there is a chance that the disease may return again. Patient's data like heart rate, oxygen level will be frequently measured and sent to server. Using a web browser Application in patient's or his caretaker's Smartphone the patient can view his health status. To continuously monitor the patient sensors are connected to a Microcontroller and a LCD display is attached to view the data. This system will continuously monitor the patient's heartbeat along with body temperature, if there is a lot of variation in the value then an alert message is sent to the Pre-saved contacts and doctor.

4. HEALTHCARE REQUIREMENTS

The various Sensors used in Medical Healthcare are Temperature sensor, ECG and Pulse oximeter connected to the Arduino.

4.1 ECG SENSOR

The AD8232 as shown in Figure 1 is a sensor for measuring ECG [1] and other bio-potential. These sensors can extract, amplify, and filter even small bio-potential signals in the presence of noise due to movement.



Fig 1 ECG Sensor

4.2 PULSE OXIMETER SENSOR

MAX30100 as shown in Figure 2 is a sensor with integrated pulse oximeter and heartrate monitor. It has two LED's, a photo-detector, optics, and analog signal processing unit with low noise for detecting pulse oximetry and heartrate signals.



Fig 2 Pulse Oximeter Sensor

4.3 TEMPERATURE SENSOR

LM35 as shown in Figure 3 is a sensor with integrated circuit which is used to measure temperature in °C.

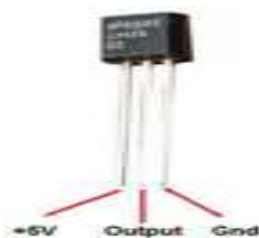


Fig 3 Temperature Sensor

4.4 ARDUINO UNO

The Arduino UNO as shown in Figure 4 is a widely used ATmega328P open-source Microcontroller board developed by Arduino.cc.



Fig 4 Arduino UNO

4.5 LCD DISPLAY

LCD display as shown in Figure 5 is a flat-panel display which uses the light-modulating properties of liquid crystals.

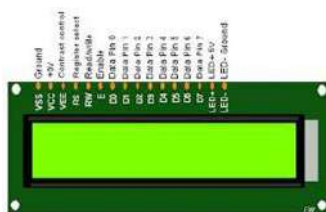


Fig 5 LCD Display

5. PROPOSED SYSTEM

The health monitoring system is a two tier architecture and they are

- Wireless Body Sensor Network(WBSN)
- Graphical User Interface

The Wireless Body Sensor Network [4] mainly consists of the wearable sensors like Pulse oximeter, temperature sensor and the heartbeat sensor. They act as data collecting units, collecting the physiological signals from the patient's body through the sensors. These collected data are then forwarded to the base station or the gateway server via serial communication. In the base station, data that is send will be stored as files for

the forthcoming purposes. When required the data can be accessed anytime by typing the corresponding IP address at the end user device like PC, laptop, tablet, etc. The last part of the architecture or the GUI is used to store, analyze and present the received data in a graphical and text format.

The Proposed work IoT based secured Healthcare consists of an Arduino UNO and the sensors are connected to the board and it is shown in the Figure 5.

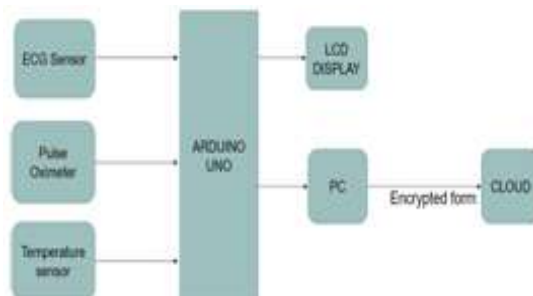


Fig 6 Flow Diagram of IoT based Secured Healthcare System

The values from the ECG [11] and Pulse oximeter sensors are sent to the Arduino by connecting the sensors using I2C configuration with Arduino UNO and the data are serially transmitted to the cloud after encryption, which is shown in the Figure 6. The following are the workflow of the proposed healthcare system

Step 1: Monitor the ECG [3], Spo2, Heart rate, Temperature of the patient.

Step 2: Find if the monitored values are within the normal range or it goes beyond the normal range.

Step 3: If the parameters are within the normal range, then no values are stored on the cloud [5] and the continuous monitoring takes place.

Step 4: If the parameters are beyond the range then the values are uploaded and saved in the cloud [6]. This technique is used in order to save the memory usage of the cloud.

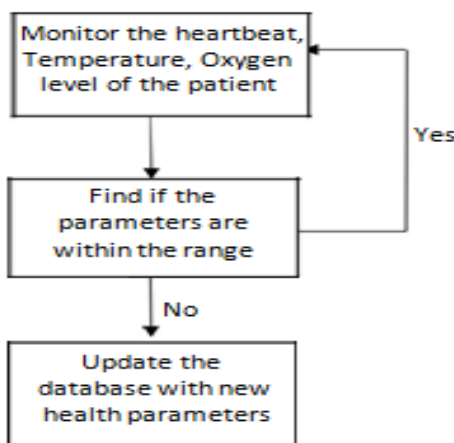


Fig 7 Flowchart of the process

6 CLOUD DEPLOYMENT

The values monitored through the ECG, Pulse oximeter, Temperature sensors are uploaded to the cloud using the visual studio software. The website for storing the monitored data in a specific server is bought from a website vendor cyber students.in, who allocates separate space in their dedicated server in which the values can be stored [8].

7 ENCRYPTION ALGORITHM

In cryptography, a message or information is encoded which is accessed only by authorized parties and unauthorized cannot access them. This encryption method can be employed to forbid intervention and prevents unauthorized from accessing. During encryption the plain text which is the intended information or message is encrypted into a cipher generating cipher text. This cipher text can be read only if decrypted using suitable decryption algorithm. The encryption [7] and decryption can be carried out either symmetric or asymmetric method. The Encryption Algorithm that is proposed in this work is Blowfish algorithm. Blowfish is a symmetric-key block cipher included in a large number of cipher suites and encryption products with 16 rounds.

9 ENCRYPTION AND DECRYPTION

The encrypted values of ECG, Temperature and Pulse oximeter sensor values done using Microsoft Visual Studio for the first person is shown in the Figure 12

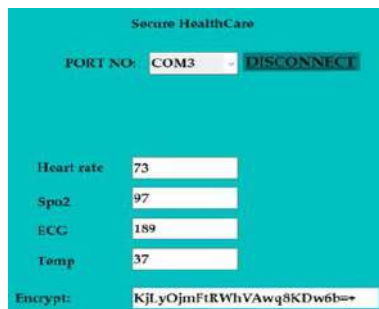


Fig 12 Encrypted Value of the Monitored Sensor Values for Person 1

This application is developed using visual studio software and the separate label and text boxes are created for each of the monitored values. Since it uses serial communication, specifying the port to which the controller is connected to the PC displays all the values in this application. The encrypted value of all the values is shown in the last label Encrypt. By connecting the PC to internet all the values are uploaded to the cloud. Similarly for the second and the Third Person the encrypted values of the monitored sensor values are shown in Figure 13 and Figure 14.

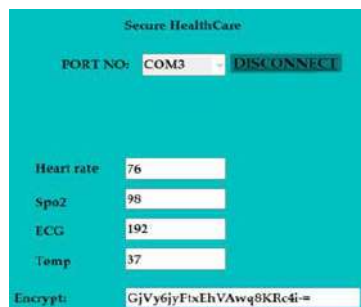


Fig 13 Encrypted Value of the Monitored Sensor Values for Person 2



Fig 14 Encrypted Value of the Monitored Sensor Values For Person 3

The values obtained from ECG, Pulse oximeter, Temperature as shown in Figure 14 are sent to the Arduino and the values are uploaded to the cloud using serial communication with the help of visual studio software [9]. The Decrypted values for the Encrypted values obtained in the Figure 15, Figure 16, and Figure 17.

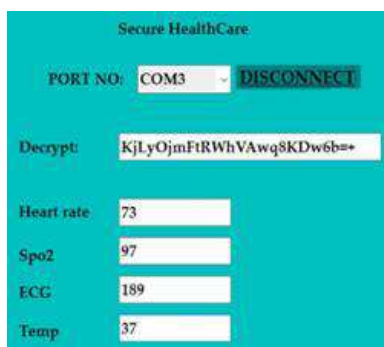


Fig 15 Decrypted Value of the Encrypted Sensor Values for Person 1

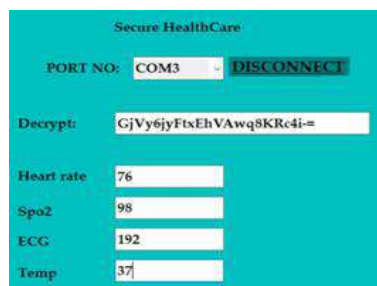


Fig 16 Decrypted Value of The Encrypted Sensor Values For Person 2



Fig 17 Decrypted Value of the Encrypted Sensor Values for Person 3

2479	000	000	012	039
2480	019	000	010	036
2481	129	093	149	039
2482	160	093	095	039
2483	058	000	015	040
2484	068	000	182	039
2485	054	000	184	039
2486	079	095	183	041
2487	079	093	183	040
2488	079	095	183	039
2489	031	095	184	038
2490	031	095	184	037
2491	030	098	010	037
2492	098	098	184	037
2493	058	098	184	034
2494	049	097	183	034
2495	037	000	188	035
2496	037	000	188	035
2497	035	000	195	034
2498	039	099	217	034
2499	063	099	219	035
2500	051	098	215	034
2501	181	067	214	035
2502	041	000	218	035
2503	055	000	204	035
2504	055	000	204	034
2505	035	097	002	034

Fig18 Sensor values uploaded in Cloud

In Figure 18, first column denotes the serial number, the second column denotes the heart rate of the patient, the third column denotes the Spo2 value, the fourth column denotes the ECG values [10] and the last column denotes the Temperature of the patient under monitoring.

10 SUMMARY

A Secured Healthcare system is discussed in this work which includes software and hardware modules such as Arduino UNO, LCD, Microsoft visual Studio, MySQL, Arduino IDE which are used in this work. For cryptography Blowfish cryptographic algorithm is used and the tasks involved in that algorithm are briefly described. The values are monitored from the patients and they are encrypted, then the values are uploaded in the cloud and decrypted using the Blowfish algorithm. Through Decryption the monitored values are obtained in the Visual Studio software and can be viewed by the Caretaker or the Doctors.

This method is implemented using ECG, Pulse oximeter, Temperature sensors interfaced with the Arduino. These Sensors are connected to the patients as wearable. Values of ECG, Pulse Oximeter and the temperature sensor are obtained in the serial monitor of Arduino IDE, encrypted and then uploaded to the cloud through serial communication using Visual Studio software.

By using the web browser in the mobile phone or PC or any other electronic gadgets the values can be monitored by accessing the URL. In this way a secured healthcare system is established. Thus patients with heart diseases can be monitored with the help of this project.

11 FUTURE ENHANCEMENTS

The further work which can be included in this project is to alert the caretaker or doctor with an alarming signal whenever the values go beyond the normal range so that no constant monitoring is needed. Moreover sensors such as EOG, Pressure, Hand and leg movement sensor can also be added to this proposed work.

12 REFERENCES:

1. Uttam U. Deshpande and Milan A.Kulkarni, "IoT based Realtime ECG Monitoring System using Cypress WICED", *IJAREEIE*, Vol 6, pp.710-720, 2017.
2. Sneha N. Malokar and Samadhan D. Mali, "An IoT Based Health Care Monitoring System-A Review", *IJIRCCE*, Vol 5, pp.11583-11589, 2017.
3. Megha Koshti and Sanjay Ganorkar, "IoT Based Health Monitoring System by using Raspberry Pi and ECG Signal", *IJRSET*, Vol 5, pp.8977-8985, 2016.
4. Farah Nasri and Abdellatif Mtibaa, "Smart Mobile Healthcare System based on WBSN and 5G", Vol.8, No.10, *IJACSA*, pp.147-156, 2017.
5. Zhifeng Xiao And Yang Xiao, "Security And Privacy In Cloud Computing", *IEEE Communications Surveys & Tutorials*, Vol.15, No.2, Second Quarter, pp 843-859, 2013.
6. Saira Varghese, S.Maria Celestin Vigila, "A Comparative Analysis on Cloud Data Security", *Proceedings of 2015 Global Conference on Communication Technologies*, pp.507-510, 2015.
7. R.Manjusha, R.Ramachandran, "Comparative Study of Attribute Based Encryption Techniques in Cloud Computing", *International Conference on Embedded Systems*, pp.116-120, 2014.
8. Kajal Chachapara, Sunny Bhadlawala, "Secure sharing with cryptography in cloud computing", 2013 Nirma University International Conference (NUiCONE), pp.1-3, 2013.
9. Hassanalieragh, A. Page, T. Soyata, G. Sharma, M. Aktas, G. Mateos, "Health Monitoring and Management Using Internet-of-Things (IoT) Sensing with Cloud-based Processing: Opportunities and Challenges", *Services Computing (SCC)*, IEEE, pp. 285-292, 2015.
10. E.M. Fong and W.Y. Chung, "Mobile Cloud-Computing Based Healthcare Service by Noncontact ECG Monitoring", *Sensors*, pp. 16451-16473, 2013.
11. Y.Wang, "Design and evaluation of a novel wireless reconstructed 3-lead ECG monitoring system", In: *Proceedings IEEE 2013 Biomedical Circuits and Systems Conference (Bio-CAS)*, pp.362-365. Rotterdam, 2013.

Covid-19 Severity Detection

M. Prethi and Ila. Vennila

Department of Electrical and Electronics Engineering, PSG College of Technology, Coimbatore, India

ABSTRACT

This paper proposes a deep convolutional layer network for the severity detection of COVID-19 disease. The rapid spread of coronavirus infection has surprised the world and has had a major impact on the lives of billions of people. Deep learning algorithms can be developed to help analyze the potentially large number of chest CT scans. However, segmenting infected regions from CT images is a difficult task and many different algorithms need to perform for identifying the affected and not affected lungs of a CT images. To address these challenges, the two techniques namely adaptive super pixel for identifying dots part and Ground Truth Segmentation is applied to separate the infected regions from chest CT images. The ResNet-50 deep convolution neural network is used to identify the symptoms of the segmented infected region. According to the pixel information the segmentation process is done. According to the segmented data the symptoms of COVID-19 are classified. The proposed methods of CNN minimize the requirements of the manual process of CT images and distinguish the different symptoms of COVID-19 patient.

Keywords-COVID-19, deep learning, CT images, classification, image processing, Convolution Neural Networks.

I. INTRODUCTION

Coronavirus disease 2019 (COVID-19) has been started widespread worldwide since December 2019 [1], [2]. It's highly contagious, and severe cases can cause acute respiratory distress or multiple organ failure [3]. On 11 March 2020, the WHO has made the assessment that COVID-19 is characterized as an epidemic. As of 8th April 2020, in total, 1,391,890 cases of COVID-19 are recorded, and thus the worth has reached 81,478 with a rapid increase of cases. The diseases are usually confirmed by using the reverse transcription-polymerase chain reaction (RT-PCR) test [4]. While diagnosis and confirming of COVID-19 patients using RT-PCR is a

Time-consuming process and it also produces false-negative cases which put into the difficult situation for the presumptive patients to be identified and treated firstly [3], [5], and [6]. As a non-invasive imaging technique, computed tomography can identify the patches like Ground glass detection, crazy paving pattern and the consolidation with the affected patient images. Hence CT may function as an important tool for COVID-19 patients to be screened and diagnosed early. Despite its advantages, CT may share some common same characteristics between COVID-19 and other chest diseases, therefore making the automated distinction is a little difficult [2]. Recently, deep learning-based AI (AI) technology has demonstrated tremendous success within the sector of medical data analysis because of its capacity of extracting rich features from multimodal clinical datasets [9]. The deep learning method was developed previously for diagnosing the disease and distinguishes different bacterial and virus infections from CT imaging data [10]. Additionally, attempts are made to detect various chest CT imaging features [11]. In the current COVID-19 pandemic, deep learning-based methods are designed efficiently for chest CT data analysis and classification of symptoms [2], [3], and [12]. Besides, deep learning algorithms are mainly focused on COVID-19 monitoring [13], screening [14] and prediction of the hospital stay [15]. Compared to X-rays images, CT screening is widely preferred because of its different slices and lungs can view at three dimensional. In recent works [4], [10], the infection signs are clearly visible through the CT slices of an image. The ground glass opacity are identified at early stages whereas the consolidation at later stage of COVID patients.

II. RELATED WORKS

A. Segmentation in Chest CT

CT imaging plays the major role for detection and diagnosis of lung infection [23], [24]. Initially the segmentation of lungs is not an easy task because there are also other diseases, so it leads to a wrong classification. For segmenting a CT images many Deep learning and machine learning algorithm were performed. The Ground truth segmentation algorithm segment the each and every pixels present in an image.

Therefore the affected regions are identified accurately.

The support vector machine (SVM) classifier is one of the machine learning algorithms to detect the lung nodules from CT slices [27]. In paper [28] the bidirectional chain code is used to segment the lung diseases and to reinforce the overall performance of the model. However, the similar visual appearances of nodules and

background of lung images put into difficult task for segmenting the nodule region. There are other several deep learning algorithms which overcome these problems [29]–[31]. The [29] central focused neural network are designed for segmenting the lung nodules from chest CT slices [30]. The GAN synthesized data are used in order to increase the number of training data which gives the better result. The residual deep network models are designed are detecting the lung tumor diseases.

B. Deep Learning

In our work, the aim is to segment the COVID-19 infection regions of the lungs for quantifying and evaluating the disease. The unsupervised machine learning algorithm identifies the affected nodules present in a CT images. Due to the limited data, the supervised learning cannot identify the diseases more accurately but using GAN synthesis more number of datasets can be created. The Transfer Learning method is the best for dealing with limited datasets [35], [36]. The transfer learning compared with each and every result initially; it identifies the affected and not affected patient. The importance of using supervised algorithm is to provide an accuracy result with the limited datasets [37]. The deep neural network method uses the supervised and unsupervised learning algorithm [38]. This supervised and unsupervised method reduces the loss of the unlabeled datasets and with the training datasets [39], [40], [41]. In [39] the cross entropy semi supervised method are being used which reduces the loss of the unlabeled datasets. In summary the existing method produces the loss and limited dataset method [41], and other approaches produces the supervision result with greater accuracy level [40]. Additionally, in medical segmentation the supervised learning plays an important role by producing results with the limited datasets and produces an unlabeled datasets [36], [42]. In [43] the pelvic segmentation using semi supervised learning produces the best result with the limited data. The residual learning methods are used in many different

applications. The advantage of using residual learning is it has a shortcuts which connects the output to the layer as an inputs. The residual connection has many interconnection blocks. The machine learning algorithm it identifies the region-attention loss is designed to proceed with the insufficient data issue for training and testing the deep learning models. In paper [44] developed segmentation of lesion using an MR images [45]. Different from these existing methods, our ground truth segmentation provides information of the affected regions.

C. Artificial Intelligence for COVID-19

Artificial Intelligent method are used in many of the application it plays a major role for identification of COVID-19 diseases [6], [15]. In artificial intelligent method it used in medical image segmentation, signal processing, satellite application, automotive and many other application. In this work, the medical segmentation are done for identifying the affected region [18], [22], [46], [47], [50]–[53], those medical datasets are based on the CT slices. For instance, in paper [46] designed a convolution neural network method to identify the affected patient and the not affected patients. Initially they trained on the different CT slices and those CT slices results are compared with the radiologist for identifying the affected region of the lungs. In [47] collected nearly 49,096 CT image slices from COVID-19 patients and normal patients who are suffering from the other several lung diseases. The CT images are trained by a U-Net architecture method to identify the affected patients. Those results are compared with the radiologist for further diagnosis of the diseases. The examples of deep learning algorithms include ResNet model, used in [18], and U-Net model [56], used in [50]. Finally, to segment, the infection regions in lung CT slices of an image the ground truth segmentation are performed for identifying the affected regions. The adaptive methods identify the total affected results.

III. PROPOSED METHOD

In this section, the Adaptive superpixel process is applied to identify the dots part of the affected patient and Ground Truth Segmentation for segmenting the most affected region. Finally, the deep convolution neural network is applied to identify the symptoms of the infected region of the COVID-19 patients

A. PREPROCESSING

Digital image processing is the application of signal processing techniques and is used in any number of medical imaging applications. Image processing is mainly focused to extract a piece of information by several image processing techniques and by their algorithms. Image processing is classified into the following three steps they are importing the images with the dataset or by digital photography. Analyzing an image which includes compression, spotting the pattern and enhancement of an image Output is the last stage of the image processing method in which the result can be altered image. The main classification of image processing is Visualization - sharpening, restoration and observation - To create a better image, image retrieval - the image of interest and measurement of pattern in the image – Measures various objects in an image. And finally an image Recognition – Distinguish the objects in an image. These are the image processing techniques.

B. Image Segmentation

In image processing, the segmentation of an image plays a major role. In image segmentation it subdivides the image into further parts like boundary, trace or line detection. This segmentation helps in further process for the better clarification and observation of the input image data. The image segmentation identifies the certain needed pixel and it gives the pixel information of the specific region that is segmented. After the preprocessing steps like image enhancement, filtering, compression and restoration the image processing techniques are applied.

C. Adaptive Superpixel Algorithm

Superpixels provide a useful pixel image representation. Firstly the superpixel methods, suffer from a minimum of a number of the drawbacks they are topology is handled heuristically, the total number of superpixels is predefined and lack of information and finally the lack of adaptiveness. As a remedy of this method, an adaptive superpixel method is introduced which helps in the better information gaining of an image and the accuracy level will also be better when compared to the superpixel method. BASS respects the topology, spatial coherence and it takes each and every pixel into an account which helps for better result accuracy. The BASS method is mainly used for focusing on the accuracy level of the performance for a medical application the accuracy level is important therefore the BASS method is mainly focused on medical application and satellite application. Qualitatively, the BASS method achieves the best results when compared to all other models and demonstration of this is not only by subjective visual inspection but also by the objective quantitative performance evaluation of the applications.

D. Ground Truth Segmentation

The Ground Truth Segmentation method is proposed in this model to segment a certain region alone. In this paper the focus is given to segment only the affected region of the chest CT images. The affected region alone is segmenting for getting a more information of an image which helps the doctor and radiologist for better results. It also helps in further treatment to the patient. Therefore, in this paper the Ground Truth Segmentation is implemented.

E. Architecture

• Residual learning

Residual learning plays a significant role in very deep layers. These residual blocks help in fast learning instead of calculating the mapping for each and every layer. This method is well suited for restoration and reconstruction problems since the output and input for these cases are similar. This approach mitigates the vanishing gradient problem also. Layer they use skip connections from the input and output images. This residual learning helps in increase of the performance and convergence of the model.

• Residual Network

Deep Residual Network contains the convolution layer, pooling layer, activation layer and fully connected layer. Each layer is stacked with one over the other layer. The residual network identifies the connection between the layer and it has a skip connection therefore, the learning process is better. A Residual block is shown in Fig. 1.

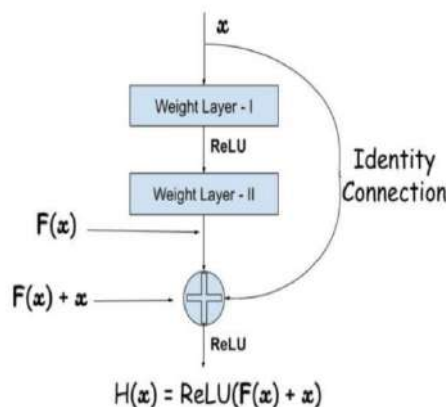


Fig.1 A Block of Deep Residual Network

• Residual Function

Residual mapping is the function that adds their input attributes to the output that is called skip connection which helps in a better learning process. Therefore, the final result of the residual function will be added up

with their input function the many attributes and information that can be gained by using a residual function. The Residual Mapping is acting as a bridge between the input and the output of the block and their representation of their residual function are described in fig.2.

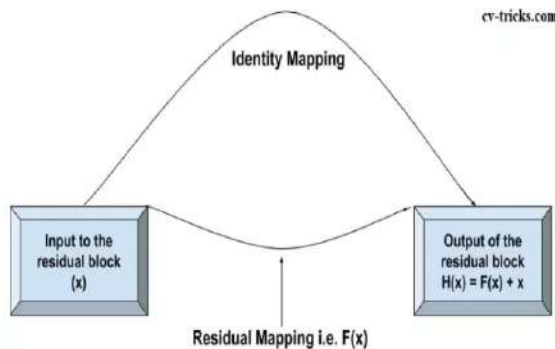


Fig.2 Intuitive representation of Residual Function

• **Architecture of RESNET-50**

The design of ResNet50 has 4 phases. The organization can take the info picture having stature, width as products of 32 and 3 as channel width. Each ResNet engineering plays out the underlying convolution and max-pooling utilizing 7×7 and 3×3 piece measures separately. A while later, Stage 1 of the organization starts and it has 3 Residual squares containing 3 layers each. The size of pieces used to play out the convolution activity in each of the 3 layers of the square of stage 1 are 64, 64 and 128 separately. The bended bolts allude to the personality association. The ran associated bolt addresses that the convolution activity in the Residual Block is performed with step 2, consequently, the size of information will be diminished to half as far as stature and width however the channel width will be multiplied. As we progress starting with one phase then onto the next, the channel width is multiplied and the size of the information is decreased to half. For deeper network like ResNet50, ResNet152, and so on, bottleneck configuration is utilized. For every remaining capacity F, 3 layers are stacked one over the other. The three layers are 1×1, 3×3, 1×1 convolutions. The 1×1 convolution layers are liable for lessening and afterward reestablishing the measurements. The 3×3 layer is left as a bottleneck with more modest info/yield measurements. The complete architecture of ResNet-50 is shown in fig.3

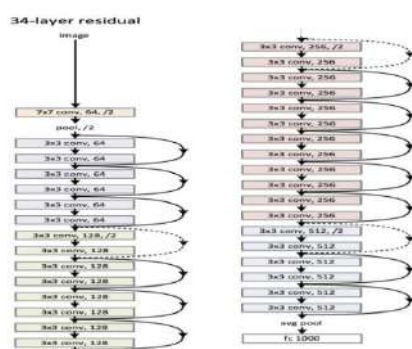


Fig.3 Architecture of ResNet-50

Each shaded square of layers address a progression of convolutions of a similar measurement. The component planning is intermittently down examined by steps convolution joined by an increment in channel profundity to save the time intricacy per layer. Specked lines indicate leftover associations in which we project the info by means of a 1x1 convolution to coordinate with the components of the new square. ResNet was not quick to utilize alternate way associations, Highway Network presented gated easy route associations. These defined entryways control how much data is permitted to stream across the alternate way. Comparable thought can be found in the Long Term Short Memory (LSTM) cell, in which there is a defined neglect door that controls how much data will stream to the following time step. Accordingly, ResNet can be considered as an uncommon instance of Highway Network.

IV. IMPLEMENTATION

MATLAB coding done by C language or any other program coding it can call the subroutines and inbuilt function in MATLAB. A covering capacity is made permitting MATLAB information types to be passed and

returned. MEX documents (MATLAB executables) are the powerfully loadable article records made by aggregating such capacities. Since 2014 expanding two-way interfacing with Python was being added. Libraries written in Perl, Java, ActiveX or .NET can be straightforwardly called from MATLAB, and numerous MATLAB libraries (for instance XML or SQL support) are carried out as coverings around Java or ActiveX libraries.

A. RESULTS

• Normal Image

The dataset are taken from the kaggle (<https://www.kaggle.com/c/covidct/data>) by using that dataset the affected and not affected by the COVID-19 disease and their affected regions are identified and segmented.



Fig.4 not affected Image

In fig.4 the original CT image of the not affected patient are taken for preprocessing and for further process. The original image is affected none of the lung diseases.



Fig.5 Result of not affected patient

Considering their dots part of the not affected CT image it is classified as normal. The fig.5 represents the result of the normal healthy patient.

• Affected Image

The patient affected by the COVID-19, CT image is taken for further processing. The fig.6 is the patient affected by the COVID-19 disease.



Fig.6 Affected Image

In the fig .6 the affected patient of images are taken and it is preprocessed and the dot parts are identified by the Adaptive Superpixel method. The dot parts represent the number of white and black pixels in the image.

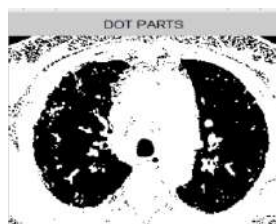


Fig.7 Dot Parts

In the Fig.7 the dots parts are identified by using an Adaptive Superpixel Algorithm it identify each and every pixel in the image and the centroid are taken in order to identify the total pixel information. The scattered and the white points are the affected portion of the patient CT image.



Fig.8 Segmented region

In the fig.8 represent the segmented portion of the affected image. According to the dots part identified by the Adaptive Superpixel Algorithm the infected region are identified. The segmentation of affected region is done by Ground Truth Segmentation method. By comparing all the pixel information the most affected regions are segmented. The less affected portion in the CT image will not give the more information of the affected patient for the further process therefore the highest affected region is segmented separately.

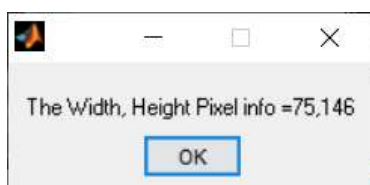


Fig.9 Pixel information

The fig.9 represents the total pixel information of affected segmented region. The 75 represent the total width size and 146 represent the height of the affected image pixel. With this information the total width and the total height affected by the patients are identified.

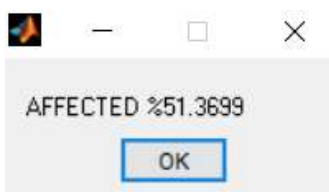


Fig.10 Affected percentage

In the fig.10 the affected percentage are calculated with the width and height pixel information. This percentage is for the segmented affected region. In the fig.8 the affected region are segmented in that region the affected percentage is 51.36. It helps the radiologist as well as doctor to identify the affected region and their total affected percentage.

The total pixel information and the affected percentage are shown in the table. 1.1.

IMAGE NUMBER	TOTAL WIDTH	TOTAL HEIGHT	AFFECTED PERCENTAGE	SYMPTOMS
D1	76	136	57.35	Ground Glass Opacity
D2	75	146	51.35	Consolidation
D3	10	12	30.54	Basic Syndrome
D4	56	83	69.87	Ground Glass Opacity
D5	33	84	39.28	Consolidation
D6	64	119	79.99	Crazy Paving Pattern
D7	50	58	86.20	Crazy Paving Pattern
D8	81	110	73.63	Ground Glass Opacity
D9	40	47	85.10	Crazy paving pattern
D10	30	90	33.33	Basic Syndrome

In the table 1.1, the parameters are displayed it includes the segmented region of the affected total width, total height, the affected percentage and the symptoms of the affected region. It helps the radiologist as well as doctor to identify the total affected and their symptoms, therefore it quicken the prediction process and start their early treatment.

V. CONCLUSION

In this paper, a deep convolution network is proposed for identifying the affected and normal patients. In the affected patient dataset, the adaptive superpixel is applied for identifying the dot part and ground truth segmentation process is applied to segment the affected region which helps the radiologists and the doctor to identify affected region more clearly. The total pixel information and the affected percentage are recalculated, which helps the radiologist in the analysis of the CT images.

REFERENCES

1. J. Chen, L. Wu, J. Zhang, L. Zhang, D. Gong, Y. Zhao, and S. Hu, "Deep learning-based model for detecting 2019 novel coronavirus pneumonia on high-resolution computed tomography: A prospective study," *Medrxiv* Jan. 2020.
2. F. Shan, Y. Gao, J. Wang, W. Shi, N. Shi, M. Han, Z. Xue, D. Shen, and Y. Shi, "Lung infection quantification of COVID-19 in CT images with deep learning," 2020, arXiv:2003.04655.
3. L. Li, L. Qin, Z. Xu, Y. Yin, X. Wang, B. Kong, J. Bai, Y. Lu, Z. Fang, Q. Song, K. Cao, D. Liu, G. Wang, Q. Xu, X. Fang, S. Zhang, J. Xia, and J. Xia, "Artificial intelligence distinguishes COVID-19 from community acquired pneumonia on chest CT," *Radiology*, vol. 19, Mar. 2020.
4. X. Xie, Z. Zhong, W. Zhao, C. Zheng, F. Wang, and J. Liu, "Chest CT for typical 2019-nCoV pneumonia: Relationship to negative RT-PCR testing," *Radiology*, vol. 12, Feb. 2020, Art. no. 200343.
5. T. Ai, Z. Yang, H. Hou, C. Zhan, C. Chen, W. Lv, Q. Tao, Z. Sun, and L. Xia, "Correlation of chest CT and RT-PCR testing in coronavirus disease 2019 (COVID-19) in China: A report of 1014 cases," *Radiology*, vol. 26, Feb. 2020, Art. no. 200642.
6. Y. Fang, H. Zhang, J. Xie, M. Lin, L. Ying, P. Pang, and W. Ji, "Sensitivity of chest CT for COVID-19: Comparison to
RT-PCR," *Radiology*, vol. 19, Feb. 2020, Art. no. 200432.
7. S. Rajaraman, S. Candemir, I. Kim, G. Thoma, and S. Antani, "Visualization and interpretation of convolutional neural network predictions in detecting pneumonia in pediatric chest radiographs," *Appl. Sci.*, vol. 8, no. 10, p. 1715, Sep. 2018.

An Intelligent System Using Deep Learning Techniques to Prevent Human-Animal Conflicts in Agricultural Lands

M. Kathiresh, P. Sweety Jose*, R. Neelaveni and C.T. Sangavi Chellam

Department of Electrical and Electronics Engineering, PSG College of Technology, Coimbatore, Tamilnadu, India – 641 004

ABSTRACT

Human - Wildlife conflict one of the main threats revolving around the forest border areas. Intrusion of wild animals into agricultural fields brings damage to both, property and lives of human beings. This creates a great need for the development of animal repellent systems. This paper proposes an Internet of Things (IoT) based smart device that effectively repels animals from the agricultural fields. In this proposed system, movement of any object in the surroundings is detected by the Passive Infrared (PIR) Sensors. When motion is detected, the thermal camera is rotated to a specific position and triggered to capture the image. The captured image is transmitted to the Raspberry Pi for detection of the animal. Three classifiers - Support Vector Machine (SVM), k - Nearest Neighbors (k-NN) and Convolutional Neural Network (CNN) are considered for detection and the best results were obtained with CNN. The proposed system achieves up to 95.24% classification accuracy with CNN. Based on the animal detected, ultrasonic waves of desired frequency range are generated to exasperate the wild animals. In addition to the above feature, the lights are also flashed at the animal to have a better repelling effect. The captured images of the animal, along with time and location information are transmitted from the embedded controller to the Forest Department through Internet. Simultaneously, a warning message is given through the Public Addressing System to warn the people living in the nearby residential area. An alert tone or text message is also transmitted to individual mobile phones from the Forest Department.

Indexterms - Animal Intrusion Monitoring; Thermal Image; Convolutional Neural Network; Animal Repeller; Internet of Things

INTRODUCTION

Animal intrusion into residential or agricultural lands is increasing nowadays due to deforestation and reduced rainfall. Serious threats are encountered by the agriculturists from thefts, natural calamities, crop losses and damages by animals, resulting in lower yields. In India, about 400 citizens are killed annually in human-animal conflict. A study carried out by the Wildlife Institute of India during 2007-2011 reported 7,381 human injury cases and 888 human deaths due to animal intrusion into human habitat. The Ministry of Environment, Forests, and Climate Change has studied about 98 casualties due to tiger attack from 1 April, 2013 to 31 March, 2017. It was also reported (thehindu.com, 22 August 2017) that the number of human deaths from 1 April, 2009 to 31 March, 2016 due to elephant attacks was 2,804. Tigers, Leopards and, Elephants are also killed in the above conflict [1]. Animal intrusion commonly occurs in places where crops attractive to the animals were grown. Expansion of human populations into wildlife habitat also aggravates this situation. More pronounced damage take place in lands adjacent to forest areas. One of the most familiar methods to avoid animal intrusion is by putting up an electric fence around the agricultural lands or forest border areas. But, this is expensive and may not be aesthetically pleasing or practicable. Traps and poisons were also used by people to prevent human-animal conflict. Nevertheless, this method is intolerable either by the Society or the Government [2]. Deterrent methods used currently are typically audible, with the primary difference being the frequency range of the deterrent. Deterrents which are audible in the range of human hearing causes nuisance for the property owner and the neighbors. This is undesirable and cannot be used near the village areas.

Ultrasonic deterrents are deterrents which produces sound waves at frequencies above the range of human hearing. Animals such as deer, wild bores, tigers etc. are sensitive to sounds in the higher frequency range [3] [4] [5]. Therefore, by producing sound in the ultrasonic range, the animal will make a rigorous effort to move away from the area to avoid hearing of ultrasonic sound. This paved way for the development of ultrasonic animal repellent systems. Herbruck Steven [6] in his patent, describes an Animal Repellent Apparatus that generates an undesirable noise for animals such as dogs and cats. This helps in frightening the animals from trespassing within certain geographical locations. An Infrared sensor mounted in the front of the animal repellent apparatus will trigger the ultrasonic transmitter, only when an animal is detected. This apparatus only serves the domestic purpose but not for the wild animals. Ray Benjamin F in [7] illustrates an Animal Repellent device which provides a safety reflector with a solar powered ultrasonic signal perceptible to deer and other animals. The apparatus also comprises a rechargeable battery, solar panel, and a sound chip for emitting the

ultrasonic signal. Thus, it helps in effectively repelling animals from human habitat. But, there is no communication system available to notify the intrusion of animals to the people and the Forest Department. Another system proposed in [8], generates ultrasonic waves of fixed frequency range when an animal is encountered. This system uses PIR Sensor to detect movement of any object. When motion is detected, the image is captured using day light cameras and processed to detect the animal. However, day light cameras are not effective for monitoring wildlife at night. Systems discussed in [9] [10] [11], monitor intrusion of animals into railway tracks, residential areas, and agricultural lands but do not have any mechanism to prevent them from entering into agricultural lands.

The proposed Smart Animal Repellent System provides online monitoring and effective repulsion of animals from human habitat by generating ultrasonic waves and light flashes. Ultrasonic waves are sound waves greater than 20 kHz, inaudible to humans but irritating to most of the animals. The system employs PIR sensor to detect movement and thermal camera to capture the images. Employment of thermal camera allows the system to detect animals in deep cover or concealed by fog. Once, an animal is detected from the captured thermal image, the image, time and location information is transmitted from the system to the Forest Department through internet. Warning signal and text messages are also simultaneously sent to alert the people living in the residential area.

Proposed Methodology

The smart animal repellent apparatus comprises of Thermal Camera mounted on a rotating frame on a pole, Stepper motor, Passive Infrared Sensor, Light sensor, Flashing LED (Light Emitting Diodes) Lights, Embedded Controller, Solar Panel, Rechargeable Batteries, Ultrasonic Wave Transmitter, Global Positioning System, and Internet connectivity module. Solar panel is used as one of the sources of power for the repelling device. The block diagram of the proposed system is shown in Fig.1. Passive Infrared Sensors are deployed around the agricultural field to detect movement in that location [12]. When a Passive Infrared Sensor detects motion, it provides a trigger pulse to the embedded controller using a wireless communication protocol. On receiving the trigger pulse, the embedded controller identifies the exact source of trigger pulse and moves the thermal camera towards that direction by the rotating the stepper motor which is mounted on the pole. The thermal camera is then made ON to capture images of animals/objects that cause movement in that area. The image captured is fed to the embedded controller for processing. The captured image is then passed to the classifier for detection of an animal. If the object detected is an animal, ultrasonic waves of desired frequency are generated to irritate the animal.

The audible frequency range differs for different kinds of animals. Based on the type of animal classified, ultrasonic waves are generated and transmitted with the help of amplifiers and speakers to the surrounding. The frequency of the ultrasonic waves is continuously varied within the range so that the animal does not get used to the sound. The light sensor measures the intensity of sun light. The measured intensity forms the significant parameter for controlling the intensity of flashing LEDs. Orientation of Flashing LED Panel is changed towards the animal movement. LEDs are flashed in addition to ultrasonic waves to have a better repelling effect. GPS (Global Positioning System) module is also added to the device to obtain the location. The captured images of the animal, along with time and location information are transmitted from the embedded controller to the monitoring station of the Forest Department through Internet. Simultaneously, a warning message is given through the public speaker to warn the people living in the nearby residential area. In addition, an alert tone or text message is transmitted to Individual mobile phones of the people from the Forest Department through Internet or Cellular Network. The sequence diagram of proposed system is as shown in Fig.2.

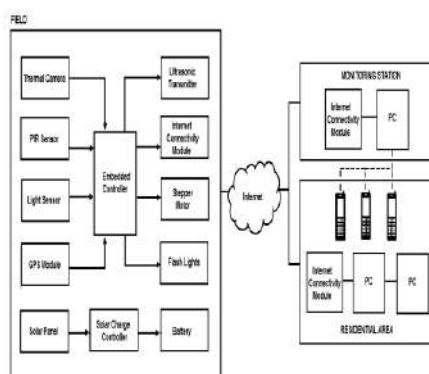


Fig. 1 Block Diagram of the Proposed System to prevent Human-Animal Conflict

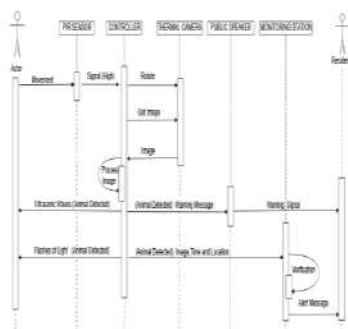


Fig. 2 Sequence Diagram of the Proposed System

SYSTEM DESIGN

In the proposed system, thermal camera is employed to capture images of the surroundings, when the animal is detected. The camera is mounted to a threaded bolt attached to the stepper motor. The stepper motor is placed on a short piece of wood. The wood is attached to the top of the pole. The pole is fitted to the ground. The circuit composed of Embedded Controller, Wireless Receiver, Amplifier, Speaker, Light sensor, Wireless Nano USB (Universal Serial Bus) Adapter, Network Gateway, and GPS module is attached to the front of the wooden piece. Proposed Physical Setup of the system is shown in Fig.3.

Passive Infrared Sensors are placed at different places in the surrounding to detect motion within 180° radius [13]. Each passive infrared sensor has three connections - V_{CC} (5V), ground and output. The output from the PIR sensor is transferred wirelessly to the embedded controller present in the circuit attached to the front of the wooden piece (placed on the pole) for processing. Wireless transfer of data is implemented by means of Serial Wireless Transceiver Module (e.g. XBeePro S₂). Transmitter is attached to the PIR sensor and the receiver is connected to the controller. When PIR Sensor detects motion, it transmits a high value wirelessly to the embedded controller by means of XBeePro S₂. The embedded controller analyses the high value and triggers the stepper motor. The stepper motor is rotated specific number of steps based on the unique identification number that is transmitted along with the measured value from the PIR sensor. Internal structure of the proposed system is shown in the Fig.4.

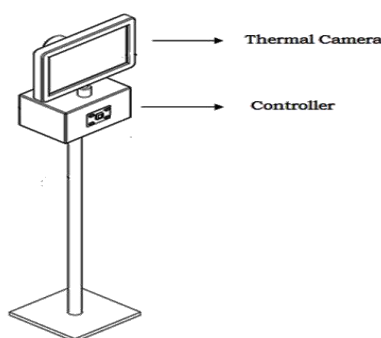


Fig. 3 Proposed Physical Setup of the Intelligent System

Animal Intrusion Monitoring

Detection of movement by the PIR sensors triggers the embedded controller to change the orientation of the thermal camera. There are several cameras that can be employed for monitoring wildlife in the surroundings. For example, Night vision camera is one of the tools used for capturing wildlife [14]. They take in small amounts of visible light, magnify and project it on the display. But, they cannot effectively detect objects in poor weather conditions like fog, light snow, light rain and smoke or scenery. Therefore, thermal cameras are considered to be the most effective tool for monitoring wild animals [15] [16]. Unlike night vision cameras, thermal cameras do not require visible light to produce images at night. This camera produces images based on heat energy emitted by the object [17] [18].

The image captured by the thermal camera is fed into the embedded controller for processing. The captured image is pre-processed and passed to the classifier for detection of the animal. Three classifiers are studied and their detection results are compared in order to select an appropriate classifier for the proposed smart repellent system. The classifiers considered for comparison are k-NN, SVM and CNN. k-NN and SVM classifiers are commonly used Machine Learning Algorithms, whereas Convolutional Neural Network is one class of Deep Learning Algorithms [19]. The main difference between machine learning and deep learning algorithms is in the feature extraction and object detection. In traditional machine learning algorithms, feature extraction is

explicitly added. By contrast, in deep learning algorithms feature extraction is done automatically by the algorithm.

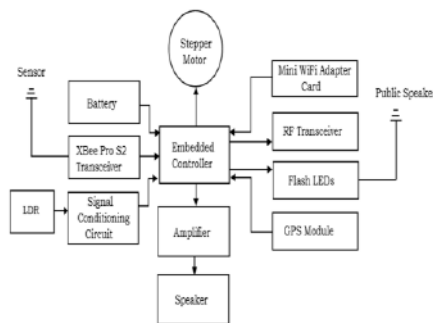


Fig. 4 Internal Structure of the Proposed Intelligent System

Machine Learning

In Machine Learning, the problem is divided into two steps: Object Detection and Object Recognition. The steps involved in Object Recognition using machine learning algorithms are shown in Fig.5. Pre-processing is the initial step involved in image processing. In pre-processing, the image acquired through thermal camera is first converted into grey scale. The grey scale converted image is resized to 100 x 200 pixels. Smoothing operation is then performed to reduce noise within the image by convolving the image with the kernel. Among various smoothing techniques, Median Smoothing technique is preferred because it preserves the edges in the thermal image whilst removing the noise. In Median Smoothing, the pattern of neighbors called the window is made to slide pixel by pixel over the grey scaled image. The median smoothing sorts the pixel values in the numerical order and replaces each pixel with the median pixel value.

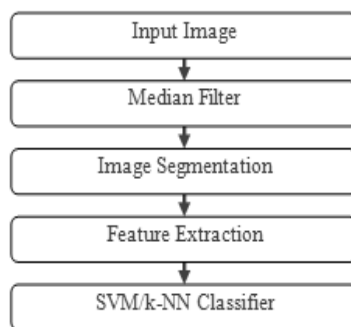


Fig. 5 Steps involved in Object Detection using Machine Learning Algorithm

Pre-processing is followed by Image Segmentation. Image Segmentation also known as binarization is the method of partitioning an image into several segments. It helps in finding the objects and boundaries in the images. Image segmentation involves Thresholding followed by Erosion and Dilation operations. Thresholding operation is performed to extract pixels from image which represent an object. It compares pixel intensity with respect to the threshold. Thresholding can be expressed as given in Equation (1).

$$T(x, y) = \begin{cases} 255, & S(x, y) > \text{threshold} \\ 0, & \text{Otherwise} \end{cases} \quad (1)$$

Where $T(x, y)$ is the intensity of pixel in the target image and $S(x, y)$ is the intensity of pixel in the source image.

Morphological operations are performed to separate the connected objects. Morphological operations include erosion and dilation. Erosion removes a layer of pixels around the object. Dilation adds a layer of pixels to the object. Contour tracing helps in detecting the object or finding the region of interest in the images. Contour is a boundary or edge of an image. Histogram of Oriented Gradient (HOG) feature extraction is employed to capture contour, silhouette and some texture information of the extracted object. Histogram of oriented gradients (HOG) is a feature extractor mainly used in image processing for detection of object. In the HOG feature descriptor, the distribution of local intensity gradients constitutes the features. Gradients are useful because the magnitude of gradients is high around the corners and edges. The extracted HOG feature vectors of the object are passed to the classifier for classification. Two classifiers under machine learning considered for comparison are:

- **k-NN classifier**

k-Nearest Neighbors Classifier is otherwise known as Non Parametric Lazy Learning Algorithm. Decision of the k-NN classifier depends on the entire training data set. The input data given to the classifier can be scalars or multidimensional vectors. k-NN works efficiently with arbitrary number of classes. A single number 'k' determines the number of neighbors that control the classification [20]. Classification of k-NN classifier depends on the majority vote of the neighbors. When k=1, it is called as nearest neighbor algorithm or When k=K, then it is termed as K- nearest neighbor algorithm. k-NN classifier is used in huge number of applications like Nearest Neighbor based Content Retrieval, Protein-Protein interaction and 3D structure prediction and Gene Expression.

- **SVM classifier**

Support Vector Machine is a supervised learning algorithm that categorizes the data into two or more classes. It can be used for both classification and regression problems. SVM is specifically designed for binary classification. During the training phase, SVM classifier plots each data point in n dimensional space and discovers the hyper plane that separates the different classes. Increasing the hyper plane

Deep Learning

Deep learning is a subset of machine learning and is widely used in variety of applications. Deep learning algorithms are complex and takes more amount of time to train the network. Compared to traditional machine learning algorithms, it has very high execution speed in the testing phase. Convolutional Neural Network is a deep learning algorithm primarily suited for image recognition and classification [21] [22]. It is a category of neural network and consists of number of convolution and sub sampling layers followed by one or more fully connected layers. The architecture of Convolution Neural Network used for thermal image processing is shown in Fig. 6.

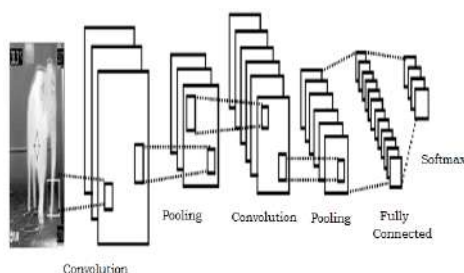


Fig. 6 Thermal Image Classification using CNN

The input image is pre-processed and fed to the Convolutional Neural Network. The input image should be of size $w \times h \times n$, where w is the width, h is the height of the image, and n is the number of channels. (e.g.) For Grey Scale Image $n = 1$ and for RGB image $n = 3$. The convolution layer will have k filters (or kernels) of size $m \times m \times q$ where m should be smaller than the dimension of the input image and q can either be the number of channels in the image ' r ' or smaller. Convolution of filter with image results in k feature maps of size $w-m+1$. The feature maps are sub sampled with mean or max pooling. Max pooling selects the largest value from the window of the image currently enclosed by the kernel. Fully connected layer at the end of the architecture flattens the high-level features that are learned by convolutional layers. It combines the features and passes it to the output layer where a softmax classifier is present to predict the input class label.

Repellent Mechanisms

Detection of an animal stimulates the repellent mechanisms present in the system. Ultrasonic wave's generation and flash lights are the two repellent mechanisms employed to repel animals away from the agricultural lands. The audible range of each animal decides the frequency range of ultrasonic waves. In case of elephants, infrasound waves are employed to repel them from human habitat. The audible hearing range of animals is listed in Table I [23].

Table 1. Audible Frequency Range of Animals

Animal	Frequency Range (Hz)
Elephant	12-12000
Deer	250-30000
Dog	67-45000
Cat	45-64000

Tiger	250 - 65000
Bison	16-40000
Leopard	30000-65000

Ultrasonic waves are generated from the embedded controller as 1 Vp-p square wave of desired frequency. The frequency of the ultrasonic waves is continuously varied within the range so that the animal does not get used to the sound. Waveforms generated by the controller is passed to the amplifier and then transmitted to the surroundings through the speaker. The lights are also flashed at the animal in addition to the ultrasonic wave generation to have a better repelling effect. Light Dependent Resistor (LDR) is used for measuring the light intensity of the surroundings. LDR is connected to the input port of the Embedded Controller. Based on the output of LDR, the intensity of the flash lights is varied. The controller controls the intensity of the flash LEDs by varying the power sent to the LED. Varying levels of power can be achieved by varying the duty cycle of the Pulse Width Modulation (PWM) signal generated from the controller to the flash LEDs. The circuit diagram of the proposed repellent system is shown in Fig. 7.

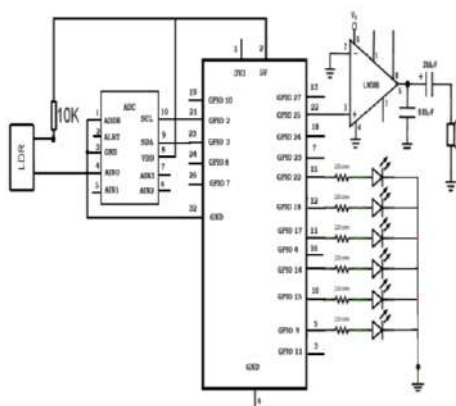


Fig. 7 Circuit Diagram of the Proposed Repellent System

When an animal is detected, the embedded controller also sends a warning message through wireless serial port communication module to the public speaker present in the residential area. The embedded controller with a wireless serial port communication module attached to the public speaker picks up the warning message, interprets and then triggers a warning signal (if the message reveals a dangerous situation) to alert the people around.

The wireless communication is implemented by a RF (Radio Frequency) transceiver module WIR-1186. The module operates at 865MHz - 869MHz band and has 5 channel options. The module has a range of about 2 kilometres, and even more if modules configured as repeaters are used. It is connected to serial Receiver and Transmitter lines of the controller and can support baud-rate of 9600 bps to 115200 bps. Global Position System (GPS) module connected to the controller provides information about the Latitude, Longitude and the Current time.

Real-Time Monitoring

Image of the animal, latitude, longitude and time information are transmitted from the controller through network gateway to the IoT platform. This provides continuous remote monitoring of forest border areas. Selection of the IoT platform plays an important role in the development of this application. There are several factors that are to be considered for selection of the platform. Some of the factors are scalability, system performance, protocol, bandwidth, interoperability, redundancy and disaster recovery. Major protocols that are supported by IoT platform are HTTP (Hypertext Transfer Protocol), CoAP (Constrained Application Protocol) and MQTT (Message Queue Telemetry Transport).

HTTP is a request-response protocol and is not always optimized for mobile devices. HTTP/2, a modern revision of HTTP is employed in many machine to machine applications. It was intended to speed up browser-side and server-side transactions. This new protocol applies multiplexing to handle the TCP (Transmission Control Protocol) requests instead of the ordered and blocking format used by HTTP, which can cause data congestion and hurt performance. MQTT is an asynchronous messaging protocol. It is extremely lightweight due to its binary nature. It follows publish/subscribe model and is best used when the node sends data at irregular intervals of time and when internet connection is unreliable. CoAP is specifically developed for resource constrained devices. It is a document transfer protocol like HTTP and follows a client/server model It

uses UDP (User Datagram Protocol) instead of TCP. It is well-suited for wireless sensor networks and a good option for low power sensors. Clients make requests to servers, servers send back responses. CoAP is a one-to-one protocol, so broadcast capabilities are not native to the protocol.

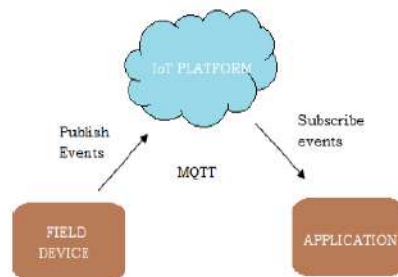


Fig. 8 MQTT Publish/Subscribe Model

Among these protocols, MQTT is best suited for this application. HTTP is not preferred for this application as it lacks security and does not support offline messaging. MQTT is used rather than CoAP owing to the unreliable internet connection around the forest border areas and asynchronous data transfer. MQTT publish/Subscribe model is as shown in Fig. 8. In order to transfer data to the IoT platform, unique id of the device should be initially registered. Registration of the device provides the user with organization credentials. These credentials are needed for transfer of data from the controller to the IoT platform. Image is converted into base64 format and then sent to the IoT platform. An application is developed using PHP and MySQL database to aid in remote monitoring of forest border areas. The application receives the data from the IoT platform, processes it and displays in the webserver for remote monitoring from the Forest Department.

RESULTS AND DISCUSSION

Thermal images of animals are required for training the classifier in the proposed system. Images (Elephants, human, deer and false images) are captured through our FLIR C2 Thermal Camera. FLIR C2 is a portable pocket-sized thermal camera intended for usage in various applications such as Counter-surveillance, Wildlife Monitoring, Cancer detection, PCB defects, etc. The images captured through FLIR (Forward-Looking Infrared) C2 camera is saved to its internal memory and is later downloaded into the computer. The camera produces 80 x 60 pixel thermal image with a 3" LCD (Liquid Crystal Display). The sample image of the elephant acquired is as shown in Fig. 9. Color intensity of the pixels in the image varies with the temperature. The vertical bar on the right side of the image defines the colors for different temperatures. The image captured through FLIR C2 thermal camera is moved to the classifier for detection of animal. The backend program of the proposed system is written in python and the user interface is built using PHP and MySQL. Various stages involved in detection of objects from the image are illustrated in the Fig. 10.

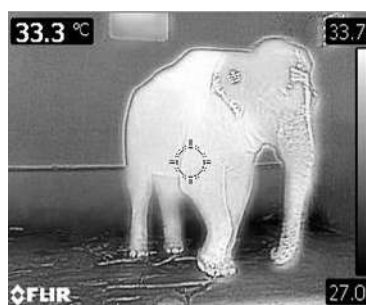


Fig. 9 Sample Thermal Image of Elephant

In Fig. 10, two regions of interest were identified from the original image. HOG features are extracted for the regions of interest. The features extracted are passed through the k-NN/SVM classifier for classification. Results of object detection for deer, elephant, human are as shown in Fig. 11. The classifiers were trained using thermal image samples of different kinds of animals. Total number of samples used for training the classifiers was 428. Accuracy and execution speed of each classifier was evaluated and compared. The performance of k-NN classifier for different k values varying from 1 to 150 is analyzed to locate the optimal value of k. Variation of classifier's accuracy with k is shown in the Fig. 12. Fig. 12 shows the depreciation of accuracy with increasing number of neighbors. When the number of neighbors 'k' increases, several neighbors from other classes tend to be included in the nearest neighbor range and one class will have more number of neighbors than the other classes. This situation may result in more number of misclassifications and as a result, the accuracy of the system decreases. Compared to the conventional Machine Learning algorithms, training of Deep Learning

algorithm consumes more time and occupies more amount of memory space. The convergence of accuracy over the validation data, with time is shown in Fig. 13.



(a)



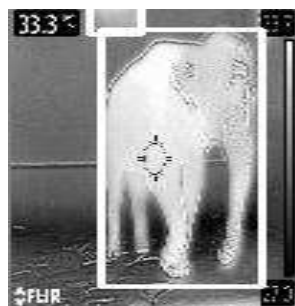
(b)



(c)



(d)



(e)

Fig. 10 Image after (a) Median Smoothing (b) Binarization (c) Erosion (d) Dilation (e) Regions of Interest

From the results shown in Fig.14 and Fig.15, it is inferred that the Convolutional Neural Network has better classification accuracy and speed than the other two classifiers. Since feature extraction is automatically performed by the deep learning algorithm, the execution time is much lesser than the execution time of the Machine Learning Algorithm.

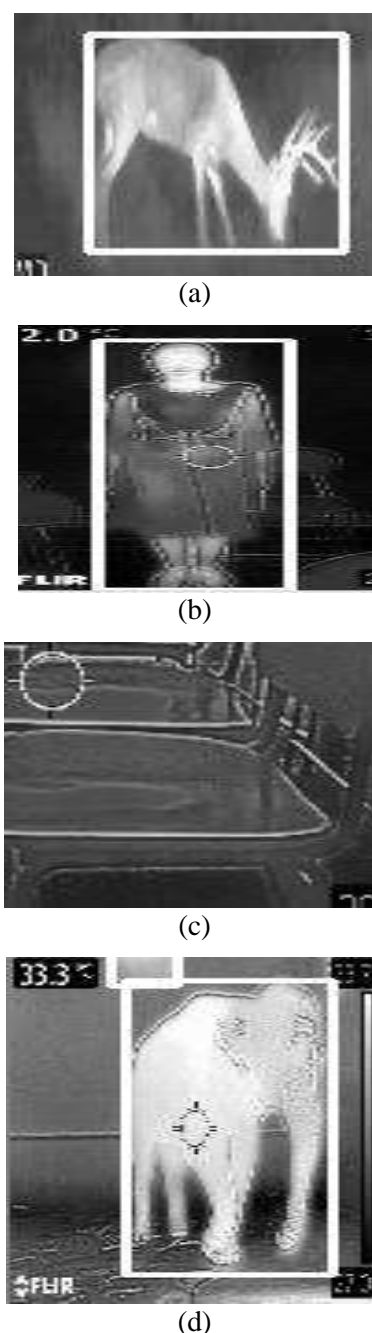


Fig. 11 Results of Object Detection for (a) deer, (b) human, (c) false image and (d) elephant

Animal detection is followed by the repellent mechanisms. The system generates ultrasonic waves and light flashes to deter wild animals away from agricultural lands. Ultrasonic waves generated from the controller at various frequencies were viewed through PiScope, a digital waveform viewer as shown in Fig. 16. The frequency of the ultrasonic waves is switched every 60 seconds. Variation of frequency within the specific range (Table 1) avoids animals from adaptation to the sound emitted through the speaker of the proposed system. Image, time and location information are also simultaneously transmitted from the controller to the IoT platform. The data was retrieved by the application and was presented to the user as shown in the Fig. 17. When an animal is detected, the application displays the name of the animal, GPS coordinates, Device ID, Time and Location information to the user. It allows the users to add resident's phone numbers in order to send alerts. Database containing phone numbers of the residents is shown in Fig. 18.

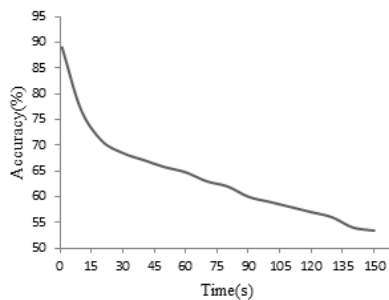


Fig. 12 Variation of Accuracy with Number of Neighbors (k)

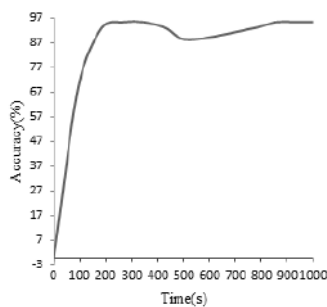


Fig. 13 Convergence of Accuracy over Validation Data with Time

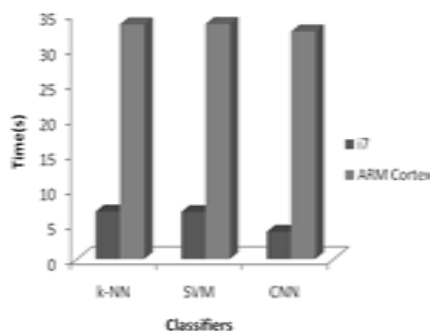


Fig. 14 Comparison of Classifiers based on Accuracy

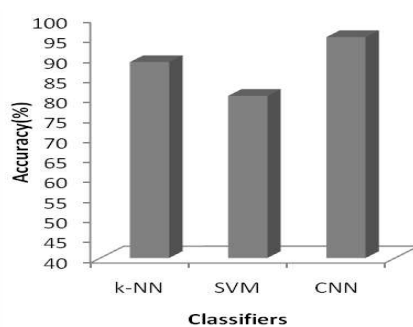


Fig. 15 Comparison of Classifiers based on Speed

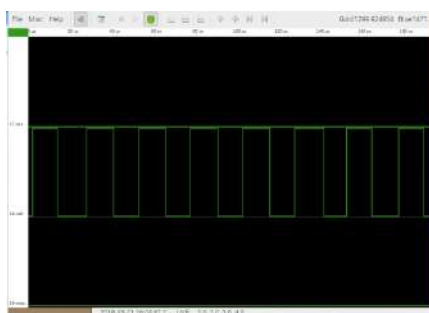


Fig. 16 Generation of Ultrasonic Waves



Fig. 17 Animal Intrusion Notification to the Forest Department in Web Browser

ID	Phone Number 1	Phone Number 2	Phone Number 3
1	+919835511000	+919421267000	+919789432100
2	+919842251700	+919876541111	+91984210770
3	+91974312400	+919842251700	+919748321700
4	+91984441700	+9194207000	
5	+919421003111	+91984420204	
6		+91972121285	
7			
8			
9			
10			
11			
12			
13			
14			
15			

Fig. 18 MySQL Database for Phone Numbers

CONCLUSION

The proposed method automatically detects wild animals and prevents Human-Wild life conflict by generating ultrasonic waves and flash lights. In this system, Thermal Camera was employed to capture images of the moving object. Use of Thermal Camera in the system helps in accurate recognition of animals in darkness, fog, mist, and rain. The captured image was processed in the controller to detect animal. Various classifiers (k-NN, SVM and CNN) were considered for animal recognition from images. The classifiers were evaluated based on accuracy and speed and their results were discussed. Animal recognition results show that Convolutional Neural Network has high classification accuracy (95.24%) and speed (3.8721s) compared to the conventional machine learning algorithms. Following recognition, the system also sends notification to the Forest Department and the public speaker in the Residential area in order to take immediate action. Implementation of the proposed system results in continuous monitoring of Forest Border Areas and prevention of animal intrusion.

REFERENCES

1. thehindu.com, Addressing the human-wildlife conflict 2014. [Online].<http://www.thehindu.com/news/national/kerala/bjps-show-of-strength-at-keezhattur/article23427857.ece> [Accessed: 22 Aug 2017]
2. Sachin Sharma, Dharmesh Shah, Rishikesh Bhavsar, Bhavesh Jaiswal, Kishor Bamniya, "Automated Detection of Animals in Context to Indian Scenario," In 5th International Conference on Intelligent Systems, Modelling and Simulation (ISMS 2014), Langkawi, Malaysia, 2014.
3. Nweke F.U., "Design, Construction and Characterization of a Solar-Powered Multi-tone Ultrasonic Rodent Repeller," International Journal of Science and Research, 2015, 4(2), pp. 144-147.
4. Humayun Rashid, Iftekhar Uddin Ahmed, Taslim Reza, S.M., Islam, M.A., "Solar Powered Smart Ultrasonic Insects Repellent with DTMF and Manual Control for Agriculture," In International Conference on Imaging, Vision & Pattern Recognition, IEEE, Dhaka, 2017.
5. Muhammad Assaqafi Mohd Fisol, Warsuzarina Mat Jubadi, "Ultrasonic and Infrared Repelling Device for Controlling The Population of Rat in Paddy Field," In Asia Pacific Conference on Circuits and Systems, IEEE, Malaysia, 2010, pp. 359-361.
6. Herbruck Steven L., "Ultrasonic Animal Repelling Apparatus", US patent 5 214 411, 25 May 1993.
7. Ray Benjamin F., Ray Sue B., "Animal repellent apparatus", US patent 8 054 186, Nov 8, 2011.
8. Wang, "F Jalaja, S., Abel Daniel, T., Gowtham Shankar, B., Kaliraj, M., Yuthish Khanna, "Real Time Animal Repellent System using Image Processing", International Journal for Scientific Research & Development, 2016, 4(2), pp. 2094-2097.

9. Prateek Mathur, Rasmus H., Nielsen, Neeli R., Prasad, Ramjee Prasad, 2014. Wildlife Conservation and Rail Track Monitoring Using Wireless Sensor Networks. In: 4th International Conference on Wireless Communications, Vehicular Technology, Information Theory and Aerospace & Electronic Systems (VITAE 2014), IEEE, Denmark, pp. 512-515.
10. Mansoor Roomi, S.Md., Rajesh, P., Jyothi Priya, R., Senthilarasi, M., "A Line Model Based Approach for Monkey Intrusion Detection," In International Conference on Signal Processing and Communications (SPCOM 2010), IEEE, Bangalore, India, 2010, pp 1-5.
11. Sanku Kumar Roy, Arijit Roy, Sudip Misra, Narendra Singh Raghuvanshi, Mohammad S., Obaidat, "AID: A prototype for Agricultural Intrusion Detection using Wireless Sensor Network," In IEEE International Conference on Communications (ICC 2015), London, 2015, pp. 7059-7064.
12. Jayanth, G.R., Sathishkumar, P., Essa Mahapatra, "An Optoelectronic Profiling and Ranging Sensor for Monitoring of Perimeters," IEEE Sensors Journal, 2015, 15(7), pp. 3692-3698.
13. Biagioni, E.S., Sasaki, G., "Wireless sensor placement for reliable and efficient data collection," In 36th Annual Hawaii International Conference of System Sciences, IEEE, Big Island, Hawaii, 2003.
14. David Forslund, Jon Bjarkefur, "Night Vision Animal Detection," In 2014 Intelligent Vehicles Symposium, IEEE, Dearborn, 2014, pp. 737-742.
15. Suseethra, S., Abraham Chandy, D., Siva Mangai, N.M., "Recognition of Elephants in Infrared Images Using Mean- shift Segmentation," In International Conference on Information Communication and Embedded Systems (ICICES 2017), IEEE, 2017, pp 1-6.
16. Siva Mangai, N.M., Shilu Tresa Vinod, Abraham Chandy, D., "Recognition of elephants in infrared images using clustering-based image segmentation," International Journal of Electronic Security and Digital Forensics, 2015, 7(3), pp. 234-244.
17. Sean Ward, Jordon Hensler, Bilal Alsalam, "Autonomous UAVs Wildlife Detection Using Thermal Imaging, Predictive Navigation and Computer Vision," In IEEE Aerospace Conference, Yellowstone Conference Center, Big Sky, Montana, 2016, pp 1-8.
18. Peter Christiansen, Kim Arild Steen, Rasmus Nyholm Jørgensen, Henrik Karstoft, "Automated Detection and Recognition of Wildlife Using Thermal Cameras", Sensors Journals, 2014, 14(8), pp. 13778-13793.
19. Hung Nguyen, Sarah J., Maclagan, Tu Dinh Nguyen, "Animal Recognition and Identification with Deep Convolutional Neural Networks for Automated Wildlife Monitoring," In IEEE International Conference on Data Science and Advanced Analytics (DSAA 2017), Tokyo, Japan, 2017, pp. 40-49
20. Yanying Li, Youlong Yang, Jinxing Che, and Long Zhang, "Predicting the Number of Nearest Neighbor for kNN Classifier," IAENG International Journal of Computer Science, 2019, 46(4), pp. 662-669
21. Ahmad Alzu'bi, Abbes Amira, and Naeem Ramzan, "Learning Transfer Using Deep Convolutional Features for Remote Sensing Image Retrieval," IAENG International Journal of Computer Science, , 2019, 46(4), pp637-644,
22. Thi Thi Zin, Cho Nilar Phyto, Pyke Tin, Hiromitsu Hama, and Ikuo Kobayashi, "Image Technology based Cow Identification System Using Deep Learning," Lecture Notes in Engineering and Computer Science: Proceedings of The International MultiConference of Engineers and Computer Scientists 2018, 14-16 March, 2018, Hong Kong, pp. 320-323
23. Jayprakash D., Sonone, Dattatray A., Patil, Kantilal P., Rane, "Irritating and Hearing Frequency Identification and Generation to Avoid Animals Accident," International Journal of Innovative Research in Science, Engineering and Technology, 2014, 3(7), pp. 14454-14464.

Advances in Sentiment Analysis of Twitter Data

T. Raveena¹, P. Saranya², Marx Rajangam³ and Engels Rajangam^{4*}

^{1,2}Department of Computer Science & Engineering, PSG College of Technology, Coimbatore, India

³Department of Computer Science & Engineering, PSG College of Technology, Coimbatore, India

³ORCID: 0000-0001-6530-3203

⁴Department of Computer Science & Engineering, PSG College of Technology, Coimbatore, India.

⁴(Corresponding author) ORCID: 0000-0003-1225-8415

ABSTRACT

Sentiment analysis deals with the analysis of emotions, opinions, facts and sentiments in audio, video and text content. When applied on text, sentiment analysis can be used to analyze sentences created by people in blogs, comments, reviews and tweets. Typically, when applied on text, sentiment analysis is used to determine whether an opinion is positive or negative about an element or a concept in the text. In this paper, a detailed analysis of various algorithms and recent techniques for sentimental analysis in the last decade has been performed and documented. Further, this paper presents an overview of the most prevalent approaches employed in sentimental analysis of twitter data.

Keywords—Sentiment analysis, classification, Twitter, Data analysis, reviews.

I. INTRODUCTION

Sentiment analysis has become one of the popular and wide scoped research areas in computer science because of the explosion of sentiment information from online audio and video content sharing platforms, social web sites, online forums, and blogs. Sentiment analysis or opinion mining is used to classify the opinions expressed by analyzing the training data. When applied to the text content, sentiment analysis is used to determine whether an opinion is positive or negative about an element or a concept in the text. Typical usage scenarios for sentiment analysis on text include an attempt to determine whether an opinion is positive or negative about an element or a concept in the text. With appropriate and adequate data handling more than two classes of opinions is also possible.

With the rapid growth and development of technology and internet, a large number of reviews on products and services are being added to the worldwide web every day. Twitter is an online platform that enables its users to create short text and multimedia content and hence has become a famous tool for sharing user sentiments on products and services. As of 2021, it is estimated that Twitter has more than 330 million monthly active users with 500 million tweets being tweeted per day. These tweets range from everyday activities to political messages. For social scientists, as well as researchers from other disciplines, this data could provide rich insight into society, politics and more.

This survey focuses mainly on analyzing tweets where opinions are highly unstructured and heterogeneous. Existing sentiment analysis methods can be divided into two broad categories as machine learning approaches and lexicon based approaches.

Machine learning approaches make use of machine learning algorithms and deal with solving the sentiment analysis problem as a text classification problem. These are further divided as supervised and unsupervised learning approaches, in which the decision classifiers, the linear, rule based and probabilistic classifiers are part of supervised learning approaches. Classifiers like SVM, Naive Bayes fall under the supervised learning approach. Supervised learning approaches depend mainly on the training documents which are labeled for performing classification. This approach deals with a set of training records in which each of the individual records are mapped and labeled with a class. The classification model has a similar relation to the features that are in the individual records to that of one of the class labels. Given an instance of unknown class, the model is used for the prediction of class label. When only one label is associated with it then it results in a hard classification problem whereas when a probabilistic instance of a class label is assigned to it then it is called a soft classification problem. There are a variety of supervised classifiers in existence.

Lexicon based approaches depend on sentiment based lexicons and is further divided as corpus and dictionary oriented approaches which employ various statistical and semantic methods for finding the polarity.

This work is organized as follows: Section 2 reviews various sentiment analysis techniques used for different problems, domains and scenarios over the last decade in technical literature. Section 3 tabulates and discusses the findings and section 4 concludes this paper with a summary.

II. Sentiment analysis techniques

A. SVM and Dictionary Based Sentiment Analysis

In a paper presented by Alexandra Balahur [1], experiments were performed for sentimental tweets task of Semantic Evaluation (SemEval2013) in English and Spanish. The main tasks handled in this work are sentiment classification for English and sentiment classification for Spanish.

The first approach used for this task was a supervised learning approach with Support vector machines sequential minimal optimization (SVM SMO) for the sentiment classification of English tweets. This method considered unigram and bigram features. The second approach was designed to be a hybrid method, and employed supervised learning with a SVM SMO with a linear kernel. This method too considered unigram and bigram features along with reference dictionaries for sentiments, emoticons, colloquial words and features of media in social networks. Dictionary based approach replaced sentiment bearing words with labels for the sentiment classification of Spanish tweets, considering the malformed formats and grammar of tweets including spelling variation and other social network specific terms and symbols.

The main conclusions obtained included that the use of minimal linguistic processing made the approach easily portable to other languages. The usage of linguistic processing like lemmatization, removal of stop words made the performance worse. The usage of unigrams and bigrams for accurate identification of sentiment polarities, to learn some general patterns in expressions. Usage of joint classifiers helped in improving the performance of monolingual classifiers.

B. TWITTER MOOD PREDICTS STOCK MARKET

A paper presented by Johan Bollena [2] focuses on Stock market prediction which uses the efficient market hypothesis and the random walk theory. Recent researches suggest that prominent indicators which can predict the news much earlier are possible to be learnt from social media interactions than any contemporary methods. In this work public mood states were tough to predict. The accuracy of these methods to predict the news was severely constrained by the indicators and is in relation with the sentiment of the public. However, this method poses complex challenges as conducting opinion surveys take a lot of time and effort, and preparing the samples for population is expensive depending on the sample size.

The first of the approaches used in this work is an opinion finder. It is publicly available tool that takes the tweets posted on a given day and analyses them to find the time series of public opinion every day. This tool can also identify the opinion polarity based on subjective sentence sentiment analysis.

The second of the approaches in this work is the Google-Profile of Mood States (GPOMS) tool. It considers various mood dimensions of the public, using the tweet text, and trying to map a view of the changes in public mood. By the inclusion of more mood and sentiment dimensions the results from GPOMS on the stock market prediction models, including accuracy, can be improved much. From the analysis of GPOMS, it is found that the tweets have a predictive effect on the people's mood variations. However, as per GPOMS, the general happiness of the people cannot be predicted by the tweets, using the public opinion finder tool.

This work is extended to take into account the social and cognitive effects in which individual agents are endowed with ability to learn from past experiments. Location and language must be given importance to avoid geographical and cultural sampling errors.

C. SEMI SUPERVISED LEARNING FRAMEWORK

A research paper by Nadia Felix [3] focuses on supervised algorithm that requires representations of labeled data for construction of the classification model. Labeled data are tedious and expensive to obtain. Semi-supervised learning uses both labeled and un-labelled data and utilizes unlabeled data in their training process. These methods are accessible in contrast to the limited number of annotated ones and acquisition of labeled tweets often requires a costly process that involves skilled experts. Most tweet sentimental analysis technique involves lexicon and corpus based approaches. In this work, Consensus between Classification and Clustering Ensembles (C3E) algorithm was integrated with the semi supervised learning mainly used for tweet classification. Due to this, tweet labeling costs are reduced as only small part of annotated data is used. This work can be strengthened by using this method for aspect based tweet sentiment classification.

D. CLASSIFIER ENSEMBLE

A paper presented by Silva [4] focuses on classifying the tweets based on classifier ensembles. This paper uses the technique of ensembles of multiple base classifiers along with the scores obtained from lexicons which can improve the tweet sentiment classification aiding to better accuracy. Comparison of bag of words and feature hashing was carried out and their advantages and disadvantages are shown. Feature representation for the

sentiment classification of tweets was carried by two methods: bag of words and feature hashing. In preprocessing, data cleaning was performed by eliminating the retweets, stop words, URL, mentions, punctuations and accentuations. Stemming is then performed. Sanders twitter sentiment corpus, Stanford twitter sentiment corpus, Obama McCain debate (OMD) and healthcare reform (HCR) were the dataset used for this work. WEKA was the tool used for multinomial Naïve bayes classifier, logical regression and Random forest. LibSvm was used for training SVM classifiers. Standard 10-fold cross validation was used with OMD and sanders twitter sentiment datasets. HCR used public resource validations. Stanford Twitter sentiment Corpus samplings from the original training set were validated and made available in the test available. On comparing the Standalone classifiers with ensemble approach, the latter provided a better accuracy.

E. RANKED WORDNET GRAPH

A paper dealing with Ranked WordNet graph for Sentiment Polarity Classification in Twitter by Arturo Montejo Raeza [5] addresses the problem of polarity classification in sentiment analysis by presenting an approach which extracts the vector of weighted nodes from graph Wordnet, which are in turn used in SentiWordNet to compute final estimation of polarity. The first method consisted of evaluation of a supervised approach like SVM using the vector space model to build the features. Preprocessing was carried out but Stop words were not removed. In this work, a personalized page rank vector consisting of a ranked sequence of WordNet synsets were weighted using a random walk algorithm called Page Rank. The results were the personalized page rank vectors (PPV). The graph of Word Net was taken where the nodes represented the synsets and axes are semantic relations between them, which is followed by an iterative process which yields to the selection of more nodes in proximity. A final list of values was retrieved. The inference obtained is that, on comparing of the proposed approach to SVM, the results are not better but they are quite close hence this unsupervised solution is an interesting alternative to supervised one. This work can be strengthened by the study of usage of negation and better data cleaning.

F. NGRAM ANALYSIS AND DYNAMIC ARTIFICIAL NEURAL NETWORK

M. Ghiassia, J. Skinner B and D. Zimbra [6] proposed a method which is a hybrid system for twitter brand sentiment analysis using dynamic artificial neural network (DAN2) and n-gram analysis. Twitter sentiment analysis uses a variety of features, which are derived from conventional text classification methods. However, it also has produced results which were inconsistent in prior that question the effectiveness of analysis. Thus for addressing this issue and reducing the number of features this work focuses on a technique of supervised feature reduction using n-gram and statistical approach for the development of a lexicon specific to the twitter data, which is also reduced to brand specific lexicon for brand related tweets. A Hybrid approach is used for feature extraction involving Dynamic artificial neural network (DAN2), SVM and N -gram analysis, and further Twitter API v1.0 tool was used for data collection. Justin Bieber's twitter corpus was considered as the dataset. The tweets were identified by using uni-grams, bi-grams and tri-grams. Feature engineering approaches were undertaken to reduce the number of features and making them manageable. From the training dataset, the vector representation of tweets with the corresponding manual calculation and the values were given as starting point input to the DAN2 algorithm. A 2-dimensional search was employed for finding the best parameter value for every iteration, and inferior results were eliminated. The Search was terminated on obtaining desired training accuracy level. The SVM model the input consisted of 187 features similar to DAN2, further a model was constructed for each individual sentiment. This approach resulted in increased sensitivity with tweets with mild sentiments, resulting in better accuracy of identification of neutral category. DAN2 model proved much better at finding the messages of interest compared to SVM. However it has a cost of offsetting false positives. This work can be strengthened by examining the performance of DAN2 in opinion analysis, sentiment detection and on other brand related and more general twitter corpora.

G. SENTIMENT CAUSAL RULE METHOD

A paper by Rahim Dekharghani [7] focused on solution to the problem of extracting important summary information from tweets by using sentimental causal rules. The sentimental causal rules are an eminent and efficient mechanism for summarizing that combines the causal relations with the sentiment embedded in the causal relationships. The dataset selected for this approach was mainly the tweets collected on three topics Kurdish and turkey, Kurdistan workers party, Kurdistan and turkey. Preprocessing of tweets was carried out such as removal of URLs, removal of Stop words, treatment of special characters and treatment of emoticons and treatment of acronyms. Then the aspect keywords were extracted from tweets, from which tweet vectors were constructed, after which the causal rules are extracted. The rules with low confidence were eliminated, and the polarity of the rules was also extracted. The aspect keyword was extracted from the tweets by using a third party commercial service (www.alchemyapi.com) which is a cloud based text mining platform. Causal Bayesian

network was used in which the nodes represent the variables and arc presents the probabilistic dependence. The main advantage of this work was the ability to summarize a large amount of information in the form of sentimental causal rules. The disadvantage was the absence of large dataset, some causalities could not be extracted due to rule structure definition, and negation of tweets were not handled which would greatly decrease the accuracy. This work can be extended by analyzing tweets from different languages.

H. OPINION MINING

A paper based on Localized Twitter opinion mining using sentiment analysis by Syed Akib Anwar Hridoy [8], focuses on utilization and interpretation of twitter data for determining the public opinions. To determine the popularity of a given product in several locations, analysis were carried out involving huge level data, for which tweets from twitter data were processed. The tweets were used as a source of data, and were extracted from twitter using the twitter API. Tweets were extracted in a fixed set of locations. These locations include New York, Los Angeles, Boston, Chicago, Dallas, San Francisco and Philadelphia. Preprocessing of the tweets was carried out, and filtering was carried out by Stanford natural language processing (SNLP) tool. The tweet sentiments were assessed using the SentiWordNet tool, which gave score for the words. Finally the net score was calculated. The limitations were that the amount of tweets collected was comparatively low, usage of Namsor, a tool that was used was not completely error free, and further the quality of tweets was low. This work can be strengthened by using a better NLP filtering mechanism and also a custom Sentiword dictionary can be utilized.

I. SENTI-CIRCLES

Hassan Saif [9] proposed a method which focused on the contextual semantics for the semantic analysis of twitter data. This concentrates on an approach called SentiCircle that attempts to build a word representation model that dynamically captures the semantics of the words, considering context. The words are assigned with polarity of sentiments and their strengths in from a referenceable sentiment lexicon.

SentiCircle performs two sentiment analysis tasks in this regard, namely sentiment identification considering entities and sentiment identification considering tweets. This paper followed two approaches for tweet-level sentiment detection namely-supervised learning and lexicon based approaches. In supervised learning approach, the output datasets are provided which are used to train the machine and get the desired outputs. From the training datasets, emoticons were used infer the tweet polarities of three classes, namely positive, negative and neutral. These polarities are then used for training the model.

The lexicon-based approaches involve calculating orientation for a document from the semantic orientation of words or phrases in the document. Such methods eliminated the dependency on training data. Word lexicons are used as references to assign sentiment orientation based weights to words and the final sentiment for the specific text is computed.

The lexicon-based approaches do accomplish the task well with conventional texts, however fail to perform with twitter data. The format and expressions in such texts are more colloquial and do not conform to grammar most of the times. To overcome these limitations, an algorithm called Senti-strength is used which employs formally coded lexicons of words and phrases which are well suited for text used in social networks such as twitter platform.

SentiStrength uses a lexicon to find strength of sentiments in the colloquial text used in social discussions. SentiStrength is confined with the fixed set of words that appear in the lexicon. The analysis of sentiments does not consider the words which are not included in the reference lexicon, and this poses a challenge when processing twitter data. This issue necessitates human intervention for coding data which is costly and may even lead to errors due to domain dependencies and lack of knowledge. To address these challenges an approach called SentiCircles is used. Senticircles approach pre-assigns strengths and polarity to words, composes an adaptive representation, and identifies the contextual semantics using a specific lexicon of sentiments. With such as approach Senticircles is able to fine tune the strengths and polarities. SentiCircles involves two distinct tasks with regards to sentiment analysis: Sentiment identification at entity level and sentiment identification at tweet level. The former detects sentiment related to a specific object, topic or entity, such as Covid-19, Life Insurance, or Cricket. The latter detects the sentimental undertone with regards to the tweets posted by an individual on the twitter platform. Senticircles has been successful at a collection of twitter tweets. As an extension of the above algorithms, the proposed model can be tested on twitter streams and may explore optimization steps for controlling size of the term index.

J. NET BRAND REPUTATION

A paper presented by Nur Azizah [10] uses Net promoter score (NPS) that collected data by acquiring customer recommendations for telecommunication and network based products and services. NPS survey was done by considering customer samples. NPS can be expensive and reported draw data but did not extend the research into a detailed analysis of the individual product based insights. To overcome these problems, a method called Net Brand Reputations (NBR) was used. It was a quantitative measurement which employed sentiment analysis for evaluating the contentment of customers. Since this study was primarily focusing on the communication domain, it evaluated the data related to 3G/4G, Short Messaging Service (SMS), data, VOIP and internet, which were the top five revenue contributors for the communication services firms. NBR also offered a comprehensive dashboard for the real time tracking and monitoring of data from academic and industrial official accounts on the twitter platform. NBR offered the possibility of extension to specific domains with insufficient training data using transfer learning. In addition, NBR was capable of collecting more data for training purposes using social media campaigns.

K. ONTOLOGY BASED TECHNIQUE

A paper by Christos Berberidis [11], focuses on a new technique for sentiment analysis of the twitter posts i.e. classification of tweets using ontology based techniques. This work tries to employ the domain ontology for computing sentiment scores in a detailed manner based on the text content of the tweets. The aim was to build a system which would accept the tweet as the corresponding to a particular subject and providing sentiment scores for every feature aspect of the subject. This work mainly constitutes of two stages, namely The process of creating an ontology for the specific domain under consideration, and the Sentiment analysis of the tweets.

The ontology creation was examined by two algorithms, namely Formal concept analysis (FCA), and Ontology Learning. In Formal Concept analysis, the aim was to generate a table of cross concepts corresponding to the ontology to the specific domain and Twitter4J tool was used to extract the tweets. In ontology learning OntoGen, a data driven semi-automatic ontology editor, was used. It deployed text mining methods through an interactive and efficient user interface that has a reduced complexity. For the purpose of combining the sets of hyponyms and synonyms to the ontology, WordNet lexical database was used for retrieval of synsets of the hyponyms and synonyms of every given word. The sentiment analysis of the tweets was performed in three steps:

- (1) The ontology was queried to retrieve the respective attributes of every object.
- (2) The related and relevant tweet messages were retrieved.
- (3) Finally sentiment analysis of the given word was performed. Open Dover was used to extract the sentiment from each sentence. Finally the recall ratios were calculated. This work can be extended by the substitution of OpenDover with a custom built sentiment classifier. It is possible to realize a fully automatic and functional ontology builder can be created, by combining a set of effective techniques for learning ontologies.

L. HOUSING PRICE AND PUBLIC SENTIMENT ESTIMATION

This work tries to estimate public sentiment about a location based on the housing prices in that area [12]. To estimate this relationship, tweets from a specific geolocation were collected and preprocessed before sentiment analysis, kernel density estimation were performed and a house pricing model linking public mood was evolved. Features of the housing included housing structure, neighborhood characteristics and building amenities. Emotional lexicons (AFINN and NRC) were used to evaluate the emotion attached to tweets. Housing transaction analysis was performed and a spatial tweet distribution of the tweets was built. These information were combined together to estimate the emotion of people based on their tweets and their locations. Finally, hotspot analysis validated the significant clusters in the overall model combining data from the various sources.

M. FILTER AND EVOLUTIONARY OPTIMIZATION

Hassonah and team propose a hybrid model with filter wrapper combination various types of reviews including movie reviews, restaurant reviews, product reviews and public opinion [13]. In this work, based on a topic, tweets were extracted various datasets. NLP tasks such as tokenization, stopword removal, and stemming were performed on these tweets. The remaining content is processed to obtain a labeled TF-IDF format. Then a feature ranking is performed followed by Multi-verse Optimization (MVO) for further fine tuning the feature selection. These identified features are processed by an SVM to classify the tweet into either as a positive, negative or neutral sentiment. This final sentiment classification was also evaluated with decision trees, random

forests and K-Nearest neighbors. This work can be extended by analyzing other methods for feature selection and other classifiers for final sentiment categorization of the tweets.

N. LEXICON OF ADVANTAGES AND DISADVANTAGES

This work explores the effect of a creating and using a lexicon of advantages and disadvantages of products based on their attributes [14]. Usage of such a lexicon resulted in a more refined classification of product related tweets. Such a lexicon reduced ambiguity and improved quality of results. Reviews regarding Xbox-one and Nintendo 2DS-XL from the Entertainment Software Association (ESA) 2017 expo were used for this study and analysis. This paper used Tandem LSTM-SVM approach for product tweet classification. The classification of products fell into three groups, positive, negative and neutral. The better ability classify product reviews could be used to improve products and services and address issues related to them.

III. DISCUSSION

The attributes of the papers analyzed in this review are summarized in Table 1.

Table 1 Sentiment Analysis Techniques and Approaches

Reference No	Year	Task and Scope	Dataset / Data resources	Algorithm/ Tool Used	Metrics Used
1	2014	Multilingual processing	SemEval 2013 Task 2 Dataset / Twitter	SVM, Dictionary based approaches	F1-measure, Accuracy
2	2011	Twitter mood effect on stock markets	Custom dataset / Twitter	Opinion Finder, Google-Profile of Mood States (GPOMS), Self-organizing Fuzzy Neural Network	Accuracy
3	2016	Sentiment understanding from Twitter reviews	SemEval 2013 Task 2 Dataset / SemEval 2014 Task 9 Dataset / Twitter	SVM, Semi-Supervised Learning, Consensus between Classification and Clustering Ensembles (C3E)	F1-measure
4	2014	Tweet representation and ensemble classification	Sanders twitter sentiment corpus, Stanford twitter sentiment corpus, Obama McCain debate (OMD) and healthcare reform (HCR)	Random forest, Naïve Bayes, SVM, Linear and Logistic Regression	Precision, Recall, F1-measure
5	2014	Sentiment polarity classification using Tweets	Twitter	Random Walk algorithm, SVM, Twitter Search API	Polarity score, F1-measure
6	2013	Brand sentiment using twitter reviews	Tweets related to Justin Bieber / Twitter	Dynamic artificial neural network, SVM and N-gram	Recall, Accuracy
7	2014	Sentimental causal rule discovery	Tweets related to Kurdish and turkey,	Local Causal Discovery (LCD), Causal Bayesian,	Polarity percentage, Class label

		using Tweets	Kurdistan workers party, Kurdistan and turkey / Twitter	SVM, neural network	
8	2015	Localized Twitter opinion mining	Tweets from seven cities in USA / Twitter	SNLP, Twitter API, POS Tagger, SentiWordNet	Count, Percentage
9	2016	Contextual sentiment analysis for Twitter reviews	Obama-McCain Debate (OMD), HealthCare Reform (HCR), Stanford Sentiment Gold Standard (STS-Gold), Stanford Twitter corpus / Twitter	Supervised approach, Lexicon based approach, Senticircles	Density, F1-measure, Accuracy
10	2015	Mobile phone Brand reputation based on Tweets	Data from official handled of mobile phone network providers from Twitter	SVM, Naïve Bayes, Decision Tree	F1-measure, Accuracy
11	2013	Sentiment analysis of Twitter reviews using Ontology	Twitter messages about mobile phones and their attributes	Opendover, Twitter4j, OntoGen, Formal Concept Analysis	Recall, Concordance
12	2021	Housing price prediction	Tweets from Manhattan	Hot-spot analysis, Kernel density estimation, Multivariate Linear regression	Ts statistic, z-score
13	2019	Filter and evolutionary wrapper for SA	Movie review, Product review, restaurant review and public opinion / Twitter	TF-IDF, OAuth Twitter endpoint and Rest API for query based tweet extraction, SVM, Multi-verse Optimization Algorithm (MVO)	Accuracy, F-measure
14	2020	Knowledge based lexicon for SA	Xbox-one and Nintendo 2DS-XL reviews from Entertainment Software Association (ESA) 2017	Tandem LSTM-SVM approach for sentiment analysis	Search interest, percentage

From the table, it is evident that this review has covered various technical approaches over the last decade used in sentiment analysis of tweets. This review has covered various domains including understanding stock markets, housing prices based on tweets, understanding brand reputation, desirability of geographical locations and more common opinion mining tasks. In addition, this review has covered various technical approaches used in the sentiment analysis task for tweets.

Based on the extensive reviews of technical aspects of sentiment analysis techniques in the reviewed techniques that span the last decade, the most widely used classifiers in sentiment analysis are identified and their usage is shown in Figure 1.

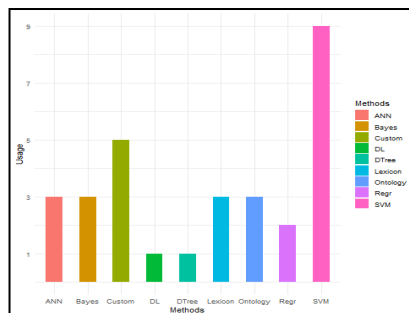


Figure 1. Classifiers and their usage in SA

SVM is the most popular and most widely used classifier for sentiment analysis and classification of tweets. This may be due to the fact that in most sentiment analysis of tweets, there are only three classes (positive, negative and neutral) and a relatively straightforward three-class linear classifier (SVM) can be effectively used. The next most popular classifiers are custom made and are closely followed by ANN and Bayesian classifiers. It is also evident from the fact that machine learning based approach for sentiment analysis of tweets is more widely used compared to the lexicon based approach. Ontology based approaches and lexicon based approaches are as common as the ANN and Bayesian classifiers. Linear and logistic regression, decision trees and deep learning methods were not as common as other prevailing methods for sentiment analysis of tweets.

Accuracy and F1-Measure (also referred to as F-Score, F-measure) are two of the highly used evaluation metrics. F1-Measure is computed in terms of Precision and Recall measures. High precision implies fewer false positives and high recall implies fewer false negatives during the classification process. Precision and Recall can be computed using Equations (1) and (2).

$$\text{Precision} = \frac{\text{True Positive}}{\text{True Positive} + \text{False Positive}} \quad (1)$$

$$\text{Recall} = \frac{\text{True Positive}}{\text{True Positive} + \text{False Negative}} \quad (2)$$

F1-Measure indicates a test's accuracy. It is the harmonic mean of precision and recall as given in Equation (3).

$$\text{F1 - Measure} = 2 \times \frac{(\text{Precision} \times \text{Recall})}{(\text{Precision} + \text{Recall})} \quad (3)$$

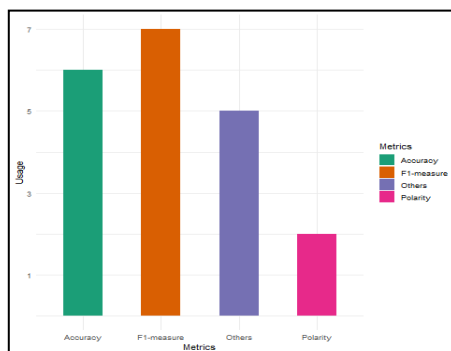


Figure 2. Evaluation metrics usage in SA

Based on this survey, the commonly used metrics for sentiment analysis tasks for tweet messages were also identified. F-measure (or F1-measure) is the most widely used metrics followed by accuracy as shown in Figure 2. Custom measures of success and straightforward polarity of the messages were also used, but not as commonly as the other metrics.

This analysis also presents information on hybrid approaches such as the classifier ensemble and n-gram analysis using AI/ML algorithms such as DAN2 that proved to yield better results. SVM and Naïve Bayes classifiers are two major widely used machine learning algorithms that are employed for the solving of sentiment classification problem. The usage of natural language processing tools has also been a prime attraction for the researchers and continues to be a trend. As in many of the applications the contexts of the text and user preferences play a major role and hence context-based sentiment analysis needs more attention in future. Contexts, concepts and topics in the tweet message texts may play a crucial role for intelligent sentiment analysis tasks. Hence, NLP tasks such as concept and knowledge representation [15] techniques and topic extraction [16] approaches may be integrated with sentiment analysis for tweets in the near future. More recent artificial intelligence and cognitive modeling [17], cognitive architectural [18] and techniques may be used in sentiment analysis tasks as well. In the recent literature, sentic computing [19] and cognitive computing [20] are starting to play a role in analysis of sentences and texts. These new frontiers of research may also soon impact sentiment analysis tasks related to tweet messages.

This survey also revealed that WordNet is used primarily as the lexicon source for different languages. Sentiment analysis may also be applied for languages other than English though it is not as common.

IV. CONCLUSION

This survey paper gives an overall view of the various approaches and methods employed in sentiment analysis of twitter data. We analyzed papers published regarding the diversified approaches of analysis of sentiments on the twitter data, and those indexed by reputed indexing houses. The results obtained from the review are presented in tabular and graphical forms for easy comprehension and comparison. This work has also presented the possible future directions for sentiment analysis for tweets.

V. REFERENCES

1. Alexandra Balahur, José M. Perea-Ortega, "Sentiment analysis system adaptation for multilingual processing: The case of tweets", *Information Processing & Management*, Volume 51, Issue 4, July 2015, pp 547-556, doi: <https://doi.org/10.1016/j.ipm.2014.10.004>
2. Johan Bollena, Huina Mao, Xiaojun Zeng, "Twitter mood predicts the stock market", *Journal of Computational Science*, Volume 2, Issue 1, March 2011, pp 1-8, doi: <https://doi.org/10.1016/j.jocs.2010.12.007>.
3. Nádia Félix Felipeda Silva, Luiz F.S. Coletta, Eduardo R. Hruschka, Estevam R. Hruschka Jr., "Using unsupervised information to improve semi-supervised tweet sentiment classification", *Information Sciences*, Volumes 355–356, 10 August 2016, pp 348-365, doi: <https://doi.org/10.1016/j.ins.2016.02.002>.
4. Nádia F.F. da Silva, Eduardo R. Hruschka, Estevam R. Hruschka Jr., "Tweet sentiment analysis with classifier ensembles", *Decision Support Systems*, Volume 66, October 2014, pp 170-179, doi: <https://doi.org/10.1016/j.dss.2014.07.003>
5. Arturo Montejo-Ráez, Eugenio Martínez-Cámara, M. Teresa Martín-Valdivia, L. Alfonso Ureña-López, "Ranked WordNet graph for Sentiment Polarity Classification in Twitter", *Computer Speech & Language*, Volume 28, Issue 1, January 2014, pp 93-107, doi: <https://doi.org/10.1016/j.csl.2013.04.001>
6. M. Ghiassi, J. Skinner, D. Zimbra, "Twitter brand sentiment analysis: A hybrid system using n-gram analysis and dynamic artificial neural network", *Expert Systems with Applications*, Volume 40, Issue 16, 15 November 2013, pp 6266-6282, doi: <https://doi.org/10.1016/j.eswa.2013.05.057>
7. Rahim Dehkharghani, Hanefi Mercan, Arsalan Javeed, Yucel Saygin, "Sentimental causal rule discovery from Twitter", *Expert Systems with Applications*, Volume 41, Issue 10, August 2014, pp 4950-4958, doi: <https://doi.org/10.1016/j.eswa.2014.02.024>
8. Syed Akib Anwar Hridoy, M. Tahmid Ekram, Mohammad Samiul Islam, Faysal Ahmed and Rashedur M. Rahman, "Localized twitter opinion mining using sentiment analysis", *Decision Analytics*, Volume 2, Issue 8, 2015, doi: <https://doi.org/10.1186/s40165-015-0016-4>
9. Hassan Saif, Yulan He, Miriam Fernandez, Harith Alani, "Contextual semantics for sentiment analysis of Twitter", *Information Processing & Management*, Volume 52, Issue 1, January 2016, pp 5-19, doi: <https://doi.org/10.1016/j.ipm.2015.01.005>

10. Nur Azizah Vidya, Mohamad Ivan Fanany, Indra Budi, "Twitter Sentiment to Analyze Net Brand Reputation of Mobile Phone Providers", *Procedia Computer Science*, Volume 72, 2015, pp 519-526, doi: <https://doi.org/10.1016/j.procs.2015.12.159>
11. Efstratios Kontopoulos, Christos Berberidis, Theologos Dergiades, Nick Bassiliades, "Ontology-based sentiment analysis of twitter posts", *Expert Systems with Applications*, Volume 40, Issue 10, August 2013, pp 4065-4074, doi: <https://doi.org/10.1016/j.eswa.2013.01.001>
12. Mark Junjie Tan, Cheng He Guan, "Are people happier in locations of high property value? Spatial temporal analytics of activity frequency, public sentiment and housing price using twitter data", *Applied Geography*, Volume 132, July 2021, doi: <https://doi.org/10.1016/j.apgeog.2021.102474>
13. Mohammad A. Hassonaha, Rizik Al-Sayyeda, Ali Rodana,b, Ala' M. Al-Zoubia, Ibrahim Aljaraha, Hossam Farisa, "An efficient hybrid filter and evolutionary wrapper approach for sentiment analysis of various topics on Twitter", *Knowledge-Based Systems* (2019), doi: <https://doi.org/10.1016/j.knosys.2019.105353>
14. Filippo Chiarello, Andrea Bonaccorsi *, Gualtiero Fantoni, "Technical Sentiment Analysis. Measuring Advantages and Drawbacks of New Products Using Social Media", *Computers in Industry* 123 (2020), 103299, doi: <https://doi.org/10.1016/j.compind.2020.103299>
15. Engels Rajangam, Chitra Annamalai, "Graph Models for Knowledge Representation and Reasoning for Contemporary and Emerging Needs – A Survey", *I.J. Information Technology and Computer Science*, 2016, 2, 14-22, MECS (<http://www.mecs-press.org/>), doi:<https://doi.org/10.5815/ijitcs.2016.02.02>
16. Engels Rajangam, Chitra Annamalai, 'Topic extraction using local graph centrality and semantic similarity', *Concurrency and Computation - Practice & Experience*, vol. e5054, pp. 1-16, ISSN : 1532-0634. November 2018, doi: <https://doi.org/10.1002/cpe.5054>
17. Marx Rajangam, Annamalai C., "Extractive document summarization using an adaptive, knowledge based cognitive model", *Cognitive Systems Research*, Volume 56, Year 2019, Pages 56-71, doi:<https://doi.org/10.1016/j.cogsys.2018.11.005>
18. Marx Rajangam, Annamalai C., "Contemporary Cognitive Architectures: A Comparative Study of Structures and Adaptability", *International Journal of Artificial Intelligence and Soft Computing*, Volume 5 (4), Year 2017, pp 263 - 284, doi: <https://doi.org/10.1504/IJAISC.2016.081343>
19. Grissette, H., Nfaoui, E.H, "Affective Concept-Based Encoding of Patient Narratives via Sentic Computing and Neural Networks", *Cognitive Computing*, 2021, doi: <https://doi.org/10.1007/s12559-021-09903-z>
20. Park, SM., Kim, YG, "Root Cause Analysis Based on Relations Among Sentiment Words", *Cognitive Computing*, Volume 13, pp903–918, 2021, doi: <https://doi.org/10.1007/s12559-021-09872-3>

Design and Hardware Implementation of Three-Phase Multi-Level Active Front End PWM Rectifier

R. Srinivashkannan, M. Sundaram, B. Vinod, J.Chelladurai and M. Anand
EEE Department, PSG College of Technology, Coimbatore, India

ABSTRACT

The design, modelling, and realisation of hardware of a 3-phase multi-level (3PML) unidirectional active PWM rectifier is presented in this paper to improve the power factor close to unity with lower order dominating harmonics as per IEEE standard 519-1992 and lower interface voltage tension on devices. 3PML PWM rectifier system is for industrial DC bus supply with high voltage DC (HVDC) bus in comparison to grid. The primary circuit is a three step three wire non-generative front end PWM rectifier, with a control strategy dependent on Direct power control with space vector PWM. A highly efficient direct power control strategy is used to reduce current harmonic injection into the grid and topology proposed with help of MATLAB/Simulink and 15kW hardware implemented and results presented in this paper. The high-power factor achieved 0.996 and input current harmonic distortion (ITHD) observed 2.13% at full load condition.

Keywords-Unidirectional active front end PWM rectifier, Space vector-PWM. Direct control Scheme, Vienna rectifier

I. INTRODUCTION

The 3-phase AC is converted to DC power in a wide range of power electronics and drives, including Electric Vehicles, Industrial Automation Drives, Power supply systems, and energy storage systems. A 3-phase, 3-switch, 3-level controlled PWM rectifier was designed using a combination of an uncontrolled 3-phase diode bridge rectifier and a DC converter with gain more than unity to increase the output voltage based on input variation. Instantaneous sine current control, better output voltage regulation, and peak inverse voltage stress on the power BJTs are some of its characteristics. [1]. In addition to the desired fundamental voltage at the rectifier output, pulse width modulation techniques produce a high frequency harmonic component in the input current. The use of an output DC bus capacitor will greatly minimize switching frequency ripple [2].

The PWM pulse generation circuit for controlling the VIENNA Rectifier II, is built based on a study of simple realization possibilities of isolation with transformer. The input currents have a constant sinusoidal time behaviour and the output voltage is isolated at high frequencies and regulated within one quickest scanning cycle. Compared to 6-pulse controlled and uncontrolled rectifiers, the Vienna rectifier is the preferred choice due to its benefits such as half the number of switches, a compact structure, large power density, and the potential to achieve unity power factor with the right control technique. [3] - [5]

The vector control method is employed to construct and test a 230 – 395 V, 1000 W converter as a prototype to learn the control dynamics, and it is compared to the traditional hysteresis control method. The pure sinusoidal shape of input currents with output capacitor voltages of same magnitude along with unity power factor is achieved in the proposed control method. In this multi-level 3-switch Vienna rectifier, voltage referenced control is proposed along vector control strategy with same magnitude of voltage across the output of capacitor. A complex space vector system is replaced in the proposed control method for the Vienna rectifier. A single carrier control signal is used to vary the modulation index of the pulse width modulated (PWM) switching sequence. The Vienna rectifier topology is preferred due to its simple boosting of multi-level switch topology and generation of 3-level voltage. Vienna rectifier output has distortion-free voltage and current waveforms with unity power factor operation. The control signal brings back the output voltages followed by the grid currents, whenever it detects grid currents are out of phase with the reference voltages. The distortions created by the Vienna rectifier's non unity power factor operation are evaluated. [6]-[8]. For the 3-phase multi-level Vienna rectifier, a different analog-based critical conduction mode (CRM) control system is proposed. Easy analogue CRM control in each step of the Vienna rectifier can be accomplished. Cost effective, easily available analogue control based controllers are used to execute all of the control schemes. In 3.2 kW, 3-phase Vienna rectifier, zero-voltage-switching (ZVS) and switching during demagnetising of inductor with power factor of 0.994 is measured [9]. The design of 3-phase, three-level unity power factor based rectifier with MATLAB/Simulink and hardware setup was discussed in detail. [10]. The concept of centre aligned SVPWM for 3-phase Vienna rectifier is discussed in [11].

II. 3- PHASE MULTI-LEVEL PWM RECTIFIER

Fig. 1 presents a 3-phase, multi-level active front end PWM rectifier capable of unidirectional power processing. From the output side common neutral point available between the two dc bus capacitor. Output filter capacitor also reduces the high frequency ripple and high frequency harmonics on the output side. Neutral point considered as null potential when duty cycle is on. The upper (Da1,Db1,Dc1) and lower (Da2,Db2,Dc2) diodes are having blocking voltage of 800Vdc at duty cycle is off(1-D) and switches (Sa,Sb,Sc) blocking voltage of 400Vdc at duty cycle is on.

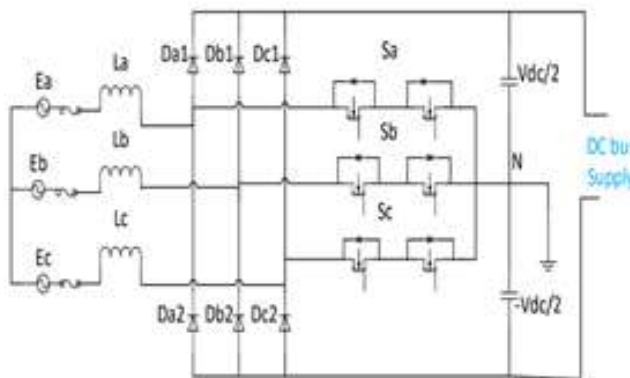


Fig. 1 Three-phase multi-level active front end PWM rectifier

The input filter inductor current should capable to follow the input phase voltage fundamental frequency as per equations given below equation (1) to (6). Here the equations (1),(2),(3) are input fundamental phase voltages and input line waveforms equations are (4),(5),(6).

$$E_a = V_m \sin \omega t \quad (1)$$

$$E_b = V_m \sin(\omega t - 2\pi/3) \quad (2)$$

$$E_c = V_m \sin(\omega t - 4\pi/3) \quad (3)$$

$$I_a = I_m \sin \omega t \quad (4)$$

$$I_b = I_m \sin(\omega t - 2\pi/3) \quad (5)$$

$$I_c = I_m \sin(\omega t - 4\pi/3) \quad (6)$$

III. DESIGN CALCULATIONS & HARDWARE COMPONENTS

Table I Design Specifications

Input Voltage	370Vrms to 530Vrms
Input supply frequency	47-52Hz
Maximum Input Power	17000W
Input current	23Arms
Input current ripple allowable	7.07A
Switching Frequency	25kHz
Output Voltage	750Vmin – 800Vmax
Output Power	15000W
Output voltage ripple	30Vdc

3.1 Inductor Selection

Inductors are connected in series with input line of converter to suppress input current ripple in the 3-phase multi-level PWM rectifier. In industrial practices, line filter inductor value is calculated from the formula represented as equation 7. Here, $L = L_a = L_b = L_c$

$$L = \left(\frac{V_{dc}}{2}\right) * \left(\frac{1}{4}\right) * \left(\frac{1}{F_{sw}}\right) * \left(\frac{1}{\Delta I_L}\right) \quad (7)$$

$$L = 506 \mu H$$

Selected inductor material is AMCC40

3.2 Capacitor Selection

The required capacitor is sized using the equation 8. The input and output current ripples are being reduced significantly by choosing Output filter capacitor as per the equation 8 and voltage ripple is brought to the level as per the industrial standard.

$$C \geq \frac{Po * 2 * F_{SW}}{\Delta V_o} \quad (8)$$

$$C_u = C_b = C = 1.4 \text{mF}$$

Electrolytic capacitor selected for DC bus application.

3.3 Diode Selection

Diodes Da1, Db1, Dc1, Da2, Db2, Dc3 should carry high current capable of 45A its 20 % of rated current and voltage 1200Vdc its 20% of rated voltage. Selected diode is IDWD40G120C5

3.4 Power MOSFET Selection

The MOSFET selection was done based on both dynamic and static characteristics of the load. Quick turn-on and turn-off, minimum on state resistance, optimal miller plateau near middle of gate voltage range are considered for optimum switching and conduction losses to get desired peak efficiency. The switch is selected with a drain-source voltage to withstand voltage spike of 20% more than its rating. Power MOSFET is IPW65R019 is selected based on the design considerations

3.5 Gate Driver Selection

To select the gate driver IC the awareness of current control mode, gate voltage of the MOSFET and gate charge of selected device is considered as key features. The number of channels of operating circuit switches, totem poles or no of pole of circuits is considerable. Source and Sink current calculation is advisable.

Selected gate driver is 1ED3124MU12H

3.8 Microcontroller Selection

The selected micro controller is 32 bit TMS320C28377. Its operating frequency is 200MHz, single- precision Floating-Point unit(TMU), Trigonometric Math unit, clock and system control, on-chip crystal oscillator and etc.

IV. CONTROL APPROACH & SPACE VECTOR PWM

To achieve unity power factor with reduced THD direct power control technique is used in this paper. The space vector PWM is used to generate the modulations index with respective to output voltage demand or output voltage reference voltage. In Fig. 2, it is shown that, control of input line current with respect to phase voltage fundamental frequency is achieved by using phase locked loop(PLL) control scheme. The 3-phase quantities are considered as stationary axis(α & β) then converted as direct axis and quadrature axis (d&q axis). There phase quantities to two phase rotating quantities is achieved through below mathematical expressions call park-transformation shows in Fig. 3&Fig. 4.

$$E_\alpha = \left(\frac{3}{2}\right) E_a \quad (9)$$

$$E_\beta = \left(\frac{\sqrt{3}}{2}\right) (E_b - E_c) \quad (10)$$

$$E_d = E_\alpha \cos\theta + E_\beta \sin\theta \quad (11)$$

$$E_q = E_\alpha \sin\theta - E_\beta \cos\theta \quad (12)$$

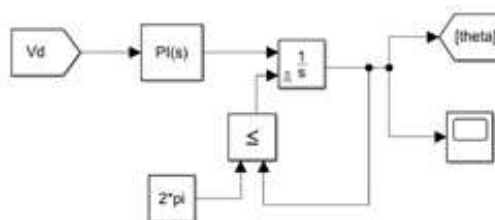


Fig. 2 Phase Locked Loop

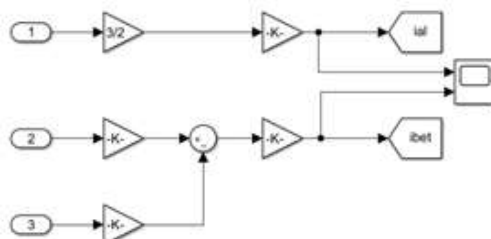


Fig.3 Three-phase Quantities to Two-phase stationary quantities

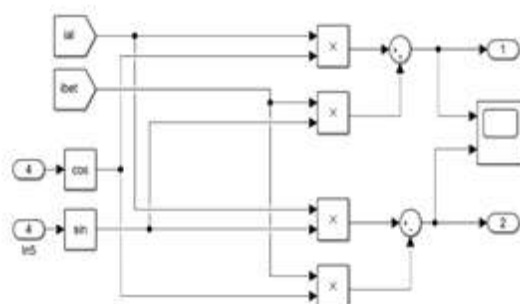


Fig. 4 Two-phase Stationary Quantities to Two- phase Rotating Quantities

space vector PWM is synthesised using the inverse park transformation to convert the 2- phase rotating quantities to 3-phase quantities. In this system, the inner current and outer voltage compensations loops are used to help the system with less harmonics on the input side. To control the both inner current loop bandwidth should be more than 5 to 10 times of outer voltage loop compensation bandwidth.

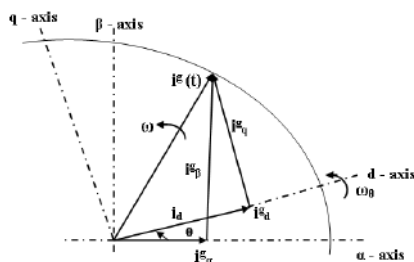


Fig. 5 Vector diagram of Park Transformation

In Fig. 5, ω is fundamental frequency $i_g(t)$ resultant vector of i_d and i_q rotating vectors.

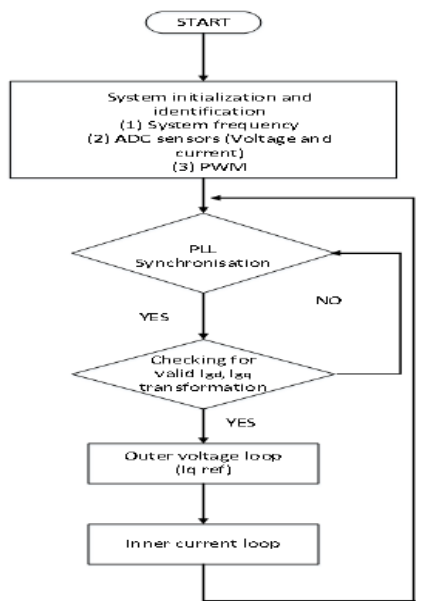


Fig. 6 Flow Chart of Control Loop

Space vector pulse width modulation is more suitable for low harmonic distortion at the input side and it also effectively use the three phase grid current in-phase with the fundamental input voltage source. 3PML PWM rectifier modulation is done by space vector quantities. Modulation of the space vector pulse width is applied for the voltage output and the regulation of the input current. The switching vectors are generated to regulate both input current and output voltage based on the proposed control scheme is the unique advantage. For a sufficiently tiny time interval, a collection of stationary vectors produced by park transformation. If the collected sample time for 3PML PWM rectifier provides error, then reference voltage and current vector rotates to a new angular position at the next sampling instant to the correspond new set of stationary vectors.

V. MATLAB/SIMULINK SCHEMATIC AND RESULTS

Fig. 7 shows the 3PML PWM rectifier power circuit.

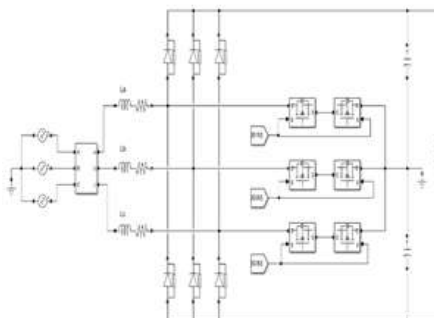


Fig. 7 3PML PWM Rectifier Power Circuit

The circuit is designed up to input power 17kW and output power 15kW.

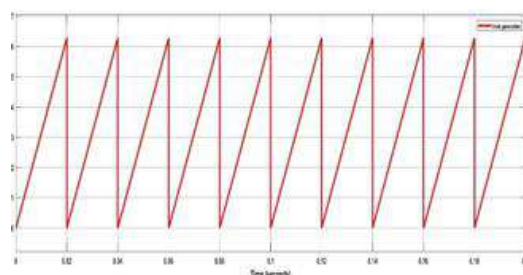


Fig.8 Theta(θ) Generation

Fig. 8 is output of the phase locked loop for zero cross detection and theta generation used to make the help to follow input voltage waveform to input current waveform.

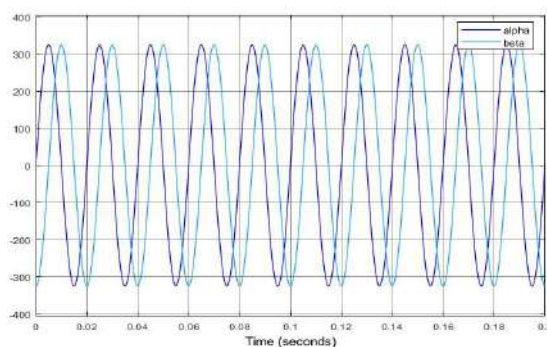


Fig.9 abc to $\alpha\beta$ Quantities

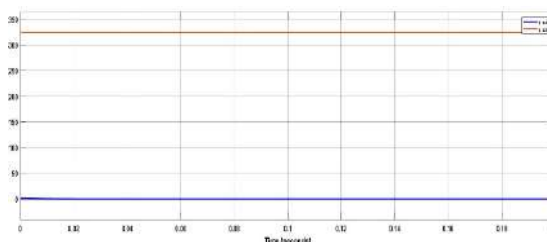


Fig.10 $\alpha\beta$ to dq

Fig. 9 shows the output of block Fig. 4 and Fig. 10 shows the output of $\alpha\beta$ to dq transformation of input voltage waveform.

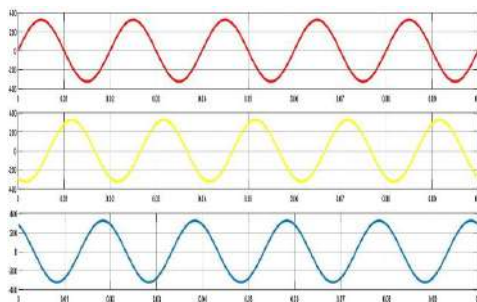


Fig. 11 Input Voltage Waveform with Peak Magnitude of 325V

From Fig. 11 & Fig. 12 we can find the both input voltage and input current with phase difference 0. But normally without direct power control with space vector PWM is not possible. Input current maximum up-to 23A Irms observed when phase to line voltage 230Vrms.

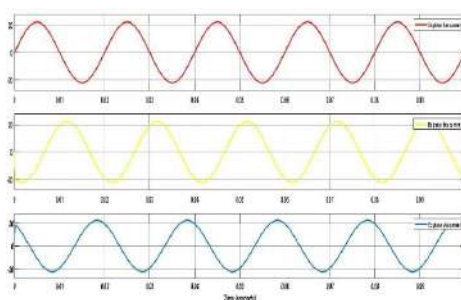


Fig. 12 Input Current Waveform

Fig. 12 shows the less distortion from input voltage frequency.

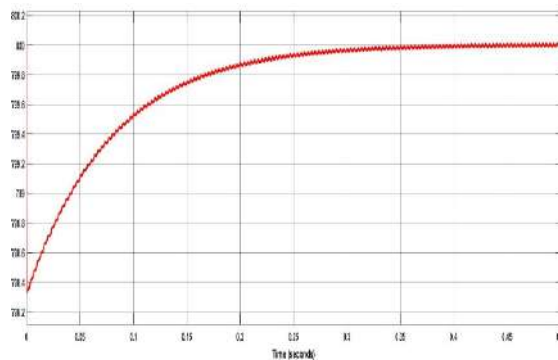


Fig. 13 DC Bus Capacitor Voltage with Magnitude of 800V

VI. EXPERIMENTAL RESULTS AND DISCUSSION

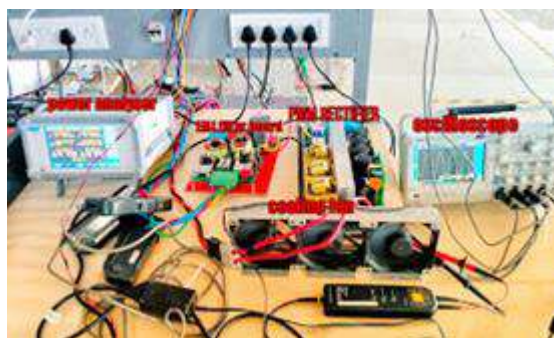


Fig. 14 Experimental Test Setup Showing 3PML PWM Rectifier

The 3PML PWM rectifier is whole setup is included with gate driver, 32-bit Digital signal processor TMS320C28377. While loading the PWM rectifier at nominal input voltage 415V then the observation of %ITHD and power factor is possible. The power factor and % ITHD with respective to the various loads are

within recommended limits. Gate driver waveforms and modulation waveforms and pole voltage waveforms and diode voltage waveforms at load condition are shown in this paper below.

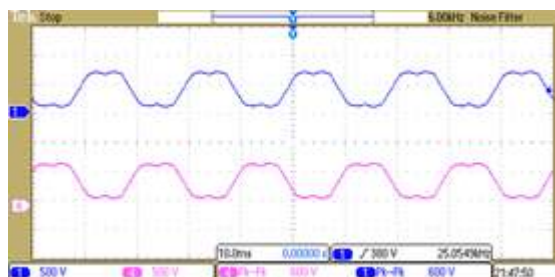


Fig.15 Space Vector PWM Modulation Wave

Above Fig.15 shows the two-phase space vector PWM which are amongst three phase modulation waves. This modulation wave having capable of lower harmonic production towards the grid. This result wave form captured across Eaphase pole. This wave form reflects the power MOSFET voltage stress on its own.

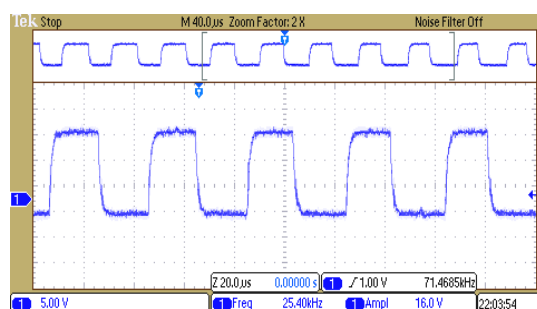


Fig.16 Gate Driver Waveform

Fig.16 shows the gate driver output waveform with 25kHz switching frequency and amplitude of 16V

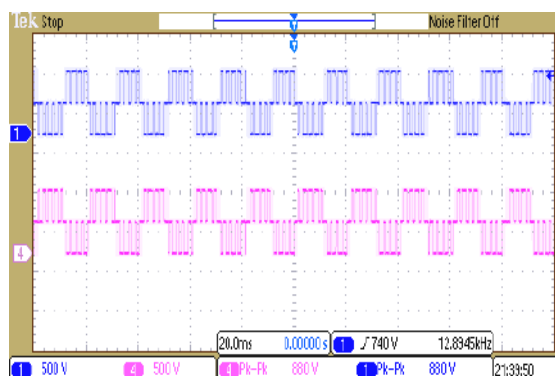


Fig.17 Voltage Across the Diode of Da1, Da2

Fig. 17 shows the voltage across the Da1, Da2. Blue colour wave forms represent voltage across Da1 and another pink colour represents the Da2 its lower diode of Ea phase at the condition of duty cycle is on.

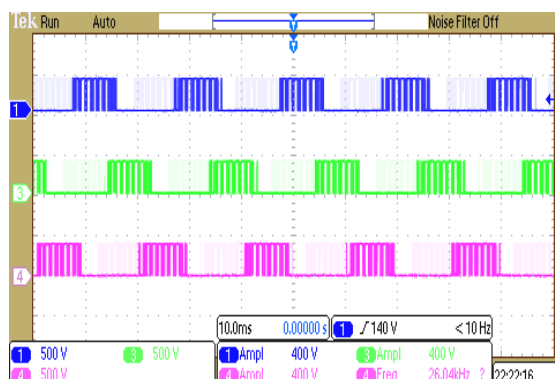


Fig.18 Voltage Waveform Across the Sa,Sb,Sc

Above Fig.18 shows the pole voltage i.e pole voltage when duty cycle is on.

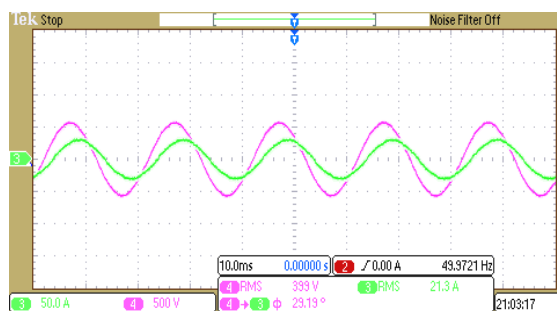


Fig.19 Phase-to-Phase Voltage and Line-Line Current Phase Difference of Single-Phase

Fig. 19 shows the phase difference between two waveforms are 29.19° approximately 30° . The phase to phase voltage and line current waveforms having phase difference reflecting less harmonic distortion.

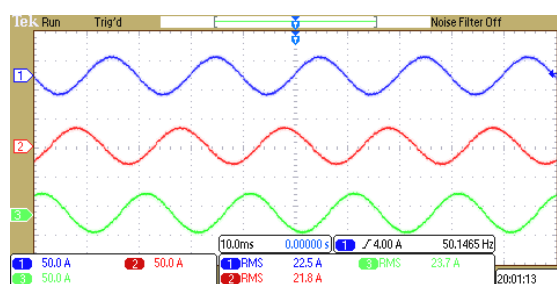


Fig. 20 Input Line Current Waveforms

Fig. 20 shows the input line Current waveforms of 3 phase. Form the experimental set up the power factor and ITHD observations with value of 0.996 at nominal voltage 415Vac(line to line voltage) or 234Vac line to phase voltage and nominal load 15kW at output side and 2.13% Total harmonics distortion achieved in input inductor line current.

VI. CONCLUSION

In this work, a control approach for operation of 3P3L rectifier with direct power control is proposed with MATLAB/Simulink and results presented. The control of the hardware has been implemented using a Texas instruments based DSP TMS320C28377 platform. The hardware observed high power factor of 0.996 and less % ITHD of 2.13%, delivering a power of 15116.62 W. Input rated line voltage and phase voltage of 415Vac and 234Vac, respectively. The RMS input current and output current is measured as 23A, 18.54 A respectively.

REFERENCES

1. IEEE Standard 519-1992, IEEE Recommended Practices and Requirements for Harmonic Control in Electrical Power Systems
2. J. W. Kolar, "A novel three-phase utility interface minimizing line current harmonics of high-power telecommunications rectifier modules," IEEE Trans. Ind. Electron., vol. 44, no. 4, pp. 456–467, 1997.
3. X. Yu, K. Jin, Q. Chen, and J. Chang, "Control study of Vienna-type rectifiers for high DC-link voltage utilization and high power factor," 2013 4th IEEE Int. Symp. Power Electron. Distrib. Gener. Syst. PEDG 2013 - Conf. Proc., no. 1, 2013.
4. T. Shimizu, T. Fujita, G. Kimura, and J. Hirose, "Unity-power-factor PWM converter with DC ripple compensation," Electr. Eng. Japan (English Transl. Denki Gakkai Ronbunshi), vol. 123, no. 1, pp. 51–62, 1998.
5. J. W. Kolar, U. Drofenik, and F. C. Zach, "VIENNA rectifier II - a novel single-stage high-frequency isolated three-phase PWM rectifier system," IEEE Trans. Ind. Electron., vol. 46, no. 4, pp. 674–691, 1999.
6. S. A. Shaon and K. M. A. Salam, "Study of Vienna rectifier and a highly efficient single phase two stage inverter with low THD," 8th Int. Conf. Electr. Comput. Eng. Adv. Technol. a Better Tomorrow, ICECE 2014, pp. 619–622, 2015.
7. J. Adhikari, I. V. Prasanna, and S. K. Panda, "Voltage oriented control of the three-level Vienna rectifier using vector control method," Conf. Proc. - IEEE Appl. Power Electron. Conf. Expo. - APEC, vol. 2016-May, pp. 9–16, 2016.
8. D. A. Molligoda, J. Pou, C. J. Gajanayake, and A. K. Gupta, "Analysis of the Vienna Rectifier under

-
- Nonunity Power Factor Operation,” 2018 Asian Conf. Energy, Power Transp. Electrification. ACEPT 2018, no. 1, pp. 1–7, 2019.
9. Wang, J., Feng, S., & Kurokawa, F. (2020, September). Critical Conduction Mode Three-Phase Vienna Rectifier. In 2020 9th International Conference on Renewable Energy Research and Application (ICRERA) (pp. 418-422). IEEE.
 10. MJ, Krishna Kumar. "Design, hardware implementation and control of a 3-phase, 3-level unity power factor rectifier." PhD diss., Indian Institute of Science Bangalore-560 012 India, 2012.
 11. K. Siriphan and P. Khamphakdi, "Analysis of Center-Aligned Space Vector Pulse Width Modulation Realization for Three-Phase Vienna Rectifier," Proc. 2019 Int. Conf. Power, Energy Innov. ICPEI 2019, no. 2, pp. 44–47, 2019.

Estimation of Remaining Useful Life (RUL) for Turbofan Engines Using Automl: A Self Service Analytics Approach

¹Banu Rekha B, ²Somasundaram B, ³Manoj J and ⁴Ramesh S

¹Department of Biomedical Engineering, PSG College of Technology

²Senior Member, International Society for Automation

³Postdoctoral Fellow, Liverpool John Moores University, U.K.

⁴Associate Member, Institution of Engineers, India

ABSTRACT

Industry 4.0 enables a manufacturing plant to mitigate risk and retain its profitability by performing predictive analytics. To achieve I4.0 standards, data analytics techniques have to be applied in the entire value chain of a manufacturing plant to create a better decision support system for the management. The Aviation Industry offers opportunities in predictive analytics by virtue of its aggregation of functional data. One such challenge is the estimation of Remaining Useful Life (RUL) of Turbofan Engines. A Turbofan engine is a type of jet engine that encompasses a variety of processes and mechanisms primarily driven by fluid dynamics. Prediction of RUL leads to reduced maintenance costs and incidence of failures. In this work, the PHM08 challenge dataset from prognostic data repository is considered. The work focuses on development of RUL prediction algorithm using a self service analytics approach. The prediction model was developed in a format that could be deployed on a EDGE Device as suggested by Industrial Internet Consortium Analytical Framework. The results of the work suggest that self service analytics methods such as AutoML could be used by the Aviation industry by scaling up for economical deployment in portable smart devices with limited computational capabilities to achieve level 5 as per Digital Maturity Assessment (DMA) guidelines of International Society of Automation (ISA).

I.INTRODUCTION

The World Economic Forum observes that the Fourth Industrial Revolution (I4.0) is building on its predecessor, the digital revolution, and that the boundaries between the physical, digital and biological spheres are softened [1]. The industrial machines built with intelligent controllers and sensor systems during the era of Industry 3.0 are now getting connected to form an Industrial Internet of Things (IIOT) with the advancement in Information and communication technology. Research studies conducted on data across various fields have given key insights into hitherto unexplained grey areas. Thus, these data have great deal of value in terms of facilitating knowledge and also possesses monetary value. Hence, this research work aims to provide a substantial contribution towards the emerging technological trends in Data Science. The role of Data Analyst in the Aviation Industry is considered vital to refine out insights from flight data collected so as to imbibe data driven decisions like improving productivity or utilization, improve efficiency of process or method, improve life or predict failures in machines etc. The article [2] presents the impact of I4.0 in aviation industry as the creation of a unique data system, emergence of new digital production technologies, centralized control room and man-machine interaction. Still, definite use cases for the public or the academic world in accordance with the Industry Internet Consortium (IIC) Analytical Framework [3] is limited. This knowledge is necessary to achieve Digital Maturity levels in the data analytics endeavours. While traditional machine learning techniques have been used in the aviation industry for improving customer service, disruption prediction and emergency management, this work focuses on applying Automated Machine Learning (AutoML) techniques on prediction of Remaining Useful Life (RUL) of Turbofan Engines that are widely used in jet aircrafts. Though the concept of Industry 4.0 was introduced to the world in 2011, there is a high volume of publications and research articles available as journals and other peer reviewed resources. Philipp Zehnder et. al. [4] discussed on digital representations of real-world assets in industrial environment with a single data analytics pipeline paves a way of creating a digital twin & optimize / test the asset using a non-invasive method. Vachálek et. Al. [5] discussed on how the digital twin of an industrial production line within the industry 4.0 concept be created and different hypothesis of achieving various KPIs can be validated in an automobile industry for maintenance engineering, production engineering, computing various production planning strategies. Aanedo [6] provided the specific requirement of IIOT (Industrial Internet of Things) for creating a Digital Twin where the total effort of making the digital thread is managed using a Digital Thread across various platforms. Luo et. al. [7] demonstrated the application of multidomain unified modelling for self-sensing using soft sensors for autonomous / self-prediction of maintenance intervals. They also defined

the Edge analytics requirements for executing the Unified modelling language for Mathematical Computational modelling with the data from different sensors of a CNC. Ishibashi et. al [8] predicted the Remaining Useful Life (RUL) of a generic system when a higher level of interpretability of the prediction model is desired. They demonstrated that GFRBS can work with the uncertainty of the PHM problems and can be used as an accurate prediction model that, at the same time, presents good interpretability. Javed et. al. [9] proposed a prognostics model that integrated two new algorithms, a Summation Wavelet Extreme Learning Machine (SWELM) and Subtractive-Maximum Entropy Fuzzy Clustering (S-MEFC) to predict degrading behavior, automatically identify the states of degrading machinery, and to dynamically assign Failure Threshold. Xi et al. [10] proposed an idea to first build statistical relationship between failure time and the time realizations at specified degradation levels on the basis of off-line training data sets, and then identify possible failure times for on-line testing units based on the constructed statistical model and available on-line testing data. Health degradation of engineering systems was represented by a one-dimensional and non-decreasing degradation curve. Baraldi et. al. [11] developed the prognostic model in the case in which some observations indicating the equipment degradation level are available, although affected by uncertainty. In the ensemble approach, BAGGING technique was used for the generation of diverse models. Ji et al. have predicted the Remaining Useful Life Airplane Engine Based on PCA-BLSTM technique [12] and reported that their hybrid model showed better prediction accuracy and performance. From the literature, it is deduced that although multiple machine learning approaches have been applied to bring out industry specific insights on functional data, there were few or trivial works reported on usage of Stacked Ensemble methods and AutoML methods. Hence, this research work focuses on the application of AutoML techniques to predict the RUL of Turbofan engines. We report the results of applying three machine learning techniques. The first one is based on building a linear regression model on the sensor data to estimate the RUL. In the second technique, a binary classification approach is carried out using AutoML by dividing the engine dataset into two classes based on the estimated RUL above 30 cycles and below 30 cycles. Finally, a multiclass classification approach is carried out by dividing the dataset into estimated RUL within 15 cycles, between 15 and 30 cycles and above 30 cycles.

II. MATERIALS AND METHODOLOGY

In this work the Prognostics and Health Management PHM08 Data Set from NASA Ames Prognostics CoE is considered [13]. PCoE Datasets are publicly available datasets that are used to support development of prognostic algorithms. This dataset is the collection of engine degradation simulation studies done using C-MAPSS technique. Fault evolution was characterized using data from several sensors. Though PHM08 Data Set is a simulated dataset, the business understanding of this challenge data set is to use the aggregated data of 21 different sensors per operation placed in a turbofan engine and predict the Remaining Useful Life (RUL). There are three operational settings that describe its functioning: Mach Number (Speed), Altitude of operation & Maximum Throttle during operation. The settings of the aircraft engine are visualized as shown in Fig 1. From the figure, it is inferred that the data have to be segmented before using for analysis since the sensor pertaining to each setting are different and would relate to the RUL of the engine.

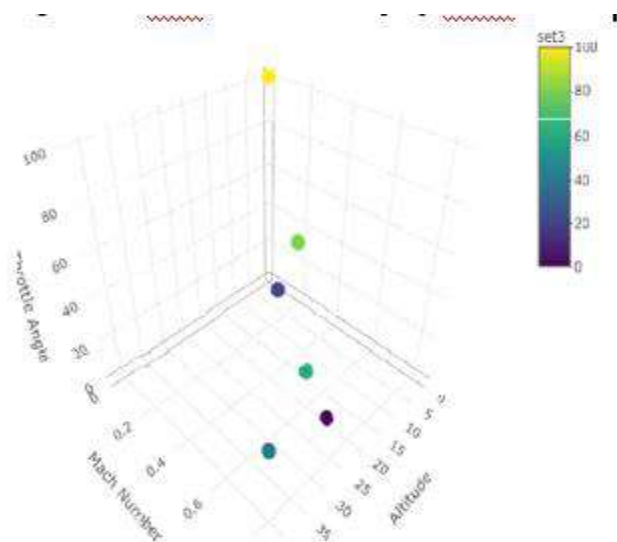


Fig. 1 3-D Visualization of Operational Settings in the PHM08 Data Set

A. Exploratory Data Analysis

The dataset consists of 45918 rows in the training dataset and 29820 rows in the test dataset with 27 features. To ascertain the validity of the sensor data, the distribution of the 21 sensor data is visualized through box plot analysis as shown in Figure 2. From the figure, it is inferred that values from sensor number 13 and 15 does not show any appreciable variation and has low standard deviation. Hence, the sensor data with low standard deviation were eliminated from the computation. Figures 3 and 4 represent the Histogram of Train Data of maximum possible cycles of Turbofan Engines and Histogram of Train Data for each setting. The Remaining Useful Life (RUL) of the aircraft engine was numerically calculated using Equation 1, where (i) represent the id of the engine.

Remaining Useful Life (RUL) = Maximum Life of the Engine (i) - Cycle of that Engine (i) of that row (1)

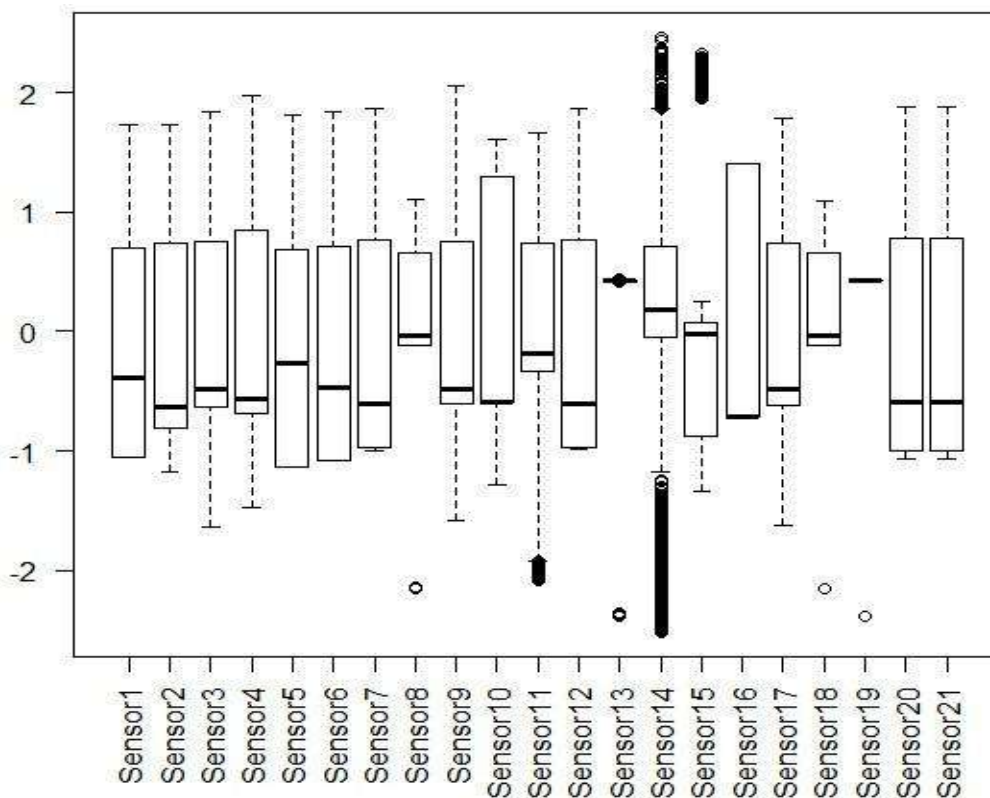


Fig. 2. Box plot visualization of distribution of sensor data from PHM08 dataset

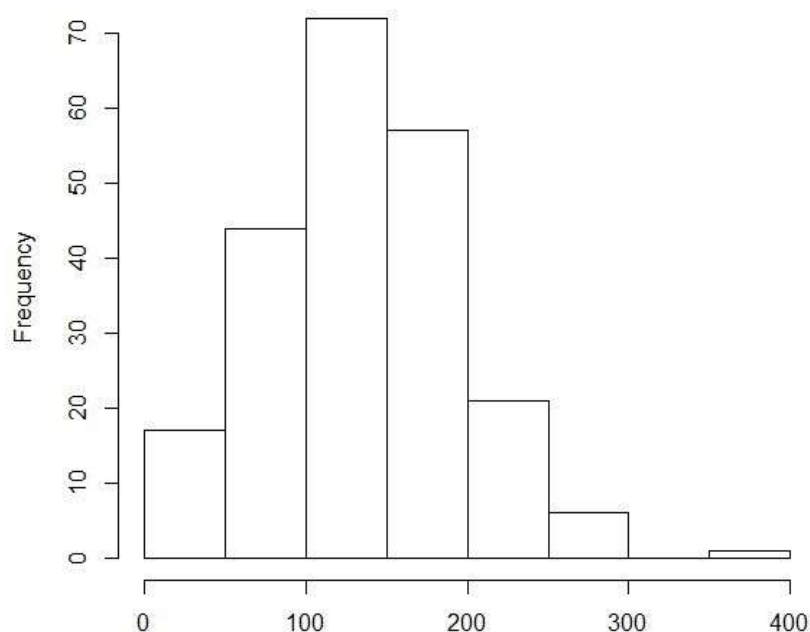


Fig. 3. Histogram visualization of PHM08 training dataset with maximum possible cycles of engines

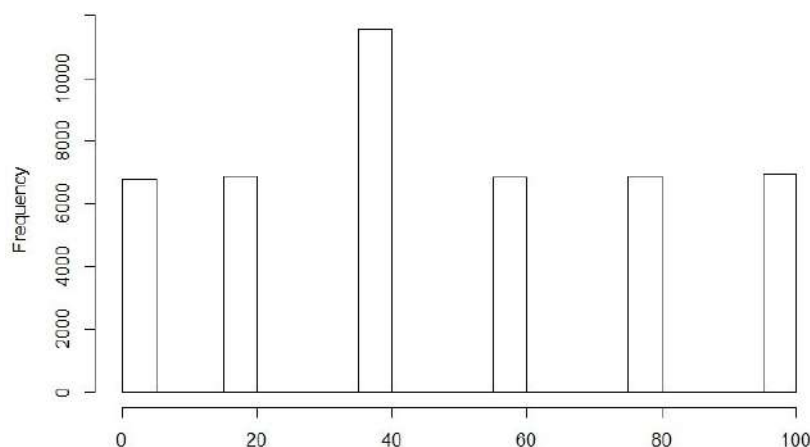


Fig. 4. Histogram visualization of PHM08 training dataset for each operational setting

B. Principal Component Analysis

As discussed in section 2.A, data from two sensors are not included in the second stage of RUL computation based on their statistical analysis. Principal Component Analysis (PCA) is a machine learning technique used to reduce the number of features in a dataset, otherwise known as dimensionality reduction. PCA captures the variance in the dataset and creates a reduced set of principal components that preserve the data while eliminating the noise. Eigenvalue provides the magnitude of the variance and Eigenvector provides the corresponding direction of variance in the data space. The number of Principal Components would be equal to the number of features in the dataset. Let there be n dimensional feature vectors of a given dataset denoted by A_1, A_2, \dots, A_n . These are converted into Principal components $\tilde{A}_1, \tilde{A}_2, \dots, \tilde{A}_k$. Equation (2) is used to compute covariance matrix E of the original vectors. From the covariance matrix E , the eigen values are calculated. The corresponding eigen vector matrix \tilde{E} for each eigen value are given in Equation (3). The expression for the Principal Components is given in Equation (4). The equations (2) – (4) are shown in figure 5.

$$E = \sum_{i=1}^n (A_i - \bar{A})(A_i - \bar{A})^T \quad (2)$$

$$\tilde{E} = \begin{cases} e_1 = e_{11} + e_{12} + \dots + e_{1n} \\ \vdots \\ e_k = e_{k1} + e_{k2} + \dots + e_{kn} \end{cases} \quad (3)$$

$$\begin{cases} \tilde{A}_1 = e_{11} A_1 + e_{12} A_2 + \dots + e_{1n} A_n \\ \vdots \\ \tilde{A}_k = e_{k1} A_1 + e_{k2} A_2 + \dots + e_{kn} A_n \end{cases} \quad (4)$$

Fig. 5. Equations (2), (3) and (4) for the PCA analysis

After pre-processing the sensor data, the PCA is performed. Figure 6 shows the Scree plot of the Principal Components. It is observed that the first two principal components contribute to the majority of variance. Hence, PCA1 and PCA2 are considered for further computation. For performing binary and multi-class classification, a dummy variable called “label1” was created for the rows of data where the RUL was greater than or equal to 30 cycles. Another dummy variable “label2” was created where the value was ‘2’ for rows of data in which RUL is greater than or equal to 15 cycles and ‘1’ for rows of data where the RUL was greater than or equal to 30 cycles. To validate the segmentation, a scatter plot of the PC1 and PC2 versus the estimated RUL was plotted. Figures 7 and 8 illustrate the clear distinction between the different classes based on the Principal Components 1 and 2.

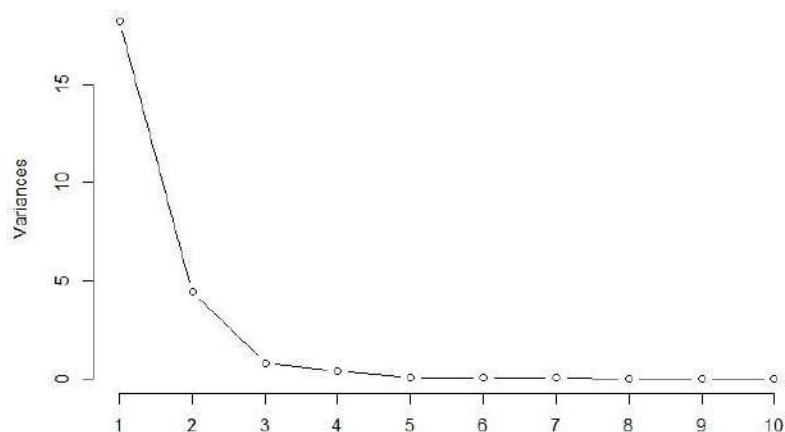


Fig. 6 Scree plot of Principal Components Vs Variance of sensor values

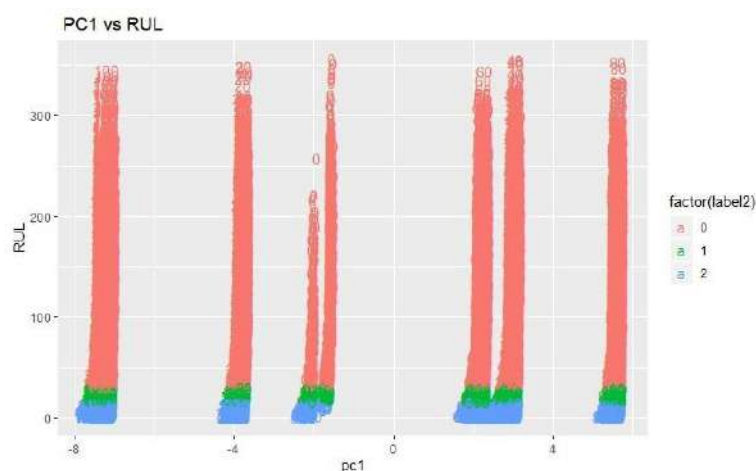


Fig. 7 Scatter Plot of Principal Component 1 Vs Remaining Useful Life

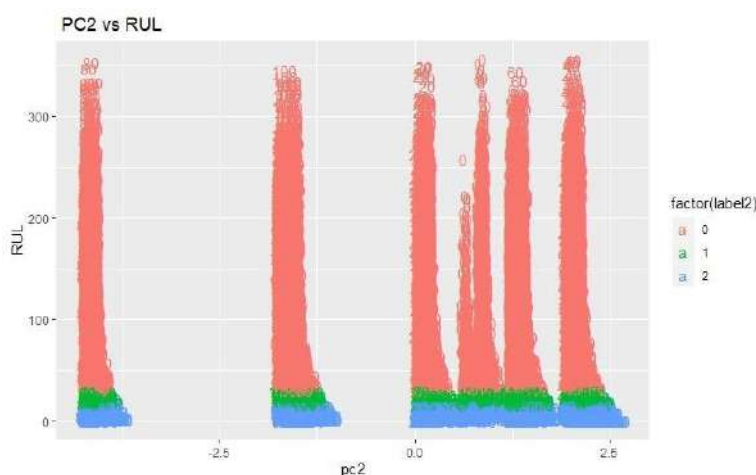


Fig.8 Scatter Plot of Principal Component 2 Vs Remaining Useful Life

To deploy the algorithm in an edge device, the equation of the Principal Component can be created using the Equation (5), in which i varies from 1 to Max no. of Principal Components

$$PC = \text{Data } (i) - \text{Center value}(i) \text{ of the PC} / \text{scale}(i) * \text{rotation}(i) \text{ value of the PC} \quad (5)$$

C. Linear Regression Model using ML

The primary purpose of the work is about creating a data analysis model and deploy it in Industrial IIOT devices where basic mathematical functions like addition, multiplication, subtraction and division are alone feasible. Hence, with the Principal Components and the sensor values, a Multiple Linear Regression Model is built to estimate the RUL. From the model equation, it is seen that this purpose can be achieved by converting the equations into a format suitable for computation in edge devices such as PLCs, microcontrollers, etc. The regression model is given by Equation (6).

$$\begin{aligned} \text{RUL} = & 14519.52 + (-9.34) * \text{Sensor2} + (-0.73) * \text{Sensor3} + (-1.25) * \text{Sensor4} + (-281.73) * \text{Sensor6} + \\ & (2.71) * \text{Sensor7} + (14.5) * \text{Sensor8} + (-0.47) * \text{Sensor9} + (-60.21) * \text{Sensor11} \\ & + (5.27) * \text{Sensor12} + (-11.68) * \text{Sensor13} + (-317.55) * \text{Sensor15} + (-3.53) * \text{Sensor17} + (6.44) * \\ & \text{Sensor20} + (19.66) * \text{Sensor21} + (-66.08) * \text{pc2} \end{aligned} \quad (6)$$

Machine Learning techniques require optimization of hyper parameters for higher efficiency and Deep learning techniques based on Artificial Neural Networks are primarily used for automatically extracting parameters. Amidst these shortfalls, AutoML algorithms are gaining popularity as they can automatically tune the hyper parameters and help in optimization of the machine learning and deep learning techniques. AutoML algorithms enable the reduction of human interaction needed in traditional machine learning methods. They focus on two important aspects such as data collection and the prediction of outcomes. The performance of machine learning models is dependent on the intuition and experience of data scientists [14]. Pipelining refers to the various steps involved in the tuning of Machine learning algorithms. In AutoML, the pipelines of Machine Learning are optimized such that people with limited knowledge of Machine Learning are able to achieve better results in their areas of deployment. AutoML techniques such as Auto-WEKA, Auto-sklearn, TPOT, Auto-ml, Auto-KERAS, H2O and Darwin were standalone applications that supported the efforts of automating Machine learning tasks. Few other cloud applications such as Google Cloud AutoML, Microsoft AzureML, Transmogri AI and Ludwig were added to the AutoML domain. able to create pipelines for processing and has superior feature engineering techniques to optimize its pipelines. It is well suited for classification applications and provides a leader board facility that displays the techniques that provide the prominent results for the current optimization process. The H2O AutoML algorithm was applied to the PHM08 dataset to perform linear regression. The results given in Table 1 shows the leader board statistics. The leader board showed 51 rows and 8 columns that imply that 51 Models were tried by the autoML algorithm with deviance as the criteria for selection. H2O had selected 37 GBM models, 9 Deep learning Models, 2 Stacked Ensemble models, 1 DRF model, 1 GLM model and 1 XRT model. It was observed that Stacked Ensemble models topped the leader board. The Top 5 meta learners of this stacked ensemble model that emerged as leader are given in Table 2 with the corresponding relative and scaled importance value. Figure 9 shows the graph of H2O models with respect to their corresponding relative importance. From the graph, it is inferred that these top 5 meta learners contribute to significant metrics in the stacked ensemble method. While testing the model with the test dataset, a correlation of 0.803 was achieved between the expected outcome and the predicted outcome.

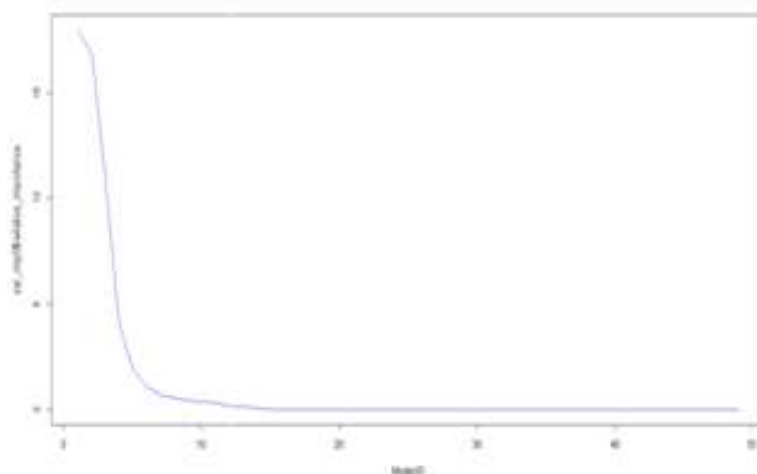


Fig.9 Relative Importance of Top Five metalearners of Stacked Ensemble Model

For performing Binary Class Classification, the PHM08 dataset was segmented into two groups. The first group had data with RUL less than 30 cycles and the second group had data with RUL more than or equal to 30 cycles. Table 1 summarizes the performance metrics of the classifiers implemented by the H2O platform. The input features were the two principal components. During the binary classification task using training dataset, a maximum accuracy of 99.78% was achieved by the ensemble model of GBM and Random Forest. While the specificity and sensitivity given individually by the GBM and Random Forests were comparatively lesser, it is noted that their ensemble combination achieved more than 99% specificity and sensitivity on the training dataset. From Table 2, it is noted that the accuracy, specificity and sensitivity values were drastically lower when used on the test dataset. In spite of being tuned, the ensemble learning was not able to produce appreciable results on the test dataset.

To improve the accuracy of the classification task, the first 4 Principal Components were considered for classification. The results of the AutoML training on the training dataset and cross validation dataset are presented in Table 1. The classification task was also carried out with the first 4 Principal Components along with the sensor values. The results of the classification task are summarized in Table 1. From Table 1, it is understood that the combination of PCs with sensor values are giving better results in the cross-validation phase compared with the training phase. Multiclass classification model training of PHM08 prognostics data set to predict classes 0, 1 and 2 was carried out using AutoML with the first 4 PC's. Table 2 presents the performance statistics of the H2O platform on both the PHM08 training dataset and test dataset. Due to the unbalanced nature of the classes, the AutoML was assigned with unbalance data management attribute as true. The relative importance levels of the meta learners of the AutoML training and shown in fig 10.

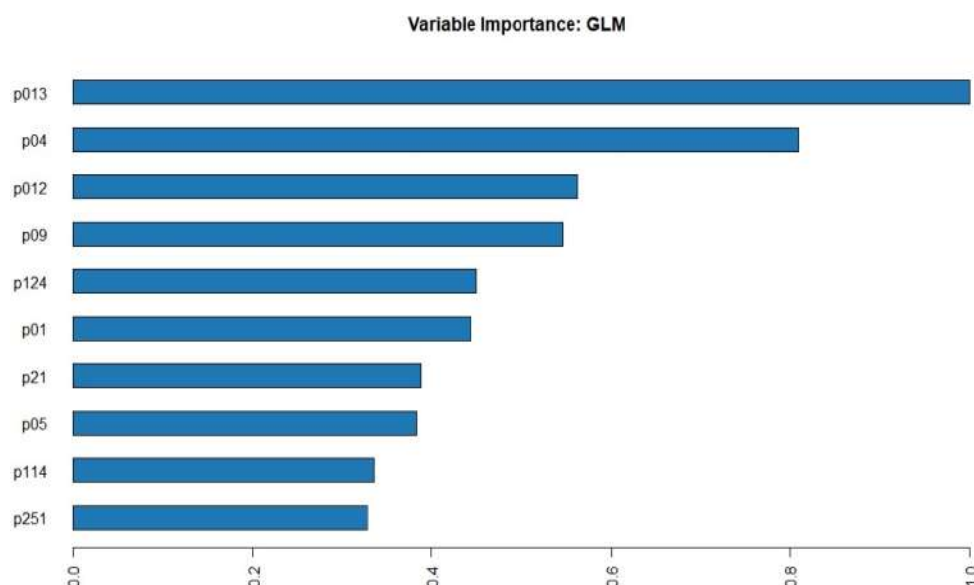


Fig. 10 Relative importance of the meta learners

IV. RESULTS AND DISCUSSION

In this work, three approaches were followed for estimating the Remaining Useful Life (RUL) of Turbofan engines. The Prognostic Database PHM08 was considered due to its popularity in enabling predictive analytics and being a mission critical database in the aviation industry. The first phase of work involved creating a Linear Regression Model using sensor data and the first two principal components of the features. Equation 6 provided the numerical expression of the Linear Regression Model that was found to be suitable for implementing in edge devices. Then, AutoML techniques were applied on the dataset to perform regression, binary class classification and multi class classification. The regression model was built using several models by the H2O platform. Out of these, the winner was the stacked ensemble method. In spite of the AutoML application, the RMSE value achieved by the stacked ensemble method was around 40 that is considerably high when compared with the recent literature that quoted the dataset. The binary classification and multiclass classification was performed by segmenting the dataset on the basis of RUL values. The thresholds were arrived as 15 and 30 cycles as the RUL of the turbofan engines.

ID	model Type	mean residual _deviance	rmse	mse	mae	training_ time_ms	predict time _per_row_ms
1	Stacked Ensemble	1611.13	40.14	1611.1 3	29.27	40708.00	1.65
2	Stacked Ensemble	1617.79	40.22	1617.7 9	29.29	1063.00	0.03
3	GBM	1638.59	40.48	1638.5 9	29.56	874.00	0.009
4	XRT	1641.71	40.52	1641.7 1	29.64	6508.00	0.012
5	GBM	1644.88	40.56	1644.8 8	29.68	606.00	0.018

TABLE I LEADER BOARD TOP 5 MODELS WITH PERFORMANCE ON PHM08 DATASET USING H2O AUTOML

ID	Variable (meta learner name)	Relative importance	Scaled importance
1	GBM_5_AutoML_20200215_143949	15.355	1
2	GBM_grid 1_AutoML_20200215_143949_model_14	14.856	0.967
3	GBM_grid 1_AutoML_20200215_143949_model_1	14.488	0.943
4	GBM_grid 1_AutoML_20200215_143949_model_3	7.508	0.489
5	XRT_1_AutoML_20200215_143949	1.397	0.091

TABLE II TOP FIVE METALEARNERS OF STACKED ENSEMBLE MODEL IN H2O PLATFORM

V. CONCLUSION

The aim of this research work was to develop a use case with open industrial datasets with two specific objectives as (i) perform data analytics in the context I4.0 in accordance with IIC and ISA standards (ii) explore H2O AutoML package for the PHM08 Challenge dataset. The data was pre processed through Exploratory Data Analysis (EDA) and validated. From this analysis, it was observed that the aircraft was operated at six different settings and two of the sensor data did not show appreciable variation in the estimation of RUL. Based on the remaining sensor data and the extracted Principal Components, an attempt was made to estimate RUL using regression, binary classification and multiclass classification. While several research studies based on the dataset were able to achieve higher accuracy values by virtue of the hyper tuning methods and deep learning methods, we have presented about a research framework to employ Automated Machine Learning methods to analyze the Turbofan Degradation data. In the Industry 4.0 scenario, by empowering the engineers with the knowledge of AutoML techniques such as H2O, meaningful insights into the data can be achieved even with a limited knowledge of data science.

REFERENCES

1. The Fourth Industrial Revolution: what it means, how to respond. Available at : <https://www.weforum.org> [Accessed 12th March, 2021]
2. The four impacts of industry 4.0 on aeronautics. Available at :<https://ignition.altran.com/en/article/> [Accessed 12th March, 2021]
3. Diab, H and Lin, S, "Industrial Analytics: The Engine Driving the IIoT Revolution", IIC:PUB:T3:V1.00:PB:20171023, March 2017
4. Philipp, Z and Dominik, R, 'Representing Industrial Data Streams in Digital Twins using Semantic Labeling' IEEE International Conference on Big Data, 2018, pp. 4223 – 4226.
5. Vachálek, J., Bartalský, L., Rovný, O, Šišmišová, D., Morháč, M. and Lokšík, M., "The digital twin of an industrial production line within the industry 4.0 concept," 2017 21st International Conference on Process Control (PC), StrbskePleso, 2017, pp. 258-262.
6. A, Anedo, "Industrial IoT lifecycle via digital twins," International Conference on Hardware/Software Codesign and System Synthesis (CODES+ISSS), Pittsburgh, PA, 2016, pp. 1-1.
7. Luo, W., Hu, T., Zhu, W. and Tao, F., "Digital twin modeling method for CNC machine tool," 2018 IEEE 15th International Conference on Networking, Sensing and Control (ICNSC), Zhuhai, 2018, pp. 1- 4.
8. Ishibashi, R. and Lucio, C., "GFRBS-PHM: A Genetic Fuzzy Rule-Based System for PHM with Improved Interpretability", 2013 IEEE Conference on Prognostics and Health Management (PHM), pp. 1--7, 2013.
9. Javed, K., Gouriveau, R. and Zerhouni, N., "SW-ELM: A summation wavelet extreme learning machine algorithm with a priori parameter initialization", Neurocomputing, Vol. 123, pp. 299--307, 2014.
10. Xi, Z., Jing, R., Wang, P. and Hu, C., "A Copula-based sampling method for data-driven prognostics and health management", 2013 IEEE Conference on Prognostics and Health Management (PHM), pp. 1--10, 2013.
11. Baraldi, P., Compare, M., Saucio, S. and Zio, E., "Ensemble neural network-based particle filtering for prognostics", Mechanical Systems and Signal Processing, Vol. 41 No. 1, pp. 288--300, 2013.

12. Ji, S., Han, X., Hou, Y., Song, Y., & Du, Q. (2020). Remaining Useful Life Prediction of Airplane Engine Based on PCA-BLSTM. *Sensors (Basel, Switzerland)*, 20(16), 4537. <https://doi.org/10.3390/s20164537>
13. A. Saxena and K. Goebel (2008). "PHM08 Challenge Data Set", NASA Ames Prognostics Data Repository (<http://ti.arc.nasa.gov/project/prognostic-data-repository>), NASA Ames Research Center, Moffett Field, CA
14. A. Truong, A. Walters, J. Goodsitt, K. Hines, C. B. Bruss and R. Farivar, "Towards Automated Machine Learning: Evaluation and Comparison of AutoML Approaches and Tools," 2019 IEEE 31st International Conference on Tools with Artificial Intelligence (ICTAI), 2019, pp. 1471-1479, doi: 10.1109/ICTAI.2019.00209
15. AutoML capabilities of H2O library. Available at: <https://www.kaggle.com> [Accessed 12th March, 2021]

Improving Sewing Line Performance and Rejection Analysis in a Garment Industry

Mathivanank¹, Jayachitra R², Punitharani K³ and Prabhakarank⁴

^{1,2,3}PSG College of Technology, Coimbatore

⁴Industrial Engineer, Jay Jay Mills (India) Pvt. Ltd., SIPCOT, Perundurai

ABSTRACT

Garment manufacturing is a traditional industry with global competition. The most critical manufacturing process is sewing, as it generally involves a lot of operations. Now-a-days to fulfill the customer's demand within leadtime and to fulfill their requirements, their whole productive system and their operators must be fully efficient and capable. A balanced sewing line can reduce the production time of garment, increase production efficiency and reduce production cycle time. Sometimes due to the rapid changes in the style of apparel products, excessive pressure the workers won't retain pace with the given manufacture target. In this context, many movements practiced by the operators are unnecessary. This affects the productivity of the organization. In this paper, the Work-in-progress inventory are determined and the non-value-added activities are located using industrial engineering tools. Various tools and techniques like time study, Flexsim, method study, efficiency calculation, SOP, Pareto chart analysis, solution matrix have been applied to reduce the production time and rejection of garments. These significant improvements can be achieved applying below mentioned tools and techniques.

Keywords— WIP operations, time study, Flexsim, line balancing, method study, efficiency calculation, Pareto chart analysis, solution matrix.

I. INTRODUCTION

The production process of garments is separated into four main phases, designing, clothing, pattern generation, fabric cutting, sewing, ironing and packing. Manufacturing engineers are alarmed with the steadiness of the lines by allocating to work spaces as similarly as conceivable. This sewing line consists of a set of workstations in which a specific task in a predefined sequence is processed. Inappropriate workstation assignment will lead to the increase of labor cost, WIP, cycle time, and lead times or standard allowed minute is used to measure task or work content of a garment. This term is widely used by industrial engineers and production system. All the garments industries are labor intensive, so the best utilization of labours of the industry will assure the highest profit of company. In the present scenario apparel engineering industries are annoying to growth in recent manufacture system and condition and uninterruptedly observing for new manufacture tools and methods to retain pace with the quick alterations of the trend in clients of apparel goods. To agreement with the recent condition and fulfil client request inside lead time, entire manufacture system should be extra capable and effective. Full apparel is created based on the performance and involvement of distinct performance level where they are accomplished. If we note a garments production line, we will realize that there are lots of in-progress inventory and wait time among early each consecutive operation. Some methods are agreed in the factory and enduring are outsourced based on the need. The major problems faced in the garment manufacturing company is stitching area. Most of the failures to meet delivery time is because of stitching.

II. PROBLEM DEFINITION

Currently, Carter's body suit processing time is high at 6.87 min for single garment in sewing line. This fails in meeting of standard minute value 4.08 min. The processing time of body suit is delayed by 2.79 min. There are lots of WIP inventory between the workstations because of non-value-added activities. Hence, its output is quite less. The operators and the line supervisors are not aware about the standard working procedure. Thus, lots of rejection piece occurs during inspection.

III. OBJECTIVES

To increase the line efficiency by 10% of current efficiency.

To develop standard operating procedure (SOP) for operators who fail to meet the SMV.

To reduce the processing time of garment pieces through removing non-value-added activities

To improve production performance using lean concepts and industrial engineering tools.

To reduce the defects in the garments.

IV. DATACOLLECTION

Time study has been conducted on the sewing line. The results are shown in Table I. The operations performed in the carter's body suit production are

S.No	IDNo	Operation	SMV min	Actual time in min
1	12815	Heat-seal	0.20	0.18
2	11915	Twill tape attach	0.17	0.38
3	11235	Twill tape close	0.18	0.32
4	11839	Neck binding	0.24	0.41
5	11713	Sleeve hemming	0.17	0.44
6	12764	Lap shouldertack	0.32	0.56
7	7844	Lap shouldertack	0.32	0.56
8	10718	Sleeve attach 1	0.48	0.69
9	11829	Sleeve attach 2	0.48	0.69
10	11880	Side seam 1	0.44	0.69
11	8082	Side seam 2	0.44	0.39
12	12766	Side seam 3	0.44	1.02
13	7262	Bottom binding	0.21	0.38
14	11111	Sleeve and bottom tack	0.50	0.14
15	7837	Gusset iron	0.15	0.13
16	12572	Button top	0.12	0.68
17	11652	Button bottom	0.12	0.68
18	11828	Ironing	0.35	0.59
19	12827	Ironing	0.35	0.59
20	10201	Packing	0.35	0.98
21	7739	Binding cut	0.08	0.08

Table 1. Time study

V. ANALYSIS AND INTERPRETATION

A. Sewing Process flow

Sewing process flow is a method of visually documenting the stages involved in performing a certain procedure. The process flow of sewing a carter's body suit is shown in Fig 1.

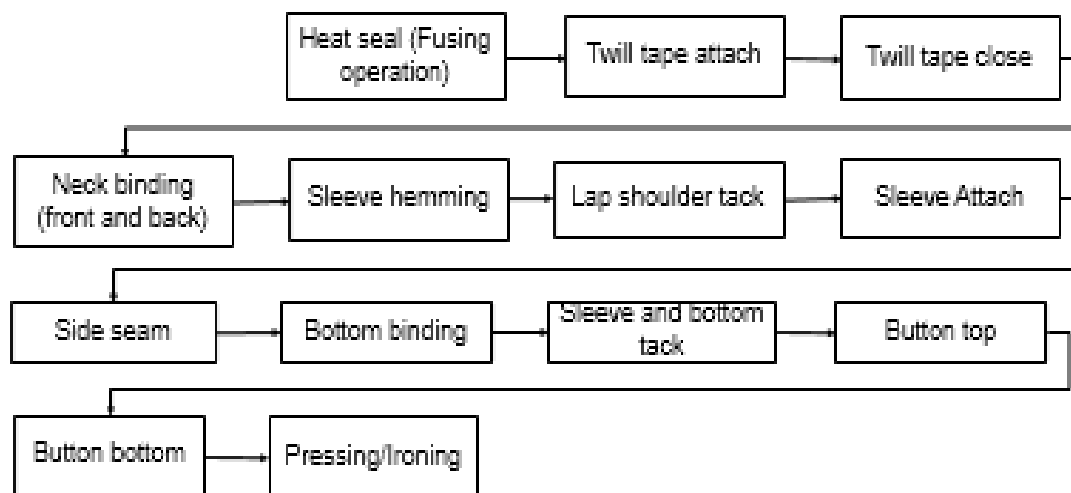


Fig.1 Process flow

B. Network diagram for linebalancing

The network diagram is a quality management tool that charts the flow of activity between separate tasks. It graphically displays independent relationships between the tasks. A network diagram is developed to understand the flow of the process in Fig2.

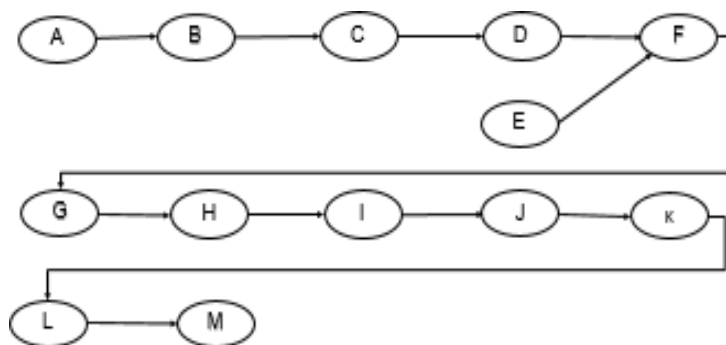


Fig.2 Network diagram

C. Efficiency calculation

The comparison of what is actually produced or performed with what can be achieved with the same consumption of resources is known as efficiency. To calculate the efficiency of each operator, the efficiency chart has been developed and through the chart, the bottleneck operations have been identified. Shift timing is 8 hours, 21 manpower for single wing line, from this standard allocated minute is calculated. The standard minute value of producing single garment is 4.08 minutes.

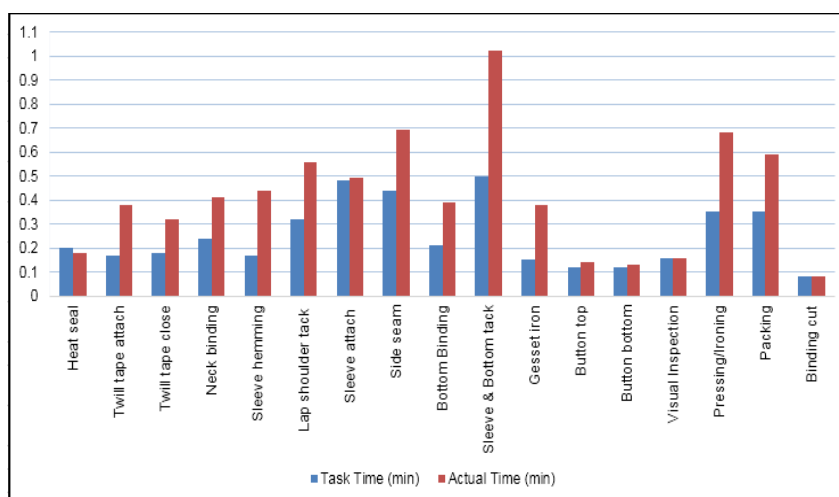


Fig.3 Efficiency chart

Fig.3 shows the graphical representation of the efficiency of each operator. In a manufacture sewing line, where source collected, manufacture goes under volume and lots of garment's parts one exact work plan remain uncommitted, those zones are called as holdup areas and which mechanism as a restriction for flat flow of manufacture is called as bottleneck.

D. Takt time calculation

Takt time is the average time between the start of production of one unit and the start of production of the next unit. Takt time is calculated using the formula,

$$\text{Takt time} = \frac{\text{Net available time for production}}{\text{Monthly demand}}$$

Monthly demand

The monthly demand of body suits is 115065 pieces and the net available time for production is 12480 hours. In one shift 480 minutes, 12 shifts per week, total working days in a month is 26, and demand is 29640.

Takt time	=	480x26
	=	29640
	=	0.19433 minutes

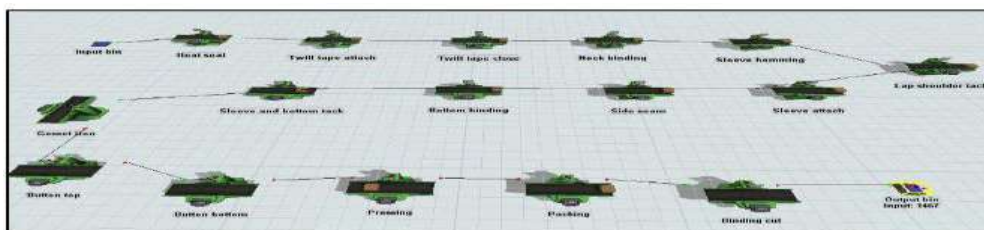


Fig.4 Flexsim–Currentmodel

VI. Simulation Result

The current model of line is simulated using Flexsim software as shown in Fig.4

The assumptions made before simulating the existingsewingline are,

All themachines are available at thetime zero

The successor machine is idle when the product is processingat the precedence machine

In realtime,the successo rmachine will be loadedwithanother garment, itwillnotbe idle

Processing of garment is based on priority system.(FIFO –FirstinFirstOut

Object	input	output	processing
Heatseal	1479	1478	677.4
Twilltapeclose	1477	1476	358.4
Sleevehemming	1475	1474	923.5
Twilltapeattach	1478	1477	399.4
Neckbinding	1476	1475	014.4
Sleeve andbottomtack	1470	1469	957.4
Bottombinding	1471	1470	421.4
Gessetiron	1469	1469	787.9
Buttontop	1469	1469	339.6
Sideseam	1472	1471	940.8
Buttonbottom	1469	1469	458.2
Sleeveattach	1473	1472	306.2
Lapshouldertack	1474	1473	526.4
Pressing	1469	1468	603.6
Packing	1468	1467	567.1
Bindingcut	1467	1467	7041.6
Outputbin	1467	0	0

TableII Simulationreport

A.LARGEST CANDIDATERULE ALGORITHM

Linebalance is to allocate the entire job on as consistently as probable,it is used to combining the related processing time processes. Its helps steadiness the line. The dissimilarinleastrationally work component time and the superioritycotrols the two among the components. The LCR accounts for effort thecomponents to be organized in a sliding order. For each station valuewhich is notextraordinarily the acceptable preceded. The superiority relations and is the instantaneouspredecessor among these jobs. A task can be done bymachinesofdifferenttypesandalsoby labourtypes.Theprocessing time of any task is a variable determined bytheskilllevel andefficiency.

Using largestcandidaterule formed thework stations depends on the precedence and processing time of the garments. Work element assigned to stations details areShowninthe Table III.

Station	TaskAssigned	Taskdescription	Tasktime(min)	No.ofoperators
1	A	Heat seal	0.2	1
	E	Sleevehemming	0.17	1
2	B	Twilltapeattach	0.17	1
	C	Twilltapeclose	0.18	1
	D	Neckbinding	0.24	

3	F	Lapshouldertack	0.32	2
4	G	Sleeveattach	0.48	3
5	H	Sideseam	0.44	3
6	I	Bottombinding	0.21	1
	J	Sleeveandbottomtack	0.5	3
7	K	Buttontop	0.12	1
	L	Buttonbottom	0.12	1

Table III Workelement assigned to stations

B. Cause and effect diagram

Cause and effect diagram show the causes of a specific event and the effect of the event. This diagram is used to identify the major defects occurring in the garment. The fishbone diagram for the rejection due to defects and over processing are shown in Fig. 5 & 6

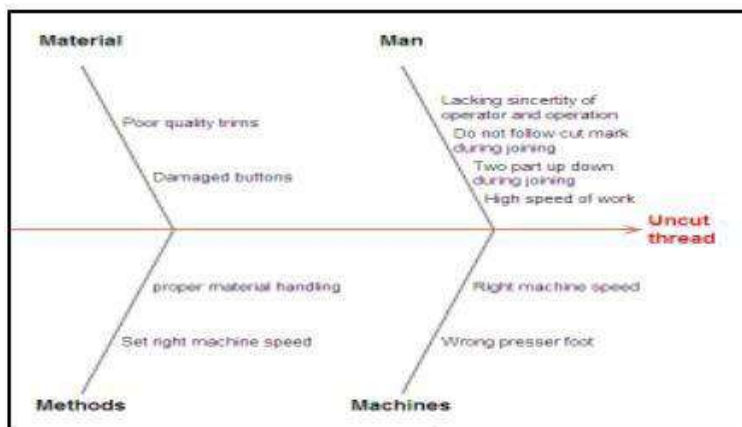


Fig.5 Uncut thread due to defects – fishbone diagram

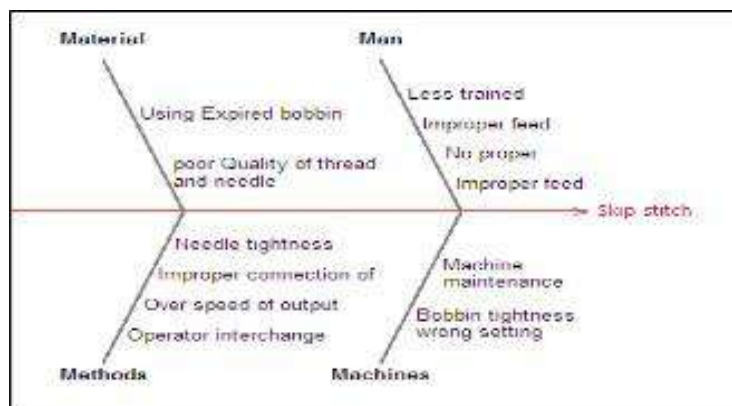


Fig.6 skip stitch due to defects – fishbone diagram

VII. REJECTION ANALYSIS

Sale order no carter's body suit number CAR – 484 Total demand of carter's bodysuit in form of single sale order. In this demand split into two different shipment date. Fabric initially comes from the processing division that stored in the finished fabric knitted store. Cutting, embroidery, Chest printing and sewing are the four main sections for producing the garments. Rejection quantity in a sewing line/month 2911 pieces. Total demand of carter's bodysuit in sale order 239735. Actual production of carter's bodysuit 243522. production of garments without rejection 234229. In the time of shipment, the lack of pieces 9293. This situation learning has been steered in a designated

A. Various defects in garments

Yarn mistake thick/thin yarn, holes, needle line, button mistake, fabric defects, fusing defects, color shading, center out, printing, Embroidery, broken stitches, shape out, SPI, singer stitch, puckering, loose stitch twisted, bowing double stitch joint stitch. The operators should be fully aware about all the basic operations of bodysuit and should be trained properly to operate all the operations. The operators should be allowed to regular production line only after attaining the efficiency of 80% in the training line. They should be aware about the basic mechanisms and should be able to repair it when some problems occur.

VII. PARETOCHARTANALYSIS

The Pareto chart analysis is a method used for judgement creating based on the 80/20 rule. It is a judgement creating method that statistically divides a in adequate quantity of input factors consuming the highest effect on a result, either that is needed or objectionable. Pareto study is founded on the knowledge that 80% of a project's benefit can be realized by undertaking 20% of the work or conversely 80% difficulties are traced to 20% of the causes. A Pareto graph that comprises both bars and a line graph, where distinct values are signified in sliding order by bars, and the collective total is denoted by the line. The values are in declining order and the cumulative function is a concave function. Pareto diagram high points the probable problems from a set of problems. It can be used to recognize most mutual sources of defects, the maximum occurring type of defect, or the most frequent reasons for customer complaints etc.

The graphical representation of the rejection rate chart of the various divisions is shown in Fig. 8

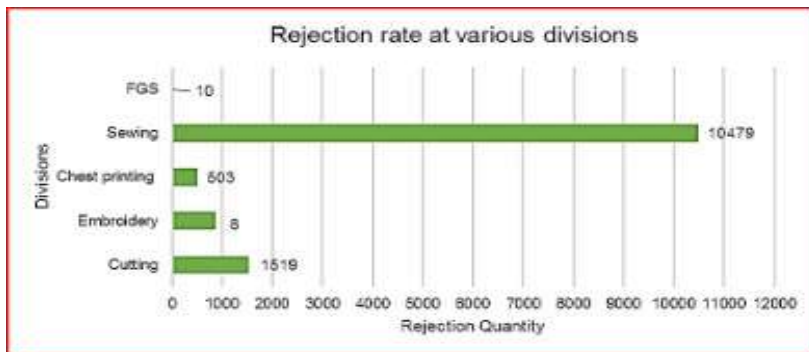


Fig 7 Rejection rate defects

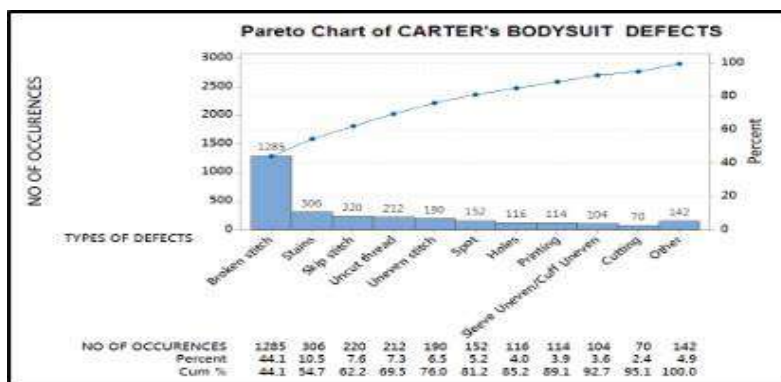


Fig.8 Paretochart

Pareto chart is used to graphically summarize and display the relative importance of the differences between groups of data. It is a bar diagram. The length of the bars signify regularity and are organized with the longest bars on the left and the shortest to the right. In that method the chart visually portrays which parts are more important.

VIII. SOLUTION MATRIX

Defects minimization is the first condition of reducing production cost and improving the quality. It will also reduce the cycle time by reducing rework and finally result higher productivity. Quality problems which lead to defects and rework in production is a major reason for increased lead time. Finally, some potential solutions are suggested to overcome the causes as shown in solution matrix in table IV.

Type	Major causes	Solution
Man	Less trained	Proper training for workers and SOP
	Dirty hand	Keep hands clean while handling material
	Cutting the stitch while trimming	Trim only using trimmer not by scissor
	Improper checking	Inline checkers for critical operations.
Machine	Improper maintenance	Do regular maintenance before starting new style
	Overheating of needles	Single piece flow avoids machine overstarting
Method	Unwanted material movement	Reduce material movement bring line system

Table iv Isolutionmatrix

This transportation cost can be reduced using the method of cost analysis and rejection analysis

	Existing	Improved
Lagged pieces	9293 pieces	6245 pieces
Transportation cost	Rs.69675	Rs.46800

Table V Cost analysis comparison

IX. CONCLUSION

Production time of the carter's bodysuit selected has been reduced from 6.87 minutes to 5.25 minutes. Number of operators have been utilized to line the sewing line. Rejection pieces has been reduced; the main reduction is due to defects of garment pieces. Sewing line effectiveness has been improved from 59.3% to 77.7%. Existing simulation model and proposed simulation model is developed in Flexsim software. An Existing model was created and analysed for potential areas of improvement. Industrial engineering tools and software were used to create a proposed model. The Flexsim mode that a better production time reduction through the use of line balancing. Simulation model is established in order to enable accepting and confirming that the model signifies the actual system.

Usually, employees have to do their processes in a hurry and frequently by being in a static position, which is dissimilar from their normal life. So, the effort situation wants to be matched and well-planned to them as much as possible. Seeing these facts, working station normalization to make workers calm and sense them unrestricted to work is very greatly essential to accept the extreme yield with suitable quality from them. In accumulation to these, sewing line furthermore wants to be very much well-adjusted to increase hourly production volume. By confirming the appropriate work spreading among the workers, the planned productivity can be attained without consuming overtime. Even a slight strategy variation to the sewing floor or any exact process can effect in very positively. Hence, the like type apparel industries, those who need to diagnose and correct their difficulties, and imagine for the improved production effectiveness through the enhancement of the little performing workers, the investigation results can be worthwhile and useful to them.

REFERENCES

1. International Journal of Scientific & Engineering Research, 4(2), 1-10.
2. Mukunda A, Aman Prasad B.H, Rajeswara Rao KVS, K. N. Subramanya (2014), "Ergonomic Evaluation of the Workstations in a Garment Manufacturing Industry – An Exploratory Study", International Journal of Mechanical and Production Engineering, ISSN: 2320-2092, Vol. 2, Issue 4.
3. Md. Mazedul Islam et.al., "Minimization of Reworks in Quality and Productivity Improvement in the Apparel.
4. Khatun, M.M. (2013). Application of Industrial Engineering Technique for Better Productivity in Garments Production. International Journal of Science, Environment and Technology, 2(6), 1361-1369.
5. Kapuria, T. K., Rahman, M., & Haldar, S. (2017). Root Cause Analysis and Productivity Improvement of An Apparel Industry Through Kaizen Implementation. Journal of Applied Research on Industrial Engineering, 4(4), 227-239.
6. Hodge, G.L., Goforth Ross, K., Joines, J.A., & Thoney, K. (2011). Adapting lean manufacturing principles to the textile industry. Production Planning & Control, 22(3), 237-247.
7. Baset, M. A., & Rahman, M. M. (2016). Application of Industrial Engineering in Garments Industry for Increasing Productivity of Sewing Line. International Journal of Current Engineering and Technology, 6(3), 2347-5161.
8. Sohail Ahmed and Md. Shafiqul Islam Chowdhury, "Increase the Efficiency and Productivity of Sewing Section through Low Performing Operators Improvement by using Eight Wastes of Lean Methodology", Global Journal of Researches in Engineering: J General Engineering, Volume 18 Issue 2 Version 1.0 Year 2018, Online ISSN: 2249-4596 & Print ISSN: 0975-5861.
9. Taposh Kumar Kapuria et.al., "Root Cause Analysis and Productivity Improvement of an Apparel Industry in Bangladesh through Kaizen Implementation", Journal of Applied Research on Industrial Engineering, Vol. 4, No.4 (2017) 227-239.
10. Md. Ahasan Habib et.al., "Improving Productivity

of Apparel Manufacturing System using Value Stream Mapping and Production Control Tools focusing on Printing Section”, *IJRET: International Journal of Research in Engineering and Technology*, Volume: 02 Issue: 09 | Sep-2013, eISSN: 2319-1163 | pISSN: 2321-7308.

11. Pranjali Chandurkar, Madhuri Kakde, Abhishek Bhadane, “Improve the Productivity with help of Industrial Engineering Techniques”, *International Journal on Textile Engineering and Processes*, ISSN: 2395-3578 Vol1, Issue4, October 2015.
12. Amal S Das, P V Gopinathan, “Productivity Improvement Using Industrial Engineering Tools – Case Study Of a Typical Spinning Mill”, *International Journal of Engineering Development and Research*, Volume 4, Issue3, ISSN:2321-9939.
13. M. M. Islam, A. M. Khan and M. M. Islam, (2013), “Application of Lean Manufacturing to Higher Productivity in the Apparel Industry in Bangladesh”, *International Journal of Scientific & Engineering Research*, 4(2), 1-10.
14. Mukunda A, Aman Prasad B.H, Rajeswara Rao KVS, K. N. Subramanya (2014), “Ergonomic Evaluation of the Workstations in a Garment Manufacturing Industry – An Exploratory Study”, *International Journal of Mechanical and Production Engineering*, ISSN: 2320-2092, Vol. 2, Issue4.
15. H M A Pfaira et.al., “The Use of Productivity Improvement Tools and Techniques in the Botswana Textile Industry”, *International Journal of Mining, Metallurgy & Mechanical Engineering (IJMMME)*, Volume 3, Issue 3(2015) ISSN 2320-4060 (Online).

Design of a Smart Waste Segregation System

R. Jayachitra, Udit Sanyal, Ayush Singh and Thangaraju Naveen
Department of Mechanical Engineering, PSG College of Technology

ABSTRACT

Waste segregation is an important process which directly effects the environment. Effective separation of different types of waste at collection point increases the efficiency of the process. A literature survey was carried out to understand the waste segregation process and the difficulties faced by the existing methods. Estimated data was then found out about the amount of waste produced in an area. Various stages were allocated for the segregation process which would give the optimum result. Then a design was proposed for the smart waste segregator according to the stages and required workflow. 3D models were made according to the design for all the part and the whole system all together. The main objective of this waste segregator system is to separate dry waste. The final modal will be useful to segregate waste at the collection point itself which will reduce the wastage of resources. Moreover the segregation of different waste at different plant increased the net carbon dioxide emission in the process, whereas this model is capable of segregating most of the waste at a single point itself.

I. INTRODUCTION

"Waste segregation" means dividing waste into dry and wet. Dry waste includes wood and related products, metals and glass. Wet waste naturally refers to organic waste usually generated by eating establishments and are heavy in weight due to dampness. Waste can also be economic concern. Waste Segregation is different from Waste Categorization. Waste Segregation means to group Waste into different Categories. Each waste goes into its category at the point of dumping or collection. Categorization comes after collection or dumping.

II. PROBLEM STATEMENT AND OBJECTIVE

There is a need of a smart waste segregation equipment to separate dry waste into its different constituent at a single location with reduced human contact to increase the efficiency and safety of waste segregation process. The following objectives are defined for this problem,

- To design a smart waste segregation system to segregate glass, ferrous and non-ferrous metallic waste.
- To check the feasibility of the waste segregation system.

III. LITERATURE SURVEY

From the literature review, we see all the techniques of sorting, different types of wastes and methods to identify different types of wastes.

(1)Magnetic Separator (2) Eddy current separator. (3) Inductor sorting. (4) Near infrared sensors. (5) Noted the quantity of waste is collected in Municipal Solid waste Management. (6) For small particles star screens can be used which is followed by glass breaker screen to separate glass particles

The entire system will be made automated so as to reduce human contact.

IV. METHODOLOGY

Based on the information obtained from the literature review, the problem has been identified, and the methodology to progress through the course of the project has been formulated

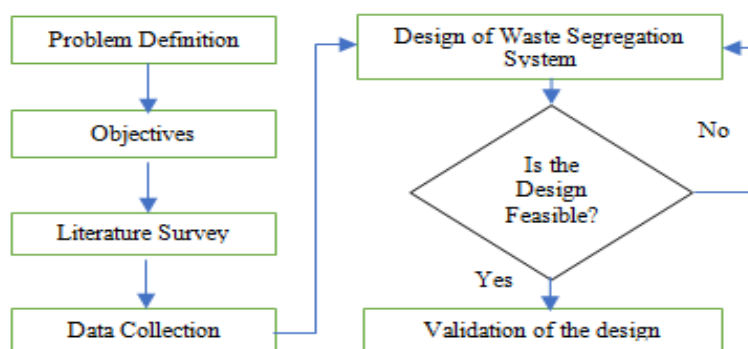


FIG. 1 METHODOLOGY FLOWCHART

Literature survey is done to understand what has already been done in this field and what challenges are being faced for it. This gives a clear idea about how to proceed with our project by finding the gaps in the literature survey and doing what has not been done before. Various data on waste storage and waste generation in households are taken from municipal corporations to understand the quantity of waste that is to be dealt with. Using the literature survey, waste segregation system is designed that is unique and deals with the problems caused as brought up by the data collection and literature survey. Finally feasibility of the design is checked, if it isn't feasible, the system is designed again, and if it is feasible then design calculations are done to validate the model.

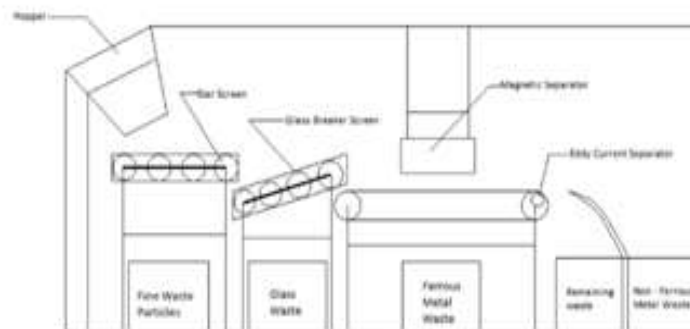


FIG. 2 DIAGRAMATIC REPRESENTATION OF THE WASTE SEGREGATION SYSTEM

V. DESIGN AND WORKING

The waste segregator was designed such that the segregation takes place in stages. Four different stages were identified for which the segregation will take place in series one after another. Each stage has its own dedicated bin for the purpose of collection of the corresponding waste. Finally the remaining unsegregated waste is collected in a separate bin.

Design of the segregation system

As shown in the diagrammatic representation of the waste segregation system in fig 2, a hopper is used to collect all the waste on daily basis and this is where the work of the machine begins. At the end of the hopper the segregation process starts. First the material falls on the star screen where smaller waste particles are removed. Then rest of the waste moves on to the glass breaker screen where glass is segregated by breaking them into smaller pieces. For the next stage the waste falls on the conveyer belt from which the ferrous waste is removed by another overhead magnetic separator. At the end of conveyer eddy current separator removes the non-ferrous waste from the mainstream waste. All the remaining waste then falls in a separate bin. Fig 3 shows the CAD model of this system.

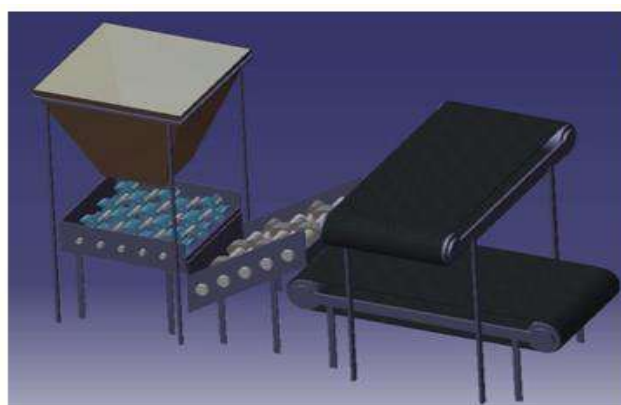


FIG. 3 CAD MODEL OF THE SYSTEM

Waste storage/hopper

The hopper is designed to store waste until the machine is turned on. It is shaped like a truncated pyramid with the larger diameter serving as the inlet for the waste, and the smaller diameter serving as the outlet of the storage system. The outlet of this hopper leads to the entry of the flow control mechanism. A movable disk is attached via a mechanical link that serves to separate the wastes. This disk opens and closes alternatively allowing only a few material to enter at one time onto the conveyer belt. Fig 4 shows the image of the hopper.

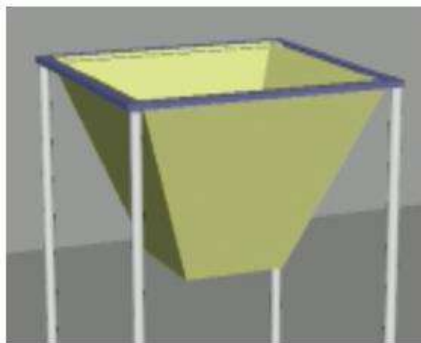


FIG 4 HOPPER

Star Screen

Star and disc screens consist of many shafts aligned parallel and at the same distance to each other which are fitted with side-by-side rotating star or disc type wheels. The screening stars or discs are arranged so that square or rectangular openings are produced. The shaft spacing governs the size of the respective openings.

The star and disk screening machines are fed by a dosing system or conveyor belt. The smaller fraction falls through between the stars, while the larger fraction is moved along further on the screening surface by the rotation of the shafts. The greater fraction is moved along the screening surface by the rotating shafts until it is thrown off at the end of the screen.

Star and disc screens can be used horizontally or at a slight incline. They are categorised by vibration-free operation and, due to the fact that they do not clog easily, they are suitable for grading damp and hard to screen bulk solids as well as for screening out over-lengths.

Disc screens and star screens are used in the wood processing industry (sawmills, waste wood incineration plants, power stations, by manufacturers of wood fuels), in the recycling industry (waste wood processing plants, waste wood operations, recycling processes, RDF plants or refuse derived fuel plants, composting sites) as well as in many other industries. The screening deck has different shafts with rubber stars of diameter 50 mm. The shaft is made of solid steel. It is driven by 12v DC motor

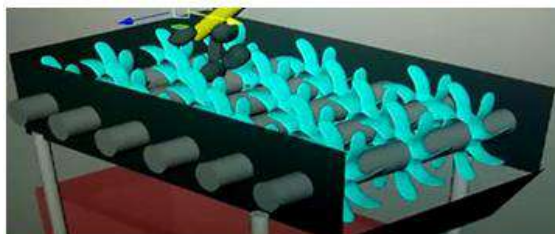


FIG. 5 STAR SCREEN

Glass breaker screen

The glass breaker deck has different shafts with steel elliptical disks of major diameter 50 mm and minor diameter 30 mm. It is tilted at an angle between 20 degrees so that glass material keep rolling back until they are shattered. It makes separation of glass waste easy. The glass breaks and the smaller pieces fall through the gaps between the stars. Reference for the dimensions were taken from Manufacturers Catalogue of Bollegraaf Recycling Machinery (Technical Information Sheet – Glass Breaker Screen, Page 2).

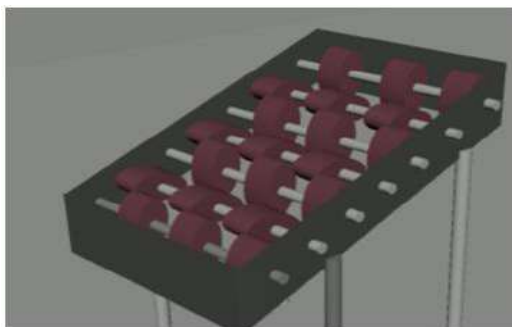


FIG. 6 GLASS BREAKER SCREEN

Magnetic separator

A magnetic separator consists of a mighty magnet that is placed or suspended from a ceiling or device. The magnetic separator creates a magnetic field of high intensity and very high gradient capable of attracting very weak materials such as iron oxides, weak magnetic powders and a high amount of paramagnetic.

Materials can be passed over a table top magnetic separator, while suspended magnetic separators often hang over a material to remove its impurities. Magnetic separators are influential, portable and can be adjusted to remove various types of magnetic materials from a liquid or solid. They are most effective when used in a liquid, although it is also possible to remove solid contaminations.

Magnetic separators are very adaptable and incredibly simple in design. In fact, a basic magnetic separator can be built at any time, using only a powerful magnet such as neodymium magnets and a clamp to hold the material down.

The main disadvantage of a magnetic separator is that it must be constantly maintained. The magnetic separator should be washed or cleaned to remove accumulated magnetic materials, while oil should be added to moving parts. In the case of an electromagnetic separator, the electromagnets must be able to be switched off at any time in case of emergency. Hence to save cost and time, electromagnet is used that is designed according to the pull force that is required by the machine to generate for it to function properly.

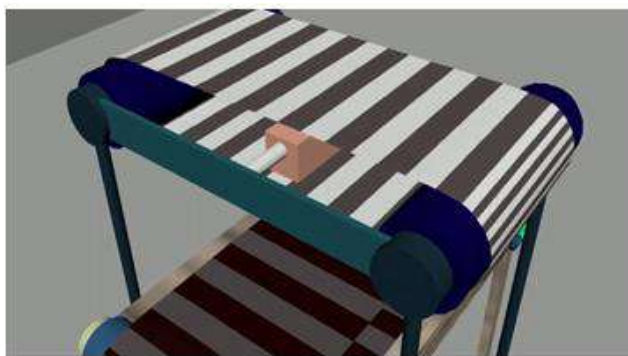


FIG. 7 MAGNETIC SEPARATOR

Eddy current separator

An eddy current separator is a dual pulley conveyor system, where the non-metallic rotor cover houses an independently rotating high-speed magnetic rotor. Separation occurs when a non-ferrous metal particle (e.g. aluminium, copper or zinc) is conveyed into the magnetic zone. It uses a powerful magnetic field to separate non-ferrous metals from waste.

Eddy current separators are not designed to sort ferrous metals which become hot inside the eddy current field. This can lead to damage of the eddy current separator unit belt.

The eddy current separator is applied to a conveyor belt carrying a thin layer of mixed waste. At the end of the conveyor belt is an eddy current rotor. Non-ferrous metals are thrown forward from the belt into a product bin, while non-metals simply fall off the belt due to gravity.

Eddy current separators may use a rotating drum with permanent magnets, or may use an electromagnet depending on the type of separator.

This separation is in accord with two laws they are:

- Faraday's Law of induction: where electrical currents are induced when conductors enter a revolving magnetic field (e.g. non-ferrous metals such as aluminium)
- Lenz's Law: where the induced eddy currents create a magnetic field that opposes the magnetic field that created it. This results in the repulsion of a conductor away from the magnetic source

Investigations into the connection between the magnetic rotor speed and the throw distance of a non-ferrous metal particle identified that the amount of repulsive energy induced into a non-ferrous metal particle is proportional to the dwell time in the field.

In practice, there is an optimal rotational speed for every magnetic rotor design to produce the best level of non-ferrous metal movement for each application.

This is commonly between 2,000 and 5,000 RPM. The insight that increased rotor speed always produces a higher level of non-ferrous metal separator is misguided.

Key design parameter is focusing on reducing the distance between the magnet pole and the surface of the belt for there is a significant reduction in magnetic field at distance.

- Carbon fibre wrap: The magnets sit on the rotor's magnet carrier, which rotates freely inside the non-magnetic shell. Carbon fibre tape, wrapped around the rotor, securely hold the magnets to the carrier
- The Air Gap: The air gap between the surface of the carbon fibre tape and inside of the shell must be sufficient to ensure no contact, even when the rotor is spinning at high speeds and there may be a small degree of flexing
- Shell Thickness: Due to the hard working environments of the recycling industry, the thickness of the shell must be sufficient to withstand wear
- Belt Thickness: This also applies to the belt thickness, with some applications requiring thicker and more healthy feed belt designs.

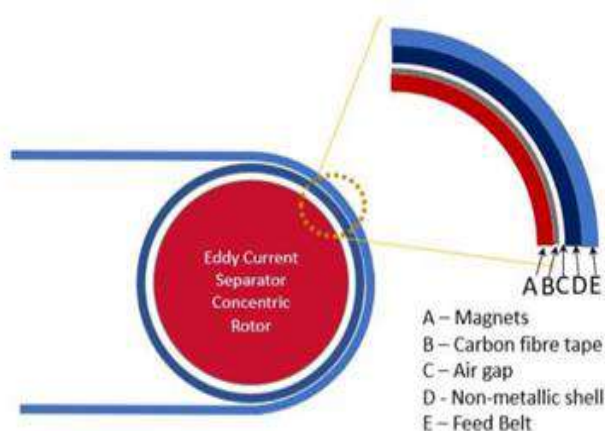


FIG. 8 COMPONENTS OF AN EDDY CURRENT ROTOR

The dimensions of the permanent magnet (both in length around the rotor and thickness) dictate the throw of magnetic field. Longer and thicker magnets produce deeper magnetic fields. Shorter and thinner magnets produce low intense magnetic fields.

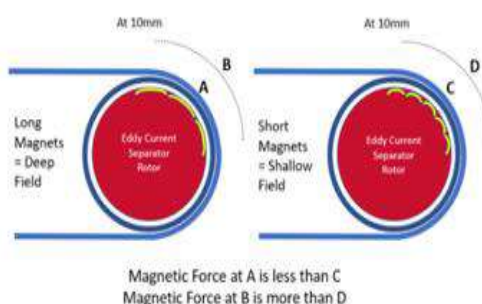


FIG. 9 EDDY CURRENT SEPARATOR ROTOR

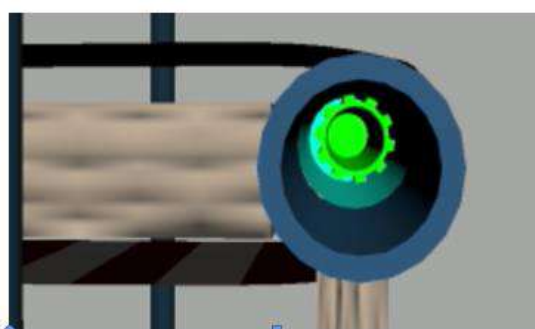


FIG. 10 EDDY CURRENT SEPARATOR

Working

The waste is stored in the hopper. As the machine is turned on, waste falls on the star screen deck which removes smaller inseparable wastes. Rest of the waste moves on to the glass breaker screen where the glass waste breaks and fall into the bin. Waste then moves on to the conveyer system where ferrous metal is removed by the overhead magnetic separator. At the end of the conveyer eddy current separator helps to remove the non-ferrous metals.

VI. SPECIFICATIONS

MOTOR

Rated Voltage = 12 V (DC)

Load Current = 9 A

RPM = 30 rev/min

Stall Torque = 25 Kg cm

HOPPER

Top length and breadth of hopper = 250 mm

Bottom length and breadth of hopper = 100 mm

Height of hopper = 200 mm

Capacity = 0.006m³

BIN

Five 150 mm length cubes

Conveyer Belt

Conveyor belt is used for transfer material from one place to another.

Belt width = 0.2m; Conveyer length = 0.4m

Belt capacity = 252 kg/hr

Dimension of the system

The overall dimensions of the system are:

Length = 1.1 m.; Width = 0.25 m; Height = 0.48 m

Design of hopper

As shows in the fig 11, the dimensions of the hopper are:

Top side a=0.25 m

Base side b=0.10 m

Height h=0.20 m

Volume of hopper = $((a^2+ab + b^2) h)/3 = ((0.06+0.02+0.01)0.20)/3 = 0.006m^3$

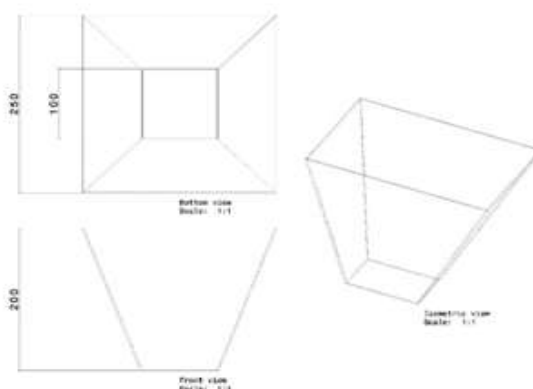


FIG. 11 SKETCH OF THE HOPPER

Design of shaft for star screen

Power transmitted by each shaft = 7.7 W

Speed of the shaft = 30 rpm

Assuming stress for the mild steel shaft as 30 MPa

The shaft is subjected to both bending and twisting

Fig 12 shows the image of a star screen disk. The circular variant of the star screen has been chosen for the ease of calculation.

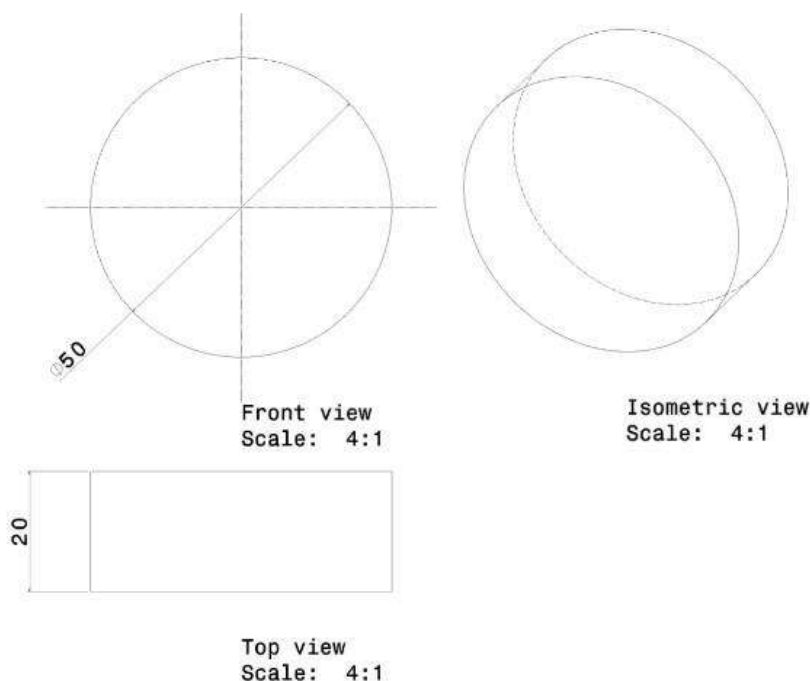


FIG. 12 STAR SCREEN DISK

$$\text{Mass of the disks (m)} = \rho V = 1.57 \times 10^{-4} \times 1522 = 0.24 \text{ kg (Density of hard rubber = } 1522 \text{ kg/m}^3\text{)}$$

$$\text{Force exerted by each disk} = mg = 0.24 \times 9.81 = 2.34 \text{ N}$$

$$\text{Power transmitted (P)} = \frac{2\pi NT}{60}$$

$$\text{Twisting moment (T)} = \frac{60P}{2\pi N} = \frac{60 \times 7.7}{2\pi \times 30} = 2.45 \text{ Nm}$$

To find the bending moment;

Fig 13 shows the image of a star screen shaft with the disks attached. From this a free body diagram is made showing all the forces acting on the shaft as in fig 14.

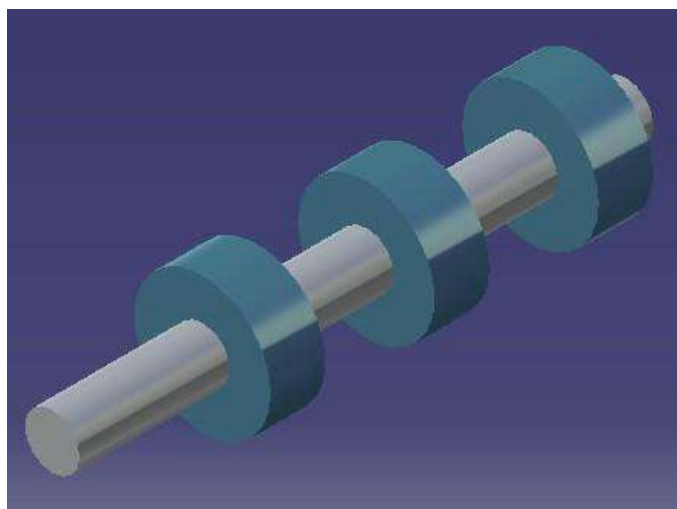


FIG. 13 STAR SCREEN SHAFT

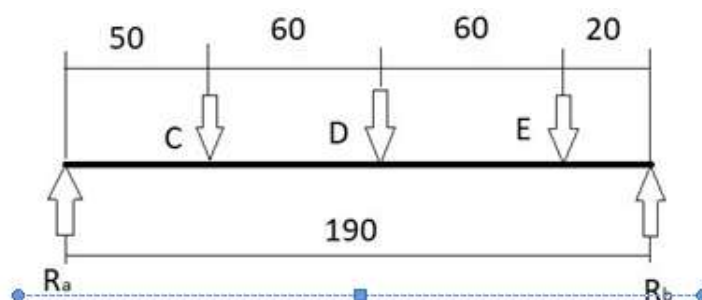


FIG. 14 FORCES ACTING ON THE SHAFT

Referring fig 14;

Total vertical force = 0

$$\Rightarrow R_a + R_b - 3 \times 2.34 = 0$$

$$\Rightarrow R_a + R_b = 7.03 \text{ N}$$

Total Moment at A = 0

$$\Rightarrow R_a(0) - 0.05(2.34) - 0.11(2.34) - 0.17(2.34) + 0.19(R_b) = 0$$

$$\Rightarrow R_b = 4.06 \text{ N}$$

$$\Rightarrow R_a = 2.97 \text{ N}$$

Finding the bending moments at C, D and E;

$$M_c = 0.05(2.97) = 0.15 \text{ Nm}$$

$$M_D = 0.11(2.97) - 0.06(2.34) = 0.19 \text{ Nm}$$

$$M_E = 0.17(2.97) - 0.12(2.34) - 0.06(2.34) = 0.08 \text{ Nm}$$

Since bending moment at D is maximum

Considering $M = 0.19 \text{ Nm}$

Equivalent twisting moment

$$T_{eq} = \sqrt{T^2 + M^2} = \sqrt{2.45^2 + 0.19^2} = 2.16 \text{ Nm}$$

For strength criteria;

$$\frac{T}{J} = \frac{\tau}{r}$$

Polar moment of inertia (J) = $\pi D^4/16$

Simplifying for shaft of diameter D;

$$T_{eq} = (\pi/16) D^3 \tau$$

To find the diameter of the shaft

$$D^3 = \frac{16 T_{eq}}{\pi \tau} = (16 \times 2.16) / (30 \times 10^6 \times \pi)$$

$$\Rightarrow D = 0.007 \text{ m} = 7 \text{ mm} \approx 10 \text{ mm}$$

Therefore each shaft for star screen is selected to be 10 mm in diameter

Design of shaft for glass breaker screen

Power transmitted by each shaft = 7.7 W

Speed of the shaft = 30 rpm

Assuming stress for the mild steel shaft as 30 MPa

The shaft is subjected to both bending and twisting. Fig 15 shows the sketch of a glass breaker disk. For the elliptical disks, major diameter is 50 mm and minor diameter is 30 mm.

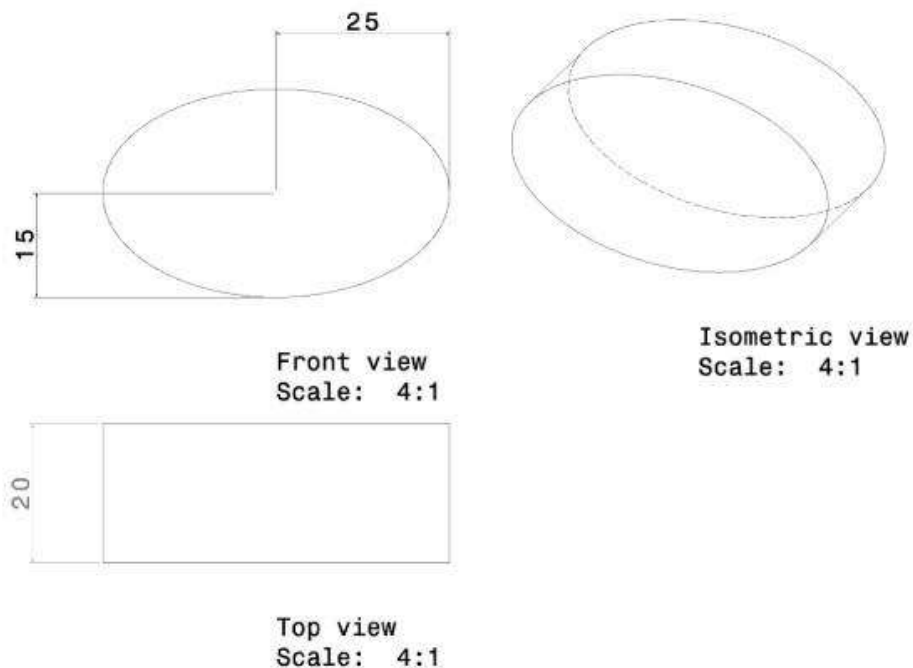


FIG. 15 GLASS BREAKER DISK

$$\text{Volume of each disk (v)} = \pi ab l = \pi \times 0.05 \times 0.03 \times 0.02 = 9.42 \times 10^{-5} \text{ m}^3$$

$$\text{Mass of the disks (m)} = \rho v = 9.42 \times 10^{-5} \times 7850 = 0.74 \text{ kg (Density of mild steel = 7850 kg/m}^3\text{)}$$

$$\text{Force exerted by each disk} = mg = 0.74 \times 9.81 = 7.26 \text{ N}$$

$$\text{Power transmitted (P)} = \frac{2\pi NT}{60}$$

$$\text{Twisting moment (T)} = \frac{60P}{2\pi N} = \frac{60 \times 7.7}{2\pi \times 30} = 2.45 \text{ Nm}$$

To find the bending moment,

Fig 16 shows the image of a glass breaker shaft with the disks attached. From this a free body diagram

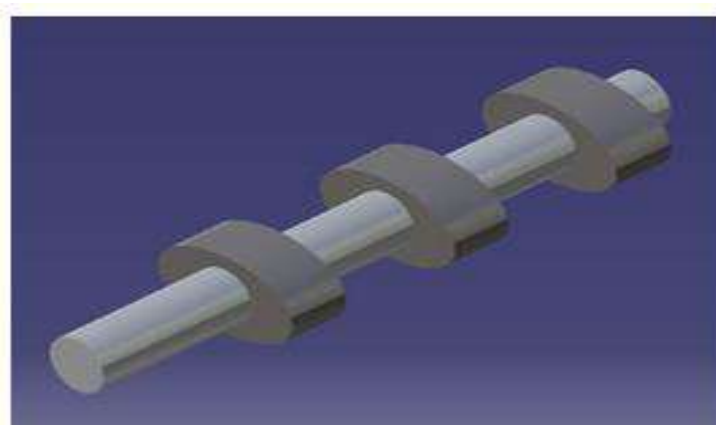


FIG. 16 GLASS BREAKER SHAFT

Referring fig 17;

Total vertical force = 0

$$\Rightarrow R_A + R_B - 3 \times 7.26 = 0$$

$$\Rightarrow R_A + R_B = 21.78 \text{ N}$$

Total Moment at A = 0

$$\Rightarrow R_A (0) - 0.05(7.26) - 0.11(7.26) - 0.17(7.26) + 0.19(R_B) = 0$$

$$\Rightarrow R_B = 12.61 \text{ N}$$

$$\Rightarrow R_A = 9.17 \text{ N}$$

Finding the bending moments at C, D and E;

$$M_C = 0.05(9.17) = 0.46 \text{ Nm}$$

$$M_D = 0.11(9.17) - 0.06(7.26) = 0.57 \text{ Nm}$$

$$M_E = 0.17(9.17) - 0.12(7.26) - 0.06(7.26) = 0.25 \text{ Nm}$$

Since bending moment at D is maximum

Considering $M = 0.57 \text{ Nm}$

Equivalent twisting moment

$$T_{eq} = \sqrt{T^2 + M^2} = \sqrt{2.45^2 + 0.57^2} = 2.51 \text{ Nm}$$

For strength criteria;

$$\frac{T}{J} = \frac{\tau}{r}$$

Polar moment of inertia (J) = $\pi D^4/16$

Simplifying for shaft of diameter D;

$$T_{eq} = (\pi/16) D^3 \tau$$

To find the diameter of the shaft

$$D^3 = \frac{16T_{eq}}{\tau \times \pi} = (16 \times 2.51) / (30 \times 10^6 \times \pi)$$

$$\Rightarrow D = 0.008 \text{ m} = 8 \text{ mm} \approx 10 \text{ mm}$$

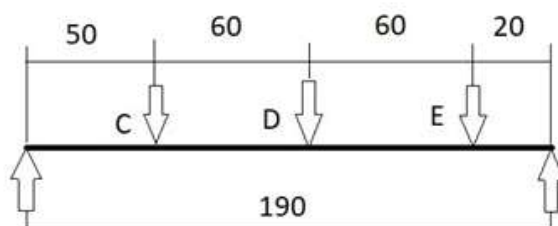


FIG. 17 FORCES ACTING ON THE SHAFT

Glass breaker inclination

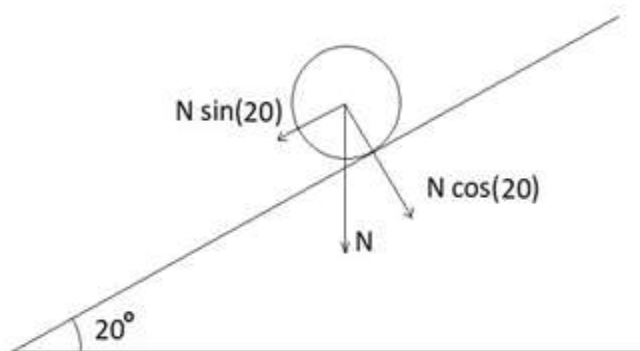


FIG. 18 FORCES ACTING ON THE GLASS BOTTLE

$$F_f = \mu N$$

Coefficient of friction of metal with glass = 0.3

Mass of an average empty 750ml glass bottle = 0.3 kg

$$N = 0.3 \times 9.81 = 2.94\text{N}$$

$$F_f = 2.94 \times 0.3 = 0.882\text{N}$$

Gravitational force pulling the bottle down at 20° inclination

$$N_G = N \sin 20^\circ = 2.94 \times 0.34 = 1.00\text{N}$$

Since $F_f < N_G$; 35° inclination for Glass breaker screen is optimum

Power Transmission

Design of V-belt drive system

Power to be transmitted = 7.7 W = 0.008 kW (motor specification)

Speed of the driving motor = 30 rpm (motor specification)

Selection of V-Belt Sections

(Referred from Design Data Book, Page 7.58, Table- Data on Standard V-belt sections)

Selecting Type A, for load less than 5 kW

Selection of Pulley Diameter

(Referred from Design Data Book, Page 7.54, Table- Recommended series of pulley diameter and tolerance)

Selecting $d = D = 40$ mm (Since Driver and driven pulley has same diameter)

Selection of centre distance

Given, $C = 37$ mm

Nominal Pitch Length of the belt

(Referred from Design Data Book, Page 7.61)

$$L = 2C + \frac{\pi}{2}(D + d) + \frac{(D-d)^2}{4C}$$

$$= 2(37) + \pi(40)$$

$$= 199.66 \text{ mm}$$

Load correction factor

For normal load;

$$F_c = 1.00$$

Correction factor for arc of contact

(Referred from Design Data Book, Page 7.68)

$$\text{Arc of contact} = 180^\circ - \frac{D-d}{C}(60^\circ)$$

$$= 180^\circ$$

Therefore, correction factor $F_D = 1.00$

Selection of service factor

(Referred from Design Data Book, Page 7.69, Table- Correction factor for industrial service)

$F_a = 1.1$ (for light load and working less than 16 hrs. per day)

Calculation of maximum power capacity

(Referred from Design Data Book, Page 7.62)

For Type A;

$$kW = (0.45 S^{-0.09} - \frac{19.62}{d_e} - 0.765 \times 10^{-4} S^2)S$$

Now,

$$S = \frac{\pi dn}{60 \times 1000} = \frac{\pi \times 40 \times 30}{60 \times 1000} = 0.06 \text{ m/s}$$

$$d_e = d_p \times F_b = 40 \times 1 = 40 \text{ mm (Since } D/d = 1, F_b = 1)$$

$$kW = (0.45 (0.06)^{-0.09} - \frac{19.62}{40} - 0.765 \times 10^{-4} (0.06)^2)0.06$$

$$kW = 0.005 \text{ kW}$$

(Referred from Design Data Book, Page 7.70)

$$N = \frac{P \times F_\alpha}{kW \times F_c \times F_d}$$

$$N = \frac{0.008 \times 1.1}{0.005 \times 1 \times 1} = 1.76 \approx 2 \text{ Belts}$$

Actual centre distance

(Referred from Design Data Book, Page 7.61)

$$C = A + \sqrt{A^2 - B}$$

$$A = (L/4) - \pi \frac{D+d}{8}$$

$$A = (199.66/4) - \pi \frac{40+40}{8} = 18.5 \text{ mm}$$

$$B = \frac{(D-d)^2}{8} = 0 \text{ mm}$$

$$\text{Therefore, actual centre distance, } C = 18.5 + \sqrt{18.5^2 - 0} = 37 \text{ mm}$$

Pull force of electromagnet

$$F = (N \cdot I)^2 \mu_0 A / (2 g^2)$$

Where,

μ_0 is the permeability of free space which is equal to $4\pi \times 10^{-7} \text{ N/A}^2$

F is the force in Newton

N is the number of turns

I is the current in Amps

A is the area in length units squared

g is the length of the gap between the solenoid and a piece of metal

Selecting a copper wire of 30m of 26 gauge

I.e. radius of wire = 0.2mm

Resistivity of copper wire $\rho = 0.0171 \text{ ohm mm}^2/\text{m}$

Resistance (R) = $\rho L/A$

$$= (0.0171) (30) / \pi (0.2^2)$$

$$= 4.08 \text{ ohm}$$

Battery selected: 12 v car battery

Coil resistance = 4.08 ohm.

Using Ohm's law,

$$V = IR$$

$$12 = I (4.08)$$

$$I = 2.94 \text{ A} \approx 3 \text{ A (approx.)}$$

The current is calculated to be 3 amp.

$$\text{Gap} = 0.15 \text{ m}$$

$$\text{Radius of iron core} = 5 \text{ cm}$$

$$\text{Area of solenoid} = \pi r^2 = 0.00785 \text{ m}^2$$

$$\text{Number of turns} = 1000$$

$$F = (N \times I)^2 \mu_0 A / (2 g^2)$$

$$= (1000 \times 3)^2 (4\pi \times 10^{-7}) (0.00785) / (2 \times 0.15^2)$$

$$= 1.9719 \text{ N}$$

$$= 2 \text{ N (approx.)}$$

This means the electromagnet can pull up to 2N of weight to it when placed at a distance of 0.15m

Design of conveyer belt

Design parameters:

- Belt Speed
- Belt Capacity
- Belt Power

Belt speed

The relationship between the maximum belt speed, roller diameter and the relative revolution per minute is given as

$$v = \pi D n / 60,000$$

Where,

n= no of revolution per minute; (30)

D= roller diameter (60.33mm); and

v= belt speed (m/s)

$$v = \pi \times 60.33 \times 30 / 60,000$$

$$v = 0.09 \text{ m/s}$$

Belt capacity

$$\text{Conveyer Belt Capacity} = 3.6 A p v \text{ (kg/s)}$$

Where;

A = Load cross section area perpendicular to the load on the belt (m^2)

p = Approximate density of material conveyed (514 kg/m^3)

v = Belt Speed (0.09 m/s)

[As stated in *Design and Development of Waste Sorting Machine. American Journal of Engineering and Applied Science*]

$$A = 0.16 B^2 C \tan \theta$$

Where,

B = Belt width (0.2m)

C = Conveyer length (0.4m)

Also,

$$\theta = 0.35 \text{ (angle of repose)}$$

$$\theta = 0.35(25^\circ) = 8.75^\circ$$

Hence,

$$A = 0.16 \times 0.2^2 \times 0.4 \tan(8.75)$$

$$A = 0.0004 \text{ m}^2$$

$$\text{Conveyer Belt Capacity} = 3.6 \times 0.0004 \times 514 \times 0.09 = 0.07 \text{ kg/s}$$

Belt power

The power P (W) at drive pulley drum is

$$P = F v$$

Where,

F = Total tangential force at the periphery of drive pulley (N);

v = Belt speed (0.09 m/s)

Density of ASTM A525 Galvanized Steel = $7.8 \text{ g/cc} = 7800 \text{ kg/m}^3$

$$\begin{aligned} \text{Volume of the Roller (V)} &= \pi (R^2 - r^2) L = \pi (0.06^2 - 0.05^2) 0.20 \\ &= 0.0007 \text{ m}^3 \end{aligned}$$

$$\text{Mass of the roller (m)} = V \rho = 0.0007 \times 7800 = 5.46 \text{ kg}$$

$$\text{Moment of Inertia (I)} = m (R^2 + r^2)/2 = 5.46(0.06^2 + 0.05^2)/2 = 0.017 \text{ kgm}^2$$

$$\text{Angular Velocity } (\omega) = 2\pi N/60 = 2\pi (30/60) = 3.14 \text{ s}^{-1}$$

Assuming acceleration time = 0.1s

$$\text{Angular Acceleration } (\alpha) = 3.14/0.1 = 31.4 \text{ s}^{-2}$$

$$\text{Torque (T)} = I\alpha = 0.017 \times 31.4 = 0.53 \text{ N m}$$

Hence,

$$F = T/R = 0.53/0.06 = 8.83 \text{ N}$$

Therefore,

$$P = 8.83 \times 0.09 = 0.8 \text{ W}$$

Waste segregation rate

Dry waste is 37% of the total Municipal Solid Waste in India

Glass = 2%; Ferrous metal = 2%; Non Ferrous metal = 3% [Source: *Journal of Civil Engineering and Environmental Technology*]

Waste less than 5mm is approximately 10% of the total waste [Source: *Particle Size Distribution in Municipal Solid Waste Pre-Treated for Bioprocessing*]

$$\text{Conveyer capacity of our system} = 0.07 \text{ kg/s} = 252 \text{ kg/hr}$$

I.e. Waste Processing rate of the system = 252 kg/hr

$$\text{Considering 100\% waste (Dry, wet and other wastes)} = 681.08 \text{ kg/hr}$$

Segregation rate of:

$$\text{Small Waste} = 0.1 \times 681.08 = 68.11 \text{ kg/hr}$$

$$\begin{aligned} \text{Glass Waste} &= 0.02 \times 681.08 - 0.1(0.02 \times 681.08) = 13.62 - 1.36 \\ &= 12.26 \text{ kg/hr} \end{aligned}$$

$$\begin{aligned} \text{Ferrous Metal} &= 0.02 \times 681.08 - 0.1(0.02 \times 681.08) = 13.62 - 1.36 \\ &= 12.26 \text{ kg/hr} \end{aligned}$$

$$\text{Non-Ferrous Metal} = 0.03 \times 681.08 - 0.1(0.03 \times 681.08)$$

$$= 20.43 - 2.04 = 18.39 \text{ kg/hr}$$

$$\text{Remaining Waste} = 0.3 \times 681.08 - 0.1(0.3 \times 681.08) = 204.32 - 20.43$$

$$= 183.89 \text{ kg/hr}$$

VII. CONCLUSION

The basic design of the smart waste segregation system was made. Specifications for the design was determined. Different stages of the segregation process was identified and a workflow was designed for optimum effectiveness of the system. 3D models were developed for each component as well as the whole system. Various design calculations were done to validate the model in real time conditions. Studied about the waste generation rates and percentage of each components of dry waste. Finally a video was animated using Autodesk Maya to aid the visualisation of the project.

VIII. REFERENCES

1. Aleena V.J., Kavya Balakrishnan, Rosmi T.B., Swathy Krishna K.J., Sreejith S, Subha T. D. 2017. Automatic Waste Segregator and Monitoring System. *Stmjournals*.
2. Ebikapade Amasuomo, Jim Baird. 2016. The Concept of Waste and Waste Management. *Journal of Management and Sustainability*.
3. Biswajit Ruj, Vivek Pandey, Priyajit Jash, Srivastava V. K. 2015. Sorting of plastic waste for effective recycling. *International Journal of Applied Sciences and Engineering Research*.
4. Harshith R, Karthik Y, Pruthivishri Hegde, Sharma B, Tejas N, Shivalingappa D and Kumarswamy H. S. 2020. Development and Fabrication of Smart Waste Segregator. Springer Nature Singapore Pte Ltd.
5. Moni M Mondal, Christopher J Speier, Dirk Weichgrebe. 2018. Multi-stage optimization approach for sustainable municipal solid waste collection systems in urban areas of Asia's newly industrialized countries. Institute of Sanitary Engineering and Waste Management (ISAH), Leibniz Universität Hannover, Welfengarten, Hannover 30167, Germany.
6. Payal Srivastava, Vikas Deep, Naveen Garg and Purushottam Sharma. 2019. SWS—Smart Waste Segregator Using IOT Approach. Springer Nature Singapore Pte Ltd.
7. Pradip Baishya, Shanjenbam Brojendro Singh, Mahanta D. K. 2015. Fabrication & testing of dry waste sorting machine. *International Research Journal of Engineering and Technology (IRJET)*.
8. Saranya K. C., Vijayaraj Sujana, Balasubramanian Abivishaq and Nithish Kanna K. 2020. Smart Bin with Automated Metal Segregation and Optimal Distribution of the Bins. Springer Nature Singapore Pte Ltd.
9. Soumiya M., Balakrishnan M, Shanthi K. 2018. Composition of Municipal Solid Waste Accumulated in Vellore Dump Yard from Coimbatore City. *Life Science Informatics Publications*.
10. Faculty of Mechanical Engineering. PSG College of Technology, "Design Data Book", M/s. Kalaikathir Publishers, Coimbatore, 2012.

Fabrication of Rice Husk Gasifier Stove by Improving Efficiency

Kannan K, Babu S and Dhiraviyapandiyam P

Department of Mechanical Engineering, PSG College of Technology, Coimbatore

ABSTRACT

Researchers are seeking methods to ensure clean combustion using low-value dry biomass in residential cooking. The process of obtaining combustible gases from dry biomass is termed as gasification. A state of art method in combustion technology is 'Top-lit Up draft' (T-LUD) gasification. The fuel I am using is rice husk. My interest is to make the stove eco friendly stove with lowering emission as well as improving thermal efficiency by producing blue flame to 29% similar to LPG. The prominent features are low cost, population specific design, safety in operation, economical and ecofriendly. Rice husk has a better calorific value of 3000kcal/kg.

Keywords: rice husk; gasification; thermal efficiency; blue flame

1. INTRODUCTION

Abundance of rice husk biomass is found in India. Carbon dioxide emission from LPG can be minimized by replacing it with rice husk. Specifically a ton of rice husk replaces 23 tanks (11 kg each) of LPG fuel. Normally rice husk is dumped and burnt along the roadside which contributes to pollution. It can be mimimized of it is used as a fuel in stove. One kg of rice husk can be loaded in a single burner stove. It will produce blue flame while operating with limited air supply With the rocket increase in the LPG fuel price rice husk will make a good alternative .Like LPG stove we can also control the flame by adjusting the air supply. It is more safe as it burns in the atmospheric pressure comparative LPG .This stove did not have any complicated devices hence it is more economical and has a very high life time compared to LPG.

2. Experimental section

Various parts of the Rice Husk Gas Stove are,

1. Gasifier Reactor
2. Control
3. Pot Support
4. Switch
5. Safety shield
6. Chamber
7. Fan
8. Burner
9. Char

2.1 The Gasifier Stove Reactor

The rice husk is placed and burned in gasifier stove reactor with limited air supply. Depending upon the output power, the radius of the cylindrically shaped reactor is varied. Based on the operating time, height is varied. On the inside, it is made up of a stainless steel sheet gauge no. 20 and galvanized iron sheet of gauge no. 18 in the outside. Insulation is provided between outer and inner chamber. Safety shields outside of the cylinder are provided to prevent touching of hot reactor chamber.

2.2 The Fan Assembly

The fan provides the air needed by the fuel during gasification. It is usually fastened on the bottom chamber, either at the door or at the chamber itself, to directly push the air into the column of rice husks in the reactor. It has a power input of 16 watts using a 220 volt AC. A rotary switch is used to control the speed of the fan which controls the flow of gas to the burner.

2.3 The Burner

The burner converts the combustible gas to a bluish flame. It consists of holes, where combustible gas passes through .The secondary holes located at the outside of the burner are used to supply the air for the combustion of gases. On top of the burner is a utensil holder that holds the pot in place during cooking. The burner is removable for loading of fuel into the reactor and is set during operation.

2.4 Principle of operation:

Follows the Principle of production of combustion gases

- More the air supply bluish will be the flame.
- 4.7kg of air is required to burn 1kg of husk.

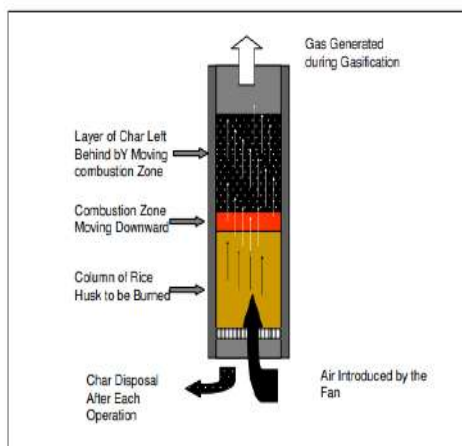
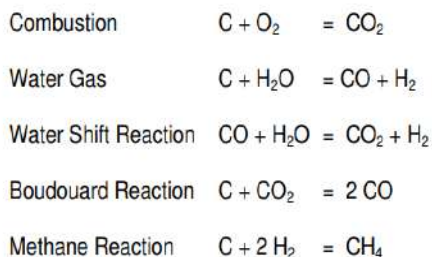


Figure 2 Principle of operation

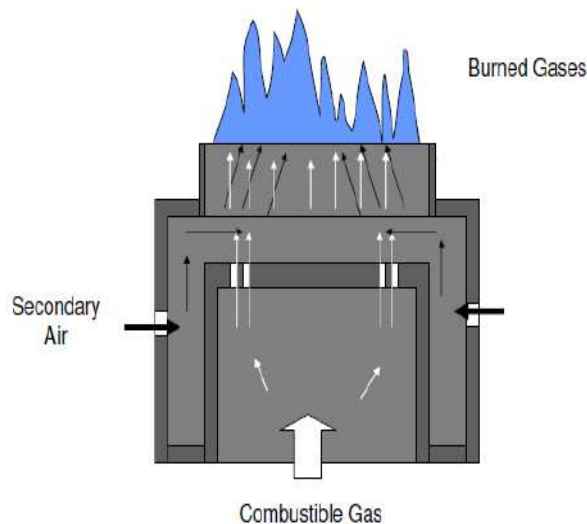


Figure 2 Secondary air intake

3. Design Procedure

- Problem to design a stove for two persons for one serving (Breakfast)
- Considering rice, water, vegetable and milk to be cooked in their diet
- Calorific value of rice husk =3000kcal/kg
- Specific gasification rate=110-210 kg/m²-hr
- Density of rice husk=90-150 m³

Food	Specific Heat (Kcal/kg-°C)	Total Energy Needed (Kcal/kg)*
Rice	0.42 – 0.44	79.3
Meat	0.48 – 0.93	56.5
Vegetables	0.93	74.5
Water	1.0	72

*At 72°C temperature difference

Table 1 Energy need by different foods

Energy needed

- The amount of energy needed to cook food can be computed using the formula,

- $Q_n = M_f \times E_s / T$

where:

- Q_n - energy needed, Kcal/hr
- M_f - mass of food, kg
- E_s - specific energy, KCal/kg
- T - cooking time, hr
- For 200g of rice in 15 minutes=63.44kcal/hour
- For 2liters of water in 15 min.=576kcal/hour
- For .5kg of veg. in 15 min. = 149kcal/hour
- For 1liter of milk in 15 min.=284.4kcal/hour

$Q_n(\text{Total})=1072.84 \text{ kcal/hour}$

- Energy input
- $FCR = Q_n / (HV_f \times \epsilon_g)$

where:

- FCR - fuel consumption rate, kg/hr
- Q_n - heat energy needed, Kcal/hr
- HV_f - heating value of fuel, Kcal/kg
- ϵ_g - gasifier stove efficiency, %
- **$FCR = 1.19 \text{ Kg husk/hour}$**

Reactor diameter

- It be computed using the formula,
- **$D = (1.27 FCR)^{0.5} / SGR$**

where:

- D - diameter of reactor, m
- FCR - fuel consumption rate, kg/hr
- SGR - specific gasification rate of rice husk,
- 110-210 kg/m²-hr(110)
- **$D = 0.11 \text{ m}$**
- **Height of the Reactor**
- **$H = (SGR \times T) / \rho r_h$**

where:

- H - length of the reactor, m
- SGR - specific gasification rate of rice husk, kg/m²-hr
- T - time required to consume rice husk, hr
- ρ_{rh} - rice husk density, kg/m³
- **H=1.1m**

- **Time to Consume Rice Husk**

- $T = (\rho_{rh} \times V_r) / FCR$

- where:

- T - time required to consume the rice husk, hr
- V_r - volume of the reactor, m³
- ρ_{rh} - rice husk density, kg/m³

- FCR - rate of consumption of rice husk, kg/hr

- **T = 0.87 or 52.2 minutes**

- **Amount of Air Needed for Gasification**

- $AFR = (e \times FCR \times SA) / \rho_a$

- where:

- AFR - air flow rate, m³/hr
- e - equivalence ratio, 0.3 to 0.4
- FCR - rate of consumption of rice husk, kg/hr
- SA - stoichiometric air of rice husk, 4.5 kg air

- per kg rice husk

- ρ_a - air density, 1.25 kg/m³

- **AFR=1.28 m³/hr**

- **Superficial Air Velocity**

$$V_s = 4 AFR / \pi (D)^2$$

- where:

- V_s - superficial gas velocity, m/s
- AFR - air flow rate, m³/hr
- D - diameter of reactor, m

- **V_s = 0.03 m/s**

4. Comparative cost analysis

Investment cost	Rice husk gasifier	LPG stove
Stove	Rs.6000.00	Rs.2000.00
Tank		Rs.900.00
Total	Rs.6000.00	Rs.2900.00
Fuel consumption	Rs.9.00/day	Rs.21.00/day
Electricity	Rs.1.50/day	
Total	Rs.10.50/day	Rs.21.00/day
Operating time	3 hours/day	3 hours/day
Operating cost/hour	Rs.3.50/hour	Rs.7.00/hour
Yearly savings on fuel	Rs.3840.00	

Table 2 Comparative cost analysis

5. Pictures of designed model



Figure 3.12volt fan



Figure 4 Burner



Figure5Reactor

6. RESULT AND DISCUSSION

From the obtained design data it is obvious that all standards of the rice husk gasifier design are met hence the rice husk gasifier can be successfully designed for two members usage. It is also made compact for portable usage.

7. CONCLUSION

Application area for this gasifier includes water heating, boiling, cooking etc. In future the size of the stove can be tailored for specific needs such as Institutions, restaurant.

REFERENCES

1. Reed, T.B. & Larson, R. A Wood-gas Stove for Developing Countries. In: Wood Fires that Fit. Appropriate Technology Journey to Forever. Retrieved November 22, 2005 from http://journeytoforever.org/at_woodfire.html
2. Reed, T.B., Anselmo, E., & Kircher, K. Testing and Modeling the Wood-gas Turbo Stove. In: Wood Fires that Fit. Appropriate Technology Journey to Forever. Retrieved November 22, 2005 http://journeytoforever.org/at_woodfire.html
3. Reed, T.B. & Walt, R. The "Turbo" Wood-Gas Stove. BEF and CPC. Retrieved November 22, 2005 <http://www.repp.org/discussiongroups/resources/stoves/Reed/Turbo2.htm>
4. Regional Energy Technologies in Asia. A Regional Research and Dissemination Programme. Retrieved november 21, 2005 from <http://www.retsasia.ait.ac.th/photogallery.htm>
5. Sharma, S.K. (1993). Improved Solid Biomass Burning Cookstoves: A Development Manual. RWEDP in Asia. United Nations: Food Agriculture Organization.
6. Stanley, R. & Venter, K. Holey Briquette Gasifier Stove Development. Retrieved November 22, 2005 from <http://www.rep.org/discussiongroups/resources/stoves/Stanley/BriqGassstove.htm>
7. Stickney, R. E., Piamonte, V. N. & Belonio, A. T. (1989, July). Converting Rice Hull to Gaseous Fuel. Appropriate Technology. 16(1). Southampton Row, London, UK: IT publications Ltd. p. 14-16.
8. Stickney, R. E., Piamonte, V. N. & Belonio, A. T. (1989, March). DA-IRRI Rice Hull Gasifier. IRRI, Los Baños, Laguna: Department of Agricultural Engineering.
9. The New Turbo Wood-Gas Stove. A Bioenergy Innovation from Community Power Corporation. Retrieved November 21, 2005 from <http://www.repp.org/discussiongroups/resources/stoves/Reed/Turbo.htm>.
10. Wimberly, J. E. (1983). Technical Handbook for the Paddy Rice Postharvest Industry in Developing Countries.
11. Win, U.T. San San Rice Husk Gasifier Stove. Retrieved November 22, 2005 from <http://www.myanmarbioenergy.com/sansanrice.htm>

Study of Heat Transfer Characteristics during Phase Change in a Latent Heat TES System

Muthamilselvan N and Kannan K

Department of Mechanical Engineering, PSG College of Technology, Coimbatore

ABSTRACT

The Thermal Energy Storage (TES) system is not a new concept and it is used for decades. PCM are employed in the TES system to reduce time or rate mismatch between energy supply and energy demand. In this paper, Erythritol is used as PCM to store the energy in the medium temperature TES system. Aim of this work is to characterize the heat exchanged between Heat Transfer Fluid & PCM and its phase change are investigated. To verify the behaviour and nature of the PCM in the system for a charging cycle an experiment and a CFD model has been developed. The results obtained can be used as guidelines for subsequent analysis and optimisation process.

Keywords : Phase Change Material; CFD; thermal storage system.

1. INTRODUCTION

A Thermal Energy Storage (TES) system is being employed in solar, refrigeration and temperature control systems to store the surplus energy when the supply and consumption do not match. This mismatch issue can be adjusted to a certain extent without causing any pollution to the environment when the energy is efficiently stored and retrieved in the thermal energy storage systems. TES systems can store energy as sensible heat, latent heat or chemical reactions. Compared with Sensible Thermal Energy Storage (STES), Latent Thermal Energy Storage (LTES) with phase change materials offers a number of advantages such as quasi-isothermal charging/discharging process and high energy density. Thus, the LTES has great potential in the field of solar energy building applications, heat load shifting and electronics cooling components [1].

The heat storage in the form of latent heat can be effectively achieved by means of PCMs (Phase Change Material). PCM must have high heat of fusion so that they can absorb a lot of energy during melting or solidifying. A PCM temperature remains constant during the phase change, which is useful for keeping the subject at a uniform temperature. The selection of the correct storage material and the knowledge of its thermal properties is a key step to accomplish the requirements of the application and the final performance of the system. The PCM are classified into: Organic, Inorganic. The Organic materials have many advantages such as: congruent melting ; non- corrosive behaviour; high latent heat of fusion; broad range of melting temperatures; minimum tendency to sub-cooling; chemical stability; no toxicity. The main drawback is low thermal conductivity, where the formation of high temperature gradients is experienced during the transient heat transfer. The main advantage of inorganic PCMs is the high latent heat of fusion than organic. Their main drawback is that they melt in an incongruent way.

In thermal energy storage system material selection plays a key role which is chosen based on its latent heat and melting point(or range). Other requirements are no inflammability, higher heat of fusion and no separation of phases.

Moreover, selecting a material with its appropriate property is more difficult for any application. Commercially available PCMs like hydroquinone, erythritol, D-mannitol and other paraffins are investigated in abundance, but a clear picture of database of PCMs suitable for required application, their limitations, explored solutions etc are missing [2].

The design process of a heat exchanger is dominated by the identification of effective solutions in order to increase the heat flux inside the storage material. Adine et al [3] used Shell and tube heat exchanger to predict the thermal behaviour and performance of a latent heat storage units, using two phase change material in shell side for each units and while the heat transfer fluid, hot water, flows in tube side for both units and its efficiencies are reported.

Fornarell et al. [4] investigated the melting process in a shell and tube latent heat storage numerically where analysis on the convection effect on the heat transfer respect to a pure conductive mode is done. Arena et al [5] presented different geometrical configuration for a TES system to identify the best solution as regards thermal energy storage with PCM materials and impact on the performance of the phase change process.

The objective of this work is to study the behaviour of the PCM and the TES system for medium temperature applications experimentally and numerically. This information can be further used for the performance enhancement and design optimisation of the required system.

2. DESIGN OF TEST SYSTEM

The shell and tube heat exchanger is used for the analysis of TES systems. The shell side is made of Polycarbonate material which is transparent, to observe the behaviour of the PCM and is made of rectangular shape. The dimension of shell side is 150*150*200 mm with thickness of 5mm. Single tube is kept in the middle section of the shell which is of SS and Heat Transfer Fluid (HTF) is passed through the tube. The HTF used is steam and it enters at $T_{in} = 431\text{K}$, $P_{in} = 5\text{ bar}$. Tube has an inner radius $R_i = 23.4\text{ mm}$ and a thickness of, $s = 1\text{ mm}$. A Teflon bush is placed to avoid the direct heating of shell in the system with $r_{bi} = 25.4\text{ mm}$. The PCM used in the system is erythritol, whose properties are listed in the Table 1.

Thermal properties	Value	Units
Melting Temperature	391	K
Thermal conductivity solid/liquid	0.733/0.33	W/mK
C_p solid/liquid	1.35/2.76	kJ/kgK
Density solid/liquid	1480/1300	Kg/m ³
Coefficient of thermal expansion	$2.94 \cdot 10^{-5}$	K ⁻¹
Heat of fusion	339	kJ/kg

Table 1 Properties of Erythritol

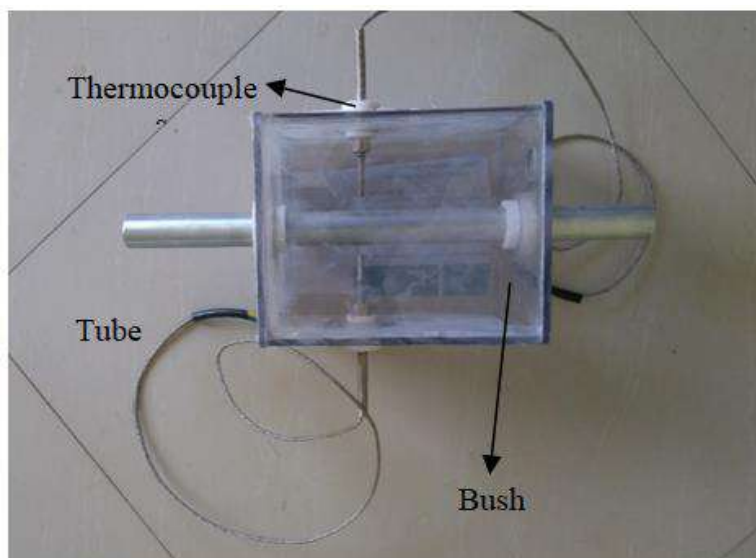


Fig. 1. Fabricated model of TES system.

3. MATHEMATICAL MODEL

The mathematical model to study the PCM during the storage of energy is presented. The HTF is flowing axial direction around the tube. When HTF runs through the TES system, heat is transferred between HTF and PCM. The assumptions for the model are: the HTF is incompressible and viscous, the PCM is homogeneous, the problem is axi-symmetric, the thermo-physical properties of HTF and PCM are constant, the wall conduction is neglected, the conduction heat transfer within the PCM in axial direction is neglected.

The energy conservation equation for the HTF only through convection is,

$$\rho_{HTF} A_{HTF} C_{HTF} \frac{\partial T_{HTF}}{\partial t} = h \pi D_i \Delta T_{HTF} \quad (1)$$

The energy balance of the PCM is only by conduction and given by,

$$\frac{\rho_{PCM} A_{PCM} \Delta H_{PCM}}{t} = k_{PCM} \Delta T_{PCM} \quad (2)$$

Nomenclature	
HTF	Heat Transfer Fluid
ρ_{HTF}	density of heat transfer fluid, kg /m ³
A_{HTF}	area of heat transfer fluid, m ²
C_{HTF}	specific heat of heat transfer fluid , J/ kg/ K
ΔT	change in temperature, k
h	heat transfer coefficient, W /m ² /K
D_i	diameter of inner tube, m
ρ_{PCM}	density of PCM, kg /m ³
A_{PCM}	area filled by PCM, m ²
g	gravitational constant, m/s ²
k_{pcm}	thermal conductivity, W /m/K
s	thickness, m
r_{bi}	bush inner radius, m
S	source term
H_{sen}	sensible heat enthalpy, J/ kg
H_{lat}	latent heat enthalpy, J/ kg
β	liquid fraction
b,c	constant
μ	viscosity, mPa s
T_{ref}	reference temperature, k

4. NUMERICAL MODEL

The 3D axis symmetric problem has been solved in ANSYS FLUENT for the melting process. To model the phase change phenomenon, enthalpy-porosity technique is applied. This model depends on the liquid volume fraction ζ which denotes the ratio of volume of liquid to the total volume in each cell. In this technique the melting is calculated by the quantity of liquid fraction ζ computed at each time step for every cell based on enthalpy balance.

Thus the energy equation used here is,

$$\frac{\partial(\rho H)}{\partial t} + \nabla(\rho V H) = \nabla(k \Delta Y) + S_E \quad (3)$$

Where,

$$H = H_{Sen} + H_{Lat} \quad (4)$$

$$H_{Sen} = H_{ref} + \int_{T_{ref}}^T C_p dT \quad (5)$$

$$H_{Lat} = \beta L \quad (6)$$

In using a fixed-grid approach for the analysis of melting and solidification systems, a main difficulty is in accounting for mass and heat transfer conditions in the vicinity of the phase change. The basic approach for overcoming this problem is to define appropriate volume source terms for the governing equations. In the enthalpy-porosity approach, the latent heat is accounted for by defining source term in the energy equation.

$$\beta = 0 \quad \text{if } T < T_{solids}$$

$$\beta = 1 \quad \text{if } T > T_{solids}$$

$$\beta = \frac{T - T_{solids}}{T_{liquids} - T_{solids}} \quad \text{if } T_{solids} < T < T_{liquids}$$

The continuity equation is given by,

$$\frac{\partial \rho}{\partial t} = \nabla(\rho V) = 0 \quad (7)$$

The momentum equation is given by,

$$\frac{\partial(\rho V)}{\partial t} + \rho V(\nabla V) = -\nabla p + \nabla(2\mu\beta V) + A_c(\beta)V + S_m\beta^3(1-\beta)^2 \quad (8)$$

$$A_c(\beta) = \frac{-c(1-\beta)^2}{\beta^3 + b} \quad (9)$$

5. EXPERIMENTATION RESULTS



Fig. 2. Experimental setup of TES system

The steam from Parabolic Trough collector is used as the heat source for conducting the experiment. The experimental setup is shown in Fig. 2. The PCM is kept at the ambient temperature at the beginning of the experiment and measured using RTD. 3kg of Erythritol is poured inside the shell container through a provision at the top side. The PCM is not completely filled to visualize the melting behaviour. Two thermocouples are provided at the side wall in equal distance from the bottom i.e. 80mm and one thermocouple is provided at the top of the system. The flow is controlled using a ball valve at the exit and steam residence time can be varied. The infrared thermometer is used to measure the steam temperature.

The experiment was carried out for 2.5 hours. During this time the melting was initialized at 1.15 hours. The melting was only at the region that is very near to the tube wall Fig 3. Scales of PCM are deposited on the walls of the tube which retarded the heat propagation to the material and to the subsequent layers.



Fig. 3. Initialization of melting near tube walls.

The agglomeration of PCM taken place inside the system which in turn increases the melting time. Buoyancy effects were not felt throughout the run time and pure conduction dominated the overall charging cycle. Small time experiments were conducted separately to check the stability of the PCM during melting and solidification. A 50g of erythritol is taken in an aluminium vessel with silver coatings. As mentioned above, during melting the cluster formation occurs and then becomes liquid completely. But during the solidification process, erythritol structure changes.



Fig. 4. Crystalline formation after solidification

Initially the erythritol is taken as powdered form and after solidification it forms an irregular crystalline structure with varying sizes. Next, with same amount of PCM experiment repeated with a mechanical stirrer, to avoid clogging of material and to enhance the heat transfer performance. It is observed during the process, that time taken is reduced thrice the time of process without the stirrer. It is for the both the melting and solidification process but in solidification the scaling and irregular crystalline structure formation increases.



Fig.5. Small time experiment in a aluminium vessel

6. NUMERICAL RESULTS

A 3D simulation of the storage system with the actual boundary conditions were modelled using ANSYS Fluent software. The effects to be captured during simulation are the melting, heat transfer and the natural convection effects. The model was meshed using face meshing for entire surface with medium relevance center. The boundary condition given to the tube side is velocity=30m/s and the temperature is 431k and pressure at 5 bar, similar to the experiment.

The time taken for complete melting of PCM is 9.45 hrs for the TES system in the simulation. The convection effect in the shell side happens only near the tube walls. A graph is plotted for Heat transfer coefficient and nusselt number for several intervals of time at different height of the system near tube walls.

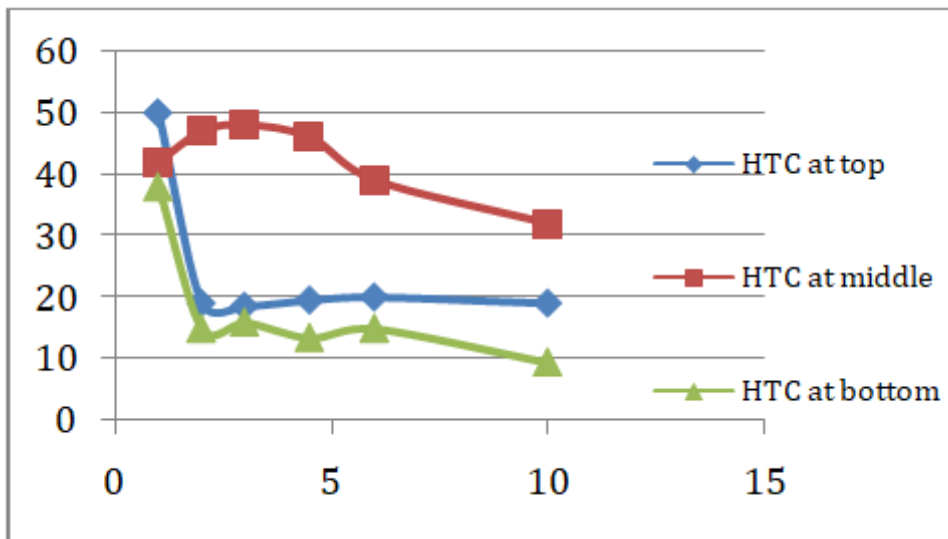


Fig. 6. Heat transfer coefficient vs Time

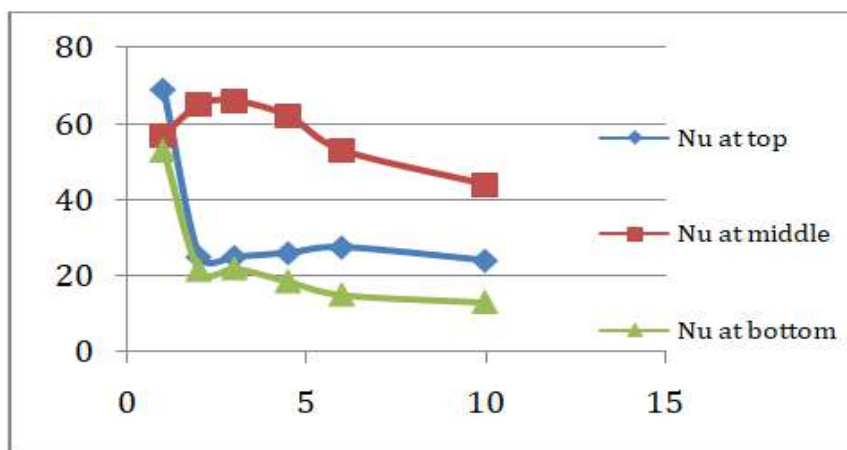


Fig. 7. Nusselt number vs Time

From graph fig 6 and 7 it is observed that at the middle section of the system, convection effect is dominant. The convection effects fall after 5 mm radial from the tube side and becomes nil. The melting in the simulation actually happens mostly in radial direction and in angular direction near the shell walls.

The contours of liquid fraction for various intervals of time at different cross section of the system are listed in the fig 8.

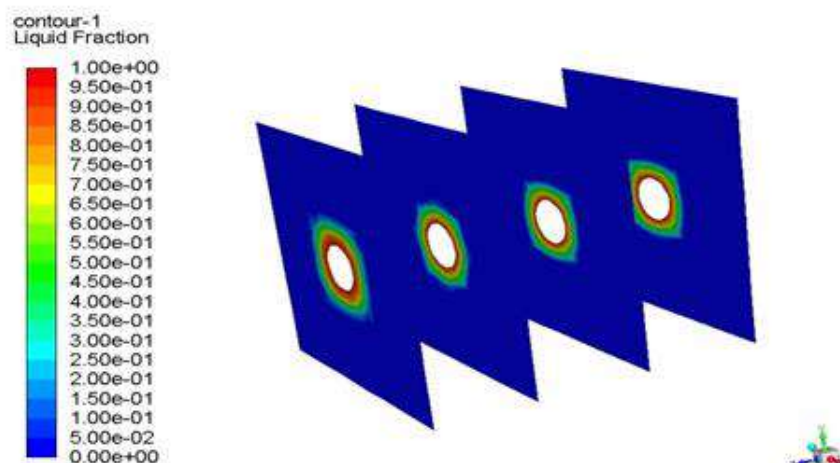


Fig. 8.a Liquid fraction contours at 1 hour.

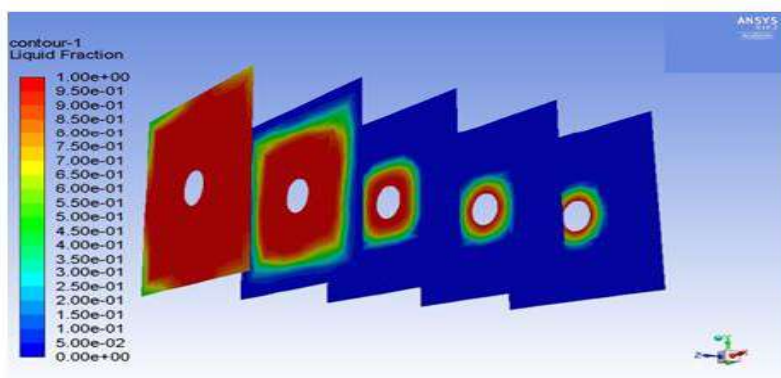


Fig. 8.b Liquid fraction contours at 3 hours.

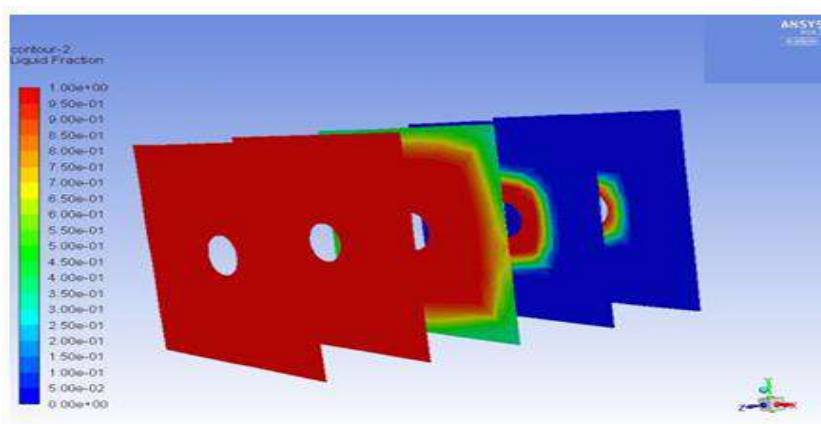


Fig. 8.c Liquid fraction contours at 4.5 hours

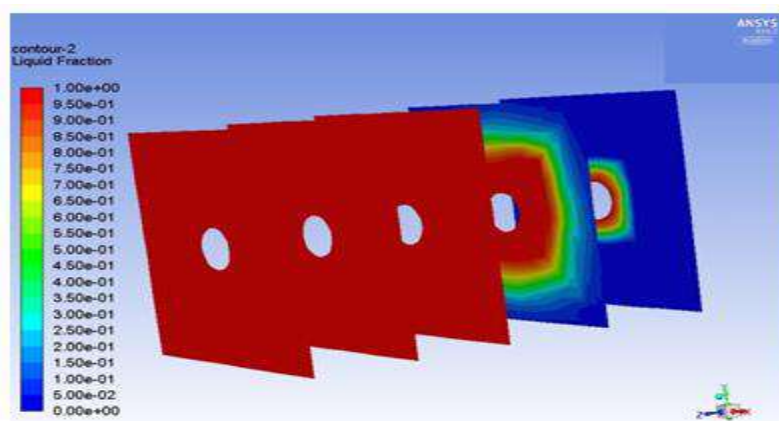


Fig. 8.d Liquid fraction contours at 6 hours.

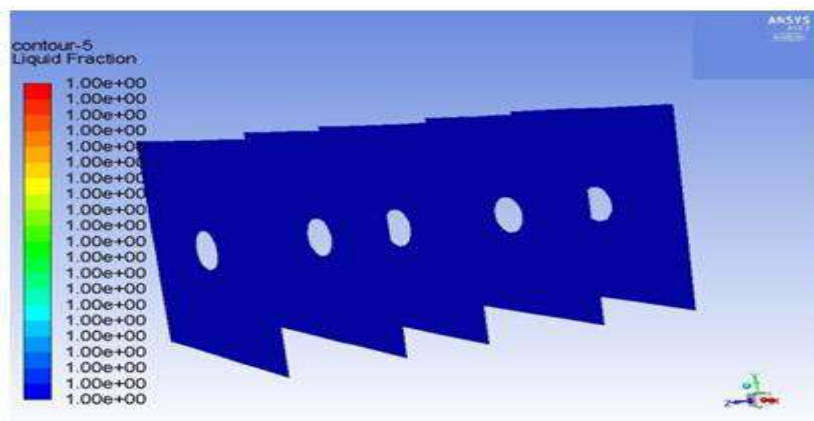


Fig. 8.e Liquid fraction contours at 10 hours.

As it is observed that the melting begins at the top of the system, the initialization of melting begins at 50 minutes, where in the experimental it was at 90 minutes. The energy stored in the PCM is plotted against time intervals is show in fig 9. The temperature attained in the system is plotted in fig 10.

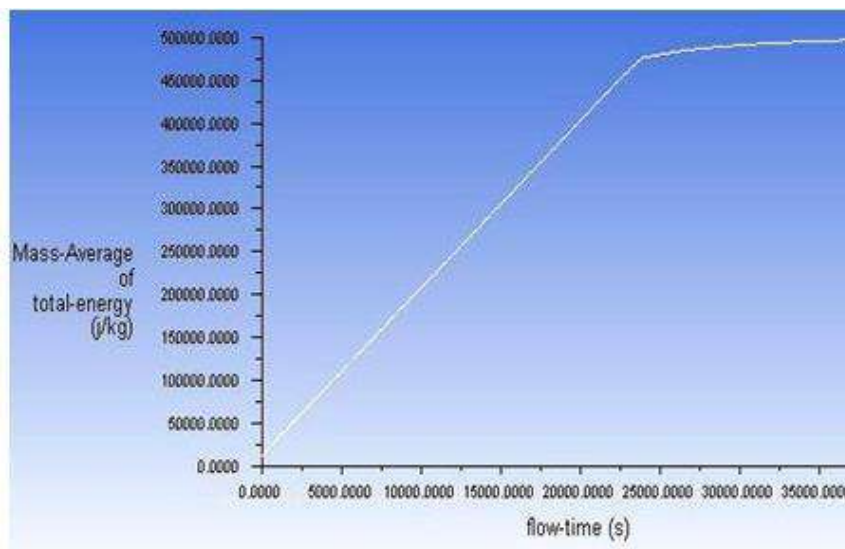


Fig 9. Energy vs time

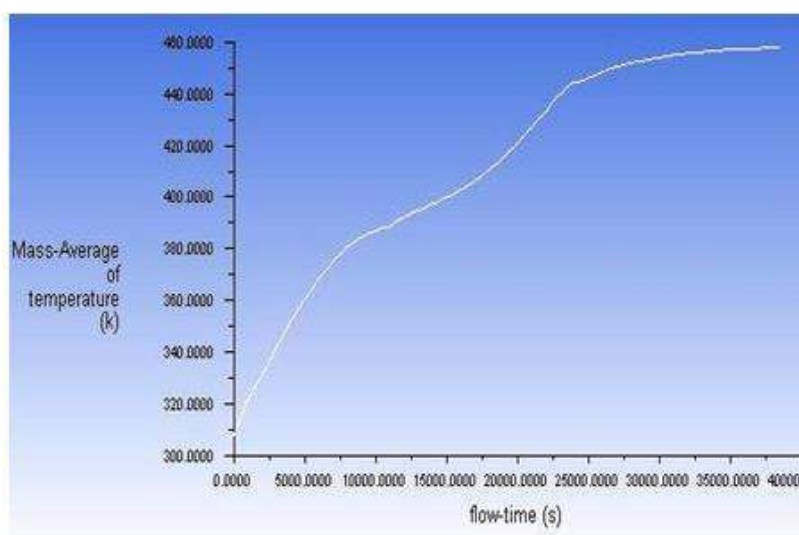


Fig. 10. Temperature vs Time

From the graphs it is observed that the energy stored and temperature obtained becomes a straight line after the completion of melting and the stored energy is only because of sensible heat energy after complete melting.

Thus, the convection effect in the system is only at a certain distance and for a particular time. The Boussinesq effects used in the simulation does not provide a better effects in the simulation but there is a slight effect of convection in the system due to this. The slighter effect of convection enhance the heat transfer mode and reduces the time than the experimentation.

7. CONCLUSION

In this work, the behaviour of PCM and the Heat transfer characteristics by both experimentally and numerically are analysed. By experimental study it is observed that the structural/chemical stability of the PCM selected i.e. erythritol is not good. Even after melting, liquid PCM doesn't flow on the surface of tubes owing to its less self-weight. It sticks to the surface of the tube walls and agglomeration starts to take place which reduces the heat transfer rate and increases the melting time. PCM attains a meta stable state during melting and active energy has to be supplied externally to completely melt the PCM. The heat transfer rate can be increased by providing continuous stirring for the reduction in melting time from the small experiments conducted. But stirring should be avoided during solidification. New blends of PCM can be used to avoid the clogging of materials.

The numerical 3D simulation of the TES system shows the swirl formed due to the gravitational pull reduces the melting time. The natural convection included in the system by Boussinesq equation, enhance the heat transfer rate little higher than the actual experimental system where it happens only through conduction. The complete melting time taken in the simulation is lesser than the actual system since the structural instability of PCM is not considered.

The main advantage of the simple shell and tube model proposed in this work is the simplicity in computational and experimental. To correlate the experimental study with the numerical results of the PCM used, for proper validation. This study is useful for the future work in design optimisation of the TES system for large applications where the problems can be neglected.

REFERENCES

1. Peilun Wang, Hua Yao, ZhipengLan, ZhijianPeng, Yun Huang, Yulong Ding, “Numerical investigation of PCM melting process in sleeve tube with internal fins”, *Energy Conversion and Management*, 2015.
2. Mohammed Mumtaz A. Khan, R. Saidur, Fahad A. Al-Sulaiman, “A review for phase change materials (PCMs) in solar absorption refrigeration systems”, *Renewable and Sustainable Energy Reviews*. 76, 105–137, 2017.
3. F. Fornarelli, S.M. Camporeale, B. Fortunato, M. Torresi, P. Oresta , L. Magliocchetti, A. Miliozzi, G. Santo, “CFD analysis of melting process in a shell-and-tube latent heat storage for concentrated solar power plants”, *Applied Energy*. 164, 711–722, 2016.
4. S Arena, G Cau, C Palomba, “CFD Simulation of Melting and Solidification of PCM in Thermal Energy Storage Systems of Different Geometry”, *Journal of Physics*. 655, 012-051, 2015.
5. S. Harikrishnan, M. Deenadhayalan, S. Kalaiselvam, “Experimental investigation of solidification and melting characteristics of composite PCMs for building heating application”, *Energy Conversion and Management*. 86, 864–872, 2014.
6. N.H.S. Tay, M. Belusko, M. Liu, F. Bruno, “Investigation of the effect of dynamic melting in a tube-in-tank PCM system using a CFD model”, *Applied Energy*. 137 738–747, 2015.
7. Camila Barreneche, Helena Navarro, Susana Serrano, Luisa F. Cabeza, A. Inés Fernández, “New database on phase change materials for thermal energy storage in buildings to help PCM selection”, *Energy Procedia*. 57, 2408 – 2415, 2014.
8. Lin Qiu, Min Yan, “Numerical Simulation and Analysis Of PCM on Phase Change Process Consider Natural Convection Influence”, *International Conference on Computer Application and*
9. Ammar M. Abdulateef, Sohif Mat, JasimAbdulateef, KamaruzzamanSopiana,Abduljalil A. Al-Abidi, “Geometric and design parameters of fins employed for enhancing thermal energy storage systems: a review”, *Renewable and Sustainable Energy Reviews*.
10. G. Kumaresan, V.S. Vigneswaran, S. Esakkimuthu, R. Velraja, “Performance assessment of a solar domestic cooking unit integrated with thermal energy storage system”, *Journal of Energy Storage* 6 (2016) 70–79.
11. M. Shinn, K. Nithyanandam, A. Barde, R.E. Wirz, “Sulfur-based thermal energy storage system using intermodal containment: Design and performance analysis”, *Applied Thermal Engineering*. 128,1009–1021, 2018.

Productivity Improvement in Robot Welding through Experimentation by Varying Process Parameters

Jayachitra R and Viswanathan P

Department of Mechanical Engineering, PSG College of Technology

ABSTRACT

This paper deals with an experimental investigation through industrial engineering tools was carried to study the outcome of several welding constraint ssuch as, welding current, voltage, feedrate, number of welding passes, coildiameter, weldingpathetc.,to increase theproductivity of transfer case cover welding. Detailed methodology provides the number of iterations done to achieve the optimized parameter reading form aximum productivity. The cycle time calculation reports the present capacity of the robotic welding, which needs to be improved more than thrice of the existing production rate. This paper also provides details analysis report on the cost aspect on varying productivity affecting factors suchas; weldingparameters, robotspecialfeatures, coildiameter, layout arrangement and allocation of man power. Results observed in this paper are useful for setting welding parameter and guide show to plan cost effective production.

I. INTRODUCTION

Robot welding machine taken for experimentation is KUKA robot with Fronius [6] welding setup (Fig 1). Experiments are carried out by analyzing the factors influencing robotic welding by varying welding parameters, utilizing special features and advancements in robot welding to monitor the welding capacity of the machine. The productivity improvements are carried out by analyzing the cycle time, utilization of special fixtures andmaterial handlingtime. This paper discusses on various welding techniques used andweldingd effects found during the fabrication of transfer case cover. Welding plays very important role in fabrication industry and to ensure the qualityof fabrication, all the welding shallbe defects free.By way ofwelding issues can considerably disturb weld performance and longevity, early detection and rectification is significant toconfirm that welds can transfer out their intended purpose [7]. For ensuring the quality of welding joints and finally the integrity of the equipment, various inspection and testing methods are available in today's modern industries.

A. About Roboticwelding

Real market situations are merely well-matched with light/medium lot production, due to robust competition and dynamical behaviour of themarket.



Fig 1 Roboticweldingsetup

In that situations, robotic manufacture arrangements display the greatest “cost per unit” enactment if linked with manual work and with rigid computerized arrangements(Fig 2).

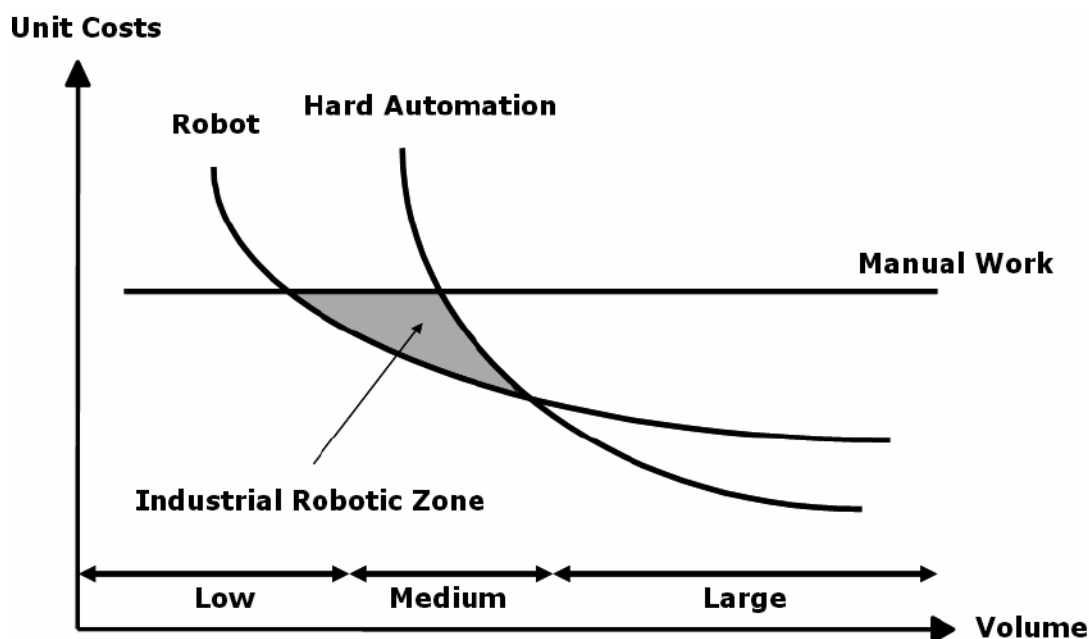


Fig1.2 Industrial robot zone

Industrial Robotic Welding is by the most prevalent use of robotics globally[8].

B. About Transfer case housing

The transmission case covering (Fig 3), situated below the vehicle, is persistently out to the elements. It can oxidized or improve cracks and leaks, producing it to fail lubrication. Leaking fluid over the transmission case would be a cautionary sign that the transmission case is in distress and may necessity to be resealed or exchanged.



Fig 3 Transfer case cover

C. About the process

Robotic welding is by distant the greatest widespread application of industrial robots. Very upright research works, attaining very exciting outcomes, were completed since the early 1980s[5], concentrating disputes like the welding method itself. Robot automation structures are quickly taking the place of the human work power. One of the welfares is that this modification delivers the human work force with the period to spend on extra imaginative jobs. The amount of arc welding automation robot stations is rising very quickly. The two best mutual stations are the GMAW (Gas Metal Arc Welding) station and the GTAW (Gas Tungsten Arc Welding) place[1]. This effort grants the automation of the welding method with protected electrodes, joining the elasticity of the method and the repeatability and protection of the computerization [2].

The metallic inert gas welding procedure[12] contains of heating, melting and solidification of parental metal and a filler solid in confined fusion sector by brief heat basis to create a joint. MIG welding parameters are the greatest essential factors disturbing the superiority, efficiency and price of welded joint. The input variables openly disturb the profile factor. The input variables deliberate for examination are as follows [3].

Welding current : It is the greatest essential variable for welding, since it controls the string off amount of rod, fusion depth and weld geometry.

Welding voltage : It defines the figure of fusion zone and weld strengthening height.

Welding speed: It is termed as the amount of travel workpiece under electrode.

Heat Input

Speed of welding (s) = Travel of electrode / arc time mm/min

Heat input rate = $(V \times A \times 60) / S$ joules per mm, V is arc energy in volts,

A is welding current in ampere,

Shape Factor

This is the relation of Penetration depth to Weld Width. Shape factor = Penetration depth / Weld Width. The beyond factors i.e. arc current, arc voltage and welding speediness and their connections play an important part in defining the weld bead shape features.

II. LITERATURE REVIEW

Literature Name	Author	Inference	Co-relation to this project
Optimal pass planning for robotic welding of large-dimension joints with deep grooves	S.J. Yan, S.K. Ong, A.Y.C. Nee	For the pass planning of deep groove welding, this paper proposes an optimization method with the objective to maximize the section area of the weld bead, so that the number of passes can be minimized.	Relationship between bead dimensions and welding parameters
Effect of Welding Parameters on Tensile & Yield Strength of IS 2062 grade Steel Using Design of Experiment Approach	K. R. Jagtapa, M. S. Rojekara, S. V. Dravidb, A. R. Deshpande	1. Effect of input parameters on mechanical properties. 2. Analysis of variance (ANOVA) was used to predict the impact of welding parameters on the response.	1. DOE on welding parameters 2. Helps to find out optimum welding parameters.
Automated planning of robotic MAG welding based on adaptive gap model	Alexander Kussa, Thomas Dietza, Felix Spennrath, Alexander Verlb	A gap model has been developed that represents the relation between welding parameters and a changing gap geometry due to assembly variations resulting i.e. from errors in manual tack welding.	How to plan for and experimental validation
Welding Seam Tracking in Robotic Gas Metal Arc Welding	Yanling Xu, Na Lv, Gu Fang, Shaofeng Du, Wenjun Zhao, Zhen Ye, Shanben Chen	Vision based robotic GMAW welding seam tracking system	Related to welding quality improvements

Table 1. Literature survey

III. OBJECTIVE

The following is the problem case on productivity.

❑ ComponentName :Transfercasecover

❑ Current, Robotwelding

production rate :24nos.pershift(8hrs.)

❑ Component requirement :150nos.perday

❑ Operatingshifts :2

❑ Production allotted days :10

The following objectives are framed to fulfil the requirement of this report.

❑ To analyse and improve the productivity of robot welding by reducing welding cycletime

❑ To simplify welding processes

❑ To reduce welding rejections

IV. METHODOLOGY

The objective of the work is to increase the productivityof robotic welding. The methodology followed to achieveisdepicted intheFig. 1.4.

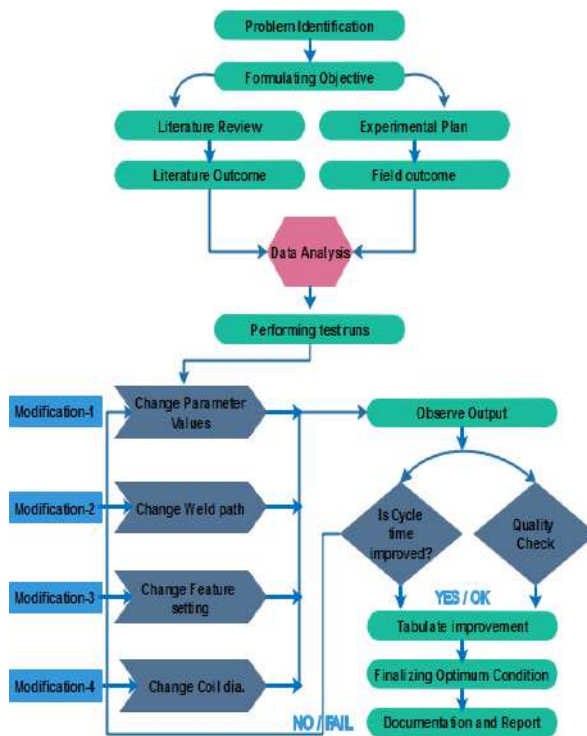


Fig. 4Flowchartformethodology

The above methodology gives fairideaon how thisproject flows. The factors to be considered for improving the productivity of robotic welding as follows[11];

❑ Weldingparameters :Sheetthickness, Voltage, Current andTravel speed

❑ No.of passes duringwelding

❑ Welding path

❑ Thickness of the weldingcoil:0.8mm,1.2mm,1.6mm

❑ Failtouse automatic accessories:Positione rmotionand auto cleaner

❑ Operator fatigue

By modifying the above factorsr results areobtained.The obtained results are tabulated and monitored to achieve the required productivity

V. EXPERIMENTAL SETUP

Below is the experimental setup area to weld transfer case cover. There are two such positioners on both sides of the robotic welding machine (Fig 1.5). First set of six transfer case covers are placed in one of the positioner for top side welding. Once the operation is completed, these are taken to the operator side table (Fig 1.6) for deburring and fettling. On completion of the manual activities, these transfer case covers are loaded to the second positioner for bottom side welding.



Fig. 5 Robot welding side

Once bottom side welding is under process, another six sets of transfer case covers are loaded in first positioner for top side welding. Meanwhile bottom side welding gets completed in the second positioner, the completed jobs are taken to the rear side table for fettling and de burring. These six numbers of components are called for inspection. On getting inspection cleared, finally number punch made one very transfer case over and loaded in the specially done transporting pallet for moving to next operation.



Fig..6 Robot welding operator side

VI. EXISTING PRODUCTION RATE AND DISCUSSIONS

A. Current production output cycle time

TC Cover - Robo welding - Time study									
Starting time		8:00:00	am	1 hr capacity		End Time		9:00:00	am
Topside welding		Bottom side welding		Others		Total cycle time		Time	No of components produced
Min	Sec	Min	Sec	Min	Sec	Min	Sec		
9	34	7	54	0	20	17	48	8:17:48	1
9	34	7	54	0	20	17	48	8:35:36	2
9	34	7	54	0	20	17	48	8:53:24	3

Table.2 Current cycle time

Above Table 2 gives the details cycle time analysis report on an hour production rate. As per this table it is clearly visible that an hour production rate is three components. Objective of this project is to improve this

cycle time by analyzing the factors influencing this welding cycle time. On improving this cycle time and achieving the required component of 150 numbers per day will give a cost saving of Rs. 6,80,000 per month only on robotic welding as per Table 3.

Robot welding cost saving details/month	
Hour rate	₹2,000.00
Current production qty./day	48
Process cost per component	₹666.67
On achieving production qty./day	150
Process cost per component	₹213.33
Cost saving/component	₹453.33
Total order qty./month	1500
Total cost saving/month	₹6,80,000.00

Table 3 Robotic welding cost

Detailed analysis on the process cost of each and every process is listed in Table 4. Other costs such as material, man power and overheads are also included in process cost calculation of per component

Process flow and Process cost					
Sl. No.	Process	Process done at	Resource used		Process cost/unit
			Mach ine	Man power	
1	Gas cutting	Equipment division	1	1+1	₹ 119.00
2	Sub parts machining	Machine shop	1	1	₹ 215.00
3	Manual setting welding	Equipment division	1	1	₹ 45.00
4	Robo welding	Equipment division	1	1	₹ 666.67
5	Stress relieving	OSP	-	-	₹ 65.70
6	Shot blasting	Equipment division	1	1	₹ 43.80
7	Painting	Equipment division	-	1	₹ 43.80
8	Final machining	Machine shop	1	1	₹ 1,850.00
9	Oiling, Packing & Dispatch	Machine shop	-	2	₹ 180.00
			Raw material cost		₹ 2,856.00
			Overheads		₹ 304.25
	Customer PO Price / unit	₹ 11,650.00	Total expenses/ unit:		₹ 6,270.22
	Current profit / unit	₹ 5,379.79			
	Monthly order Qty.	1500	Total Billing Value		₹ 1,74,75,000.00

Table 4 Process flow and cost

VII. AMPLIFIED PRODUCTION RATE AND DISCUSSIONS

A. Range of welding parameters range

- ☐ Travelspeed: 0.20-0.32m/min
- ☐ Voltage : 18.9-39volts
- ☐ WeldingGas : 100%CO₂(or)75% Ar&25% CO₂
- ☐ Flowrate : 15-18CFH(7.05–8.46 L/min)
- ☐ Coildia. : 0.8,1.2 & 1.6mm

Physical trials[10] are taken with multiple combinations for travel speed and voltage [9], finally ended with optimized parameters shown in Table 6. Table 5 gives the existing welding parameter reading with current production output of 24nos.per shift. Where as, iteration 18 parameter gives maximum production output without and defects of about 84 nos.pershift.

Existing Robotic welding machine parameter readings	
WeldingParameter	ExistingReading
Travelspeed	0.21m/min
Voltage	39volts
WeldingGas	100%CO ₂
Coildia.	1.2mm

Table 5 Current welding parameter reading

Physical trials: Iteration 18	
WeldingParameter	TrialReading -optimized
Travelspeed	0.25m/min
Voltage	28volts
WeldingGas	75% Ar&25% CO ₂
Coildia.	1.6mm

Table.6 Optimized welding parameter

VIII. CONCLUSION

Thus transfer case housing robotic welding productivity was improved by taking physical trials by varying welding parameters. Although, productivity was increased, cost of welding increased by 20% since 75% Ar & 25% CO₂ mixed gases was used instead of CO₂ alone as shielding gas, which produces more spatter. Also, welding coil diameter was changed from 1.2 mm to 1.6mm. Software investigation includes demonstrating key features or performances of a physical or intangible system. Simulation can be pursued to display the ultimate actual properties of another situations and sequences of achievement. This was planned by using software's such as Flexsim and Arena to find out the idle time, idle material and man Movement manual work cycle time to Reduce overall cost of the component.

REFERENCES

1. V.V.Ruiwale, A.A.Kadam, S.M.Kulkarni, and M.S.Jadhao, "A Review on Recent Trends in Robotic Welding", *International Journal of Engineering Science and Innovative Technology (IJESIT)* Volume 4, Issue 5, September 2015
2. K. Abbasi, S. Alam and Dr. M.I. Khan, "An Experimental Study on the Effect of MIG Welding parameters on the Weld-Bead Shape Characteristics", *IRACST – Engineering Science and Technology: An International Journal (ESTIJ)*, ISSN: 2250-3498, Vol. 2, No. 4, August 2012.
3. S.P.Tewari, Ankur Gupta, Jyoti Prakash, "Effect of welding parameters on the weldability of material", *International Journal of Engineering Science and Technology*, Vol. 2(4), 2010, 512-516.
4. A. Ghosh., A. K. Mallik., 2005. "Manufacturing Science." 23rd ed. New Delhi. Eastern western press pvt. Ltd. p319. Fronius, "CMT: Cold Metal Transfer", Brochure, 2004.

5. L.Jarvis.,K.Barton,“KeyholeGTAWUserguide”,CSIROManufacturing&Infrastructure Technology,Australia,2000.
6. Pires, J. Norberto, “Welding robots: technology, systems issues and applications”.Springer-VerlagLondonLimited2006
7. S. R. Meshram, N. S Phokar, “Optimization of Process Parameter ofGasMetalArcWeldingtoImprovethQualityofWeldBeadGeometry”,InternationalJournalofEngineering,Bu sinessandEnterpriseApplication,5(1)June-August2013,pp.46-52
8. Gautam Kocher, Sandeep Kumar, Gurcharan Singh, “ExperimentalAnalysis in MIG Welding with Is 2062e250 A Steel with ariousEffects”,InternationalJournalofAdvancedEngineeringTechnology, Vol.III/IssueII/April-June,2012,pp.158-162
9. S.R.Patil,C.A.Waghmare,“OptimizationofMIGweldingparametersforimprovingstrengthof Welded joints”, International Journal of Advanced EngineeringResearchandStudies,Vol.II,Issue IV,July-Sept.2013,pp.14-16
10. N.B. Mostafa, M.N. Khajavi, “Optimization of welding parametersforweldpenetrationinFCAW”AchievementsinmaterialandManufacturingEngineeringVol.16ISSUE 1-2May-June2006.

Design and Analysis of Flow Patterns and Thermal Behaviour in a Refrigeration Truck Using CFD

Archana J, Punitharani K and Jayachitra R

Department of Mechanical Engineering, PSG College of Technology, Coimbatore

ABSTRACT

The demand and scope of the refrigerated transport system, plays a crucial role in cold supply chain. Refrigerated trucks are designed to maintain a low temperature inside the cabin in order to transport food product without any spoilage. The airflow patterns and thermal behavior are the two major factors influencing the storage quality of the food products. The contemporary work is focused towards the design and analysis of flow pattern and thermal behavior inside the truck cab in for transportation of chick in live condition. It is observed that, poorer air velocity and better product temperature at their end of the truck cabin. So, the number of plenum hole and positions are changed to obtain a rapid and uniformity in cooling of product. A Computational Fluid Dynamics (CFD) modeling is agreed out for examination and comparison of the temperature, velocity and pressure circulation in the actual refrigerated truck and the modified truck design.

Keywords — Refrigerated truck, thermalbehaviour, airvelocity, pressure, plenum holes and Computational fluid dynamics.

INTRODUCTION

In India road transport is a main mode of transport for goods and chattels over large distances. The atmospheric temperature in few parts of India touches 45°C. In such condition reports shows that the temperature inside the cabin of a transport truck even exceeds 55°C. Especially for chick transportation, refrigeration trucks are used widely by the poultry industries. The ambient air in the truck is maintained at 15°C to 21°C. Upholding of even temperature throughout the cabin is essential in order to preserve the quality, safety and shelf life of product within the refrigerated enclosure, the temperature level and its similarity are directly governed by airflow pattern. The design of the air-distribution system should permit This air flow to compensate heat fluxes exchanged over the insulated walls or generated by the products. This process is vital in order to decrease temperature difference throughout the refrigerated truck. The VCRS (Vapour compression refrigeration system) is used in the truck, the input power to initiative the compressor of the refrigeration system is haggard from the power of the engine shaft. Refrigerant R134a is commercially used in domestic refrigerator all over the world. R134a has poor ozone depletion potential and has excessive global warming potential with a value of 1430. This research is commenced to high point the airflow characteristics, temperature and heat transfer related problematic issues of the refrigerated truck. Thus, by changing the number of plenum holes and its position to obtain a uniform cooling effect inside the cabin. A Computational Fluid Dynamics (CFD) modelling is agreed out for examination and comparison of the temperature, velocity and pressure circulation in the actual refrigerated truck and the modified truck design.

Objectives

To design the refrigeration truck cabin for storage of food products using software Solidworks-2019

Then analyse the flow pattern and thermal behavior inside the truck by means of CFD (Computationalfluidynamics)software.

To obtain the uniform flow distribution in the truck cabin by varying the air velocity and plenum size.

II. HEAT LOAD CALCULATION

Heat load factors naturally studied in a cold storage design

$$Q_{total} = Q_{product} + Q_{air} + Q_{infiltratedair} + Q_{walls} + Q_{equipment} + Q_{person}$$

Given conditions: Capacity–576 kg

Initial temperature – 42 °C

Storage temperature – 18 °C

Specific heat – 4.65 kJ/kg-k

Transportingtime–10 hours

Product load: $Q = m \times CP \times (T_0 - T_1)$

$$Q = 576 \times 4.65 \times (42 - 18)$$

$$Q = 64281.6 \text{ kJ}$$

$$= \frac{64281.610}{360 \times 60} = 1.79 \text{ kW}$$

Respiration load:

$$Q = 576 \times 11.72$$

$$= 6.751 \text{ kW}$$

$$\text{Total product load} = 1.79 + 6.751$$

$$= 8.54 \text{ kW}$$

$$\text{Ton of refrigeration} = \frac{8.54}{3.52} = 2.43 \text{ TR}$$

ii. Airload:

Volume of air = Total truck volume – Total volume of product

$$= 16.96 - 7.88 = 9.08 \text{ m}^3$$

Density of air = 1.117 kg/m³

Mass of air

$$= 1.117 \times 9.08$$

$$= 10 \text{ kg of air}$$

$$Q_{\text{air}} = m \times CP \times \Delta T$$

$$= 10 \times 1.005 \times (40 - 18)$$

$$= 221.1 \text{ kJ}$$

Given conditions: Capacity – 576 kg

Transmission load:

PPGI thickness (T1) – 0.5 mm

Thermal conductivity (k1) – 0.0299 W/m.K

PUF thickness (T2) – 79 mm

Thermal conductivity (k2) – 0.028 W/m.K

Stainless steel (T3) – 0.5 mm

Thermal conductivity (k3) – 14.2 W/m.K

Opposite two walls will have similar area, thus

wall1: 9.513 m²

wall2: 20 m²

wall1	73.74 kJ
wall2	155.03 kJ
Total	228.77 kJ

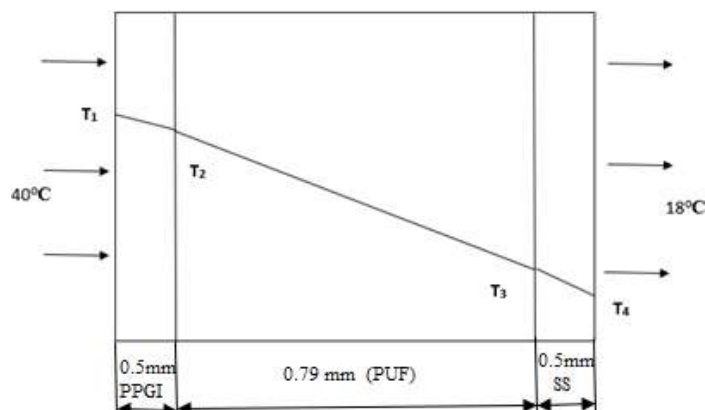


Fig.1 Heat transfer through insulation wall

$$k_1 = 0.02998 \text{ W/m.K}$$

$$k_2 = 0.028 \text{ W/m.K}$$

$$k_3 = 14.2 \text{ W/m.K}$$

$$Q = \frac{\Delta T}{\left(\frac{\Delta x}{KA}\right)}$$

$$R_1 = \frac{0.01667}{A}; R_2 = \frac{2.821}{A}; R_3 = \frac{3.086 \times 10^{-5}}{A}$$

$$R_{NET} = \frac{2.837}{A} \text{ K/W}$$

From above calculation,

$$Q = 6.3 \text{ W/m}^2$$

$$T_2 = 39.89^\circ\text{C}; T_3 = 22.12^\circ\text{C}$$

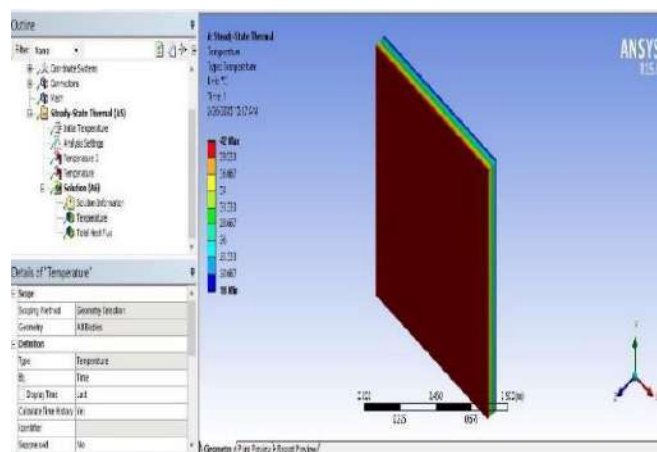


Fig.2 Steady-state thermal analysis of insulation material

The thermal analysis of insulation material at steady-state condition is shown in the figure 2. The PUF (Polyurethane foam) reduces the heat transfer rate, when compared to other insulation materials.

$$\text{Airload} + \text{transmission load} = 221.1 + 228.77$$

$$= 449.87 \text{ kJ} = 0.0124 \text{ kW}$$

$$\text{Total load} = 8.54 + 0.0131 = 8.55 \text{ kW} = 2.43 \text{ TR}$$

Safety factor	0.3
Ton of Refrigeration	TR

III. SELECTION OF REFRIGERANT AND REFRIGERATION SYSTEM COMPONENTS

Selection of Refrigerant

The selection of a refrigerant plays a major role in refrigeration system for various applications. It should be selected based on its physical, chemical and thermodynamic properties. Refrigerant R134a is a hydro fluoro carbon (HFC) that has zero potential to root the depletion of the ozone layer and few green house effect. R134a is the non-flammable and non-explosive, has toxicity within limits and decent chemical stability. Coming from the HFC(hydrofluorocarbons) family of refrigerants, R134a is also known as tetrafluoroethane(CH₂FCF₃).

No	Properties	R-134a
1	Boiling Point	-14.9° For -26.1°C
2	Auto-Ignition Temperature	1418° For 770°C
3	Ozone Depletion Level	0
4	Solubility in Water	0.11% by weight at 77°F Or 25°C
5	Critical Temperature	252° For 122°C
6	Cylinder Colour Code	Light Blue
7	Global Warming Potential (GWP)	1430

Table1. Properties of R134a refrigerant

Refrigeration Cycle

Before a detailed examination of truck cabin for the operating conditions, it is compulsory to understand how the air conditioning system works.

Mechanical refrigeration is talented by endlessly circulating, evaporating, and condensing a fixed supply of refrigerant in a closed system. Low pressure and low temperature super heated refrigerant vapor from the evaporator enter the compressor (State 1) and departs as high pressure and temperature superheated vapor (State 2).

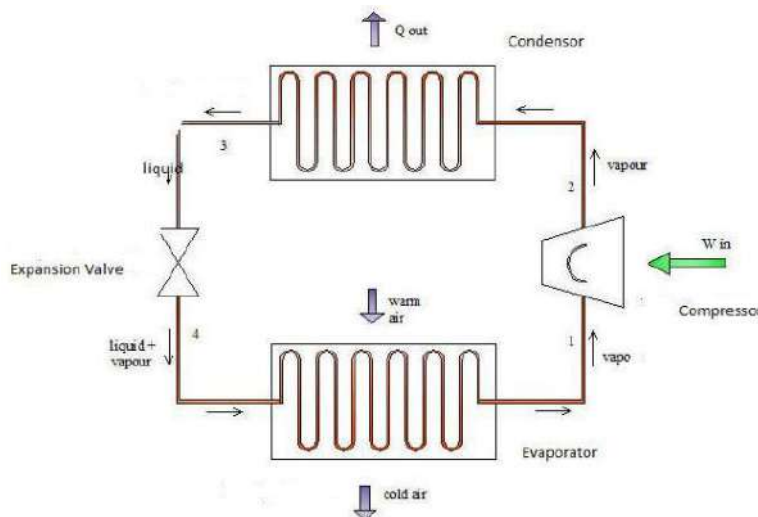


Fig.3 Refrigeration Cycle Equipment

This vapor arrives the condenser where heat is disallowed to out door air that is required over the condenser coils. The refrigerant vapor is cooled to the saturation temperature (State 2s), condensed to a liquid (State 3s), and cooled below the saturation point (State 3a). The high-pressure liquid is required through an expansion valve into the evaporator (State 4). The pressure in the evaporator is much lower than the pressure in the condenser, so the refrigerant arrives the evaporator as a liquid-vapormix at low temperature and pressure. The refrigerant soaks up the heat from warm indoor air that is blown over the evaporator coils. The refrigerant is totally evaporated (State 1s) and heated above the saturation temperature before entering the compressor. The indoor air is cooled and dehumidified as it streams over the evaporator and repaid to the living space. The refrigeration cycle is shown in Figure 4.

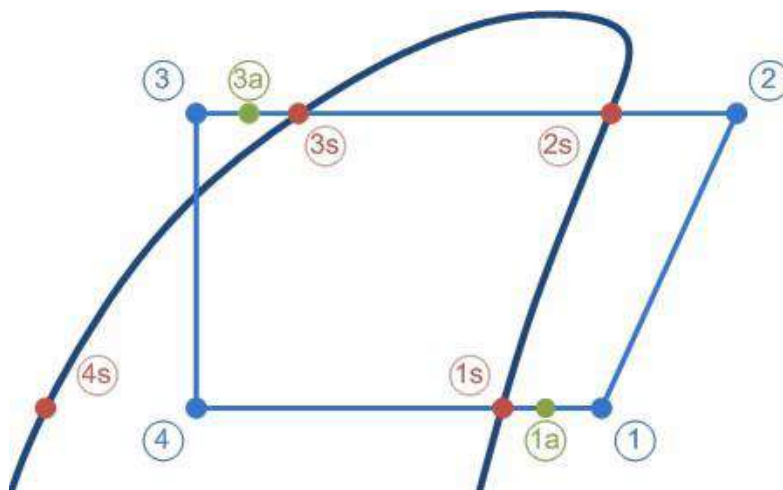


Fig.4 Pressure– Enthalpydiagram

	T	P	h	s
Description	[°C]	[bar]	[kJ/kg]	[kJ/kg.K]
1. Compressor suction	18.0	4.147	412	1.749
2. Compressor discharge	82.6	14.55	460/1	1.809
2s. Condensation dewpoint	54.0	14.55	425.8	1.709
3s. Condensation bubble point	54.0	14.55	278.8	1.259
3a. Condenser out	52.0	14.55	275.6	1.25
3. Including Additional sub cooling	52.0	14.55	275.6	1.25
4. After expansion valve	10.0	4.147	275.6	1.268
4s. Evaporation Bubble point	10.0	4.147	213.8	1.049
1s. Evaporation dew point	10.0	4.147	404.5	1.723
1a. evaporator	18.0	4.147	412	1.749

Table2. Performance details of refrigerant at various stages

With the above collected data, the mass flow rate, compressor work, condenser work and coefficient of performance are calculated by using the below formulas as follows,

Work done by evaporator

$$\dot{Q}_e = \dot{m}(h_1 - h_4)$$

$$10.55 = \dot{m}(412 - 275.6)$$

$$\dot{m} = 0.077 \text{ kg/s}$$

Work done by Compressor

$$\dot{W}_c = \dot{m}(h_2 - h_1)$$

$$= 0.11(460.1 - 412)$$

$$\dot{W}_c = 3.7 \text{ kW}$$

Work done by Condenser

$$\dot{Q}_c = \dot{m}(h_2 - h_3)$$

$$= 0.077(460.1 - 275.6)$$

$$\dot{Q}_c = 14.21 \text{ kW}$$

Work done by Compressor

$$\text{COP} = 2.25$$

Selection of refrigerant components

There are four basic components of refrigeration system viz. compressor, condenser, expansion valve and evaporator. The compressor is considered the heart of the refrigeration system.

In our project, the selection of compressor is based on the Danfoss Cool-selector software and on market survey which suits to work well with R134 a refrigerant. The compressor selected is reciprocating compressor with 0.077 kg/s mass flow rate. The purpose of the evaporator is by using the liquid refrigerant to remove unwanted heat from the product. The liquid refrigerant limited within the evaporator is boiling at low pressure. The evaporator coils are created of copper and provided with aluminum fins.

It causes more uniform distribution of cooling effect inside the truck cabin. The expansion valve is situated at the finale of the liquid line, before the evaporator. The valve then reduces the pressure of the refrigerant as it passes over and done with the orifice, which is located inside the valve. The expansion valve selected is TE5-55 thermostatic expansion valve. The commitment of the condenser is to extract heat from the refrigerant to the outside air. A natural air-cooled condenser is selected as the condenser type, with coil surface area is 12.47 m² and coil fin spacing 8 mm. The details of the selected refrigeration components are given in the table 3.

Sl. No	Component	Description
1	Discharge Pressure Gauge(Pd)	14.55 bar
2	Suction Pressure Gauge(Ps)	4.147 bar
3	Compressor type	Reciprocating compressor
4	Mass flow rate in evaporator	0.077 kg/s
5	Compressor power supply [V/Ph/Hz]	220-240/3/50-60
6	Coil surface area	12.47 m ²
7	Coil fin spacing	8 mm
8	Fan quantity & size	2 nos. & 600 mm
9	Air volume	3500

Table 3. Refrigeration system components

IV.DESIGN OF TRUCK CABIN

In this project work, small-scale refrigerated trucks of 3 – ton capacity were considered. These types of trucks are the most common vehicle used in the food cold-chain.

The refrigerated truck had length, width and height of 4232 mm, 1852 mm and height 2164 mm, respectively.

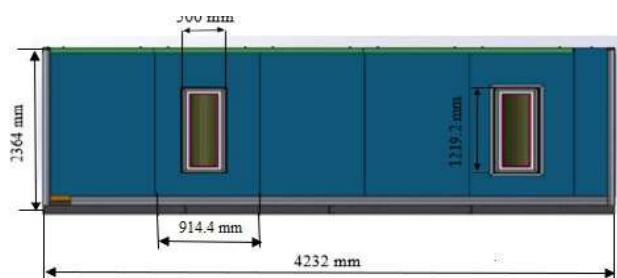


Fig.5 Truck cabin design

The geometry of the truck cabin consists of chicks which are placed inside the boxes. There are 72 chicks are placed in each chick box. Totally 8 trolleys are arranged inside the truck cabin. In the truck, plenum plate is placed on the upper side of the cabin. The plenum plate consists of 46 holes, where the cold air blows over the product.

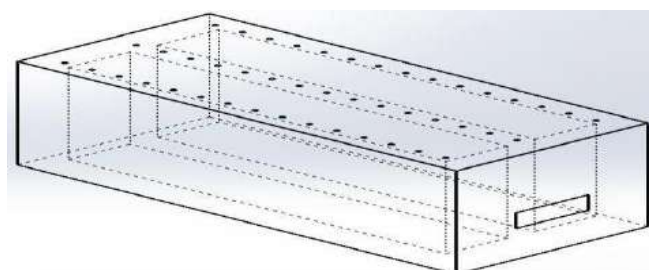


Fig.6 Truck cabin geometry

The above truck cabin geometry is used to perform simulation of air flow and heat dissipation using computational fluid dynamics (CFD). In the actual system contain of two plenum plate are shown in the figure 6. The dimension of two plenum plates is not same. One plenum plate consists of uniform holes on both sides, but in another plate only one side holes are placed. Hence, the trolley on one side gets uniform cooling of product than the other.

Modified truck cabin design

The simulation results, lead to some modification in the actual system design. This will increase the flow rate of air and remove the product heat more effectively compared to the actual system.

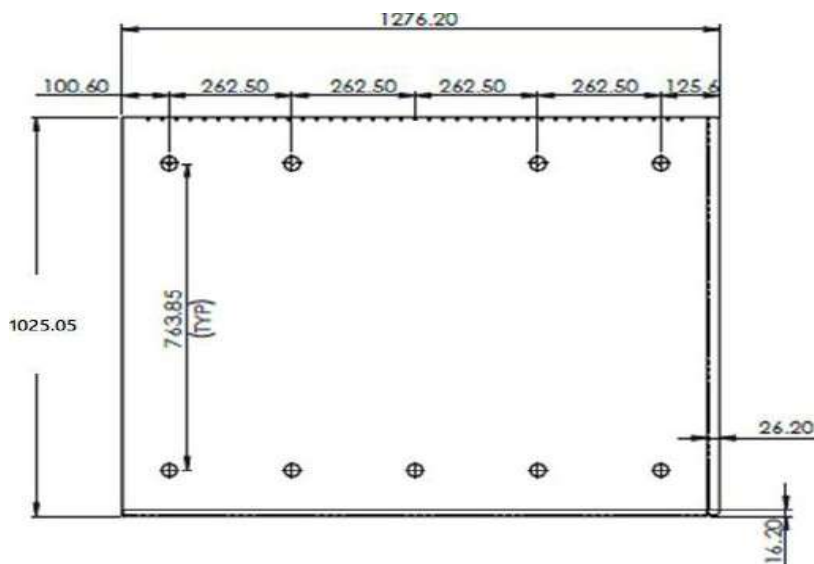


Fig.7 Modified plenum design (All dimensions are in mm)

For obtaining uniform cooling effect inside the cabin, the plenum plate design is modified is shown in figure 7. So, the two plenum plates are designed with same dimension, which leads to get uniform air distribution on both side of the trolley. The air filter area is also increased with length and width of 700 mm and 600 mm. Its helps to circulate more air inside the cabin.

V. COMPUTATIONAL MODELLING AND MESHING

Initially import the geometry file from Solid works to Ansys software. Then create a named section and name the plenum holes as in let and air filter area on the side of the cabin as outlet.

Meshing & Boundary conditions

The commercial software package ANSYS Fluent was new for the generation of the model. The cooling performance of a loaded cold truck in cooling process using transient three-dimensional computational fluid dynamics model. The model accounted for turbulence by worth of the standard k- Epsilon 00model with standard wall profiles. The air inside the refrigerated chamber is assumed to be in compressible fluid. The cut-cell cartesian methodology is used, where the mesh fits perfectly with the geometry, falling the number of inaccuracies that propagate through the rest of the domain.

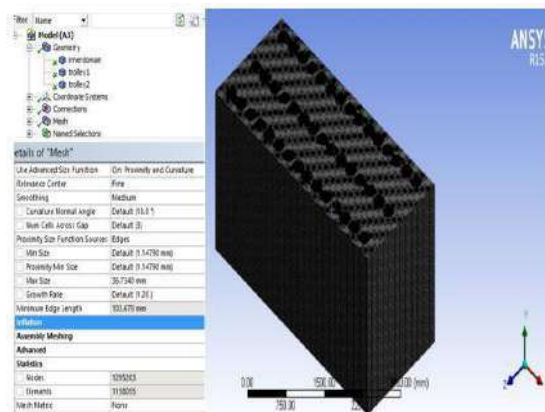


Fig.8 Meshed Model

To account for the effects of turbulence, the SST k-Epsilon model was employed. The transient state condition is used to run the simulation, because the temperature of the product is changed according to the time. The applied boundary conditions for the analysis is shown in the tables below

S.No	BoundaryZones	BoundaryConditions
1	Inlet	Velocity inlet
2	Outlet	Pressure Outlet

Table 4. Boundary Conditions

S.N	Solver	Options
1	Type	Energyon
2	Time	Transient
3	Viscous	K-Epsilon
4	Material	Chick
5	velocity	5m/s&6m/s

Table 5. Model setup

Thus, the SST k-Epsilon turbulent model is used, which reasons for transport of turbulent shear stress and gives highly accurate predictions. It solves for two variables: k – the turbulence kineticenergy and ϵ – the rate of dissipation. It is well – suited for high Reynolds number.

VI. RESULT AND DISCUSSION

Velocity – Contour of Actual Truck

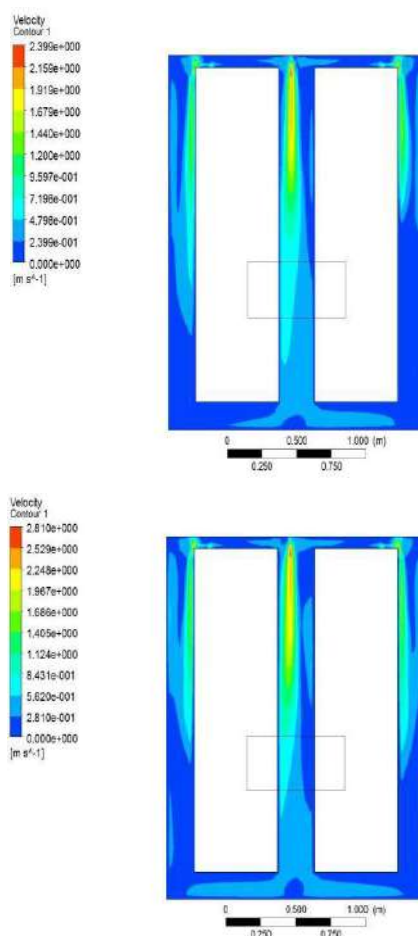


Fig.9 Front view and of truck cabin – velocity contour at 5 &6 m/s

This above result shows, that the average velocity of air inside the cabin for 5 and 6 m/s inlet condition is 2 m/s and 2.5 m/s. Therefore, average velocity inside the cabin is more in second inlet condition.

Temperature – Contour of Actual Truck

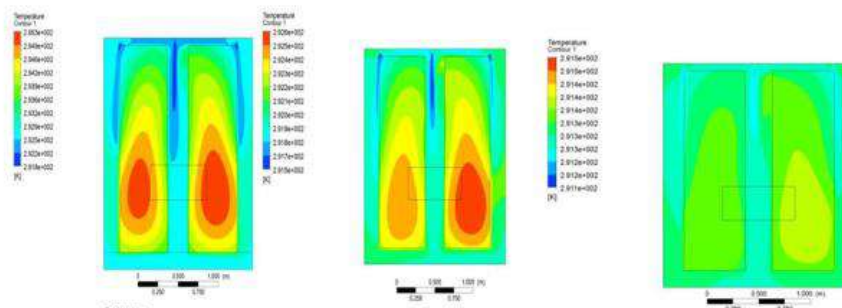


Fig.10 Front view of truck cabin–Temperature contour at 5m/s at (1hr,2hr &3hr)

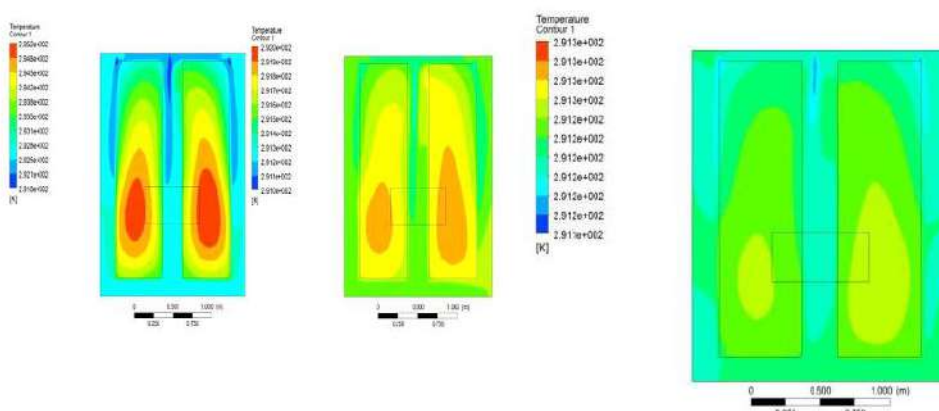


Fig.11 Front view of truck cabin–Temperature contour at 6m/s at (1hr,2hr &3hr)

For both 5 m/s and 6 m/s inlet condition, the temperature contour for different time period is shown in the fig 10 & 11. The time taken to attain 18°C is almost 3 hours in both the inlet condition. It is clearly understood, that the temperature of one trolley is reduced quickly compared to others.

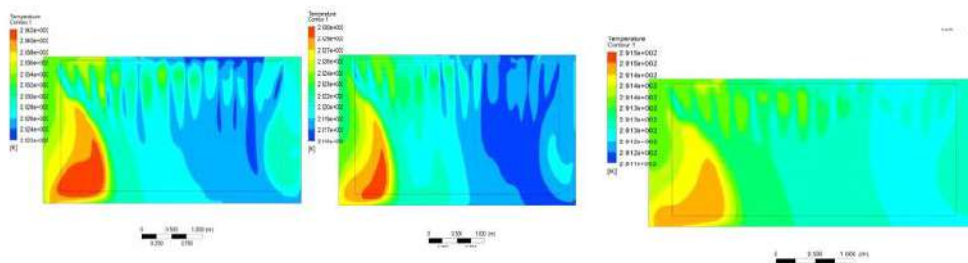


Fig.12 Side view of truck cabin–Temperature contour at 5m/s at (1hr,2hr &3hr)

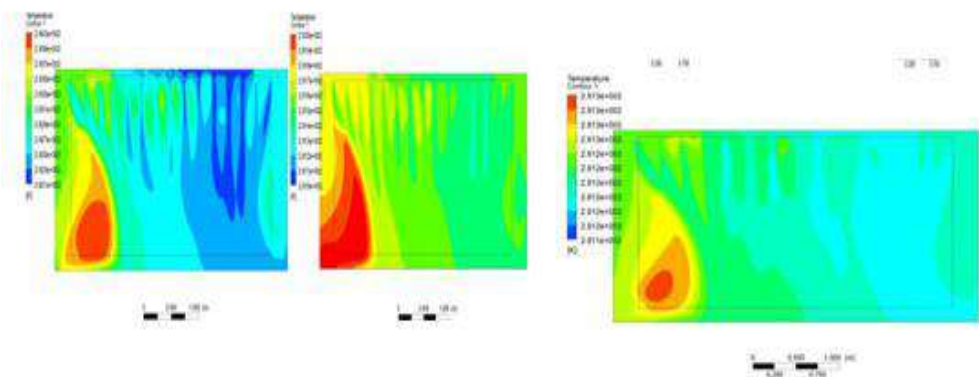


Fig.13 Side view of truck cabin–Temperature contour at 6 m/s (1hr,2hr &3hr)

Some amount of heat is still presented on the back side of the truck is shown in the fig 12 & 13. So non-uniform cooling of product is experiencing inside the truck cabin for both the inlet condition.

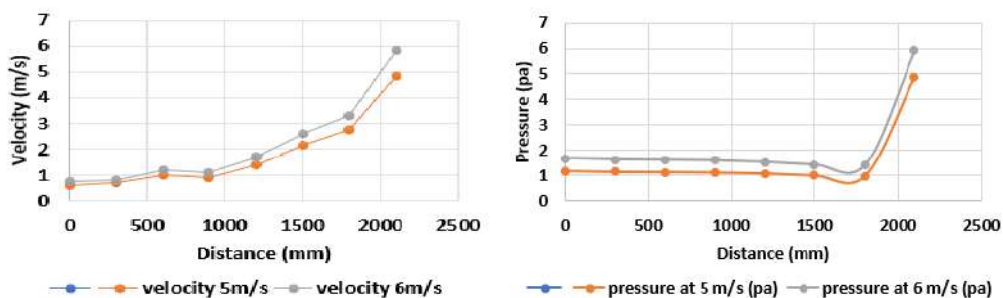


Fig14. Velocity and pressure distribution graph at 5m/s & 6m/s

For both the inlet condition 5 m/s and 6 m/s, the velocity and pressure distribution over the various plane are given in the graph 14.

Temperature–Contour of Modified Truck

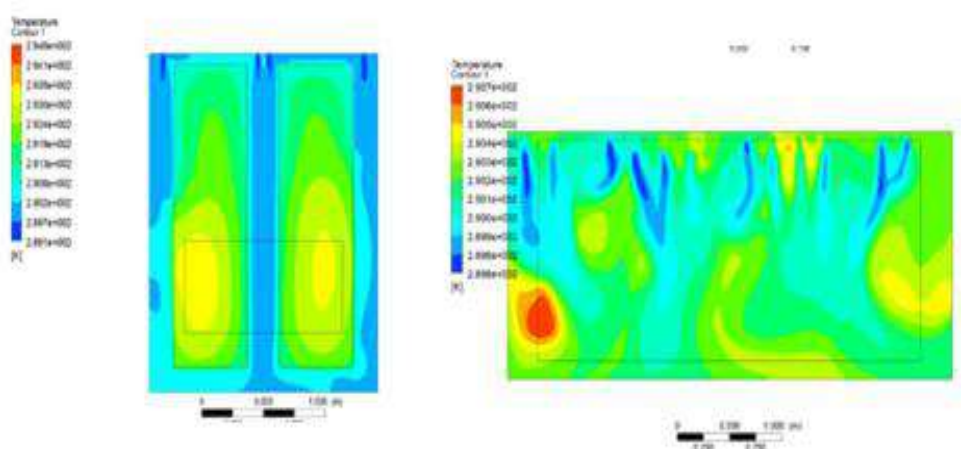


Fig.15 Front & Side view of truck cabin–Temperature contour at 5m/s at (1hr)

From the above figure, it is clearly understanding, that both the trolley attains uniform cooling and temperature on the back-side of the truck cabin is also removed.

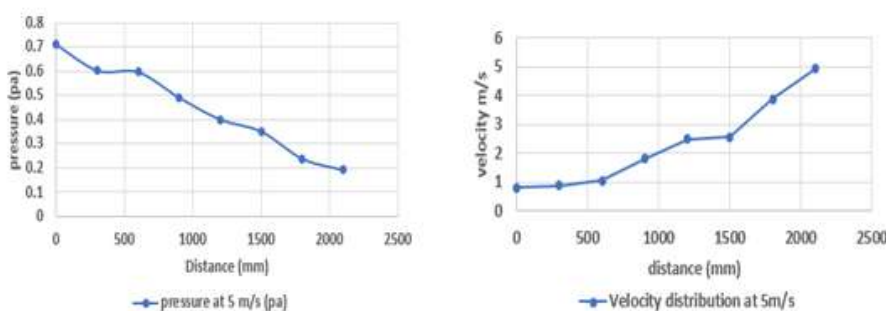


Fig16. Pressure and velocity distribution graph

From these results, it is evident that, the modified truck design is more efficient than the Actual truck design. The average velocity inside the truck cabin is 2.5 m/s. Hence the time taken to obtain a required cooling effect is reduced from 3 hours to 1hour.

VII.CONCLUSION

The Actual truck cabin is designed by using Solid works – 2019. Then the Computational Fluid Dynamics (CFD) modelling and comparison of the temperature, velocity and pressure distribution inside the truck cabin is carried out. Thus, the result shows non – uniform air flow pattern and cooling effect of the product. So, the truck design is changed by increasing the number of plenum holes and positions are changed to obtain a rapid and uniformity in cooling of product. Hence the time taken to obtain a required cooling effect is reduced from 3

hours to 1 hour. From the analysis, it is evident that the modified truck design is more efficient than the Actual truck design.

REFERENCES

1. Amr Kaood, Essam E. Khalil and Gamal M. El-Hariry, "Flow Patterns and Thermal Behaviour in a Large Refrigerated Store, Faculty of Engineering" Cairo University, Egypt, Volume 13, Issue 2 Ver.III, PP81 - 92, 2016.
2. Turkey Yildiz, "CFD Characteristics of Refrigerated Trailers and Improvement of Air flow for Preserving Perishable Foods Department of Information Technology (B.I.D.B.), Izmir Institute of Technology, 35430 Izmir, Turkey, 2019.
3. [3] Moureh, J., Menia, N., & Flick, D. Numerical and experimental study of air flow in a typical refrigerated truck configuration loaded with pallets. *Computers and Electronics in Agriculture*, 34 (1-3), 25-42, 2002.
4. Mehran Islam, Asif Kabir, Arnab Mustafi Arka, and Md. Ashiqur Rahman. "Assessment of the Transport Refrigeration System in Bangladesh and Numerical Simulation of the Refrigeration Performance" AIP Conference Proceedings 2121, 030013, 2019.
5. Tanaka, F., & Konishi. The use of CFD to improve the performance of a partially loaded cold store. *Journal of Food storage and transportation*, 35 (6), 874-880, 2012.
6. Yi, T., Jing, X.I.E., Jin-feng, W., Chen, M., & Yi, Z. Computational Fluid Dynamics Simulation about Comparison of Different Forms of Return Air in a Small Cold Store, 517, 1133-1138, 2012.
7. Getahun, S. Ambaw A. Delele M. Meyer C.J. Opara, U.L. "Analysis of air flow and heat transfer inside fruit packed refrigerated shipping container: Part I—Model development and validation" *J. Food Eng.*, 203, 58-68, 2017.
8. Han J.W, Zhao C.J, Yang X.T, Qian J.P, Xing B, "Computational fluid dynamic simulation to determine combined mode to conserve energy in refrigerated vehicles" *J. Food Process. Eng.* 39, 186-195, 2016.
9. Alam S, "A Proposed model for Utilizing Exhaust Heat to run Automobile Air-conditioner", The 2nd Joint International Conference on Sustainable Energy and Environment 21-23 November 2006, Bangkok, Thailand, 2006.
10. Amit M. Patel and Prof. R. I. Patel, "Optimization of different Parameters of cold storage for energy conservation", *International Journal of Modern Engineering Research*. Vol.2, Issue3, 2012

A Phoneme-Based Method to Recognise Visual Speech Using Deep Learning Model

¹Bineeshia J, ²Vinoth Kumar B, ³Monirhithikka S. P and ⁴Sarayumiththira V. C

^{1,3,4}Department of Computer Science and Engineering, PSG College of Technology, Coimbatore, India

²Department of Information and Technology, PSG College of Technology, Coimbatore, India

ABSTRACT

Lip reading is a skill to identify the words uttered by a person based on visual information. As different characters generate relatively similar lip sequence, it is misleading at the word level, which is challenging for a novice to master. For example, the characters 'a' and 'e' have the same lip sequence. However, given the context of adjacent words in a sentence and a language model, such inconsistencies can be rectified to some extent. A system that can identify the words uttered is achievable using computer vision due to the availability of a large training dataset and neural network models. Our system is designed as a visual encoder - decoder, with visual content being collected and interpreted using convolutional neural networks and generates enhanced speech at the output layer. The system has been testified on a challenging dataset. End to end approach is used to train the model. The proposed system's experimental results show that it has good robustness.

Keywords—CNN, deep learning, lip reading

I. INTRODUCTION

Lip reading is an ability to decode speech by looking at the motion of the lips. [1]. It is often called “a third ear,” and it's not easy to comprehend a single word by reading a speaker's lips. When confronted with the obstacles and daily distractions that exist in our environment, it is quite easy to miss a word, a phrase, or perhaps a whole sentence. In recent years, several improvements have been achieved in the field today of automated lip-reading, with an increasing diversity of machine learning-based approaches being used. Automation of lip reading can be performed either with audio or without audio. It is called as Visual speech recognition when lip reading is done without audio. For words like “th” and “f”, it is difficult to decipher since the shapes made by the lips are similar. People describe the experience of being able to read lips as the world opening up again because they can communicate more effectively.

Listeners gain confidence, active participation, and stronger connections with people as a result of their capacity to understand what is being said. Being unable to grasp what is being aforementioned will cause a way of frustration and isolation. Communication plays a major role in human life and it is essential for human contact. Learning to read lips can also help communication specialists since it gives them the tools they need to speak more efficiently with deaf and hard-of-hearing people. Lip reading, which is defined as the ability to estimate one's said word or entire sentence only based on visual cues, is a difficult yet fascinating exercise. because of different kinds of individuals, their languages and articulations [1]. It's a hard topic that has not yet been fully resolved and is a great challenge for solving using artificial intelligence and machine learning methods. A machine that is able to read the lips is possible by tasks involving computer vision, such as the usage of image classification, object detection, neural network models, tracking the region of mouth from the given visual data. At times when audio is corrupted, the visual recognition system serves as a solution. The convolutional neural network model accepts the input in the form of video, converting into photo frames and outputs the corresponding phoneme spoke.

The remainder of the paper is organised in the following manner. In literature review, an overview of several research papers are discussed. In section 3, the architecture of the system is mentioned. Its components and working methodologies are also discussed in detail. A discussion of the experimental results relating to the proposed system is provided in section 4. Towards the end, in section 5, conclusions and ideas for future work are given.

II. LITERATURE REVIEW

In this work [2], It is mentioned that the state-of-the-art model for recognising single words in the wild has been developed. Its major components are a residual network and Bidirectional Gated Recurrent Unit (BGRU) layers. In Fenghour et al [3] a lip reading system based on neural networks is proposed. A specialized transformer is used to classify visemes in continuous speech which in turn is used as a schema to classify lip reading sentences. Perplexity analysis is used for the conversion of visemes to words, thus enhancing the accuracy of lip reading sentences. A method for dataset building from programs like talk show, speech and news for Mandarin

sentence level lip reading is put forward by Xuejuan Chen et al [4]. To convert Hanyu Pinyin into Chinese characters, this model uses a 3D convolutional layer with DenseNet and residual bidirectional long short-term memory, as well as a model with a stack of multi-head attention. The main objective of the Lip by Speech (LIBS) method is to improve the efficiency of lip reading that can be learned using speech recognition software. This method is proposed by Ya Zhao et al [5] and by obtaining the new state-of-the-art performance on the CMLR and LRS2 datasets, it outperforms the baseline by a margin of 7.66 percent and 2.75 percent in character error rate, respectively. The WLAS (Watch, Listen, Attend, and Spell) model that helps in lip reading the sentences is mainly focused in the paper proposed by J.S.Chung et al [6]. Convolution Neural network is mainly used to capture the smallest unit of sound and its visual equivalent from still images. This model, utilises character-level outputs, to learn a language model and features a new dual attention mechanism that can work with either visual or audio input or both. Video is converted to viseme, and then viseme is converted to a character by using separate models. Such a method was proposed by JavadPeymanfard et al [7]. Using LRS2 (BBC-Oxford Lip Reading Sentences 2) dataset, the word mistake rate improved by 4% when compared to the typical sequence to sequence lip-reading model. MingshuangLuo et al [8] offer a unique pseudo-convolutional policy gradient (PCPG) based method to overcome two problems: the exposure bias caused by the "teacher-forcing" approach, and the ambiguity between the discriminative optimization aim and the appraisal metric. Thus making significant improvements over other related methods which certainly demonstrates the benefits of our method. To enhance and improve the relations of the global sequence's level and local feature's level, Xing Zhao et al [9] proposed mutual constraints on both of them. The results show that the suggested technique is effective because it is both discriminative and resilient, and on both standards, it reports new state-of-the-art performance. Pingchuan Ma et al [10] proposed a stream of ideas to bridge the gap between the criteria for optimal lip-reading deployment in real-world circumstances and the current methodologies that are as follows. Using self-distillation, state-of-the-art performance on LRW and LRW-1000 is increased by a large margin to 88.5 percent and 46.6 percent, respectively. The computational cost is a quarter of what it was in the original model by applying a few architectural changes thereby making it possible to apply lip-reading models in practical applications. Kenji Matsui et al [11] investigate a lip-reading system that recognises by registering the words you wish to pronounce and is optimised for the user using a limited amount of data. The training data set was created using Variational Auto Encoder for the word recognition model, in which 36 viseme pictures were transformed into tiny data. The devices which best suited the lip-reading type speech enhancement concerning both small vocabulary recognition accuracy and usability were the embedding mobile devices. Chenzhao Yang et al [12] present a new deep neural network (DNN) to increase lip-reading efficiency in the speaker-independent circumstance.

III. METHODOLOGY

Neurons that possess learnable bias and weights make up the convolutional neural network. With the input it receives each neuron does a dot product and, if desired, a non-linearity. Deep artificial neural networks called convolutional neural networks are being used to categorize images, cluster them by resemblance, and recognise objects within scenarios.

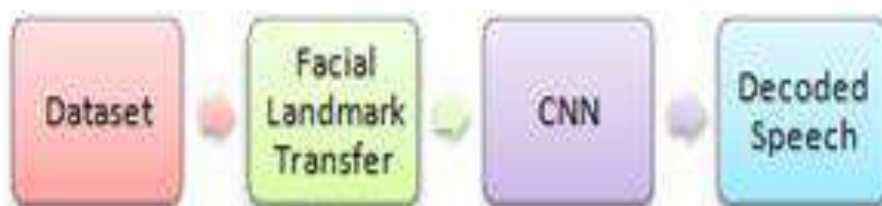


Fig. 1 Architecture

Fig. 1 Components of the system

A. Architecture

Initially, the video is given as input in the form of data images which is followed by facial landmark transfer. The algorithm is followed by CNN. Finally, the decoded speech is obtained as output. The overall framework of the system is briefly illustrated in Fig. 1.

B. DATA

The video recordings of a bee dataset movie script with a duration nearly five hours and more is used, and it is spoken by multiple speakers. The recorded script is based on the English language, which contains 30,000 words and 900 sentences. The statements are structured in such a way that each word has a different pronunciation feature. In total there are 42 categories of phonemes. The utterances do not exceed 3-4 seconds.

The speakers were filmed from the front and the words were captured in a quiet, well-lit location. Videos were captured at 30 fps with a resolution of 720 pixels by 480 pixels. The training set has 4 lakh frames and the testing set consists of 31000 frames.

C. Data pre-processing

In the pre-processing stage, the goal is to process the data from raw video to get only the region of interest - the mouth. Although feeding non-pre-processed videos and letting the neural network learn the features and the area of interest itself from a bigger frame might be also possible, focusing solely on the mouth area will speed up the training process. Therefore, video processing is done first. Video processing converts video into individual frames. One second of video consists of 30 frames. i.e. converting one second of video we obtain 30 colour images. Second step is identifying and cropping the mouth region from the individual frames.

Pre-processing the videos is done in accordance with the stages shown in Fig. 2. Videos are captured at 25 frames per second and comprises of 160 by 160-pixel images with RGB pixel values. Initially, recordings are sampled to generate image frames, and then face detection is performed. As the area of interest and the input of the visual frontend is a person's lips who is speaking, location of facial landmarks is required. A CNN-based detector known as the Single Shot MultiBox Detector (SSD) is used for detecting the appearance of faces. Faces pointing at different angles could also be recognized. A reduced image size of $112 \times 112 \times N$ (N refers to the no. of image frames) is produced by digitizing the video frames in greyscale, scaling, and then cropping them around the boundary of the facial landmarks.

The process of cropping the mouth region requires vertices of top and bottom lip of the face. By using the face landmarks function, the vertices of the individual top and bottom lip is obtained which outputs the actual size of the mouth region. Finally iterate all the frames to extract the mouth region and grouped the images into a frame neighbourhood. Gentle transcript aligner is a web application used to classify the audio based on phonemes which gives the desired output for each frame neighbourhood in the form of a json file. The generated json file consists of categories of phonemes aligned with individual timestamps of the video at which the phoneme occurred. Imbalanced dataset is very prone to overfitting and biased results to the majority class even with data augmentation and weighting loss functions.

D. Neural Network

Given a video of a person speaking, the network has to guess the spoken words. A series of images of the mouth regions is given as input to the network.

In the domains of computer vision and machine learning, the convolutional neural network (CNN) is by far the most efficient and popular choice for understanding visual information. In the form of the following equation (1), at the coordinate (i,j) the feature map at layer h with input x pixel is obtained.



Fig. 2. Stages of video image pre-processing

$$h_{ij} = a * ((W * x)_{ij} + b) \quad (1)$$

with a as non-linearity activation function, b - bias vector (feature map filter), W - weight-matrix, and h_{ij} - hidden layer of the coordinates (i,j) .

Cropped mouth region and aligned phoneme json file is fed into a convolutional layer. The system is an auto encoder as shown in Fig. 3 Auto encoders are a family of neural networks for which the input is the same as the output. The output is reconstructed from the latent space representation which is obtained by compressing the input data. The first process of auto encoding is convolution. The convolutional layer is used to convolve the given input image and using a filter, features from the source image is retracted by scanning. Size of the filter is 5×5 pixels i.e. the system moves the filter over the given images with the dimension of 5×5 pixels. Dot products between the image pixel values and the weights values defined in the filter are obtained in order to reduce dimensionality of the images. An activation function is used as a gate function to evaluate whether the particular neuron should be activated or not. The ReLU() expanded as Rectified Linear Unit function is a non-linear activation function. The ReLU function does not activate all the neurons at the same time unlike the other

functions which makes it preferable here. This is used to add non linearity to avoid system convergence. $\text{Relit}(x) = \max(0, x)$ with x as the matrix of the input image. The maximum or largest value in each patch of each feature map is calculated by Maxpool() operation. Max pooling is used to detect the sharp patterns in the given images. The aligned phoneme (json) file is used to identify the total number of categories of the phoneme and its repetitions which is present in the dataset. The pooling layer's output is given into the upcoming convolution layer, and the process is continued. In the end, the pooling layer's output is converted in the form of neuron weights. Three layers make up the neural network: the input layer, the hidden layer, and the output layer. 1000 neurons are present in the input layer, 300 neurons in the hidden layer and 41 neurons in the output layer. Weights of neurons are updated for each iteration and each output neuron has the probability of phoneme. The output corresponding to the highest probability value will be the predicted phoneme. The output that is obtained at the output layer is matched with the phoneme that is present in the json file. The predicted output is converted to text by referencing the key file.

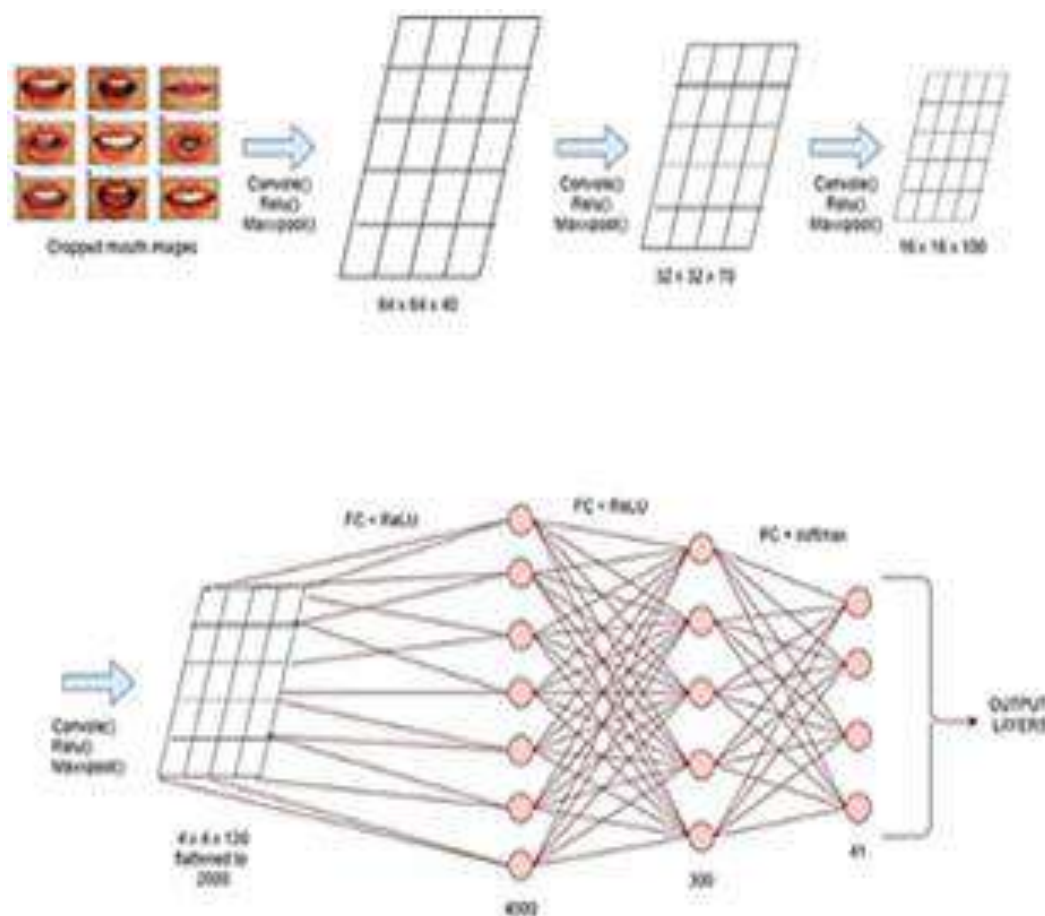


Fig. 3. Structure of auto encoder

E. Illumination

Once trained, the entire architecture of the proposed lip reading system has been evaluated under several degree of illumination, in order to evaluate its robustness to lighting changes. The illumination was achieved by varying the pixel brightness. After sampling the video, the illumination is exerted to the image frames. The intensity of pixel components in the images of videos taken from the dataset consisting of RGB pixels ranges from zero to 255. The first phase of the algorithm is to normalise all the pixels, which entails the minimum-maximum normalising of pixels. The pixel values are translated to $[0, 1]$ from the range $[0, 255]$. This is followed by adjusting the pixel values according to equation (2), where M denotes a matrix of pixels, γ a scalar value, and R the resulting matrix of pixels after the gamma correction. This is known as gamma correction.

$$R = M^{1/\gamma} \quad (2)$$

Images will darken when γ values are less than 1.0, whereas images will brighten when γ values are greater than 1.0. In this paper, the γ values used for gamma correction are 0.5 and 1.5. A gamma correction occurs after re-normalizing all pixels' values, in order that all pixel values are mapped back to a certain range that is from $[0, 1]$ to $[0, 255]$.

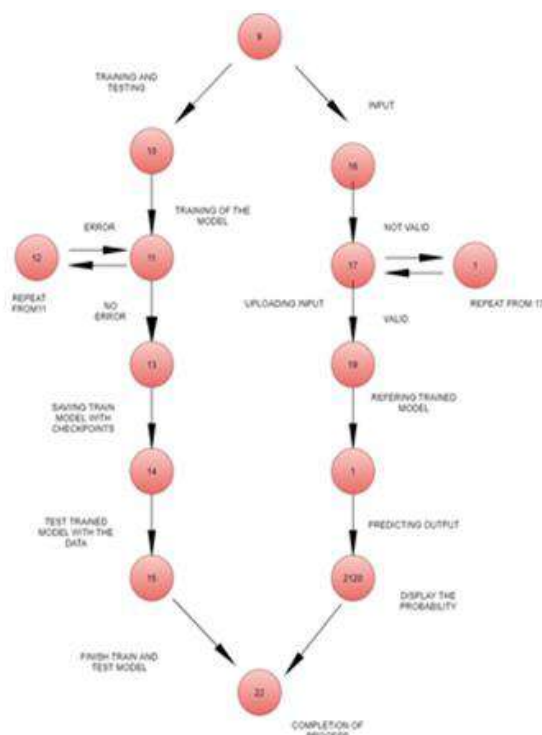


Fig. 4. Cyclomatic Complexity

IV. EXPERIMENT AND RESULT

A. Cyclomatic Complexity

In order to find the complexity of the source code that is being correlated to coding errors, the cyclomatic complexity is calculated as shown in Fig.4.. By developing the control flow graph for the particular code, it is calculated.

$$V(G) = P + 1 = 6 \text{ (P – no of conditional statement)}$$

$$V(G) = R = 6 \text{ (R – no of regions)}$$

$$V(G) = 26 - 2 \cdot 2 + 2 = 6$$

B. Independent paths

Independent paths are the available paths that traverse at least one new edge in the flow graph. If the number of independent paths and $V(G)$ is equal then the white box testing is valid.

The primary evaluation metric takes the form of a confusion matrix. A classification algorithm's performance is summarised using the technique of a confusion matrix. It can give a better idea of what classes the model predicts wrongly the most and for which words they are being confused. The generated and plotted confusion matrix for our model can be seen in Fig. 5. The values are not normalized and the number in each individual cell represents how much is the given word being confused with another one. The darker background illustrates a higher confusion rate. For example, the class label of 0 from both the x and y axis has a value of 6943 i.e. 6943 times the model predicts that class correctly from the total set of images.

Another example, the class label of 0 from x axis and 1 from y axis has a value of 186 i.e. 186 times the model wrongly predicts the 'silence' (class label 0) as 'k' (class label 1). In Table I, the confusion matrix's class label is given and in Table II, the independent paths are shown.

Table I. Class Label for Confusion Matrix

0	silence	21	uh
1	k	22	f
2	ao	23	ay
3	r	24	s
4	d	25	aa
5	ih	26	uw
6	ng	27	m
7	t	28	g

8	ah	29	ae
9	l	30	aw
10	n	31	hh
11	ow	32	y
12	z	33	th
13	b	34	p
14	ey	35	oov
15	iy	36	er
16	sh	37	jh
17	dh	38	ch
18	eh	39	oy
19	w	40	zh
20	b		

1	2	3	4	7	8	9	10	11	13	15	22	
1	2	3	4	7	8	9	16	17	19	20	21	22
1	2	3	5	7	8	9	10	11	13	14	15	22
1	2	3	5	7	8	9	16	17	19	20	21	22
1	2	3	6	7	8	9	10	11	13	14	15	22
1	2	3	6	7	8	9	16	17	19	20	21	22

TABLE II. INDEPENDENT PATHS

For a certain period of time, recognition independent of the speaker was a goal which was unachievable. Even for human lip-readers who are very skilled, speaker dependent reading was found to give high performance. The proposed model accepts the input as a sequence of images. It displays the probability of phonemes for all types of phonemes for each frame, then identifies the maximum value of the probability for each frame to interpret the output of the image and converts into textual description.

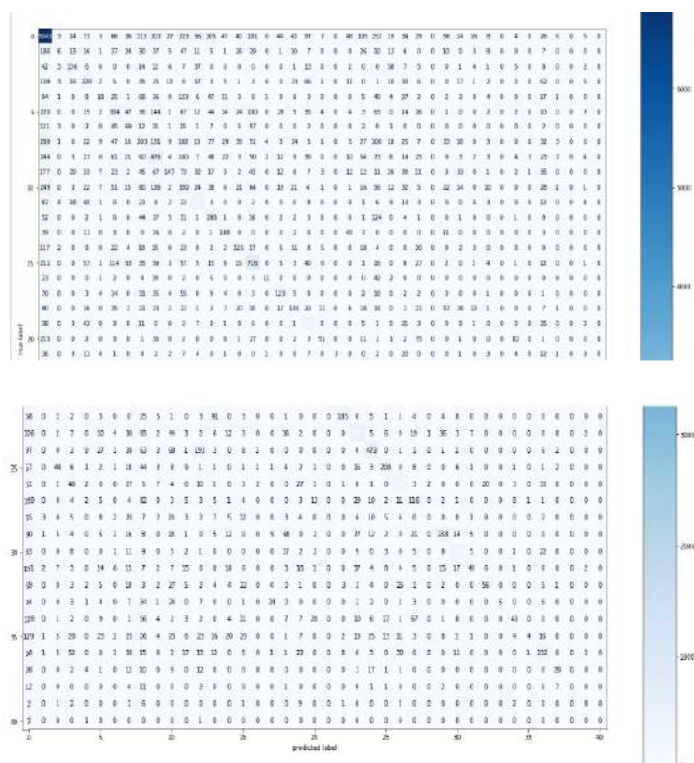


Fig. 5. Confusion matrix

V. CONCLUSION

In this work a phoneme-based method to identify lip reading by using deep learning methodology is reported. In the proposed model input is given in the form of a sequence of images and output is given in the form of the image's probability of phoneme. The best results were achieved using the convolutional neural network (CNN) architecture. The architecture to classify temporal sequences of images and learning of features were achieved

through two layers of fully connected hidden network structure which is an auto encoder, and the softmax is used for predicting output.

The primary evaluation metric is a confusion matrix. This is due to the nature of the problem where our priority is to detect all incorrect values and not label an incorrect value as the correct value. Phoneme based lip reading methodology gives an accuracy of 45% for a multiple speaker model. Multiple speaker model has an accuracy of less than 50% due to the fact that this method needs enough sample data. Although a 45 percent accuracy rate for a multi-speaker model does not appear to be successful, this accuracy is good when the neural network is chosen from 41 different phonemes. The accuracy achieved by our model is also high compared to human level lip reading accuracy, which is ranged from 12% to 53%. It is necessary for the model to learn to identify new sentences from a huge content. The future directions of the work is to standardize the sample data and improve the algorithm to do multi-view tracking of the mouth region which is a more complex feature than a single view.

REFERENCES

1. Chung, Joon Son & Zisserman, Andrew. (2017). Lip Reading in Profile. 10.5244/C.31.155. British Machine Vision Conference.
2. Martinez, Brais & Ma, Pingchuan & Petridis, Stavros & Pantic, Maja. (2020). Lipreading Using Temporal Convolutional Networks. 6319-6323. 10.1109/ICASSP40776.2020.9053841.
3. Souheil Fenghour, Daqing Chen, Kun Guo, Perry Xiao ; Lip Reading Sentences Using Deep Learning With Only Visual Cues; 2020 IEEE Access; volume 8.
4. Chen, Xuejuan & Du, Jixiang & Zhang, Hongbo. (2020). Lipreading with DenseNet and resBi-LSTM. Signal, Image and Video Processing. 14. 10.1007/s11760-019-01630-1.
5. Ya Zhao, Rui Xu, Xinchao Wang, Peng Hou, Haihong Tang, Mingli Song; Hearing Lips-Improving Lip Reading by Distilling Speech Recognizers; AAAI 2020.
6. Joon Son Chung, Andrew Senior, Oriol Vinyals, Andrew Zisserman; lip reading sentences in wild; 2017 IEEE Conference on Computer Vision and Pattern Recognition (CVPR).
7. Peymanfard, Javad & Mohammadi, Mohammad Reza & Zeinali, Hossein & Mozayani, Nasser. (2021). Lip reading using external viseme decoding.
8. Luo, Mingshuang & Yang, Shuang & Shan, Shiguang & Chen, Xilin. (2020). Pseudo-Convolutional Policy Gradient for Sequence-to-Sequence Lip-Reading. 273-280. 10.1109/FG47880.2020.00010.
9. Zhao, Xing & Yang, Shuang & Shan, Shiguang & Chen, Xilin. (2020). Mutual Information Maximization for Effective Lip Reading.
10. Ma, Pingchuan & Martinez, Brais & Petridis, Stavros & Pantic, Maja. (2020). Towards practical lipreading with distilled and efficient models.
11. Kenji Matsui, Kohei Fukuyama, Yoshihisa Nakatoh, Yumiko O. Kato; Speech Enhancement System Using Lip-reading; 2020 IEEE 2nd International Conference on Artificial Intelligence in Engineering and Technology (IICAET).
12. Chenzhao Yang, Shilin Wang, Xingxuan Zhang, Yun Zhu; Speaker-Independent Lip-reading With Limited Data; 2020 IEEE International Conference on Image Processing (ICIP).
13. Iryna Anina, Ziheng Zhou, Guoying Zhao, Matti Pietikäinen; a multi-view audio-visual database for non-rigid mouth motion analysis; 2015 11th IEEE International Conference and Workshops on Automatic Face and Gesture Recognition (FG); volume 1.
14. Wand, Michael & Koutnik, Jan & Schmidhuber, Jürgen. (2016). Lipreading with long short-term memory. 6115-6119. 10.1109/ICASSP.2016.7472852.
15. Du Tran, Lubomir Bourdev, Rob Fergus, Lorenzo Torresani, Manohar Paluri; Learning spatiotemporal features with 3D convolutional networks; 2015 ICCV.
16. Jen-Cheng Hou, Syu-Siang Wang, Ying-Hui Lai, Yu Tsao, Hsiu-Wen Chang, Hsin-Min Wang; Audio-Visual Speech Enhancement Using Multimodal Deep Convolutional Neural Networks; 2018 IEEE Transactions on Emerging Topics in Computational Intelligence; volume 2.

17. KwanchivaThangthai, Richard Harvey, Stephen Cox, Barry-John Theobald; Improving lip-reading performance for robust audiovisual speech recognition using DNNs; 2015 AVSP.
18. Lee, Daehyun& Lee, Jongmin& Kim, Kee-Eung. (2017). Multi-view Automatic Lip-Reading Using Neural Network. 290-302. 10.1007/978-3-319-54427-4_22.
19. Zhu, Mei-li & Wang, Qing-qing&Luo, Jiang-lin. (2019). Lip-Reading Based on Deep Learning Model. 10.1007/978-3-662-59351-6_4.
20. KarelPalecek; Experimenting with lip-reading for large vocabulary continuous speech recognition; 2018 Journal on Multimodal User Interfaces.
21. Yong Xu, Jun Du, Li-Rong Dai, Chin Hui Lee; A regression approach to speech enhancement based on deep neural networks; 2015 IEEE/ACM Transactions on Audio, Speech, and Language Processing; volume 23.
22. SubhashiniVenugopalan, Marcus Rohrbach, Jeff Donahue, Raymond Mooney, Trevor Darrell, Kate Saenko; Sequence to sequence-video to text; 2015 ICCV.
23. Ziheng Zhou, Xiaopeng Hong, Guoying Zhao, and MattiPietikäinen; A compact representation of visual speech data using latent variables; 2014 IEEE Transactions on Pattern Analysis and Machine Intelligence; volume 36.

An Extensive Survey on Memetic Differential Evolution

¹Prakash J and ²Vinoth Kumar B

¹Department of CSE, PSG College of Technology, Coimbatore

²Department of Information Technology, PSG College of Technology, Coimbatore

ABSTRACT

Differential Evolution is one among the most robust and adaptable evolutionary optimization techniques in continual parameter spaces that has been developed in recent years. Differential evolution works in a similar way to a typical evolutionary technique on the basis of computing stages. Differential Evolution is one among the most adaptable and reliable population-based algorithms available, with multi-modal resilience. Since the introduction of differential evolution, it has attracted the attentions of numerous academicians across the world which has resulted in a variety of improved versions of the fundamental algorithm. Given the rapid advancement of Differential Evolution research as well as its application in a variety of fields of science and technology, we believe it is time to give a critical assessment of the most recent studies and to identify some significant future directions. Although several questions remain unanswered, new application areas are developing. This paper discusses some of the current Differential evolution trends in memetic algorithm like Knowledge Based Differential Evolution, Surrogate Model Differential Evolution, Hybrid Differential Evolution, Local Search Based Differential Evolution and some of the performance measures used to determine the effectiveness of the algorithm along with the various applications that the evolutionary algorithm can be deployed.

Keywords: Memetic Algorithm, Local Search Based Differential Evolution, Hybrid Differential Evolution, Surrogate Model Differential Evolution, Knowledge Based Differential Evolution.

I. INTRODUCTION

Differential Evolution (DE) was presented by Storn and Price in a progression to papers a decade ago, which is still a crust area for the researchers. Differential Evolution is primarily a global optimization method that uses a population-based stochastic algorithm. As of late differential evolution has acquired expanding interest for tackling optimization problems in numerous technical and scientific fields.

Differential Evolution is now regarded as the optimization approaches that are often utilized for continuous optimization problems. Differential evolution techniques are a kind of evolutionary technique, however unlike most other evolutionary algorithms, it doesn't have a natural paradigm and isn't physiologically based. Differential Evolution has performed admirably in a wide range of optimization tasks from diverse scientific domains.

Differential Evolution technique are a metaheuristic search technique based on population that improves a candidate solution through an evolutionary procedure. These algorithms will make few, if any, assumptions about the original optimization problem and will be able to rapidly explore large design spaces. With multi-modal problem robustness, the Differential Evolution approach is one of the most adaptive and stable population-based search techniques accessible.

Researchers have been motivated to design new or hybrid techniques for optimization algorithm as a result of evolutionary algorithms ability to produce closest solutions, such as hybrid MA, immune clonal algorithm, quantum evolutionary clustering technique, and so on. The use of evolutionary algorithms to large-scale challenges has inspired the scientific community's interest [24-28].

Despite the fact that research on and with Differential Evolution has progressed significantly over the last ten years, there are still numerous unresolved questions and new application areas to be explored. The search logic of the Differential Evolution structure has some limits because it contains a too limited set of investigation changes. This aspect has prompted numerous computer scientists to propose changes to the original algorithm in order to improve the existing Differential Evolutionary Technique. This paper discusses some of the most recent developments in DE research.

The objective of the paper is to provide an overview of various variants of memetic differential evolutionary techniques that are available in the literature, this paper also provide a study of different performance measures that shall be used in determining the efficiency of the evolutionary methods. Also the several applications where the evolutionary techniques can be used also been discussed.

The organization of the paper is organized as the variants of Differential evolutionary techniques in section 2, followed by the memetic algorithms in Section 3 followed by the performance measures in section 4 and application of evolutionary techniques in Section 5 followed by conclusion at section 6.

II. Variants of Differential Evolution

Since the proposal of Differential evolution by Prince and Storn in the 1990, It has become more powerful and successful technique in the field of optimization. With the popularity and usage in the various domain the differential evolution has advanced to a greater extends, with the number of variants in differential evolution are proposed and used by many researchers. Table 1 shows the information on the common and popular variants of DE [29-33]. In this section we will discuss on five of the following variants in DE shown in Table

1. Standard Differential Evolution (DE)
2. Self-adaptive Control Parameters Differential Evolution (JDE)
3. Self-Adaptive differential evolution (SADE)
4. Adaptive Differential Evolution with optional external archive (JADE)
5. Composite Differential Evolution (CoDE)

Table 1 Variants of Differential Evolution Technique

Variant of DE	Year	Author
DE	1997	Storn et al.,
JDE	2006	Brest et al.,
SADE	2009	Qin et al.,
JADE	2009	Zhang et al.,
CoDE	2011	Wang et al.,

A) Standard Differential Evolution (DE)

The Standard Differential Evolution method is a simple and straightforward evolutionary algorithm. This operates on the basis of cycle of stages. The various stages of standard differential evolution include: Initialization, mutation, Crossover / recombination, Selection.

- **Stage -1:** In initialization stage, based on the problem's total variables, the population will be initialized with random numbers. This stage will be followed by mutation,
- **Stage 2:** In mutation stage, the vector difference is determined, the appropriate mutation scheme for a given optimization issue is determined by the problem. Some of the mutation scheme like DE/rand-to-best/1, DE/best/1, DE/rand/1, etc.,
- **Stage 3:** The Crossover stage is used to increase the population vector's diversity. Where, it simply facilitates the creation of an offspring by combining elements from the current element and those produced via mutation. Binomial and Exponential are the major two types of crossover variants.
- **Stage 4:** The final stage of Selection is performed to determine the need for exclusive replacement, by identifying whether or not the trial or the goal vector survives to the following generation.

B) JADE

In Differential evolution, the performance may have a significant impact depending on the values selected for crossover probability (CR) and mutation factor (F). Researchers have proposed a number of self-adaptive techniques to handle these problems in order to dynamically adjust the control parameters without previous knowledge of the problem's features. JADE was suggested to enhance the conventional DE's performance by adding a novel mutation mechanism that adaptively changes control settings.

By adopting a novel mutation technique DE/current-to-p-best/ with an updating control parameters and optional external archive in an adaptive way, JADE is suggested to enhance optimization efficiency. The archive operation employs historical data to provide progress direction information, whereas the DE/current-to-p-best/ is a generalisation of the usual DE/current-to-best/.

Parameter adaptation in JADE automatically changes control parameters to appropriate values, the user's prior understanding of the link among parameter choices and optimization problem features is no longer required. As a result, it is useful for increasing the algorithm's robustness. In terms of convergence performance, JADE

outperforms or is comparable to other standard particle swarm optimization, adaptive or classic DE algorithms and other evolutionary algorithms in the literature. For problems that have reasonably high dimensionality, JADE with an external archive yields good results.

C) Composite DE (CoDE)

Wang et al. [32] recommend Composite Differential Evolution (CoDE) is one of the best Differential Evolution variations for global optimization. The primary goal of CoDE is to increase Differential evolutions performance by combining various efficient trial vector generation algorithms with many appropriate DE parameter settings that have complementing qualities.

- **Step-1:** In Composite Differential Evolution, a strategy pool is built in advance, that includes three very much examined trial vector generation techniques (i.e.,) (i) DE/rand/1/bin, (ii) DE/rand/2/bin and (iii) DE/current-to-rand/1.
- **Step-2:** A parameter pool including three pairs of CR and F is built in advance: (i) CR=0.2 & F=0.8, (ii) CR=0.1 & F=1.0 and (iii) CR=0.9 & F=1.0.
- **Step-3:** By adopting the three trial vector generation techniques in the strategy pool one at a time, three offspring are generated for every target vector.
- **Step-4:** Furthermore, every trial vector generation approach has a set of CR and F parameters picked at random from the parameter pool. As a result, the fittest of the three offspring is chosen as the trial vector.
- **Step-5:** Finally, the best individual from the target and trial vectors is chosen as the next generation's potential individual.

D) Self-adaptive control parameter differential evolution (JDE)

Brest et al., [29] proposed a technique, JDE which is a self-adaptive control parameter differential evolution that has demonstrated satisfactory results on benchmark problems. In JDE, the optimization method parameters are fine-tuned using the concept of evolution of the evolution process. Even though concept is appealing, proving that self-adaptation methods are convergent is a challenging task in practice.

The parameter control approach used in JDE depend on the self-adaptation of the DE evolutionary process's parameters CR and F, resulting in a flexible Differential evolution that adapts itself to reach the optimal optimization result. However, self-adaptive Differential evolution has a lot more parameters and all benchmark functions have fixed values. Those additional parameters do not need to be changed by the user.

The user does not have to guess which numbers are suitable and which are problem-specific when using the JDE approach. Because the principles for self-adapting control parameters is straightforward, this variant of the Differential evolution algorithm doesn't quite add to the time complexity of the original DE method.

E) SADE

The control parameters are the sole structural variation between the standard DE and SADE algorithm. Differential evolution uses three control parameters: (i) population size, (ii) crossover rate and (iii) mutation rate. Selection of appropriate parameter settings may increase DE efficiency, however selecting appropriate parameters is a complex and problem-dependent process in and of itself. Although a few parameters in the SADE algorithm must be fixed, the mutation operation is more crucial in the DE method's performance. Yet have numerous appealing characteristics, it has been found that Differential evolution does not always work as well as expected. Even if the population has not converged to a local optimum, scientific studies of Differential evolution has revealed that it may stop progressing toward a global optimum. It is self-adaptive in the

fact that the values of the control parameters CR and F vary based on various simple manipulations in each generation. The various stages of SADE include

- **Initialization:** Since the SADE population is based on stochastic search strategy, the initial population is necessary to begin the DE algorithm search. Every initial population is produced by evenly randomising individuals across the search space. Furthermore, for every initial individual real-valued string, starting values of the crossover rate and mutation factor are produced at random within a specified range.
- **Mutation:** Every vector in the existing population is considered as the target vector even before mutation operator is performed. A mutant vector is created for every target vector by combining the weighted differences between two random vectors to the third vector from the current population.

- Crossover: A trial vector is created by utilising a crossover procedure similar to uniform crossover to pick solution threshold value from either the mutant vector or its matching target vector.
- Selection: The objective function for every trial vector is assessed after crossover. Next, in terms of objective function values, every trial vector is matched to the appropriate target vector. For the next generation, the vector with the lower goal function value survives.

III. Memetic Algorithm

Memetic algorithms are variant of a classic evolutionary algorithm that attempts to model this behaviour. To increase the chances of early convergence, it employs a local search approach. The term Memetic algorithm is now frequently used to describe a problem-solving strategy that combines evolution or other population-based technique with distinct local improvement or individual learning procedures. In this section we will discuss on the different alternates of memetic DE algorithms like Knowledge based differential evolution, Surrogate Model Differential Evolution, Hybrid Differential Evolution, Local Search Based Differential Evolution. Table 2 shows the variants of memetic algorithm with their applications and performance measure [1-16].

Table 2: Details of the Variant of De with its Application and Performance Metrics

Year	Author	Variant of ME	Application	Performance Metrics
2019	Alam et al.,	Knowledge Based Differential Evolution	Image Compression	<ul style="list-style-type: none"> • Mean Square error • Compression ratio
2018	Qi et al.,		Industrial Internet of things.	<ul style="list-style-type: none"> • Response Time • Availability • Throughput • Trust
2016	Kumar et al.,		Image Compression	<ul style="list-style-type: none"> • Successful performance (SP). • Average number of function Evaluations (AFES) • Probability of convergence, • Optimization accuracy,
2019	Narloch et al.,		Protein structure prediction	<ul style="list-style-type: none"> • Energy Function
2021	Chen et al.,	Surrogate Model Differential Evolution	High-dimensional expensive optimization	<ul style="list-style-type: none"> • BEST • Worst • Mean • Standard deviation, • Wilcoxon test
2020	Zhao et al.,		Production optimization with nonlinear state constraints	<ul style="list-style-type: none"> • Ackley function • Rastrigin function
2019	Yang et al.,		Optimization problems with both equality and inequality constraints	<ul style="list-style-type: none"> • Effective Rate (ER) • Mean • Standard deviation, • t-test
2019	Wang et al.,		Expensive constrained optimization problems with inequality constraints.	<ul style="list-style-type: none"> • Successful Rate (SR) • Acceleration Rate (AR)
2020	Hassan et al.,	Hybrid Differential Evolution	Feature selection	<ul style="list-style-type: none"> • Time cost • Complexity of the network • Number of selected features, • Standard deviation, • Worst • Mean • BEST • Classification accuracy
2021	Rauf , et		Classification problems	<ul style="list-style-type: none"> • Standard deviation,

	al.,			<ul style="list-style-type: none"> • Worst • Mean • Best
2019	Nguyen et al.,		Resource constrained job scheduling	<ul style="list-style-type: none"> • Tightness of the instance constraints • Comparing by iterations • Comparing by run-time
2020	Wang et al.,		Image Classification	<ul style="list-style-type: none"> • Error rate
2019	Wu et al.,	Local Search Based Differential Evolution	Machine scheduling	<ul style="list-style-type: none"> • The average distance • Computational time • The ratio of non-dominated solutions
2017	Peng et al.,		Improved contraction criterion	<ul style="list-style-type: none"> • Friedman's test • Wilcoxon's signed-rank test • Function error value
2017	Wang et al.,		College students' comprehensive quality evaluation.	<ul style="list-style-type: none"> • Function error value • Wilcoxon's signed-rank test
2021	Mansueto et al.,		Clustering problems	<ul style="list-style-type: none"> • Gap(%)

3.1. Knowledge Based Differential Evolution

In KBDE the knowledge and characteristics are incorporated into the operations of differential evolution to obtain the enhanced outcome. This knowledge-based technique is proposed mainly to reduce the search.

- The knowledge shall be incorporated into the differential evolution operations as follows
- The chromosome is initialised using knowledge.
- Knowledge is incorporated in the selection of parent at different steps of mutation.
- Crossover operation is incorporated with knowledge.

The Differential evolution method has a low convergence rate, despite its outstanding global search capacity. The Differential evolution methods can employ characteristics and knowledge of the problem that will speed up the convergence rate, which is known as KBDE.

To accelerate the search, the information about the problem is used a knowledge base which are been unified into operators like initialization, mutation, and crossover.

- **Initialization:** Chromosomes are generated at random, but to build a better starting population than random ones, a knowledge base is employed.
- **Evaluation:** The goal is to calculate the survival probability of each chromosome. In this case, the problem's knowledge is employed in parent selection, accelerating up the search for the optimal solution.
- **Crossover:** The crossover operator combines the target and mutant chromosomes, and the knowledge is used to direct the search to the most viable solution.

Pseudocode 3.1: Knowledge-Based Differential Evolution

Step-1: Using Knowledge base, create a chromosome population.

Step-2: Examine the chromosomes.

Step-3: While the Max Population has not been achieved do

Step-3.1: Consider better N chromosomes with a lower unfitness value.

Step-3.2: Form sub-populations with the chromosomes that yield higher quality.

Step-3.3: Do all of the chromosomes

Step-3.3.1: The target chromosome is chosen;

Step-3.3.2: Three chromosomes are selected randomly from the subpopulation;

Step-3.3.3: Calculate the chromosome of the mutant;

Step-3.3.4: To make a trial chromosome, perform Knowledge base between the mutant and target chromosomes.

Step-3.3.5: Examine the chromosome of the trial;

Step-3.3.6: Replace the target chromosome with the trial chromosome if the trial chromosome's unfitness rating is smaller than the target chromosome's.

Step-4: End While

Step-5: Return the best-performing chromosome;

3.2. Surrogate Model Differential Evolution

In the recent years, Surrogates have demonstrated their ability to aid evolutionary techniques in tackling computationally intensive restricted optimization problems. Many approaches are used to create the surrogate model, including Kriging, neural network, polynomial regression, support vector regression and radial basis function.

This method generates an initial population, evaluates initial solutions, and then initialises the exclusive solution. After then, the algorithm continues the iterations until the completion criteria is met. To approximate the true aim and every constraint, Krigings are constructed at the start of each generation by employing the database's selected solutions as global surrogates. Secondly, a trial vector generation process generates offspring solutions for each parent solution. Following that, current population are modified using the classical Differential evolution selection operator. Then, to every solution, local Krigings is created to resemble the actual objective function. Then, for every solution, a localized search is performed to create a heir solution. Finally, the solutions that are feasible and impossible set are grouped into many clusters using fuzzy clustering. A optimal option then is chosen in each cluster using a restricted approach. The population of the later generation is also updated.

Pseudocode 3.3: Surrogate Model Differential Evolution

Step-1: Initialization: Randomly individual NP are generated

Step-2: Perform Differential Mutation

Step-2.1: Generate an individual affinity matrix for the current population.

Step-2.2: Individual probability matrices should be calculated.

Step-2.3: Select an individual at random from current population, then calculate the probability vector.

Step-2.4: Create the matching mutant individual for each person.

Step-3: To do recombination, use the conventional binomial crossover operator.

Step-4: Evaluation and selection: Utilise the surrogate model to estimate the objective value for each individual in the current population.

Step-5: Individuals who have been properly evaluated are utilised to progressively train the surrogate model at each iteration, resulting in a stronger model.

3.3. Hybrid Differential Evolution

Varied mutation methods have different effects on Differential evolutions performance. In hybrid differential evolution techniques, the novel mutation approach shall be incorporated with the different required procedure into classical differential evolution. This in hybridized with the methodology of PSO will improve the convergence rate and performance. In some cases, the strategy of novel population is combined by torus distribution to modify population range.

Pseudocode 3.3: Hybrid Differential Evolution

Step-1: Initial population is generated

Step-2: Evaluate the initialized population

Step-3: for Generation 1 to max do

Step-4: for individual 1 to total population do

Step-5: Random instance are selected that belong to the individuals

Step-6: Generate trial vector from minimum mutant vectors for total dimensions.

Step-7: Compute the mutant vector for every target vector.

Step-8: If Random individual population \leq Crossover

Step-9: Then trial vector = mutant vector.

Step-10: End If Trial vector = target vector

Step-11: End for if f(Trial vector = target vector) then

Step-12: Global fitness vector = trial vector

Step-13: End if Global fitness vector = target vector

Step-14: End for Generation = Generation + 1

Step-15: End for

3.4. Local Search Based Differential Evolution

Memetic algorithms have a number of advantages, one of which is that they allow Local search and Evolutionary algorithm methods to complement one and others in a form that compensates for both evolutionary algorithms deficiencies in local exploitation and local search inadequacies in global exploration.

The use of Differential evolution to tackle real-world issues has grown in recent times. A major reason for development is that, contrast to previous optimization approaches, differential evolution simply needs fitness values, making it relevant to a broader range of situations. Differential evolution has demonstrated its effectiveness in a variety of real-world settings, including developing optimum harmonic filters, and improving satellite pictures brightness and contrast, Greenhouse process modelling. In other applications, however, differential evolution confronts two issues: sluggish local optima stagnation and convergence speed.

To address these issues, Memetic differential evolution algorithms have recently been presented as an improvement to traditional DE techniques by including LS. In this regard, certain local search methods, as well as hybridizations of them, have been created and used to improve local modification of individuals in the process of global search. In cases when a standard differential evolutionary algorithm faces from local stagnation, a correctly integrated local search function is predicted to not only boost convergence and also generate more precise results.

Pseudocode 3.4: local search based differential evolution

Step-1: Generate N initial Target vectors randomly

Step-2: Target vectors of every Fitness is calculated

Step-3: Initial value is set

Step-4: Repeat

Step-5: Target vector is sorted

Step-6: If Generation local search frequency = 0

Step-7: Then local search is activated

Step-8: End If

Step-9: For every population do

Step-10: Set mutants and trials

Step-11: Calculate the fitness of trials and select new target.

Step-12: End for

Step-13: Using control methods update the levels

Step-14: Generation = Generation + 1

Step-15: until Maximum Fitness evaluation is reached

IV. Performance Evaluation

It is necessary to evaluate the developed evolutionary models to determine how efficiently does it work. To assess such performance, a variety of performance measures must be considered. These metrics are critical during the assessment and comparison of studied methods rely on their better outcomes. Even though there are numerous such performance measures in the field which can evaluate performance in these kinds of activities, there has yet to be a systematic study done to offer proof of their use. The primary focus of this section is to examine and quantify the several types of performance measures used in differential evolutionary research. The following performance metrics are being explored in the paper regarding the differential evolution.

a) Hypervolume (HV)

The hypervolume indicator is among the most frequently utilized set-quality indicators in evolutionary multiobjective optimization methods and stochastic multiobjective optimization. It is a measure determines the objective space region concealed by nondominated sets derived by multiobjective evolutionary algorithms with all objectives to also be reduced. The hypervolume may be calculated using the formula below in Eq .1.

$$\text{Hypervolume} = \text{Volume} \left(\bigcup_{j=1}^{|A|} X_j \right) \quad \rightarrow (1)$$

b) Pareto Front Size (PFS):

Pareto front size shows the every globally nondominated points generated at the evolutionary technique as the total generations is expanded. Turning a multi-objective optimization issue into a sequence of single-objective optimization problems is a common way to create Pareto fronts or by applying evolutionary techniques to create a collection of potential solutions to the Pareto set over time.

c) Generational distance (GD)

It is to determine how near the choices are to the true Pareto front. When Generational distance are equal to zero, then all non dominated solutions created that are found in the true Pareto front. The Generational distance is computed by below equation in Eq .2.

$$\text{Generational Distance} = \frac{\sqrt{\sum_{j=1}^N X_j}}{N} \quad \rightarrow (2)$$

d) Inverted generational distance (IGD)

Inverted generational distance was introduced as a better alternative to Generational distance due to the simple notion of inverting the sequence of the fronts that the Generational distance considers as input. The Inverted generational distance is computed by below equation in Eq .3.

$$\text{Inverted Generational Distance} = \frac{1}{|X|} \left(\sum_{i=1}^{|X|} d_i^a \right)^{\frac{1}{a}} \quad \rightarrow (3)$$

e) Spacing

The spacing metric is used to determine how evenly dispersed the nondominated set is. The method operates better when the spacing is minimal. The Spacing is computed by below equation in Eq .4.

$$\text{Spacing} = \sqrt{\frac{1}{N} \sum_{j=1}^N (d_i - d_a)^2} \quad \rightarrow (4)$$

f) Maximum Pareto Front Error(MPFE)

In the worst-case situation, MPFE determines the maximum distance in objective space between each person in the approximations front and the closest vector in the actual Pareto front as shown in in Eq .5. The algorithm is said to be better if the MPFE value is lower.

$$\text{Maximum Pareto Front Error} = \max d \quad \rightarrow (5)$$

Where, in objective space, d is the distances between the closest Pareto front solution and the nondominated solution.

g) Error Ratio:

Error ration is defined as the fraction of Pareto points that aren't true. The Error ratio is computed by below equation in Eq .6.

$$\text{Error Ratio} = \frac{\sum_{j=1}^N e(t_j)}{N} \quad \rightarrow (6)$$

Here, I represent the Individuals that are present in the approximation front and number of individuals is denoted as N. Smaller Error Ratio values indicate that there are fewer non-true Pareto points in X, and therefore stronger non-dominated groups.

h) Overall Non dominated vector generation Ratio (ONVGR)

During multiobjective evolutionary algorithms evolution, the number of non-dominated individuals identified in an approximation front is measured as Overall Non dominated vector generation. ONVGR is determined by below equation in Eq .7.

$$\text{Overall Non dominated vector generation Ratio}(C, N) = \frac{|C|}{|N|} \rightarrow (7)$$

It is determined as the ratio of optimal solution sets cardinality to the number of points in Pareto set.

i) Mean squared error (MSE)

Mean Squared Error is the most often used metric for determining the average square root between both the actual and derived solutions. Mean Squared Error is determined by below equation in Eq .8.

$$\text{Mean Square Error} = \frac{1}{N} \sum_{j=1}^N (P - Q)^2 \rightarrow (8)$$

j) Convergence

Convergence is defined as the algorithm's rate or speed. These variables will determine how quickly an algorithm achieves the target value. The estimated and actual effort may be used to determine the convergence process as shown in the equation in Eq .9.

$$\text{Convergence} = \sqrt{\frac{1}{N} \sum (P - Q)} \rightarrow (9)$$

V. Applications of Differential Evolution Techniques

Differential evolution, with its popularity and simplicity, it is used by the various researchers in their respective field based on their essentials. In this section we will discuss on the various areas of research, where the differential evolution and its variants are applied. Some of the areas include: Video Based Vehicle Classification, Power Plant Control, Healthcare, Text Summarization, Sentimental Analysis, Financial Time Series, Internet of Things, Remote Sensing, Cloud Computing, Software Engineering, etc.,

a) Job scheduling

Job scheduling issues with limited resources are common in real-world supply chain management and logistics. Organizations can more effectively use logistical resources and increase delivery performance by solving certain optimization challenges. Finding the best answer is difficult due to their intricacy. Existing solution approaches based on meta-heuristics and integer programming have demonstrated impressive outcomes for small instances, but when applied to large-scale instances with hundreds of jobs, they become inefficient. To handle resource restricted task scheduling issues, a hybrid optimisation strategy that combines the power of differential evolution, iterated greedy search, mixed integer programming, and parallel computing can be applied [3].

b) Image Classification

Convolutional Neural Networks has proven to be superior in image categorization, and evolutionary computation approaches have lately exploded in popularity as a way to automatically create CNN structures, saving the time and effort of manually designing CNNs. In image classification, the architectures of CNNs of any length are developed using an unique hybrid differential evolution approach with a newly introduced crossover operator called DECNN. [4].

c) Classification Problems

Differential evolution is simple and powerful technique in evolutionary methodology, which are been used to solve a variety of difficult optimization issues in a variety of scientific and engineering areas. DE has various drawbacks, such as a poor convergence rate and premature convergence, which results in the worst DE execution configuration. To address the difficulties noted above, two types of DE variants have been used: chaotic map hybridization and adaptive parameter selection-based DE (APSDE) based on PSO (CMHDE-PSO) and DE [2].

d) Power system:

The operation of the electrical system is becoming increasingly difficult in the current environment. Load frequency management is the most critical circumstance in power system control. To regulate the frequency of

electrical power systems, a hybrid differential evolution and pattern search (HDE-PS) approach shall be applied [17].

e) Feature selection

Because of its nonlinearity, Artificial Neural Networks (ANN) have been widely employed in scientific challenges and have attracted a large number of researchers as the most preferred tool for pattern classification, regression, and identification. The selection of number of nodes in each layer, number of layers, and proper weights is the most difficult aspect of ANN models. Because the number of layers and nodes affects the network's complexity, the training procedure will become more complicated. The multi-variant differential evolution (MVDE) method, a new population-based stochastic search technique, would be utilised to solve fifteen well-known real-world issues [1].

f) Protein Structure Prediction

In computational complexity theory, three-dimensional protein structure prediction is characterised as an NP-complete issue. Because precise algorithms are unable to handle this sort of issue, metaheuristics have emerged as effective tactics for locating answers in a reasonable amount of time. Protein Structure Prediction would be done using a Knowledge Based Differential Evolution Algorithm. [12].

g) Retinal Blood Vessel Segmentation

The automated or computer-assisted diagnosis of retinopathy relies heavily on retinal blood vessel segmentation. Blood vessel segmentation by hand takes a long time and requires a lot of topic expertise. The blood vessels are also only a few pixels wide and entirely obscure the fundus image. It makes them much more difficult for contemporary algorithms to properly automate retinal blood vessel segmentation. To perform autonomous retinal blood vessel segmentation, a modified differential evolution method would be used, in which the modified DE uses cross-communication across several populations [34].

h) Machine scheduling

Energy is critical to our survival as individuals and as a community. A challenge with scheduling unconnected parallel machines that is both energy-efficient and bi-objective with the goal of reducing both the manufacture span and overall energy consumption. The parallel machines have the ability to increase their processing speed. To solve these issues, a memetic differential evolution method is applied [13].

i) Clustering problems

Clustering is one of the most well-studied unsupervised learning issues. Its goal is to arrange a set of objects into logical groupings called clusters. Minimum Sum-of-Squares in Euclidean Geometry is one of a prominent model for a clustering problem is the MSSC. The topic continues to garner a lot of interest in the scientific literature due to its NP-hardness, and numerous heuristic techniques have been presented. Recent research has focused on improving the basic K-Means algorithm, by choosing the right initial configuration or including as a local search technique within a global optimization algorithm. A Memetic Differential Evolution method constructed on the frequent implementation of this algorithm from chosen configurations and particularly tailored for the MSSC issue to solve this problem [16].

VI. CONCLUSION

This paper offers an overview of the many variations of differential evolutionary approaches that are known in the literature, with the variants of differential evolution technique like DE, SADE, CoDE, JDE, JADE are discussed, Also a study of different memetic algorithm strategies like Knowledge Based Differential Evolution, Surrogate Model Differential Evolution, Hybrid Differential Evolution, Local Search Based Differential Evolution is presented. The several performance metrics that shall be used to determine the effectiveness of the evolutionary methods like Hypervolume (HV), Maximum Pareto Front Error(MPFE), Inverted generational distance (IGD), Pareto front size (PFS), Overall Non dominated vector generation Ratio (ONVGR), Generational distance (GD), Spacing, Error Ratio(ER), Mean squared error (MSE), Convergence and the various application fields in which evolutionary methods can be applied have also been addressed.

REFERENCES

1. Hassan, S., Hemeida, A. M., Alkhalaf, S., Mohamed, A., & Senjyu, T. (2020). Multi-variant differential evolution algorithm for feature selection. *Scientific Reports*, 10(1). <https://doi.org/10.1038/s41598-020-74228-0>
2. Rauf, H. T., Bangyal, W. H., & Lali, M. I. (2021). An adaptive hybrid differential evolution algorithm for continuous optimization and classification problems. *Neural Computing and Applications*. <https://doi.org/10.1007/s00521-021-06216-y>

3. Nguyen, S., Thiruvady, D., Ernst, A. T., & Alahakoon, D. (2019). A hybrid differential evolution algorithm with column generation for resource constrained job scheduling. *Computers & Operations Research*, 109, 273-287. <https://doi.org/10.1016/j.cor.2019.05.009>
4. Wang, B., Sun, Y., Xue, B., & Zhang, M. (2020). A hybrid differential evolution approach to designing deep convolutional neural networks for image classification. <https://doi.org/10.26686/wgtn.13158293.v1>
5. Chen, G., Li, Y., Zhang, K., Xue, X., Wang, J., Luo, Q., Yao, C., & Yao, J. (2021). Efficient hierarchical surrogate-assisted differential evolution for high-dimensional expensive optimization. *Information Sciences*, 542, 228-246. <https://doi.org/10.1016/j.ins.2020.06.045>
6. Yang, Z., Qiu, H., Gao, L., Jiang, C., Chen, L., & Cai, X. (2019). A novel surrogate-assisted differential evolution for expensive optimization problems with both equality and inequality constraints. *2019 IEEE Congress on Evolutionary Computation (CEC)*. <https://doi.org/10.1109/cec.2019.8790113>
7. Zhao, X., Zhang, K., Chen, G., Xue, X., Yao, C., Wang, J., Yang, Y., Zhao, H., & Yao, J. (2020). Surrogate-assisted differential evolution for production optimization with nonlinear state constraints. *Journal of Petroleum Science and Engineering*, 194, 107441. <https://doi.org/10.1016/j.petrol.2020.107441>
8. Wang, Y., Yin, D., Yang, S., & Sun, G. (2019). Global and local surrogate-assisted differential evolution for expensive constrained optimization problems with inequality constraints. *IEEE Transactions on Cybernetics*, 49(5), 1642-1656. <https://doi.org/10.1109/tcyb.2018.2809430>
9. Alam, Lamia & Dhar, Pranab & Hasan, Mirza & Golam, Mohammed & Bhuyan, Sarwar & Daiyan, Golam. (2019). An Improved JPEG Image Compression Algorithm by Modifying Luminance Quantization Table.
10. Qi, J., Wang, Z., Xu, B., Wu, M., Gao, Z., & Sun, Y. (2018). Qos-driven adaptive trust service coordination in the industrial Internet of things. *Sensors*, 18(8), 2449. <https://doi.org/10.3390/s18082449>
11. Kumar, B. V., & Karpagam, G. (2016). Knowledge-based differential evolution approach to quantisation table generation for the JPEG baseline algorithm. *International Journal of Advanced Intelligence Paradigms*, 8(1), 20. <https://doi.org/10.1504/ijaip.2016.074776>
12. Narloch, P. H., & Dorn, M. (2019). A knowledge based self-adaptive differential evolution algorithm for protein structure prediction. *Lecture Notes in Computer Science*, 87-100. https://doi.org/10.1007/978-3-030-22744-9_7
13. Wu, X., & Che, A. (2019). A memetic differential evolution algorithm for energy-efficient parallel machine scheduling. *Omega*, 82, 155-165. <https://doi.org/10.1016/j.omega.2018.01.001>
14. Peng, L., Zhang, Y., Dai, G., & Wang, M. (2017). Memetic differential evolution with an improved contraction criterion. *Computational Intelligence and Neuroscience*, 2017, 1-12. <https://doi.org/10.1155/2017/1395025>
15. Wang, Y., Ding, Z., Zuo, M., & Peng, L. (2017). An improved memetic differential evolution for college students' comprehensive quality evaluation. *International Journal of Wireless and Mobile Computing*, 13(3), 193. <https://doi.org/10.1504/ijwmc.2017.088528>
16. Mansueto, P., & Schoen, F. (2021). Memetic differential evolution methods for clustering problems. *Pattern Recognition*, 114, 107849. <https://doi.org/10.1016/j.patcog.2021.107849>
17. J. H. Van Sickle, K. Y. Lee and J. S. Heo, "Differential Evolution and its Applications to Power Plant Control," 2007 International Conference on Intelligent Systems Applications to Power Systems, 2007, pp. 1-6, doi: 10.1109/ISAP.2007.4441675.
18. Ling, S.H.; Lam, H.K. Evolutionary Algorithms in Health Technologies. *Algorithms* 2019, 12, 202. <https://doi.org/10.3390/a12100202>
19. S. Karwa and N. Chatterjee, "Discrete Differential Evolution for Text Summarization," 2014 International Conference on Information Technology, 2014, pp. 129-133, doi: 10.1109/ICIT.2014.28.
20. Onan, Aytug & Korukoğlu, Serdar & Bulut, Hasan. (2016). A Multiobjective Weighted Voting Ensemble Classifier Based on Differential Evolution Algorithm for Text Sentiment Classification. *Expert Systems with Applications*. 62. 10.1016/j.eswa.2016.06.005.

21. J. Li, J. Liu and J. Wang, "An Improved Differential Evolution Task Scheduling Algorithm Based on Cloud Computing," 2018 17th International Symposium on Distributed Computing and Applications for Business Engineering and Science (DCABES), 2018, pp. 30-35, doi: 10.1109/DCABES.2018.00018.
22. Shailendra Pratap Singh, Vibhav Prakash Singh, Ashok Kumar Mehta, Differential evolution using homeostasis adaption based mutation operator and its application for software cost estimation, *Journal of King Saud University - Computer and Information Sciences*, Volume 33, Issue 6, 2021, Pages 740-752, ISSN 1319-1578, <https://doi.org/10.1016/j.jksuci.2018.05.009>.
23. Dawar, Deepak & Ludwig, Simone. (2018). A Differential Evolution Based Multiclass Vehicle Detector and Classifier for Urban Environments. 10.4018/978-1-5225-5643-5.ch067.
24. Viswajaa S, Vinoth Kumar B, Karpagam GR. Survey on Nature Inspired Meta-Heuristics Algorithms in Optimizing the Quantization Table for the JPEG Baseline Algorithm. *International Advanced Research Journal in Science, Engineering and Technology*. 2015;2(4):14–123.
25. Vinoth Kumar B, Karpagam GR, Zhao Y. Evolutionary algorithm with memetic search capability for optic disc localization in retinal fundus images. In: *Intelligent Data Analysis for Biomedical Applications*. Elsevier; 2019. p. 191–207.
26. Rajesh R, Mathivanan B. Predicting Flight Delay using ANN with Multicore Map reduce framework, *Communication and Power Engineering*. In Walter de Gruyter GmbH & Co KG; 2017.
27. Kumar BV, Jeneessha P, Nivethitha M. A differential evolutionary algorithm for image segmentation of white blood cells in acute lymphoblastic leukaemia images. In: 2020 Fourth International Conference on Inventive Systems and Control (ICISC). IEEE; 2020.
28. Hemanth DJ, Kumar BV, Manavalan GR. Recent advances on Memetic algorithms and its applications in image processing. Springer Nature; 2019.
29. Brest, Janez & Greiner, Sao & Bošković, Borko & Mernik, Marjan & Zumer, Viljem. (2007). Self-Adapting Control Parameters in Differential Evolution: A Comparative Study on Numerical Benchmark Problems. *Evolutionary Computation, IEEE Transactions on*. 10. 646 - 657. 10.1109/TEVC.2006.872133.
30. Storn, R., Price, K. Differential Evolution – A Simple and Efficient Heuristic for global Optimization over Continuous Spaces. *Journal of Global Optimization* 11, 341–359 (1997). <https://doi.org/10.1023/A:1008202821328>
31. Zhang, Jingqiao & Sanderson, A.C.. (2009). JADE: Adaptive Differential Evolution With Optional External Archive. *Evolutionary Computation, IEEE Transactions on*. 13. 945 - 958. 10.1109/TEVC.2009.2014613.
32. Wang, Yong & Cai, Zixing & Zhang, Qingfu. (2011). Differential Evolution With Composite Trial Vector Generation Strategies and Control Parameters. *Evolutionary Computation, IEEE Transactions on*. 15. 55 - 66. 10.1109/TEVC.2010.2087271.
33. A. Sivasuriyan, D. S. Vijayan, R. Munusami, and P. Devarajan, "Health assessment of dams under various environmental conditions using structural health monitoring techniques: a state-of-art review," *Environmental Science and Pollution Research*, Oct. 2021, doi: 10.1007/s11356-021-16749-3.
34. Qin, A., Huang, V., & Suganthan, P. (2009). Differential evolution algorithm with strategy adaptation for global numerical optimization. *IEEE Transactions on Evolutionary Computation*, 13(2), 398-417. <https://doi.org/10.1109/tevc.2008.927706>
35. Kamlesh Mistry, Biju Issac, Seibu Mary Jacob, Jyoti Jasekar and Li Zhang. (2018). Multi-Population Differential Evolution for Retinal Blood Vessel Segmentation. *International Conference on Control, Automation, Robotics and Vision (ICARCV)*, 978-1-5386-9582-1

Design and Fabrication of Control Circuit for Boost Converter of Solar Panel in Wind-Solar Hybrid System

P. Sweety Jose¹, P. Subha Hency Jose² and Amirtha R. S³

^{1,3}Department of EEE, PSG College of Technology, Coimbatore

²Department of Biomedical Engineering, PSG College of Technology

ABSTRACT

In this paper, a MW class wind-solar hybrid park has been studied and design of control circuit for the boost converter of solar panel is presented. The solar panel is integrated with the already running Wind turbine. An analog control circuit has been designed using PLECS software to generate PWM pulse for constant output voltage of 1200V from the boost converter in accordance with the varying solar input. Using the voltage feedback approach, a boost converter may step up from a fluctuating or changing input voltage to a greater constant dc output voltage. The output of the converter is measured and compared to a reference voltage using this approach. The difference between the two values will be utilized to generate a pulse width modulation signal that will be used to operate a switch in the boost converter.

Keywords—hybrid, boost converter, controller, solar panel, PLECS

I. INTRODUCTION

One of the most basic requirements for a country's economic success is a stable and constant electricity supply. Fossil fuel sources are rapidly diminishing over the planet. In the current context, fossil fuels meet the vast bulk of energy demand. Renewable energy methods such as solar, biomass, geothermal, and wind meet a modest portion of the demand [1]. There will soon come a time when the entire planet will be suffering from a catastrophic fuel scarcity. Solar and wind energy have grown at an astonishingly quick rate in recent years. Both are renewable energy sources with plenty of power.

Asia Pacific countries utilise a huge amount of energy due to their rapid economic expansion. Despite the global financial crisis, these countries' energy demand is increasing. In comparison to Japan, Russia, and China, India utilises the most energy for residential, agricultural, and commercial reasons.

An ideal wind and solar hybrid system creates electrical energy by combining wind turbines and solar PV with an effectively shared infrastructure, enabling for improved economic and social usage of all resources[4]. Wind Solar True Hybrid is a concept in which the electricity provided by both wind and solar generators is combined at the system or inverter level. The wind-solar hybrid system comprises of a wind turbine, a solar photovoltaic battery, a controller, a battery, an alternating current/direct current load, and other components. The Controller is in charge of the PV array's and wind turbine's energy management, as well as battery charging. [3]. The power capacity of the wind turbine is limited by the inverter, power transformer, and evacuation lines (1.5MW in test case). The majority of the solar panels are installed on the site designated for the wind turbine. This allows the hybrid system to optimally utilise the whole shared infrastructure between wind and solar and give higher advantages to society[5]. Individual measurements at the solar and wind portions are recommended to determine the generation breakdown.

The advantages of a hybrid system include greater grid stability, better utilization of land, better plant load factor, reduced cost of evacuation, higher efficiency of inverter, faster execution[2].

II.BACKGROUND

A. Boost Converter

Boost converters are widely employed in the regulation of switch mode DC power supply. Normally, the converter's DC input voltage swings, therefore the average output voltage must be adjusted to be equivalent to the target value[6].

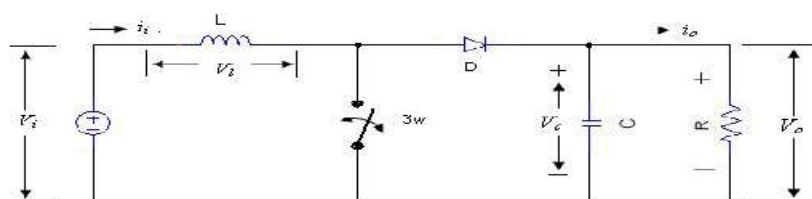


Fig. 1. Boost converter circuit

As illustrated in Fig. 1, the output voltage of the boost converter circuit may be changed from the input voltage up to many times the input voltage. The energy is stored in the inductor's magnetic field (L). The inductor (L) conducts current (i_L), and the voltage across the inductor equals the input voltage (V_i).

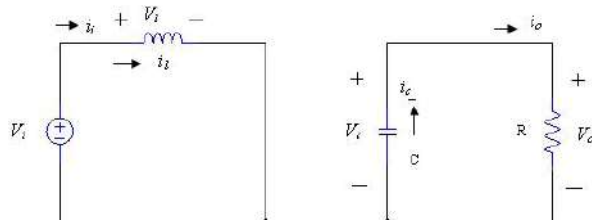


Fig. 2. Converter circuit when the switch Sw is closed

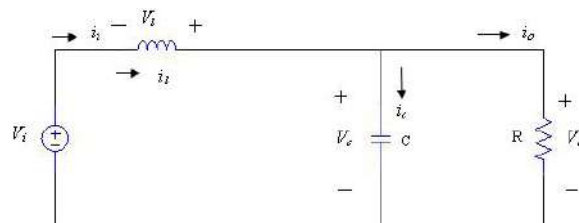


Fig. 3. Converter circuit when the switch Sw is open

When the switch is open, as illustrated in Fig. 3, the inductor's stored energy is transmitted to the capacitor (C) and the load (R) via the diode (D). To raise the output voltage (V_o), the voltage across the inductor reverses and adds to the input voltage (V_i)

$$V_o = V_i / (1 - D)$$

Where D is the duty ratio which is the ratio of the width of the pulse (T_{on}) to the total time period of the waveform (T).

III. DESIGN OF CONTROL CIRCUIT

A. Overall block diagram of wind-solar true hybrid

Fig. 4 shows the overall block diagram of wind-solar true hybrid.

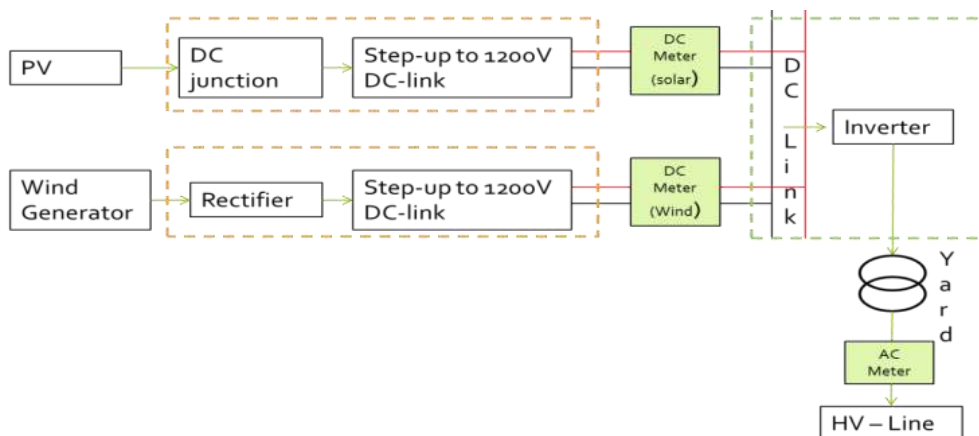


Fig. 4. Overall block diagram of wind-solar true hybrid

the wind generator's (pmsg - changing ac) energy is converted into dc and stepped up to a constant dc voltage through a step-up chopper. this continuous dc is distributed over a massive capacitor bank (the dc-link capacitors). the energy generated by solar photovoltaic panels (spv) is a variable direct current (dc) that is stepped-up to a constant direct current voltage (same as wind) and made available via the same dc-link capacitors. the wind-solar hybrid grid-tied inverter will invert the electric power available across this common dc-link, which is then transformed and fed into the hv line (where it is metered for billing). the power evacuated from this hybrid is limited to the capacity of the wind turbine, for example 1.5mw. the hybrid inverter's control system is created in such a way that the electrical energy pumped from the solar pv and wind generators is intelligently controlled to be capped at 1.5mw (within the available evacuation limits). multi-mppt (each step-up igt section in the hybrid unit operates at individual mppt) option is enabled in the hybrid unit to generate maximum power from the solar park when integrating large solar installations (>500kwp) with the wind turbine.

IV Block diagram of the control circuit

The output of the converter is measured and compared to a reference voltage in Fig. 5. The difference between the compared values will be utilised to generate a pulse width modulation signal that will be used to drive the switch in the boost converter.

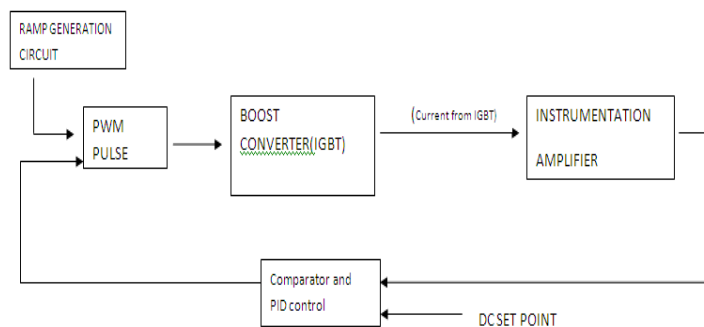


Fig. 5. Block diagram of the control circuit

Block diagram for Ramp Generation

In the below circuit, a switch is turned on and off between +10V and -10V based on a control signal. The switching on and off is controlled by the ramp pulse itself as feedback. A zero crossing detector produces the control signal of required frequency

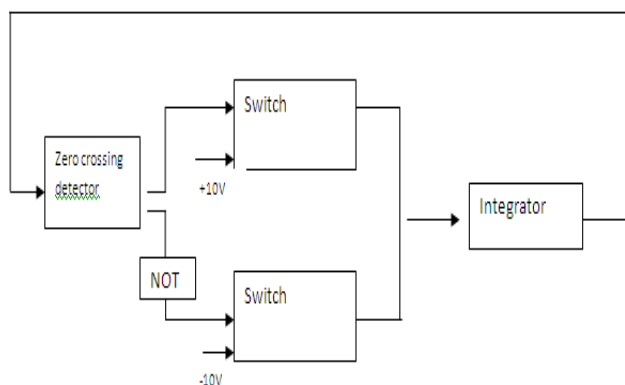


Fig. 6. Ramp Generation block diagram

IV SIMULATION

The simulation is carried out using PLECS software which is installed as a plug-in in MATLAB.

A. Simulation of overall circuit

Fig. 7 shows overall circuit which is simulated using MATLAB. It consists of three PLECS circuits namely Ramp generation circuit, PWM generation circuit and boost converter circuit.

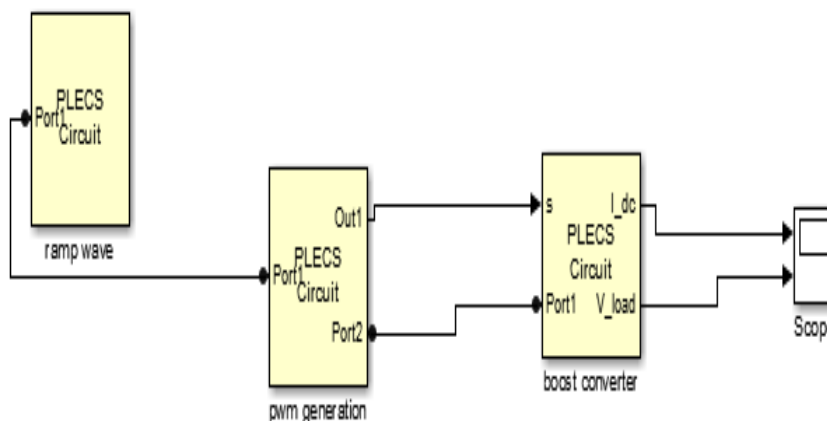


Fig. 7. Simulation of the overall circuit

B. Simulation of ramp generation circuit

Fig. 8 shows ramp generation circuit which is simulated using PLECS tool in MATLAB.

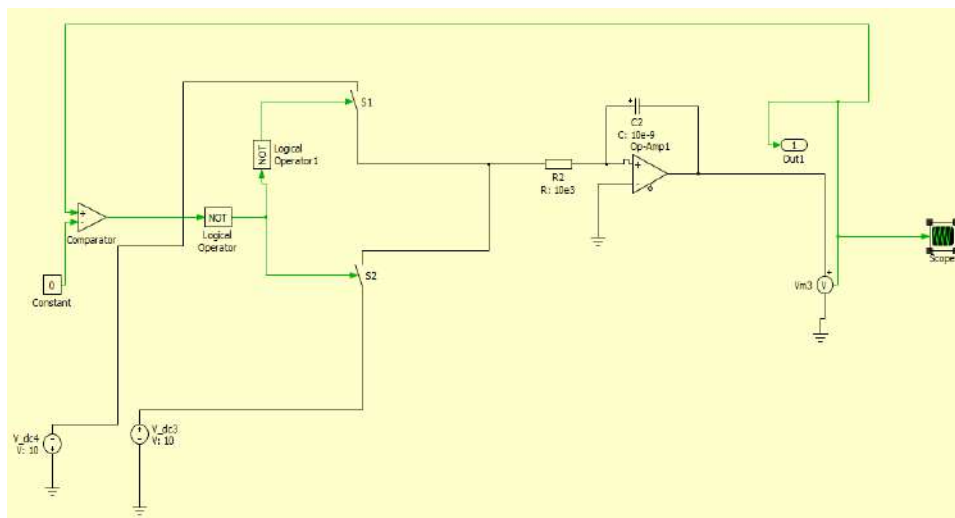


Fig. 8. Simulation of ramp generation circuit

C. Simulation of PWM generation circuit

Fig. 9 shows PWM pulse generation circuit which is simulated using PLECS tool in MATLAB.

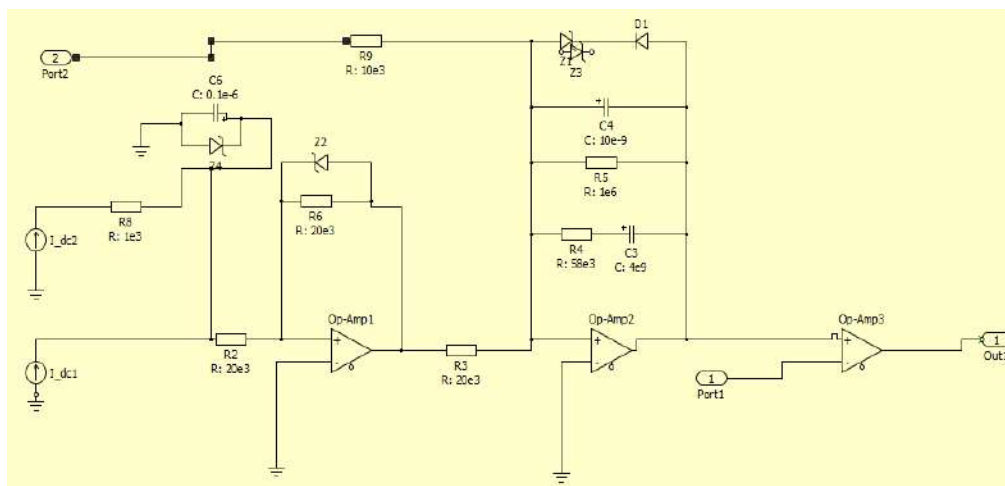


Fig. 9. Simulation of PWM generation circuit

D. Simulation of boost converter circuit

Fig. 10 shows boost converter circuit which is simulated using PLECS tool in MATLAB[7],[8].

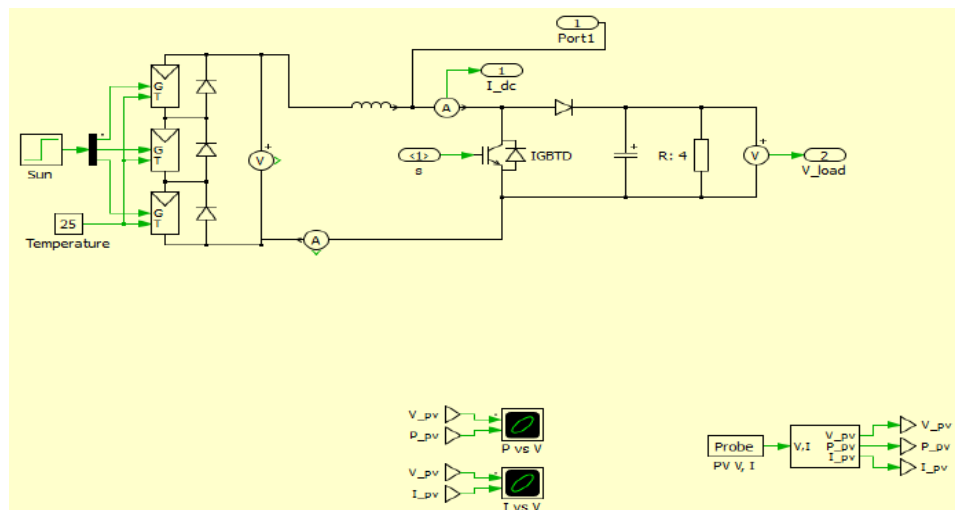


Fig. 10. Simulation of boost converter circuit

V. FABRICATION

The following ICs are used for the fabrication of the control circuit.

A. Instrumentation Amplifier

The instrumentation amplifier INA114 from Texas Instruments is utilised. The INA114 is a low-cost general-purpose instrumentation amplifier with a three-operational-amplifier (OP-AMP) architecture. A single external resistor R_g may be used to adjust any gain between 1 and 10,000.

$$\text{Gain} = 1 + (50k/R_g)$$

Figure 11 shows the functional block diagram of the Instrumentation Amplifier INA114. 11.

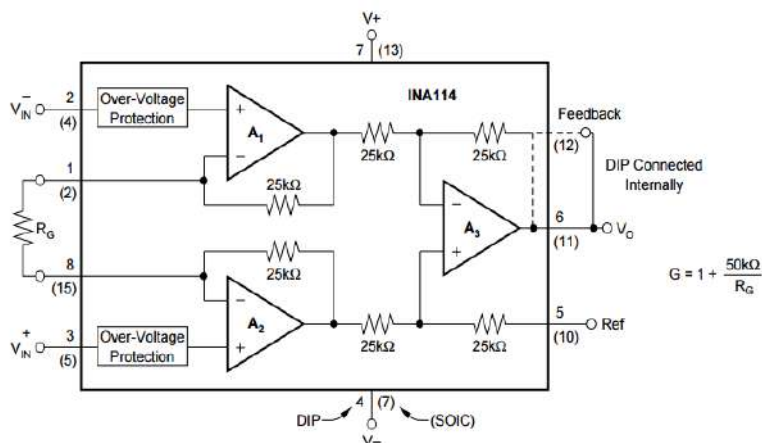


Fig. 11 .Functional block diagram of Instrumentation Amplifier INA114

B. Sawtooth Generation

Frequency is between 2.3 – 2.9 kHz .The following OP-AMPS are used in the sawtooth generation circuit

CMOS Quad 2 Input NAND Schmitt Triggers - Texas Instruments CD4093B: It is made up of four Schmitt trigger circuits. Each circuit operates as a two-input NAND gate with schmitt trigger on both inputs. For positive and negative going signals, the gate changes at various locations. The hysteresis voltage is defined as the difference between positive and negative voltage. This may be used to function as a wave shaper. The Functional block diagram of Texas Instruments CD4093B is shown in Fig. 12.

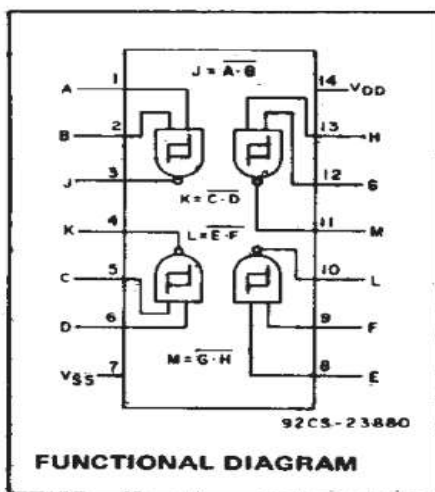


Fig. 12 .Functional block diagram of Texas Instruments CD4093B

DG444 – They are monolithic CMOS analog switches. They have four independent single pole single throw (SPST) analog switches as well as a TTL and CMOS compatible digital input.

V EXPERIMENTAL SET-UP

The control circuit which is designed using PLECS is fabricated on the PCB and shown in Fig. 13 .Then testing is done on the PCB by applying test conditions. The ramp wave and PWM pulses are obtained and the waveforms are captured in the CRO.



Fig. 13.Experimental Set-up

VI.RESULTS AND DISCUSSION

The simulation results obtained in the PLECS software are shown in Fig. 14 and Fig. 15 .

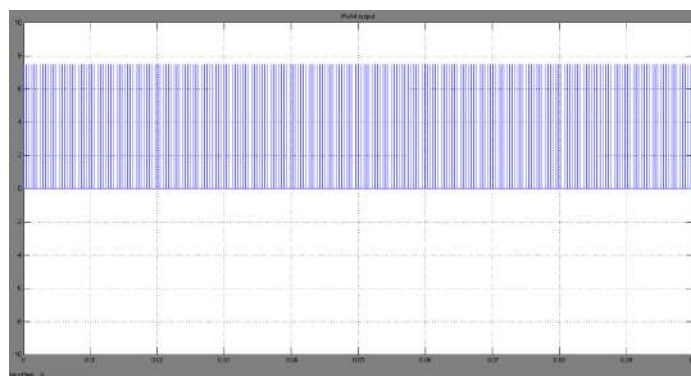


Fig. 14 .PWM pulse output

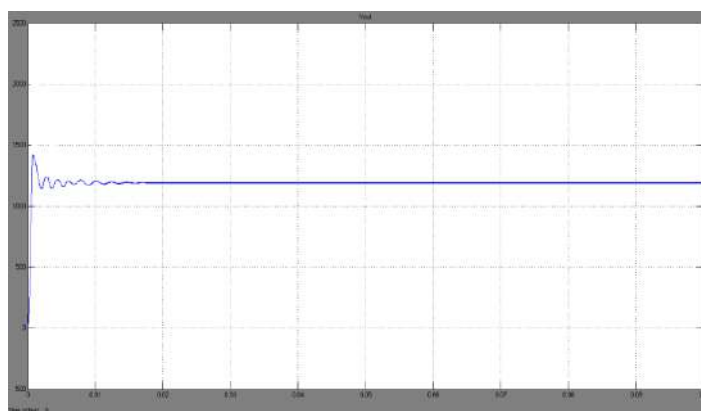


Fig. 15 .Output voltage

In Fig. 14,the PWM pulse obtained has the required frequency of 2.4kHz for the boost chopper .These PWM pulses when given as input to the IGBT in the boost chopper ,output voltage of 1200V is obtained as in Fig. 15

The ramp wave and PWM pulses generated using the experimental set-up and captured in the CRO are shown in Fig. 16 and Fig. 17 respectively.

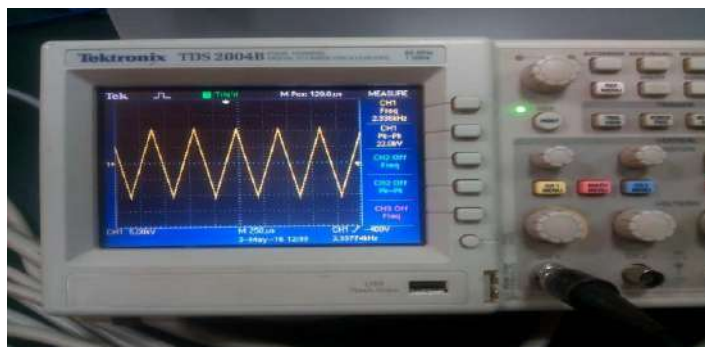


Fig. 16 .Ramp wave

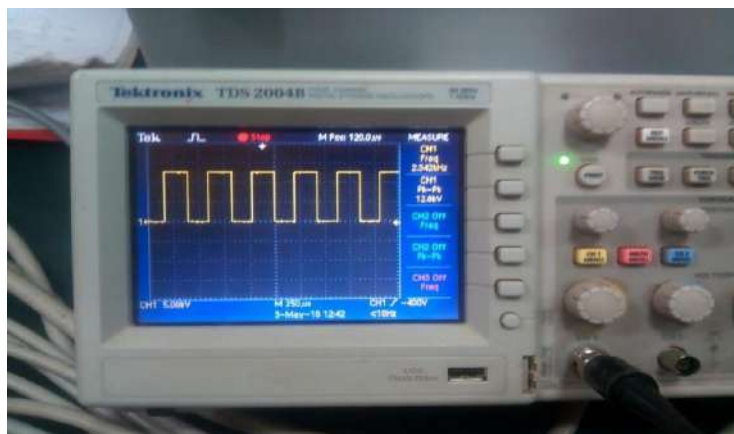


Fig. 17. PWM pulses

The ramp wave and the PWM pulses generated using the experimental set-up have frequencies in the range of 2.336 kHz and 2.342 kHz respectively.

VI. CONCLUSION

thus, a control circuit for producing pwm pulses for a constant output voltage of 1200v from the boost converter in response to fluctuating solar input has been conceived and built. the experimental set-up yielded findings that were similar to those obtained from simulation. the experimental setup has been evaluated in the laboratory under a variety of test situations and has proven to be effective. after performing basic testing on-site, the setup is ready to use with the power circuit that is integrated with the grid.

REFERENCES

1. Stanley R. Bull, —Renewable Energy Today and Tomorrow, Proceedings of the IEEE, vol. 89, no. 8, pp. 316-381, August 2001.
2. J. A. Castle , J. M. Kallis , S. M. Moite and N. A. Marshall, "Analysis of Merit of Hybrid Wind/Photovoltaic Concept for Stand Alone Systems", Proc. of the 15-th IEEE PV Specialists Conference, pp. 734-744, 198
3. Xing Zhang, Renxian Cao, Solar photovoltaic (PV) grid power generation and its control inverter. Beijing: Mechanical Industry Press
4. Mehdi dali, jamel Blhadj and Xavier Roboam: Design of a stand-alone hybrid photovoltaic-wind hybrid system with battery storage, IEEE Transaction.
5. M. Liserre, T. Sauter, J.Y. Hung :Future Energy Systems:-Integrating Renewable Energy Sources into the Smart Power Grid Through Industrial Electronics, IEEE Industrial Electronics Magazine , 2010.
6. K. Bose, Modern Power Electronics and AC Drives, Pearson Education, 2003.
7. Average Irradiance during the year, <http://solarelectricityhandbook.com/solar-irradiance.html>
8. Average Temperature during the year, <http://www.holiday-weather.co/Alexandria/averages/>

Ensemble Based Approach for Early Prediction of Alzheimer's Disease

Kavitha C, Narmatha R, Aishvarya G, Sharadha K, Thamil Vani S and Lavanya G

Department of CSE, PSG College of Technology, Coimbatore, India

ABSTRACT

Alzheimer's Disease (AD) is a neurological disorder that is capable of shrinking the brain causing cells in the brain to die, which has no cure till date. It is thought to be caused by the abnormal buildup of proteins in and around brain cells. It is difficult to notice any symptoms when the initial changes are happening, because the brain is attempting to correct them so the individual can function normally. However, with increasing neuronal damage, the brain is not able to correct them and patients start showing some cognitive decline. Researchers believe that this degeneration of neurons in the brain occurs at least 10 years before diagnosis. The significant brain structure changes can be measured by Magnetic Resonance Imaging (MRI) scan. Healthcare organizations are becoming increasingly keen on how artificial intelligence can support better patient care while reducing costs and improving efficiencies. In the recent decade, Convolutional Neural Network has been widely used for image classification tasks with excellent performance. AlexNet and Lenet are Convolution Neural Network models which have had a huge impact on the field of machine learning and computer vision. The proposed system makes use of ensembled Alexnet and Lenet machine learning models to get the best possible result for the early prediction of Alzheimer's Disease, which makes it possible for people to participate in clinical trials to test the latest therapies so that the disease can be prevented or controlled to some extent.

Keywords—Machine Learning, Ensemble, Neuroimaging

INTRODUCTION

Alzheimer's Disease (AD) is a neurological disease in which the brain cells will be dead which will cause memory loss and cognitive decline to people [1]. Generally, the people aged over 65 years are affected by this Alzheimer's disease and the younger ones are affected only by 10% [2]. Alzheimer's disease is a condition that affects the human's brain. At first, the symptoms are mild and over time it is more severe causing serious issues. There are common symptoms for this disease and these include memory loss, language problems and unpredictable behaviour. One of its main conditions is the presence of plaques and tangles in the brain [3].

Another one is the connection loss between the nerve cells, or neurons, in the brain. Connection loss means that the information cannot easily pass between the different areas of the brain. As the symptoms get worse the people who are affected find it difficult to remember the recently happened events or things and to identify the people they know well. Hence, a person affected by Alzheimer's disease must need full-time assistance.

This disease was named after Dr. Alois Alzheimer [3-4]. In 1906 he examined the brain of a woman and he found that she had died of mental illness that affected her memory which causes unpredictable behaviour. He noted abnormal clumps and tangled bundles of fibres in the patient's brain. Now they are called as amyloid plaques and neurofibrillary or tau tangles, respectively. It is now considered as one of the main symptoms of Alzheimer's disease.

Alzheimer's disease is a progressive disease, as the symptoms get worse over time/days/years. One of the main conditions is memory loss and it is found to be the first symptom to develop after a person is affected by Alzheimer's disease.

The symptoms get worse gradually, over months or years. If symptoms get worse over hours or days, that person must require immediate medical attention, because it could lead to a stroke. A person may find difficulty in reasoning, complex tasks, and judgment. It may lead to: Difficulty with the tasks that have several stages to complete, Difficulty in handling money or paying bills, Poor understanding of safety and risks, Difficulty in making proper decisions.

A person may find changes in their personality and behavioural changes which include: Poor interest in activities they do usually, Compulsive, obsessive, or socially inappropriate behaviour, Loss of empathy, Often get upset, angry, or worried more than before. This will lead to: Wandering or getting lost, Difficulty in remembering things which causes repeating questions or conversations, Difficulty in remembering their daily activity or appointment, Difficulty in remembering the things where they placed. A person may find it difficult to recognize faces or objects or be unable to use basic tools. These problems occurred due to difficulty in remembering and not due to eyesight problems.

Inside each healthy adult human brain there are about 100 billion neurons, with branching extensions that enable them to communicate with one another. The connections between neurons are called synapses, which release and detect chemicals to help the flow of information between neurons [5]. Increasing the level of the abnormal form of protein tau (tau or neurofibrillary tangles) inside the neurons and increasing the level of protein beta-amyloid (beta-amyloid plaques) outside of neurons are two of the main changes in a brain affected by Alzheimer's disease [6].

Beta-amyloid plaques interrupt the communication between neurons and cause cells to die while tau tangles block the reception of the nutrients and other essential molecules inside neurons. Because of these changes, the brains of people with severe Alzheimer's disease shrink due to cell loss [7]. In brain scans one can see the widespread debris and inflammation inside the brain as a result of the dead neurons.

Currently there is no proper diagnosis treatment which slows down the progression of Alzheimer's disease. There are some drugs available which only reduce the symptom of confusion and memory loss which is a short-term treatment [8].

LITERATURE SURVEY

L.Khedher J. Ramirez, J.M. Gorriz, in [9] presented a Computer Aided Designing system which predicts Alzheimer's Disease earlier by utilizing pictures of tissue segmented cerebrum. The system intends to classify between Mild Cognitive Impairment (MCI), Elderly Normal Control (NC), and AD and depends on a few methods like Partial Least Squares (PLS) and Principal Component Analysis (PCA).

Jack Albright in [10] developed a novel technique called All Pairs technique which involved studying the comparison of different pairs of data for patients. The method is found to be effective in classifying AD and MCI patients with an accuracy of 86.6%

Modupe Odusami, Rytis Maskeliunas, Robertas Damaševičius and Tomas Krilavicius in [11] developed an 18-layer Neural Network model called Resnet18 which performed better than the other known models present at that time. The method makes use of regularization technique during the training stage which increased the accuracy of classification.

Fedorov, Alex and Hjelm, R Devon and Abrol, Anees and Fu, Zening and Du, Yuhui and Plis, Sergey and Calhoun, Vince D in [12] developed an unsupervised machine learning model called Deep InfoMax and trained the model with datasets from Alzheimer Disease Neuroimaging Initiative (ADNI). The method shows potential utility of Deep InfoMax model in medical field.

M. Puranik, H. Shah, K. Shah and S. Bagul in [13] developed a Convolutional Neural Network model for classification of Alzheimer's disease in order to decrease the efforts and money involved in consulting a doctor. The method made use of pre trained models which involved transfer learning concepts and made use of Inception Resnet V2 model for classification.

Xia, Zaimin and Yue, Guanghui and Xu, Yanwu and Feng, Chiyu and Yang, Mengya and Wang, Tianfu and Lei, Baiying in [14] proposed a novel method which used 3D convolutional Long Short-Term Memory (3D CLSTM) to predict Alzheimer's disease. The model was trained on ADNI dataset and was highly effective in terms of accuracy.

Atif Mehmood, Shuyuan yang, Zhixi feng, Min wang, AL Smadi Ahmad, Rizwan khan, Muazzam Maqsood, Muhammad Yaqubin [15] proposed a method that uses VGG16 architecture with pre-trained weights from Transfer Learning. The model was trained on ADNI dataset and resulted in testing accuracy of 83.72%

Abed, Mahjabeen Tamanna and Fatema, Umme and Nabil, Shanewas Ahmed and Alam, Md. Ashraf and Reza, Md Tanzim in [16] developed three different Deep Neural Network models namely VGG19, Inception and Resnet. The models trained on ADNI dataset achieved an accuracy of 90%, 85% and 70% respectively.

E. Mggdadi, A. Al-Aiad, M. S. Al-Ayyad and A. Darabseh in [17] developed an efficient prediction model for Alzheimer's disease using VGG16 model which achieved an accuracy of 70.3%. The model using VGG16 worked better than 2D CNN.

Table I. Summary of The Existing Deep Learning Models for Alzheimer’s Disease Prediction

DEEP LEARNING MODEL	LIMITATIONS
VGG19	Low classification accuracy for intermediate stages like MCI
VGG16	Computational complexity is high since the architecture is complex
3D CLSTM	AD prediction accuracy is low
Inception-Resnet	Performs low in binary classification
Resnet	Requires weeks for training if the dataset is large and requires high computational power
Deep InfoMax	Requires more time for training since the model is unsupervised.

PROPOSED WORK

The proposed system involves Ensemble techniques which uses AlexNet and LeNet. Ensembles are predictive models which uses the combinations of predictions from two or more models thereby increasing the overall performance. Because AlexNet is an extremely powerful model capable of achieving high accuracies on very challenging datasets and producing good prediction results and LeNet model network learns the best internal representation from raw images automatically, the proposed system combines the AlexNet and LeNet models. Unlike VGG and Resnet, LeNet is a simple model that is easier to train. AlexNet and LeNet models are trained individually and the ensemble is used for classification which involves taking the highest vote between the results of these two models.

The Proposed System follows Majority Voting Ensemble Approach where the predictions of both AlexNet and LeNet is taken into account and the final output prediction is based on the majority of votes casted to each of the output classes by the single predictive models as shown in Fig. 1.

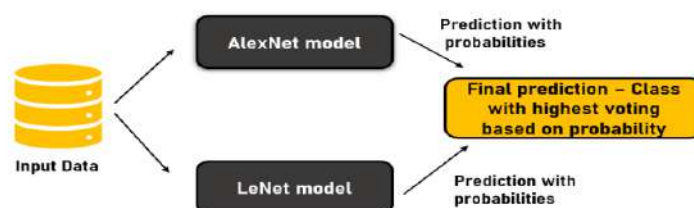


Fig. 1. Ensemble Approach based on Voting

The flow of the proposed system can be depicted as in Fig. 2.

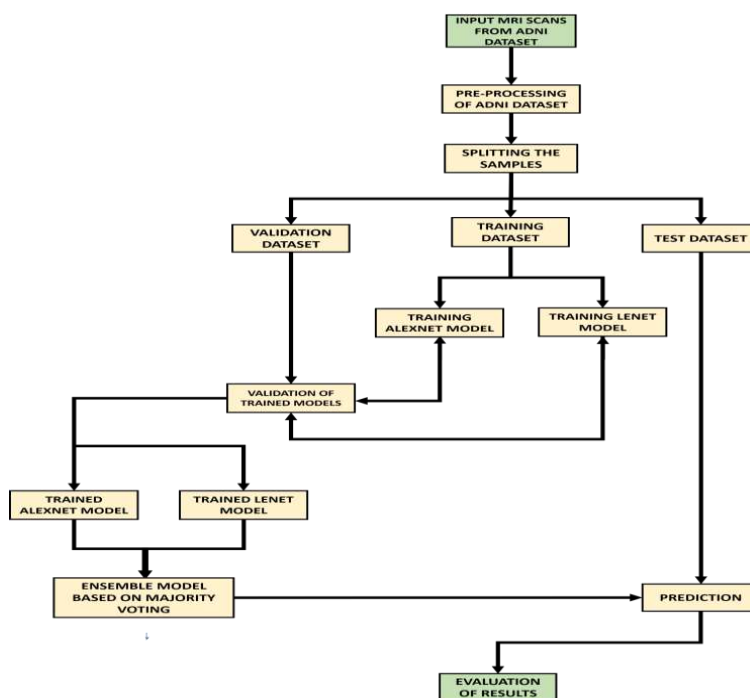


Fig. 2.System Flow

The key modules that are portrayed in the architecture diagram are explained as follows.

Input MRI Scans from ADNI Dataset

The input for the system is the MRI Scans which could in turn be given as the input to the AlexNet Model and the LeNet Model for training and testing the models individually. The dataset from various sources have been analyzed and it is finally acquired from the Alzheimer's Disease Neuroimaging Initiative (ADNI) which is a dedicated organization to help the researches with the data associated with the progression of AD collected from various sources. It includes various biomarkers like Positron emission tomography (PET) image, MRI image, biospecimen, clinical and genetic data which could be used for the research and study of Alzheimer's Disease. Among the available biomarkers, MRI is chosen since it is considered as less invasive and highly efficient.

Pre-processing of ADNI Dataset

The input data should be pre-processed before feeding into the models so that the models could avoid overfitting and underfitting problems during training phase. There are three main steps involved in pre-processing as shown in Fig. 3:

Segmentation and Normalisation are done with SPM software in MATLAB [18]. Slicing is done in Python.

1 Segmentation and Normalisation

SPM has a standard template containing the six main tissues of the brain. Accurately mapping the tissues of the acquired MRI image from ADNI Dataset [19] to the tissues of the template will increase the accuracy of prediction. Voxel Resolution of the image is changed.

2 Slicing

The brain can be viewed in three different views namely Axial View, Coronal View and Sagittal View as shown in Fig. 3. Since the brain changes due to Alzheimer's are visible clearly in Coronal View, only the Coronal View of the brain is given as input to the model.

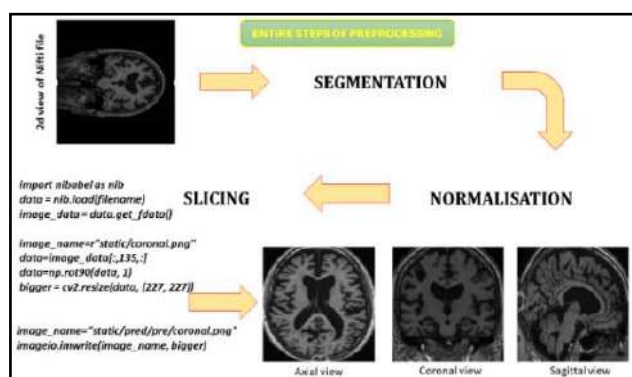


Fig. 3.Steps of Pre-processing

Performing Segmentation and Normalisation using MATLAB ensured that the preprocessed MRI had the main tissues that were required and this preprocessed dataset increased the accuracy of the model. Without this step, input cannot be given directly as MRI, since that would only decrease the performance of the model.

Splitting the Samples

The samples obtained after the pre-processing stage can be split into three categories, each of which is individually important for the training and testing of the neural network models, as shown in the Fig.4.

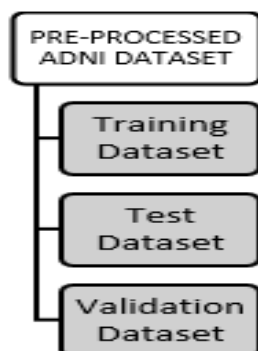


Fig. 4.Splitting of Dataset

Architecture of the AlexNet Model

The built AlexNet model contains eight learned layers: five convolutional and three fully connected layers as shown in Fig. 5. The notable parameters used in the AlexNet Model are discussed as follows.

1 ReLU Nonlinearity

The most common method of modelling a neuron's output f as a function of its input x is with $f(x) = \tanh(x)$ or $f(x) = (1 + e^{-x})^{-1}$ but this way of modelling is considered much slower than the functionality $f(x) = \max(0, x)$. When deep convolutional neural networks possess neurons with Rectified Linear Units (ReLU) as in the latter function, the training rate is several times faster. On the other hand, ReLUs have the property of Local Response Normalization wherein if at least few training samples yield a non-negative input, then the process of learning occurs seamlessly.

2 Max Pooling

Pooling layers in CNNs are assigned with the task of summarizing the values of the neighbouring neurons and giving a condensed value as an output. There are many types of pooling like Max Pooling, Min Pooling and Average Pooling among which the Max Pooling is chosen for the AlexNet Architecture. Max Pooling is basically a filtering mechanism that ensures only the maximum value out of the available values is selected for the output.

3 Overall Architecture of the AlexNet model

The AlexNet contains eight layers among which the first five layers are convolutional layers and the remaining three layers are fully connected layers. The output from the third fully connected layer is fed as input to a 3-way softmax that yields distribution over the 3 class labels such as AD, MCI and CN. The various layers, their output shapes and the number of parameters of the trained AlexNet model [20] are summarized as in the Fig.5

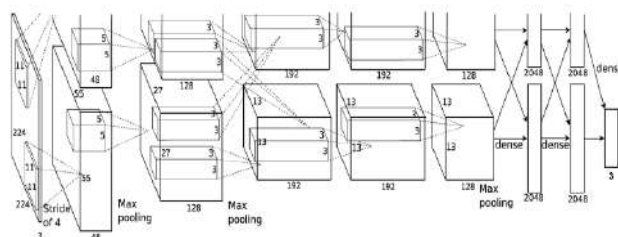


Fig. 5. Architecture of the AlexNet Model

Architecture of the LeNet Model

The built LeNet model contains five learned layers: two convolutional and three fully connected layers as shown in Fig. 6. The notable parameters used in the LeNet Model are discussed as follows.

1 Average Pooling

The usage of pooling layer after the convolutional layers is to down sample the available parameters. Among the various types of pooling like Max Pooling, Min Pooling and Average Pooling that are available, Average Pooling is chosen for the LeNet Architecture. Average Pooling is basically a filtering mechanism that ensures the average value of the available values is selected for the output.

2 Overall Architecture of the LeNet model

The LeNet contains five layers among which the first two layers are convolutional layers and the remaining three layers are fully connected layers. As like the AlexNet architecture, the output from the third fully connected layer of the LeNet is fed as input to a 3-way softmax that yields distribution over the 3 class labels such as AD, MCI and CN. The activation function that is used in the LeNet is the ReLU activation function. The various layers, their output shapes and the number of parameters of the trained LeNet model [21] are summarized as in the Fig. 6.

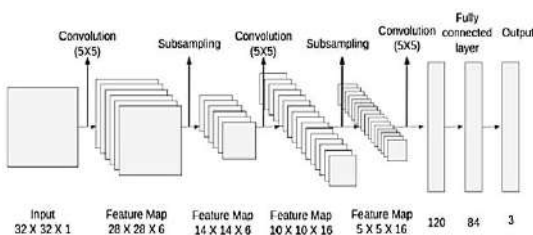


Fig. 6. Architecture of the LeNet Model

Training Phase, Prediction of Unseen Data and Evaluation of Results

The training for each of the models is carried out with the pre-processed training dataset for nearly 50 epochs and a callback has been set to terminate the training process automatically if the loss value and accuracy meet desirable values. The AlexNet model and the LeNet model are ensembled to achieve greater efficiency in comparison to each of their individual efficiencies. The final ensemble model can be given with some unseen MRI images to evaluate the model based on metrics like accuracy.

WORK FLOW

The work flow of the system is depicted in the Fig. 7.

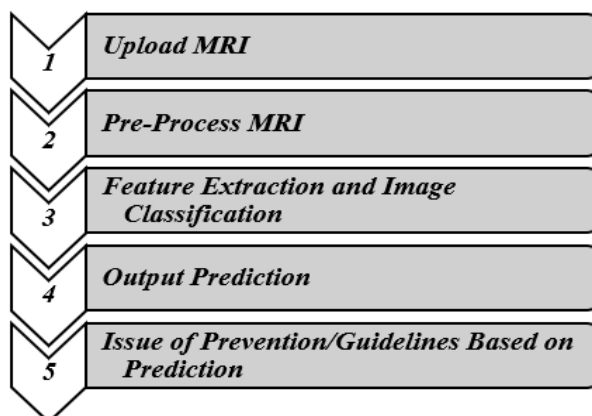


Fig. 7. Work Flow

The above depicted steps are explained as follows.

A) Upload MRI

The User has to Upload his MRI in .nii extension

B) Pre-Process MRI

The uploaded MRI will be pre-processed using MATLAB and sliced by Python

C) Feature Extraction and Image Classification

The models that have been developed will extract the features from the input image and perform Image Classification.

D) Output Prediction

Finally, Output will be predicted by the model which will return how much the given input image resembles the category of data we have fed it.

E) Prevention/Guidelines Based on Prediction

If the person tests positive for Alzheimer's, preventive ways to reduce the effect of Alzheimer's will be given.

If the person tests negative for Alzheimer's, then ways to avoid the risk of being affected with Alzheimer's in future will be given.

IMPLEMENTATION

Fig. 8 shows the page after the user uploads the MRI file. The page is redirected to MRI Visualisation page where all the three views of brain – Axial, Coronal and Sagittal views are displayed.

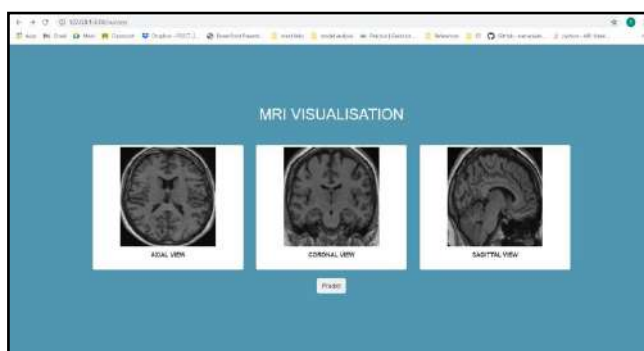


Fig. 8. MRI Visualisation Page

Fig. 9 shows the Result Displaying Page, the predicted output by the model along with the probability will be displayed.

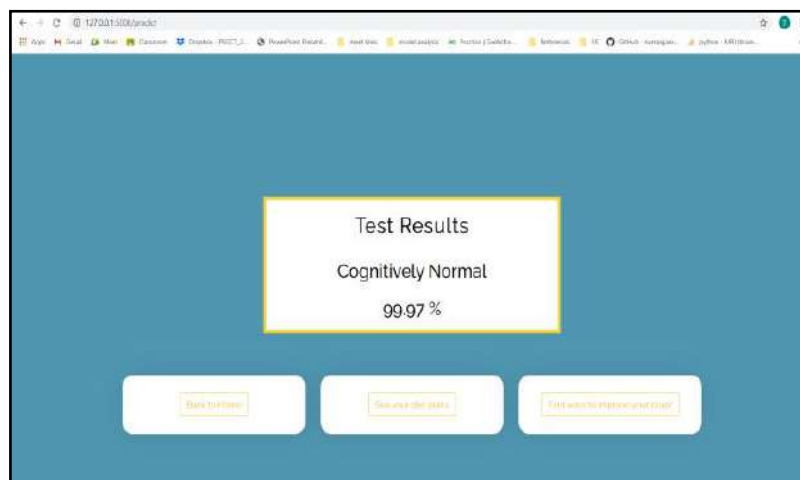


Fig. 9. Result Displaying Page

RESULTS AND CONCLUSION

RESULTS

Efficient and accurate prediction of Alzheimer's disease (AD) is very important because early prediction is the only way to provide better and effective treatment. Early prediction of AD plays a major role in therapeutic development and also for caring for patients in the right manner. Different neural network models were analysed based on neuroimaging data for early prediction. The Voting based Ensemble model [22] that is developed consists of two models: AlexNet and LeNet. The AlexNet Neural Network model that was developed was effective in predicting AD (including MCI and CN) which gave a training accuracy of 100% and testing accuracy of 87%. The LeNet Neural Network model is developed for predicting AD (including MCI and CN) which gives a training accuracy of 100% and testing accuracy of 74%. Combining these two models in Ensemble Network gives the testing accuracy of 97%. The Ensembled model accuracy is greater than the accuracy of models tested individually. Hence, the model that is developed can be used to identify Alzheimer patients at initial stages who can be good candidates for clinical trials.

The summary of the number of images in training and testing dataset is shown in Table II.

Table II. Summary Of The Images In Training And Testing Datasets

Classification	Number Of Images In Training Data	Number Of Images In Testing Data
AD (Alzheimer's Disease)	144	36
MCI (Mild Cognitive Impairment)	146	36
CN (Cognitively Normal)	152	36
Total Image Count	442	108

Accuracy Calculation

A confusion matrix [23] can be used to view the number of correct and incorrect predictions of each class. It displays how the classification model has predicted the results. Accuracy [23] can be calculated from the confusion matrix which is explained below.

True Positives (TP): These are scenarios in which the model outputs yes (they have the disease), and they do have the disease.

True Negatives (TN): The model outputs no, and they don't have the disease.

False Positives (FP): The model outputs yes, but they don't actually have the disease.

False Negatives (FN): The model outputs no, but they actually do have the disease.

$$\text{Accuracy} = \frac{\text{Number of correct predictions (TP+TN)}}{\text{Total number of predictions (TP+TN+FP+FN)}}$$

Table iii. Confusion Matrix Of Alexnet Model

	AD	CN	MCI
AD	34	1	1
CN	3	31	2
MCI	3	4	29

From Table III, it is inferred that the AlexNet model has a prediction accuracy of 87%. The AlexNet model predicts AD and CN more accurately than MCI.

Tableiv. Confusion Matrix Of Lenet Model

	AD	CN	MCI
AD	25	5	6
CN	8	23	5
MCI	2	2	32

From Table IV, it is inferred that the LeNet model has a prediction accuracy of 74%. LeNet model predicts MCI more accurately than AD and CN.

Table V. Confusion Matrix Of Ensemble Model

	AD	CN	MCI
AD	35	1	0
CN	0	36	0
MCI	2	0	34

FROM TABLE V, IT IS INFERRED THAT THE ENSEMBLE MODEL HAS A PREDICTION ACCURACY OF 97%.

From the Tables III to V, it could be concluded that the Ensemble Model has higher accuracy than the other two single predictive models.

Visualisation of AlexNet and LeNet Training

The training phase of AlexNet and LeNet involves the usage of Categorical Crossentropy [24] as loss function since the output classes involves three categories:

- i. Alzheimer's Disease
- ii. Mild Cognitive Impairment
- iii. Cognitively Normal

The training accuracy value observed during the training of AlexNet is shown in Fig. 10.

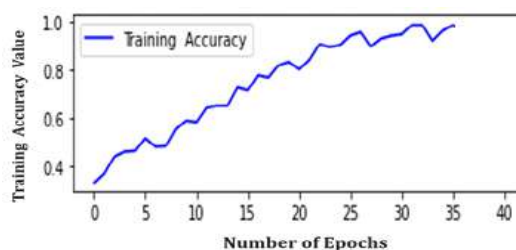


Fig. 10. Training accuracy of AlexNet

The training accuracy value observed during the training of LeNet is shown in Fig. 11.

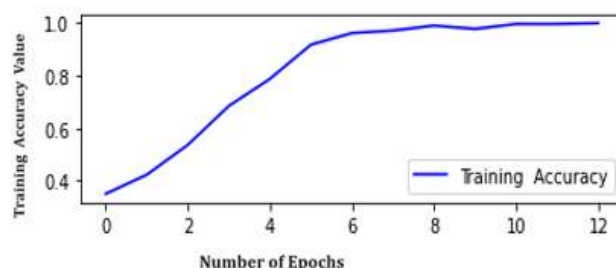


Fig. 11. Training Accuracy of LeNet

Both AlexNet and LeNet attained training accuracy value of 1.0 by training for 35 and 12 epochs respectively. The time taken to train LeNet model was comparatively lesser than AlexNet model.

Efficiency of Ensemble Approach

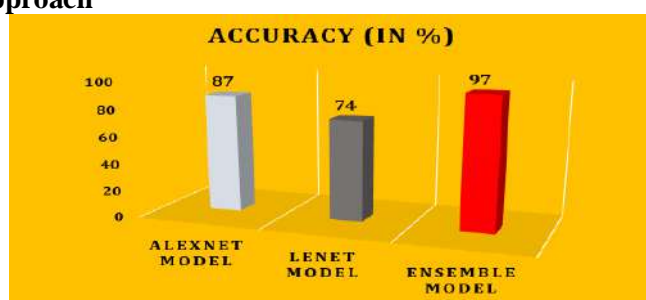


Fig. 12. Accuracy of each model

The visualization of the performance of the single predictive models and the ensemble model in terms of accuracy is shown in Fig.12. From this figure, it is clear that Ensemble approach has produced better results since Ensemble approach is mainly used for increasing the performance and robustness of the prediction process.

1. Performance

As evidently seen from the Confusion Matrix shown in Table V the Ensemble model yields higher accuracy in comparison to the single predictive models.

2. Robustness

The robustness of the Ensemble model is determined by its reliability which is far higher than the single predictive models.

The Ensemble approach improved the accuracy of the model, ideally achieving better performance than any individual predictive model used in the ensemble.

REFERENCES

1. "Alzheimer's disease", Mayo Clinic, Jun 26, 2021. Accessed on: July 20, 2021. [Online]. Available: <https://www.mayoclinic.org/diseases-conditions/alzheimers-disease/symptoms-causes/syc-20350447>
2. Alzheimer's Association, What is Alzheimer's Disease?, 2021, Accessed on : July 20, 2021. [Online]. Available: <https://www.alz.org/alzheimers-dementia/what-is-alzheimers>
3. Medical news today, What to know about Alzheimer's Disease, Sep. 22, 2020, Accessed on : Jul 20, 2021. [Online]. Available: <https://www.medicalnewstoday.com/articles/159442>
4. "Basics of Alzheimer's Disease and dementia", July. 08, 2021. Accessed on : July 20, 2021. [Online]. Available: <https://www.nia.nih.gov/health/what-alzheimers-disease>
5. "Control System", March. 21, 2018. Accessed on : July 20, 2021. [Online]. Available: <https://courses.lumenlearning.com/wmopen-biology2/chapter/control-systems/>
6. "Alzheimer's Disease and the β -Amyloid Peptide", Jan. 19, 2010. Accessed on July. 20, 2021. [Online]. Available: <https://www.ncbi.nlm.nih.gov/pmc/articles/PMC2813509/>

7. "What Are the Main Characteristics of the Brain with Alzheimer's?"; May.16,2017. Accessed on July.20,2021.[Online].Available:<https://www.nia.nih.gov/health/what-happens-brain-alzheimers-disease>
8. Alzheimer's Association,"Medications for Memory, Cognition and Dementia-Related Behaviors",2021,Accessed on July.20,2021.[Online]. Available:<https://www.alz.org/alzheimers-dementia/treatments/medications-for-memory>
9. Khedher, Laila & Ramírez, Javier & Gorriz, Juan & Brahim, Abdelbasset & Segovia, F.. (2015). Early diagnosis of Alzheimer's disease based on partial least squares, principal component analysis and support vector machine using segmented MRI images. *Neurocomputing*. 151, Part 1. 139-150. 10.1016/j.neucom.2014.09.072.
10. Albright J. Forecasting the progression of Alzheimer's disease using neural networks and a novel preprocessing algorithm. *Alzheimers Dement (N Y)*. 2019 Sep 25; 5:483-491. doi: 10.1016/j.trci.2019.07.001. PMID: 31650004; PMCID: PMC6804703.
11. Odusami M, Maskeliūnas R, Damaševičius R, Krilavičius T. Analysis of Features of Alzheimer's Disease: Detection of Early Stage from Functional Brain Changes in Magnetic Resonance Images Using a Finetuned ResNet18 Network. *Diagnostics (Basel)*. 2021 Jun 10;11(6):1071. doi: 10.3390/diagnostics11061071. PMID: 34200832; PMCID: PMC8230447.
12. Fedorov, Alex & Hjelm, R Devon & Abrol, Anees & Fu, Zening & Du, Yuhui & Plis, Sergey & Calhoun, Vince. (2019). Prediction of Progression to Alzheimer's disease with Deep InfoMax. 1-5. 10.1109/BHI.2019.8834630.
13. Puranik, Mukul, Himanshu Shah, Keval D Shah and S. Bagul. Intelligent Alzheimer's Detector Using Deep Learning. *Second International Conference on Intelligent Computing and Control Systems (ICICCS)* (2018): 318-323.
14. Xia, Zaimin & Yue, Guanghui & Xu, Yanwu & Feng, Chiyu & Yang, Mengya & Wang, Tianshu & Lei, Baiying. (2020). A Novel End-to-End Hybrid Network for Alzheimer's Disease Detection Using 3D CNN and 3D CLSTM. 1-4. 10.1109/ISBI45749.2020.9098621.
15. Mehmood A, Yang S, Feng Z, Wang M, Ahmad AS, Khan R, Maqsood M, Yaqub M. A Transfer Learning Approach for Early Diagnosis of Alzheimer's Disease on MRI Images. *Neuroscience*. 2021 Apr 15; 460:43-52. doi: 10.1016/j.neuroscience.2021.01.002. Epub 2021 Jan 17. PMID: 33465405.
16. Abed, Mahjabeen & Fatema, Umme & Nabil, Shanewas & Alam, Md. Ashraful & Reza, Md Tanzim. Alzheimer's Disease Prediction Using Convolutional Neural Network Models Leveraging Pre-existing Architecture and Transfer Learning. 1-6. 10.1109/ICIEVicIVPR48672.2020.9306649.
17. E. Mggdadi, A. Al-Aiad, M. S. Al-Ayyad and A. Darabseh, "Prediction Alzheimer's disease from MRI images using deep learning," 2021 12th International Conference on Information and Communication Systems (ICICS), 2021, pp. 120-125, doi: 10.1109/ICICS52457.2021.9464543.
18. "SPM – MATLAB Central", Feb.2,2021. Accessed on May.14,2021.[Online].Available:<https://www.mathworks.com/matlabcentral/profile/authors/7905683>
19. "Alzheimer's Disease Neuroimaging Initiative", 2017,Accessed on April.25,2021.[Online].Available:<http://adni.loni.usc.edu/>
20. Shipra Saxena,The Architecture of Lenet-5, March.18,2021.Accessed on Aug 15,2021.[Online].Available:<https://www.analyticsvidhya.com/blog/2021/03/the-architecture-of-lenet-5/>
21. Krizhevsky, Alex and Sutskever, Ilya and Hinton, Geoffrey E. ImageNet Classification with Deep Convolutional Neural Networks, Volume 25, 2012.
22. Himanshi Singh,Basic Ensemble Techniques in Machine Learning, March 10,2021.Accessed on August 15,2021.[Online].Available:<https://www.analyticsvidhya.com/blog/2021/03/the-architecture-of-lenet-5/>
23. Banso D. Wisdom. Understanding the Confusion Matrix (II),May.6,2019.Accessed on October 5,2021.[Online]. Available:<https://dev.to/overrideveloper/understanding-the-confusion-matrix-264i>
24. Understanding Categorical Cross-Entropy Loss, Binary Cross-Entropy Loss, Softmax Loss, Logistic Loss, Focal Loss and all those confusing names, Raúl Gómez blog, May 23, 2018.

Deep Learning Based Sign Language Interpreter

Kavitha C, Roshini M, Akshaya M, Selvapriya K, Poornimasri P and Vikasinit
Department of CSE PSG College of Technology Coimbatore

ABSTRACT

People affected by speech impairment can't communicate using hearing and speech and they rely on sign language for communication. The formal and informal communications of these people are affected by the requirement of a human sign language interpreter. There has been quite a significant advancement in computer vision which would enable us to easily track the hand gestures and eliminate the need of a human interpreter for communication. The proposed system tries to do a real time translation of hand gestures into equivalent English text/ audio. The proposed system takes hand gestures as input through video and translates it into speech/text which could be understood by a non-signer. By the usage of deep learning technique Convolutional Neural Network (CNN), the hand gestures are to be predicted and converted into equivalent text and by the usage of Natural Language Processing, the predicted text is to be converted to audio. The results of the developed system for sign language recognition and interpretation achieved an accuracy of around 80%. By deploying this system, the communication gap between signers and non-signers could be narrowed down. Furthermore the developed model can also be incorporated in real world applications.

I. INTRODUCTION

According to a survey conducted by the Ministry of Statistics and Programme Implementation, there are approximately 4.2 million people who suffer from speech impairments. Nearly 2.5 billion people worldwide i.e. 25% people will have a certain degree of hearing loss by 2050 according to the World's first report published by World Health Organisation (WHO) on March 21, 2020. Speech impaired people heavily rely on human speech interpreters for medical, legal, educational and training sessions. The problem is that most of the hearing people do not know how to speak by signs, thus creating a barrier making it difficult for the deaf people to have social interactions. Hence, the speech impaired and the deaf highly rely on human interpreters for communication. There isn't any infrastructure available for these speech impaired and the deaf to communicate with the non-signers without a human interpreter.

Basically, there isn't a pathway created for automation of sign language translation and hence there is a need for automation of sign language translation which would result in convenient communication between speech impaired people and the non-signers without the need of an interpreter for translation. In order to deal with these obstacles, the sign language translation system could be automated with the help of artificial intelligence techniques like Convolutional Neural Networks.

Sign language interpretation methods aim at automatically translating sign languages using vision based techniques. Sentence-level and word-level sign recognition are the two tasks involved in this process. The three main factors that determine the meaning of sign are head poses, body motions and hand gestures which imply tasks involving word-level sign recognition are tough. In this paper, word level sign language recognition and translation into equivalent text and audio is dealt with.

The aim is to build a Sign Language Interpreter which tries to do a real time translation of hand gestures into equivalent English audio. This system takes the hand gestures as input through video and converts it into text using Image-appearance based 3D Convolutional Networks and by using Natural Language Processing Techniques to convert the converted text to audio so as to ease the communication between a signer and a non-signer.

A. AMERICAN SIGN LANGUAGE

Sign language is a way of communicating using hand gestures, movements, body language and facial expressions specifically designed for the deaf and the speech impaired people. Like several languages present for communication like English, Spanish etc there are different sign languages present. There is no sign language which is said to be universal sign language. Different countries and regions use different sign languages like the spoken languages. There are somewhere between 138 and 300 different types of sign language used around the globe today. Some of the sign languages present include American Sign Language (ASL), British Sign Language (BSL), Chinese Sign Language (CSL), Arabic Sign Language etc. In this paper, the target is to deal with the ASL.

American Sign Language is the visual-gestural language which is used by most of the deaf community. It is a complete, natural language which has the same linguistic properties as that of the spoken languages but with a grammar which differs from English. ASL satisfies all the fundamental features of a language and has its own rules for word formation, pronunciation and word order. For example, the ASL users ask a question by raising their eyebrows, widening their eyes and tilting their body

forward. Fingerspelling is the ASL alphabet. Every letter of the alphabet has a sign. It is the part of ASL which is often used to spell out names and places. It is an easy way to communicate if one doesn't know or can't remember some of the ASL signs.

Figure 1 represents some of the signs used for fingerspelling in ASL:

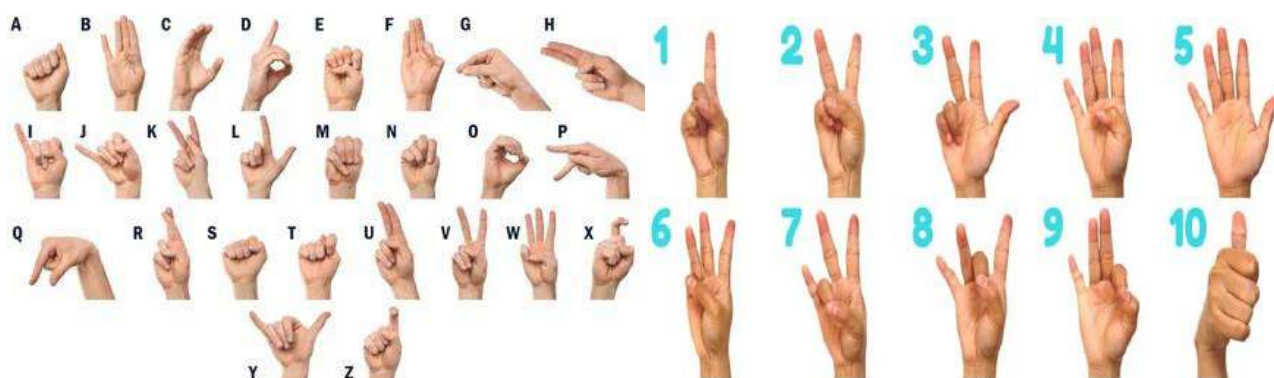


Figure 1. The ASL fingerspelling alphabets

Figure 2 represents some of the basic expressions which are used to meet and greet people in ASL.



Figure 2. Basic expressions in ASL

Even though there are numerous sign languages present and used in different regions of the world, American Sign Language is chosen in this paper to deal with because of its popularity and major usability among the people.

B. CONVOLUTIONAL NEURAL NETWORK

A Convolutional Neural Network (ConvNet) is a Deep Learning algorithm which can take in an image as input, assign importance i.e. learnable weights and biases to various objects in the image and be able to differentiate one from the other. The main role of the ConvNet is to reduce the images into a form which is easier to process, without losing features which are critical for getting a good prediction. CNN are multilayer perceptrons where it contains three main layers - convolutional layer, pooling layer and fully-connected layer. As shown below, Figure 3 depicts the layers of CNN.

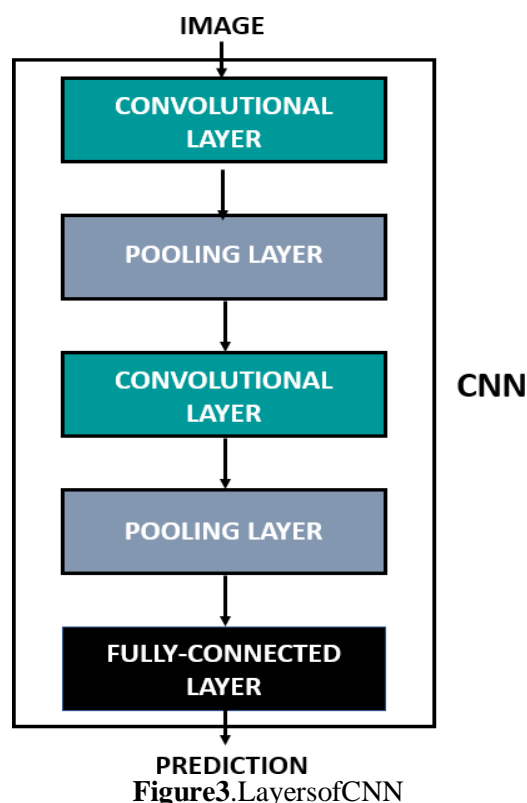


Figure 3. Layers of CNN

- **Convolutional Layer**-Convolutional layer extracts the feature by applying filters to the input image.
- **Pooling Layer**-Pooling layer carries out two different functions- Max pooling and Average pooling. Max pooling takes the maximum value and the average pooling takes the average value in order to reduce the dimensionality.
- **Fully Connected Layer**-Fully connected layer takes the position before the output and aggregates information.

ADVANTAGES

CNN has elevated accuracy and spots the significant feature without human overseeing.

II. RELATED WORKS

- [1] Sign Language Recognition using Neural Networks –The paper aims to detect hand gestures based on certain features. The features included were purely based on the meaningful shapes of the hands i.e. the orientation, centroid, thumb in terms of raised or folded and status of fingers and did not include the features like skin colour, texture etc. The system developed captures the hand gestures and converts them to words in the form of text. The system used Conventional Neural Networks (CNN) to convert the American Sign Language (ASL) to text.
- [2] Sign Language Translator using Deep Learning –This paper deals with the recognition of 26 English alphabets using the hand gestures present in the Indian Sign Language. The dataset for the Indian Sign Language was created on their own. Images of the hand gestures for the Sign Language of 26 English Alphabets were recorded and put into 26 different classes such that each class comprises nearly 2000 images corresponding to that particular alphabet. The proposed system used CNN architecture, particularly VGGNet for gesture recognition.
- [3] American Sign Language Recognition using Deep Learning and Computer Vision –The focus of this paper is to create a vision based application which offers translation of sign language to text. The model uses video sequences to extract temporal and spatial features. The spatial features were recognized using Inception, a Convolutional Neural Network (CNN). The temporal features were trained using Recurrent Neural Network (RNN). The main advantage of the system was the use of robust and accurate architecture for gesture recognition.
- [4] Quo Vadis, Action Recognition? A New Model and the Kinetics Dataset – This paper uses the Kinetics dataset which is a Human Action Video Dataset. The dataset consists of 400 different human action classes and

over 400 videos per class wherein each video lasts for 10s and is collected from the YouTube videos. The paper gave an analysis of how the available architectures such as LSTM (Long Short Term Memory), Two Stream CNN and 3D CNN work on action recognition for this particular dataset and their performance were compared.

- [5] Dynamic hand gesture recognition using RGB-D data for natural human-computer interaction – In this paper, RGB-D depth sensors have shown to outstrip dynamic hand gesture recognition by combining Euclidean distance between hand joints and shoulder centre joint with the modulus ratios of skeleton features to generate a unifying feature descriptor for each dynamic hand gesture. Improved dynamic time warping (IDTW) algorithm which is used to obtain the final recognition results, applies the weighted distance and a restricted search path to avoid the huge computation in conventional DTW and improve the recognition performance.
- [6] Handshake recognition for Argentinian Sign Language using ProbSom – In this paper, a new approach called ProbSom was proposed. The approach is a technique which is similar to Random Forests, Neural Networks and Support Vector Machines. An Argentinian Sign Language dataset is used which consists of the hand gesture images. The images are processed and the descriptors are extracted which in turn is used for hand shape classification using ProbSom. The accuracy for this approach was found to be approximately 90%.
- [7] Sign Language Recognition using Temporal Classification – This paper highlights the use of Temporal scaling, where all signs are normalized to a length (the average number of frames for each sign is 57 frames) by resampling using a fast Fourier transform. Since most of the important information is retained between the original data and the sampled version, the effect of the speed at which a sign is performed is nullified, as some signers sign at a higher speed than others. Temporarily scaling the data would normalize all signals to be roughly at the same speed. Here, several Machine Learning models like SVM, Logistic Regression, LSTM were employed for temporal classification. Another technique called Sequential Pattern Mining which was used to perform multivariate time series classification.
- [8] Using Deep Convolutional Networks for Gesture Recognition in American Sign Language – In this paper, the author proposes a CNN architecture, consisting of multiple convolutional and dense layers. The architecture includes 3 groups of 2 convolutional layers followed by a max-pool layer and a dropout layer, and two groups of fully connected layers followed by a dropout layer and one final output layer. From the paper, a conclusion can be made that the results are affected by certain factors i.e. the skin colour and the lighting variations of the images present in the dataset.
- [9] American Sign Language Recognition Using Leap Motion Controller with Machine Learning Approach – In this paper, the authors perform recognition of American Sign Language (ASL) for 26 letters and 10 digits. An optical hand tracking module called the Leap Motion Controller which captures the movements of the hands with unparalleled accuracy is used to extract features from finger and hand motions to differentiate between the static and dynamic gestures. The sign language recognition rates are 93.81% and 80.30% using Deep Neural Network (DNN) and Support Vector Machine (SVM) respectively for 26 letters and for the amalgamation of 26 letters and 10 digits, the recognition rates are 88.79% using DNN and 72.79% using SVM which is slightly lower.
- [10] Evaluation of Pooling Operations in Convolutional Architectures for Object Recognition – In this paper, the authors worked on Evaluation of Pooling Operations in Convolutional Architectures for Object Recognition. The desire is to improve insight into various functions on fixed architecture by directly comparing several common object recognition tasks. Maximum pooling makes a markable note when compared with subsampling operations based on results. There is no significance of overlapping pooling over non-overlapping pooling, in spite of shift-invariant properties.
- [11] Video-based Sign Language Recognition without Temporal Segmentation – In this paper, the author used the Modern Chinese Sign Language for gesture recognition. A novel sign recognition framework, the Hierarchical Attention Network with Latent Space (LS-HAN) was proposed which basically eliminates one of the pre-processing steps i.e. the temporal segmentation. The input is basically a video containing 16 frames. The model consists of three main parts – Video Feature Representation using Two Stream CNN, Semantic Gap Bridging using Latent Space, Latent Space based recognition using Hierarchical Attention Network (HAN).

- [12] Sign Language Recognition with Transformer Networks – In this paper, the authors propose a system where it uses OpenPose for feature extraction and CNN for end-to-end feature learning. The system was built using Flemish Sign Language and was trained using different methodologies such as PoseLSTM, Pose Transformer Network (PTN), Video Transformer Network (VTM) and Multimodal Transformer Network (MTN). In conclusion, it was found that the OpenPose key points add information which are helpful for discriminating between classes. The best method was identified to be Multimodal Transformer Network with an overall accuracy of 74.7%.
- [13] A Comparative Study of Various Object Detection Algorithms and Performance Analysis – Different object detection methods such as R-CNN, Fast R-CNN, Faster R-CNN, Single Shot Detector (SSD) and YOLOv3. All these models were retrained and compared and their performance was analysed. The models differed in terms of speed and accuracy. The speed features analysed differs as follows. R-CNN < Fast R-CNN < Faster R-CNN < SDD < YOLOv3. YOLOv3 was found to be fast and accurate. It is also beneficial as it can detect the objects directly and all objects are detected only in single time.
- [14] Real Time Object Detection Using YOLOv3 – The main objective of the paper was to detect objects using the You Only Look Once (YOLO) approach. In YOLO, the algorithm looks at the image completely by predicting the boundary boxes and class probabilities for the boxes faster than other methods. In this paper, a model was trained such that the input was a batch of images and the output was the list of boundary boxes with recognized classes.
- [15] A Review on Methods for Speech-to-Text and Text-to-Speech Conversion – The aim of this paper was to study different methods for STT (Speech-to-Text) and TTS (Text-to-Speech) conversion and analyse which one would be the best for both the cases. For STT conversion, the techniques analysed include Linear Predictive Coding (LPC), Dynamic Time Warping, Hidden Markov Model (HMM), Neural Network and Mel-Frequency Cepstrum Coefficient (MFCC). For TTS conversion, the techniques analysed include Rule Based Machine Translation (RBMT), Statistical Machine Translation (SMT) and Hidden Markov Model (HMM). The best method for STT conversion was found to be a combination of Hidden Markov Model and Deep Neural Network which could be implemented using Google Speech Recognition API module. The best method for TTS conversion was found to be the Hidden Markov Model which could be implemented using pyttsx3 or gTTS (Google Text to Speech) modules.

III. EXISTING SYSTEM

The scope of the existing sign language interpreter is limited only towards the recognition of alphabets and numbers. The existing system cannot recognize words which is a huge drawback. Hence the proposed work focuses on recognizing words. The input image is either uploaded or recorded through a web camera for a certain time and fed to the model, then the signs in the image will be converted to audio or text.

IV. PROPOSED SYSTEM

The proposed system is to recognize the signs shown by the user through a web camera in a continuous fashion and expand the recognition of signs to commonly used phrases. The proposed system is to be modeled in such a way that it also recognizes words in addition to alphabets and numbers. The sign language recognizer will be built using image-appearance based 3D Convolutional Networks (Inflated Two Stream Convolutional Networks) to recognize the signs and convert them to text and by using Natural Language Processing Techniques to convert text to speech. The proposed 3D model is a hybrid model of the 3D Convolutional Neural Networks and the Two Stream Networks. As shown in Figure 4, the approach begins with a 2 dimensional architecture and all the filters and pooling kernels are inflated so that the time dimension is also taken into account. Also parameters from a 2 Dimensional model are being trained on ImageNet during the implementation of a 3 Dimensional model. Significant importance is given to set the optimal receptive fields since a temporal dimension is involved. The proposed model would be trained and the accuracy would be analysed. The Inception module is used to make the network grow wide rather than deeper. To decrease the number of input channels 1x1x1 convolutions are used before 3x3x3 convolutions. The proposed model is trained using video datasets so that the gesture recognition would be more accurate than the existing systems.

Figure 4 describes the design of the model used for recognition of ASL

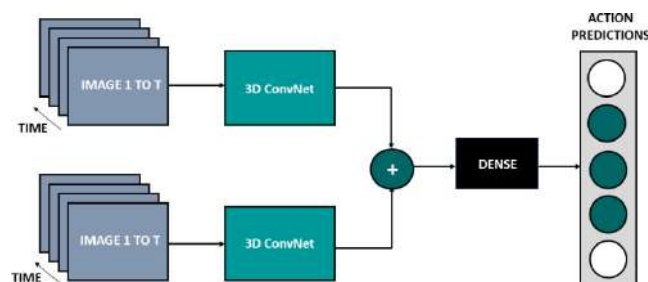


Figure 4. TwoStream3DConvNet

Figure 5 depicts the System Design Model of the Sign Language Interpreter.

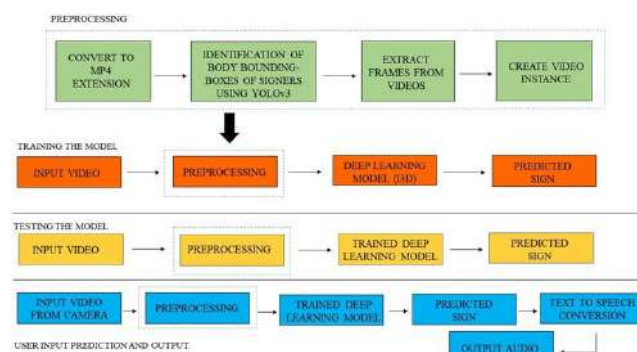


Figure 5. System Design Model of Sign Language Interpreter

As depicted in Figure 5, the system design model consists of four modules namely preprocessing, training the model, testing the model and user input predictions and output.

- The first module converts the video to mp4 extension, then the boundary box is identified for each video followed by the extraction of image frames from the videos.
- In the second module, the preprocessed videos are trained using the I3D model in order to convert the predicted sign to text.
- In the third module, the credibility of the trained I3D model is tested using a subset of the dataset.
- In the fourth module, the model is implemented to perform real time recognition. A video is recorded through a web camera which is preprocessed and fed into the trained I3D model which recognizes the performed sign into text. The text is then converted into speech by using the python module gTTS (Google Text to Speech) which is then shown as the output.

V. SYSTEM IMPLEMENTATION

dataset as shown in Figure 7 consists of the video instances with all the above variations in order to improve system performance.

A. Dataset

WLASL is a large dataset which consists of videos that are used for Word-Level American Sign Language (ASL) recognition. The dataset features 2,000 common different words in American Sign Language and consists of nearly 20,000 video instances recorded from nearly 120 different signers with each video indicating only one sign. Each sign is recorded such that it is performed by at least 3 signers.

The reasons to choose a large video dataset is as follows

- The signs mainly depend upon the movement of the hands, body posture and head poses. For example, the sign for the words 'read' and 'dance' differ only in the orientation of the hands. Hence in order to differentiate, several video instances would be required. The chosen dataset is a large dataset with nearly 20,000 video instances with each word mapped on to at least 15 videos on an average.
- The words used in the vocabulary of signs are usually large. The chosen dataset features nearly 2,000 words.
- The sign for a word may consist of a series of actions. Hence the usage of an image dataset for word level sign

language recognition would affect the system and the use of video dataset would increase the performance. For example, in Figure 6, the word “hungry” can be interpreted to be “wish” due to the similarity in some of the actions. Hence the usage of a video dataset would be more appropriate.



Figure 6. ASL for the words “Wish” and “Hungry”

- The background present in the videos, the appearance of the signers and the colour of the outfits as well affect the recognition. Hence the



Figure 7. Video instances present in the chosen dataset with the variation such as background, appearance etc.

The dataset contains

- gloss : Glossary- The English word to which the ASL has been performed.
- instances: Video Instances- consists of all the video instances of the ASL performed for the corresponding word.

The words present in the dataset which are used for recognition include book, drink, wish, hungry, read, dance, against, family, child, angry, towel etc. Each video in the dataset consists of length ranging between 0.5 and 8 seconds and the average length of all the videos ranges approximately 0.85 seconds.

B. Preprocessing

The videos in the dataset are converted to the same file extension for the purpose of uniformity. YOLOv3 is a regression-based algorithm and a refined version of YOLO and YOLOv2. YOLOv3 is used to detect the hands in the image and predict the boundary boxes of the image which is stored in the database for later processing. Boundary box detects only one object in an image. YOLOv3 is chosen because of its speed and accuracy. It uses Darknet-53 as a feature extractor which is more efficient than Darknet-19 used in YOLOv2. In terms of precision for smaller objects YOLOv3 has Average Precision of 18.3 whereas YOLOv2 has Average Precision of 5 which is a huge difference. The architecture of the YOLOv3 model is shown in Figure 8. After that the videos are converted into image sequences and fed to the I3D model for recognition.

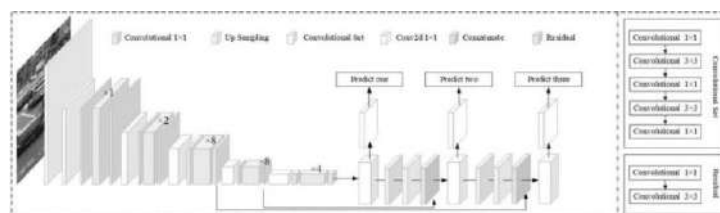


Figure 8. YOLOv3 Architecture

C. Training

The dataset is trained on Two-Stream Inflated 3D Convolutional Neural Network (I3D) which uses ImageNet-pretrained Inception-V1 as the base model. The I3D model is pre-trained on Kinetics Dataset in order to easily detect high-level features such as edges and patterns. In the experiments, the input videos are processed at 25 frames per

second. Max-pooling uses asymmetrical filters in the initial stages of the network so that time is maintained while pooling over the spatial dimension. In the later stages of the network time is included by running convolutions and pooling. During training the videos are randomly cropped both spatially and temporally and concurrently random left-right flipping is harmoniously put in for each video. Training on videos is done with standard SGD with momentum set to 0.9 with synchronous parallelization across 64 GPUs. Each subset is trained with 200 epochs. The training process is terminated once the validation accuracy stops increasing.

The steps to arrive at I3D Architecture as depicted in Figure 9 is as follows,

1. Inflating 2D Conv Nets into 3D

All the filters and pooling kernels are inflated to become 3 dimensional by adding a temporal dimension.

2. Bootstrapping 3D filters from 2D Filters

The weights of the 2 dimensional filters are repeated

N times along the temporal dimension and rescaled by dividing by N . N refers to the dimension of the filters.

3. Optimal Receptive Field

Choosing an optimal receptive field is important because if it grows fast in time with respect to space it might cause feature information loss and if it grows very slowly it may not properly capture the scene dynamics.

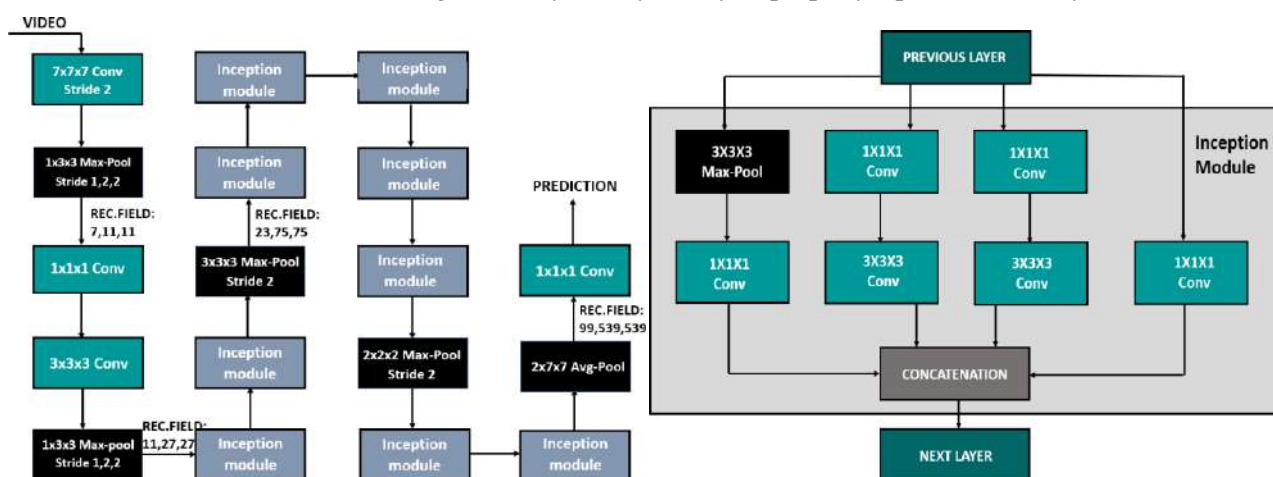


Figure 9. Architecture of I3D Model

D. Testing

Before the model can be tested the input video has to be converted into rgb frames, resized then center cropped. After which the model is set up and the input channels are defined. The dataset is divided into subsets of 100, 300, 1000, 2000 and testing is done. After the prediction is made, the evaluation regarding how accurate the model is done.

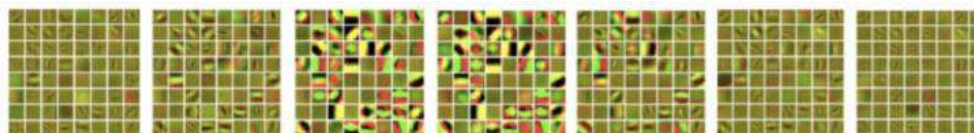


Figure 10. Flow Network Filters



Figure 11. Filters of RGB I3D Network

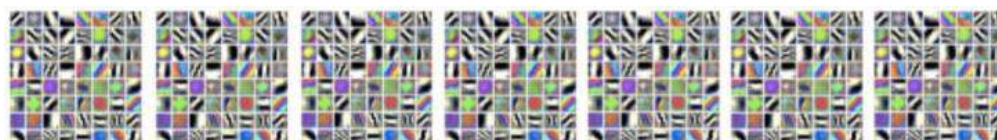


Figure 12. Filters of Inception-v1 Module

From the above figures i.e. Figure 10, Figure 11, Figure 12, it can be observed that the filters from the RGBI3D network have rich temporal structure.

E. Camera Feed

The model has been trained on the dataset. In order to test the model with user input the web camera has to be connected to provide input. In this module the user is prompted to provide the model with the input video where he/she can record a video performing the sign. Before the input video can be fed it has to be formatted suitably in order to make predictions by the model. The video is resized, center-cropped and color normalised with mean / standard deviation. Figure 13 represents the sample input video recorded in real time through the web camera.



Figure 13. Input for Sign Language - Against

F. Text To Speech

In this module, the predicted word is converted into speech by making use of the python module Google Text to Speech (gTTS) API which makes use of the Hidden Markov Model (HMM). It is a probabilistic technique which is a subclass of dynamic Bayesian models. It gives better accuracy for Text to Speech conversion. HMM is a network which is automatically trained which is an advantage. Moreover it is an effective framework for modeling temporal vector sequences. HMM has self-adapting capabilities that increase the quality of the conversion. Figure 14 depicts the architecture of gTTS. gTTS converts the text into audio as an mp3 file.

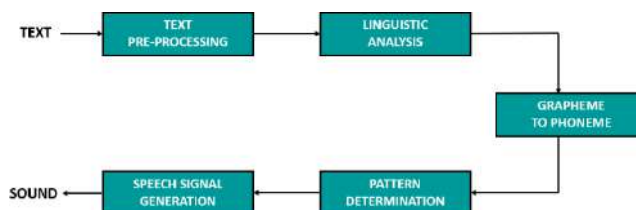


Figure 14. Architecture of gTTS

G. Accuracy Computation

Different words have very similar sign gestures which may cause errors in the classification results. However, by using contextual information some of the erroneous classification can be rectified. Therefore, for the word-level sign language recognition it is more reasonable to use top-K predicted labels. So, the accuracy is calculated using the topk method, that is if the correct answer is present in the top k predicted values, it is considered to have an accuracy of 100%. As depicted in Figure 15, the accuracy obtained with the help of the I3D model is around 80%.

top-k accuracy when k=1: 0.72173415698231346
top-k accuracy when k=5: 0.78892109754378012
top-k accuracy when k=10: 0.80173442151430889

Figure 15. Accuracy over different subsets

VI. RESULTS AND INFERENCE

This Sign Language Recognition System is developed and tested successfully.

Total data used for the work : 20000 videos
 Total training data used for the work : 14000 videos
 Total testing data used for the work: 6000 videos

As shown in Figure 16, it depicts that the model correctly predicts the performed sign.



Figure 16. Output for Sign Language - Against

A. Performance evaluation

Evaluation Metric : Top-k Accuracy

Top-k Accuracy computes the number of times where the correct label is among the top k labels predicted (ranked by predicted scores). k refers to the number of predictions taken into consideration. Top k accuracy calculates accuracy by checking whether the correct label falls under the top k predictions made by the model.

Table 1. Accuracy over different subsets

Testing Data Subset Size /k	k=1	k=5	k=10
n=100	72%	78%	80%
n=300	64%	70%	75%
n=1000	59%	67%	72%
n=2000	55%	60%	64%

The testing set is divided into subsets of 100, 300, 1000, 2000 and testing is done. As the accuracy metric is Top-k accuracy, the testing is carried out for different k values like (k = 1, 5, 10) and for different testing data subset sizes and the accuracy is examined and analysed. As shown in Table 1, the accuracy is maximized when the value of k = 10 and the testing data size is n = 100. As the testing data size increases, the accuracy gets minimized as observed in Table 1.

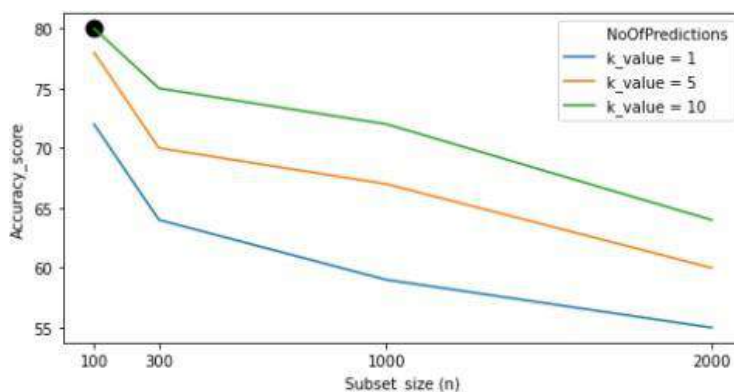


Figure 17. Accuracy over different k values and subset size

VI. CONCLUSION AND FUTURE WORK

The rudimentary idea of communication of speech impaired through sign language and the problem they face when there is absence of an interpreter is discussed. Hence the aim is to implement a sign language interpreter which will facilitate them to communicate with non-signers without any complications in the absence of a human sign language interpreter. For the sign language interpreter, the

concepts of YOLOv3 for object detection and Convolutional Neural Network for accurately and precisely classifying the hand gestures have been used and the developed system achieved an accuracy of nearly 80% at top-k accuracy with k value to be 10 and testing data subset size to be 2000. The proposed system provides a real-time and accurate translation of hand gestures.

The following are the some of the enhancement that could be included in the future,

- First potential enhancement is that the model could be used to recognize sentences by adding a gesture for word break. This can work by giving a definite gesture for word break. This would be quite beneficial for the signer to communicate with the non-signers.
- Second potential enhancement would be to classify hand gestures using RNN (Recurrent Neural Networks). The RNN is similar to other neural networks but with a major advantage which is memory as it feeds the output of a result back into itself. RNN requires a lot of processing power and large storage as it stores the output for the next epoch.
- Third potential enhancement would be to build a system which could possibly convert speech to sign language as well and also create an user interface with the combination of these two functionalities i.e. conversion of sign language to speech and conversion of speech to sign language which would aid the signers to communicate with the non-signers.

REFERENCES

1. Prof. Avinash Bagul, Shailesh Bachani, Shubham Dixit, Rohin Chandha, "Sign Language Recognition using Neural Network", April 2020.
2. Rahul Sharma, Sunil Raj, Prajay Agarwal, Saraswati Nagtilak, Uday Patil, Swaroop Patwari, "Sign Language Translator using Deep Learning", February 2020.
3. Kshitij Bantupalli, Ying Xie, "American Sign Language Recognition using Deep Learning and Computer Vision", December 2018
4. Joao Carreira, Andrew Zisserman, "Quo Vadis, Action Recognition? A New Model and the Kinetics Dataset", 2018
5. C. Linqin, C. Shuangjie and X. Min, "Dynamic hand gesture recognition using RGB-D data for natural human-computer interaction", 2017.
6. F. Ronchetti, Q. Facundo and A. E. Cesar, "Handshake recognition for Argentinian Sign Language using Probsom", 2016.
7. Hardie Cate, Fahim Dalvi, Zeshan Hussain, "Sign Language Recognition using Temporal Classification", December 2015.
8. Vivek Bheda, N. Dianna Radpour, "Using Deep Convolutional Networks for Gesture Recognition in American Sign Language", 2017.
9. Teak-Wei Chong, Boon-Giin Lee, "American Sign Language Recognition Using Leap Motion Controller with Machine Learning Approach", October 2018.
10. Sven Behnke, Andreas Muller, Dominik Scherer, "Evaluation of Pooling Operations in Convolutional Architectures for Object Recognition", September 2010.
11. Jie Huang, Wengang Zhou, Qilin Zhang, Houqiang Li, Weiping Li, "Video-based Sign Language Recognition without Temporal Segmentation", January 2018.
12. Mathieu De Coster, Mieke Van Herreweghe, Joni Dambre, "Sign Language Recognition with Transformer Networks", 2020.
13. Anand John, Divyakant Meva, "A Comparative Study of Various Object Detection Algorithms and Performance Analysis", October 2020.

14. OmkarMasurekar, OmkarJadhav, Prateek
15. Kulkarni,ShubhamPatil,“RealTimeObjectDetectionUsingYOLOv3”,March2020.
16. ShivangiNagdewani,AshikaJain,“AREviewonMethodsforSpeech-to-TextandText-to-SpeechConversion”,May2020.

Soukya - Virtual Rehabilitation and Monitoring

K. Sathiyapriya, Navenkumar D, Priyadarsan M, Mokshith M and Preetham B

Department of CSE, PSG College of Technology, Coimbatore, Tamil Nadu

ABSTRACT

Exercises can become inefficient and vain, when not done properly. Having a proper pose and proper trajectory while performing an exercise is vital for the exercise to be fruitful. Soukya is a medical tele-rehabilitation application that uses suitable and efficient Machine learning and Computer vision algorithms, which evaluate the correctness of the therapeutic exercises being done by the patient, in real time. The evaluation results provide useful feedback to the patient and also enable the physiotherapist to gain insights on the effectiveness of the exercise routine for the patient, thereby improving the overall quality of the rehabilitation.

1. INTRODUCTION

Medical Rehabilitation is considered to be crucial as it restores the health of elderly people or people who try to recover after undergoing any physical or mental trauma. It supports the patient by providing proper care to get things back to normal and to improve their fitness both physically and mentally. Rehabilitation is an essential part of healthcare and is integral for achieving universal health coverage. Rehabilitation needs are increasing globally, along with the rising prevalence of non-communicable diseases and ageing populations. National efforts must strengthen health systems to provide rehabilitation, making it available to everyone at all levels of health care, whenever needed.

The COVID-19 pandemic has disrupted healthcare services across the globe, especially in the fields of Non communicable diseases (NCB). Though the disruption of services is global, low income countries are the worst affected. "Rehabilitation services have been disrupted in almost two-thirds (63%) of countries, even though rehabilitation is key to a healthy recovery following severe illness from COVID-19", quotes the World Health Organization (WHO). Also, the elderly population, who are more in need of such rehabilitation care, is expected to grow by 13.1% in the next 10 years in India. Hence, it becomes very important to look for a feasible solution that can help all kinds of patients to continue with their rehabilitation programs in a sustainable manner.

Tele-Rehabilitation has become very much essential especially in these times. Tele rehabilitation refers to the use of information and communication technologies (ICT) to provide rehabilitation services to people remotely in their home or other environments. Such services include therapeutic interventions, remote monitoring of progress, education, consultation, training and a means of networking for people with disabilities. It aims at enhancing recovery by supplementing the existing system remotely. It enables patients practice exercises provided with a tailored treatment plan at the comfort of their homes. Physical Rehabilitation becomes difficult for senior citizens as it involves a lot of time and cost. With the growth in ageing population and a need for monitoring patients remotely, Tele rehabilitation has seen large growth recently.

The proposed application facilitates the therapist to prescribe exercises and allows them to adjust it according to the patient's condition. The effective interface allows the therapist to monitor and review the progress of the patients. The exercises are designed in a gaming environment by providing rewards for successful completion of the session which not only boosts the activity of patients but also reduces the anxiety and stress levels. The assessment data of therapy sessions of each patient are stored digitally which allows the therapist to monitor them anytime later. The work is being done in collaboration with the students of PSG Institute of Medical Science and Research.

2. PROBLEM STATEMENT

The existing systems are infeasible, due to the fact that they either heavily rely on sophisticated peripherals like Kinect sensors/virtual reality [1] [2] or the simple systems are not able to evaluate the dynamic exercises. The aim is to develop an interactive web application that enables the therapist to assign suitable exercises to the patient and monitor the effectiveness of that exercise for that patient and also observe the progress of the patient. On the patient's end, the goal is to develop an effective interface that aids the patient to learn the exercise provided and evaluate the correctness of his postures, using Machine learning and computer vision algorithms. The proposed work eludes the problems stated by using a simple interface without using any hardware devices.

3. RELATED WORK

Tele rehabilitation has gained much importance in this era of the Internet. Recently, many commercial rehabilitation products are available. If these products are analysed, it can be observed that some of them make use of wearable devices. There have been some steps taken to automatically assess the level of correctness of a movement. But most of the works are limited to either verifying the correctness of a pose or to use a single algorithm to check if the exercise is being performed correctly.

Zhao et al., [3] proposed the design and implementation of a Kinect-based system for rehabilitation exercises monitoring and guidance. The Unity framework has been chosen to implement the system because it provides a virtual reality environment to demonstrate detailed movements to the patient and to facilitate examination of the quality and quantity of the patient sessions by the clinician.

Rogez et al., [4] addressed human pose recognition from video sequences by formulating it as a classification problem. The main takeaway from this paper is a pose detection algorithm based on random forests. A bottom up approach is followed to build a decision tree by recursively clustering and merging the classes at each level. The proposed approach gives promising results with both fixed and moving cameras.

Camporesi et al., [5] presented new solutions based on Virtual Reality technologies for improving the delivery of physical therapy and rehabilitation.

Krishnanath et al., [6] have used the PoseNet algorithm for real-time pose estimation. The real-time poses of the user are captured through a webcam and processed using human pose-estimation algorithms. The selected image from the database is also processed using the same algorithm. Finally, the system compares both these poses and prompts the user whether the patient has successfully imitated the pose.

Rishan et al., [7] have developed the Infinity Yoga Tutor application which captures user movements using the mobile camera and then streamed at a resolution of 1280×720 at 30 frames per second to the detection system. The system consist of two main modules, a pose estimation module which uses OpenPose to identify 25 key points in the human body, and a pose detection module which consists of a Deep Learning model, that uses time-distributed Convolutional Neural Networks, Long Short Term Memory and SoftMax regression in order to analyse and predict user pose or asana using a sequence of frames.

Martin-Moreno et al., [8] have proposed a solution based on the use of the Wii Controller to control the exercise movements, along with software that provides the patient with an easy, intuitive and interactive control system. Web services are used to allow the remote monitoring of the treatment by physiotherapy professionals.

The complexity of the exercises may vary depending on the part of the body and also considering the health conditions of the patients. Hence more hybrid and flexible ways of evaluating the exercises are needed.

4. WEB APPLICATION

4.1. INTRODUCTION

The web application has two primary modules, one is the therapist module and the other one is the patient module. The application is responsive and developed using flask with basic HTML5 framework and Bootstrap and Google Firestore for both authentication and storage. The chief therapist will be the administrator of the entire application who can modify the data of any patients and therapist via firebase console.

4.2. Therapist Module

The therapist interacts with the application by the following tasks. The therapist adds a patient by providing his/her details which include previous treatments, current health conditions, etc. He/she would also be able to allocate rehabilitation exercises to the patient based on the health conditions. The therapist could also review the exercises that have been performed by the patients so far. The therapist will also be able to fix the date for the next review based on the exercises done by the patient. The therapist can vary the exercise parameters on observing the patient's performance over the time.

4.3. Patient Module

Patients can interact with the web application using the login credentials provided to them by the therapist at the time of admission. The patients can then begin to practice the exercise assigned to them by choosing one at a time and save the progress once the session completes. For each exercise the patient completes, points would be provided to them by monitoring at each frame of the session. The report for that session would be generated based on the performance of the patient and will be saved for the reference of the therapist. In addition to this patients can contact the assigned therapist and the patient will receive notification regarding exercise assignment, session submission and therapist call for.

5. TECHNICAL APPROACH

5.1. Architecture Overview

The Architecture diagram shown in figure 1 comprises a web application which uses flask and google firebase with patient details and their respective therapy exercise profile prescribed by the therapist. The web application model initially operates in two ways. It fetches the patient exercise profile from the database while capturing the patient motion in real time. The real time motion capture is then fed to the pose estimation model which uses the trained exercise profile to estimate the correctness of the exercise in the profile.

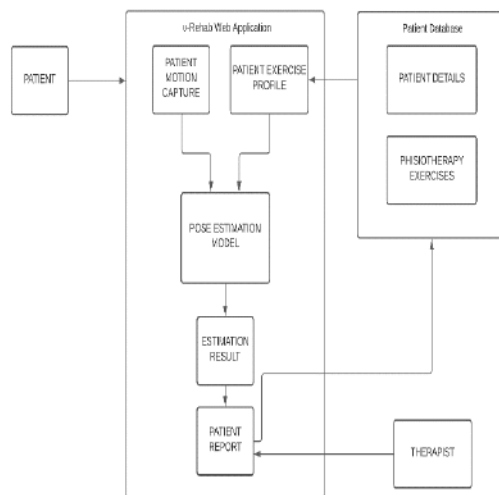


Fig.1. Architecture Diagram

The estimated pose correctness and final assessment is displayed to the patient dynamically which later generates a report for that patient and stores it into the database of the respective user. The report is then made available to both the patient and the therapist.

5.2. Dataset

Raw videos of the exercise, taken at various positions are provided by the health experts. The video is then fed into the pose estimation model [9]. The video is annotated with various angles of the joints for analysis. The angles are extracted at various positions of the exercise and the average of those angles along with variance is used to evaluate the correctness of the exercise done by the patients [10].

5.3. Pose Estimation

Pose estimation is a hard task due to little joints and impediments [11]. In this work, pose estimation is done by using a framework called Media Pipe. Media Pipe is a cross platform framework for building multi modal machine learning pipelines. It is used for various applications like face detection, multi hand tracking, pose estimation etc. The landmarks identified by Mediapipe on the body are shown in figure 2.

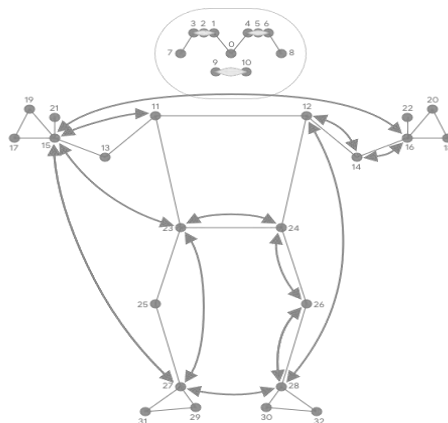


Fig.2. Pose Estimation

Media Pipe works by using a detector that first locates the pose region-of-interest (ROI) within the frame. The tracker subsequently predicts the pose landmarks and segmentation mask within the ROI using the ROI-cropped frame as input.

5.4. Parameter Tuning

The angle of various joints can be tuned depending on the various characteristics of the patient like age, gender and medical conditions. The confidence of the pose estimation model can be tuned to get better pose estimation results.

5.5. Exercise 1 - Squat

For squats, three heuristics are identified for evaluation. First, the arms should be kept straight, and should be steady throughout the exercise. This is evaluated by measuring the angle between, three landmarks, the shoulder, the elbow and the wrist. This angle should be maintained at 180 degrees ideally throughout the exercise.

Secondly, the arms should be parallel to each other and they should be at right angles with the spine, throughout the exercise. This is quantified by measuring the angle between the shoulder, hip and the elbow. This angle should be maintained at 90 degrees for the entire duration of the exercise.

Lastly, a proper squat exercise requires the person to bend the knee up to an ideal minimum point. An improper squat is one where the person bends below the ideal point, or doesn't bend enough to reach the ideal point. Through the analysis of a video provided by a health expert, it was estimated that the optimal knee angle was 45 degrees. The above angles are measured in every frame and the user is alerted whenever the joints cross the threshold. Also a certain amount of variance must be provided for various categories of patients, depending on their medical condition which is decided by the physicians. The default variance given is 5 degrees

5.6. Exercise 2 - Hip Bridge

For the hip bridge three heuristics were identified for evaluation. First the arms should be straight and inclined at 180 degrees throughout the course of the exercise laid to the surface.

Secondly the spine should be initially flat pressed against the surface and gradually rise to an angle of 180 degree, which is obtained using the joints hip, shoulder and knee. In a proper Hip bridge exercise, the spine will reach up to 180 degrees and a bridge shape is formed between the shoulder and the hip. This position should be held for 15 seconds and then the spine should gradually return the original position.

The knees should form a pyramid like shape and they should vary only slightly while the hip is being raised. Ideally they should lie in the range of 10 to 15 degrees. Using all these angle values, the patient is alerted, when any of these constraints is violated, along with suggestions to rectify the pose.

5.7. Exercise 3 - Seated Right Knee Extension

For the seated right knee extension exercise three heuristics are identified for evaluation. First, the spine should be straight and seated at 90 degrees throughout the exercise. Second, the arms should be parallel to each other and also to the spine.

Last, the legs should be seated at 90 degrees respective to the spine and knee at 90 degrees respective to the legs. The optimal knee angle on the extension of the right knee should be 180 degrees. The frames are closely monitored for the angles throughout the session and indicated to the patient if there are any errors in the action of the exercise angles. The default variance provided here is 5 degrees.

6. RESULTS

6.1. Exercise 1 – Squats

Stand straight

Seated Limit Reached
Slowly stand up



Fig.3. Squats 1

Fig.4. Squats 2

Initially, as shown in figure 3 the application instructs the patient to stand straight to come in position by monitoring the angles. As the patient slowly squats down (figure 4) the angle of the knees are closely monitored and when the default angle is met within the variance provided it instructs to stand up again indicating that the seating level is reached for the squats exercise. The angle deviations are calculated and used to provide feedback for the patient [12].

Continue squatting up
Error: Squatting too deep



Fig.5. Squats Error

The application prompts the patient that he is squatting too deep indicating that the exercise is incorrect as shown in figure 5.

6.2. Exercise 2 - Hip Bridge

Initial position set
Raise your hip



Fig.6. Hip Bridge 1

In figure 6 the patient has laid down to the surface with his arms parallel to the spine and knees bent.

Bridge formed
Hold for 15.0 seconds and lower down



Fig.7. Hip Bridge 2

The application then instructs the patient to raise the hips slowly until a bridge is formed under the hip as shown in figure 7 and then prompts the patient to hold it for 15 seconds and bring it back to initial position again.

Continue lowering your hip
Error: Raising hip too much

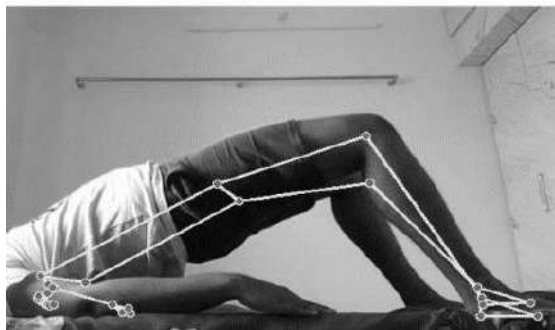


Fig.8. Hip Bridge Error

When the patient raises his hips too high as shown in figure 8 indicating that the exercise is incorrect and the application prompts the same to the patient.

6.3. Exercise 3 - Seated Right Knee Extension

Initial position set
Slowly extend the right leg



Fig.9. Seated Right Knee Extension

In figure 9 the patient is seated with his spine at 90 degrees perpendicular to the knee and legs are also at 90 degrees with respect to the knee which marks the initial position for the exercise.

Extension limit reached
Slowly lower right leg



Fig.10. Seated Right Knee Extension 2

In figure 10 the patient raises his right knee and the model prompts that the extension limit is reached when the knee angle becomes 180 degrees and then instructs to bring back to original position.



Fig.11. Seated Right Knee Extension Error

In general both the legs should clearly be visible. But in figure 11 the left legs are not visible and the error is shown.

7. CONCLUSION

There are many works that discuss the effectiveness of various remote tele-rehabilitation systems. Most of them require the patient to use additional wearable devices or sensor. They also do not provide feedback about the correctness of the exercise being done.

In this work, a computer vision based user friendly application that uses pose estimation to provide personalized feedback at real time on rehabilitation exercises has been developed. The output of pose estimation has been used to evaluate videos of rehabilitation exercises through human pose key points.

Several extensions were identified as strong opportunities for future work past this work. One path would be to evaluate the body postures of kids and people with different body figures. Another direction would be to build an application that allows users to record a video and get pose feedback at any place.

REFERENCES

1. S. K. Swee, L. Z. You, B. W. W. Hang and D. K. T. Kiang, "Development of rehabilitation system using virtual reality," 2017 International Conference on Robotics, Automation and Sciences (ICORAS), 2017, pp. 1-6, doi: 10.1109/ICORAS.2017.8308045.
2. R. Fuior, C. Luca, D. Andrițoi and C. Corciovă, "The Application of Virtual Reality Technology in Rehabilitation," 2019 11th International Symposium on Advanced Topics in Electrical Engineering (ATEE), 2019, pp. 1-4, doi: 10.1109/ATEE.2019.8724953.
3. W. Zhao, H. Feng, R. Lun, D. D. Espy and M. A. Reinthal, "A Kinect-based rehabilitation exercise monitoring and guidance system," 2014 IEEE 5th International Conference on Software Engineering and Service Science, 2014, pp. 762-765, doi: 10.1109/ICSESS.2014.6933678.
4. Rogez, J. Rihan, S. Ramalingam, C. Orrite and P. H. S. Torr, "Randomized trees for human pose detection," 2008 IEEE Conference on Computer Vision and Pattern Recognition, 2008, pp. 1-8, doi: 10.1109/CVPR.2008.4587617.
5. Camporesi, M. Kallmann and J. J. Han, "VR solutions for improving physical therapy," 2013 IEEE Virtual Reality (VR), 2013, pp. 77-78, doi: 10.1109/VR.2013.6549371.
6. Borkar, Pradnya Krishnanath et al. "Match Pose - A System for Comparing Poses," International journal of engineering research and technology 8 (2019): n. Pag.
7. Rishan, B. De Silva, S. Alawathugoda, S. Nijabdeen, L. Rupasinghe and C. Liyanapathirana, "Infinity Yoga Tutor: Yoga Posture Detection and Correction System," 2020 5th International Conference on Information Technology Research (ICITR), 2020, pp. 1-6, doi: 10.1109/ICITR51448.2020.9310832.
8. Martin-Moreno, D. Ruiz-Fernandez, A. Soriano-Paya and V. Jesus Berenguer-Miralles, "Monitoring 3D movements for the rehabilitation of joints in physiotherapy," 2008 30th Annual International Conference of the IEEE Engineering in Medicine and Biology Society, 2008, pp. 4836-4839, doi: 10.1109/IEMBS.2008.4650296.

9. Sonwani, Nitesh and Aryan Pegwar. "Auto_Fit: Workout Tracking Using Pose-Estimation and DNN." (2020).
10. Chen, S., & Yang, R.R. Pose Trainer: Correcting Exercise Posture using Pose Estimation. (2020). ArXiv, abs/2006.11718.
11. Singh, S. Agarwal, P. Nagrath, A. Saxena and N. Thakur, "Human Pose Estimation Using Convolutional Neural Networks," 2019 Amity International Conference on Artificial Intelligence (AICAI), 2019, pp. 946-952, doi: 10.1109/AICAI.2019.8701267.
12. Thar, Maybel & Winn, Khine & Funabiki, Nobuo. "A Proposal of Yoga Pose Assessment Method Using Pose Detection for Self-Learning". (2019) 137-142. 10.1109/AITC.2019.8920892.

Detection of Sensitive Data Exposure in Images

Amir Faizal, Dhilip Sanjay S, Naveen P, Vishnu Vardhan, Mouleeswaran S and L. S. Jayashree
Department of Computer Science and Engineering, PSG College of Technology, Coimbatore, Tamil Nadu

ABSTRACT

In the contemporary age of clever devices and smart telephones, any image taken the use of those devices are straight away auto uploaded to the cloud (Google Photos, iCloud, etc) or internet (Social media sites like Facebook, Twitter, and so forth). And there's an archive of all of the contents that is being uploaded to the internet within the Wayback Machine. So, one have to be careful about what is being uploaded to the internet. Unfortunately, people knowingly or unknowingly upload photos containing sensitive data like: Usernames and Passwords, Credit card or Payment Card Information (PCI), Personally Identifiable Information (PII), E-mail Addresses, Phone Numbers, Social Security Numbers, Aadhar Numbers, Protected Health Information (PHI), Customer's facts, Student's facts. All these sensitive information fall beneath 3 classes: (i) Personal and Private Information, (ii) Confidential Business Information, (iii) Classified Information. Loss, misuse, modification, or unauthorized get entry to to sensitive information can adversely affect the privacy or welfare of an man or woman, alternate secrets and techniques of a business or even the security and global members of the family of a state relying on the level of sensitivity and nature of the records. We have designed a deep studying machine that classifies the data in the snap shots as touchy or non-sensitive. On being categorised as touchy, we can warn the users that their photograph incorporates sensitive data (earlier than uploading to the cloud).

Keywords— CNN, Sensitivity Detection, Image Classification, Tesseract OCR, Text Classification

INTRODUCTION

Nowadays, any image taken using smart devices and smart phones are immediately auto uploaded to the cloud or internet. Unfortunately, people knowingly or unknowingly upload images containing sensitive data. We have designed a system that uses machine learning to prevent the exposure of sensitive data in images.

Our system will be using two machine learning models and an OCR module. Image classification model uses Convolutional Neural Networks to classify the data based on the visual features. Optical Character Recognition to extract the text from images. Text classification model which makes use of Word Embeddings and Convolutional Neural Networks to classify the data based on extracted textual features.

Our primary motivation is to prevent the exposure of sensitive data in images (before uploading to the cloud or social media platforms) and also to enlighten the people who have little or no awareness about the consequences of sensitive information exposure. This system will be useful for anyone who makes use of the internet, cloud platforms and social media platforms. It'll help prevent the exposure of sensitive data in images.

LITERATURE SURVEY

In [1] used Multi Sequencing with CNN. Data imbalance is a commonplace trouble in textual content class, especially in domain unique touchy texts. Deep Neural networks achieved promising results on textual content class responsibilities.

In [2] used TD2V, a Twitter-based Doc2Vec model and Modified Distance. The proposed technique aims to exploit the semantic and content of a report, as opposed to based on key phrases or document layout as most of existing strategies in DLP. The pre-educated document embedding version TD2V is implemented into the security and privacy area. Sensitive statistics are hard to attain considering the fact that they can contain private records approximately an character or a corporation. Therefore, custom sets of documents had been created for the experiment performed in this thesis. The performance of these algorithms notably relies upon at the statistics set and on the speed and memory demands, and each one could be a solid choice in a specific environment.

In [3] used OSVM rejection, Ensemble rejection, Center Based Similarity SVM, Deep Open Classification (CNN or LSTM), DOC with FastText. DOC took the longest time to train, due to the training process of neural networks; however, it was reasonably fast in classification. used Naive Bayes, Support Vector Machine (SVM), k-nearest neighbor algorithm and decision trees. Naive Bayes has given the highest learning of DLP text classification architect using the words weighting. Naive Bayes classifier has achieved 98.75 accuracy.

In [5] used KNN, SVM, Hybrid (SVM-KNN), Convolution Neural Network Logistic regression. This paper shows the improvement of the text classification model by using non-linear features with convolutional layers.

In [6] used Support Vector Machines (SVMs), Naive Bayesian classifiers, and Rocchio classifiers. A successful classifier have to meet numerous assessment criteria. It need to have a low fake poor rate and low fake effective price.

In [7] used Deep CNN with Tree classifiers. CNNs are trained in an end-to-quit way to allow pixel-stage prediction and type.

In [8] used Convolutional neural networks. An intrinsic characteristic of the convolutional layers in Convolutional Neural Networks is the ability to extract information from the input image into feature maps. The experiments on real-world datasets demonstrate that utility (classification accuracy)- privacy trade-off is perfectly handled via the adversarial training process.

In [9] used CNN pre trained on ImageNet, Tesseract OCR engine, one-dimensional convolutional neural network. This cease-to-quit learnable multimodal deep community that jointly learns textual content and photograph capabilities and performs the final type based on a fused heterogeneous representation of the document.

In [10] used Convolutional neural networks, Recurrent Neural Network (LSTM). Fitting a model to text and image is difficult because of the differences in the shape, size, and techniques used to process each. To improve performance of a deep learning model that is training on limited data, you need a simpler model with fewer parameters.

PROPOSED METHOD

The literature survey shows that none of the existing systems apply both image classification and text classification simultaneously for the detection of sensitive data in images. The proposed system applies both image classification and text classification simultaneously to detect sensitive data in images. On being labeled as sensitive. Warn the customers that their picture contains sensitive statistics (earlier than importing to the cloud), thereby preventing the loss, misuse or unauthorized get right of entry to to sensitive information.

Dataset Collection

The dataset used for the implementation of image classification and text classification model are described. The Image Dataset had a total of 700 images. Out of which 350 were sensitive images and the rest 350 were non-sensitive images. We split the dataset into training and validation data. Training data had 600 images and validation data had 100 images. The non-sensitive images were collected from the Kaggle dataset named Image dataset.



Fig 3.1 Non-sensitive Images

Only a part of this dataset was used for training in our model. The sensitive images were not readily available. So we scraped sensitive images like Aadhar card, PAN card, Driving License, Credit cards, Debit cards, ID cards, SSN cards, Voter's ID, Bank Passbook, Passport, Visa, Number plates, Bills and Invoices, etc. using selenium.



Fig 3.2 Sensitive Images

The text dataset had 32000 samples (approximately). Out of which 20000 examples were used for training purposes and the rest 12000 were used for validation purposes. The non-sensitive text data was collected from

the BBC News dataset and Wiki movie plots dataset. The sensitive text data was generated using publicly available fake Aadhar cards, PAN cards, Credit cards, Debit cards, Number plates, SSN cards, Bank Passbook, SSN cards, common usernames, email addresses, etc.

```

Dataset Size: 31576
Training Dataset Size: 20000
Sample Training Data: username:delany, password:ruhammad, email:delany@facebook.com, phone no:1567769561
Validation Dataset Size: 11576
Sample Validation Data: Veronica Sawyer one popular girls Hesterburg High School Sherwood, Ohio. In addition Veronica, popular clique consists three wealthy beautiful girls first name: Heather Chandler, Heather Duke, Heather McManara. Though popular students, Heathers feared hated. Veronica enough behavior forgo return old life "nerdy" friends. When new student, rebellious outsider named Jason "J.D." Dean pulls gun locks Kurt Kelly Ram Sweeney, trying bully him, fire blanks the m, Veronica finds fascinated him. When Veronica attends frat party Heather Chandler, refuses sex frat brother throws up, Heather vows des Troy reputation. J.D. shows Veronica's house end sex outside, Veronica tells J.D. wants make Heather puke guts out. The next morning, Veronica J.D. break Heather's house. J.D. serves Heather liquid claims hangover cure actually drain cleaner, killing her. J.D. urges Veronica a forge dramatic suicide note weather's handwriting. The school community look Heather's apparent suicide tragic decision made popular ostensibly troubled teenager. Heather Duke soon steps Heather Chandler's former role clique leader begins wearing red scrunchie belonged Chandler. Several days later, Kurt Ram spread false rumor Veronica giving oral sex, ruining reputation. J.D. proposes Veronica lure woods promise "make rumors true," shoot nonfatal "Ich Edge" bullets. J.D. shoots kills Ram Veronica misses Kurt, runs away. Veronica realizes bullets real; J.D. chases Kurt back towards Veronica, panics fatally shoots him. J.D. plants pay materials beside boys, suicide note stating two l overs participating suicide pact. At funeral, boys made martyrs homophobia. Although keeps dating J.D., Veronica increasingly disturbed behavior.
Martha Dumstock, obese student known "Martha Dumtruck", pins suicide note chest walks traffic. She survives, badly injured mocked trying "act like popular kids." Heather McManara calls popular radio show one night Veronica Heather Duke listening talks depression life; next day, Heather Duke tells entire school Heather McManara's radio call. McManara attempts take life overdosing pills girls' bathroom saved Veronica. Veronica tells J.D. will not participate killings. He climbs room revolver kill her, Veronica used harness make look like hanged herself. Assuming dead, rambles plan blow school pop rally. A petition circulating get band Big Fun perform campus, students signed, actually mass suicide note. Veronica confronts J.D. boiler room, rigging explosives. She shoots refuses stop bomb. As J.D. collapses, stabs timer stops. Veronica walks pop rally everyone cheering. The severely injured J.D. follows outside bomb strapped chest, offers personal eulogy, detonates bomb. Veronica confronts Heather Duke, takes red scrunchie, says "Heather love, new sheriff town," invites Martha Dumstock hang prom night watch on movies her. Martha Veronica walk hallway Heather Duke watches.
    
```

Fig 3.3 Sample Text from Dataset

System Architecture

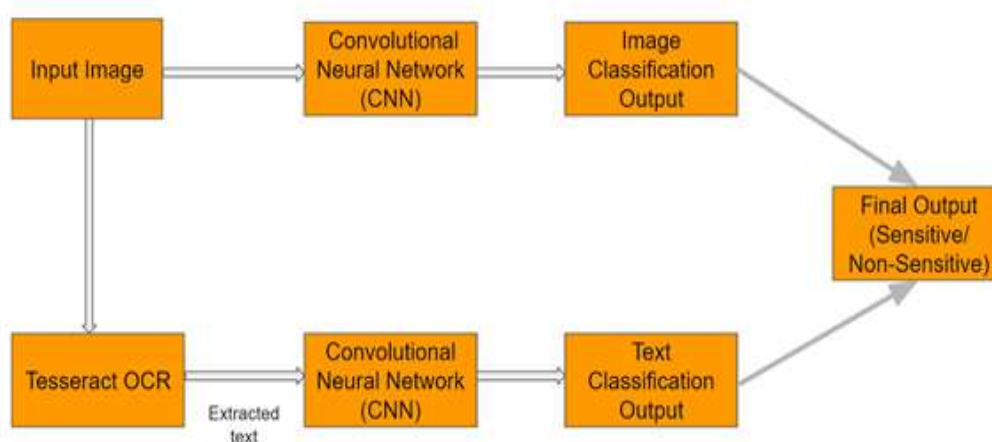


Fig 3.4 Architecture Diagram

The system architecture is shown in Fig 3.4. The architecture of the proposed system has the following components:

- **Input Image** - The input image is obtained from the user.
- **Convolutional Neural Network (CNN for Image Classification)** - The image is classified as sensitive or non-sensitive using Convolutional Neural Network.
- **Tesseract OCR** - The text in the user's image is extracted by using tesseract OCR.
- **Convolutional Neural Network (CNN for Text Classification)** - Text that is extracted from tesseract OCR is classified as sensitive or non-sensitive using the Convolutional Neural Network.
- **Image Classification Output** - The output of the image classification module is obtained.
- **Text Classification Output** - The output of the text classification module is obtained.
- **Final Output** - The image classification output and the text classification output are fused together and the result is displayed to the user as sensitive or non-sensitive.

Image Classification Model

The Layers of the Image classification model are shown in Fig 3.5 (a) and Fig 3.5 (b). The model has Convolution 2D Layers and Max Pooling 2D Layers with Relu Activation Function, Fully connected dense layers and the Output Layer. The Output Layer is a Sigmoid Activation Function. If the output of this final layer is greater than 0.5 the image contains sensitive data, else it contains non-sensitive data.

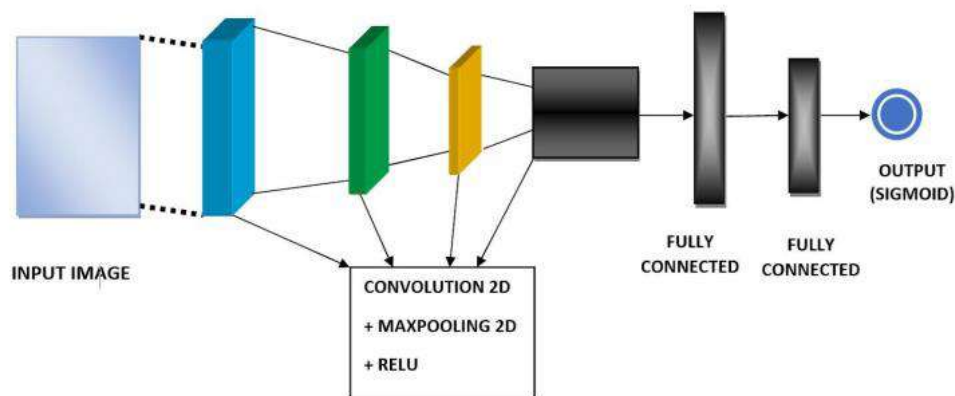


Fig 3.5 (a) Image Classification Model

Model: "sequential"

Layer (type)	Output Shape	Param #
conv2d (Conv2D)	(None, 148, 148, 32)	896
max_pooling2d (MaxPooling2D)	(None, 74, 74, 32)	0
conv2d_1 (Conv2D)	(None, 72, 72, 64)	18496
max_pooling2d_1 (MaxPooling2D)	(None, 36, 36, 64)	0
conv2d_2 (Conv2D)	(None, 34, 34, 128)	73856
max_pooling2d_2 (MaxPooling2D)	(None, 17, 17, 128)	0
conv2d_3 (Conv2D)	(None, 15, 15, 256)	295168
max_pooling2d_3 (MaxPooling2D)	(None, 7, 7, 256)	0
flatten (Flatten)	(None, 12544)	0
dense (Dense)	(None, 512)	6423040
dense_1 (Dense)	(None, 1)	513

Total params: 6,811,969
 Trainable params: 6,811,969
 Non-trainable params: 0

Fig 3.5 (b) Layers in Image Classification Model

Text Classification Model

The Layers of the Text classification model are shown in Fig 3.6 (a) and Fig 3.6 (b). The model has Embedding Layer, Convolution 1D layer with Relu Activation function, Global Average Pooling 1D layer, Fully connected dense layers and the Output Layer. The Output Layer is a Sigmoid Activation Function. If the output of this final layer is greater than 0.5 the image contains sensitive data, else the image contains non-sensitive data.

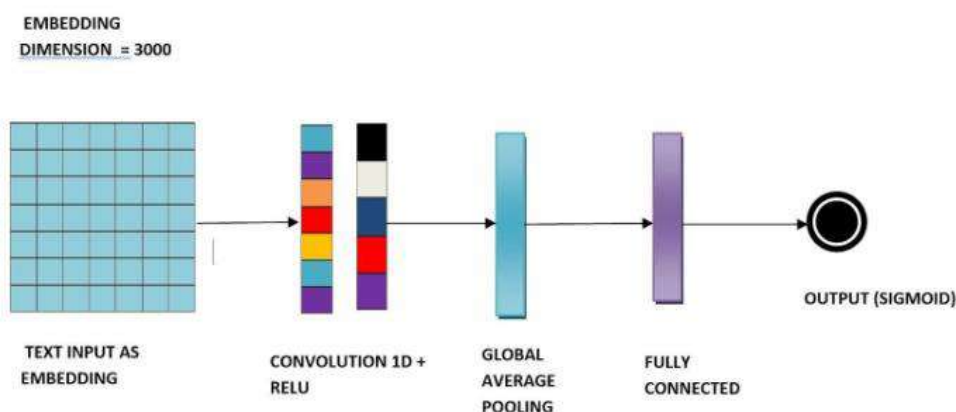


Fig 3.6 (a) Text Classification Model

```
Model: "sequential_12"
Layer (type)                Output Shape                Param #
-----
embedding_12 (Embedding)    (None, 60, 32)             96000
conv1d_12 (Conv1D)          (None, 56, 64)             10304
global_average_pooling1d_12 (None, 64)                 0
dense_20 (Dense)            (None, 24)                 1560
dense_21 (Dense)            (None, 1)                  25
-----
Total params: 107,889
Trainable params: 107,889
Non-trainable params: 0
```

Fig 3.6 (b) Layers in Text Classification Model

RESULTS

Fig 4.1 shows the output of the final model. This output consists of both text and image classification model result (Results from both the classification models are merged and output is displayed as sensitive or non-sensitive). The results of Image Classification model, Text Classification model are discussed separately. The results shown by the web application are also discussed below.



Fig 4.1 Output of final model

Image Classification Results

The image classification results with its accuracy and loss for different Hidden layers and number of epochs are tabulated in Table I. The maximum accuracy is achieved with the ADAM optimizer at 114 epochs with 11 Hidden layers.

Table I Image Classification Results

Number of Hidden Layers	Number of Epochs	Validation	
		Accuracy	Loss
11 (With RMSProp=0.1 optimizer)	116	0.9750	0.0449
11 (With RMSProp=0.1 optimizer)	120	0.9500	0.1533
11 (With ADAM optimizer)	114	1.000	0.0165
11 (With ADAM optimizer)	104	0.9500	0.1225

Fig 4.2 shows the accuracy and loss function of image classification model for both training and validation data.

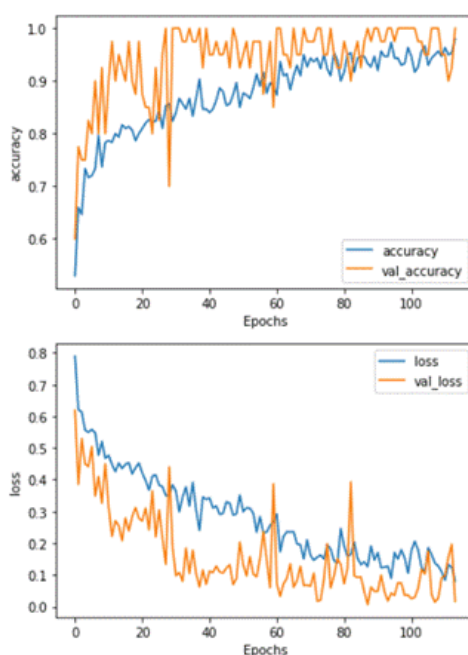


Fig 4.2 Accuracy and Loss of Image Classification Model

Fig 4.2 shows the confusion matrix of image classification. It shows the number of correct and incorrect prediction made in image classification. The image classification model has a maximum accuracy of 68 percentage.

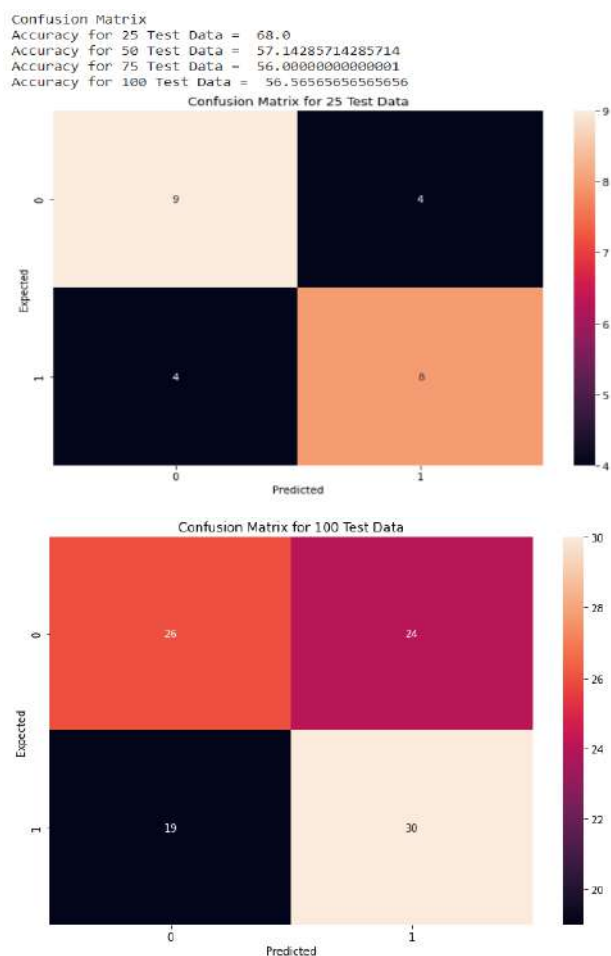


Fig 4.3 Image Classification Confusion Matrices

Text Classification Results

The text classification results with its accuracy and loss for different Hidden layers and number of epochs are tabulated in Table II. The maximum accuracy for text classification is achieved with the ADAM optimizer at 6 epochs with 5 Hidden layers.

Table II Text Classification Results

Number of Hidden Layers	Number of Epochs	Validation	
		Accuracy	Loss
5 (With ADAM optimizer)	6	1.000	4.8541e-05
5 (With ADAM optimizer)	6	1.000	7.4832e-05
4 (With ADAM optimizer)	5	0.9997	9.7882e-04

Fig 4.4 shows the accuracy and loss function of text classification model for both training and validation data.

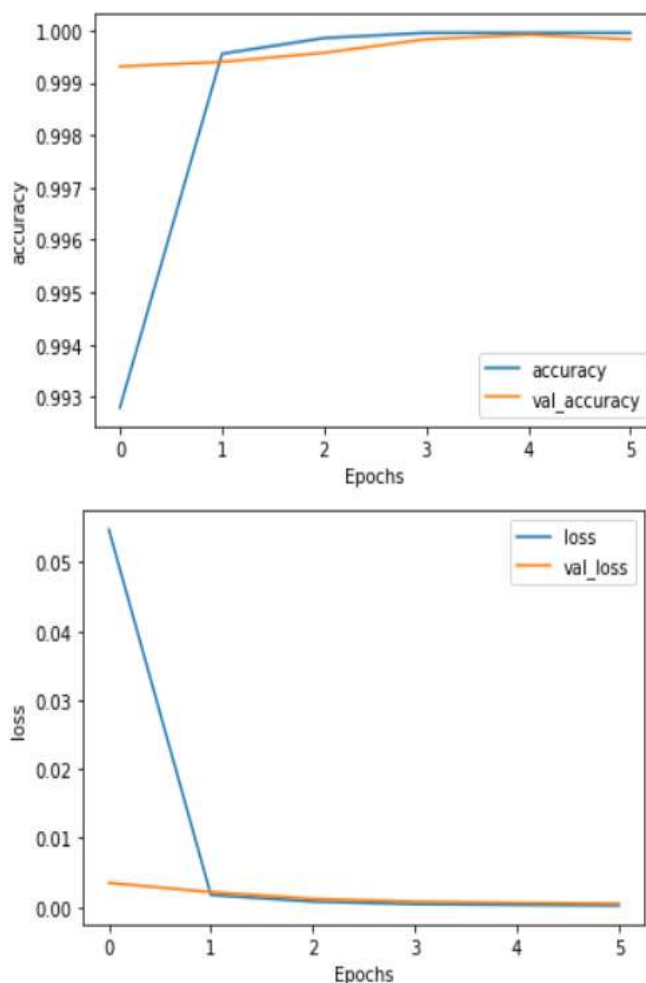


Fig 4.4 Accuracy and Loss of Text Classification Model

Fig 4.5 shows the confusion matrix of text classification. It shows the number of correct and incorrect prediction made in text classification. The image classification model has a maximum accuracy of 99 percentage.

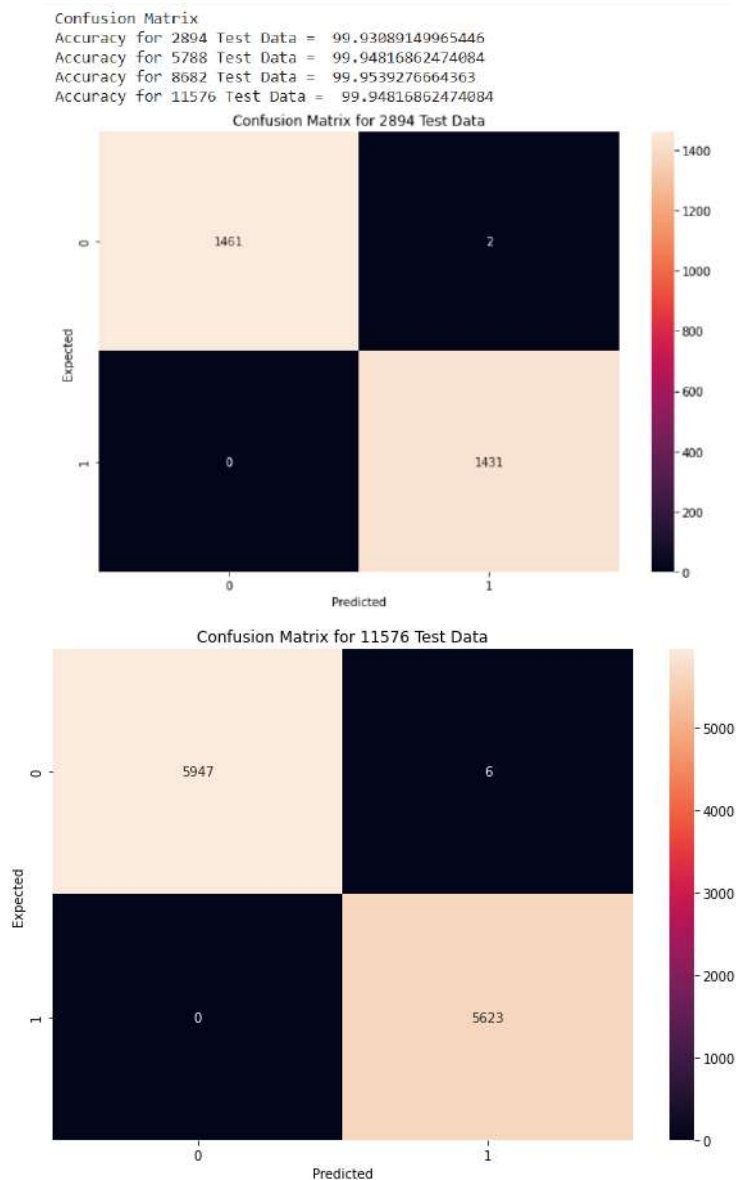


Fig 4.5 Text Classification Confusion Matrices

Results in web application

The final model is deployed as a web application using Firebase Hosting Services. The Web Application uses Tesseract OCR for extracting the text from the image, which is later given as input to the text classification model. The web application classifies the image as sensitive or non-sensitive by using both the image classification and the text classification models. The URL of the web application is <https://sensitivity-detecto.web.app>. The figures Fig 4.6 (a) and Fig 4.6 (b) shows the result obtained in web application.



Fig 4.6 (a) Classified as Sensitive

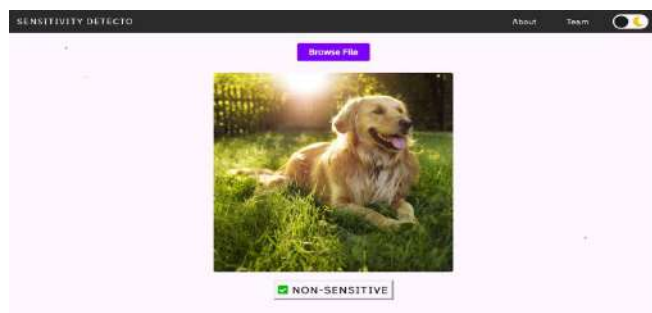


Fig 4.6 (b) Classified as Non-sensitive

CONCLUSION

In this project, the Image Classification model is used to classify the data based on the visual features. And then Optical Character Recognition is used to extract the text from the image. The Text Classification model is used to classify the data based on extracted textual features. Through this system anyone can find whether the image uploaded in the internet or cloud contains any confidential information. If it contains sensitive data our system will produce a warning stating that sensitive information is present. Thus, our system helps in detecting the sensitive information and protects the images from being misused.

REFERENCES

1. Y. Chen and D. Evans, "Auditing information leakage for distance metrics," in Privacy, Security, Risk and Trust (PASSAT) and 2011 IEEE Third International Conference on Social Computing (SocialCom), 2011 IEEE Third International Conference on. IEEE, 2011, pp. 1131–1140.
2. Harel, A. Shabtai, L. Rokach, and Y. Elovici, "M-score: estimating the potential damage of data leakage incident by assigning misuseability weight," in Proceedings of the 2010 ACM workshop on Insider threats. ACM, 2010, pp. 13–20.
3. J. Gantz and D. Reinsel, "The digital universe in 2020: Big data, bigger digital shadows, and biggest growth in the far east," IDC iView: IDC Analyze the future, vol. 2007, pp. 1–16, 2012.
4. M. Katzer and D. Crawford, "Office 365 compliance and data loss prevention," in Office 365. Springer, 2013, pp. 429–481.
5. Ouellet and R. McMillan, "Magic quadrant for content-aware data loss prevention," Gartner Group Research Note, 2011.
6. Katz, Y. Elovici, and B. Shapira, "Coban: A context based model for data leakage prevention," Information Sciences, vol. 262, pp. 137–158, 2014.
7. S. Alneyadi, E. Sithirasenan, and V. Muthukkumarasamy, "A semantics-aware classification approach for data leakage prevention," in Information Security and Privacy. Springer, 2014, pp. 413–421.
8. F. Krause, Taxicab geometry: An adventure in non-Euclidean geometry. Courier Corporation, 2012.
9. M. Hart, P. Manadhata, and R. Johnson, "Text classification for data loss prevention," in Privacy Enhancing Technologies. Springer, 2011, pp. 18–37.
10. J. M. Gomez-Hidalgo, J. M. Martin-Abreu, J. Nieves, I. Santos, F. Brezo, and P. G. Bringas, "Data leak prevention through named entity recognition," in Social Computing (SocialCom), 2010 IEEE Second International Conference on. IEEE, 2010, pp. 1129–1134.
11. Amuthadevi, D. S. Vijayan, Varatharajan Ramachandran, "Development of air quality monitoring (AQM) models using different machine learning approaches", Journal of Ambient Intelligence and Humanized Computing, <https://doi.org/10.1007/s12652-020-02724-2>.

Precision Agriculture – Coimbatore Based Crop Suggestion System Using ML and IOT

N Gopika Rani, Sneha Sridharan, Gayathri B, Poovizhi Mangai K, Praja S. S and Shivathmica C
Department of CSE PSG College of Technology, Coimbatore

ABSTRACT

Agriculture rules more than half of India's population economically. Farmers are not aware of the right crop according to their soil characteristics and site specific parameters. Due to this the yield can be low and their profits are affected. A crop recommendation system has been developed, with an intention to assist the farmers in the Coimbatore district of Tamil Nadu in helping them select appropriate crops based on the soil in their farms. The goal is to mitigate the traditional farming methods, and to achieve this, a combination of machine learning models such as Random Forest, K-Nearest Neighbor and Decision tree is used as an ensemble model. The most suitable crop to be grown depends on the soil quality which is governed by soil and environmental characteristics such as temperature, rainfall, soil type etc. This automated crop suggestion system alleviates farmers from the pitfalls of traditional farming practices and paves way for better agricultural profit and productivity. IoT sensors to measure Temperature and pH of the soil are used in this system to provide the exact values of these attributes giving reliable results. Furthermore, the ensemble model proves to give the best accuracy of 89.27% as compared to the existing ensemble model with accuracy 85.41% and ANN with accuracy 76.1%. Thus, the most precise crop to be grown in the farmer's agricultural land in Coimbatore is suggested.

Keywords—Ensemble model, Random Forest, K-Nearest Neighbor, Decision Tree, Internet of Things

I. INTRODUCTION

India is the world's second largest producer of wheat and rice and world's first producer of several other crops. [16] Coimbatore is a district in the Tamil Nadu which is located on the banks of the Noyyal River and enveloped by the Western Ghats. Coimbatore is the second largest city in the state of Tamil Nadu. The cultivable soil of the district is classified into 16 different soil series having different soil properties. [17] All sorts of traditional farming practices do exist here. Farmers of Coimbatore are unaware of the heterogeneous nature of soil. There are major changes in soil properties happening even within short distances. Growing the same crop as the neighbouring farmer will not be as profitable as it is for them. Also, choosing a crop for cultivation based only on market trends will cause adverse loss financially and worsen the quality of soil.

By taking into account of the undulating nature of the environment and soil parameters that Indian agriculture relies on, farmers don't find the most precise agriculture techniques for better yield. But they are unaware of such influencing parameters. They always prefer to trust their instincts and follow traditional farming methods. Such unsure practices may unfortunately cause the anticipated productivity and profitability become unsubstantial. Since soil is a non-renewable natural resource the soil health and land productivity may deteriorate overtime. This may lead to unpleasant implications on the farmer's life as well as the status of food security in the specific region. In the thought of extenuating this situation, smart farming techniques can be imbibed.

A crop recommendation system developed for the Coimbatore region will be beneficial. This system is developed based on certain input parameters like soil pH, EC (Electrical Conductivity), type, N, P, K and environmental conditions like temperature and rainfall. This system requires multi label classification (MLC) which can be achieved by algorithms like Random Forest, Decision Tree etc. [1,13,14] Hence, we combined the power of 3 such algorithms: Random Forest, KNN and Decision tree to form an ensemble model to get better results. The ensemble model gives more prediction and efficiency than any of its models could accomplish alone. Temperature sensors reads the accurate temperature values continuously. pH sensors detects the pH of the soil ranging from 0 to 14. [13] Sensor readings along with user inputs like soil type, rainfall is fed into the trained model to give the output. This system provides precise suggestion on the most appropriate crop to be grown in the farmer's agricultural land in Coimbatore.

II. LITERATURE SURVEY

Z. Doshi et al. (2018) discussed about environmental parameters like temperature, rainfall, farm's latitude, longitude, altitude and distance from the sea and soil characteristics such as pH value, soil type and thickness of aquifer and topsoil that has to be considered in a crop suggestion system. [1] Crops used were bajra, jowar, maize,

rice and wheat, barley, cotton, groundnut, gram, jute, other pulses, potato, ragi, tur, rapeseed and mustard, sesame, soybean, sugarcane, sunflower and tobacco crops. They compared various machine learning models that have in built support for Multi-label classification (MLC): Decision Tree, K Nearest Neighbor (K-NN), Random Forest and Neural Network and obtained 90.2%, 88.78%, 90.43% and 91% efficiency respectively.

S. Pudumalar et al.(2016) stated that a suggestion system based on site specific and soil parameters would be the most useful for farmers.[2] The attributes considered in this paper: Depth, Texture, pH, Soil Colour, Permeability, Drainage, Water holding and Erosion. The crops chosen by them include millet, groundnut, pulses, cotton, vegetables, banana, paddy, sorghum, sugarcane, coriander. A recommendation system using an ensemble model with majority voting technique was proposed. The base learners used were Random tree, CHAID, K-Nearest Neighbour and Naive Bayes and it was observed that the prediction accuracy of the model was 88%. Ensemble model is one of the most preferred for this system according to these set of papers and therefore we decided to opt for it.

Kevin Tom Thomas et al.(2020) used environmental factors like temperature, humidity etc and soil parameters such as N, P, K and pH of the soil in their input dataset.[3] The algorithms: kNN, kNN with cross validation, Decision Tree, Naïve Bayes and SVM were considered for evaluation and their respective efficiencies were 85%, 88%, 81%, 82% and 78%. It was inferred that kNN with cross validation was the ideal model and thus we decided to adopt kNN as one of the base learners in our ensemble model. The idea of adding IoT sensors to measure soil properties in their scope for improvement section inspired us to include the same in our project.

Harshitha L. et al.(2020) discussed about improving crop productivity through crop recommendation.[4] Nutritional features in soil like pH values, organic Carbon, iron, zinc, nitrogen, phosphorus, sulphur have been used as it is assumed that chemical analysis of the soil helps in improving crop production. Other attributes include rainfall and temperature. Algorithm chosen by them is Naïve Bayes Algorithm.

K.R. Akshatha et al.(2018) aimed to solve the problem of crop selection using a combination of different models.[5] It considers soil based attributes like depth, texture, pH, soil color, permeability, drainage, water holding capacity and erosion in their dataset. The crop recommendation system is built using an ensemble model – majority voting technique, using a combination of models like Random tree model, K-Nearest Neighbor model and Naïve Bayes model. The crops recommended by mapping with appropriate soil parameters are millet, groundnut, pulses, cotton, vegetables, banana, paddy, sorghum, sugarcane, coriander.

Srilakshmi A. et al.(2020) aimed to get the best solution for crop prediction and recommendation system by comparing machine learning algorithms like random forest, decision tree and SVM.[6] Accuracy obtained for random forest is 95.09%, higher than the rest of the models. The datasets are trained using SVM – grid search and random forest algorithms. The soil parameters taken into account for predicting crop based on environmental factors are temperature, humidity, pH and rainfall. The dataset consists of 3100 rows x 5 columns obtained from online that required no preprocessing. It was also found that combination of SVM and decision tree gave an accuracy of 91.8%, randomized search used on random forest gave 94.7% accuracy. Hence, it is concluded that random forest algorithm performs the best accuracy when compared to other models. Future work comprises of including more soil parameters to perform crop prediction.

Snehal S. Dahikar et al.(2014) focused on making the farmers attain maximum crop yield at minimum cost using ANN – feed forward back propagation technique.[7] The yield for a crop is predicted based on the soil specific parameters like pH, depth, nutrient contents like nitrogen, phosphate, potassium, organic carbon, magnesium, sulphur, manganese, copper, iron and environment-based parameters like temperature, and rainfall. It is concluded that ANN can be a beneficial tool for prediction.

Varsha A. et al.(2020)designed a model to predict a specific crop grown in a soil.[8] The dataset collected IoT system are soil moisture, soil pH and gas content of soil. Firstly, data mining techniques are applied on the sensor values then machine learning steps are applied. A sophisticated front end web interface is also developed for the farmers to view the recommended crop for their soil. The idea of adding IoT sensors to measure soil properties inspired us.

Avinash Kumar et al.(2019) proposed a recommendation system using soil type, average rainfall, average temperature, pH and its corresponding crop type as attributes for 15 different crops.[9] They have used 3 different algorithms individually to figure out which one provides the best accuracy (SVM – 89.66%, Decision Tree – 86.80%, Logistic Regression – 86.04%). It also provides details of Pests and its management for the recommended crop using Information Retrieval.

Tanmay Banavlikar et al.(2018) aimed to design a system that deploys soil moisture sensor, temperature sensor, humidity sensor embedded on Raspberry Pi to detect the physical parameters of the soil.[10] Artificial Neural Networks concept is used to train the datasets to suggest the appropriate crop. The attributes for training the datasets include soil moisture content, humidity, temperature and the apt crop.

Devdatta A. Bondre, et.al (2019) described how to predict crop yield based on soil nutrients and recommends fertilizers.[11] The datasets are collected for attributes such as fertilizer, location and crop yield. Crops considered are rice, wheat, soybean, sunflower, cotton, sugarcane, tobacco and dry chilli. Random Forest and Support Vector Machine were used for Crop Yield Prediction and fertilizer recommendation. They arrived at an accuracy of about 86.35% for support vector machine and 99.47% for random forest which inspired us to use random forest as one of the model for our project.

Soumya Sri Attaluri, et.al (2020) provided a crop recommendation system with a prime motive of creating economic welfare of farmers.[12] Factors such as cost of planting, cost of harvesting, rainfall, crop demand, cost of seed, cost of fertilizer and yield of crop are considered to generate a more accurate prediction of whether harvesting a crop will yield profits or not. Dataset for this research is sourced from Indian government websites published by different ministries related to agriculture.

The paper is further organized as follows. Section III explains the detailed system design with architecture definition. The mathematical model for the proposed system is depicted in Section IV. Section V describes the complete implementation of the proposed model. The result analysis is presented in Section VI. Finally, Section VII concludes the designed system and also discusses the future enhancements.

III. SYSTEM DESIGN

A detailed design of the proposed system is discussed along with the workflow of the entire system and the IoT module.

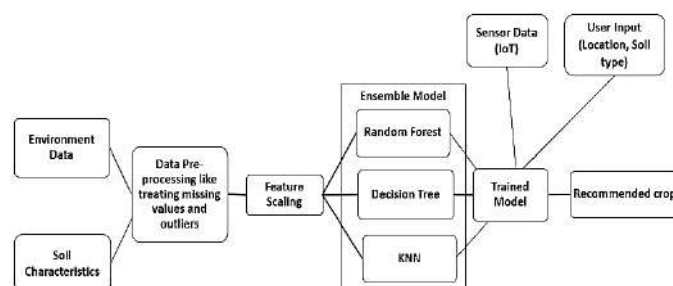


Figure 3.1 Workflow of the proposed model

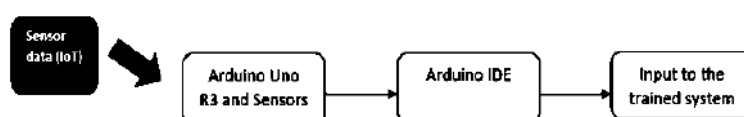


Figure 3.2 IoT Architecture

A. Architecture Definition

Figure 3.1 is described as follows:

In order to use this system in real time, the data is collected from Soil Survey department and the Tamil Nadu Agriculture University. Environmental data such as rainfall, temperature and soil characteristics like N, P, K, EC, pH and soil type are used as input parameters to correctly recommend crops for a specific area and soil type. The data collected is then pre-processed by performing one hot encoding to convert categorical features into numeric values. After pre-processing, data is z-score normalized to give equal priority to all the attributes. It is then provided as input to the ensemble model containing random forest, decision tree and kNN for training.

Sensors are deployed to provide accurate values to the final machine learning system for prediction. Temperature and pH are measured using sensors and given as inputs to the system. Figure 3.3 shows the IoT circuit connections in which the sensors are connected to the Arduino board. Data line in DT11 temperature sensor is connected to A1 pin of Arduino board and P0 line in pH sensor is connected to A0 pin of Arduino board through which the temperature and pH values are obtained and collected in the Arduino IDE. This data is then sent to serially from the Arduino IDE to python so that it can serve as input to the trained model as shown in Figure

3.2. User input and input from the IoT sensors is supplied to the trained model and the output is collected. The recommended crop is then presented as the output.

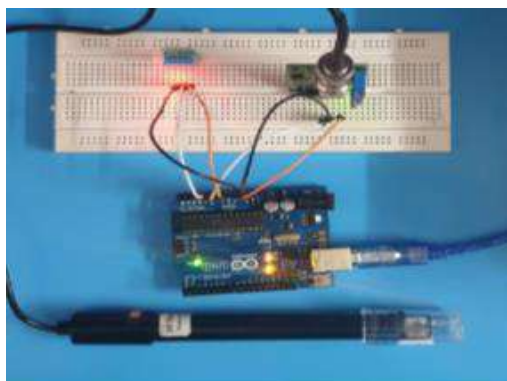


Figure 3.3 Circuit Connections

IV. Mathematical Model

1) Ensemble Learning Technique

Ensemble learning technique in machine learning integrates multiple models to achieve increased performance. It combines the power of multiple ML algorithms so that one model can correct the errors of another and predict results with much higher accuracy. Two or more models can be used as the base learners in this technique. The base learners should be chosen such that each of them perform well individually so that the combined model gives better results.

In this project, the base learners used are k-Nearest Neighbours, Decision Tree and Random Forest for the Majority Voting technique. Majority Voting is an ensemble technique that is one of the best models to solve classification problems. In this, the training set is supplied to all the models and each of them gets trained individually. The inputs for prediction is then fed to all the models separately. Each prediction result is counted as a vote and the output with the maximum number of votes is given as the final result.

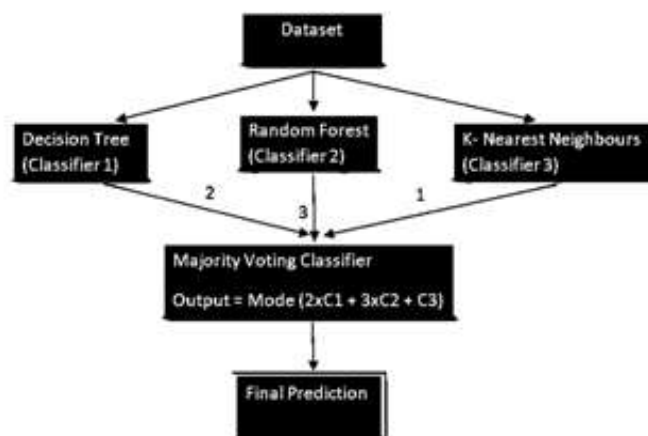


Figure 4.1 Weighted Ensemble Learning Model Flowchart

Weighted Ensemble Model = Mode (2 * (Decision Tree Output) + 3 * (Random Forest Output) + kNN Output)
(1)

Figure 4.1 represents the Weighted Ensemble model. The weight choices depend upon the importance or accuracy of the individual models. Random forest had maximum accuracy when tested individually with the same dataset and hence it is given maximum weightage of 3 followed by Decision Tree with weightage 2 and then by kNN with weightage 1.

A. Learners Used

1) Decision Tree

Decision Tree is a non-parametric supervised machine learning technique used for solving both classification and regression problems. It often mimics a human's thinking ability while making a decision. It is a tree-like structure where the internal nodes represent the features of a dataset; the branches act as the decision rules, and leaf nodes are the final result of the decisions as shown in Figure 4.2. This uses different attribute selection

measure to decide on where to split. They are namely Gini Index, Information Gain, Reduction in Variance and Chi Square. The tree algorithm depends on the selected attribute measure.

a) General Working

1. Start the tree with root node S (complete dataset)
2. Find the best attribute using Attribute Selection Measure, Information Gain. The categorical feature that will maximize the information gain value using the impurity criterion entropy is chosen at each level.

$$Entropy(T) = \sum_{i=0}^n - f_i \log(f_i) \quad (2)$$

n – number of unique values of the target variable

f_i – probability of i^{th} value of target variable

Entropy is the measure of uncertainty or impurity in the data. In a decision tree, if the output is a binary variable then higher entropy values indicate that it is difficult to predict the output as either 0 or 1.

$$Gain(T,X) = Entropy(T) - Entropy(T,X) \quad (3)$$

T = target variable

X = Feature to be split on

Entropy(T,X) = Entropy after data is split on a specific feature X

Information gain is the reduction in entropy. In a decision tree, information gain is used to predict the best split. Here, the information gained or the reduction in uncertainty is measured to predict the output class caused by a particular attribute split.

3. Divide S into subsets
4. Generate decision tree node (which contains the best attributes)
5. Recursively continue from step 3

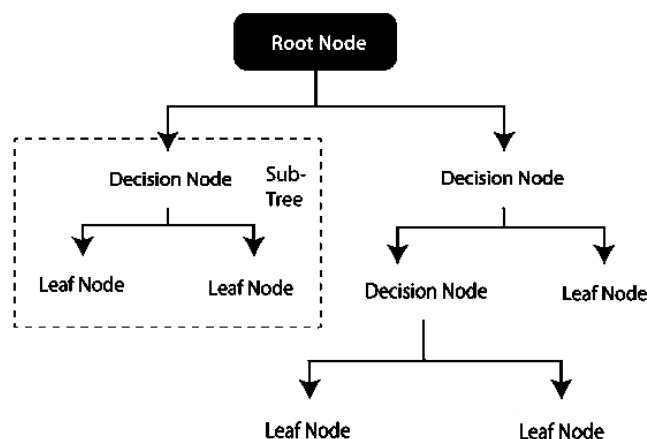


Figure 4.2 Structure of Decision Tree

2) Random Forest

Random Forest is a popular algorithm that belonging to the supervised learning technique. It basically involves the process of combining multiple classifiers to solve a complex problem and to improve the performance of the model, which is generally called as ensemble learning. As in Figure 4.3, Random Forest combines the use of many decision trees. It takes the prediction from each tree and based on the majority votes of predictions, and it predicts the final output.

a) General Working

1. Number of decision trees to be constructed is chosen as N.
2. Any random subset of the training set is considered to construct each decision tree.
3. The decision trees for the selected data points is constructed in a similar way using information gain as attribute selection measure.

4. Repeat steps 2 and 3 for N times.
5. The category of decision trees that wins the majority votes in the predictions will be assigned for the new data points.

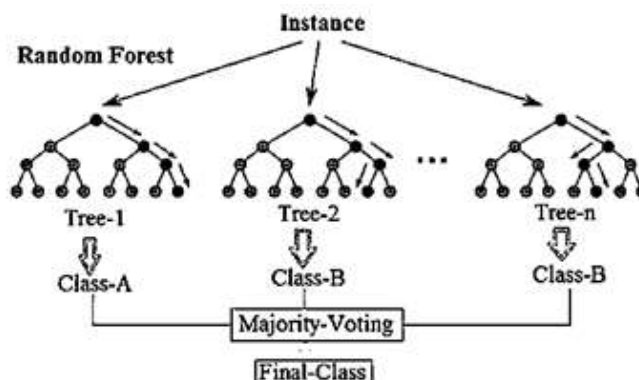


Figure 4.3 Construction of Random Forest with n-Decision Trees

3) K-Nearest Neighbours

K-NN is a non-parametric algorithm, that stores the dataset and at the time of classification, it performs an action on the dataset. For this reason, it is also called a lazy learner algorithm. K-NN algorithm checks the new data point with the available data points and puts the new point into the category that is most similar to the available categories. Figure 4.4 shows that k is chosen as 3 and class B has been chosen as the class for the input point.

b) General Working

Number K of the neighbors is selected.

The Euclidean distance (Minowski distance with $p=2$) is calculated to find the K nearest neighbors.

$$\text{Minowski Distance} = \sum_{i=0}^n \sqrt[p]{|x_i - y_i|^p} \quad (4)$$

$$\text{When } p = 2, \text{ Euclidean Distance} = \sum_{i=0}^n \sqrt{|x_i - y_i|}$$

x and y are the two points

n – number of dimensions of the two points

Euclidean distance in Euclidean space is the length of the line segment between two points. It is measured using Pythagoras theorem:

$$\text{Hypotenuse}^2 = \text{Base}^2 + \text{Height}^2 \quad (5)$$

Where the hypotenuse is the line segment between the two lines.

$$\text{Height} = (x_2 - y_2)^2, \text{ Base} = (x_1 - y_1)^2 \quad (6)$$

$$\text{Hypotenuse}^2 = (x_2 - y_2)^2 + (x_1 - y_1)^2 \quad (7)$$

$$\text{Hypotenuse} = \sqrt{(x_2 - y_2)^2 + (x_1 - y_1)^2} \quad (8)$$

The number of data points that belong to each category of target variable is counted.

The category that has the maximum number of neighbors will be assigned to the new data point.

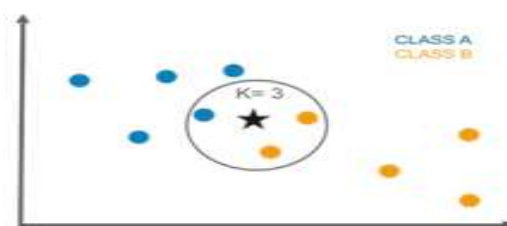


Figure 4.4 Working of K-Nearest Neighbour Algorithm

4) IoT Module

Temperature sensor and pH sensor are attached to Arduino UNO board to collect the soil attributes like temperature and pH and give it as an input for prediction.

a) Arduino UNO

Arduino is an open-source microcontroller board used for building electronics projects. It consists of a programmable circuit board and an IDE (Integrated Development Environment) to write programs using which sensor values can be obtained. Arduino IDE uses a simple version of C++.

b) DHT11 Temperature Sensor

The DHT11 is a simple, low-cost digital temperature and humidity sensor which can measure the temperature and humidity of the surroundings. It uses a thermistor to measure the input data and convert it into electronic data to record, monitor, or signal temperature changes.

b) pH Sensor

pH scale shows the acidity and basicity of a solution. It has values ranging from 0 (acidic) to 14 (basic). pH sensor consists of two main components – pH electrode and signal converter. pH electrode measures the potential between the electrodes and converts it to pH units. Signal converter is a voltage regulator chip which supports the voltage supply of 3.3-5.5V DC. pH is calculated using Nernst equation.

$$volt = avgval * 5.0 / 1024 / 6 \quad (9)$$

$$ph = -5.70 * volt + calibration_value \quad (10)$$

V. Implementation

A. Dataset Collection

The dataset is obtained from the Soil Testing Lab and Tamil Nadu Agricultural University, Coimbatore. This dataset consists of the soil and environmental parameters of all the areas in Coimbatore district. The input parameters considered are Soil N, P, K, EC, pH, Soil Type, Temperature and Rainfall. The data has 20 different crops that are widely grown here like Banana, Bengalgram, Bhendi, Brinjal, Blackgram, Onion, Paddy, Redgram, Sugarcane, Tapioca, Cotton, Cowpea, Cumbu, Greengram, Groundnut, Sorghum, Horsegram, Tomato, Turmeric, Coconut.

B. Data Preprocessing

Data pre-processing is a technique used in data mining, machine learning which is used to transform the raw data into useful datasets that can be used to perform various tasks. It is generally the first step of any learning model.

Categorical attributes need to be encoded to have numerical values for correct working of the machine learning system. One Hot Encoding is a popular technique used for the same where a binary variable is created for each of the unique values of that categorical variable. This ensures that no ordinal relationship between the different values of the variable is assumed.

C. Splitting the dataset

The data is split into 80% for train set as x_{train} , y_{train}

and 20% for test set as x_{test} , y_{test} . The model is trained using the training set and the test set is used to evaluate the machine learning model.

D. Feature Scalling

Feature scaling is a method used to normalize data in each attribute. This is mainly used to keep all attributes in the same value range to avoid giving higher priority to attributes with higher values.

The most appropriate method to do this is: Standardization (Z-score Normalization)

$$X' = \frac{X - \mu}{\sigma} \quad (11)$$

μ – mean of the sample

σ – standard deviation of the sample

Model Building

1) Machine Learning module

Random Forest, Decision Tree and kNN are combined to build the majority voting ensemble model to recommend the most suitable crop. Here, each model is first defined. Information gain is used as the criteria to decide the attributes at each level of the decision tree. In Random Forest, 10 decision trees are constructed and combined to predict the result. Euclidean distance ($p=2$) is considered to determine 26 nearest neighbours in kNN whose output value determine the predicted crop.

These results are combined with weights 2,3,1 for Decision Tree, Random Forest and kNN respectively to give the final predicted crop of the machine learning system.

2) IoT Module

Temperature sensor and pH sensor are attached to Arduino UNO board to collect the soil attributes like temperature and pH and give it as an input for prediction.

c) DHT11 Temperature Sensor

This sensor has 3 pins – Vcc, Gnd and Data. Table 5.1 shows the connections of DHT11 sensor to the Arduino Board.

Pins in Sensor	Arduino Connection
Vcc	Vin
Gnd	Gnd
Data	A1

Table 5.1 DHT11 Connections

DHT library <dht.h> is added to the Arduino. Temperature values are sensed using `DHT.read11(dht_pin)` function and the data is printed using the function `Serial.print(DHT.temperature)`

d) pH Sensor

It consists of Signal conversion module and a pH electrode. It has 6 pins – V+, Gnd, Gnd, Po, Do, To. Table 5.2 shows the connections of pH sensor to the Arduino Board.

Pins in Sensor	Arduino Connection
V+	5V
Gnd	Gnd
Po	A0

Table 5.2 pH Sensor Connections

pH electrode should be calibrated in order to get accurate values. A solution whose pH value is known is taken (distilled water pH = 7) and the electrode is dipped onto it to find the value it prints. Finally, the difference is added to the calibration value (calibration_value = 20.44). pH values are sensed using `analogRead(A0)` function. Figure 5.1 shows the Arduino circuit connections.

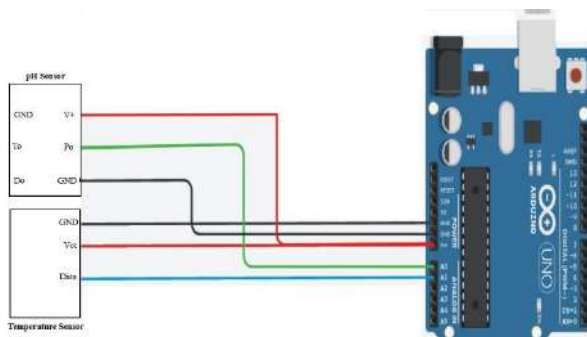


Figure 5.1 Circuit Connections

Connecting IoT module to Python

The data collected from the sensors is collected and sent via serial port. PySerial package is used to access serial port. The average of the sensor values is computed and stored for prediction.

E. User Input Prediction

The most appropriate crop is recommended to users for a user defined input. The values entered by the users for attributes such as Soil Type, Rainfall, N, P, K, EC are combined with the readings received from the Temperature and pH sensors and the most appropriate crop is predicted.

VI. RESULT ANALYSIS

The dataset obtained from Soil Testing Lab and Tamil Nadu Agricultural University, Coimbatore consists of 1162 records of crop data for different areas in Coimbatore. This is split into train and test set with 930 records in the train set and 232 record in test set. After splitting, the training set is given as input so as to train the model.

		PREDICTED																			
		BN	BG	BH	BL	BR	CO	CT	CW	CU	GG	GN	HG	ON	PA	RG	SG	SC	TP	TO	TU
ACTUAL	BN	23	0	0	0	0	0	0	1	0	0	0	0	0	0	0	0	0	0	0	0
	BG	0	5	0	0	0	0	0	0	0	0	0	0	0	0	0	0	0	0	0	0
	BH	0	0	3	0	0	1	0	0	0	0	0	0	0	0	0	0	0	0	0	0
	BL	0	0	0	1	0	0	0	0	0	0	0	0	0	0	0	0	0	0	0	0
	BR	0	0	1	0	3	0	0	0	0	0	0	0	0	0	0	0	0	0	0	0
	CO	0	0	0	0	0	33	0	0	0	0	0	0	0	0	0	0	0	0	0	0
	CT	1	0	0	0	0	0	5	0	0	0	0	0	0	0	0	0	2	0	0	0
	CW	0	0	0	0	0	0	0	13	0	0	0	0	0	0	0	3	0	0	0	0
	CU	0	0	0	0	0	0	0	0	4	0	0	0	0	0	0	1	0	0	0	0
	GG	1	0	0	0	0	0	2	0	0	7	0	1	0	0	1	0	0	0	0	0
	GN	0	0	0	0	0	0	0	3	0	0	11	1	0	0	0	3	0	0	0	0
	HG	0	0	0	0	0	0	0	1	0	0	0	8	0	0	0	0	0	0	0	0
	ON	0	0	0	0	0	0	0	1	0	0	0	0	9	0	0	0	0	0	0	0
	PA	0	0	0	0	0	0	0	0	0	0	0	0	0	4	0	0	0	0	0	0
	RG	0	0	0	0	0	0	0	0	0	0	0	0	0	0	5	0	0	0	0	0
	SG	0	0	0	0	0	0	0	0	0	0	0	0	0	0	0	45	0	0	0	0
	SC	0	0	0	0	0	0	0	0	0	0	0	0	0	0	0	0	5	0	0	0
	TP	0	0	0	0	0	0	0	0	0	0	0	0	0	0	0	0	0	7	0	0
	TO	0	0	0	0	0	0	0	0	0	0	0	0	0	0	0	0	0	0	0	14
	TU	0	0	0	0	0	1	0	0	0	0	0	0	0	0	0	0	0	0	0	3

Figure 6.1 Confusion matrix and accuracy score.

BN – Banana, BG – Bengalgram, BH – Bhendi, BL – Blackgram, BR – Brinjal, CO – Coconut, CT - Cotton, CW - Cowpea, CU - Cumbu, GG - Greengram, GN - Groundnut, HG - Horsegram, ON - Onion, PA - Paddy, RG - Redgram, SG - Sorghum, SC - Sugarcane, TP - Tapioca, TO - Tomato, TU - Turmeric

Figure 6.1 signifies the confusion matrix that we obtained for our model. It is a 20 x 20 matrix that shows the accuracy of crop predictions. The columns of the matrix represent the predicted crops and row represent the actual crops. The diagonal gives the number of correctly predicted crops and the rest shows the number of incorrect predictions. Accuracy score determines the accuracy of the system in predicting the output. It is the ratio of number of records predicted correctly (i.e. predicted and actual output value is the same) to the total number of records in test set.

$$\text{Accuracy score} = \frac{\text{Correct predictions}}{\text{Correct predictions} + \text{Incorrect predictions}} \tag{12}$$

So, the accuracy score is directly proportional to the number of correct predictions. If the recommended crop for a large number of records are predicted correctly, then the number of correct predictions increases hence improving accuracy score. The accuracy score obtained is 0.8927 which indicates that the system is 89.27% accurate.

Table 6.1 Classification Report

Crop	Precision	Recall	F1 Score	Support
Banana	0.92	0.96	0.94	24
Bengalgram	1.00	1.00	1.00	5
Bhendi	0.75	0.75	0.75	4
Blackgram	1.00	1.00	1.00	1
Brinjal	1.00	0.75	0.86	4
Coconut	0.94	1.00	0.97	33
Cotton	0.71	0.62	0.67	8
Cowpea	0.68	0.81	0.74	16
Cumbu	1.00	0.80	0.89	5
Greengram	1.00	0.58	0.74	12
Groundnut	1.00	0.61	0.76	18
Horsegram	0.80	0.89	0.84	9
Onion	1.00	0.90	0.95	10
Paddy	1.00	1.00	1.00	4

Redgram	0.83	1.00	0.91	5
Sorghum	0.83	1.00	0.91	45
Sugarcane	1.00	1.00	1.00	5
Tapioca	1.00	1.00	1.00	7
Tomato	1.00	1.00	1.00	14
Turmeric	1.00	0.75	0.86	4
Accuracy			0.89	233

Table 6.1 depicts the precision, recall, F1 score and support for each crop (output label) in our system. Precision is the ratio of correctly predicted observations (True Positive) for a crop C1 to the total predicted observations for the same crop (C1) (True Positive + False Positive). False Positive is the number of observations with actual output being a different crop but predicted as C1.

$$\text{Precision} = \text{True Positive} / (\text{True Positive} + \text{False Positive}) \quad (13)$$

Recall is the ratio of correctly predicted observations (True Positive) for a crop C1 to the total number of records with actual output label as C1 (True Positive + False Negative). False Negative is the number of observations with predicted output being a different crop but actual output is C1.

$$\text{Recall} = \text{True Positive} / (\text{True Positive} + \text{False Negative}) \quad (14)$$

F1 Score is the harmonic balance of precision and recall.

$$\text{F1 Score} = 2 * \text{Precision} * \text{Recall} / (\text{Precision} + \text{Recall}) \quad (15)$$

Support is frequency of occurrence of a particular crop in the test dataset.

Table 6.2 Readings from sensor

Sl. No.	Temperature Readings from Arduino	pH Readings from Arduino
1	26.0	7.25
2	26.0	7.25
3	26.0	7.27
4	26.0	7.44
5	26.0	7.26

Average: 26.0 °C Average: 7.29

The temperature and pH from the sensor is received from the Arduino board as presented in Table 6.2. The average of five values is taken for better accuracy.

```
Area: Pogalur
Soil type: Irugur Series
N value: 218.41
P value: 12.63
K value: 470.6
EC value: 0.27
pH: 7.29
Temperature: 26
Rainfall: 1500
Predicted Crop: Coconut
```

Figure 6.2 User Input Predictions

The required attributes are collected as input from the user as demonstrated in Figure 6.2. This is used to recommend the most suitable crop.

Sl. no	Model	Accuracy	F1 Score	Precision
1	Decision Tree	86.25	85.02	86.76
2	Kernel SVM	73.54	67.56	75.09
3	KNN	66.52	51.81	62.11
4	Naïve Bayes	48.49	52.63	64.89
5	Random Forest	86.69	82.63	85.45
6	SVM	82.82	81.17	86.78

7	Logistic Regression	74.22	68.79	79.34
8	Majority Voting (Existing): Random Forest, Decision Tree and Naïve Bayes	84.54	84.68	86
9	Majority Voting (Proposed): Random Forest, Decision Tree and kNN	89.27	88.87	92.39

Table 6.3 Comparison with existing models



Figure 6.3 Graphical Comparison with existing models (Accuracy, F1 Score, Precision)

DT – Decision Tree, KSVM – Kernel SVM, kNN – k Nearest Neighbour, NB – Naïve Bayes, RF – Random Forest, SVM – Support Vector Machine, LR – Logistic Regression, MVE – Majority Voting (Existing), MVP – Majority Voting (Proposed)

In Table 6.2 and Figure 6.3, the proposed system is compared with other existing models. The existing majority voting technique with learners such as Random Forest, Decision tree and Naïve Bayes gave an accuracy of 85.41%. Another existing system that used ANN showed an accuracy of 76.1%. Therefore, it can be inferred that the proposed system showed maximum accuracy.

VII. CONCLUSION AND FUTURE ENHANCEMENTS

The proposed system plays a major role in assisting the farmers to make a decision on the best crop to be grown on their farm land located in Coimbatore. This system considers various soil and environmental factors, and IoT sensor values to predict the accurate crop. The ensemble learning model used provides an advantage by combining the accuracies of KNN, random forest and decision tree algorithms and gives a resulting accuracy of 89.27% which is higher than the accuracy of the existing majority voting techniques and ANN which are 85.41% and 76.1% respectively.

As an enhancement of the proposed system, additional IoT sensors for other parameters can be used. Also, crop rotation can be included as a new feature to predict the crop based on the previously grown crop.

REFERENCES

1. Z. Doshi, S. Nadkarni, R. Agrawal and N. Shah, "AgroConsultant: Intelligent Crop Recommendation System Using Machine Learning Algorithms", 2018 Fourth International Conference on Computing Communication Control and Automation (ICCUBEA), Pune, India, 2018, pp. 1-6. doi-10.1109/ICCUBEA.2018.8697349.
2. S. Pudumalar, E. Ramanujam, R. H. Rajashree, C. Kavaya, T. Kiruthika and J. Nisha, "Crop recommendation system for precision agriculture", 2016 Eighth International Conference on Advanced Computing (ICoAC), Chennai, 2017, pp. 32-36. doi: 10.1109/ICoAC.2017.7951740.
3. Kevin Tom Thomas, Varsha S, Merin Mary Saji, Lisha Varghese, Er. Jinu Thomas "Crop Prediction Using Machine Learning", International Journal of Future Generation Communication and Networking Vol. 13, No. 3, (2020), pp. 1896–1901 K. Elissa, "Title of paper if known," unpublished.
4. Harshitha L, Rashmi M N, Vaishnavi I Dodamani, Yamini S, Nandini M S, "Improving Crop Productivity through Crop Recommendation", International Research Journal of Engineering and Technology (IRJET) Volume: 07 Issue: 08 | Aug 2020.

5. K. R. Akshatha, K. S. Shreedhara, "Implementation of Machine Learning Algorithms for Crop Recommendation Using Precision Agriculture", International Journal of Research in Engineering, Science and Management Volume-1, Issue-6, June 2018.
6. Srilakshmi A, Madhumitha K, Geetha K, "Machine learning approach: Recommendation of suitable crop for land using meteorological factors", Proceedings of the 2nd International Conference on IoT, Social, Mobile, Analytics & Cloud in Computational Vision & Bio-Engineering (ISMAC-CVB 2020).
7. Miss Snehal S.Dahikar, Dr.Sandeep V.Rode, Agricultural Crop Yield Prediction Using Artificial Neural Network Approach", International Journal Of Innovative Research In Electrical, Electronics, Instrumentation And Control Engineering, Vol. 2, Issue 1, January 2014.
8. Varsha A, Midhuna V M,Rilty, Assistant Prof. Divya R, "Soil Classification and Crop recommendation using IoT and Machine Learning", International Journal of Scientific Research & Engineering Trends Volume 6, Issue 3, May-June-2020, ISSN (Online): 2395-566X.
9. Avinash Kumar, Sobhangi Sarkar and Chittaranjan Pradhan, "Recommendation System for Crop Identification and Pest Control Technique in Agriculture", International Conference on Communication and Signal Processing, April 4-6, 2019, India.
10. Tanmay Banavlikar, Aqsa Mahir, Mayuresh Budukh, Soham Dhodapkar, "Recommendation System Using Neural Networks", International Research Journal of Engineering and Technology(IRJET) Volume: 05 Issue: 05.
11. Devdatta A. Bondre, Santosh Mahagaonkar, "Prediction of crop yield and fertilizer recommendation using machine learning algorithms", International Journal of Engineering Applied Sciences and Technology, 2019, Vol. 4, Issue 5, ISSN No. 2455-2143
12. Soumya Sri Attaluri, Nowshath K Batcha, Raheem Mafas "Crop Plantation Recommendation using Feature Extraction and Machine Learning Techniques", Journal of Applied Technology and Innovation (e -ISSN: 2600-7304) vol. 4, no. 4, (2020)
13. Preethi G, Rathi Priya V, Sanjula S M, Lalitha S D, Vijaya Bindhu B. "Agro based crop and fertilizer recommendation system using machine learning", European Journal of Molecular & Clinical Medicine Volume 7, Issue 4, 2020.
14. Sivanandhini, P., & Prakash, J. Comparative Analysis of Machine Learning Techniques for Crop Yield Prediction. International Journal of Advanced Research in Computer and Communication Engineering. 2020;9(6):289–93.
15. Rajesh R, Mathivanan B. Predicting Flight Delay using ANN with Multicore Map reduce framework, Communication and Power Engineering. In Walter de Gruyter GmbH & Co KG; 2017.
16. "Agriculture in India" article available in Wikipedia Link: https://en.wikipedia.org/wiki/Agriculture_in_India
17. Amuthadevi, D. S. Vijayan, Varatharajan Ramachandran, "Development of air quality monitoring (AQM) models using different machine learning approaches", Journal of Ambient Intelligence and Humanized Computing, <https://doi.org/10.1007/s12652-020-02724-2>

Effective Industrial Workstation Design Using Ergonomic Analysis for Employees in a Pump Manufacturing Industry

Jayachitra R and Arunprabhu R

Department of Mechanical Engineering, PSG College of Technology, Coimbatore, Tamil Nadu, India

ABSTRACT

This study investigates a work posture of an employees to improve comfort and to improve productivity of an organization. This study will include ergonomics practices in work station. In case of any mismatch of employee's anthropometry with work station leads to disorders of the soft tissues (muscles, tendons, ligaments, joints, and cartilage) and especially at lower back pain, it will lead to musculoskeletal disorder (MSD). musculoskeletal disorder causes pain in joints, muscles and ligaments. It will lead to fatigue concentration in work postural, decreases the productivity etc. Hence this study focus on human fatigues on work posture of an operator in a pump manufacturing company A questionnaires was framed and provided to employee and so that fatigue concentration is prioritized. RULA (Rapid Upper Limb Assessment) & NIOSH (National Institute for Occupational Safety and Health) assessment is conducted to know severity in fatigue concentration while doing an operation and while lifting a job respectively. This project aims to develop a newly ergonomically designed workstation in order to reduce postural stress and to improve productivity. To study a simulation on work posture fatigue it is necessary to know the anthropometry of an employee's and statistical study on anthropometry data is done to know the impact percentile populations such as P5, P50 & P95. Based on statistical study high impact percentile population is provided as input for simulation. The ergonomic simulation software 3DSSPP is used to develop a 3d model of work posture of an operator in work station and analysed to know fatigue level and simulation is done to improve a comfort while doing an operation.

Keywords: musculoskeletal disorder, anthropometry, questionnaires, RULA, NIOSH, fatigue, percentile populations and work posture.

1 INTRODUCTION

In manufacturing industries, efficiency of worker plays an important role. Productivity of worker greatly depends upon ergonomic design of workstation. Ergonomics is designing a job to fit the worker so the work is safer and more efficient. Implementing ergonomic solutions can make employees more comfortable. Efficient ergonomics in workstation design shows better interaction between man-machine systems. Lot of research has been done on analyzing and improving ergonomics of workstation, facility layout and tool design. Study regarding operator performance and comfort in repetitive task has been done.

2 LITERATURE REVIEW

Anthropometric Difference In Postural Analysis

Raffaele Castellone et al. [9] the study investigates three manual assembly operations from a car production line were selected as case studies. For the first case study the upper arm elevation angle is greater and leads to an unacceptable posture of the upper limb.

Design On Reducing Musculoskeletal Risk Factors

Baba MdDeros et al [4], this study was conducted at an automotive component manufacturer. The measurement shows the current workbench height is 87cm from the floor, which is too low. Ro-Ting Lin et al [10], a prospective study was focused on reducing shoulder loadings by redesigning nine workstations. The original workstation resulted in shoulder angles greater than 400 which leads to elbow pain and redesigned work station resulted in 250 to avoid shoulder and elbow pain.

Rapid Upper Limb Assessment

Mahendra K C et al [7], this study was to identify the discomfort/pain experienced by the workers. The discomfort level of the workers can be evaluated by designing a detailed questionnaire and checklist to be present to the respondent. Discomfort level is minimized with above 50% of welders in the improved RULA control graph.

National Institute Occupational Safety And Health (Niosh)

Anukriti Sahni et al [2], This paper focuses on presenting literature on the NIOSH lifting equation, ergonomic redesign includes load being brought closer to worker (by training). Nor Hafeezah Kamarudin et al [8], an

ergonomic intervention assessment tool that used to calculate the recommended weight limit (RWL) for lifting tasks and to identify the hazardous lifting tasks.

3. Problem Statement

- Mismatching of workers anthropometry and work station design will leads to poor reach ability and poor accessibility of worker to do operation.
- Repeatedly lifting of weights from shorter height to longer height more than allowable weight will cause musculoskeletal disorders (MSD).
- Workers prolonged postures will tends to increase fatigue level in humans postural stress.

4. OBJECTIVE

The general objective of this study was to examine the relationship between the suitability of workstation and work posture equipment designs on the job satisfaction on working posture of an employees.

- To frame and conduct questionnaires to study the difficulties faced by employees on workstation.
- To collect anthropometric data for employees.
- To minimize postural stress and fatigue for employees.
- To develop an ergonomically designed work station.

5. METHODOLOGY

Purpose of the study is to find out fatigue stress in working posture and to reduce musculoskeletal disorders and to suggest ergonomically designed workstation. Methodology of the project is shown in Fig. 1

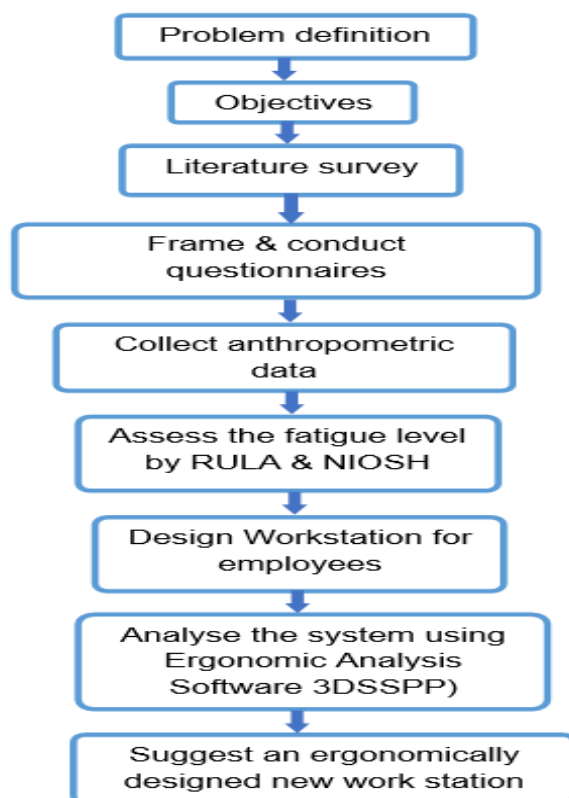


Fig. 1 Methodology of the Project

The Fig. 1 shows the methodology of the project. Observation is done on machine shop to identify the fatigues faced by employees while doing the task. The fatigue level is prioritised by framing questionnaires and by performing on ergonomic assessment tools such as RULA & NIOSH.

5.1 Selection of Case Studies

Three specific operations were selected as potentially critical for the posture to do operations such as Inlet bracket inspection, lifting of stator and filing operation in a pump manufacturing industry is shown in Fig 2, 3 & 4 respectively.



Fig. 2 Inlet Bracket Inspection



Fig. 3 Stator Lifting



Fig. 4 Filing

6. Assessment Tools

6.1 Questionnaires

Questionnaires help to know the problems faced by some employees. It helps prioritize fatigue level faced by employees by ranking the risk factor. Questionnaires are framed to ensure whether a work environment is safely built or not and ergonomically designed or not.

Table. 1 Quick Exposure Checklist for Inlet Bracket Inspection

Exposure Level	Back	Shoulder/arm	Wrist/hand	Neck	Work Pace	Stress
Very High	1	1	1	1	-	-
High	6	6	6	6	-	4
Moderate	-	-	-	-	5	3
Low	-	-	-	-	2	-

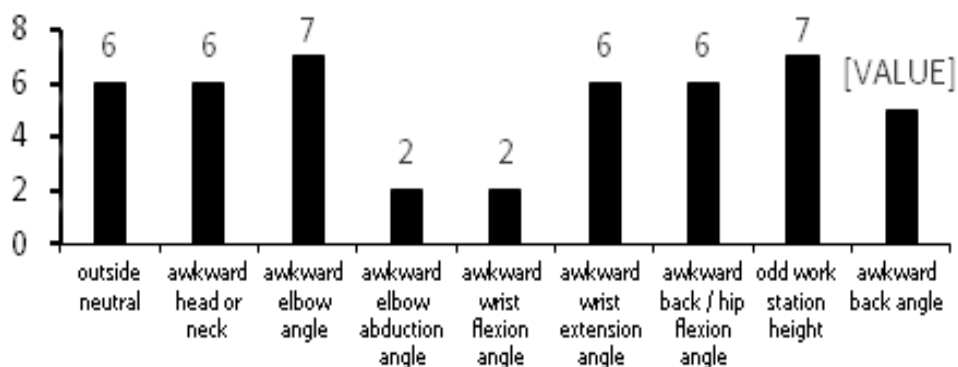


Fig. 5 Ergonomic Assessment Checklist Result for Inlet Bracket Inspection

Table. 2 Quick Exposure Checklist Result for Stator Lifting

Exposure Level	Back	Shoulder/arm	Wrist/ hand	Neck	Work Pace	Stress
Very High	10	-	-	-	-	-
High	-	10	10	10	3	5
Moderate	-	-	-	-	7	5
Low	-	-	-	-	-	-

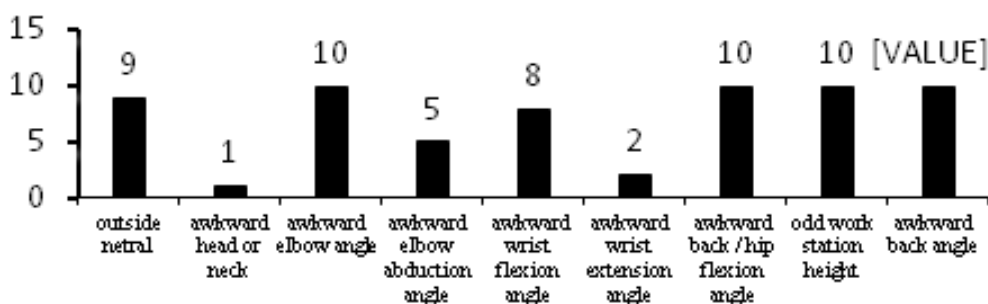


Fig. 6 Ergonomic Assessment Checklist Result for Stator Lifting

Table. 3 Quick Exposure Checklist Result for FILING

Exposure Level	Back	Shoulder/arm	Wrist/ hand	Neck	Work Pace	Stress
Very High	1	3	-	3	-	-
High	2	-	3	-	-	-
Moderate	-	-	-	-	3	3
Low	-	-	-	-	-	-

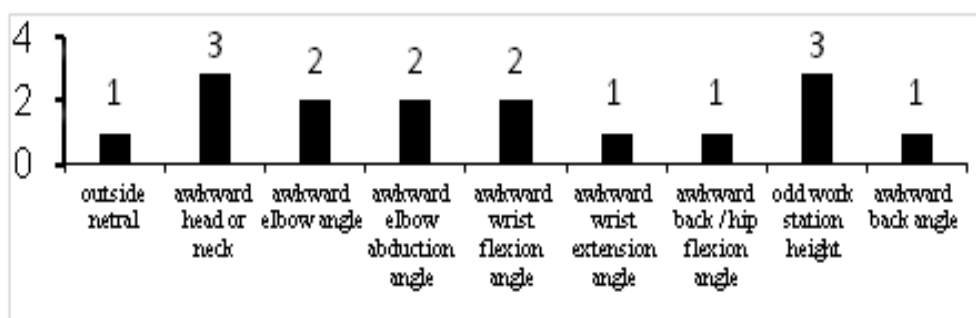


Fig. 7 Ergonomic Assessment Checklist Result for Filing

Quick Exposure Checklist survey results is shown in Table 1, 2 & 3. Ergonomic Assessment Checklist survey results are plotted in graph is shown in Fig 5, 6 & 7.

6.2 RULA

RULA is a screening tool that assesses biomechanical and postural loading on the whole body with particular attention to the neck, trunk and upper limbs. It is method developed for ergonomic analysis of workstations where upper limb activities are reported to be hazardous.

Table. 4 RULA Score

Case	RULA Score	Action
Stator Lifting	7	Very high risk, implement change now
Filing	7	Very high risk, implement change now

RULA score is calculated and shown in Table. 4 workers are at high risk while doing an operation and immediate action has to be taken to change the work posture.

6.3 NIOSH

NIOSH is a tool used to assess the manual material handling risks associated with lifting and lowering tasks in the workplace.

- **NIOSH Lifting Equation:** $LC (51) \times HM \times VM \times DM \times AM \times FM \times CM = RWL$

LC = Load Constant (51 lbs = 23.13kg)

H = Horizontal location of the object relative to the body (H)

F = Frequency and duration of lifting activity (F)

C = Coupling or quality of the workers grip on the object (C)

- **Lifting Index (LI):** $\text{Weight} \div \text{RWL} = \text{LI}$

Table. 5 NIOSH Assessment Stator Lifting

Stator Lifting	H	V	D	A	C	F (lifts/min)	Load Weight (lbs)	RWL (lbs)	LI
origin	18	10	0	0°	Fair	1	33.07	17.29	1.91
Destination	20	43.5	33.5	0°	Fair	1	33.07	11.85	2.79

from the above Table. 5, it is clear states that Lifting Index is greater than 1 which means a case is at very high risk and need to implement a ergonomic workposture change immediately.

7. Anthropometry

Anthropometry of an employees is collected for inlet bracket inspection, stator lifting and filing cases is shown in Table. 8, 9 and 10 respectively. Since work place dimension is not a standard one because anthropometry varies from person to person so fatigue is purely depend on anthropometry. Designing of workplace needs direct involvement of anthropometric data. Body dimension is essential for doing simulation in 3DSSPP is listed in Table 6 Measuring instruments used for measurements is listed in Table 7.

Table. 6 Body Parts for Measurements

S.No	Body Measurements
1	Neck Height (NH)
2	Shoulder Height (SH)
3	Shoulder Width (SW)
4	Upper Arm (UA)
5	Lower Arm (LA)
6	Head Radius (HR)
7	Tragion (T)
8	Wrist (W)
9	Upper Leg (UL)
10	Lower Leg (LL)
11	Foot (F)

Table. 7 Measuring Instruments

S.No	Measuring Instruments
1	Measuring Tape
2	Goniometer
3	Small Bone Calliper

Table. 8 Anthropometry and percentile population of Inlet bracket inspection

name	age	neck height	shoulder width	shoulder height	upper arm	lower arm	wrist	upper leg	lower leg	foot	tragion	head radius
1	22	2.50	19.75	23.00	12.00	13.00	8.00	20.00	18.13	10.00	1.00	4.10
2	23	2.75	18.00	20.50	12.00	11.50	8.25	17.50	18.13	8.00	1.25	4.00
3	22	2.13	18.50	20.75	13.50	11.13	8.25	18.75	17.50	10.00	1.00	4.00
4	24	2.75	18.13	18.50	12.50	11.75	6.75	20.50	17.13	8.00	1.00	4.10
5	23	2.13	19.13	18.50	11.50	12.25	7.00	20.00	17.75	9.00	1.25	4.00
6	22	3.00	19.00	20.00	12.13	12.50	8.50	19.13	18.13	10.00	1.50	4.30
7	24	2.75	17.75	20.75	13.00	11.50	8.13	20.00	18.25	10.00	1.25	4.15
8	23	1.50	18.00	19.00	10.75	9.75	6.50	16.00	16.00	7.00	1.00	4.10
mean		2.44	18.53	20.13	12.17	11.67	7.67	18.98	17.63	9.00	1.16	4.09
SD		0.46	0.65	1.40	0.80	0.92	0.74	1.44	0.71	1.12	0.17	0.09

P5		1.68	17.46	17.81	10.86	10.15	6.46	16.61	16.45	7.16	0.87	3.94
P50		2.44	18.53	20.13	12.17	11.67	7.67	18.98	17.63	9.00	1.16	4.09
P95		3.20	19.61	22.44	13.49	13.20	8.89	21.36	18.80	10.84	1.44	4.25

Table. 9 Anthropometry and percentile population of stator lifting

name	age	neck height	shoulder width	shoulder height	upper arm	lower arm	wrist	upper leg	lower leg	foot	tragon	head radius
1	22	2.50	17.50	23.00	12.50	12.25	7.50	18.00	18.00	8.00	1.00	4.10
2	22	3.00	17.00	19.00	11.50	13.00	7.00	18.75	17.00	9.00	1.25	4.15
3	22	2.75	17.00	20.00	12.50	13.00	7.00	19.00	18.00	10.00	1.00	4.00
4	22	2.50	16.13	18.00	11.50	10.75	7.00	17.00	16.00	9.00	1.00	4.00
5	23	2.75	17.50	20.50	12.00	11.50	7.50	17.50	18.00	9.00	1.00	4.10
6	21	2.50	16.75	21.00	12.75	12.13	7.00	18.50	19.00	10.00	1.00	4.15
7	22	3.50	18.25	20.50	12.00	11.75	8.00	18.50	16.50	8.00	1.50	4.15
8	20	3.75	17.25	19.25	13.00	11.00	7.75	20.00	18.00	9.00	1.50	4.30
9	22	3.13	18.50	22.50	13.00	12.00	8.50	20.00	16.00	10.00	1.25	4.15
mean	21	2.75	16.25	18.25	11.50	11.50	7.00	18.00	17.50	8.00	1.25	4.00
SD		2.91	17.21	20.20	12.23	11.89	7.43	18.53	17.40	9.00	1.18	4.11
P5		0.41	0.73	1.58	0.58	0.71	0.50	0.93	0.94	0.77	0.20	0.09
P50		2.23	16.01	17.59	11.28	10.71	6.60	17.00	15.84	7.72	0.85	3.96
P95		2.91	17.21	20.20	12.23	11.89	7.43	18.53	17.40	9.00	1.18	4.11

Table. 10 Anthropometry and percentile population of filing

name	age	neck height	shoulder width	shoulder height	upper arm	lower arm	wrist	upper leg	lower leg	foot	tragon	head radius
1	51	3.00	18.50	19.50	11.00	12.50	7.50	19.00	16.50	7.00	1.50	4.00
2	22	3.00	17.00	20.25	10.75	12.00	7.00	18.00	18.13	9.00	1.25	4.15
3	24	3.25	16.13	17.50	11.00	11.00	7.50	16.50	16.50	6.00	1.50	4.10
mean		3.08	17.21	19.08	10.92	11.83	7.33	17.83	17.04	7.33	1.42	4.08
SD		0.12	0.98	1.16	0.12	0.62	0.24	1.03	0.77	1.25	0.12	0.06
P5		2.89	15.59	17.17	10.72	10.80	6.94	16.14	15.78	5.28	1.22	3.98
P50		3.08	17.21	19.08	10.92	11.83	7.33	17.83	17.04	7.33	1.42	4.08
P95		3.28	18.83	21.00	11.11	12.86	7.72	19.53	18.31	9.39	1.61	4.19

7.1 Percentile calculation

In this study three different percentile population is studied such as P5, P50 & P95.

$$P5 = \text{mean} - 1,65 * SD$$

$$P50 = \text{mean}$$

$$P95 = \text{mean} + 1,65 * SD$$

7.2 Histogram Plot

A histogram plot is plotted to know the distribution pattern of anthropometry data. Only by knowing the distribution of anthropometry data a respective statistical study will be carried out. Hence Histogram plot is carried out in both cases.

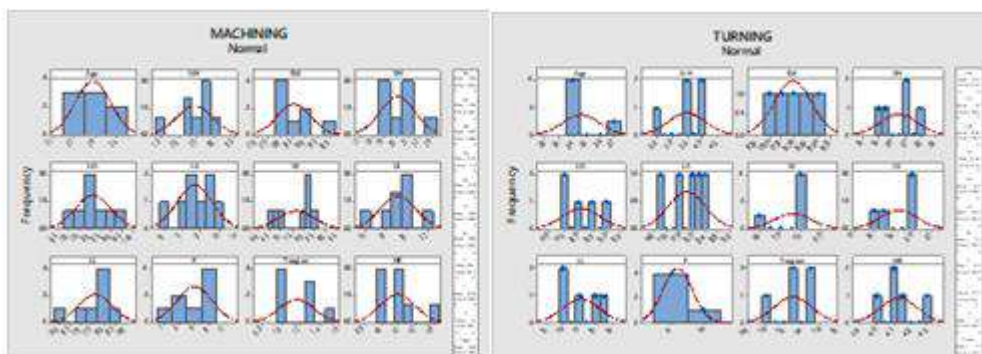


Fig. 8 Histogram Plot of Inlet Bracket Inspection

Fig. 9 Histogram Plot of Stator Lifting

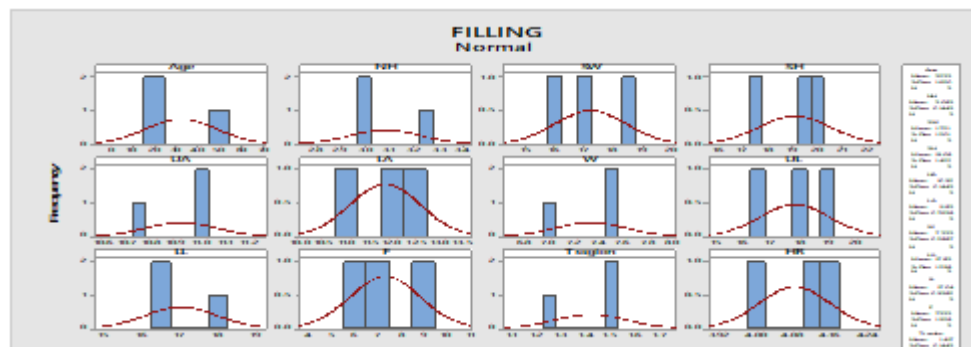


Fig. 10 Histogram plot of Filing

Histogram plot is plotted for Inlet bracket Inspection, stator lifting and filing is shown in Fig 8, 9 & 10. From the Fig 8, 9 & 10. It clearly shows that anthropometry data for all the cases follows normal Distribution.

7.3 Hypothesis Test

Hypothesis test is done to know on which percentile a major population falls, so one sample z-test hypothesis test is done. This p-value has the range of $(0 < p < 1)$.

P > 0.05 Null hypothesis is not rejected

P < 0.05 Null hypothesis is rejected

Table. 11 Hypothesis Test of Inlet Bracket Inspection

S No	Body Parts	P5	P50	P95
1	Neck Height	0	.988	0
2	Shoulder Width	0	.996	0
3	Shoulder Height	0	.992	0
4	Upper Arm	0	.995	0
5	Lower Arm	0	.995	0
6	Wrist	0	.947	0
7	Upper Leg	0	.752	0
8	Lower Leg	0	.984	0
9	Foot	0	1	0
10	Tragion	0	.95	0
11	Head Radius	0	.906	0

Table. 12 Hypothesis Test of Stator Lifting

S No	Body Parts	P5	P50	P95
1	Neck Height	0	.985	0
2	Shoulder Width	0	.991	0
3	Shoulder Height	0	1	0
4	Upper Arm	0	.978	0
5	Lower Arm	0	.991	0
6	Wrist	0	.975	0
7	Upper Leg	0	.986	0
8	Lower Leg	0	.866	0

9	Foot	0	1.0	0
10	Tragion	0	.937	0
11	Head Radius	0	1.0	0

Table. 13 Hypothesis Test of Filing

S No	Body Parts	P5	P50	P95
1	Neck Height	0.005	.998	0.005
2	Shoulder Width	0.004	.998	0.004
3	Shoulder Height	0.004	.996	0.004
4	Upper Arm	0.005	.962	0.005
5	Lower Arm	0.004	.993	0.004
6	Wrist	0.005	.981	0.005
7	Upper Leg	0	.996	0.004
8	Lower Leg	0.005	.997	0.004
9	Foot	0.004	.996	0.004
10	Tragion	0.005	.962	0.005
11	Head Radius	0.003	.923	0.002

From the above table. 11, 12 & 13. p-value is greater than 0.05 (α) in percentile 50, and hence null hypothesis is not rejected. It denotes that major population falls on P50 percentile population. Hence P50 anthropometry data is taken for simulation study.

8. Simulation

Ergonomic analysis is done on 3DSSPP Simulation software. Based on output of hypothesis test P50 percentile population anthropometry data is taken as an input for simulation study.

In stator lifting operators L4/L5 back compression is of 889 lb which falls in yellow region which severity is high and centre of pressure falls outside yellow area which means body is in unbalance posture. And Maximum Exertion Duty % which is in red colour it means severity is high.

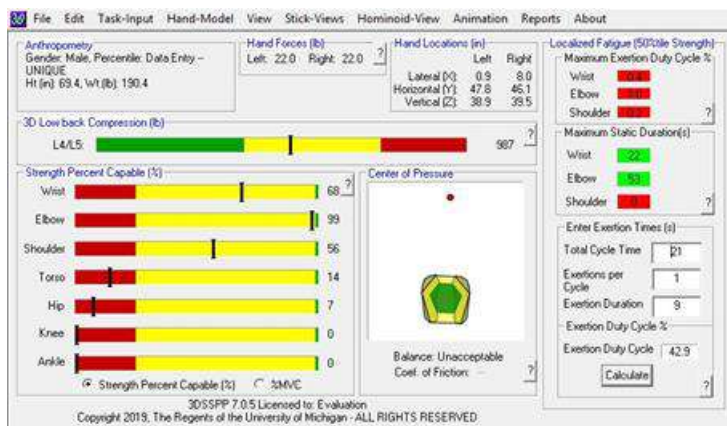


Fig. 11 Analysis Summary Report – Existing Inlet Bracket Inspection



Fig. 12 Simulation Model – Existing Stator Lifting

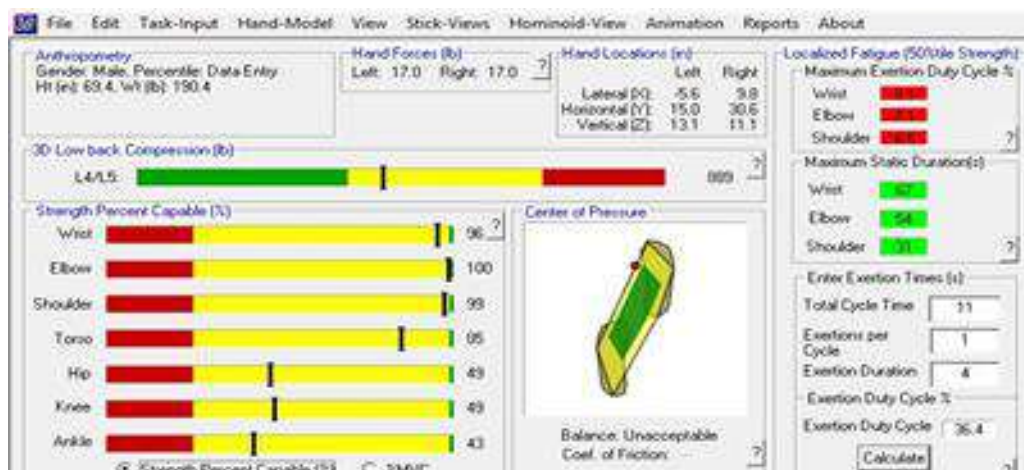


Fig. 13 Analysis Summary Report – Existing Stator Lifting

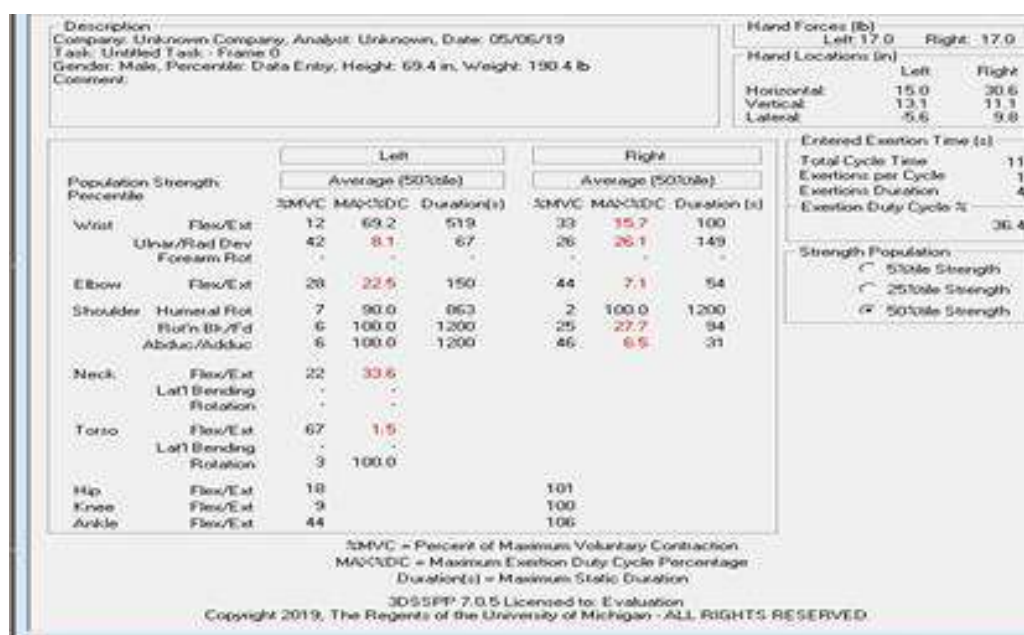


Fig. 14 Localized Summary Report - Existing Stator Lifting

8.2 SUGGESTIONS

To avoid human fatigue and awkward posture while doing operation some suggestions are provided

Lifting

- A pallet tilter is suggested that operator no needs bend while lifting because tilter will adjust the height and provides angular rotation of pallets.
- It is advised to lift at a vertical location of the object relative to the floor of 30 inches and horizontal location of the object relative to the body of 10 inches.

Inspection

- In Inlet Bracket Inspection table height is increased to 40 inches before it was 28 inches.
- Roller conveyor is suggested over the table so that inspected component will be freely moved to other end of table and hence measuring instruments is kept within reachable area so bending of operator is avoided.

Proposed simulation model of Inlet Bracket Inspection, Stator lifting and Filing is shown in Fig 15&18 respectively.

In stator lifting after suggestions operators L4/L5 back compression is of 617 lb which falls in green region which is in safer zone as shown in Fig 16 and centre of pressure falls inside green area which means body is in balance posture as shown in Fig 16. Maximum Exertion Duty % which is in green colour for wrist, elbow and shoulder as shown in Fig 17 it means severity is low and maximum static duration is improved.

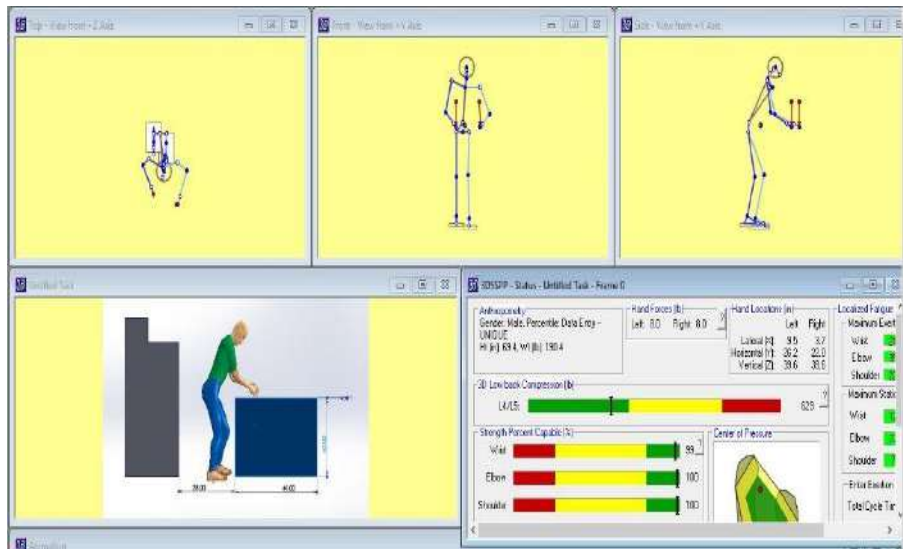


Fig. 15 Simulation Model – Proposed Inlet Bracket Inspection

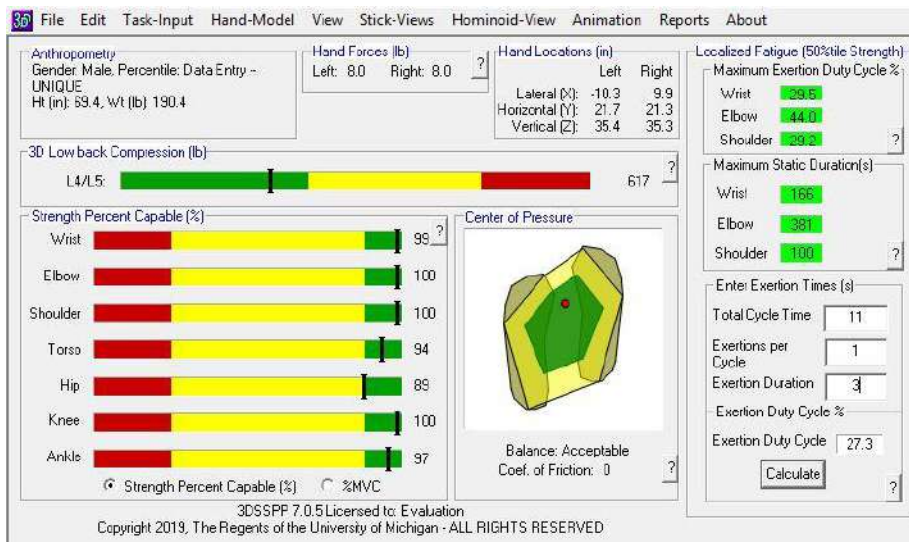


Fig. 16 Analysis Summary Report – Proposed Stator Lifting

Population Strength Percentile		Left			Right		
		%MVC	MAX%DC	Duration (s)	%MVC	MAX%DC	Duration (s)
Wrist	Flex/Ext	20	39.9	228	17	47.7	205
	Ulnar/Rad Dev	24	29.5	166	23	31.9	180
	Forearm Rot	-	-	-	-	-	-
Elbow	Flex/Ext	18	44.0	381	16	51.6	511
	Rot'n Bk/Fd	-	-	-	-	-	-
Shoulder	Humeral Rot	18	43.6	164	14	58.1	259
	Abduc/Adduc	24	29.2	100	22	35.2	123
Neck	Flex/Ext	14	61.4	-	-	-	-
	Lat'l Bending	-	-	-	-	-	-
	Rotation	-	-	-	-	-	-
Torso	Flex/Ext	50	4.7	-	-	-	-
	Lat'l Bending	-	-	-	-	-	-
	Rotation	1	100.0	-	-	-	-
Hip	Flex/Ext	36	-	-	51	-	-
Knee	Flex/Ext	-	-	-	21	-	-
Ankle	Flex/Ext	35	-	-	40	-	-

Fig. 17 Localized Summary Report - Proposed Stator Lifting

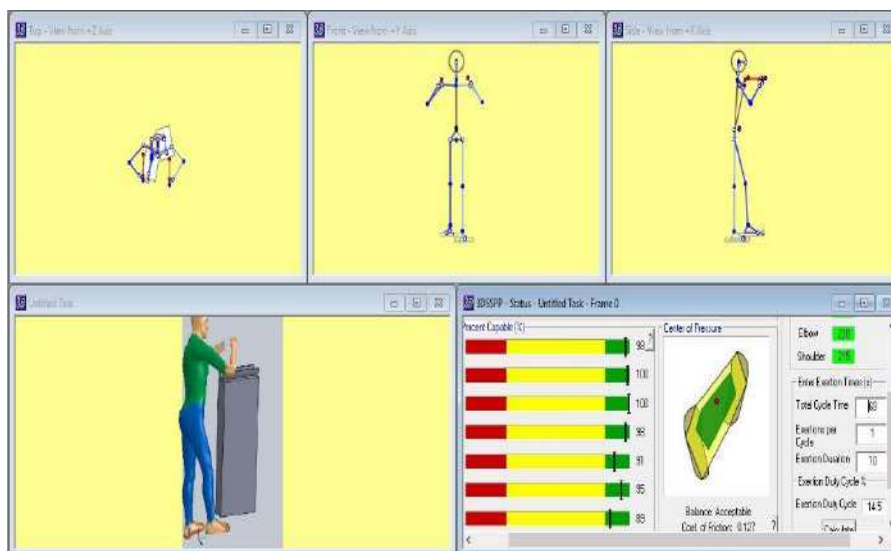


Fig. 18 Simulation Model in 3DSSPP Software - Proposed FILING

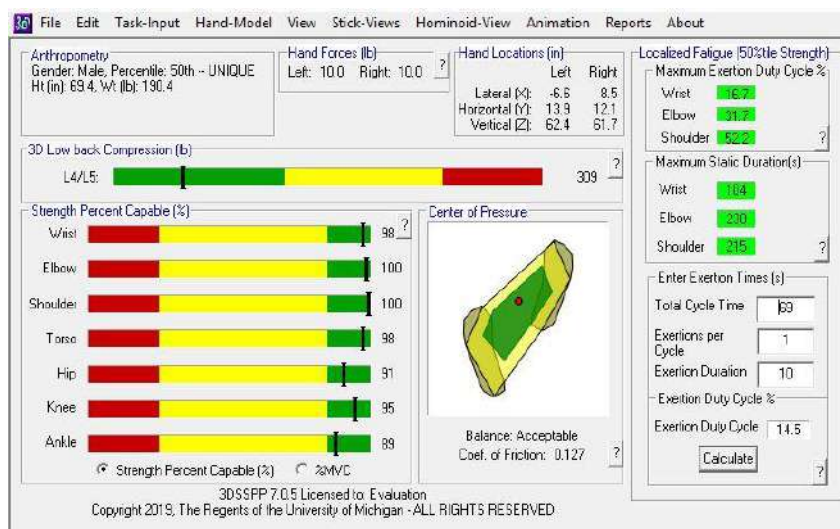


Fig. 19 Analysis Summary Report – Proposed FILING

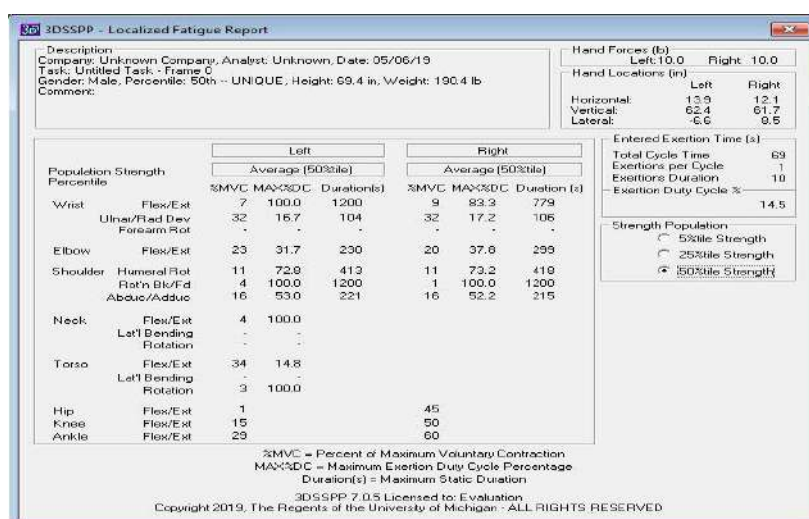


Fig.20 Localized Summary Report - Proposed FILING

9. RESULT AND CONCLUSION

The ergonomic analysis is done on Inlet Bracket Inspection, Stator lifting and Filingwork posture results shows that in In Inlet Bracket Inspection operators L4/L5 back compression of 987 lb is reduced to 629 lb which is in green region as shown in Fig. 15 and body also in well balanced posture. In stator Lifting operators L4/L5 back compression is of 889 lb is reduced to 617 lb which is in green region as shown in Fig 16 and since centre of

pressure falls within green region as shown in Fig. 16 body is in balanced position. Maximum Exertion Duty Cycle % and Maximum Static Duration(s) gets increased in proposed model as compared to existing model in both a cases as shown in Fig. 14,17& 20. To avoid high fatigue and awkward posture suggestions are provided based on anthropometry, so that bending is avoided and reachability is improved and in stator lifting a pallet tilter is suggested so that operator no needs bend while lifting. Finally L4/L5 back compression is reduced in both the cases.

REFERENCES

1. Amare Matebu and Birhanu Dagneu, "Design of manual material handling system through computer aided ergonomics: a case study at bdtsc textile firm", *International Journal for Quality Research.*, vol. 8, pp. 557-568, Nov, 2014
2. Anukritisahni and Dr.R.B. Shahu," The NIOSH Lifting Equation for manual Lifting: A Literature Review", *International Journal of innovations in engineering and Technology.* vol. 6,pp. 1058-1064,2012.
3. N. A. Ansari and Dr. M. J. Sheikh, "Evaluation of work Posture by RULA and REBA: A Case Study", *IOSR Journal of Mechanical and Civil Engineering.*, vol. 11, pp.18-23, july. 2014.
4. Baba MdDeros, Nor KamalianaKhamis, Ahmad Rasdan Ismail, HarisJamaluddin, Azmi Mat Adam and SarudinRosli, "An Ergonomics Study on Assembly Line Workstation Design", *American Journal of Applied Sciences.*, vol. 11,pp. 1195-1201, 2011.
5. IvaniriaTecillaGuimaraes Souza, Celia Roberta Buss Buski, Eduardo Concepcion Batiz, and Ana Lucia Berretta Hurtado, "Ergonomic analysis of a clothing design station", *Applied Human Factors and Ergonomics Procedia Manufacturing.*, vol. 3, pp. 4362-4369, 2015.
6. P.N.Kaleand, R.T.Vyavahare, "Ergonomic Analysis Tools: A Review", *International Journal of Current Engineering and Technology.* vol. 6,No. 4, pp. 2347-2351,Aug, 2016.
7. K c .Mahendra and Dr. A thimmanagouda, "Ergonomic Analysis of Welding Operator Postures", *International Journal of Mechanical and Production Engineering.*, vol. 4, pp. 2092-2101, June. 2016.
8. Nor HafeezahKamarudin ,SitiAnom Ahmad , MohdKhair Hassan , RosnahMohdYusuff and SitiZawiahMdDawa, "A Review of the NIOSH Lifting Equation and Ergonomics Analysis", *Advanced Engineering Forum.*, vol. 10, pp. 214-219, 2013.
9. Raffaele Castellone, Stefania Spada, Giovanni Caiazzo, and Maria Pia Cavatorta, "Assessment of Anthropometric Differences in the Design of Workstations: Case Studies of an Automotive Assembly Line", *International Journal of Applied Engineering Research.* , Volume 12, Number 14, pp. 4549-4555, 2017.
10. Ro-Ting Lin, and Chang-chuanchan, "Effectiveness of workstation design on reducing musculoskeletal risk factors and symptoms among semiconductor fabrication room workers", *International Journal of Industrial Ergonomics.*, vol. 37, pp. 35-42, 2007.

Box-Behnken Analysis on Crystallinity of Microwave Air Plasma Treated Micro Crystalline Cellulose (MCC) Powder

K. Vaideki^{*}, M. Surendhar and C. Veeramani

Department of Applied Science, PSG College of Technology, Coimbatore, India

ABSTRACT

The paper describes the influence of microwave plasma treatment on the degree of crystallinity of microcrystalline cellulose (MCC) powder isolated from raw cotton fiber using acid hydrolysis process. The attribute of crystallinity viz., Total Crystallinity Index (TCI) that can be calculated using FTIR spectral data is altered during plasma treatment. This study aims to obtain maximum positive crystallinity change within controllable range of plasma parameters. Design of experiments (DOE) approach is applied to study effects of individual process parameters and interaction effects on changes in crystallinity of MCC powder after microwave plasma treatment. Box-Behnken design (BBD) is utilized to develop statistical experimental model to reduce time and resource involved to obtain efficient plasma parameter combinations for better positive crystallinity index change. Based on the statistical analysis and experimental verification, change in degree of crystallinity has been optimized based on maximizing the positive change, because MCC powders with higher degree of crystallinity is considered as an efficient particle reinforcement material.

Keywords: Microcrystalline cellulose (MCC), Crystallinity, Microwave plasma, Box-Behnken method, Design of Experiments (DOE), Optimization.

1. INTRODUCTION

MCC is depolymerized cotton widely used for various purposes. The crystallinity of MCC powder affects the quality of resultant product as crystallinity defines the stability and bonding tendency of MCC (1). This study is concentrated in improving the crystallinity of MCC powder using microwave plasma treatment. The properties of plasma depend on the source of input energy used for ionization (2). In general, a constant energy is supplied to neutral gas forming plasma species (electrons, ions, radicals and excited atoms) along with visible light radiation. In this study, plasma is generated using microwaves. The electric field is produced by microwave discharge. Microwave plasma produces effective surface modifications in materials under treatment enhancing quality and properties of the final products (3, 4). The change in crystallinity is dependent upon the nature and property of plasma used. The crystallinity of cotton has been found to be varied by microwave plasma (5).

Experimental process optimization is an iterative process involving mathematical techniques, performed either manually or using software tools like Design Expert. It is a statistical tool constructed to design experiments efficiently, screen characteristic features, perform comparative tests, optimize processes etc.,. Design of experiments is a multi-purpose technique (6). It extends its usage to simulate experiments (7) in addition to doing experiments physically. Design of experiments is a statistical methodology used for obtaining the relationship between input and output parameters in a process. This is a mathematical technique used widely by manufacturing industries to characterize the input combination to achieve desired result. Statistical significance and impact due to individual factors are achieved by ANOVA (Analysis of Variance) and graphical simulation tools (8, 9, 10). The focus of experimental design is to study and analyze the relation between the factors and the response(s) of a process, the factors are independent variables and the response is dependent variable. The study also includes prominent interactions along with the effects due to individual factors. The focus lies on minimizing the number of runs of experiment performed to obtain an optimum result. Box-Behnken and Central Composite are certain DOE designs (11).

Box-Behnken is a second order rotatable design built by three-level incomplete factorial design. The center point and the midpoint of edges of the factor cube (Figure 1) are focused by Box-Behnken for test runs excluding the extreme points to get satisfactory results. This design is efficient in fitting second order polynomials to response surfaces. Fewer points are required in comparison to Central Composite design.

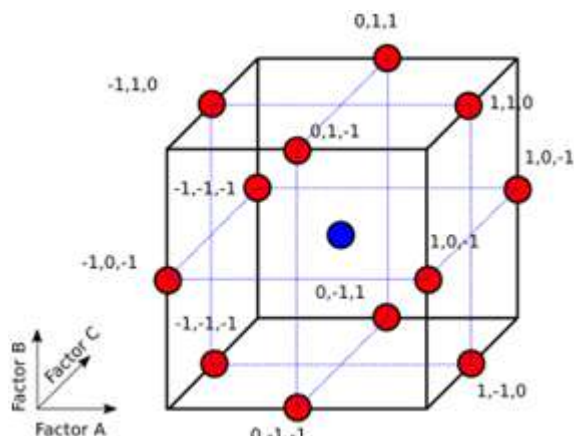


Figure 1: Box-Behnken design consideration

(Courtesy: [https://develve.net/Box-Behnken design.html](https://develve.net/Box-Behnken%20design.html))

In line with this, the current study is performed to analyze the relation between plasma parameters and its influence on resultant change in crystallinity of MCC sample using Box-Behnken optimization method.

2. METHODOLOGY:

2.1 Synthesis of MCC powder

One gram of raw cotton is weighed in electronic balance and is placed in hot air oven for a period of 1 hour to remove moisture content absorbed by cotton from atmosphere. The dry cotton obtained from oven is weighed and introduced into a conical flask with 20ml of 2.5N HCl. The mixture of cotton and HCl is placed in a magnetic stirrer for 75 minutes at 45° C under closed conditions. Cotton gets depolymerized during the process and after the process time, cold water is poured into the reaction mixture.

The mixture settles after a day and the filtrate is drained. The residue obtained is MCC contaminated with the acid used. Residue is centrifuged 4-5 times to remove the acid contamination and is verified by examining the pH. Residue is transferred to a petri dish, dried using hot air oven and grinded to obtain MCC particles. To confirm the MCC nature, small amount of sample is dispersed in 2 ml of iodinated zinc chloride solution taken in watch glass and the violet-blue color appearance confirms the micro crystalline nature of the powder.

2.2 Microwave plasma treatment:

The synthesized MCC powder was treated with microwave plasma. The chamber used for producing microwave plasma is shown below in Figure 2.

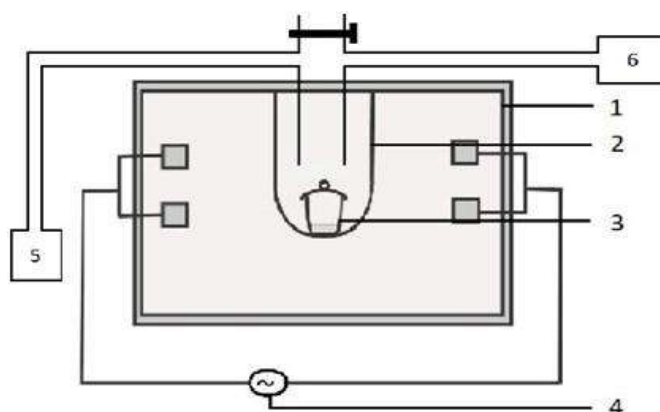


Figure 2: Microwave plasma chamber

1. Densely insulated steel chamber
2. Quartz chamber
3. Calcite crucible for sample loading
4. Microwave power source with two pairs of klystrons of 1.1KW each
5. Rotary pump
6. Pressure gauge

The dense metal chamber isolates the generated field of micro waves from escaping into surrounding. The quartz chamber allows produced beams of microwaves to pass through minimizing the area of plasma generation concentrating the field toward the sample. Calcite crucible holds good properties in withstanding high temperature and good permeability nature for microwaves and the MCC sample is placed inside this chamber. Two pairs of klystrons each capable of producing an electrical power of 1.1 kW generates the field necessary to produce plasma. The rotary pump evacuates the metal chamber to maintain required range of pressure which is measured using a pressure gauge. In the present study commercial grade air is used as process gas. Power percentage of klystron pair, pressure inside vacuum chamber and time of treatment are the plasma process parameters that can affect the plasma parameters (viz., electron, ion temperature and energies) and in turn the structure of the micro crystalline cellulose particles upon interaction. The upper and lower range selected for these plasma process parameters are presented in Table 1.

Table 1: Microwave plasma process parameters

Factor	Upper Range	Lower Range
Time	1 min	3 min
Pressure	0.5 mbar	1.5 mbar
Power Percentage	53% of 2.2 KW	57% of 2.2 KW

The experimental runs suggested by Box-Behnken design when the upper and lower ranges of the plasma process parameters were fed as input for the design are presented in Table 2.

Table 2: Box – Behnken experimental runs

Run	Factor A Pressure (mbar)	Factor B Power percentage (%)	Factor C Time (min)
1	1.5	57	2
2	1.0	53	3
3	0.5	55	3
4	1.0	55	2
5	0.5	53	2
6	1.0	55	2
7	1.0	55	2
8	1.5	55	3
9	1.5	53	2
10	1.0	53	1
11	1.0	55	2
12	0.5	55	1
13	1.0	57	3
14	1.0	57	1
15	0.5	57	2
16	1.5	55	1
17	1.0	55	2

0.03 gm of MCC powder was taken for every single experimental run. The MCC powder was subjected to FTIR analysis before and after the plasma treatment to calculate total crystallinity index before and after plasma treatment. The difference in total crystallinity index was fed as response into the Box-Behnken design table.

2.3 ATR-Fourier Transform Infrared Spectroscopic Analysis

The crystallinity of MCC powder before and after plasma treatment has been analyzed using ATR-FTIR spectra. The spectra were recorded using a Perkin Elmer (Spectrum 100) FTIR spectrometer in the range of 4000–500 cm^{-1} with a resolution of 1 cm^{-1} . The total crystallinity index of the cellulose powder was calculated using the IR spectra. TCI has been calculated using the ratio between the absorbance values of the bands at 1372 and 2900 cm^{-1} (12).

3. RESULTS AND DISCUSSION

The difference in total crystallinity index ($\Delta \text{TCI} = \text{TCI after plasma treatment} - \text{TCI before plasma treatment}$) of the MCC powder before and after the microwave air plasma treatment was fed as the response into the design table for ever single experimental run (Table 3)

Table 3: Box-Behnken Design with Response

Run	Factor A Pressure (mbar)	Factor B Power percentage (%)	Factor C Time (min)	Response Δ TCI
1	1.5	57	2	-0.03
2	1.0	53	3	0.15
3	0.5	55	3	-0.01
4	1.0	55	2	-0.01
5	0.5	53	2	-0.02
6	1.0	55	2	-0.04
7	1.0	55	2	-0.06
8	1.5	55	3	-0.04
9	1.5	53	2	-0.07
10	1.0	53	1	0.06
11	1.0	55	2	-0.02
12	0.5	55	1	-0.03
13	1.0	57	3	-0.01
14	1.0	57	1	0.01
15	0.5	57	2	0.00
16	1.5	55	1	0.03
17	1.0	55	2	-0.08

3.1 BOX-BEHNKEN DESIGN ANALYSIS

Attributes are analyzed individually accounting for the results obtained by performing the experiments. The analysis consists of components like Fit summary, Model function, ANOVA, Diagnostics, Model graphs providing information about the data fit to the considered design and variation with respect to change in factors.

3.2 Δ TCI Analysis

3.2.1 Transformation

Analysis of TCI response is effective without a transformation applied to the design data to neutralize the discrepancies in input data. The normal probability plot shown in Figure 3 explains redundant transformation function.

3.2.2 Fit summary

i. Sequential model sum of squares

This attribute of fit summary provides the significance of terms involved in the construction of the model equation.

Table 4: Sequential model Sum of Squares

Source	Sum of Squares	Df	Mean squares	F value	p-value prob > F
Mean vs Total	0.0017	1	0.0017	-	-
Linear vs Mean	0.0032	3	0.0011	0.32	0.8120
2FI vs Linear	0.0052	3	0.0017	0.45	0.7223
Quadratic vs 2FI	0.022	3	0.0075	3.32	0.0864
Cubic vs Quadra	0.012	3	0.0041	5.05	0.0758
Residual	0.0033	4	0.0008	-	-
Total	0.048	17	0.0028	-	-

The sequential sum of squares calculates the feasibility of having different kinds of terms in the model as addition of more terms to the model increases the correctness of the predicted result and hence a model that allows addition of terms the most is considered the best fit model and as seen from Table 4, quadratic vs 2FI

model provides higher F-value with descent p-value and hence the model of choice. Though cubic vs quadratic provides the highest F-value this is not a suggested one as this is an aliased model.

ii. Lack of fit test

Lack of fit test compares residual error to pure error and provides the initial image of deviation of predicted response from the actual response obtained.

Table 5: Lack of Fit Tests

Source	Sum of Squares	Df	Mean Square	F value	p-value prob>F
Linear	0.040	9	0.0044	5.41	0.0595
2FI	0.035	6	0.0058	7.07	0.0396
Quadratic	0.012	3	0.0041	5.05	0.0758
Cubic	0.000	0	-	-	-
Pure Error	0.0033	4	0.0008	-	-

The lack of fit sum of square is a portion of residual sum of square obtained due to specific model not fitting the data. The lack of fit F value compares the residual error to the pure error. Studying the contents of Table 5 provides a conclusion that quadratic model possess the lowest sum of squares value, greater p-value compared to other models and it is not aliased.

iii. Model summary statistics

Table 6: Model Summary Statistics

Source	Std. Dev	R-Squared	Adjusted R-Squared	Predicted R-Squared	PRESS
Linear	0.058	0.0684	-0.1466	-0.7754	0.082
2FI	0.062	0.1794	-0.3129	-2.4902	0.16
Quadratic	0.047	0.6615	0.2264	-3.3949	0.20
Cubic	0.029	0.9293	0.7172	-	-

Examining **Table 6** values, **Quadratic model** is considered the best fit model as the standard deviation of error for this model is less compared to other non-aliased models. In addition to the std-dev value this model shows greater R- squared, adjusted R-squared, PRESS values that explain certain portion of lack of fit in the model. Comparatively higher PRESS value explains the predicted quadratic model best fits the actual design points with minimal deviations than others.

3.2.3 Model function [f(x)]

Considering the results obtained from the lack of fit tests, the quadratic model is chosen as the appropriate model that fits the experimental scenario to a greater extent than the other models included in the design. This model includes the certain terms for further studies as mentioned in **Table 7**.

Table 7: Quadratic model terms

Selected terms
Intercept
A-pressure
B-power percentage
C-time
AB
AC
BC
A ²
B ²
C ²

3.2.4 ANOVA for response surface quadratic model

Table 8: Analysis of variance table

Source	Sum of Squares	df	Mean square	F-value	p-value Prob> F
Model	0.031	9	0.0034	1.52	0.2972
A-pressure	0.0003	1	0.0003	0.14	0.7200
B-power percentage	0.0028	1	0.0028	1.25	0.2998
C-time	0.00005	1	0.00005	0.022	0.8855
AB	0.0001	1	0.0001	0.045	0.8388
AC	0.0020	1	0.0020	0.90	0.3737
BC	0.0030	1	0.0030	1.35	0.2836
A ²	0.0029	1	0.0029	1.32	0.2887
B ²	0.0062	1	0.0062	2.78	0.1393
C ²	0.013	1	0.013	5.89	0.0457

Residual	0.016	7	0.0022	-	-
Lack of fit	0.012	3	0.0041	5.05	0.0758
Pure error	0.0033	4	0.0008	-	-
Correlation total	0.046	16	-	-	-

Table 8 concentrates on the effect of individual terms to the model result .F-value of the model is 1.52; stating the model is non-significant to noise (disturbances) and a 29.72% chance that model F-value of this large could occur due to noise. The lack of fit F-value of 5.05 implies that there is 7.58% chance that a lack of it F- value this large could occur due to noise.

Table 9: Model ANOVA Values

Term	Value
Standard Deviation	0.047
Mean	-0.010
Coefficient of variance%	473.66
PRESS	0.20
R-squared	0.6615
Adjusted R-Squared	0.2264
Predicted R-squared	-3.3949
Adequate precision	4.163

Adequate precision in Table 9 measures the signal to the noise ratio. The value 4.163 is very significant and provides the information that the obtained data is an adequate signal as value more than 4 is desirable. This model can be used to navigate through the design space.

Table 10: Estimated co-efficient and significance

Factor	Coefficient Estimate	df	Standard Error	95% CL		VIF
				Low	High	
Intercept	-0.042	1	0.021	-0.092	0.0081	1.00
A-pressure	-0.0063	1	0.017	-0.046	0.033	1.00
B-Power percentage	-0.019	1	0.017	-0.058	0.021	1.00
C-time	0.0025	1	0.017	-0.037	0.042	1.00

AB	0.0050	1	0.024	-0.051	0.061	1.00
AC	-0.023	1	0.024	-0.079	0.034	1.00
BC	-0.028	1	0.024	-0.084	0.029	1.00
A ²	-0.027	1	0.023	-0.081	0.028	1.01
B ²	0.038	1	0.023	-0.016	0.093	1.01
C ²	0.058	1	0.023	0.0014	0.11	1.01

The model equation is constructed using the ANOVA and the coded coefficients of terms are mentioned in **Table 10**. A VIF (Variance Inflation Factor) closer or equal to one state's that the system is orthogonal. All the terms involved in the study are orthogonal and hence there are effects due to the terms that deviates the predicted response value farther from the actual response obtained as the result. The model equation that significantly fits the system is,

$$\Delta TCI = -0.042 - 0.0063*A - 0.019*B + 0.0025*C + 0.005*AB - 0.023*AC - 0.028*BC - 0.027*A^2 + 0.038*B^2 + 0.056*C^2 \dots \dots \dots \text{(Final equation in terms of coded factors)}$$

$$\Delta TCI = +28.3875 + 0.0145*Pressure - 1.0456*Power \text{ percentage} + 0.5797*Time + 0.005*Pressure*Power \text{ percentage} - 0.045*Pressure*Time - 0.01375*Power \text{ percentage}*Time - 0.106*Pressure^2 + 0.00963*Power \text{ percentage}^2 + 0.056*Time^2 \text{(Final equation in terms of actual factors)}$$

The equation in terms of actual factors define the response surface of TCI and the response value for any combination of factors within the experimental range can be predicted using the same.

3.2.5. Diagnostics case statistics report

The report comprises of various statistical graphical plots that ensures the reliability of the model over the desired response

i. Normal Plot of Residuals

Normal probability plot is used to indicate nature of residuals. Internally studentized residuals forming nearly a straight line as shown in Figure 3 implies normal distribution. Absence of curves or patterns in the plot reveals that a transformation not required.

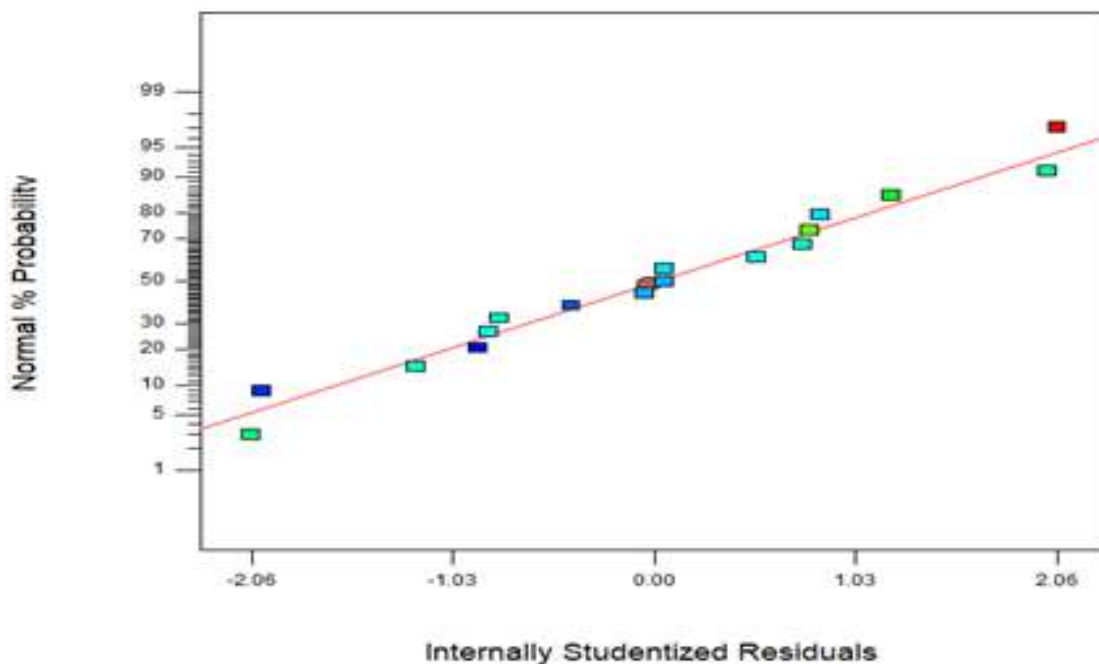


Figure 3: Normal plot of residuals of ΔTCI

ii. Studentized residuals Vs Predicted values Plot

This is the internally studentized residuals versus predicted response value in ascending order. The plot is used to visualize the assumption of constant variance. The plot must be a random scatter rather than a megaphone pattern indicating that a need for a transformation is not required. The points in the plot shown in Figure 4 are within the range, indicating the correctness of constant variance assumption.

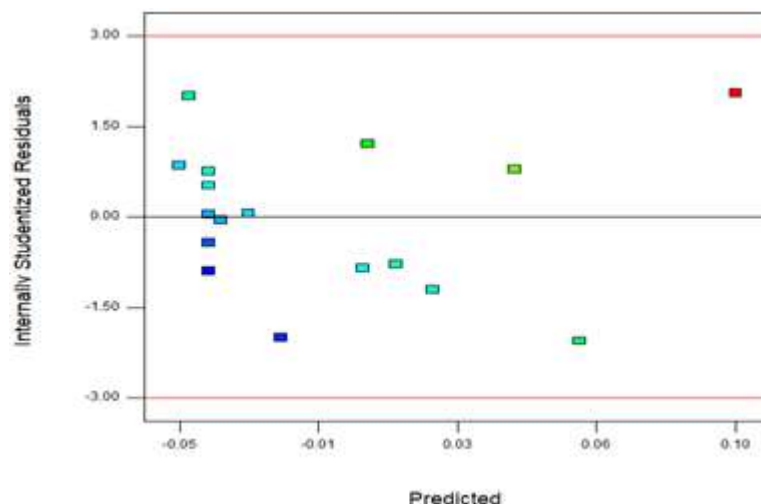


Figure 4: Studentized residuals vs. predicted values plot of Δ TCI

iii. Predicted Vs Actual values Plot

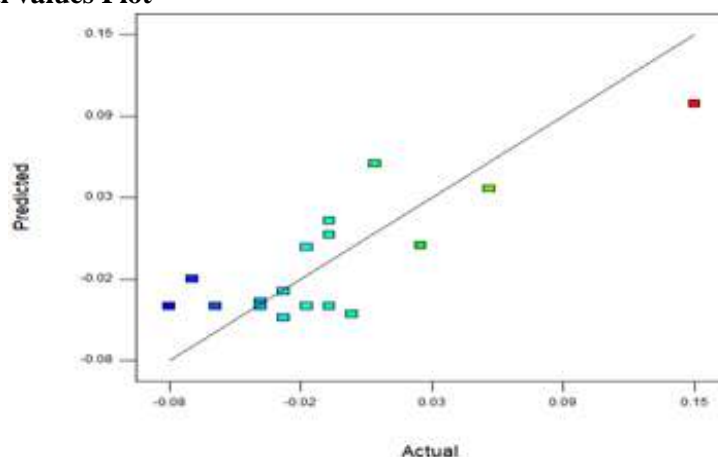


Figure 5: Actual vs. Predicted plot of Δ TCI

The variation in the obtained experimental value (actual) and predicted value by the model for similar runs is graphically shown in Figure 5. The graphical points follow a straight line with some minor deviations. Hence the actual and predicted values nearly correspond to each other showing better efficacy of model.

iv. Externally Studentized Residuals Plot

This statistical plot is a measure of determining, number of times standard deviation of actual value varies from the predicted values, after removing the outlier point using control limit to find the influential points (or the outliers) in the standard deviation. Figure 6 discloses that the control limit is actually set by the design at 4.82 in magnitude. The absence of outliers within this limit indicates that all the response values can be used as such for statistical analysis.

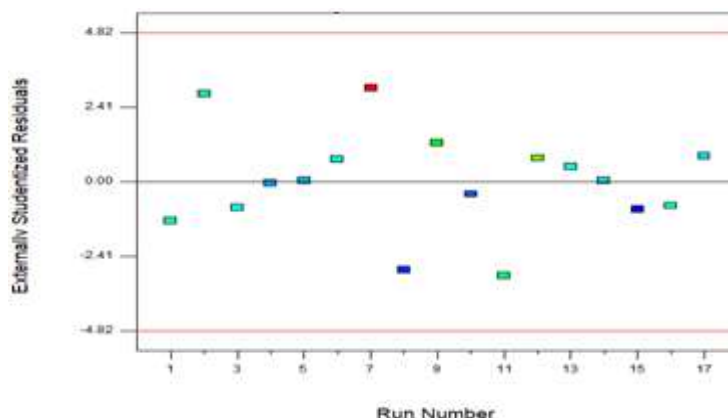


Figure 6: Externally studentized residuals plot of Δ TCI

v. Box-Cox power transform plot

A natural log value of residuals vs lambda plot is a tool to determine the appropriate power transformation to apply for response data to make the prediction more relative to obtain accurate results. The lowest power on box-cox plot represents the value of lambda, providing minimal residual sum of squares in transformed model. Plot below indicates a lambda value of 1, indicating no requirement for a transformation, strengthened by the range between high and low confidence index limits being less than 3 (low=-0.15,high=1.4).

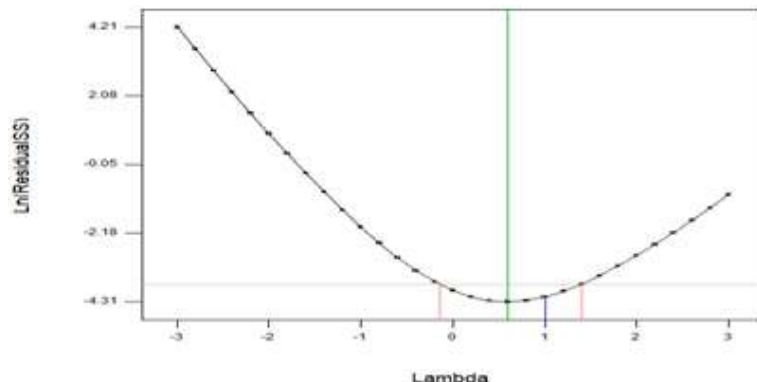


Figure 6: Box-Cox power transform plot for Δ TCI

3.2.6. Model graphs

i. Influence of one factor on Δ TCI

The tool provides a graphical representation of the influence of individual factors over the response under study. One factor graph provides linear effect of changing the levels of a single factor. The graphs below represent the individual influences, constructed by taking 2 of 3 influencing factors constant respectively. Additionally all three factors are also involved in interaction.

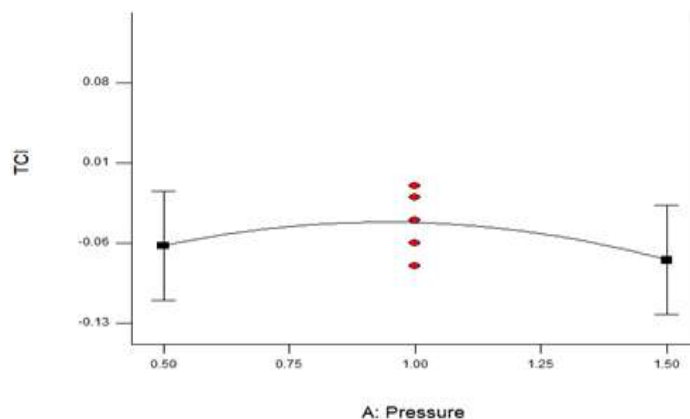


Figure 7: Predicted influence of Pressure on Δ TCI

Maintaining a constant power percentage and exposure time, it can be inferred from figure 7 that as the pressure increases the Δ TCI values increases up to a pressure of 1 mbar and decreases thereafter. This is because the mean free path of the plasma species decreases with pressure thereby increasing the collision rate, and hence decreasing the effective interaction between the plasma species and MCC surface.

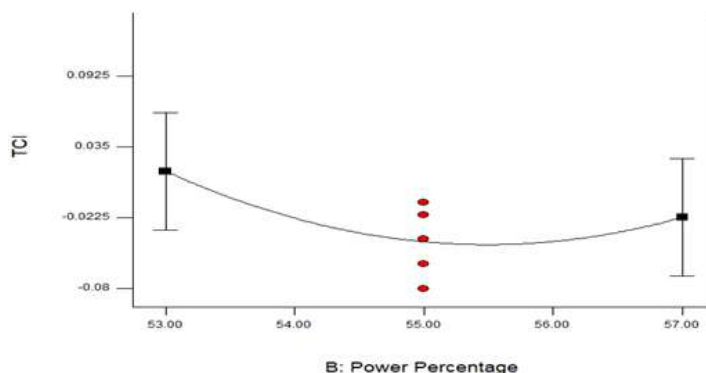


Figure 8: Predicted influence of Power percentage on Δ TCI

Figure 8 shows the variation of ΔTCI with respect to power percentage, while maintaining a constant pressure and exposure time; it can be inferred from figure 8 that as the power percentage increases the ΔTCI values decreases up to 55% and almost remains constant. This is because as the electrical power is increase, the collisions increase and mean free path decreases thus decreasing the effective interaction between the plasma species and MCC surface.

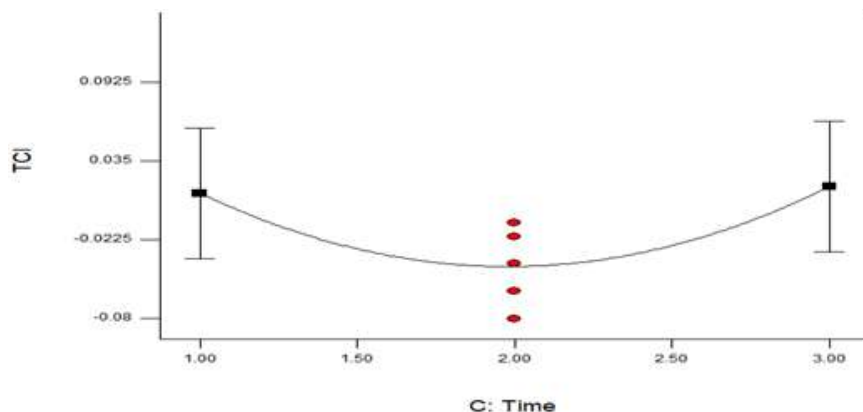


Figure 9: Predicted influence of Time on ΔTCI

As the exposure time increases maintaining constant pressure and power percentage, the ΔTCI value decreases up to 2 minutes and increases thereafter. This could be attributed to effective surface oxidation that takes place when the MCC powder is exposed to microwave air plasma for about two minutes and formation of intra and inter hydrogen bonds thereafter up to 3 minutes.

ii. Influence of interacting factors on ΔTCI

Including factors interaction provides results with high standards of prediction. The influence of interacting factors over ΔTCI is shown in following graphs (Figure 10, Figure 11 and Figure 12) where one among the three factors involved in the interaction is taken as constant.

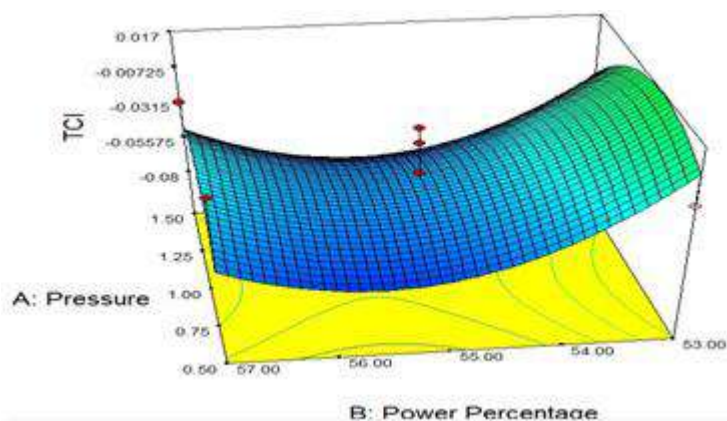


Figure 10: Predicted influence of pressure-power percentage interaction on ΔTCI

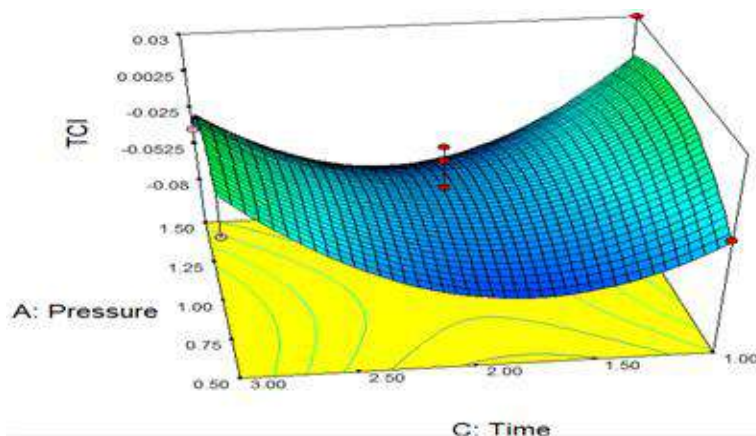


Figure 11: Predicted influence of pressure-time interaction on ΔTCI

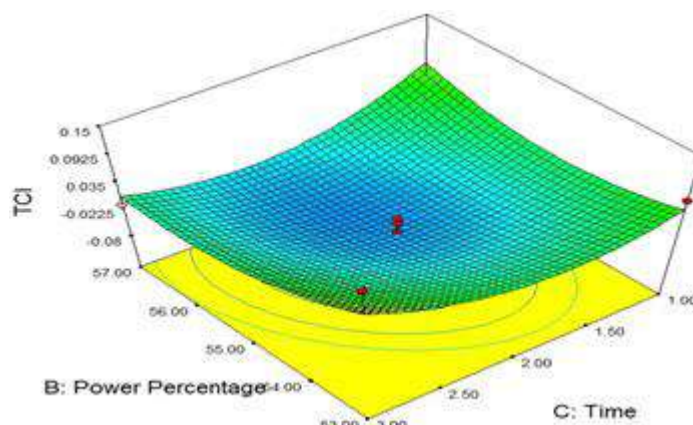


Figure 12: Predicted influence of time-power percentage interaction on Δ TCI

3.2.7 Δ TCI Optimization

Optimization process performed for maximizing the Δ TCI provides a range of combination of runs with respective desirability (higher) closer to 1 as shown in Table 11.

Table 11: Optimization outcomes of design for maximum Δ TCI

Number	Pressure	Power Percentage	Time	Δ TCI	Desirability
1	0.68	53.00	3.00	0.111	0.835
2	0.69	53.00	3.00	0.111	0.835
3	0.70	53.00	3.00	0.111	0.832
4	0.65	53.04	3.00	0.109	0.824
5	0.84	53.00	3.00	0.109	0.823
6	0.51	53.00	3.00	0.109	0.822
7	0.67	53.00	2.97	0.107	0.817
8	0.72	53.00	2.94	0.103	0.797
9	1.01	53.00	3.00	0.100	0.785
10	1.04	53.00	3.00	0.099	0.777

To experimentally confirm the desirability test, MCC powder was treated with microwave plasma using the following process parameters: Pressure: 0.70 mbar, power percentage: 53%, Time of treatment: 3 minutes. The ATR-FTIR spectra were taken before and after plasma treatment and TCI was calculated using the spectral absorbance values. The Δ TCI value calculated using these readings was found to be 0.10 which is close to the desirability test result. Hence it can be concluded that the Box-Behnken simulation holds good for maximizing the Δ TCI value of microwave plasma treated MCC powder within the said range of process parameters.

4. CONCLUSION

The optimized process parameters to obtain maximum Δ TCI within the working range have been formulated using the Box-Behnken design. The equation generated from the design additionally aids in prediction of response for any set of process parameters confined in working range. The experimental process is estimated to fit a quadratic model and hence the attributes of crystallinity should align with the same to obtain better predictions. The Δ TCI is aligned with the process model trend and hence the predictions have enhanced reliability for expected results.

REFERENCES

1. Sunkya Park, John O Baker, Micheal E Hammer, Philip A Parilla and David K Johnson, "Cellulose crystallinity crystallinity index: Measurement techniques and their impact on interpreting cellulose performance", *Biotechnol Biofuels*, (2010) ; doi: 10.1186/1754-6834-3-10, PMID: 20497524, Free PMC article.
2. H. Conrads and M Schmidt, "Plasma generation and plasma sources", *Plasma sources science technology*. 9 (2000).
3. M Kaiser, K.M Baumgartner and A Mathews, "Microwave plasma sources- application in industries", Wiley online library, (2012).
4. J Musil, "Microwave plasma: its characteristics and applications in thin film technology", *Institute of physics, Vacuum*, (1986), 36(1-3), 161-169.

5. S Prabhu, K Vaideki, S Anitha, "Effect of microwave argon plasma on the glycosidic and hydrogen bonding system of cotton cellulose", *Carbohydrate polymers*, (2017), 156, 34-44.
6. Box, G.E., Hunter, W.G. and Hunter, J.S. *Statics for Experiments*. 2nd Edition, Wiley, New York, (2005).
7. Law, A.M and Kelton, W.D. *Simulation Modeling and Analysis*. 3rd Edition Mc Graw Hill, New York. (2000)
8. S.L.CFerreira, R.E.Brush, H.SFerreira, G.DMatos, J.MDavid, G.CBrando, E.G.Pda Silva, L.A Portugal, P.S dos Reis, A.S Souza and W.N.I dos Santos, "Box-Behnken design: An alternative for the optimization of analytical methods", *Analytica chimicia Acta*, (2007), 597.
9. R.Konda, K.P. Rajurkar, R.RBishu, A.Guhaand, M.Parson, "Design of experiments to study and optimize process performance", *international journal of quality and reliability management*, (2005).
10. Steven A. weissmen and Neal G. Anderson 'Design of experiments (DOE) and process optimization: A review of Recent Publications', ACS publications, (2014).
11. S. Anitha, K Vaideki, S Prabhu and S Jayakumar," ATR-FTIR analysis on the hydrogen bonding network and glycosidic bond of DC air plasma processed cellulose", *Journal of molecular structure*, (2019), 1180.
12. Nelson, Mary L., and Robert T. O'Connor.. "Relation of Certain Infrared Bands to Cellulose Crystallinity and Crystal Lattice Type. Part II. A New Infrared Ratio for Estimation of Crystallinity in Celluloses I and II." *Journal of Applied Polymer Science*, (1964),8(3):1325-41.

Analysis on OAT Systems for RFID Devices

Senthil Prabha R, Sangeetha B, Ravitharajalakshmi N and Keerthi P

Department of IT, PSG College of Technology, Tamil Nadu, India

ABSTRACT

OAT Merchandise Visibility provides retailers real-time visibility into the inventory of RFID tagged merchandise through the supply chain and in stores. OAT Merchandise Visibility provides an end to end solution for the retail supply chain right from manufacturing to distribution and also through out the store. It provides insight into their operations and execution challenges, from the point of manufacture through point of sale. This is done by integrating RFID from the point of manufacture through logistics and distribution operations and the stores. The various scenarios are deployed and developed from the handheld. Existing .NET CE SDK cannot be customized for new cases. So OAT Mobile SDK for iOS helps in terms of both customization and portability.

Keywords: RFID, Mobile SDK, Hybrid Mobile Architecture, OAT

INTRODUCTION

Automatic Identification includes RFID. RFID uses radio waves to automatically track objects. RFID is a quick technology that requires no line-of-sight scanning. The RFID system includes an RFID tag with a microchip and an antenna, and a reader with an antenna. The information is stored in RFID tags that are attached to the objects for identification. Each object has an Electronic Product Code. The EPC number on each object's RFID tag uniquely identifies it. The antenna on the tag's microchip captures the reader's radio waves, allowing the chip to transmit the identification information to the reader. These radio waves are decoded by the reader and converted to digital data for processing by a server. RFID systems are used in retail and manufacturing to help prevent theft and manage inventory. Figure 1.1 shows RFID tags, readers, antennas, and a host computer running application software. The OAT Foundation Suite is a tried-and-true middleware platform that integrates enterprise applications with real-time data from Auto-ID, Wi-Fi, RTLS, and GPS inputs in a two-way process. OAT Foundation Suite architecture consists of several components that work together to provide a complete and customizable Radio Frequency Identification solution. There are three major components in OAT. They are OAT Enterprise Administrator, OAT Express and OAT Enterprise Data Administrator. OAT Express provides RFID middleware for data capture and aggregation, device management and monitoring, EPC number and product management. An OAT Express server is associated with one store or many stores of the same organization and these servers migrate their collected data to the OAT Enterprise Data Manager for analysis. OAT Enterprise Administrator manages and monitors all OAT Express servers in an enterprise. It stores and distributes master data such as locations of stores, products of stores and EPC number ranges to the relevant OAT Express servers and central OAT EDM server. OAT Enterprise Data Manager serves as a single point to collect data from OAT Express servers. This aggregated data will be analysed and used for reporting. Reports will be useful for customers for decision making purposes. In order to improve business processes, OAT solutions provide real-time visibility into systems. The built solutions are OAT Asset Tracking and Merchandise. In-store and distribution OAT Merchandise Visibility covers the entire retail supply chain. They have operational and execution issues from manufacturing to retail. RFID is used in manufacturing, logistics, distribution, and retail. OAT Merchandise Visibility increases retailer visibility. It also helps retailers stand out. It tracks assets and work-in-progress. A supply chain-wide asset tagging system allows manufacturers to locate assets, contents and components. Asset tracking is designed to address issues in manufacturing and distribution. ATA targets aerospace manufacturers, logistics companies, and airlines to ensure part documentation accuracy and aircraft safety. High-memory RFID tags identify aircraft parts.

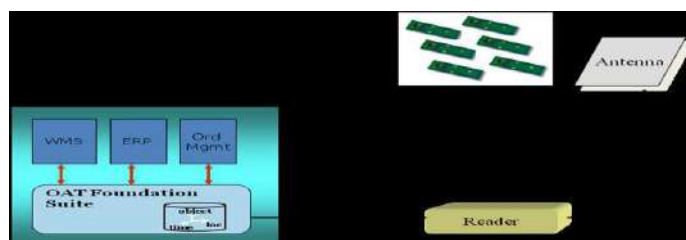


Fig1 Components of RFID system

2. LITERATURE SURVEY

OAT Merchandise Visibility provides retailers real-time visibility into the inventory of RFID tagged merchandise through the supply chain and in stores. It leverages the combined strengths and capabilities of Checkpoint's Tagging/ Labelling Solutions and the OAT Foundation Suite to deliver a complete solution. OAT Merchandise Visibility provides an end-to-end solution for the retail supply chain right from manufacturing to distribution and also throughout the store. It provides insight into their operations and execution challenges, from the point of manufacture through point of sale. This is done by integrating RFID from the point of manufacture through logistics and distribution operations and the stores. The various scenarios are deployed and developed from the handheld are as follows. Cycle Count, Filtered Cycle Count, Locate item, Locate item and offline are the various use cases deployed from the Handheld. The in depth knowledge of these scenarios are studied. Through the Windows Mobile Centre the device is connected to the PC. Through this information is passed from the Handheld to the Oatxpress. The existing RFID reader is native and it is not capable of running applications that could run on different platforms, it is not portable and so we are going to build a framework that is hybrid, such that it can run on various platforms like Blackberry, Apple, Windows and Android. Key decisions are taken based on the technology specifications and values. Checks the parameter values between existing and proposed values and chooses the best implementation method. Existing .NET CE SDK cannot be customized for new cases. So, iOS SDK is capable in terms of both customization and portability. Merchandise Visibility solution scenarios are currently built in .NET CE framework and can be used only with readers compatible with that framework. The framework can be executed only in that corresponding platform. Many customers doesn't recommend the native platform because their functionalities may be working with multiple platforms. So, .NET CE framework cannot be used in cross level of platforms for the customer's requirements.

2.1 NATIVE VERSUS HYBRID APPLICATION

Fig 2 and Fig 3 depicts the development process for native app and hybrid app respectively.

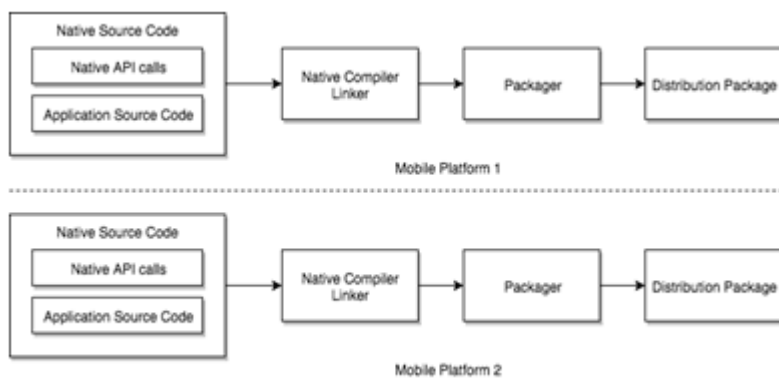


Fig2. Native Application development process

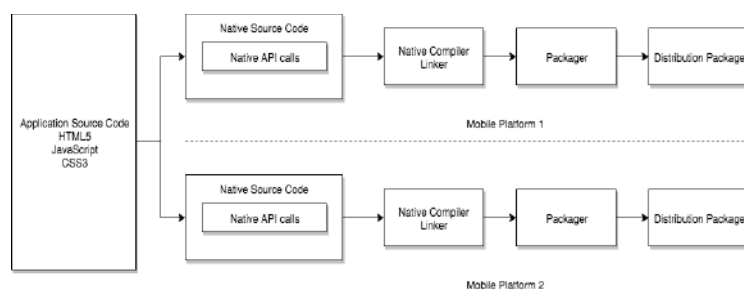


Fig3 Hybrid Application development process

Native application has all components developed using platform specific software language while the Hybrid APP has application source code developed using cross platform software languages and native drivers developed using platform specific languages.

2.2 OBJECTIVES

OAT mobile follows Hybrid mobile architecture while building applications in multiple platforms. It is solved by using standards based web technologies to bridge web applications and mobile devices. The RFID readers are paired to the mobil

edevelopedusingBluetoothandcommunicationbetweenthemis channelledthroughCordovaJavaScript Bridge.TheSDKistargetedforAppleiOSplatform, as the applications developed using the SDK is targeted for modern days smart devices; memory is assumed to be available for exclusive use for the app (150MB 400MB operating memory). The SDK is targeted for the currently supported RFID readers. The targeted users of this SDK are developers who has JavaScript, AngularJS, iOS and HTML5. Thus performance need not be equivalent to the ones developed on specific native stacks. But efforts will be made to bring near native performance. Hybrid mobile architecture is implemented using web technologies. UI is based on HTML5 and business logic is implemented using JavaScript. AngularJS is used as the client side Merchandise Visibility web framework. Onsen UI as mobile responsive design platform which can be further optimised based on the customer's requirements. The RFID readers are paired to the mobile devices using Bluetooth and communication between them is channelled through Apache Cordova JavaScript Bridge. Cordova plugins like RFD8500 and TSL were created for native communication. Apache Cordova PhoneGap plugin is made set up to deploy the hybrid application on the top of any platforms. Hybrid strategy helps in porting the business logic to multiple mobile OS platforms by retaining majority of common code. This helps in maintaining almost a single code base for all platforms. Table 1 depicts key point comparison between these two approaches.

Table 1 Comparison between native and hybrid technologies

Feature	Native app	Hybrid App
Scripting Languages	Native only	Native / Web / Web
Flexibility of the source code	None	High
Device-specific functions	High	Medium
Utilize what is known	Low	High
Graphics technology	High	Medium
Adaptability	Low	Medium
Working knowledge of installation	High	High
Performance	High	Medium
Accessibility of the Device	Full	Full
Consistency	Low	High

3 PROPOSED CORDOVA HYBRID ARCHITECTURE

The platform agnostic source codes are developed using HTML5, JavaScript and CSS. This common code will be then compiled for specific platforms and will be run using Cordova's JS Bridge. MVP and MVVM are two popular UI architectural patterns aiming at separation of concerns. In MVP, the Presenter updates the View based on the requested actions it performs on the Model, but the View is not Model aware. Thus it is possible to share models between the views. Usually the binding between View and presenter is one to one. In MVVM, the View Model has no information about the View, despite the fact that the View holds a reference to it. This is why a one-to-many mapping between multiple Views and a single View Model is possible. In the MVVM pattern, the View has no knowledge of the Model. This is because the View Model is its "Model" as far as it is aware. Data binding isolates the View from having to understand what's really going on behind the scenes. The issues at hand are UI, UI gestures, and data. The SDK's architecture is depicted in Figure 2.

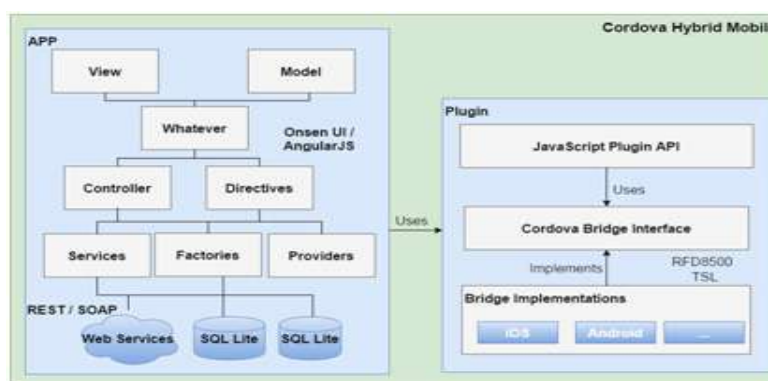


Fig 4 Cordova Hybrid Architecture

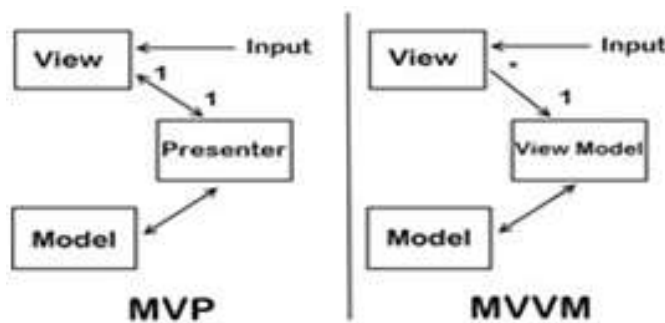


Fig5. MVP Vs MVVM

As view model can be shared across the views, it gives us great flexibility in plugging new views. It also preserves all qualities of presenter. AngularJS is chosen as the merchandise visibility framework for clean separation of concerns. AngularJS is based on JavaScript and has components to support enterprise grade application development. The views are created using HTML5 and uses HTML5 feature extensions to build custom HTML tags. Dependency Injection feature in AngularJS opens up opportunities for loose coupling and unit testability.

4 SYSTEM DESIGN

It is concerned with the overall system's architecture and design. It explains about various technologies used in development of the system.

Fig 6 depicts the System Architecture Framework that mainly focuses on the Customization of the use cases. SDK will adopt "Aspect" oriented overrides for realizing the customizations. The customizable units are composed as "Commands" and a set of commands can form an "Event". Each of these commands and events can be overridden using "Aspects". The aspects are "Before", "After" and "Around".

The "Aspects" written for "Before" will execute before the command execution and "After" executes after the command execution. "Around" aspects will override the original implementations. Thus "Aspect" oriented overrides will allow controlled customizations; whereas the frameworks provided extension facilities can be used for developing new functionalities.

The command framework for SDK will be based on "Command Angular" command framework, which is in turn based on AngularJS. OAT mobile SDK architecture can be designed around Cordova, NodeJS and AngularJS. Fig 6 depicts the Workflow of the services. It shows how the system's functionality and responsibilities are partitioned and assigned to subsystems or components. Architecture of SDK will be as follows. Use case engine is the core of SDK and this will be the foundation used for developing Merchandise Visibility scenarios. Components are cross cutting concerns. Tools are utilities to use the SDK. This methodology deals with the entire system architecture and ways to implement with the necessary technology.

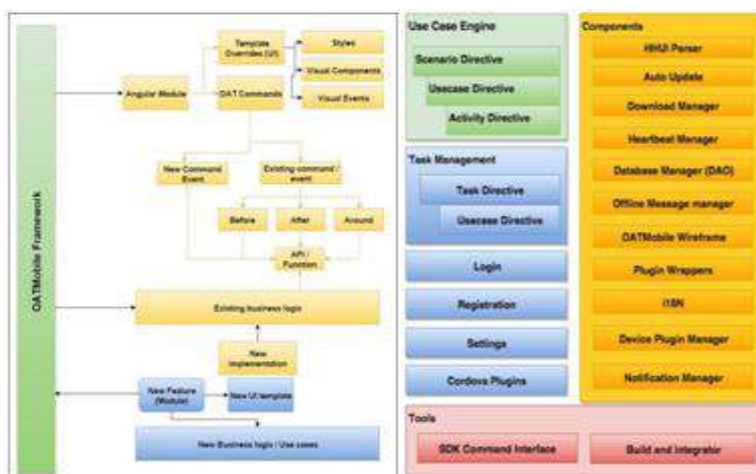


Fig6 System Architecture Fig7 Services Workflow

4.1 APPLICATION LAYER ARCHITECTURE

UI follows Merchandise Visibility patterns. Business logic is developed as AngularJS services. Overrideable component are developed as commands, which can be invoked from controller and business logic layer. DAO is based on the repository pattern. Native layer calls are made through Cordova JS Bridge. OFS REST calls are made from

business logic orthroughcommands.Fig8 depictstheApplication Layered ViewoftheSDK.OAT mobile SDK will include a registration module to register handheld devices withOFS.Registrationisinitiatedwhentheapplicationisstarted.Sequenceisdescribedaboveandflowgoesthroughth evariousparameters.Theoriginalimplementationofnavigates to registration UI. This can be overridden to go withanycustomimplementationwhichthendispatchesRegister.OATmobileSDKfollows OFS login. The client will execute the authentication strategy set from theserver basedonthefollowingdesign. OAT mobile SDK can have either OAT Login or External login. A new implementationcan be done to override either of these authentication mechanisms. The strategy is decided attheserver.

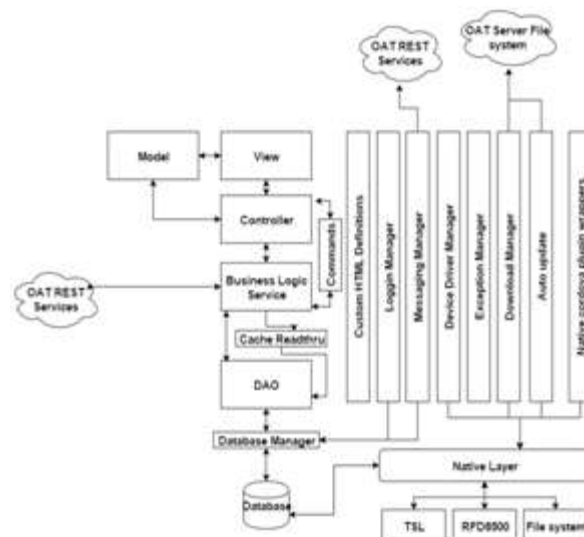


Fig8 ApplicationLayer

Handheld UI xml is the input for these directives. The scenario directive maps to the scenario tag in HHUI.xml. Thisdirective will construct a collection of scenario tags and represent them as dashboard iconson the screen. The mapping is now based on the class Name attribute, but eventually it has to bebased onascenario/use caseID. Theseusedirectiveiscomposedofmanyoat-activitydirectives. UsecaseService willbean angularservice, andwillberesponsiblefor navigatingbetweenactivitiesin the use case and controlling the use case termination. All use case related properties areaccessedthroughthisdelegate. Customization can be done by editing the usecase.html. A copy of the folder iscreated,ifbothoriginalandcustomizedusecaseshavetoberetained.Theoriginalimplementationwillbeoverriddenifthe copiedfolderwasgivensamenamethetheoriginal.OATActivityDirective defines an activity within a use case. Multiple activities make up a usecase. Anactivity canbeUIbased or anaction.The sequence of operations whenconstructing the activities are:ReadtheUI template,extract andrenderit ifitisUIbasedactivity.Delegatetheoperation torespectiveservice,iftheactivityisnon-UIbased. Every UIactivity shouldhave a templateURL. ThisURL shouldrepresentan htmlpage.Thecontrollerscanlistenfor“activity”enterandleaveevents.OATScenarioDirective maps to the scenario tag in HHUI.xml. This directive willconstructacollectionofscenariotagsandrepresentthemasdashboardiconsonthescreen.The mapping is now based on the class Name attribute, but eventually it has to be based ona scenario/use caseID.

5. Experimentalresult Analysis

This section elaborates on the techniques and procedures used during the system's testing process. Execution transforms the theoretical design into a functional system. Implementation requires research into the system and its constraints. After retrieving the OATxpress database, the system checks for presence of the site name. If the site name is present, download products, locations, filters, and other parameters, and register the device id. Otherwise, the error message reads “Device not reachable, Site ID not found.” For example, to register the device with a store, Click the OAT mobile icon to launch the app and enter the server URL. Register by entering the site/store name. Registration occurs after server configuration and based on the customer's needs. Enabling OAuth requires entering the system administrator's username and password. As soon as you register, a server-side sync occurs, downloading and configuring all products, locations, and other configurations The server will provide the username and password. Users typically generate their OATxpress username and password from the OAT Systems support site. An email with username and password will be sent to the user's mail I To access the home page, the user must first log in. Successful application login returns user to Home

page. Check OATxpress is online before starting OAT Merchandise Visibility. This syncs the iPod's time with the OATxpress. Simultaneously displaying and disabling OATxpress scenarios. The home page displays all configured scenarios and settings. They are synchronized using RFXML script on the server side. Fig 9 shows how to configure the home screen and the server. The configuration table status allows for four different ways to sync data from the server to the handheld side. Product, Location, Filter, and Configuration are the four methods. Only the association values and history are stored in each OATxpress DB, while the entire object state containing all attribute values is stored in a new schema called the product model. The model is now a product model. The server-to-handheld synchronization is based on handheld UI RFXML configuration scenarios used to identify aircraft parts.



Fig9 Configuring Homepage and Serverpage

By selecting Location from the list, the expected number of items is shown in Fig 11. If it can connect to the server, it scans the object. The progress bar advances with the scan count. OFF/release hard trigger to stop scanning. View scan accuracy in Detail View. The Scan Accuracy Page shows the following. When the MissingItemsThreshold is set to '0', a pop-up screen appears. This pop up screen appears if the cycle counted inventory is less than 80% of the expected inventory, or if the difference between the expected and cycle counted inventory is 20% or more. No pop-up message is displayed if the Missing Items Threshold is set to 100. Filtered Cycle Count, like Cycle Count, verifies inventory at various store locations but with a specific product. Store Associate scans items in a specific section of the store with an iPod. Start typing. All attribute values are auto-completed. Actual Total is the number of items in the store inventory that match the filter. Fig 12 shows filtered cycle counting.



Fig11Count Analysis



Fig13LocateItem

Fig. 13 shows the scanned UPC, its description, and default Filter attributes values. To find the item, turn on Trigger Hold. Begin walking with the iPod device with the trigger pressed, and follow the beeps and progress bar value to the nearest product location. The iPod starts looking for it. The progress bar and audio beep frequency indicate the tag's distance. The beep stops when the item is found. The new commissioned EPC is written onto the tags and is only available in the online mode. Any number of items can be encoded at the same time. This scenario is only available online and will be disabled in offline mode. From the Home page, select the Encode Item scenario. Using the keypad, a store associate can scan or enter the UPC/SKU. The product details will be displayed if you tap out of the text box. After scanning the UPC and viewing the details, place the RFID reader on the tag to be encoded. The EPC is read implicitly, without the need for the store associate to pull the trigger. Only after the product details are displayed will the EPC field be enabled. When an EPC scan is successful, a beep is and the beam is turned off. Both the product information and the EPC have been cleared.

CONCLUSION

The hybrid solution of application has been created which solves all the problems of portability, cost effectiveness and customization concerns. The platform agnostic sourcecodes has been developed using HTML5, JavaScript and CSS, which helps in creating common code which will be then compiled for specific platforms and will be run using Cordova's JS Bridge. MVP and MVVM are two popular UI architectural patterns aiming at separation of concerns which has been successfully analyzed and implemented combining the advantage factors of both these parameters. The command framework for SDK implemented which is in turn based on AngularJS features. The communication between the applications developed using the SDK and the OAT servers will be on "REST" protocol using JSON as medium. Offline data capability will be achieved through SQLite. Application would manage a database for storing configuration and message information; while few other databases will be downloaded from OAT server.

BIBLIOGRAPHY

1. N. Ahmed, S. Butler and U. Ramachandran, "GuardianAngel: An RFID-based indoor guidance and monitoring system," 2010 8th IEEE International Conference on Pervasive Computing and Communications Workshops (PERCOM Workshops), 2010, pp. 546-551, doi: 10.1109/PERCOMW.2010.5470498.
2. <https://cordova.apache.org/docs/en/10.x/guide/overview/>
3. <https://www.hirist.com/j/hybrid-developer-middleware-cordova-1-3-yrs-553756.html?ref=googlejob>
4. N. Ahmed, S. Butler and U. Ramachandran, "GuardianAngel: An RFID-based indoor guidance and monitoring system," 2010 8th IEEE International Conference on Pervasive Computing and Communications Workshops (PERCOM Workshops), 2010, pp. 546-551, doi: 10.1109/PERCOMW.2010.5470498.
5. Agarwal, Shilpa. "The impact of Auto-ID technology on process performance—RFID in the FMCG supply chain."
6. <https://www.rfidsolutionsonline.com/doc/oatsystems-oat-foundation-suite-0001>
7. <https://rfidworld.ca/tag/oat-foundation-suite>
8. <https://www.businesswire.com/news/home/20130429005073/en/OATSystems-a-Division-of-Checkpoint-Systems-Providing-Passive-RFID-Asset-Tracking-for-Five-Year-Veterans-Affairs-Hospital-Contract>
9. OATSystemsEngineeringTeam, 2012, "OATMerchandiseVisibilityUserGuide", OATSystems.
10. HareesSeniSyed, 2015, "OATMobileSDK, Highlevel design document", OATSystemsInc.
11. HareesSeniSyed, 2015, "OATMobileSDK—ProposedArchitecture", OATSystemsInc.
12. SwethaKuppuswamy & AshaMS, 2015, "OATmobileStoreAssociateManualv1.2", OATSystems Inc.
13. SymboltechnologiesTeam, 2015, "MC319ZRFIDMobileComputerIntegratorGuide-RevisionA".
14. <http://www.skyscanner.net/blogs/developing-mobile-cross-platform-library-part-3-javascript>.
15. <https://developer.apple.com/library/ios/documentation/Performance/Conceptual/PerformanceOverview/PerformanceTools/PerformanceTools.html>.
16. <https://www.fiercehealthcare.com/it/oatsystems-a-division-checkpoint-systems-providing-passive-rfid-asset-tracking-for-five-year>
17. <https://www.rfidsolutionsonline.com/doc/oatsystems-oat-foundation-suite-0001>

Optimized Semantic Mapping of XML Elements

Sangeetha B, Senthil Prabha R, Ravitha Rajalakshmi N and Srilam K

Department of Information Technology, PSG College of Technology, Coimbatore, India, TamilNadu – 641004

ABSTRACT

Interoperability is a major concern for many data sources as each individual data sources are defined with a different schema. Many business systems, such as CRM and marketing data, are merged to create a unified picture of the data from which new consumer insights can be derived. Data integration is a method of presenting a unified view of data. The Extensible Markup Language (XML) is rapidly gaining popularity as a data exchange format and a data model for databases, industry applications, and internet services. Data sources differ in schema but may include similar data, necessitating the development of data integration tools for XML data. It is necessary to construct semantic mapping in order to merge data from disparate data sources. The mapping is accomplished by determining how the data sources are semantically related. The proposed system uses bi-partite graph representation and apply Kuhn-Munkres algorithm for mapping the sources. The weights between the graphs is obtained using the syntactic and semantic similarity measures. Reeds and Washington State University's xml data sources are used for experimentation to evaluate the system. The performance of the system is analyzed using precision, recall and f-measure.

Keywords: Semantic mapping, Jaro-Winkler Winkler, Cosine Similarity, Minkowski ,Edit distance, Bi-partite graph Hungarian, Kuhn-Munkres

1 INTRODUCTION

XML is an Extensible markup language used to carry the structure and semantic information. It plays an important role to transfer and share information across the web. XML has been widely used in e-business to exchange data across their partners because of its interoperable property. Since XML uses user-defined tags, organization and enterprises can define their own document to describe its structure and content. Due to the tremendous increase of data in XML format, integration [11] of XML data sources comes into reality. This leads to the integration problem since the representation of data may differ for the same concepts. Integration means data from different sources are combined thereby it provides the user with meaningful information. The structural and semantic mapping between the given data sources must be generated by this integration system. [6, 9]. But, XML does not support well for data integration due to its heterogeneity in structure and vocabularies. To resolve this problem, semantics of the XML data has to be found. This is done by the identification of relationships between the schemas. In order to find the semantic relations, different string based distance measures are used. The main objective is to find the semantic relationship between the heterogeneous data sources and further this heterogeneous data can be accessible by providing semantic mapping. The system is developed by considering XML document as a bipartite graph and for optimal mapping bi-partite graph matching algorithms are used. Data integration finds its application in various fields like e-shopping, banking, e- business, search engines etc.

The highlights of the proposed work are given below:

- A semantic mapping for data integration between the elements of the xml data sources is established.
- Bipartite graph is used for data source representation where each xml data source is treated as a set
- Kuhn-Munkres algorithm is used for finding the maximum weight of the bipartite graph to find similar elements

The remaining part of the paper is structured as follows. Section II presents survey of the related works. System design is discussed in Section III. Section IV and V depicts the implementation and result analysis of the model. Section VI presents the concluding remarks.

1 RELATED WORKS

String based similarity measures use the given terms in the xml file for finding the relevance value which normally lies between 0 and 1. The granularity of data used differs from one similarity measure to the other. A score of '0' indicates no similarity and '1' indicates high similarity.

2.1 Distance Based Similarity

The number of bits required to change string 1 to string 2 is known as the Hamming distance [13], and it is defined as the number of bits required if both strings are the same size. If two strings are 1000111 and 1011001, the hamming distance is four bits.

Jaro similarity measure is the measure indicating closeness of the concept based on the number of matching characters. The Jaro distance between the given strings are computed as given in equation 3.5.

$$d_j = \begin{cases} 0, & \text{if } m = 0 \\ \frac{1}{3} \left(\frac{m}{|s1|} + \frac{m}{|s2|} + \frac{m-t}{m} \right), & \text{otherwise} \end{cases} \quad (1)$$

where m – represents the number of matching characters

t – represents the number of transpositions (The number of matching but different sequence order characters divided by 2)

s_1, s_2 – length of the 1st and 2nd string

Dice co-efficient is similar to Jaccard similarity but gives twice the commonalities between the sets to the total number of properties. The value ranges from 0 to 1.

$$\text{Dice coefficient} = 2 \frac{|A \cap B|}{|A| + |B|} \quad (2)$$

N-gram is defined as the contiguous sequence of 'n' characters from a given string. N-grams of size 1, 2 and 3 are called uni-grams, bi-grams and tri-grams respectively.

The cosine similarity is the measure of the angle between two vectors, which focuses on the angle between the vectors and not on the magnitude between them. The cosine of the angle is computed to identify the similarity between the given vectors. If the vectors are found orthogonal, they are considered to be not similar, whereas an angle of 0° indicates that the vectors are in the same direction and hence they are considered to be similar. The formula for computing the cosine similarity is given below in equation 3.

$$\text{Cosine_similarity} = \frac{V_1 \cdot V_2}{\|V_1\| \|V_2\|} = \frac{\sum_{i=1}^n V_{1i} \cdot V_{2i}}{\sqrt{\sum_{i=1}^n V_{1i}^2} \sqrt{\sum_{i=1}^n V_{2i}^2}} \quad (3)$$

where

v_1 – Vector of terms in document 1

v_2 – Vector of terms in document 2

Substring similarity finds the similarity based on the longest common substring

Overlap coefficient is similar to the Jaccard index which computes the commonalities between the sets. The Overlap measure is given by,

$$O(X, Y) = |B_x \cap B_y| \quad (4)$$

B_x - set of tokens generated for string X

B_y - set of tokens generated for string Y

Monge-Elkan distance uses semantic similarity and each substring is evaluated against the most similar substring in the comparison entity names

Euclidean distance is based on the distance between input vectors and is independent of cosine rule. The Euclidean distance between two vectors is given by,

$$\text{ecu}(q, r) = (\sum_y (q(y) - r(y))^2)^{1/2} \quad (5)$$

Needleman-Wunsch is the global alignment measure which computes the similarity scores by computing the score matrix with edit costs.

Smith-waterman distance is a local alignment measure which finds the similarity between the sequences of strings. This algorithm optimizes the similarity value by considering all the possible length of the strings.

Structural similarity [7] finds the similarity between the XML documents by taking the entire structure into account. This approach is based on the edit distance cost between the documents.

Resnik [9] uses information content for identifying the similarity measure and is stated in equation 6.

$$\text{sim}(c1,c2) = \max(-\log[P(c)]) \quad (6)$$

where c is the set of concepts that subsume both $c1$ and $c2$.

Given two concepts or terms $c1$ and $c2$, Lin (Warin 2004) considers the information content shared by two concepts and the information content of each concept separately as given in equation 7.

$$\text{sim}(c1, c2) = \frac{(2*IC(c))}{(IC(c1)+IC(c2))} \quad (7)$$

where $IC(c)$ is the information content of the concepts

Jiang and Cornath use the difference between the information content of the subsuming concept and the independent concepts to scale the relatedness of two concepts. Edge counting and information content are combined to improve correlation. The mathematical representation of the Jiang and Cornath measure, given two terms $c1$ and $c2$ is stated in equations 8 and 9.

$$\text{dist}(c1,c2)=IC(c1)+IC(c2)-2*IC(c) \quad (8)$$

$$\text{sim}(c1,c2)= 1/\text{dist}(c1,c2) \quad (9)$$

2 SYSTEM DESIGN

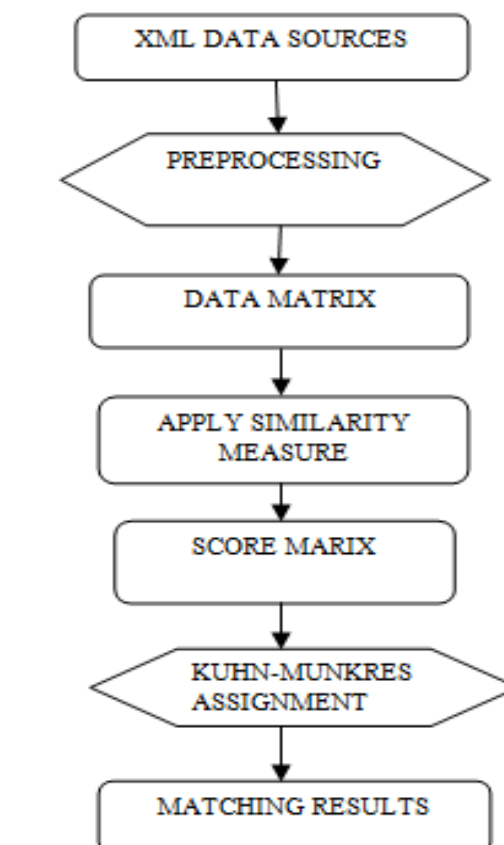


Figure 1: System Design

The different similarity measures have been applied to the xml data sources for finding the similarity between the two data sources. This results in the mapping of both the xml documents. The mapping is achieved by identifying the semantic relatedness between the data sources. Then, the performances of these algorithms are computed by comparing with other algorithms. The XML data sources are preprocessed using SAX/DOM parser to extract the elements and are stored in matrix format. Then, the score matrix is obtained by applying similarity metrics to the data sources. In the last step, score matrix is given to Kuhn-Munkres bipartite graph optimal matching algorithm and the process is repeated until optimal matching is obtained. As a result mapping between both XML data sources occurs.

3 IMPLEMENTATION

This section involves the implementation methodology used for finding the similarity between different XML data sources. The dataset used is the courses handled in universities like Reed College and Washington State University. The similarity between the data sources are found using different distance measures like edit distance, Jaro Winkler distance, Jaccard similarity and Structural similarity

```
<?xml version="1.0"?>
- <root>
  - <course>
    <reg_num>10577</reg_num>
    <subj>ANTH</subj>
    <crse>211</crse>
    <sect>F01</sect>
    <title>Introduction to Anthropology</title>
    <units>1.0</units>
    <instructor>Brightman</instructor>
    <days>M-W</days>
  - <time>
    <start_time>03:10PM</start_time>
    <end_time>04:30</end_time>
  </time>
  - <place>
    <building>ELIOT</building>
    <room>414</room>
  </place>
</course>
</root>
```

```
<?xml version="1.0"?>
- <root>
  - <course>
    <sln>10637</sln>
    <sub>ACCTG</sub>
    <crs>230</crs>
    <lab/>
    <sect>01</sect>
    <title>INT FIN ACCT</title>
    <credit>3.0</credit>
    <days>TU,TH</days>
  - <times>
    <start>7:45</start>
    <end>9</end>
  </times>
  - <place>
    <bldg>TODD</bldg>
    <room>230</room>
  </place>
    <instructor>B. MCELDFOWNEY</instructor>
    <limit>0112</limit>
    <enrolled>0108</enrolled>
  </course>
</root>
```

Dataset of Reed College

Dataset of Washington State University

Figure 2: Snapshot of Reed and Washington State Dataset

4 RESULT ANALYSIS

The system is implemented and the similarity between two XML documents was computed and their performances was analyzed by comparing with the similarity measures like edit distance, Jaro Winkler distance, Jaccard distance and Structural similarity.

The performance of these similarity measures are computed by using this formula,

$$\text{Precision} = \frac{\text{raw score}}{\text{length_file_2}} \quad (10)$$

$$\text{Recall} = \frac{\text{raw score}}{\text{length_file_1}} \quad (11)$$

Table 1: Performance Calculation Table

Similarity Measures	Precision	Recall
Edit distance	0.875	0.7368
Jaro-Winkler distance	0.9375	0.8421
Jaccard Similarity	0.5	0.4210
Structural Similarity	0.5	0.4210

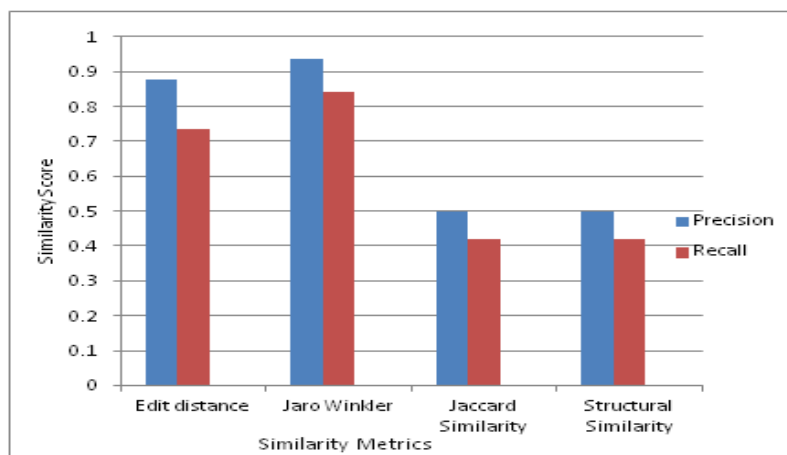


Figure 3: Comparison of various similarity measures

The above figure shows the comparison chart for describing the performance measures of various similarity measures. The graph has been plotted against datasets and similarity measures with the threshold value of $\lambda=0.5$ for all the measures. From the above figure, it is very clear that Jaro Winkler distance similarity measure has higher accuracy, when comparing to other algorithms.

5 CONCLUSION

The proposed method focuses on integrating the data residing at different sources by applying different similarity measures like edit distance, Jaro Winkler distance, Jaccard similarity and Structural similarity. These approaches have been presented for measuring semantic similarity between the XML data sources, which is useful in the integration of data sources. By varying the threshold value, performance of the algorithms were analyzed. It has been found that, Jaro Winkler distance has the highest accuracy and scope when compared to other algorithms. The XML data source is represented as a bipartite graph and the Kuhn-Munkers algorithm is used for finding the maximal weight to indicate the similarity between the concepts. The future work focuses on improving the accuracy of similarity values by introducing various distance measures and bipartite graph matching algorithms.

REFERENCES

1. Lukasz Kurgan, Waldemar Swiercz, and Krzysztof J. Cios, "Semantic Mapping of XML Tags using Inductive Machine Learning", In Proceedings of ICMLA, 99-109, 2002.
2. Zhang Na, Zhang Dongzhan, Yu Ye and Duan Jiangjiao, "An improved method for classifying XML documents based on structure and content", Proceedings of the Third International Symposium on Computer Science and Computational Technology, 2010.
3. Azadeh Haratian Nezhadi, Bitra Shadgar and Alireza Osareh, "Ontology Alignment using Machine Learning Techniques", International Journal of Computer Science & Information Technology (IJCSIT), 2011.
4. William W. Cohen, Pradeep Ravikumar and Stephen E. Fienberg, "A Comparison of String Distance Metrics for Name-Matching Tasks", American Association for Artificial intelligence, 2003
5. Suphakit Niwattanakul, Jatsada Singthongchai, Ekkachai Naenudorn and Supachanun Wanapu, "Using of Jaccard Coefficient for Keyword Similarity", Proceedings of the International MultiConference of Engineers and Computer Scientists, 2013.
6. Joe Tekli, Richard Chbeir and Kokou Yetongno, "Efficient XML Structural Similarity Detection using Sub-tree Commonalities", SIGMOID, 2007.
7. Sam's string Metrics; www.coli.uni-saarland.de/courses/LT1/2011/slides
8. P. Resnik, "Semantic Similarity in a Taxonomy: An Information-Based Measure and its Application to Problems of Ambiguity in Natural Language", AI Access Foundation and Morgan Kaufmann Publishers, 1999.
9. Lin, "Using syntactic dependency as a local context to resolve word sense ambiguity", In Proceedings of the 35th Annual Meeting of the Association for Computational Linguistics, pp. 64-71, 1997.
10. Jiang and D. Conrath, "Semantic similarity based on corpus statistics and lexical taxonomy", In Proceedings on International Conference on Research in Computational Linguistics, 1997.
11. Samuelsen, J., Chen, W. & Wasson, B, "Integrating multiple data sources for learning analytics—review of literature", RPTTEL 14, 11 (2019). <https://doi.org/10.1186/s41039-019-0105-4>
12. Amuthadevi, D. S. Vijayan, Varatharajan Ramachandran, "Development of air quality monitoring (AQM) models using different machine learning approaches", Journal of Ambient Intelligence and Humanized Computing, <https://doi.org/10.1007/s12652-020-02724-2>

Hybrid Feature Selection Using Multiple Feature Ranking and Clustering Techniques

Vandna V, Renukadevi T N, Indhumadhi M, Janani R, Iswaryaa G P and Ramesh A. C
PSG College of Technology, Coimbatore, TamilNadu

ABSTRACT

With the immense machine learning models and algorithms developed, feature selection and feature ranking play an essential role as they not only facilitate the machine learning algorithm to train faster but also makes the machine learning model less complex, easily interpretable and more accurate. In Feature selection, the redundant or irrelevant variables in the input data are eliminated and in feature ranking, the features will be ordered based on some scoring function which in turn is based on the relevance of the features. Most of the feature selection methods known work only with a single feature ranking technique. There exists a new way [1] where the clustering of variables are combined with various feature ranking techniques in order to select the best feature subset. In the feature selection framework, the feature ranking subsection identifies relevant features and the clustering subsection discards the redundant features. But, there are certain flaws in the above-mentioned technique. The threshold value was not set based on a specific criteria, it was randomly selected and the union of all the clusters results in a large set of features and this must be optimized further. In the proposed method we aim at developing a hybrid solution that improves the accuracy of the feature selection mechanism. Our method eliminates the need to explicitly set the threshold and it performs better than all other evaluated feature selection techniques on testing, with an accuracy of 94% for Ionosphere dataset, 97% for Wine dataset, 51% for Vowel dataset and 95% for WDBC dataset.

I. INTRODUCTION

Machine learning datasets have grown in size in recent years, and in a few circumstances, the number of input variables now are high in number when compared to the number of samples. Machine learning models that appear to lack an embedded feature selection mechanism would accumulate minor noisy contributions to the predicted variable for each noise variable. If there are a large number of little noisy contributions, the sum will lead to a greater prediction error [2]. Feature ranking algorithms individually focus on different aspects of the data. Feature selection techniques work on the assumption that discriminative features do not depend on the features that are nor relevant or redundant, and they tend to hold a part of the original dataset [3]. Feature selection based on just one of the ranking techniques will not give the best expected results.

A hybrid feature selection algorithm that combines the best qualities of multiple feature ranking techniques will perform comparatively better than any of the other feature ranking methods. Our aim is to develop a hybrid feature selection technique by combining multiple feature ranking techniques that outperforms the existing feature selection methods and evaluate the performance of our algorithm using multiple datasets. In this way, optimal features can be selected from the dataset, thus increasing the accuracy and efficiency of the algorithm.

II. RELATED WORKS

[1] Combining Multiple Feature-Ranking Techniques and Clustering of Variables for Feature Selection – A feature selection framework that incorporates variable clustering with several feature ranking approaches to choose the best feature subset. The feature ranking module detects relevant characteristics, whereas the clustering module removes the features that are relevant. The threshold criteria stated in this paper is a manually fixed number that needs to be reviewed further. The union operation (computing cluster heads for all models) yields a bigger subset that must be further improved.

[4] Mini-Batch Normalized Mutual Information: A Hybrid Feature Selection Method - Integration of feature ranking and optimal feature selection, incorporating the advantages of both methods. All the features are added to the selected list one by one, If adding the feature to the list improves the accuracy of prediction, the feature is added to the selected list (from highest to lowest rank). If the inclusion of a feature reduces accuracy, that feature is removed. Training and determining accuracy to determine the selected set of features take quite a long time. Optimizing the time required to obtain the selected features would assist in reducing the time complexity, and improved metrics may be devised to obtain the actual connections among the features, allowing the redundant features to be discarded.

[5] An Integrated Framework With Feature Selection for Dropout Prediction in Massive Open Online Courses – The high dropout rate in Massive Open Online Courses has had a significant environmental impact. Conventional methods rely on manually extracted features, making the ultimate prediction effect difficult to

predict. To address this issue, this research provides an integrated framework with feature selection (FSPred) to forecast dropout in MOOCs (Massive Open Online Courses), which covers feature generation, feature selection, and dropout prediction.

[6] Novel Feature Selection and Voting Classifier Algorithms for COVID-19 Classification in CT image – For coronavirus detection both CT scan and X rays play a vital role in diagnosis. The framework developed has three phases. Initially, from CT scan, features are extracted and Guided Whale Optimization Algorithm is performed. LSH SMOTE balances the selected features. It further improves the results of classification. Finally a voting classifier selects the most voted class.

[7] Visualization, Feature Selection, Machine Learning: Identifying the Responsible Group for Extreme Acts of Violence – The violent acts are visualised using linear and non-linear dimensionality reduction techniques. The generalisation accuracy of three machine learning models - decision tree, linear and nonlinear SVM - is used to identify sequential forward features. Based on the selected features of a violent event, the multilayer perceptron is used to forecast the VEO (Violent Extremist Organization). This has been done with the assumption that each violent activity is the responsibility of a single VEO. If numerous VEOs engage in a specific activity, deeper multilayer perceptrons are required and this will increase the problem's complexity.

[8] A Hybrid Meta-Heuristic Feature Selection Method Using Golden Ratio and Equilibrium Optimization Algorithms for Speech Emotion Recognition – Methods called GREO (Golden Ratio based Equilibrium Optimization) algorithm after combining with GRO (Golden Ratio Optimization) and EO (Equilibrium Optimization) is devised as hybrid meta-heuristic Feature selection. These algorithms are used for SER from the audio signals. The No Free Lunch (NFL) algorithm states that there is no such optimization algorithm, which could optimize every single problem. Therefore, it concludes that hybrid methods for optimization can improve the overall performance.

III. Existing system

In the existing system, the input variables are ranked using machine learning models like Logistic Regression, Support Vector Machines and Random Forests. For each of the aforementioned methods, the dataset features that are ranked lower than a particular threshold are discarded. The features that are ranked higher than the threshold are grouped into clusters. The highest-ranked feature among all the features in each of the clusters is collected. The threshold value here is chosen at random and is not based on any particular criteria. The union of all the clusters results in a very large set of features which results in increased complexity and that requires further optimization.

IV. Proposed system

The scope of this project is to design and implement a hybrid feature selection technique, by modifying the MFSS algorithm by eliminating the need for manually setting the threshold, solving the union problem and improving the feature selection accuracy. Then, evaluate the performance of the technique by comparing the results with various existing feature selection methods. Four datasets (Wine, Ionosphere, Vowel, WDBC) from the UCI machine learning repository [9] will be used for the evaluation of the proposed methods.

Feature Selection

Feature selection is the process of selecting a subset of features by removing features that are either irrelevant or do not contribute to the prediction of the target variable. The MFSS (Multi Filter Feature Selection) algorithm and a few feature selection methods (Mini Batch Feature Addition, Mini Batch Feature Removal, Random features Boruta) that do not require setting a threshold are discussed below.

Multi-Filter Feature Selection (MFSS)

The Multi Filter Feature Selection method combines variable clustering techniques with multiple feature ranking techniques. The feature ranking technique is used in classifying the relevant features and the clustering module eliminates the redundant features. Three methods has been used to rank the input variables:

- Logistic regression: Predicts the feature importance
- Support Vector Machine: Separates data into different classes
- Random Forests - Creates a collection of decision trees.

After ranking the features, n lowest-ranked features are eliminated. The value of n is manually set and is common to all three rankings. All the selected features per ranking are then clustered using the Affinity Propagation (clustering algorithm) method. This method was used since the number of clusters need not be

explicitly mentioned. Linear correlation and Info Gain are both used to create a distance matrix to be used for affinity propagation methods. From each of the clusters, the highest-ranked feature is selected and the rest are discarded. A union of features selected by all three rankings after clustering is performed to obtain the final set of features. Though this technique performs better than other methods, there are certain drawbacks to it; the threshold value is randomly set, and the union of clusters often results in a large set of features so that the optimal set of features are not obtained.

Mini Batch Feature Addition

Ranking of the features is performed using any of the ranking techniques. By starting with an empty set, features are added one by one to the set in the increasing order of ranks (from best ranked). After each addition, the feature set is evaluated against a model. If the performance deteriorates, the feature is ignored. Otherwise, the feature is selected. The same process is repeated for all features.

Mini Batch Feature Removal

This method is similar to the above method. After performing the ranking, the method starts with selecting the full feature set. Features are removed one by one from the set in the decreasing order of ranks (ranked). After each removal, the performance is calculated. If performance goes down, the feature is selected, otherwise, it is discarded.

Random Features

Three new features are added to the dataset:

- Boolean
- Fraction between 0 and 1
- Any positive integer

Ranking is performed for all the features and the features that are ranked worse than the random features are eliminated.

Boruta

For each feature, a shadow feature is added. The shadow feature is populated by shuffling the actual feature's values. Feature ranking is then performed for all the original and shadow features together. All features that are ranked worse than their shadow are eliminated

Modified MFFS

The proposed algorithm is a modification of the MFFS algorithm. After performing the rankings, instead of selecting top n features by setting the value of n randomly, one of the below algorithms can be used:

- Mini batch – feature addition
- Mini batch – feature removal
- Random features
- Boruta

The resultant features can be clustered as per the MFFS algorithm. The original MFFS algorithm and the modified MFFS algorithm are depicted in Figure 1 and Figure 2.

In the Multi Filter Feature Selection Algorithm, the top n features are selected for clustering.

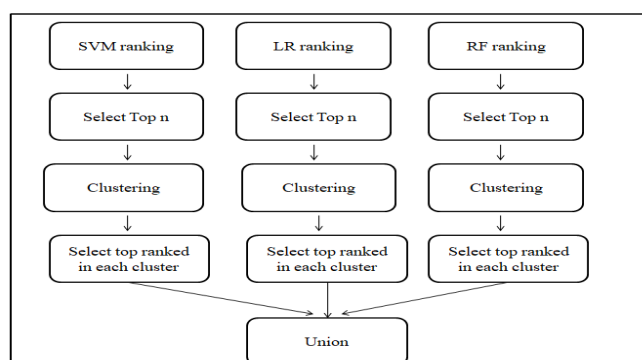


Figure 1. MFFS Algorithm

In Modified Multi Filter Feature Selection Algorithm, instead of selecting top n features, we use features selected by mini batch or boruta or Random features methods.

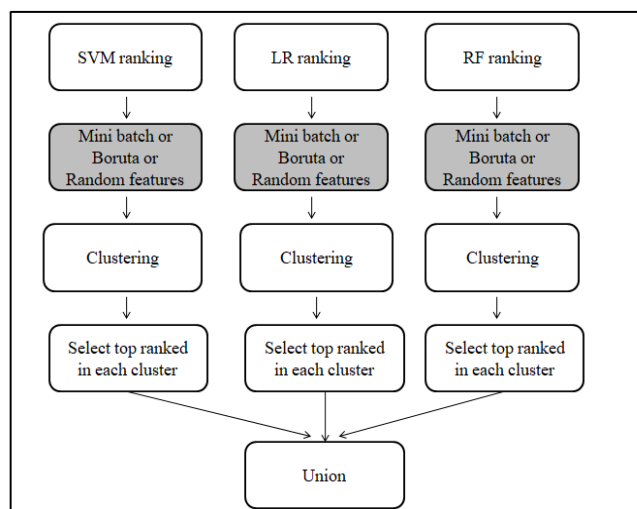


Figure 2. Modified MFFS Algorithm

V. SYSTEM IMPLEMENTATION

A. Dataset

Four datasets (Ionosphere, Wine, Vowel and WDBC) were used to evaluate the performance of the feature selection methods proposed. The dataset details are described in Table I.

TABLE I
DATASETS USED FOR EVALUATION

	Ionosphere	Wine	Vowel	WDBC
No.of columns (Input/Target)	34(33/1)	13(12/1)	11(10/1)	31(30/1)
No.of rows (Training/Testing)	351(200/151)	178(142/36)	990(528/462)	569(455/144)
Classes	2	3	11	2

B. Performance

The performance of all the algorithms with the accuracy and features are presented in Table II (Ionosphere) , Table III (Wine), Table IV (Vowel) and Table V (WDBC). In the column *Accuracy*, grey highlights on the cells denote an increase in accuracy in comparison to the original MFFS(Multi Filter Feature Selection algorithm). A decrease in the number of features selected while having no decrease in the accuracy is denoted as a grey highlight in the *No. of features* column. For Multi Filter Feature Selection algorithm and Mini batch algorithms(Mini batch addition,Mini batch removal), the model needs to be trained n times, where n is the number of features before the important features can be identified. Whereas, for Random features and Boruta, no extra training of the model is required to determine the set of features.

TABLE II
RESULTS FOR IONOSPHERE DATASET

Algorithm	Accuracy	No. of features selected	Features selected	No. of times model is trained to determine n
All features	0.928	34	F1,F2,F3,F4,F5, F6,F7,F8,F9,F10, F11,F12,F13,F14, F15,F16,F17,F18, F19,F20,F21,F22, F23,F24,F25,F26, F27,F28,F29,F30, F31,F32,F33,F34	-
MFFS - LC (dropped 3)	0.934	10	F5,F6,F4,F24,F7,F2, F8,F25,F3,F1	n
MFFS - IG (dropped 3)	0.921	11	F1,F5,F6,F15,F24, F27,F7,F8,F16,F10, F29	n
Mini batch (add) - LC	0.941	6	F6,F5,F27,F20,F1,F29	n
Mini batch (add) - IG	0.915	6	F5,F27,F29,F6,F32,F1	n
Mini batch (remove) - LC	0.954	9	F2,F5,F33,F27,F10, F29,F6,F25,F4	n
Mini batch (remove) - IG	0.934	10	F2,F12,F5,F27,F15,F29,F6,F25,F32,F19	n
Random Features - LC	0.928	11	F5,F17,F3,F1,F8,F7, F6,F25,F23,F28,F4	0
Random Features - IG	0.947	14	F5,F26,F27,F17,F3,F1,F14,F6,F25,F23, F24,F21,F28,F4	0
Boruta - LC	0.934	8	F1,F4,F6,F8,F18,F23,F7,F3	0
Boruta - IG	0.934	11	F10,F21,F24,F1,F4,F11,F5,F23,F25,F12,F3	0

TABLE III
RESULTS FOR WINE DATASET

Algorithm	Accuracy	No. of features selected	Features selected	No. of times model is trained to determine n
All features	0.972	13	F1, F2, F3, F4, F5, F6, F7, F8, F9, F10, F11, F12, F13	-
MFFS - LC (dropped 3)	0.944	5	F3, F13, F12, F7, F2	n
MFFS - IG (dropped 3)	0.916	4	F3, F13, F1, F7	n
Mini batch (add) - LC	0.916	4	F7, F2, F13, F3	n
Mini batch (add) - IG	0.972	4	F7, F3, F13, F1	n
Mini batch (remove) - LC	0.972	6	F5, F3, F2, F12, F7, F1	n
Mini batch (remove) - IG	0.916	5	F4, F3, F2, F7, F1	n
Random Features - LC	0.972	7	F13, F1, F7, F12, F5, F3, F2	0
Random Features - IG	0.888	5	F10, F13, F1, F3, F2	0
Boruta - LC	0.972	5	F3, F2, F7, F6, F1	0
Boruta - IG	0.833	2	F1, F2	0

TABLE IV
RESULTS FOR VOWEL DATASET

Algorithm	Accuracy	No. of features selected	Features selected	No. of times model is trained to determine n
All features	0.508	10	F1, F2, F3, F4, F5, F6, F7, F8, F9, F10	-
MFFS - LC (dropped 3)	0.430	6	F6, F7, F2, F4, F1, F3	n
MFFS - IG (dropped 3)	0.478	6	F7, F2, F5, F4, F1, F3	n
Mini batch (add) - LC	0.517	7	F7, F5, F2, F4, F3, F1, F8	n
Mini batch (add) - IG	0.331	5	F3, F5, F7, F2, F4	n
Mini batch (remove) - LC	0.331	5	F3, F9, F7, F1, F4	n
Mini batch (remove) - IG	0.285	4	F10, F7, F1, F6	n
Random Features - LC	0.426	5	F7, F2, F3, F4, F1	0
Random Features - IG	0.450	6	F7, F4, F2, F6, F1, F5	0
Boruta - LC	0.510	5	F4, F3, F1, F2, F5	0
Boruta - IG	0.510	5	F4, F3, F1, F2, F5	0

TABLE V
RESULTS FOR WDBC DATASET

Algorithm	Accuracy	No. of features selected	Features selected	No. of times model is trained to determine n
All features	0.938	30	F1, F2, F3, F4, F5, F6, F7, F8, F9, F10, F11, F12, F13, F14, F15, F16, F17, F18, F19, F20, F21, F22, F23, F24, F25, F26, F27, F28, F29, F30	-
MFFS - LC (dropped 3)	0.929	11	F21, F14, F22, F24, F29, F2, F18, F7, F11, F28, F10	n
MFFS - IG (dropped 3)	0.938	14	F1, F4, F21, F14, F22, F24, F29, F2, F18, F25, F11, F28, F30, F10	n
Mini batch (add) - LC	0.956	8	F24, F18, F28, F22, F25, F26, F2, F21	n
Mini batch (add) - IG	0.956	8	F24, F18, F28, F22, F25, F26, F2, F21	n
Mini batch (remove) - LC	0.964	9	F22, F2, F21, F11, F16, F7, F29, F30, F14	n
Mini batch (remove) - IG	0.964	11	F22, F2, F21, F11, F25, F16, F7, F29, F8, F30, F14	n
Random Features - LC	0.947	10	F11, F14, F27, F29, F22, F23, F28, F25, F8, F17	0
Random Features - IG	0.929	11	F11, F14, F3, F27, F29, F30, F22, F23, F28, F25, F8	0
Boruta - LC	0.947	6	F11, F2, F1, F9, F7, F15	0
Boruta - IG	0.921	11	F2, F10, F15, F20, F5, F1, F9, F21, F6, F7, F11	0

C. Analysis of Results

For the Ionosphere, WDBC and Wine datasets, all four methods performed better than MFFS. For the Vowels dataset, mini-batch (add) and Boruta performed better. Furthermore, for Ionosphere, Boruta and mini-batch algorithms selected a lesser number of features in spite of giving higher accuracy. For the wine dataset, Mini-batch (addition) selected lesser features and for Vowels, Boruta selected less. All four methods selected lesser features for the WDBC dataset. Boruta and Mini batch (addition) performed better than the MFFS method for all 4 datasets. Mini batch (addition) gave higher accuracy than Boruta for all datasets. Boruta & Mini Batch reduced no. of selected features in 75% of the datasets (compared to MFFS). Selected feature count is much less than the number of features in the dataset as mentioned in Table VI. Boruta reduced feature selection time by removing the need for additional model training to estimate the value of n.

TABLE VI
NO. OF FEATURES SELECTED BY BORUTA AND MINI BATCH(ADD)

Dataset	Boruta	Mini batch(add)
Ionosphere	8/34	6/34
Wine	5/13	4/13
Vowel	5/10	7/10
WDBC	6/30	8/30

VI. CONCLUSION AND FUTURE WORK

With the growing size of Machine learning datasets, it is high time we identify and use the most relevant feature for the classification of targets. Though there are many feature selection algorithms, most of the time, the features selected are not highly relevant. So, a combination of these feature selection algorithms, the MFFS algorithm would give us better results when compared to the individual algorithms. The modified MFFS algorithm is the better version of MFFS algorithm addressing the issues in the MFFS algorithm. The modified MFFS algorithm gave better accuracy for both mini batch addition and Boruta algorithms in all four tested datasets. The number of features selected was also much lesser compared to the original MFFS algorithm. Of the two algorithms, Boruta determines the value of n in constant time whereas Mini batch addition requires training the model n times to obtain the list of selected features. Thus, modified MFFS using Boruta is a preferable option when there is a time or computation resource constraint. Modified MFFS with Mini batch addition is preferred when the required computation resources and time is available since it gives a slightly better performance.

A line of future work is to perform clustering post Union operation and check for accuracy. It is also of interest to experiment with various feature ranking techniques and check for the efficiency and accuracy of the algorithm. The algorithm can also be tested with various other regression datasets.

REFERENCES

1. A. U. Haq, D. Zhang, H. Peng and S. U. Rahman, "Combining Multiple Feature-Ranking Techniques and Clustering of Variables for Feature Selection," in *IEEE Access*, vol. 7, pp. 151482-151492, 2019, doi: 10.1109/ACCESS.2019.2947701.
2. J. Fan and Y. Fan, "High dimensional classification using features annealed independence rules," *Ann. Statist.*, vol. 36, no. 6, pp. 2605–2637, 2008.
3. M. H. C. Law, M. A. T. Figueiredo, and A. K. Jain, "Simultaneous feature selection and clustering using mixture models," *IEEE Trans. Pattern Anal. Mach. Intell.*, vol. 26, no. 9, pp. 1154–1166, Sep. 2004.
4. G. S. Thejas, S. R. Joshi, S. S. Iyengar, N. R. Sunitha and P. Badrinath, "Mini-Batch Normalized Mutual Information: A Hybrid Feature Selection Method," in *IEEE Access*, vol. 7, pp. 116875- 116885, 2019, doi: 10.1109/ACCESS.2019.2936346.
5. L. Qiu, Y. Liu and Y. Liu, "An Integrated Framework With Feature Selection for Dropout Prediction in Massive Open Online Courses," in *IEEE Access*, vol. 6, pp. 71474-71484, 2018, doi: 10.1109/ACCESS.2018.2881275.
6. E. -S. M. El-Kenawy, A. Ibrahim, S. Mirjalili, M. M. Eid and S. E. Hussein, "Novel Feature Selection and Voting Classifier Algorithms for COVID-19 Classification in CT Images," in *IEEE Access*, vol. 8, pp. 179317-179335, 2020, doi: 10.1109/ACCESS.2020.3028012.
7. M. Hashemi and M. Hall, "Visualization, Feature Selection, Machine Learning: Identifying the Responsible Group for Extreme Acts of Violence," in *IEEE Access*, vol. 6, pp. 70164-70171, 2018, doi: 10.1109/ACCESS.2018.2879056.
8. A. Dey, S. Chattopadhyay, P. K. Singh, A. Ahmadian, M. Ferrara and R. Sarkar, "A Hybrid Meta-Heuristic Feature Selection Method Using Golden Ratio and Equilibrium Optimization Algorithms for Speech Emotion Recognition," in *IEEE Access*, vol. 8, pp. 200953-200970, 2020, doi: 10.1109/ACCESS.2020.3035531.
9. Dua, D. and Graff, C. (2019). UCI Machine Learning Repository [<http://archive.ics.uci.edu/ml>]. Irvine, CA: University of California, School of Information and Computer Science.

RAGE - A Versatile Drug Target for Alzheimer's disease

Palaniswamy Rani*, Balasubramanian Ayshwariya and Saravana Kumar Vinodh

Department of Biotechnology, PSG College of Technology, Coimbatore, Tamilnadu 641004, India

ABSTRACT

Alzheimer's disease (AD) is a chronic neurodegenerative disease which accounts for 60–70% cases of dementia. Worldwide, around 50 million people are affected by dementia and every year nearly 10 million new cases are being reported. Major cause of AD is abnormal accumulation of amyloid beta in the brain cells which in turn forms neurofibrillary tangles that leads to failure of synaptic transmission and neuronal degeneration. Deposition of amyloid beta is governed by various factors in which Receptor for advanced glycation end products (RAGE) plays a critical role in pathogenesis of AD. RAGE is a key pattern recognition receptor of the innate immune response and mediates diverse physiological and pathological effects through cellular signaling pathways leading to inflammatory reactions. In this context, the potential role of RAGE in cognitive impairment and as therapeutic target for AD is an interesting topic to review. In this essence, this review emphasis on RAGE and its isoforms in human, pattern recognition of RAGE for diverse ligands, role of RAGE in AD through RAGE and amyloid beta interaction, involvement of RAGE activated signaling pathways in neuro-inflammation, role of sRAGE in amyloid beta clearance, sRAGE as therapeutics for AD and development of RAGE inhibitors. This chapter overviews RAGE as potential therapeutic targets for Alzheimer's disease.

Keywords: Alzheimer's disease, Cognitive impairment, RAGE, Amyloid Beta, Neurodegeneration, Drug, development

INTRODUCTION

Dementia is a root cause for progressive cognitive decline and is caused by various disease conditions that include Huntington's disease, Alzheimer's disease (AD), etc. Dementia patients are facing vulnerable conditions in terms of physical and mental health which presents a serious challenge to the healthcare systems and requires early diagnosis and therapy. The incidence of dementia is mostly observed in geriatric populations over the age of 65 years and above. Alzheimer's disease is the leading cause of dementia, accounting for 50% to 70% of cases. The pattern of symptoms and biomarkers helps to identify Alzheimer's disease. AD generates short-term memory decline, manifestation and repetitive questioning state in patients. Dementia affects essential functions which are memory function, executive ability, language ability, visuospatial ability, and personality and behavior conditions. The association of dementia with pathophysiological conditions observed in normal aging, complicates the early identification and leads to overt cognitive decline which give rise to functional impairment. The biomarkers accustomed to AD are extracellularly accumulated amyloid beta and intracellular tangles of hyperphosphorylated tau and both of them affect synaptic function that leads to neuronal signal loss. Hippocampal atrophy in the medial temporal lobe also causes early symptoms in AD. Oxidative stress in brain cells increases with age, as a result AGEs (Advanced glycation end-products) are generated rapidly. This enhanced AGEs activates RAGE (Receptor for Advanced Glycation Endproducts), a pattern recognition receptor which binds to variety of ligands. RAGE has been linked to AD and other neurological diseases since its activation leads to inflammatory reactions. This activated RAGE can transport peripheral A β to the brain and amyloid peptides also bind to RAGE which is further eliciting an inflammatory response through the NF- κ B (Nuclear factor kappa B) pathways. Therefore, RAGE the key player in AD pathology [1,2,3].

FUNCTIONAL SIGNIFICANCE OF RAGE IN AD

RAGE is a member of immunoglobulin superfamily with a molecular weight of 35kDa. The RAGE gene is located in the chromosome 6. The full-length RAGE consists of V domain with 23-116 amino acid residues, C1 domain with 124-221 amino acid residues, C2 domain with 227-317 amino acid residues, transmembrane region with 343-363 amino acid residues and the cytoplasmic tail domain with 363-404 amino acid residues [4,5,6,7]. The V and C2 domains are composed of 8 strands linked through 6 loops forming 2 β sheets attached by disulfide bonds respectively whereas the C2 domain folds as C-type immunoglobulin domain. The transmembrane domain contains the "GxxxG" motif which is essential for homodimerization of receptor and signal transduction [8,9]. The cytoplasmic tail has 3 units such as membrane proximal domain (17 amino acids), central domain (17 amino acids) and unstructured C terminus [10]. These structural units are essential for mediating the interaction between RAGE and effector molecules. RAGE binds with a diverse range of ligands relevant to distinct pathological conditions such, cardiovascular disease, AD and cancer. RAGE, ligand binding mediates cellular signal transduction pathways such as NF- κ B, MAPK (mitogen-activated protein kinase), and

others. The expression of RAGE has been demonstrated in various brain tissues namely astrocytes, hippocampus, superior frontal gyrus neurons, entorhinal cortex, and cerebral endothelial cells. Increased RAGE expression in the Blood Brain Barrier (BBB) enhances influx of A β to brain and this in return activates RAGE expression. Simultaneously, it increases the activity of the A β -producing-secretase enzyme (BACE1) in neurons, results in neuroinflammation, A β accumulation, and tau hyperphosphorylation. The accumulation of amyloid peptides mainly A β_{1-40} and A β_{1-42} causes RAGE-mediated apoptosis in neurons [11,12,13].

Alternative splicing of RAGE gene and proteolytic cleavage of full length RAGE (fRAGE) are majorly involved in producing RAGE isoforms. These variants are responsible for a variety of pathophysiological processes depending on the interaction of ligands. Eventually, all the isoforms exhibit similar affinity towards RAGE ligands. In order to understand RAGE-mediated signaling pathways it is important to comprehend the interaction and function of RAGE isoforms. Majorly, three isoforms of RAGE represented as a key player in mediating signaling pathways which are full-length RAGE (fRAGE), Dominant Negative RAGE (DNRAGE) and soluble RAGE (sRAGE). Aside from these three variants, other forms of RAGE reported in the human brain are C domain modified sRAGE (sRAGEB), N truncated RAGE (NRAGE), intracellular modified RAGE (RAGEB) and C domain modified DNRAGE (DNRAGEB) (figure 1). Elucidating the role of these isoforms helps to understand the functional perspective of signaling pathways in neuronal disorders [2,14,15,16].

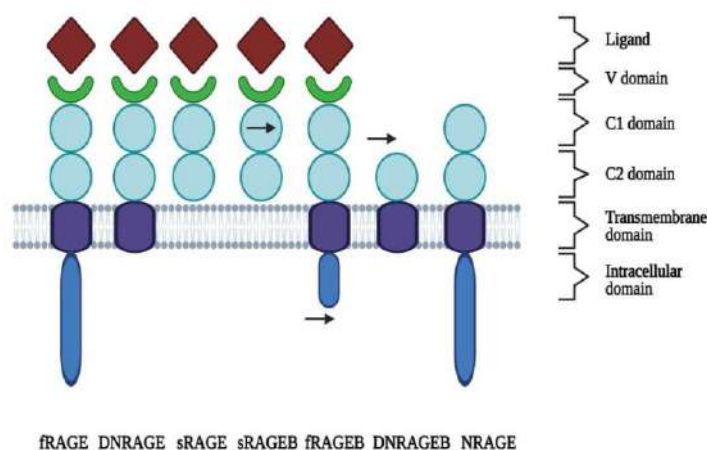


Figure 1: Structure and Isoforms of RAGE. Arrow mark indicates modifications in the domain (Created with BioRender.com)

Full-length RAGE (fRAGE)

This isoform governs a major role in pathophysiological pathways such as chemotaxis, apoptosis, proliferation, and inflammation. It consists of V, C1 and C2, transmembrane domain and also intracellular cytoplasmic tail. The intracellular cytoplasmic domain is essential for activating various signaling pathways such as NF- κ B, MAPK etc [17,18,19,20]. Presence of fRAGE induces more accelerated and sustained signaling pathways than the other forms of RAGE. Since, DNRAGE and sRAGE are involved in decaying the binding of ligands towards fRAGE presumably involved in suppressing the effect of fRAGE mediating signaling. Therefore, sRAGE and DNRAGE gained an important role in study of inhibitors in various chronic neuronal diseases. Additionally, interaction of ligands with RAGE generates reactive oxidative species (ROS) which regulate the intracellular signaling pathways [21,22]. RAGE-ligand interactions had shown cell specific effects and the activation of signaling pathway is determined by the cell types.

Soluble RAGE (sRAGE)

sRAGE is structurally similar to fRAGE but lacks transmembrane domain and cytoplasmic tail leading to release of sRAGE into the extracellular space. The other subtypes of sRAGE that exists are endogenous secretory RAGE (esRAGE) which is generated from pre-mRNA via alternative splicing and cleaved RAGE (cRAGE) which is formed from the cleavage of RAGE's extracellular domain [2,14]. The sRAGE is a key player in decaying fRAGE mediated signaling pathways because sRAGE binds to the RAGE ligands prior to the fRAGE [1,23]. When sRAGE binds with early monomeric or soluble ligands, it further prevents the formation of insoluble complexes. Therefore, sRAGE amends the formation of insoluble aggregates of ligands and thereby prevents the efficacious activation of fRAGE signaling pathway [2,24,25,26].

Dominant Negative RAGE (DNRAGE)

DNRAGE has V and C domain similar to fRAGE but lacks an intracellular cytoplasmic tail domain. DNRAGE competes with fRAGE for binding with ligands to block the fRAGE mediating signal transduction due to lack

of intracellular cytoplasmic tail domain. DNRAGE interaction with ligands prevents the initial binding of fRAGE with ligands. At the same time, accumulation of ligands on the surface of the cells further activates influx of more ligands which in turn causes aggregation of ligands and oxidative stress that promotes fRAGE activation [25, 27].

Structural feature of RAGE for diverse ligands

RAGE interacted with a diverse variety of ligands with different size and symmetry. The rationale behind the multi-ligand recognition property of RAGE elucidated by negatively charged VC1 domain and ligand-driven multimodal dimerization [4,5]. Since RAGE interacted with acidic ligands and oligomerization had provided high stability between RAGE and ligand interaction. The basic (positive charge) nature of the V domain is provided by the presence of highly conserved Arginine and Lysine residues. At the same time, the C2 domain composed of large negative charge mediates the efficient binding of ligands on VC1 domain by repelling the negatively charged ligands towards VC1 domain. Therefore, the conserved basic cavity exhibited by the RAGE receptor is essential for recognizing multi diverse ligands [4,5,8,35].

ROLE OF RAGE LIGANDS IN AD

Studies have been reported that RAGE binds with diverse group of ligands mainly A β , S100 proteins (S100A12, S100B, S100A7, S100A8/A9 complex), advanced glycation end products (AGE), Mac-1 (Macrophage-1 antigen), HMGB1 (High mobility group box) and Phosphatidylserine [28,29,30].

AGE are the forms of modified proteins that are subjected to glycation and progressively involved in various modifications that in turn result in formation of insoluble cross links. Various types of AGE are reported such as glyoxal-lysine dimer (GOLD), methylglyoxal-lysine dimer (MOLD), Carboxyethyl-lysine (CEL), Pentosidine, and Carboxymethyl-lysine (CML). The rate of AGE formation is influenced by different environmental factors. Accumulation of AGE in intracellular and extracellular space recruits various neuronal related disorders. During aging, oxidative stress is elevated in brain cells which lead to the formation of AGE which in turn activates RAGE. The activated RAGE mediates the A β influx from the blood to brain, leading to RAGE-A β interactions which induces NF- κ B inflammatory signaling pathways [31,32,33,34].

AGEs are mostly located in pyramidal neurons and its concentration had increased in AD patients. As AD progress, the elevated level of AGE positive neurons leads to hyperphosphorylation of tau protein which finally causes senile plaques and neurofibrillary tangles (NFTs) [38,39]. AGEs-RAGE interaction leads to dephosphorylation of Nuclear factor activated T-cells (NFAT-1) and increased BACE1 expression. NFAT-1 is an important regulator of BACE1 expression which in turn regulates APP processing [40,41]. Regulation of detoxifying mechanisms such as Glyoxalase 1 (GLO1) detoxifying pre-AGEs methylglyoxal (MG) is prominent activity to mitigate the AD pathogenesis. But glutathione depletion (essential enzyme cofactor) in AD patients down regulates the GLO1-AGE detoxifying system, thus mediating the elevated production of AGEs [42,43,44,45].

RAGE AND AMYLOID PATHOLOGY

Amyloid Beta (A β), a pathological marker of AD is toxic to neuronal cells since it produces reactive oxygen species and causes accumulation of lipid peroxides and hydrogen peroxide. In primary neurons and astrocytes, it is a strong inducer of NF- κ B activation pathway. The chemotactic nature of A β causes microglia to migrate and accumulate around the amyloid plaques. fRAGE interacts with both the monomeric and complex forms of A β , leading to secretion of cytokines (Interleukin IL-6, IL-8, and IL-1b) by activated human astrocytoma cells, resulting in neuronal damage [4,5,32].

Failure in RAGE regulation tends to disrupt the production and clearance of A β peptides within the brain. RAGE is a key player in generating neurotoxicity. RAGE interaction with A β oligomers activates proinflammatory responses, ROS activation which causes amyloid pathological change followed by neuronal cell death (figure 2) [36,37].

RAGE is a critical player in AD as follows; i) RAGE increase the formation of A β and neurofibrillary tangles (tau hyperphosphorylation). ii) Activates microglia and astrocytes into inflammatory states which tend to develop cellular stress. iii) Enhanced neurodegeneration leads to cognitive impairment. iv) This process continues as a cyclic process and leads to progression of AD [46,47,48,49,50,51,52].

RAGE and A β clearance

RAGE is a transporter responsible for mediating influx of A β inside the brain whereas efflux of A β is controlled by LRP-1 and P-glycoprotein transporters. It has been demonstrated that AD affected brain samples had shown elevated expression of RAGE receptors and decreased level of LRP1 receptors [37]. The influx of peripheral A β

peptides into the brain is caused by the upregulation of RAGE and the downregulation of LRP1 receptors. Further activation of β secretases and also γ secretases leads to the generation of A β [36]. It is evident that A β accumulation distorts the BBB junction via Ca²⁺ calcineurin pathway [53,54,55]. Abundant RAGE-A β interaction drives the RAGE-DIAPH1 signaling pathway which is a prominent mediator for activating inflammation and cellular dysfunction [42,56].

Oxidative stress in AD

The interaction of RAGE-AGEs tends to raise ROS levels, affecting various antioxidant defense systems including glutathione-related enzymes, catalase, superoxide dismutase, and as well as activating protein kinase C [57]. The presence of metal ions along with AGEs initiates the generation of ROS that affects the cellular processes. Peptidyl radicals and nitroxyl radicals are sources for oxidative stress [58,59].

RAGE: Signaling pathways in AD pathology

Neuronal inflammation is a major reason for enhanced generation of A β and hyperphosphorylation of tau protein. Interaction of RAGE and A β induces various cellular signaling pathways [60]. As shown in Figure 2, RAGE-A β mediates the activation of the CaMKK-AMPK signaling pathway, which causes oxidative stress, tau hyperphosphorylation and chronic neuroinflammation [51,61]. Phosphorylation of ERK1/2 increases A β binding and tau kinase levels [62,63,64]. RAGE mediated GSK-3 (Glycogen synthase kinase 3) signaling pathway induces the hyperphosphorylation of tau protein [11,45,65]. RAGE mediated NF- κ B signaling pathway induces the release of cytokines which leads to oxidative stress and inflammation [66,67,68].

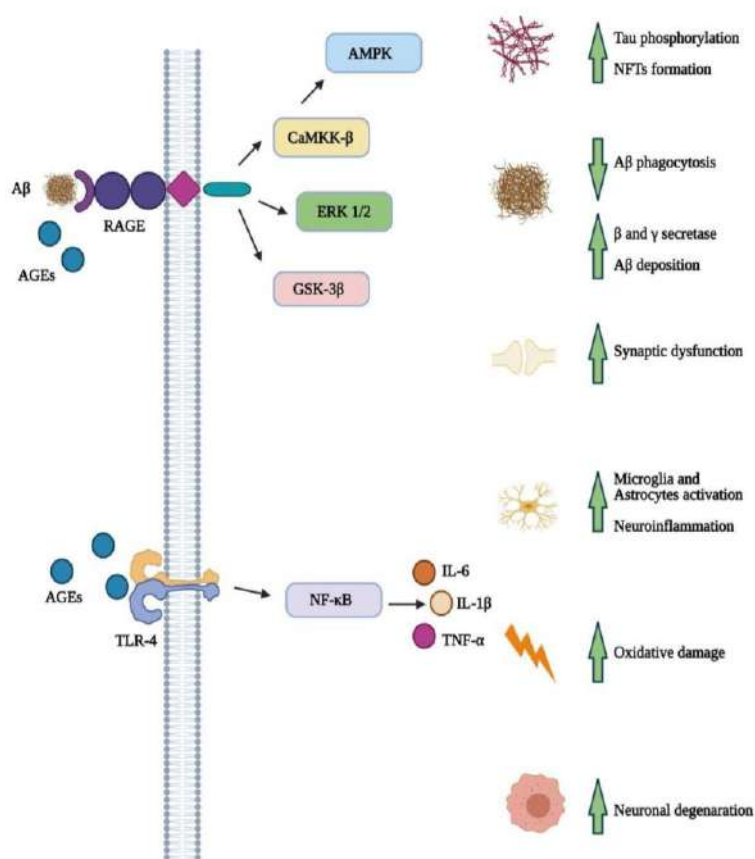


Figure 2: Pathological process in AD mediated by RAGE-A β interaction (Created with BioRender.com).

Interaction between sRAGE and A β

sRAGE had an inhibitory effect on fRAGE signaling pathways. Elevated aggregation of A β leads to formation of highly cross-linked complex structures. It is evident that fRAGE mostly binds with highly cross-linked structures than the monomeric A β . Therefore, when sRAGE binds with A β prior to the membrane bound RAGE, thereby prevents the fRAGE activation and RAGE ligand generation [24] as represented in figure 3. sRAGE administration into the circulatory system also increases peripheral nerve regeneration, prevents A β crossing from blood, and reduces AGE binding to the endothelial cell surface [73,74,75]. Additionally, most of the sRAGE is generated by ADAM10 sheddase and polymorphism in ADAM10 might be responsible for decreased concentration of sRAGE leading to the progression of AD [76,77,78,79,80].

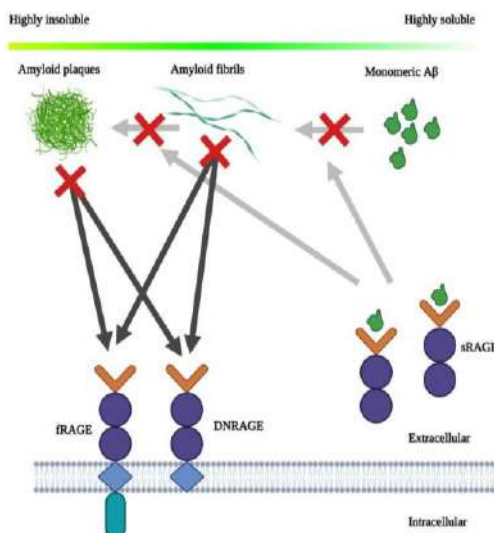


Figure 3: sRAGE as therapeutics for A β clearance in AD. Binding of sRAGE with monomeric A β prevents the formation of complex A β structures thereby preventing fRAGE interaction and proinflammatory signaling pathways. (Created with BioRender.com)

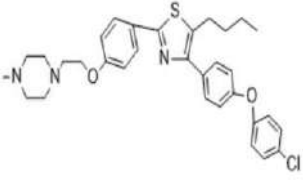
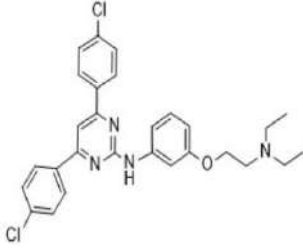
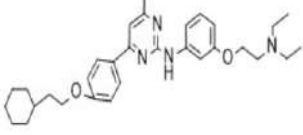
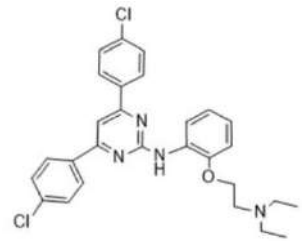
DEVELOPMENT OF RAGE INHIBITORS

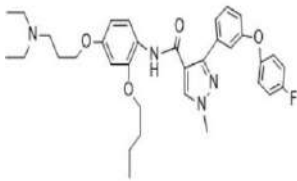
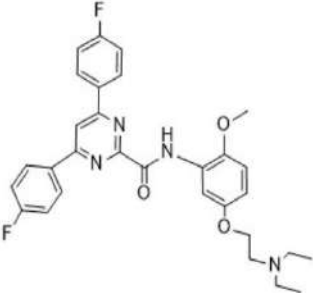
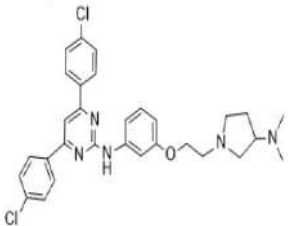
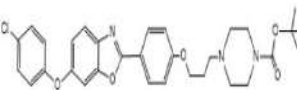
Existing knowledge on the mechanism of RAGE-A β interaction in AD pathology paves way for development of RAGE antagonists for AD treatment. Various strategies have been developed for blocking the RAGE-A β interaction such as synthetic RAGE analogs and RAGE antibodies to decay the RAGE mediated inflammatory response [81]. Anti-RAGE antibody administration hampered inflammatory signalling pathways, resulting in decreased cytokine expression and interruption of RAGE up-regulation. Anti-RAGE antibodies also prevent the A β mediated monocyte infiltration which induce pro-inflammatory responses and cause neurotoxicity in AD. Even though anti-RAGE antibodies seem to be beneficial, its permeability through blood brain barrier is still implausible [82, 83]. Hence, the development of synthetic RAGE inhibitors gained attractiveness.

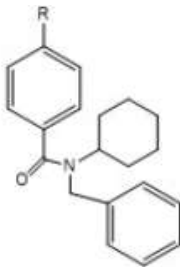
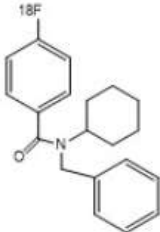
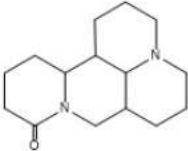
In the recent years, various synthetic RAGE inhibitors are developed in rapid pace such as 2-aminopyrimidine series of inhibitors, pyrazole-5-carboximide series of inhibitors, 6-phenoxy-2-phenylbenzoxazole series of inhibitors, FPS-ZM1, [18 F] RAGER and Matrine. The details of synthetic RAGE inhibitors are given in table 1.

Table 1: Development of Synthetic inhibitors for RAGE

Inhibitor classification	Inhibitor	Inhibitor name	Inhibitor structure	RAGE inhibitory activity	Model system and method used for RAGE-drug interaction	Therapeutic Effects	References
2-aminopyrimidines analog series	1	PF-04494700 or TTP488 (3-[4-[2-butyl-1-[4-(4-chlorophenoxy)phenyl]imidazol-4yl]phenoxy]-N,N-		$K_d = 500$ nM	Phase III clinical trial Study includes mild to moderate participants of AD Fluorescent polarization with	RAGE-A β binding inhibition Reduction of inflammatory markers Cognitive function improvement	84,85,86,87

		diethylprop an-1- amine)			sRAGE Mouse model of systemic amyloidosis		
	2	2,4-phenyl- substituted thiazole derivatives of 2 aminopyri midines		$IC_{50} = 1.21 \mu M$	Study performed using SAR (Structure- Activity relationshi p study)	Inhibition of $A\beta$ influx through BBB Downregulati on of NF- κ B Blocking RAGE- $A\beta$ interaction	88
	3	4,6-Bis(4- chlorophen yl)-N-(3-(2- (diethylami no) ethoxy) phenyl)- pyrimidin- 2-amine		$K_d = 102 \mu M$ $IC_{50} = 16.4 \mu M$	Acute model study- mice model Surface plasmon Resonance (SPR) using human RAGE	Inhibition of $A\beta$ BBB entry Downregulati on of NF- κ B activation Improvement of cognitive function Inhibition of $A\beta$ accumulation	89,90
	4	4-(4-(2- Cyclohexyl ethoxy) phenyl)-N- (3-(2- (diethylami no) ethoxy)- phenyl)-6- methylpyri midin-2- amine		Perce nt inhibit ion = 49.6 ± 4.4	Acute animal model study- mice model	Inhibition of $A\beta$ -RAGE binding Blocking of $A\beta$ entry into BBB Downregulati on of NF- κ B of activation	89
	5	4,6-Bis(4- chlorophen yl)-N-(2-(2- (diethylami no) ethoxy) phenyl)- pyrimidin- 2-amine		$IC_{50} = 4.6 \mu M$	Acute animal model study- mice model SPR using human RAGE	Inhibition of $A\beta$ accumulation Inhibition of $A\beta$ entry into BBB Downregulati on of NF- κ B activation	89
Pyrazole-5- carboximid e analog series	6	N-(2- butoxy-4- (3- (diethylami no) propoxy)		$K_d = 43.4 \mu M$ $IC_{50} = 1.9 \mu M$	SAR study mice model study SPR	Inhibition of $A\beta$ -RAGE binding Inhibition of $A\beta$ entry into BBB	89,90

		phenyl)-3-(4-(4-fluorophenoxy)phenyl)-1-methyl-1H-pyrazole-5-carboxamide)			analysis		
	7	N-(2-(2-(Diethylamino)ethoxy)-5-methoxyphenyl)-4,6-bis(4-fluorophenyl)pyrimidine-2-carboxamide)		-	ELISA on human RAGE-Aβ ₁₋₄₂	Inhibition of Aβ-RAGE binding Improved hydrophilicity and reduced cytotoxicity	90
	8	4, 6-Bis(4-chlorophenyl)-N-(3-(2-(3(dimethylamino)pyrrolidin-1-yl)ethoxy)phenyl)pyrimidin-2-amine)		-	Molecular docking study RAGE-Aβ ₁₋₄₂ interaction using ELISA	Inhibition of Aβ-RAGE binding Improved analog binding efficiency	92
6-phenoxy-2-phenylbenzoxazole analog series	9	4-(3-{4-[6-(4-Chlorophenoxy)-benzoxazol-2-yl]-phenoxy}-propyl)-piperazine-1-carboxylic acid tert-butyl ester)		40% inhibition at 4 μM	AD mice model study Assay performed -FRET (Fluorescence resonance energy transfer)	Blocks Aβ penetration across the BBB Reduction of amyloid aggregation Analogues are protective against cytotoxicity	93

	10	FPS-ZM1 (N-Benzyl-N-cyclohexyl-4-chlorobenzamide)		Ki for $A\beta_{1-40}$ = 25 nM	Rat model study RAGE- $A\beta_{1-42}$ and RAGE- $A\beta_{1-40}$ using ELISA	Up-regulated antioxidant defense system Down-regulated AGE-mediated pro-inflammatory cytokines Decreased $A\beta_{1-40}$ and $A\beta_{1-42}$ production as well as oxidative stress Improved cognitive function	94,95
	11	[^{18}F] RAGER		K_d = 15 nM	Molecular docking study Autoradiography	Inhibition of $A\beta$ -RAGE binding	96
	12	Matrine		K_d = 24 mM	AD mice model study ELISA on human RAGE- $A\beta_{1-42}$	Inhibits the cytotoxicity induced by $A\beta_{42}$ Inhibition of accumulation of $A\beta_{42}$ Suppressed the $A\beta$ /RAGE signaling pathway, proinflammatory cytokines and plaque formation Improved cognitive function	97

2-aminopyrimidines series of inhibitors are derived from one of the RAGE ligand called argpyrimidine-1 which is served as a template for the design of inhibitor. This argpyrimidine 1 has two essential moieties which are pyrimidine moiety and amino acid moiety (two parts – linker part and terminal polar part). The modification in these two moieties gave rise to a new class of aminopyrimidines of the RAGE antagonists (Inhibitor 1-5). These inhibitors had a pharmacophore made up of two aromatic groups, an alkyl chain with protonable nitrogen and a

pyrimidine central core. [84-89]. Pyrazole-5-carboximide series of inhibitors are designed by introduction of electronegative substituent and modification of ethoxy moiety (Inhibitor 6-8) [90-92]. 6-phenoxy-2-phenylbenzoxazole series of inhibitors have three parts such as 6-phenoxy region, 2-phenyl benzoxazole core and amino alkoxy region. Compounds with a (4-(alkoxycarbonyl) piperazin-1-yl) alkyloxy side chain in the 6-phenoxy-2-phenylbenzoxazole class of inhibitors inhibited RAGE-A β interactions significantly [93]. The first tested radiotracer (small molecule) that accumulated in the areas of high RAGE expression is RAGER [18F] [96]. Matrine (Mat) is derived from *Sophora flavescens* Ait, a chinese herb medicine used to treat dementia. Matrine could inhibit cytotoxicity induced by A β 42, preventing A β 42 aggregation and reducing RAGE-A β interaction [97]. Even though various small molecules of RAGE inhibitor are under trial, they are unable to interact with larger surface areas of the protein interface and thus block protein-protein interactions. Thereupon, peptides inhibitors gained essential attractiveness in therapeutics due to its advantages over small molecule antagonists [98].

CONCLUSION AND FUTURE ASPECTS

RAGE-amyloid interactions have a significant part in the pathophysiology of AD through neuroinflammation and amyloid mediated pathogenesis. Blocking this interaction by synthetic small molecule inhibitors, anti-RAGE antibodies and peptides antagonists are novel therapeutic strategy for AD. However, no RAGE inhibitors have been approved for clinical use so far, because of the limitations in bioavailability and transport of the drug candidates through BBB. Future research on developing drug therapeutics with good bioavailability, permeability, maximum safety and efficacy is warranted.

CONFLICT OF INTEREST

NONE DECLARE

REFERENCES

1. Cai Z, Liu N, Wang C, Qin B, Zhou Y, Xiao M et al. Role of RAGE in Alzheimer's Disease. *Cellular and Molecular Neurobiology*. 2015;36(4):483-49
2. Ding Q, Keller J. Evaluation of rage isoforms, ligands, and signaling in the brain. *Biochimica et Biophysica Acta (BBA) - Molecular Cell Research*. 2005;1746(1):18- 27.
3. Korczyn A. Mixed Dementia-the Most Common Cause of Dementia. *Annals of the New York Academy of Sciences*. 2002;977(1):129-134.
4. Yatime L, Andersen G. Structural insights into the oligomerization mode of the human receptor for advanced glycation end-products. *FEBS Journal*. 2013;280(24):6556-6568.
5. Xue J, Rai V, Singer D, Chabierski S, Xie J, Reverdatto S et al. Advanced Glycation End Product Recognition by the Receptor for AGEs. *Structure*. 2011;19(5):722- 732.
6. Neeper M, Schmidt A, Brett J, Yan S, Wang F, Pan Y et al. Cloning and expression of a cell surface receptor for advanced glycosylation end products of proteins. *Journal of Biological Chemistry*. 1992;267(21):14998-15004.
7. AGER - Advanced glycosylation end product-specific receptor precursor - Homo sapiens (Human) - AGER gene & protein [Internet]. Uniprot.org. 2021 [cited 23 January 2021]. Available from: <https://www.uniprot.org/uniprot/Q15109>
8. Dattilo B, Fritz G, Leclerc E, Vander Kooi C, Heizmann C, Chazin W. The Extracellular Region of the Receptor for Advanced Glycation End Products Is Composed of Two Independent Structural Units†. *Biochemistry*. 2007;46(23):6957-6970.
9. Sakaguchi M, Murata H, Yamamoto K, Ono T, Sakaguchi Y, Motoyama A et al. TIRAP, an Adaptor Protein for TLR2/4, Transduces a Signal from RAGE Phosphorylated upon Ligand Binding. *PLoS ONE*. 2011;6(8): e23132.
10. Rai V, Maldonado A, Burz D, Reverdatto S, Yan S, Schmidt A et al. Signal transduction in receptor for advanced glycation end products (RAGE). Solution Structure Of C-Terminal Rage (Ctrage) And Its Binding to Mdia1. *Journal of Biological Chemistry*. 2012;287(14):11283.
11. Li J, Liu D, Sun L, Lu Y, Zhang Z. Advanced glycation end products and neurodegenerative diseases: Mechanisms and perspective. *Journal of the Neurological Sciences*. 2012;317(1-2):1-5.

12. Röcken C, Kientsch-Engel R, Mansfeld S, Stix B, Stubenrauch K, Weigle B et al. Advanced Glycation End Products and Receptor for Advanced Glycation End Products in AA Amyloidosis. *The American Journal of Pathology*. 2003;162(4):1213-1220.
13. Ramasamy R, Vannucci S, Yan S, Herold K, Yan S, Schmidt A. Advanced glycation end products and RAGE: a common thread in aging, diabetes, neurodegeneration, and inflammation. *Glycobiology*. 2005;15(7):16R-28R.
14. Hudson B, Carter A, Harja E, Kalea A, Arriero M, Yang H et al. Identification, classification, and expression of RAGE gene splice variants. *The FASEB Journal*. 2007;22(5):1572-1580.
15. Kaji Y, Usui T, Ishida S, Yamashiro K, Moore T, Moore J et al. Inhibition of Diabetic Leukostasis and Blood-Retinal Barrier Breakdown with a Soluble Form of a Receptor for Advanced Glycation End Products. *Investigative Ophthalmology & Visual Science*. 2007;48(2):858.
16. Yonekura H, Yamamoto Y, Sakurai S, Petrova R, Abedin M, Li H et al. Novel splice variants of the receptor for advanced glycation end-products expressed in human vascular endothelial cells and pericytes, and their putative roles in diabetes-induced vascular injury. *Biochemical Journal*. 2003;370(3):1097-1109.
17. Yeh C, Sturgis L, Haidacher J, Zhang X, Sherwood S, Bjercke R et al. Requirement for p38 and p44/p42 Mitogen-Activated Protein Kinases in RAGE-Mediated Nuclear Factor- κ B Transcriptional Activation and Cytokine Secretion. *Diabetes*. 2001;50(6):1495-1504.
18. Li J, Wang W, Huang X, Oldfield M, Schmidt A, Cooper M et al. Advanced Glycation End Products Induce Tubular Epithelial-Myofibroblast Transition through the RAGE-ERK1/2 MAP Kinase Signaling Pathway. *The American Journal of Pathology*. 2004;164(4):1389-1397.
19. Dukic-Stefanovic S, Gasic-Milenkovic J, Deuther-Conrad W, Münch G. Signal transduction pathways in mouse microglia N-11 cells activated by advanced glycation endproducts (AGEs). *Journal of Neurochemistry*. 2003;87(1):44-55.
20. Haslbeck K, Bierhaus A, Erwin S, Kirchner A, Nawroth P, Schlötzer U et al. Receptor for advanced glycation endproduct (RAGE)-mediated nuclear factor- κ B activation in vasculitic neuropathy. *Muscle & Nerve*. 2004;29(6):853-860.
21. Habib S. Alterations in tubular epithelial cells in diabetic nephropathy. *Journal of Nephrology*. 2013;26(5):865-869.
22. Mohamed A, Bierhaus A, Schiekofer S, Tritschler H, Ziegler R, Nawroth P. The role of oxidative stress and NF- κ B activation in late diabetic complications. *BioFactors*. 1999;10(2-3):157-167.
23. Yu S, Wong C, Szeto C, Li E, Cai Z, Tam L. Members of the receptor for advanced glycation end products axis as potential therapeutic targets in patients with lupus nephritis. *Lupus*. 2014;24(7):675-686.
24. Chaney M, Stine W, Kokjohn T, Kuo Y, Esh C, Rahman A et al. RAGE and amyloid beta interactions: Atomic force microscopy and molecular modeling. *Biochimica et Biophysica Acta (BBA) - Molecular Basis of Disease*. 2005;1741(1-2):199-205.
25. Yan S, Chen X, Fu J, Chen M, Zhu H, Roher A et al. RAGE and amyloid- β peptide neurotoxicity in Alzheimer's disease. *Nature*. 1996;382(6593):685-691
26. Lue L, Walker D, Brachova L, Beach T, Rogers J, Schmidt A et al. Involvement of Microglial Receptor for Advanced Glycation Endproducts (RAGE) in Alzheimer's Disease: Identification of a Cellular Activation Mechanism. *Experimental Neurology*. 2001;171(1):29-45.
27. Du Yan S, Zhu H, Fu J, Yan S, Roher A, Tourtellotte W et al. Amyloid- peptide-Receptor for Advanced Glycation Endproduct interaction elicits neuronal expression of macrophage-colony stimulating factor: A proinflammatory pathway in Alzheimer disease. *Proceedings of the National Academy of Sciences*. 1997;94(10):5296-5301.
28. Schmidt A, Yan S, Yan S, Stern D. The biology of the receptor for advanced glycation end products and its ligands. *Biochimica et Biophysica Acta (BBA) - Molecular Cell Research*. 2000;1498(2-3):99-111.
29. Schmidt A, Yan S, Yan S, Stern D. The multiligand receptor RAGE as a progression factor amplifying immune and inflammatory responses. *Journal of Clinical Investigation*. 2001;108(7):949-955.

30. Bucciarelli L, Wendt T, Rong L, Lalla E, Hofmann M, Goova M et al. RAGE is a multiligand receptor of the immunoglobulin superfamily: implications for homeostasis and chronic disease. *Cellular and Molecular Life Sciences (CMLS)*. 2002;59(7):1117-1128.
31. Ray R, Juranek J, Rai V. RAGE axis in neuroinflammation, neurodegeneration and its emerging role in the pathogenesis of amyotrophic lateral sclerosis. *Neuroscience & Biobehavioral Reviews*. 2016;62: 48-55.
32. Emanuele E, D'Angelo A, Tomaino C, Binetti G, Ghidoni R, Politi P et al. Circulating Levels of Soluble Receptor for Advanced Glycation End Products in Alzheimer Disease and Vascular Dementia. *Archives of Neurology*. 2005;62(11):1734.
33. Teissier T, Boulanger É. The receptor for advanced glycation end-products (RAGE) is an important pattern recognition receptor (PRR) for inflammaging. *Biogerontology*. 2019;20(3):279-301.
34. Xie J, Reverdatto S, Frolov A, Hoffmann R, Burz D, Shekhtman A. Structural Basis for Pattern Recognition by the Receptor for Advanced Glycation End Products (RAGE). *Journal of Biological Chemistry*. 2008;283(40):27255-27269.
35. Koch M, Chitayat S, Dattilo B, Schiefner A, Diez J, Chazin W et al. Structural Basis for Ligand Recognition and Activation of RAGE. *Structure*. 2010;18(10):1342-1352.
36. Khter F, Akhter A, Kesari K, Javed R, Ruokolainen J, Vuorinen T. RAGE Exacerbate Amyloid Beta (A β) Induced Alzheimer Pathology: A Systemic Overview. 2021.
37. Liu R, Wu C, Zhou D, Yang F, Tian S, Zhang L et al. Pinocembrin protects against β -amyloid-induced toxicity in neurons through inhibiting receptor for advanced glycation end products (RAGE)-independent signaling pathways and regulating mitochondrion-mediated apoptosis. *BMC Medicine*. 2012;10(1).
38. Luth H. Age- and Stage-dependent Accumulation of Advanced Glycation End Products in Intracellular Deposits in Normal and Alzheimer's Disease Brains. *Cerebral Cortex*. 2004;15(2):211-220.
39. Choi B, Cho W, Kim J, Lee H, Chung C, Jeon W et al. Increased expression of the receptor for advanced glycation end products in neurons and astrocytes in a triple transgenic mouse model of Alzheimer's disease. *Experimental & Molecular Medicine*. 2014;46(2):e75-e75.
40. Cho H, Son S, Jin S, Hong H, Shin D, Kim S et al. RAGE regulates BACE1 and A β generation via NFAT1 activation in Alzheimer's disease animal model. *The FASEB Journal*. 2009;23(8):2639-2649.
41. Loske C, Gerdemann A, Schepl W, Wycislo M, Schinzel R, Palm D et al. Transition metal-mediated glycooxidation accelerates cross-linking of β -amyloid peptide. *European Journal of Biochemistry*. 2000;267(13):4171-4178.
42. Derk J, MacLean M, Juranek J, Schmidt A. The Receptor for Advanced Glycation Endproducts (RAGE) and Mediation of Inflammatory Neurodegeneration. *Journal of Alzheimer's Disease & Parkinsonism*. 2018;08(01).
43. Kuhla B, Boeck K, Schmidt A, Ogunlade V, Arendt T, Münch G et al. Age- and stage-dependent glyoxalase I expression and its activity in normal and Alzheimer's disease brains. *Neurobiology of Aging*. 2007;28(1):29-41.
44. More S, Vartak A, Vince R. Restoration of Glyoxalase Enzyme Activity Precludes Cognitive Dysfunction in a Mouse Model of Alzheimer's Disease. *ACS Chemical Neuroscience*. 2012;4(2):330-338.
45. Li X, Xie J, Jiang X, Lv B, Cheng X, Du L et al. Methylglyoxal Induces Tau Hyperphosphorylation via Promoting AGEs Formation. *NeuroMolecular Medicine*. 2012;14(4):338-348.
46. Cunnane S, Nugent S, Roy M, Courchesne-Loyer A, Croteau E, Tremblay S et al. Brain fuel metabolism, aging, and Alzheimer's disease. *Nutrition*. 2011;27(1):3-20.
47. Rapoport S, Hatanpää K, Brady D, Chandrasekaran K. Brain Energy Metabolism, Cognitive Function and Down-regulated Oxidative Phosphorylation in Alzheimer Disease. *Neurodegeneration*. 1996;5(4):473-476.
48. Yan S. RAGE is a key cellular target for A β -induced perturbation in Alzheimer's disease. *Frontiers in Bioscience*. 2012; S4(1):240-250.

49. Chaney M, Stine W, Kokjohn T, Kuo Y, Esh C, Rahman A et al. RAGE and amyloid beta interactions: Atomic force microscopy and molecular modeling. *Biochimica et Biophysica Acta (BBA) - Molecular Basis of Disease*. 2005;1741(1-2):199-205.
50. Zong H, Madden A, Ward M, Mooney M, Elliott C, Stitt A. Homodimerization Is Essential for the Receptor for Advanced Glycation End Products (RAGE)-mediated Signal Transduction. *Journal of Biological Chemistry*. 2010;285(30):23137-23146.
51. Son S, Jung E, Shin H, Byun J, Mook-Jung I. A β -induced formation of autophagosomes is mediated by RAGE-CaMKK β -AMPK signaling. *Neurobiology of Aging*. 2012;33(5): 1006.e11-1006.e23.
52. Marksteiner J, Imarhiagbe D, DeFrancesco M, Deisenhammer E, Kemmler G, Humpel C. Analysis of 27 vascular-related proteins reveals that NT-proBNP is a potential biomarker for Alzheimer's disease and mild cognitive impairment: A pilot-study. *Experimental Gerontology*. 2014;50: 114-121.
53. Watson R, Prabhala R, Plezia P, Alberts D. Effect of β -carotene on lymphocyte subpopulations in elderly humans: evidence for a dose-response relationship. *The American Journal of Clinical Nutrition*. 1991;53(1):90-94.
54. Wan W, Chen H, Li Y. The potential mechanisms of A β -receptor for advanced glycation end-products interaction disrupting tight junctions of the blood-brain barrier in Alzheimer's disease. *International Journal of Neuroscience*. 2013;124(2):75-81.
55. Kook S, Seok Hong H, Moon M, Mook-Jung I. Disruption of blood-brain barrier in Alzheimer disease pathogenesis. *Tissue Barriers*. 2013;1(2):e23993.
56. Qosa H, LeVine H, Keller J, Kaddoumi A. Mixed oligomers and monomeric amyloid- β disrupts endothelial cells integrity and reduces monomeric amyloid- β transport across hCMEC/D3 cell line as an in vitro blood-brain barrier model. *Biochimica et Biophysica Acta (BBA) - Molecular Basis of Disease*. 2014;1842(9):1806-1815.
57. Jiang JM, Wang Z, Li DD. Effects of AGEs on oxidation stress and antioxidation abilities in cultured astrocytes. *Biomed Environ Sci*. 2004;17(1):79-86.
58. Durany N, Münch G, Michel T, Riederer P. Investigations on oxidative stress and therapeutical implications in dementia. *European Archives of Psychiatry and Clinical Neurosciences*. 1999;249(S3):S68-S73.
59. Ramasamy R, Vannucci S, Yan S, Herold K, Yan S, Schmidt A. Advanced glycation end products and RAGE: a common thread in aging, diabetes, neurodegeneration, and inflammation. *Glycobiology*. 2005;15(7):16R-28R.
60. Fernández J, Rojo L, Kuljis R, Maccioni R. The Damage Signals Hypothesis of Alzheimer's Disease Pathogenesis. *Journal of Alzheimer's Disease*. 2008;14(3):329-333.
61. Salminen A, Kaarniranta K, Haapasalo A, Soininen H, Hiltunen M. AMP-activated protein kinase: a potential player in Alzheimer's disease. *Journal of Neurochemistry*. 2011;118(4):460-474.
62. Webster B, Hansen L, Adame A, Crews L, Torrance M, Thal L et al. Astroglial Activation of Extracellular-Regulated Kinase in Early Stages of Alzheimer Disease. *Journal of Neuropathology and Experimental Neurology*. 2006;65(2):142-151.
63. Slowik A, Merres J, Elfgen A, Jansen S, Mohr F, Wruck C et al. Involvement of formyl peptide receptors in receptor for advanced glycation end products (RAGE) - and amyloid beta 1-42-induced signal transduction in glial cells. *Molecular Neurodegeneration*. 2012;7(1):55.
64. Barroso E, del Valle J, Porquet D, Vieira Santos A, Salvadó L, Rodríguez-Rodríguez R et al. Tau hyperphosphorylation and increased BACE1 and RAGE levels in the cortex of PPAR β / δ -null mice. *Biochimica et Biophysica Acta (BBA) - Molecular Basis of Disease*. 2013;1832(8):1241-1248.
65. Li X, Lv B, Xie J, Liu J, Zhou X, Wang J. AGEs induce Alzheimer-like tau pathology and memory deficit via RAGE-mediated GSK-3 activation. *Neurobiology of Aging*. 2012;33(7):1400-1410.
66. Wang C, Xie J, Xu Y, Wang T, Cai J, Wang X et al. Trientine Reduces BACE1 Activity and Mitigates Amyloidosis via the AGE/RAGE/NF- κ B Pathway in a Transgenic Mouse Model of Alzheimer's Disease. *Antioxidants & Redox Signaling*. 2013;19(17):2024-2039.

67. Wang X, Yu S, Hu J, Wang C, Wang Y, Liu H et al. Streptozotocin-induced diabetes increases amyloid plaque deposition in AD transgenic mice through modulating AGEs/RAGE/NF- κ B pathway. *International Journal of Neuroscience*. 2013;124(8):601-608.
68. Lukiw W. NF- κ B-regulated, proinflammatory miRNAs in Alzheimer's disease. *Alzheimer's Research & Therapy*. 2012;4(6):47.
69. Hudson B, Stickland M, Grant P. Identification of polymorphisms in the receptor for advanced glycation end products (RAGE) gene: prevalence in type 2 diabetes and ethnic groups. *Diabetes*. 1998;47(7):1155-1157.
70. Prevost G, Fajardy I, Fontaine P, Danze P, Besmond C. Human RAGE GLY82SER dimorphism and HLA class II DRB1-DQA1-DQB1 haplotypes in type 1 diabetes. *European Journal of Immunogenetics*. 1999;26(5):343-348.
71. Rani P. G82S RAGE polymorphism is associated with Alzheimer's disease. *Frontiers in Bioscience*. 2020;12(1):150-161.
72. Hofmann M, Drury S, Hudson B, Gleason M, Qu W, Lu Y et al. RAGE and arthritis: the G82S polymorphism amplifies the inflammatory response. *Genes & Immunity*. 2002;3(3):123-135.
73. Park L, Raman K, Lee K, Lu Y, Ferran L, Chow W et al. Suppression of accelerated diabetic atherosclerosis by the soluble receptor for advanced glycation endproducts. *Nature Medicine*. 1998;4(9):1025-1031.
74. Wear-Maggitti K, Lee J, Conejero A, Schmidt A, Grant R, Breitbart A. Use of Topical sRAGE in Diabetic Wounds Increases Neovascularization and Granulation Tissue Formation. *Annals of Plastic Surgery*. 2004;52(5):519-521.
75. LaRue B, Hogg E, Sagare A, Jovanovic S, Maness L, Maurer C et al. Method for measurement of the blood-brain barrier permeability in the perfused mouse brain: application to amyloid- β peptide in wild type and Alzheimer's Tg2576 mice. *Journal of Neuroscience Methods*. 2004;138(1-2):233-242.
76. Li X, Du L, Cheng X, Jiang X, Zhang Y, Lv B et al. Glycation exacerbates the neuronal toxicity of β -amyloid. *Cell Death & Disease*. 2013;4(6): e673-e673.
77. Quade-Lyssy P, Kanarek A, Baiersdörfer M, Postina R, Kojro E. Statins stimulate the production of a soluble form of the receptor for advanced glycation end products. *Journal of Lipid Research*. 2013;54(11):3052-3061.
78. Yamagishi S. Soluble form of a receptor for advanced glycation end products sRAGE as a biomarker. *Frontiers in Bioscience*. 2010; E2(4):1184-1195.
79. Sugihara T, Munesue S, Yamamoto Y, Sakurai S, Akhter N, Kitamura Y et al. Endogenous Secretory Receptor for Advanced Glycation End-Products Inhibits Amyloid- β 1-42 Uptake into Mouse Brain. *Journal of Alzheimer's Disease*. 2012;28(3):709-720.
80. Huang W, Chen W, Jiang L, Yang Y, Yao L, Li K. Influence of ADAM10 Polymorphisms on Plasma Level of Soluble Receptor for Advanced Glycation End Products and The Association with Alzheimer's Disease Risk. *Frontiers in Genetics*. 2018;9.
81. Bongarzone S, Savickas V, Luzi F, Gee A. Targeting the Receptor for Advanced Glycation Endproducts (RAGE): A Medicinal Chemistry Perspective. *Journal of Medicinal Chemistry*. 2017;60(17):7213-7232.
82. Matsumoto H, Matsumoto N, Shimazaki J, Nakagawa J, Imamura Y, Yamakawa K et al. Therapeutic Effectiveness of Anti-RAGE Antibody Administration in a Rat Model of Crush Injury. *Scientific Reports*. 2017;7(1): 12255.
83. Kozyrev N, Albers S, Yang J, Prado V, Prado M, Fonseca G et al. Infiltrating Hematogenous Macrophages Aggregate Around β -Amyloid Plaques in an Age- and Sex-Dependent Manner in a Mouse Model of Alzheimer Disease. *Journal of Neuropathology & Experimental Neurology*. 2020;79(11):1147-1162.
84. Galasko D, Bell J, Mancuso J, Kupiec J, Sabbagh M, van Dyck C et al. Clinical trial of an inhibitor of RAGE-A interactions in Alzheimer disease. *Neurology*. 2014;82(17):1536-1542.

85. Burstein A, Grimes I, Galasko D, Aisen P, Sabbagh M, Mjalli A. Effect of TTP488 in patients with mild to moderate Alzheimer's disease. *BMC Neurology*. 2014;14(1).
86. Diseases A, derivatives a, derivatives a, derivatives g, derivatives i, compositions p et al. WO2011041198A1 - Substituted imidazole derivatives for treatment of alzheimers disease - Google Patents [Internet]. Patents.google.com. 2021 [cited 25 January 2021]. Available from: <https://patents.google.com/patent/WO2011041198A1/en>
87. Sabbagh M, Agro A, Bell J, Aisen P, Schweizer E, Galasko D. PF-04494700, an Oral Inhibitor of Receptor for Advanced Glycation End Products (RAGE), in Alzheimer Disease. *Alzheimer Disease & Associated Disorders*. 2011;25(3):206-212.
88. Lee Y, Kim H, Kim Y, Roh E, Han H, Shin K. Synthesis and structure–activity relationships of tri-substituted thiazoles as RAGE antagonists for the treatment of Alzheimer's disease. *Bioorganic & Medicinal Chemistry Letters*. 2012;22(24):7555-7561.
89. Han Y, Choi G, Son D, Kim N, Yun H, Lee S et al. Ligand-Based Design, Synthesis, and Biological Evaluation of 2-Aminopyrimidines, a Novel Series of Receptor for Advanced Glycation End Products (RAGE) Inhibitors. *Journal of Medicinal Chemistry*. 2012;55(21):9120-9135.
90. Kim S, Han Y. Design, synthesis, and biological evaluation of pyrimidine-2-carboxamide analogs: investigation for novel RAGE inhibitors with reduced hydrophobicity and toxicity. *Archives of Pharmacal Research*. 2015;38(11):1952-1962.
91. Han Y, Kim K, Choi G, An H, Son D, Kim H et al. Pyrazole-5-carboxamides, novel inhibitors of receptor for advanced glycation end products (RAGE). *European Journal of Medicinal Chemistry*. 2014;79: 128-142.
92. Han Y, Kim K, Son D, An H, Kim H, Lee J et al. Fine tuning of 4,6-bisphenyl-2-(3-alkoxyanilino) pyrimidine focusing on the activity-sensitive aminoalkoxy moiety for a therapeutically useful inhibitor of receptor for advanced glycation end products (RAGE). *Bioorganic & Medicinal Chemistry*. 2015;23(3):579-587.
93. Choi K, Lim K, Shin J, Kim S, Suh Y, Hong H et al. 6-Phenoxy-2-phenylbenzoxazoles, novel inhibitors of receptor for advanced glycation end products (RAGE). *Bioorganic & Medicinal Chemistry*. 2015;23(15):4919-4935.
94. Deane R, Singh I, Sagare A, Bell R, Ross N, LaRue B et al. A multimodal RAGE-specific inhibitor reduces amyloid β –mediated brain disorder in a mouse model of Alzheimer disease. *Journal of Clinical Investigation*. 2012;122(4):1377-1392.
95. Hong Y, Shen C, Yin Q, Sun M, Ma Y, Liu X. Effects of RAGE-Specific Inhibitor FPS-ZM1 on Amyloid- β Metabolism and AGEs-Induced Inflammation and Oxidative Stress in Rat Hippocampus. *Neurochemical Research*. 2016;41(5):1192-1199.
96. Cary B, Brooks A, Fawaz M, Drake L, Desmond T, Sherman P et al. Synthesis and Evaluation of [18F] RAGER: A First Generation Small-Molecule PET Radioligand Targeting the Receptor for Advanced Glycation Endproducts. *ACS Chemical Neuroscience*. 2016;7(3):391-398.
97. Cui L, Cai Y, Cheng W, Liu G, Zhao J, Cao H et al. A Novel, Multi-Target Natural Drug Candidate, Matrine, Improves Cognitive Dessficits in Alzheimer's Disease Transgenic Mice by Inhibiting A β Aggregation and Blocking the RAGE/A β Axis. *Molecular Neurobiology*. 2016;54(3):1939-1952.
98. Lee A, Harris J, Khanna K, Hong J. A Comprehensive Review on Current Advances in Peptide Drug Development and Design. *International Journal of Molecular Sciences*. 2019;20(10):2383.

Recurrent Neural Network Based Predictive Virtual Machine Migration in Hybrid Cloud

E.G. Radhika, S. P. Rajamohana and K. Khavya

Department of Information Technology, PSG College of Technology, Coimbatore, Tamil Nadu, 641004, India

ABSTRACT

In recent years, Cloud computing has evolved as a widely accepted technology. Security and data availability are some of the key features of the cloud. During critical times like natural disaster or unexpected server downtime in the data center, Virtual Machine (VM) migration technology helps to preserve the data by moving the resources from one physical server to the other. The process of moving VM's from one physical server to other parts of the same server or to other server within same data center or to other data center is known as VM migration. Few of the challenges in VM migration are security issues, network bandwidth, and volume of data to be transferred. VM migration is to be done with compliance of the Service Level Agreement (SLA). Few of the techniques for migration the VM are statistical approach, machine learning (ML) and neural network approach. This work surveys various VM migration techniques, evaluates the best migration technique for multi-user cloud environment. The results shown that Recurrent Neural Network(RNN) algorithm is found to be best suited since it produces best results compared to the traditional algorithms.

Keywords—Cloud computing, migration, Service Level Agreement, private cloud, RNN.

I. INTRODUCTION

VM migration is the process that moves a running VM from one server to other. The main reason for opting for VM migration is data recovery. The data centers of Cloud Service Providers (CSP) are generally placed in regions where there are minimal chances of natural calamities like earthquake such that there is no damage to the servers present in those data centers. There are two types of VM migration namely,

A. Hot Migration

It is also known as live migration. Virtual machines will be live during this process. Users will not be interrupted during this process and the downtime of the server will be in seconds.

B. Cold Migration

In this process, the VMs will not be functioning and there will be interruptions in this case. Applications which functions 24*7 and which must not have any delay like banking applications cannot opt for live migration and other application that can accept the delay can opt for the cold migration. However, the cost of live migration is huge compared to cold migration since hot migration involves transferring resources on the fly which needs at most care and highly secured environment. Whereas in cold migration, the VMs are turned off and then the resources will be migrated. Live migration in turn has different phases such as,

a) **Pre-copy memory migration-** It has two phases. The initial phase is warm up where all the contents are migrated from running VM to other. The next phase is stop and copy where the dirty pages are recopied and at the final stage the running VMs are turned off and remaining contents are migrated.

b) **Post-copy memory migration-** It refers to the process of copying the contents in the target VM after it is been transferred from source VM. It initially copies the memory state and finally the processors on to the target VM.

II. RELATED RESEARCH WORKS

There are different techniques in VM migration such as statistical method with deals with working on setting up metrics like threshold and fine tuning the metrics to reach the threshold level and it is more related to statistical methods wherein it involves numerous mathematical notations that helps in developing a complex system that can be used for VM migration technique, machine learning method is based on implementing ML algorithms for VM migration and hybrid approach deals with implementing VM migration techniques by combining two or more methods. The survey is made to find the best VM migration technique and the results are discussed in table 1.

Table I. Summary of related works

Details of the papers surveyed	Features compared in research work
--------------------------------	------------------------------------

Name of the Author and year	Title of the paper	Data set used	Proactive/Reactive approach	Metrics chosen for evaluation	Algorithm used/ proposed for VM migration with accuracy
Debabrota Basu, et al., & 2019 [1]	Learn-as-you-go with Megh: Efficient Live Migration of Virtual Machines	PlanetLab Dataset and Google Cluster Dataset used in CloudSim toolkit.	This paper is based on predictive approach as it focuses on eliminating the live migration issues found in other existing approaches.	Execution time, total cost for migration, number of active hosts and total number of VM migration.	Reinforcement learning based Megh algorithm – Performance evaluation is better than THRMMT, IQRMMT, MADMMT, LRMMT and LRRMMT. Reduces the cost of VM migration.
Elsaid, M, et al., & 2019 [2]	Machine Learning Approach for Live Migration Cost Prediction in VMware Environments	Own data collection phase is included that collects 144 readings (last 12 hours data before conducting experiment is taken) from the VM cluster.	This paper is based on predictive approach as it focuses on eliminating the main cost issue in live migration by using ML technique for prediction.	The input parameters are power consumption, CPU overhead, migration time, IP network overhead,	Machine learning algorithm with two phases training and prediction in VMware environment. The accuracy is 90%.
Kaur, Ramandeep & 2017 [3]	A Hybrid Approach for Virtual Machine Migration in Cloud Computing Environment	The work includes the simulation setup. So, it doesn't have any real-time datasets used.	This paper is proactive strategy as it formulates the strategy and compares the work with other existing methods and finds the proposed work to be optimal.	The metrics are number of migrations, SLA violations, energy consumption and number of VMs	Artificial Neural network with bee colony approach. Performance better than TVMM and ACOVMM.
Hassan, M. K, & 2018 [4]	Machine Learning Based Approach for Virtual Machine Migration	Real time data sets from three different servers namely venus, alaadin and chinmay	This paper is proactive strategy as it compares between three approaches such as KNN, regression trees and SVM and finds the non-suitable	The metrics considered are CPU utilization, memory and Inter VM bandwidth utilization.	KNN, SVM and regression trees. KNN has less performance than SVM and regression trees.

Zhou, A., et al & 2019 [5]	Towards Service Composition Aware Virtual Machine Migration Approach in the Cloud	Real time live data center costs are considered	approach. This is the proactive technique which employs PSO and LSP technique for evaluating the performance of the data center	Only the network cost is been considered	Proposed INLP technique in order to solve NP Hard problems and LP solvers are used to evaluate the correctness of this problem.
E G Radhika, et al. & 2018 [6]	An Efficient Predictive technique to Autoscale the Resources for Web applications in Private cloud	Real time data servers are used to collect and analyze the data.	This is the predictive approach that uses RNN to predict future workload for VM provision.	The metrics considered are CPU utilization and memory.	Proposed RNN algorithm is implemented in private cloud for web applications.
E G Radhika, et al. & 2018 [7]	An RNN-LSTM Based Flavor Recommender Framework in Hybrid Cloud	Real time data servers are used to collect and analyze the data.	To predict future resources RNN is used and recommended flavor for hybrid cloud that is cost efficient.	The metrics considered are CPU and RAM utilization.	Proposed flavor recommender framework is implemented in hybrid cloud for web applications.

III. INFERENCES & OBSERVATION

In accordance with the above detailed study on various types of VM migration techniques, it is inferred that the neural network related algorithm holds good in case of live VM migration technique. The neural network algorithm is the most efficient method for effective VM migration is found in this study. It is also observed that the proactive approach will be best suited approach since it focuses on a problem statement and finds the solution for the problem. E.G. Radhika et al.[7] also referred RNN to predict future workload in cloud environment to recommend best suitable flavor for the customer. In addition, predictive approach which is the sub class of the proactive approach might hold good in cases of VM migration because in predictive approach, initial prediction of the approach is made then based on the obtained results are compared. If there is a deviation, then the parameters are fine tuned to obtain the expected throughput. Hence it is inferred that the proactive approach and the neural network related techniques will hold good for the VM migration.

IV. IMPLEMENTATION

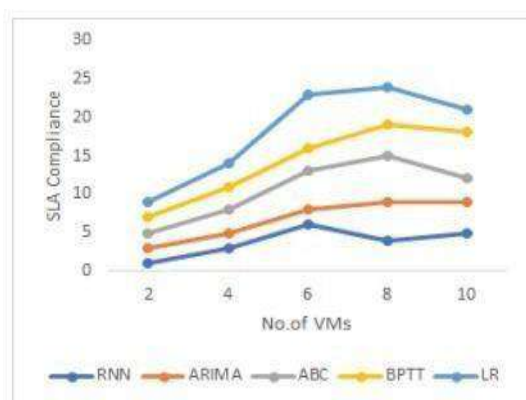
As inferred that neural network approach suits best for the hybrid cloud setup, cloud model is setup using two openstack private clouds. For simplicity, web application is considered and hosted in hybrid cloud using two private clouds. This proposed application consists of 12 web servers, 6 application servers and 3 DB servers running with OS as Ubuntu Linux and compute instance type as m1.medium. The real-time data sets are used for training and testing. The process carried out in this implementation is as follows. Firstly, initialize the cloud framework by hosting the virtual machines. RNN algorithm is implemented for

the VM migration and deployed in VMs. Then the migration metrics like bandwidth, number of VMs migrated, SLA violations, CPU utilization and energy consumption are accounted. The obtained results are compared with the traditional algorithms like Auto Regressive Integrated Moving Average (ARIMA), Back Propagation Through Time (BPTT), Linear Regression (LR) and Artificial Bee Colony (ABC). The results found that RNN algorithm performs better than other traditional algorithms. Table II given below depicts

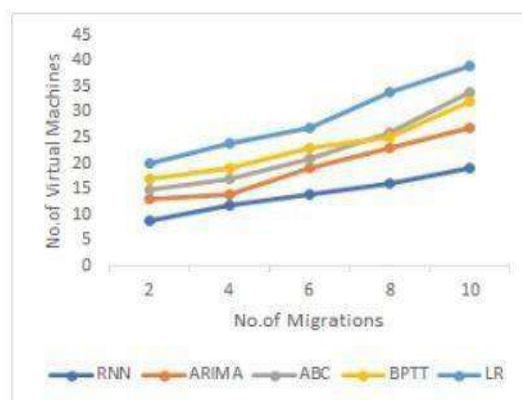
Table II. Results obtained while using RNN algorithm in the hybrid cloud environment

No. of VMs	Migration count	Bandwidth in Gpbs	CPU utilization	Energy consumption in KWH	SLA Violation
2	1	0.5	0.25	50	16
4	2	1.3	0.36	88	27
6	4	2.5	0.42	124	32
8	6	3.9	0.59	149	39
10	8	4.6	0.71	162	44

the results obtained by implementing the RNN algorithm in the hybrid cloud using openstack framework. The proposed work is compared with the existing traditional VM migration algorithms. The results are discussed in detail further.



(1)

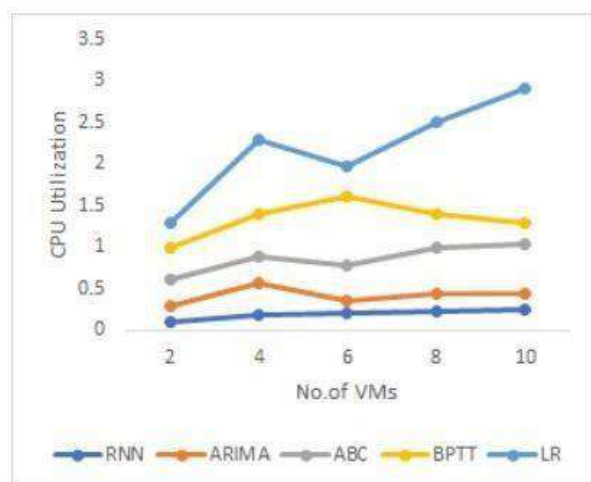


(2)

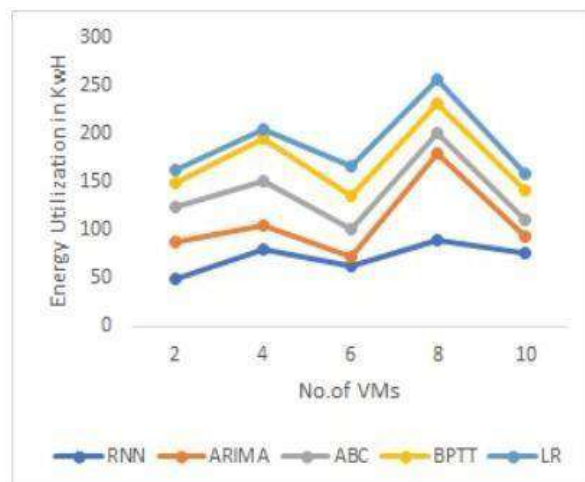
Fig. 1. Comparison SLA compliance with traditional algorithm and RNN algorithm

Fig. 2. Comparison of migration count with traditional algorithm and RNN alg

Figure 1 illustrates the SLA compliance vs the total no. of VMs for traditional and RNN algorithm. Figure 2 represents the migration count vs the total no. of migrations for traditional and RNN algorithm. RNN algorithm has lesser number of migrations compared to the existing traditional VM migration algorithm. The



(3)



(4)

Fig. 3. Comparison of CPU Utilization with traditional algorithm

Fig. 4. Comparison of Energy utilization with traditional and RNN and RNN algorithm algorithm

RNN algorithm has lesser number of migrations compared to the existing traditional VM migration algorithm. Figure 3, Figure 4 and Figure 5 shows the relationship between the various metrics like CPU utilization, energy utilization and bandwidth utilization vs total No. of VMs. The results depicts that RNN algorithm has a better performance than the other traditional algorithms.

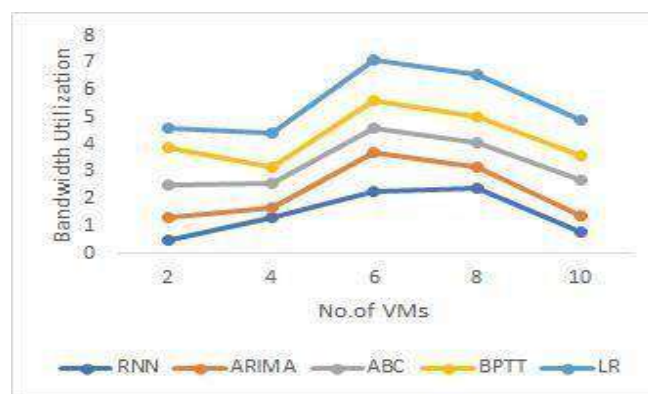


Fig. 5. Comparison Bandwidth utilization with traditional algorithm and RNN algorithm

V.CONCLUSION

VM migration is an important strategy in cloud computing. There are two different types of VM migration in which live migration is handy during critical hours. This work surveys the different types of live migration techniques and finds neural network approach would be optimal for VM migration. RNN algorithm is implemented with hybrid cloud simulation with openstack cloud and it produces best results compared to the other existing traditional algorithms like LR, BPTT, ARIMA and ABC.

REFERENCES

1. Basu, D., Wang, X., Hong, Y., Chen, H., & Bressan, S. (2019). Learn- as-you-go with megh: Efficient live migration of virtual machines. *IEEE Transactions on Parallel and Distributed Systems*.
2. Elsaid, M.; Abbas, H. and Meinel, C. (2019). Machine Learning Approach for Live Migration Cost Prediction in VMware Environments. In *Proceedings of the 9th International Conference on Cloud Computing and Services Science - Volume 1: CLOSER*.
3. KAUR, Ramandeep.(2017) A Hybrid Approach for Virtual Machine Migration in Cloud Computing Environment. *International Journal of Advanced Research in Computer Science and Software Engineering*, [S.l.], v. 7, n. 9, p. 30-35.
4. Hassan, M. K., Babiker, A., Zobli, S., Amien, M. B., & Kanona, E. A. Machine Learning Based Approach for Virtual Machine Migration.
5. Zhou, A., Wang, S., Ma, X., & Yau, S. S. (2019). Towards Service Composition Aware Virtual Machine Migration Approach in the Cloud. *IEEE Transactions on Services Computing*.
6. Radhika, E. G., Sadasivam, G. S., & Naomi, J. F. (2018). An efficient predictive technique to autoscale the resources for web applications in private cloud. In 2018 Fourth International Conference on Advances in Electrical, Electronics, Information, Communication and Bio-Informatics (AEEICB) (pp. 1-7). IEEE.
7. Radhika, E. G., & Sadhasivam, S. G. (2018). An RNN-LSTM Based Flavor Recommender Framework in Hybrid Cloud. In 2018 17th IEEE International Conference on Machine Learning and Applications (ICMLA) (pp. 270-277). IEEE.
8. C. Amuthadevi, D. S. Vijayan, Varatharajan Ramachandran, "Development of air quality monitoring (AQM) models using different machine learning approaches", *Journal of Ambient Intelligence and Humanized Computing*, <https://doi.org/10.1007/s12652-020-02724-2>

Leadership and Employees' Attrition in Manufacturing Companies

Shankar R

Department of Humanities, PSG College of Technology, Coimbatore

ABSTRACT

Considering today's competitive market, managing an organization's competent and qualified human resources is critical to success. In order to attract staff, the industry usually raises executive compensation. It's a difficult task for any leader in charge of more than one staff in a corporation. Administrators are frequently untrained on how to keep employees from quitting. Employers view turnover as a loss of productive employees and talent. However, there's more to attrition than a shrinking population. Entrepreneurs take with them the necessary skills and qualifications they gained throughout their time as employees departing a company. Here is where leadership styles, as well as skills, play a critical influence in lowering attrition rates. The current study examines the impact of leadership styles on the many factors of attrition in the manufacturing sector in this context.

Keywords: Human Resource, Leadership Styles, Attrition, Manufacturing sector.

INTRODUCTION AND PROBLEM DEFINITION

Since the turn of the century, the field of leadership — both in theory and in practice — has been a rapidly expanding part of management science. Leadership is a given and fundamental role in most concepts of management and organization in enforcing rules, inspiring personnel, and expressing future goals and visions to aim towards. In most companies, leadership is thought to offer a unique, important, and valuable difference to based intervention, and the role of the manager has consequently been consumed with the never-ending work of discovering identities or practices associated with effective management. The area of organizational leadership has typically been leader-centered, focusing on the individual executives and their characteristics, skills, and deeds, and therefore putting the abstract phenomena of 'leadership' into separate individuals who are removed from their cultural context. This one was important in the early twentieth century's innovations in operations research, in which the greatest leaders were to be found and chosen based on their fitness and formal merits rather than pre-modern criteria like kinship or magnetism. The issue of determining what made a suitable leader remained unsolved, and this topic spawned a slew of diverse thought schools. One school of thought attempted to discover personality attributes that set great leaders apart from others. Others countered that leadership was about the interaction between leaders and followers, and also that different kinds of interaction had different outcomes.

In modern texts, a leader is characterized as a collective with special abilities to impact the group, and governance is therefore a series of complex interactions in which leaders inspire followers by developing shared meaningful visions of the future. The dividing line between transaction processing and revelatory governance, showing the difference between governance as a contracting party's leader and followers and leadership as a social relationship in which followers' aspirations is raised to those of the leaders themselves, is at the heart of the argument. In recent years, there seems to be a growing debate in the areas of leadership studies over shared and distributed leadership viewpoints, with the emphasis on leadership as a group activity rather than the actions of official leaders. Along with management decisions and entrepreneurship activity activities, the leaders are in a position to resolve all employee-related problems. The galloping need for talented personnel throughout the last decade of the twenty-first century has had a crucial impact on all employment-related concerns in organizations experiencing employee attrition. Employers are particularly concerned about the implications for needs that go far beyond ground attrition and the repercussions on corporate performance, as well as the necessity for ongoing recruiting and the associated expenditures. When a person is employed, it is customary for him to remain working for the organization during his long career.

Consequently, once someone is fit for work in terms of the job circumstances and his standards, the employer that hires him is expected to provide him with work. This implies that associations are mutually and reciprocally interested in the definition and reinterpretation of their partnership structure. India is rapidly establishing itself as a global industrial hub. Either industrial enterprises, such as autos or computer components, durable goods, or technical goods, are manufactured in India by multinationals. According to a report by the Federation of Indian Chambers of Commerce and Industry (FICCI) and Yes Bank, India is on track to become the global manufacturing center for luxury goods in the next five years, with the development of luxury goods expected to be a US\$ 500 million industry. India possesses all of the requisite talents in product, process, and capital

engineering because of its long manufacturing legacy and higher education institutions. India's low-cost, well-educated labor draws a wide range of businesses from various industries, transforming the country into a global manufacturing powerhouse. The enormous domestic sector in India, as well as the access to low labor with superior technological skills, has enticed a growing number of multinationals to establish manufacturing bases in the country.

Following the advent of globalization, the industry underwent a major transformation. The success of manufacturing and promotion is entirely dependent on skilled and well-trained employees. The company's retailers are given systematic training to help them increase their knowledge. However, following good training, workers demonstrate their abilities by aggressively exhibiting their abilities through violent performance. The flippant attitude or actions of important bosses create resentment, and smart and skilled salespeople depart their employment or resign swiftly. This creates a tremendous void as a result of their unexpected departure, and the company suffers greatly as a result of their absence. At the same time, massive financial losses were incurred in the development of new employers through detailed and meticulous planning. At this point, it's more necessary to figure out what's causing manufacturing attrition. At the same time, the damage done to the company's reputation and the prestige lost as a result of reference marketing by qualified employees had to be assessed. The worker who leaves the organization still spreads the negative comment through recommendation marketing and demonstrates the hostile work environment. This is also the chief's job to recognize and respond to worker complaints on a timely basis. The current research tries to find a solution to the research objective using the framework outlined above.

1. To investigate the impact of leadership on the elements that contributes to attrition in the Manufacturing sector.

LITERATURE SAMPLES

Sudha et al. (2015) investigated why employees quit their jobs and made recommendations for retaining employees in the retail sector, with a focus on a study of selected organized stores in Salem, Tamilnadu. A total of 150 people were polled from ten well-organized Salem shops. According to the findings, there is a link between corporate objectives and retention, as well as numerous personal factors such as higher education, work development, popularity, and family, all of which have a major impact on the respondent's present employability.

The initial survey was conducted with a questionnaire survey among 156 employees questioned by Rajasshrie Pillai et al (2016) to explore the causes of workforce attrition. Controlled interviews were also conducted to have a better understanding of the HR experience. Their report also talked about the company's workforce goals. Their research focuses on managerial attrition reasons and planned store retention approaches.

METHODOLOGY

For the study, the top 10 manufacturing enterprises in Coimbatore based on turnover are chosen, from which the sample respondents are drawn. Purposive sampling is used to pick 200 respondents who are workers of the select companies. The study's data is obtained using structured questionnaires and sorted in a way that allow for analysis. The study has a restriction in that the data are only available for a specific place.

Analyses and Discussion

Kaiser-Meyer-Olkin (KMO) Measure of Sampling Adequacy

Table 1: KMO and Bartlett's Test

Kaiser-Meyer-Olkin Measure of Sampling Adequacy.		.937
Bartlett's Test of Sphericity	Approx. Chi-Square	265.31
	df	200
	Sig.	.007

The KMO value 0.937 states that the variables chosen for the study are positively correlated with the Bartlett's test of significance value at 0.07 and hence it is valid that Factor Analysis can be performed for the selected variable.

4.5.2 Communalities

Principal Component Analysis can be used to extract the communalities for the variable and that is followed as;

Table 2: Communalities

Factors	Initial	Extraction
Induction and training	1.000	.631
Collective team work	1.000	.581
Leadership	1.000	.636
Innovation	1.000	.723
Lack of Recognition	1.000	.610
Quality of Supervision	1.000	.541
Control	1.000	.609
Job expectations vs reality	1.000	.617
Shifts in Management Strategies	1.000	.539
Career development	1.000	.555
Co-operation	1.000	.609
Family Welfare	1.000	.681
Representation	1.000	.630
Job Satisfaction	1.000	.646
Salary and Benefits	1.000	.591
Job environment	1.000	.599
Meeting deadlines	1.000	.668
Effective communication	1.000	.607
Initiative	1.000	.590

Extraction Method: Principal Source: Primary data

This leads to the verification of individual variances has shown in the communalities that the 19 variables have their variances ranging from 0.541 to 0.723 this implies the 19 variables are statistically significant.

Rotated Component Matrix

Rotated Component Matrix indicated the correlation of each variable with each factor. After factor analysis eight factors have been arrived from nineteen statements. Variable with high factor loading are considered first and have great importance. Such factors are identified and names are given for each factor as follows;

Table 3: Rotated Component Matrix

Factors	Components			Factor name
	1	2	3	
Orientation and initial training	.741			In-house factors
Representation	.692			
Job Satisfaction	.662			
Salary and Benefits	.702			
Quality of Supervision	.631			
Job expectations vs reality	.663			
Shifts in Management Strategies	.602			
Co-operation	.639			
Lack of Recognition		.589		General factors
Control		.612		
Career development		.671		
Family Welfare		.599		
Working environment		.681		
Collective team work			.625	Personal factors
Leadership			.582	
Representation			.571	
Meeting deadlines			.509	
Effective communication			.600	
Initiative			.623	

Extraction Method: Principal Component Analysis.

Rotation Method: Varimax with Kaiser Normalization. a. Rotation converged in 6 iterations.

From the above table it is shown that on the basis of given relationship, eight variables on first factor are loaded and those factors are named as in-house factors. On the Second Factor, five variables are loaded and they are named as general factors. On the Third Factor, six variables are loaded and named as personal factors.

Multivariate analysis of variance to test the impact of attrition on the development and productivity of selected companies

Multivariate Analysis of Variance has been used to analyze the significance of differences between the employees' attrition and the development and productivity of the selected companies.

H₀₁: There is no significant difference between leadership and factors of employees' attrition of the selected companies.

General Linear Model: Leadership styles versus Employees' attrition

Table 4: Multivariate analysis of variance

MANOVA for Employees' attrition S = 2 m = - 0.5 n = 100			
Criterion	Test Statistic	F	P
Wilk's	0.58241	12.56213	0.00**
Lawley-Hotelling	0.41238	9.41241	0.00**
Pillai's	0.72135	10.78412	0.00**
Roy's	0.44563		0.00**

Source: Primary data

The table 2 presents the multivariate analysis between the leadership styles and employees' attrition. It is inferred that the p values are being significant and lead to the rejection of null hypothesis and confined that the various leadership styles will have significant difference in the employees' attrition.

RECOMMENDATION AND CONCLUSION

Over the previous decade, India's manufacturing industry has undergone various transformations, including a major shift in the nature and spread of the globalized economy. India has a robust industry, with clients from various socioeconomic groups all around the country. The proliferated growth of the organized retail business in India has also created the issue of workforce depletion. The huge issue of turnover has risen in today's different company cultures around the world. Workforce turnover has been a modest but steady stumbling block to an organization's growth and competitiveness. Companies must build comprehensive retention strategies to handle the high incidence of attrition. Employees must develop a clear grasp of the job profile and performance evaluation. When responsibilities, skills, and judgment must be dispersed over numerous individuals instead of one, leadership is best practiced as a cooperative and collective role. Finally, manufacturing enterprises in Coimbatore must encourage diversity and devise strategies to retain personnel in a variety of positions, ages, and functional areas by offering resources for their growth and reminding people that they're the only firm's most valuable and important asset.

REFERENCES

1. Alinibzberg 1980, Man and his Work: Managing People at Work, Macmillan Publishing Company Inc., New York.
2. Alshahrani Ahmed Saeed, Alqahtani Abdulaziz Mubark and Alshahrani Bander Sayaf 2015, 'Exploring Human Resource Management System of Saudi Electricity Company', International Journal of Management Science and Business Administration, Vol.1, Issue 5, pp.25-40.
3. Amarja Satish Nargunde 2013, 'Role of hr in retail sector in India', International Journal of Management, Vol.4, Issue 6, pp.221-226.
4. Arunkumar 2017, A study oin employee attrition in organized retailing sector with reference to Coimbatore city, Ph.D.Thesis submitted to Anna University
5. Chih Y, Kiazad K, Zhou L, Capezio A, Li M and Restubog S 2016, 'Investigating Employee Turnover in the Construction Industry: A Psychological Contract Perspective', Journal of Construction Engineering and Management, Vol.142, Issue 6.
6. Lucia Crevani, Monica Lindgren, Johann Packendorff (2010), 'Leadership, not leaders: On the study of leadership as practices and interactions', Scandinavian Journal of Management, 26, 77—86

7. Rajasshrie Pillai, Ravi Teja Mamidi and Hamsini Kuchibhotla 2016, 'A Study of Employee Turnover and Retention Strategies in Organised Retail in Pune City', *MERC Global's International Journal of Social Science & Management*, Vol.3, Issue 3, pp.83-87.
8. Sudha P, Prasannakumaran C & Aswini M M (2015), 'An empirical analysis on employee retention policies of selected organized retailers with special reference to Salem city, Tamilnadu', *Asia Pacific Journal of Marketing & Management Review*, Vol.4, No.1, pp.24-35.
9. Vuyisile Mabindisa 2013, 'Impact of staff turnover on organizational effectiveness and employee performance at the department of home affairs in the eastern cape province', unpublished Dissertation submitted to Durban University of Technology.
10. Yamonaa Thevey 2014, 'A study on employee's turnover intention in banking industry', Thesis submitted to University Utara Malaysia, Kedah.
11. Yongbeom Hur 2007, 'Organizational performance, turnover, and human resource management: Focusing on municipal police services', *University of Kentucky Doctoral Dissertations Paper 524*. http://uknowledge.uky.edu/gradschool_diss/524. Accessed on 24.03.2016.

Static Analysis of Vulnerabilities Using LUA

R Senthilprabha, Ravitha Rajalakshmi N, B Sangeetha and Kaaviya S

Department of IT, PSG College of Technology, Coimbatore 641004

ABSTRACT

As technology advances, cybercrime is becoming more prevalent. New methods for detecting inconsistencies that may harm the network are being developed. Many businesses have utilized vulnerability scanning to detect security flaws. The term "vulnerability" refers to the flaws in a system that allow it to be attacked. Vulnerability assessments allow for the development of current solutions to safeguard the system from being compromised. Several scanners are available now that use a programming language to detect and attack network vulnerabilities. The goal of this paper is to create a vulnerability scanner that uses the host's network functionality to discover security vulnerabilities using LUA scripts. The proposed method can be used to decrease the host's memory footprint.

Indexterms— authorize; cyberspace; scripts; security; scanner; target host; vulnerability

1. INTRODUCTION

Consumer security preferences have become increasingly significant as information technology has advanced. The vast majority of software developers write applications to simply execute them in their intended state, but they are unaware of the numerous security safeguards that must be taken. Developers frequently ignore the flaws brought into the system by the programming language and fail to protect users from the possibility of unwanted access. It becomes evident that new safeguards must be established to protect users from security breaches. In addition to the hazards that users face as a result of software development flaws, network performance plays a key role in jeopardizing their security. Knowledge and a complete understanding of these dangers are required to detect and eliminate them. Understanding how these vulnerabilities function and mitigating risk requires a fundamental understanding of how it manifests themselves in the system, what flaws must be addressed to reduce vulnerabilities, and what alternate options can be formed. The proposed work would create a vulnerability scanner that will use LUA scripts to find faults in the network functionalities of the host and network. The scanner examines various vulnerabilities and reports on whether or not the target host is vulnerable.

II. EXISTING SYSTEM

To gain access to any computer connected to a network, Nessus does remote security scanning. It can scan both inside and outside. The inner scan only scans hosts connected to a router. The outside scan looks for hosts not directly connected to a router (a remote host). Scanning can be done in the initial instance or using a template for a given host. Numerous hosts can also be scanned. Nessus operates by analyzing each port on a system, identifying the service it runs and testing it for vulnerabilities that could be exploited by a hacker to conduct a hostile assault. Nessus is client-server software. Clients control sessions while servers test them. The severity categories are High, Medium, Low, and Informal [2]. Also, results are saved instantly after a host scan. The results are split into two categories: plug-in and host vulnerabilities. The plugins category categorizes all detected vulnerabilities and displays impacted hosts. During the scan, the host category identifies all hosts and vulnerabilities. [12]. It can be exported in any format. Nessus makes no assumptions about the server's setup. It is an extensible open-source project. Incomplete security because vulnerabilities exist until the administrator fixes them. Niko is a command-line scanner for malicious files/CGIs, outdated server software, and other concerns. It inspects both generic and specific servers. It also records and prints any cookies received. It relies on the Perl programming language for several of its capabilities. On-line services such as CGI scripts, Dynamic Web Applications, and Web Server Configurations are susceptible to Nikto. It does it by sending HTTP requests to the webserver and evaluating their responses. It can match patterns in returned responses and accept data from header variables or form submissions. Nikto's scan requests are URLs. A server configuration or web application is detected by Nikto by querying this database. Because of its subtlety, this detection method is trusted [1]. Nikto can also send data to servers using GET variables or POST data. Nikto checks server responses. This allows it to test for cross-site scripting and SQL injection. The application lacks a graphical user interface and is solely command-line driven. In addition to SQL Server, MBSA detects missing security updates and configuration settings for Internet Explorer, Internet Explorer, and the IIS web server [5]. Since SP3, the Windows Update agent determines which security updates are available for MBSA. The VA checks are based on the hard-coded registry and file checks. Some IIS directories have

relatively low permissions, allowing outsiders to make needless changes. Angry IP scanner is a lightweight IP scanner. It can scan an infinite number of IP addresses and ports. It's modest and universal. By pinging an IP address, you may resolve hostname, MAC address, and ports. Plugins help collect more data. Also retrievable are the workgroup name, NetBIOS information, web server detection, and regularly used IP address ranges.

III. PROPOSED SYSTEM

The suggested scanner was written in LUA and includes a Python interface that enables the programmer to determine whether or not a given host is vulnerable. Lua, a lightweight and platform-independent scripting language, is employed. Compilation of Lua programs into bytecode and execution on the Lua virtual machine It is not parsed straight from the Lua text file. Compilation takes place in the background and is completely transparent to the user. To reduce the memory footprint of the host environment it can be done offline by leaving the compiler. Vulnerability scanning scripts are being done using the LUA scripting engine for various network-based vulnerabilities. The basic architecture for the scanner is given in Figure 1.

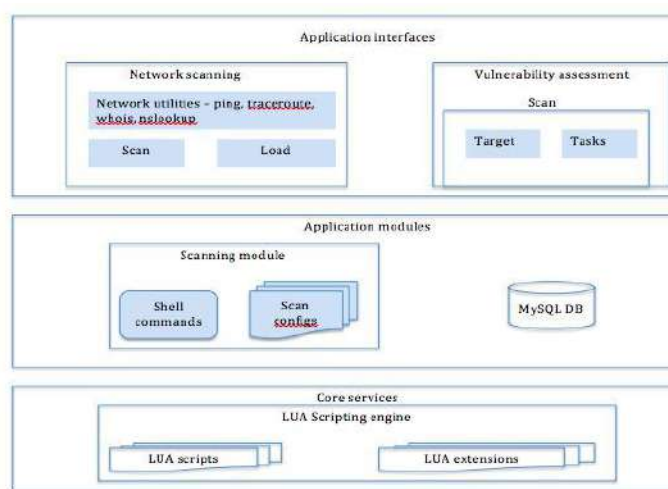


Figure 1. Vulnerability scanner Architecture

IV. IMPLEMENTATION



Figure 2. Vulnerability scanner tool UI

The suggested system employs several vulnerability scanning scripts that are executed against the host to determine its vulnerability. Python is being used to create the user interface. Some of the proposed vulnerability scanning scripts are tabulated in Table 1.

Table 1: Vulnerability scanning scripts

Authen_owners	By contacting an auth daemon running on the target machine, it attempts to determine who owns an open TCP port. Identd, the authentication service, is frequently available on port 113.
Authen_spoof	Identifies the identd server that is spoofing its responses.
Firewalk	It utilizes the IP TTL expiration method, which is usually referred to as firewalking, to identify firewall rules.
Firewalk_bypass	A vulnerability exists in the Netfilter and firewall protocols that can be exploited to open ports dynamically using helpers.
Finger	When the finger service is called, it returns a list of usernames.

Iplic_brute	This was used in iPhoto Library to do brute force password audits.
Dns_zeus	ZTDNS @ abuse.ch can be used to see if a host IP range is part of the Zeus botnet.
Dns_curupdate	In some instances, it may require root capabilities to do a dynamic DNS update.
Dns_rand_srcport	Predictable-port recursion vulnerability found in DNS servers with predictable source ports is susceptible to cache poisoning attacks.
Dns_rand_txid	TXID DNS recursion vulnerability is predictable. Cache poisoning attacks are possible on DNS servers with predictable TXID values.
ftp_lib	Tests for OPIE off-by-one stack overflow in the FTP daemon. If launched on a susceptible target host, this script will crash.
http_authen	Used to gather information about the authentication scheme of a web service. It is also used to find the realm of a web service that needs authentication.
http_authen_finder	Scanning the web for form-based or HTTP-based authentication may help. As a result, a table containing each URL and method is returned.
http_adobe_cold_fusion	By exploiting an authentication bypass vulnerability in Adobe Coldfusion servers, it was possible to get the administrator session cookie.
http_dom_based_xss	Finds places where attacker-controlled DOM information can trivially alter JavaScript execution.
http_fileupload_exploit	Exploits web applications' file upload forms by changing the Content-type header and creating valid picture files with the payload in the comment.
http_google_phish	Used to check if the target hosts are on Google's harmful phishing and malware blacklist. The Google blacklist is part of Google's Safe Browsing service.
http_iis_web_vuln	By searching and attempting to access a password-protected folder it is used to find a vulnerability in IIS 5.1/6.0. The vulnerability allows unwanted users to access secure WebDAV folders.
http_malware_target	Used to find the target host that is being compromised for the malicious purpose by searching for the signature of known server compromises.
http_php_admin_dir_traversal	Used to gather remote files on the webserver by exploiting a directory traversal vulnerability in phpMyAdmin server.
http_shell_shock	This script exploits the "shellshock" vulnerability in web applications. Bash accidentally executes commands when they are appended to the end of function definitions contained in environment variables.
http_stored_xss	Checks for stored XSS on the target host. It occurs when the server retains the attacker's data and displays it on pages returned to other users during normal browsing without adequate HTML escaping. If the script returns an unfiltered answer, XSS.
arises.http_waf_print	Used to find whether a web application firewall is present along with its type and version
telnet_encrypt	This method is used to determine whether the target host is vulnerable to stored XSS. It happens when the attacker's data is retained by the server and is persistently displayed on pages returned to other users during normal browsing without sufficient HTML escaping. If the script produces an unfiltered response, an XSS vulnerability arises.
stuxnet_detection	To realize if the target host has been infected with the Stuxnet worm, use this command.
oracle_stealth	The O5LOGIN flaw connects the session key to a password hash. This script exploits the Oracle O5 LOGIN authentication flaw. An authenticated user gets a salt and session key from the server. A login attempt is not recorded as the script disconnects as soon credentials are received. The session key and salt can be used to find the user's password.
netbus_authen_bypass	Used to find whether the NetBus server allows full access without the password by exploiting an authentication bypass vulnerability.
ajp_authen	Used to gather information about the authentication scheme of Apache

	JServ Protocol. It is also used to find the realm of AJP service that needs authentication.
ajp_brute_force	Used to do brute force auditing of passwords by running against the Apache JServ protocol. The AJP service is usually used by web servers to interact with Java back-end application server containers.
ajp_header	Used to return the server response headers by doing a HEAD or GET request against the root directory or any directory of Apache JServ Protocol server.
ajp_method	Used to list potentially risky methods by sending an OPTIONS request and finds the options supported by the AJP server.
ajp_req	The Apache JServ Protocol accepts URI requests via HEAD, PUT, GET, TRACE, and DELETE. The results are saved. Web servers commonly employ the AJP service to communicate with Java back-end application servers.
http_apache_negotiate	Whether the target HTTP server supports mod negotiate. The script operates by requesting resources like home and index without an extension. The target would respond with a content-location header containing target resources like index.html and "negotiate" if the mod negotiate option is enabled depending on settings.
http_avaya_office_users	Used to capture user data in Avaya IP Office systems. The URI '/system/user/scn user list' returns an XML file providing useful information such as display name, full name, and extension number.
http_awstats_exec	Used to exploit a GETvariable sort in Awstats Totals to allow remote code execution. The script sends a command payload encoded with PHP's chr () function.
http_axis2_traversal	A crafted request to the xsd parameter exploits a directory traversal issue in Apache Axis2. Before exploiting this flaw, extract a genuine service from /listServices. It will try to acquire the Axis2 service configuration file '/conf/axis2.xml' by default using the path '/axis2/services/'.
ms_sql_brute_force	Used to do password guessing against Microsoft SQL Server. When combined with broadcast-ms-SQL-discover script it gives better results.
ms_sql_dac_port	When conventional database connection attempts fail, the Dedicated Admin Connection port is used. For example, when the server runs out of RAM or other issues arise. The DAC port also enables administrators to access system items usually inaccessible. A remote admin connection is enabled by default on the loopback adapter but can be disabled by changing the value to 1. In rare circumstances, the SQL browser may show DAC as available when it is not. This script requests the SQL browser service and connects to the reported port.
ms-SQL-hasdbaccess	Retrieves a user's database access list from MS SQL Server instances. Authentication using SQL Server is required. If a user with the sysadmin server role is present, the script will run. The script attempts to run a command for each set of credentials available by iterating over them.

```

-- PORT      STATE SERVICE
-- 8009/tcp  open  ajp13
-- | ajp-brute:
-- |   Accounts
-- |   root:secret - Valid credentials
-- |   Statistics
-- |_   Performed 1946 guesses in 23 seconds, average tps: 82
    
```

Figure 3. ajp_brute_force scan result


```
Starting Nmap 7.01 ( https://nmap.org ) at 2016-03-21 04:16
Nmap scan report for 192.168.1.2
Host is up (0.00044s latency).
PORT      STATE SERVICE
8009/tcp  closed ajp13

Nmap done: 1 IP address (1 host up) scanned in 13.61 seconds
Kaaviyas-MacBook-Air:Python Kaaviya$ python desk.py
Below is the output from the script in terminal

Starting Nmap 7.01 ( https://nmap.org ) at 2016-03-21 04:27
Nmap scan report for 192.168.1.2
Host is up (0.00052s latency).
PORT      STATE SERVICE
8009/tcp  filtered ajp13

Nmap done: 1 IP address (1 host up) scanned in 2.12 seconds
Kaaviyas-MacBook-Air:Python Kaaviya$
```

Figure 4. ajp-header scan result

```
Starting Nmap 7.01 ( https://nmap.org ) at 2016-03-21 05:17 IST
Nmap scan report for 192.168.1.3
Host is up (0.0015s latency).
Not shown: 993 filtered ports
PORT      STATE SERVICE      VERSION
80/tcp    open  http         Microsoft HTTPAPI httpd 2.0 (SSDP/UPnP)
|_http-server-header: Microsoft-HTTPAPI/2.0
110/tcp   open  pop3?
135/tcp   open  msrpc        Microsoft Windows RPC
139/tcp   open  netbios-ssn Microsoft Windows 98 netbios-ssn
143/tcp   open  imap?
445/tcp   open  microsoft-ds Microsoft Windows 10 microsoft-ds
5357/tcp  open  http         Microsoft HTTPAPI httpd 2.0 (SSDP/UPnP)
|_http-server-header: Microsoft-HTTPAPI/2.0
Service Info: OSs: Windows, Windows 98, Windows 10; CPE: cpe:/o:microsoft:windows, cpe:/o:microsoft:windows_98, cpe:/o:microsoft:windows_10

Service detection performed. Please report any incorrect results at https://nmap.org/submit/ .
Nmap done: 1 IP address (1 host up) scanned in 58.24 seconds
```

Figure 5 . http_awstats_exec scan result

```
Starting Nmap 7.01 ( https://nmap.org ) at 2016-03-21 05:52 IST
Nmap scan report for 192.168.1.3
Host is up (0.00034s latency).
PORT      STATE SERVICE
445/tcp   open  microsoft-ds

Host script results:
| ms-sql-brute:
|   [192.168.1.3\MSSQLSERVER]
|     No credentials found
|     Errors:
|       No network protocols enabled.
|       Failed to load usernames list.
|   [192.168.1.3\MSSQLSERVER007]
|     No credentials found
|     Errors:
|       Failed to load usernames list.
|_

Nmap done: 1 IP address (1 host up) scanned in 1.18 seconds
```

Figure 6. ms_sql_brute_force scan result

§ ms-sql-info

Used to find version and configuration information for Microsoft SQL Server instances. The script uses two ways of getting information regarding the version of SQL Server instances:

a. SQL Server Browser service querying

It provides version information and runs by default on UDP port 1434 on servers that have SQL Server installed. Without affecting the functionality of the instances, this service may be disabled.

b. Sending a probe to the instance

It responds with information including the exact version number. It is the same way that Nmap follows for service versioning. This script can do for pipes (instances accessible via Windows) and can also target instances listed by the SQL Server Browser service.

§ **ms-sql-ntlm-info**

It collects data from remote Microsoft SQL servers that have NTLM authentication enabled. When an MS-TDS NTLM authentication request with an invalid domain and null credentials is received, the remote service will respond with an NTLMSSP response containing information about NetBIOS, DNS, and OS build version.

- s-sql-query

Used to query ms-SQL Server instances.

SQL Server credentials required.

§ **ms-sql-table**

Server is queried for a list of tables for each database. Credentials for SQL Server are required.

This script will only execute against SQL Server services if the mssql. instance-name, mssql. instance-all, and mssql. instance-port script arguments are not provided. Everyone should be able to access the system database table. Iterate over a list of databases with an account that has DB or sysadmin rights to extract table names. As a result, enumeration continues until all tables in all databases have been found. Table 2 shows the final comparison of the vulnerabilities examined by the various scanners.

```
Starting Nmap 7.01 ( https://nmap.org ) at 2016-03-21 09:27 IST
Nmap scan report for 192.168.1.4
Host is up (0.0025s latency).
Not shown: 994 closed ports
PORT      STATE SERVICE  VERSION
80/tcp    open  tcpwrapped
88/tcp    open  tcpwrapped
110/tcp   open  tcpwrapped
143/tcp   open  tcpwrapped
548/tcp   open  afp      Apple AFP (name: Soorya.s MacBook Pro; protocol 3.4; Mac 0:
5900/tcp  open  vnc      Apple remote desktop vnc
Service Info: OS: Mac OS X; CPE: cpe:/o:apple:mac_os_x:10.9, cpe:/o:apple:mac_os_x

Service detection performed. Please report any incorrect results at https://nmap.org.
Nmap done: 1 IP address (1 host up) scanned in 33.65 seconds
```

Figure 7. ms_sql_config scan result

```
ms-sql-config:
[192.168.100.25\MSSQLSERVER]
Databases
  name      db_size  owner
  =====  =====  =====
  nmap      2.74 MB  MAC-MINI\david
Configuration
  name      value    inuse    description
  =====  =====  =====  =====
  SQL Mail XPs 0        0        Enable or disable SQL Mail XPs
  Database Mail XPs 0        0        Enable or disable Database Mail XPs
  SMO and DMO XPs 1        1        Enable or disable SMO and DMO XPs
  Ole Automation Procedures 0        0        Enable or disable Ole Automatio
  xp_cmdshell 0        0        Enable or disable command shell
  Ad Hoc Distributed Queries 0        0        Enable or disable Ad Ho
  Replication XPs 0        0        Enable or disable Replication XPs
Linked Servers
  srvname    srvproduct  providername
  =====  =====  =====
  MAC-MINI  SQL Server  SQLOLEDB
```

Figure 8. ms_sql_dac_port scan result

V. CONCLUSION AND FUTURE WORK

Vulnerability assessment is critical for securing the system's network perimeter. This article discussed a variety of scripts for scanning for vulnerabilities. A thorough investigation of the vulnerabilities that the tool is capable of identifying was conducted by running each script on a variety of vulnerable targets. The data indicate that while the scanner is capable of identifying many types of vulnerabilities, it is not capable of detecting all types of vulnerabilities as a single scanner. If many tools are integrated, the total number of vulnerabilities discovered by each tool will be greater than the number discovered by each tool independently. A thorough understanding of how various scanning tools work may alleviate some of the burden associated with establishing tool

integration by focusing exclusively on specific functionalities. The research is centered on the establishment of a testbed in which various scanners will be combined based on their capabilities.

Table 2 Comparison on Vulnerability Assessment

Scannersrd	Angry IPscanner	Nessus	Nikto	MBSA (only for Windows)	Vulnerability scanner using Lua
Businesslogic web applications		√	√		
Technical vulnerabilities custom web applications		√		√	√
Webserver	√	√	√	√	√
Database	√		√		√
OS	√	√	√	√	√
Network	√	√		√	√
Applications	√		√	√	√

REFERENCES

- Du, Xiaoning, Bihuan Chen, Yuekang Li, Jianmin Guo, Yaqin Zhou, Yang Liu, and Yu Jiang. "Leopard: Identifying vulnerable code for vulnerability assessment through program metrics." In 2019 IEEE/ACM 41st International Conference on Software Engineering (ICSE), pp. 60-71. IEEE, 2019.
- A. Costin, "Lua Code: Security Overview and Practical Approaches to Static Analysis," 2017 IEEE Security and Privacy Workshops (SPW), 2017, pp. 132-142, doi: 10.1109/SPW.2017.38.
- Peng, L. (2019). Attack surface analysis and code coverage improvement for fuzzing. Master's thesis, Nanyang Technological University, Singapore.
- A. Costin, "Lua Code: Security Overview and Practical Approaches to Static Analysis," 2017 IEEE Security and Privacy Workshops (SPW), 2017, pp. 132-142, DOI: 10.1109/SPW.2017.38.
- <https://www.syhunt.com/en/index.php?n=Articles.LuaVulnerabilities>
- Peng Li and Baojiang Cui, December 2010, "A Comparative Study on Software Vulnerability Static Analysis Techniques and Tools", in Proceedings of the IEEE International Conference on Information Theory and Information Security (ICITIS), pp.521-524
- Nilima R. Patil and Nitin N. Patil, April, 2012. "A comparative study of network vulnerability analysis using attack graph", in Proceedings of
- National Conference on Emerging Trends in Computer Technology (NCETCT-2012)
- Xia Yiming, 2006. "Security Vulnerability Detection Study Based on Static Analysis," Computer Science, 33(10), pp. 279-283, Symposium, 18-22 May 2008, pp. 143-157.
- Oleg Sheyner, Joshua Haines, Somesh Jha, R. Lippman, and J. M. Wing, May 2002. "Automated generation and analysis of attack graphs", in Proceedings of IEEE Symposium on Security and Privacy.
- Nilsson J., 2006, "Vulnerability Scanners", Master of Science Thesis at Department of Computer and System Sciences, Royal Institute of Technology, Kista, Sweden.
- Vulnerability assessment tool report, IATAC, 6th edition, 2014.
- Identifying malware by observing abnormalities, White paper, Tenable security.
- Nexpose vulnerability scanning, White paper, Rapid7.
- "Lua 5.1 Reference Manual", 2014.
- https://www.owasp.org/index.php/Vulnerability_Scanning_Tools
- <http://www.lua.org/pil/1.4.html>
- <http://www.tenable.com/products/nessus/nessus-professional>

Ameliorated End-To-End Deep Learning System for Self Learning Cars

R. Thirumahal and Balajimuthazhagan T

Department of Computer Science & Engineering PSG College of Technology, Coimbatore – 641004

ABSTRACT

The introduction of self-driving automobiles in today's society necessitates the development of high-quality algorithms to guide them. Convolutional neural networks are extensively utilised because of their ability to classify images based on observed attributes. The proposed solution entails steering a car autonomously using just the windshield view as input. This is accomplished by using Convolutional neural networks in an end-to-end deep learning strategy, as proposed by NVIDIA for self-driving automobiles. To improve the accuracy of existing models, the neural network will be supported with inputs from image processing modules that identify lane markers and cars. Reduced costs, increased safety, and increased mobility are all advantages of providing such an algorithm for retrofitting existing cars.

Keywords- Autonomous Vehicles, Self-driving car, End-to-End Deep learning, Convolutional Neural Networks, Feature Extraction, Classification Tools

I. INTRODUCTION

Autonomous automobiles, often known as self-driving cars, are vehicles that can steer and drive themselves. For more than a decade, academics and industrial R&D departments have been researching emerging autonomous driving solutions. In the not-too-distant future, Level-3/4 autonomous vehicles may become a reality. A combination of interlocking trends, including the renaissance of deep learning [17], [18], the rapid progression of sensing and in-vehicle computing devices, the accumulation of data with annotations, and technical breakthroughs in related research fields, are the primary reasons for drastic technical achievement in recent years. In research, the levels of automation pertaining to vehicle steering vary from Level 0 (zero autonomous features) to Level 5 (operate entirely without the presence of a driver) with the current multitude of cars operating with an autonomy of Level 1 (driver assistance is mandatory). Various automobile manufacturers and software giants have shown interest in increasing this autonomy for safer travel, lower operational costs, and increased mobility. The goal of this research is to improve an end-to-end deep learning system with assisting image processing modules in order to attain Level 3 autonomy. (automated driving with optional driver engagement). The image processing modules will focus on identifying lane markings and vehicles to suggest the applicable steering angle. Just like in the case of a human driver, the system will receive only the windshield view of the vehicle as input. The system will then predict the direction and a quantified measure of steering. The project is largely inspired by a paper published by NVIDIA towards autonomous steering which prescribes a pure end-to-end deep learning approach. By implementing a better pipeline and having aiding modules on top of it will lead to better prediction of steering angles.

II. LITERATURE REVIEW

A. Autonomous Vehicles

Waymo, Uber, Tesla, Nissan, and other companies are devoting a significant amount of engineering resources to developing self-driving vehicles. Figure 1 depicts the similarities between autonomous cars and human-driven automobiles.

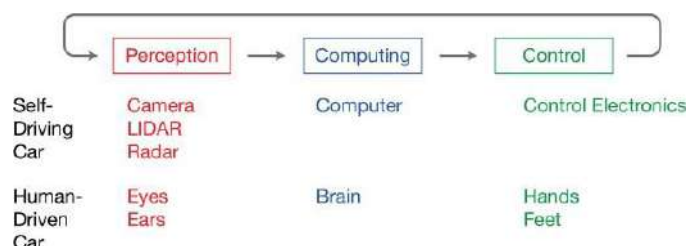


Fig.1 Similarities between Autonomous Vehicles and Human-driven Vehicles.

The entire process of Vehicle steering can be broken up into 3 parts [1]:

- Perception – This refers to the vehicle's ability to receive visual and other important information.

The self-driving car's perception can be achieved through various methods. 360° vision cameras are good in identifying shapes and the corresponding colour of the environment but are not useful in determining the

distance to the objects. LIDAR (Light Detection and Ranging) contains a constantly rotating beam which helps in judging the distance, location of objects and shapes. Radar is used in addition to 360° vision cameras and LIDAR for fine tuning.



- Control – Deals with the mechanical component of driving the vehicle after the computing stage.
- Computing – Deals with how the visual data must be processed in order to acquire meaningful information.

The steering wheel will receive input from the Computing stage in order to steer the vehicle. The three processes can be combined in order to emulate an autonomous vehicle.

B. Convolutional Neural Network Methods

The arduous nature of pattern recognition has been simplified using Convolutional Neural Networks. Before these of CNNs, the entire process used to be split into two parts: Feature extraction and Classification [2]. Through CNN, features can now be automatically learned through training examples.

1) ALVINN

The first approach to using a neural network for autonomous vehicle navigation was ALVINN (Autonomous Land Vehicle in a Neural Network). Pomerleau was the one who came up with it (1989). The model structure was simple, and the network predicted actions from pixel inputs. The predicted actions were then mapped on to typical driving circumstances. It showed that neural networks can be used to create an end-to-end navigation system [3].

2) DAVE

The Defense Advanced Research Projects Agency (DARPA) began an experiment in which a radio-controlled automobile was driven through several locations. The car was also steered with the help of a human being to record the steering angle. Two cameras placed in the front of the vehicle recorded the video input. This along with the steering angle was populated to form the training data [4].

3) DAVE-2 System

The DAVE-2 system was proposed by NVIDIA in 2016. The collection system for the training data is shown in Fig 1

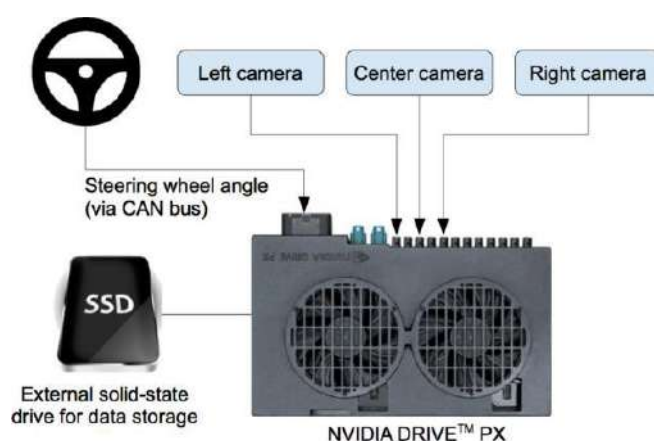


Fig 1. High-level view of the data collection system

Behind the windshield, three cameras are mounted, and timestamped video from the cameras is captured simultaneously with the steering angle applied by the human driver. $1/r$, where r is the turning radius in meters, is used as the steering component to make the calculations independent of the vehicle's geometry [2] [13].

The training data contained images coupled with the respective steering component ($1/r$). Human driven data alone is not enough, the network must be able to recover from the mistakes. Additional images with different steering actions are recorded and are added to the training data in order to make it more reliable [2]. By introducing a varied training data, the model trained will be less prone to errors.

C. Object Localization for Vehicle Detection

Though computer vision is expected to play a large role in self-driving cars, it has low precision, and hence it is coupled with road models, which uses multiple sensors for object detection. The aim is to get the detections using sensors in conjunction with a Kalman filter, and then filter out the false positives using road models. A neural network is used to make predictions and it is trained to predict the depth value of each object based on the labels. Further, a convolutional neural network (CNN) is used to extract the features. Initially, R-CNN used selective search for proposing regions and AlexNet to classify them. But it remained impractical for real-time implementations. Instead, Overfeat architecture has been used due to its high efficacy and ability to make a single forward pass by reusing the layers of the CNN efficiently [5].

While there has been a significant improvement in image recognition systems, the real-time part of it has not been considered. In [5] it has been applied to a laptop GPU which operates at a frequency greater than 10Hz and high image resolutions of 640 x 480. Overfeat CNN detector is used to make a single forward pass by reusing layers of the CNN. It converts an image recognition CNN into a sliding window, which converts the fully connected layers to convolutional layers. A grid of final feature vectors is produced, which is used to predict the presence of an object. After the object has been detected, a single bounding box is predicted using regression, using the same features. The network used in [5] has a context-view of 355 x 355 pixels. There is a problem of ambiguity where the prediction of two bounding box locations for two objects, is incorrectly handled since it predicts that there should be a third box in between [5].



D. End-to-end deeplearningsystem

The task is divided into lane detection [9][15], path planning [15][16], and control logic [7] in the primitive method. Lane keeping is a fundamental feature for self-driving cars. Despite many sensors installed on autonomous cars such as radar, LiDAR, ultrasonic sensor and infrared cameras, the ordinary color cameras are still very important for their low cost and ability to obtain rich information. Given an image captured by camera, one of the most important tasks for a self-driving car is to find the proper vehicle control input to maintain it in lane [6]. The lane markers can be recognised using various image processing techniques such as Hough transform, canny edge detection, and so on. Following that, path planning and control logic can be implemented. The quality of feature extraction and its interpretation of visual data is crucial to the accuracy of such an approach. The rules obtained manually are not perfect and are prone to errors.

Only Convolutional neural networks are used in an end-to-end deep learning strategy to take in images as input and produce the control signal. There is no manual intervention in the model's optimization because it is solely reliant on the training data. This eliminates the need to identify and categorise pre-defined object categories [8].

Before training the CNN model, the data need to be further processed. First of all, to simplify the problem, driving at night is not considered in this paper and all four clips recorded at night are not considered. Second, the data contains many scenarios such as driving forward, changing lanes, making turns, driving on straight or curved roads, driving in normal speed or moving slowly in a traffic jam, etc. To train a lane keeping model, the data that meet the following criteria are selected: driving in normal speed, no lane changes or turns, and both straight and curved roads. Endtoenddeep leaninglargelyreducedthehumanerrorwhichisinvolved.

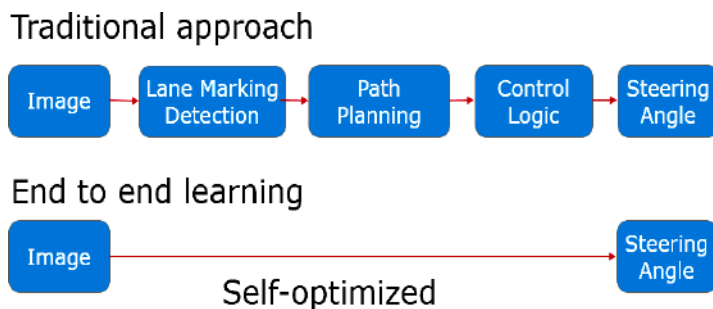


Fig.2.Traditional approachvs Endtoenddeeplearning.

III. SYSTEM DESIGN

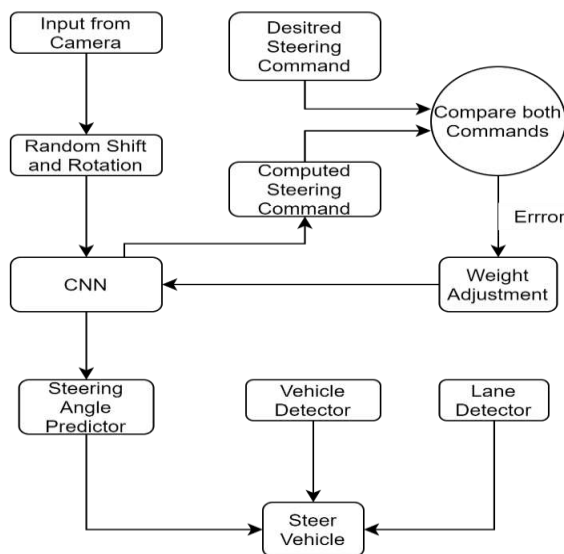


Fig 3. Training the neural network.

Our training system is depicted in Figure 3 as a block diagram. Images are sent into a CNN, which then calculates a steering command. The proposed command for the image is compared to the desired command, and the CNN weights are changed to get the CNN output closer to the desired output. Back propagation is used to make the weight change.

The agent can either be an intelligent agent which is trying to invoke the application backend or an actual user who is trying to interact with the application. Steer Vehicle functionality incorporates inputs from three different functionalities - Steering Angle Predictor, Lane Detector and Vehicle Detector and display the final output. Steering Angle Predictor is responsible for predicting the steering angle from the given input frame. Lane Detector is responsible for identifying the lanes from the given input image. Vehicle Detector functionality is responsible for identifying the vehicles from the given input images using bounding boxes. Then train the model using the neural network and export it. Finally, load the model along with the pre-trained weights

IV IMPLEMENTATION

The entire system can be broadly split up into two majormodules.

1. Steeringanglepredictionusingend-to-endnetworks
2. Straightlinelanetrackingusingimageprocessingtechniques

A. Steering angle predictor using end to end deep learningneuralnetworks

An end-to-end convolutional neural network was used to create the steering angle predictor. The windshield view is taken astheinputandtheneuralnetworkanalyzesandoutputsasteering angle. The datasets used for to deploy and test theSteeringAnglePredictormodules areasfollows:

Table I Datasetsfortrainingend-To-Endcnn

SNo	DatasetName	Alias	Contents
1	RanchoPalosVerdesDataset	D1	45,500images,2.2GB

			Dataformat :filename.jpgangle
2	SanPedroDataset	D2	63,000images,3.1GB
			Data format:filename.jpgangle,year-mm-ddhr:min:sec:millisec

Two CNN Models were considered to implement the end-to-enddeeplearningsystem

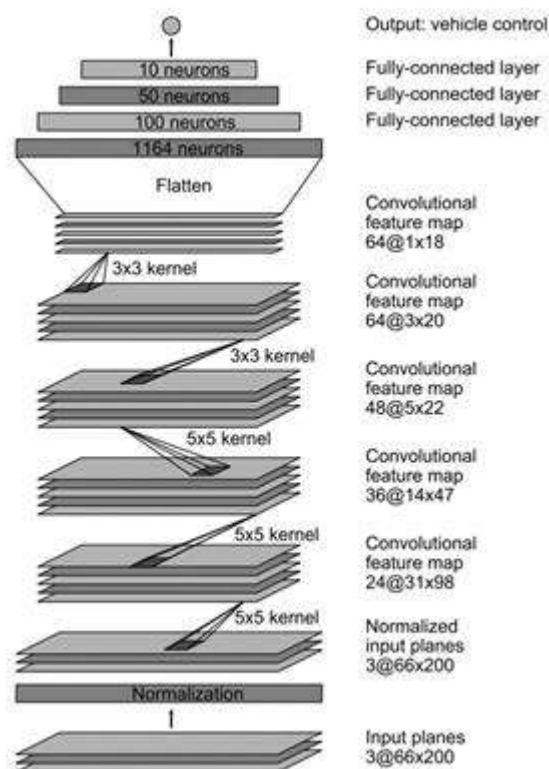


Fig.4.CNN Model1,Architectureproposedin[2]

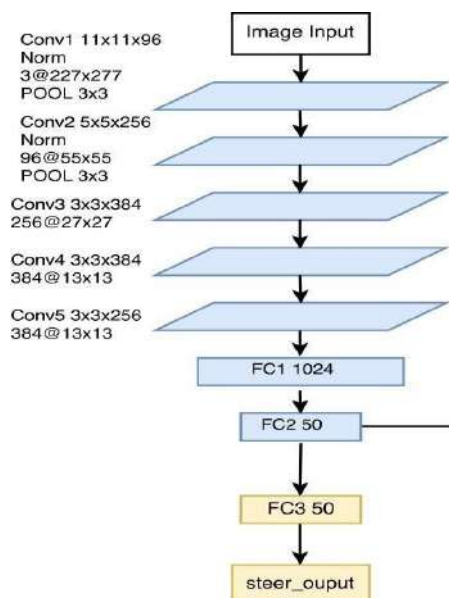


Fig.5.CNN Model2, Architecture proposedin [10][11]

The pipeline was trained, and the model was saved in alocal repository. The summary of the results are tabulated asfollows:

Table. I Rmsevaluesforcnnmodelvsdataset

SNo.	CNNModel	RMSEonD1	RMSEonD2
1	CNNModel1	0.0567	0.2034
2	CNNModel2	0.0789	0.3023

Fig 5 shows that by providing the windshield view as the input, the steering angle is successfully predicted and represented in the form of a steering wheel. The two different datasets covered varied types of lanes ranging from straight lanes to curved lanes. However the RMSE values indicate that the model is not completely accurate and can be improved with the help of aiding modules.



Fig. 6. Steering Angle predictor Implementation.

The model was able to predict good results, however from the tabulation it is imperative that the accuracy of the model should be increased.

B. Straightline lane detection

For lane tracking only image processing techniques were used to identify the yellow and white markings present on the road.



Fig.7. Basic lane detection Implementation.

The straight lines are identified based on the yellow and white markings present on the road.

Table III. Image Processing Techniques Used For Lane Detection

S No.	Methodname	Description
1	RGBtoHLS	The first step is to select only the yellow and white colors of the image. The image is converted from RGB to HLS.
2	Grayscale	The image is thereafter converted into a grayscale format.
3	GaussianBlur	Gaussian smoothing is applied to remove the noise or soft edges since there will be a rapid change in the pixel intensity when a lane is identified.
4	Canny EdgeDetection	The edge detection approach is Canny edge detection.
5	Region of Interest	A region of interest based on the edges of the lane is selected to be processed.
6	Hough Line Transform	Averaging and extrapolating multiple lines which appear in the image: The slopes of all the lines will be found and whichever slope is negative will be considered as a right lane's line and whichever slope is positive will be considered as a left lane's line. Using the polyfit function, the combined slope and intercept values are found out, which will be used for finding out the x and y values separately for both left and right directions.

7	Removing the distortion	Since each camera lens will have some radial distortions it is necessary to remove them. For that, undistort function is used for removing out all the distortions from the image.
8	Image Pre processing	Pre-processing steps are done to the undistorted images and noise is removed.
9	Perspective Transform	When the image is given as input, the lanes will look as if it is going to converge at some point. Because of this, lanes can't be detected properly. So the image is changed to a different perspective, where the image is now seen from the top. This is much easier to isolate the lane lines and to fit the curve.
10	Sliding Window Algorithm	This algorithm is used to find out all the non-zero pixels that are present in the image. Using a histogram the starting point of the lane is identified in both the directions. A box is drawn over the lane and it is restructured based on the lane's direction. The non-zero pixels which are present inside the box are used to plot the curve. Then a curve is fitted in both the directions
11	Plotting it to the image.	A polygon is drawn based on the curve values. After this step the image is turned back to its original perspective: from top-down to front view.
12	Radius of curvature	Radius of curvature is found using a mathematical formula and the offset from the center of the road is calculated. This is used to account for a probabilistic steering angle.

C. Vehicle Object Identification

The feature vector is created by using the method of the Histogram of Gradients (HOG) which uses spatial binning and various parameters like orientation, number of bins, etc. Later the features are extracted, and the hog features of the image is displayed. Support Vector Machine classification algorithm is used for training the data set having 5967 vehicles and 5232 non vehicles. Classifier Accuracy obtained was 98.78%



Fig. 8. Vehicle Detector Module Output

The vehicle detection module draws bounding boxes around the vehicles present in the image. The bounding boxes give an account of whether an obstruction is present in the view or not.

D. Integration of steering angle and lane prediction

The Basic lane detection was successfully integrated with the Steering Angle Prediction module. The below formula from [12] can be used to better the accuracy of the steering angle and reduce the RMSE.



Fig. 9. Steering Angle predictor Implementation.

The model was able to predict good results, however from the tabulation it is imperative that the accuracy of the model should be increased.

Post integration the RMSE values decreased suggesting that the aiding module helped in improving the accuracy of the deeplearningsystem.

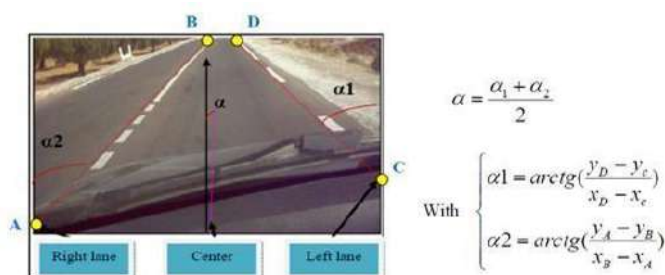


Fig.10.Integrationoflanedetectionwithsteeringangleprediction.

The accuracy of the model increasedwith the help of the aiding module.

Table iv. Rmsevaluesafterintegration

SNo.	CNNModel	RMSEonD1	RMSEonD2
1	CNNModel1	0.0540	0.2019
2	CNNModel2	0.0679	0.3018

E. Final Phase Integration

During the final phase all the three modules were successfully integrated and the steering angle was predicted based on the input of all the three resulting modules. The steering angle predictor backed by end-to-end deep learning network, the vehicle detection and curved lane tracking modules backed by image processing techniques has improved the overall prediction of the system.



Fig 11. Final integration output

From the figure we can see that all the three modules were combined into a single pipeline. The pipeline executes all the three modules simultaneously and arrives at the steering angle.

IV. CONCLUSIONANDFUTUREWORK

Theend-to-enddeeplearningsystemwassuccessfullyintegrated with the aiding module and was able to lower theRMSE values.This suggests that by coupling image processing modules with a deep learning model, we are able to achievebetterresultsthanexistingmodels.

Reduced costs, increased safety, and increased mobility are all advantages of providing such an algorithm for retrofitting existing cars.Theproject focused on particular datasets with suitable lightingconditions and lowerobstructions. However,by enforcing a longer training time on varied datasets this restriction can beremoved.

Future work includes the integration of an advanced lanefinding model along with vehicle detection strategies in ordertofurtherincreasingtheaccuracyofexistingmodules.

REFERENCES

- 1 Science in the News. (2018). Self-driving Cars: The technology, risks and possibilities - Science in the News. [online] Available at:<http://sitn.hms.harvard.edu/flash/2017/self-driving-cars-technology-risks-possibilities/> [Accessed 17 Dec. 2018].
- 2 Bojarski, M., Del Testa, D., Dworakowski, D., Firner, B., Flepp, B., Goyal, P., Jackel, L.D., Monfort, M.,

- Muller, U., Zhang, J. and Zhang, X., 2016. End to end learning for self-driving cars. arXiv preprint arXiv:1604.07316.
- 3 Pomerleau, D.A., 1989. Alvin: An autonomous land vehicle in a neural network. In *Advances in neural information processing systems* (pp. 305- 313).
- 4 Net scale Technologies. Autonomous off-road vehicle control using end- to-end learning, July 2004. [online] Available at: <http://net-scale.com/doc/net-scale-dave-report.pdf> [Accessed 19 Dec. 2018].
- 5 Huval, B., Wang, T., Tandon, S., Kiske, J., Song, W., Pazhayampallil, J., Andriluka, M., Rajpurkar, P., Migimatsu, T., Cheng-Yue, R. and Mujica, F., 2015. An empirical evaluation of deep learning on highway driving. arXiv preprint arXiv:1504.01716.
- 6 Chen, Z. and Huang, X., 2017, June. End-to-end learning for lane keeping of self-driving cars. In *Intelligent Vehicles Symposium (IV), 2017 IEEE* (pp. 1856-1860). IEEE.
- 7 Humaidi, A.J. and Fadhel, M.A., 2016, May. Performance comparison for lane detection and tracking with two different techniques. In *Multidisciplinary in IT and Communication Science and Applications (AIC-MITCSA), Al-Sadeq International Conference on* (pp. 1-6).IEEE.
- 8 The comma.ai driving dataset. [Online]. Available: <https://github.com/commaai/research> [Accessed 22 Dec. 2018].
- 9 A. J. Humaidi and M. A. Fadhel, "Performance comparison for lane detection and tracking with two different techniques," in *2016 Al-Sadeq International Conference on Multidisciplinary in IT and Communication Science and Applications (AIC-MITCSA)*, May 2016, pp. 1–6
- 10 Yang, Z., Zhang, Y., Yu, J., Cai, J. and Luo, J., 2018, August. End-to- end Multi-Modal Multi-Task Vehicle Control for Self-Driving Cars with Visual Perceptions. In *2018 24th International Conference on Pattern Recognition (ICPR)* (pp. 2289-2294). IEEE.
- 11 Ferreira, A., Almeida, A. and Vidal, F. (2018). Autonomous Vehicle Steering Wheel Estimation from a Video using Multichannel Convolutional Neural Networks. *Proceedings of the 15th International Conference on Informatics in Control, Automation and Robotics*.
- 12 Hechri, A. and Mtibaa, A., 2011. Lanes and road signs recognition for driver assistance system. *IJCSI international journal of computer science issues*, 8(6).
- 13 H. Xu, Y. Gao, F. Yu, and T. Darrell, "End-to-end learning of driving models from large-scale video datasets," in *CVPR*, 2017.
- 14 J. Zhao, B. Xie, and X. Huang, "Real-time lane departure and front collision warning system on an fpga," in *2014 IEEE High Performance Extreme Computing Conference (HPEC)*, Sept 2014, pp. 1–5.
- 15 C. Li, J. Wang, X. Wang, and Y. Zhang, "A model based path planning algorithm for self-driving cars in dynamic environment," in *2015 Chinese Automation Congress (CAC)*, Nov 2015, pp. 1123–1128.
- 16 S. Yoon, S. E. Yoon, U. Lee, and D. H. Shim, "Recursive path planning using reduced states for car-like vehicles on grid maps," *IEEE Transactions on Intelligent Transportation Systems*, vol. 16, no. 5, pp. 2797–2813, Oct 2015.
- 17 I. Goodfellow, Y. Bengio, and A. Courville, *Deep Learning*. MIT Press, 2016, <http://www.deeplearningbook.org>.
- 18 Y. Jia, E. Shelhamer, J. Donahue, S. Karayev, J. Long, R. B. Girshick, S. Guadarrama, and T. Darrell, "Caffe: Convolutional architecture for fast feature embedding," *CoRR*, vol. abs/1408.5093, 2014.

Predicting Autism Spectrum Disorder Using Stacking Based Ensemble Model

K. Anitha Kumari, V. Nivethidha, D. Apoorva, T. Subitsha and S. Muhil Varsini

Department of IT, PSG College of Technology, Coimbatore, India

ABSTRACT

Autism Spectrum Disorder(ASD) is a group of developmental disorders that result in behavioral and social challenges to the ones that possess them. Patients with ASD are different from most others in the manner they interact, communicate, learn and behave. They struggle with various routine chores and often need extra care. ASD is often misapprehended as an Intellectual Disability. Some people with ASD may show high intelligence while others do not. Some do well during social interactions while others do not. This kind of unpredictable and wide range of symptoms and characteristics are denoted by the term spectrum in Autism Spectrum Disorder. Due to the complexity and variety of ASD, it commonly takes a long term from detection of the behavioral symptoms and symptoms to the definitive diagnosis, which unavoidably ends in the lagging of crucial remedies or intervention. Early confirmation of ASD will improve the general mental wellness of the patients. With the advancement of machine learning, it has become possible for neurologists to use machine-learning algorithms to perform early diagnosis of ASD. In this paper, an effective classifier model based on ensemble learning is applied to predict the presence of ASD with more accuracy. In the stacking-based ensemble, heterogeneous weak learning models work in parallel. The individual outputs are combined by training a meta-model to predict based on the different weak models' predictions. XGBoost is used as the meta-model as it performs various system optimizations and algorithmic enhancements. The results show that stacking with XGBoost achieves higher accuracy compared to individual classifier models.

Keywords— Autism Spectrum Disorder [ASD], Supervised Machine Learning, Ensemble learning, Stacking, XGBoost.

I. INTRODUCTION

Neurodevelopmental disorders predominantly affect the performance of one's nervous system, especially the brain. They can range from mild disabilities, allowing the affected people to live comparatively normal lives, to severe impacts that require lifelong monitoring and care. One such kind of neurodevelopmental disorder, ASD is defined by significant behavioural, social and communication challenges. It is usually a life-long condition. It includes a wide range of disorders like Asperger's syndrome, autistic disorder, childhood disintegrative disorder etc. Despite the fact that persons with ASDs have some symptoms, ASDs impact different people in different ways [10]. The symptoms may range from mild to severe in patients. Due to this very reason, the treatment plan is individualized to meet specific needs. There is currently no single danger element that is sufficient to produce ASD. As a result, each individual is likely to be affected by a combination of genetic and environmental risk factors. Sometimes ASD diagnosis is skipped until adolescence or adulthood, especially in those kids with better adaptive functions and subtle symptoms. Receiving an earlier diagnosis of ASD has a significant impact on an individual, especially their family, which helps them seek the required help and support that the child needs [14]. But diagnosing ASD is lengthy, time-consuming, and a complex process that requires specific clinical expertise.

When machine learning methods are used in predicting diseases, they give preferable results [16][20]. Recently, many machine learning and deep learning algorithms [8] are employed to indicate the presence of ASD in children. In this paper, an effective stacking-based ensemble model is suggested using XGBoost as a meta-learner and other classifier models like SVM, LDA, KNN, Decision tree, Naïve Bayes, and Random Forest as base-learners [19]. Each of these classifier models is diverse in its way and work well on a certain type of data. As an ensemble machine learning algorithm [15], the Stacking method has a higher prediction accuracy than a single learning algorithm. And XGBoost is a straightforward, robust, and sparsity-aware algorithm [18].

II. LITERATURE SURVEY

Several papers and applications on ASD and Ensemble learning have been used as a reference for this paper. The inferences gained from the research are discussed below.

K. S. Omar, P. Mondal, N. S. Khan, M. R. K. Rizvi and M. N. Islam built a model for predicting autism that combines Random Forest-CART (CART-Classification and Regression Trees) and Random Forest-Id3(Id3-Iterative Dichotomiser) to predict ASD for individuals irrespective of age. With respect to the evaluation metrics, the proposed prediction model significantly outperforms other models (False Positive Rate). [1].

S. Mostafa, L. Tang and F. Wu generated neural network-based characteristics for the diagnosis of ASD in this study. The 264 region-based parcellation approach was used to construct a brain network that was tested using a functional magnetic resonance imaging (fMRI) scan. The 264 eigenvalues of the brain network's Laplacian matrix were then used to produce 264 raw brain characteristics, while network centralities were used to define three additional features. The study results in identifying 64 discriminating features using a feature selection technique. Furthermore, using the ABIDE (Autism Brain Imaging Data Exchange) dataset, multiple machine learning models were trained for diagnosing ASD. The linear discriminant analysis produced a higher accuracy with our derived features [2].

To find gene biomarkers using genomic data, Sekaran, K, and Sudha devised a unique gene selection technique. The pattern of gene expression demonstrates a strong association between genes linked to a variety of disorders. However, gene expressions are very marginally influenced by irregular molecular interactions and reactions that occur throughout the transcription process. It has an adverse influence on the detection of disease-related biological markers. The proposed system here helps to overcome this defect [3].

Ray C, Kumar Tripathy H and Mishra S. Bhateja V., Satapathy S., Zhang YD., Aradhya V suggested a machine learning-based approach to assess autistic disorder. It is concerned with the categorization of datasets of suspected autistic patients using many classifiers in the WEKA tool, in order to uncover the model with greater accuracy and precision, allowing one to predict whether or not the child is truly autistic [4]. A general review of predicting autism spectrum disorder is performed by Kalpana and Anitha Kumari [19].

Yufei Wang, Jianxin Wang, Fang-Xiang Wu, Rahmatjan Hayrat, and Jin Liu studied on how to identify autism spectrum disorder. This paper presents an approach to identify ASD using ensemble learning and multi-atlas deep feature representation. The multi-atlas deep feature representation method with stacked denoising auto-encoder aids in obtaining additional discriminative features for ASD detection. A model combining multilayer perceptron and ensemble learning performs the final ASD identification challenge [5].

III. PROPOSED SYSTEM

The system's flow is represented in Fig 1. The phases involved are Data Collection, Data Preprocessing, Training Base learners and Meta learner models, Result Evaluation and Prediction of ASD. The project is implemented in Python. The data is collected from four datasets of UCI public repository.

A) Dataset Description:

The dataset for this research was obtained from the UCI repository which is public. The dataset has 20 attributes in which ten are behavioural attributes and remaining are individual characteristics. The attribute types are continuous, categorical and binary. The various attributes included are shown in the Table 1.

The ASD questionnaires are used to assess whether the people have any autistic traits in them. This questionnaire test does not require any specific knowledge. Anyone who knows the person can take the test for them. It is not used to diagnose individuals for ASD because there may be some wrong judgments from people. It is only developed as a screening tool which helps clinicians to take further steps [6].

DATASET ATTRIBUTES AND TYPES

Attribute	Type
Age	Number
Gender	String
Ethnicity	String
Inbred with jaundice	Boolean (0,1)
Kith and Kin with PDD	Boolean (0,1)
Who is finalizing the test	String
Country	String

First time user or not	Boolean (0,1)
Type of the Screening Method	Integer
Question 1 - 10 Answers	Binary (0, 1)
Screening Score	Integer

B) Data Preprocessing

Data preprocessing includes handling missing data, noisy data and transforming data into appropriate forms suitable for machine learning. Usually, real world dataset often contains noise and unrelated data. Hence, data pre-processing becomes an essential process before training the model with the data. For pre-processing, the null values are removed along with the insignificant features in the dataset. The dataset is partitioned into training and testing datasets after it has been pre-processed.

C) Base Learner Algorithms

The base learner models – SVM(Support Vector Machine), LDA(Linear Discriminant Analysis), KNN(K-nearest Neighbors), Random Forest, Naïve Bayes, Decision Tree are trained with the training set[13].

a) *SVM-Support Vector Machine*: SVM is a supervised linear model. Though it is specifically used in classification problems, it can also be used to regression challenges. In SVM, each data item is represented as a point in a multi-dimensional space, with the number of dimensions equaling the number of features, and the value of each and every feature denoting the value of a certain coordinate. Then, the hyper-plane is found to perform classification. This hyper-plane differentiates the two classes. The coordinates of individual observation are the support vectors. Hyperplanes or lines are used to classify the dataset classes.

b) *Random forest*: Random forest is a supervised learning method that has been used for classification and regression[7], but it is most commonly employed for classification. A forest is made up of many solitary trees, and the number of separate trees enhances the strength of the forest. Similarly, in the random forest technique, several decision trees are formed using data samples, after which each decision tree's prediction is obtained, and final voting is utilised to determine the best option. Overfitting in a random forest is mitigated by averaging the findings of many decision trees, resulting in better results than a single decision tree. [12].

c) *Linear discriminant analysis*: Linear discriminant analysis is a technique for identifying linear combinations of characteristics that distinguish various classes. The linear classifier uses a mixture of the results. The LDA classes are widely dispersed. LDA, like principal component analysis, can be used to reduce dimensionality and classify data [11]. The prior probability for class 1 and class 2 are p_1 and p_2 , respectively, for a dataset with two classes; μ_1 , μ_2 , and μ are the class means and overall mean respectively; and cov_1 and cov_2 are the class variances respectively.

$$\mu = p_1 \times \mu_1 + p_2 \times \mu_2 \quad (1)$$

Within-class and between-class scatters should then be used to express the required requirements for class separability. The scatter measure calculation for a multiclass case is presented below:

$$S_w = \sum_{j=1}^n p_j cov_j \quad (2)$$

where n denotes the no of classes and

$$cov_j = (x_j - \mu_j)(x_j - \mu_j)^T \quad (3)$$

The calculation for between-class scatter is shown as follows:

$$S_b = \frac{1}{n} \sum_{j=1}^n (\mu_j - \mu)(\mu_j - \mu)^T \quad (4)$$

The next step is to find a discriminant plane that maximises the ratio of between-class to within-class scatters:

$$J_{LDA} = \frac{w S_b w^T}{w S_w w^T} \quad (5)$$

d) *Decision tree*: Decision tree is a supervised learning algorithm in machine learning. Although it is mainly used for addressing Classification problems, it is also used to solve Regression problems. Decision is a tree-structured classifier in which the internal nodes reflect dataset attributes, branches represent decision rules, and each leaf node represents the conclusion. It is a graphical depiction that presents all viable solutions to a problem/decision for a particular situation

e) *K-Nearest Neighbor*: KNN can be applied for classification[17] as well as regression problems. It is the most commonly used model for classified problems since the computation time is less compared to algorithms. K-NN presumes that comparable things lie in close contiguity, that is comparable matters are close to each other. It uses of similarity of characteristics to anticipate the values. Euclidean distance is used to calculate the distance between test dataset and training dataset.

f) *Multinomial Naive Bayes*: Multinomial Naive Bayes is an algorithm which uses probabilistic classifier. This is most preferably used in NLP and classification problems. Bayes theorem is base for this algorithm. This is used to predict the tag of a text then for all tags its probability is calculated, finally the tag which has more probability is produced as result. Naive Bayes classifier is a assortment of different algorithms in which one common principal is shared by all the algorithms, and which implies every character being classified isn't relating to the other character. If one feature is present or absent it is not related if the other feature is present or absent.

D) Ensemble Learning Technique – Stacking

Stacking comes under one of the ensemble machine learning algorithms. It is used when the multiple machine learning models have skill on the dataset in distinct ways. Stacking is an advanced implementation of Model Averaging Ensemble technique. In this technique each sub-models contributes equally and with respect to their performance weights to a combined prediction. The contributions from each sub model are combined to train an entirely new model(meta-learner) and generate the best predictions. The final model is stacked on top of other models; hence it is called stacking.

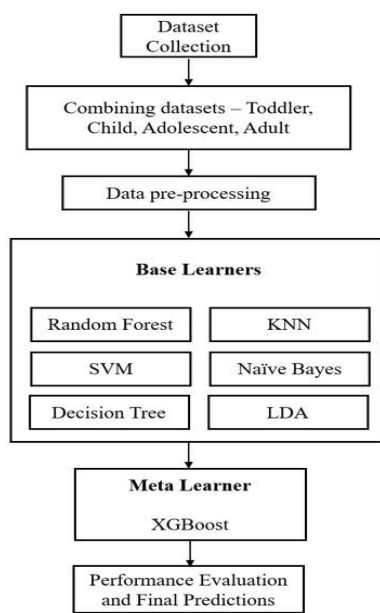


Fig.1 System Design

E) Meta learner

XGBoost is an improvised technique of the gradient boost algorithm and its open-source. Multiple decision trees are blended and that is used to provide one final prediction in the Gradient Boosting Machine. Gradient boost calculates a target variable by blending the results of various simpler, weaker models accurately.

The training is accomplished iteratively through including new trees that are used to find the residuals and the mistakes of earlier trees that are then combined with the preceding trees and this is used to calculate the final prediction. This set of rules is referred to as gradient boosting as it follows a gradient descent algorithm to decrease the loss while including new models.

XGBoost, a library of gradient boosting methods, is employed as a meta learner. XGBoost is specifically designed for today's data science concerns and technologies. It makes use of boosting algorithms and is

available in an easy-to-use library. XGBoost has several advantages, including being highly scalable, parallelizable, and quick to perform. It typically outperforms many other algorithms because it has excessive predictive strength and is sort of 10 instances quicker than the alternative gradient boosting strategies.

The predictions from the base learners are used as an input to the meta learner which is XGBoost and final predictions are made from the meta learner.

IV. Result Analysis

Fig 2 shows the proportion of ASD cases with normal cases for the chosen dataset.



Fig2. ASD class with yes and no

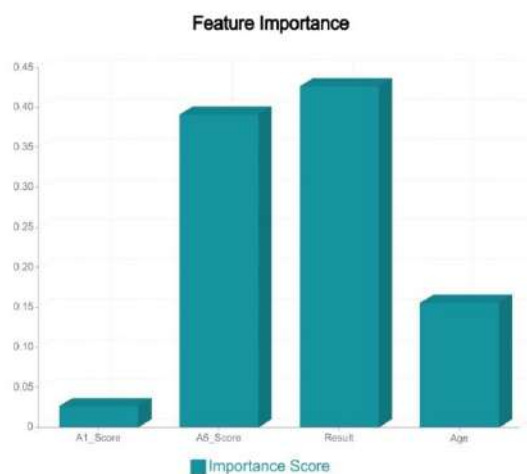


Fig.3 Four most important features of Stacking + XGBoost model

Identifying the features that are most important in determining the outcome are also of great importance. Fig 3 shows the score of the four most important features of the chosen dataset - A1 Score, A2 Score, Questionnaire result and Age.

In this paper, accuracy [9], f1 score, precision, specificity and recall are considered for analysing performance of the classifiers.

1) Accuracy: It answers the question 'How many children have been correctly predicted?'

$$\text{Accuracy} = (\text{TN} + \text{TP}) / (\text{FN} + \text{TN} + \text{TP} + \text{FP})$$

where,

TP denotes True Positive,

TN denotes True Negative,

FP denotes False positive,

FN denotes False Negative,

2) **Precision:** 'How many of those who were labelled as having ASD are affected by ASD?'

$$\text{Precision} = \text{TP} / (\text{FP} + \text{TP})$$

3) **Recall:** 'Among all the people who are affected by ASD, how many of those have been correctly predicted by the model?'

$$\text{Recall} = \text{TP} / (\text{FN} + \text{TP})$$

4) **F1-score:** It is the mean of the recall and precision.

$$\text{F1 Score} = 2 * (\text{P} * \text{R}) / (\text{P} + \text{R})$$

where P denotes Precision and R denotes Recall.

5) **Specificity:** 'Of all the people who do not suffer from ASD, how many of those did the model correctly predict?'

$$\text{Specificity} = \text{TN} / (\text{TN} + \text{FP})$$

SVM, LDA, KNN, Random Forest, Decision tree, Naive Bayes, Stacking with XGBoost - all these models are compared by these performance analysis as shown in Table 1 and Fig 4.

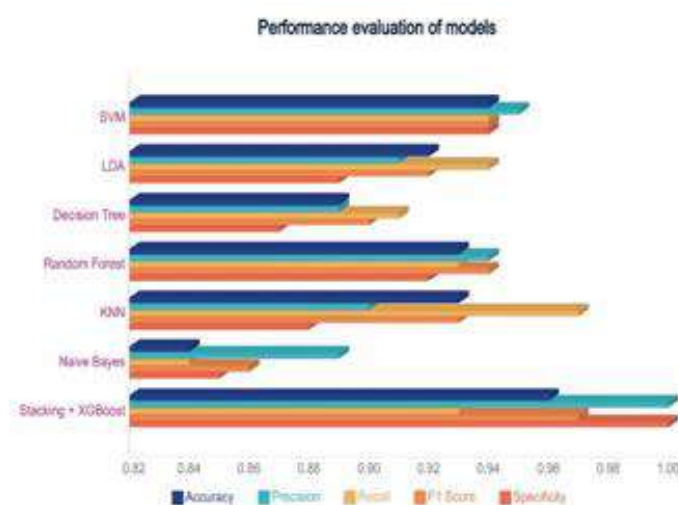


Fig.4 Comparison of algorithms based on evaluation metrics

Table 1 Performance ANALYSIS of different classifiers

Algorithm	Accuracy	Precision	Recall	F1 Score	Specificity
SVM	0.94	0.95	0.94	0.94	0.94
LDA	0.92	0.91	0.94	0.92	0.89
Decision Tree	0.89	0.89	0.91	0.90	0.87
Random Forest	0.93	0.94	0.93	0.94	0.92
KNN	0.93	0.90	0.97	0.93	0.88
Naive Bayes	0.84	0.89	0.84	0.86	0.85
Stacking+ XGBoost	0.96	1.00	0.93	0.97	1.00

KNN algorithm shows high recall as 97%. Stacking with XGBoost algorithm shows the high accuracy as 96%, high precision and sensitivity as 100%, and high f1 score as 97%. Thus, stacking with XGBoost model surpasses the other classifier models with respect to precision, accuracy, F1 score and specificity.

V. CONCLUSION

In this proposed work, prediction of ASD was done using different machine learning techniques and a stacking-based ensemble technique. Numerous evaluation indicators were utilised to assess the efficacy of the models deployed for ASD prediction using a combined dataset from four age groups: toddlers, children, adolescents, and adults. While comparing the various models, the stacking-based ensemble method with XGBoost gave a higher accuracy when compared with other models. This result strongly suggests that the proposed model can be preferred over conventional machine learning classifiers. Clinicians can make better decisions with such a high-performing model. This way, ASD can be quickly diagnosed; and the needs of ASD-affected children can be aptly met.

REFERENCES

- 1 K. S. Omar, P. Mondal, N. S. Khan, M. R. K. Rizvi and M. N. Islam, "A Machine Learning Approach to Predict Autism Spectrum Disorder", International Conference on Electrical, Computer and Communication Engineering (ECCE), IEEE, pp. 1-6, 2019.
- 2 S. Mostafa, L. Tang and F. Wu, "Diagnosis of Autism Spectrum Disorder Based on Eigenvalues of Brain Networks", IEEE Access, vol. 7, pp. 128474-128486, 2019
- 3 Sekaran, K., Sudha, M. "Predicting autism spectrum disorder from associative genetic markers of phenotypic groups using machine learning", J Ambient Intel Human Comput 12, pp. 3257–3270, Springer, 2021.
- 4 Ray C, Kumar Tripathy H & Mishra S, "Assessment of Autistic Disorder Using Machine Learning Approach", In: Bhateja V., Satapathy S., Zhang YD., Aradhya V. (eds) Intelligent Computing and Communication. ICICC. Advances in Intelligent Systems and Computing, vol 1034, Springer, Singapore, 2019.
- 5 Yufei Wang, Jianxin Wang, Fang-Xiang Wu, Rahmatjan Hayrat & Jin Liu, "AIMAFE: Autism spectrum disorder identification with multi-atlas deep feature representation and ensemble learning", Journal of Neuroscience Methods, Volume 343, Elsevier, 2020.
- 6 Granpeesheh, Dennis Dixon and Erik Linstead, "A cluster Analysis of challenging Behaviors in Autism Spectrum Disorder". 2017 16th IEEE International Conference on Machine Learning and Applications (ICMLA), 2017.
- 7 Omar, K. S., Mondal, P., Khan, N. S., Rizvi, M. R. K., & Islam, M. N.,—A Machine Learning Approach to Predict Autism Spectrum Disorder. 2019 International Conference on Electrical, Computer and Communication Engineering (ECCE). doi:10.1109/ecace.2019.8679454, 2019.
- 8 Heinsfeld, A. S., Franco, A. R., Craddock, R. C., Buchweitz, A., & Meneguzzi, F. — Identification of autism spectrum disorder using deep learning and the ABIDE dataset. NeuroImagel: Clinical, 17, 16–23. doi:10.1016/j.nicl.2017.08.017, 2018.
- 9 Duda, M., Kosmicki, J. A., & Wall, D. P., — Testing the accuracy of an observation-based classifier for rapid detection of autism risk. Translational Psychiatry, 4(8), e424–e424. doi:10.1038/tp.2014.65, 2014.
- 10 Kosmicki, J. A., Sochat, V., Duda, M., & Wall, D. P. — Searching for a minimal set of behaviors for autism detection through feature selection-based machine learning. Translational Psychiatry, 5(2), e514–e514. doi:10.1038/tp.2015.7, 2015.
- 11 Jain, A., & Huang, J., — Integrating independent components and linear discriminant analysis for gender classification. Sixth IEEE International Conference on Automatic Face and Gesture Recognition, 2004. Proceedings. doi:10.1109/afgr.2004.1301524, 2004.
- 12 Aparna Shenoy, K.V. Viswanatha, Raju Ramakrishna Gondkar, "Early Sepsis Prediction in Intensive Care Patients using Random Forest Classifier", International Journal of Computer Sciences and Engineering, Vol.8, Issue.1, pp.17-22, 2020.
- 13 Hyde, K. K., Novack, M. N., LaHaye, N., Parlett-Pelleriti, C., Anden, R., Dixon, D. R., & Linstead, E., — Applications of Supervised Machine Learning in Autism Spectrum Disorder Research: a Review. Review Journal of Autism and Developmental Disorders. doi:10.1007/s40489-019-00158-x, 2019
- 14 Stevens, E., Atchison, A., Stevens, L., Hong, E., Granpeesheh, D., Dixon, D., & Linstead, E., — A Cluster Analysis of Challenging Behaviors in Autism Spectrum Disorder. 2017 16th IEEE International Conference on Machine Learning and Applications (ICMLA). doi:10.1109/icmla.2017.00-85, 2017.
- 15 Rakhimberdina, Zarina, Xin Liu, and Tsuyoshi Murata. 2020. "Population Graph-Based Multi-Model Ensemble Method for Diagnosing Autism Spectrum Disorder" Sensors 20, no. 21: 6001. <https://doi.org/10.3390/s20216001>
- 16 Pal, R., Poray, J., & Sen, M, — Application of machine learning algorithms on diabetic retinopathy. 2017 2nd IEEE International Conference on Recent Trends in Electronics, Information & Communication Technology (RTEICT). doi:10.1109/rteict.2017.8256959, 2017.

- 17 Altay, O., & Ulas, M., —Prediction of the autism spectrum disorder diagnosis with linear discriminant analysis classifier and K-nearest neighbor in children. 2018 6th International Symposium on Digital Forensic and Security (ISDFS). doi:10.1109/isdfs.2018.8355354, 2018.
- 18 Budholiya, Kartik & Shrivastava, Shailendra & Sharma, Vivek. (2020). An optimized XGBoost based diagnostic system for effective prediction of heart disease. Journal of King Saud University - Computer and Information Sciences. 10.1016/j.jksuci.2020.10.013.
- 19 Kalpana, C., & Anitha Kumari K., — Predicting Autism Spectrum Disorder Using Machine Learning Algorithms: A Review. International Journal of Computer Sciences and Engineering [IJCSE], vol.8, iss 5, 2020, pp.no: 31 – 36, doi: <https://doi.org/10.26438/ijcse/v8i5.3136>
- 20 Sonar, P., & JayaMalini, K., — Diabetes Prediction Using Different Machine Learning Approaches. 2019 3rd International Conference on Computing Methodologies and Communication (ICCMC). doi:10.1109/iccmc.2019.8819841, 2019.
- 21 C. Amuthadevi, D. S. Vijayan, Varatharajan Ramachandran, “Development of air quality monitoring (AQM) models using different machine learning approaches”, Journal of Ambient Intelligence and Humanized Computing, <https://doi.org/10.1007/s12652-020-02724-2>

Color Correction Using Color Checkers

Senthil Kumaran V and Hashini S. S

Department of Applied Mathematics and Computational Sciences, PSG College of Technology, Coimbatore – 641 004, India

ABSTRACT

In this work, we present a simple but a different approach to correct colors of digital photographs. Pictures taken on digital cameras do not portray the actual colors of the photo that a naked eye can see. This is because of the surroundings and the lighting conditions a photo is captured in. The problem of colors is solved here using an external component called a color checker. The algorithm takes 2 inputs and gives a color corrected output which helps photographers and a few other areas of work where pictures play an important role. The method we propose has been tuned and tested on various image data. The paper deals with image processing and machine learning for color calibration and to detect the colorchecker on the target image and uses Python programming language to get the output.

Keywords — Color Correction, Macbeth Colorchecker, Xrite, DotProduct, EigenValues, Color Pixel Values, WhiteBalance, ColorCast

1. INTRODUCTION

Photographs are a story that we fail to put in words. A picture holds a million emotions. A camera in which the picture is taken is light sensitive [1]. The changes in colors of images are dependent not only on the surface properties of the objects in the frame, but also depends mainly on the lighting conditions which are like the angle the object is placed, the illuminant colors etc., and on the characteristics of the digital camera we use. Human vision brilliantly captures the true colors but imaging devices do not do so because they cannot easily adapt to the spectral responses to cope up with different conditions and as a result, the digitised image creates an undesirable shift in the entire color range. The great spread of digital cameras, be it Dslr's or a simple phone camera have brought in a new era for digital images depicting a huge variety of subjects. In this frame of reference, we have developed an algorithm that makes it possible to recognize and remove a superimposed color in a digital image. The algorithm is structured in two main parts: computing the color correction matrix and subtracting or adding it to the captured image. Few other methods to this problem and the advantages of this method are discussed in this paper. Future developments are also illustrated.

Color analysis deals with a major problem which is controlling the lighting condition while clicking a picture. A particular color in the target frame appears to be measured as a different color for pictures taken under the same environment. Fields like healthcare, space research, food industries and other color-managed areas apply color calibration on a daily basis. This work deals with a physical object that helps correct colors called the colorchecker. The ColorChecker Color Rendition Chart, this very well known chart with an array of 4 x 6 color patches, is an icon of the imaging industry. It was formally presented in a 1976 article by C. S. McCamy and his colleagues from the Macbeth Company, a Division of Kollmorgen Corporation at the time [4].

2. BACKGROUND STUDY

The methods used in this paper revolve around colors, lighting and the algorithm is all about matrices and eigenvalues.

2.1 The XRite Color Checker

The Xrite Color Checker is a device (color rendition chart) used in industries to solve the problem of color correction. It is originally known as the Macbeth color checker. It is a color calibration target of a rectangular framed cardboard arrangement of 24 squares (6x4) of painted samples/colors/shades. This color checker will take care of the white balance too. We have a neutral grey scale for white balance (it corrects the light and make it as white as possible). Each of the 24 color patches represents the colors of natural objects, such as sky blue, flesh tones and leaf green and each patch reflects light just like its real world counterpart [1]. Each square is individually colored using a solid tone to produce pure, flat, rich color without dots or mixed tints. Figure 1 shows the XRite Color Checker.



Figure 1. Xrite Color Checker

2.2 White Balance

Whenever we do a photoshoot, we expect the pictures to come out realistically, mostly similar to how we see it in person. For faithful reproduction, we adjust or remove unrealistic color casts, so that objects which appear white in person are rendered white in our photo is known as the White balance. Relative warmth or coolness of white light is referred to as color temperature. The camera's white balance has to take into account the "color temperature" of a light source. Cameras can create unsightly blue, orange, or even green color casts because our eyes are excellent at judging what's white under different light sources, but digital cameras often have great difficulty with auto white balance (AWB). A white balance setting in a professional camera is a numerical value (Kelvin temperature). In order to improve our photos under a wider range of lighting conditions, understanding digital white balance plays a major role thereby avoiding these color casts [7].

3. RELATED WORKS

There are many other methods that can solve the problem of color correction which is discussed in this section. They have their own advantages and disadvantages over the algorithm discussed in this paper, which depends on the necessity to use photographs and digitise images.

3.1 Adobe Lightroom

We take a raw picture of the target and the reference Xrite ColorChecker and then upload it to the adobeLightroom. We then convert the RAW file to DNG using a DNG Converter. Then open the DNG in the colorchecker calibration app and we save it as a profile. Importing that profile into lightroom is the major step and we then apply it to all the pictures. We can also check white balance if needed and at the end we copy the profile to all the related pictures that needs to be color corrected [6]. This is indeed a good way to correct colors and it produces the best results, but this depends on a few external software which makes us propose this method described in our paper.

3.2 Pantone Card

Pantone Card is similar to an Xrite Color Checker which works with our phone cameras to measure and match colored objects, materials, and surfaces to their Pantone Color equivalents. Placing the color correction card over the shade that needs to be matched is the first step. Then we open Pantone's smartphone app on our mobile device and take a snap of the card. The app is designed such a way that it automatically performs color matching and then returns the most similar shades [5]. This can be used to correct colors too the same way we use the color checker. Figure 2 shows the Pantone card.



Figure 2. Pantone Card

3.3 Supervised Learning for Color Calibration

The image has a set of known color regions like a color checker and we need to find the actual colors of the image. The actual colors of the 24 squares can be extracted from the image using Python's OpenCV. We take it as input, x. We know the colors of these 24 squares from the Macbeth ColorChecker chart. We take it as output y. Using the extracted color of as input(X) and actual colors of the known color region as output(Y), we need to find the transformation relationship (function) between X and Y. Using the transformation relationship, we can calibrate the color of the unknown regions in the image. This can be taken as a machine learning's regression problem that used regression analysis because the values are continuous. This method uses multivariate regression for further results [3].

4. DATASET

In order to color correct images and produce best results, the algorithm needs 2 inputs, one image is the target image with the color checker, and the other is the ideal colors checker image, provided both the inputs are under the same lighting conditions. We can compare both the data using the pixel values stored as csv format and then correct the color of the output image. This method has been tried on a variety of objects and has been trained accordingly. The RGB values of a color checker under ideal conditions are shown in Figure 3.

ColorChecker 2005	xyY (CIE D50)	L*a*b* (CIE D50)	Adobe			Apple			ProPhoto			sRGB			sRGB (GMB)		
			x	y	Y	R'	G'	B'	R'	G'	B'	R'	G'	B'	R'	G'	B'
0	illuminant	0.3457 0.3585 100	100	0	0	255	255	255	255	255	255	255	255	255	255	255	255
1	dark skin	0.4316 0.3777 10.08	37.99	13.56	14.06	107	82	70	94	63	51	81	67	54	116	81	67
2	light skin	0.4197 0.3744 34.95	65.71	18.13	17.81	184	146	129	183	128	109	159	135	114	199	147	129
3	blue sky	0.2760 0.3016 18.36	49.93	-4.88	-21.93	101	122	153	74	103	139	94	102	133	91	122	156
4	foliage	0.3703 0.4499 13.25	43.14	-13.10	21.91	95	107	69	73	89	48	75	86	55	90	108	64
5	blue flower	0.2999 0.2856 23.04	55.11	8.84	-25.40	128	127	173	110	108	162	118	111	154	130	128	176
6	bluish green	0.2848 0.3911 41.78	70.72	-33.40	-0.20	129	188	171	84	178	155	127	168	157	92	190	172
7	orange	0.5295 0.4055 31.18	62.66	36.07	57.10	201	123	56	211	102	30	167	118	54	224	124	47
8	purplish blue	0.2305 0.2106 11.26	40.02	10.41	-45.96	77	92	166	52	71	156	79	74	145	68	91	170
9	neutral red	0.5012 0.3273 19.38	51.32	48.24	16.25	174	83	97	180	59	79	141	83	80	198	82	97
10	purple	0.3319 0.2482 6.37	30.33	22.98	-21.59	86	61	104	73	42	88	68	49	82	94	58	106
11	yellow green	0.3984 0.5008 44.46	72.53	-23.71	57.26	167	188	75	145	177	39	144	170	74	159	189	63
12	orange yellow	0.4957 0.4427 43.57	71.94	19.36	67.86	213	160	55	220	143	39	181	152	60	230	162	39
13	blue	0.2018 0.1692 5.75	28.78	14.18	-50.30	49	65	143	26	47	131	57	50	120	35	63	147
14	green	0.3253 0.5032 23.18	55.26	-38.34	31.37	99	148	80	60	133	54	85	123	69	67	149	74
15	red	0.5686 0.3303 12.57	42.10	53.38	28.19	155	52	59	159	29	43	120	59	46	180	49	57
16	yellow	0.4697 0.4734 59.81	81.73	4.04	79.82	227	197	52	232	187	0	199	188	66	238	198	20
17	magenta	0.4159 0.2688 20.09	51.94	49.99	-14.57	169	85	147	174	60	134	143	85	127	193	84	151
18	cyan	0.2131 0.3023 19.30	51.04	-28.63	-28.64	61	135	167	0	118	154	78	111	148	0	136	170
19	white 9.5 (85 D)	0.3469 0.3608 91.31	96.54	-0.43	1.19	245	245	242	242	243	239	242	243	240	245	245	243
20	neutral 8 (23 D)	0.3440 0.3584 58.94	81.26	-0.64	-0.34	200	201	201	189	191	191	189	190	191	200	202	202
21	neutral 6.5 (44 D)	0.3432 0.3581 36.32	66.77	-0.73	-0.50	160	161	162	144	146	146	145	146	146	161	163	163
22	neutral 5 (70 D)	0.3446 0.3579 19.15	50.87	-0.15	-0.27	120	120	121	101	102	102	102	102	102	121	121	122
23	neutral 3.5 (185 D)	0.3401 0.3548 8.83	35.66	-0.42	-1.23	84	85	86	65	66	68	66	66	68	82	84	86
24	black 2 (1.5 D)	0.3406 0.3537 3.11	20.46	-0.08	-0.97	52	53	54	37	37	38	37	37	38	49	49	51

Figure 3. Color coordinates of an ideal color checker

5. METHODOLOGY

Different input images are passed through the algorithm written to produce a color corrected output. The algorithm goes through different phases which majorly includes the detection of the color checker and the matrix calculation. The algorithm takes help of image processing where we have numerical values called "pixels" and they represent an image. These matrix entries are the pixel values which forms a whole image (Figure 4). The algorithm is as follows:

- Input-1:** Picture of the target image with the colorchecker.
- Input-2:** Picture of the colorchecker alone as a reference under the same lighting conditions.
- Step 1:** Take a picture of the target image along with the colorchecker on any digital lens
- Step 2 :** Take a picture of the color checker alone under the same surroundings and the same lighting conditions.
- Step 3 :** An algorithm to detect the coordinates of the color checker is devised.



Figure 4. ColorChecker Detection

Step 4: Find the color coordinates (or) the r,g,b values of all the 24 colors

Step 5: Repeat step 4 and 5 for input-2 also

Step 6: Store the pixel values (color coordinates) of both the inputs in a csv file

Step 7: Compute the dot product of the 2 pixel valued matrices.

Step 8: Correct input - 1 with the color corrected matrix.

Step 9: Convert the pixel valued matrix to a corrected image.

Output:Color Corrected target image.

The workflow of this paper and the algorithm is depicted as a flowchart in Figure 5.

5.1 Color Checker Detection

The target image (input-1) contains the color checker. In order to get the color pixels of each color in the checker, we need to find their coordinates. So we devise an algorithm to find the x, y coordinates and then compute the RGB values at that point. This method will return 'found' when it finds a checker on the image and it will return an image overlaid with circles on each patch of the color. The outer circle is the "reference" value, the inner circle is the average value from the actual image. The coordinates as output is stored as a csv file and its first 24 lines contains the x, y values of each color locations and the average values. [2]

x, y, r, g, b (csv format)

In addition to this, the size of the color square of the checker is also stored in the last two lines. The alignment of the color squares are in order of the typical MacBeth color checker ("dark skin" top left, "black" bottom right).

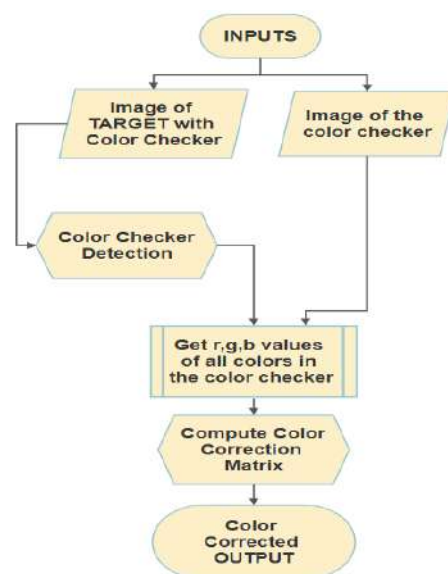


Figure 5. Work-Flow

6. RESULTS AND ANALYSIS

The aim of this paper is to bring out and reproduce the original colors of an image as seen from a human eye. We compute Color Correction Matrix (CCM) 'A'. We can describe it as a 4x3 matrix A which approximate the following equation:

“Let P be a reference color checker matrix (24 x 3) and C be a color checker matrix to correct (24 x 3).”

$$P = [C \ 1] A$$

Results observed here in Figure 9 and 10 shows a prodigious difference in the input and output. Figure 6 shows the snippet of the code written in python where the dot product is computed and the color correction matrix is printed. Figure 7 shows the type of variable the CCM is and how the matrix is calculated. Figure 8 shows the format in which the CCM is stored. Figure 9 and 10 are calculated and trained on different inputs and that is why the numerical values of the CCM vary.

```
source_xyz_hm = np.append(source_xyz, np.ones((24, 1)), axis=1)
ccm = np.linalg.pinv(source_xyz_hm).dot(reference_xyz)

print('CCM:')
```

Figure 6. Code Snippet

```
PS D:\tri3d\webglshift\color_correction\colorcorrectionmatrix> python computeCCM.py data\xrite_photo_actual.csv data\xrite_overlay_rendered.csv ccm_overlay.csv
>>
CCM:
[[ 1.05951799 -0.30504165  0.51257974]
 [ 0.09436276  1.38234374 -0.54956426]
 [ 0.04144909  0.0771739  1.36439536]
 [-13.17272893 11.80768251 26.5275649 ]]
```

Figure 7. Color Correction Matrix

	A	B	C	D
1	1.597667	-0.30919	0.933348	
2	-0.53326	1.30948	-1.67546	
3	-0.04434	-0.15581	2.182076	
4	-23.1037	-24.7029	-29.2919	
5				

Figure 8. CSV format of the matrix



Figure 9 Result



Figure 10 Color Calibration

7. CONCLUSION AND FUTURE WORK

ColorCheckers, be it any color targets can be captured by digital cameras, lens and other color input bias, and the performing image affair can be compared to the original map, or to reference measures, to check the degree to which image accession reduplication systems and processes compare the mortal visual systems. It also can be used to color correct one print with the map in it (that may have a special color cast, for case thanks to a lighting achromatism difference) to a different" reference" print with the map in it. Because of its wide vacuity and use, its careful design, and its thickness, and because comprehensive spectrophotometric measures are available, the ColorChecker has also been used in academic exploration into motifs similar as spectral imaging.

This work model gives a decent color corrected output taking in account of a few conditions, like lighting, camera angles and more. The method described in this paper uses an external, physical object - a colorchecker which is pretty expensive in the market. So in the future, we can optimise a few steps and also try to create a fully automated way to correct colors instead of depending on a materialistic thing. We should try to reproduce the original colors or try to print the colors rather than buying a whole new product. Also the colorcheck detection algorithm is pretty technical and we can work on improving it. Other methods such as using a pantone card, or using the method of histogram matching or using other unsupervised or deep learning algorithms can be taken into account to yield best results.

REFERENCES

- 1 Gasparini, F., & Schettini, R. (2003, September). Color correction for digital photographs. In 12th International Conference on Image Analysis and Processing, 2003. Proceedings. (pp. 646-651). IEEE.
- 2 Fernández, P. D. M., Peña, F. A. G., Ren, T. I., & Leandro, J. J. (2019). Fast and robust multiple colorchecker detection using deep convolutional neural networks. *Image and Vision Computing*, 81, 15-24.
- 3 Rizzi, A., Gatta, C., & Marini, D. (2003). A new algorithm for unsupervised global and local color correction. *Pattern Recognition Letters*, 24(11), 1663-1677.
- 4 Varghese, D., Wanat, R., & Mantiuk, R. K. (2014). Colorimetric calibration of high dynamic range images with a ColorChecker chart. *Proceedings of the HDRi*.
- 5 Ciocca, G., Marini, D., Rizzi, A., Schettini, R., & Zuffi, S. (2003). Retinex preprocessing of uncalibrated images for color based image retrieval. *Journal of Electronic Imaging*, 12(1), 161-172.
- 6 Marini, D., & Rizzi, A. (2000). A computational approach to color adaptation effects. *Image and Vision Computing*, 18(13), 1005-1014.
- 7 Barnard, K., Cardei, V., & Funt, B. (2002). A comparison of computational color constancy algorithms. I: Methodology and experiments with synthesized data. *IEEE transactions on Image Processing*, 11(9), 972-984.

Efficiency Improvement in an Assembly Line by Using Line Balancing Method and Value Stream Mapping

R. Jayachitra and K. S Gowtham Kumar

Department of Mechanical Engineering, PSG College of Technology

ABSTRACT

The focus of this paper is on the improvement of the assembly line by means of assembly line balancing approaches. The assembly line balancing is about evenly distribution of the work load among the workstations without violating the precedence and cycle time specifications. The two assembly line balancing tactics specifically Largest candidate rule method (LCR) and Kilbridge and Westercolumn method (KWC) are utilized to strengthen the efficiency of assembly line by minimizing the number of workstations and thereby reducing the balance delay of the assembly line. Line balancing is an effective method to enhance the throughput of assembly line by reducing non-value-added activities. The technique followed includes calculation of cycle time of the process, identifying the non-value-added activities, calculating overall work load on station and distribution of work load on each station by the method of line balancing. This paper broadens the productivity and effectivity of an Excavator Assembly line in ABC organization. Line balancing is used to measure the efficiency of the line and later used to measure the effectiveness of the proposed solution. Multiple approaches have been proposed based on the time study carried out. Evaluation of the outcomes of the proposed assembly line suggests that the line efficiency of the excavator's assembly line is improved from 71.27% to 77.44%

Keywords: About Assembly line balancing, Cycle time study, Non-Value added activities, Work load

INTRODUCTION

Costs discount is currently one of the foremost goals for enterprises. The enterprises try to decrease costs in dissimilar ways. One way is the inventory levels reduction. In order to decrease the quantity of raw materials, work in process (WIP) and inventory level of prepared goods enterprises have to find and remove dissimilar kinds of problems which are linked to the large amount of inventory. The problems can concern the little superiority of goods, which causes the requirement of growing the amount of manufactured products in order to confirm that a particular amount of good goods will be prepared to be sent to a customer. A more processes variability is alternative kind of problem. In this condition a firm can manufacture dissimilar number of nonconforming goods daily, therefore, a firm not ever recognizes whether it will be prepared to encounter the clients' demands. Thus, it keeps a enormous inventory level just in case. Moreover, machine failures and production downtimes caused by different reasons can force companies to keep high inventory level.

At the similar time, insufficient manufacturing line organization or inappropriate manufacture control can lead to appearance of too much inventories. If a week plan is created and then each work station works at their own pace, an unrestrained WIP can seem producing additional costs. Namely, the costs of extra space to keep WIP, costs of extra shipping tasks, costs of needless movements, costs of capital spent in materials, costs of nonconforming goods which seemed because of inappropriate WIP protection, etc. For these reasons levels of inventories should be organized to avoid extra costs. The impact of current inventory levels on a company lead time (LT) can be examined with the use of Value Stream Mapping (VSM) and Value Stream Analysis (VSA). Inappropriately, it provides us only a static data about the present situation without the opportunity to examine inventory levels in time. That is why, additional studies are essential to be performed in order to see the dynamics of a manufacturing system (MS) and, predominantly, the dynamics of inventory levels. Therefore, it is essential to use a dynamics system analysis.

1.1 Value stream mapping and value stream analysis

Value stream mapping and value stream analysis are well identified procedures used in industrial processes analysis. The main goal of VSM is the appearance of a value movement along with the industrial process. The data collected directly from an industrial line are presented in the form of Current Stream Map, which are next examined. In order to progress Current Stream Map unusual symbols are used. The map offers data regarding just one product family. A product family is defined as a collection of goods that pass through similar industrial procedures and over common apparatus in the downstream procedures in the industrial system. The map is constructed on the basis of the data regarding a representative of the product family i.e. usually a product which is created the most often. First of all, in order to create Current Stream Map it is essential to collect the following data concerning a manufacturing procedure?

- A orderof manufacturing procedures,

- Cycle time of the industrial processes measured in a time study, which provides data about how frequently single piece of a product leaves a process understood on a workstation,
- Existing working period which can be used for manufacturing processes,
- Machineries or work stations accessibility for manufacture of this product family,
- Rate of materials distributions and the quantity of distributed materials,
- Rate of complete products shipment to a customer and a quantity of products in a shipment

1.2 Line Balancing

The scope of this learning is to discover the understanding of Production-line industrial and balancing, Types of Line balancing, apparatus balancing and its failure and analysis. A production line is said to be in balance when every worker's job takes the same quantity of time. Line balancing is a manufacturing-engineering purpose in which whole group of production-line tasks are divided into equal portions. Well-balanced lines avoid labour idealness and increase productivity. Line-balancing approach is to make production lines flexible enough to absorb exterior and interior irregularities. There are two types of line balancing, which we have explained as –

- Static Balance – Refers to long-term changes in capacity over a period of several hours or longer. Static imbalance results in underutilization of workstations, machines and people.
- Dynamic Balance – Refers to short-term changes in capacity, like, over a period of minutes, hours at most. Dynamic inequity arises from product mix changes and variations in work time dissimilar to product mix.

LITERATURE REVIEW

The ideas and ideas essential for the assignment were considered and composed from numerous journals or books printed in the ground of industrial engineering and lean engineering practices for reducing takt tie then eliminating non value added activities in an assembly line.

Reichhart A, Holweg M, Taj S had approached lean emphases on rejecting all non-value added activities from order of record to receipt of payment, lead time and work in process drop (WIP), quality enhancement, enhanced elasticity, condensed transactions, shortened scheduling, enhanced communications, reduced costs, better on time deliveries, improved sales and space utilization are all probable through the real planning and execution of lean production [1,2].

Womack JP, Jones DT researchers approved that LM could be a cost saving mechanism and can be used to monitor to be world class association by its popular tools like 5s, TPM, pokayoke, kanban, cellular manufacturing SMED, kaizen, value stream for the improved efficiency, decrease in WIP inventory, enhancement in excellence, reducing space utilization and better work place organization. Detecting what creates value for customers. The Lean approach can be shortened Identify what generates value from the customer's perspective, while in process, if consumer does not pay for non-value added actions and should be removed from the process [3].

Lasa IS et al. explained that VSM has been systematically examined and a team produced to increase the creative system of a production application, it is a graphical device which is produced using a predefined set of standardized icons that helps the organization to see and understand the flow of material and data as the product goes along different stages [4].

Liker JK, Belokar RM et al. identified that after sketch the value stream it aids the association to separate value adding activities from non-value adding activities from recent condition and find kaizen opportunities. The real advantage is, it gets the firm away from isolated point kaizen and builds towards a true organization based on the flow of materials and data across the whole value stream, alteration of inner wheel housing process line by considering case study of an automobile industry with effective cycle time decrease is made clearly, assembly lines are still essential to get the smoothing of production system in any medium organization [5, 6].

Work study including time and process study which is used for inspecting human operational, all its condition and which lead to a effective enquiry of all the features which distress the effectiveness of the condition that is revised to make enhancements the look deals with an outline to work study [7].

Problem Statement

- It is a leading automobile spare manufacturing company which is a subcontracting industry with Daimler, Brakes India and Ashok Leyland as its major customers. It is facing increased machine operator time which leads to more man power in the assembly line.
- Productivity decreases due to more number of defective products and low quality products produced which also incurs additional cost for rework.
- Want to improve their output and productivity to achieve their yearly target by eliminating causes and production time that affect profit for company.

OBJECTIVES

- To reduce man power and to implement optimized layout.
- To increase the product quality and reducing non value added activities to eliminate process.
- To introduce the single piece flow in the assembly line.

value stream mapping

The connection of current state value stream mapping for the brakes assembly line of all four types of components is shown in Fig 1a, 1b, 1c, 1d. For each components the processes varies at very small amount.

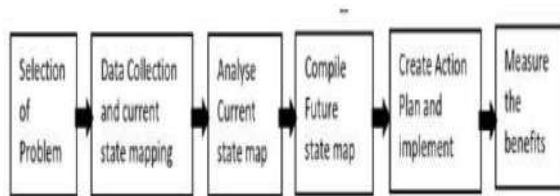


Fig.0 VSM Methodology

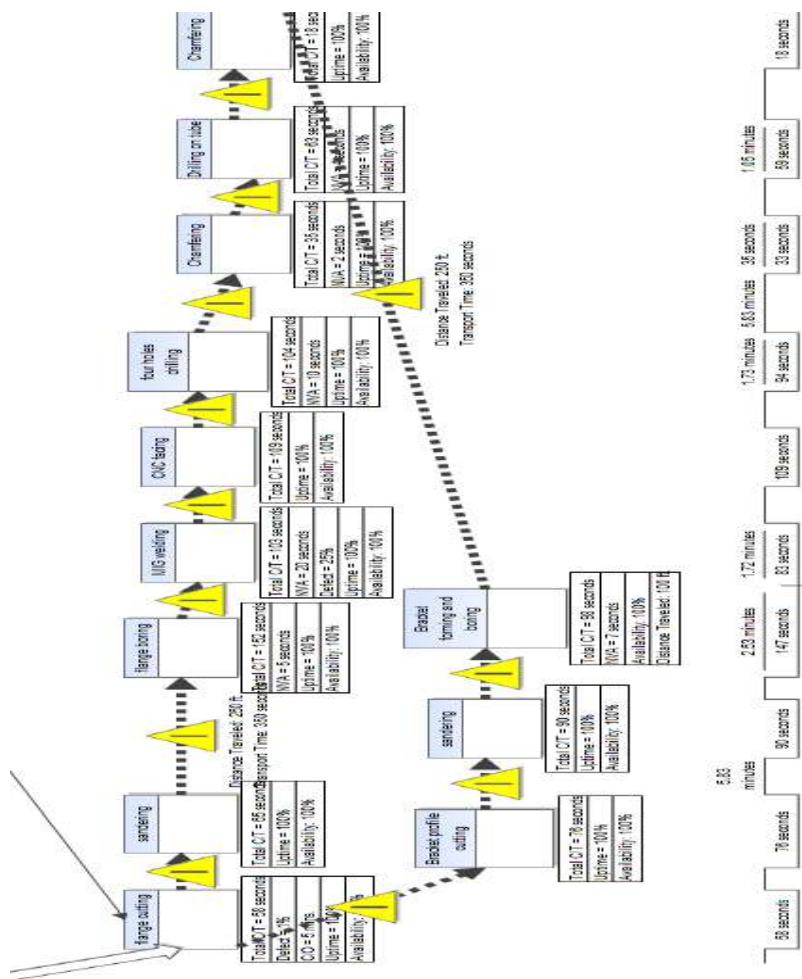


Fig 1a: Current State Value Stream Mapping

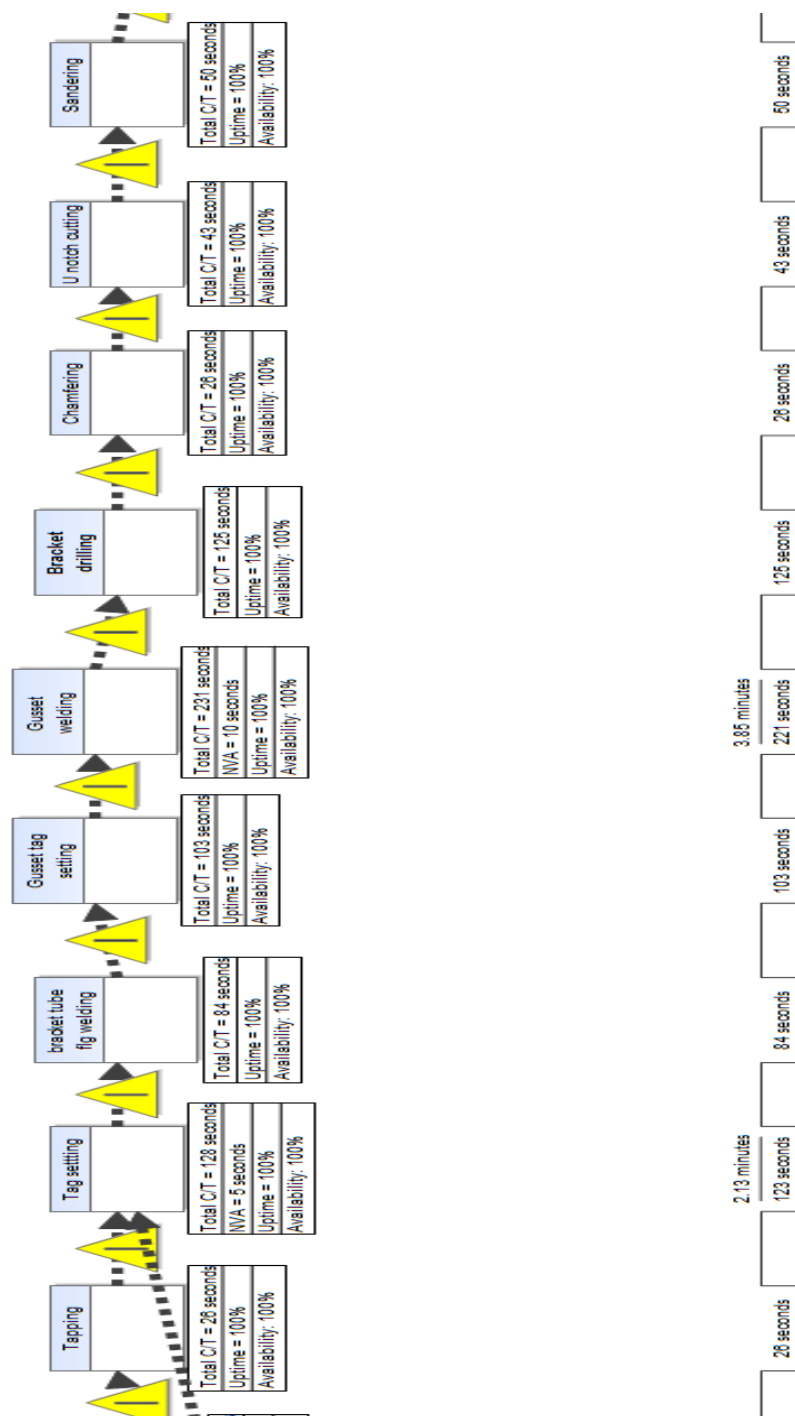


Fig 1b: Current State Value Stream Mapping

(Fig 1a, 1b, 1c, 1d) shows the connection of current state value stream mapping and its takt time is calculated as follows,

- Hours per Shift = 8 hrs.
- Number of Shifts = 2 Shifts
- Break time per Shift = 50 mins
- Days per week = 6 days
- Days per month = 26 days
- Customer Demand = 6240 components/ month
- Takt time = $\frac{((8 * 2 * 60) - 120) * 26}{6240}$
- = 3.5 * 60 = **210 secs.**

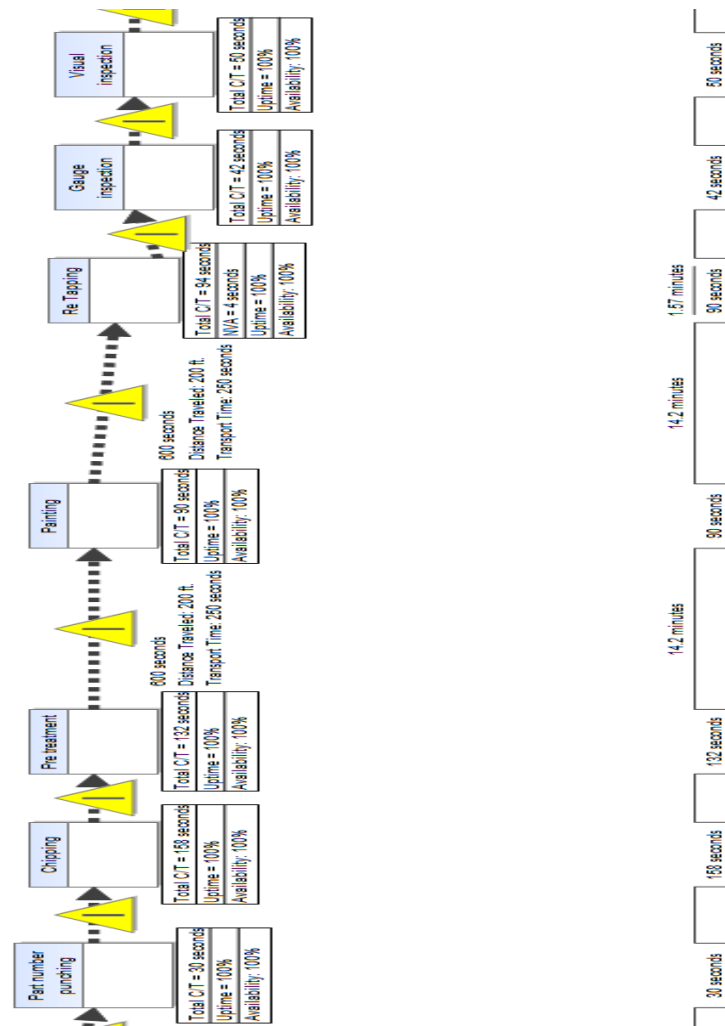


Fig 1c: Current State Value Stream Mapping

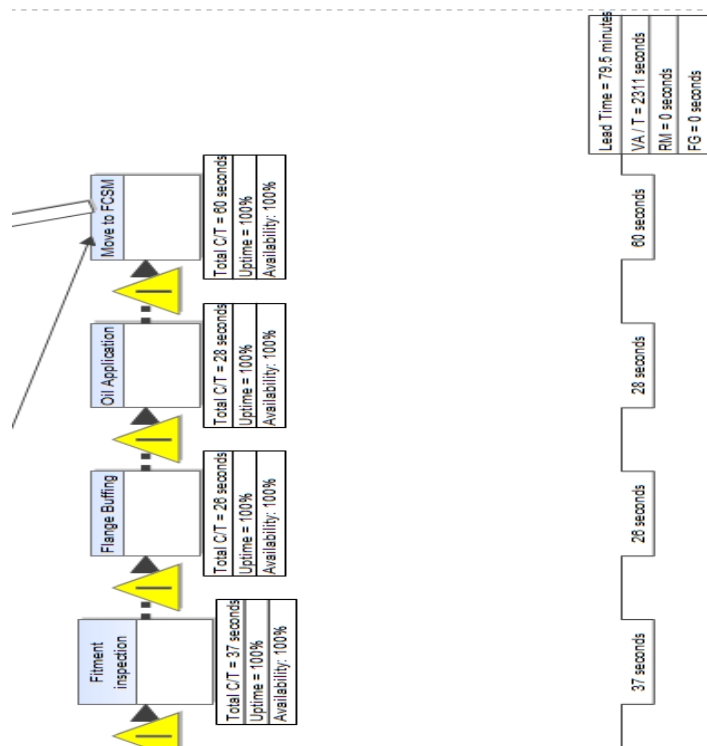


Fig 1d: Current State Value Stream Mapping

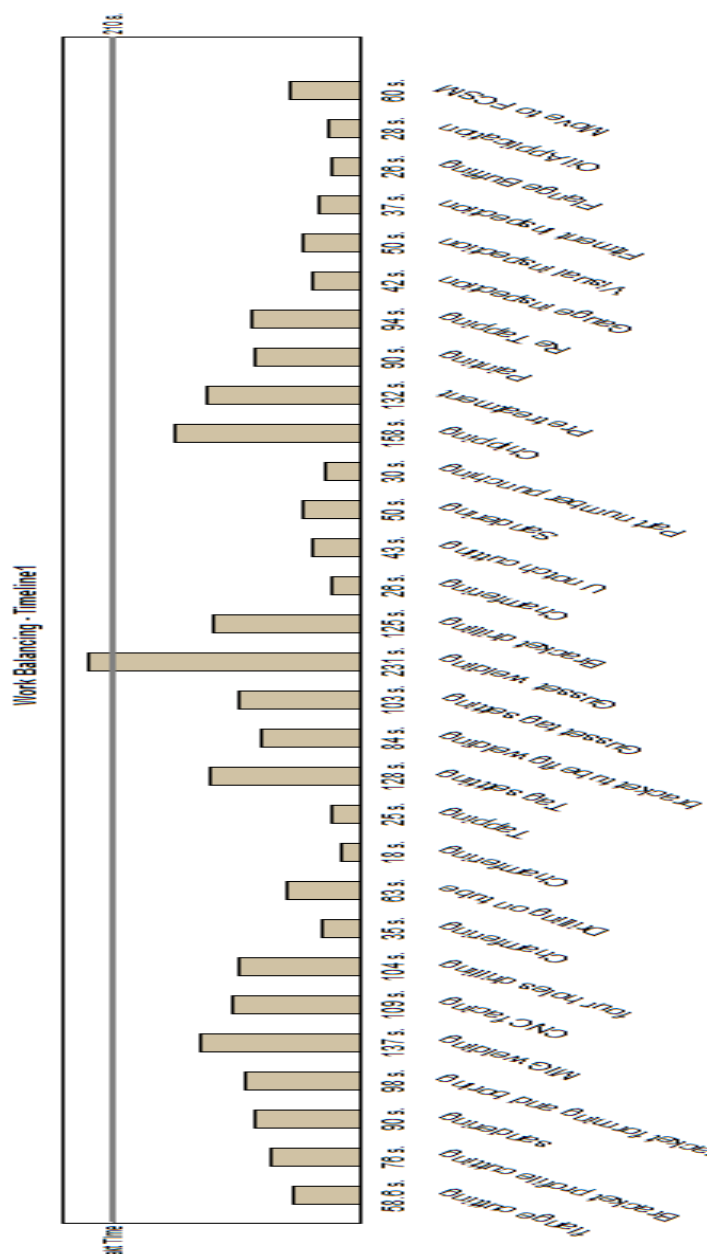


Fig 2: Work Balancing Time Line

LINE BALANCING

Line balancing for whole assembly process is shown in (Fig 5, 6, 7, 8) and workstations are aligned based on number of workers. A manufacture line is thought to be in equilibrium when each worker's job takes the similar quantity of time.

No	Workstation #	Work Area	Elem Task Description	ST	Elem Task #	Prac
1	1		Flange Boring	97	1	
2	2		MIG Welding	103	2	1
3	3		CNC Facing	109	3	2
4	4		Four Holes Drilling	103	4	3
5	5		Brazing	25	5	4
6			Chamfering	35	6	5
7			Drilling on tube	62	7	6
8			Chamfering	17	8	7
9	6		Bracket Forming and Boring	112	9	8
10	7		Tag setting	128	10	9



Fig 5: Line balancing for first half processes

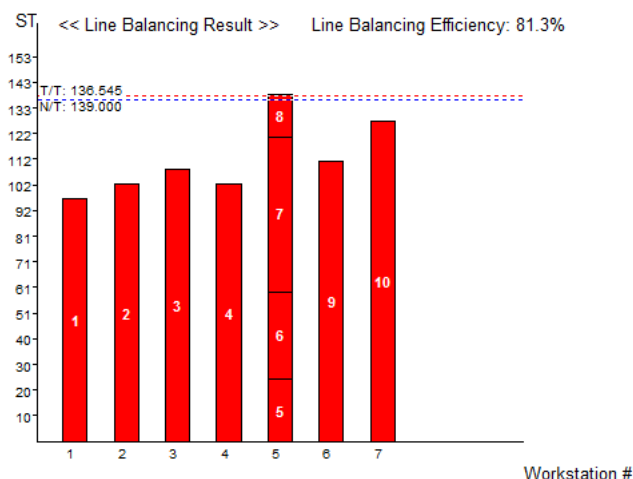


Fig 6: Workstations for first half processes

First half of the processes consists of 10 processes which is aligned into 7 workstation based on 7 workers. The CNC operator having an idle time of 84 secs so CNC operator can be aligned for four holes and two holes chamfering process. So the chamfering machine should be moved near to CNC machine. So the maximum time 139 secs can be further reduced.

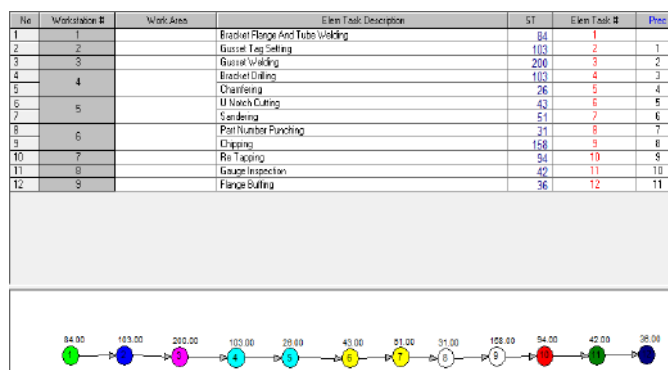


Fig 7: Line balancing for second half processes

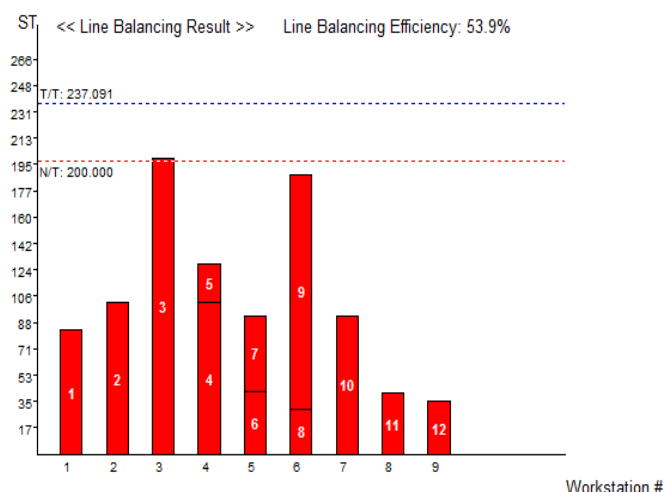


Fig 8: Workstations for second half processes

Second half of the processes consists of 12 processes which is aligned into 9 workstation based on 9 workers. Bracket drilling and chamfering processes, part number punching and chipping processes, U-notch cutting and sandering processes are aligned into same workstation. The maximum station time is 200 secs.

RESULTS AND DISCUSSION

In future state mapping the re-tapping process is eliminated and painting process is carried out after completing the painting process. So one process and one man power can be eliminated as shown in Fig 9a, 9b, 9c, 9d.

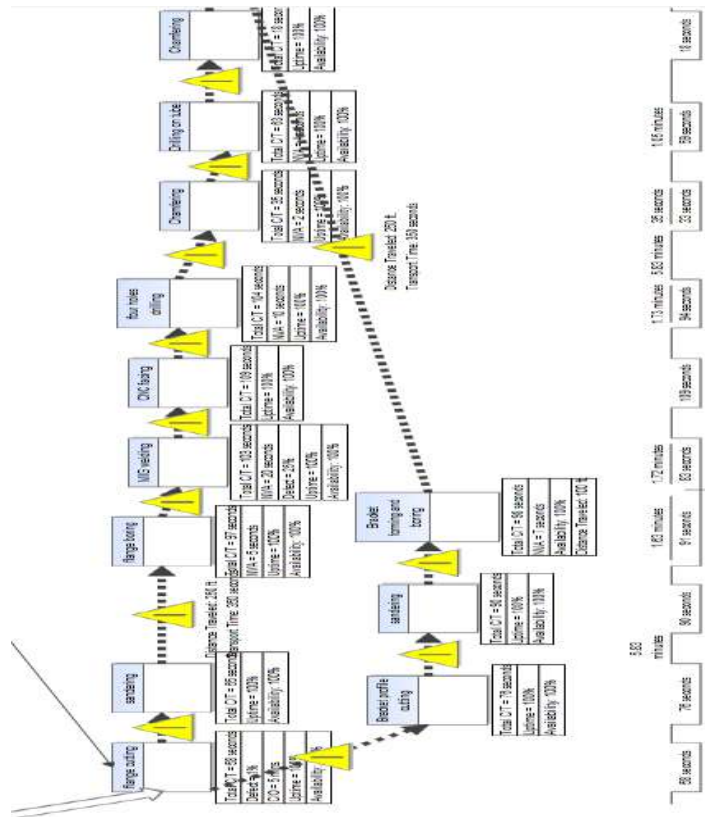


Fig 9a: Future state value stream mapping

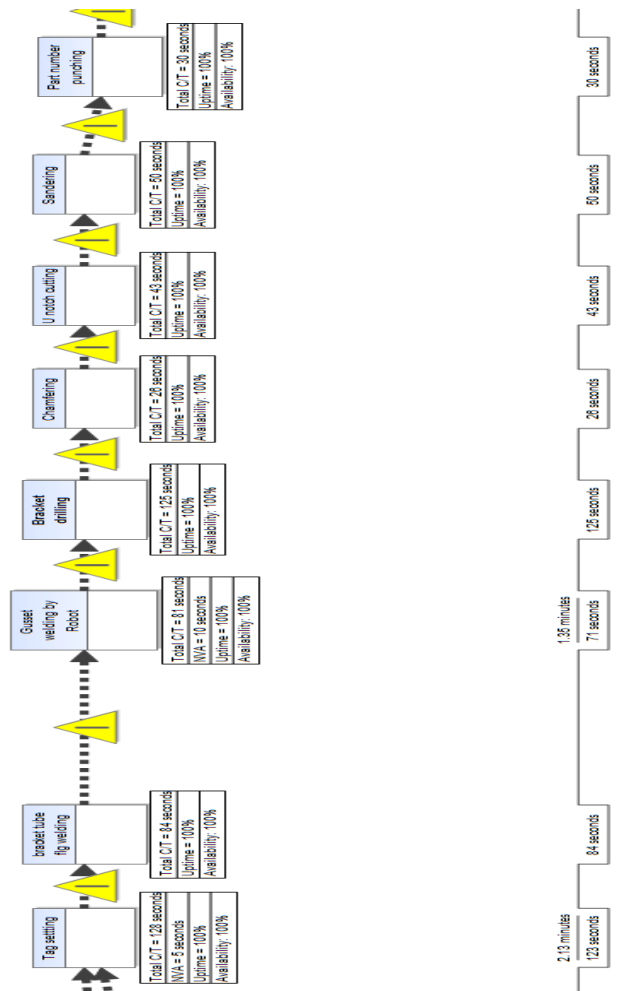


Fig 9b: Future state value stream mapping

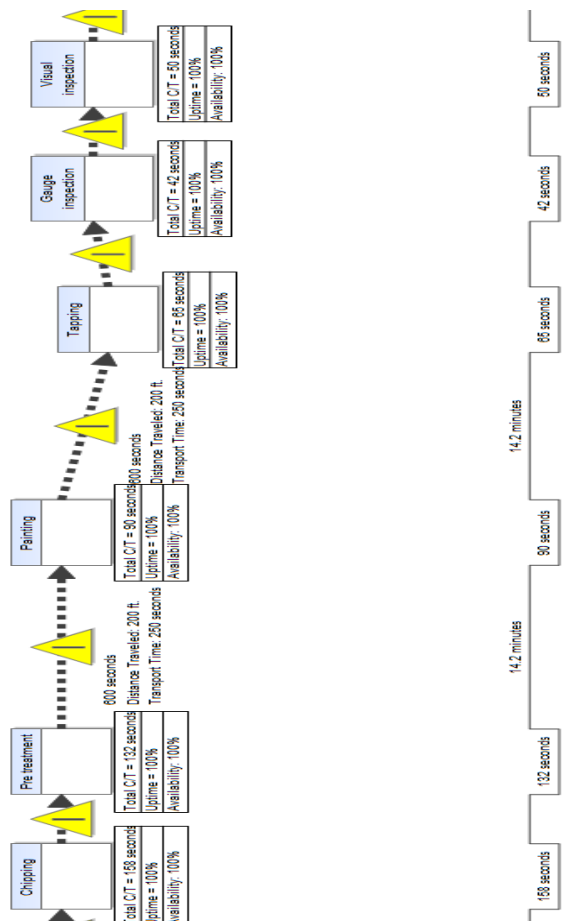


Fig 9c: Future state value stream mapping

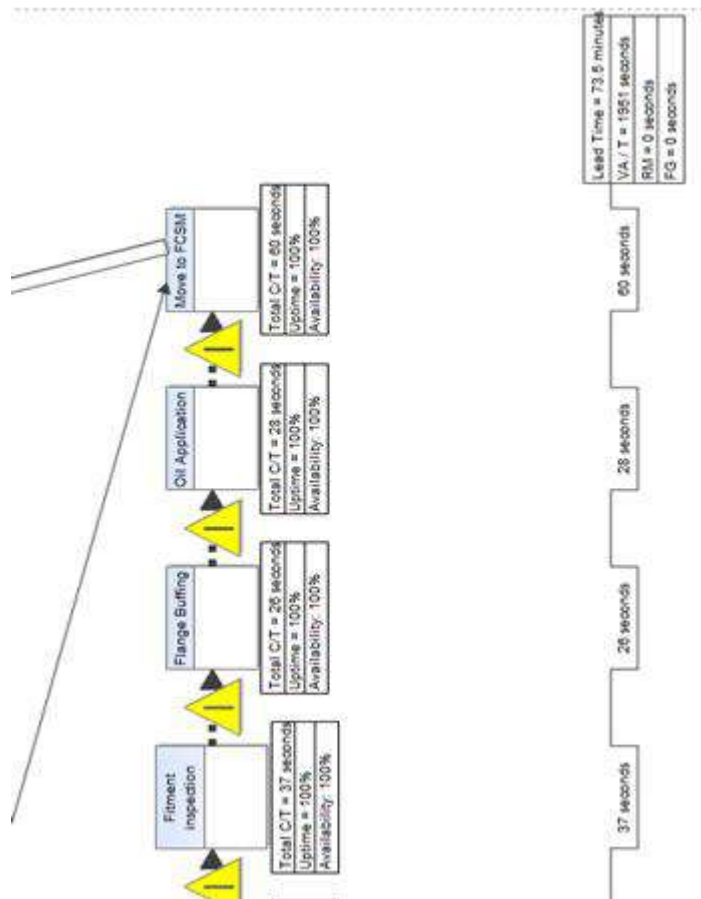


Fig 9d: Future state value stream mapping

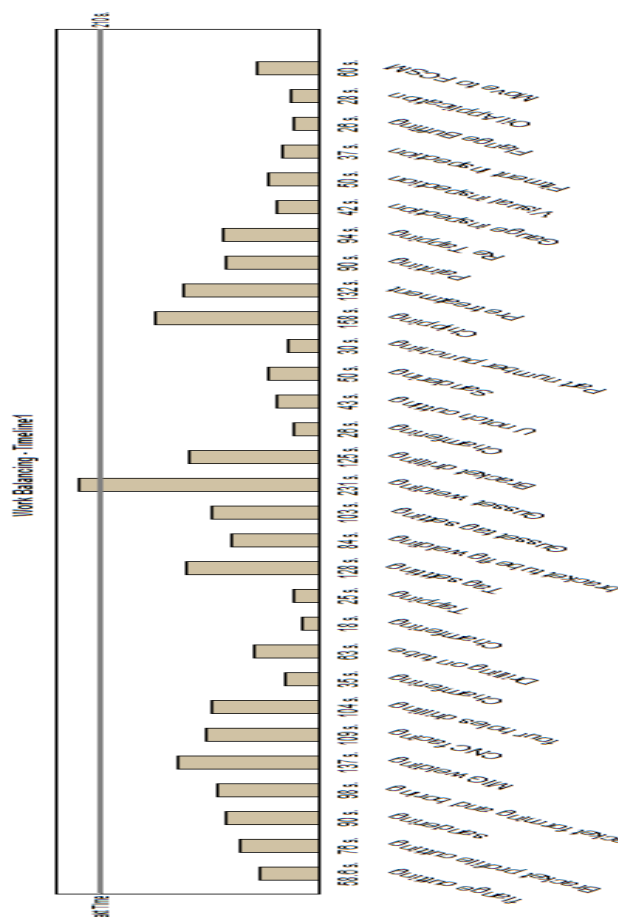


Fig 10: Work Balancing Time Line

- T_{wc} = An assemble product requires a certain total amount of time to build, called the work content time (T_{wc}) = 1412.33 minutes
- w = no of work station = 12
- T_c = the maximum available cycle time = 152 minutes
- Balance delay (d) = $(\eta_{actual} * T_s - \sum T_{wc}) / (\eta_{actual} * T_s)$
 $= (12 * 152 - 1412.33) / (12 * 152)$
 $= (1824 - 1412.33) / 1824$
 $= 411.67 / 1824$
 $d = 0.2256$
- Line efficiency (η) = $(1-d) * 100$
 $= (1-0.2256) * 100$
 $\eta = 77.44\%$

CONCLUSION

The detailed study of the excavator assembly line identified the importance of cycle time study and the line balance. This led to identification of those activities which were duplicated and added no value to the assembly line, rather it added extra time to the activities. This led to the improvement in the assembly line. Initially the efficiency was found to be 71.27%. By removing the duplication and unnecessary work in the stations and feeders led to the improvement in the efficiency and few standard operations were implemented. Thus, by applying LCR method we have found the increase in efficiency in the proposed layout i.e. 77.44% with the improvement of 6.17%. Line balancing is used to align the process to number of workers available so that the workers can be effectively utilized and minimum number of workers needed can be identified. This paper describes assembly line balancing is one of the major steps to be taken into consideration while increasing productivity of Excavator industries. Line balancing is done with taking in account the takt time, cycle time and downtime and thus reduces the production lead time with increased number efficiency. Continuous improvement is the step to reduce unnecessary downtime losses

REFERENCES

1. Reichhart A, Holweg M (2007) Lean distribution: Concepts, Contributions, Conflicts. *Int J Prod Res* 45: 3699-3722.
2. Taj S (2007) Lean manufacturing performance in china: assessment of 65 manufacturing parts. *Journal of Manufacturing Technology Management* 19: 2179-237.
3. Womack JP, Jones DT (2003) *Lean Thinking (2nd edn.)* Simon & Schuster, Inc., New York, pp. 16 -26.
4. Lasa IS, Labura CO, Castro Vila RD (2008) An evaluation of Value Stream Mapping Tool. *Business process management Journal* 14: 39-52.
5. Liker JK, Meier D (2007) *The Toyota Way Field Book*. Tata McGraw -Hill Edition, New Delhi, p. 41.
6. Belokar RM, Kharb SS, Kumar V (2012) An Application of Value Stream Mapping In Automobile Industry: A Case Study. *International Journal of Innovative Technology and Exploring Engineering* 1: 2278-3075.
7. International labour office, G. Kanawaty, *Introduction to work study*, 1992.
8. Keyte B, Locher D (2004) *The Complete Lean Enterprise: Value Stream Mapping for Administrative and Office Processes*. New York.
9. Tapping D, Shuker T (2003) *Value Stream Management for the Lean Office*. Productivity press, New York.
10. Martin K, Osterling M (2013) *Value Stream Mapping: How to visualize work and align leadership for organizational transformation*. McGraw-Hill, New York.
11. ArunKanti Bose, "Application of Fishbone Analysis for Evaluating Supply Chain and Business Process- A Case Study on the ST James Hospital," *International Journal of Managing Value and Supply Chains.*, vol. 3, no 2, pp. 17-24, 2012.

Numerical Investigation of Coated AISI 4140 Steel by Nitrided Substance

Babu S¹, Raja V², Dinesh Kumar R³, Madhan Muthu Ganesh K⁴ and Mohamed Anwaru⁵

^{1,2,5}Mechanical Engineering Department, PSG College of Technology, Coimbatore

³Mechanical Engineering Department, NIT Srinagar, Jammu & Kashmir

⁴Aeronautical Department, M.A.M. School of Engineering, Trichy

ABSTRACT

In the present study, samples made of AISI 4140 steel, pre-treated with plasma nitriding (PN) and coated with coatings like Titanium Nitride (TiN), Titanium Carbo Nitride (TiCN), Chromium Nitride (CrN), Aluminium Titanium Nitride (AlTiN) using Physical Vapour Deposition (PVD) technique, were investigated in terms of their dry and wet sliding wear behaviour. Wear tests, were performed with a pin-on-disc machine. The results of the duplex treated samples were compared with the conventional hard chrome coated AISI 4140 steel. The results showed improved wear properties of the duplex-treated specimens compared to the hard chrome coated AISI 4140 steel. TiCN coated and nitrided 4140 steel has shown the best performance among the investigated materials. Furthermore, the compound layer formed during nitriding was found to act as an intermediate hard layer leading to superior sliding wear properties. The improved performance of the duplex treated samples can be attributed to the presence of a nitrided subsurface.

Keywords– Adhesion, Duplex Treatment, Plasma Nitriding, PVD, Tribology, Wear

I. INTRODUCTION

The stress-strain curve for hardened work material is mainly used to tensile properties measurements. AISI 4140 steel is used in various mechanical drives and machine tool components such as gears, bolts, couplings, etc. AISI 4140 is quenched-tempered steel so that it has a tempered martensite phase after heat treatment [1-3]. For the estimation of both elastic and plastic deformation of the hardened work material, this study provides tensile tests result at room and higher temperature. For the tensile properties of these materials, hardness is the important factor over the effect of strain rate [4-5, 9]. Hardened work material is subjected to tensile test, to find the tensile properties like ultimate strength, Yield strength, young's modulus of the steel. Thus, main aim of this paper is to obtain tensile property data of AISI 4140 steel using experimental method, in which V-notch is introduced in the specimen.

From Literature review, it is inferred that there is need for deformation measurement and strain localization characteristics study on hardened V-notch specimen material at room temperature and higher temperature condition in combination with fractography technique.

Hardened steel strain was obtained using conventional UTM experimental results. For any simulation in Finite Element Method, the properties of high strength material are required for input data.

II. MATERIAL SELECTION

AISI 4140 (EN 19) is classified as medium carbon steel in which percentage carbon amount is varying from 0.38 to 0.43%. It has lower percentages of alloys namely Manganese, Silicon, Chromium and Molybdenum. The chemical composition is tabulated in table I.

Table I. Chemical Composition Of Aisi 4140 Steel

Steel	C	Mn	Si	Cr	Mo
AISI 4140	0.38 - 0.43	0.75 - 1	0.20 - 0.35	0.80- 1.10	0.15 - 0.25

This material was chosen in view of its ability to be nitride without losing its toughness. The material was given as a bar, from which samples of 8 mm diameter and 30 mm height were cut. The ends of specimens were polished so as to achieve the surface roughness of approximately 0.4 μm , as indicated in the standard, ASTM G99-04. Preceding nitriding, the samples were polished with alumina, followed by cleaning with acetone. The nitriding of the specimens was performed by plasma nitriding (PN) process at $\sim 5400\text{C}$ in a 75% H_2 -25% N_2 atmosphere, at a pressure of 450-500Pa, for ~ 16 hrs. The process parameters were selected based on the literature [2-3, 10, 13] which suggested that nitride results have direct relation with concentration of nitrogen, treatment temperature, and treatment time. Moreover, higher treatment temperature helps in achieving greater diffusivity of nitrogen into the surface [10].

III. RESPONSE MEASUREMENTS

Wear tests were carried out on duplex treated samples. The schematic of the experimental setup is shown in Fig. 1.

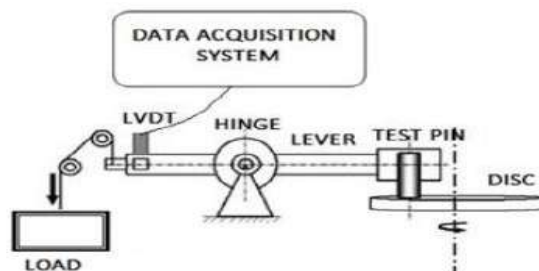


Figure 1: Schematic of Experimental Setup



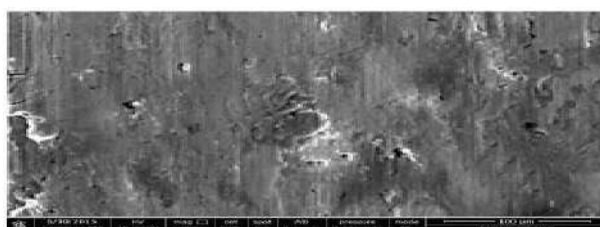
Figure 2: Actual Experimental Setup

Scanning Electron Microscopy (SEM) techniques were used. Field Emission Gun-Scanning Electron Microscope (FEG-SEM) JSM-7600F was used to acquire the SEM micrographs of the cross sections of untreated and PN treated specimens. The PN treated specimen was chemically characterized using Energy Dispersive X-Ray analysis (EDX), where, the electron beam from the SEM serves to excite characteristic X-rays from the area of the specimen being probed. The actual experimental test setup is as shown in Fig. 2.

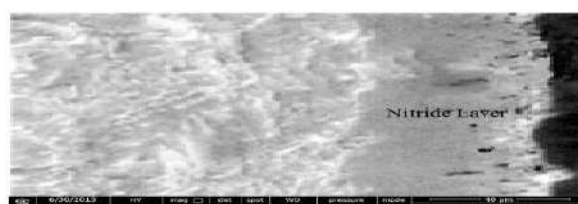
IV. RESULTS AND DISCUSSION

A cross sectional SEM micrograph of untreated AISI 4140

and that of PN treated 4140 specimen is shown in Fig. 3a, and 3b, respectively. Fig 3a illustrates typical microstructure of AISI 4140 steel employed in the present work. Plasma nitriding of the steel substrate gave rise to the development of nitride layer. The cross sectional SEM micrograph (Fig. 3b) reveals that the average thickness of the PN layer which was measured with the help of image analysis technique, and, it was found to be $\sim 45 \mu\text{m}$. EDX Spectrum of cross-section of nitrided 4140 is presented in Fig. 3c which clearly indicates the presence of nitrogen. It shows the element composition of 83.25 at. % Fe and traces of Cr, Si, etc., in addition to the presence of nitrogen. Nitrogen observed on the surface supports the formation of Cr- and Fe- nitrides on the surface [10].



(a)



(b)

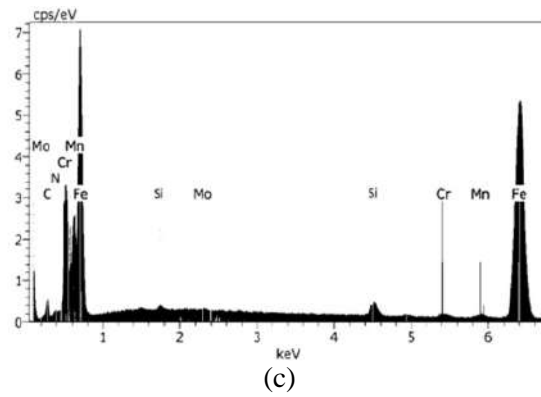


Figure 3: SEM micrograph of (a) cross-section of AISI 4140, (b) cross-section of nitrided 4140 and (c) EDX Spectrum of cross section of nitrided 4140

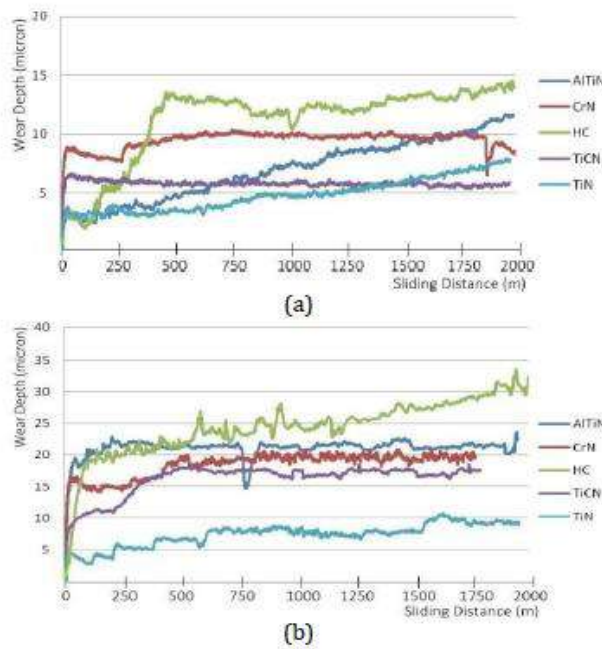


Figure 4: Variation of wear track depth in dry sliding condition at (a) 10N and (b) 20N load

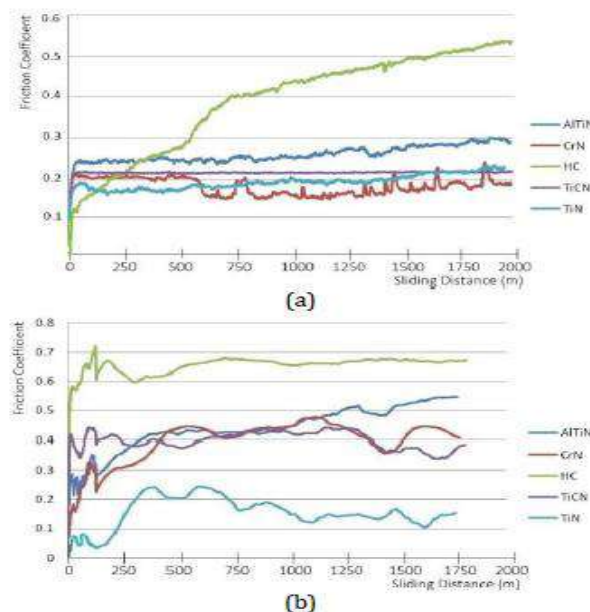


Figure 5: Variation of friction coefficient in dry sliding condition at (a) 10N and (b) 20N load

As evident from Fig. 4, wear track depth goes on increasing

with increase in load. HC coated 4140 has shown sudden rise in wear track depth. It shows sudden increase in friction coefficient (refer Fig. 5a and 5b) at 250-300m of sliding distance, which is an indication of adhesion of work material to the tool surface [1-2, 4]. However, no such sudden rise is observed in case of duplex treated specimens. Among the duplex treated specimens, N-TiN 4140 has shown the lowest wear track depth among the materials under investigation. As load increases from 10N to 20N, the friction coefficient increases for all the materials. It is observed that for duplex treated specimens, at 10N load, the friction coefficient shows very constant value throughout the test. Its average value for duplex treated samples ranges between 0.15 and 0.25. N-TiCN 4140 has shown extremely constant friction coefficient of 0.22 throughout the test. However, as load increases from 10N to 20N, the friction coefficient increases rapidly. At 20N normal load, the average values of friction coefficient, for the entire duplex treated specimens, lie between 0.15 and 0.45, as against 0.65 for HC coated 4140. The oscillations observed in the friction curve [12] indicate that debris of both coating and counterpart is produced, which moves away from the contact area. For all the materials, at 20N load, the friction coefficient increases rapidly during first 200m displacement and thereafter, it remains fairly steady. In order to study the effect of sliding speed on wear characteristics, the tests were conducted at 4.19 m/s and 5.23 m/s with normal load of 10N. Fig. 6a and 6b show variation of wear track depth in dry sliding condition at 4.19 m/s and 5.23 m/s, respectively. It has been observed that as sliding speed increases, wear track depth goes on reducing, for all the materials under investigation. Reduced wear is attributed to the reduced friction (refer Fig. 7 and Fig. 8) due to hydrodynamic squeeze film action, discussed later. It has been observed that N-TiCN 4140 has shown a very constant wear depth throughout the test.

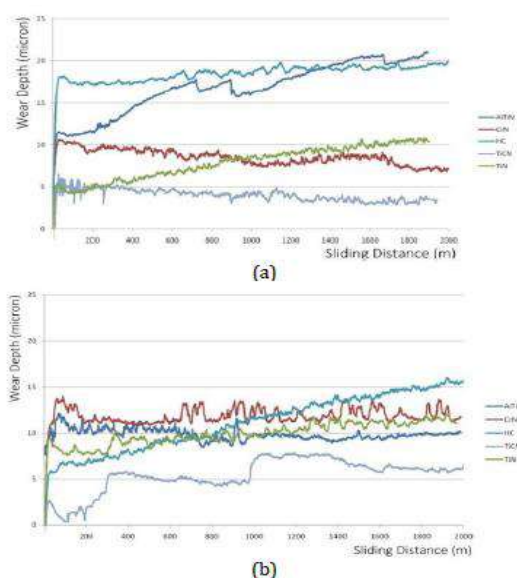


Figure 6: Variation of wear track depth in dry sliding condition at

(a) 4.19 m/s and (b) 5.23 m/s

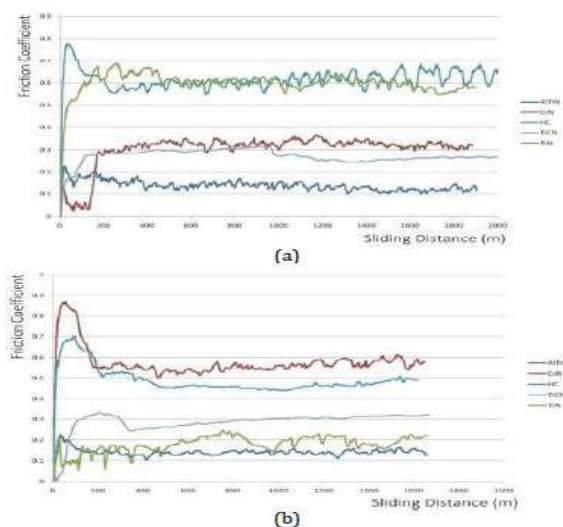


Figure 7: Variation of friction coefficient at 4.19 m/s in (a) dry and

(b) wet sliding condition

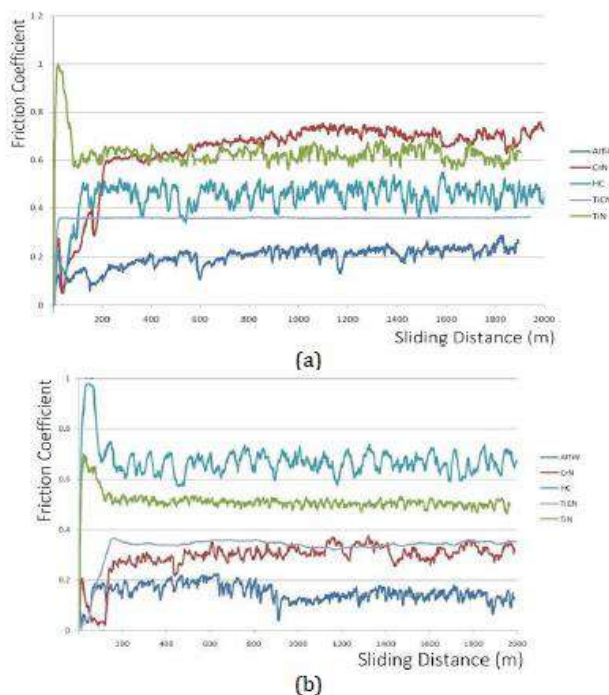


Figure 8: Variation of friction coefficient at 5.23 m/s in (a) dry and

(b) wet sliding condition

It has been observed that as sliding speed increases, friction coefficient goes on reducing. It is due to the fact that as speed of the disc increases, the radial and tangential components of the centrifugal force tend to draw more lubricant into the space between stationary pin and the rotating disc. This hydrodynamic squeeze film action is responsible for reduction in friction coefficient which ultimately leads to reduced wear. Among all the materials under investigation, N-TiCN 4140 has shown very constant

and consistent value of friction coefficient under all the conditions of load and sliding speed. Low values of friction

coefficient in case of duplex treated specimens are in good

agreement with previous results [9]. At increased sliding speed, duplex treated specimens produce much better results than at lower sliding speed [3]. Basically, nitriding of steel prior to PVD coating improves wear resistance of steel [8]. In general, deposition of the coatings on PN treated specimens decreased the pin wear significantly. It may be noted that the wear of the investigated coatings decreases with increased substrate hardness due to nitriding. Compared to untreated substrates, the duplex treated specimens showed improved sliding wear resistance, which can mainly be attributed to the higher substrate hardness, and improved coating-substrate adhesion [19]. Adhesion of the coat to the substrate may be attributed to the presence of interface layer between the coat and the substrate [12, 14]. Increased wear resistance may be attributed to the formation of this layer which further leads to improved coating-substrate adhesion.

V. CONCLUSION

TiN, TiCN, CrN and AlTiN coatings were deposited on plasma nitrided AISI 4140 steel, using PVD process. Also, conventional hard chrome was coated on untreated AISI 4140 steel and the tribological characteristics were studied, in detail. Following conclusions are drawn from the test results: The wear experiments that have been conducted indicate that nitriding of 4140 steel prior to coating the steel substrate, deposited by PVD process, leads to improved friction and wear behaviour. The nitriding process applied to the steel substrate was found to provide satisfactory load carrying support which leads to the improved tribological

behaviour of the coated system. Reduction in friction may be attributed to the long treatment duration that helps nitrogen penetrate deeper into the surface, which ultimately leads to the formation of thick nitride layer. In case of TiCN coated tribo-system, the nitrided zone prior to coating improves coating-substrate adhesion, most probably through the inter-diffusion between iron nitride at the nitrided surface and thin Ti interlayer deposited at the beginning of the coating process. TiCN coated on PN treated 4140 has proved to be the best suitable coating in terms of steady friction behaviour, among the investigated coating materials.

REFERENCES

1. Y. B. Guo, C. R. Liu, Mechanical Properties of Hardened AISI 52100 steel in Hard Machining Processes.
2. Babu, S, Manisekar, K, Dinakarn, V, Gajendran, C, A Study of Mechanical Properties of Nuclear Reactor Bearing's Steels Using Digital Image Correlation Technique, Lecture Notes in Mechanical Engineering, 2020, pp. 571–579.
3. A.H. Meysami, R. Ghasemzadeh, S.H. Seyedein, M.R. Aboutalebi, An investigation on the microstructure and mechanical properties of direct-quenched and tempered AISI 4140 steel
4. C. V. Gorwade, A. S. Alghamdi, I. A. Ashcroft, V. V. Silberschmidt, M. Song, Finite element analysis of the high strain rate testing of polymeric materials.
5. Babu, S., Manisekar, K., KalaiSelvi, S, Heat transfer analysis of slewing ring bearing for high thermal applications, Journal of Thermal Science and Engineering Applications, 2017, 9(1), 011006
6. Marichamy, M., Babu, S, Experimental study and taguchi optimization of process parameter on mechanical properties of A319 aluminum alloy using friction stir welding, Materials Today: Proceedings, 2020, 39, pp. 1527–1531,ISSN:2214-7853.
7. Babu, S., Manisekar, K, Experimental study of heat distribution in polished bearing surfaces for design and development of large diameter slewing ring bearing for FBR, Procedia Engineering, 2014, 86, pp. 350–358
8. Marichamy, M., Babu, S, The selection of optimum process parameters on A319 aluminum alloy in friction stir welding MCDM method, Materials Today: Proceedings, 2020, 37(Part 2), pp. 228–231, ISSN:2214-7853
9. Gbadebo Owolabi, Oluwamayowa Okeyoyin, Oluwakayode Bamiduro, Adewale Olasumboye, Horace Whitworth, The effects of notch size and material microstructure on the notch sensitivity factor for notched components.

Process Improvement Transformation in Petroleum Using Neural Network Approach

R. Ramprakash and V. Jaiganesh

Department of Mechanical Engineering, PSG College of Technology, Coimbatore- 641004, TN, India

ABSTRACT

In the Oil and Gas industry, the implementation of artificial intelligence techniques gives advantages of better use of existing infrastructure. It provides better future outcomes, which makes it an essential technology in the operations of the industry. In this paper, the implementation of artificial intelligence techniques for good planning, determination of reservoir rock properties, drilling optimization and production facilities are reviewed. With precise knowledge of permeability and porosity, reservoir engineers can develop robust reservoir development plan and manage hydrocarbon recovery effectively. For porosity prediction, wire-line log data and seismic attributes are used in artificial intelligence-based models. Permeability prediction has been discussed by considering the different types of well-log data in the modeling of artificial intelligence techniques to predict single-phase fluid. Solution of specific developed problems during the determination of permeability in the actual experiment is also mentioned. Artificial intelligence techniques are used in the design and accurate analysis of the drilling fluid. It assists in the selection of drill bit and drilling-related problems. If a reservoir cannot produce naturally, we can select a suitable artificial lift and design the production system using Artificial intelligence techniques.

Keywords – Artificial neural network, Enhanced oil recovery Fuzzy logic system, Artificial lift, Permeability Porosity

1. INTRODUCTION

In terms of the transportation of petroleum fluids around the globe, pipelines are becoming more critical. With the increasing number of applications, pipelines are subject to different failures under different conditions [1]. Pipelines are extended to several km for various purposes, to transport oil and gas for industrial and household use [2]. In other words, pipeline safety and security are related to a country's social and economic development. Although the pipelines are the safest mode of transportation, there are chances of flow leakage and interruption while running due to various reasons [3]. Cracks and leaks in a pipeline system can be a reason for economic loss, waste of resources, and sometimes even human deaths due to system failure. Inspection and checking of the pipeline condition are, therefore, mandatory on a timely basis. The damage that occurs due to a few reasons, such as welding defects, mechanical factors, external damage, natural hazards, corrosion, has a significant impact on the life of the pipeline. It is, therefore, mandatory for a pipeline to undergo regular inspection in order to avoid accidents and pipeline failure. The application of Artificial intelligence tools such as fuzzy logic and neural networks is evolving as oilfield technology. In 1996 PRRC researchers used fuzzy logics to compute the significance of mini-permeameter permeability measurement. One of the goals of artificial intelligence in upstream operations is personnel strategy optimization to minimize risk. Artificial intelligence can affect drilling space positively. There are many advantages of artificial intelligence in the petroleum industry. ANNs are computational systems whose architecture and operation are inspired by biological neural cells in the brain. ANN's primary function can be defined either as computational models for linear and nonlinear approximation, clustering and classification of data, or as model simulation. The Feed-Forward (FF) network is commonly used along with Back Propagation to train neural networks. Feed-Forward Back Propagation Network (FFBPN)'s main use is to learn and map the relationships between inputs and outputs. In addition, the FFBPN learning rule is used to adjust a system's weight values and threshold values to achieve the minimum error. It can also be described as a complex relationship between the input and output values of a network set. Each node or neuron has a value that is determined by the input received from other network system units. Each input signal is multiplied by the corresponding input line weight value.

2. Proposed Feed Forward Back Propagation Network (FFBPN) Approach

The overall methodology is presented in Figure 1. The first step comprises of collecting the data from the crude oil industry. Six parameters were identified, based explicitly on the higher impact on the pipeline condition. The FFBPN technique was used for training a model which is the performance of two-way iterations. The first way includes the forward step computation of input weights and the second way is backward step computation for updating weights and calculating errors. The training data was normalized within the range of [0–1]. Seventy

percent of collected data was used for training the model, whereas 30% of the data is divided equally for the testing and validation, respectively.

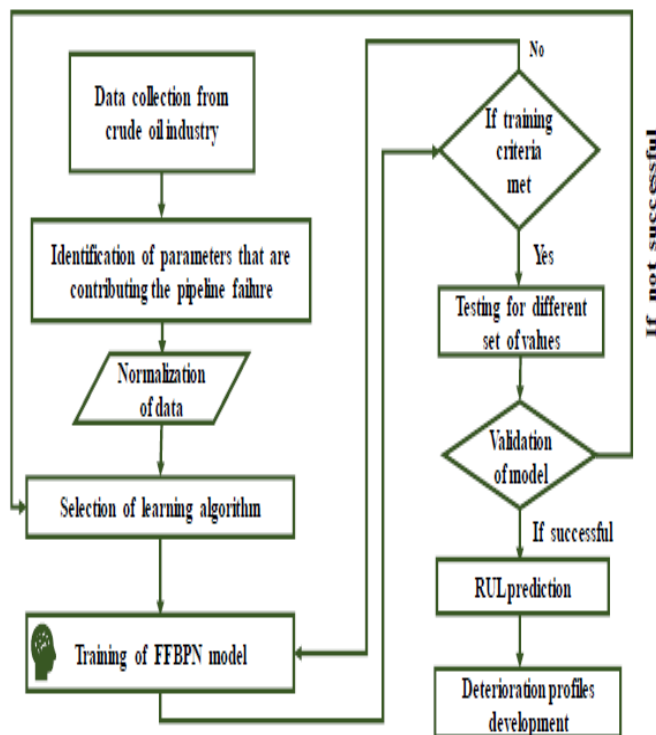


Figure 1. FFBN approach workflow.

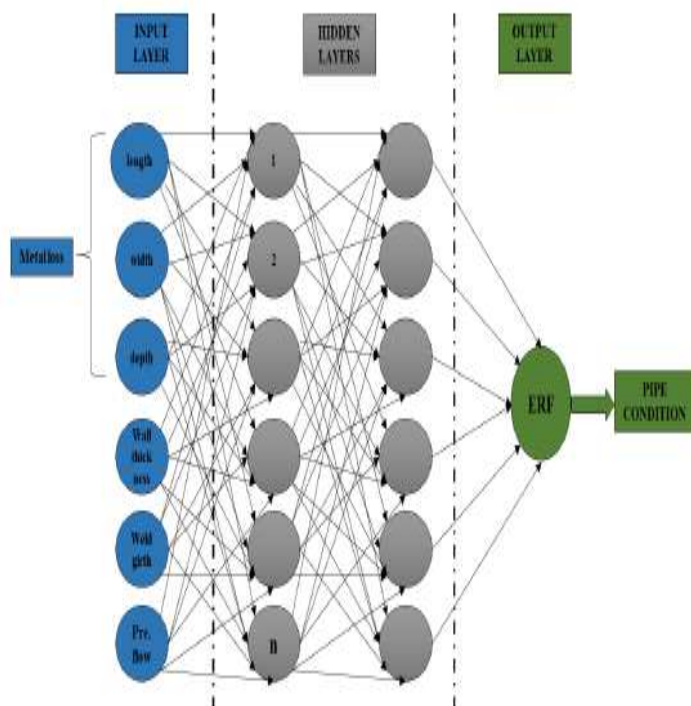


Figure 2. Proposed Neural Network architecture.

A neural network system solved the problem related to estimating technically and economically EOR methods. However, economic examination, which was not clear up by this system, now clear up by the neural network approach. To design two separate networks, one which has aimed to get the technically successful project and can be applied under reservoir condition. Moreover, examine the project by applying a second neural network whether the project is beneficial

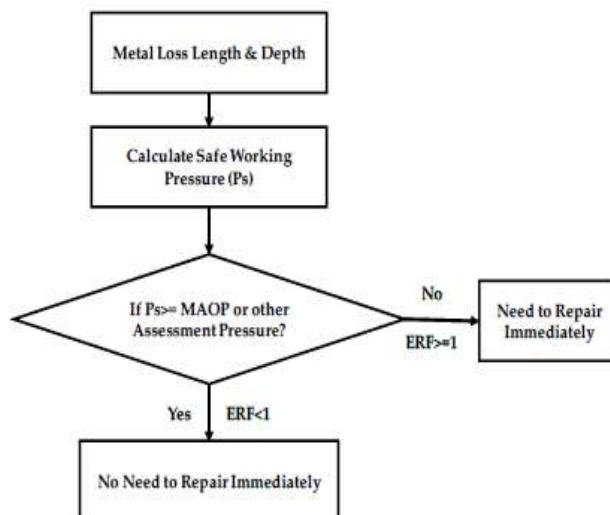


Figure 3. Flowchart for determination of Estimated Repair Factor.

Finally, the model was validated for its reliability with a new (unknown) data set and the results were found to be satisfactory.

The six parameters including metal loss (length, width and depth), wall thickness, weld girth and pressure were considered from the data and given as inputs, and Estimated Repair Factor (ERF) is taken as output to develop the FFBN model as shown in Figure 2. The model was developed in three stages, namely training, testing and validation, in which 70%, 15% and 15% of data were used, respectively. If the training criteria are met in the first stage, then the model proceeds to the test stage where it is tested to measure its performance for a given testing data sample values; otherwise, it is recalled for retraining in the first stage. The model is successfully developed and validated after the

testing stage..

3. FFBN Model Development

MATLAB 2018a was used to develop the FFBN model. During the initial training stage, the FFBN-based model is trained using the available historical data. If the model fails to meet expectations, it will allow the process to be re-propagated until it reaches the best requirement using. The six parameters mentioned above have been used as inputs and ERF has been used as a target

for the model development. Notably, the model was trained with a different number of neurons, out of which, 16 neurons gave the best predicted output and the selected number of data sets were sufficient to train, validate and test the model. A FFBN neural network has been developed to predict a crude oil pipeline's life condition. Specific factors have been considered as inputs for model development as limited data were available. The model developed was trained on the basis of Equation (1) and the Levenberg-Marquardt backpropagation algorithm; the model has been later validated and tested by providing all possible data sets. The R2 value has been predominantly changed as the number of hidden neurons was varied, starting from a minimum of 6 to a maximum of 20, as shown in Figure 5. . The input layer receives the input signals from the other source; the role of the hidden layer is to transform the signals into something that the output signal can use in some way. The proposed neural network architecture with 'tansig' and 'purelin'.

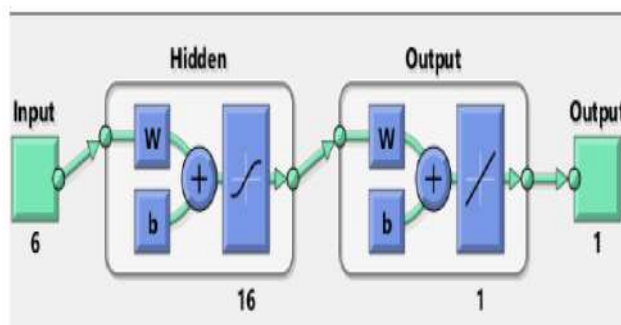


Figure 4. Proposed network architecture with functions

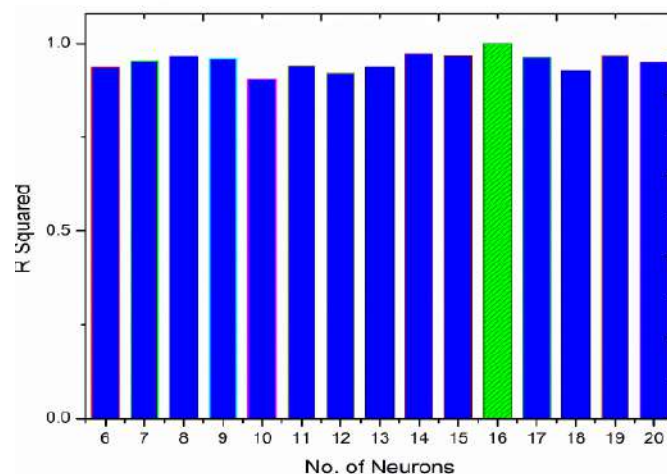


Figure 5. Variation of R2 value over number of hidden neurons.

The accuracy of the developed model has been found to be highly sensitive to the number of hidden neurons. Table 2 shows the overall R2 values against the respective number of hidden neurons, with MSE and R2 values, in all stages. The best network architecture was found to be [6 _ 16 _ 1]. Variations in R2 and MSE values along typical ANN stages with 16 hidden neurons are illustrated in Figure 6. The overall R2 values are found to be consistent with the number of neurons ranging from

12 to 18, the detailed results obtained against these neurons are presented here. During the selection of optimum network structure, the error for the existing state of the neural network must be assessed constantly. This needs the selection of an error function, conventionally called a loss function, which can be used to estimate the loss of the model, so that the weights can be updated to reduce the loss on the next evaluation. In this study, MSE has been used as loss function to compute the performance of neural network.

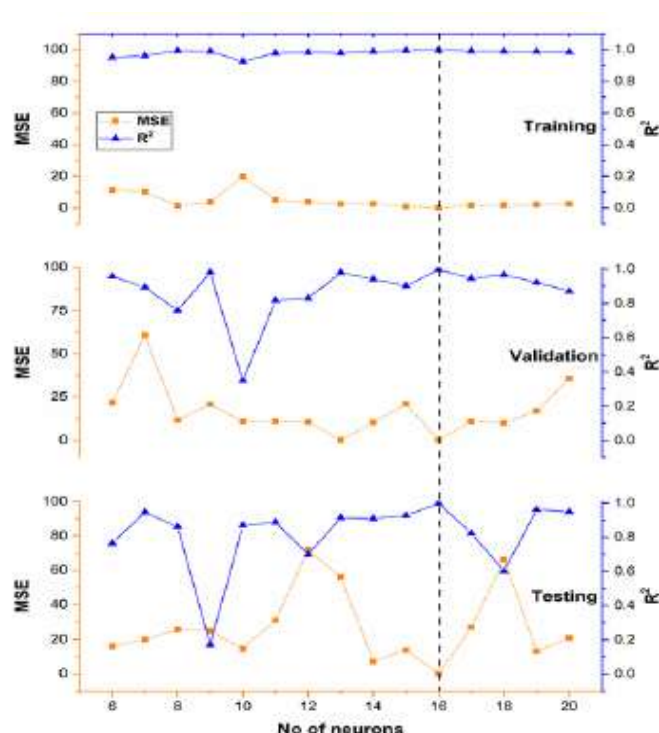


Figure 6. Variations in MSE and R2 values with number of neurons

The variations in the value of MSE and R2 over the number of hidden neurons are clearly represented in Figure 6. Notably, all stages have R2 values close to 1.0 and MSE values close to 0, with 16 hidden neurons shown in the Figure 6 by a dotted line.

Figure 7 represents the summary of R2 plots in training, testing and validation stages during the training process. For the training data set, an overall R2 value of 0.9998 has been obtained. The neural network was

trained and validated using available historical data set to develop a robust model with the finest predicted accuracy of the output. The results have been found to be satisfactory, as the overall R2 value is close to 1.0. Notably, the R2 value in each stage is close to 1.0, i.e., 0.9997, 0.9999 and 0.9999 for training.

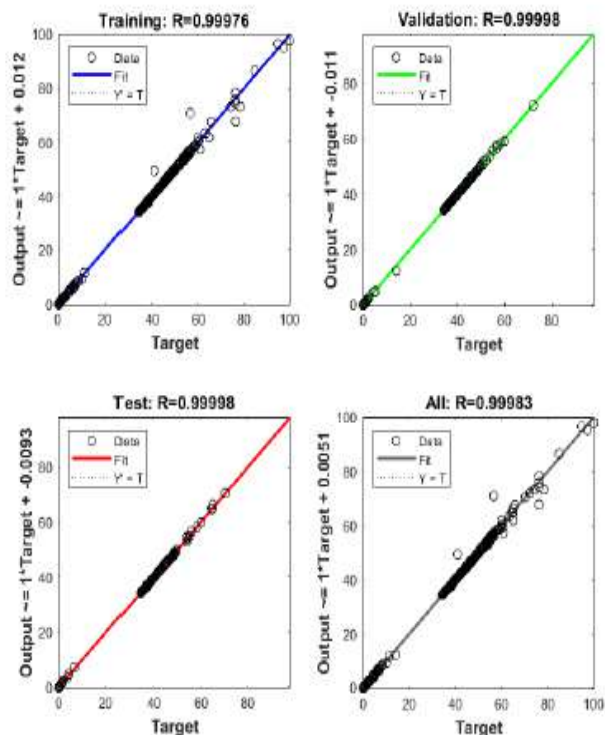


Figure 7. Training, Testing, Validation

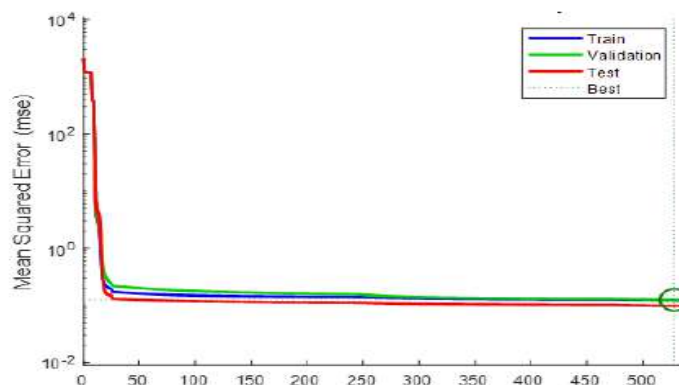


Figure 8. Best validation performance plot

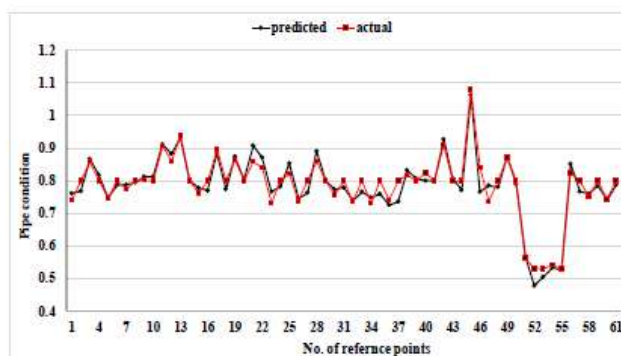


Figure 9. Plot for actual ERF vs predicted ERF.

4. CONCLUSIONS

The prediction model to assess the condition of the crude oil pipeline was developed using the Back Propagation Neural Network technique focused on specific factors such as metal loss anomalies (across length, width and depth), wall thickness, weld girth and pressure flow. _ The results of FFBN model found to be satisfactory based on an R2 value of 0.9998. The predicted output accuracy was found to be highly dependent on the number of neurons. _ The model was tested with a new data set and the results were found to be good, with the R2 value of 0.99. _ The FFBN model was validated using a new sample data and the results were found to be accurate with Root Mean Square Error (RMSE) and Mean Absolute Percentage Error (MAPE) values of 0.02514 and 0.02526, respectively. _ The deterioration curves were generated to know the effect of each factor selected on the pipeline condition; it was found that pressure has a major negative effect on pipeline condition and weld girth has a minor negative effect on pipeline condition. _ The proposed FFBN was validated with other published models for its robustness and it was found that FFBN performed better than the previous approaches based on R2 and RMSE. _ In terms of maintenance scheduling, the proposed approach will be beneficial. The developed model can be applied to real-time data to help pipeline operators take the necessary actions to prevent product losses in the oil and gas pipeline industries.

REFERENCES

1. Aimin Yang, Yang Han, Yuhang Pan, Hongwei Xing, Jinze Li—Optimum surface roughness prediction for titanium alloy by adopting response surface methodology, *International Journal of Results in Physics* 7(2017)1046–1050.
2. Aezhisai Vallavi Muthusamy Subramaniana, Mohan Das Gandhi Nachimuthu, Velmurugan Cinnasamy,—Assessment of cutting force and surface roughness in LM6/SiCp using response surface methodology, *Journal of Applied Research and Technology* 15(2017)283–296.
3. João Eduardo Ribeiro, Manuel Braz César, Hernâni Lopes —Optimization of machine parameters to improve the surface quality, *Procedia Structural Integrity* 5(2017)355-362.
4. M. Subramanian, M. Sakthivel, K. Soorya Prakash, R. Sudhakaran —Optimization of Cutting Parameters for Cutting Force in Shoulder Milling of Al7075-T6 Using Response Surface Methodology and Genetic Algorithm, *Procedia Engineering* 64(2013)690–700.
5. Montgomery DC—Introduction to statistical quality control, Wiley (1996), New York.

The Impact of Inventory Management Practice on Firm's Competitiveness and Organizational Performance

B. Vaishnavi and R. Ilakkiya

Department of Mechanical Engineering, PSG College of Technology, Coimbatore

ABSTRACT

This study aimed to empirically examine the impact of inventory management practice on firms' competitiveness and organizational performance. Data for the study were collected from 188 micro and small enterprises (MSEs) operating in the manufacturing sub-sector and the relationships and hypothesis proposed in the conceptual framework were tested using structural equation modeling (SEM). The results indicate that higher levels of inventory management practice can lead to an enhanced competitive advantage and improved organizational performance. Also, competitive advantage can have a direct, positive impact on organizational performance. Therefore, it is recommended that policy makers, universities, NGOs and any concerned party who are engaged in supporting of MSEs need to work on providing the necessary training and resource to promote the inventory management practice of MSEs which will result in increasing their competitiveness and organizational performance. That would enhance their contribution to the economic development of the country. Note that, the conclusion obtained from this study may not be used to generalize to large and medium scale as well as overall sectors since its focus is only from the MSEs' manufacturing sub-sector points of view.

Keywords — Inventory management, ABC analysis, Multi bin system, Periodic review policies, Continuous review policies

I. INTRODUCTION

Inventory management, which is a part of the internal company's function, is one of the areas of supply chain management. If the firm can properly and efficiently manage its inventory system, it may be able to save money on operational costs. Good stock management will maximise corporate benefits, whereas vice versa lead to lack of stock control and will result in a loss of company benefit [1]. The continuous review policy and the periodic review policy are two replenishment policies that are frequently utilised in practise. According to the continuous review policy, the inventory status is continually maintained, and ordering according to lot size (Q) was done when the level reached the designated inventory reorder threshold. The periodic review policy indicates that the inventory status was tracked at regular periodic intervals and reorders were made to raise the inventory level to the predefined point. These inventory system policies aren't exhaustive, but they're good enough to address issues with the inventory management system's security. The effectiveness and efficiency of an inventory management system may have a major impact on supply chain management, improving cycle service levels and lowering costs [2]. The benefit of a continuous review strategy is that it may solve situations where demand is strong, but the drawback is that order quantities are changeable. The supplier is more likely to make mistakes, thus clients who bought the fixed order quantity are preferred. With the periodic review policy, the situation is the inverse [3]. To ensure a successful supply of raw materials, the Kanban method necessitates supplier commitment to offering quick services. Essentially, the Kanban method simply necessitates a minimal number of stocks in the production line, with inventories equal to output numbers. As a result, supplier commitment is critical in ensuring that manufacturing lines run smoothly and effectively. Quality, desire to collaborate, technical expertise, geography, and pricing are five essential characteristics to consider while selecting suppliers. Just in time aims to remove stocks rather than transfer them to a different point in the supply chain.

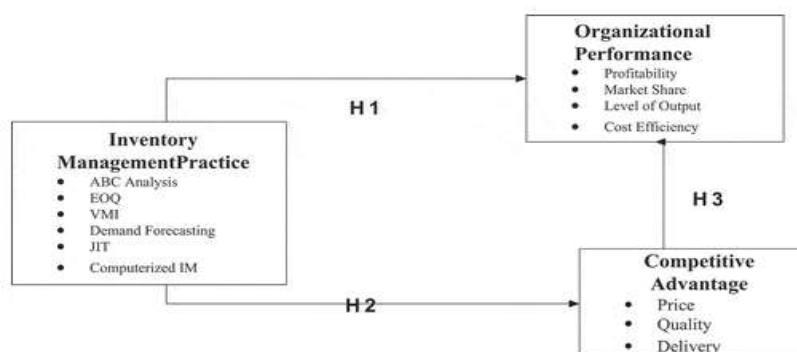


Figure 1. Conceptual framework of the study

II. METHODOLOGY

The process for developing a Kanban system as well as procurement policies are provided as follows that includes gathering essential parameters is the first step in developing a Kanban system and calculating Kanban quantity. Finally establishing a pull mechanism and rule. Whereas the procedure for developing procurement policy includes collecting relevant data, Safety stock, reorder point, economic order quantity calculations and average inventory level calculations. Contrasting the policies of continuous and periodic evaluation.

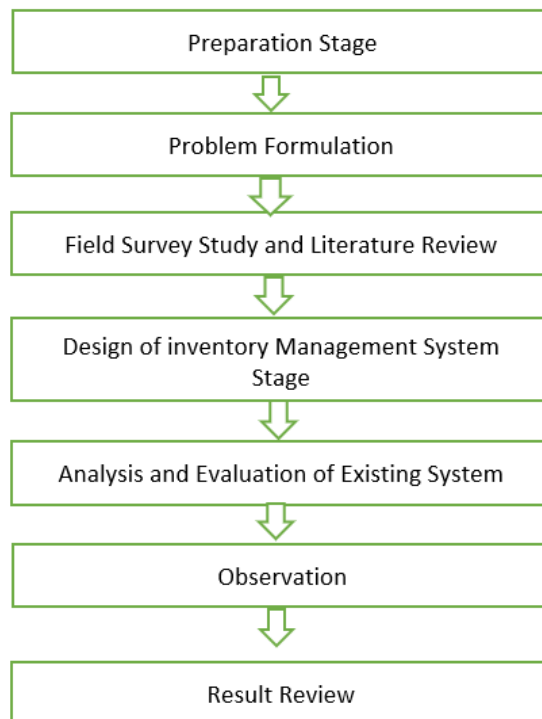


Figure 2: Methodology of the Process

III. CASE STUDY

The research methodology is directly translated to the case study. The procedures involved in the methodology are explained as below

1. Forward cover system

The 'Push system,' which sought to retain a big inventory of product according to consumer projection, is at the heart of traditional production strategy. However, this has been a significant problem for individuals, since raw material stockpiles have increased, production processes have become disjointed, and unnecessary stock has been produced. The problems with the front cover system are that the requirements which are not met must be identified, this need must be placed in the context of procurement, there must be a high degree of leadership and staff commitment, and the capacity to make a strong enough forward commitment to produce the needed market pull. Forward contracts include counterparty credit risk because no money is exchanged at the outset. Because one can rely on the counterparty to deliver the asset, which might end up to lose money if the counterparty defaults between the initial agreement date and the delivery date.

1.1 Procurement policy

- Capital investment in inventories is high
- Raw material inventory is high as compare to usage.
- Safety stock amount for each product is high as compared to usage

2. ABC ANALYSIS

ABC analysis is a method of inventory classification that divides into three categories: A, B, and C. The most valuable goods are A, while the least valuable items are C. The ABC analysis in Ats-Elgi limited is listed in table 1 and 2

A Category – 5% to 10% of the items represent 70% to 75% of the money value.

B Category – 15% to 20% of the items represent 15% to 20% of the money.

C Category – The remaining number of the items represent 5% to 10% of the money value.

TYPE OF ITEM	NUMBER OF ITEM	INVENTORY VALUE
A-ITEM	291	30999531.82
B-ITEM	469	5831012.144
C-ITEM	1951	1918426.878

Table 1: Type of item and Inventory value

TYPE OF ITEM	% OF USAGE	% OF INVENTORY VALUE
ITEM A	11%	80%
ITEM B	17%	15%
ITEM C	72%	5%

Table 2: Percentage of Usage and Percentage of Inventory value

3. Multi bin Kanban system

The supplier tops up the bins at regular intervals in a multi-bin Kanban system. They frequently have numerous locations inside the plant, and the operators will simply take full bins and return empty bins for restocking. The following is how the Multi-bin system works. Items are organised into many containers. The first bin is placed on top of the second bin, or in front of it. On the bottom of each bin is a reorder card. The first bin is the only one from which material is taken. When the first bin is full, it is swapped out for the second. The reorder card is used to replenish the first bin's contents. While waiting for the material on order to arrive, material is pulled from the second bin. When the new material arrives, it is placed in the empty bin, and the reorder card is placed back in its original location in the bin. The practise is repeated until all of the material in one bin has been used up. The reordering card is then used to refill the material.

Description	Replenishment lead time(days)	Batch size	Number of cards
Wheel aligner kit dya 1000w	90	4	6
Kit wb f7d	90	11	6
Power pack with motor assy-f	90	6	6
Blower fan model ta/r 18-18	90	12	3
Vacuum pump	90	32	3
Wrench impact 1/2" sp1140ex	90	8	7
French ratchet 1/2" sp1133sx	90	8	7
Power pack	90	4	3
Burner bantona - b30a/as47cpu	60	12	3
Electric 3hp ind motor	60	47	4
3hp electric motor b3 b14	60	19	7

Table 3: Proposed batch size and number of cards for Multi bin system

IV. Basic simulation using c program

1. Flow chart using c program

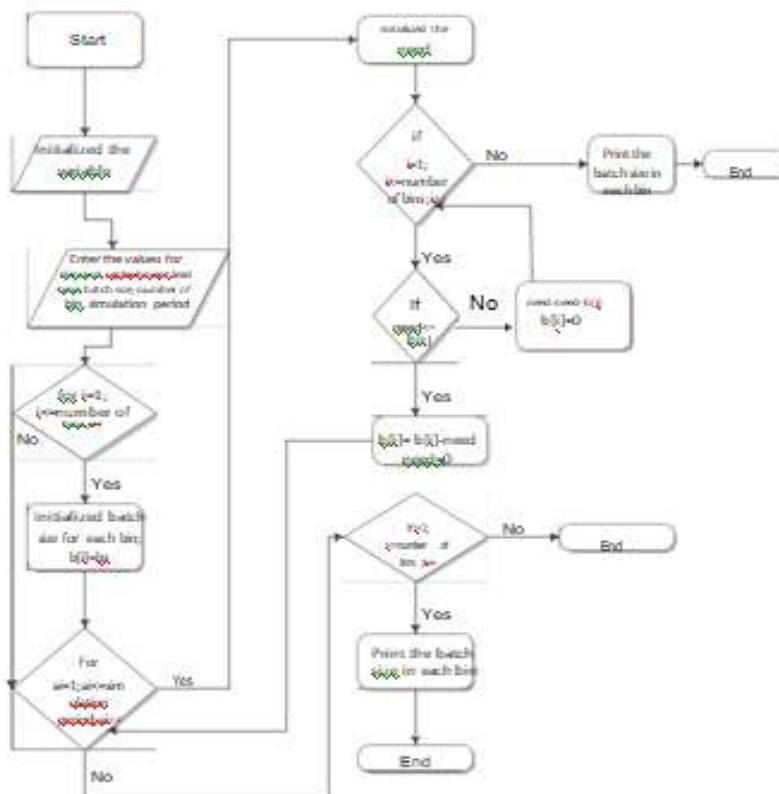


Fig 3: Flow chart using c program

2. C Program code

```
#include<stdio.h>
#include<conio.h>
void main()
{
int ai,i,d,bs,nb,nee,m,lt,tmp=0,opt,b[100]; clrscr();
printf("\n Enter demand value = ");
scanf("%d",&d);
printf("\n Enter number of bins = "); scanf("%d",&nb);
printf("\n Enter batch size = " );
printf("\n Enter manufacturing lead time in months = " ); scanf("%d",&lt);
printf("\n The Monthly demand is = %d\n Number of bins
= %d\n Batch size = %d\n Manufacturing lead time =%d months \n ",d,nb,bs,lt);
printf("\n Enter the simulation period in months ="); scanf("%d",&m);
for(i=1;i<=nb;i++)
{
b[i]=bs;
printf("\n Bin %d = %d",i,b[i]);
}
}
```

```

for(ai=1;ai<=m;ai++)
{
nee=d;
for(i=1;i<=nb;i++)
{
if(nee<=b[i])
b[i]=b[i]-nee;
nee=0;
}
else
{
nee=nee-b[i];
tmp=tmp+b[i];
b[i]=0;
}
}
for(i=1;i<=nb;i++)
{
printf("\n\n Bin %d = %d",i,b[i]);
}
getch();
}
    
```

V.Simulation using arena

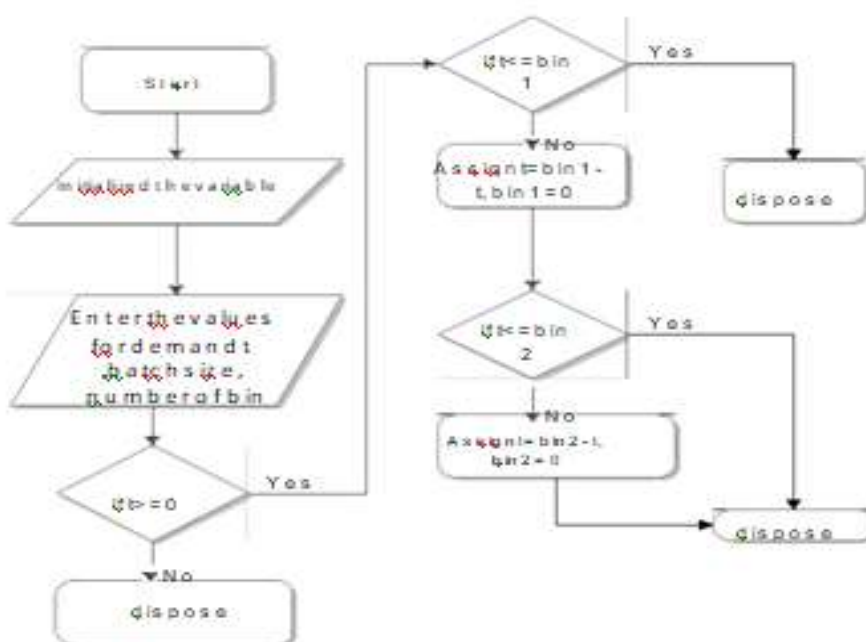


Fig 4: Flow chart-2 bin system

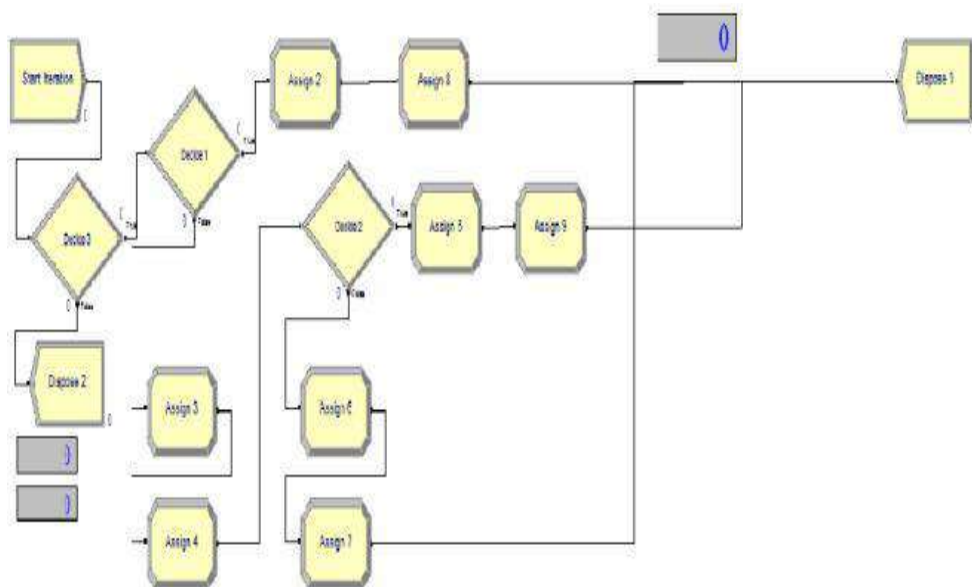


Fig 5: Simulation model-2 bin system

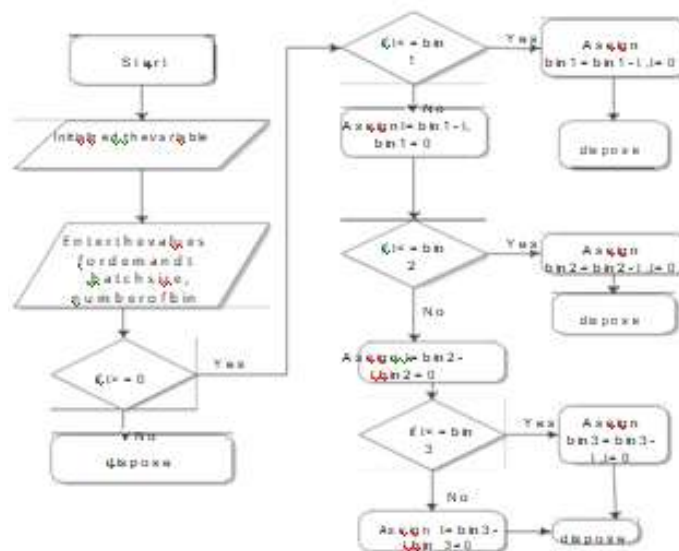


Fig 6: Flow chart-3 bin system

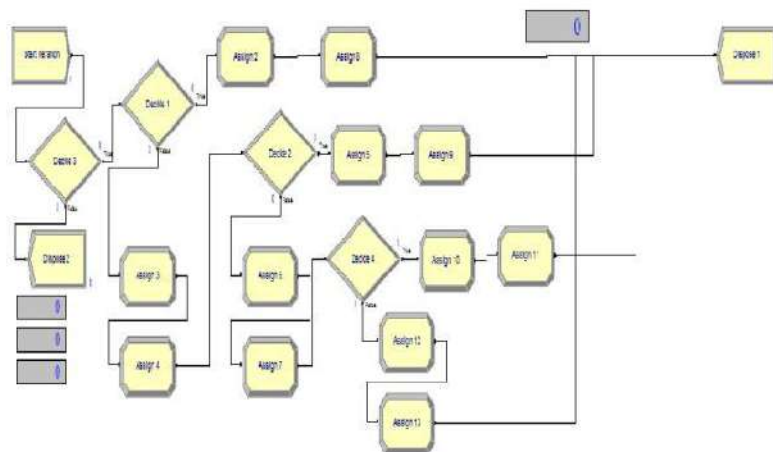


Fig 7: Simulation model-3 bin system

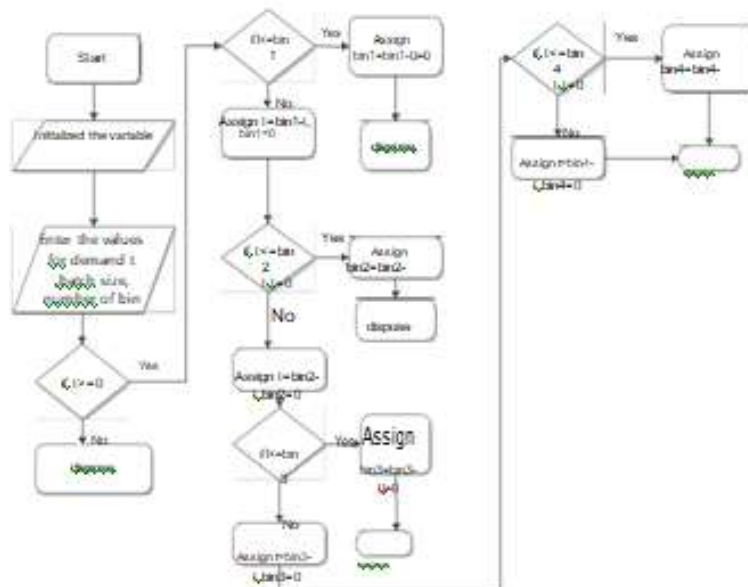


Fig 8: Flow chart-4 bin system

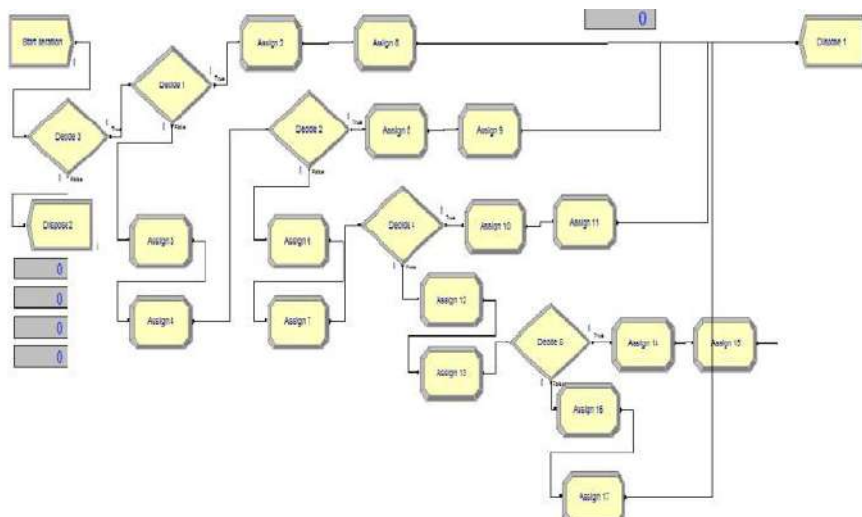


Fig 9: Simulation model-4 bin system

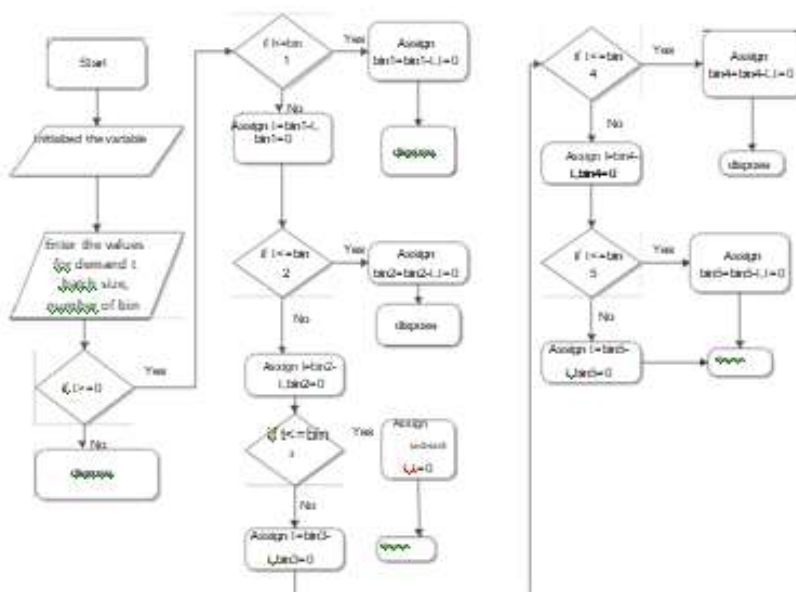


Fig 10: Flow chart-5 bin system

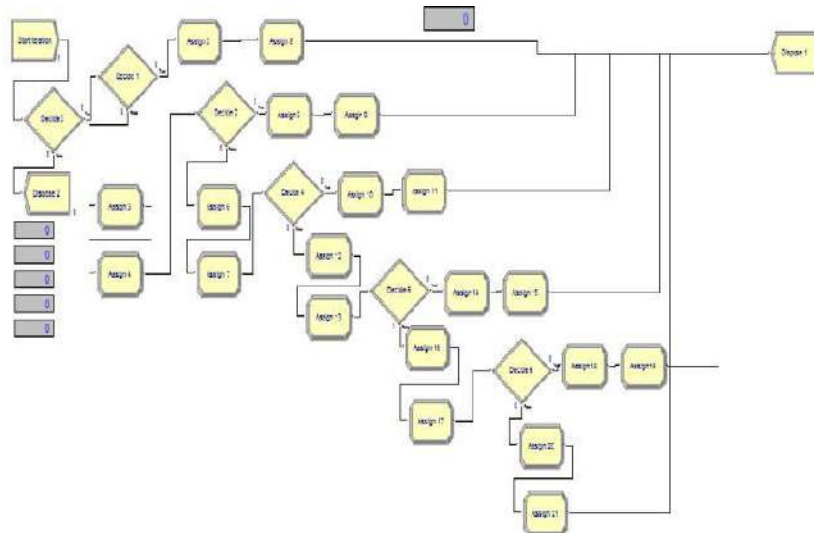


Fig 11: Simulation model-5 bin system

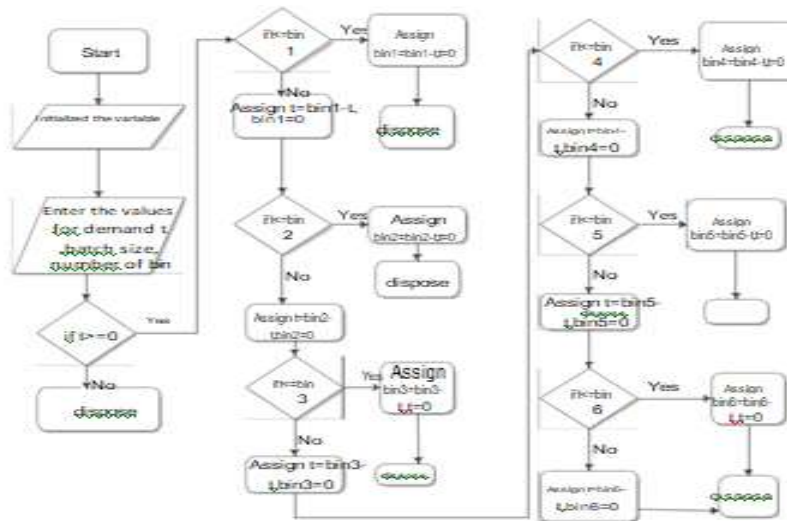


Fig 12: Flow chart-6 bin system

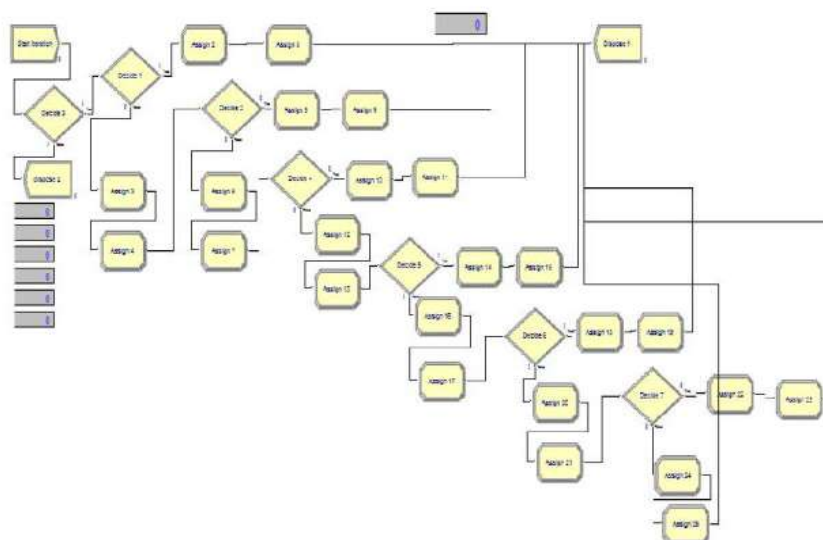


Fig 13: Simulation model-6 bin system

VI. Inventory management system-procurement policies

1. Continuous Review (Q method)

1. $ROP = FS - 1 (CSL) \times \sigma L$ (1) $ROP = DL + SS$ (2)

$$CI = Q/2 \quad (3) \quad AIL = CI + SS \quad (4) \quad DL = DL \quad (5)$$

$$\sigma L = \sqrt{L}\sigma D \quad (6)$$

$$Q = \sqrt{(2DeS)/hC} \quad (7)$$

2 Periodic Review (P method)

$$SS = F_s - 1(CSL) \times \sigma_{T+L} \quad (8) \quad DT+L = (T + L) D \quad (9)$$

$$\sigma_{T+L} = \sqrt{(T+L)} \sigma D \quad (10) \quad OUL = DT+L + SS \quad (11) \quad AIL = (DT)/2 + SS. \quad (12)$$

This is the definition of a few terms:

SS = safety stock

CSL = cycle service level

CI = cycle inventory

ROP = reorder point

F_s-1 = normsinv

σ_{T+L} = standard deviation of demand during T+L

T = review interval

L = average lead time for replenishment

D = average demand per period

σD = standard deviation of demand per period

σL = standard deviation of demand during lead time $DT+L$ = mean demand during T+L

OUL = order up to level

AIL = average inventory level

Q = lot size

De = annual demand

S = order cost per lot

h = holding cost

c = unit cost

1. Comparison of continuous review policy and periodic review policy

Description	Cycle inventory	Average inventory level	Average inventory value(rupees)
Power pack with motor assy-f	17	26	374887
Sensor head kit truck align	1	1	240278
Blower fan model ta'r 18-18	17	55	682351
Ramp assembly	5	8	110270
Vacuum pump	48	118	414696
Wrench impact 1/2" sp1140ex	24	41	217398
Wrench ratchet 1/2" sp1133sx	24	44	123035
Blower 8000 cmh. italy.ta-s15	1	3	28489
Electric 3hp induction motor	93	137	732998
Oxygen sensor	46	78	207501

Table 4: Proposed continuous review policy inventory system

Description	Order up to level	Average inventory level	Average inventory value(rupees)
Power pack with motor assy-f	38	14	212450
Sensor head kit truck align	2	2	400464
Blower fan model ta/r 18-18	73	48	599265
Ramp assembly	16	25	335875
Vacuum pump	161	95	332052
Wrench impact 1/2" sp1140ex	60	27	139376
Wrench ratchet 1/2" sp1133sx	63	30	82697
Blower 8000 cmh italy.ta-s15	4	2	24378
Electric 3hp induction motor	208	92	494674
Oxygen sensor	116	57	151304

Table 5: Proposed periodic review policy inventory system

VII.RESULTS AND DISCUSSION

1. Analysis of Procurement policy

Safety stock, Reorder level, Average inventory level, Average inventory value and savings in inventory cost were analysed. Based on the results of the inventory policy of each item, it is evident that the Periodic review policy is having less inventory value as compare to continuous review policy

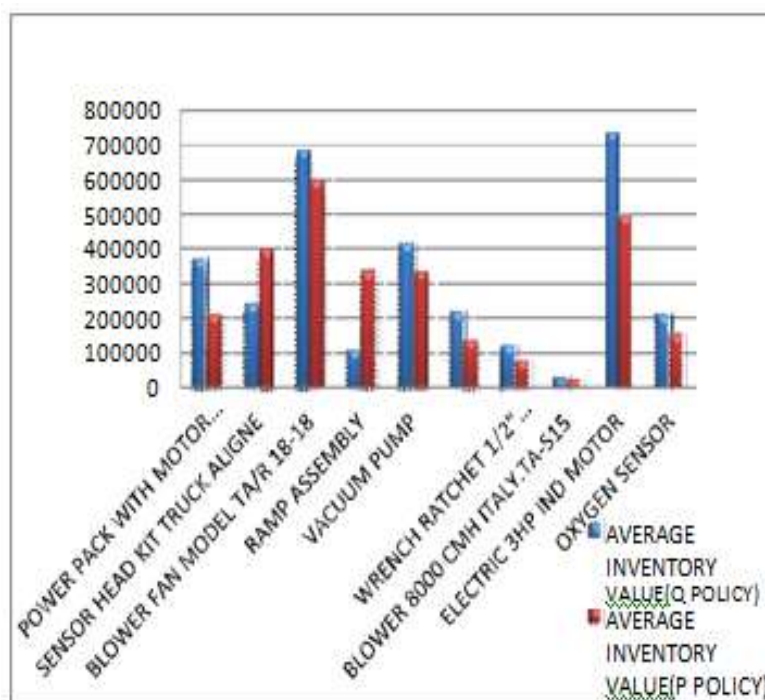


Fig 14: Comparison of average of inventory value

Description	Average inventory value (q-policy)	Average inventory value (p-policy)	Average Inventory value (old)	Q-policy savings (%)	P-policy savings (%)
Power pack with motor	374887	212450	1316531	72	83
Sensor head kit truck align	240278	400464	2838854	92	91
Blower fan model ta/r 18-18	682351	599265	2314605	71	74
Ramp assembly	110270	335875	1980629	94	83
Vacuum pump	414696	332052	1648759	75	80
Wrench impact 1/2" sp1140ex	217398	139376	438373	50	68
Wrench ratchet 1/2" sp1133sx	123035	82697	247959	50	67
Blower 8000 cmh 8000-15	28489	24378	851863	97	97
Electric 3hp induction motor	732998	494674	5149854	86	90
Oxygen sensor	207501	151304	1395075	85	89

Table 6: Comparison of p-policy savings(%) and q-policy savings(%)

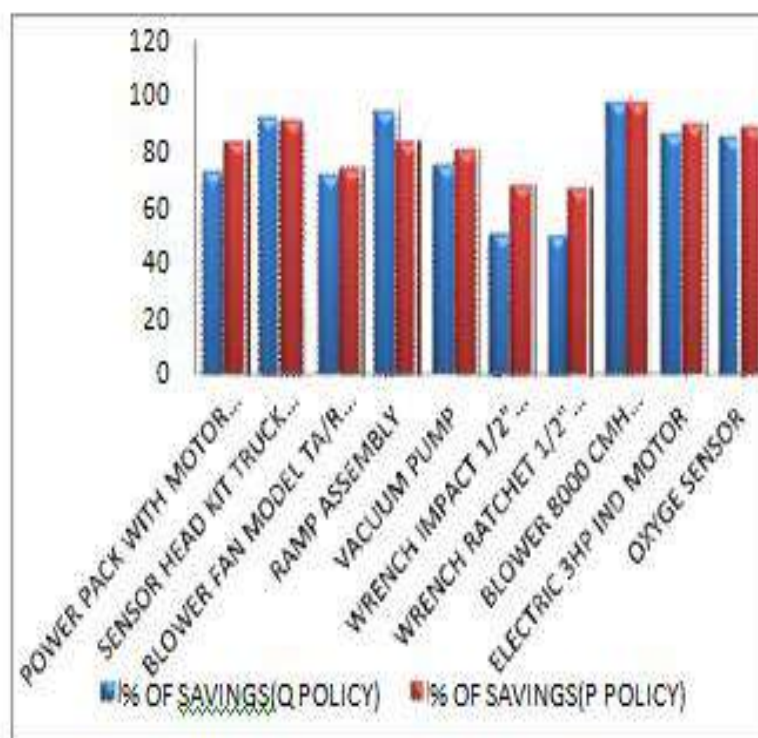


Fig 15: Comparison of p-policy savings (%) and q-policy savings (%)

2. Analysis of multi bin Kanban system

Based on simulation result, multi bin system keeps down the inventory cost as compared to forward cover system.

Description	Apr'15 - qty	May'15 - qty	June'15 - qty	July'15 - qty
Wheel aligner kit dwa 1000w	2	3	2	2
kit wb f7d	2	12	7	3
Power pack with motor assy-f	3	2	6	6
Sensor head kit truck align	0	0	0	0
Blower fan model ta/r 18-18	26	51	17	41
Vacuum pump	13	13	10	9
Wrench ratchet 1/2" sp1133sx	5	4	4	4
Power pack	39	36	18	34
Blower 8000 cmh italy.ta-s15	5	4	4	4
Power pack	39	36	18	34
Burner bentone - b30a/as47cpu	17	20	9	14
Electric 3hp ind motor	62	83	40	35
3hp electric motor b3 b14	39	49	97	82

Table 7: Forward cover system-inventory in terms of quantity

Description	Apr'15- value	May'15- value	June'15 - value	July'15- value
Wheel aligner kit dwa 1000 w	372505.1	542765.3	384651.2	393834.5
Kit wb f7d	110825.5	681200.9	397367.2	166226
Power pack with motor assy-f	50550	29400	88200	88200
Sensor head kit truck align	0	0	0	0
Blower fan model ta/r 18-18	81897.66	160645.4	53548.47	141260.6
Vacuum pump	36220.73	36220.73	27862.1	25075.89
Wrench ratchet 1/2" sp1133sx	53967.75	43174.2	43174.2	43174.2
Power pack	334501.8	309722.4	158168.5	299795.7
Blower 8000 cmh italy.ta-s15	53967.75	43174.2	43174.2	43174.2
Power pack	334501.8	309722.4	158168.5	299795.7
Burner bentone - b30a/as47cpu	407839.2	490315	217252.5	344241.2
Electric 3hp induction motor	351557.4	470633.2	209792.8	184292.5
3hp electric motor b3 b14	222337.1	279346.6	534211	453382.1

Table 8: Forward cover system-inventory value in terms of rupees

Description	April 15- qty	May15- qty	June15 qty	July15 qty
Wheel aligner kit dwa 1000w	2	3	1	2
Kit wb f/d	2	4	8	1
Power pack with motor assy-f	1	2	4	5
Sensor head kit truck align	0	0	0	0
Blower fan model ta/r 18-18	6	6	6	6
Vacuum pump	20	25	30	35
Wrench ratchet 1/2" sp1133sx	6	8	10	4
Power pack	3	4	4	4
Blower 8000 cmh italy.ta-s15	0	0	0	0
Power pack	24	48	1	24
Burner bentone - b30a/as47cpu	16	8	8	12
Electric 3hp induction motor	16	32	1	16
3hp electric motor b3 b14	24	30	36	23

Table 9: Multi bin system-inventory in terms of quantity

Description	April 15- value	May 15- value	June15 value	July15 value
Wheel aligner kit dwa 1000w	415147	622720	103787	415147
Kit wb f/d	119931	239863	479725	29983
Power pack with motor assy-f	7350	29400	51450	73500
Sensor head kit truck align	0	0	0	0
Blower fan model ta/r 18-18	74180	74180	74180	74180
Vacuum pump	70189	87737	105284	122831
Wrench ratchet 1/2" sp1133sx	16717	22290	27862	11145
Power pack	25761	34348	34348	34348
Blower 8000 cmh italy.ta-s15	0	0	0	0
Power pack	206073	412146	8586	206073
Burner bentone - b30a/as47cpu	392266	196133	196133	294199
Electric 3hp induction motor	85813	171627	5363	85813
3hp electric motor b3 b14	135162	168953	202744	129531

Table 10: Multi bin system-inventory value in terms of rupees

VIII. CONCLUSION

This study contains proper observation of inventory management in the company. A better inventory management can solve all the problems occur in inventory and helping the company to face the problems by following proper techniques and controlling. This will reduce the huge money investment problems and it will lead the way for avoiding such circumstances. Inventory is timely changing physical asset which is sold or being a dead stock have by the company. It creates way for the production process if shortage occurs in the production and also it gets more even after the production. An efficient inventory management can control and make the company to grow more and if in inefficient way it will ruin the company business. Companies are

always concentrates on domestic as well as international in order to increase the business globally based on trends. This study is on leading brake manufacturing company conducting ABC analysis for items predicting the future demands which should be forecasted by the company. From the study it is shown that buying of materials and shortage occurs due to improper way of forecasting the demand. ABC analysis is carried to find out the materials which are moves fast and important to the company and which is differs from sales and volume in the inventory.

REFERENCES

- 1 S. Chopra and P. Meindl, *Supply Chain Management Strategy, Planning and Operation*, 4th Ed, Pearson, 2010.
- 2 F. D. Hedrick *et al*, "Inventory Management. Purchasing for Owners of Small Plants," *Buying for Retail Stores and Inventory Management*, 2012.
- 3 C. Laeiddee, "Improvement of Re-Order Point for Drug Inventory Management at Ramathibodi Hospital," *Master Thesis*, Mahidol University, 2010.
- 4 Muris Lage Junior, Moacir Godinho Filho, Variations of the kanban system: Literature review and classification, *Int. J. Production Economics* 125 (2010) 13–21
- 5 Sipper, D, Bulfin Jr, R.L. *Production: Planning, Control, and Integration*, McGraw-Hill, New York, 1997.
- 6 Performance, *Academy of Management Journal*. Vol.38, No.5, p. 1325-1360. Heizer, J. and Render, B. 2005. *Flexible Version: Operation Management*, 7th edition, New Jersey: Prentice Hall.
- 7 Kobbacy K., Liang Y. 1999. Towards the development of an intelligent inventory management system, *Integrated Manufacturing Systems*. p. 354-366.
- 8 Donald W., 2003. *Inventory Control and Management*, 2nd Edition, John Wiley & Sons Ltd.

Thermal Performance Analysis of the Sustainable Solar Air-Conditioner System by Solar Cooling Tube

Babu S¹, Hariprakasham K², Premkumar T³, Subaasini M G⁴ and Mathanbabum⁵

^{1,4}Mechanical Engineering Department, PSG College of Technology, Coimbatore-004

²Senior Data Analyst at Solver minds Solutions & Technologies Pvt. Ltd Chennai

³Mechanical Engineering Department, PSG Institute of Technology and Applied Research, CBE-062

⁵Research Scholar, Mechanical Engineering Department, Government College of Engg. Bargur

ABSTRACT

A solar air conditioner using thermal performance method was experimentally studied in this paper. The coefficient of performance (COP) of the solar cooling tube was mostly affected by the vacuum degree of the system. In past research, the thermal vacuum method, using an electric oven and iodine-tungsten lamp to heat up the adsorbent bed and H₂O vapor to expel the air from the solar cooling tube, was used to manufacture solar cooling tubes. This paper presents a novel thermal vacuum combined with vacuum pump method allowing an increased vacuum state for producing solar cooling tubes. The following conclusions are reached: the adsorbent bed temperature of solar cooling tube could reach up to 233°C, and this temperature is sufficient to meet desorption demand; the refrigerator power of a single solar cooling tube varies from 1W to 12W; the total supply refrigerating capacity is about 287 kJ; and the COP of this solar cooling tube is about 0.215.

Keywords – Solar energy, Air conditioner system, solar tube

1. INTRODUCTION

With the improvement of people's living standard, the demand for air conditioner is increasing. Use of CFCs for refrigeration compression has global warming potential (GWP) and ozone depletion potential (ODP), so their use should be minimized. The energy problem has become a major problem facing human development, and has led to efforts to reduce fossil fuel usage. Solar energy, one of the most abundant resources, has many advantages, most importantly that it is environmentally friendly. This has led to attention from the worldwide research community.

Adsorption refrigeration uses nature working pairs as refrigerants and solar energy as a heat resource, so it consumes no fossil fuels during refrigeration process and is environment friendly. Ferreira Leite et al. [1] presented the characterization and the pre-dimensioning of an adsorption chiller as part of a 20kW air conditioning central unit for cooling a set of rooms that comprises an area of 110m². The adsorption chiller's expected coefficient of performance (COP) was found to be around 0.6. Khattab [2] presented the description and operation of a simple structure, low cost solar-powered adsorption refrigeration module. Test results showed that a module using bed technique Type 4 and reflector arrangement Type C provided the best performance. Wang et al. [3, 4] used a compound adsorbent of CaCl₂ and activated carbon as working pairs and to produce an ice-making test unit for fishing boats. At evaporating temperatures of -35°C and -25°C, the cooling powers are 0.89 and 1.18kW respectively. Clause [5] explored the possibility to perform heating and air-conditioning of a state-of-the-art building located near Paris in France. For air-conditioning, thermal comfort was achieved as indoor temperature was kept below 25°C during five consecutive hot days.

2. SOLAR ENERGY

India is a tropical country is blessed with a lot of sunshine whose availability extends to more than nine months in a year. It is one of the most promising sources of clean energy. However the major problems encountered with the utilization of solar energy are its low energy content on earth, which rarely exceeds 1 kW/m² which is low value of technological utilization like drying & Secondly the limited hours of availability. Information on solar radiation is needed in application fields dealing with the exploitation of solar energy. An important input parameter is the global solar radiation received. This in turn is a function of several variables such as the nature and extent of cloud cover, water vapor content and other atmospheric constituents such as O₂, N₂, CO₂, O₃, dust etc., It is therefore not always possible to predict the actual of irradiant for a given location. Nevertheless the analysis of long term meteorological data on solar radiation makes it possible not only the interrelationship between its components, but also the types of parameters governing the statistics of their characteristic distributions. Attempts have been made to determine the hourly values of total radiation through its relationship with the daily solar radiation. Accurate methods of determining incident and transmitted solar radiation values on inclined surfaces from horizontal solar data are usually required in the design, dynamic performance evaluation and control of solar energy systems and devices. Most meteorological data give only the global or

total radiation on horizontal surfaces. In order to determine the radiation values on inclines surfaces from horizontal total solar radiation data, correlation procedure is required to separate the direct and diffuse components of the horizontal global radiation. The direct and diffuse radiation has quite distinct characteristics of their collection and transmission of transparent materials comparison of the performance and relative cost different stationary reflector design are required for prospective manufactures of stationary solar collectors. For many applications (for domestic hot water, low pressure steam for industry) a symmetrical reflector is appropriate. Hence a thorough study about the structure, energy of the sun becomes very essential.

3. MANUFACTURE OF THE SOLAR COOLING TUBE

The manufacturing process of solar cooling tube is mainly

composed of three steps: (1) the preparation filling process; (2) preliminary drying of the solar cooling tube; (3) operating vacuum state by means of thermal/vacuum method. The steps are as follows. First, the 13X zeolite is activated in the 325°C oven for 8 hours, and then an appropriate amount of highly pure sodium silicate and pure water is added to prepare the adsorption compound. The resulting adsorbent compound has better thermal conductivity and formability than 13X powder [15]. An electric mixer is used to stir the mixture until it becomes liquid state. A funnel is used to fill the confected the compound adsorbent into all-glass tubular solar collector and preliminary dries it by iodine-tungsten lamp. Second, put the all-glass tubular solar collector filled with the compound adsorbent into a high borosilicate glass and welding pipe using glass welding lathe, then the semifinished solar cooling tube was made. Third, 200mL pure water is placed into the semi-finished solar cooling tube. The tube is then placed into an electric dry oven, and welding the solar cooling tube with adsorption bottle, jointing pot beaker and vacuum pump. Figure 1 is a photograph of the production equipment. After several hours discharging



Figure 1: Photograph of manufacturing solar cooling tube.

4. PRINCIPLE OF SOLAR COOLING TUBE

The structure of the solar cooling tube is shown in Figure 3. The solar cooling tube contains these major components: solar collector, adsorbent bed, condenser, inner tube, and evaporator. The solar collector, condenser, inner tube, and evaporator are made of hard borosilicate glass. Using 13X zeolite, the temperature difference between daytime and nighttime corresponds to the adsorption capability difference of refrigerant water; hence, the solar cooling tube achieves refrigeration cycle.

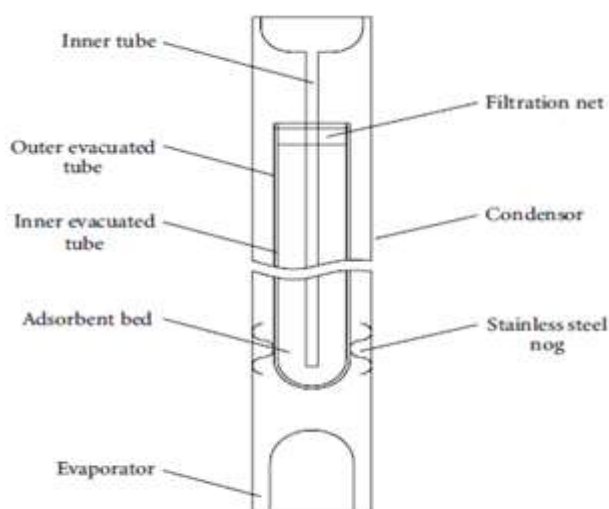


Figure 2: Sketch of the solar cooling tube.

5. EXPERIMENT SETUP

The sketch and photograph of the experiment in solar cooling tube was shown in Figures 3. The main apparatus used for this experiment are as follows: 2700 Multimeter/ Data Acquisition system of Keithley Co., was used for collecting the data of temperature measurement, T-type thermocouples and K-type thermocouples are the temperature sensors for lower temperature and higher temperature testing, respectively, the model TRM-123 temperature and radiation instrument produced by Jinzhou was used for testing the solar radiation density, and the model RYQ- 1 automatic surface meteorological station was used for measuring the environmental temperature and air relative humidity.

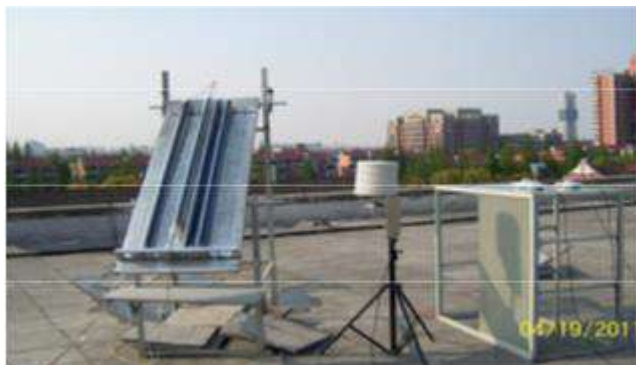


Figure 3: The photograph of the experiment.

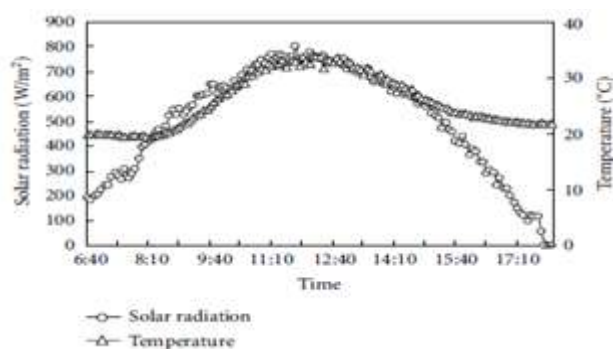


Figure 4: Solar radiation and ambient temperature variation

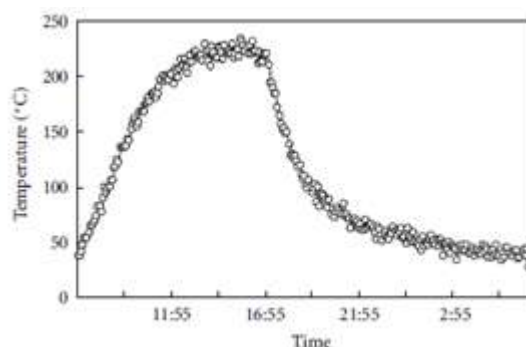


Figure 5: The adsorbent bed temperature variation of the solar cooling tube.

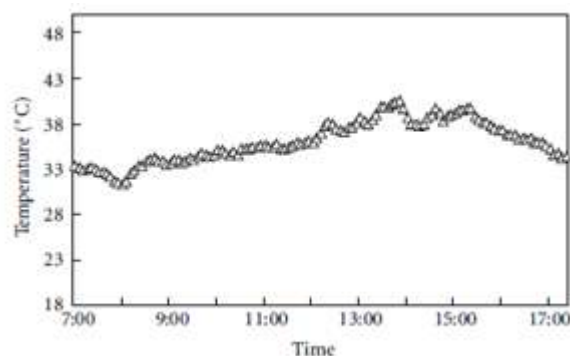


Figure 6: The condensation temperature variation.

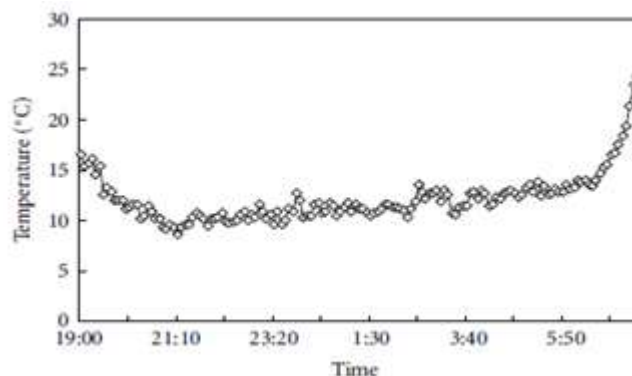


Figure 7: The evaporation temperature variation.

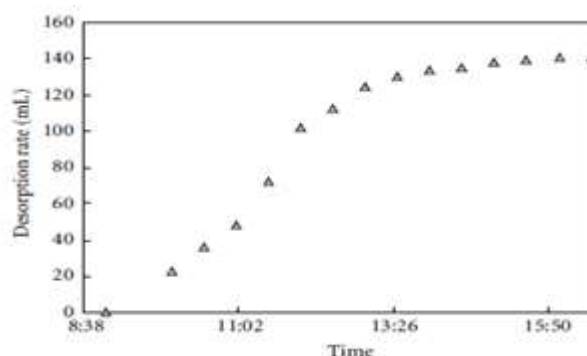


Figure 8: The desorption capacity variation of the solar cooling tube.

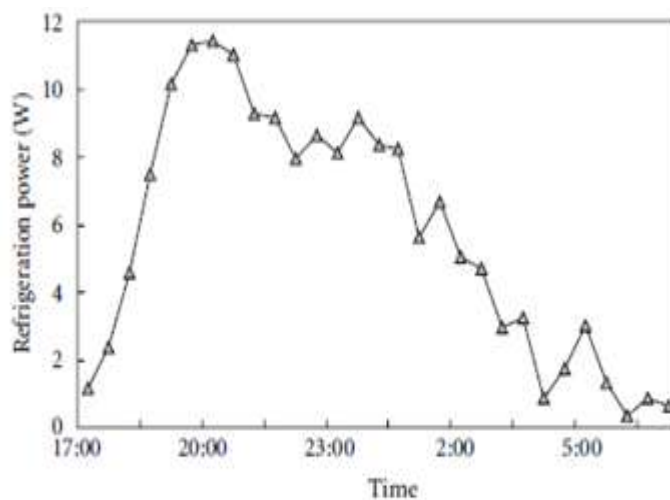


Figure 9: The refrigerator power of a single solar cooling tube.

6. CONCLUSION

This paper focused on an experimental study of a solar cooling tube using a thermal/vacuum emptying method. The solar cooling tube uses solar energy as a heating resource to complete the adsorption cycle, reducing damage to the environment compared to common alternatives. The performance of solar cooling tube was experimentally studied in this research and the following conclusions can be drawn:

- (1) When ambient temperature is about 19.4°C–33.8°C, and the solar radiation is about $20.1 \text{ MJ} \cdot \text{d}^{-1} \text{ m}^{-2}$, the adsorbent bed temperature of solar cooling tube reaches up to 233°C. This temperature can meet desorption demand.
- (2) At the nighttime, the adsorbent bed temperature of the solar cooling tube cooled down to the minimum temperature about 33°C and this temperature can meet adsorption demand. The temperature difference between adsorbent bed and ambient temperature is about 14°C.
- (3) The refrigerator power of a single solar cooling tube varied from 12W to 1W. The total supply refrigerating capacity is about 287 kJ and the COP of this solar cooling tube is about 0.215.

REFERENCES

- 1 Babu S, Franklin, G, Nirmal Kumar, T V. &KasiAswin, K (2018) 'Refrigeration Using Waste Heat Recovery From Exhaust Gas Of Engine, . (ISBN: 978-1-5386-4021-0), IEEE Xplore28, DOI: 10.1109/TAPENERGY.2017.8397314.
- 2 Mithat, (2008) 'Thermal energy storage performance of paraffin in a novel tube in shell system', Applied Thermal Engineering Vol.28,PP: 405– 413.
- 3 Demirbas, M. Fatih, (2006), 'Thermal Energy Storage and Phase Change Materials: An Overview', Energy Sources, Part B, Vol.1 and PP:85 – 95.
- 4 Babu S, Senthilvel S, Paul Gregory F, Gopi T, (2020) 'Investigations on Improving the Efficiency of Solar Air Heater Using Extended Surfaces', Springer Proceedings in Energy, ISSN: 2352-2534, doi.org/10.1007/978-981-15-2662-6_25.
- 5 Babu S, R. Sriram, S. Gopikrishnan, and A. Praveen "Solar Energy Simulation of Fresnel lens Concentrated System for Thermal Electric Generator" Lecture Notes in Mechanical Engineering, Springer Nature, August 2021, PP: 833-839, ISBN: 978-981-16-0698-4.
- 6 Babu S, ShyamSashvat R R, Daniel Susai, and Ajay N, (2021) 'FEM analysis of novel Fresnel sheet solar concentrating system for TEG', IOP Conf. Series: Materials Science and Engineering 1130 012028, doi:10.1088/1757-899X/1130/1/012028.
- 7 Demirbas, M. Fatih, (2006), 'Thermal Energy Storage and Phase Change Materials: An Overview', Energy Sources, Part B, 1:85 – 95.

